THE JOURNAL
OF
CHEMICAL PHYSICS

VOLUME 34, NUMBER 2 FEBRUARY, 1961

Heats of Mixing in Liquid Alkali Nitrate Systems

O. J. KLEPPA AND L. S. HERSH

Institute for the Study of Metals and Department of Chemistry, University of Chicago, Chicago, Illinois

(Received July 29, 1960)

The enthalpies of mixing in binary liquid alkali nitrate systems have been measured, and are all negative. It is found that the magnitude of the molar mixing enthalpy (ΔH^M) increases in a regular fashion with increasing difference in size between the two participating cations, according to the following approximate relation

$$\Delta H^M \cong -X(1-X)U[(d_1-d_2)/(d_1+d_2)]^2.$$

Here X and $(1-X)$ are the mole fractions of the two components, U is the lattice energy of the mixture, while d_1 and d_2 are the interionic distances characteristic of the two pure components. The results are in accord with the view that in these systems the principal source of the enthalpy of mixing is the reduction in Coulombic repulsion between the second nearest neighbor cations. For binary systems with negative enthalpies of mixing of the order of RT there is evidence for short-range order among the cations.

INTRODUCTION

DURING recent years physical and inorganic chemists have shown increasing interest in the properties of fused salts. As a result, a great deal of new information has become available regarding the structure, equilibrium properties, and transport properties of such systems.[1]

There are, nevertheless, still surprisingly large gaps in our knowledge, even regarding some of the more obvious and fundamental points. For example, we still know very little about how the thermodynamic properties of fused salt mixtures depend on the size, charge, and structure of the participating ions. The experimental picture is particularly inadequate if we consider the relative importance of heat and entropy in the departure of fused salt mixtures from ideal behavior.

In the present study we shall consider only the simplest possible type of mixture, namely, binary systems of salts which have a common anion. This problem already has received some attention in the past, notably in the well-known emf study by Hildebrand and Salstrom[2] of liquid mixtures of silver bromide with different alkali bromides. However, since silver bromide can hardly be considered as a prototype of an *ionic* substance, these earlier results do not permit general predictions to be made regarding typically ionic systems.

By means of the new high-temperature reaction calorimeter described in another communication,[3] we have made direct and precise determinations of the heats of mixing in binary alkali nitrates. Unfortunately, the new calorimeter is not designed for operation at the high temperatures required for studies of the fused alkali halides. Nevertheless, since the corresponding nitrates show important analogies with the halides, we believe that our results may serve also as a guide to the behavior of the theoretically more interesting halide mixtures. It is our plan to return to this problem later, when calorimetric equipment and techniques which permit operation at the higher temperatures have been developed.

In an earlier communication we presented detailed heat data for liquid mixtures of sodium-potassium nitrate. In the present work we give a report on the other nine binary alkali nitrate systems. For six of these we report reasonably detailed data, while for the remaining three [(K-Rb)NO_3, (Rb-Cs)NO_3, (Li-Cs)NO_3] our results serve mainly to establish the order of magnitude of the excess enthalpy: In lithium-cesium nitrate the heat of mixing is larger than for all the other systems explored (max about -800 cal/mole). However, lithium nitrate is already undergoing

[1] See H. A. Levy, P. A. Agron, M. A. Bredig, and M. D. Danford, Ann. N. Y. Acad. Sci. **79**, 761 (1960).

[2] J. H. Hildebrand and E. J. Salstrom, J. Am. Chem. Soc. **54**, 4257 (1932).

[3] O. J. Kleppa, J. Phys. Chem. (to be published).

Copyright © 1961 by the American Institute of Physics

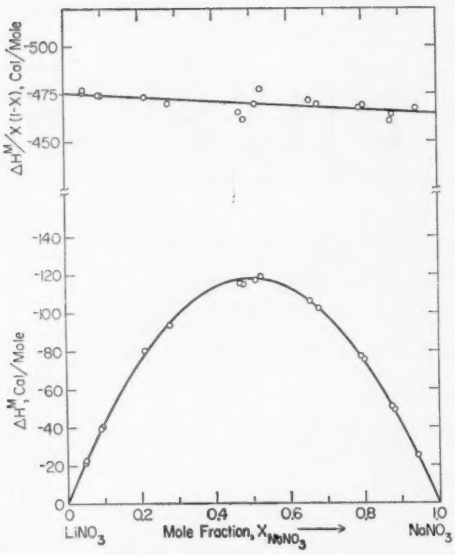

FIG. 1. Molar integral heats of mixing (ΔH^M) in mixtures of lithium nitrate-sodium nitrate at 345°.

some thermal decomposition at the temperature where cesium nitrate melts (414°C). Therefore, precise measurements were not attempted. For potassium-rubidium nitrate and for rubidium-cesium nitrate the heats of mixing are so small (−15 cal/mole or less) that precise values could not be obtained.

EXPERIMENTAL

The mixing experiments reported were performed at 345° and 450°C. The calorimeter temperature was determined by means of an iron-constantan thermocouple, which was checked every two weeks against a N.B.S. calibrated Pt-10% PtRh couple. Owing to imperfections in the controller system the operating temperature of the calorimeter changed slightly from day to day and from week to week. However, it generally was within about 2 deg of the stated mean temperatures.

The lithium, sodium, and potassium nitrates used in the present work were all Mallinckrodt Analytical Reagents. The salts assayed 99.88% $LiNO_3$, 100.04% $NaNO_3$ and 100.03% KNO_3, respectively, as determined by the ion-exchange method. The salts melted to form clear colorless liquids, and were used without further purification after drying in the air at 130°C.

As purchased, the rubidium and cesium nitrates were of nominal "99.9%" purity (from the Millmaster Chemical Corporation). Before use these nitrates were recrystallized once from distilled water. Samples of the recrystallized salts assayed 100.27% $RbNO_3$ and 100.01% $CsNO_3$, respectively, and they melted to form clear and colorless liquids.

In the present work Pyrex glass containers were used, as described in the work cited in footnote 3. In the work with $LiNO_3$ at 345°C the glass, after only one run, took on a somewhat opaque appearance, suggesting a slight chemical attack. However, no significant increase in opaqueness resulted from additional runs, and the glass containers showed no change in weight. There was no indication of any attack on the glass by the other nitrates.

In most experiments reported below we used the "balanced heat effect" method, i.e., 90–100% of the exothermic heat of mixing was compensated through a drop of gold from room temperature into the calorimeter.[3] The total amount of salt used in each experiment was 0.05 to 0.2 mole. The actually observed heats of mixing ranged from 0.3$_0$ cal [for about 0.1 moles of a (Rb-Cs)NO_3 mixture) to about 50 cal [for (Li-Cs)NO_3 and (Li-Rb)NO_3]. The correction for ampoule breakage and manipulation was 0.05 (±0.03) cal. The uncertainty in this figure represents the major source of error for the experiments involving small heats of mixing.

RESULTS

The experimental results for the six binary systems which were explored in detail are presented graphically in Figs. 1–6. In these figures are plotted both the molar heat of mixing, ΔH^M, and the quantity $\Delta H^M/X(1-X)$.

It will be noted that for potassium-cesium nitrate and for lithium-sodium nitrate this quantity appears to depend linearly, or very nearly linearly, on composition.

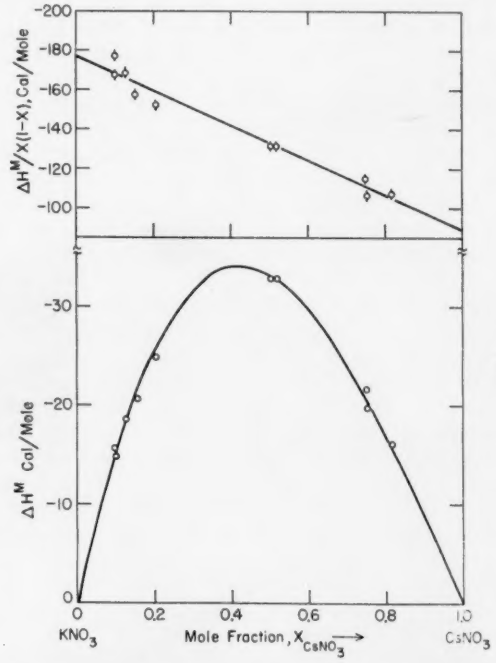

FIG. 2. Molar integral heats of mixing (ΔH^M) in mixtures of potassium nitrate-cesium nitrate at 450°.

A near-linear dependence of $\Delta H^M/X(1-X)$ on X was previously observed for sodium-potassium nitrate.[3] We derived the following expressions for ΔH^M by the least-squares method,

$$(\text{K-Cs})\text{NO}_3,\ 450°: \Delta H^M = -X(1-X)(89.5+87.5X) \text{ cal/mole}$$

$$(\text{Li-Na})\text{NO}_3,\ 345°: \Delta H^M = -X(1-X)(464+11.5X) \text{ cal/mole.}$$

In these expressions X is the mole fraction of the nitrate of the *smaller* ion.

For the remaining four systems it is apparent that the experimental values of $\Delta H^M/X(1-X)$ cannot be represented by straight lines. For these systems we have fitted the data by analytical expressions of the type

$$\Delta H^M = X(1-X)[a+bX+cX(1-X)]. \qquad (1)$$

Values of a, b, and c were derived by the least-squares method. (In all cases X is the mole fraction of the nitrate of the *smaller* ion.)

All values of these constants, and the corresponding values for sodium-potassium nitrate, are given in Table I. This table demonstrates some very interesting facts:

(a) The magnitude of the (negative) enthalpy of mixing, as measured by the constant a, increases in a regular fashion with increasing separation of the two alkali metals in the periodic system. We shall demonstrate below that there is a simple, semiempirical relation between the excess enthalpy and the relative difference in size of the two solution partners.

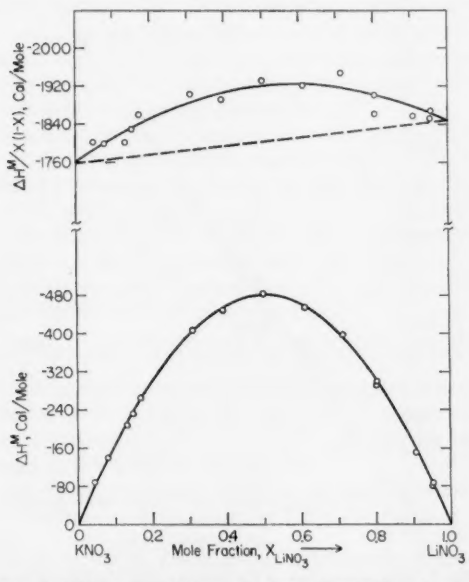

FIG. 3. Molar integral heats of mixing (ΔH^M) in mixtures of lithium nitrate-potassium nitrate at 345°.

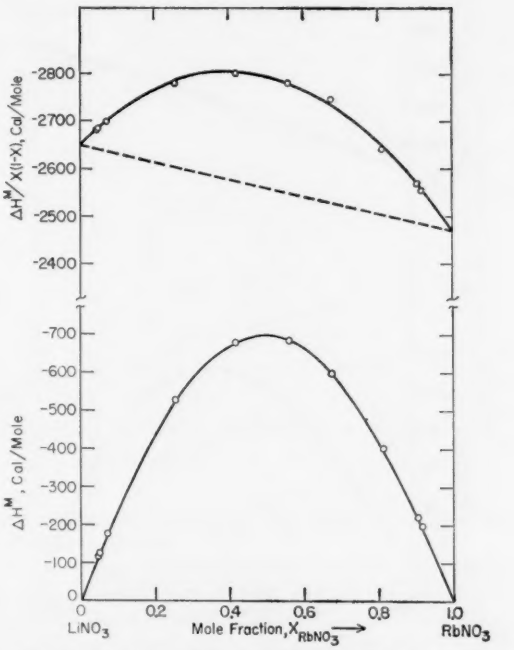

FIG. 4. Molar integral heats of mixing (ΔH^M) in mixtures of lithium nitrate-rubidium nitrate at 345°.

(b) All systems exhibit energetic asymmetry, a measure of which is the value of the constant b, the difference between the two limiting heats of solution. It will be noted that the b's are all negative. Thus the limiting enthalpy of solution of the salt of the larger ion in the salt of the smaller ion is always more negative than that for the opposite process.

(c) Note finally that the deviation of $\Delta H^M/X(1-X)$ from a linear dependence on composition increases with increasing negative values of ΔH^M. Thus in $(\text{Na-Rb})\text{NO}_3$, the value of c is -36 cal (about 1% departure from linearity), while in $(\text{Li-Rb})\text{NO}_3$ it is -945 cal (about 9%). We shall demonstrate below that these departures from linearity probably arise from short-range order in the second nearest neighbor shells (i.e., among the cations).

Another summary of the experimental results is presented in Fig. 7. In this figure we have plotted the quantity $\Delta H^M/X(1-X)$ at 50-50 composition along the ordinate axis. Along the abscissa we plot the "Tobolsky parameter"[4] $[(d_1-d_2)/(d_1-d_2)]^2$, where d_1 and d_2 are the interionic distances characteristic of the two pure salts. For the four systems in which we found a curvature in $\Delta H^M/X(1-X)$ two points are plotted. The open circles give the actual experimental values, while the filled circles give the values obtained by omit-

[4] A. V. Tobolsky, J. Chem. Phys. **10**, 187 (1942).

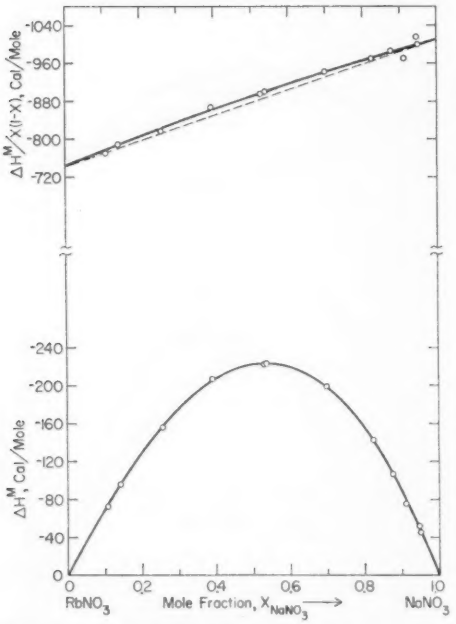

FIG. 5. Molar integral heats of mixing (ΔH^M) in mixtures of sodium nitrate-rubidium nitrate at 345°.

TABLE I. Summary of heat of mixing data for binary alkali nitrate systems (in cal/mole).

System, °C	a	b	c
(Li—Na)NO_3; 345°	−464	−11.5	~0
(Li—K)NO_3; 345°	−1759	−87	−463
(Li—Rb)NO_3; 345°	−2471	−178	−945
(Li—Cs)NO_3; 450°	(−3000)	...	...
(Na—K)NO_3; 345–450°	−408.5	−68	~0
(Na—Rb)NO_3; 345°	−744.5	−268	−36
(Na—Cs)NO_3; 450°	−1041	−435	−93
(K—Rb)NO_3; 345°	(−60)	...	...
(K—Cs)NO_3; 450°	−89.5	−87.5	~0
(Rb—Cs)NO_3; 450°	(−14)	...	...

ting the quadratic terms in Eq. (1); i.e., the values of $\Delta H^M/X(1-X)$ derived by linear interpolation between the two terminal values.

In the usual approximation we have

$$d_{MeNO_3} = r_{Me^+} + r_{NO_3^-}.$$

For the lithium, sodium, potassium, and rubidium nitrates we have used Pauling's crystal radii for

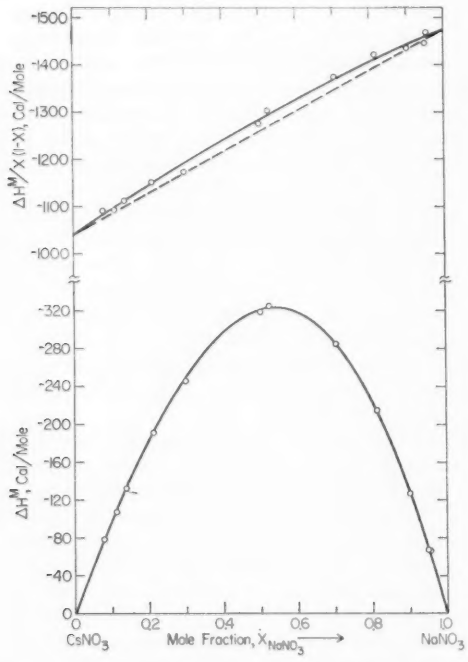

FIG. 6. Molar integral heats of mixing (ΔH^M) in mixtures of sodium nitrate-cesium nitrate at 450°.

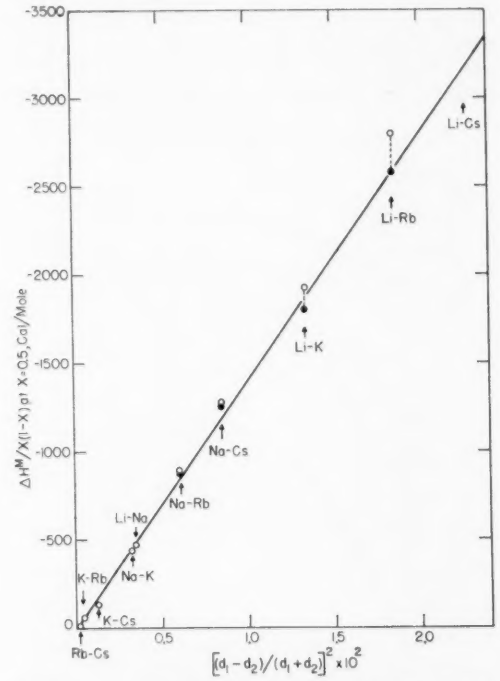

FIG. 7. The dependence of the magnitude of the heat of mixing ($4\Delta H^M_{0.5}$) on the Tobolsky parameter (open circles: experimental values; filled circles: interpolated values).

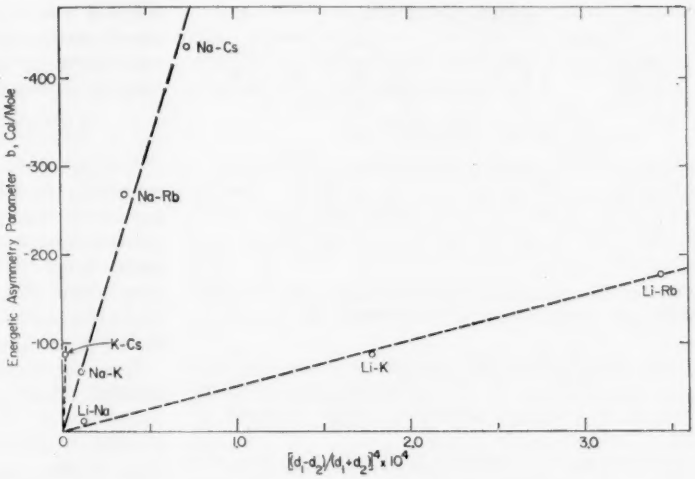

FIG. 8. The dependence of the energetic asymmetry (b) on the Tobolsky parameter.

r_{Me^+}. A value of $r_{NO_3^-}$ was obtained by the following procedure. It is known that $RbNO_3$, $TlNO_3$, and $CsNO_3$ have high-temperature cubic (CsCl) modifications.[5] From the lattice parameters of these salts we calculated values of d_{MeNO_3}, making a 3% correction for the change in coordination number from 8 to 6. These values are given in the third column of Table II.

If we now assume that the cations in these salts have the usual ionic radii[6] (column 4), we obtain the values of $d_{NO_3^-}$ given in the last column. It will be seen that the values of $d_{NO_3^-}$ from the data on $RbNO_3$ and $TlNO_3$ are in quite good agreement, yielding an average of 4.37 A, i.e., the size of the NO_3^- ion is comparable to that of I^-. Note, however, that the value derived from the lattice parameter of $CsNO_3$ deviates significantly. For the mixtures involving liquid cesium nitrate we used the value of d_{CsNO_3} recorded in Table I to calculate the Tobolsky parameter.

It should finally be noted that the slope in Fig. 7, i.e., the "constant" which relates $-4\Delta H_{0.5}{}^M$ to the Tobolsky parameter, is about 140 kcal. This quantity is of the order of magnitude of the lattice energy (U) for the alkali nitrates. Neglecting finer points in our results, we accordingly may write the following approximate empirical expression for the heat of mixing in all the binary liquid alkali nitrates

$$\Delta H^M \cong -X(1-X)U[(d_1-d_2)/(d_1+d_2)]^2 \text{ cal/mole.}$$

Here U is the lattice energy of the considered mixture.

So far we do not know to what extent this expression may apply also in other fused ionic systems. We shall return to this problem subsequently.

For the seven systems for which we have the required information, we have plotted in Fig. 8 the values of the asymmetry parameter b vs the *fourth* power of the Tobolsky parameter.

It is of considerable interest to note that for a systematic sequence of systems such as $(Li\text{-}Na)NO_3$—$(Li\text{-}K)NO_3$—$(Li\text{-}Rb)NO_3$, the values of b fall on a straight line. This holds also for the mixtures of $NaNO_3$ with KNO_3, $RbNO_3$ and $CsNO_3$, although in this case the slope of the line is larger than for the lithium systems by a factor of the order of 12! If we consider the ratio b/a, we find that this ratio changes from 0.025 for lithium-sodium nitrate to 0.166 for sodium-potassium nitrate and to 0.98(!) for potassium-cesium nitrate. We have as yet no satisfactory quantitative explanation for these striking variations in energetic asymmetry.

DISCUSSION

It is of interest to consider how the present results differ from similar data already available for simple ionic solid solutions (such as KBr-NaBr, etc.). We shall preface this discussion with a brief outline of the structure of molten salts as it is known today.

It is recalled that simple ionic solids may be considered to consist of two interpenetrating "lattices," one of which contains all the cations, while the other one holds all the anions. In the simplest case, the

TABLE II. Ionic sizes in rubidium, cesium and thallium nitrate. Data in angström units.

Salt	Lattice parameter, a[a]	$0.97\,a\sqrt{3} = 2d_{MeNO_3}$	d_{Me^+}[b]	$d_{NO_3^-}$ (calc)
$RbNO_3$	4.37	7.34	2.96	4.38
$CsNO_3$	4.49	7.54	3.38	4.16
$TlNO_3$	4.31	7.24	2.88	4.36

[a] R. W. G. Wycoff.[5]
[b] L. Pauling.[6]

[5] R. W. G. Wycoff, *Crystal Structures* (Interscience Publishers, Inc., New York, 1951), Vol. I.
[6] L. Pauling, *Nature of the Chemical Bond* (Cornell University Press, Ithaca, New York, 1948), 2nd ed.

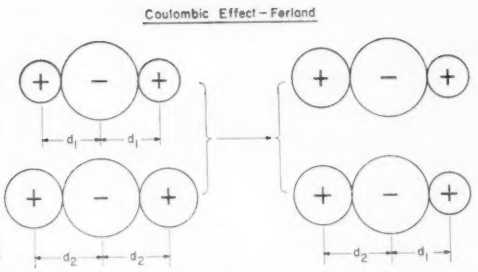

FIG. 9. Model illustrating change in second nearest-neighbor repulsion on mixing (see work cited in footnote 14).

sodium chloride structure, each cation is contained in a "cage" consisting of six anions. Outside this cage is the shell of next nearest neighbors, which contains 12 cations, and so on.

It seems to be characteristic of ionic salts that the process of fusion is associated with a very considerable increase in volume. For alkali halides this volume change is of the order of 20%, for the nitrates the change is 10–15%.[7] Very recent measurements [H. Schinke and F. Sauerwald, Z. anorg. u. allgem. Chem. **304,** 25 (1960)] indicate even smaller values. (For metals and for "nonionic" salts such as the silver halides, this expansion characteristically is much smaller, often of the order of 4–5%. If we make the naive approximation that the individual ions have characteristic radii, we conclude that the major portion of this volume change on fusion must give rise to empty sites in the two interpenetrating structural networks. This will lower the coordination number in the nearest-neighbor shells from six (in solid sodium chloride) to a value closer to five. Coordination numbers of this magnitude have, in fact, been found in fused alkali halides in recent x-ray and neutron diffraction studies.[8]

Note that the energy associated with placing an anion on a cation site, or vice versa, is of the order of the lattice energy both in the liquid and in the solid state. In either case there will be no significant "mixing" of anion and cation sites at ordinary temperatures.

Note also that in the fused salt, as in the corresponding solid, the structural arrangement of the nearest neighbors probably in large measure is governed by the repulsion (Coulombic+core) between the large negatively charged ions. For a family of salts with a common anion, we might accordingly expect extensive structural similarity from one member of the family to the next.

When a solid solution is formed from two *ionic* salts which have cations of the same charge and a common anion (i.e., alkali halides), the process is always associated with a positive excess enthalpy. By use of a simple lattice model, Tobolsky[4] showed that in this case the molar enthalpy of mixing can be estimated from the expression

$$\Delta H^M \cong X(1-X)U[d_1-d_2)/(d_1+d_2)]^2.$$

Except for the positive sign, we recognize that this expression is identical with our own approximate formula for the liquid nitrates! It is not as yet known to what extent our formula may be applied also in other fused ionic systems. However, preliminary calorimetric data on liquid (K-Li)F, (K-Li)Cl, and (K-Li)Br recently quoted by Aukrust *et al.*,[9] seem to be in general agreement with our expression.

Since the work of Tobolsky,[4] there have been more detailed theoretical studies of the energy change associated with the formation of ionic solid solutions, notably by Wallace,[10] by Wasastjerna,[11] and by Durham and Hawkins.[12]

On the whole, these studies do not seem of particular importance from the point of view of the investigator of fused salt mixtures. However, a point of considerable interest is discussed in some detail by Durham and Hawkins. These authors show that if all ions in a mixed crystal are forced to stay on the true lattice sites, the calculated (positive) enthalpies of mixing are much too large. However, there is a very considerable gain in energy when the ions are allowed to settle in local energy minima. This brings the calculated heat of mixing into reasonable agreement with experiment.

If we carry these ideas over into the liquid state, it seems probable that the observed negative enthalpies of mixing in fused salts are related in a simple way to the loose liquid structure. This structure offers the individual ions excellent opportunities to find local energy minima. This points toward possible quantitative calculations of the Coulombic energy change on mixing in its dependence on the size of the common ion, and on the fraction of empty sites. As far as is known no detailed and rigorous calculations of this type have as yet been made. Therefore we shall in the following explore the problem from a less quantitative point of view.

From a simple analysis it seems likely that the major part of the Coulombic heat of mixing in fused salts which have a common ion must arise either from changes in the nearest-neighbor shell, or in the second nearest-neighbor shell.

If, for example, the process of mixing is associated with a certain increase or decrease in the number of nearest neighbors, this rearrangement might be expected to give rise to significant and correlated changes

[7] W. J. Davis, S. E. Rogers, and A. R. Ubbelohde, Proc. Roy. Soc. (London) **A220,** 14 (1953).

[8] H. A. Levy, P. A. Agron, M. A. Bredig, and M. D. Danford, Ann. N. Y. Acad. Sci. **79,** 762 (1960).

[9] E. Aukrust, B. Björge, H. Flood, and T. Förland, Ann. N. Y. Acad. Sci. **79,** 830 (1960).

[10] W. E. Wallace, J. Chem. Phys. **17,** 1095 (1949).

[11] J. A. Wasastjerna, Soc. Sci. Fennica, Commentationes Phys.-Math. **15,** 3 (1949).

[12] G. S. Durham and J. A. Hawkins, J. Chem. Phys. **19,** 149 (1951).

in energy and in volume. Now it is known that the volume change on mixing in sodium-potassium nitrate is small and positive,[13] while we have shown in the present work that the corresponding change in enthalpy is negative. Thus it seems unlikely that a change in the nearest-neighbor shell is the principal source of the mixing enthalpy (energy). In fact, the sign, the magnitude, and the observed correlation with the Tobolsky parameter indicate that the enthalpy of mixing probably arises, at least in part, from changes which occur in the second nearest-neighbor shell. We shall illustrate this by means of a crude structural model which is due to Förland,[14] and which is reproduced in Fig. 9.

Let us evaluate the change in Coulombic energy on "mixing" for this hard-sphere charged ion model. Since the nearest-neighbor configurations are unchanged, the total change in energy arises from a reduction in second nearest neighbor repulsion. Thus we obtain a gain in energy,

$$\Delta E = -(e^2/2)(1/d_1+1/d_2)[(d_1-d_2)/(d_1+d_2)]^2.$$

It is clearly fortuitous that this "model," which neglects the three-dimensional character of our problem and disregards all higher order terms in the total Coulombic energy, gives an expression for the energy change which is correct as to sign, order of magnitude, and functional dependence on the Tobolsky parameter. Nevertheless, the agreement suggests that further work along this line might be worthwhile.

At the present time detailed and realistic calculations of this type have not, to the knowledge of the authors, been attempted. However, through the courtesy of Dr. Milton Blander of Oak Ridge we have received the results of some unpublished calculations carried out by him.[15] Blander improves Förland's model by considering solutions in an infinite linear ionic chain. Specifically, he calculates the energy change associated with the dissolution of one molecule of a one-dimensional solute consisting of hard-sphere charged ions, and with an interionic distance of $r(1+\Delta)$, into a solvent consisting of hard-sphere charged ions of interionic distance r.

Blander finds (a) that the energy change is always negative and of magnitude comparable to the experimental values for the fused nitrates; (b) that for small Δ's the relation between the energy change and Δ is roughly parabolic; and (c) that his model shows a small but definite energetic asymmetry.

His calculations seem to confirm that the major part of the negative enthalpy of mixing may indeed arise from the reduction in second nearest-neighbor repulsion. This effect is symmetrical; i.e., for this term the energy change for the transfer of KNO_3 into $NaNO_3$ does not differ from that for the inverse process. However, changes in the interactions between more distant neighbors give rise to energetic asymmetry. These asymmetries are in the same direction as those observed experimentally.

SHORT-RANGE ORDER

It is well known from elementary solution theory that for solutions with a nonzero heat (energy) of mixing, departures from a random distribution of the two components in the mixture are to be expected. Therefore, if we are correct in our tentative conclusion that the principal source of the heat of mixing in the considered fused salt mixtures is the change in second nearest neighbor interactions, we should be able to make quantitative estimates regarding departures from random mixing among the two cations. We should also be able to estimate the corresponding contributions to the various excess thermodynamic functions.

Let us designate the potential energy of the arrangement $\cdots A^+C^-A^+\cdots$ with v_{11}, that of $\cdots B^+C^-B^+\cdots$ with v_{22}, and that of the mixed arrangement $\cdots B^+C^-A^+\cdots$ with v_{12}. If we assume that the coordination number for the *next*-nearest neighbors is z, we obtain from the lattice theory of solution[16] the following expression for the molar heat of mixing

$$X(1-X)\lambda[1-X(1-X)2\lambda/zRT-\cdots]. \qquad (2)$$

Here $\lambda=(Nz/2)[2v_{12}-(v_{11}+v_{22})]$; N is Avogadro's number. For values of λ small compared to $zRT/2$, this expression reduces to the well-known form

$$\Delta H^M \cong X(1-X)\lambda, \qquad (3)$$

which corresponds to the zeroth or random mixing approximation.

In strict applications of this theory it is assumed that v_{11}, v_{22}, and v_{12} are independent of composition, i.e., the potential energies v do not depend on the local environment of the considered configurations. Therefore λ is considered to be a true "constant," and a plot of $\Delta H^M/X(1-X)$ vs X should give a straight line with a zero slope.

It is apparent from our experimental data that this assumption is not valid for the fused nitrate mixtures, since these all exhibit a certain measure of energetic asymmetry. In order to proceed, we make the additional arbitrary assumption that our expressions for ΔH^M still hold if we let λ vary linearly with concentration.

Under these circumstances we predict that systems with weak interaction (i.e., with small numerical values of λ or ΔH^M) should exhibit essentially random mixing. These should have a linear or near linear dependence of $\Delta H/X(1-X)$ on X. This is borne out by the data for (K-Cs)NO_3, (Na-K)NO_3, and (Li-Na)NO_3. How-

[13] O. J. Kleppa and D. Bearcroft (unpublished results).
[14] T. Förland, *On the Properties of Some Mixtures of Fused Salts* (N. T. H. Trykk, Trondheim, Norway, 1958).
[15] M. Blander (unpublished).
[16] See, e.g., J. H. Hildebrand and R. L. Scott, *Solubility of Non-Electrolytes* (Reinhold Publishing Corporation, New York, 1950), p. 146.

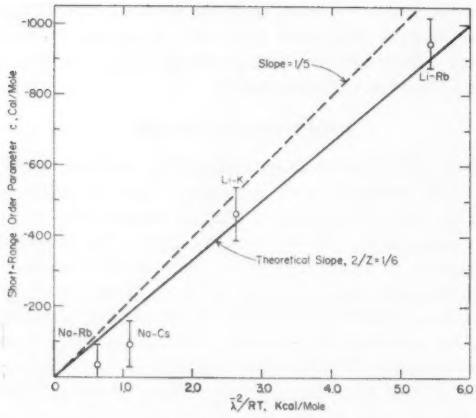

FIG. 10. The dependence of short-range order parameter (c) on the strength of interaction (λ).

ever, in systems with stronger interaction, a parabolic term in $\Delta H^M/X(1-X)$ is predicted. The magnitude of this term should be related in a simple, quantitative way to the magnitude of λ (or ΔH^M).

By comparison of Eq. (2) with Eq. (1), we note that an average value of λ may be obtained by setting $\bar{\lambda}=a+b/2$. We may similarly identify c with $-2\lambda^2/zRT$. If Eq. (2) is valid, we accordingly expect that a plot of c vs λ^2/RT should yield a straight line, with a numerical value of the slope of $2/z$. For the four systems (Na-Rb)NO_3, (Na-Cs)NO_3, (Li-K)NO_3, and (Li-Rb)NO_3, such a plot is given in Fig. 10. It will be noted that within experimental error these four systems do indeed give a straight line which passes through the origin. We see, furthermore, that the slope of this line is near $\frac{1}{6}$, which is the theoretical value derived from the number of second nearest neighbors in the sodium chloride structure. For the considered fused nitrates, the slope might be expected to be somewhat larger, perhaps between $\frac{1}{6}$ and $\frac{1}{5}$. In view of the possible error in our values of c, the agreement must be considered as very satisfactory.

CONCLUDING REMARKS

In the present paper we have discussed the properties of mixtures of fused salts from the simplest possible point of view, i.e., we have considered the ions as hard spheres of appropriate charge. Our results demonstrate that this naive model represents a useful zeroth approximation, just as in the corresponding theory of cohesion in ionic solids. It should be kept in mind, however, that in this discussion we have deliberately neglected other important contributions to cohesion in ionic systems, such as the possible effect of polarization, the influence of van der Waals forces, possible variations in the repulsive potential, etc. In view of the very restricted amount of experimental information which is as yet available, we believe an attempt at discussing these factors would be premature.

At the present time we are extending the scope of this investigation: Recently we have initiated additional work on other "low-melting" salt melts, and we are planning similar work on fused halides at more elevated temperatures. In these studies we hope to produce a sound experimental basis for future discussions of the dependence of the heat of mixing on the nature of the ions involved.

Later on we plan to measure also the free energy of mixing in typical fused salt systems. By comparing these free energies with the corresponding heats of mixing we hope to obtain a deeper understanding of the interesting problems associated with the entropy of mixing.[14]

ACKNOWLEDGMENTS

The authors wish to acknowledge discussions with other workers in the fused salt field, and with several staff members of the Institute for the Study of Metals, the University of Chicago. We are particularly indebted to Dr. Milton Blander of Oak Ridge National Laboratory for furnishing us with the results of his unpublished calculations. The chemical analyses were performed by Miss M. C. Bachelder.

This work was supported by the Office of Naval Research at the University of Chicago.

Solution at High Density to the Born-Green Equation

A. A. BROYLES

The RAND Corporation, Santa Monica, California, and the University of Florida, Gainesville, Florida

(Received June 22, 1960)

A solution to the Born-Green integral equation with the Lennard-Jones potential at $v/v^*=n^{-1}a^{-3}=0.9$ is presented. Its asymptotic form is found to be $1-38.9r^{-6}\sin(2\pi r-2.928)$, and its integral over the volume r of the system is $r-2.06$. The value of E'/RT is found to be -2.6 and of pv/RT is 3.8. The magnitudes of these thermodynamic quantities are compared with those obtained by the Monte Carlo method.

A RECENT paper[1] has compared solutions of the Born-Green integral equation for the radial distribution function with those obtained by Wood and Parker[2] employing a Monte Carlo technique. The Lennard-Jones pair potential was used so that the pair potential energy was given by

$$\phi(r)=4\epsilon[(a/r)^{12}-(a/r)^{6}]. \tag{1}$$

The value of kT/ϵ was taken to be 2.74 for all cases. By choosing the unit of length to be the parameter a in Eq. (1), we leave only the number of particles per cubic centimeter n remaining to be varied.

Wood and Parker[2] have chosen the parameter v/v^* equal to $n^{-1}a^{-3}$. The comparisons between the two distribution functions already made[1] are for $v/v^*=2.5$, 1.2, and 1.0. Figure 1 extends this comparison down to $v/v^*=0.9$ where the crystal structure is already appearing in the Monte Carlo function.

A discussion of the checks on the accuracy of these solutions is contained in footnote 1. Those checks were used to assure us that the solution to the Born-Green equation in Fig. 1 lies well within 1% of the correct solution for that part of the curve lying to the right of the first $g=1$ point. The curve to the left of this point has a comparable absolute accuracy. A further check was employed by finding iterated solutions that approached the solution in Fig. 1 entirely from below and entirely from above. The solution was finally obtained using an interval of 0.025 in r/a.

There is a general belief among workers in the field that a solution to the Born-Green equation will not exist when the density of the fluid exceeds a certain critical value. This would be a very interesting phenomenon since it might correspond to the freezing of the liquid. Since the value of v/v^* equal to 0.9 is believed by Wood and Parker[2] to be a density where the substance has solidified, it is particularly interesting that it was possible to obtain the solution in Fig. 1. To remove the objection that this solution may have been possible only because the integrations were not carried beyond $r/a=4.0$, a comparison was made between the solutions obtained at an interval of 0.1 but with upper limits of 4.0 and 5.6. These solutions differed by less than 1% in the range from 1.0 to 4.0. Since these solutions differed from the final one (at interval 0.025) by only 10% in this range, it was concluded that the final solution in Fig. 1 would not be altered by more than a few percent if the upper limit were increased.

It is possible to make the following argument that the integral in the Born-Green equation will exist if it can be assumed that $g(r)$ approaches unity, regardless of how slowly. Let us consider the Born-Green equation in the form of Eq. (6.8) of footnote 3. In the notation and units ($a=1$) of footnote reference 1, it may be written as

$$rf(r)=n\pi\int_{s=-\infty}^{\infty}F(s+r)G(s)\,ds, \tag{2}$$

where

$$F(x)=x[g(x)-1], \tag{3}$$

and

$$G(s)=\int_{|s|}^{\infty}(y^2-s^2)\,g(y)\beta\phi(y)\,dy. \tag{4}$$

The asymptotic expression for $G(s)$ may be obtained by assuming that $g(y)$ has become unity and that $\phi(r)$ is asymptotic to $4\epsilon/r^6$ (we take $a=1$). It is

$$G(s)\sim 2\beta\epsilon/s^4. \tag{5}$$

We see then that $G(s)$ falls off rapidly enough at large $|s|$ to make the integral in Eq. (2) convergent. Actually, since $G(s)$ falls off so fast for large $|s|$, we could probably relax this condition on $g(r)$ to some extent without destroying the existence of the integral.

The existence of the integral in Eq. (2) does not prove the finiteness of the integral,

$$I=4\pi\int_0^{\infty}(1-g)\,r^2dr, \tag{6}$$

which we know[4] should have the value n^{-1} of 0.9 for $v/v^*=0.9$.

To evaluate I it is necessary to know the asymptotic form of $g-1$ or f. Although this asymptotic form has

[1] A. A. Broyles, J. Chem. Phys. **33**, 456 (1960).
[2] W. W. Wood and F. R. Parker, J. Chem. Phys. **27**, 720 (1957).
[3] Herbert S. Green, *The Molecular Theory of Fluids* (Interscience Publishers, Inc., New York, 1952), 1st ed., p. 77.
[4] Terrell L. Hill, *Statistical Mechanics* (McGraw-Hill Book Company, Inc., New York, 1956), 1st ed., p. 185. Eq. (29.35).

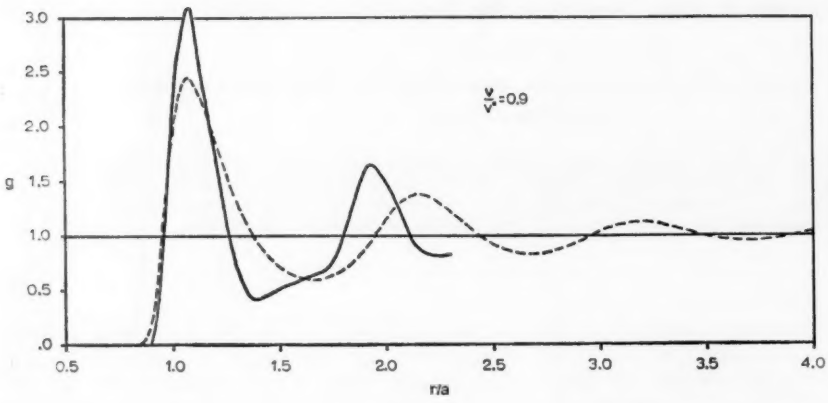

FIG. 1. Radial distribution function g vs r/a for $v/v^* = n^{-1}a^{-3} = 0.9$ from the Monte Carlo method (solid curve) and the Born-Green equation (dashed curve).

not been derived from Eq. (2), a fit to $g-1$ has been obtained to within the accuracy of the numerical calculations (1%) for the last cycle of the solution shown in Fig. 1. This fit is over the range from r equal 3.0 to 4.0. It has the form

$$g-1 \sim -38.9r^{-5}\sin(2\pi(r-2.928)). \qquad (7)$$

With this asymptotic form of $g-1$, the value of I as defined by Eq. (6) may be obtained. The value of I, when the integration from r equal zero to 3.962 is carried out, is 0.84, and from r equal 3.962 to infinitiy is 1.22, to give a total value for I of 2.06 instead of the desired 0.9.

It is not surprising that $g(r)$ has approached its asymptotic form beyond $r=3.0$ since Eq. (5) indicated that $G(3)$ is quite small. Since $G(s)$ contains the characteristics of ϕ in Eq. (2), it is reasonable to expect that its range would determine how quickly the solution approaches its asymptotic value.

TABLE I. Thermodynamic functions for $v/v^*=0.9$.

	E'/RT	pv/RT
Born-Green	−2.6	3.8
Monte Carlo	−1.9	7.7

Figure 1 indicates that there is considerable difference between the Born-Green and Monte Carlo radial distribution functions for $v/v^*=0.9$. For this reason, it is not surprising to find poor agreement in the thermodynamic functions computed from them. Table I shows the values of E'/RT and pv/RT computed from Wood and Parker's[2] Eqs. (24) and (25) using the Born-Green solution for a v/v^* of 0.9. The corresponding Monte Carlo values obtained by Wood and Parker are also shown.

The calculations were coded for the RAND Corporation "Johniac" electronic computer by C. L. Lowery. He is responsible for developing the technique of approaching the correct solution from two sides.

Note added in proof: By mistake, g from the Monte Carlo method was plotted against $1.037\ r/a$ in Fig. 1. Thus it should be moved slightly to the left.

THE JOURNAL OF CHEMICAL PHYSICS VOLUME 34, NUMBER 2 FEBRUARY, 1961

Quantum Calculations of the Velocity Dependence of the Differential and Total Cross Sections for Elastic Scattering of Molecular Beams*

RICHARD B. BERNSTEIN

Chemistry Department, The University of Michigan, Ann Arbor, Michigan

(Received August 10, 1960)

The partial wave treatment (phase shift analysis) of the elastic scattering of molecular beams [J. Chem. Phys. **33,** 795 (1960)] is applied to the calculation of the velocity dependence of the differential and total cross sections for an assumed L-J (12, 6) potential. For most of the calculations, the ϵ, σ values are chosen to correspond to the H_2-Hg system. The range of the velocity parameter $A \equiv k\sigma = \mu v\sigma/\hbar$ is from 3 to 30; this is equivalent to a 100-fold variation in H_2 beam temperature (approx 8.2–820°K). Computations of the angular distribution of the scattering $d\sigma(\theta)/d\Omega$ and the total cross section Q as a function of A are reported. A correlation of the interference maxima in $d\sigma(\theta)/d\Omega$ is presented. The Massey-Mohr approximation for $Q(A)$ for an inverse sixth-power attractive potential is compared with the present calculations for the L-J (12, 6) potential. Significant undulatory deviations are noted at low A; this effect is attributed to the existence of the broad maximum in the phase shift curve $\eta(l)$, which, in turn, originates from the negative repulsive phases at low l. Consideration is given to the question of the sensitivity of the scattering to the repulsive part of the potential.

INTRODUCTION

It is well-known that the classical treatment of elastic scattering[1,2] is inapplicable under certain conditions, and in particular, yields no information regarding low-angle differential scattering or the total cross section. Massey and Mohr[3] applied the quantum-mechanical (partial wave) method to the molecular scattering problem, obtaining an exact solution for the rigid-sphere model[3a] and an approximate one for a general inverse-power intermolecular potential.[3b] For the latter case a simple approximation for the total cross section Q was derived; for the potential

$$V(r) = -C/r^6, \tag{1}$$

the Massey-Mohr equation takes the form

$$Q = b(C/v)^{2/5}, \tag{2}$$

where v is the relative velocity and b a known constant. The differential scattering cross section $d\sigma(\theta)/d\Omega$ [alternatively written $I(\theta)$] could not be expressed in simple terms.

In a previous paper[4] a partial wave treatment (phase shift analysis) was presented for the scattering of molecules subject to a Lennard-Jones (12, 6) potential,

$$V(r) = 4\epsilon[(\sigma/r)^{12} - (\sigma/r)^6]. \tag{3}$$

The repulsive part of the potential leads to negative phase shifts (η_l) for the lower order partial waves and thus gives rise to a maximum in $\eta(l)$, whose location and value are dependent upon the velocity parameter

$$A \equiv k\sigma = \mu v\sigma/\hbar. \tag{4}$$

It is the purpose of the present paper to investigate the influence of the repulsion (via the phase shifts) upon the differential and total scattering cross sections and their velocity dependence. In this connection it has been of interest to investigate the applicability of the Born approximation and the validity of the Massey-Mohr equation when applied to molecular scattering according to an L-J (12, 6) potential.

PROCEDURE

The symbols used are those of I. The two parameters found convenient to characterize the scattering system are

$$A = k\sigma, \qquad B = \epsilon\sigma^2 2\mu/\hbar^2, \tag{5}$$

where $k = 2\pi/\lambda = \mu v/\hbar$ is the propagation number, μ the reduced mass, and v is the (initial) relative velocity. For most of the calculations to be presented, the parameters ϵ and σ have been chosen the same as in I, to correspond fairly closely to the H_2-Hg system: $\epsilon = 2.46\times10^{-14}$ erg, $\sigma = 2.91$ A. Here $B = 125$ and A has been varied from 3 to 30. This is equivalent to a 100-fold range in the H_2 beam temperature (i.e., from 8.2–820°K, assuming (from I) the equivalence: $T = 295$°K at $A = 18$).

Phase shifts were taken from Table III of I, suitably extended to higher l (always until $\eta_l \lesssim 0.03$) by means of the Born approximation (to be discussed below). On using the standard Mott-Massey[5a] equations, $I(\theta)$ and Q were computed from the phases at $A =$ 3, 5, 7, 9, 10, 14.1, 15, 18, 20, 24, and 30 using an

* The author acknowledges with thanks financial support of this work from the U. S. Atomic Energy Commission, Division of Research, and from the Alfred P. Sloan Foundation.

[1] J. F. Hirschfelder, C. F. Curtiss, and R. B. Bird, *Molecular Theory of Gases and Liquids* (John Wiley & Sons, Inc., New York, 1954).

[2] E. A. Mason, J. Chem. Phys. **26,** 667 (1957).

[3] (a) H. S. W. Massey and C. B. O. Mohr, Proc. Roy. Soc. (London) **A141,** 434 (1933); (b) **A144,** 188 (1934).

[4] R. B. Bernstein, J. Chem. Phys. **33,** 795 (1960), hereafter referred to as I.

[5] N. F. Mott and H. S. W. Massey, *The Theory of Atomic Collisions* (Clarendon Press, Oxford, 1949), 2nd ed.; (a) p. 24; (b) p. 118.

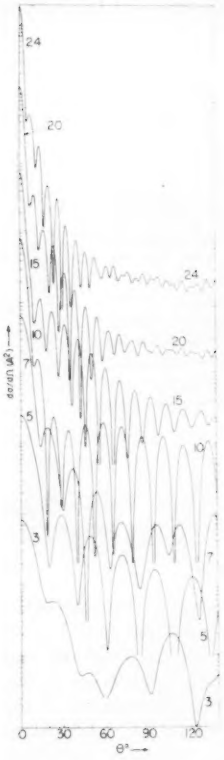

FIG. 1. Typical calculated angular distributions. Parameter: A. $B=125$ for all curves. Note that the vertical (log) scale has been shifted by one cycle progressively for each succeeding curve (see text).

IBM 704 computer. The program yielded $I(\theta)$ (in A^2) and $I^*(\theta)\equiv I(\theta)/\pi\sigma^2$ from 0, (0.5), 180° as well as Q (in A^2) and $Q^*\equiv Q/\pi\sigma^2$. Computing time for one given value of A varied from 0.5 to 1.5 min (in the latter case the calculation involved 120 phases).

VELOCITY DEPENDENCE OF THE ANGULAR DISTRIBUTION

Figure 1 shows some typical angular distributions. Here $A=3$, 5, 7, 10, 15, 20, and 24; θ extends to 140°. For clarity of presentation, the vertical (logarithmic) scale has been shifted by one cycle progressively for each succeeding curve. To fix the location of the curves, the values of the intercepts $[I(0)$ in $A^2]$ are listed, as follows,

A	3	5	7	10	15	20	24
$10^{-3}\times I(0)\,(A_2)$	0.82	2.51	6.48	8.14	7.33	13.1	21.4.

The positions of the interference maxima and minima are correlated in Fig. 2.[6] The index N is an integer for a maximum, half-integer for a minimum. As pointed out in I, the periodicity of the undulations in the angular distributions is governed primarily by A. This is seen quite clearly in Figs. 1 and 2.

It would be desirable to construct a unique "reduced scattering curve," i.e., a universal representation for the velocity-dependent angular distributions (Fig. 1). This cannot be expected, however, due to the complexity of the problem when the reduced relative kinetic energy

$$K\equiv\tfrac{1}{2}\mu v^2/\epsilon=A^2/B \tag{6}$$

is of order unity and the incident deBroglie wave is seriously distorted by the scattering potential. As pointed out in I, this distortion is also dependent upon A (or, equivalently, the ratio of the wavelength to the extension of the force field).

A step in this direction may be taken if one restricts attention to the scattering at low angles and at high A, where the wave is not much diffracted by the scattering field (conditions appropriate for the Born approximation; see the following). Here the undulations in the angular distribution $I(\theta)$ should be determined primarily [5b] by the variable ks, where

$$s=2\sin(\theta/2), \tag{7}$$

or, equivalently, by the dimensionless quantity

$$ks\sigma=2A\sin(\theta/2). \tag{8}$$

Figure 3 is a plot with abscissa[7] $2A\sin(\theta/2)$, for $A=$ 15, 20, 24, and 30. In the low-angle region particularly, the curves show similarity; the major part of the velocity dependence is thus fairly well correlated. For smaller velocities ($A\leq 10$), the correlation is less satisfactory, as anticipated.

RELATION BETWEEN $I(0)$ AND Q

Massey and Mohr[3a] have considered the limiting case when a very large number of phase shifts are re-

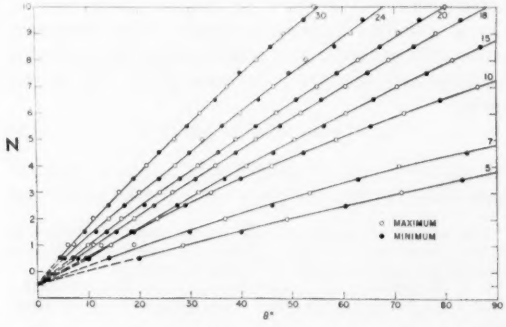

FIG. 2. Correlation of interference peaks in angular distributions. Parameter: A. $B=125$ for all curves. The index N is an integer for a maximum, half-integer for a minimum.

[6] For $A\leq 10$ the undulations in $d\sigma(\theta)/d\Omega$ are noticeably less regular; this is seen (to a lesser extent) in Fig. 2. As discussed in I, for $B=125$ and $A\leq 10$ penetration of the centrifugal barrier occurs (classically, the condition for orbiting is $K\leq 0.8$) giving rise to one or more discontinuities in the $\eta(l)$ curves; this factor may be of some importance here.

[7] The ordinate is $(1/A^2)d\sigma(\theta)/d\Omega$. The rationale for this choice is presented in the next section.

quired in the calculation of $I(\theta)$, and the phases (after removing multiples of π) are essentially random numbers (η_l oscillating rapidly with l). Under these conditions one finds that

$$I(0)=(kQ/4\pi)^2. \tag{9}$$

For the "rigid-sphere" potential Q is velocity independent; for a realistic intermolecular potential Q is a relatively insensitive function of velocity (see discussion following). With the approximation of nearly constant Q, Eq. (9) implies $I(0)/k^2\cong$ constant. To remove the major velocity dependence of $I(0)$ the ordinate in Fig. 3 was therefore chosen to be $(1/A^2)d\sigma/d\Omega$.

It is convenient to rewrite Eq. (9) in terms of the reduced quantities $I^*(\theta)$ and Q^*. Thus

$$I^*(0)\cong(AQ^*/4\pi^{\frac{1}{2}})^2. \tag{10}$$

The ratio $j(A)$ is defined,

$$j(A)\equiv I^*(0)/(AQ^*/4\pi^{\frac{1}{2}})^2, \tag{11}$$

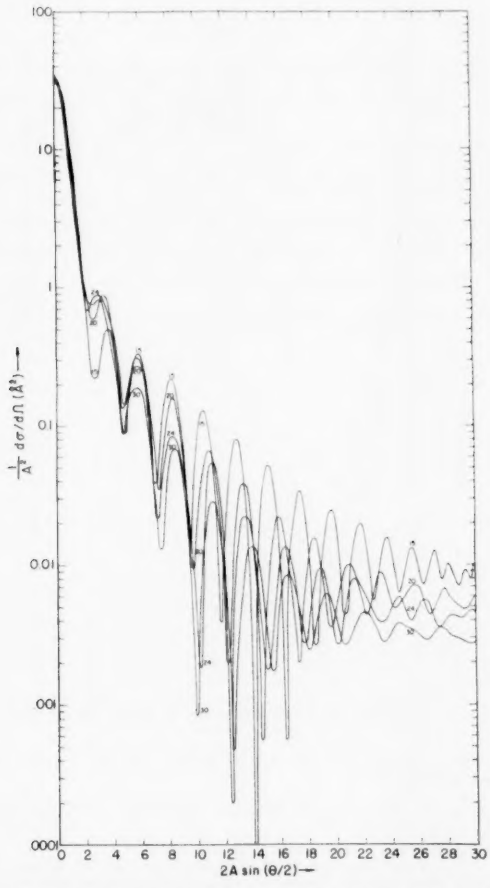

FIG. 3. Reduced scattering curves. Parameter: A. $B=125$ for all curves.

TABLE I. Relation between $I^*(0)$ and Q^*.

	L.-J. (12,6); $B=125$				Rigid sphere
A	$I^*(0)$	Q^*	$I^*(0)/A^2$	$j(A)$	$j(A)$
3	30.8	7.27	3.42	3.25	1.47
5	94.3	13.17	3.77	1.09	1.26
7	244	14.06	4.98	1.27	
9	299	10.69	3.69	1.62	
10	306	9.16	3.06	1.83	1.11
14.1	245	6.58	1.23	1.43	
15	275	6.67	1.22	1.38	
18	395	7.16	1.22	1.20	
20	491	7.41	1.23	1.12	1.05
24	806	7.60	1.40	1.22	
30	1208	7.08	1.34	1.35	
40[a]	(1750)	(5.80)	(1.09)	(1.63)	

[a] These computations less reliable than others.

which, for the rigid-sphere model at least, should approach unity in the high velocity limit.

Table I lists the calculated values[8] of $I^*(0)$, Q^*, $I^*(0)/A^2$, and $j(A)$. Given in the last column for comparison are several values of $j(A)$ for the rigid-sphere model, as calculated from the phases of Massey and Mohr.[3a] From the present results for the L-J (12,6) potential it appears that Eq. (10) does not adequately describe the relation between $I^*(0)$ and Q^*. The velocity dependence of Q^* is discussed later.

BORN APPROXIMATION FOR THE PHASES (L.-J. POTENTIAL)

For any L-J potential of the form

$$V(r)=(a/r^q)-(b/r^s), \tag{12}$$

the Born approximation for the higher order phases may readily be evaluated by an obvious extension of the treatment of Massey and Mohr.[3b] The result of the integration is simply

$$\eta=\eta^{(a)}+\eta^{(q)}, \tag{13}$$

where the phases $\eta^{(a)}$ and $\eta^{(q)}$ are obtained from Eq. (39) of footnote 3b.

For the L-J (12,6) potential, using symbols concordant with those of footnote 3b,

$$\alpha V=-\left(\frac{C^{(6)}}{r^6}+\frac{C^{(12)}}{r^{12}}\right), \tag{14}$$

where

$$\alpha=2\mu/\hbar^2, \tag{15}$$

$$C^{(6)}=4\epsilon\sigma^6\alpha=4B\sigma^4,$$

and

$$C^{(12)}=-4\epsilon\sigma^{12}\alpha=-4B\sigma^{10}. \tag{16}$$

[8] The calculated values of $I(O)$ and Q are somewhat sensitive to the cutoff phase (number of higher order phases used). Sample calculations indicate that $j(A)$ may be uncertain by a few percent.

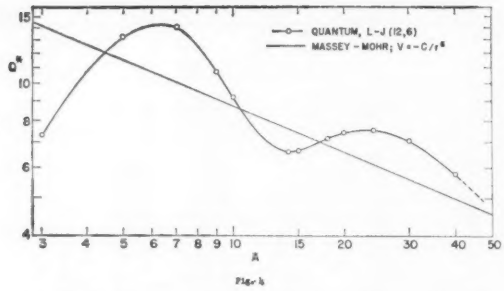

FIG. 4. Velocity dependence of total cross section. $Q^*\equiv Q/\pi\sigma^2$. $B=125$.

For large l (replacing $l+\frac{1}{2}$ by l) one obtains the useful approximation formulas for the phases

$$\eta^{(6)}=(3\pi/8)BA^4/l^5 \quad \text{(attractive)}, \tag{17}$$

$$\eta^{(12)}=-(63\pi/256)BA^{10}/l^{11} \quad \text{(repulsive)}. \tag{18}$$

A quantity of interest is the ratio

$$-\eta^{(12)}/\eta^{(6)}=0.656(A/l)^6. \tag{19}$$

Thus for $l\geqslant 2A$ the repulsive contribution to the Born phase is $<1\%$ of the attractive term. As mentioned in I, for the example investigated, Eq. (17) reproduced accurately (± 0.02) all directly calculated higher order phases (i.e., for $l\geqslant 2A$ and $\eta\leqslant 0.5$).

APPLICABILITY OF THE MASSEY-MOHR EQUATION FOR THE TOTAL CROSS SECTION

Massey and Mohr[3b] derived a simple formula for the total cross section Q for the potential $\alpha V=-C/r^s$, making use of the Born approximation for the higher order phases and utilizing the essentially random character of the lower order phases (mentioned previously). For $s=6$ the Massey-Mohr equation may be written in the following equivalent forms,[9]

$$Q=5.720(C/k)^{2/5}=5.720\sigma^2(4B/A)^{2/5}$$

$$=4.662\times 10^{11}(C'/v)^{2/5}, \tag{20}$$

where

$$C'=C/\alpha=4\epsilon\sigma^6.$$

In terms of $Q^*\equiv Q/\pi\sigma^2$, one obtains a "reduced" form of Eq. (20)

$$Q^*=3.170(B/A)^{2/5}. \tag{21}$$

It is of interest to investigate the influence of the repulsive part of the potential upon Q. Figure 4 shows data taken from Table I [the quantum calculations for the L-J (12,6) potential] plotted in the form $\log Q^*$ vs $\log A$. For comparison the appropriate straight line corresponding to Eq. (21) is shown.

Significant undulating deviations are noted (which are attributed to the repulsive contribution to the potential). This effect is thought to be a consequence of the broad maximum in the $\eta(l)$ curve (see Fig. 6 of I) which, in turn, originates from the negative repulsive phases at low l. Although the sign of η in itself does not affect $\sin^2\eta$ (and thus Q) the existence of the maximum in $\eta(l)$ gives rise to a certain concentration of *nonrandom* phases near the maximum. These phases (depending on whether $\sin^2\eta>\frac{1}{2}$ or $<\frac{1}{2}$) either add to or subtract from the Q calculated for random phases. The directions of the deviations in Fig. 4 seem to be fairly well accounted for on the basis of these considerations.

The deviations are expected to diminish in magnitude with increasing A, as the fraction of the total number of (non-Born) phases which are nonrandom decreases. Thus the velocity dependence of the cross section should approach $v^{-2/5}$ as the "semiclassical"[10] conditions are achieved, as appears to be the case experimentally.[11,12a] However, deviations similar to those of Fig.

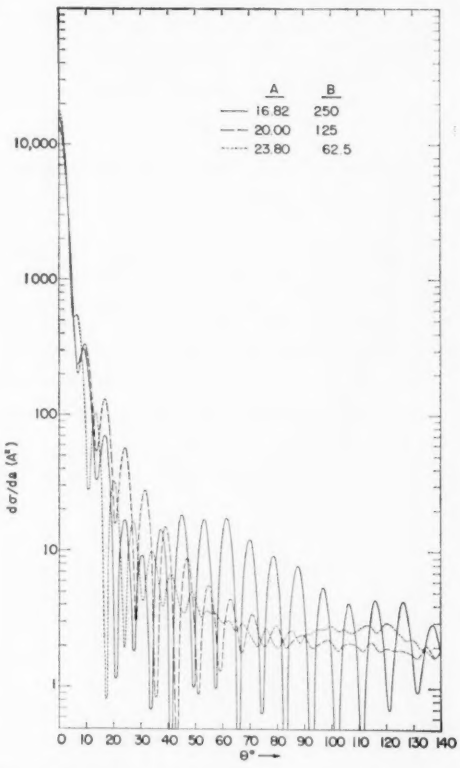

FIG. 5. Influence of A and B (at constant BA^4) upon the angular distribution.

[9] E. W. Rothe and R. B. Bernstein, J. Chem. Phys. **31**, 1619 (1959).

[10] K. W. Ford and J. A. Wheeler, Ann. Phys. (N. Y.) **7**, 259, 287 (1959).

[11] H. Pauly, Z. Naturforsch. **15a**, 277 (1960).

[12] (a) H. Schumacher, R. B. Bernstein, and E. W. Rothe, J. Chem. Phys. **33**, 584 (1960). (b) Observations of quantum effects in the scattering of Li by Hg have been reported [H. U. Hostettler and R. B. Bernstein, Phys. Rev. Letters **5**, 318 (1960)].

4 should be observable[12b] for beams of the lighter gases at low temperatures.

In the very high velocity region (large A and K), nearly all phases would be negative; the velocity dependence of Q should (eventually) change from $v^{-2/5}$ to $v^{-2/11}$. This important consideration has not been treated quantitatively in the present study.

SENSITIVITY OF THE SCATTERING TO THE REPULSIVE PART OF THE POTENTIAL

Studies of the scattering of thermal velocity molecular beams are expected[9,13,14] to yield information primarily on the long-range attractive part of the intermolecular potential (via the constant $C' \equiv 4\epsilon\sigma^6$). However, in view of the discussion of the previous section it is of importance to ascertain the sensitivity of the scattering to the repulsive part.

According to the Massey-Mohr equation, for a given relative velocity or k the total cross section should be independent of ϵ and σ provided C' is held constant. In the present notation this is equivalent to the condition

$$BA^4 = \text{const} \qquad (22)$$

(at constant k, of course). Equation (22) implies [through Eq. (17)] also that all the Born attractive phases will remain unchanged.

A set of calculations was carried out to investigate the effect (on both $d\sigma/d\Omega$ and Q) of varying A and B at constant k, maintaining $BA^4 = 2.00 \times 10^{-7}$. Table II lists the results for $I(0)$ and Q. The parameters were chosen to avoid the "bounded region" discussed in I, enabling the use of the Q-i-K curves (the "reduced phase" treatment) to estimate the phases for $K = 1.13$ and 9.06. The Massey-Mohr equation (20) yields $Q = 176$ A^2 (for the three cases).

TABLE II. Influence of A and B (at constant BA^4) upon $I(0)$ and Q.

K	A	B	σ(A)	$10^{-3} \times I(0)$ (A^2)	Q(A^2)
1.13[a]	16.82	250	2.447	15.7	207
3.20[b]	20.00	125	2.910	13.8	198
9.06[a]	23.80	62.5	3.460	18.2	184

[a] Phases estimated using Q-i-K curves from I (extended).
[b] Phases from Table III of I (extended).

Figure 5 shows a comparison of the three calculated angular distributions. Although the curves are easily distinguishable, the problem of deriving a unique or "best" set of parameters ϵ, σ for a given observed angular distribution (i.e., the "inversion" problem) appears to be a formidable one indeed.

One may conclude that while the influence of the repulsive part of the potential is important (and should be observable under certain conditions), the attractive term dominates in determining the scattering of thermal velocity molecular beams.

ACKNOWLEDGMENTS

The author wishes to express his appreciation to Professor P. J. W. Debye (Senior Scientist, Institute of Science and Technology, University of Michigan) for a number of valuable discussions and suggestions. The assistance of Mrs. H. Schumacher in plotting graphs and arranging tables is acknowledged with thanks.

[13] H. S. W. Massey and R. A. Buckingham, Nature **138**, 77 (1936).
[14] H. U. Hostettler and R. B. Bernstein, J. Chem. Phys. **31**, 1422 (1959).

Calculation of the Diamagnetic Susceptibility of N_2

H. F. HAMEKA

Department of Chemistry, The Johns Hopkins University, Baltimore, Maryland

(Received July 19, 1960)

The diamagnetic susceptibility of the nitrogen molecule has been calculated from wave functions that are constructed from gauge invariant atomic orbitals. The result is -13.539×10^{-6} which agrees satisfactorily with the average experimental value -13.3×10^{-6}.

I. INTRODUCTION

IT has been suggested in recent work [1] that it may be profitable to employ gauge invariant atomic orbitals to calculate the magnetic properties of molecules. A method was developed for calculating diamagnetic susceptibilities and proton shielding constants for molecules, which is applicable if the molecular wave functions may be constructed from atomic orbitals with a suitable degree of accuracy. The method was successfully applied to a calculation of the magnetic susceptibility and the proton shielding constant of the hydrogen molecule[1] and to a calculation of the magnetic susceptibility of methane.[2] In this paper the magnetic susceptibility of the nitrogen molecule will be calculated. The wave functions which will be employed in this calculation were obtained by Scherr[3] from an SCF LCAO MO treatment of the nitrogen molecule.

The only previous calculation[4] of the susceptibility of N_2 that was reported in the literature gave a value of -24.6×10^{-6} which is almost double the average experimental value[5] -13.3×10^{-6}. It will be shown that the accuracy of theoretical results may be improved considerably by employing gauge invariant atomic orbitals.

The procedure that will be followed in this calculation was reported previously for the hydrogen molecule.[1] In the present calculation the method will have to be generalized to some extent; therefore it will be discussed briefly here.

In the absence of a magnetic field the Hamiltonian of our N electron system is

$$\mathcal{H}_\sigma=\sum_{j=1}^{N}-(\hbar^2/2m)\Delta_j+V(\mathbf{r}_1,\ \mathbf{r}_2,\ \cdots,\ \mathbf{r}_N), \quad (1)$$

where Δ_j stands for the Laplace operator. In the presence of a magnetic field $\mathbf{H}$ this becomes

$$\mathcal{H}_\sigma^{(q)}=\sum_{j=1}^{N}\Lambda^{(q)}(j)+V(\mathbf{r}_1,\ \mathbf{r}_2,\ \cdots,\ \mathbf{r}_N)$$

$$\Lambda^{(q)}(j)=-(\hbar^2/2m)\Delta_j-(e\hbar/mci)(\mathbf{A}_j^{(q)}\nabla_j)+(e^2/2mc^2)(\mathbf{A}_j^{(q)})^2$$

$$A_j^{(q)}=\tfrac{1}{2}[\mathbf{H},\ \mathbf{r}_j-\mathbf{q}], \quad (2)$$

where $\mathbf{q}$ is called the gauge of the vector potential.[6]

It will be assumed that the function Ψ_0 is the exact eigenfunction of the ground state of $\mathcal{H}_\sigma'$ and that Ψ_0 may be constructed from atomic orbitals ϕ_{ka}, where the first subscript denotes the functional form of the orbital and the second subscript denotes the corresponding nucleus. Further it will be assumed that the functions Ψ_n, which also may be constructed from atomic orbitals, together with Ψ_0 form a complete set. To every function Ψ_n corresponds an approximate eigenvalue E_n of the operator $\mathcal{H}_\sigma'$.

In the presence of a magnetic field $\mathbf{H}$ it is now profitable to assign the same gauge to the atomic orbitals ϕ_{ka} as was previously defined for $\mathbf{A}_j$ in Eq. (2). According to the theory of gauge transformations[6] the functions Ψ_0 and Ψ_n are then transformed to

$$\Psi_0^{(q)}=\Psi_0(\phi_{ka}^{(q)},\ \phi_{lb}^{(q)},\ \phi_{mc}^{(q)},\ \cdots)$$

$$\Psi_n^{(q)}=\Psi_n(\phi_{ka}^{(q)},\ \phi_{lb}^{(q)},\ \phi_{mc}^{(q)},\ \cdots)$$

$$\phi_{ka}^{(q)}=\phi_{ka}\exp[ie\Phi(\mathbf{q}-\mathbf{a})/\hbar c]$$

$$\Phi(\mathbf{u})=\tfrac{1}{2}([\mathbf{Hu}]\mathbf{r}). \quad (3)$$

Although the functions Ψ_0 and Ψ_n are supposed to be orthogonal this need not necessarily be true for the functions $\Psi_0^{(q)}$ and $\Psi_n^{(q)}$.

A good variational wave function for our N electron system is

$$\Psi=B_0\Psi_0^{(q)}+\sum_{n=1}^{\infty}B_n\Psi_n^{(q)}, \quad (4)$$

where $B_n\ll B_0$. A variational calculation of the ground-state energy from the function Ψ will yield, to a second

[1] H. F. Hameka, Z. Naturforsch. **14a**, 599 (1959).
[2] H. F. Hameka, Physica **25**, 626 (1959).
[3] C. W. Scherr, J. Chem. Phys. **23**, 569 (1955).
[4] J. V. Bonet and A. V. Bushkovititch, J. Chem. Phys. **21**, 2199 (1953).
[5] L. Hector, Phys. Rev. **24**, 229 (1924); F. Bitter, *ibid.* **36**, 1648 (1930); V. I. Vaidyanathan, Phil. Mag. **5**, 380 (1928).
[6] I.. A. Kramers, *Quantentheorie des Elektrons und der Strahlung* (Akademie Verlag Gesellschaft, Leipzig, Germany, 1938), p. 270.

approximation,

$$E_0(H)=\frac{E_{00}}{S_{00}}-\sum_{j=1}^{\infty}\frac{(S_{00}E_{0j}-S_{0j}E_{00})(S_{00}E_{j0}-S_{j0}E_{00})}{S_{00}^2(S_{00}E_{jj}-S_{jj}E_{00})}$$

$$E_{kl}=\langle\Psi_k^{(q)}\mid\mathcal{H}_\sigma^{(q)}\mid\Psi_l^{(q)}\rangle$$

$$S_{kl}=\langle\Psi_k^{(q)}\mid\Psi_l^{(q)}\rangle. \tag{5}$$

The matrix elements E_{kl} and S_{kl} are both independent of $\mathbf{q}$ and may be expressed in terms of the following matrix elements,

$$V_{kl}=\langle\Psi_k^{(q)}\mid V(\mathbf{r}_1,\mathbf{r}_2,\cdots,\mathbf{r}_N)\mid\Psi_l^{(q)}\rangle$$

$$T(ku;lv)=\langle\phi_{ku}^{(q)}\mid\Lambda^{(q)}\mid\phi_{lv}^{(q)}\rangle$$

$$S(ku;lv)=\langle\phi_{ku}^{(q)}\mid\phi_{lv}^{(q)}\rangle, \tag{6}$$

all of which are independent of $\mathbf{q}$. Consequently, for a calculation of E_{kl} and S_{kl} it is permissible to choose definite and different values of $\mathbf{q}$ in each different quantity V_{kl}, $T(ku,lv)$, and $S(ku,lv)$ without affecting the values of either E_{kl} or S_{kl}. The most practical choice for $\mathbf{q}$ is the position of the nucleus corresponding to the atomic orbital following the operator. Therefore, throughout the calculation the following matrix elements will be evaluated

$$T(ku,lv)=\langle\phi_{ku}^{(v)}\mid\Lambda^{(v)}\mid\phi_{lv}\rangle$$

$$S(ku,lv)=\langle\phi_{ku}^{(v)}\mid\phi_{lv}\rangle. \tag{7}$$

It will appear that the V_{kl} do not contribute to the magnetic susceptibility. Now that for each term $T(ku,lv)$ the gauge has been clearly defined it is possible to expand in each different $T(ku,lv)$ the operator $\Lambda^{(v)}$ as a power series in H:

$$\Lambda^{(v)}(j)=\Lambda_0^{(v)}(j)+H\Lambda_1^{(v)}(j)+H^2\Lambda_2^{(v)}(j)$$

$$\Lambda_0^{(v)}(j)=-(\hbar^2/2m)\Delta_j$$

$$H\Lambda_1^{(v)}(j)=(e\hbar i/2mc)(\mathbf{H}[\mathbf{r}_{jv}\nabla_j])$$

$$H^2\Lambda_2^{(v)}(j)=(e^2/8mc^2)\sum_k H_k^2(r_{jv}^2-r_{jvk}^2)\quad k=x,y,z, \tag{8}$$

where $\mathbf{r}_{jv}$ denotes the position of electron j with respect to nucleus v. The operators defined in Eq. (8) contain the angles between magnetic field and molecular orientation but it is intended to average over these angles at the end of the calculation. In calculating E_{kl} we will take all contributions of $\Lambda_0^{(v)}(j)$ together and denote their sum by $E_{kl}^{(0)}$; similarly $E_{kl}^{(1)}$ and $E_{kl}^{(2)}$ are defined. Thus

$$E_{kl}=V_{kl}+E_{kl}^{(0)}+E_{kl}^{(1)}H+E_{kl}^{(2)}H^2. \tag{9}$$

From our assumption that Ψ_0 is the exact ground-state eigenfunction of $\mathcal{H}_\sigma'$ it follows that

$$V_{k0}+E_{k0}^{(0)}=E_0S_{k0}, \tag{10}$$

where E_0 is the lowest eigenvalue of $\mathcal{H}_\sigma'$.

Let us now reconsider Eq. (5) and neglect higher powers in H than the second in $E_0(H)$. By making use of Eq. (10) it may be rewritten as

$$E_0(H)=\frac{E_{00}}{S_{00}}-H^2\sum_{j=1}^{\infty}\frac{E_{0j}^{(1)}E_{j0}^{(1)}}{S_{00}E_j-S_{jj}E_0}, \tag{11}$$

where E_{00} and E_{jj} in the denominator have been replaced by the energy values E_0 and E_j which are independent of H. The molar diamagnetic susceptibility is given by

$$\chi=-2N\left\{\frac{E_{00}^{(2)}}{S_{00}}-\sum_{j=1}^{\infty}\frac{E_{0j}^{(1)}E_{j0}^{(1)}}{S_{00}E_j-S_{jj}E_0}\right\}$$

$$-2N\left[\frac{\partial^2}{\partial H^2}\left\{\frac{HE_{00}^{(1)}}{S_{00}}\right\}\right]_{H=0}. \tag{12}$$

This formula was derived previously for the hydrogen molecule[1]; in this paper it has been extended to more complicated systems and also some parts of the derivation have been proved more rigorously.

II. CALCULATIONS

Equation (12) has been derived on the assumption that Ψ_0 is the ground-state eigenfunction of $\mathcal{H}_\sigma'$. If a suitable approximate function is inserted into Eq. (12) an approximate value of χ will be obtained. It is convenient to split χ into three parts:

$$\chi=-\chi_1-\chi_2+\chi_3$$

$$\chi_1=-2NE_{00}^{(2)}/S_{00}$$

$$\chi_2=-2N[\partial^2/\partial H^2\{HE_{00}^{(1)}/S_{00}\}]_{H=0}$$

$$\chi_3=2N\sum_{j=0}^{\infty}E_{0j}^{(1)}E_{j0}^{(1)}/(S_{00}E_j-S_{jj}E_0). \tag{13}$$

The wave functions that will be employed in this calculation were obtained by Scherr[3] from an SCF LCAO MO treatment of N_2. Starting from the atomic orbitals $1s_a$, $1s_b$, $2s_a$, $2s_b$, $2p_{xa}$, $2p_{xb}$, $2p_{za}$, $2p_{zb}$, $2p_{ya}$, and $2p_{yb}$, where the subscripts a and b denote the corresponding nuclei, Scherr obtained molecular orbitals as linear combinations of these atomic orbitals. Following the notation of Scherr the ground-state wave function becomes then

$$F_0=(14!)^{-\frac{1}{2}}\sum_P P\delta_P(1\sigma_g)_1(1\sigma_g)_2(1\sigma_u)_3(1\sigma_u)_4(2\sigma_g)_5(2\sigma_g)_6$$

$$\times(2\sigma_u)_7(2\sigma_u)_8(1\pi_{xu})_9(1\pi_{xu})_{10}(1\pi_{yu})_{11}(1\pi_{yu})_{12}$$

$$\times(3\sigma_g)_{13}(3\sigma_g)_{14}\alpha_1\beta_2\alpha_3\beta_4\alpha_5\beta_6\alpha_7\beta_8\alpha_9\beta_{10}\alpha_{11}\beta_{12}\alpha_{13}\beta_{14}. \tag{14}$$

The excited-states wave functions that are of interest in this calculation may be obtained by transferring one electron from a bonding to an antibonding orbital. A typical example is

$$F(1\sigma_g;1\pi_{xg})=2^{-\frac{1}{2}}(14!)^{-\frac{1}{2}}\sum_P P\delta_P\{(1\pi_{xg})_1(1\sigma_g)_2$$

$$+(1\sigma_g)_1(1\pi_{xg})_2\}(1\sigma_u)_3(1\sigma_u)_4(2\sigma_g)_5(2\sigma_g)_6(2\sigma_u)_7$$

$$\times(2\sigma_u)_8(1\pi_{xu})_9(1\pi_{xu})_{10}(1\pi_{yu})_{11}(1\pi_{yu})_{12}(3\sigma_g)_{13}$$

$$\times(3\sigma_g)_{14}\alpha_1\beta_2\alpha_3\beta_4\alpha_5\beta_6\alpha_7\beta_8\alpha_9\beta_{10}\alpha_{11}\beta_{12}\alpha_{13}\beta_{14}. \tag{15}$$

The diamagnetic susceptibility may now be calculated from Eq. (13) with the aid of the wave functions above. It should be borne in mind that in each operator $\Lambda_k^{(v)}(j)$ the gauge $\mathbf{v}$ should be taken as the position of the nucleus corresponding to the atomic orbital on which the operator works. The operator $\Lambda_2^{(v)}(j)$ may be simplified by averaging over all possible orientations of the molecule,

$$\Lambda_2^{(v)}(j)=(e^2/12mc^2)r_{jv}^2. \tag{16}$$

The calculation of χ_1 reduces now to the evaluation of various one- and two-center integrals of r_{jv}^2. The numerical values may be obtained by introducing elliptic coordinates and by making use of the tables of Miller, Gerhauser, and Matsen.[7] The result is $\chi_1=21.151\,313(a_0^2e^2N/6mc^2)$.

In order to calculate χ_2 and χ_3 it is helpful to determine the function

$$\begin{aligned}[\sum_j H\Lambda_1^{(v)}(j)]F_0=H_x\sqrt{2}[&0.00257F(1\sigma_g;1\pi_{yg})\\&+0.33907F(2\sigma_g;1\pi_{yg})-0.85312F(3\sigma_g;1\pi_{yg})\\&-0.88313F(1\pi_{xu};\sigma_u 2p)]-H_y\sqrt{2}[0.00257F(1\sigma_g;1\pi_{xg})\\&+0.33907F(2\sigma_g;1\pi_{xg})-0.85312F(3\sigma_g;1\pi_{xg})\\&-0.88313F(1\pi_{yu};\sigma_u 2p)],\end{aligned} \tag{17}$$

where the function $F(1\pi_{yu};\sigma_u 2p)$ may be written as a linear combination of $F(1\pi_{yu};1\sigma_u)$, $F(1\pi_{yu};2\sigma_u)$ and $F(1\pi_{yu};3\sigma_u)$. For a calculation of χ_3 from Eq. (13) we may now restrict ourselves to the excited states whose wave functions occur in Eq. (17) since it was assumed that the functions Ψ_n form a complete set. It is then found that $\chi_3=4.146\,676(a_0^2e^2N/6mc^2)$ after averaging over all possible molecular orientations.

Equation (17) also serves to calculate $HE_{00}^{(1)}$. From the definition of $\phi_{ka}^{(q)}$ in Eq. (3) it follows that

$$\begin{aligned}HE_{00}^{(1)}/S_{00}=(H_x^2+H_y^2)(&-0.139950A+0.270451B\\&-0.157047C)\end{aligned}$$

$$A=\langle 1s_a \mid x \mid 2p_{xb}\rangle$$

$$B=\langle 2s_a \mid x \mid 2p_{xb}\rangle$$

$$C=\langle 2p_{za} \mid x \mid 2p_{xb}\rangle. \tag{18}$$

The integrals A, B, and C may be obtained from the tables of Miller, Gerhauser, and Matsen,[7] it is then found that $\chi_2=0.141\,738(a_0^2e^2N/6mc^2)$.

By combining the values of χ_1, χ_2, and χ_3 it is found that $\chi=-17.146\,375\ (a_0^2e^2N/6mc^2)$, or since $a_0^2e^2N/6mc^2=0.789\,601\times10^{-6}$ $\chi=-13.539\times10^{-6}$. The various experimental values range from -11×10^{-6} to -14×10^{-6}, their average is -13.3×10^{-6}, so the agreement between theory and experiment is well within the limits of experimental error.

[7] J. Miller, J. M. Gerhauser, and F. A. Matsen, *Quantum Chemistry Integrals and Tables* (University of Texas Press, Austin, Texas, 1958).

THE JOURNAL OF CHEMICAL PHYSICS VOLUME 34, NUMBER 2 FEBRUARY, 1961

Vibrational Relaxation in Liquids

MARSHALL FIXMAN

Mellon Institute, Pittsburgh, Pennsylvania

(Received August 5, 1960)

Attempts have been made to apply the binary collision theory of vibrational deactivation to the liquid phase. The change of collision frequency with density was approximately accounted for, but the transition probability per collision was assumed independent of density. This latter assumption is investigated here by an addition, to the direct intermolecular force, of the frictional and random forces of Brownian motion theory. It is found that the frictional force has negligible effect, but the random force makes low-energy collisions much more effective in causing transitions than is predicted for an isolated binary collision by the semiclassical theory of Zener, Landau, and Teller. As a consequence, the isolated binary collision theory cannot be applied to liquids although it should be adequate for fairly dense gases. Probably the Brownian motion theory exaggerates the neighbor effects in liquids; the point is discussed.

I. INTRODUCTION

THE binary collision theory of vibrational relaxation in gases has had considerable success.[1,2] In this theory the frequency of vibrational deactivation is separated into two factors: the probability of deactivation per collision and the collision frequency. Attempts have been made to develop a theory of vibrational relaxation in liquids from the same point of view[3,4]; that is, the transition probability per collision was assumed to be unaffected by the change in phase and density, but one or another theory of liquids was applied to account for the change in collision frequency with density. Litovitz found that when the cell model was used to calculate collision frequencies, this theory gave an excellent account of the temperature and pressure dependence of the vibrational relaxation time of liquid CS_2. Moreover, the probabilities of energy exchange per collision in the liquid and gas were found to be in close agreement.

This success of the binary collision model for the liquid state, and the corresponding failure of a collective model due to Herzfeld,[5] was naturally regarded as a vindication[4,5] of the physical postulates of the binary collision model. It was observed that in a gas, vibrational energy transfer is caused predominantly by collisions of very high energy, in which the colliding pair of molecules come very close together. The probability of a third molecule perturbing this intimate event seems, *prima facie*, to be negligible.

The theory of nonequilibrium processes in liquids is so difficult, and in such a primitive state, that the applicability of such a simple model as has been mentioned is greatly to be desired. Yet its experimental success does not furnish an unambiguous confirmation of the postulates. The collision frequency was calculated with the assumption of hard-sphere molecules, and the cell model which was used has not been very successful even in the calculation of equilibrium properties of fluids. Thus the success of the binary collision model, though extremely interesting and important, may result from a cancellation of errors in the collision frequency and the probability of energy transfer per collision, and does not even preclude a complete breakdown of the concept of binary collisions applied to liquids.

The last possibility raised is naturally a quantative rather than a qualitative question. *If* the intermolecular energy of a pair of molecules must be arbitrarily large to produce a given event, then the interaction energy of the pair with the rest of the system must be arbitrarily small (subject to fixed total volume), to produce the event, because of the microcanonical or canonical distribution of the total energy of the systems.

A bit of evidence will be presented here to the effect that the energy of a binary collision which is required to cause vibrational deactivation in a liquid is not large enough to allow neglect of the interaction of the pair with the rest of the systems. It must be stressed that the somewhat arbitrary separation of the transition probability into a collision frequency and a transition probability per collision is here maintained; only the latter factor is discussed. The physical basis of the calculation is an addition of the frictional and random forces of Brownian motion theory[6] to the intermolecular force exerted by a pair. The point of view of the calculation is negative in the following sense, the effect of the rest of the system on the dynamics of a binary collision will be computed on the assumption that the effect is small. If the resulting perturbation on the deactivation probability turns out to be small, then the binary collision approximation is vindicated. If the perturbation turns out to be large, then the binary collision approximation is shown to be, at the very least, inconsistent. What actually happens is that the former

[1] K. F. Herzfeld and T. A. Litovitz, *Absorption and Dispersion of Ultrasonic Waves* (Academic Press, Inc., New York, 1959).
[2] Footnote reference 1, Chap. VII.
[3] C. Kittel, J. Chem. Phys. **14**, 614 (1946).
[4] T. A. Litovitz, J. Chem. Phys. **26**, 469 (1957).
[5] Footnote reference 1, pp. 405 and 406.
[6] S. Chandrasekhar, Revs. Modern Phys. **15**, 1 (1943).

result holds for a gas, the latter for a liquid. As far as the predictive value of the binary collision theory, there is no point in using a perturbation which is small. Neither theory nor experiment is good enough.

II. THEORETICAL BASIS

1. Preliminaries

A semiclassical theory[7] of the vibrational deactivation process was devised by Zener, and discussed also by Landau and Teller.[2,8] A lucid comparison of the semiclassical and quantum mechanical theories bas been given by Widom and Bauer.[9] In the semiclassical theory the potential energy of a system consisting of two molecules, one of them with an internal vibrational coordinate, is expanded to first order in the vibrational coordinate. The latter is given a quantum-mechanical treatment in which the expanded potential energy is a function of the classical motion of the internuclear coordinate. First-order time-dependent perturbation theory gives for the probability P of a transition between the ith and jth vibrational states in a single collision

$$P=(1/\hbar^2)\left|\int_{-\infty}^{+\infty}V_{ij}[x(t)]\exp i\omega t dt\right|^2, \tag{1}$$

where

$$\hbar\omega=|E_i-E_j| \tag{2}$$

and V_{ij} is the matrix element of the potential energy between the ith and jth states. We shall use the semiclassical theory and it appears that[9] it gives an adequate account of the binary collision down to as low collision energies as need be considered. It is a desirable refinement to use, in the classical calculation of the pair separation $x(t)$, an intermolecular potential and total energy which have been symmetrized with respect to the initial and final states, but for the very reasonable numerical example given at the end of this work, the symmetrization produces a quantitatively minor effect which will be neglected.

Only head-on collisions will be considered here, that is, the relative motion will be confined to a line. Most of the early work was done with this restriction. It has given qualitatively reasonable results which here should be all the more reliable, in that the absolute value of P is not of interest, but only the relative values of P for the unperturbed binary collision, and for the collision perturbed by Brownian forces.

The common exponential intermolecular potential

$$V(x)=K\exp(-ax) \tag{3}$$

will be used here also, and $V_{ij}(x)$ will be taken proportional to $V(x)$. Arbitrarily, we take the proportionality constant to be $\hbar/K$, so that

$$P=\left|\int_{-\infty}^{+\infty}\exp[-ax(t)+i\omega t]dt\right|^2. \tag{4}$$

2. Brownian Motion Equations

The basic assumption which defines the model is that the relative motion of an assigned molecular pair is the same as the motion of a Brownian particle in a field of force.[10] This model is very close to Kirkwood's calculation[11] of transport properties in liquids, but the language here will deal with the actual trajectory $x(t)$ rather than distribution functions, and the resemblance will not be pursued. Specifically, the assumption is

$$d^2x/dt^2=-\beta x/dt-m^{-1}dV(x)/dx+A(t), \tag{5}$$

where x is the separation of the two molecules, m is the reduced mass, and $A(t)$ is the random acceleration of Brownian motion theory and is characterized by its autocorrelation function

$$\langle A(t_1)A(t_3)\rangle=\beta(2kT/m)\delta(t_1-t_3)$$
$$\langle A(t)\rangle=0, \tag{6}$$

$\delta(\ )$ is a Dirac delta function[12] and β is a friction constant in units of $\sec^{-1}$.

Equation (5) is nonlinear and inhomogeneous as written, and we have found no way to solve it for the (now) stochastic variable $x(t)$. However, in view of the severely limited question to which this calculation is addressed, a perturbation treatment should suffice. This is not solely a move of desperation, for if the isolated binary collision is not an excellent or, indeed, an entirely adequate model, even a rigorous solution of Eq. (5) would not be a satisfactory replacement. Rather an investigation of the origins of Eq. (1) would have to be made to determine the validity of one of the approximations in it, namely, the assumption that the vibrational coordinate of one molecule interacts with only *one* other molecule. Here this assumption is taken for granted, and only the question of the time dependence of the single intermolecular coordinate $x(t)$ is allowed to be influenced by the remainder of the system. What will be assumed, then, is

$$x(t)=x_0(t)+p(t), \tag{7}$$

where $x_0(t)$ is the solution of Eq. (5) with β and $A(t)$ set equal to zero, and $p(t)$ is a small perturbation. More precisely, since $x(t)$ is a stochastic variable it is assumed that the probability of large $p(t)$ is negligibly small if t lies within the collision time interval. Now according to Eqs. (5) and (6), this assumption is expected to be true only if β is small, so that when Eq. (7) is used in Eq. (5), and the equation linearized with

[7] C. Zener, Phys. Rev. **38**, 277 (1931).
[8] L. Landau and E. Teller, Physik. Z. Sowjetunion **10**, 34 (1936).
[9] B. Widom and S. H. Bauer, J. Chem. Phys. **21**, 1670 (1953).
[10] That is, the relative motion satisfies the Langevin equation.
[11] J. G. Kirkwood, J. Chem. Phys. **14**, 180 (1946).
[12] M. C. Wang and G. E. Uhlenbeck, Revs. Modern Phys. **17**, 323 (1945).

respect to p, it is also reasonable to suppress $\beta dp/dt$. The result is

$$d^2x_0/dt^2 = -m^{-1}dV(x_0)/dx_0, \tag{8}$$

$$d^2p/dt^2+m^{-1}[d^2V(x_0)/dx_0^2]p = -\beta dx_0/dt+A(t). \tag{9}$$

The procedure now is to obtain $x_0(t)$ from Eq. (8) and substitute $x_0(t)$ into Eq. (9), the result being an equation in which p is the dependent, t the independent variable.

In the solution of Eq. (8) it is convenient to take $t=0$ as the time of closest approach, that is, the maximum of $x_0(t)$ is $x_0(0)$. Further, let ϵ be the potential energy of the pair at $t=0$. Then it is known, and most easily verified from

$$(m/2)(dx_0/dt)^2+V(x_0) = \epsilon \tag{10}$$

which is equivalent to Eq. (8), that the solution of Eq. (8) is

$$V[x_0(t)] = K\exp[-ax_0(t)] = \epsilon\,\mathrm{sech}^2ct, \tag{11}$$

where

$$c = a(\epsilon/2m)^{\frac{1}{2}}. \tag{12}$$

Let us put

$$\tau = ct$$

and agree not to use a different notation for a function where its argument is changed from t to τ. Thus $p(t)=p(\tau)$.

When the independent variable of Eq. (9) is changed from t to τ, and V and x_0 substituted from Eq. (11), Eq. (9) becomes

$$d^2p/d\tau^2+2(\mathrm{sech}^2\tau)p = R(\tau), \tag{13}$$

$$R(\tau) = R_a(\tau)+R_b(\tau)$$

$$R_a(\tau) = c^{-2}A(t), \tag{14}$$

$$R_b(\tau) = -(2\beta/ac)\tanh\tau. \tag{15}$$

III. DIFFERENTIAL EQUATION

The solution of Eq. (13) can be obtained by the method of variation of parameters.[13] What is required first is a pair of linearly independent solutions of the homogeneous equation,

$$d^2p_i/d\tau^2+2(\mathrm{sech}^2\tau)p_i = 0; \quad i=1,2. \tag{16}$$

Equation (16) closely resembles a tabulated equation[14] and it may readily be verified that

$$p_1 = \tanh\tau,$$

$$p_2 = 1-\tau\tanh\tau, \tag{17}$$

are satisfactory solutions. From them the general solution of Eq. (13) is determined[13] as

$$p = -p_1(\tau)\int_0^\tau \frac{p_2(\tau_2)R(\tau_2)}{W(\tau_2)}d\tau_2+p_2(\tau)\int_0^\tau \frac{p_1(\tau_2)R(\tau_2)}{W(\tau_2)}d\tau_2 + c_1p_1(\tau)+c_2p_2(\tau), \tag{18}$$

where

$$W(\tau) \equiv p_1(\tau)dp_2(\tau)/d\tau-p_2(\tau)dp_1(\tau)/d\tau = -1.$$

The constants c_1 and c_2 are chosen to satisfy initial conditions, which are taken to be $dx/dt=0$ at $t=0$, and $x(0)=x_0(0)$. The former condition gives $c_1=0$, and the latter gives $c_2=0$. Therefore,

$$p = p_1(\tau)\int_0^\tau p_2(\tau_2)R(\tau_2)d\tau_2-p_2(\tau)\int_0^\tau R(\tau_2)p_1(\tau_2)d\tau_2, \tag{19}$$

$$= p_a+p_b. \tag{20}$$

It will be convenient to have broken up in Eq. (20) the two parts of p which arise from the two parts of R in Eqs. (14) and (15); p_a is a functional of $A(t)$ and is consequently the stochastic part of p, while p_b is determined solely from the initial conditions.

IV. TRANSITION PROBABILITY

According to Eq. (4),

$$P = \langle |I|^2\rangle, \tag{21}$$

where

$$I = \int_{-\infty}^{+\infty}\exp[-ax(t)+i\omega t]dt. \tag{22}$$

The brackets $\langle\ \rangle$ signify an average over $A(t)$. Consideration of the initial energy, also a random variable, will be deferred until later. With $x=x_0+p=x_0+p_a+p_b$, an expansion of the integral in Eq. (22) gives

$$I = I_0+I_a+I_b,$$

$$I_0 = \int_{-\infty}^{+\infty}\exp[-ax_0(t)+i\omega t]dt,$$

$$I_a = -a\int_{-\infty}^{+\infty}P_a(t)\exp[-ax_0(t)+i\omega t]dt,$$

$$I_b = -a\int_{-\infty}^{+\infty}p_b(t)\exp[-ax_0(t)+i\omega t]dt. \tag{23}$$

For the computation of P, it may be observed from Eqs. (14) and (19) that $\langle I_a\rangle=0$. From Eqs. (15) and (19) it follows that $|I_b|^2$ is proportional to β^2, and is therefore neglected. What is left in P is

$$P = I_0^2+2I_0\,\mathrm{Re}I_b+\langle |I_a|^2\rangle.$$

Now the evaluation of I_b from Eqs. (15), (19), and (23) is fairly straightforward. Neither the calculation

[13] L. R. Ford, *Differential Equations* (McGraw-Hill Book Company, Inc., New York, 1933), p. 76.

[14] E. Kamke, *Differentialgleichungen* (Akademische Verlagsgesellschaft, Leipzig, 1943), Vol. 1, p. 504.

nor the results will be presented, for it turns out that I_b is very uninteresting. It vanishes at high frequencies as $\exp[-\pi\omega/2c]$, the same as I_0, whereas it turns out that $\langle |I_a|^2 \rangle$ lacks this exponential decay, and therefore forms a much more significant perturbation on the binary collision model than I_b, for the vibrational frequencies which are significant. In sum, the random force of the Brownian motion model will be retained, but the frictional force will be discarded,

$$P = I_0^2 + \langle |I_a|^2 \rangle. \tag{24}$$

From Eq. (23)

$$\langle |I_a|^2 \rangle = a^2 \int_{-\infty}^{+\infty}\int_{-\infty}^{+\infty} \langle p_a(t_1)\, p_a(t_3) \rangle \times \exp[-ax_0(t_1) - ax_0(t_3) + i\omega(t_1 - t_3)]\, dt_1 dt_3. \tag{25}$$

We now discuss the evaluation of this complicated double integral for the pertinent case of large ω.

V. STOCHASTIC TRANSITIONS

1. Correlation

The first problem is the evaluation of $\langle p_a(t_1)\, p_a(t_3) \rangle$. From Eqs. (14) and (19), write

$$p_a(t_1) = c^{-2} \int_0^{\tau_1} A(t_2) f(\tau_1, \tau_2)\, d\tau_2, \tag{26}$$

where

$$f(\tau_1, \tau_2) \equiv p_1(\tau_1)\, p_2(\tau_2) - p_2(\tau_1)\, p_1(\tau_2). \tag{27}$$

Then

$$\begin{aligned}
&\langle p_a(t_1)\, p_a(t_3) \rangle \\
&= c^{-4} \int_{\tau_2=0}^{\tau_1}\int_{\tau_4=0}^{\tau_3} \langle A(t_2)\, A(t_4) \rangle f(\tau_1, \tau_2) f(\tau_3, \tau_4)\, d\tau_2 d\tau_4 \\
&= (2\beta kT/mc^4) \int_0^{\tau_1} f(\tau_1, \tau_2) f(\tau_3, \tau_2) \left[\int_0^{\tau_2} \delta(t_4 - t_2)\, d\tau_4 \right] d\tau_2,
\end{aligned} \tag{28}$$

where the last equation follows from Eq. (6). Now

$$\begin{aligned}
\int_0^{t_3} \delta(t_4 - t_2)\, d\tau_4 &= c \int_0^{t_3} \delta(t_4 - t_2)\, dt_4 \\
&= c\{H(t_3 - t_2) H(t_2) - H(-t_2) H(t_2 - t_3)\},
\end{aligned} \tag{29}$$

where $H(x)$ is the step function

$$H(x) = \begin{cases} 1 & \text{if } x > 0 \\ 0 & \text{if } x < 0 \end{cases}.$$

To see this, put

$$\int_0^{t_3} \delta(t_4 - t_2)\, dt_4 = \int_{-t_2}^{t_3 - t_2} \delta(x)\, dx.$$

The integral is unity if and only if $t_3 - t_2 > 0$, $t_2 > 0$, and minus unity if and only if $t_3 - t_2 < 0$, $t_2 < 0$. Otherwise, the integral is zero. This is the content of Eq. (29). Substitution of Eq. (29) into Eq. (28) gives

$$\begin{aligned}
&\langle p_a(t_1)\, p_a(t_3) \rangle \\
&= (2\beta kT/mc^2) \Big\{ H(t_1) \int_0^{t_1} H(t_3 - t_2) f(\tau_1, \tau_2) f(\tau_3, \tau_2)\, dt_2 \\
&\qquad - H(-t_1) \int_0^{t_2} H(t_2 - t_3) f(\tau_1, \tau_2) f(\tau_3, \tau_2)\, dt_2 \Big\} \\
&= (2\beta kT/mc^2) \Big\{ H(t_1) H(t_3 - t_1) \int_0^{t_1} f(\tau_1, \tau_2) f(\tau_3, \tau_2)\, dt_2 \\
&\qquad + H(t_3) H(t_1 - t_3) \int_0^{t_3} f(\tau_1, \tau_2) f(\tau_3, \tau_2)\, dt_2 \\
&\qquad - H(-t_1) H(t_1 - t_3) \int_0^{t_1} f(\tau_1, \tau_2) f(\tau_3, \tau_2)\, dt_2 \\
&\qquad - H(-t_3) H(t_3 - t_1) \int_0^{t_3} f(\tau_1, \tau_2) f(\tau_3, \tau_2)\, dt_2 \Big\}.
\end{aligned} \tag{30}$$

Now observe that $\langle |I_a|^2 \rangle$ is necessarily a positive real number, so that the integrand in Eq. (25) excluding $\langle p_a(t_1)\, p_a(t_3) \rangle$ is invariant to the exchange of t_1 and t_3, or the substitution $(t_1, t_3) \to (-t_1, -t_3)$. This means that in any of the terms on the rhs of Eq. (30), we can exchange t_1 and t_3, or make the substitution $(t_1, t_3) \to (-t_1, -t_3)$, keep the rest of the integrand (and the limits) in Eq. (25) unchanged, and still get the same value of the integral. Therefore, in the second and fourth terms on the rhs of Eq. (30), exchange t_3 and t_1. This gives for $\langle p_a(t_1)\, p_a(t_3) \rangle$ the expression

$$\begin{aligned}
&(4\beta kT/mc^2)[H(t_1) H(t_3 - t_1) - H(-t_1) H(t_1 - t_3)] \\
&\qquad \times \int_0^{t_1} f(\tau_1, \tau_2) f(\tau_3, \tau_2)\, dt_2.
\end{aligned} \tag{31}$$

Define

$$Q(\tau_1, \tau_3) \equiv \int_0^{\tau_1} f(\tau_1, \tau_2) f(\tau_3, \tau_2)\, d\tau_2.$$

The definitions (17) and (27), and an elementary integration over τ_2 give

$$\begin{aligned}
Q(\tau_1, \tau_3) &= p_1(\tau_1)\, p_1(\tau_3)[\tau_1 - \tau_1^2 \tanh\tau_1 + \tau_1^3/3] \\
&\quad - [p_1(\tau_1)\, p_2(\tau_3) + p_2(\tau_1)\, p_1(\tau_3)][\tau_1 \tanh\tau_1 - \tau_1^2/2] \\
&\quad + p_2(\tau_1)\, p_2(\tau_3)[\tau_1 - \tanh\tau_1].
\end{aligned} \tag{32}$$

It follows that $Q(-\tau_1, -\tau_3) = -Q(\tau_1, \tau_3)$, and we can make the substitution $(\tau_1, \tau_3) \to (-\tau_1, -\tau_3)$ in (31) to obtain a final expression for $\langle p_a(t_1)\, p_a(t_3) \rangle$,

$$(8\beta kT/mc^3) H(t_1) H(t_3 - t_1) Q(\tau_1, \tau_3).$$

Consequently, Eq. (25) becomes

$$\begin{aligned}
\langle |I_a|^2 \rangle &= \mathrm{Re}(8a^2\beta kT/mc^3) \int_0^{\infty} dt_1 \int_{-\infty}^{\infty} dt_3 H(t_3 - t_1) Q(\tau_1, \tau_3) \\
&\quad \times \exp[-ax_0(t_1) - ax_0(t_3) + i\omega(t_1 - t_3)].
\end{aligned} \tag{33}$$

2. Integration

It is now useful to represent the step function as a Fourier integral[15]

$$H(t_3-t_1)=\int_{-\infty}^{+\infty} g(y)\,\exp[iy(t_3-t_1)]dy$$

$$g(y)=\tfrac{1}{2}\delta(y)+(2\pi iy)^{-1}. \tag{34}$$

The change of variables to $\tau=ct$ in Eq. (33), and the substitution of Eq. (34) yield

$$\langle\,|\,I_a\,|^2\rangle$$

$$=\mathrm{Re}(8a^2\beta kT/mc^5)\int_{-\infty}^{\infty}dy g(y)\int_0^{\infty}d\tau_1\int_{-\infty}^{\infty}d\tau_3 Q(\tau_1,\tau_3)$$

$$\times\exp[-ax_0(\tau_1)-ax_0(\tau_3)+i\theta(\tau_1-\tau_3)], \tag{35}$$

where

$$\theta=c^{-1}(\omega-y).$$

Consider first that part of the integral in (35) which arises from the real part of $g(y)$, i.e., $\frac{1}{2}\delta(y)$. This part will be proportional to

$$\mathrm{Re}\int_0^{\infty}d\tau_1\int_{-\infty}^{\infty}d\tau_3 Q(\tau_1,\tau_3)$$

$$\times\exp[-ax_0(\tau_1)-ax_0(\tau_3)+i(\omega/c)(\tau_1-\tau_3)]. \tag{36}$$

Now $Q(\tau_1,\tau_3)$ may be broken down into a sum of products $u(\tau_1)w(\tau_3)$, as is shown in Eq. (32). Consequently the double integral (36) may be written as a sum of products of two integrals, one over τ_1, the other over τ_3, say

$$\mathrm{Re}\sum\left\{\int_0^{\infty}d\tau_1 u(\tau_1)\,\exp[-ax_0(\tau_1)+i(\omega/c)\tau_1]\right\}$$

$$\times\left\{\int_{-\infty}^{+\infty}d\tau_3 w(\tau_3)\,\exp[-ax_0(\tau_3)+i(\omega/c)\tau_3]\right\}. \tag{37}$$

From Eq. (11), $\exp[-ax_0(\tau)]$ is proportional to $\mathrm{sech}^2\tau$ and an inspection of a table of Fourier transforms for the functions $w(\tau_3)$ which occur in Q [Eq. (32)], will show that the τ_3 integral in (37) vanishes as $\exp(-\pi\omega/2c)$ where ω is large.[16] The τ_1 integration will probably contain terms of nonexponential decay, but the net result will still be a total exponential decay, so that these terms will be negligible compared to those eventually retained, when ω is large.

The imaginary part of $g(y)$ must be multiplied by the imaginary part of the remainder of the integral of Eq. (35). It can readily be verified that the imaginary part of the integral over τ_1 and τ_3 does not change under the substitution $(\tau_1,\tau_3)\rightarrow(-\tau_1,-\tau_3)$, except to change the limits on the τ_1 integration from $0<\tau_1<\infty$ to $-\infty<\tau_1<0$. The two expressions for the integral can be added together to give

$$\langle\,|\,I_a\,|^2\rangle=\mathrm{Im}(2a^2\beta kT/\pi mc^5)\int_{-\infty}^{\infty}y^{-1}Fdy, \tag{38}$$

where

$$F=\int_{-\infty}^{\infty}d\tau_1\int_{-\infty}^{\infty}d\tau_3 Q(\tau_1,\tau_3)$$

$$\times\exp[-ax_0(\tau_1)-ax_0(\tau_3)+i\theta(\tau_1-\tau_3)]. \tag{39}$$

F meets all the qualifications of a "good function," in the terminology of Lighthill.[15] F is everywhere differentiable any number of times wrt y, and goes to zero sufficiently rapidly as $|\,y\,|\rightarrow\infty$. In fact,[16] F goes to zero as $\exp(-\pi\,|\,\theta\,|\,)$ as $|\,y\,|\rightarrow\infty$. Consequently,[17] the integral

$$\int y^{-1}Fdy$$

is to be interpreted as a Cauchy principal value

$$g\equiv\int_{-\infty}^{\infty}y^{-1}Fdy=-\int_{-\infty}^{+\infty}\ln|\,y\,|\,(\partial F/\partial y)dy. \tag{40}$$

Change the integration variable in (40) to $\theta=c^{-1}(\omega-y)$,

$$g=\int_{-\infty}^{\infty}[\ln\omega+\ln|\,1-c\theta\omega^{-1}\,|\,]\partial F/\partial\theta d\theta$$

$$=\int_{-\infty}^{+\infty}\ln|\,1-c\theta\omega^{-1}\,|\,\partial F/\partial\theta d\theta, \tag{41}$$

where the last step follows from the exponential decay of F at $|\,\theta\,|\rightarrow\infty$. It is now beneficial to divide the integral into three parts:

$$g=g_1+g_2+g_3,$$

$$g_1=\int_{-\infty}^{-\omega/c}[\ln(1-c\theta/\omega)]\partial F/\partial\theta d\theta,$$

$$g_2=\int_{-\omega/c}^{+\omega/c}[\ln(1-c\theta/\omega)]\partial F/\partial\theta d\theta,$$

$$g_3=\int_{+\omega/c}^{\infty}[\ln(-1+c\theta/\omega)]\partial F/\partial\theta d\theta. \tag{42}$$

In the first and third integrals, g_1 and g_3, $|\,\theta\,|$ is $\geq\omega/c$ throughout the range of integration. Consequently, the asymptotic form of F can be used in g_1 and g_3; $F=o(\theta^N\exp-\pi\,|\,\theta\,|\,)$, where N is a small integer. It readily follows that g_1 and g_3 decay exponentially with ω for large ω, and can be neglected. On the other hand, g_2 is much larger.

[15] M. J. Lighthill, *Fourier Analysis and Generalized Functions* (Cambridge University Press, New York, 1958).

[16] A. Erdelyi, Editor, *Tables of Integral Transforms* (McGraw-Hill Book Company, Inc., New York, 1954), Vol. 1. The required transforms can all be worked down to No. 2, p. 30.

[17] Footnote reference 15, p. 37.

A convergent expansion of g_2 results from an expansion of the logarithm,

$$g_2=-\sum_{n=1}^{\infty}n^{-1}(c/\omega)^n\int_{-\omega/c}^{+\omega/c}\theta^n\partial F/\partial\theta d\theta. \tag{43}$$

The limits may now be allowed to approach $\pm\infty$ without introduction of any new error,

$$g_2=\sum_{n=1}^{\infty}(c/\omega)^n\int_{-\infty}^{+\infty}\theta^{n-1}F(\theta)d\theta. \tag{44}$$

Equation (39) gives

$$\int_{-\infty}^{+\infty}\theta^{n-1}F(\theta)d\theta=\int_{-\infty}^{\infty}d\tau_1\int_{-\infty}^{\infty}d\tau_3Q(\tau_1,\tau_3)\times\exp[-ax_0(\tau_1)-ax_0(\tau_3)]\times\frac{d^{n-1}}{d(-i\tau_3)^{n-1}}\int_{-\infty}^{+\infty}\exp[i\theta(\tau_1-\tau_3)]d\theta, \tag{45}$$

but the derivative of the last integral in Eq. (45) is

$$2\pi(i)^{n-1}[d^{n-1}/(d\tau_3^{n-1})]\delta(\tau_3-\tau_1).$$

Consequently,[18]

$$\int_{-\infty}^{\infty}\theta^{n-1}F(\theta)d\theta=(2\pi/i^{n-1})\int_{-\infty}^{+\infty}\exp[-ax_0(\tau)]\times\{(d^{n-1}/d\tau_3^{n-1})\exp[-ax_0(\tau_3)]Q(\tau,\tau_3)\}_{\tau_3=\tau}d\tau. \tag{46}$$

The determination of the integral in Eq. (46) by a straightforward appeal to Eq. (32) is tremendously complicated. A more feasible procedure begins with the definition of Q which gives, after $\exp[-ax_0(\tau)]$ is introduced from Eq. (11),

$$\int_{-\infty}^{\infty}\theta^{n-1}F(\theta)d\theta=(2\pi/i^{n-1})(\epsilon/K)^2\int_{-\infty}^{\infty}d\tau\int_0^{\tau}d\tau_2h(\tau,\tau_2)[d^{n-1}h(\tau,\tau_2)/d\tau^{n-1}], \tag{47}$$

where

$$h(\tau,\tau_2)\equiv\operatorname{sech}^2\tau f(\tau,\tau_2). \tag{48}$$

Now it may be seen from Eq. (46) that the integral vanishes for odd n, because $Q(\tau,\tau)$ is an odd function of τ. It also turns out that the lowest n for which the integral is nonvanishing is $n=4$.

Consider first $n=2$ in Eq. (47). The double integral in Eq. (47) is

$$\tfrac{1}{2}\int_{-\infty}^{\infty}\int_0^{\tau}(d/d\tau)[h(\tau,\tau_2)]^2d\tau_2d\tau. \tag{49}$$

Since

$$(d/d\tau)\int_0^{\tau}[h(\tau,\tau_2)]^2d\tau_2=[h(\tau,\tau)]^2+\int_0^{\tau}\frac{d[h(\tau,\tau_2)]^2}{d\tau}d\tau_2$$

and $h(\tau,\tau)=0$, because $f(\tau,\tau)=0$ [see Eq. (27)], the integral (49) becomes

$$\tfrac{1}{2}\int_{-\infty}^{\infty}(d/d\tau)\left[\int_0^{\tau}[h(\tau,\tau_2)^2]d\tau_2\right]d\tau=\tfrac{1}{2}\int_0^{\infty}[h(\infty,\tau_2)]^2d\tau_2-\tfrac{1}{2}\int_0^{-\infty}[h(-\infty,\tau_2)]^2d\tau_2,$$

but $h(\pm\infty,\tau_2)=0$, and consequently the integral in Eq. (47) vanishes for $n=2$.

A similar but slightly more involved calculation gives for $n=4$, and with no approximations,

$$\int_{-\infty}^{\infty}d\tau\int_0^{\tau}d\tau_2h(\tau,\tau_2)d^3h(\tau,\tau_2)/d\tau^3=\tfrac{1}{2}\int_{-\infty}^{\infty}d\tau\left[\frac{dh(\tau,\tau_2)}{d\tau}\right]^2_{\tau_2=\tau}=\tfrac{1}{2}\int_{-\infty}^{\infty}\operatorname{sech}^4\tau d\tau, \tag{50}$$

where the last step follows readily from Eqs. (48), (27), and (17). With

$$\int_{-\infty}^{\infty}\operatorname{sech}^4d\tau=4/3,$$

Eqs. (50), (47), (44), and (38) give

$$\langle|I_a|^2\rangle=8a^2\beta kT\epsilon^2/3mc\omega^4K^2. \tag{51}$$

This is to be compared with I_0^2. Equations (23) and (11) give

$$I_0^2=(\pi^2\epsilon^2\omega^2/c^4K^2)\exp(-\pi\omega/c). \tag{52}$$

VI. DISCUSSION

The first observation to make about $\langle|I_a|^2\rangle$ is the unexpected dependence of this perturbation to the transition probability on the energy of the binary collision. Since c^2 is proportional to ϵ [Eq. (12)], I_0^2 drops to zero exponentially as ϵ is decreased, while $\langle|I_a|^2\rangle$ goes to zero only as $\epsilon^{\frac{1}{2}}$. The calculation being completed, a rationalization is not very difficult. Equation (4) shows that, for large ω, only high-frequency components of the time-dependent intermolecular potential, contribute to the transition probability. In an isolated binary collision, such high-frequency motions occur only at high energies, but when the binary collision is perturbed by a random impulse force $A(t)$, it is evident that even a collision with a small relative velocity may for a brief period, during which the impulse acts, have components of high frequency. Moreover, the slower the relative motion, the more likely it is that the force $A(t)$ will act during a collision. It may be repeated that the frictional part of the Brownian motion model is negligible.

In order for the binary collision theory to be applicable to liquids, we must require at least the condition that α,

$$\alpha\equiv\langle|I_a|^2\rangle/I_0^2=\beta[(8a^2kTc^3/3\pi^2m\omega^6)\exp(\pi\omega/c)], \tag{53}$$

[18] Footnote reference 15, p. 19.

be much less than unity for the energies which the binary collision theory indicates are important. This energy turns out to be

$$\epsilon=\tfrac{1}{2}mv_0^2,$$

where[2]

$$v_0=(2\pi\omega kT/am)^{\frac{1}{2}}.$$

Let us calculate α for liquid CS_2, the substance to which Litovitz[4] applied the binary collision theory. Take[2,4]

$$\omega=2\pi\times397\times3\times10^{10}\ \text{sec}^{-1},$$

$$a=5\times10^{8}\ \text{cm}^{-1},$$

$$T=300°.$$

Then

$$\alpha=1.4\beta\times10^{-13}\ \text{sec}.$$

If β is estimated from the Einstein relation $\beta=kT/Dm$, where D is a diffusion constant, $\alpha\ll1$ for gases up to quite high densities. But for the liquid state itself, $\beta\cong10^{13}$ sec^{-1}, and there is no escaping the result, α is not small, and the binary collision model does not apply to liquids.

One may of course reject the use of the Brownian motion model, and consequently this calculation, entirely. Certainly the model gives only a rough account of what is to be expected of the liquid state. Very probably, the error produced by the model is an exaggeration of the perturbation. This seems likely, though not at all certain, because of the delta-function autocorrelation which the Brownian motion model ascribes to $A(t)$. A more realistic autocorrelation would have a spectrum which is less dense in the high-frequency range, and presumably, therefore, less effective in causing transitions. It would be interesting to test this speculation by the selection of a Gaussian autocorrelation for $A(t)$, with a variable second moment.

In any case, refinements[2,4] of the repulsive potential to include the longer range attractive part, cannot be taken seriously when the binary collision model is applied to liquids.

THE JOURNAL OF CHEMICAL PHYSICS VOLUME 34, NUMBER 2 FEBRUARY, 1961

Nuclear Magnetic Resonance Study of the Proton Transfer in Water

S. MEIBOOM

Bell Telephone Laboratories, Inc., Murray Hill, New Jersey

(Received June 6, 1960)

Measurements of the nuclear relaxation in water are reported. The transverse relaxation rate $(1/T_2)$ of the proton resonance is pH dependent. The effect is shown to be due to a spin-spin splitting of the proton resonance by O^{17} (spin 5/2), which is only partially averaged out by proton exchange. The increase of relaxation rate is observable in natural water (0.037% O^{17}), and becomes very appreciable in water enriched in O^{17}. Additional information can be obtained by measuring relaxation rates in the presence of an rf field H_1, using a method due to Solomon. A study of the width of the O^{17} resonance as a function of pH is in quantitative agreement with the results of the proton resonance. The observations provide a direct determination of the rate constants of the exchange reactions:

$$H_2O+H_3O^+\xrightarrow{k_1}H_3O^++H_2O \text{ and } H_2O+HO^-\xrightarrow{k_2}HO^-+H_2O.$$

It is found that $k_1=(10.6\pm4)\times10^9$ liter mole^{-1} sec^{-1} and $k_2=(3.8\pm1.5)\times10^9$ liter mole^{-1} sec^{-1}. The spin-spin interaction between H and O^{17} in water is determined as 92 ± 15 cps. In the Appendices, theoretical equations for the exchange contribution to the relaxation rate are derived.

I. INTRODUCTION

THE anomalous mobilities of the hydrogen and hydroxyl ions in water find their explanation in the occurrence of fast proton transfers between these ions and neutral water molecules.[1] Formally, the proton transfer processes can be written as

$$H_2O+\overset{+}{H_3O}\xrightarrow{k_1}\overset{+}{H_2O}H+H_2O \qquad (I)$$

$$OH_2+\overset{-}{O}H\xrightarrow{k_2}\overset{-}{O}H+HOH. \qquad (II)$$

A number of different models for the detailed mechanism of these reactions have been advanced. It is probable that the actual proton transfer between suitably oriented molecules is very fast and consists of quantum mechanical tunneling; the rate-determining step of the reaction is the necessary reorientation of the water molecules between successive exchanges. There is strong evidence for the existence of an $H_9O_4^+$ complex, held together by very strong hydrogen bonds. In this model, the rate-determining step would be migration of these strong hydrogen bonds ("structural diffusion").

The anomalous mobilities of the hydronium and hydroxyl ions are closely related to the rate of reactions (I) and (II), but the quantitative relation will depend

[1] For a review and references see M. Eigen and L. DeMayer, Proc. Roy. Soc. (London) **A247**, 505 (1958); also, their chapter in *The Structure of Electrolytic Solutions*, edited by W. J. Hammer (John Wiley & Sons, Inc., New York, 1959).

on the details of the transfer mechanism. It is, therefore, of interest to measure the rate of these reactions directly. In this paper such measurements by means of the nuclear magnetic resonance (NMR) technique[2] will be reported.

A necessary condition for the applicability of the NMR method to a specific system is that the nuclei involved in the exchange can be in at least two different "environments," characterized by different local magnetic fields, and accordingly different Larmor frequencies of the nuclei. The exchange process will transfer nuclei from one environment to another, with an accompanying switch of their resonance frequency to a different value. It is thus possible to track the exchange reaction, because the nuclei are "labeled" by their Larmor frequency. The experimentally determined quantity is the increase in linewidth in the NMR spectrum caused by these frequency changes. Qualitatively the changes observed in the NMR spectrum of a system as its exchange rate is increased gradually from zero to a high value are as follows: A gradual broadening of the resonance lines involved in the exchange will be observed initially. This broadening will increase until the individual lines overlap and a single broad line is observed. On continued increase of the exchange rate this line will narrow, and at very fast rates a single sharp line, at the center of gravity of the contributing lines is observed. The first stage of broadened individual lines will be called "lifetime broadening," because the broadening can be considered as resulting from the finite time a nucleus stays in a definite frequency state. The second stage, in which there is a single collapsed line, is referred to as "exchange narrowing." In this stage, the exchange is fast enough for an averaging of the individual resonance frequencies to occur, and the width of the observed line decreases with increasing exchange rate.

In water the exchange is both acid- and base-catalyzed, and the rate is so fast that, except for a small *p*H range around neutral, exchange narrowing applies. We should, therefore, expect that, if any effect of the exchange on linewidth would occur, the addition of acid or base would increase the exchange rate and, therefore, decrease the width of the resonance. Such a behavior of the linewidth as function of *p*H has been reported previously by Meiboom, Luz, and Gill[3] and is confirmed by the present work. It is now clear, however, that the interpretation given in the previous note is incorrect. The interpretation hinges on the cause of the multiple proton frequencies. As already stated, at least two different proton frequencies must be present in the system in order for a broadening to occur at all. In footnote reference 3, it was assumed that the two relevant frequencies corresponded to hydrogen bonded and "free" protons, respectively. However, the new measurements show that the dominant factor is the splitting of the proton resonance by spin-spin interaction with O^{17}. (The O^{17} isotope has a spin of $\frac{5}{2}$, while the two other stable oxygen isotopes, O^{16} and O^{18}, have zero spin.) This follows from the observation that the magnitude of the broadening is about proportional to the O^{17} concentration in the water (see Fig. 3). The fact that the predominant splitting is due to a spin-spin interaction rather than to a chemical shift is confirmed by the observation that the present measurements, which were done at 60 Mc, give the same magnitude for the broadening as the previous measurements,[3] which were done at 31 Mc. As the broadening in the case of fast exchange is proportional to the square of the frequency difference between the individual lines, a chemical shift splitting would result in an increase of width with frequency.

It should be mentioned that the presence of deuterium, of course, also results in a splitting of the proton resonance by spin-spin interaction. However, this splitting can be expected to be much smaller than the one caused by O^{17} and can be neglected for the present purpose. This is confirmed by the observation that the broadening of the proton resonance in deuterium-enriched water is not appreciably larger than in water with natural deuterium abundance.[4]

II. MEASURING METHODS

A. Proton Relaxation in Water

The observed proton resonance in water consists of a single Lorentzian line, with a width of less than one cps. Direct width measurements by slow passage cannot be done with any accuracy on such narrow lines because of the unavoidable inhomogeneity of the magnetic field.

For a Lorentzian line, the full width at half-amplitude in cps, Δ, is related to the transverse relaxation time T_2 by the equation

$$\Delta = 1/\pi T_2. \tag{1}$$

There are a number of methods of measuring T_2 which eliminate the effect of field inhomogeneity. The most widely used one is the spin-echo method. In the work reported here, however, a different method, first given by Solomon,[5] has been employed. Besides giving the "natural" T_2, this method gives additional useful information, as discussed in the following.

[2] The first paper giving a theory of exchange broadening is H. S. Gutowsky, D. W. McCall, and C. P. Slichter, J. Chem. Phys. **21,** 279 (1953). Other papers developing the theory are: H. S. Gutowsky and A. Saika, J. Chem. Phys. **21,** 1688 (1953); H. S. Gutowsky and C. H. Holm, *ibid.* **25,** 1228 (1956); P. W. Anderson, J. Phys. Soc. Japan **9,** 316 (1954); J. I. Kaplan, J. Chem. Phys. **28,** 278 (1958); R. A. Sack, Mol. Phys. **1,** 163 (1958); H. M. McConnell, J. Chem. Phys. **28,** 430 (1958). For a simple, qualitative exposition of the basic principles see S. Meiboom, Z. Elektrochem. **64,** 50 (1960).

[3] S. Meiboom, Z. Luz, and D. Gill, J. Chem. Phys. **28,** 1611 (1957).

[4] D. Gill, thesis, Jerusalem (unpublished).

[5] I. Solomon, Compt. rend. **248,** 92 (1959); **249,** 1631 (1959).

It is well known that the nuclear magnetization can be flipped through 180° by an adiabatic fast passage through the resonance.[6] In Solomon's method, an adiabatic fast passage is made halfway through the resonance, i.e., the sweep is stopped when the center of the resonance line is reached. The rf field $\mathbf{H}_1$ is kept on all the time. We shall call this an adiabatic half-passage. After such a passage, the magnetization will be parallel to $\mathbf{H}_1$, and as γH_1 is large compared to $1/T_1$, the magnetization will keep this direction also after the passage. The magnitude of the magnetization, however, will decay with a time constant to be denoted by $T(H_1)$. An essential feature of the method is that $T(H_1)$ is not appreciably affected by inhomogeneity of the applied magnetic field $\mathbf{H}_0$, if the variation of $\mathbf{H}_0$ over the sample volume is small compared to $\mathbf{H}_1$. The rf field $\mathbf{H}_1$ should be reasonably homogeneous over the active volume of the sample. The crossed coil probe of the Varian spectrometer fulfills this requirement.

After an adiabatic half-passage, the magnetization is perpendicular to $\mathbf{H}_0$, and it may be thought that $T(H_1)$ would be identical with the ordinary transverse relaxation time T_2. However, in general this is not so. The difference arises from the fact that $T(H_1)$ is observed in the presence of the rf field $\mathbf{H}_1$, while T_2 characterizes the relaxation in the absence of such a field. Even though in practice $\mathbf{H}_1$ is much smaller than $\mathbf{H}_0$, the former can have a pronounced effect if slow processes, such as chemical exchange, occur in the system. A theoretical treatment is given in Appendix A. The approach used there is based on the Bloch equations[6] generalized to include exchange.[7] Although such a treatment has limited applicability, it is a good approximation for the case of interest here. Explicit solutions for $T(H_1)$ as a function of H_1 and of the exchange rate can be obtained for some special cases. The one most useful here applies when the resonance consists of one dominant line, all other resonances being much weaker. We can then neglect the direct contribution of the weak lines to the observed signal, and consider them only as far as they contribute to the width of the dominant line through the exchange process. For the proton resonance in water this is an excellent approximation, as the highest O^{17} concentration used was only about 0.2%. Subject to the above restriction, the following equation is derived in Appendix A:

$$1/T(H_1)=(1/T')+\tau\sum_i \frac{P_i\delta_i^2}{1+\tau^2(\delta_i^2+\omega_1^2)}, \qquad (2)$$

where τ is the average lifetime between successive exchanges, i.e., the average time a proton is bonded to a specific oxygen atom ($1/\tau$ is the specific rate of exchange), P_i the relative intensity of the ith line, δ_i the frequency difference (in rad/sec) between the ith line and the dominant line, and $\omega_1\equiv\gamma H_1$, γ being the gyromagnetic ratio. The quantity T' characterizes the transverse relaxation due to mechanisms other than the exchange. If all these mechanisms involve short correlation times T' will be equal to the longitudinal relaxation time T_1. This will be assumed to hold in what follows. The validity of Eq. (2) is subject to one additional condition. This is that the probability for a nucleus to change its frequency to the ith line as a result of an exchange is independent of its initial environment. This condition is fulfilled for the proton resonance in water, because the protons transfer in a random way between different oxygen atoms. (This is not so for the O^{17} resonance, as here only one of the two coupled protons exchange at a time. For a detailed discussion see Appendix A.)

In the limit $\omega_1\rightarrow 0$ the relaxation time $T(H_1)$ will approach T_2. Equation (2) then becomes

$$(1/T_2)-(1/T_1)=\tau\sum_i \frac{P_i\delta_i^2}{1+\tau^2\delta_i^2}, \qquad (3)$$

where T' has been replaced by T_1. Equations (2) and (3) will be used in the interpretation of the experimental results.

B. O^{17} Relaxation in Water

The O^{17} resonance in water is much broader than the proton resonance. The main relaxation mechanism is provided by the coupling of the quadrupole moment of the O^{17} nucleus with electrical field gradients in the molecule, and a T_1 for O^{17} of about 4×10^{-3} sec results. Direct linewidth measurements from slow passage records can, therefore, be used for the O^{17} resonance. In fact, the relaxation methods would be impracticable in this case, because of the low abundance of O^{17} even in the enriched samples. In order to obtain a workable signal to noise ratio very slow passage and heavy filtering are necessary, and the latter would be impossible in the transient methods.

Fortunately, the exchange broadening of the O^{17} is of the same order of magnitude as its natural linewidth. In contrast to the proton resonance, it is not reduced by the low O^{17} concentration. A proton exchange in an O^{17} molecule has a 50% chance of switching the O^{17} resonance frequency to another line of the spin-spin triplet. It can be assumed that in water an exchange process replaces only one hydrogen atom at a time, so that only frequency switches between adjacent lines of the O^{17} spin-spin triplet occur. Equations for this case have been calculated by Loewenstein and Meiboom,[8] and the graphs given in Fig. 2 of that paper will be used in interpreting the O^{17} results.

[6] F. Bloch, Phys. Rev. **70**, 460 (1946).
[7] H. M. McConnell, J. Chem. Phys. **28**, 430 (1958). McConnell's procedure is equivalent to the treatment given by Gutowsky, McCall, and Slichter.[2]
[8] A. Loewenstein and S. Meiboom, J. Chem. Phys. **27**, 1067 (1957).

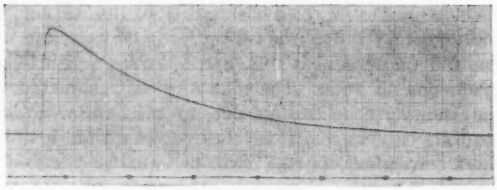

FIG. 1. Typical record obtained in the proton relaxation measurements by adiabatic 90° flip. The lower trace gives time marks at one-second intervals.

III. EXPERIMENTAL

A Varian high-resolution magnet and spectrometer were used in making the measurements. The proton resonance was studied at 60 Mc. The fast single sweep necessary to obtain an adiabatic half-passage was obtained by interrupting a dc current through the modulation coils on the probe. The circuit consisted of three large dry cells (4.5 v) connected through a variable 1000-ohm resistor and an on-off switch to the modulation coils. An electrolytic capacitor of 500 μfarad was shunted on the modulation coils to give a time constant of about 0.01 sec. The measuring procedure was as follows: Using the standard linear sweep, the proton resonance was centered on the scope and the phase adjusted to the dispersion mode. The modulation coils were then connected to the single sweep circuit described previously, and the current adjusted so as to be just outside the resonance. The necessary current was about 200 ma for the strongest rf fields used (rf attenuator at 0 db) and about 5 ma for the weakest (rf attenuator at 40 db). The current was then switched off, and the resulting signal recorded on a Sanborn recorder. A typical record is shown in Fig. 1.

Failure of the trace to return to the base line after the relaxation is completed indicates off resonance condition. If the trace stays above the base line, the center of the resonance was not reached in the fast passage. If it drops below the base line, the center has been passed. This is easily seen by remembering that the final position of the trace is determined by the slow passage dispersion curve, which crosses the base line at the center of the resonance. In general, a few trials, and suitable adjustments of the magnetic field, were necessary to obtain a satisfactory record. The recorded decay curve was plotted on semilog paper and the slope of the straight line so obtained gave the relaxation time $T(H_1)$.

Two changes in the standard Varian 4311 rf unit proved necessary in order to obtain satisfactory results. As delivered, this unit always has a low-pass filter in the output to the recorder, and will, therefore, distort rapidly changing signals. Actually positions "1" and "2" of the "frequency response" knob have identical filtering, and the unit was rewired to eliminate filtering in the "1" position. The second change arose from the observation of some nonlinearity in the function of the phase detector. The cause of this was traced to a detuning of the last i.f. transformer of the receiver by the diode detector connected to it. The rectifier in this detector has an effective capacitance, the value of which depends on the bias and, therefore, on the signal amplitude. The effect was eliminated by providing separate i.f. stages for the diode detector and the phase detector.

The relaxation time $T(H_1)$ of the protons in each water sample was measured as function of H_1. The attenuator setting was calibrated in terms of H_1 using the double irradiation method given by Anderson.[9,10] The longitudinal relaxation time T_1 of the protons was measured by a method consisting of an adiabiatic 180° flip followed by a sampling of the magnetization on the return sweep.[10,11]

In the study of the O^{17} resonance, a variable frequency rf unit (Varian 4210A) was used at 7.1 Mc. In order to improve the frequency stability, the transmitter was locked in with a crystal controlled oscillator. A field modulation of 20 cps was used and the derivative of the absorption mode recorded.

The relaxation times, T_1 and T_2, were obtained from linewidth and saturation measurements, as follows. Resonances were recorded for a number of different H_1 values and the amplitude of the signal plotted as function of H_1. From this curve the H_1 value $H_{\max}$ giving the maximum signal amplitude was determined. For a Lorentzian line we have the relation

$$T_1T_2=[2(\gamma H_{\max})^2]^{-1}. \tag{4}$$

The width of the observed resonance is given by

$$\Delta=(\pi\sqrt{3})^{-1}T_2^{-1}[1+(\gamma H_1)^2T_1T_2]^{\frac{1}{2}}, \tag{5}$$

where Δ is the peak to peak separation of the derivative of the absorption curve, in cps. On combining (4) and (5),

$$\Delta=(\pi\sqrt{3})^{-1}T_2^{-1}[1+(H_1^2/2H_{\max}^2)]^{\frac{1}{2}}. \tag{6}$$

On using (4) and (6), T_1 and T_2 were calculated from the observed linewidths and $H_{\max}$.

The calibration of the H_1 field was obtained by measuring the induced rf voltage in a small two turn coil, of known dimensions, inserted in the probe instead of the sample.

In all three series of measurements were made:

(1) proton relaxation as function of pH in water with natural O^{17} abundance (0.037%);

(2) proton relaxation as function of pH in water enriched in O^{17} (0.2%). The sample contained about 3% deuterium;

[9] W. A. Anderson, Phys. Rev. **102,** 151 (1956).

[10] For experimental details see W. A. Anderson and L. F. Johnson, *Special Operating Techniques* (Instrument Division, Varian Associates, Palo Alto, California, 1959).

[11] R. L. Conger and P. W. Selwood, J. Chem. Phys. **20,** 323 (1952); G. Chiarotti, G. Cristiani, L. Giulotto, and G. Lansi, Nuovo cimento **12,** 519 (1954).

(3) O^{17} relaxation as function of pH in water containing about 0.8% O^{17}, and about 10% deuterium. In the first series, the water sample was contained in a Teflon tube; in the two other series, in a glass tube. The pH was adjusted by the addition of small amounts of HCl or KOH solution and measured with semimicro glass and reference electrodes and a Beckman pH meter. The pH was measured both before and after the relaxation measurements. As the sample was not buffered, some drift in pH often occurred of the order of a few tenths of a pH unit. The average of the initial and final pH was then adopted. In the first series of measurements, distilled water from a quartz still was used, fresh water being taken for each pH value. In this series, at least part of the dissolved oxygen was removed by bubbling argon gas through the sample for about one hour before the measurements. The enriched samples used in the second and third series were obtained through Dajak Laboratories and Isomet Corporation, respectively, and were used without further purification. In each of these series, the same sample was used for all the pH values. During a series, the pH was changed a number of times from acidic to basic and vice versa, in order to fill in points on the experimental curve. A certain amount of salt, less than 0.1 M, accumulated, therefore, in the sample as the measurements progressed. This apparently did not affect the results, as no systematic deviation of the later points relative to the earlier ones was found. In these two series no attempt was made to remove dissolved oxygen.

For the interpretation of the second series, the concentration of O^{17} in the sample has to be known. This concentration was measured by comparing the amplitude of the O^{17} resonance in the sample with that in a sample of ordinary water. At the beginning of the series, the concentration was found to be 0.24 at.% O^{17} and at the end 0.20%. The decrease can be ascribed to dilution by the acid and base, and partially to exchange with atmospheric humidity. The measured proton relaxation times were corrected for this change in concentration, it being assumed that the same fraction of O^{17} was lost in each pH adjustment.

The deuterium content of the sample used in series 3 was determined by comparing the amplitude of the deuterium resonance with that in a sample of known deuterium content. The deuterium concentration was about 10%.

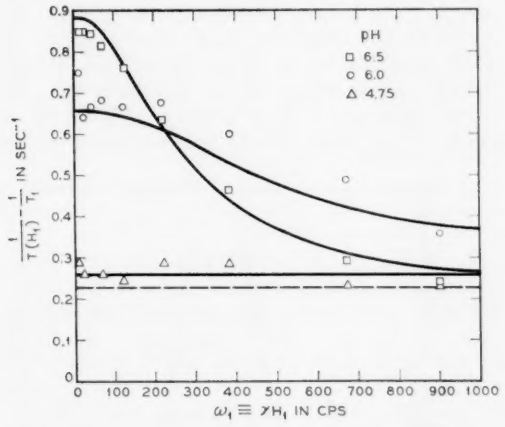

FIG. 2. Proton relaxation rates in water containing 0.2% O^{17}. T_1 is the longitudinal relaxation time and $T(H_1)$ the transverse relaxation time in the presence of an rf field H_1. The abscissa gives the magnitude of H_1 in terms of $\omega_1 \equiv \gamma H_1$. The points indicate experimental results, while the curves have been calculated as described in Sec. IV.

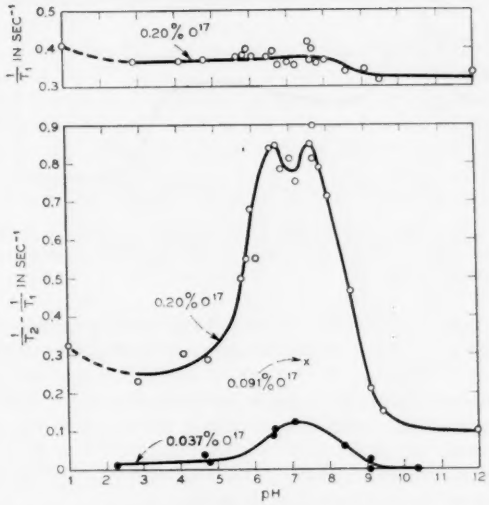

FIG. 3. In the upper figure is plotted the observed longitudinal proton relaxation rate $(1/T_1)$ in O^{17} enriched water as function of pH. The lower figure gives the difference between the observed transverse and longitudinal relaxation rates as function of pH.

IV. RESULTS AND INTERPRETATIONS

Typical results for the proton relaxation in O^{17} enriched water are shown in Fig. 2. In this figure, the quantity $\{[T(H_1)]^{-1}-T_1^{-1}\}$, which gives the contribution of the exchange process to the relaxation, has been plotted against the magnitude of the rf field, given in terms of $\omega_1=\gamma H_1$. The points indicate the results of actual measurements, while the curves were calculated from Eq. (2), as discussed below. Figure 2 is for a water sample containing 0.20% O^{17} and for the three pH values indicated. Similar curves were obtained for 22 different pH values in the pH range between 1 and 12.

Extrapolation of the measured relaxation times to $\omega_1 \to 0$ gives $(1/T_2-1/T_1)$, the difference between the transverse and longitudinal relaxation rates. This quantity has been plotted in the lower part of Fig. 3. The points in this figure give the results for all the solutions measured. The measurements on the enriched

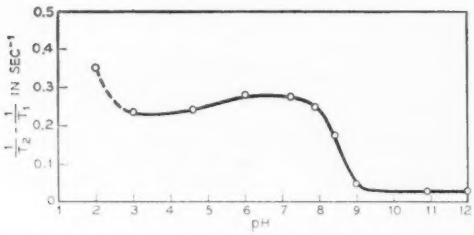

FIG. 4. Difference between transverse and longitudinal relaxation rates in water containing 5×10^{-6} mole liter^{-1} $MnCl_2$ as function of pH.

samples (0.20% O^{17}) were done at a temperature of 25 ± 1°C. Those on the water with natural O^{17} abundance (0.037%) were made at 30 ± 4°C (these measurements were made before an adequate temperature control was installed). A single measurement on a sample with 0.091% O^{17} is also indicated in the figure. In the upper part of Fig. 3, the measured values of $1/T_1$ for the enriched samples are given.

Referring to Fig. 3, it is seen that the maximum value of $(1/T_2-1/T_1)$ is, within the accuracy of the measurements, proportional to the O^{17} concentration.

A feature of the curves in Fig. 3 is that in the enriched sample $(1/T_2-1/T_1)$ does not approach zero at low and high pH values as it should if the O^{17} interaction were the sole cause of the broadening. This effect is not due to a systematic error in the T_1 or T_2 measurements because it is not present to an appreciable extent in the water with natural O^{17} abundance, which was measured by the same methods. As any interaction with the O^{17} will be averaged out by fast exchange, the observed "wings" can only be explained by some other interaction unaffected by exchange. The most probable cause is the presence of a paramagnetic impurity. Specifically, Mn^{++} ions are known to reduce the T_2 of water much more than the T_1.[12] From the results given in footnote reference 12, it can be estimated that 0.5×10^{-5} mole liter^{-1} Mn^{++} ions would give the observed values of $(1/T_2-1/T_1)$ in the wings of the curve. In Fig. 4 are given measured values of $(1/T_2-1/T_1)$ for a 0.5×10^{-5} mole liter^{-1} solution of $MnCl_2$. The effect is much larger in acidic solutions than in basic ones, the transition occurring between pH 8 and 9. This is roughly what would be expected from the solubility product of $Mn(OH)_2$ (4×10^{-19}). The behavior of the wings in Fig. 3 can therefore be explained by assuming the presence of Mn impurity. This is corroborated by the behavior of T_1 (top of Fig. 3), which also shows a change between pH 8 and 9. An attempt to prove the presence of Mn by chemical methods was unsuccessful, the sample being lost in a mishap.

[12] J. R. Zimmerman, J. Chem. Phys. **22,** 950 (1954). For a key to later references see L. O. Morgan and A. W. Nolle, J. Chem. Phys. **31,** 365 (1959). R. Hauser and G. Laukien, Z. Physik **153,** 394 (1959).

In order to eliminate the contribution of paramagnetic ions to the broadening, we have lowered the experimental points in Fig. 3 by 0.23 in the acidic range and by 0.1 in the basic range, with a transition between pH 8 and 9. In this way, the points of Fig. 5 were obtained. The curve is a calculated one and will be discussed in the following. Although we did not succeed in actually proving the presence of manganese impurity, it is thought that this way of correcting the data is essentially correct, whatever the reason for the additional broadening may be. This is based on the fact that the curves of $(1/T(H_1)-1/T_1)$ vs H_1 (three of which are given in Fig. 2) approach a limiting value for large H_1 which is not zero but rather equal to the applied correction. This shows that the mechanism responsible for the additional broadening has a correlation time which is much shorter than the exchange time; the curves will presumably drop to zero at some higher H_1 value, outside the experimental range. We can, therefore, consider the additional broadening to be constant over the range of interest and subtract it from the observed values.

The results given in Fig. 5 can be interpreted in terms of the exchange reactions (I) and (II) by means of Eq. (3). The specific rates of exchange for the two reactions (I) and (II) are, respectively,

$$\tau_{\text{acid}}^{-1}=\{[H_2O]^{-1}(d[H_2O]/dt)\}_{\text{I}}=k_1[H_3O^+], \quad (7)$$

$$\tau_{\text{base}}^{-1}=\{[H_2O]^{-1}(d[H_2O]/dt)\}_{\text{II}}=k_2[OH^-]$$
$$=k_2(K_W/[H_3O^+]), \quad (8)$$

where K_W is the dissociation constant of water, taken as 10^{-14} mole^2 liter^{-2} at 25°C. The expression $[H_2O]^{-1}(d[H_2O]/dt)$ should be understood here as the fraction of water molecules which exchange protons per unit time. We have to relate the preceding rates with the quantity $1/\tau$ of Eq. (3) which denotes the exchange rate of an hydrogen atom. The chance that a specific hydrogen atom will be transferred in reaction (I) is $\frac{1}{3}$, because the transfer mechanism consists of the addition of a proton to a water molecule, followed by the transfer of one of the three hydrogen atoms of the ion.

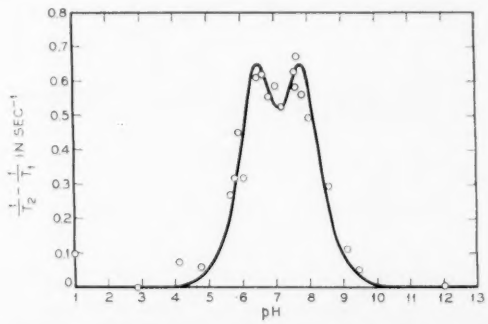

FIG. 5. Corrected proton relaxation rates in water. The curve has been calculated as described in Sec. IV.

The chance for a specific hydrogen atom to be transferred to another oxygen atom is therefore $\frac{1}{3}$. A similar agrument gives a factor $\frac{1}{2}$ for reaction (II). We have, therefore,

$$\tau^{-1}=(1/3\tau_{\text{acid}})+(1/2\tau_{\text{base}})=\tfrac{1}{3}k_1[\text{H}^+]+\tfrac{1}{2}k_2(K_W/[\text{H}^+]). \quad (9)$$

Equations (3) and (9) determine the theoretical curve for $(1/T_2-1/T_1)$ as function of pH. Three parameters have to be adjusted in fitting a theoretical curve to the observed points. These are the spin-spin interaction between the protons and the O^{17} (2δ), and the two rate constants k_1 and k_2. It is easily seen that the shape of the curve is determined solely by δ and the geometrical average of the two rate constants $(k_1k_2)^{\frac{1}{2}}$, while the position of the curve along the pH axis depends on the ratio k_1/k_2.

In calculating a theoretical curve, the following procedure has been adopted. For the case of water, the quantities in Eq. (3) are $\delta_1=0$; $\delta_2=5\delta$; $\delta_3=3\delta$; $\delta_4=\delta$; $\delta_5=-\delta$; $\delta_6=-3\delta$; $\delta_7=-5\delta$, where 2δ is the spin-spin interaction in radians sec^{-1}; $P_1=1-p$; $P_2=P_3=\cdots P_7=p/6$, where p is the abundance of O^{17} in the sample. In order to determine δ, we observe that the expression on the right-hand side of Eq. (3), considered as a function of τ, has a maximum which by a simple plot is found to occur at $\tau\delta=0.26$, while the magnitude of the maximum is $1.37\ p\delta$. If in nearly neutral water the exchange becomes slow enough for $\tau\delta>0.26$, then maxima in the relaxation rate will be expected to occur at the two pH values (one acidic and one basic) for which $\tau\delta=0.26$. Referring to the experimental results in Fig. 5, it will be seen that the points indeed indicate two maxima of the relaxation rate, at pH values of about 6.5 and 7.5, respectively. It may be objected that the scatter of the points is such that this result could be fortuitous. Even if this is admitted, we can still conclude that the maximum broadening does occur in nearly neutral water from the fact that the observed relaxation rate is nearly constant over the pH range of about 6.5 to 8. From Eq. (9) it follows that at the limits of this pH range the exchange rate is about a factor three larger than at the center and an appreciable change in relaxation rate would be expected if we were not in the region of maximum broadening. In other words, any attempt to fit a theoretical curve to the observed points on the assumption that the maximum broadening is not reached, results in a curve with a much smaller width to height ratio than the one actually observed.

Taking the maximum of $(1/T_2-1/T_1)$ as $0.65\ \text{sec}^{-1}$, we have $0.65=1.38\ p\delta$, which gives $\delta=235$ rad sec^{-1}. Once δ is known, k_1 is calculated by fitting one point on the part of the curve in the acidic range (the base catalyzed exchange can be neglected here), and similarly k_2 from a point in the basic range. We obtain $k_1=8.8\times10^9$ mole^{-1} liter sec^{-1} and $k_2=3.1\times10^9$ mole^{-1} liter sec^{-1}.

In deriving Eq. (3), the effect of quadrupole relaxation of the O^{17} nucleus has been neglected. This relaxation will result in a switching of the proton frequency between different lines of the O^{17} multiplet and can only be neglected if the average lifetime between quadrupole transitions of the O^{17} is large compared to the average lifetime between proton exchanges. The most serious effect of the O^{17} relaxation occurs, therefore, at the lower rates of exchange, and in the above analysis of the experimental results it will affect mainly the estimate of the spin-spin interaction from the maximum value of $(1/T_2-1/T_1)$. (An error in δ will of course indirectly affect the values for k_1 and k_2, as their calculation involves δ.)

That the O^{17} relaxation indeed affects the results appreciably, can be seen as follows. The maximum of $(1/T_2-1/T_1)$ was found to occur when $\tau\delta=0.26$, or $\tau=1.1\times10^{-3}$ sec. This has to be compared with the rate of O^{17} relaxation, which is characterized by the longitudinal relaxation time of the O^{17}. (We shall denote this time by T^1 in order to differentiate it from the T_1 of the protons.) From measurements of the O^{17} resonance (given in more detail in the following) $T^1=4.4\times10^{-3}$ sec. This is only four times as large as τ at the maximum.

The effect of the O^{17} relaxation can be considered as a partial frequency averaging over the multiplet lines, and can be taken into account by introducing an effective spin-spin interaction, δ_{eff}, in Eq. (3), instead of the real δ. This is discussed in more detail in Appendix B, where the following equation is derived:

$$\delta_{\text{eff}}=\delta[T^1/(T^1+\tau)]. \quad (10)$$

Replacing δ by δ_{eff} in Eq. (3), the values of δ, k_1, and k_2, corrected for quadrupole relaxation, are

$k_1=(10.6\pm4)\ 10^9$ mole^{-1} liter sec^{-1}

at $25\pm1°\text{C}$

$k_2=(3.8\pm1.5)\ 10^9$ mole^{-1} liter sec^{-1}

$\delta=290\pm40$ rad sec^{-1}.

The spin-spin interaction in cps is $\delta/\pi=92\pm15$ cps. The probable errors were estimated as follows. The main sources of error in the calculation of the spin-spin interaction are in the determination of the maximum value of the relaxation rate and in the concentration of O^{17} in the sample (p). The probable error in each of these quantities is estimated as 10%, giving a probable error of 14% in δ. The calculated rate constants depend critically on the pH values in the steep parts of the curve in Fig. 5. The accuracy of the pH measurements in this region is estimated as ±0.1 pH unit, corresponding to a probable error of 26%. In addition, the calculated rate constants are about proportional to δ^2, and an error of 28% is contributed from this source.

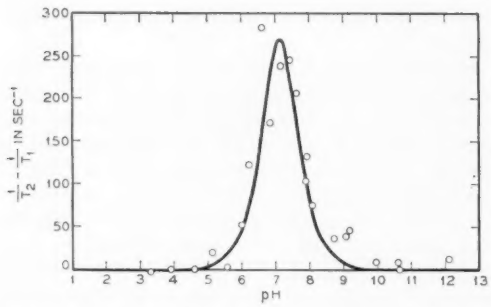

FIG. 6. Relaxation rates of O^{17} in water as function of pH. The points indicate the observed values, while the curve has been calculated, using the rate constants and spin-spin interaction obtained from the proton resonance.

We thus obtain a probable error in the rate constants of about 40%.

The curve in Fig. 5 has been calculated with the above values of k_1, k_2, and δ, using Eqs. (3), (9), and (10).

A check on this interpretation can be obtained from the dependence of the relaxation rate $1/T(H_1)$ on H_1. The lines in Fig. 2 have been calculated with the rate constants and spin-spin interaction given previously, using Eqs. (2), (9), and (10). The calculated lines have been shifted upwards by 0.23 sec^{-1}, which is the contribution from the paramagnetic impurities as discussed before. This value is indicated by the dashed line in the figure. The agreement with the experimental points is satisfactory, especially in view of the fact that the curves are quite sensitive to changes in exchange rate.

An additional check is provided by the linewidth measurements of the O^{17} resonance. The T_1 and T_2 of this resonance were determined as described in the previous section. The T_1 is independent of pH within the accuracy of the measurements, and an average value of $1/T_1=230$ sec^{-1} has been adopted. The linewidth, characterized by T_2, is, however, pH dependent, the line being about twice as wide in neutral water as in acidic or basic water. In Fig. 6 the quantity $(1/T_2-1/T_1)$, which gives the contribution of the exchange to the linewidth, has been plotted as a function of pH. The points indicate the experimental results while the curve has been calculated from the rate constants and spin-spin interaction obtained from the proton resonance. As the O^{17} resonance is a spin-spin triplet, and only one proton at a time is exchanged, the curves of Fig. 2 of footnote reference 8 have been used in obtaining the calculated linewidths. In this case we have to take τ as the average lifetime between exchanges of either of the protons of the water molecule, and have, therefore,

$$1/\tau=\tfrac{2}{3}k_1[H^+]+k_2(K_W/[H^+], \qquad (11)$$

rather than Eq. (9) as used for the proton resonance. The factor $\frac{2}{3}$ is the probability that reaction (I) will result in a proton exchange in the water molecule, because there is a $\frac{1}{3}$ chance that the incoming and outgoing proton will be the same. Reaction (II) will always result in the exchange of a proton and the statistical factor is one. The difference of a factor two between Eqs. (11) and (9) can also be looked upon as being due to the fact that the concentration of the oxygen atoms is half that of the protons. An oxygen atom is, therefore, involved in an exchange twice as often as a proton is.

In correcting for the quadrupole relaxation of the O^{17}, a correction factor derived by Piette and Anderson[13] has been used—see Eq. (55) in Appendix B. In applying this equation, we can assume that T_2 in the absence of exchange is equal to the longitudinal relaxation time T^1.

It will be noted that the O^{17} curve (Fig. 6) is narrower than the corresponding curve for the proton resonance (Fig. 5). This is also reflected in the experimental points. Two main factors contribute to this difference in behavior. The first is the faster switching rate of the O^{17} i.e., the factor of two difference of Eq. (11) vs Eq. (9). The second is the larger frequency separation of the outermost lines of the proton sextuplet (which contribute most to the broadening) compared to the frequency separation of the O^{17} triplet.

V. DISCUSSION

The rate constants of the transfer reactions (I) and (II) obtained by the NMR method can be compared with those expected from the observed anomalous mobilities of the water ions. As a simple model we assume that a transfer reaction (I) or (II) results in the shift of an electron charge (e) by the average O–O distance in water (x), and that successive transfers are completely uncorrelated. The anomalous mobility, μ, is then related to the average lifetime between transfers (τ) by the relations

$$\mu=(e/kT)D \qquad (12)$$

$$D=\langle x^2\rangle/6\tau. \qquad (13)$$

The proton mobility in water is 36.2×10^{-4} cm^2 v^{-1} sec^{-1}. If we assume that the mobility of the hydronium ion as a unit (i.e., excluding transfers) is about equal to that of the Na^+ ion (5.3×10^{-4}), we obtain for the anomalous contribution to the mobility 30.9×10^{-4} cm^2 v^{-1} sec^{-1}. Similarly, we subtract from the mobility of the OH^- ion (19.8×10^{-4}) that of the Cl^- ion (7.9×10^{-4}) to obtain for the anomalous contribution 11.9×10^{-4} cm^2 v^{-1} sec^{-1}.

On introducing these values in (12) and (13), and putting for the O–O distances $x=2.76$ A, we obtain

$$k_1=(1/[H_2O])\,(1/\tau H_3O^+)=11.2\times10^9 \text{ liter mole}^{-1}\text{ sec}^{-1}$$

$$k_2=(1/[H_2O])\,(1/\tau_{OH^-})=4.3\times10^9 \text{ liter mole}^{-1}\text{ sec}^{-1}.$$

[13] L. H. Piette and W. A. Anderson, J. Chem. Phys. **30**, 899 (1959).

This is in agreement with the rate constants obtained by the NMR method.

$[k_1=(10.6\pm4)\ 10^9$ and

$$k_2=(3.8\pm1.5)\ 10^9 \text{ liter mole}^{-1} \text{ sec}^{-1}].$$

A simple mechanism consisting of the transfer of a proton between an ion and an adjacent water molecule is, therefore, consistent with the observed rate constants.

ACKNOWLEDGMENT

The author wants to acknowledge the assistance of J. P. O'Brien, who made most of the measurements reported here.

APPENDIX A. EQUATIONS FOR THE RELAXATION RATE IN THE PRESENCE OF EXCHANGE

1. General Formulation

The following treatment applies if any relevant spin-spin interactions, as well as the rate of exchange, are small compared to the frequency difference of the interacting nuclei.[14] In the water system investigated in this paper, this condition is always fulfilled.

The problem to be treated can be stated as follows: Consider a system of identical nuclei, the members of which can be in any one of n different environments. By the environment of a nucleus is meant here any factor which will influence its average local field, such as chemical shift or the spin state of an interacting nucleus. Subject to the condition stated at the beginning of this section, the ith environment can be characterized by the Larmor frequency ν_i $(i=1, 2 \cdots n)$ of the nuclei in it. The fraction of the nuclei in the ith environment will be denoted by P_i. Obviously

$$\sum_{i=1}^{n} P_i=1. \tag{14}$$

If no transfer of nuclei between different environments takes place, the NMR spectrum will consist of n lines, of frequencies ν_i and relative intensities P_i. We wish, however, to treat the case that the nuclei do transfer from one environment to another, a transfer being accompanied by the switching of their Larmor frequency from one ν_i to another. A transfer can be the result of an actual chemical exchange of the nuclei of which the resonance spectrum is being considered, or of the exchange of some other nuclei with which they have spin-spin interaction. Other possible processes are hindered rotation in the molecule and quadrupole relaxation of an interacting nucleus. For lack of a better term we shall call the occurrence of any of these processes a "collision." The probability that, as a result of a collision, a nucleus will switch from environment j to environment i will be denoted by a_{ij}.[15]

The following relations hold, the second one following from the principle of detailed balancing

$$\sum_{i=1}^{n} a_{ij}=1 \tag{15}$$

$$P_j a_{ij}=P_i a_{ji}. \tag{16}$$

The system investigated in this paper (water) provides a good example for illustrating the above definitions. For simplicity we shall assume that no deuterium is present in the water, but we do consider the presence of O^{17}, which is the main factor causing exchange broadening. We first consider the proton resonance. If no exchange were taking place, the proton spectrum would consist of seven lines: A central line due to the protons bonded to O^{16} or O^{18} (spin 0), and six equally spaced lines due to the protons bonded to O^{17} (spin $\frac{5}{2}$). We have accordingly,

$$P_1=1-p$$

$$P_2=P_3=\cdots P_7=\tfrac{1}{6}p, \tag{17}$$

where p is the atom fraction of O^{17} in the sample. An exchange collision will result in the transfer of a proton to a new oxygen atom, the probability of a transfer to the ith line being independent of the initial state and simply equal to P_i. Therefore,

$$a_{1j}=1-p$$

$$a_{2j}=a_{3j}=\cdots a_{7j}=\tfrac{1}{6}p;$$

$$j=1\cdots7. \tag{18}$$

We next consider the O^{17} resonance. In the absence of exchange, this resonance would consist of a spin-spin triplet due to spin-spin interaction with two equivalent protons. Accordingly,

$$P_1=P_3=\tfrac{1}{4}$$

$$P_2=\tfrac{1}{2}. \tag{19}$$

An exchange collision will result in the replacement of one of the two protons. The probability that the incoming proton is in the same spin state as the outgoing one is $\frac{1}{2}$. In this case, the frequency of the O^{17} precession will be unchanged. On the other hand, if the incoming proton is in a spin state opposite to that of the outgoing one, the frequency of the O^{17} will be switched to an adjacent line. From a consideration of

[14] J. I. Kaplan, J. Chem. Phys. **28**, 278 (1958).

[15] It should perhaps be stated explicitly that this definition does not imply that a collision always causes a switch in the frequency of the nucleus involved. The fraction of the collisions which are ineffective in this respect is expressed by a_{ii}.

all possible cases, we find

$$a_{11}=a_{22}=a_{33}=a_{21}=a_{23}=\tfrac{1}{2}$$

$$a_{12}=a_{32}=\tfrac{1}{4}$$

$$a_{13}=a_{31}=0. \tag{20}$$

Subject to the conditions mentioned at the beginning of this Appendix, the behavior of the nuclei in the ith environment can be described by a set of Bloch equations.[6] A simple way of generalizing these equations to take exchange into account has been given by McConnell.[7] The generalized equations are

$$(dM_x^{(i)}/dt)+(1/T_2^{(i)})M_x^{(i)}+\gamma(M_y^{(i)}H_z^{(i)}-M_z^{(i)}H_y^{(i)})+\tau^{-1}M_x^{(i)}-\sum_{j=1}^{n}\tau^{-1}M_x^{(j)}a_{ij}=0$$

$$(dM_y^{(i)}/dt)+(1/T_2^{(i)})M_y^{(i)}+\gamma(M_z^{(i)}H_x^{(i)}-M_x^{(i)}H_z^{(i)})+\tau^{-1}M_y^{(i)}-\sum_{j=1}^{n}\tau^{-1}M_y^{(j)}a_{ij}=0$$

$$(dM_z^{(i)}/dt)+(1/T_1^{(i)})(M_z^{(i)}-M_0^{(i)})+\gamma(M_x^{(i)}H_y-M_y^{(i)}H_x^{(i)})+\tau^{-1}M_z^{(i)}-\sum_{j=1}^{n}\tau^{-1}M_z^{(j)}a_{ij}=0, \tag{21}$$

where $\mathbf{M}^{(i)}$ is the magnetization of the nuclei in the ith environment, $\mathbf{M}_0^{(i)}$ its equilibrium value, τ the average lifetime of a molecule between successive collisions, T_2 the transverse relaxation time in the absence of exchange, T_1 the longitudinal relaxation time, $\mathbf{H}^{(i)}$ the total magnetic field in the ith environment, and γ the gyromagnetic ratio of the nuclei.

The first three terms in each equation are the well-known Bloch terms. The fourth term represents the rate at which magnetization is lost by the nuclei in the ith environment as a result of collisions, while the last term gives the rate at which magnetizating is gained by transfer of nuclei from other environments.[16] The magnetic field $\mathbf{H}^{(i)}$ is the sum of the strong field $\mathbf{H}_0$ along the z axis, the rotating rf field $\mathbf{H}_1$ perpendicular to the z axis, and the local fields $\mathbf{h}_z^{(i)}$ characterizing the chemical shift and the spin-spin interactions. Equations (21) are transformed to a coordinate system rotating with $\mathbf{H}_1$ by the usual procedure.[17] The x axis of the rotating coordinate system is taken to coincide with $\mathbf{H}_1$. The transformed equations are

$$(dM_x^{(i)}/dt)+[(1/T_2^{(i)})+\tau^{-1}]M_x^{(i)}-\tau^{-1}\sum_{j=1}^{n}M_x^{(j)}a_{ij}+(\delta_i-\Delta\omega)M_y^{(i)}=0$$

$$(dM_y^{(i)}/dt)+[(1/T_2^{(i)})+\tau^{-1}]M_y^{(i)}-\tau^{-1}\sum_{j=1}^{n}M_y^{(j)}a_{ij}+\omega_1M_z^{(i)}-(\delta_i-\Delta\omega)M_x^{(i)}=0$$

$$(dM_z^{(i)}/dt)+[(1/T_1^{(i)})+\tau^{-1}]M_z^{(i)}-\tau^{-1}\sum_{j=1}^{n}M_z^{(j)}a_{ij}-\omega_1M_y^{(i)}=(1/T_1^{(i)})M_0^{(i)}, \tag{22}$$

where $\delta_i\equiv\gamma h_z^{(i)}$ is the frequency shift in the ith environment, $\Delta\omega$ the difference between γH_0 and the frequency of the applied rf field, and $\omega_1\equiv\gamma H_1$. In practice, the absolute values of the δ_i are unknown, as only relative chemical shifts are measured; however, a constant contribution to the δ_i can be absorbed into γH_0 without loss of generality. For the present purpose, it is most convenient to choose this contribution so that

$$\sum_i P_i\delta_i=0. \tag{23}$$

In order to solve Eq. (22), we have to specify $\Delta\omega$ and ω_i as a function of time and adopt a suitable set of initial conditions. The slow passage spectrum is given by the stationary solutions of (22) when $\Delta\omega$ and ω_1 are constants. Such solutions are given in footnote reference 2.

We are here interested in solutions describing the relaxation of the total magnetization after the latter has been flipped from its equilibrium position through 90° by adiabatic half-passage. During this relaxation, the rf field is kept constant, i.e., ω_i and $\Delta\omega$ are independent of time. In order to obtain the initial conditions in a rigorous way, it would be necessary to solve (22) for the time interval of the adiabatic flip. This will not be attempted here. Instead, in order to keep the problem manageable, we shall treat only two special cases, characterized by the fact that the resonance on slow passage consists of a single, nearly Lorentzian line. This is the case if either the exchange is very fast, so that the separate resonance frequencies are nearly averaged out into a single broadened line, or if one line is very much stronger than the others, say $P_1\gg P_2,\ P_3\cdots$. We shall treat these two cases in the next two sections.

2. Equations for the Case of Fast Exchange

Fast exchange is defined by the condition

$$\delta_i\tau\ll 1. \tag{24}$$

If this equation holds, the resonance on slow passage

[16] It should be noted that the third term includes all collisions, even those which do not involve a change of environment. However, this is compensated for by including in the summation range of the fourth term the value $j=i$.

[17] I. I. Rabi, N. F. Ramsey, and J. Schwinger, Revs. Modern Phys. **26**, 167 (1954).

will consist of a single, nearly Lorentzian line. In the method of Solomon as described in the paper, we execute an adiabatic fast passage to the center of the line and observe the subsequent relaxation of the magnetization. As the line has a Lorentzian shape, it can be expected that the decay will be exponential, and this is indeed observed. Moreover, as the magnitude of $\mathbf{H}_1$ is always taken large enough to saturate the resonance almost completely, the magnetization will relax to a value much smaller than its value immediately after the adiabatic flip, which is equal to M_0. It is, therefore, sufficient for our purpose to seek the special solution of Eq. (22), which has the character of an exponential decay to zero magnetization. It should be noted that it is implicitly assumed in the preceding arguments that the passage is adiabatic also in respect to the exchange rate, i.e., during the passage the effective magnetic field in the rotating coordinate system changes its direction but slightly during a mean exchange time τ. For in the opposite case—passage fast compared to mean exchange time—each component $\mathbf{M}^{(i)}$ of the magnetization would execute its own independent flip and end up in a direction determined by its chemical shift δ_i. The exchange process transfers effectively magnetization from one $\mathbf{M}^{(i)}$ to another, and thus will cause a change in direction of the individual $\mathbf{M}^{(i)}$ after the passage. This corresponds to other solutions of Eq. (22), which will not be considered here.

Guided by these physical considerations, we shall now find a suitable solution of (22). In addition to condition (24), we shall assume for simplicity that

$$1/T_1^{(i)}=1/T_2^{(i)}=1/T_1. \tag{25}$$

Physically this means that the exchange is the only slow process, all other relaxation processes being fast compared to the Larmor frequency and contributing equally to T_1 and T_2. Equation (25) also implies that the relaxation rate is the same in the different environments.

As after the adiabatic passage the rf frequency is at the center of the resonance line, we substitute in (22) $\Delta\omega=0$. Also, as mentioned previously, $\mathbf{H}_1$ is large enough to saturate the resonance and the magnetization will be nearly zero in the stationary state (the absorption component is saturated and the dispersion component is zero at the center of the line). For the case under consideration, it is, therefore, sufficient to solve the homogeneous equations corresponding to (22). The stationary special solution of the inhomogeneous equations, which has to be added to the solution of the homogeneous equations, is very nearly zero.

We look for solutions of the form

$$M^{(i)}(t)=M^{(i)}(0)\,\exp[-t(1/T+1/T_1)]. \tag{26}$$

On substituting (26) into the homogeneous equations corresponding to (22), we obtain[18]

$$\begin{vmatrix} \tau/T[I]+[A] & -[\Delta] & \\ +[\Delta] & \tau/T[I]+[A] & -\omega_1\tau[I] \\ & \omega_1\tau[I] & \tau/T[I]+[A] \end{vmatrix}=0, \tag{27}$$

where

$$[A]\equiv\begin{bmatrix} a_{11}-1 & a_{12} & a_{13}\cdots a_{1n} \\ a_{21} & a_{22}-1 & a_{23}\cdots a_{2n} \\ \vdots & \vdots & \vdots \\ a_{n-1} & a_{n2}-1 & a_{n3}\cdots a_{nn}-1 \end{bmatrix}, \tag{28}$$

$$[\Delta]\equiv\begin{bmatrix} \delta_1\tau & & & & \\ & \delta_2\tau & & & \\ & & \cdot & & \\ & & & \cdot & \\ & & & & \delta_n\tau \end{bmatrix}, \tag{29}$$

and $[I]$ is the identity matrix. Note that, as a result of Eq. (15), the determinant of the matrix $[A]$ is zero:

$$|A|=0. \tag{30}$$

Equation (27) is of order $3n$ in $1/T$ and has accordingly $3n$ roots. However, as discussed before, the dominant root for the case of fast exchange is real and goes to zero as τ goes to zero. The latter statement follows from the fact that the exchange broadening tends to zero as τ tends to zero. In view of Eq. (24), we expand Eq. (27) in powers of τ/T retaining only terms of the lowest significant order. Terms of zero order in τ/T cancel, because by putting $\tau=0$, Eq. (27) is identically fulfilled by virtue of Eq. (30). Moreover, only terms containing even orders of $\delta_i\tau$ will appear in the expansion of (27), as can be seen by a simple inspection. We retain, therefore, only terms of the first order in τ/T and terms of the second order in $\delta_i\tau$. In this approximation (27) is equivalent to

$$\begin{vmatrix} \tau/T[I]+[A] & -[\Delta] & \\ [\Delta] & [A] & -\omega_1\tau[I] \\ & \omega_1\tau[I] & [A] \end{vmatrix}=0. \tag{31}$$

We shall now reduce the order of the determinant (31) from $3n$ to n, by a process which consists essentially of adding rows and columns. Define

$$[B]\equiv\begin{bmatrix} [A] & -\omega_1\tau[I] \\ \omega_1\tau[I] & [A] \end{bmatrix}. \tag{32}$$

[18] Brackets indicate matrices and vertical lines determinents.

Equation (31) can then be written as

$$\begin{bmatrix} \tau/T[I]+[A] & -[\Delta] & 0 \\ [\Delta] & & \\ & & [B] \\ 0 & & \end{bmatrix}=0. \quad (33)$$

Multiply the matrices in the lower partitions of (33) from the left by the reciprocal matrix of $[B]$, denoted by $[B^{-1}]$. The determinant then reduces to order $2n$ and Eq. (33) can be written as

$$\begin{vmatrix} \tau/T[I]+[A] & -[\Delta] \\ [C] \quad [\Delta] & [I] \end{vmatrix}=0, \quad (34)$$

where $[C]$ is the submatrix of $[B^{-1}]$ containing the first n rows and columns. In (34) multiply the lower partitions by $[\Delta]$ from the left and add the result to the upper ones. Equation (34) then reduces to

$$|\tau/T[I]+[A]+[\Delta][C][\Delta]|=0. \quad (35)$$

As $[\Delta]$ is a diagonal matrix, the ijth element of the product matrix $[\Delta][C][\Delta]$ is $\tau^2\delta_i\delta_j c_{ij}$, where c_{ij} denotes the ijth element of $[C]$. Expanding the determinant in (35), retaining only terms of first power in τ/T and second power in $\delta_i\tau$, and using Eq. (30), we obtain

$$\tau/T\sum_{i=1}^{n}|A_{ii}|+\tau^2\sum_{i,j=1}^{n}|A_{ij}|\,\delta_i\delta_j c_{ij}=0, \quad (36)$$

where $|A_{ij}|$ denotes the cofactor of $|A|$ belonging to the ijth element.

Equation (36) can be further simplified by making use of the relations (14)–(16). The following relations between the cofactors of $|A|$ exist:

$$|A_{ij}|=|A_{jj}| \quad (37)$$

$$P_i|A_{ij}|=P_j|A_{ji}|. \quad (38)$$

The proof of (37) is as follows: The cofactor $|A_{ij}|$ can be obtained by replacing the element a_{ij} in $|A|$ by 1 and all other elements in the jth column by zeros. In the determinant so obtained, add all other rows to the jth row. By virtue of Eq. (15) the elements in the jth row then becomes zeros, except for the element in the jth column, which becomes 1. The new determinant is seen to be equal to $|A_{jj}|$.

The proof of (38) is similar. Obtain $|A_{ij}|$ by replacing a_{ij} in $|A|$ by 1 and all other elements in the ith row and jth column by zeros. Multiply the first column by P_1, the second by P_2, and so on for all columns. Divide the first row by P_1, the second row by P_2, and so on. This will leave the value of the determinant unchanged. However, using Eq. (16), it is seen that any element a_{kl} will be changed into a a_{lk}, while the element 1 is changed into P_j/P_i. Transposing the resulting determinant, it is seen to be equal to $(P_j/P_i)|A_{ji}|$.

From (14), (37), and (38) it follows that

$$\sum_i|A_{ii}|=\sum_i|A_{ji}|=\sum_i(P_i/P_j)|A_{ij}|$$
$$=\sum_i(P_i/P_j)|A_{jj}|=|A_{jj}|/P_j=|A_{ij}|/P_j. \quad (39)$$

Equation (36) therefore reduces to

$$T^{-1}=\tau\sum_{i,j=1}^{n}(-P_j\delta_i\delta_j c_{ij}). \quad (40)$$

This expression gives the contribution of the exchange to the relaxation rate. The quantities c_{ij} were defined as elements of the matrix $[B^{-1}]$ [Eq. (32)] and can be written as

$$c_{ij}=|B_{ji}|/|B|, \quad (41)$$

where $|B_{ji}|$ is the cofactor in $|B|$ belonging to the jith element. Clearly both $|B_{ji}|$ and $|B|$ are polynomials in $(\tau\omega_i)^2$. The dependence of $1/T$ on the magnitude of the rf field (i.e., on $\omega_1\equiv\gamma H_1$) is therefore in general a rather complicated one.

Equation (40) can be much simplified for the case that $a_{ij}=P_i$, that is when the probability of transfer to the ith environment is independent of the initial environment. This case applies to the proton resonance in water (but not to the oxygen resonance). The sum in Eq. (40) can be written as a bordered determinant. On using (32) and (41), we have

$$T^{-1}=\tau/|B|\begin{vmatrix} & \delta_1 & \delta_2 & \cdots & \delta_n & & & & \\ P_1\delta_1 & P_1-1 & P_1 & \cdots & P_1 & -\omega_1\tau & & & \\ P_2\delta_2 & P_2 & P_2-1 & \cdots & P_2 & & -\omega_1\tau & & \\ \cdot & \cdot & \cdot & & \cdot & & & \cdot & \\ \cdot & \cdot & \cdot & & \cdot & & & & \cdot \\ \cdot & \cdot & \cdot & & \cdot & & & & \cdot \\ & \omega_1\tau & & & & P_1-1 & P_1 & \cdots & P_1 \\ & & \omega_1\tau & & & P_2 & P_2-1 & \cdots & P_2 \\ & & & \cdot & & \cdot & \cdot & & \cdot \\ & & & \cdot & & \cdot & \cdot & & \cdot \\ & & & \cdot & & \cdot & \cdot & & \cdot \end{vmatrix}. \quad (42)$$

The determinant in this expression can be factored by adding or subtracting rows (or columns) and using Eqs. (14) and (23). In order to conserve space we will only indicate the necessary operations. Add to row 2 the rows 3, 4, $\cdots n+1$, and to row $(n+2)$ the rows $(n+3)$, $(n+4)$, $\cdots(2n+1)$. As a result of Eqs. (14) and (23) row 2 will have zeros in the first and second partitions and row $(n+2)$ in the third partition. Subtract column 2 from columns 3, 4, $\cdots(n+1)$, and column $(n+2)$ from columns $(n+3)$, $(n+4)$, $\cdots(2n+1)$. It is then possible to factorize out $-\tau^2\omega_1^2$. The remaining determinant will have diagonal matrices in all four square partitions. Subtract $\omega_1\tau$ times the rows in the lower partition from the corresponding rows in the middle partition. All the elements in the 2, 3 partition will then be zero and the remaining determinant can be expanded to give

$$-\tau^2\omega_1^2\sum_{i=1}^{n}P_i\delta_i^2(1+\tau^2\omega_1^2)^{n-2}.$$

By applying the same operations to $|B|$, we find

$$|B|=+\tau^2\omega_1^2(1+\tau^2\omega_1^2)^{n-1}.$$

For the case $a_{ij}=P_i$, Eq. (40) reduces therefore to

$$T^{-1}=\frac{\tau}{1+\tau^2\omega_1^2}\sum_{i=1}^{n}P_i\delta_i^2. \tag{43}$$

The observed rate of relaxation is given by Eq. (26), and is therefore characterized by a relaxation time given by

$$1/T(H_1)=(1/T_1+1/T). \tag{44}$$

For the limit $\omega_1\to 0$ Eq. (43) reduces to an equation given by Piette and Anderson.[13]

3. Equations for the Case of One Dominant Line

In this section we drop the restriction to fast exchange [Eq. (24)], and shall instead assume that the number of nuclei in one environment is much larger than the number of nuclei in all other environments.

$$P_1\gg\sum_{i\neq 1}P_i. \tag{45}$$

To a good approximation the resonance will then consist of a single line and thus the considerations at the beginning of Sec. 2 still hold. For the sake of simplicity, we shall only treat the case

$$a_{ij}=P_i.$$

In the present approximation we retain powers up to the first in τ/T and in P_i/P_1; however, we include all powers of $\tau\delta_i$.

Our starting point will be Eq. (35). An inspection of the steps leading to this equation shows that they are also valid in the present approximation [use has to be made of the fact that $\delta_1\ll\delta_{i\neq 1}$; this follows from (23) and (45)]. On writing out Eq. (35), we have

$$\begin{vmatrix} (\tau/T)+P_1-1+\tau^2\delta_1^2c_{11} & P_1+\tau^2\delta_1\delta_2c_{12} & \cdots \\ P_2+\tau^2\delta_2\delta_1c_{21} & (\tau/T)+P_2-1+\tau^2\delta_2^2c_{22} & \cdots \\ \vdots & \vdots & \end{vmatrix} =0. \tag{46}$$

We expand (46), keeping only terms of the lowest relevant order as specified above. We first note that of the quantities c_{ij} we have only to keep c_{22}, $c_{33}\cdots c_{nn}$. This is seen as follows. The c_{ij} are defined in Eq. (41) in terms of the cofactors $|B_{ji}|$ of $|B|$. If $|B|$ is written out, a simple inspection will show that the $|B_{ii}|$ and $|B_{i1}|$ $(i=2\cdots n)$ have terms of zero order in P_2, $P_3\cdots P_n$, while all the other cofactors have only terms of first and higher order in these quantities. In Eq. (46) the $|B_{i1}|$ are always associated with δ_1 and from Eqs. (23) and (45) it follows that δ_1 is an order of magnitude smaller than the other δ_i. We can, therefore, consider the terms containing the $|B_{i1}|$ as having the same order as the other off-diagonal terms. As in an expansion of (46) the off-diagonal elements will always appear in pairs, the off-diagonal c_{ij} will only contribute terms of second or higher order in $P_2\cdots P_n$ and can be neglected.

Inspection of $[B]$ shows that the c_{ii} $(i=2\cdots n)$ contain only terms of even order in $P_2\cdots P_n$, and thus we need to take the zero-order terms only. The latter are easily obtained by putting $P_2=P_3=\cdots P_n=0$ in $|B|$. The result is

$$c_{22}=c_{33}=\cdots c_{nn}=-(1+\tau^2\omega_1^2)^{-1}. \tag{47}$$

Substitution of $c_{11}=0$ and $c_{ij}=0$ $(i\neq k)$ into (46), and expansion of the determinant, keeping only terms up to first power in τ/T, gives

$$|D|+(\tau/T)\sum_i|D_{ii}|=0, \tag{48}$$

where

$$|D|=\begin{vmatrix} P_1-1 & P_1 & P_1 & \cdots \\ P_2 & P_2-1+\tau^2(\delta^{(2)})^2c_{22} & P_2 & \cdots \\ P_3 & P_3 & P_3-1+\tau^2(\delta^{(3)})^2c_{33} & \cdots \\ \vdots & \vdots & \vdots & \end{vmatrix} \tag{49}$$

and $|D_{ii}|$ is the principal minor of $|D|$ belonging to the iith element.

Neglecting again terms of second and higher order in $P_2 \cdots P_n$, as well as crossterms containing both τ/T and $P_2 \cdots P_n$, we obtain

$$(P_1-1)\prod_{i\neq 1}[-1+\tau^2\delta_i^2 c_{ii}]-P_1\sum_{j\neq 1}P_j\prod_{i\neq 1,j}[-1+\tau^2\delta_i^2 c_{ii}] +(\tau/T)\prod_{i\neq 1}[-1+\tau^2\delta_i^2 c_{ii}]=0. \quad (50)$$

This reduces to

$$(\tau/\tau)=(1-P_1)+P_1\sum_{j\neq 1}\frac{P_j}{[-1+\tau^2\delta_j^2 c_{jj}]}, \quad (51)$$

and finally, using (47) and noting that $1-P_1=\sum_{j\neq 1}P_j$ [Eq. (14)]

$$T^{-1}=\tau\sum_{j\neq 1}^{n}\frac{P_j\delta_j^2}{1+\tau^2[\omega_1^2+\delta_j^2]}. \quad (52)$$

The summation can be taken to include $j=1$, because δ_1 is an order of magnitude smaller than the other δ_i.

Obviously Eq. (52) reduces to Eq. (43) if condition (24) applies. In the other extreme, if $\tau\delta_i \gg 1$, and for $\omega_1 \ll \delta_i$, Eq. (52) reduces to $1/T=1/\tau$, which is the expected result.

APPENDIX B. CORRECTION FOR QUADRUPOLE RELAXATION OF THE O^{17}

The quadrupole relaxation of the O^{17} nucleus will cause a switching of the proton frequencies between the different lines of the O^{17} multiplet. The pertinent residence times can be calculated in terms of the T_1 of the O^{17} resonance by a procedure given by Pople.[19] Additional terms, describing the O^{17} relaxation, can easily be introduced in Eq. (21). However, when this is done, the approximations used in Appendix A do not apply any more, and it seems impossible to obtain a simple expression for $T(H_1)$ by this procedure.

A good estimate of the correction for quadrupole relaxation can, however, be obtained from the following considerations. If no quadrupole relaxation of the O^{17} were present, a proton would spend on the average a time τ in a definite line of the O^{17} multiplet, before returning to the central line (for low O^{17} concentrations we can neglect transitions between lines of the O^{17} multiplet). On the other hand, if quadrupole relaxation does take place, transitions to other lines of the O^{17} multiplet may take place before an exchange returns the proton frequency to the central line. The effect of such transitions will be a partial averaging of the δ_i, and quadrupole relaxation can be taken into account by introducing a set of effective frequencies, $\delta_{i\,eff}$, which are smaller than the corresponding δ_i. In estimating $\delta_{i\,eff}$ we shall ignore the discrete structure of the O^{17} multiplet and do the calculations as if the z component of the O^{17} spin, and, therefore, the frequency of the proton, were relaxing continuously with the longitudinal relaxation time of the O^{17} (to be denoted by T^1 in order to differentiate it from the proton relaxation time T_1). We write accordingly

$$\delta_i(t)=\delta_i\exp(-t/T^1), \quad (53)$$

where $\delta_i(t)$ is the frequency of the proton (relative to the center of the multiplet), a time t after an exchange switched its frequency to δ_i.

The quantity we wish to calculate, $\delta_{i\,eff}$, is the average of $\delta_i(t)$, at some arbitrary time, over all the protons which started off with the frequency δ_i and have not yet returned to the central line. We chose the time at which the average is taken as the zero of the time scale. At the time $t=0$ a proton which switched to the frequency δ_i at the time $-t$ will have relaxed to a frequency $\delta_i(t)$ given by Eq. (53). However, the proton should be included in the average only if its frequency has not switched back to the central line between $-t$ and 0. The probability of survival is $P(t)=e^{-t/\tau}$ and the average of $\delta_i(t)$ is

$$\delta_{i\,eff}=\int_0^\infty \delta_i\exp(-t/T^1)e^{-t/\tau}dt \Big/ \int_0^\infty e^{-t/\tau}dt$$
$$=\delta_i[T^1/(T^1+\tau)]. \quad (54)$$

This result can be compared with a similar equation derived by Piette and Anderson.[13] Their Eq. (20), derived for the case of fast exchange only, is in our notation equivalent to

$$\delta_{i\,eff}=\delta_i[T_2/(T_2+\tau)], \quad (55)$$

where T_2 characterizes the linewidth of the proton multiplet lines in the absence of exchange. For the case of fast exchange, $\tau \ll T_2$ and Eqs. (54) and (55) will be identical if $T_2=\frac{1}{2}T^1$. The T_2's of the multiplet lines can be equated to the residence times τ given in footnote reference 19. Piette and Anderson derive their equation on the assumption that the T_2's of the different multiplet lines are equal, but we shall not be much off if we take an average τ, weighing each line according to its contribution to the exchange broadening. For fast exchange the contribution is proportional to δ_i^2, and for the O^{17} multiplet the weighing factors are therefore 25:9:1. We thus get $T_2=\tau_{Av}=(17/35)T_1\approx\frac{1}{2}T_1$. Equation (55) agrees therefore with (54) in the case of fast exchange.

[19] J. A. Pople, Mol. Phys. **1**, 168 (1958). Pople states that for spin larger than 1 the definition of T_1 presents difficulties, but actually his treatment can easily be applied to spin values higher than 1. A straightforward definition of T_1 is obtained by substituting the expressions for the quadrupole transition probabilities in the suitable generalization of Eq. (2.11) of Pople's paper. For the case of spin 5/2 we obtain for the residence times: $\tau_{\pm 5/2}=8/15\ T_1$; $\tau_{\pm\frac{3}{2}}=8/23\ T_1$; and $\tau_{\pm\frac{1}{2}}=4/9\ T_1$. The result that the predominance of quadrupole relaxation is a sufficient condition for the existence of a T_1 has been proved in general by R. K. Wangsness and F. Bloch, Phys. Rev. **89**, 728 (1953).

Choice of Parameters for the Hückel π-Electronic Structure of Furan: Tentative Extension to Pyrrole and Thiophene

FRANK L. PILAR AND JOHN R. MORRIS, II

*Department of Chemistry, University of New Hampshire, Durham, New Hampshire**

(Received July 15, 1960)

A comparison of the experimental bond lengths of furan with empirical bond length/bond energy relations for carbon-oxygen bonds leads to the conclusion that the ratio of the carbon-oxygen resonance integral to the carbon-carbon resonance integral of furan is between about 0.1 to 0.3. Use of this value along with a Coulombic integral parameter based upon the ultraviolet absorption spectrum of furan leads to a Hückel molecular orbital picture of the π-electronic structure of furan which is compatible with the known chemical reactivity of the molecule. The same[3] approach is used to suggest resonance and Coulombic parameters for the Hückel molecular orbital treatment of pyrrole and thiophene. The treatment yields atom localization energies and para-localization energies consistent with the relative chemistries of furan, pyrrole, and thiophene.

INTRODUCTION

THE use of the Hückel approximation in the molecular orbital treatment of furan and other heterocyclic compounds has been the subject of many theoretical papers during recent years.[1–3] Perhaps an essential feature, or at least a prevailing one, of the majority of these papers dealing with furan has been the value assigned to the resonance integral parameter k defined by

$$k=\beta_{CO}/\beta_{CC}, \tag{1}$$

where β_{CO} and β_{CC} are the resonance integrals of the carbon-oxygen and carbon-carbon bonds, respectively. In all of the papers known to the present authors, k has been chosen to have a value rather close to unity—usually in the range 1 to 1.5. Since β_{CO} is related to the order of the carbon-oxygen bond, such a value of k leads to a π-electronic structure in which the oxygen atom of furan is an important contributor to the so-called aromatic sextet, i.e., the carbon-oxygen mobile bond order is appreciably greater than zero and the total electronic charge density of the oxygen atom is considerably less than two. Purely chemical evidence, on the other hand, shows that the diene nature of furan (as evidenced in the Diels-Alder reaction) is very pronounced—a fact which previous molecular orbital treatments do not neatly explain since it is difficult to reconcile extensive participation of the oxygen atom in the conjugated system of furan with the undeniable diene nature of the molecule.

THE RESONANCE INTEGRAL PARAMETER

If one assumes that the equation for k adapted from the treatment by Lennard-Jones[4], i.e.,

$$k=(E_{C=O}-E_{C-O})/E_{C=C}-E_{C-C}, \tag{2}$$

is correct, then knowledge of the proper bond energies should suffice to determine k. Whereas previous workers have interpreted $E_{C=O}$ as the energy of the double bond in a carbonyl compound such as formaldehyde (a standard carbon-oxygen double-bond energy, so to speak), we believe that this term should be interpreted as the *actual* energy of the carbon-oxygen bond in furan. Such a bond energy may be estimated from bond length/bond energy relations such as those given by Glockler[5] or by a thermochemical method such as discussed by Pilar.[6] As shown in this latter paper, the carbon-oxygen bond energy of furan is about 91 kcal/mole. Comparing this to the C—O bond energy of an alkyl ether (84 kcal/mole) and the C—O bond energy of formaldehyde (170 kcal/mole), one is led to suspect that the C—O bond of furan is much more like a single bond than a double bond. This, then, should lead to a small value of k in Eq. (2) which, in turn, should produce a small value for the mobile bond order of the C—O bond in furan. In the paper just quoted, it has been shown that this mobile bond order is very likely on the order of 0.1. It is easy to see that if one uses the bond energy of formaldehyde for $E_{C=O}$, as others have invariably done, then k becomes larger than unity and, of course, leads to a large degree of double-bond character in the furan C—O bond.

Since the carbon-oxygen bond length of furan is not definitely established at this time, Eq. (2) will yield the range within which k should vary. This uncertainty results from the fact that in the estimation of the C—O bond energy of furan one must resort to empirical bond length/bond energy relations at some stage of the estimation. Bak[7] favors a value of $r_{CO}>1.37$ A based on microwave spectroscopy as compared to 1.40 A$\pm$ 0.03 A obtained by Schomaker and Pauling[8] by electron diffraction techniques. This shows that $E_{C=O}$ in furan lies between 85 and 110 kcal/mole. Supplying other

* Part of this work was carried out at the Massachusetts Institute of Technology Computation Center, Cambridge, Massachusetts.

[1] R. D. Brown and B. A. W. Coller, Australian J. Chem. **12**, 152 (1959).

[2] M. M. Kreevoy, J. Am. Chem. Soc. **80**, 5543 (1958).

[3] L. E. Orgel *et al.*, Trans. Faraday Soc. **47**, 113 (1951).

[4] J. Lennard-Jones, Proc. Roy. Soc. (London) **A158**, 280 (1937).

[5] G. Glockler, J. Phys. Chem. **62**, 1049 (1958).

[6] F. L. Pilar, J. Mol. Spectroscopy **5**, 72 (1960).

[7] B. Bak, L. Hansen, and J. Rastrup-Anderson, Discussions Faraday Soc. **19**, 30 (1955).

[8] V. Schomaker and L. Pauling, J. Am. Chem. Soc. **61**, 1769 (1939).

TABLE I. Indices of chemical reactivity for furan with $k=0.1$, 0.15, 0.20 and $h=0.5$.

	Atom or bond[a]	k, h 0.1, 0.5	0.15, 0.5	0.2, 0.5
Atom charge density	1	1.978	1.951	1.917
	2	1.005	1.011	1.018
	3	0.996	1.014	1.023
Mobile bond order	12	0.127	0.186	0.242
	23	0.888	0.880	0.870
	34	0.453	0.461	0.470
Free valence number	2	0.717	0.666	0.620
	3	0.389	0.391	0.392
Atom localization energy[b]	2	−1.647	−1.652	−1.659
	3	−2.453	−2.431	−2.405
Para-localization energy	2, 5	−2.50	−2.53	−2.57

[a] The heteroatom is No. 1 and the other atoms are numbered consecutively therefrom.

[b] All energies are in units of β_{CC}.

bond energies from Pauling[9] and setting $E_{C-O}=85$ kcal/mole (as in an alkyl ether), Eq. (2) shows that $0.1\leq k\leq 0.3$ with a great likelihood, in our opinion, that the most probable value lies closer to 0.1 than to 0.3.

We have, of course, assumed that $E_{C=C}$ and E_{C-C} may be interpreted as the bond energies of ethylene and ethane, respectively. Obviously, such an assumption has no theoretical justification. In actuality, however, the *most* unrealistic assumption lies in the choice of *equal* carbon-carbon resonance integrals. Using the bond lengths of Schomaker and Pauling[8] and appropriate bond energies, one obtains the approximate relations: $\beta_{CO}/\beta_{23}=0.14$ and $\beta_{23}/\beta_{34}=2.3$. Clearly, the two carbon-carbon resonance integrals are far from being equal. However, in keeping with the usual Hückel approximation as far as possible, we have adopted the assumption of equal carbon-carbon resonance integrals, in which case our interpretation of $E_{C=C}$ and E_{C-C} in Eq. (2) leads to essentially the β_{CO}/β_{23} ratio of 0.1 to 0.3.

THE COULOMBIC INTEGRAL PARAMETER

The Coulombic integral parameter h is defined by

$$\alpha_0=\alpha_C+h\beta_{CC}, \tag{3}$$

where the α's represent Coulombic integrals for the atoms indicated via subscript. For want of a more rigorous approach, h is frequently based upon relative electronegativities or else chosen in a purely empirical manner. We have chosen h so that the resulting π-electronic structure of furan (using k as chosen above) is in qualitative agreement with the ultraviolet absorption spectrum of furan.

Based primarily upon the work of Pickett[10] we have correlated the *ca* 1750 A band group with an $n\rightarrow\sigma^*$ transition, the *ca* 1900 A band group with a $\pi\rightarrow\pi^*$ transition and the *ca* 2600 A band group with an $n\rightarrow\pi^*$ transition. Only the latter two of these are significant with respect to h. If these assignments are *relatively* correct, then it is apparent that the energy $h\beta_{CC}$ (a nonbonding level containing the lone pair electrons of oxygen which do not participate in the sextet) must lie *above* the highest occupied π-electronic level. Calculations with $0.1\leq k\leq 0.3$ show that $h=0.5$ satisfies the spectrally imposed requirement. The quantitative agreement with regard to the relative energies of the $n\rightarrow\pi^*$ and $\pi\rightarrow\pi^*$ transitions is not good but would hardly be expected to be otherwise when based upon such a crude theory as the Hückel approximation.

RESULTS WITH FURAN

Table I lists values of several indices of chemical reactivity for furan based upon $k=0.1$, 0.15, 0.20 and $h=0.5$. As will be noted, the noncrossing rule is not obeyed except for $k=0.1$. However, we feel that atom charge densities are not particularly significant reaction indices, and, thus, we prefer to focus attention upon the atom localization energies and free valence numbers instead. It is of some comfort to note that these latter two indices are in agreement in all of the calculations of this paper. In alternant hydrocarbons it has been shown by the Pullmans[11] that the free valence number is a universal criterion of chemical reactivity and, furthermore, parallels the atom localization energies. Although furan is not an alternant hydrocarbon, the low degree of conjugation of oxygen should lead to quasi-alternant hydrocarbon behavior for the molecule.

It is apparent that the pertinent indices correctly predict the α reactivity of furan and its diene nature. The para-localization energy, which is a measure of the diene nature, may be compared to that of benzene (-4β) and that of 1,3-butadiene (-2.48β). Using maleic anhydride as a reference dieneophile, it is well known that both furan and 1,3-butadiene form normal Diels-Alder adducts with this molecule while benzene is completely unreactive. This diene nature is the most obvious manifestation of the quasi-alternant hydrocarbon behavior of furan.

In Fig. 1, we have depicted the electronic structure of furan based upon $k=0.2$ and $h=0.5$. Calculations show that the energy levels labeled π_2 and π_5^* are independent of k and h. This turns out to be a result of the fact that these two levels belong to the eigenfunctions which are antisymmetric with respect to reflection in the symmetry plane of the molecule. Thus the associated eigenvectors for the oxygen atom are identically zero for these two levels.

[9] L. Pauling, *Nature of the Chemical Bond* (Cornell University Press, Ithaca, New York, 1960), pp. 85 and 189.

[10] L. Pickett, J. Chem. Phys. **8**, 293 (1940); J. Am. Chem. Soc. **73**, 4865 (1951).

[11] B. Pullman and A. Pullman, *Les Théories Électroniques de la Chimie Organique* (Masson et Cie, Paris, 1952).

It is of interest to note that our results parallel very closely those of the valence bond treatment of Simonetta[12] and the interpretation given by Schomaker and Pauling to their electron diffraction results.[8]

The fairly great difference between the atom localization energies of the 2- and 3-positions plus the fact that electronic effects should not be transmitted very effectively through the oxygen atom predict that the presence of an α substituent in furan should not greatly alter the reactivity of the remaining α position. This agrees with experimental fact, for it is found that electrophilic substitution in furan occurs predominantly in the α position regardless of the electronic nature of a substituent already in an α position.[13] Of course, this would not be expected to hold true for substituents which can strongly conjugate with the furan nucleus. In such a case, a strongly electron-withdrawing group could conceivably activate the β position so that this position was more reactive than the α position.

In a previous communication[14] we had discussed the π-electronic structure of furan based on $k=0.1$ and $h=1.0$. While the indices of chemical reactivity obtained from these parameters are entirely compatible with those of the present paper, it is apparent that a value of $h=1.0$ must be ruled out upon the basis of the electronic spectrum. This is assuming that our use of Eq. (2) is a realistic way of obtaining k.

EXTENSION TO PYRROLE AND THIOPHENE

Pyrrole

Bond length/bond energy relations for carbon-nitrogen compounds are not as easily estimated as for carbon-oxygen compounds. Table II represents the data on carbon-nitrogen bonds which we have used to estimate the carbon-nitrogen bond energy of pyrrole. The bond distances of Table II were obtained from the compilation of Wheland[15] and the bond energies from tables by Pauling.[9] The estimation is based upon the assumption that bond energies vary in a roughly linear fashion with bond lengths. We have used other methods, e.g., the equation of Gordy,[16] and find little significant variation in the resulting bond energy. The use of Gordy's equation is unfortunately hampered by the impossibility of assigning a realistic value for the bond energy of a pure double bond in carbon-nitrogen compounds.

Use of the pyrrole carbon-nitrogen bond energy from Table II leads to a value of about 0.5 for k. For this molecule $n\rightarrow\pi^*$ transitions are absent and thus it is not possible to choose h in the same manner as was done for furan. For want of a more rigorous approach we have assumed that h for nitrogen should be roughly halfway between that of carbon and that of oxygen, i.e., about 0.25.

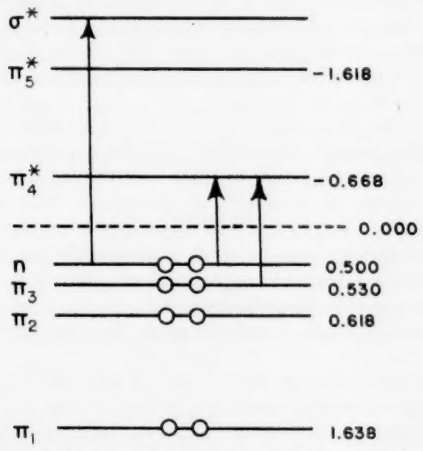

FIG. 1. Molecular orbital energy levels of furan (not to scale). The energies are relative to the Coulombic integral of carbon and are all expressed in units of β_{CC}.

TABLE II. Bond length/bond energy relations for carbon-nitrogen bonds.

Bond	r (A)	Bond energy kcal/mole)
C—N	1.47[a]	70[a]
C=N	1.34[b]	147[c]
C⋮N	1.42[d]	(100)

[a] Diethyl and dimethyl amines.
[b] p-Isopropylideneaminophenol.
[c] n-Butylisobutylideneamine.
[d] Pyrrole.

TABLE III. Indices of chemical reactivity for pyrrole with $k=0.5$ and $h=0.25$.[a]

	Atom or bond	
Atom charge density	1	1.562
	2	1.107
	3	1.112
Mobile bond order	12	0.520
	23	0.766
	34	0.599
Free valence number	2	0.446
	3	0.407
Atom localization energy	2	−1.714
	3	−2.171
Para-localization energy	2, 5	−3.11

[a] Numbering system and units same as for Table I.

[12] M. Simonetta, J. Chim. Phys. **49**, 68 (1952).
[13] R. C. Fuson, *Advanced Organic Chemistry* (John Wiley & Sons, Inc., New York, 1950), p. 598.
[14] J. R. Morris and F. L. Pilar, Chem. & Ind. (London) **1960**, 469.
[15] G. W. Wheland, *Resonance in Organic Chemistry* (John Wiley & Sons, Inc., New York, 1955), pp. 695 ff.
[16] W. Gordy, J. Chem. Phys. **15**, 81 (1947).

TABLE IV. Bond length/bond energy relations for carbon-sulfur bonds.[a]

Bond	r (A)	Bond energy (kcal/mole)
C—S	1.81[b]	62[b]
C=S	1.71[c]	114[c]
C⋯S	1.74[d]	(98)

[a] Data from Wheland (footnote 15) and Pauling (footnote 9).
[b] Thioethers.
[c] Thiocarbonyls.
[d] Thiophene.

The indices of reactivity based on the above values of h and k are listed in Table III. Noteworthy is the fact that although the free valence numbers and atom localization energies unambiguously predict α reactivity for the molecule, the atom localization energies for the 2- and 3-atoms are not as widely separated as in furan (the same is true, of course, for the free valence numbers). Thus one might understand why pyrrole does not show the tendency to undergo substitution exclusively in the α position as does furan.

Another point of interest is the para-localization energy of pyrrole which is much higher than that of furan. Evidently the nitrogen atom of pyrrole is sufficiently conjugated with the ring to destroy most of the diene nature of the molecule. Pyrrole, as is well known, does not form a normal adduct with a dieneophile such as maleic anhydride.

Thiophene

Longuet-Higgins[17] has proposed that it is necessary to consider $3p3d^2$ hybridization of the sulfur atom in the molecular orbital treatment of thiophene. Although the use of this scheme has the advantage of pointing out various interesting analogies between thiophene and benzene,[18] we feel that it is slightly simpler mathematically and, for most practical purposes, quite satisfactory to ignore the d-orbitals of sulfur when discussing much of the chemical reactivity of thiophene.

The resonance integral parameter was chosen as for pyrrole using the data of Table IV. Use of these data in the Lennard-Jones equation yielded $k=0.6$. By comparison, the value of k estimated by Longuet-Higgins in the d-orbital hybrid was 0.8.

Since carbon and sulfur have very similar electronegativities on the Pauling scale, we chose to set $h=0$. This choice is in qualitative agreement with comparable choices for furan and pyrrole. Thiophene shows a $\pi\rightarrow\pi^*$ transition at *ca* 2300 A,[19] but the transitions in the vacuum ultraviolet are not known well enough for us to use such information to choose h. The indices of reactivity calculated from $k=0.6$ and $h=0$ are given in Table V. Again it is apparent that α reactivity is predicted and that unlike furan and like pyrrole, the α reactivity may be easily influenced by substituents in an opposite α position.

TABLE V. Indices of chemical reactivity for thiophene with $k=0.6$ and $h=0$[a].

	Atom or bond	
Atom charge density	1	1.359
	2	1.168
	3	1.152
Mobile bond order	12	0.597
	23	0.710
	34	0.600
Free valence number	2	0.425
	3	0.422
Atom localization energy	2	−1.696
	3	−2.052
Para-localization energy	2, 5	−3.47

[a] Numbering system and units same as in Table I.

The relatively high value of the para-localization energy is compatible with the lack of diene character in thiophene with respect to participation in the Diels-Alder reaction. It is also of interest that the bond orders listed in Table V differ very little from those reported by Longuet-Higgins.[17]

SUMMARY

Resonance integral parameters for furan, pyrrole, and thiophene were chosen on the basis of published bond lengths, bond energies, and the Lennard-Jones equation. The Coulombic integral parameter for furan was chosen on the basis of the ultraviolet absorption spectrum, and the Coulombic integral parameters for pyrrole and thiophene were chosen relative to furan on the basis of the relative electronegativities of the heteroatoms.

The indices of chemical reactivity calculated from the Hückel molecular orbital approximation correctly reflect the diene nature of furan and the lack of such diene nature in pyrrole and thiophene. The atom localization energies and free valence numbers of these three molecules may be used to rationalize the facts that all three molecules undergo electrophilic substitution primarily in the α-position and, furthermore, that furan exhibits such a tendency to the most pronounced extent.

The bond orders listed in Tables I, III, and V could be used to estimate bond lengths by the use of bond length/bond order relations found in the literature.[6,20] Although the results of such a correlation appear quite satisfactory, the complications due to the effects of hybridization upon bond lengths make it hazardous to attribute undue significance to such correlations.

[17] H. C. Longuet-Higgins, Trans. Faraday Soc. **45**, 173 (1949).
[18] M. J. S. Dewar and E. A. C. Lucken, J. Chem. Soc. **1959**, 426.
[19] W. E. Haines *et al.*, J. Phys. Chem. **58**, 274 (1954).
[20] C. A. Coulson, *Theoretical Organic Chemistry* (Butterworths Scientific Publications, Ltd., London, 1959), Kekulé Symposium, London, September, 1958, pp. 49 ff.

Interpretation of Viscosity Data for Concentrated Polymer Solutions

HIROSHI FUJITA AND AKIRA KISHIMOTO

Physical Chemistry Laboratory, Department of Fisheries, University of Kyoto, Maizuru, Japan

(Received June 16, 1960)

An empirical viscosity vs concentration relation for concentrated polymer solutions is derived in terms of a simple free volume theory, and its applicability is tested with some available data for amorphous polymer+solvent systems. It is found that the derived relation fits well those data over the range of polymer concentrations so concentrated that interchain entanglements occur to form a weak network structure throughout the solution. In the region of relative low polymer concentrations, however, it shows deviation of a common feature from the experimental results. Two temperature-dependent parameters are contained in the viscosity equation derived; one is characteristic of the polymer species and the other is dependent upon the particular combination of polymer and diluent. These parameters are evaluated from comparisons with experimental data, and their variations with temperature are discussed.

INTRODUCTION

ACCORDING to a recent review article by Fox, Gratch, and Loshaek,[1] our present knowledge about the variation of viscosities of polymer solutions with diluent concentration appears as yet to be very incomplete or otherwise insufficient. Thus, on the one hand, published data covering a wide range of concentration are available only for a limited number of systems, and, on the other hand, few empirical relationships of wide applicability have been established. In a recent paper[2] we have shown that the dependence on diluent concentration and also on temperature of viscoelastic properties of amorphous polymers in the presence of small amounts of a low-molecular-weight diluent can be described fairly well in terms of a simple free volume theory. The purpose of the present article is to apply a similar theory to the viscosity of concentrated polymer solutions, in the hope of establishing a viscosity vs concentration relationship of wide applicability. An illustration of the potentiality of the viscosity relation derived here has been shown in a recent short communication.[3] In the present study we will subject this equation to more extensive comparison with experimental data, in order to obtain information about its limitation, as well as its applicability.

THEORY

Consider a uniform mixture composed of a volume V_1 of a low-molecular-weight substance (which will hereafter be referred to as "solvent") and a volume V_2 of a linear amorphous polymeric material. To avoid the complexity which may arise from the presence of crystalline parts we will confine the present discussion to systems of amorphous polymers. The total volume of the system will be denoted by V. Then

$$V=V_1+V_2. \tag{1}$$

According to currently accepted concepts, the local looseness of a solution or of a solid in bulk may be conveniently expressed in terms of the magnitude of a volume generally called the "free volume." We denote the average free volume in the mixture by V_f and write it in the form

$$V_f=(V_f)_1+(V_f)_2. \tag{2}$$

Here $(V_f)_2$ denotes the average free volume in the pure polymer at the same temperature as that of the mixture considered. Hence $(V_f)_1$ represents the free volume newly produced in the system by the addition of the solvent. It is considered that the magnitude of $(V_f)_1$ increases with increasing V_1 but the proportionality factor between these two volumes may depend upon the amount of the polymer with which the given solvent is to be mixed. Also this factor may vary with the temperature T of the system. In the present treatment we assume that it is a function of T only, characteristic of the given polymer-solvent pair, and denote it by the symbol $\gamma(T)$. Then

$$V_f=(V_f)_2+\gamma(T)V_1. \tag{3}$$

Division of Eq. (3) by Eq. (1) and rearrangement, gives for the average fractional free volume f

$$f=(V_f)_2/V_2+[\gamma(T)-(V_f)_2/V_2]v_1, \tag{4}$$

where v_1 is the volume fraction of the solvent in the mixture. The ratio $(V_f)_2/V_2$ equals the value of f at $v_1=0$, i.e., the average fractional free volume of the pure polymer at temperature T, and may be written $f(T,0)$ if we use the notation $f(T,v_1)$ for the value of f for the mixture of temperature T in which the volume fraction of the solvent is v_1. Equation (4) may then be put in the form

$$f(T,v_1)=f(T,0)+\beta'(T)v_1, \tag{5}$$

where

$$\beta'(T)=\gamma(T)-f(T,0). \tag{6}$$

Equation (5) is the same in form as Eq. (6) of footnote 2 but differs from the latter in that f is a linear function

[1] T. G Fox, B. Gratch, and S. Loshaek, in *Rheology*, edited by F. Eirich (Academic Press Inc., New York, 1956), Vol. I, Chap. 12.
[2] H. Fujita and A. Kishimoto, J. Polymer Sci. **28**, 547 (1958).
[3] H. Fujita and A. Kishimoto, Bull. Chem. Soc. Japan **33**, 274 (1960).

of v_1 rather than C (grams of solvent per gram of dry polymer).

If we neglect the contribution of the solvent, the macroscopic viscosity η of a polymer solution may be expressed by the general relation

$$\eta = FN_2\zeta_2. \tag{7}$$

Here N_2 is the total number of monomer units of polymer chains contained in a unit volume of the solution, ζ_2 is the friction coefficient of an individual monomer, and F is a proportionality factor. The coefficient ζ_2 represents the reciprocal of the ease with which each monomer can jump from one position to another by thermal agitation in the local field of molecular forces around it. Therefore, it becomes smaller as the local looseness of the solution is increased. Since the latter property may depend upon the average fractional free volume f of the solution, it would be reasonable to assume an explicit relation between ζ_2 and f. Here we assume for this relation a form similar to that which was proposed by Doolittle[4] in his treatment of the viscosity of simple liquids. Thus

$$\ln\zeta_2 = \ln A + 1/f(T, v_1), \tag{8}$$

where A is a constant dependent upon the size and the shape of the monomer unit as well as upon the particular combination of monomer and solvent. In the original equation of Doolittle a constant B appeared as the coefficient for the term $1/f$, but in the present treatment this will be simply set equal to unity. This is due to the following reason. In the derivation of Eq. (5) for $f(T, v_1)$ we have not given any explicit definition for the free volume. This is because no unique manner of defining this volume has as yet been established. Accordingly, our V_f represents at best something which is proportional to the "true" free volume. In other words, though it will be stated, for convenience of description, as the fractional free volume, the quantity f is left undetermined by an yet unknown proportionality factor. The constant B in the original Doolittle viscosity expression may be included in this unknown factor unless we define V_f in some univocal manner. This is mathematically equivalent to setting B simply equal to unity.

The factor F in Eq. (7) is related to the physical requirement that in the viscous flow of a polymer in bulk or in solution the jumps of respective monomer units cannot take place completely independent of each other but must be coordinated.[1] This is due, on the one hand, to the fact that the monomers belonging to a polymer chain are linked together through covalent bonds and, on the other hand, to the condition that if the solution is sufficiently concentrated in polymer, interchain entanglements occur and make relative movements of neighboring polymer molecules less free. Recent work[1] shows that if the solution of a polymer is so concentrated as to permit interchain entanglements, its viscosity at fixed concentration and temperature increases linearly with the 3.4 power of the molecular weight M of the polymer (when the polymer is polydisperse, as is generally the case, M should be replaced by M_w, the weight-average molecular weight of the polymer), regardless of polymer species or of whether the chain is linear or branched. This fact allows us to express the factor F in the form

$$F = KM^{3.4} \tag{9}$$

provided the polymer concentration is sufficiently high. No definite information concerning the proportionality factor K is as yet available, but it appears reasonable to suppose that for a given polymer-solvent pair K depends upon the density of interchain entanglements in solution.

It is reported[1] that the 3.4 power dependence of F on M changes to a less sensitive M dependence below a certain critical molecular weight M_e and that the value of M_e is, for a given polymer-solvent pair, a function of v_1 only such that

$$M_e = M_{e0}/(1-v_1). \tag{10}$$

Here M_{e0} is the value of M_e for the undiluted polymer. Data available indicate that $M_{e0} \approx 3.5\times10^4$ for polystyrene[5] and $\approx 1.0\times10^4$ for polymethyl methacrylate.[6] The real implication of M_e is as yet unknown, but it is generally argued that the polymer chains having molecular weights smaller than M_e can no longer overlap enough to cause effective interchain entanglements in solutions of concentration v_1. Our treatment in the present paper will be concerned with solutions so concentrated that the molecular weight of the given sample is always above this critical molecular weight.

Since no definite information about K is available,[7] we here assume that it may be treated as constant, independent of temperature and concentration, although this may be open to considerable criticism. Substitution of Eqs. (8) and (9) into Eq. (7) then yields

$$\eta(T, v_1) = K'M^{3.4}N_2 \exp[1/f(T, v_1)], \tag{11}$$

where K' is a constant defined by

$$K' = KA. \tag{12}$$

Division of $\eta(T, v_1)$ by $\eta(T, v_1^*)$ gives

$$\eta(T, v_1)/\eta(T, v_1^*) = [(N_2)_{v_1=v_1}/(N_2)_{v_1=v_1^*}] \times \exp\{[1/f(T, v_1)]-[1/f(T, v_1^*)]\}. \tag{13}$$

[4] A. K. Doolittle, J. Appl. Phys. **22**, 1471 (1951); **23**, 236 (1952).

[5] M. L. Williams, J. Appl. Phys. **29**, 1395 (1958).

[6] F. Bueche, J. Appl. Phys. **26**, 738 (1955).

[7] Experimentally, only the combination of K and ζ_2 may be measured as a function of solvent concentration. Therefore, definite information can be obtained for K only when there becomes available a procedure by which the dependence of ζ_2 on v_1 may be isolated from the observed results.

Here v_1^* denotes the value of v_1 chosen as a reference for the comparison of viscosities for different concentrations at a fixed temperature; it is, of course, necessary to take it in the range of solvent concentration where η obeys Eq. (11). It is a simple matter to show that at constant temperature

$$(N_2)_{v_1=v_1}/(N_2)_{v_1=v_1^*}=(1-v_1)/(1-v_1^*). \quad (14)$$

A quantity a_c defined by

$$a_c=\eta(T, v_1)(1-v_1^*)/\eta(T, v_1^*)(1-v_1) \quad (15)$$

therefore takes the form

$$\ln a_c=[1/f(T, v_1)]-[1/f(T, v_1^*)]. \quad (16)$$

Equation (5) may now be introduced into this equation to give

$$-\ln a_c=\frac{\beta'(T)(v_1-v_1^*)}{f(T, v_1^*)[f(T, v_1^*)+\beta'(T)(v_1-v_1^*)]}, \quad (17)$$

which may be rewritten in the form

$$-\frac{1}{\ln a_c}=f(T, v_1^*)+\frac{[f(T, v_1^*)]^2}{\beta'(T)}\cdot\frac{1}{(v_1-v_1^*)}. \quad (18)$$

The dimensionless quantity a_c may be calculated as a function of v_1 when data for isothermal viscosity are obtained over a range of solvent concentration; the lowest of the v_1's at which the viscosity values have been taken may be chosen as the reference concentration v_1^*. Equation (18) indicates that when those a_c data are plotted in the form of $-1/\ln a_c$ against $1/(v_1-v_1^*)$ there is obtained a straight line which gives $f(T, v_1^*)$ and $\beta'(T)$ from the intercept on the ordinate axis and the slope. Substitution of the values of $f(T, v_1^*)$ and $\beta'(T)$ obtained into Eq. (5) leads to the determination of $f(T, 0)$, which in turn allows evaluation of $\gamma(T)$ when it is inserted into Eq. (6) together with the foregoing $\beta'(T)$ value.

In the following we shall examine how well the predicted linearity between $1/\ln a_c$ and $1/(v_1-v_1^*)$ is obeyed by available data for the isothermal viscosity of concentrated polymer solutions. The data to be compared with the theory should be for solutions sufficiently concentrated in polymer that the 3.4 power dependence of F on M is satisfied. Unfortunately, there are available at present a very limited number of published data which cover a sufficiently wide range of polymer concentration and thus meet with this requirement. The extensive check of the theory presented must therefore await the accumulation of further experimental results.

COMPARISON WITH EXPERIMENTAL DATA

Polymethyl Methacrylate (PMMA)+Diethyl Phthalate

Bueche[6] reported fairly extensive viscosity measurements for a sample of PMMA (viscosity-average molecular weight, M_v, is 6.3×10^4) in diethyl phthalate over a wide range in concentration and temperature. From Table I of his paper, values of a_c were calculated as a function of v_1 and T,[8] and the results are plotted in Figs. 1(a) and 1(b) in the form suggested by Eq. (18). The value of v_1^* chosen at each temperature is indicated in these graphs. It is seen that for all the cases the data are represented fairly well by a straight line, in agreement with the theoretical prediction, although at some temperatures the plots show a downward deviation from linearity in the region of small values of $1/(v_1-v_1^*)$. This type of deviation is more appreciable in the data on the system polystyrene+diethyl benzene which will be discussed in the next section.

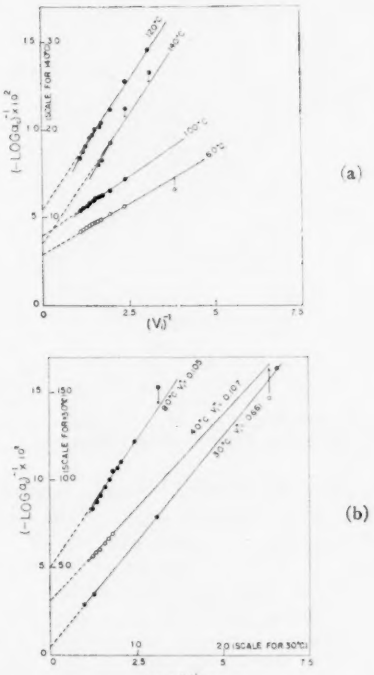

FIG. 1. (a) and (b). Plots of $-1/\log a_c$ vs $1/(v_1-v_1^*)$ for the system PMMA+diethyl phthalate studied by Bueche.[6]

Figure 2 plots the values of $f(T, 0)$, $\beta'(T)$, and $\gamma(T)$ determined from the intercepts and the slopes of the straight lines drawn in Figs. 1(a) and 1(b).

Polystyrene (PS)+Diethyl Benzene

Figure 3 shows plots for $-1/\log a_c$ against $1/(v_1-v_1^*)$ derived from the viscosity data given in Table I

[8] To convert weight fraction of polymer, in which Bueche reported his data, to volume fraction of polymer we used a value of 1.120 for the density of diethyl phthalate and the equation of Fox *et al.* for the temperature variation of the density of PMMA; T. G Fox and S. Loshaek, J. Polymer Sci. **15**, 371 (1955).

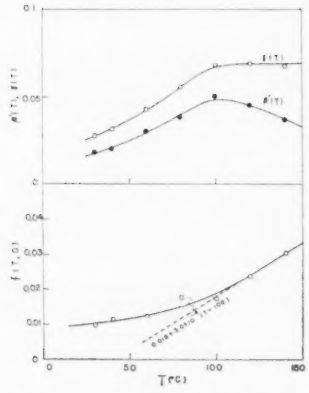

FIG. 2. Variations of $f(T, 0)$, $\beta'(T)$, and $\gamma(T)$ with temperature for the system PMMA+diethyl phthalate.

of the paper by Bueche.[9,10] Bueche reported that the weight-average molecular weight of the PS sample for which these data were taken was 7.2×10^5.

From Fig. 3 we see that for all the cases examined the predicted linear relation is fairly well obeyed by the experimental data down to the value of the abscissa which corresponds roughly to $v_1=0.55$. For values of v_1 greater than this all the plots exhibit distinct downward curvature. This similar behavior has already been noted, though far less noticeable, in some of the plots for PMMA+diethyl phthalate. In Fig. 4 are shown graphically the values of $f(T, 0)$, $\beta'(T)$, and $\gamma(T)$ derived from the straight lines drawn in Fig. 3.

Polystyrene+Dibenzyl Ether

Probably the most complete of the viscosity data so far reported for polymer+solvent systems is that due to Fox, Gratch, and Loshaek[1] for a PS sample ($M_w=7\times10^4$) in dibenzyl ether. Unfortunately, their data are as yet available only in a graphical form. Based on the viscosity values read from their published graph, we have calculated[11] $\log a_c$ as a function of v_1 and T and have plotted them in Figs. 5(a) and 5(b) in the form of $-1/\log a_c$ against $1/(v_1-v_1^*)$. For all the temperatures examined the predicted linear relation is well obeyed over the entire range of the abscissa, although this statement must be reserved for the lowest three temperatures at which only two or three points are available. It is worthwhile to note that these plots do not show any apparent downward curvature in the region of high solvent concentration. The values of $f(T, 0)$, $\beta'(T)$, and $\gamma(T)$ determined from the straight lines in Figs. 5(a) and 5(b) are plotted in Fig. 4.

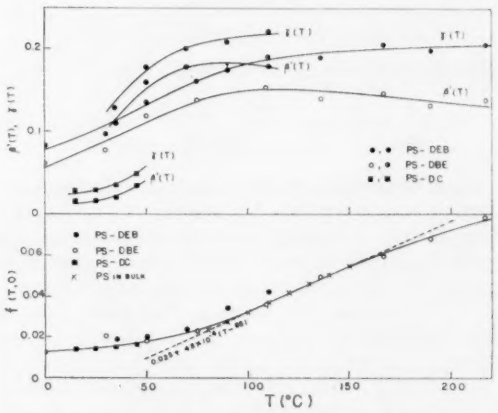

FIG. 4. Variations of $f(T, 0)$, $\beta'(T)$, and $\gamma(T)$ with temperature for PS+various solvents.

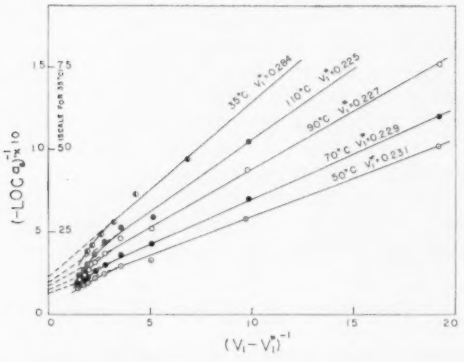

FIG. 3. Plots of $-1/\log a_c$ vs $1/(v_1-v_1^*)$ for the system PS+diethyl benzene studied by Bueche.[9]

Polystyrene+Decalin

From the literature there are available more viscosity data for solutions of polystyrene. However, these cover only regions of relatively low concentrations of polymer and hence are not very appropriate for the test of the present theory. In Fig. 6 are shown the plots calculated from the data of Ferry, Gradine, and Udy[12] for a PS sample ($M_w=3.7\times10^5$) in decalin. All the curves exhibit distinct downward curvature for v_1 greater than about 0.75. The values for $f(T, 0)$, $\beta'(T)$, and $\gamma(T)$ calculated from the straight lines in Fig. 6 (there is considerable arbitrariness in drawing these lines) are shown in Fig. 4.

It was found that the viscosity data of Ferry *et al.*[12] for the same PS sample in xylene, plotted in the form of Fig. 6, give plots which show, at all the temperatures

[9] F. Bueche, J. Appl. Phys. **24**, 423 (1953).

[10] In converting reported polymer weight fractions to volume fractions we used a value of 0.864 for the density of diethyl benzene and the equation of Fox *et al.* for the density of PS; T. G Fox and S. Loshaek, J. Polymer Sci. **15**, 371 (1955).

[11] To convert reported polymer weight fractions to volume fractions the density of dibenzyl ether was taken as 1.043. For PS the above-cited equation of Fox and Loshaek was employed.

[12] J. D. Ferry, L. D. Granding, and D. C. Udy, J. Colloid Sci. **8**, 529 (1953).

examined, no definite linear portion but downward curvature. Plots of a similar nature were obtained also from the viscosity data of Spencer and Williams[13] for PS in isopropyl benzene. These failures of the theory are not unexpected because, as has been noted previously, the data of these workers cover relatively low polymer concentrations only.

DISCUSSION

Several examples shown above suggest that at least for the range of polymer concentrations in which sufficient interchain entanglements occur the variation of η for solutions of amorphous linear polymers with concentration may be adequately represented by Eq. (11). According to this equation, the primary factor for the concentration dependence of η is the variation of the monomer friction coefficient with the volume fraction of the solvent, and the success of the equation is largely due to the choice of an expression of the Doolittle type for the relation between this coefficient and the average fractional free volume of the solution. As far as the region of sufficiently high polymer concentrations is concerned, it appears that the dependence of the factor F on concentration may be ignored or otherwise may be said to be of little importance. Recently, there have been many indications that the form of the Doolittle type is very pertinent to the quantitative description of frictional properties of polymeric solids[2,14,15] and of small molecules diffusing in such solids.[16] The study presented in this paper provides more evidence of the basic importance of the Doolittle equation for the description of frictional properties of polymeric systems. In this connection, it is very gratifying that Cohen and Turnball[17] have quite recently succeeded in giving a theoretical justification for the form of the Doolittle equation.

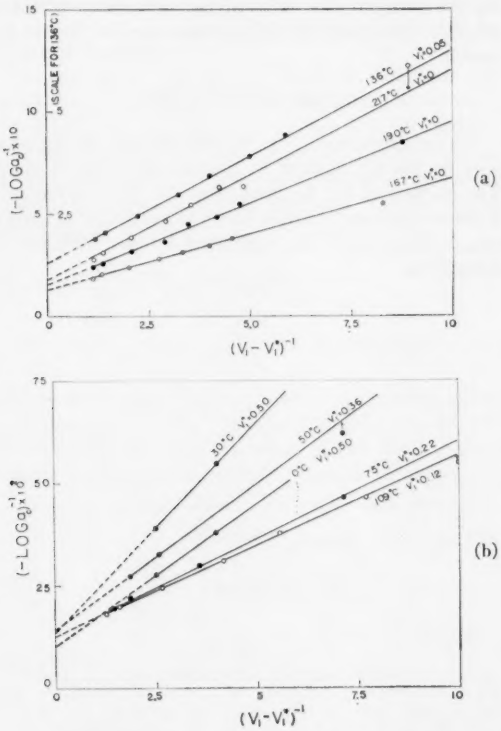

FIG. 5. (a) and (b). Plots of $-1/\log a_c$ vs $1/(v_1-v_1^*)$ for the system PS+dibenzyl ether studied by Fox, Gratch, and Loshaek.[1]

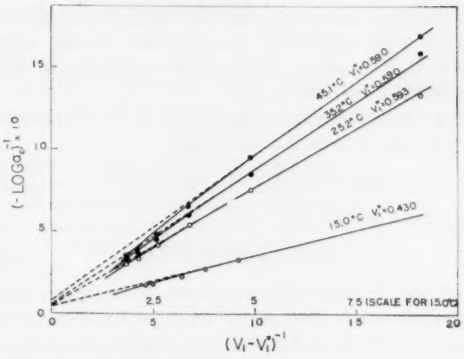

FIG. 6. Plots of $-1/\log a_c$ vs $1/(v_1-v_1^*)$ for the system PS+decalin studied by Ferry, Grandine, and Udy.[12]

$f(T, 0)$

According to our formulation, the function $f(T, 0)$ must be characteristic of the species of the polymer concerned; it is expected that this function is independent of the molecular weight (provided it is sufficiently high so that the effect of chain ends on the free volume is negligible) and also of the solvent in which the viscosity data are to be taken. The results shown in Fig. 4 indicate that our $f(T, 0)$ data for PS nearly fulfill these requirements; that is, the values of $f(T, 0)$ determined for different combinations of molecular weight and solvent fall approximately along a single curve. It is of interest to note that this curve is approximately represented by two straight lines intersecting in the region of the glass transition temperature ($\approx$80–100°C) of pure PS. As shown by a dashed line in Fig. 4, the curve in the range from 80 to 170°C is approximated by the equation $f(T, 0) = 0.025 + 4.5\times10^{-4}\ (T-80)$, where T is expressed in °C. It is often argued[18] that the free volume in a polymeric solid is *frozen-in* at temperatures below the glass transition temperature T_g. The present

[13] R. S. Spencer and J. L. Williams, J. Colloid Sci. **2**, 116 **(1947)**.

[14] M. L. Williams, R. F. Landel, and J. D. Ferry, J. Am. Chem. Soc. **77**, 3701 (1955).

[15] H. Fujita and A. Kishimoto, J. Colloid Sci. **13**, 418 (1958).

[16] H. Fujita, A. Kishimoto, and K. Matsumoto, Trans. Faraday Soc. **56**, 424 (1960).

[17] M. H. Cohen and D. Turnball, J. Chem. Phys. **31**, 1164 (1959).

[18] T. G Fox and P. J. Flory, J. Appl. Phys. **21**, 581 (1950).

data indicate, however, that this volume actually decreases with decreasing temperature in the region below T_g, though its temperature coefficient is much smaller than that above T_g.

If we neglect a slight dependence of N_2 on temperature, it follows from Eq. (11) that

$$\ln a_T = [1/f(T,0)] - [1/f(T^*,0)], \tag{19}$$

where a_T is defined by

$$a_T = \eta(T,0)/\eta(T^*,0), \tag{20}$$

and T^* is an arbitrarily chosen reference temperature. If data for a_T as a function of T are available and if the value of $f(T^*,0)$ is known, it is possible to calculate $f(T,0)$ at temperatures other than T^*, by means of Eq. (19). We have applied this procedure to the a_T curve previously reported by Fujita and Ninomiya[19] for a sample of PS, with $T^* = 135°C$ and $f(135°C, 0) = 0.0478$ interpolated from the $f(T,0)$ curve in Fig. 4. The values of $f(T,0)$ obtained are indicated by crosses in Fig. 4 and are seen to be in gratifying agreement with those derived from the analysis of a_c data.

The behavior of the $f(T,0)$ curve for PMMA in Fig. 2 is similar to that for PS discussed previously. Above $T = 100°C$ the curve is approximately fitted by the equation $f(T,0) = 0.018 + 3.0\times10^{-4}\ (T-100)$, where T is expressed in °C. Below T_g of this polymer ($\approx$80–100°C) the free volume is not constant but decreases slightly with decreasing temperature. By correlating viscoelastic and dilatometric data for a series of poly-*n*-alkyl methacrylates we have recently shown that the value of $f(T,0)$ for PMMA at 100°C is 0.019_1.[15] This value is in good agreement with the value 0.018_7 interpolated for this temperature from the $f(T,0)$ curve of Fig. 2.

[19] H. Fujita and K. Ninomiya, J. Polymer Sci. **24**, 233 (1957).

$\beta'(T)$ and $\gamma(T)$

In general, the values of $f(T,0)$ or of $f(T,v^*)$ are so small that there is a considerable uncertainty in determining them from the intercept of a straight line drawn through points of $-1/\log a_c$ against $1/(v_1 - v_1^*)$. In the evaluation of $\beta'(T)$ this uncertainty is squared, so that the resulting values of $\beta'(T)$ and hence of $\gamma(T)$ should be less accurate. Therefore not much can be said about the magnitudes as well as the temperature dependences of these parameters shown in Figs. 2 and 4. However, one may point out from these graphs some features which appear to be general for amorphous polymer+solvent systems. Those are as follows: (a) in the region of T lower than T_g both $\beta'(T)$ and $\gamma(T)$ increase rather sharply with increasing temperature; (b) at a temperature near T_g $\beta'(T)$ reaches a maximum and then gradually decreases as T increases; and (c) $\gamma(T)$ remains almost constant or slightly increases in the corresponding region of T. Also there can be seen such a general trend that for a given polymer the larger the molecular size of the solvent, the values of $\gamma(T)$ at fixed temperatures become smaller. This implies that if it is miscible with the given polymer the addition of a solvent of a smaller size is more effective for plasticizing the material. We wish to leave consideration of the physical meanings of these parameters for future research.

ACKNOWLEDGMENTS

We are indebted to Mr. M. Sakamoto of this Laboratory for his aid in some of the numerical calculations. The interest of Dr. K. Ninomiya, the Japan Synthetic Rubber Company, in this study is gratefully acknowledged. This work was supported by the Ministry of Education.

Zero-Field Splitting of Molecular Zeeman Levels

R. McWEENY*

Departments of Mathematics, Physics, and Chemistry, University College of North Staffordshire, Keele, Staffordshire, England

(Received July 11, 1960)

Electron spin-spin coupling, responsible for zero-field splitting of Zeeman levels, may be discussed very generally by means of a "coupling anisotropy function" defined in terms of the components of the two-electron density matrix. The properties of this function are fully discussed elsewhere: the present note is concerned with zero-field splitting of triplet levels and with the series of approximations which lead from the general results to simple (orbital theory) approximations. A numerical calculation on the phosphorescent triplet states of naphthalene gives reasonable agreement with experiment.

ZERO-FIELD splitting of the triplet states of naphthalene and other aromatic hydrocarbons has been observed by Hutchison and Mangum[1] and by van der Waals and de Groot.[2] The latter authors have given a theoretical discussion based upon a simple two-electron model, while Gouterman and Moffitt[3] made rough theoretical estimates of principal splitting constants, using simple Huckel MO's and nearest-neighbor integral approximations. The purpose of this note is to indicate how the problem may be formulated and solved most generally and to examine the series of approximations which lead to the results just cited. A full account of the underlying general theory will be published elsewhere.

We take as a manifold of electronic functions the $2S+1$ members (Φ_κ) of the multiplet of interest, with $\kappa=(S, M)$ and $M=-S, -S+1, \cdots S$, and assume for simplicity (though generalization is straightforward) that there is no *spatial* degeneracy. The matrix element, between any pair of functions (Φ_κ, Φ_λ) of the spin coupling operator

$$\mathcal{H}_{\mathrm{dip}}=\tfrac{1}{2}g^2\beta^2\sum_{i,j}{}'r_{ij}^{-5}[r_{ij}^2\mathbb{S}(i)\cdot\mathbb{S}(j) -3(\mathbf{r}_{ij}\cdot\mathbb{S}(i))(\mathbf{r}_{ij}\cdot\mathbb{S}(j))] \quad (1)$$

may then be expressed in terms of a *coupling anisotropy function* for the "standard state" with $M=S$. This function is defined in terms of the spinless components of the two-electron density matrix (McWeeny[4]),

$$\rho_2(\kappa\lambda\mid 1,2;,1',2') = P_2(\kappa\lambda\mid \overset{+}{1},\overset{+}{2};\overset{+}{1'},\overset{+}{2'})\alpha(1)\alpha(2)\alpha^*(1')\alpha^*(2') + P_2(\kappa\lambda\mid \overset{+}{1},\overset{+}{2};\overset{+}{1'},\overset{-}{2'})\alpha(1)\alpha(2)\alpha^*(1')\beta^*(2')+\cdots \quad (2)$$

in which 1 and 2 symbolize space and/or spin variables of two particles, according to context, and the superscript + and − signs are part of the function symbols denoting the various *spinless* components. The coupling anisotropy function for the standard state ($M=S$) is, with an obvious abbreviation of the components in (2),

$$Q_{\mathrm{cn}}(1,2;1',2')=[(++\mid++)-(+-\mid+-) -(-+\mid-+)+(--\mid--)]_{\mathrm{st}}-[(-+\mid+-) +(+-\mid-+)]_{\mathrm{st}}, \quad (3)$$

The "diagonal element," $1'=1, 2'=2$, may be integrated over all positions of the two particles to give

$$\tfrac{1}{2}\int Q_{\mathrm{cn}}(1,2;1,2)\,dv_1dv_2 = \langle\sum_{i,j}{}'[3\mathbb{S}_z(i)\mathbb{S}_z(j)-\mathbb{S}(i)\cdot\mathbb{S}(j)]\rangle_{\mathrm{av}}, \quad (4)$$

the expectation value of an operator which measures the anisotropy of spin coupling associated with sharpness of the z component. To give one example, the matrix of $g\beta\mathbf{H}\cdot\mathbb{S}+\mathcal{H}_{\mathrm{dip}}$ ($\mathbf{H}$ being the applied field) for a set of triplet functions is[5]

$$\begin{bmatrix} -\frac{1}{8}g^2\beta^2I_1+g\beta H_z & \frac{1}{2}\sqrt{2}g\beta(H_x-iH_y) & -\frac{3}{8}g^2\beta^2I_2 \\ \frac{1}{2}\sqrt{2}g\beta(H_x+iH_y) & \frac{1}{4}g^2\beta^2I_1 & \frac{1}{2}\sqrt{2}g\beta(H_x-iH_y) \\ -\frac{3}{8}g^2\beta^2I_2 & \frac{1}{2}\sqrt{2}g\beta(H_x+iH_y) & -\frac{1}{8}g^2\beta^2I_1-g\beta H_z \end{bmatrix} \begin{matrix}(M=+1)\\(M=0)\\(M=-1)\end{matrix} \quad (5)$$

* Present address (1960–1961): Quantum Chemistry Group, University of Uppsala, Uppsala, Sweden.

[1] C. A. Hutchison and B. W. Mangum, J. Chem. Phys. **29**, 952 (1958).

[2] J. H. van der Waals and M. S. de Groot, Mol. Phys. **2**, 333 (1959); **3**, 190 (1960).

[3] M. Gouterman and W. Moffitt, J. Chem. Phys. **30**, 1107, 1369 (1959).

[4] R. McWeeny, Proc. Roy. Soc. (London) **A253**, 242 (1959); Revs. Modern Phys. **32**, 335 (1960).

[5] g may be given the free-electron value 2 in the field-independent terms. The same value would apply elsewhere only in the absence of configuration interaction—whose effect may be simulated by using an effective g value quite close to 2.

in which

$$I_1=\int\frac{2z_{12}^2-x_{12}^2-y_{12}^2}{r_{12}^5}Q_{ca}(1,2;1,2)dv_1dv_2,\qquad I_2=\int\frac{x_{12}^2-y_{12}^2}{r_{12}^5}Q_{ca}(1,2;1,2)dv_1dv_2 \tag{6}$$

and the coordinates are referred to principal axes. In the zero field case, the functions with $M=\pm1$ are mixed to give the symmetry adapted combinations used by van der Waals and de Groot (1959)[2] and the zero-field coupling energies are $E=X,\ Y,\ Z$, where $Z=\beta^2I_1$, and $X,\ Y$ are obtained by cyclic permutation of $x_{12},\ y_{12},\ z_{12}$. For a two-electron wave function these quantities coincide with those defined by van der Waals and de Groot. On the other hand, the wave function from which $Q_{ca}(1,2;1,2)$ is determined may be an *exact* eigenfunction of the spinless *many*-electron Hamiltonian. We now distinguish various approximations.

First, we recognize a "closed shell" (A, say) of N_A electrons described by an antisymmetric function $\Phi_A(1,2,\cdots N_A)$ and suppose the remaining N_B "outer" electrons similarly described by $\Phi_B(N_A+1,\cdots N_A+N_B)$. A state of the system of (N_A+N_B) electrons may then be represented, in this approximation, by an antisymmetrized product of the "group" functions Φ_A and Φ_B; and for orthogonal groups we find (extending the analysis of McWeeny, 1959[4])

$$Q_{ca}(1,2;1',2')=\sum_R Q_{ca}{}^R(1,2;1',2')$$
$$+\sum_{R,S}{}'Q_1{}^R(1;1')Q_1{}^S(2;2')-\sum_{R,S}{}'Q_1{}^R(2;1')Q_1{}^S(1;2')$$
$$(R,\ S=A,\ B) \tag{7}$$

where, for instance, $Q_1{}^R(1;1')$ is the *spin density matrix* for the R group (in the notation of McWeeny 1960[4]). Now a closed shell may be defined most generally as a group of electrons in a lowest energy *singlet* state and in this case the A-group spin density vanishes and (7) reduces to

$$Q_{ca}(1,2;1',2')=Q_{ca}{}^B(1,2;1',2'). \tag{8}$$

It is therefore sufficient, in discussing the spin coupling, to consider the *outer electrons alone*. This result does not depend on the usual doubly occupied orbital description of a closed shell and therefore applies very generally.

A second reduction occurs when we adopt an orbital approximation, using singly occupied (α) orbitals to describe the outer electrons in the standard state with $M=S$. In this case, considering only the outer shell and dropping the superscript B,

$$Q_{ca}(1,2;1',2')=Q_1(1;1')Q_1(2;2')-Q_1(2;1')Q_1(1;2') \tag{9}$$

in terms of the (*one*-electron) spin density matrix alone. This result arises from the familiar fact that in one-determinant approximation

$$\rho_2(1,2;1',2')=\rho_1(1;1')\rho_1(2;2')-\rho_1(2;1')\rho_1(1;2'). \tag{10}$$

The third approximation consists of expanding the outer shell orbitals in terms of basis functions $\phi_1,\ \phi_2,\cdots$(e.g., atomic orbitals giving the LCAO approximation) in which case the spin density becomes

$$Q_1(1;1')=\sum_{i,j}\phi_i(1)Q_{1ij}\phi_j{}^*(1'), \tag{11}$$

where $\mathbf{Q}_1$ (first introduced by McConnell, 1958[6]; see also McWeeny, 1960[4]) is analogous to the charge and bond order matrix but refers to the singly occupied MO's alone and therefore gives an LCAO picture of the distribution of spin angular momentum. The matrix $\mathbf{Q}_1$ is easily determined from the AO coefficients of the singly occupied MO's: if these are collected as the columns of a matrix $\mathbf{T}$, then $\mathbf{Q}_1=\mathbf{T}\mathbf{T}\dagger$. Basic quantities of the form (6) may then be expressed in terms of integrals such as

$$I_x=\int(x_{12}^2/r_{12}^5)Q_{ca}(1,2;1,2)dv_1dv_2$$
$$=\sum_{i,j,k,l}[Q_{1ij}Q_{1kl}-Q_{1kj}Q_{1il}](\phi_j\phi_l\mid x_{12}^2/r_{12}^5\mid\phi_i\phi_k). \tag{12}$$

Finally, it is useful to approximate the AO integrals in (12). If the AO's are orthogonal it is customary to neglect such integrals unless $i=j$ and $k=1$. This gives

$$I_x\simeq2\sum_{i<k}[Q_{1ii}Q_{1kk}-Q_{1ik}{}^2]\gamma_{ik}{}^x. \tag{13}$$

The $\gamma_{ik}{}^x$ integrals may then be expressed in terms of $\gamma_{ik}{}^{||}$, $\gamma_{ik}{}^{\perp}$, and $\gamma_{ik}{}^z$—referring, respectively, to x parallel and perpendicular to link i—k, in the plane, and normal to the molecular plane. As Gouterman and Moffitt have remarked, these integrals are unpleasant. A crude approximation which we have found useful consists of replacing each $2p$ orbital by a point charge of half an electron in each "lobe" at the most probable electron-nuclear distance (a device which gives electron repulsion integrals with about 95% accuracy). It is important, however, to recognize that a nearest-neighbor approximation (Gouterman and Moffitt[3]) is inadequate since neither the integrals nor their coefficients fall off rapidly with distance: in the case of naphthalene, for example, nearest neighbors contribute only about half the value of an integral such as (13).

The approximations which lead to the reduction of (7) are in no way essential and it would be interesting

[6] H. M. McConnell, J. Chem. Phys. **28,** 1188 (1958); Proc. Natl. Acad. Sci. U.S. **45,** 172 (1959).

to obtain the coupling anisotropy function using accurate wave functions. But the present analysis suggests that quite crude functions may often be adequate. In the first place, the tightly bound inner electrons can be rigorously excluded in so far as the wave function can be written as an antisymmetrized product of two parts. Second, $Q_{ca}(1, 2; 1', 2')$ is antisymmetric in each pair of variables (1, 2 and 1′, 2′) and Q_{ca} (1, 2; 1, 2) therefore vanishes at least as rapidly as r_{12}^2 as two particles approach (cf. McConnell 1959[6]); it is therefore unnecessary that the wave function shall accurately describe electron correlation. And, finally, integrals such as (12) appear to be rather insensitive to the values of $\gamma_{ik}^{||}, \gamma_{ik}^{\perp}, \gamma_{ik}^{s}$ and to be determined largely by molecular geometry. In conclusion therefore we report some calculations for naphthalene, in which all the above approximations were made. The triplet state was described by promoting one electron from the top bonding orbital into the lowest antibonding, both being taken as Huckel orbitals. All pairs of atoms were considered in evaluating (12) and substitution in (6) led to

$$X/hc=0.85\times10^{-2}, \qquad Y/hc=4.91\times10^{-2},$$
$$Z/hc=-5.77\times10^{-2}\ \text{cm}^{-1}$$

(x and y axes being in the plane, with x along the central bond). The zero-field splittings are then

$$(Y-Z)/hc=0.107\ \text{cm}^{-1}, \quad (X-Z)/hc=0.066\ \text{cm}^{-1}$$

and are in reasonable agreement with the observed values of 0.1143 and 0.0863 cm^{-1}, respectively.

THE JOURNAL OF CHEMICAL PHYSICS VOLUME 34, NUMBER 2 FEBRUARY, 1961

Valence Bond Treatment on the *B* State of the Hydrogen Molecule

CARMEN S. TSCHUDI* AND NORAH V. COHAN

Facultad de Ciencias Exactas y Naturales, Universidad Nacional de Buenos Aires, Peru 222, Buenos Aires, Argentina

(Received May 23, 1960)

The potential energy of the lowest $^1\Sigma_u^+$ state of the hydrogen molecule is given as a function of the internuclear distance. Calculations were carried out by the valence bond method using Slater 1*s* and 2*p* atomic orbitals. Both ionic and covalent structures were considered. The 1*s* orbitals of the ionic and covalent functions included a variational parameter but the orbital exponent of the 2*p* orbital was kept constant. It is found that the introduction of the 2*p* orbital into the wave function results in a considerable improvement of the dissociation energy and that further the state is essentially covalent in character rather than ionic, as previously reported.

INTRODUCTION

FOR a long time it has been assumed that the state of lowest energy of symmetry $^1\Sigma_u^+$ of the hydrogen molecule, often called *B* or *V* state, is ionic.[1–3] The large equilibrium internuclear distance, and also the unusually slow approach of potential energy curve to its asymptotic value with increasing internuclear distance were thought to be properties belonging to an ionic, rather than a covalent state. Another important fact supporting this idea was that the only possible wave function with the right symmetry made up from 1*s* orbitals is the ionic function, $s_a(1)\ s_a(2)-s_b(1)\ s_b(2)$, where *a* and *b* are the nuclei, and 1 and 2 the electrons. In order to have a covalent wave function a higher energy orbital is needed, for example a 2*p* orbital. It was assumed that such a covalent wave function would have very small weight on account of the high energy of the excited orbital used.

In spite of the above considerations, calculations were not conclusive. Zener and Guillemin[4] were not able to decide whether the *B* state was ionic or not. Brackman's calculations, published by Altmann and Cohan,[5] using the above ionic function, give a very poor value for the dissociation energy at the equilibrium internuclear distance: 0.44 ev compared with the experimental value of 3.7 ev. Phillipson and Mulliken[6] calculated the energy of the *B* state applying the molecular orbital theory. The wave function they use is the antisymmetrized product of molecular orbitals σ_g and σ_u, which are made up from linear combinations of 1*s* atomic orbitals; they take the exponential parameters of these orbitals, ζ_g and ζ_u, as variation parameters. Their results also suggest that the ionic structure alone must be a poor approximation. In fact, their wave function reduces to the ionic function mentioned above when both exponential parameters are equal, but when $\zeta_g \neq \zeta_u$ a considerable improvement of the results is obtained. Huzinaga[7] performed a molecular orbital

* Present address: Department of Chemistry, The Florida State University, Tallahassee, Florida.

[1] R. S. Mulliken, Phys. Rev. **50**, 1017 (1936).
[2] R. S. Mulliken, Phys. Rev. **50**, 1028 (1936).
[3] R. S. Mulliken, J. Chem. Phys. **7**, 20 (1939).
[4] C. Zener and V. Guillemin, Phys. Rev. **34**, 999 (1929).
[5] S. L. Altmann and N. V. Cohan, Trans. Faraday Soc. **50**, 1151 (1954).
[6] P. E. Phillipson and R. S. Mulliken, J. Chem. Phys. **28**, 1248 (1958).
[7] S. Huzinaga, Progr. Theoret. Phys. (Kyoto) **20**, 15 (1958).

treatment, similar to the treatment of Phillipson and Mulliken, of the $^1\Sigma_u^+$ state for internuclear distances up to and including 2.0 a.u. His results also indicate that different exponential parameters give better results than a single parameter. Huzinaga[8] also performed a calculation of this state based on the one center expansion method using wave functions which exhibit 2p character. The energy values so obtained are higher than the values of Phillipson and Mulliken[6] for comparable distances.

It seems therefore worthwhile to study the $^1\Sigma_u^+$ state of the hydrogen molecule by the valence bond method, using both the ionic function and a covalent function made up from $1s$ and $2p$ orbitals. Different screening constants for the $1s$ orbitals in the ionic and covalent functions are used as parameters in a variational treatment. It is also useful to observe the values of the screening constants which minimize the energy, in order to compare the results with those obtained by similar treatments for the ground state of the hydrogen molecule, by Weinbaum[9] first and later by Altmann and Cohan.[5] They concluded that a better result for the dissociation energy is obtained when both screening constants, the one associated with the $1s$ orbital of the covalent function and the other with the ionic function, are the same. Scherr[10] suggested that an improvement is obtained when the Slater's rules of atoms are extraploated to the molecular case, instead of using both screening constants equal to unity. Altmann and Cohan[5] showed that the improvement found by Scherr was only due to a local maximum error. The effective nuclear charge for the $2p$ orbital in our work is kept constant, and equal to one. We believe that this approximation does not introduce a serious error, for the extreme values of the effective nuclear charge for the $2p$ orbital in the united atom (He in configuration $1s2p$) and in the separated atoms $[H(1s)+H(2s)]$ are 1.15 and 1.0, respectively, while for the $1s$ orbital in the covalent function they vary from 2.0 to 1.0, according to Slater rules. In order to study the variation of the parameters with the internuclear distance, this is taken as a further variational parameter.

METHODS AND RESULTS

The wave function used is $\Psi=c_c\phi_c+c_i\phi_i$ where

$$\phi_c=N_c[s_a^c(1)\,p_b(2)+p_b(1)\,s_a^c(2)+s_b^c(1)\,p_a(2)+p_a(1)\,s_b^c(2)],$$

$$\phi_i=N_i[s_a^i(1)\,s_a^i(2)-s_b^i(1)\,s_b^i(2)],$$

$$s_m^k(j)=Z_k^{\frac{3}{2}}\pi^{-\frac{1}{2}}\exp(-Z_k r_{mj})$$

$$p_m(j)=\tfrac{1}{4}Z^{5/2}(2\pi)^{-\frac{1}{2}}r_{mj}\cos\theta_{mj}\exp[-(Z/2)r_{mj}],\quad(\text{with } Z=1.0)$$

and N_c and N_i are normalization factors. The index m indicates the nucleus a or b, j the electron 1 or 2 and k the canonical structure covalent (c) or ionic (i). The $2p$ orbitals are defined so that the direction z is along the internuclear axis from a to b.

The secular determinant therefore is

$$\begin{vmatrix} H_{cc}-E & H_{ci}-ES_{ci} \\ H_{ic}-ES_{ic} & H_{ii}-E \end{vmatrix}=0,$$

where

$$H_{cc}=E_c=\int\phi_c\mathcal{H}\phi_c d\tau,\qquad H_{ii}=E_i=\int\phi_i\mathcal{H}\phi_i d\tau,$$

$$H_{ci}=H_{ic}=\int\phi_c\mathcal{H}\phi_i d\tau,\ \text{and}\quad S_{ci}=S_{ic}=\int\phi_c\phi_i d\tau,$$

$\mathcal{H}$ is the complete Hamiltonian operator of the molecule.

All the one-electron integrals and the Coulomb two-electron integrals were computed from the analytical expressions given by Coulson[11] and Roothaan,[12] respectively. The last-mentioned integrals were also checked by four and six point interpolation from Roothaan's[13] numerical tables. The numerical values for the exchange and resonance two-electron integrals were made available to us.[14] Atomic units (a.u.) are used throughout the calculations, the unit of length being $a_0=0.5292$ A and the unit of energy $e^2/a_0=27.206$ ev.

Calculations were made for internuclear distances ρ, varying from 1.6 to 7.0 a.u. with a fairly small interval in the neighborhood of the equilibrium internuclear distance ρ_e which has been taken equal to 1.293 A($\rho_e=2.4433\ a_0$). The effective nuclear charges for both canonical structures were varied from 0.6 to 1.4 in steps of 0.2 and in some cases of 0.1. Final results of the energy are given in ev.

Results of the present work are given in Table I, Table II, Table III, and Fig. 1. Table I gives the values of the effective nuclear charges Z_c and Z_i which minimize the covalent and ionic energy, respectively, and $\bar{Z}_c$ and $\bar{Z}_i$ which minimize the total energy. In Fig. 1 energies are plotted against the internuclear distances. The potential energy curves calculated by Phillipson and Mulliken[6] are also shown in order to compare their results with ours. Table II gives the best values obtained for the covalent, ionic, and total energies. Table III gives the values of the approximate weights of the covalent and ionic functions. They were calculated for

[8] S. Huzinaga, Progr. Theoret. Phys. (Kyoto) **17**, 162 (1957).
[9] S. Weinbaum, J. Chem. Phys. **1**, 593 (1933).
[10] C. W. Scherr, J. Chem. Phys. **22**, 149 (1954).
[11] C. A. Coulson, Proc. Cambridge Phil. Soc. **38**, 210 (1942).
[12] C. C. J. Roothaan, J. Chem. Phys. **19**, 1445 (1951).
[13] C. C. J. Roothaan, "Tables of two center coulomb integrals between $1s$, $2s$ and $2p$ orbitals," Special Technical Report, University of Chicago (1955).
[14] These integrals were computed in the Laboratory of Molecular Structure and Spectra at the University of Chicago on a general program for the Univac Scientific WADC, Dayton, Ohio, computing machine. We wish to thank Professor C. C. J. Roothaan and especially Dr. B. Ransil for making available the computation of these integrals.

the set of values of effective nuclear charges nearest to the ones that minimize the total energy.

DISCUSSION

Table I shows that for the B state of the hydrogen molecule, Z_e is greater than one, while as already shown by Brackman,[5] the Z_i is less than one, for the equilibrium internuclear distance. We also conclude that as the internuclear distance increases both Z_e and Z_i decrease, approaching the values given by Slater's rules as ρ tends to infinity. This is also true for the ground state, as pointed out by Hirschfelder and Linnett.[15] According to an empirical formula given by Musulin,[16] the dependence of Z_e on the internuclear distance can be expressed approximately by an exponential function that approaches the values for the united and separated atoms, according to Slater rules. It follows then that Z_e depends on: (i) the values of the effective nuclear charge for the united and separated atoms, and (ii) the internuclear distance. Then it is not surprising to find $Z_e=1.166$ for the ground state[17] and $Z_e=1.16\pm0.02$ for the state B. In fact, effect (i) tends to increase the value of Z_e when going from the ground to the B state, for the values of Z_e for the united atoms corresponding to the two states are 1.7 and 2.0, respectively. But effect (ii) is just the opposite because the large equilibrium internuclear distance of the state B relative to that of the ground state tends to decrease Z_e, so that both effects are just balanced.

The variation of Z_i with the internuclear distance is almost linear and very slow and the Slater rules are approximately valid in this case. For the ground state and the equilibrium internuclear distance, the value of Z_i is greater than 1.0. Altmann and Cohan[5] suggested that the difference in symmetry of the two states is responsible for this difference in behavior. Due to the antisymmetry of the wave function of the B state, which involves the existence of a node between the nuclei, the electron cloud tends to be outside this region, the attraction of one nucleus upon the electron cloud attached to the other is small compared with the electron repulsion; this causes an expansion of the electron cloud and hence a diminution of the effective nuclear charge Z_i.

TABLE I. Values of the effective nuclear charges which minimize the covalent, ionic, and total energies.[a]

ρ(a.u.)	Z_c	Z_i	$\bar{Z}_c$	$\bar{Z}_i$
1.6	1.33	...	1.33	...
2.1	1.22	0.81	1.22	1.15
2.4433	1.16	0.80	1.15	1.04
2.8	1.12	0.78	1.12	1.00
3.1	1.09	0.77	1.10	0.91
4.0	1.03	0.74	1.06	0.84
7.0	1.00	0.69	1.00	0.76

[a] All values have an estimated error of ±0.02.

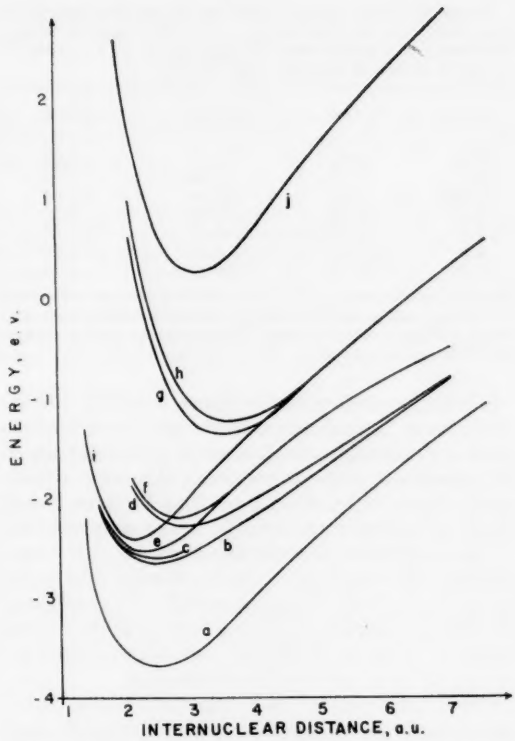

FIG. 1. Potential energy curves. (a) Experimental, according to the data given by Phillipson and Mulliken; (b) using the best total wave function of the present calculation; (c) using the total wave function with $\bar{Z}_e=\bar{Z}_i$ [curve (c) is only approximate because we had not calculated enough values of E so as to be able to make a full variational treatment. The only important feature for the following discussion is that curve (c) lies just above curve (b) as indicated]; (d) using the total wave function with $\bar{Z}_e=1.0$ and $\bar{Z}_i=0.7$ (Slater rules); (e) using the best covalent wave function; (f) using the covalent wave function with $Z_e=1.0$ (Slater rules); (g) using the best ionic wave function; (h) using the ionic wave function with $Z_i=0.7$ (Slater rules); (i) the curve obtained by Phillipson and Mulliken using different screening constants [Phillipson and Mulliken report 10.98 ev at 4.0 A; it should be 10.79 ev. This corrected energy value was obtained by the referee from private communication with the authors]; (j) the curve obtained by Phillipson and Mulliken with $\zeta_g=\zeta_u=1.0$ coincident with our ionic wave function when $Z_i=1.0$.

The results of the last two columns of Table I are rather surprising. $\bar{Z}_c$, which minimizes the total energy, is practically the same as Z_c, which minimizes the covalent energy E_c for each value of the internuclear distance. However the same is not true for $\bar{Z}_i$. This effective nuclear charge increases unexpectedly and, for values of ρ near the equilibrium internuclear distance it is greater than unity. Therefore it seems that the above explanation given by Altmann and Cohan[5] for the ionic function alone does not apply when it mixes with the covalent function.

[15] J. O. Hirschfelder and J. W. Linnett, J. Chem. Phys. **18**, 130 (1950).
[16] B. Musulin, J. Chem. Phys. **25**, 801 (1956).
[17] S. C. Wang, Phys. Rev. **31**, 579 (1928).

TABLE II. Best values obtained for the covalent energy E_c, ionic energy E_i, and total energy E. The zero energy is taken as the energy of a ground-state hydrogen atom [H(1s)] plus the energy of an excited hydrogen atom [H(2s)].

ρ(a.u.)	E_c (ev)	E_i (ev)	E (ev)
1.6[a]	−2.07	...	−2.07
2.1	−2.55	0.64	−2.57
2.4433	−2.54	−0.44	−2.64
2.8	−2.41	−1.03	−2.59
3.1	−2.26	−1.27	−2.54
4.0	−1.71	−1.26	−2.18
7.0	−0.48	−0.33	−0.78

[a] The ionic function was not included in the final calculations of the total energy, at this value of the internuclear distance, on account of the extremely small weight of this function.

TABLE III. Values of the approximate weights of the covalent and ionic functions.

ρ(a.u.)	$\bar{Z}_c$	$\bar{Z}_i$	$\lvert c_c \rvert^2$	$\lvert c_i \rvert^2$
2.1	1.2	1.2	0.92	0.01
2.4433	1.2	1.0	0.80	0.03
2.8	1.2	1.0	0.71	0.05
3.1	1.0	1.0	0.64	0.08
4.0	1.0	0.8	0.41	0.19
7.0	1.0	0.7	0.57	0.15

Several conclusions can be drawn from Fig. 1. First of all, curve (g) indicates that the ionic wave function alone is a poor approximation to the energy of state B. As pointed out in the introduction, this result was already suggested by Brackman's and Phillipson's and Mulliken's calculations. It is also a poor approximation to the equilibrium internuclear distance (1.9 A approximately) which is much larger than the experimental value of 1.293 A. Curve (h) with $Z_i=0.7$ throughout is not very different from the former while $Z_i=1.0$ (curve j) tried by Phillipson and Mulliken and recalculated by us gives much worse results.

Curve (e) shows the most important feature of the present work, namely, that the covalent structure alone gives a much better result than the ionic wave function with a dissociation energy of 2.56 ev and an equilibrium internuclear distance close to 1.2 A. That is, *state B seems to be mainly covalent instead of ionic, as was supposed up to now.* The inclusion of an excited $2p$ orbital is necessary in order to obtain a reasonable value for the dissociation energy. When $Z_c=1.0$ throughout, only slightly worse results are obtained (curve f). It could be argued that, as suggested by Chandrasekhar[18] and Arai,[19] the ionic wave function used is a rather bad wave function. In fact, it is known that as ρ tends to infinity it gives an energy of −0.472656 a.u. instead of the best theoretical value of −0.52756 a.u.[20] as calculated by Henrich.[21] Although the ionic wave function could be improved, it seems to us improbably that a different ionic wave function would give a potential energy curve below curve (e). If this is the situation, the mixing of such an ionic wave function with our covalent wave function would be so great as to lower the energy almost to the value of experimental dissociation energy, and this seems highly improbable without explicit introduction of the r_{12} terms into the wave function.

Curve (b) is our best potential energy curve, and it differs only slightly from curve (e) where only the covalent wave function is used. In fact the weight of the ionic wave function is very small for ρ_e (of the order of 3% as shown in Table III); it increases considerably for ρ around 5 a_0, and then decreases again. It is worth noting that a better result is obtained when only one variational parameter $\bar{Z}_c=\bar{Z}_i$ is used (curve c) than when using the Slater values for the molecule $\bar{Z}_c=1.0$ and $\bar{Z}_i=0.7$ (curve d); this is true for the excited as well as for the ground state. As a consequence of the small weight of the ionic wave function at the equilibrium internuclear distance, a small variation of $\bar{Z}_i$ has a negligible effect on the total energy, while a small variation of $\bar{Z}_c$ modifies it considerably, in accordance with similar results obtained for the ground state.[5]

Finally, in the present calculation we obtain a dissociation energy of 2.64±0.02 ev and $\rho_e=1.30\pm0.01$ A. For comparison, Zener and Guillemin,[4] using a different type of wave function with three parameters,[22] obtained 2.57 ev and with a further variational parameter they improved the calculated energy up to 2.64 ev. Phillipson and Mulliken[6] with their molecular orbital type of wave function with two variational parameters obtained 2.330 ev. Kolos and Roothaan[23] using a 34 term correlated wave function obtained an energy of 3.5130 ev as compared with the experimental value 3.5802 ev. They obtained a value for the equilibrium internuclear distance equal to 1.258 A compared to the observed value of 1.2926 A.

ACKNOWLEDGMENTS

We wish to thank Dr. Simon L. Altmann for suggesting this problem to us, and Dr. Bruno Linder for his assistance in preparing the manuscript. One of us (C.S.T.) is also indebted to the Consejo Nacional de Investigaciones Cientificas y Tecnicas, Buenos Aires, for a fellowship during the course of the present work.

[18] S. Chandrasekhar, Astrophys. J. **100**, 176 (1944).
[19] T. Arai, J. Chem. Phys. **26**, 451 (1957).
[20] The zero of energy is taken here as the energy of nuclei and electrons at infinite separation.
[21] L. R. Henrich, Astrophys. J. **99**, 59 (1944).
[22] Zener and Guillemin started with five parameters but one turned out to be zero and another infinite.
[23] W. Kolos and C. C. J. Roothaan, Technical Report, part 2, page 169 (1957–9), Laboratory of Molecular Structure and Spectra, The University of Chicago.

Theory of Light Scattering by Thin Rodlike Macromolecules in a Liquid Subjected to Shear*

K. OKANO AND E. WADA†

The Institute of Physical and Chemical Research, Tokyo, Japan and Department of Chemistry, Wayne State University, Detroit, Michigan

(Received August 2, 1960)

The light scattering by thin rodlike particles in a liquid subjected to shear is calculated on the basis of the Rayleigh-Gans treatment. The calculations are made for both unidirectional laminary flow and for flow of periodically alternating direction. The calculation is carried out by two methods: the interference factor P is expressed in terms of a power series of G/D, where G and D are the rate of shear and the rotatory diffusion constant, respectively, of the rod rotating around its minor axis. This treatment is applicable to sufficiently low G/D values. The result for a very wide range of rate of shear is obtained by using the Peterlin distribution function of particle axis. Numerical calculation shows that both results agree in a region of G/D below about two if the axial ratio is large enough. The theoretical results appear to agree with the experimental ones.

THE light scattering by anisometric particles in a liquid subjected to shear not only provides a direct method of studying the behavior of the particles in the flowing medium but also provides a new means of determining their shape and size.[1]

Several theories have been proposed on this subject for various types of macromolecules. Peterlin, Heller, and Nakagaki[2] have developed a theory for flexible linear polymers composed of identical segments, each of which has an isotropic polarizability. This theory has been extended by Stevenson and Bhatnagar[3] to the case that the polarizability of the segment is anisotropic. Nakagaki and Heller[4] in an alternate approach approximated the polymer molecule by an isotropic spheroid of variable axial ratio. Stevenson[5] using a second approximation to the Rayleigh treatment has calculated the scattered light intensity for rigid spheroidal particles, his results being valid if α does not exceed about 0.8; here $\alpha=2\pi a/\lambda'$, where a is the semimajor axis of the particle and λ' the wavelength in the surrounding medium.

For the purpose of covering a wider range of particle (molecular) size, the light scattering of thin rodlike particles in a medium subjected to shear is calculated on the basis of the Rayleigh-Gans theory. The calculations are made for both unidirectional laminar flow[6] and for flow of periodically alternating direction.

It is assumed that the particle (molecule) can be approximated by a thin rod particle having an axial ratio $p\geq 20$, and that it is suspended (dissolved) in a liquid subjected to shear of the rate G. If the Rayleigh-Gans theory can be applied (small relative refractive index m) the "interference factor" of the particle

$$P(\mathbf{s})=\int_0^{2\pi}\int_0^{\pi}\frac{\sin^2(x\cos\gamma)}{(x\cos\gamma)^2}f(\vartheta,\phi)\sin\vartheta d\vartheta d\phi, \quad (1)$$

with

$$x=(2\pi/\lambda')L\sin(\theta/2),$$

with

$$\mathbf{s}=\mathbf{s}'-\mathbf{s}_0', \quad (2)$$

$$\mathbf{s}=2\sin(\theta/2)(\sin\delta\cos\psi, \sin\delta\sin\psi, \cos\delta), \quad (3)$$

where $\mathbf{s}'$ and $\mathbf{s}_0'$ are the unit vectors in the directions of scattered and incident light beams, L the length of the rod axis, γ the angle between the axis and the bisectrix of the direction of $\mathbf{s}'$ and $-\mathbf{s}_0$, λ' the wavelength in the surrounding liquid, θ the angle of observation with respect to the incident beam, ϑ (or δ) and ϕ (or ψ)[7] the polar and aximutal angles of the particle axis (or $\mathbf{s}$) as shown in Fig. 1, and $f(\vartheta,\phi)$ the probability distribution function of the axis.

The velocity of the surrounding liquid at a point R (Fig. 1) from the center of mass of the particle is given by

$$V=Ge^{i\omega' t}(\mathbf{R}\cdot\mathbf{e}_z)\mathbf{e}_y, \qquad \mathbf{R}=(x,y,z), \quad (4)$$

where G is the rate of shear, ω' the angular frequency of the rate of shear and e_x and e_y are unit vectors in the x and y directions.

In this case, $f(\vartheta,\phi)$ is obtained by solving the diffusion equation for the Brownian motion of the particles. In order to facilitate the calculation, $f(\vartheta,\phi)$ is expressed

* A preliminary account was given at the 137th National Meeting of the American Chemical Society, Cleveland, Ohio, April 5, 1960. This work was supported in part by the Office of Naval Research.

† On leave from the Institute of Physical and Chemical Research, Tokyo, Japan.

[1] W. Heller, Revs. Modern Phys. **31,** 1072 (1959).

[2] A. Peterlin, W. Heller, and M. Nakagaki, J. Chem. Phys. **28,** 470 (1958).

[3] A. F. Stevenson and H. L. Bhatnagar, J. Chem. Phys. **29,** 1336 (1958).

[4] M. Nakagaki and W. Heller, J. Polymer Sci. **38,** 117 (1959).

[5] A. F. Stevenson, presented at the March, 1960 American Physical Society Meeting, Detroit, March 23, 1960.

[6] G. Wippler, J. Chem. Phys. **51,** 122 (1954).

[7] The angle ω in the previous theory[2] is $(90°-\psi)$. The angle ψ is used for the sake of simplicity of the equations derived here.

by the powers of G/D. D is the rotatory diffusion constant of the particle around its minor axis,[8]

$$D=3kT(2p-0.8)/8\pi\eta_0 a^3, \tag{5}$$

with

$$p=a/b, \tag{6}$$

where k is the Boltzmann's constant, T the absolute temperature, η_0 the viscosity of the surrounding liquid, and a and b the major and minor axes of the particle, respectively. The power series expression for the probability distribution function of the axis of a thin rod is

$$f(\vartheta,\phi)=\frac{1}{4\pi}\{\rho_0+\rho_1(G/D)e^{i\omega' t}+\rho_2(G/D)^2e^{i2\omega' t}+\rho_3(G/D)^3e^{i3\omega' t}+\cdots\}, \tag{7}$$

with

$$\rho_0=1, \tag{8}$$

$$\rho_1=[(1+i\omega'/6D)]^{-1}\tfrac{1}{12}P_2^2(\cos\vartheta)\sin 2\phi, \tag{9}$$

$$\rho_2=-[(1+i\omega'/3D)(1+i\omega'/6D)]^{-1}\{\tfrac{1}{84}P_2(\cos\vartheta)+\tfrac{1}{72}P_2^2(\cos\vartheta)\cos 2\phi\}$$
$$+[(1+i\omega'/6D)(1+i\omega'/10D)]^{-1}\{\tfrac{1}{280}P_4(\cos\vartheta)-\tfrac{1}{6720}P_4^4(\cos\vartheta)\cos 4\phi\}, \tag{10}$$

$$\rho_3=-[(1+i\omega'/2D)(1+i\omega'/6D)(1+i\omega'/10D)]^{-1}\tfrac{1}{2940}P_2^2(\cos\vartheta)\sin 2\phi$$
$$-[(1+i\omega'/2D)(1+i\omega'/3D)(1+i\omega'/6D)]^{-1}\tfrac{1}{10584}P_2^2(\cos\vartheta)\sin 2\phi$$
$$-[(1+i\omega'/3D)(1+i\omega'/6D)(1+i3\omega'/20D)]^{-1}\{\tfrac{1}{40320}P_4^4(\cos\vartheta)\sin 4\phi+\tfrac{1}{23520}P_4^2(\cos\vartheta)\sin 2\phi\}$$
$$-[(1+i\omega'/6D)(1+13\omega'/20D)(1+i\omega'/10D)]^{-1}\{\tfrac{1}{67200}P_4^4(\cos\vartheta)\sin 4\phi+\tfrac{1}{86240}P_4^2(\cos\vartheta)\sin 2\phi\}$$
$$+[(1+i\omega'/6D)(1+i\omega'/10D)(1+i\omega'/14D)]^{-1}\{\tfrac{1}{221760}P_6^2(\cos\vartheta)\sin 2\phi-\tfrac{1}{15966720}P_6^6(\cos\vartheta)\sin 6\phi\}, \tag{11}$$

where $P_{2n}(\cos\vartheta)$ is a Legendre polynomial of the first kind and

$$P_{2n}{}^{2m}=\sin^{2m}\vartheta d^{2m}P_{2n}/d(\cos\vartheta)^{2m}. \tag{12}$$

The interference factor of the rod is obtained by substituting Eq. (7) into Eq. (1), viz.,

$$P(\mathbf{s})=J_0+\left(\frac{G}{D}\right)e^{i\omega' t}\frac{J_2}{1+i\omega'/6D}\frac{1}{12}P_2^2(\cos\delta)\sin 2\psi+\left(\frac{G}{D}\right)^2e^{i2\omega' t}\Bigg[-\frac{J_2}{(1+i\omega'/3D)(1+i\omega'/6D)}$$
$$\times\{\tfrac{1}{84}P_2(\cos\delta)+\tfrac{1}{72}P_2^2(\cos\delta)\cos 2\psi\}+\frac{J_4}{(1+i\omega'/6D)(1+i\omega'/10D)}\{\tfrac{1}{280}P_4(\cos\delta)-\tfrac{1}{6720}P_4^4(\cos\delta)\cos 4\psi\}\Bigg]$$
$$+\left(\frac{G}{D}\right)^3e^{i3\omega' t}\Bigg[-\frac{J_2}{(1+i\omega'/2D)(1+i\omega'/6D)(1+i\omega'/10D)}\tfrac{1}{2940}P_2^2(\cos\delta)\sin 2\psi$$
$$-\frac{J_2}{(1+i\omega'/2D)(1+i\omega'/3D)(1+i\omega'/6D)}\tfrac{23}{10584}P_2^2(\cos\delta)\sin 2\psi$$
$$-\frac{J_4}{(1+i\omega'/3D)(1+i\omega'/6D)(1+3i\omega'/20D)}\{\tfrac{1}{40320}P_4^4(\cos\delta)\sin 4\psi+\tfrac{1}{23520}P_4^2(\cos\delta)\sin 2\psi\}$$
$$-\frac{J_4}{(1+i\omega'/6D)(1+3i\omega'/20D)(1+i\omega'/10D)}\{\tfrac{1}{67200}P_4^4(\cos\delta)\sin 4\psi+\tfrac{1}{86240}P_4^2(\cos\delta)\sin 2\psi\}$$
$$+\frac{J_6}{(1+i\omega'/6D)(1+i\omega'/10D)(1+i\omega'/14D)}\{\tfrac{1}{221760}P_6^2(\cos\delta)\sin 2\psi-\tfrac{1}{15966720}P_6^6(\cos\delta)\sin 6\psi\}\Bigg]+0(G/D)^4, \tag{13}$$

with

$$Jn=\tfrac{1}{2}\int_0\frac{\sin^2(x\cos\gamma)}{(x\cos\gamma)^2}Pn(\cos\gamma)\sin\gamma d\gamma. \tag{14}$$

[8] Equation (5) has recently been improved by S. Broersma [J. Chem. Phys. **32**, 1626 (1960); however, the present theory is unaffected by this change.

For $n=0$, 2, 4, and 6,

$$J_0=x^{-1}\int_0^{2x}(\sin u/u)\,du-(\sin^2 x/x^2). \tag{15}$$

$$J_2=-\tfrac{1}{2}\left[x^{-1}\int_0^{2x}(\sin u/u)\,du-(\sin^2 x/x^2)\right]+\tfrac{3}{2}[(2x^2)^{-1}-(4x^3)^{-1}\sin 2x]. \tag{16}$$

$$J_4=\tfrac{3}{8}\left[x^{-1}\int_0^{2x}(\sin u/u)\,du-(\sin^2 x/x^2)\right]-\tfrac{30}{8}[(2x^2)^{-1}-(4x^3)^{-1}\sin 2x]$$
$$+\tfrac{35}{8}[(6x^2)^{-1}-(4x^3)^{-1}\sin 2x-(4x^4)^{-1}\cos 2x+(8x^5)^{-1}\sin 2x]. \tag{17}$$

$$J_6=-\tfrac{5}{16}\left[x^{-1}\int_0^{2x}(\sin u/u)\,du-(\sin^2 x/x^2)\right]+\tfrac{105}{16}[(2x^2)^{-1}-(4x^3)^{-1}\sin 2x]$$
$$-\tfrac{315}{16}[(6x^2)^{-1}-(4x^3)^{-1}\sin 2x-(4x^4)^{-1}\cos 2x+(8x^5)^{-1}\sin 2x]$$
$$+\tfrac{231}{16}\left(\frac{1}{10x^2}-\frac{1}{4x^3}\sin 2x-\frac{1}{2x^4}\cos 2x+\frac{3}{4x^5}\sin 2x+\frac{3}{4x^6}\cos 2x-\frac{3}{8x^7}\sin 2x\right). \tag{18}$$

Equation (15) is well known as the interference factor of thin rodlike particles at $G=0$.

Since $P(\mathbf{s})$ is given in powers of (G/D), the applicability of Eq. (13) is limited in a range of low rate of shear. The exact result which is valid for the whole range of rate of shear for unidirectional laminar flow is obtained by using the following Peterlin distribution function,[9,10]

$$f(\vartheta,\phi)=\tfrac{1}{2}\sum_{n=0}^{\infty}a_{n0}P_{2n}(\cos\vartheta)$$
$$+\sum_{n=1}^{\infty}\sum_{m=1}^{n}(a_{nm}\cos 2m\phi+b_{nm}\sin 2m\phi)\,P_{2n}^{2m}(\cos\vartheta), \tag{19}$$

with

$$\int_0^{2\pi}d\phi\int_0^{\pi}f(\vartheta,\phi)\,\sin\vartheta\,d\vartheta=1, \tag{20}$$

$$a_{00}=\tfrac{1}{2}\pi, \tag{21}$$

$$a_{n0}=\sum_{j=0}^{\infty}a_{n0,j}[(p^2-1)/(p^2+1)]^j, \tag{22}$$

$$a_{nm}=\sum_{j=0}^{\infty}a_{nm,j}[(p^2-1)/(p^2+1)]^j, \tag{23}$$

where a's and b's are functions of G/D. Integration of

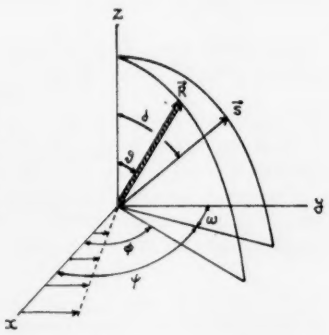

FIG. 1. Illustration of the coordinate system. *Note.* Letters with overhead arrows correspond to boldface letters in the text.

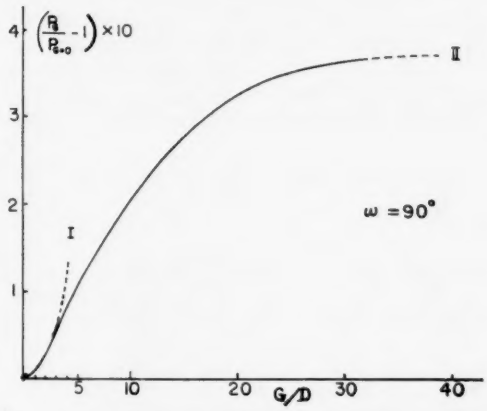

FIG. 2. Comparison of Eqs. (13) and (24). $(P_G/P_{G=0})-1$ at $\omega=90°$ and $\theta=90°$ is plotted against G/D. The curves I and II represent Eqs. (13) and (24), respectively. $p=20$, $L=300$ mμ, and $\lambda'=408$ mμ.

[9] A. Peterlin, Z. Physik **111**, 232 (1938); A. Peterlin and H. A. Stuart, *ibid.* **112**, 1 (1939).

[10] Though this distribution function is derived for spheroids, it is practically applicable also with sufficient accuracy for rodlike particles of large p value.

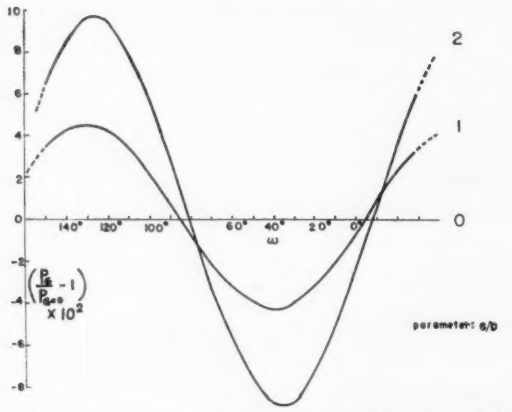

FIG. 3. Transverse angular dependence of the scattered light intensity. $(P_G/P_{G=0})-1$ at $\theta=90°$ is plotted against ω. $p=20$, $L=300$ mμ, and $\lambda'=408$ mμ.

Eq. (1) with Eq. (19) yields $P(\mathbf{s})$,

$$P(\mathbf{s})=\sum_{n=0}^{\infty}J_{2n}\Big[2\pi a_{n0}P_{2n}(\cos\delta)+\sum_{m=1}^{n}4\pi(a_{nm}\cos 2m\psi+b_{nm}\sin 2m\psi)\,P_{2n}{}^{2m}(\cos\delta)\Big]. \quad (24)$$

J_{2n} is given in Eq. (14).

By using the coefficients $a_{n,m,j}$, supplied by the Harvard Computation Laboratory,[11] the numerical calculation of Eq. (24) is carried out for the particle of 300 mμ in length and 15 mμ in diam, which corresponds to a monomer of tobacco mosaic virus. The results are plotted in Fig. 2 together with the curve representing Eq. (13). Both curves coincide in the region of G/D less than about two.

In Fig. 3, ω dependence of $P(\mathbf{s})$ is plotted according to Eq. (13). Maximum and minimum of $(P_G/P_{G=0})-1$ appear at the angles which correspond to the extinction angles of flow birefringence measurements.

The results of preliminary experiments,[12] concerned with ω dependence and G/D dependence of scattering, using tobacco mosaic virus suspensions seem to verify this theory.

ACKNOWLEDGMENT

The authors wish to express their hearty thanks to Professor W. Heller for his encouragement and many interesting and valuable discussions.

[11] The authors wish to thank Professor Scheraga of the Chemistry Department of Cornell University for having made the respective coefficients available to this laboratory.

[12] Work carried out at Wayne State University in association with W. Heller and L. Papazian and to be published shortly.

Approximate Theory of Transport in Simple Dense Fluid Mixtures*

STUART A. RICE† AND ALAN R. ALLNATT‡

Department of Chemistry and Institute for the Study of Metals, University of Chicago, Chicago 37, Illinois

(Received July 6, 1960)

The theory of transport proposed by Rice and Kirkwood is extended to the case of multicomponent systems. As in the previous case, the intermolecular force contributions to the shear and bulk viscosities and the thermal conductance are displayed as functions of the diffusion coefficient and the thermodynamic properties of the mixture. The self-diffusion coefficient is related to the intermolecular forces and molecular distribution function, thereby completing the molecular basis of the computation. Formulas are also given for the thermal diffusion factor and the heat of transport. The reader is referred to Eqs. (91), (104), (106), and (109). The theory presented predicts a form of volume fraction mixing. For example, the shear viscosity becomes

$$\eta = (v_1^*/v)^2\eta_1^* + (v_2^*/v)^2\eta_2^* + 2(v_1^* v_2^*/v^2)\eta_{12}^*,$$

with v_1^* and v_2^* the volume of N_1 molecules of component one and of N_2 molecules of component two, respectively, at the same temperature and pressure as the mixture. The quantities η_1^*, η_2^*, η_{12}^* are composition dependent so that the predicted mixing law is not pure volume fraction mixing except in the case of an ideal solution. The theory is compared with experimental measurements of the viscosity of benzene–carbon tetrachloride mixtures, and good agreement is found. The agreement between theory and experiment is discussed with reference to the mechanism of irreversibility.

I. INTRODUCTION

In a recent communication, Rice and Kirkwood[1] have developed an approximate theory of transport in simple dense fluids. The theory is primarily based on the hypothesis that a diffusive displacement in a dense fluid is small relative to the average intermolecular spacing. Using the exact statistical mechanical equations of transport for the case of the pure liquid,[2] Rice and Kirkwood evaluated the transport coefficients making use of three independent approximations. These were that:

(a) the gradient of the pair interaction potential between molecules at time $t+s$ could be expanded in a Taylor series about the gradient at time t and terms of higher order than the second could be neglected;

(b) the distribution function in pair space could be approximated as the product of the local equilibrium radial distribution function in coordinate space and the zeroth-order distribution function in momentum space; and

(c) the diffusion tensor in pair space could be approximated as the direct sum of the diffusion tensors (diagonal) in singlet space.

Absolute calculations of the transport coefficients for liquid argon were within a factor of two of experiment. Moreover, the use of any two out of three of the set diffusion coefficient, coefficient of thermal expansion, and coefficient of shear viscosity to predict the third member of the set, yielded calculations in complete agreement with experiment.

The purpose of the present paper is to extend the theory to the case of multicomponent systems using the same set of assumptions. Linear relations between the gradients of temperature and chemical potential and the fluxes of heat and matter are derived which are of the same form as the general equations of Bearman and Kirkwood.[3] The transport coefficients in the mixture are computed and the relationship to the theorem of corresponding states explored.[4]

II. FRICTION AND SELF-DIFFUSION COEFFICIENTS

We consider a ν component system consisting of N molecules which are not chemically reacting, labeling each component by a number α which runs from 1 to ν. There are N_α molecules of species α, the molecules of the species being labeled by numbers 1, 2, $\cdots$, N_α. The dynamical state of the system is specified by a distribution function $f^{(N)}(\mathbf{R}^{(N)}, \mathbf{p}^{(N)}; t)$, which satisfies the Liouville equation with $\mathbf{R}^{(N)}$, $\mathbf{p}^{(N)}$ representing the N position and momentum vectors. $\mathbf{R}_{\alpha_1}$, $\mathbf{R}_{\alpha_2}$, $\cdots$, $\mathbf{R}_{\nu N_\nu}$, $\mathbf{p}_{\alpha_1}$, $\mathbf{p}_{\alpha_2}$, $\cdots$, $\mathbf{p}_{\nu N_\nu}$. A time-smoothed distribution function, $\bar{f}^{(N)}(\mathbf{R}^{(N)}, \mathbf{p}^{(N)}; t)$ is defined by the relation

$$\bar{f}^{(N)}(\mathbf{R}^{(N)}, \mathbf{p}^{(N)}; t) = (1/\tau)\cdot\int_0^\tau f^{(N)}(\mathbf{R}^{(N)}, p^{(N)}; t+s)\,ds, \tag{1}$$

where τ is the interval of coarse graining. Given the distribution function $f^{(N)}$, the expectation value of a dynamical variable $\phi(\mathbf{R}^{(N)}, p^{(N)}; t)$ may be written as

$$\langle\phi; \bar{f}^{(N)}\rangle = \int\phi\bar{f}^{(N)}(\mathbf{R}^{(N)}, \mathbf{p}^{(N)}; t)\,d\mathbf{R}^{(N)}d\mathbf{p}^{(N)} \tag{2}$$

* This work was supported by grants from the Alfred P. Sloan Foundation and the Petroleum Research Fund of the American Chemical Society.

† Alfred P. Sloan Fellow.

‡ N.A.T.O. Fellow.

[1] S. A. Rice and J. G. Kirkwood, J. Chem. Phys. **31**, 901 (1959).

[2] J. H. Irving and J. G. Kirkwood, J. Chem. Phys. **18**, 817 (1950).

[3] R. J. Bearman and J. G. Kirkwood, J. Chem. Phys. **28**, 136 (1958).

[4] E. Helfand and S. A. Rice, J. Chem. Phys. **32**, 1642 (1960).

and it can be shown[5] that the order of integration over Γ space and time may be commuted so that

$$\langle \phi; \bar{f}^{(N)} \rangle = \langle \bar{\phi}; f^{(N)} \rangle, \tag{3}$$

where

$$\bar{\phi} = (1/\tau) \int_0^\tau \phi(t+s)\, ds. \tag{4}$$

We calculate first the average intermolecular force $\langle \mathbf{F}_{\alpha_1} \rangle$ acting on a representative molecule 1 of the species α due to the remaining $(N-1)$ molecules of the system. The instantaneous force on the molecule, when the total potential energy of interaction can be regarded as the sum of pair potentials, is[6]

$$F_{\alpha_1}(\mathbf{R}_{\alpha_1}{}^0) = \sum_{\beta}^{\nu} \sum_{\substack{j \\ \beta j \neq \alpha 1}}^{N_\beta} \nabla_{R_{\alpha 1 \beta j}} V_{\alpha\beta}(R_{\alpha 1 \beta j}{}^0). \tag{5}$$

The potential energy $V_{\alpha\beta}(R_{\alpha i \beta j}{}^0)$ of a pair of molecules of species α and β is a function only of $R_{\alpha i \beta j}{}^0$; the distance between the molecules. The average force on the molecules is thus given by

$$\begin{aligned}
&(1/v)\langle \mathbf{F}_{\alpha_1} \rangle \\
&= \int \Bigg[\int \cdots \int (1/\tau) \int_0^\tau \sum_{\substack{\beta \\ \beta j \neq \alpha 1}} \sum_{j} \nabla_{R_{\alpha 1 \beta j}} V_{\alpha\beta}(R_{\alpha 1 \beta j}(t+s)) f(t)^{(N)} \\
&\times \delta(\mathbf{R}_{\alpha 1} - R_{\alpha 1}{}^0)\, \delta(\mathbf{R}_{\beta j} - R_{\beta j}{}^0)\, ds d\mathbf{R}^{(N)} d\mathbf{p}^{(N)} \Bigg] d\mathbf{R}_{\beta j}{}^0,
\end{aligned} \tag{6}$$

where v is the volume of the system. The averaging process has been divided into two steps in the manner described by Rice and Kirkwood.[1] Noting that all molecules of the same species make the same contribution to the average force at $\mathbf{R}_{\alpha 1}{}^0$, Eq. (6) may be rewritten as

$$\begin{aligned}
&\langle \mathbf{F}_{\alpha_1} \rangle / v \\
&= \sum_{\beta \neq \alpha = 1} (N_\beta/\tau) \int \Bigg[\int \cdots \int_0^\tau \nabla_{R_{\alpha\beta}} V_{\alpha\beta}[R_{\alpha\beta}(t+s)] f(t)^{(N)} \\
&\times \delta(\mathbf{R}_\alpha - \mathbf{R}_1{}^0)\, \delta(\mathbf{R}_\beta - \mathbf{R}_2{}^0)\, ds d\mathbf{R}^{(N)} d\mathbf{p}^{(N)} \Bigg] d\mathbf{R}_2{}^0.
\end{aligned} \tag{7}$$

We evaluate this expression using the approximations outlined in Sec. I. Expanding the pair interaction potential in a Taylor series and retaining only the first two terms one finds

$$\begin{aligned}
\nabla_{R_{\alpha\beta}} V_{\alpha\beta}[R_{\alpha\beta}(t+s)] &= \nabla_{R_{\alpha\beta}} V_{\alpha\beta}[R_{\alpha\beta}(t)] \\
&+ \Delta\mathbf{R}_{\alpha\beta} \cdot \nabla_{R_{\alpha\beta}} \nabla_{R_{\alpha\beta}} V_{\alpha\beta}[R_{\alpha\beta}(t)] + \cdots.
\end{aligned} \tag{8}$$

It is convenient to introduce the reduced distribution functions $f^{(n)}$ which are related to the probability density $f^{(N)}$ by the definition

$$\begin{aligned}
&f^{(N)}(\mathbf{R}^{(n)}, \mathbf{p}^{(n)}, \mathbf{R}^{(N-n)}, \mathbf{p}^{(N-n)}; t) \\
&= f^{(n)}(\mathbf{R}^{(n)}, \mathbf{p}^{(n)}; t) f^{(n/N-n)}(\mathbf{R}^{(N-n)}, \mathbf{p}^{(N-n)}; t),
\end{aligned} \tag{9}$$

where $f^{(n/N-n)}$ is the relative probability density in the subspace $\mathbf{R}^{(N-n)}\mathbf{p}^{(N-n)}$ given that particles 1, 2, $\cdots$, n have specified coordinates and momenta. In the case that the positions and momenta of a pair of molecules of species α and β are specified, we assume that the pair distribution function $f_{\alpha\beta}{}^{(2)}$ can be approximated, in the isothermal case, by

$$\begin{aligned}
f_{\alpha\beta}{}^{(2)} &= \frac{g_{\alpha\beta}{}^{(2,0)}(R_{\alpha\beta})}{v^2} \\
&\cdot \frac{\exp[-p_{\alpha\beta}{}^2/2m_{\alpha\beta}kT]}{(2\pi m_{\alpha\beta}kT)^{\frac{3}{2}}} \left[1 + \frac{\mathbf{p}_{\alpha\beta} \cdot \mathbf{u}_{\alpha\beta}}{kT} \right],
\end{aligned} \tag{10}$$

where $\mathbf{p}_{\alpha\beta}$ is the relative momentum of the two molecules of species α and β at $\mathbf{R}_1$ and $\mathbf{R}_2$, respectively, $m_{\alpha\beta}$ is the reduced mass of the pair, and the mean relative velocity $\mathbf{u}_{\alpha\beta}$ may be expressed in the form

$$\mathbf{u}_{\alpha\beta} = \mathbf{u}_\beta(\mathbf{R}_1) - \mathbf{u}_\alpha(\mathbf{R}_1) + O(\nabla \mathbf{u}), \tag{11}$$

with $\mathbf{u}_\alpha$ and $\mathbf{u}_\beta$ the mean velocities of the separate species. Finally, $g_{\alpha\beta}{}^{(2,0)}(R_{\alpha\beta})$ is the pair correlation function evaluated under the assumption of local equilibrium in configuration space.[7] Substitution of Eqs. (8)–(10) in Eq. (7) followed by an integration over angles leads to the relation

$$\begin{aligned}
\langle \mathbf{F}_{\alpha 1} \rangle &= \sum_{\beta \neq \alpha = 1}^{\nu} \frac{N_\beta v}{3kT} \int\int_0^\tau \nabla_{R_{\alpha\beta}}{}^2 V_{\alpha\beta}(R_{\alpha\beta})\, \mathbf{u}_{\alpha\beta} \\
&\cdot \langle \mathbf{p}_{\alpha\beta} \Delta\mathbf{R}_{\alpha\beta}(s) \rangle^{\alpha,\beta} f_{\alpha\beta}{}^{(2)} ds d\mathbf{p}_{\alpha\beta} d\mathbf{R}_{\alpha\beta}{}^0,
\end{aligned} \tag{12}$$

where

$$\begin{aligned}
&\langle \mathbf{p}_{\alpha\beta} \Delta\mathbf{R}_{\alpha\beta}(s) \rangle^{\alpha,\beta} \\
&= \int \cdots \int \mathbf{p}_{\alpha\beta} \Delta\mathbf{R}_{\alpha\beta}(s) f^{(2/N-2)}(\alpha\beta/N-2)\, d\mathbf{p}^{(N-2)} d\mathbf{R}^{(N-2)},
\end{aligned} \tag{13}$$

the argument $(\alpha\beta/N-2)$ of $f^{(2/N-2)}$ indicates that the subset 2 consists of one molecule of species α and one molecule of species β.

To obtain Eq. (12), we have used the fact that the integral of the product of $\nabla_{R_{\alpha\beta}} V_{\alpha\beta}(R_{\alpha\beta})$ and $\mathbf{p}_{\alpha\beta}$ vanishes since $\nabla_{R_{\alpha\beta}} V_{\alpha\beta}(R_{\alpha\beta})$ is independent of $\mathbf{p}_{\alpha\beta}$ and the integrand is thus an odd function over an even interval. In addition, the product of $f_{\alpha\beta}{}^{(2,0)}$ and the expansion of the gradient of the potential vanishes since the average force on a molecule at equilibrium is

[5] J. G. Kirkwood, J. Chem. Phys. **14**, 180 (1946).

[6] For simplicity we will not carry the usual minus sign throughout Eqs. (5)–(17) since it combines with another minus sign (also not carried) in the definition of the frictional coefficient as the proportionality constant between force and fluid velocity.

[7] The pair distribution function $f_{\alpha\beta}{}^2$ is, of course, not the same as the pair distribution function satisfying the Fokker-Planck equation of Kirkwood's theory of transport.[5] The form of the distribution function chosen in Eq. (10) forms one of the three principal assumptions of the theory since it is possible that terms have been neglected which are not in fact negligible.

zero. We note that

$$d(\Delta\mathbf{R}_{\alpha\beta})/ds=\mathbf{p}_{\alpha\beta}/m_{\alpha\beta}, \tag{14}$$

so that a change of the variable of integration gives

$$(1/\tau)\int_0^\tau \langle \mathbf{p}_{\alpha\beta}\Delta\mathbf{R}_{\alpha\beta}\rangle^{\alpha,\beta}ds=(m_{\alpha\beta}/\tau)\int_0^\tau \langle d(\Delta\mathbf{R}_{\alpha\beta})\Delta\mathbf{R}_{\alpha\beta}\rangle^{\alpha,\beta}$$

$$=m_{\alpha\beta}\mathbf{D}_{\alpha\beta}{}^{(2)}, \tag{15}$$

where the analog of the Einstein relation has been used to define the diffusion tensor in pair space, $\mathbf{D}_{\alpha\beta}{}^{(2)}$. We shall assume that

$$\mathbf{D}_{\alpha\beta}{}^{(2)}=D_\alpha\mathbf{1}_\alpha\oplus D_\beta\mathbf{1}_\beta, \tag{16}$$

with the symbol $\oplus$ indicating a direct sum and D_α, D_β are the singlet diffusion coefficients in the spaces of molecules α and β, respectively. By combination of Eqs. (12), (15), and (16), we find that

$$\langle \mathbf{F}_{\alpha 1}\rangle=\sum_\beta^\nu \Lambda_{\alpha\beta}c_\beta m_{\alpha\beta}[(1/\zeta_\alpha)+(1/\zeta_\beta)](\mathbf{u}_\beta-\mathbf{u}_\alpha), \tag{17}$$

and

$$\Lambda_{\alpha\beta}=\tfrac{1}{3}\int \nabla_{R_{\alpha\beta}}{}^2V_{\alpha\beta}(R_{\alpha\beta})g_{\alpha\beta}{}^{(2,0)}d^3R_{\alpha\beta}, \tag{18}$$

with $c_\alpha\equiv N_\alpha/v$ the concentration of species α (molecules per unit volume). The friction constants ζ_α and ζ_β are defined by the standard relations

$$D_\alpha=kT/\zeta_\alpha$$

$$D_\beta=kT/\zeta_\beta, \tag{19}$$

whereupon the result embodied in Eq. (17) can be conveniently written in the form

$$\langle \mathbf{F}_{\alpha 1}\rangle=\sum_\beta^\nu c_\beta\zeta_{\alpha\beta}(\mathbf{u}_\beta-\mathbf{u}_\alpha), \tag{20}$$

where

$$\zeta_{\alpha\beta}=\Lambda_{\alpha\beta}m_{\alpha\beta}[(1/\zeta_\alpha)+(1/\zeta_\beta)], \tag{21}$$

and

$$\zeta_\alpha=\sum_\beta^\nu c_\beta\zeta_{\alpha\beta}. \tag{22}$$

In the case of a nonisothermal system, allowance must be made for the dependence of the pair distribution function on the gradient of temperature. We consider here only the perturbation to the distribution function in a system with no bulk matter flow. Starting from Eq. (10), we expand the pair distribution function in a Taylor series retaining only the term linear in the temperature gradient, and neglecting deviations from local equilibrium,

$$f_{\alpha\beta}{}^{(2)}(\mathbf{R}_{\alpha\beta},\mathbf{R}_\alpha,\mathbf{p}_{\alpha\beta},T)=f_{\alpha\beta}{}^{(2,0)}+\mathbf{R}_{\alpha\beta}\cdot\nabla_{R_{\alpha\beta}}f_{\alpha\beta}{}^{(2,0)}+\cdots$$

$$\mathbf{R}_{\alpha\beta}\cdot\nabla_{R_{\alpha\beta}}f_{\alpha\beta}{}^{(2,0)}=(\partial f_{\alpha\beta}{}^{(2,0)}/\partial T)_p\mathbf{R}_{\alpha\beta}\cdot\nabla_{R_{\alpha\beta}}T, \tag{23}$$

so that

$$f_{\alpha\beta}{}^{(2)}(\mathbf{R}_{\alpha\beta},\mathbf{R}_\alpha,\mathbf{p}_{\alpha\beta},T)$$

$$=f_{\alpha\beta}{}^{(2,0)}\left[1+\frac{(p_{\alpha\beta}{}^2-3m_{\alpha\beta}kT)}{2m_{\alpha\beta}kT^2}\mathbf{R}_{\alpha\beta}\cdot\nabla T\right.$$

$$\left.+(\partial/\partial T)\ln(g_{\alpha\beta}{}^{(2,0)}/v^2)_p\mathbf{R}_{\alpha\beta}\cdot\nabla T\right. \tag{24}$$

The temperature appearing in these equations refers to the midpoint between the molecules. By substituting Eq. (24) into Eq. (7), the terms dependent on the gradient of temperature are found to yield

$$\sum_\beta N_\beta v\int \nabla_{R_{\alpha\beta}}V_{\alpha\beta}(R_{\alpha\beta}(t))\mathbf{R}_{\alpha\beta}(\partial/\partial T)(g_{\alpha\beta}{}^{(2,0)}/v^2)_p$$

$$\times d\mathbf{R}_{\alpha\beta}{}^0\cdot\nabla T,$$

where only the first term in the expansion of the potential gradient operator in Eq. (8) has been retained. Performing an integration over angles, the final result for the mean force acting on the representative molecule can be written in the form

$$\langle \mathbf{F}_{\alpha 1}\rangle=\sum_\beta^\nu c_\beta\zeta_{\alpha\beta}(\mathbf{u}_\beta-\mathbf{u}_\alpha)-\gamma_{\alpha 0}{}^{\dagger(1)}\nabla\ln T$$

$$-\sum_\sigma \psi_{\alpha\sigma}{}^{\dagger(1)}\nabla x_\sigma, \tag{25}$$

where

$$\gamma_{\alpha 0}{}^{\dagger(1)}=-\sum_\beta^\nu\frac{c_\beta\bar{v}^2T}{3}\int R_{\alpha\beta}\frac{dV_{\alpha\beta}}{dR_{\alpha\beta}}\left(\frac{\partial(g_{\alpha\beta}{}^{(2,0)}/v^2)}{\partial T}\right)_{p,c_\gamma}d\mathbf{R}_{\alpha\beta} \tag{26a}$$

$$\psi_{\alpha 0}{}^{\dagger(1)}=-\sum_\beta^\nu\frac{c_\beta\bar{v}^2T}{3}\int R_{\alpha\beta}\frac{dV_{\alpha\beta}}{dR_{\alpha\beta}}\left(\frac{\partial(g_{\alpha\beta}{}^{(2,0)}/v^2)}{\partial x_\sigma}\right)_{P,T}d\mathbf{R}_{\alpha\beta}, \tag{26b}$$

and x_σ is the mole fraction of component σ. By introduction of the well-known expression for the partial pressure[8]

$$p_\alpha=c_\alpha kT-\tfrac{1}{6}\sum_\beta^\nu c_\alpha c_\beta\int R_{\alpha\beta}\frac{dV_{\alpha\beta}}{dR_{\alpha\beta}}g_{\alpha\beta}{}^{(2,0)}d\mathbf{R}_{\alpha\beta}, \tag{27}$$

the first of Eqs. (26) may be rewritten as

$$\gamma_{\alpha 0}{}^{\dagger(1)}=2[(T/c_\alpha)(\partial p_\alpha/\partial T)_{c_\gamma,p}-kT]. \tag{26a'}$$

To relate the calculated mean force to the matter fluxes or to the gradients of chemical potential in the system, we make use of a result due to Bearman and Kirkwood.[3] A state of local equilibrium corresponding to arbitrary local concentrations and temperature and arbitrary gradients of concentration can exist when external forces equal to the gradients of chemical potential of the components are imposed on the system. In such a state, the force density acting on component α can be written as $c_\alpha\langle \mathbf{F}_\alpha{}^{(1,0)}\rangle$. In the non-

[8] See for example, T. L. Hill, *Statistical Mechanics* (McGraw-Hill Book Company, Inc., New York, 1956).

equilibrium case the total force density acting on component α can be written

$$c_\alpha\langle \mathbf{F}_\alpha^{(1)}\rangle = c_\alpha\langle \mathbf{F}_\alpha^{(1,0)}\rangle + c_\alpha\langle \mathbf{F}_\alpha^{(1,1)}\rangle. \tag{28}$$

We identify $\langle \mathbf{F}_{\alpha_1}\rangle + \sum_\sigma \psi_{\alpha\sigma}{}^{\dagger(1)}\nabla x_\sigma$ with the perturbation term $\langle \mathbf{F}_\alpha^{(1,1)}\rangle$. It can be shown[9] that

$$\langle \mathbf{F}_\alpha^{(1,1)}\rangle = \nabla_T\mu_\alpha + k\nabla T$$

$$\nabla_T = \nabla - (\partial/\partial T)_{c_\gamma}\nabla T. \tag{29}$$

A simple combination of Eqs. (24) and (25) yields the linear equations

$$\nabla_T\mu_\alpha = -\sum_\beta^\nu R_{\alpha\beta}\mathbf{j}_\beta - R_{\alpha 0}\nabla \ln T, \tag{30}$$

where

$$R_{\alpha\beta} = -\zeta_{\alpha\beta} \qquad (\alpha \neq \beta)$$

$$R_{\alpha\alpha} = \sum_{\beta\neq\alpha=1} \zeta_{\alpha\beta}$$

$$R_{\alpha 0} = \gamma_{\alpha 0}{}^{\dagger(1)} + kT \tag{31}$$

$$\mathbf{j}_\beta = c_\beta(\mathbf{u}_\beta - \mathbf{u}). \tag{32}$$

The coefficients $\zeta_{\alpha\beta}$ appearing in these equations have already been defined in terms of the friction coefficients ζ_α and the quantities $\Lambda_{\alpha\beta}$.

For the case of a binary mixture, with components 1 and 2, the friction coefficients are readily calculated in terms of the integrals Λ_{11}, Λ_{12}, Λ_{22} defined by Eq. (18). It is convenient to introduce the new variables

$$\gamma = \zeta_1/\zeta_2$$

$$\alpha_{11} = m_1c_1\Lambda_{11}; \qquad \alpha_{22} = m_2c_2\Lambda_{22}$$

$$\alpha_{12} = m_{12}c_2\Lambda_{12}; \qquad \alpha_{21} = m_{12}c_1\Lambda_{12}. \tag{33}$$

By substitution of Eqs. (33) into Eqs. (21) and (22), we find

$$\zeta_1 = (\alpha_{11}+\alpha_{12})/\zeta_1 + \alpha_{12}/\zeta_2$$

$$\zeta_2 = (\alpha_{22}+\alpha_{21})/\zeta_2 + \alpha_{21}/\zeta_1. \tag{34}$$

Elimination of ζ_2 between these equations gives

$$\zeta_1{}^2 = (\alpha_{11}+\alpha_{12})(1+\sigma) \tag{35}$$

$$\sigma = \alpha_{12}\tilde{\gamma}/(\alpha_{11}+\alpha_{12}). \tag{36}$$

To evaluate the quantity denoted by $\tilde{\gamma}$ we observe that, from Eqs. (33) and (34),

$$\tilde{\gamma}^2 = \frac{\alpha_{11}+\alpha_{12}+\alpha_{12}\tilde{\gamma}}{\alpha_{22}+\alpha_{21}+\alpha_{21}/\tilde{\gamma}}. \tag{37}$$

Equation (37) is a quadratic equation for $\tilde{\gamma}$ which is conveniently rewritten in the form

$$\sigma^2 - 2\beta_1\sigma - \beta_2 = 0, \tag{38}$$

where

$$\beta_1 = \alpha_{12}{}^2/(\alpha_{11}+\alpha_{12})(\alpha_{22}+\alpha_{21})$$

$$\beta_2 = \alpha_{12}(\alpha_{12}-\alpha_{21})/2(\alpha_{22}+\alpha_{21})(\alpha_{11}+\alpha_{21}). \tag{39}$$

From Eqs. (35), (36), and (38), the friction constant ζ_1 can be calculated in terms of the integrals $\Lambda_{\alpha\beta}$.

The various isothermal diffusion coefficients are, of course, related to the frictional coefficients. For example, the interdiffusion coefficient defined by

$$\mathbf{J}_2 = -D_{21}\nabla c_2 = c_2(\mathbf{u}_2 - \mathbf{u}_1) \tag{40}$$

can be found using Eq. (30). The result is

$$D_{21} = \frac{kT1[+(\partial \ln\gamma_2/\partial \ln c_2)_{T_1P}]}{c_1m_{12}\Lambda_{21}(1/\zeta_1+1/\zeta_2)}. \tag{41}$$

Correspondingly, the self-diffusion coefficient $D_2 = kT/\zeta_2$ can be written as

$$D_2 = \frac{kT}{c_1m_{12}\Lambda_{12}(1/\zeta_1+1/\zeta_2)+c_2m_2\Lambda_{22}/\zeta_2}. \tag{42}$$

For the case of isotopic diffusion, for which $\Lambda_{11} = \Lambda_{12} = \Lambda_{22}$, we have, therefore,

$$D_{21}/D_2 = 1+[m_2c_2\zeta_1/m_{12}c_1(\zeta_1+\zeta_2)]. \tag{43}$$

The coefficients of self-diffusion, D_1 and D_2, are the coefficients measured by a tracer diffusion experiment at the given concentration; the coefficient of mutual diffusion, D_{21}, is defined in Eq. (40).

III. STRESS TENSOR

The intermolecular force contribution to the multicomponent stress tensor was derived by Bearman and Kirkwood,[3] and may be written in the form

$$\mathbf{d}_v = \tfrac{1}{2}\sum_{\beta=1}^{\nu}\sum_{\alpha=1}^{\nu}\int\cdots\int(1/\tau)\int_0^\tau\sum_{k=1}^{N_\beta}\sum_{j=1}^{N_\alpha}\mathbf{R}_{\alpha j\beta k}\nabla_{R\alpha j\beta k}V_{\alpha\beta}(R_{\alpha\beta})$$

$$\times f^{(N)}\delta(\mathbf{R}_{\alpha j}-\mathbf{R}_1)\,\delta(\mathbf{R}_{\beta k}-\mathbf{R}_2)\,ds\,d\mathbf{R}^{(N)}d\mathbf{p}^{(N)}d\mathbf{R}_{\alpha j\beta k}. \tag{44}$$

This general equation may be simplified to

$$\mathbf{d}_v = \tfrac{1}{2}\sum_{\beta=1}^{\nu}\sum_{\alpha=1}^{\nu}(N_\alpha N_\beta/\tau)\int_0^\tau\int\langle \mathbf{R}_{\alpha\beta}\nabla_{R_{\alpha\beta}}V_{\alpha\beta}(R_{\alpha\beta})\rangle^{\alpha,\beta}f_{\alpha\beta}{}^{(2)}$$

$$\times d\mathbf{R}_{\alpha\beta}d\mathbf{p}_\alpha d\mathbf{p}_\beta ds, \tag{45}$$

where, in accord with the previous notation,

$$\langle \mathbf{R}_{\alpha\beta}\nabla_{R_{\alpha\beta}}V_{\alpha\beta}(R_{\alpha\beta})\rangle^{\alpha,\beta}$$

$$= \int\cdots\int\mathbf{R}_{\alpha\beta}\nabla_{R_{\alpha\beta}}V_{\alpha\beta}(R_{\alpha\beta})$$

$$\times f^{(2/N-2)}(\alpha\beta/N-2)\,d\mathbf{p}^{(N-2)}d\mathbf{R}^{(N-2)}. \tag{46}$$

The expression displayed in Eq. (45) may be evaluated using the Taylor series expansion for the gradient of potential of Eq. (8) and the distribution function of Eq. (10). On separating the intermolecular force contribution to the hydrostatic pressure from the

[9] See, for example, R. J. Bearman, J. Chem. Phys. **29**, 1278 (1958), in particular Eqs. (4.12) and (4.13).

remainder of the stress tensor, we then have

$$\mathfrak{d}_v=\mathfrak{d}_v^{(\mathrm{equil})}+\sum_{\alpha=1}^{\nu}\sum_{\beta=1}^{\nu}\frac{N_\alpha N_\beta}{2kT\tau}\int_0^\tau\int[\langle\mathbf{R}_{\alpha\beta}\nabla_{R_{\alpha\beta}}V_{\alpha\beta}\mathbf{p}_{\alpha\beta}\cdot\mathbf{u}_{\alpha\beta}\rangle^{\alpha,\beta}+\langle\Delta\mathbf{R}_{\alpha\beta}\nabla_{R_{\alpha\beta}}V_{\alpha\beta}\mathbf{p}_{\alpha\beta}\cdot\mathbf{u}_{\alpha\beta}\rangle^{\alpha,\beta}+\langle\mathbf{R}_{\alpha\beta}\Delta\mathbf{R}_{\alpha\beta}\cdot\nabla_{R_{\alpha\beta}}\nabla_{R_{\alpha\beta}}V_{\alpha\beta}\mathbf{p}_{\alpha\beta}\cdot\mathbf{u}_{\alpha\beta}\rangle^{\alpha,\beta}]f_{\alpha\beta}^{(2,0)}\times d\mathbf{p}_\alpha d\mathbf{p}_\beta d\mathbf{R}_{\alpha\beta}ds,\quad(47)$$

where terms of the order $(\Delta R_{\alpha\beta})^2$ have been neglected.

To obtain the dissipative terms in the expression for the Newtonian stress tensor, we must now retain the terms of order $\nabla\mathbf{u}$ in the expansion for $\mathbf{u}_{\alpha\beta}$. That is to say, we write for $\mathbf{u}_{\alpha\beta}$ the first two terms in the Taylor series expansion[10]

$$\mathbf{u}_{\alpha\beta}=\mathbf{u}_\beta(\mathbf{R}_\alpha)-\mathbf{u}_\alpha(\mathbf{R}_\alpha)+\mathbf{R}_{\alpha\beta}\cdot\nabla_{R_{\alpha\beta}}\mathbf{u}.\quad(48)$$

On using the definition of the diffusion tensor, Eq. (15), the relation in Eq. (48), and the identity

$$\nabla_{R_{\alpha\beta}}\nabla_{R_{\alpha\beta}}V_{\alpha\beta}=\mathbf{e}_{R_{\alpha\beta}}\mathbf{e}_{R_{\alpha\beta}}(V_{\alpha\beta}''-V_{\alpha\beta}'/R_{\alpha\beta})+(V_{\alpha\beta}'/R_{\alpha\beta})\mathbf{1},\quad(49)$$

where the prime refers to differentiation with respect to $R_{\alpha\beta}$ and $\mathbf{e}_{\alpha\beta}$ is a unit vector pointing along $\mathbf{R}_{\alpha\beta}$, the expression for the stress tensor is transformed to the relation

$$\mathfrak{d}_v=\mathfrak{d}_v^{(\mathrm{equil})}+\sum_{\alpha=1}^{\nu}\sum_{\beta=1}^{\nu}\frac{m_{\alpha\beta}(D_\alpha+D_\beta)N_\alpha N_\beta}{2kTv^2}\int\mathbf{R}_{\alpha\beta}\mathbf{R}_{\alpha\beta}\cdot\nabla\mathbf{u}\cdot[\mathbf{e}_{R_{\alpha\beta}}\mathbf{e}_{R_{\alpha\beta}}(V_{\alpha\beta}''-V_{\alpha\beta}'/R_{\alpha\beta})+2(V_{\alpha\beta}'/R_{\alpha\beta})\mathbf{1}]g_{\alpha\beta}^{(2,0)}d^3R_{\alpha\beta}.\quad(50)$$

The Newtonian stress tensor can be written in the form

$$\mathfrak{d}=-p\mathbf{1}+2\eta[\dot{\boldsymbol{\epsilon}}-\tfrac{1}{3}\nabla\cdot\mathbf{u}\mathbf{1}]+\phi\nabla\cdot\mathbf{u}\mathbf{1},\quad(51)$$

with η and ϕ the coefficients of shear and bulk viscosity, respectively, and $\dot{\boldsymbol{\epsilon}}$ the rate of strain tensor. By writing $\mathbf{R}_{\alpha\beta}$, $\mathbf{e}_{R_{\alpha\beta}}$, and $\nabla\mathbf{u}$ in spherical polar coordinates and integrating over angles, it is found that the stress tensor in Eq. (50) can be written as the sum of partial stress tensors,

$$\mathfrak{d}_v=\sum_\alpha\mathfrak{d}_{v\alpha},\quad(52a)$$

where

$$\mathfrak{d}_{v\alpha}=-p_\alpha\mathbf{1}+2\eta_\alpha[\dot{\boldsymbol{\epsilon}}-\tfrac{1}{3}\nabla\cdot\mathbf{u}\mathbf{1}]+\phi_\alpha\nabla\cdot\mathbf{u}\mathbf{1},\quad(52b)$$

and

$$\eta_\alpha=\sum_\beta(m_{\alpha\beta}/30)(1/\zeta_\alpha+1/\zeta_\beta)c_\alpha c_\beta\int R_{\alpha\beta}^2\times(V_{\alpha\beta}''+4V_{\alpha\beta}'/R_{\alpha\beta})g_{\alpha\beta}^{(2,0)}(R_{\alpha\beta})d^3R_{\alpha\beta}\quad(53)$$

$$\phi_\alpha=\sum_\beta(m_{\alpha\beta}/18)(1/\zeta_\alpha+1/\zeta_\beta)c_\alpha c_\beta\int R_{\alpha\beta}^2\times(V_{\alpha\beta}''+V_{\alpha\beta}'/R_{\alpha\beta})g_{\alpha\beta}^{(2,0)}(R_{\alpha\beta})d^3R_{\alpha\beta}.\quad(54)$$

Note that in the limit of the one-component system, Eqs. (53) and (54) reduce to the corresponding formulas given by Rice and Kirkwood.[1]

IV. THERMAL CONDUCTIVITY

Bearman and Kirkwood[3] have shown that the intermolecular force contribution to the heat flux in a multicomponent system has the form

$$\mathbf{q}_v=\tfrac{1}{2}\sum_{\alpha=1}^{\nu}\sum_{\beta=1}^{\nu}\int(1/\tau)\int_0^\tau[V_{\alpha\beta}(R_{\alpha\beta})\mathbf{1}-\mathbf{R}_{\alpha\beta}\nabla_{R_{\alpha\beta}}V_{\alpha\beta}]\cdot[\sum_{i=1}^{N_\alpha}\sum_{j=1}^{N_\beta}\langle(\mathbf{p}_{i\alpha}/m_\alpha)\delta(\mathbf{R}_{i\alpha}-\mathbf{R}_1)\delta(\mathbf{R}_{j\beta}-\mathbf{R}_2);f^{(N)}\rangle-\mathbf{u}\langle\delta(\mathbf{R}_{i\alpha}-\mathbf{R}_1)\delta(\mathbf{R}_{j\beta}-\mathbf{R}_2);f^{(N)}\rangle]d\mathbf{R}_{\alpha\beta}ds-\sum_\alpha\mathbf{j}_\alpha\bar{H}_\alpha.\quad(55)$$

Here $\bar{H}_\alpha$ is the partial molecular enthalpy of component α. In the following, we shall neglect the kinetic contribution to the heat flux since it is small relative to the intermolecular force contribution. To evaluate Eq. (55), we rewrite it in the following form:

$$\mathbf{q}_v=\tfrac{1}{2}\sum_{\alpha=1}^{\nu}\sum_{\beta=1}^{\nu}\int(N_\alpha N_\beta/\tau)\int_0^\tau\langle[V_{\alpha\beta}\mathbf{1}-\mathbf{R}_{\alpha\beta}\nabla V_{\alpha\beta}]\cdot(\mathbf{p}_{1\alpha}/m_\alpha-\mathbf{u})\delta(\mathbf{R}_{2\beta}-\mathbf{R}_2)\rangle^{\alpha,\beta}\times f_{\alpha\beta}^{(2)}d\mathbf{p}_{1\alpha}d\mathbf{p}_{2\beta}d\mathbf{R}_{\alpha\beta}d\mathbf{R}_{2\beta}ds.\quad(56)$$

The symbols $\mathbf{p}_{1\alpha}$ and $\mathbf{p}_{2\beta}$ refer, respectively, to particles of species α and β with momenta $\mathbf{p}_1$ and $\mathbf{p}_2$. The Dirac delta function may be expanded as a Taylor series in the displacement $\Delta\mathbf{R}_{1\alpha}(s)$ of the particle with unspecified position (i.e., not fixed).

$$\delta(\mathbf{R}_{2\beta}(t+s)-\mathbf{R}_2)=\delta(\mathbf{R}_{2\beta}(t)-\mathbf{R}_2)+\Delta\mathbf{R}_{1\alpha}(s)\cdot\nabla_{R_{1\alpha}}\delta(\mathbf{R}_{2\beta}(t)-\mathbf{R}_2)+\cdots.\quad(57)$$

Consider first the contribution from the first term of this Taylor series expansion when (57) is substituted into Eq. (56). On using the expansion for the gradient of the pair potential given in Eq. (8) and neglecting terms of the order of $(\Delta R_{\alpha\beta})^2$, this is

$$\tfrac{1}{2}\sum_{\alpha=1}^{\nu}\sum_{\beta=1}^{\nu}\int(N_\alpha N_\beta/\tau)\int_0^\tau\langle(V_{\alpha\beta}+\Delta\mathbf{R}_{\alpha\beta}\cdot\nabla V_{\alpha\beta})\mathbf{1}-(\mathbf{R}_{\alpha\beta}\nabla V_{\alpha\beta}+\mathbf{R}_{\alpha\beta}\Delta\mathbf{R}_{\alpha\beta}\cdot\nabla\nabla V_{\alpha\beta}+\Delta\mathbf{R}_{\alpha\beta}\nabla V_{\alpha\beta})(\mathbf{p}_{\alpha\beta}/m_{\alpha\beta})\rangle^{\alpha,\beta}f_{\alpha\beta}^{(2)}d\mathbf{p}_{\alpha\beta}d\mathbf{R}_{\alpha\beta}ds.\quad(58)$$

[10] Note that in using this expansion we are making use of the fact that a measurement of the viscosity of a mixture treats the mixture as a homogeneous fluid for the purposes of hydrodynamics, i.e., there is for the mixture a stress tensor with a single shear viscosity, and the relevant variable is the gradient of bulk velocity, etc.

On using the distribution function displayed in Eq. (24), and the definition of the pair diffusion tensor, Eq. (16), the expression reduces (neglecting terms which vanish on integration) to

$$-\tfrac{1}{2}\sum_{\alpha=1}^{\nu}\sum_{\beta=1}^{\nu}N_\alpha N_\beta\int\mathbf{D}_{\alpha\beta}{}^{(2)}[\mathbf{R}_{\alpha\beta}\cdot\nabla\nabla V_{\alpha\beta}+2\nabla V_{\alpha\beta}]f_{\alpha\beta}{}^{(2)}d\mathbf{p}_{\alpha\beta}d\mathbf{R}_{\alpha\beta}$$

$$=-\sum_{\alpha=1}^{\nu}\sum_{\beta=1}^{\nu}N_\alpha N_\beta(D_\alpha/3)\int R_{\alpha\beta}{}^2\nabla^2V_{\alpha\beta}(\partial/\partial T)\,(g_{\alpha\beta}{}^{(2,0)}/v^2)d^3R_{\alpha\beta}\nabla T. \quad (59)$$

The contribution from the second term of the Taylor series' expansion for $\delta(\mathbf{R}_{2\beta}-\mathbf{R}_2)$ is

$$\sum_\alpha\sum_\beta(N_\alpha N_\beta/2\tau)\int(1/\tau)\int_0^\tau\langle[V_{\alpha\beta}\mathbf{1}-\mathbf{R}_{\alpha\beta}\nabla V_{\alpha\beta}]\cdot[(p_{1\alpha}/m_\alpha)-\mathbf{u}]$$

$$\times\Delta\mathbf{R}_{1\alpha}(s)\cdot\nabla_{R1\alpha}\delta(\mathbf{R}_{2\beta}-\mathbf{R}_2)\,\rangle^{\alpha,\beta}f_{\alpha\beta}{}^{(2)}d\mathbf{p}_{1\alpha}d\mathbf{p}_{2\beta}d\mathbf{R}_{\alpha\beta}d\mathbf{R}_{2\beta}ds. \quad (60)$$

We now expand $\nabla V_{\alpha\beta}$, $V_{\alpha\beta}$, and $\mathbf{R}_{\alpha\beta}$ in Taylor series in $\Delta\mathbf{R}_{\alpha\beta}$ as before, and neglect terms of the order $\Delta\mathbf{R}_{\alpha\beta}\Delta\mathbf{R}_{1\alpha}$. On using the Einstein relation for the singlet diffusion coefficient[11]

$$\langle\Delta\mathbf{R}_{1\alpha}\Delta\mathbf{R}_{1\alpha}\rangle/2\tau=D_\alpha\mathbf{1}, \quad (61)$$

the expression simplifies, after an integration over angles, to

$$\sum_\alpha\sum_\beta N_\alpha N_\beta D_\alpha\nabla\int(V_{\alpha\beta}-\tfrac{1}{3}R_{\alpha\beta}V_{\alpha\beta}')\,(g_{\alpha\beta}{}^{(2,0)}/v^2)d^3R_{\alpha\beta}. \quad (62)$$

Terms arising from the perturbation of the distribution function by the temperature gradient have been neglected.

Equations (59) and (62) give the contribution to the heat flux in the steady state. In the presence of mass transport, additional terms arise from the perturbation of the distribution function in the manner described in Eq. (10). On retaining only the first term from the expansion of $\delta(\mathbf{R}_{2\beta}-\mathbf{R}_2)$ in the expression for the heat flux, Eq. (56), the terms arising from the perturbation to the distribution function indicated in Eq. (10) are

$$\tfrac{1}{2}\sum_{\alpha=1}^{\nu}\sum_{\beta=1}^{\nu}\int(N_\alpha N_\beta/\tau)\int_0^\tau\langle[V_{\alpha\beta}\mathbf{1}-\mathbf{R}_{\alpha\beta}\nabla V_{\alpha\beta}]\cdot[(\mathbf{p}_{1\alpha}/m_\alpha)-\mathbf{u}]$$

$$\times\delta(\mathbf{R}_{2\beta}-\mathbf{R}_2)\,\rangle^{\alpha,\beta}f_{\alpha\beta}{}^{(2,0)}[(\mathbf{p}_{\alpha\beta}\cdot\mathbf{u}_{\alpha\beta})/kT]d\mathbf{p}_{\alpha\beta}d\mathbf{R}_{\alpha\beta}d\mathbf{R}_{2\beta}ds. \quad (63)$$

Again expanding $\nabla V_{\alpha\beta}$, $V_{\alpha\beta}$, and $\mathbf{R}_{\alpha\beta}$ in Taylor series' and retaining only the first terms arising from the time dependence of $\mathbf{p}_{\alpha\beta}$, the expression reduces to

$$\tfrac{1}{2}\sum_\alpha\sum_\beta(N_\alpha N_\beta\mathbf{u}_\alpha/m_{\alpha\beta}kT)\int[V_{\alpha\beta}\mathbf{1}-\mathbf{R}_{\alpha\beta}\nabla V_{\alpha\beta}]\cdot\mathbf{p}_{\alpha\beta}\mathbf{p}_{\alpha\beta}f_{\alpha\beta}{}^{(2,0)}d\mathbf{p}_{\alpha\beta}d\mathbf{R}_{\alpha\beta}. \quad (64)$$

Performing the integration over relative momentum and integrating the resultant expression over angles, leads to the final result

$$\tfrac{1}{2}\sum_\alpha\sum_\beta(N_\alpha N_\beta/v^2)\,\mathbf{u}_\alpha\int[V_{\alpha\beta}-(R_{\alpha\beta}/3)\,V_{\alpha\beta}']g_{\alpha\beta}{}^{(2,0)}d^3R_{\alpha\beta}. \quad (65)$$

With the convenient definition

$$h_{\alpha\beta}=h_{\beta\alpha}=\tfrac{1}{2}\int[V_{\alpha\beta}-(R_{\alpha\beta}/3)\,V_{\alpha\beta}']g_{\alpha\beta}{}^{(2,0)}d^3R_{\alpha\beta}, \quad (66)$$

the total heat flux is found from Eqs. (59), (62), and (65) to be[12]

$$\mathbf{q}_v=\sum_{\alpha=1}^{\nu}Q_\alpha{}^*\mathbf{j}_\alpha-\tfrac{1}{3}\sum_\alpha\sum_\beta N_\alpha N_\beta D_\alpha\int R_{\alpha\beta}{}^2\nabla^2V_{\alpha\beta}[(\partial/\partial T)\,(g_{\alpha\beta}{}^{(2,0)}/v^2)]_p d^3R_{\alpha\beta}\nabla T$$

$$+\sum_\alpha\sum_\beta 2N_\alpha N_\beta D_\alpha[(\partial/\partial T)\,(h_{\alpha\beta}/v^2)]_p\nabla T, \quad (67)$$

[11] The factor 2 is used in place of 6 because these displacements are constrained by the condition that the relative position of particles one and two is fixed.

[12] This result differs negligibly from the corresponding heat flux in a pure fluid. The very small difference which persists in the pure component limit arises from the multiplication of a large number of Taylor expansions. The number of expansions needed in the multicomponent case greatly exceeds that used in the one component case.

where

$$Q_\alpha^* = \sum_\beta c_\beta h_{\alpha\beta} - \bar{H}_\alpha. \tag{68}$$

It is convenient to separate the temperature and concentration dependence of the terms by writing Eq. (67) in the form

$$\mathbf{q}_v = \sum_\alpha Q_\alpha^* \mathbf{j}_\alpha - \kappa \nabla T - \sum_{\sigma=2} (\Omega_{0\sigma}' - \Omega_{01}') \nabla x_\sigma, \tag{69}$$

where

$$\kappa = \sum_\alpha \sum_\beta D_\alpha (\partial I_{\alpha\beta}/\partial T)_{x_\sigma, p} - \sum_\alpha \sum_\beta D_\alpha (\partial J_{\alpha\beta}/\partial T)_{x_\sigma, p}$$

$$\Omega_{0\sigma}' = \sum_\alpha \sum_\beta D_\alpha (\partial I_{\alpha\beta}/\partial x_\sigma)_{T,p} - \sum_\alpha \sum_\beta D_\alpha (\partial J_{\alpha\beta}/\partial x_\sigma)_{T,p}. \tag{70}$$

As usual, x_σ is the mole fraction of component σ, and the integrals $I_{\alpha\beta}$, $J_{\alpha\beta}$ are defined as

$$I_{\alpha\beta} = (c_\alpha c_\beta/3) \int R_{\alpha\beta}^2 \nabla^2 V_{\alpha\beta} g_{\alpha\beta}^{(2,0)} d^3 R_{\alpha\beta}$$

$$J_{\alpha\beta} = 2 c_\alpha c_\beta h_{\alpha\beta}. \tag{71}$$

Now,

$$\nabla \mu_\alpha = \sum_{\sigma=2} (\partial \mu_\alpha/\partial x_\sigma)_{p,T,x_\gamma} \nabla x_\sigma, \tag{72}$$

which may be written as

$$\nabla x_\sigma = \sum_{\alpha=2} (\Delta_{\sigma\alpha}/\Delta) \nabla \mu_\alpha, \tag{73}$$

with Δ the determinant with elements $(\partial \mu_\alpha/\partial x_\sigma)_{p,T,x_\gamma}$ and $\Delta_{\sigma\alpha}$ the cofactor of the σ, αth element. The last term of Eq. (69) can, therefore, be written in the form

$$\sum_{\sigma=2} (\Omega_{0\sigma}' - \Omega_{01}') \nabla x_\sigma = \sum_{\alpha=2} \tilde{\Omega}_{0\alpha} \nabla \mu_\alpha, \tag{74}$$

with

$$\tilde{\Omega}_{0\alpha} = \sum_m \sum_n D_m \sum_{\sigma=2} (\Delta_{\sigma\alpha}/\Delta) [(\partial I_{mn}'/\partial x_\sigma)_{p,T} - (\partial I_{mn}'/\partial x_1)_{p,T}]$$

$$I_{mn}' = I_{mn} - J_{mn}. \tag{75}$$

The discussion will now be restricted to a system of two components in which there is zero pressure gradient. In this case we have

$$\tilde{\Omega}_{02} \nabla \mu_2 = 2x_2 [D_1 [(\partial I_{11}'/\partial x_2)_{p,T} + (\partial I_{12}'/\partial x_2)_{p,T}] + D_2 [(\partial I_{21}'/\partial x_2)_{p,T} + (\partial I_{22}'/\partial x_2)_{p,T}]] \nabla \mu_2/kT [1 + (\partial \ln f_2/\partial \ln x_2)_{p,T}]. \tag{76}$$

When we consider the special case of regular solutions for which $g_{\alpha\beta}^{(2,0)}$ may be taken as independent of concentration, the differentiations may be carried out, giving

$$\tilde{\Omega}_{02} \nabla \mu_2 = \frac{4x_2(\bar{v}_1 - \bar{v}_2)[D_1(I_{11}' + I_{12}') + D_2(I_{21}' + I_{22}')] \nabla \mu_2}{\bar{v} kT [1 + (\partial \ln f_2/\partial \ln x_2)_{p,T}]}, \tag{77}$$

with $\bar{v}_1$ and $\bar{v}_2$ the partial molecular volumes of components one and two, respectively, and $\bar{v}$ the mean molecular volume. The heat flux in the steady state ($\mathbf{j}_\alpha = 0$) can be found by substitution of Eq. (77) into Eq. (69), followed by the elimination of the gradient of chemical potential by means of Eq. (30). The coefficient of thermal conductivity defined by

$$\mathbf{q}_v = -\kappa_v \nabla T \tag{78}$$

is found to be

$$\kappa_v = D_1 [(\partial I_{11}'/\partial T)_{p,x_\sigma} + (\partial I_{12}'/\partial T)_{p,x_\sigma}] + D_2 [(\partial I_{21}'/\partial T)_{p,x_\sigma} + (\partial I_{22}'/\partial T)_{p,x_\sigma}] - \frac{4x_2(\bar{v}_1 - \bar{v}_2)[D_1(I_{11}' + I_{12}') + D_2(I_{21}' + I_{22}')] R_{20}}{\bar{v} kT^2 [1 + (\partial \ln f_2/\partial \ln x_2)_{p,T}]} \tag{79}$$

$$R_{20} = (2T/c_2)(\partial p_2/\partial T)_{c_\gamma, p} - kT$$

$$R_{20} = 2pT v_2 (2\alpha_2^E - \alpha^E) + (kT/\bar{v}) x_1 (v_1 - v_2) - kT - (kT^2 x_1/\bar{v}) [2\alpha^E (v_1 - v_2) + (\alpha_1^E + \alpha_2^E)(v_2 - v_1) + (v_2 \alpha_2^E - v_1 \alpha_1^E)], \tag{80}$$

and $\alpha^E = \bar{v}^{-1} (\partial \bar{v}/\partial T)_{p,x}$ is the coefficient of thermal expansion.

We emphasize that in this section we have calculated only the intermolecular force constribution to the thermal conductivity and the heat of transport.

V. THERMAL DIFFUSION FACTOR

The thermal diffusion factor for a binary mixture, defined by the relation

$$\nabla x_1 - \alpha x_1 x_2 \nabla \ln T = 0, \tag{81}$$

can be calculated in a manner analogous to that discussed above. In the steady state the flux equation, Eq. (30), gives

$$\nabla_T\mu_1+R_{10}\nabla\ln T=0. \tag{82}$$

In the absence of a pressure gradient, we also have

$$\nabla_T\mu_1=(\partial\mu_1/\partial x_1)_{T,p}\nabla x_1-(\bar{v}_1\alpha^E T/\beta)\nabla\ln T$$
$$\alpha^E=(1/\bar{v})(\partial\bar{v}/\partial T)_{p,x_1},\qquad \beta=-(1/\bar{v})(\partial\bar{v}/\partial p)_{T,x_1}. \tag{83}$$

On combining Eqs. (81)–(83), the thermal diffusion factor is found to be

$$\alpha=[(\bar{v}_1\alpha^E T/\beta)-R_{10}]/x_2kT[1+(\partial\ln f_2/\partial\ln x_2)_{T,p}], \tag{84}$$

and from Eqs. (26) and (31)

$$R_{10}=(2/c_1)(\partial p_1/\partial\ln T)_{c_1c_2p}-kT. \tag{85}$$

Once more the result may be simplified by the introduction of the hypothesis of regular solution theory, that the volumes of the components are additive and that the radial distribution functions are independent of composition at constant temperature and pressure. From the definition of partial pressure, Eq. (24), we have

$$p_1=x_1(x_1p_{11}+x_2p_{12})$$
$$p_{11}=kT/v-(1/6v^2)\int R_{11}V_{11}'g_{11}^{(2,0)}d^3R_{11}$$
$$p_{12}=kT/v-(1/6v^2)\int R_{12}V_{12}'g_{12}^{(2,0)}d^3R_{12} \tag{86}$$
$$v=x_1v_1+x_2v_2. \tag{87}$$

The set of equations (86) and (87) has the solution

$$p_{\alpha\beta}-kT/v=(v_\alpha v_\beta/v^2)[p-(kT/2)(1/v_\alpha+1/v_\beta)], \tag{88}$$

where α, $\beta=1$, 2. From Eqs. (88) and the expression for the total pressure

$$p=x_1^2p_{11}+2x_1x_2p_{12}+x_2^2p_{22}, \tag{89}$$

it is found that

$$p_1=\frac{x_1pv_1}{v}+\frac{kTx_1x_2(v_2-v_1)}{2v^2}. \tag{90}$$

By differentiation of Eq. (90) with respect to temperature and combination with Eqs. (84) and (85), the thermal diffusion factor is found to be

$$\alpha=\Bigg[\frac{\bar{v}_1\alpha^E}{\beta}-2pv_1(2\alpha_1^E-\alpha^E)+\frac{kx_2}{v}(v_2-v_1)-k-\frac{kTx_2}{v}\{2\alpha^E(v_2-v_1)-(v_2\alpha_2^E-v_1\alpha_1^E)-(\alpha_1^E+\alpha_2^E)(v_2-v_1)\}\Bigg]\Bigg/x_2k\left[1+\left(\frac{\partial\ln f_1}{\partial\ln x_1}\right)_{T,p}\right]. \tag{91}$$

VI. CONCENTRATION DEPENDENCE OF THE TRANSPORT COEFFICIENTS AND THE RELATION TO THERMODYNAMIC PROPERTIES

In this section, we discuss the relationship of the coefficients of shear viscosity and thermal conductivity to the thermodynamic properties of the mixture and pure components, and also the concentration dependence of the transport coefficients. We consider first the coefficient of shear viscosity for a binary mixture. From Eq. (53) this can be written in the form

$$\eta=(v_1^*/v)^2\eta_1^*+(v_2^*/v)^2\eta_2^*+2(v_1^*v_2^*/v^2)\eta_{12}^*, \tag{92}$$

where

$$\eta_1^*=\frac{m_1D_1}{30kT}(N_1/v_1^*)^2\int R_{11}^2(V_{11}''+4V_{11}'/R_{11})g_{11}^{(2,0)}d^3R_{11}$$
$$\eta_2^*=\frac{m_2D_2}{30kT}(N_2/v_2^*)^2\int R_{22}^2(V_{22}''+4V_{22}'/R_{22})g_{22}^{(2,0)}d^3R_{22}$$
$$\eta_{12}^*=\frac{m_{12}(D_1+D_2)}{30kT}\frac{N_1N_2}{v_1^*v_2^*}\int R_{12}^2\left(V_{12}''+\frac{4V_{12}'}{R_{12}}\right)g_{12}^{(2,0)}d^3R_{12}, \tag{93}$$

with v_1^* and v_2^* the volumes of N_1 molecules of component one and of N_2 molecules of component two, respectively, at the same temperature and pressure as the mixture.

Note that Eq. (93) predicts a volume fraction mixing relation rather than the more usual mole fraction mixing relations. The quantities η_1^*, η_2^*, and η_{12}^* are, however, not independent of concentration, so this is not a simple rule for the viscosity of mixtures. Only for an ideal solution is a simple volume fraction mixing predicted. In the case of a regular solution, the concentration dependence of η_1^*, η_2^*, and η_{12}^* arises only from the concentration dependence of the self-diffusion coefficients in the mixture. Let η_1^0, D_1^0 and η_2^0, D_2^0 denote the transport coefficients in the pure fluids one and two, respectively, so that

$$\eta_1^*=\eta_1^0[1+(\Delta D_1/D_1^0)],$$
$$\eta_2^*=\eta_2^0[1+(\Delta D_2/D_2^0)], \tag{94}$$

where

$$\Delta D_1=D_1-D_1^0,\qquad \Delta D_2=D_2-D_2^0. \tag{95}$$

It will be convenient to relate the viscosity of the mixture to the thermodynamic properties of the mixture and the pure components. To this end, we assume that the pair potentials are of the Lennard-Jones form

$$V_{\alpha\beta}(R_{\alpha\beta})=4\epsilon_{\alpha\beta}[(a_{\alpha\beta}/R_{\alpha\beta})^{12}-(a_{\alpha\beta}/R_{\alpha\beta})^6]. \tag{96}$$

With the definition

$$B_m^{(\alpha,\beta)}=4\epsilon_{\alpha\beta}\frac{N_\alpha N_\beta}{(v_\alpha^*v_\beta^*)^{\frac{1}{2}}}\int(a_{\alpha\beta}/R_{\alpha\beta})^m g_{\alpha\beta}^{(2,0)}d^3R_{\alpha\beta}, \tag{97}$$

the set of Eqs. (93) may be reduced to

$$\eta_1^*=\frac{3m_1D_1}{5kTv_1^*}(6B_{12}^{(11)}-B_6^{(11)})$$
$$\eta_2^*=\frac{3m_2D_2}{5kTv_2^*}(6B_{12}^{(22)}-B_6^{(22)})$$
$$\eta_{12}^*=\frac{3m_{12}(D_1+D_2)}{5kT(v_1^*v_2^*)^{\frac{1}{2}}}(6B_{12}^{(12)}-B_6^{(12)}). \tag{98}$$

The energy of the fluid L, which is related to the pair distribution function by

$$L=-\sum_{\alpha}\sum_{\beta}(N_\alpha N_\beta/2v)\int V_{\alpha\beta}g_{\alpha\beta}^{(2,0)}d^3R_{\alpha\beta}, \tag{99}$$

can be written

$$L=\sum_{\alpha}\sum_{\beta}(v_\alpha^*v_\beta^*/4v^2)^{\frac{1}{2}}(B^{(\alpha\beta)}-B_{12}^{\alpha\beta}). \tag{100}$$

Similarly, from Eq. (27) for the partial pressures, we have

$$kT-pv=\sum_{\alpha}\sum_{\beta}(v_\alpha^*v_\beta^*/v^2)^{\frac{1}{2}}(B_6^{(\alpha\beta)}-2B_{12}^{(\alpha\beta)}). \tag{101}$$

For a binary mixture it is found, from Eqs. (99) and (100), that

$$2(v_1^*v_2^*/v^2)^{\frac{1}{2}}B_{12}^{(12)}=2L+pv-kT-(v_1^*/v)B_{12}^{(11)}-(v_2^*/v)B_{12}^{(22)}$$

$$2(v_1^*v_2^*/v^2)^{\frac{1}{2}}B_6^{(12)}=4L+pv-kT-(v_1^*/v)B_6^{(11)}-(v_2^*/v)B_6^{(22)}, \tag{102}$$

whereas for the pure components we have

$$B_{12}^{(11)}=2L_1+pv_1^*-kT$$

$$B_6^{(11)}=4L_1+pv_1^*-kT, \tag{103}$$

with L_1 the energy of the pure fluid one, and similar relations hold for component two. Equations (102) and (103) may be used to eliminate the integrals $B_m^{(\alpha,\beta)}$ and express the viscosity solely in terms of the diffusion coefficients and the thermodynamic properties of the mixture and components. The result is

$$\eta=(3m_1v_1^*/5kTv^2)[8L_1+5pv_1^*-5kT]\left[D_1-(v_1^*v_2^*/v^2)^{\frac{1}{2}}\frac{m_2(D_1+D_2)}{(m_1+m_2)}\right]$$

$$+(3m_2v_2^*/5kTv^2)[8L_2+5pv_2^*-5kT]\left[D_2-(v_1^*v_2^*/v^2)^{\frac{1}{2}}\frac{m_1(D_1+D_2)}{(m_1+m_2)}\right]$$

$$+\frac{3m_{12}(D_1+D_2)}{5kTv}[8L+5pv-5kT](v_1^*v_2^*/v^2)^{\frac{1}{2}}. \tag{104}$$

A parallel treatment may be made of the thermal conductance, although the equations are somewhat cumbersome. For a regular solution, the coefficient of thermal conductance is given by Eq. (79). The integrals $I_{\alpha\beta}'$ appearing therein may be written for the case of the Lennard-Jones potential function as

$$I_{\alpha\beta}'=[(v_\alpha^*v_\beta^*)^{\frac{1}{2}}/3v^2](165B_{12}^{\alpha\beta}-53B_6^{\alpha\beta}). \tag{105}$$

For a binary mixture elimination of the integrals $B_m^{(\alpha,\beta)}$ in terms of thermodynamic functions leads to

$$\kappa_v=\frac{D_1}{3v}\Bigg[-\alpha^E\Bigg\{118\left(L-\frac{v_2^*L_2}{v}\right)+112pv[1-(v_2/v)^2]$$

$$-112kT\left(1-\frac{v_2^*}{v}\right)\Bigg\}+118\left\{(\partial L/\partial T)_p-(v_2^*/v)(\partial L_2/\partial T)_p-\frac{L_2v_2^*}{v}(\alpha_2^E-\alpha^E)\right\}$$

$$+112pv\{\alpha^E[1+(v_2^*/v)^2]-2(v_2^*/v)^2\alpha_2^E\}-112k\{1-(v_2^*/v)-(Tv_2^*/v)(\alpha_2^E-\alpha)\}\Bigg]$$

$$+\frac{D_2}{3v}\Bigg[-\alpha^E\Bigg\{118\left(L-\frac{v_1^*L_1}{v}\right)+112pv[1-(v_1/v)^2]$$

$$-112kT\left(1-\frac{v_1^*}{v}\right)+118\left\{\left(\frac{\partial L}{\partial T}\right)_p-\frac{v_1^*}{v}\left(\frac{\partial L_1}{\partial T}\right)_p-\frac{L_1v_1^*}{v}(\alpha_1^E-\alpha^E)\right\}$$

$$+112pv\left\{\alpha^E\left(1-\frac{v_1^*}{v}\right)-\frac{Tv_1^*}{v}(\alpha_1^E-\alpha)\right\}\Bigg]-\frac{4x_2(v_1^*-v_2^*)R_{20}}{vkT^2[1+(\partial\ln f_2/\partial\ln x_2)_{T,p}]}\Bigg[\frac{D_1}{3v}\Bigg\{118\left(L-\frac{v_2^*L_2}{v}\right)$$

$$+112p\left(v-\frac{v_2^{*2}}{v}\right)-112kT\left(1-\frac{v_2^*}{v}\right)\Bigg\}+\frac{D_2}{3v}\Bigg\{118\left(L-\frac{v_1^*L_1}{v}\right)+112p\left(v-\frac{v_1^{*2}}{v}\right)-112kT\left(1-\frac{v_1^*}{v}\right)\Bigg\}\Bigg], \tag{106}$$

with R_{20} defined by Eq. (80).

VII. COMPARISON OF THEORY AND EXPERIMENT

The comparison of theory and experiment is severely handicapped by the lack of suitable data. In order to make use of the meager data available, the relationships between the transport coefficients and other properties must be further reduced by use of suitable approximations. In particular, from the principle of corresponding states we find

$$\frac{B_m^{(\alpha,\beta)}}{B_m^{(\alpha,\alpha)}}=\left(\frac{\epsilon_{\beta\beta}}{\epsilon_{\alpha\alpha}}\right)^{\frac{1}{2}}\frac{x_\beta}{x_\alpha}\left(\frac{v_\alpha^*}{v_\beta^*}\right)^{\frac{1}{2}}\left(\frac{a_{\alpha\beta}}{a_{\alpha\alpha}}\right)^3, \tag{107}$$

where we have also set

$$\epsilon_{\alpha\beta}=(\epsilon_{\alpha\alpha}\epsilon_{\beta\beta})^{\frac{1}{2}}. \tag{108}$$

With the use of Eqs. (107) and (108), Eq. (92) may be reduced to the form

$$\eta=\left(\frac{v_1^*}{v}\right)^2\eta_1^0\left[1+\frac{2m_2}{m_1+m_2}\left(\frac{\epsilon_{22}}{\epsilon_{11}}\right)^{\frac{1}{2}}\frac{x_2}{x_1}\left(\frac{a_{12}}{a_{11}}\right)^3\right]\left[1+\frac{\Delta D_1}{D_1^0}\right]+\left(\frac{v_2^*}{v}\right)^2\eta_2^0\left[1+\frac{2m_1}{m_1+m_2}\left(\frac{\epsilon_{11}}{\epsilon_{22}}\right)^{\frac{1}{2}}\frac{x_1}{x_2}\left(\frac{a_{12}}{a_{22}}\right)^3\right]\left[1+\frac{\Delta D_2}{D_2^0}\right]. \tag{109}$$

The results obtained in this paper may here be briefly summarized. Expressions for the diffusion coefficients [Eqs. (40)–(43)], coefficients of viscosity [Eqs. (53) and (54)], thermal conductivity [Eq. (67)], heat of transport [Eq. (68)], and thermal diffusion factor [Eq. (84)], were derived in terms of molecular parameters. For the case of regular solutions, simplified expressions for the thermal conductivity [Eq. (79)] and thermal diffusion factor [Eq. (91)] were derived, the latter expression being particularly suitable for comparison with experiment. For the coefficients of shear viscosity and thermal conductivity, the expressions most suitable for comparison with experiment are those [Eqs. (104) and (106), respectively] relating the coefficients to thermodynamic properties of the mixture and pure components and to the diffusion coefficients. Since sufficient thermodynamic data are not always available for such a comparison, it was shown how the formula for shear viscosity may be simplified by means of a corresponding states argument to relate the viscosity of the mixture to that of the pure components, the coefficients of self-diffusion, and the Lennard-Jones potential constants of the pure components [Eq. (109)].

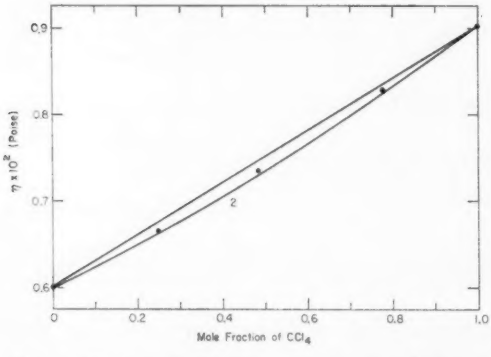

FIG. 1. Viscosity of mixtures of carbon tetrachloride and benzene as function of mole fraction of carbon tetrachloride.

The concentration dependence of the viscosity of a binary mixture predicted by Eq. (109) was tested for the system carbon tetrachloride-benzene. The molar volumes at 25°C were obtained from Wood and Brusie[13] and were assumed to be additive. Self-diffusion coefficients were obtained from the data of Graupner and Winter[14] and of Watts, Alder, and Hildebrand;[15] and mutual diffusion coefficients at infinite dilution from the data of Caldwell and Babb.[16] At infinite dilution, the mutual diffusion coefficient approaches the self-diffusion coefficient for the species present in vanishingly small concentration. The plot of the self-diffusion coefficient versus composition has been shown by Johnson and Babb[17] to be nearly linear for carbon tetrachloride at 25°C. It was assumed that the relationship was linear for both carbon tetrachloride and benzene at 25°C. The viscosity data were taken from the work of Grunberg.[18] The Lennard-Jones potential parameters used were the values given by Hirschfelder, Curtiss, and Bird.[19]

The observed values of the viscosity and those calculated from Eq. (109) are shown in Fig. 1. It is evident that the theory predicts the form of the curve correctly, although agreement is not quantitative. In Fig. 2, the excess viscosity, defined as the difference between the viscosity assuming a linear dependence of viscosity on concentration (mole fraction) minus the actual viscosity, is plotted as a function of mole fraction. It is interesting to note that if the calculated excess viscosity is divided by 1.5, then the observed and calculated excess viscosities agree within bounds corresponding to a one-quarter percent error in the measured viscosity.

[13] S. E. Wood and J. P. Brusie, J. Am. Chem. Soc. **65**, 1891 (1943).
[14] K. Graupner and E. R. S. Winter, J. Chem. Soc. **1952**, 1145.
[15] H. Watts, B. J. Alder, and J. Hildebrand, J. Chem. Phys. **23**, 659 (1955).
[16] C. S. Caldwell and A. L. Babb, J. Phys. Chem. **60**, 51 (1956).
[17] P. A. Johnson and A. L. Babb, J. Phys. Chem. **60**, 14 (1956).
[18] L. Grunberg, Trans. Faraday Soc. **50**, 1293 (1954).
[19] J. Hirschfelder, C. F. Curtiss, and R. B. Bird, *The Molecular Theory of Gases and Liquids* (John Wiley & Sons, Inc., New York, 1954).

In view of the difference between the system actually treated and the fluid composed of simple monatomic molecules envisaged by the theory, and also the probable errors in some of the experimental parameters, the agreement between theory and experiment is satisfactory. It should be emphasized that two assumptions have been made in the derivation of Eq. (109) from Eq. (92). It was assumed that the Lennard-Jones potential was valid for both pure components and the mixture, and it was assumed that the principle of corresponding states was applicable. The first assumption is probably by no means a wholly adequate representation of the potential functions of the molecules considered. As regards the second assumption, we may note that it has been found that although methane and oxygen obey the corresponding states principle to good approximation for equilibrium properties (when compared to the behavior of the fluids argon, krypton and xenon), the approximation is much poorer for transport properties such as viscosity.[20] It is likely that a part of the difference between theory and experiment is due to the sensitivity of the corresponding states principle to differences in the shapes of the molecules in this particular example.

In concluding this comparison of theory and experiment, it is pertinent to point out that our relationship between D and η differs from the usual Stokes law form. The substantial agreement with experiment we have found argues once again that a macroscopic Stokes law argument, even if it agrees with experiment, does not *necessarily* describe the transport process correctly. That is, experimental agreement with a functional form $D \propto \eta^{-1}$ need not imply that macroscopic hydrodynamics applies at the molecular level.

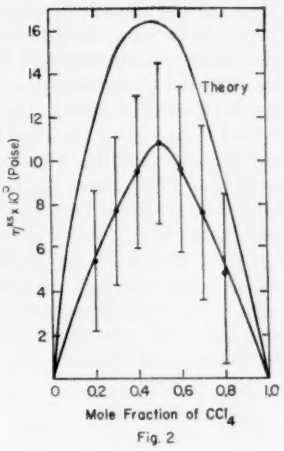

Fig. 2

FIG. 2. Excess viscosity (i.e., viscosity found minus viscosity predicted assuming a linear dependence of viscosity on mole fraction) as a function of mole fraction of carbon tetrachloride for mixtures of carbon tetrachloride and benzene. Vertical lines correspond to $\pm\frac{1}{4}\%$ error in experimental viscosities.

VIII. DISCUSSION

The primary purpose of this communication has been to obtain relations for the fluxes of matter, momentum, and energy in a multicomponent dense system which is not in thermodynamic equilibrium. The analysis has been carried out thus far without any discussion of the assumptions from which the theory is constructed. We now wish to consider the connection between the fundamental approximations of the proposed theory and the nature of the irreversible event.

The postulate that the average diffusive displacement is small relative to the mean intermolecular spacing is closely related to the idea that the average force exerted on a given molecule or a given pair of molecules by the rest of the system is analogous to the frictional force exerted by a fluid or a Brownian particle of semimacroscopic dimensions. That is, a molecule in a dense fluid is in continuous interaction with a large number of its neighbors. The relative positions of the central molecule and the neighbors alter with very high frequency due to thermal agitation. Concommitant with an alteration of intermolecular separations is a change in potential energy, and hence also of the instantaneous force field. Although the force may be expected to fluctuate rapidly in time, the implication of the identification of molecular motion with Brownian motion is that there exists a time scale on which the basic dynamical event may be considered to be independent of both prior and future events. The time evolution of the distribution function is then described only in coarse grained intervals of length τ, where τ is to be chosen by the criterion of independence stated.

It is clear that the spirit of the preceding analysis is consistent with Eq. (15), which relation is based on the tacit assumption that the conditions required for the definition of a diffusion coefficient are satisfied. Rice[21] has examined the autocorrelation function for single particle momentum in the dense fluid and concluded that the basic model is valid if the correlation vanishes after times of the order 10^{-13} to 10^{-12} sec. In the case of the dense rigid sphere fluid[22] and in the case of self-diffusion in crystals,[23,24] there is experimental evidence supporting theoretical arguments which indicate that the correlation functions for several simple types of dynamical events indeed vanish after times of this order of magnitude. While the particular situation under investigation has not been investigated in detail, the analogy with the other dense systems cited suggests that the correlation probably vanishes in a sufficiently short time to make the analysis valid.

The only other serious attempt to construct a theory of transport in fluid mixtures is due to Bearman.[25]

[20] C. Gini-Castagnoli, A. Pizzella, and P. Ricci, Nuovo cimento **11**, 466 (1959).

[21] S. A. Rice, J. Chem. Phys. **33**, 1376 (1960).

[22] R. A. Harris and S. A. Rice, J. Chem. Phys. **33**, 1055 (1960).

[23] A. R. Allnatt and S. A. Rice, J. Chem. Phys. **33**, 573 (1960).

[24] S. A. Rice and H. L. Frisch, Ann. Rev. Phys. Chem. **11**, 187 (1960).

[25] R. J. Bearman, J. Chem. Phys. **29**, 1278 (1958); **30**, 835 (1959); **31**, 751 (1959); and others to be published.

Although the philosophy underlying Bearman's calculations is in some senses similar to ours, the mathematical techniques employed by him are quite different. To date, it has proven rather difficult to reduce Bearman's expressions (which are in principle more nearly correct than ours) to practical form. Where comparison with experiment has been made, the agreement appears to be of about the same quality as that cited herein. There are a very few differences in functional form between our predictions and those of Bearman and Bearman does not predict the volume fraction mixing which we find. At this time, we believe it important to obtain experimental values of the transport coefficients for very simple fluid mixtures and to test the theory in all detail.

After such a program is complete, a detailed analysis of the similarities and differences between our theory and that due to Bearman appears to be called for. At present, such an analysis would be premature.

IX. ACKNOWLEDGMENTS

The material presented herein represents a natural development of earlier work carried out with Professor J. G. Kirkwood.[1] Although Professor Kirkwood had no direct connection with this work, we are still indebted to him for the spirit of the analysis and for an over-all philosophy which aided our programs at several points.

We wish to thank the Alfred P. Sloan Foundation and the Petroleum Research Fund of the American Chemical Society for financial support.

THE JOURNAL OF CHEMICAL PHYSICS VOLUME 34, NUMBER 2 FEBRUARY, 1961

Spectroscopy of Fluorine Flames. I. Hydrogen-Fluorine Flame and the Vibration-Rotation Emission Spectrum of HF

D. E. Mann, B. A. Thrush,* D. R. Lide, Jr., J. J. Ball, and N. Acquista

National Bureau of Standards, Washington, D. C.

(Received July 21, 1960)

The hydrogen fluoride vibration-rotation emission spectrum from a hydrogen-fluorine diffusion flame has been studied under high dispersion from 3200 cm^{-1} in the infrared to about 5500 A in the visible. Measurements were made on the rotational lines in 23 bands including (1–0), (2–1), and (3–2) of the $\Delta v=1$ sequence; (2–0), (3–1), (4–2), (5–3), and (6–4) of $\Delta v=2$; (3–0), (4–1), (5–2), and (6–3) of $\Delta v=3$; (4–0), (5–1), (6–2), (7–3), (8–4), and (9–5) of $\Delta v=4$; and (5–0), (6–1), (7–2), (8–3), and (9–4) of $\Delta v=5$. Complete rotational and vibrational analyses were carried out. The constants B_v, D_v, and H_v are given for $v=0$ to 9. The data were extensive and precise enough to warrant an extended Dunham treatment from which 18 coefficients could be determined, including those for terms in $(v+\frac{1}{2})^6$ and $J^4(J+1)^4$. Band centers for 22 bands and the vibrational term values E_v for $v=0$ to 9 are given.

I. INTRODUCTION

THE vibration-rotation spectrum of HF has been intensively studied by several investigators beginning with Imes[1] who in 1919 reported measurements on the fundamental (1–0) band. Somewhat later Schaeffer and Thomas[2] recorded their observations on the first overtone (2–0) band. More recently, Kirkpatrick and Salant[3] photographed the structure of the (3–0) and (4–0) bands, and Naudé and Verleger[4] the (2–0), (3–0), and (4–0) bands. Nielsen and his co-workers[5,6] have studied the fine structure of the (1–0) and (2–0) bands with moderately high dispersion. All of these measurements were made in absorption and in no case extended beyond the $J=11$ line in either the P or R branches.

The only previously reported investigation of the vibration-rotation spectrum of HF in emission is that of Benedict, Bullock, Silverman, and Grosse.[7] They made observations on a hydrogen-fluorine flame with a quartz-prism monochromator and were able to measure a number of lines in the (1–0), (2–1), (3–2), (3–1),

* Permanent address: Department of Physical Chemistry, University of Cambridge, Cambridge, England.

[1] E. S. Imes, Astrophys. J. **50**, 251 (1919).
[2] C. Schaeffer and M. Thomas, Z. Physik **12**, 330 (1923).
[3] D. E. Kirkpatrick and E. O. Salant, Phys. Rev. **48**, 945 (1935).
[4] S. M. Naudé and H. Verleger, Proc. Phys. Soc. (London) **A63**, 470 (1950).
[5] R. M. Talley, H. M. Kaylor, and A. H. Nielsen, Phys. Rev. **77**, 529 (1950).
[6] G. A. Kuipers, D. F. Smith, and A. H. Nielsen, J. Chem. Phys. **25**, 275 (1956).
[7] W. S. Benedict, B. W. Bullock, S. Silverman, and A. V. Grosse, J. Opt. Soc. Am. **43**, 1106 (1953).

(4–2), and (5–3) bands. Only head measurements were possible on the (2–0), (3–0), (4–1), (5–2), (6–3), and (7–4) bands. In spite of the low resolution available, the spectra were sufficiently extensive because of the very high flame temperature (3500–4000°K) to enable improved values of several molecular constants to be determined. Clearly, a detailed investigation of the HF emission from the H_2-F_2 flame with sufficiently high resolution may be expected to yield very precise constants and rather complete vibrational and rotational energy formulas. This has proved to be the case and the results of such an investigation are reported in the present paper.

Our observations on the H_2-F_2 flame spectrum revealed the following bands: (1–0), (2–1), and (3–2) of the $\Delta v=1$ (or fundamental) sequence; (2–0), (3–1), (4–2), (5–3), and (6–4) of $\Delta v=2$; (3–0), (4–1), (5–2), and (6–3) of $\Delta v=3$; (4–0), (5–1), (6–2), (7–3), (8–4), and (9–5) of $\Delta v=4$; and (5–0), (6–1), (7–2), (8–3), and (9–4) of $\Delta v=5$. Both P and R branches were observed in almost every band. Moreover, lines with J as high as 16 were measured for more than half of the former, and with J as high as 20 for the majority of the latter. The data proved to be extensive and accurate enough to warrant the use of $(v+\frac{1}{2})^5$ and $J^4(J+1)^4$ terms in the analysis.

Very recently Johns and Barrow[8] succeeded in observing for the first time a banded electronic emission spectrum of HF by means of a hollow-cathode source. They were able to show that the transition involves the $^1\Sigma^+$ ground state of HF and carried out a complete vibrational and rotational analysis. The lowest rotation-vibration level of the HF ground state identified and measured by Johns and Barrow was $J=27$ in $v=9$. The lowest vibrational level in which a $J=0$ line was observed is $v=13$. The present study and that of Johns and Barrow therefore do not quite overlap. The gap that remains is, however, relatively very small. Together, the results of these investigations thus serve to define the HF constants from their ground-state equilibrium values up to dissociation.

II. EXPERIMENTAL

An apparatus which has proved satisfactory for the spectroscopic study of various fluorine flames has already been described briefly.[9,10] It consists of three main parts: a gas handling system, a burner and combustion chamber, and a disposal unit which serves to eliminate the effluent gases. Commercial fluorine under pressure is led into the metering system through several needle valves and nickel tubing, the former enabling fairly close regulation of the upstream pressure to be maintained. Hoke needle valves manufactured from

[8] J. W. C. Johns and R. F. Barrow, Proc. Roy. Soc. (London) **A251**, 504 (1959).
[9] D. E. Mann, Spec. Rept. No. 12, Ohio State University Experiment Station (June, 1960).
[10] D. E. Mann (unpublished).

TABLE I. Vacuum wave numbers of $\Delta v=1$ sequence.

J	$P(J)$	Δ(obs-calc)	$R(J)$	Δ(obs-calc)
	1–0 band ($\nu_0=3961.60$ cm^{-1})			
5	3741.66	0.00		
6	693.64	0.04		
7	644.24	−0.06	4230.85	0.06
8	593.89	0.04	256.32	−0.03
9	542.21	−0.06	279.91	−0.07
10	489.67	0.03	301.55	−0.10
11	436.08	0.06	321.28	−0.05
12	381.45	−0.02	339.15	0.16
13	326.00	−0.05	354.66	0.06
14	269.85	0.02	368.12	−0.03
15	212.88	0.01	379.67	0.07
16			389.01	0.07
17			396.12	−0.04
18			401.21	−0.04
19			404.10	−0.05
20			404.87	−0.04
21			403.45	−0.05
22			399.89	−0.04
23			394.20	0.02
24			386.37	0.12
25			376.28	0.10
26			363.78	−0.15
27			349.57	0.02
	2–1 band ($\nu_0=3789.42$ cm^{-1})			
0			3827.49	0.00
1	3749.91	0.05	863.97	−0.03
2	708.88	0.05	898.90	−0.01
3	666.42	0.01	932.16	−0.01
4	622.58	−0.05	963.70	−0.04
5	577.52	−0.03	993.55	−0.03
6	531.20	−0.02	4021.70	0.05
7	483.71	0.01	047.98	0.08
8	435.10	0.06	072.24	−0.07
9	385.23	−0.06	094.85	0.02
10	334.48	−0.01	115.38	−0.06
11	282.76	0.05	134.14	0.03
12	229.97	−0.02	150.84	0.03
13			165.50	−0.02
14			178.21	0.00
15			188.86	0.01
16			197.50	0.05
18			208.42	0.02
19			210.68	−0.04
20			210.81	−0.13
21			209.05	0.02
22			205.05	0.05
23			198.93	0.11
24			190.41	−0.08
	3–2 band ($\nu_0=3622.02$ cm^{-1})			
0			3658.59	−0.02
1	3583.95	−0.02	693.64	−0.05
2	544.48	−0.01	727.25	0.05
3	503.68	0.04	759.13	0.01
4	461.54	0.07		
5	417.99	−0.04	817.94	−0.02
6	373.32	−0.04	844.87	0.06
7	327.49	−0.03	869.85	−0.04
8	280.63	0.07	893.19	0.01
9	232.51	−0.02	914.61	−0.01
10			934.26	0.06
11			951.84	−0.04
12			967.60	−0.04
13			981.40	−0.03
14			993.23	−0.01
15			4003.11	0.05
16			010.90	0.04
17			016.63	0.01
18			020.30	−0.04
21			019.00	−0.03
22			014.47	0.02

TABLE II. Vacuum wave numbers of $\Delta v = 2$ sequence.

J	$P(J)$	Δ(obs-calc)	$R(J)$	Δ(obs-calc)
	2–0 band (ν_0=7750.98 cm^{-1})			
1	7709.78	−0.09		
2	666.00	0.24	7855.83	0.02
3	618.57	−0.13	884.33	0.10
4	586.66	−0.09	909.99	0.16
5	515.94	−0.02	932.01	0.05
6	460.39	−0.02	950.91	0.12
7	402.02	−0.12	966.33	0.04
8	341.34	0.11	978.39	−0.05
9	277.96	0.22	987.09	−0.13
10	211.70	−0.04	992.58	−0.02
11	143.14	−0.15	994.55	−0.01
12	072.57	0.09	992.94	−0.16
13	6999.31	−0.05	988.07	−0.14
14	923.91	−0.10	979.86	−0.02
15	846.57	0.06	968.13	0.02
16	766.93	0.01	953.11	0.22
17	685.36	0.04	934.37	0.14
18	601.75	−0.04	912.34	0.20
19	516.36	−0.03	886.49	−0.13
20	429.23	0.02	857.68	−0.01
21	340.41	0.10	825.14	−0.21
22	249.84	0.08	789.66	0.04
23	157.64	−0.01	750.66	0.14
24	063.94	−0.10	707.79	−0.27
25	5968.88	−0.13	662.46	0.20
26	872.65	0.02	613.10	−0.03
27	775.10	0.13		
28	676.05	−0.05		
	3–1 band (ν_0=7411.45 cm^{-1})			
0			7448.01	−0.05
1	7372.07	0.20	481.66	0.01
2	329.42	0.05	512.10	−0.08
3	284.00	−0.01	539.56	−0.05
4	235.95	0.12	563.69	−0.20
5	185.01	0.11	584.88	−0.11
6	131.19	−0.07	602.94	0.06
7	074.99	0.00	617.58	0.06
8	016.04	−0.10	629.01	0.13
9	6954.62	−0.14	636.95	0.01
10	890.84	−0.10	641.62	−0.06
11	824.52	−0.20	643.23	0.15
12	756.26	0.08	641.06	−0.06
13	685.81	0.43	635.78	−0.02
14	612.16	−0.23	627.26	0.16
15	537.41	0.12	615.13	0.11
16	460.41	0.28	599.59	0.03
17	380.92	−0.07	580.46	−0.26
18	299.89	−0.06	558.27	−0.24
19	216.79	−0.29	532.93	0.00
20	132.37	−0.08	504.11	0.11
21	046.16	0.02	471.88	0.14
22	5958.34	0.11	436.12	−0.04
23	868.88	0.08	397.21	−0.07
24	778.03	0.10	355.32	0.19
25	685.59	−0.12	309.61	−0.12
	4–2 band (ν_0=7080.85 cm^{-1})			
0			7115.97	−0.05
1	7042.61	−0.18	148.12	−0.11
2	001.90	0.03	177.35	−0.10
3	6958.18	0.03	203.60	−0.04
4	911.54	−0.13	226.89	0.13
5	862.73	0.23	246.99	0.22
6	810.56	−0.12	263.79	0.16
7	756.26	−0.03	277.43	0.10
8	699.37	0.00	287.77	−0.06
9	640.08	0.09	295.08	−0.02
10	578.39	0.18	299.06	−0.07
11	514.05	−0.04	299.74	−0.15
12	447.87	0.17	297.33	−0.05
13	379.05	−0.05	291.53	−0.04
14	308.17	−0.19	282.38	−0.08
15	235.41	−0.14	270.17	0.14
16	160.74	0.01	254.34	0.05
17	083.99	0.03	235.26	0.03
18	005.34	0.03	212.84	−0.02
19	5924.78	−0.07	187.27	0.10
20	842.83	0.19	158.00	−0.18
21	758.72	−0.02	125.95	0.06
22	673.17	−0.05	090.43	0.12
23			051.31	−0.15
24			009.41	0.05
	5–3 band (ν_0=6758.22 cm^{-1})			
0			6791.95	−0.02
1	6721.59	−0.04	822.61	−0.21
2	682.27	0.02	850.86	0.12
3	640.19	0.08	875.78	0.09
4	595.14	−0.13	897.65	0.02
5	547.96	0.17		
6	497.70	−0.02	932.18	−0.17
7	445.24	0.12	945.12	0.05
8	389.97	−0.07		
9	332.51	−0.04	961.22	0.13
10	272.75	0.05	964.38	0.04
11	210.50	−0.06	964.38	−0.01
12	145.96	−0.22	961.22	−0.01
13	079.74	0.10		
14	011.17	0.19	945.12	−0.07
15	5940.23	−0.05	932.29	0.00
16	867.55	−0.03	915.99	−0.13
17	792.94	−0.01	896.70	0.02
18	716.45	0.00	874.06	0.12
19			847.98	0.07
20			818.48	−0.08
	6–4 band (ν_0=6442.10 cm^{-1})			
0			6774.59	0.11
1	6406.89	−0.03	503.95	−0.08
2	369.07	0.06	530.76	0.06
3	328.33	−0.07	554.60	0.15
4	285.18	0.03	575.34	0.10
5	239.30	−0.01	592.99	−0.05
6	190.92	0.00	607.63	−0.18
7	139.78	−0.27	619.39	−0.13
8	086.85	0.10	628.09	−0.06
9	031.23	0.16	633.68	0.02
10	5972.91	−0.16	636.09	0.06
11	912.82	0.02	635.39	0.14
12	850.44	0.12	631.32	0.02
13	785.79	0.09	624.07	−0.09
14	718.85	−0.12	613.76	−0.08
15			600.33	0.02
16			583.66	0.06
17			563.77	0.08
18			540.51	−0.08

TABLE III. Vacuum wave numbers of $\Delta v=3$ sequence.

J	$P(J)$	Δ(obs-calc)	$R(J)$	Δ(obs-calc)	J	$P(J)$	Δ(obs-calc)	$R(J)$	Δ(obs-calc)
	3–0 band ($\nu_0=11372.92$ cm^{-1})					5–2 band ($\nu_0=10380.29$ cm^{-1})			
0			11409.51	0.00	0			10414.07	0.03
1	11331.81	−0.01	441.59	0.06	1	10342.17	−0.06	443.43	−0.01
2	286.18	−0.06	468.95	0.00	2	299.94	0.03	468.45	0.00
3	236.24	−0.01	491.73	0.01	3	253.41	0.03	488.98	−0.03
4	181.94	0.03	509.79	−0.01	4	202.68	−0.01	505.17	0.06
5	123.27	−0.01	523.19	0.01	5	147.91	0.00	516.68	−0.02
6	060.44	0.03	531.82	0.00	6	089.07	0.00	523.74	−0.02
7	10993.36	−0.03	535.66	−0.04	7	026.20	−0.03	526.25	−0.01
8	922.30	0.02	534.82	0.01	8	9959.45	0.02	524.20	0.00
9	847.18	0.03	529.10	−0.02	9			517.55	0.00
10	768.09	0.00	518.63	−0.01	10			506.31	0.01
11			503.36	0.01	11			490.46	0.01
12	598.45	−0.03	483.29	0.03	12			470.02	0.03
13	508.10	0.01	458.39	0.03	13			444.90	−0.03
14	414.07	−0.03	428.66	−0.01	14			415.24	−0.02
15	316.59	0.01	394.16	−0.03	15			380.98	−0.02
16	215.63	0.01	354.95	0.00	16			342.17	0.03
17	111.34	0.03	310.95	0.00	17			298.69	−0.00
18	003.69	−0.04	262.18	−0.03	18			250.65	−0.01
19	9892.97	0.01	208.82	0.04	19			198.07	0.03
20			150.65	0.00	20			140.82	−0.02
21			087.88	−0.01					
	4–1 band ($\nu_0=10870.37$ cm^{-1})					6–3 band (calc $\nu_0=9900.99$ cm^{-1})[a]			
0			10905.50	−0.03					
1	10830.82	0.02			1			9961.49	
2	786.88	0.01	962.44	0.00	2			985.21	
3	738.63	0.00	984.11	0.00	3			10004.62	
4	686.14	0.00	11001.21	0.00	4			019.75	
5	629.48	0.01	013.71	0.00	5			030.35	
6	568.68	0.01	021.58	0.00	6			036.57	
7	503.82	0.01	024.81	0.01	7			038.31	
8	434.92	−0.04	023.35	0.00	8			035.54	
9	362.17	−0.02	017.23	0.00	9			028.28	
10	285.57	0.01	006.40	−0.01	10			016.49	
11	205.17	0.00	10990.91	0.01	11			000.19	
12	121.08	0.02	970.69	0.00	12			9979.33	
13	033.33	0.00	945.75	−0.02	13			953.95	
14	9942.03	−0.01	916.18	0.01					

[a] Reliable constants could not be obtained from the 6-3 band because only one branch was available.

Monel bar-stock and equipped with Teflon packing have proved satisfactory. Fluorine flow is measured with Brooks Rotameters made of Kel-F and fitted with Monel balls. Pressure in the fluorine lines is monitored with Helicoid bourdon-tube gauges. These have Monel tubes and fittings and are manufactured expressly for fluorine service.

The combustion chamber is a section of nickel tube 11 in. long and having 4 in. o.d. and $\frac{1}{8}$-in. wall thickness. It is fitted with top and bottom flanges, four optical parts, and a pair of ignition electrodes. All flange seals are made with Teflon O-rings. A burner is attached to the bottom flange and a flexible exhaust tube to the upper flange. Optical windows, usually 5-cm diam sapphire, are sealed to the side ports.

The exhaust gases are efficiently disposed of by either of two means. A Schütte-Koerting commercial fume scrubber mounted outside the laboratory has proved effective but results in the presence of the 3064-A OH band in the spectrum. When one desires to minimize the presence of OH, a tower filled with soda-lime has proved a convenient means of eliminating both fluorine and hydrogen fluoride from the effluent gases.

In normal operation fluorine flows of 3–4 liters/min are used. Stable diffusion flames several cm high have been sustained for as long as 20 hr. The burner most commonly used in this work consisted of three concentric nickel tubes with $\frac{3}{8}$, $\frac{1}{4}$, and $\frac{1}{8}$ in. o.d., respectively, and each having 0.035-in. wall thickness. Normally, the inner tube carried the fuel, while an inert gas and fluorine were flowed through the middle and outer annuli, respectively. The purpose of the inert spacer gas is to keep the burner lip comparatively cool. An inert gas could also be introduced at the base of the burner in order to sheath the flame and thereby minimize recirculation and flickering. The ratio of hydrogen to fluorine flow was ordinarily adjusted to give maximum HF intensity and was usually not far from a stoichiometric proportion. The flow of inert spacer gas was kept as low as possible to avoid undue cooling of the

TABLE IV. Vacuum wave numbers of $\Delta v=4$ sequence.

J	$P(J)$	Δ(obs-calc)	$R(J)$	Δ(obs-calc)
	4–0 band (ν_0=14831.75 cm^{-1})			
0			14866.92	0.01
1	14790.63	−0.01	896.08	0.01
2	743.60	−0.02	919.19	0.01
3	690.77	0.01	936.22	−0.01
4	632.12	0.01	947.14	−0.02
5	567.75	0.01	951.94	−0.02
6	497.72	0.00	950.62	0.00
7	422.12	0.00	943.11	0.00
8	341.00	−0.02	929.42	0.00
9	254.50	0.00	909.57	0.01
10	162.65	0.00	883.54	0.02
11	065.56	0.01	851.33	0.02
12	13963.28	−0.02	812.96	0.02
13	856.00	0.00	768.41	−0.02
14	743.74	0.01	717.73	−0.06
15	626.61	0.00	661.06	0.00
16	504.71	−0.01	598.29	0.02
17	378.16	−0.01	529.47	0.02
18	247.08	0.02	454.60	−0.03
19	111.48	−0.01	373.87	0.00
20			287.25	0.04
21			194.67	−0.02
	5–1 band (ν_0=14169.64)			
0			14203.36	−0.03
1	14130.06	−0.02	231.26	−0.02
2	084.72	−0.02	253.26	0.00
3	033.68	−0.02	269.32	0.01
4	13977.01	0.01	279.40	0.01
5	914.70	0.00	283.50	0.02
6	846.92	0.04	281.58	0.02
7	773.62	0.01	273.62	0.01
8	694.98	0.02	259.63	0.01
9	611.01	0.01	239.58	0.00
10	521.83	0.00	213.48	−0.02
11	427.52	0.00	181.38	−0.01
12	328.13	−0.02	143.22	−0.02
13	223.84	0.00	099.06	−0.01
14	114.61	−0.04	048.89	0.00
15	000.68	−0.02		
16	12882.08	0.02	13930.63	0.00
17	758.88	0.03	862.61	0.01
18	631.18	0.02	788.69	0.02
19	499.07	−0.02	708.88	0.00
20	362.75	0.01	623.26	−0.01
21	222.22	0.01	531.86	−0.01
22	077.60	−0.01		
23			331.91	0.00
	6–2 band (ν_0=13523.02 cm^{-1})			
0			13555.38	−0.01
1	13484.93	−0.03	582.02	0.00
2	441.29	0.04	602.88	0.01
3	391.95	0.01	617.94	0.03
4	337.09	−0.01	627.12	0.02
5	276.78	0.00	630.41	−0.01
6	211.04	0.00	627.84	−0.01
7	139.96	0.00	619.36	0.00
8	063.60	−0.01	604.94	−0.02
9	12982.04	−0.01	584.61	−0.01
10	895.36	−0.01	558.34	−0.01
11	803.66	0.01	526.14	−0.01
12	706.96	0.00	488.02	0.01
13	605.40	0.00	444.00	0.04
14	499.06	0.02	394.00	0.00
15	388.00	0.02	338.14	−0.01
16	272.30	0.00		
17	152.09	−0.01	208.86	0.01
18	027.45	−0.01	135.42	−0.04
19	11898.47	0.00	056.29	0.02
20	765.24	0.01	12971.30	−0.01
21			880.63	0.01
	7–3 band (ν_0=12889.53 cm^{-1})			
0			12920.48	−0.05
1			945.89	0.00
2	12810.81	0.01	965.60	0.02
3	763.20	0.03	979.56	0.00
4	710.11	0.02	987.79	−0.01
5	651.64	0.00	990.26	−0.01
6	587.85	−0.01	986.95	0.01
7	518.84	0.01	977.82	0.01
8	444.61	0.01	962.85	0.00
9	365.22	−0.04	942.05	0.00
10	280.85	−0.01	915.39	−0.02
11	191.48	−0.01	882.91	−0.01
12	097.21	−0.01	844.60	0.03
13	11998.15	0.02	800.40	0.02
14	894.32	0.02	750.37	0.02
15	785.81	0.01	694.48	−0.01
16	672.69	−0.02	632.79	−0.02
17			565.32	−0.01
18			492.05	0.00
19			413.02	0.01
	8–4 band (ν_0=12266.46 cm^{-1})			
1			12320.17	−0.01
2	12190.67	−0.01		
3	144.63	−0.01	351.55	0.02
4	093.24	0.01	358.73	0.00
5	036.52	0.00	360.25	0.01
6	11974.56	0.01	356.05	0.01
7	907.37	−0.02		
8	835.12	0.02	330.39	−0.01
9	757.72	−0.02	308.89	−0.05
10	675.37	0.00	281.72	0.02
11	588.07	0.00	248.67	0.01
12			209.85	0.02
13			165.18	−0.01
14			114.74	0.00
15			058.45	−0.01
16			11996.37	0.01
	9–5 band (ν_0=11650.72 cm^{-1})			
3			11731.11	0.00
4			737.53	−0.01
6			734.03	0.01
7			724.06	0.00
8			708.61	−0.02
9			687.75	0.01

flame by dilution. No attempt was made to operate a premixed H_2-F_2 flame by the method of Grosse and Kirschenbaum.[11]

[11] A. V. Grosse and A. D. Kirschenbaum, J. Am. Chem. Soc. 77, 5012 (1955).

The final spectroscopic observations in the photographic region were made with a Jarrell-Ash 3.4-m instrument equipped either with a Bausch and Lomb 600 lines/mm plane replica grating blazed for the third-order green, or with a similar one blazed for the

TABLE V. Vacuum wave numbers of $\Delta v=5$ sequence.

J	$P(J)$	Δ(obs-calc)	$R(J)$	Δ(obs-calc)
	5–0 band (ν_0=18131.10 cm^{-1})			
1	18091	[a]	18191.17	0.01
2	042	[a]	210	[a]
3	17986	[a]	222	[a]
4	923.09	0.01	225.37	0.00
5	853.10	0.00	222	[a]
6	776.05	0.00	210	[a]
7	692.02	0.00	192.02	0.07
8	601.10	−0.01	165.72	−0.01
9	503.37	−0.01	131.90	−0.08
10	399	[a]	090.75	0.05
11	288	[a]	042	[a]
12	170.41	0.01	17986	[a]
13	046.51	0.02	921.89	0.00
14	16916.31	−0.02		
	6–1 band (ν_0=17312.42 cm^{-1})			
1			17370.01	0.07
2	17226.07	−0.03	387.82	0.02
3	172.22	−0.06	398.35	0.01
4	111.40	−0.02	401.51	−0.02
5	043.64	0.04	397.36	0.01
6	16968.88	0.00	385.77	−0.02
7	887.32	−0.03	366.83	−0.01
8			340.49	0.01
9	704.21	0.07	306.76	0.02
10	602.62	−0.01	265.54	−0.06
11	494.64	−0.01		
12	380.29	0.02	161.24	−0.01
13	259.62	0.01	098.15	0.06
14	132.70	−0.06	027.64	0.00
15	15999.82	0.00	16949.94	−0.02
16	860.91	0.02	865.09	0.00
	7–2 band (ν_0=16511.60 cm^{-1})			
2	16428.46	0.00	16583.25	0.01
3	376.39	−0.03	592.80	−0.01
4	317.46	−0.02	595.22	0.04
5	251.72	0.02	590.32	0.00
6	179.14	0.00	578.23	0.01
7	099.87	−0.02	558.87	0.01
8	014.04	0.03	532.23	−0.02
9	15921.59	0.00	498.39	0.02
10	822.70	0.00	457.23	−0.01
11	717.42	−0.03	408.84	−0.02
12	605.96	0.06	353.23	−0.01
13	488.17	0.01	290.40	0.00
14	364.28	−0.04	220.29	−0.06
15	234.48	0.02	143.16	0.04
16	098.61	−0.06	058.77	0.04
17	14957.10	0.04	15967.21	0.01
18	809.71	0.00	868.55	−0.02
	8–3 band (ν_0=15725.33 cm^{-1})			
0			15754.93	−0.04
1	15688.82	0.07	777.58	−0.03
2	645.29	0.03	793.21	−0.02
3	594.94	0.02	801.80	0.01
4	537.82	0.03	803.27	0.01
5	473.89	−0.02	797.62	0.00
6	403.30	−0.07	784.85	0.01
7	326.16	−0.05	764.90	−0.02
8	242.59	0.06	737.84	0.01
9	152.34	−0.03	703.54	−0.04
10	055.81	−0.03	662.16	0.00
11	14953.06	0.06	613.61	0.04
12			557.84	0.03
13			494.90	0.01
14	607.48	−0.01	424.76	−0.06
15	480.28	0.00	347.63	0.01
16			263.33	0.04
17			171.85	0.01
18			073.27	−0.04
20			14855.06	0.01
21			735.37	0.01
	9–4 band (ν_0=14949.94)			
0			14978.30	0.05
1			999.62	−0.03
2	14872.74	−0.04	15014.13	0.03
3	823.98	−0.03	021.60	0.04
4			021.99	−0.02
5			015.36	−0.06
6	637.75	0.06	001.78	0.01
7	562.43	−0.01	14981.05	0.02
8	480.73	−0.01		
9			918.28	0.05
10			876.12	−0.04
11			826.94	−0.02
14			636.67	0.04
15			558.94	−0.02

[a] Overlapped lines; not used in calculations.

second order of 5000 A. Eastman Kodak spectroscopic plates variously sensitized for the region of interest were used throughout. Standard hypersensitization was also used for M, Q, and Z plates. Exposure times varied from a few minutes to about 6 hr. An iron arc was used to provide the comparison spectra for wavelength measurements.

The fundamental and first overtone sequences were studied with a Perkin-Elmer Model 99 double-pass monochromator equipped with a Bausch and Lomb 600 lines/mm replica grating in place of the prism, and with an uncooled PbS cell as the detector. The optical arrangement and performance were similar to that described by Lord and McCubbin.[12] The grating was used in first order for the $\Delta v=1$ sequence and in second order for the $\Delta v=2$ sequence. The very precise measurements of Benedict, Plyler, and Tidwell[13] of the NH_3 spectrum were used for calibration purposes in the 4410–4340 cm^{-1} region of the (1–0) band. Similarly precise measurements on CO by Rank and his co-workers[14] were used to establish wavelengths in the 4340–

[12] R. C. Lord and T. K. McCubbin, J. Opt. Soc. Am. **45**, 441 (1955).

[13] W. S. Benedict, E. K. Plyler, and E. D. Tidwell, J. Research Natl. Bur. Standards **61**, 123 (1958).

[14] D. H. Rank, A. H. Guenther, G. D. Saksena, J. N. Shearer, and T. A. Wiggins, J. Opt. Soc. Am. **47**, 686 (1957).

TABLE VI. Coefficients from rotational analysis (in cm^{-1}).[a]

Band	c_0	c_1	c_2	$c_3\times10^3$	$c_4\times10^5$	$c_5\times10^7$	$c_6\times10^7$	$c_7\times10^{11}$
1–0	3961.60	40.3322	−0.77372	−8.199	0.0574	4.46	0.089	[b]
	(0.06)	(0.0065)	(0.00093)	(0.079)	(0.0031)	(2.59)	(0.061)	
2–1	3789.42	38.8244	−0.75246	−8.237	0.0510	16.2	−0.26	...
	(0.02)	(0.0044)	(0.00068)	(0.079)	(0.0036)	(4.2)	(0.10)	
3–2	3622.02	37.3305	−0.73381	−7.832	0.0411	9.82	...	[b]
	(0.02)	(0.0040)	(0.00060)	(0.051)	(0.0064)	(1.79)		
2–0	7750.98	39.5931	−1.52636	−8.300	0.1144	11.08	−0.130	−23.6
	(0.04)	(0.0069)	(0.00063)	(0.064)	(0.0022)	(1.70)	(0.020)	(13.4)
3–1	7411.45	38.1019	−1.48444	−8.124	0.0935	11.18	0.009	−29.6
	(0.05)	(0.0093)	(0.0087)	(0.100)	(0.0035)	(3.08)	(0.038)	(28.1)
4–2	7080.85	36.6215	−1.45149	−7.850	0.0961	8.25	−0.114	...
	(0.04)	(0.0058)	(0.00080)	(0.043)	(0.0038)	(0.72)	(0.049)	
5–3	6758.22	35.1745	−1.42291	−7.631	0.0989	7.83	−0.302	...
	(0.04)	(0.0075)	(0.00117)	(0.081)	(0.0080)	(2.00)	(0.150)	
6–4	6442.10	33.7844	−1.39472	−7.677	0.0738	12.6	...	...
	(0.04)	0.0078	(0.00113)	(0.104)	(0.0057)	(3.7)		
3–0	11372.92	38.8553	−2.25945	−8.117	0.1654	7.71	−0.262	16
	(0.01)	(0.0023)	(0.00032)	(0.037)	(0.0022)	(1.79)	(0.040)	(27)
4–1	10870.37	37.3743	−2.20517	−8.040	0.1589	12.8	−0.471	...
	(0.01)	(0.0015)	(0.00037)	(0.028)	(0.0045)	(1.1)	(0.146)	
5–2	10380.29	35.9160	−2.15391	−7.955	0.1084	48.8	−1.30	...
	(0.01)	(0.0031)	(0.00089)	(0.080)	(0.0108)	(10.4)	(0.26)	
4–0	14831.75	38.1429	−2.97721	−8.056	0.2100	8.20	−0.274	9
	(0.01)	(0.0017)	(0.00023)	(0.027)	(0.0016)	(1.30)	(0.029)	(19)
5–1	14169.64	36.6645	−2.90862	−7.852	0.1952	8.60	−0.251	−12.4
	(0.01)	(0.0013)	(0.00014)	(0.017)	(0.0007)	(0.66)	(0.010)	(7.4)
6–2	13523.02	35.2245	−2.84788	−7.708	0.1786	8.92	−0.265	−12.6
	(0.01)	(0.0014)	(0.00017)	(0.022)	(0.0011)	(1.00)	(0.017)	(13.7)
7–3	12889.53	33.8033	−2.79633	−7.516	0.1593	7.83	−0.298	
	(0.01)	(0.0015)	(0.00024)	(0.021)	(0.0019)	(0.64)	(0.044)	...
8–4	12266.46	32.4059	−2.75685	−7.400	0.1464	12.4	−0.79	...
	(0.01)	(0.0026)	(0.00042)	(0.068)	(0.0046)	4.2	(0.22)	
9–5	11650.72	31.0280	−2.73253	b	b	b	b	b
	(0.09)	(0.0278)	(0.00200)					
5–0	18131.10	37.4190	−3.68110	−7.678	0.2473	−0.3	...	...
	(0.03)	(0.0051)	(0.00066)	(0.099)	(0.0031)	(4.0)		
6–1	17312.42	35.9926	−3.59973	−8.016	0.2252	14.2	−0.130	...
	(0.02)	(0.0031)	(0.00073)	(0.043)	(0.0066)	(1.4)	(0.162)	
7–2	16511.60	34.5387	−3.53215	−7.636	0.2203	8.39	−0.547	...
	(0.02)	(0.0020)	(0.00045)	(0.023)	(0.0032)	(0.57)	(0.063)	
8–3	15725.33	33.1181	−3.47435	−7.348	0.1849	3.92	−0.360	...
	(0.01)	(0.0035)	(0.00039)	(0.056)	(0.0028)	(1.93)	(0.083)	
9–4	14949.94	31.7478	−3.43322	−7.494	0.1637	−0.7	...	...
	(0.02)	(0.0060)	(0.00159)	(0.104)	(0.0217)	(10.5)		

[a] When no entry is given, the term was omitted from the least-squares fit.

[b] Calculated values of these coefficients were used to correct the observed wave numbers before making the least-squares fit. This procedure enabled some information to be obtained from bands in which many more lines were available in the R branch than in the P branch.

4100 cm^{-1} region of the (1–0) band and the 4211−4100 cm^{-1} region of the (2–1) HF band. Plyler and Tidwell's[15] measurements of the H_2O spectrum were used in the 4100–3200, 4100–3200, and 4022–3200 cm^{-1} regions of the (1–0), (2–1), and (3–2) HF bands, respectively. Twelve R branch lines in the 3800–3500 cm^{-1} region of the (4–3) were observed but were not used in the subsequent analysis. The bands of the $\Delta v=2$ sequence were measured with the aid of neon, argon, krypton, and xenon emission lines superimposed simultaneously with the HF spectra. When the more precise results from the photographic measurements were used to calculate the positions of the lines observed in the PbS region it was found the agreement was excellent and well within the stated uncertainty.

The results of all the measurements, converted to vacuum wave numbers, are listed systematically together with the values of all band centers in Tables I–V.

ROTATIONAL ANALYSIS

The wave numbers of the lines in a given vibration-rotation band may be expressed as

$$\nu_m=\sum_{k=0}^{N}c_k m^k, \qquad (1)$$

[15] E. K. Plyler and E. D. Tidwell, Mem. soc. roy. sci. Liège **18**, 426 (1957).

where $m=J+1$ for the R branch and $m=-J$ for the P branch. The first eight c_k's are defined in terms of the usual spectroscopic constants by

$$\begin{aligned} c_0&=\nu_0 \text{ (band center)}\\ c_1&=B'+B''\\ c_2&=(B'-B'')-(D'-D'')\\ c_3&=-2(D'+D'')+(H'+H'')\\ c_4&=-(D'-D'')+3(H'-H'')\\ c_5&=3(H'+H'')+8Y_{04}\\ c_6&=(H'-H'')\\ c_7&=8Y_{04}. \end{aligned} \tag{2}$$

The use of the Dunham constant Y_{04} (see the following)[16,17] in these definitions is a valid approximation in the present analysis, since it is not possible to detect the variation with vibrational state of the $J^4(J+1)^4$ term in the rotational energy. No information could be obtained on the coefficients beyond c_7.

A least-squares fit of the observed wave numbers to Eq. (1) was carried out for each band on the IBM 704 computer at the National Bureau of Standards. This calculation gave values of the coefficients c_k and their estimated standard deviations, as well as the difference between calculated and observed wave numbers. The results of the calculations are given in Table VI for all bands.

TABLE VII. Observed[a] and calculated[b] B_v, D_v, H_v (in cm^{-1}).

	B_v		$D_v\times10^6$		$H_v\times10^7$	
v	obs	calc	obs	calc	obs	calc
0	20.5590 (0.0010)[c]	20.5606	2.119 (0.010)	2.122	1.61 (0.10)	1.65
1	19.7883 (0.0010)	19.7874	2.073 (0.010)	2.064	1.60 (0.10)	1.58
2	19.0355 (0.0010)	19.0349	2.019 (0.010)	2.010	1.68 (0.10)	1.52
3	18.2988 (0.0010)	18.3008	1.954 (0.010)	1.960	1.43 (0.10)	1.45
4	17.5837 (0.0010)	17.5831	1.919 (0.010)	1.915	1.23 (0.15)	1.39
5	16.8775 (0.0015)	16.8791	1.864 (0.015)	1.873	1.31 (0.15)	1.32
6	16.1895 (0.0015)	16.1864	1.838 (0.015)	1.835	1.35 (0.15)	1.26
7	15.5033 (0.0015)	15.5024	1.799 (0.015)	1.802	1.16 (0.15)	1.19
8	14.8235 (0.0020)	14.8239	...	1.772	...	1.13
9	14.1476 (0.0030)	14.1483	...	1.747	...	1.06

[a] Average over-all bands.
[b] Calculated from Dunham coefficients in Table IX.
[c] Estimated standard deviation.

TABLE VIII. First differences in B_v (in cm^{-1}).

v	obs (B_v-B_{v+1})	calc (B_v-B_{v+1})[a]	Δ(obs-calc)
0	0.7731	0.7732	−0.0001
1	0.7527	0.7525	0.0002
2	0.7336	0.7339	−0.0003
3	0.7182	0.7177	0.0005
4	0.7034	0.7038	−0.0004
5	0.6924	0.6925	−0.0001
6	0.6843	0.6839	0.0004
7	0.6780	0.6781	−0.0001

[a] From Dunham coefficients in Table IX.

In carrying out the least-squares calculation the proper choice for N, the degree of the polynomial in Eq. (1), presented certain difficulties. Although a given term $c_k m^k$ may be known to make an experimentally significant contribution to the position of some lines of a band, it does not necessarily follow that c_k can be determined from the analysis. In many of the HF bands it was found that the contribution of a coefficient c_k, which might amount to several cm^{-1} for large values of J, could be essentially completely absorbed into the lower coefficients. This was particularly apparent when more lines were available in one branch than in the other. In such cases the inclusion of a kth term in the least-squares calculation often yielded an absurdly large value of c_k (and a correspondingly large standard deviation). This apparent divergence of the power series biased the lower coefficients very badly. The following procedure was adopted in an effort to minimize this bias. The constants c_k were estimated from a preliminary analysis of all bands and from theoretical considerations. A least-squares calculation with a polynomial of degree N (generally starting with $N=7$) was then carried out for each band, and the resulting standard deviation in c_N was compared with the predicted value of c_N. When the ratio of standard deviation to predicted value was greater than two, the calculation was repeated with a polynomial of degree $N-1$. This process was continued until the highest coefficient in the polynomial satisfied the criterion that its standard deviation be less than twice its predicted value.

The omission of an experimentally significant term c_N by the foregoing criterion causes some bias, particularly on the c_{N-1} and c_{N-2} coefficients. It must be recognized, therefore, that the standard deviations given in Table VI do not always reflect the true uncertainties in the coefficients. For the coefficients c_0 through c_3 we believe that the uncertainty which results from the

[16] J. L. Dunham, Phys. Rev. **41**, 721 (1932).
[17] C. H. Townes and A. L. Schawlow, *Microwave Spectroscopy* (McGraw-Hill Book Company, Inc., New York, 1955), pp. 9–11.

TABLE IX. Dunham coefficients for HF.

Dunham coeff.	Approx. iden.	Obs Y_{ij} (cm^{-1})	Calc Y_{ij}	Results of Kuipers *et al.* (footnote reference 6)
Y_{10}	ω_e	4138.73±0.20[a]	b	4138.25_3
Y_{20}	$-\omega_e x_e$	−90.05±0.12	b	-88.72_6
Y_{30}	$\omega_e y_e$	0.932±0.030	b	0.533_4
Y_{40}	$\omega_e z_e$	$-(1.42\pm0.33)\times10^{-2}$		$-2.1_1\times10^{-2}$
Y_{50}		$-(5.9\pm1.3)\times10^{-4}$		c
Y_{01}	B_e	20.9555±0.0015[a]	b	20.945_6
Y_{11}	$-\alpha_e$	−0.7958±0.0007	b	-0.788_8
Y_{21}	γ_e	$(1.182\pm0.040)\times10^{-2}$	b	$0.87_3\times10^{-2}$
Y_{31}		$-(3.11\pm0.73)\times10^{-4}$		c
Y_{41}		$-(5.8\pm4.6)\times10^{-6}$		c
Y_{02}	$-D_e$	$-(2.153\pm0.006)\times10^{-3}$	-2.149×10^{-3}	$-2.13_1\times10^{-3}$
Y_{12}	β_e	$(6.23\pm0.10)\times10^{-5}$	5.95×10^{-5}	$-3._8\times10^{-6}$
Y_{22}		$-(2.06\pm0.20)\times10^{-6}$	-1.75×10^{-6}	c
Y_{03}	H_e	$(1.68\pm0.07)\times10^{-7}$	1.65×10^{-7}	c
Y_{13}		$-(6.5\pm0.3)\times10^{-9}$	-3.57×10^{-9}	c
Y_{04}		$-(1.9\pm0.8)\times10^{-11}$	-1.53×10^{-11}	c

[a] After Dunham correction is applied, $\omega_e=4139.04$ cm^{-1} and $B_e=20.9560$ cm^{-1}.
[b] Used in calculation of potential constants.
[c] No value determined.

indeterminacy of the higher coefficients is probably no greater than the indicated standard deviation. However, a comparison of observed and calculated values of c_4, c_5, and c_6 suggests that systematic errors as large as three standard deviations may be present in a few cases. Only an order-of-magnitude value was obtained for c_7.

The constants B_v, D_v, H_v, and Y_{04} may be calculated from the c_k values in Table VI by the use of Eq. (2). From two to seven independent determinations are thus available for each constant. These values were weighted in accordance with the standard deviations of the c_k's and averages were taken. The average values are listed in the "observed" volume of Table VII. In taking the averages, values were excluded when they appeared to be strongly biased by omission of higher coefficients; e.g., only those H_v values were used which came from bands in which c_7 was determined. Rough estimates of the uncertainty in these average constants are indicated in Table VII. These estimates are based on both the standard deviations of the c_k coefficients and the scatter of the various determinations, and therefore take into account, as far as possible, the systematic errors discussed in the last paragraph.

The constants B_v, D_v, and H_v may be expressed as power series in $(v+\frac{1}{2})$. In the notation of Dunham we write

$$B_v=\sum_l Y_{l1}(v+\tfrac{1}{2})^l, \qquad (3)$$

where $Y_{01}\approx B_e$, $Y_{11}\approx-\alpha_e$, etc. The Y_{l1} have been determined from the observed B_v by a least-squares calculation. However, more accurate values can be obtained from the differences $B'-B''$, which are determined with greater precision than the individual B_v's. The first differences B_v-B_{v+1} were calculated from the c_2 coefficients in all possible ways which involved no more than binary combinations, i.e., B_1-B_0 is given by c_2 for the (1–0) band, by the difference of c_2 coefficients for the (2–0) and (2–1) bands, etc. (after correction for the $D'-D''$ term). The averages B_v-B_{v+1} values are listed in Table VIII. The Dunham coefficients Y_{11}, Y_{21}, ⋯ were determined from a least-squares fit of these first differences to a power series in $(v+\frac{1}{2})$. Y_{41} was the last coefficient for which a meaningful estimate could be obtained. The leading coefficient Y_{01} ($\approx B_e$) was then chosen to give the best agreement with the observed B_v. The final Y_{l1} values are listed in Table IX. The Y_{l1} calculated directly from the observed B_v agree satisfactorily with the values in Table IX, but the standard deviations are from two to three times as large.

The B_v values calculated from the final Y_{l1} are compared with the observed B_v in Table VII. The root mean square deviation between calculated and observed B_v is about 0.0015 cm^{-1}, which is in line with the estimated uncertainties in the observed B_v. It should be emphasized that this comparison is a meaningful one, since the chief uncertainty in the observed B_v comes

from the c_1 coefficients, while the information used in the calculated B_v (aside from Y_{01}) is derived from the c_2's.

The D_v constant is expressed as

$$D_v = \sum_l Y_{l2}(v+\tfrac{1}{2})^l. \qquad (4)$$

The procedure used for B_v is less satisfactory here, because the calculation of $D_v - D_{v+1}$ involves an accumulation of experimental errors. It proved better to fit the c_4 coefficients for a given vibrational sequence to a power series in $(v+\frac{1}{2})$. This was carried out for the $\Delta v=4$ and $\Delta v=5$ sequences, where c_4 is most accurately determined. The results agreed satisfactorily and gave well-determined values for Y_{12} and Y_{22}. No information could be obtained on the higher coefficients. Finally, Y_{02} ($\approx -D_l$) was chosen to fit the observed D_v. The final values are listed in Table IX, and the D_v calculated from these values are given in Table VII. The rms deviation between observed and calculated D_v is 0.006×10^{-3} cm^{-1}.

The H_v calculation was handled in a similar manner. Only Y_{13} could be determined from the c_6 coefficients, i.e., $H'-H''$ was found to be proportional to Δv within the statistical uncertainty. The rms deviation between observed and calculated H_v (Table VII) is about 0.09×10^{-7} cm^{-1}.

The best estimates for c_7 were obtained from the (5–1), (6–2), and (2–0) bands. The average of the three values, weighted according to the standard deviations, gives $Y_{04}=-(1.9\pm0.8)\times10^{-11}$.[18]

POTENTIAL FUNCTION

Dunham has given expressions for the Y_{lj} coefficients in terms of constants a_k in the power-series expansion of the molecular potential function

$$V(\xi)=(\omega_e^2/4B_e)\xi^2(1+a_1\xi+a_2\xi^2+\cdots), \qquad (5)$$

where $\xi=(r-r_e)/r_e$ and r_e is the equilibrium internuclear distance. If we identify Y_{10} with ω_e and Y_{01} with B_e, which is an adequate approximation for the present purpose, the a_k may be calculated from the Dunham coefficients which are associated with E_v and B_v (i.e., from the Y_{l0} and Y_{l1}). Thus we may calculate a_1 from Y_{11}, a_2 from Y_{20}, a_3 from Y_{21}, and a_4 from Y_{30}. The results of this procedure are

$$a_1=-2.2500, \qquad a_3=-4.457,$$
$$a_2=3.4633, \qquad a_4=4.891.$$

It is not possible to obtain a reliable value of a_5 from the present data.

The Dunham coefficients associated with D_v, H_v, etc., are functions only of the potential constants a_1, a_2, a_3, a_4 and may therefore be predicted from the values just obtained. The calculated Y_{1j} for $j=2$, 3, 4 are included in Table IX. The agreement between observed and calculated values is excellent for all coefficients except Y_{13}, where the discrepancy appears to be outside the experimental uncertainty. However, the calculation of Y_{13} from the potential constants involves considerable cancellation, and it is probable that the discrepancy could be reduced by slight readjustment of all the constants. We may conclude that the Dunham formulation gives a satisfactory representation of the HF energy levels.

The Dunham treatment shows that the classical oscillation frequency for infinitesimal amplitudes ω_e and the equilibrium rotational constant $B_e=\hbar^2/2\mu r_e^2$ are not strictly identical with the spectroscopic constants Y_{10} and Y_{01}. The correction terms may be calculated from the potential constants a_1 through a_4. One finds that $Y_{10}=(1-7.4\times10^{-5})\omega_e$, so that the true $\omega_e=4139.04$ cm^{-1}. Likewise, Y_{01} is 0.0005 cm^{-1} smaller than B_e, which gives

$$B_e=20.9560 \text{ cm}^{-1},$$

and

$$r_e=0.91680 \text{ A}.$$

The Dunham corrections for both ω_e and B_e are of the order of the experimental uncertainty in these constants.

VIBRATIONAL ENERGY

The 22 band centers have been used to determine the first nine vibrational term values. The choice of term values which gives the best over-all agreement is listed in Table X. In arriving at these values the $\Delta v=1$ and $\Delta v=2$ bands were weighted most heavily, since these results, while not as precise as the photographic data, are less susceptible to systematic errors. As a check on systematic errors, band centers were calculated from

TABLE X. Vibrational term values (in cm^{-1}).

v	Obs E_v[a]	Calc E_v[c]
0	2046.97	2046.97
1	6008.57±0.07[b]	6008.56
2	9797.97±0.07	9797.98
3	13420.00±0.07	13419.99
4	16878.82±0.07	16878.84
5	20178.22±0.07	20178.17
6	23320.94±0.07	23320.98
7	26309.56±0.15	26309.54
8	29145.30±0.15	29145.30
9	31828.85±0.15	31828.85

[a] Relative to potential minimum. The calculated zero-point energy of 2046.97 cm^{-1} has been added to the observed term values.
[b] Estimated standard deviation.
[c] Calculated from the Dunham coefficients listed in Table IX.

[18] Johns and Barrow (see footnote reference 8) use the letter L to designate the coefficient of the $J^4(J+1)^4$ term in the rotational energy.

TABLE XI. Observed and calculated[a] band centers (cm^{-1}).

v'	$v''=0$	1	2	3	4	5
1	3961.60 (3961.59)[b]					
2	7750.98 (7751.01)	3789.42 (3789.42)				
3	11372.92 (11373.02)	7411.45 (7411.43)	3622.02 (3622.01)			
4	14831.75 (14831.87)	10870.37 (10870.28)	7080.85 (7080.86)			
5	18131.10 (18131.20)	14169.64 (14169.61)	10380.29 (10380.19)	6758.22 (6758.18)		
6		17312.42 (17312.42)	13523.02 (13523.00)	... (9900.99)	6442.10 (6442.14)	
7			16511.60 (16511.56)	12889.53 (12889.55)		
8				15725.33 (15725.31)	12266.46 (12266.46)	
9					14944.94 (14950.01)	11650.72 (11650.68)

[a] From the calculated term values in Table X.
[b] Calculated values in parentheses.

the Dunham coefficients which resulted from the reduction of the vibrational term values. The 22 observed band centers agree quite satisfactorily with those calculated from the five Dunham coefficients, as shown in Table XI. The maximum deviation is 0.12 cm^{-1}, and the average is about 0.04 cm^{-1}. Therefore, we may conclude that systematic errors in the measured wave numbers are no greater than 0.1–0.2 cm^{-1}.

In the Dunham expansion of the total energy the vibrational terms are given by

$$E_v=\sum_i Y_{i0}(v+\tfrac{1}{2})^i. \qquad (6)$$

In order to obtain an idea of the sensitivity of the Y_{i0} to the number of levels fitted to Eq. (6) and to the degree of the polynomial, least-squares calculations were run for several choices of input data. Table XII shows the variation in the Dunham coefficients when the first six, first seven, etc., levels are used with a fifth-degree polynomial. Although the Y_{50} term contributes about 7 cm^{-1} to the energy at $v=6$, it is seen that levels through $v=9$ are required to determine Y_{50} with any certainty. The last column of Table XII gives the result of fitting levels $v=0$–9 to a sixth-degree polynomial. Clearly, Y_{60} cannot be determined at all, and its inclusion in the calculation interferes with the determination of the lower coefficients. The best choice available is therefore the next-to-last column of Table XII. These values are included in the general tabulation of Dunham coefficients in Table IX.

The uncertainties given in Table IX are the estimated standard deviations which result from the least-squares calculations. From the general trends presented here we may conclude that these strictly statistical uncertainties provide fairly reliable estimates for the true accuracy of the Y_{10}, Y_{20}, and Y_{30} values. However, the best values for Y_{40} and Y_{50} may be biased by the omission of the undetermined (but probably significant) higher coefficients, so that larger uncertainties should be assigned. Thus the apparently anomalous sign of Y_{50} may simply reflect its absorption of the contributions of the higher Y's.

The present results for Y_{10} and Y_{20} (i.e., ω_e and $-\omega_e x_e$) differ by about 1.5 cm^{-1} from previously accepted values. These changes are due chiefly to the inclusion of more vibrational levels in the calculation, which allowed a better determination of the higher coefficients. They illustrate the difficulty in obtaining very precise information on potential functions from a limited amount of spectroscopic data.

CONCLUSIONS

The present results in conjunction with those of Johns and Barrow[8] for the higher rotational and vibrational states define the molecular and spectroscopic constants of the HF molecule in its $X\,^1\Sigma^+$ state from their equilibrium values up to the dissociation limit with the exception of some levels in $v=9$ to 12.[19]

The lowest rotational level observed by Johns and Barrow[8] in $v=9$ is $J=27$ with energy 41521.2 cm^{-1}. The energy calculated for this level from our constants for $v=9$ is 41566.1 cm^{-1}. The difference is about equal

[19] Footnote reference 8, note added in proof.

TABLE XII. Effect of input data on Dunham coefficients.

	Levels used in calculation				
	$v=0$–6	$v=0$–7	$v=0$–8	$v=0$–9	$v=0$–9[a]
E_0	−2046.91	−2047.09	−2046.98	−2046.97	−2047.03
Y_{10}	4138.53±0.47	4139.11±0.42	4138.76±0.34	4138.73±0.20	4138.93±0.47
Y_{20}	−89.84±0.38	−90.36±0.31	−90.07±0.23	−90.05±0.12	−90.22±0.39
Y_{30}	0.84±0.14	1.04±0.10	0.940±0.063	0.932±0.030	0.997±0.140
$Y_{40}\times10^3$	2.4±22.0	−30±13	−15.2±7.7	−14.2±3.3	−26±25
$Y_{50}\times10^3$	1.7±1.3	0.2±0.7	−0.54±0.34	−0.59±0.13	0.5±2.2
$Y_{60}\times10^3$	...	...	...	...	−0.03±0.07

[a] With six-degree polynomial.

to the estimated uncertainty in our constants. On the other hand the value for B_9 obtained in this work should be more accurate since it was determined from low J lines. The actual difference in values for B_9 is about 0.07 cm^{-1}.

The lowest vibrational level in which Johns and Barrow[6] measured a $J=0$ line is $v=13$. Extrapolation of our formula for E_v yields 41018.2 cm^{-1} at $v=13$ whereas their term is 40973.1 cm^{-1}. This is probably as good agreement as can be expected under the circumstances and serves to illustrate the errors likely to be encountered in this type of extrapolation. Johns and Barrow[8] determined their formula for E_v by fitting their observations on $v=10$–19 together with the older infrared data on $v=0-4$. It predicts $E_8=29131.8$ and $E_9=31810.0$ cm^{-1}. The observed values from our measurements are 29145.30 and 31828.85 cm^{-1}, respectively. It must therefore be concluded that the results available for $v=10$, 11, and 12 are not yet very precise. This is hardly surprising in view of the long extrapolations from high J required for their determination. It seems likely that the true values lie between the results quoted by Johns and Barrow[7] and the values calculated from our formulas.

ACKNOWLEDGMENTS

Partial support by the Chemistry Branch, Air Force Office of Scientific Research during the early stages of this research is gratefully acknowledged. The authors also wish to express their appreciation to Dr. Shirleigh Silverman and Dr. Gordon E. Moore for helpful discussions.

Quasi-Lattice Model of Reciprocal Salt Systems. A Generalized Calculation

MILTON BLANDER

Oak Ridge National Laboratory, Oak Ridge, Tennessee*

(Received July 21, 1960)

A generalized statistical-mechanical calculation of the solution thermodynamics of the reciprocal molten salt system A^+, B^+, C^-, and D^- dilute in A^+ ions has been made. The calculation is based on the quasi-lattice model of reciprocal salt systems and treats the problem as an order-disorder problem. Associations of the A^+ and C^- ions as

$$A^+ + C^- \rightleftharpoons AC \quad \text{(A)}$$

$$AC + C^- \rightleftharpoons AC_2^- \quad \text{(B)}$$

$$AC_2^- + C^- \rightleftharpoons AC_3^- \quad \text{(C)}$$

are taken into account. In terms of the conventional equilibrium constants K_1, K_2, and K_3 for (A), (B), and (C), respectively,

$$K_1 = Z(\beta_1 - 1) \quad (1)$$

$$K_1K_2 = \frac{Z(Z-1)}{2!}(\beta_1\beta_2 - 2\beta_1 + 1) \quad (2)$$

$$K_1K_2K_3 = \frac{Z(Z-1)(Z-2)}{3!}(\beta_1\beta_2\beta_3 - 3\beta_1\beta_2 + 3\beta_1 - 1), \quad (3)$$

where Z is the quasi-lattice coordination number, $\beta_j = \exp(-\Delta A_j/kT)$ and ΔA_j may be termed a specific bond free energy of the jth C^- ion and is the specific Helmholtz free energy change for the formation of the jth bond. Equations (1), (2), and (3) demonstrate the surprising fact that the higher order association constants are dependent on the magnitude of the lower order association constants not only through the factor containing Z but also through the values of the β_i for the lower association constants. If $\beta_1 = \beta_2 = \beta_3 = \cdots$ etc., the equations reduce to the statistical ratios of Bjerrum. The higher association constants can be shown to be smaller for a case in which the bonding is directional (e.g., linear AC_2^-), than if they are nondirectional, as in Eqs. (2) and (3), even if the bond free energies are equal in the two cases.

INTRODUCTION

A QUASI-lattice model[1] of the molten reciprocal salt system A^+, B^+, C^-, and D^- dilute in A^+ and C^- ions has led to a potentially useful prediction of the temperature coefficients of the conventional association constant for the equilibrium

$$A^+ + C^- \rightleftharpoons AC.$$

The calculations made previously are generally not correct for any of the higher association constants. In this paper a generalization of the asymmetric[1b,1e] approximation based on the quasi-lattice model will be given and the correspondence of the parameters defined by the model to conventional mass law equilibrium constants will be shown. The generalization given here should apply to some of the higher association constants.

THE MODEL

A reciprocal salt system is a mixture of salts containing at least two cations and two anions. For simplicity, the simplest member of this class of systems—that containing the two cations A^+ and B^+ and the two anions C^- and D^-—will be discussed. The lattice model for this system consists of two interlocking sublattices, one exclusively of cations and the other exclusively of anions. The nearest neighbors of each cation are Z anions and of each anion are Z cations where Z is the lattice coordination number. By making the A^+ ion the same size as the B^+ and the C^- ion the same size as the D^- ion, any differences in the Coulombic interactions of the ions is eliminated and the model is restricted to extra-Coulombic interactions, which are here assumed to be nearest-neighbor interactions. The anion portion of the lattice is then divided into two regions, a and b. Region a contains all positions adjacent to one A^+ ion and $(Z-1)B^+$ ions and region b contains all positions adjacent to ZB^+ ions. The model is restricted to solutions dilute enough in A^+ ions to neglect anion positions adjacent to two A^+ ions. An extra-Coulombic interaction of ions is assumed so that the interchange of a C^- ion in region b with a D^- ion in region a leads to an energy change. Up to now the model is identical with the one discussed previously.[1b] The difference in the approximation considered here from that given previously is that all the positions in region a are not equivalent. The manner of occupation of the anion sites adjacent to a given A^+ ion will influence the energy change for replacing a D^- ion adjacent to a

* Operated for the U. S. Atomic Energy Commission by Union Carbide Nuclear Company.

[1] (a) M. Blander, F. F. Blankenship, and R. F. Newton, J. Phys. Chem. **63**, 1259 (1959); (b) M. Blander, *ibid.* **63**, 1262 (1959); (c) J. Braunstein and M. Blander, *ibid.* **64**, 10 (1960); (d) D. G. Hill, J. Braunstein, and M. Blander, *ibid.* **64**, 1038 1960), (e) M. Blander and J. Braunstein, Ann. N. Y. Acad. Sci. **79**, 838 (1960).

given A^+ ion by a C^- ion; in other words, the hypothesis of the interference of pair interactions will be included in the model.

This can be written as

$$AC_{j-1}^{+(2-j)}+C^- \rightleftharpoons AC_j^{+(1-j)}\ \Delta E_j\ 1\leq j\leq Z, \quad (1)$$

where it is understood that the symbol $AC_j^{+(1-j)}$ stands for an A^+ ion having jC^- ions and $(Z-j)D^-$ ions adjacent to it and the symbol C^- stands for a C^- ion having only B^+ ions as nearest neighbors, and where ΔE_j is the energy change for the indicated "reaction." In general

$$\Delta E_1 \neq \Delta E_2 \neq \Delta E_3 \neq \cdots \neq \Delta E_Z. \quad (2)$$

STATISTICAL CALCULATION

The problem is to calculate the thermodynamic properties, specifically, the chemical potentials of individual components, of the model system. To do this a total partition function for the entire assembly of ions will be calculated. Tables I, II, and III list the symbols assigned to the energy, partition function, and total number of ions for three of the four ions in all states of these three ions.

Any differences in the energy or partition function for B^+ ions due to differences in nearest neighbors can be arbitrarily assigned to the nearest-neighbor ion causing the difference and the B^+ ion is assigned the energy E_B and the partition function s for all positions. The differences between different types of A^+ ions could likewise have been arbitrarily assigned to the environmental C^- ions. Such differences were included in the partition function of A^+ ions, however, to demonstrate the validity of this arbitrary assignment.

In Table I the symbols characterizing the A^+ ion having between 0 and Z C^- ions as nearest neighbors are listed; n_A is the total number of A^+ ions, n_1' is the number of A^+ ions having one or more C^- ions as nearest neighbors and, in general, n_j' is the number of A^+ ions having j or more nearest neighbors. Thus, n_A-n_1' is the number of A^+ ions having no C^- ions as nearest neighbors and $(n_j'-n_{j+1}')$ is the number having only j C^- ions as nearest neighbors. In Table II, the energy and partition function of the j C^- ions which are members of $AC_j^{+(1-j)}$ groupings are given in columns 3 and 4. The factorial in the denominator of the expression for the partition function $(j!)$ arises because of the indistinguishability of the j C^- ions in the $AC_j^{+(1-j)}$ grouping. The total number of C^- ions in region a adjacent to all the A^+ ions is

$$Zn_Z+\sum_1^{Z-1} i(n_i'-n_{i+1}')=\sum_1^Z n_i'. \quad (3)$$

The total number of C^- ions is n_C and the number of C^- ions in region b is $n_C-\sum_1^Z n_i'$.

The quantities in Table III are self-evident. The total number of D^- ions is n_D. The number of D^- ions in regions a and b is equal to the number of positions in each of these regions not filled by C^- ions.

The combinatory factor for all the anions can be calculated as if the j positions containing C^- ions adjacent to a given A^+ ion having only j C^- ions adjacent to it were distinguishable, since the factor correcting for the indistinguishability of these j C^- ions has been included in the partition functions for the individual groups of C^- ions. Thus, the combinatory factor can be written in a way which is very much like a similar factor calculated for multilayer adsorption.[2,3] The number of independent ways of putting n_1' indistinguishable C^- ions onto the Zn_A positions adjacent to all the A^+ ions so that no more than one C^- ion is a nearest neighbor to any one A^+ ion is

$$g_0=\frac{Zn_A(Zn_A-Z)(Zn_A-2Z)\cdots[Zn_A-(n_1'-1)Z]}{n_1'!}=\frac{Z^{n_1'}n_A!}{n_1'!(n_A-n_1')!} \quad (4)$$

In a similar manner it can be shown that the number of ways of putting n_{j+1}' C^- ions onto all the A^+ ions having j C^- ions adjacent to them so that no more than $j+1$ C^- ions are adjacent to any one A^+ ion is

$$g_j=[(Z-j)^{n_{j+1}'}n_j'!]/[n_{j+1}'!(n_j'-n_{j+1}')!] \qquad 1\leq j\leq Z-1. \quad (5)$$

The combinatory factor for the $(n_C-\sum_1^Z n_i')$ C^- ions and the $(n_D-Zn_A+\sum_1^Z n_i')$ D^- ions on the $(n_C+n_D-Zn_A)$ positions in region b is[4]

$$g_b=(n_C+n_D-Zn_A)!\Big/[(n_C-\sum_1^Z n_i')!(n_D-Zn_A+\sum_1^Z n_i')!]. \quad (6)$$

TABLE I. Symbols for the A^+ ion.

State	Energy	Partition function	Number
A^+	$(E_A)_0$	r_0	n_A-n_1'
AC	$(E_A)_1$	r_1	$n_1'-n_2'$
AC_2^-	$(E_A)_2$	r_2	$n_2'-n_3'$
.	.	.	.
.	.	.	.
.	.	.	.
$AC_Z^{+(1-Z)}$	$(E_A)_Z$	r_Z	n_Z'

[2] Terrell L. Hill, J. Chem. Phys. **14**, 263 (1946).
[3] Malcolm Dole, J. Chem. Phys. **16**, 25 (1948).

TABLE II. Symbols for the C^- ions.

State	Number of ions referred to by columns 3 and 4	Energy	Partition function	Total number
AC	1	E_1	q_1	$n_1'-n_2'$
AC_2^-	2	E_1+E_2	$q_1q_2/2!$	$(n_2'-n_3')2$
$AC_3^{=}$	3	$E_1+E_2+E_3$	$q_1q_2q_3/3!$	$(n_3'-n_4')3$
$\vdots$	$\vdots$	$\vdots$	$\vdots$	$\vdots$
$AC_j^{+(1-j)}$	j	$\sum_1^j E_i$	$\prod_1^j q_i/j!$	$(n_j'-n_{j+1}')j$
$\vdots$	$\vdots$	$\vdots$	$\vdots$	$\vdots$
$AC_Z^{+(1-Z)}$	Z	$\sum_1^Z E_i$	$\prod_1^Z q_i/Z!$	$n_Z'Z$
C^- (region b)	1	E_0	q_0	$n_c-\sum_1^Z n_i'$

After the C^- ions are placed in any given configuration there is only one way to place the indistinguishable D^- ions in the remaining lattice sites so that there is no contribution to the combinatory factor from the D^- ions.

The combinatory factor for the cations is[4]

$$g_c=(n_A+n_B)\,!/n_A!n_B! \tag{7}$$

assuming that the solution is dilute enough in A^+ ions so that A^+ ions are independent of each other.

The total partition function Q_T can be written as

$$\ln Q_T=\sum \ln Q, \tag{8}$$

where the sums are taken over all possible combinations of values of n_1', $n_2'\cdots$ and n_Z' and where

$$Q=g_bg_cg_0[\prod_1^{Z-1}g_j][\prod_{j=1}^{Z}(\prod_1^j q_i/j!)^{n_j'-n_{j+1}'}]q_0^{n_C-\Sigma n_j'}p_a^{Zn_A-\Sigma n_j'}p_b^{n_D-Zn_A+\Sigma n_j'}r_0^{n_A-n_1'}r_Z^{n_Z'}(\prod_1^{Z-1}r_j^{n_j'-n_{j+1}'})s^{n_B}. \tag{9}$$

Combining and canceling some terms and simplifying the expression, one obtains

$$Q=\frac{(n_A+n_B)\,!(n_C+n_D-Zn_A)\,!n_A!(Z\beta_1)^{n_1'}\{[(Z-1)/2]\beta_2\}^{n_2'}\cdots(Z^{-1}\beta_Z)^{n_Z'}q_0^{n_C}(p_a/p_b)^{Zn_A}p_b^{n_D}r_0^{n_A}s^{n_B}}{n_A!n_B!(n_C-\sum n_j')\,!(n_D-Zn_A+\sum n_j')\,!(n_A-n_1')\,!(n_1'-n_2')\,!\cdots(n_{Z-1}'-n_Z')\,!n_Z'!}, \tag{10}$$

where

$$\beta_i=q_ip_br_i/q_0p_ar_{i-1}\qquad 1\le i\le Z;$$

$\ln Q_T$ is very well approximated by the maximum term in the summation, $\ln Q_{\max}$. The values of n_i' in the maximum term are calculated by maximizing $\ln Q$ with respect to all the n_i' at constant composition

$$\partial \ln Q/\partial n_i'=0\qquad 1\le i\le Z. \tag{11}$$

The following set of Z equations is obtained for the values of n_i' in the maximum term of $\ln Q_T$ using Stirling's approximation for the factorials,

$$\begin{aligned}
n_1-n_2&=(n_A-n_1)Z\beta_1 f\\
n_2-n_3&=(n_1-n_2)[(Z-1)/2]\beta_2 f=(n_A-n_1)[Z(Z-1)/2!]\beta_1\beta_2 f^2\\
&\ \ \vdots\qquad\quad\vdots\qquad\quad\vdots\qquad\quad\vdots\qquad\quad\vdots\\
n_{Z-1}-n_Z&=(n_{Z-2}-n_{Z-1})[2/(Z-1)]\beta_{Z-1}f=(n_A-n_1)[Z!/(Z-1)\,!]\beta_1\cdots\beta_{Z-1}f^{Z-1}\\
n_Z&=(n_{Z-1}-n_Z)(1/Z)\beta_Z f=(n_A-n_1)\beta_1\cdots\beta_Z\cdot f^Z,
\end{aligned} \tag{12}$$

[4] Randomness of mixing of C^- and D^- ions in region b and of A^+ and B^+ on the cation lattice is assumed. Corrections for non-random mixing can be made but would complicate the calculations with what I believe would be no significant gain in the value of the calculation at the present state of development of the field.

TABLE III. Symbols for the D^-ion.

State	Number of ions referred to by columns 3 and 4	Energy	Partition function	Total number
Region a	1	$(E_D)_a$	p_a	$Zn_A-\sum_1^Z n_i'$
Region b	1	$(E_D)_b$	p_b	$n_D-Zn_A+\sum_1^Z n_i'$

where the lack of a prime on the n_i denotes the value of n_i' in the maximum term and where

$$f=(n_C-\sum_1^Z n_i)/(n_D-Zn_A+\sum_1^Z n_i). \tag{13}$$

The Helmholtz free energy A is calculated from

$$A=-kT\ln Q_{\max} \tag{14}$$

and the chemical potential of any component can be computed by taking the proper derivative of A. For the component AD, for example,

$$(\partial A/\partial n_A)+(\partial A/\partial n_D)=\mu_{AD}, \tag{15}$$

where μ_{AD} is the chemical potential of the component AD.[5] The calculation[6] leads to

$$\mu_{AD}/kT=\ln[(n_A-n_1)/n_A]-(1-Z)\ln(1+f)-\ln p_b+\ln[n_A/(n_A+n_B)]-Z\ln(p_a/p_b)-\ln r_0 \tag{16}$$

if the assumption is made that the β_i, p_a, p_b, r_0, and s are independent of n_A and n_D.

If

$$\mu_{AD}^*/kT=-\ln p_b-Z\ln(p_a/p_b)-\ln r_0, \tag{17}$$

where μ_{AD}^* is the chemical potential of the standard state of the component AD, then

$$(\mu_{AD}-\mu_{AD}^*)/kT=\ln[(n_A-n_1)/n_A]+(Z-1)\ln(1+f)+\ln[n_A/(n_A+n_B)]. \tag{18}$$

By summing the left- and right-hand sides, respectively, of the set of Eqs. (12) and then adding n_A-n_1 to both sides, one obtains

$$n_A=(n_A-n_1)(1+Z\beta_1 f+[Z(Z-1)/2!]\beta_1\beta_2 f^2+\cdots+[Z!/(Z-1)!]\beta_1\cdots\beta_{Z-1}f^{Z-1}+\beta_1\cdots\beta_Z f^Z). \tag{19}$$

Defining an activity coefficient by

$$(\mu_{AD}-\mu_{AD}^*)/kT=\ln N_{A^+}N_{D^-}\gamma_{AD};$$

where the ion fractions

$$N_{A^+}=n_A/(n_A+n_B)=1-N_{B^+}$$

and

$$N_{D^-}=n_D/(n_C+n_D)=1-N_{C^-}$$

then

$$\gamma_{AD}^{-1}=\frac{N_{D^-}(1+Z\beta_1 f+[Z(Z-1)/2!]\beta_1\beta_2 f^2+\cdots+[Z!/(Z-1)!]\beta_1\cdots\beta_{Z-1}f^{Z-1}+\beta_1\cdots\beta_Z f^Z}{(1+f)^{Z-1}}. \tag{20}$$

Taking the limit as $N_{A^+}\longrightarrow 0$ simplifies the calculations, since as

$$N_{A^+}\longrightarrow 0, \qquad f\rightarrow[N_{C^-}/(1-N_{C^-})]$$

[5] It should be noted that if the condition for electroneutrality $n_D=n_A+n_B-n_C$ is used to replace all the n_D in the expression for A, then $\partial A/\partial n_D$ which is termed the single ion chemical potential of D^- ion is arbitrarily set at zero. This is equivalent to replacing the n_A, n_B, n_C, and n_D by the numbers of molecules of three of the possible components, n_{AD}, n_{BD}, and n_{BC}. In such a substitution $n_A=n_{AD}$, $n_B=n_{BD}+n_{BC}$, $n_C=n_{BC}$, and $\partial A/\partial n_A=\partial A/\partial n_{AD}=\mu_{AD}$.

[6] Appendix A.

and

$$\lim_{N_{A^+}\to 0} \gamma_{AD}^{-1} = \{(1-N_{C^-})^Z + Z\beta_1 N_{C^-}(1-N_{C^-})^{Z-1} + [Z(Z-1)/2!]\beta_1\beta_2 N_{C^-}{}^2(1-N_{C^-})^{Z-2} + [Z(Z-1)(Z-2)/3!]\beta_1\beta_2\beta_3 N_{C^-}{}^3(1-N_{C^-})^{Z-3} + \cdots\}. \quad (21)$$

Correspondence of the parameters in Eq. (21) to conventional equilibrium or mass law constants can be made as follows. In the conventional "chemical" approach, the equilibria

$$A^+ + C^- \rightleftharpoons AC$$

$$AC + C^- \rightleftharpoons AC_2^-,$$

$$AC_2^- + C^- \rightleftharpoons AC_3^{2-}, \quad \text{etc.}$$

having the equilibrium quotients

$$K_1 = N_{AC}/N_{A^+}{}^f N_{C^-}{}^f \quad (22)$$

$$K_2 = N_{AC_2^-}/N_{AC}N_{C^-}{}^f \quad (23)$$

$$K_3 = N_{AC_3^{2+}}/N_{AC_2^-}N_{C^-}{}^f \quad \text{etc.} \quad (24)$$

are assumed, where the N refers to ion fractions or mole fractions of the ions or molecules and the superscript f denotes the "free" or "uncomplexed" ions. The total stoichiometric concentration of A^+ ion is equal to the sum of the concentrations of the species containing A^+ ion and

$$N_{A^+} = N_{A^+}{}^f + N_{AC} + N_{AC_2^-} + N_{AC_3^{2-}} + \cdots. \quad (25)$$

Substituting for N_{AC}, $N_{AC_2^-}$, and $N_{AC_3^{2-}}$ in Eq. (25) from Eqs. (22), (23), and (24) and following the conventional assumption that the activity coefficient of the component AD is equal to $N_{A^+}{}^f/N_{A^+}$ and then taking the limit as $N_{A^+}\to 0$, one obtains

$$\lim_{N_{A^+}\to 0} \gamma_{AD}^{-1} = 1 + K_1 N_{C^-} + K_1 K N_{C^-}{}^2 + K_1 K_2 K_3 N_{C^-}{}^3 + \cdots \quad (26)$$

remembering that as $N_{A^+}\to 0$, $N_{C^-}{}^f \to N_{C^-}$.

Expanding the individual terms in (21) and equating the coefficients of N_{C^-}, $N_{C^-}{}^2$, and $N_{C^-}{}^3$, etc., to the corresponding terms of Eq. (26) one obtains

$$K_1 = Z(\beta_1 - 1) \quad (27)$$

$$K_1K_2 = [Z(Z-1)/2!](\beta_1\beta_2 - 2\beta_1 + 1), \quad (28a)$$

from which

$$K_2 = [(Z-1)/2]\{(\beta_2 - 1) + [(\beta_2 - \beta_1)/(\beta_1 - 1)]\} \quad (28b)$$

and

$$K_1K_2K_3 = \frac{Z(Z-1)(Z-2)}{3!}[\beta_1\beta_2\beta_3 - 3\beta_1\beta_2 + 3\beta_1 - 1] \quad (29)$$

$$K_1K_2K_3K_4 = \frac{Z(Z-1)(Z-2)(Z-3)}{4!}[\beta_1\beta_2\beta_3\beta_4 - 4\beta_1\beta_2\beta_3 + 6\beta_1\beta_2 - 4\beta_1 + 1]. \quad (30)$$

The terms in Z may be termed spatial (or configurational) and statistical factors and the terms in β_i are related to bond free energies.

DISCUSSION

Equations (27), (28), (29), and (30) show the relationship of conventional equilibrium constants to the parameters defined in the lattice model where nondirectional "bonding" is involved. If the partition functions for the individual ions are separable so that

$$q_i = \bar{q}_i \exp(-Ei/kT) \quad (31)$$

$$p_b = \bar{p}_b \exp[-(E_D)_b/kT] \quad (32)$$

$$r_i = \bar{r}_i \exp[-(E_A)_i/kT] \quad (33)$$

$$p_a = \bar{p}_a \exp[-(E_D)_a/kT], \quad (34)$$

where the bar $(^-)$ denotes the internal partition function then

$$\beta_i = (\bar{q}_i\bar{p}_b\bar{r}_i/\bar{q}_0\bar{p}_a\bar{r}_{i-1}) \exp(-\Delta E_i/kT), \quad (35)$$

where

$$\Delta E_i = E_i + (E_D)_b + (E_A)_i - E_0 - (E_D)_a - (E_A)_{i-1}. \quad (36)$$

If the internal degrees of freedom of the ions involved in an association process are not significantly changed[7] in association, then

$$\beta_i = \exp(-\Delta E_i/kT). \quad (37)$$

For $i=1$ Eq. (37) has been derived previously[1d] and has been demonstrated empirically[1e,1d] in the Ag^+, K^+, Cl^-, NO_3^-, and the Ag^+, Na^+, Cl^-, NO_3^- systems. This can be stated in other words. If the quantity $-kT\ln\beta_i$ is defined as ΔA_i, then ΔA_i is the specific Helmholtz free energy for forming the ith "bond" and might be termed the specific bond free energy.

[7] It is actually the products of the ratio of the final to the initial partition functions of the ions involved in the association process which enters and hence nothing can be deduced about any one ion.

If

$$\Delta A_i = \Delta E_i - T\Delta S_i,$$

where

$$\Delta S_i = -R \ln(\tilde{q}_i \tilde{p}_b \tilde{r}_i / \tilde{q}_0 \tilde{p}_a \tilde{r}_{i-1}), \quad (38)$$

then ΔS_i is a specific entropy of association which includes only internal degrees of freedom and excludes the spatial and statistical combinatory factors. The demonstration of the validity of Eq. (37) for associations of Ag^+ and Cl^- ions to form the ion pair Ag-Cl in the molten solvents $NaNO_3$ and KNO_3 means the $\Delta S_1 \cong 0$ in these two systems. It is to be hoped that the validity of this relation can be demonstrated more generally, at least for cases in which all the ions in a system are monatomic and probably do not exhibit appreciable changes in their internal degrees of freedom upon association.

The derived Eqs. (27)–(30) lead to some unusual and surprising results. Equation (28b) gives the second association constant K_2 in terms of the lattice parameters. Although the factor containing β_1 is probably small, it cannot be factored from the expression for K_2. This surprising result means that K_2 is a function not only of β_2 but also of β_1. The effect of β_1 on K_2 is relatively significant if β_2 is small. In fact, if β_2 is less than two but greater than one, it can be seen from Eq. (28a) that K_2 might be negative even though there exists a tendency for the association of the AC pair with a C^- ion (i.e., $\beta_2 > 1$). This unusual result, which is similar for the higher association constants, arises because of the requirement that the conventional equilibrium constants K_i be almost zero in an almost ideal solution containing A^+, B^+, C^-, and D^- ions. These results cannot always be described in a thermodynamically self-consistent manner and the defined standard states for some of the associated species in this commonly accepted method of describing associations in solution cannot be understood in a simple way.

The equations derived here can be related to previous work. For example, taking the special case in which all the specific bond free energies for the attachment of successive C^- ions are equal so that

$$\Delta A_1 = \Delta A_2 = \Delta A_3 = \cdots = \Delta A_Z$$

and

$$\beta_1 = \beta_2 = \beta_3 = \cdots = \beta_Z$$

then

$$K_1/Z = 2K_2/(Z-1) = 3K_3/(Z-2) = \cdots = ZK_Z. \quad (39)$$

This particular result, obtained from the general expressions derived here for the absolute values of the association constants, was obtained by N. Bjerrum.[8]

In the calculations leading to Eqs. (27)–(30) it has been assumed that the second C^- ion attaching itself to an A^+ ion can do so in $(Z-1)$ different positions. If only a linear grouping AC_2^- can be formed, for example, so that the second C^- ion can have a nonzero value of ΔA_2 in only one of the $(Z-1)$ sites then for this linear AC_2^-

$$K_1 K_2' = [Z(Z-1)/2!]\{[\beta_1\beta_2/(Z-1)]+1 - [Z/(Z-1)]\beta_1\}. \quad (40)$$

It is easy to show that K_2' in Eq. (37) will be lower than K_2 of Eq. (28a) for the same values of Z, β_1, and β_2. We may conclude that a direct comparison of the second association constants (i.e., K_2) for two different substances which may have the same coordination number may not be a direct measure of the specific bond free energy of the "bond." *The greater the tendency towards "directionality" in a "bond" the lower will be the association constant, if all other factors (i.e., Z, β_1, β_2, etc.) are equal.* The same sort of conclusions hold for some of the higher association constants. If we take the case in which $\beta_1 = \beta_2 \gg 1$ to illustrate some of the consequences of Eq. (40) then

$$K_1/K_2' \cong 2Z, \quad (41)$$

where it is to be remembered that Z is a *maximum coordination number*. The result expressed by Eq. (41), which is a special case of Eq. (40), is at variance with statements of Bjerrum[9] who has stated that the ratio K_1/K_2' is given by $2N$ where N is a *characteristic coordination number*. For a case, which appears to be quite common in aqueous solutions, in which $\beta_3 \ll \beta_2$, Bjerrum's characteristic coordination number, N, would be two and hence much smaller than Z.

Expressions for many other possible configurations can be derived from this model for comparison with experimental measurements in specific systems. It is hoped that the relations derived from the lattice model will lead to an insight into the meaning and interpretation of associations in solution and will prove to be generally useful in predicting the temperature coefficients of some thermodynamic properties of reciprocal salt solutions. Although the calculations made here were derived for molten salts, they can probably be justified for more general use. The relations described here will probably prove most useful for molten salts because of the innate simplicity of molten salt solutions.

APPENDIX A

Using Stirling's approximation for the factorials $\ln F! = F \ln F - F$ and taking the derivatives of $\ln Q_{max}$

[8] (a) N. Bjerrum, Z. physik. Chem. **106**, 222 (1923); (b) see also I. M. Klotz, Arch. Biochem. **9**, 109 (1946).

[9] J. Bjerrum, Chem. Revs. **46**, 381 (1950).

with respect to n_A and n_D one obtains

$$\frac{\partial \ln Q_{\max}}{\partial n_A}=\frac{1}{kT}\frac{\partial A}{\partial n_A}=\frac{\partial(n_A \ln n_A-n_A)}{\partial n_A}-\frac{\partial[(n_A-n_1)\ln(n_A-n_1)-(n_A-n_1)]}{\partial n_A}$$

$$+\frac{\partial[(n_A+n_B)\ln(n_A+n_B)-(n_A+n_B)]}{\partial n_A}-\frac{\partial(n_A \ln n_A-n_A)}{\partial n_A}$$

$$+\frac{\partial[(n_C+n_D-Zn_A)\ln(n_C+n_D-Zn_A)-(n_C+n_D-Zn_A)]}{\partial n_A}$$

$$-\frac{\partial[(n_D-Zn_A+\sum_1^Z n_j)\ln(n_D-Zn_A+\sum_1^Z n_j)-(n_D-Zn_A+\sum_1^Z n_j)]}{\partial n_A}+Z\ln(p_a/p_b)+\ln r_0$$

$$=\ln n_A-\ln(n_A-n_1)+\ln(n_A+n_B)-\ln n_A-Z\ln(n_C+n_D-Zn_A)$$

$$+Z\ln(n_D-Zn_A+\sum_1^Z n_j)+Z\ln(p_a/p_b)+\ln r_0 \quad \text{(i)}$$

$$\frac{\partial \ln Q_{\max}}{\partial n_D}=\frac{1}{kT}\frac{\partial A}{\partial n_D}=\frac{\partial[(n_C+n_D-Zn_A)\ln(n_C+n_D-Zn_A)-(n_C+n_D-Zn_A)]}{\partial n_D}$$

$$-\frac{\partial[(n_D-Zn_A+\sum_1^Z n_j)\ln(n_D-Zn_A+\sum_1^Z n_j)-(n_D-Zn_A+\sum_1^Z n_j)}{\partial n_D}+\ln p_b$$

$$=\ln(n_C+n_D-Zn_A)-\ln(n_D-Zn_A+\sum_1^Z n_j)+\ln p_b. \quad \text{(ii)}$$

Although the terms n_j are functions of n_A and n_D the calculation is simplified since the sum of the terms in the derivative which contain $(\partial n_j/\partial n_A)$ and $(\partial n_j/\partial n_D)$ will be zero as a consequence of Eq. (11).[10] That is, the relation

$$\sum_1^Z(\partial \ln Q/\partial n_j')(\partial n_j/\partial n_A)+\sum_1^Z(\partial \ln Q/\partial n_j')(\partial n_j/\partial n_D)=0 \quad \text{(iii)}$$

holds at $Q=Q_{\max}$. It should be remembered that the set of partial derivatives $(\partial \ln Q/\partial n_j')$ are at constant values of n_A, n_B, n_C, n_D, and of $n_i \neq n_j$. The two sets of partial derivatives $(\partial n_j/\partial n_A)$ and $(\partial n_j/\partial n_D)$ are at constant n_B and n_C. The sum of Eqs. (i) and (ii) leads to Eq. (16).

[10] See, for example, E. A. Guggenheim, *Mixtures* (Oxford University Press, London, 1952), p. 45.

Effect of Solvent and Solute Structure on Scintillator Pulse Heights. I. Correlation of Pulse Heights for Ring Substituted Styrene Plastic Scintillators with Hammett Substituent Constants*

STANLEY R. SANDLER AND SAMUEL LOSHAEK

Central Research Laboratory, Borden Chemical Company, Philadelphia, Pennsylvania

(Received July 25, 1960)

A group of different ring substituted styrene plastic scintillators were prepared with a constant concentration of *p*-terphenyl as the fluor and POPOP as the waveshifter. The effect of this variation in the structure of the polymer phase on pulse-height response to β and γ radiation was determined. It was found that correlations exist between the relative pulse height and the Hammett (σ) and Taft (σ_I) substituent constants for the substituted polystyrenes. Pulse heights increase with an increase in the negative value of the substituent constant, i.e., with an increase in the electron-donating power of the ring substituent on the polystyrene. It was found that markedly lower relative pulse heights were obtained for a series of styrene plastics in which the α-hydrogen in the backbone chain was substituted by a methyl group. This suggests that an α-hydrogen in the backbone chain is required for an efficient plastic solvent.

INTRODUCTION

THE generally accepted mechanism[1-4] of scintillation resulting from the absorption of ionizing irradiation in plastic and organic liquid scintillators is outlined below:

energy absorption by the solvent and excitation

$$S+E/w_0 \longrightarrow S^*, \tag{1}$$

fluorescence emission from the solvent

$$S^* \xrightarrow{p_{es}} S+h\nu_1, \tag{2}$$

solvent self-quenching

$$S^*+S \xrightarrow{p_{ss}} S+S, \tag{3}$$

energy transfer from solvent to solvent

$$S^*+S \xrightarrow{p_{ts}} S+S^*, \tag{4}$$

energy transfer to fluor

$$S^*+F \xrightarrow{p_t} S+F^*, \tag{5}$$

fluorescence emission from fluor

$$F^* \xrightarrow{p_{ef}} F+h\nu_2, \tag{6}$$

fluor self-quenching

$$F^*+F \xrightarrow{p_{ff}} F+F, \tag{7}$$

fluor internal quenching by solvent interaction

$$F^*+S \xrightarrow{p_i} F+S, \tag{8}$$

fluor internal quenching

$$F^* \xrightarrow{p_i} F. \tag{8a}$$

In these equations, S and F represent the solvent and fluor concentrations, respectively, the p's are the probabilities ($1/\tau$) of the various processes, E is the absorbed particle energy, and w_0 is the average dissipated particle energy required to produce one fluorescent excitation in the solvent.

On the basis of the above mechanism, Kallmann and Furst[1,2] derived an equation which predicts the dependence of pulse height (PH) on fluor concentration. Swank and Buck[4] found that the same equation held for plastic scintillators and included the refinement of fluorescent emission by the solvent. This basic equation has appeared in various forms[1-4] but all are mathematically equivalent to Eq. (9),

$$\mathrm{PH}=(E/w_0)q_f\delta[(q_0+kc)/(1+kc)][(1+mc)^{-1}], \tag{9}$$

where $kc=p_t/(p_{ss}+p_{es})$, $mc=p_{ff}/(p_{ef}+p_i)$, $q_f=p_{ef}/(p_{ef}+p_i)$ is the quantum yield of the fluor exclusive of fluor self-quenching, q_0 is the quantum yield of the solvent (very small in comparison to kc) and δ is a factor (includes photocathode efficiency, instrument factors, etc.) which converts the number of emitted quanta from the scintillator to an observed pulse height voltage.

In the case of liquid organic scintillators,[2] some progress has been made in determining the role of the various steps in this mechanism by varying the composition and concentration of both the solvent and the solute and observing the resulting effect on the pulse height response to α, β, and γ radiation. A similar

* This work was supported by the U. S. Atomic Energy Commission.

[1] H. Kallmann and M. Furst, Phys. Rev. **79**, 857 (1950).
[2] M. Furst and H. Kallmann, Phys. Rev. **85**, 816 (1952).
[3] G. T. Reynolds, Nucleonics **10**, 46 (1952).
[4] R. K. Swank and W. L. Buck, Nucleonics **91**, 927 (1953).

study[4] has been reported for plastic scintillators on the effect of fluor composition and concentration. However, an extensive study has not been made on the effect of solvent composition in plastic scintillators because of the unavailability of monomers which would afford a systematic variation in composition, and which, in addition, could be polymerized into optically clear scintillators. The objective in the present work, therefore, was to study the role of the solvent phase on the pulse-height response of plastic scintillators. This has been accomplished by the synthesis of a family of optically clear substituted styrene plastics having ring substituents differing greatly in their electron affinities.

Most of the interpretation of the mechanism of scintillation has thus far been primarily phenomenological, in that the various probability parameters which appear in Eq. (9) have not been related to the molecular architecture of the solvent and fluor. The present approach, on the other hand, offers a means of relating the molecular structure of the solvent phase with pulse heights in plastic scintillators. The same method also appears to show promise in treating pulse height data on organic liquid scintillators.[5]

Characterization of Polarity and Resonance in Polymeric Solvents by Hammett and Taft Substituent Constants

It is well known that mainly liquid and solid solutions containing double bonds, and particularly conjugated double-bond systems, make the best solvents for scintillators. This indicates that the electrons involved in these bonds and their mobility are important in the absorption of that portion of the incident energy which can potentially be emitted as light, and in the transfer of such energy from the solvent to the fluorescent molecule. Dipole-dipole interaction might also be a factor in the transfer of energy from solvent to solute[4,6] and this again would be favored by electron displacements within the molecule. It is reasonable to expect, therefore, that a suitable parameter which characterizes electron density distribution in a solvent molecule would bear some relation to the observed pulse height.

With the substituted styrenes used here, it is possible to place a relative numerical value on the extent to which the substituents either donate or withdraw electrons from the benzene ring as compared to the hydrogen atom. These are the Hammett sigma values[7] (hereafter abbreviated as σ) which have been interpreted as a measure of the electronegativity of the substitutents, and which have been used successfully to explain the rates and equilibria of many chemical reactions.

Recently, Taft[8,9] has shown that for meta- and para-benezene substituents (σ) can be divided into inductive (σ_I) and resonance (σ_R) components, i.e., $\sigma=\sigma_I+\sigma_R$. It has been found that the order of inductive effects obtained from the aliphatic series applies to the inductive contributions in the aromatic series. An inductive aromatic substituent content for the group X has been defined as $\sigma_x=0.45\sigma^*XCH_2-$ where σ^*XCH_2- is the inductive substituent constant for the group X in a given aliphatic series. The latter values are given relative to $\sigma^*HCH_2-=0$ and the factor of 0.45 places the value relative to the hydrogen atom as zero (σ_I for H=0). Greater physical significance is given to the inductive substituent constant by noting that it is proportional to the dipole moment of the substituent group.[8]

The application of the Hammett and Taft substituent constants to pulse-height data will be considered in the discussion of results.

RESULTS

Pulse Heights of Substituted Styrene Scintillators with β Radiation

Plastic scintillators were prepared[4] from a series of substituted styrenes whose substituent groups differed considerably in electronegativity. Para-terphenyl at 2 or 3% by weight and 0.05% POPOP were used throughout as the primary fluor and waveshifter, respectively. Monomer purity was determined by infrared spectral analysis and vapor phase chromatography. Average pulse heights relative to an anthracene crystal of the same dimensions were determined as previously described[9] ($Pa^{234}\beta$, 2.32 Mev). The pulse height values on the dimethyl styrene plastics were confirmed within experimental error in two other laboratories.[10] The results are summarized in Table I.

Pulse Heights of Selected Substituted Styrene Scintillators with γ Radiation

The relative pulse heights with γ radiation (Cs^{137}, 0.66 Mev) of a few selected substituted styrene plastic scintillators are also given in Table I.

Pulse Heights of Plastic Scintillators Based on Copolymers with Styrene or Vinyltoluene with β Radiation

In order to show the effect on pulse height of combining two monomers with different electronegativity in the solvent phase, a series of scintillators were prepared wherein the solvent phase consisted of copolymers of

[5] S. R. Sandler and Samuel Loshaek, J. Chem. Phys. **34**, 444 (1961).
[6] T. Forster, Ann. Physik **2**, 55 (1948).
[7] L. P. Hammett, Chem. Revs. **17**, 125 (1935).
[8] R. W. Taft, Jr., *Steric Effects in Organic Chemistry*, edited by M. S. Newman (John Wiley & Sons, Inc., New York, 1956), Chap. 13.
[9] R. W. Taft, Jr., N. C. Deno, and P. S. Skell, Ann. Rev. Phys. Chem. **9**, 287 (1958).
[10] We gratefully acknowledge the help of Dr. L. J. Basile of the Argonne National Laboratory and Dr. Newton F. Hayes of the Los Alamos Laboratory in making these measurements for us.

TABLE I. Relative pulse heights (β and γ radiation) for plastic scintillators[a] prepared from ring substituted styrenes.

Styrene substituent	RPH±2 for β	RPH±2 for γ
None	39	39
Mixed methyl isomers[b]	45	44
p-Ethyl	42	...
Mixed diethyl isomers[c]	48	...
3,4-Dimethyl	59	52
2,4-Dimethyl	62	55
2,5-Dimethyl	55	...
Mixed dimethyl isomers[d]	60	...
Mixed dimethyl isomers[e]	56	...
Mixed dimethyl isomers[f]	53	...
p-Isopropyl	43	...
p-*n*-Butyl[g]	32	...
p-sec-Butyl[g]	32	...
p-*t*-Butyl[g]	31	...
p-Benzyl	38	...
p-Methoxy	24	20
p-Chloro	2.5	0
m-Chloro	1.8	0
p-Dodecyl[g]	31	...
α-Methyl	5[h]	...
p-Methyl-α-methyl	6[h]	...
p-Isopropyl-α-methyl	3[h]	...

[a] All plastic scintillators contain 3% PTP and 0.05% POPOP except where noted.
[b] Vinyl toluene obtained from Dow.
[c] Diethyl benzene obtained from Dow was used to prepare this monomer.
[d] Mixture contains 51% 2,4-dimethyl styrene (DMS), 17% 3,4-DMS, and 32% 2,5-DMS.
[e] Mixture contains equal weights of 2,4-DMS, 3,4-DMS, and 2,5-DMS.
[f] The composition of this mixture determined by vapor phase chromatography was 30% 2,5-DMS, 49% 2,4-DMS, and 21% 3,4-DMS. This monomer was synthesized directly from Barrett Company commercial xylene.
[g] These scintillators were not optically clear.
[h] Value obtained by extrapolation of copolymer data—see Table II and Fig. 2.

TABLE II. Relative pulse heights of copolymer scintillators.[a]

Monomer composition %[b]					
Styrene	DMS	VT[c]	AMS	MAMS	RPH±2
	100[c]				62
	50[c]	50			51
	20[c]	80			44
		100			40
	100[d]				59
50	50[d]				48
60	40[d]				47
100					39
90			10		36
80			20		25
70			30		28
60			40		28
50			50		22
			100		5[f]
90				10	37
80				20	31
70				30	29
60				40	27
				100	6[f]

[a] All scintillators contain 3% PTP and 0.05% POPOP.
[b] DMS=dimethyl styrene; VT=vinyl toluene; AMS=α-methyl styrene; MAMS=*p*-methyl-α-methyl styrene; compositions are in % by weight.
[c] 2,4-DMS.
[d] 3,4-DMS.
[e] An undistilled monomer was used which gave a relative pulse height of 40%.
[f] Extrapolated values.

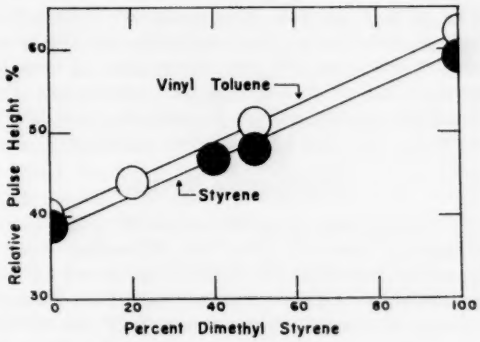

FIG. 1. Pulse heights of polydimethyl styrene copolymer scintillators with styrene and vinyl toluene.

dimethyl styrene with styrene or vinyl toluene. The results are presented in Table II and Fig. 1. This technique was useful in obtaining a knowledge of the pulse heights of scintillators prepared from α-methyl styrene and *p*-methyl-α-methyl styrene. Neither of these monomers can be polymerized alone to high molecular weight plastics but each could be copolymerized with styrene. Plastic scintillators based on copolymers of styrene with each of the foregoing monomers were prepared with as high a concentration of the

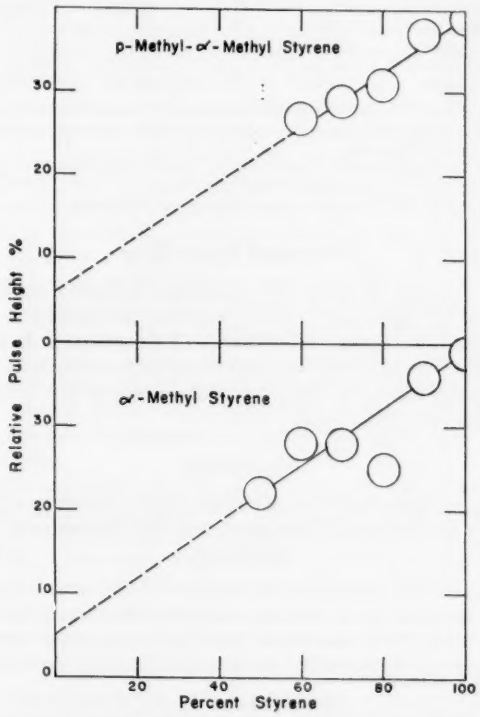

FIG. 2. Pulse heights of copolymer scintillators of styrene with α-methyl styrene and *p*-methyl-α-methyl styrene.

latter as was practical. The results are presented in Table II and Fig. 2. The pulse height of each homopolymer was obtained by extrapolation of the copolymer data to that of the pure component. This procedure appears amply justified in view of the results shown in Fig. 1 for the other copolymers.

Fluorescence Spectra

The fluorescence emission spectra of many plastic scintillators were obtained to determine whether differences in pulse height could be accounted for with these data. Spectra of a given polymer alone, the polymer with PTP and the polymer with PTP and POPOP were obtained for a large number of samples. The spectra of the plastics alone were very similar in detail in all cases as were the spectra with solutes.

TABLE III. Relative pulse height (β radiation) and σ values of substituted styrene plastic scintillators.

Styrene substituent	RPH ±2	Reference for σ, σ_I	σ	σ_I[a]
None	39		0	0
Methyl	45	7, 8	−0.16	−0.045
p-Ethyl	42	12, 7	−0.151	−0.0517
p-Isopropyl	43	12, 7	−0.151	−0.0563
3,4-Dimethyl	58	7, 8	−0.23	−0.090
2,4-Dimethyl	61	7, 8	(−0.32)[b]	−0.090
2,5-Dimethyl	54	7, 8	(−0.23)[b]	−0.090
Diethyl	49	12, 7	−0.302	−0.0134
p-Benzyl	38	7	...	+0.036
p-Methoxy	24	7, 8	−0.26	+0.25
p-Chloro	2.5	7, 8	+0.226	+0.47
m-Chloro	1.8	7, 8	+0.373	+0.47[c]

[a] For disubstituted styrenes the σ_I was obtained by taking the sum of the σ_I for two methyl groups.

[b] These values were obtained by assuming that the *o*-methyl and *p*-methyl values are the same and that the values are additive.

[c] σ_I was assumed to be the same as for the *p*-chloro substituent.

Fluorescent Decay Time

The rate of decay of luminescence following excitation by high-energy cathode rays was determined on a dimethyl styrene scintillator.[11] Two distinct decay rates were observed. The first decay rate corresponds to a decay time of 2.8×10^{-9} sec and the second to a decay time of 5.2×10^{-9} sec.

DISCUSSION

Correlation Between Relative Pulse Heights with β Radiation and Hammett and Taft Substituent Constants

Values of relative pulse heights (RPH) and σ and σ_I reported in the literature for the substituents used on the styrene monomers, which lead to polymers with good optical properties, are given in Table III. In order

[11] We gratefully acknowledge the help of Professor M. Burton of the University of Notre Dame in making these measurements for us.

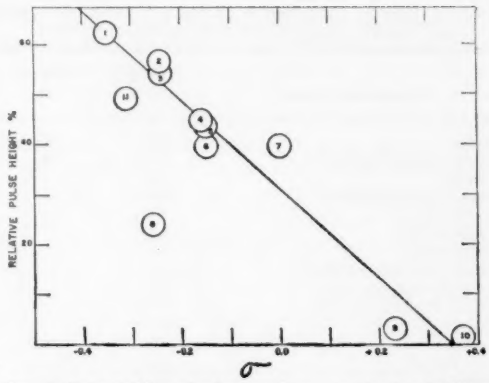

FIG. 3. Pulse heights of substituted styrene plastic scintillators vs σ. (1) 2,4-dimethyl styrene (DMS); (2) 3,4-DMS; (3) 2,5-DMS; (4) methyl styrene; (5) *p*-isopropyl styrene; (6) *p*-ethyl styrene; (7) styrene; (8) *p*-methoxy styrene; (9) *p*-chloro styrene; (10) *m*-chloro styrene; (11) diethyl styrene.

to obtain σ values for the dimethyl styrenes, the total σ for the molecule was taken as the sum for two methyl groups. Additivity has been shown to hold for substituents in the 3, 4, and 5 positions.[7,12] Thus, the values given for the 2,4- and 2,5-dimethyl derivatives can be considered only as an approximation. The additivity principle was also assumed to hold for the σ_I values for the dimethyl styrenes. The relative pulse heights are plotted against σ and σ_I in Figs. 3 and 4, respectively.

The data in Figs. 3 and 4 show a correlation between RPH and σ and σ_I, while the correlation with σ_R was

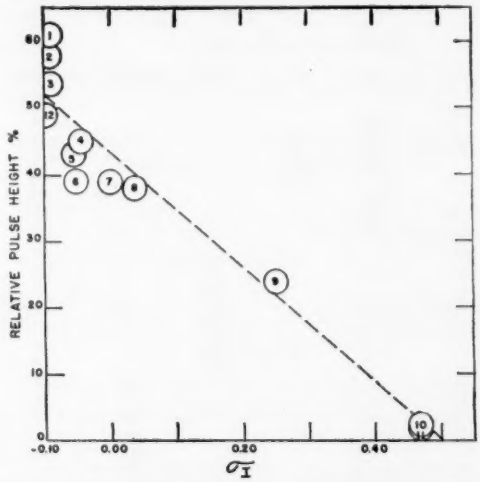

FIG. 4. Pulse height of substituted styrene plastic scintillators vs σ_I. (1) 2,4-DMS; (2) 3,4-DMS; (3) 2,5-DMS; (4) methyl styrene; (5) *p*-isopropyl styrene; (6) *p*-ethyl styrene; (7) styrene; (8) *p*-benzyl styrene; (9) *p*-methoxy styrene; (10) *p*-chloro styrene; (11) *m*-chloro styrene; (12) diethyl styrene.

[12] H. H. Jaffe, Chem. Revs. **53**, 191 (1953).

poor. The RPH increases with an increase in the negative value of σ and σ_I, i.e., with an increase in the electron donating power of the substituent. The correlation is better with σ except for *p*-methoxy styrene where the correlation is much better with σ_I. Of course, there is some uncertainty in the σ_I values assigned for the dimethyl styrenes. Thus, the correlation with σ_I is very good for the monosubstituted styrenes alone. The tendency for the dimethyl substituents to lie above the line for the monosubstituents may be due to additional enhancement effects in the former, or because of the approximate nature of the σ_I values assigned to these compounds. It would be more desirable to compare the dimethyl styrenes with other disubstituted styrenes.

The data for γ radiation shows a similar trend to the data with β radiation even though the absolute pulse heights are slightly lower.

From Fig. 1 for the copolymer data, it is seen that the RPH of a copolymer of two styrenes with different σ is approximately proportional to the weight fraction of each component.

Some Aspects of the Mechanism of Scintillation

The over-all scintillation mechanism can be best visualized in terms of Eq. (9). It has been seen that the RPH is dependent on the structure of the plastic solvent which can be characterized electronically by a σ value. It now remains to determine which of the parameters in Eq. (9) is associated with the solvent structure.

The term q_0 may be neglected since it is much less than kc in plastics[4] in the concentration range employed. The term m has been shown[4] to be small for PTP in polystyrene and polyvinyltoluene and moderate variations in its magnitude should not have a significant effect on the RPH. The term E is a constant characteristic of the radiation employed and δ is a constant. It has been reported[4] that the value of k in Eq. (9) varies greatly with the fluor used in polystyrene scintillators, but in the present work the same fluor was used throughout. In the one case where data was reported on tetraphenyl butadiene in both polystyrene and polyvinyl toluene, the value of k does not differ greatly for these two solvents, suggesting that the observed variations in in RPH are not due to a change in k resulting from a change in solvent type. On the other hand, Furst and Kallmann[2] associate the parameter $k(1/Q$ in their notation) in liquid scintillators with the solvent. Their results for aromatic solvents show that k does not vary by more than about a factor of two. If this is the order of magnitude of variation to be expected in a similar class of plastics, then the observed increase in the RPH for the dimethyl styrenes cannot be accounted for solely by a change in k.

The observed variation in RPH with change in solvent must therefore be attributed to: (1) a change in w_0, or since E is a constant, a change in E/w_0, the number of photons which are produced which are capable of fluorescing, or (2) a change in q_f, or both. Of the terms in q_f, it is reasonable to assume that p_{sf} will be dependent on fluor composition alone which has been kept constant. The term p_i, however, might be dependent on solvent type if in the internal quenching process solvent interaction is important [Eq. (8)]. If, however, internal quenching is dependent only on fluor composition [Eq. (8a), then the observed changes in RPH must be attributed to a change in w_0. Although the latter explanation is more plausible, the data at hand do not allow a definite conclusion. Furst and Kallmann[2] appear to favor a change in q_f (through p_i) as an explanation for the change of RPH with solvent composition in liquid scintillators, but with some reservations.

On the basis of the foregoing discussion, it appears highly probable that at least a good part of the observed change in RPH with solvent structure is due to an increase or decrease in the absorbed energy which can produce excited molecules capable of fluorescing. It is of further interest to determine more about this energy absorptive process. Some information on this point is offered by a comparison of the RPH's (see Table I) of the scintillators from polymers of styrene, vinyltoluene, α-methyl styrene, *p*-methyl-α-methyl styrene, *p*-isopropyl-α-methyl styrene, and *p*-isopropyl styrene. The substitution of a methyl group for the α hydrogen in the backbone of the polystyrene chain reduced the RPH from 39 to 5. Placing a methyl group in the *p* position of poly-α-methyl styrene does not increase the RPH as it does with styrene, suggesting that the methyl substituent in the ring is not primarily involved in the absorptive process. The substitution of a *p*-isopropyl group in poly-α-methyl styrene provides an α hydrogen similar to that in the backbone of a polystyrene chain and yet the RPH is not increased. This suggests that the α hydrogen must be in the backbone of the polymer chain to be effective in scintillation. This is further supported by the RPH of *p*-isopropyl styrene which is not substantially increased above that of styrene and is about the same as polymethyl styrene as expected from its σ value, even though two α hydrogens are present in the same monomer unit.

The specificity of the α hydrogen in the energy absorptive process appears to be related to the observations on the irradiation of polystyrene[13] and poly-α-methyl styrene with β and γ rays.[14] In the former, crosslinking occurs as a result of the absorption of energy at the α-hydrogen bond to give free radicals which can recombine to form crosslinks. In poly-α-methyl styrene irradiation causes chain scission, which suggests that

[13] A. Charlesby, J. Polymer Sci. **11**, 513 (1953).
[14] E. J. Lawton, A. M. Bueche, and J. S. Balwit, Nature **172**, 76 (1953).

energy is not absorbed at the α position when the hydrogen is replaced with a methyl group.

In summary, an over-all scintillation mechanism for polystyrene-type scintillators which would be in harmony with the present observations requires, first, an absorption of a fraction of the dissipated particle energy by the polymeric solvent, the α hydrogen to carbon bond in the polystyrene backbone being a preferred absorption center. On absorption of this energy, the excitation of the plastic solvent may be facilitated by the presence of nuclear substituents which donate electrons to the benzene conjugated-bond system. The transfer of energy from solvent to the fluor may then be facilitated by a favorable electron density distribution between the two. Thus, it might be that energy transfer occurs by a π-bond overlap between the excited solvent (S^*) and the flour (F).

EXPERIMENTAL

Synthesis of Monomers

The general methods of preparing the 16 alkyl styrenes has been described.[15–22] The purity of all the monomers was determined by vapor phase chromatography and infrared spectroscopy.

[15] D. T. Mowry, M. Renoll, and W. F. Huber, J. Am. Chem. Soc. **68**, 1105 (1946).
[16] C. S. Marvel, J. H. Saunders, and C. G. Overberger, J. Am. Chem. Soc. **68**, 1085 (1946).
[17] C. S. Marvel and D. W. Hein, J. Am. Chem. Soc. **70**, 1895 (1948).
[18] C. S. Marvel, R. E. Allen, and C. G. Overberger, J. Am. Chem. Soc. **68**, 1088 (1946).
[19] M. Tiffeneau, Ann. chim. et phys. **10**, 158 (1903).
[20] C. S. Marvel and G. L. Schertz, J. Am. Chem. Soc. **65**, 2054 (1943).
[21] C. G. Overberger, C. Frazier, J. Mandelman, and H. F. Smith, J. Am. Chem. Soc. **75**, 3324 (1953).
[22] L. A. Brooks, J. Am. Chem. Soc. **66**, 1295 (1944).

Preparation of Plastic Scintillators

The plastic scintillators were prepared[4] as cylindrical disks $\frac{1}{2}$ in. high by $\frac{13}{16}$ in. in diameter by polymerizing the substituted styrenes in glass vials of the right diameter (outgassed under vacuum) and machining to the desired height.

Determination of Pulse Height

The method and apparatus for determining the relative pulse heights has been described.[4] For β irradiation, a Pa^{234} (0.01 μC, 2.3-Mev source was used, and for γ irradiation a Cs^{137} source (1 μC, 0.662 Mev). All pulse heights are relative to an anthracene crystal of the same dimensions. The values obtained on several dimethyl styrene scintillators were checked in two other laboratories by other methods and showed excellent agreement.[10]

Determination of Fluorescence Spectra of Plastic Scintillators

The fluorescence spectrophotometer at the Naval Research Laboratory in Washington, D.C.,[23] was used to obtain the fluorescent spectra of the plastic scintillators. The exciting radiation (Hg $\lambda = 2375$ A) impinged on the flat roughened face of the cylindrical plastic scintillator. From the monochromator the light was passed to an IP 28 photomultiplier tube whose current output was recorded on an Esterline Angus recorder as relative fluorescent intensity versus wavelength.

ACKNOWLEDGMENTS

We are grateful to H. Goldberg and H. Dickens for their help in carrying out some of the experiments.

[23] We gratefully acknowledge the help of The Naval Research Laboratory in Washington, D. C., for making their facilities available to us and P. Bernstein for making the measurements for us.

THE JOURNAL OF CHEMICAL PHYSICS VOLUME 34, NUMBER 2 FEBRUARY, 1961

Effect of Solvent and Solute Structure on Scintillator Pulse Heights. II. Correlation of Pulse Heights for Aromatic Liquid Organic Scintillators with Hammett Substituent Constants*

STANLEY R. SANDLER AND SAMUEL LOSHAEK

The Central Research Laboratory of The Borden Chemical Company, Philadelphia, Pennsylvania

(Received July 25, 1960)

It has been found that numerous data in the literature on aromatic organic liquid scintillators could be interpreted in terms of the resonance and polarity of the constituent solvents and fluors. The resonance and polarity of the ring substituted aromatic compounds were characterized quantitatively by Hammett substituent constants (σ). For a number of liquid scintillator systems in which the fluor composition was kept constant and the structure of the aromatic solvent was varied, pulse heights increased approximately linearly with increasing electron donating (negative σ values) power of the substituents on the aromatic molecule. This correlation held for nine different fluors in each of seven different aromatic solvents. A similar correlation was found for a series of fluors consisting of substituted 2,5-diphenyl-1,3,4-oxadiazoles and 2,5-diphenyl 1,3-oxazoles in which toluene was used as the sole solvent. Pulse heights varied much more with a change in substituent groups on the solvent than with a similar change in the fluors. The observed correlation affords a means of organizing a large body of data and of gaining a further insight into the mechanism of scintillation.

IN the previous paper[1] a correlation was found between the relative pulse heights (R.P.H.) of plastic scintillators and the σ value for the aromatic substituents on the styrene ring. The object of the present work was to investigate whether a similar correlation held for solvents and solutes in liquid organic scintillators.

It is assumed that the same over-all processes hold for scintillation in plastic and liquid scintillators, thus the pulse height equation given previously[1] is used here

$$\text{P.H.}=(E/w_0)q_f\delta[(q_0+kc)/(1+kc)][1/(1+mc)], \quad (1)$$

where $kc=p_t/(p_{ss}+p_{es})$, $mc=p_{ff}/(p_{ef}+p_i)$, and $q_f=p_{ef}/(p_{ef}+p_i)$ is the quantum yield of the fluor exclusive of fluor self-quenching, c is the concentration of fluor, p_t, p_{ss}, p_{es}, $p_i=\beta c$, p_{ef}, and p_i are, respectively, the probabilities of transfer from the solvent to the fluor, solvent quenching, direct emission by the solvent (very small), self-quenching of the fluor, emission by the fluor and internal quenching by the fluor, β is a constant, E is the particle energy which is completely absorbed by the scintillator, w_0 is the average dissipated particle energy required to produce one fluorescent excitation in the solvent, q_0 is the quantum yield of the solvent (very small in comparison to kc), and δ is a factor (includes photocathode efficiency, instrument factors, etc.) which converts the number of emitted quanta from the scintillator to an observed pulse height voltage.

* This work was supported by the U. S. Atomic Energy Commission.

[1] S. R. Sandler and S. Loshaek, J. Chem. Phys. **34**, 438 (1961), preceding article.

I. RESULTS

A. Correlation of Pulse Heights with σ Values for Liquid Aromatic Solvents

Furst and Kallmann[2] have determined the constants in Eq. (1) from a study of scintillation pulse height versus fluor concentration for a number of liquid solvent-fluor concentrations and calculated a "limiting relative pulse height" which represents the hypothetical state of zero fluor self-quenching at infinite fluor concentration. The limiting relative pulse height (P/R in the notation of Furst and Kallman), is given by E/w_0q_f since $m=0$ and $(q_0+kc)/(1+kc)=1$. It is seen to be analogous to the relative pulse heights obtained with the PTP plastic scintillators[1] in which fluor self-quenching is low and the concentration of PTP is in the range where a maximum pulse height has been obtained which does not change appreciably with further moderate increases in its concentration.[3]

The limiting relative pulse heights (relative to anthracene) which are used for the correlation with the Hammett σ values for the aromatic solvents were taken from the data of Furst and Kallman[2] (Table XI of their paper). In order to emphasize the importance of the molecular unit in the absorption process the values are adjusted to an equal number of moles per gram of solvent by multiplying by the ratio of the molecular weight of the substituted benzene to that of benzene. The correlation for the plastic scintillators presented previously[1] is not significantly altered if the relative pulse heights are placed on a mole per gram basis, since the molecular weights of the styrenes do not differ greatly.

[2] M. Furst and H. Kallmann, Phys. Rev. **85**, 816 (1952).

[3] R. K. Swank and W. L. Buck, Phys. Rev. **91**, 927 (1953).

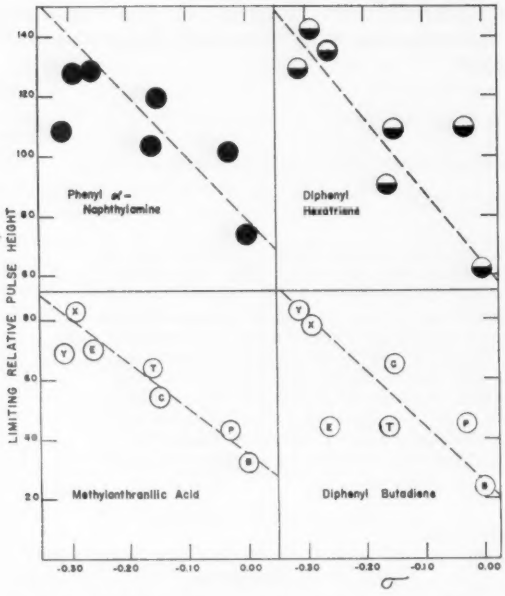

FIG. 1. Limiting relative pulse height vs σ for the indicated solutes in the following solvents: (B) benzene, (P) phenylether, (C) cumene, (T) toluene, (X) xylene, (Y) p-cymene, (E) phenetole.

Figures 1 and 2 show, for each of nine different fluorescent solutes, plots of limiting relative pulse height versus the Hammett σ values with seven aromatic solvents. The σ values[4] for the solvents are: benzene (0), phenylether (−0.03), cumene (−0.16), toluene (−0.15), xylene (−0.29), *p*-cymene (−0.32), phenetole (−0.26).

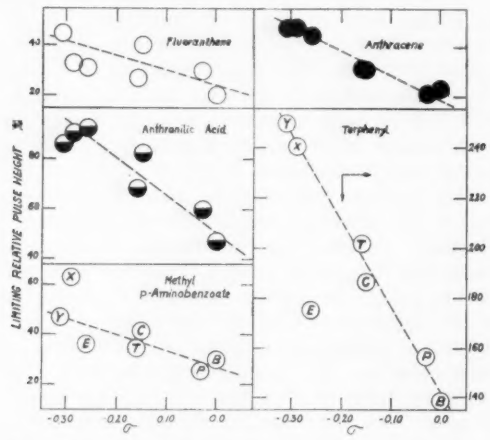

FIG. 2. Limiting relative pulse height vs σ for the indicated solutes in the following solvents: (B) benzene, (P) phenyl-ether, (C) cumene, (T) toluene, (X) xylene, (Y) *p*-cymene, (E) phenetole.

[4] J. Hine, *Physical Organic Chemistry* (McGraw-Hill Book Company, Inc., New York, 1956), p. 72.

TABLE I. Maximum relative pulse heights vs σ for 2,5-substituted diphenyl-1,3,4-oxadiazole systems in toluene.

Substituent[a]	No. in Fig. 3(a)	σ[b]	Max. R.P.H.[c]
2,5-di-*p*-methoxy	1	−0.52	1.1
2,5-di-*p*-methyl	2	−0.32	1.0
2,5-di-*p*-diphenyl	3	−0.02	0.92
none	4	0.0	0.89
2,5-di-*p*-fluoro	5	+0.16	0.85
2,5-di-*p*-chloro	6	+0.46	1.0
2,5-di-*p*-bromo	7	+0.46	0.42

[a] These refer to the substituents *X* in

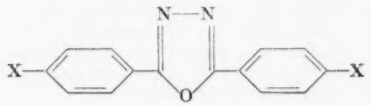

[b] Values obtained from footnote 4. The sigma values are taken as the sums for the para substituents (*X* in footnote a) on each benzene ring in the 2,5-positions.

[c] See footnote 5.

B. Correlation of Pulse Heights with σ Values for Fluorescent Solutes in Toluene

Relative pulse height (R.P.H.) data in a single solvent for fluorescent solutes with a systematic variation in structure which can be characterized by

TABLE II. Maximum relative pulse heights versus σ for substituted 2,5-diphenyl-1,3-oxazole systems in toluene.[a]

Substituent[b]	No. in Fig. 3(b)	σ[c]	Max. R.P.H.[a]
2-*p*-methoxy	1	−0.26	1.02
2-*p*-methyl	2	−0.16	1.01
none	3	0.00	1.01
2-*p*-fluoro	4	−10.75	0.96
2-*p*-chloro	5	+0.23	0.94
2-(3,4-dichloro)	6	+0.60	0.92
2-*p*-bromo	7	+0.23	0.28
2-*p*-iodo	8	+0.28	0

[a] See footnote 6.

[b] These refer to the substituents *X* in

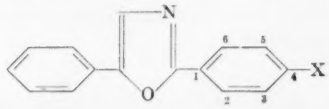

except for the 3,4-dichloro derivative. For the latter the total sigma was taken as the sum of the *m* and *p*-chloro groups.

[c] The values were taken from footnote 4.

Hammett σ values are available for the substituted 2,5-diphenyl-1,3,4-oxadiazoles[5] and 2,5-diphenyl 1,3-oxazoles.[6] For each fluor the values of the relative pulse height reported corresponds to that concentration in toluene which gives the maximum R.P.H. In order to place the correlation for each fluor system on an equal basis it must be assumed that the extent of fluor self-quenching [m in Eq. (1)] is the same for each system. This has some justification since the basic molecular structure is maintained throughout each system. Also, at the maximum, the effect of flour self-quenching is of less effect percentagewise than at other concentrations of fluor. It would be desirable to have limiting relative pulse height data for these systems.

The pulse height data and σ values are summarized in Tables I and II and are plotted in Fig. 3.

II. DISCUSSION

The data of Figs. 1 and 2 show an approximate linear correlation between the limiting relative pulse height and Hammett σ for each of nine different fluors in seven different substituted benzene solvents. For each of the fluors in the same series of solvents the slopes of the maximum relative pulse height versus σ line were very similar. Since the limiting relative pulse height is given by $(E/w_0)q_f$ the variation in pulse height can only be accounted for by a variation in w_0, the dissipated average particle energy required to produce one fluorescent excitation in the solvent, and/or $q_f = p_{ef}/p_{ef}+p_i$), the fluorescent quantum yield of the fluor exclusive of fluor self-quenching. It is postulated here that by varying the solvent the major change in the limiting relative pulse height arises from a change in the absorption process as characterized by w_0. If the probability of internal quenching (p_i) is determined by solvent-fluor interactions as frequently proposed, then with the rather great changes in fluor structure considered here, it seems unlikely that the interaction would be the same between each fluor with each solvent as indicated by the similarity of slopes in the σ correlation. Of course a compensatory variation in p_{ef} with a change in solvent could account for this observation but such a variation is probably too small considering that the fluor composition is fixed for each series of solvents.

When the solvent type was kept constant and the aromatic substituents of the fluor were varied a σ versus maximum relative pulse height correlation was also obtained (Fig. 3) for substituted 2,5-diphenyl-1,3,4-oxadiazoles and 2,5-diphenyl-1,3-oxazoles. Recently a paper by Shvaika and Grekov[7] has come to the authors' attention wherein they point out that

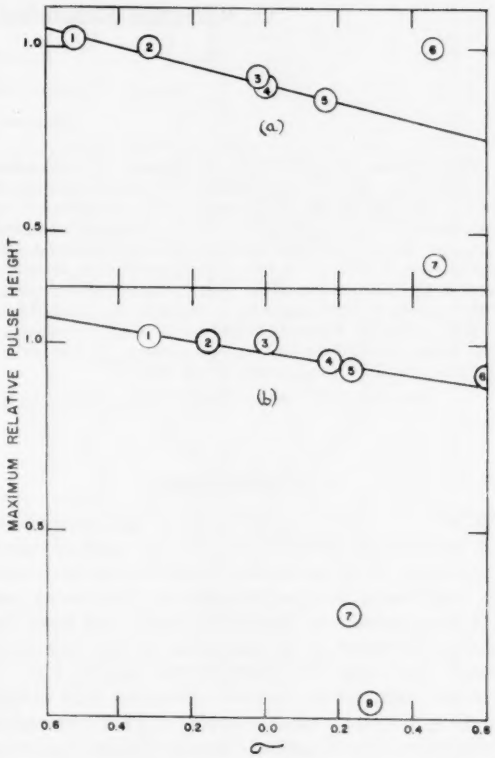

FIG. 3. Maximum relative pulse height vs σ for (a) substituted 2,5-diphenyl-1,3,4-oxadiazoles and (b) 2,5-diphenyl-1,3-oxazoles in toluene.

electron-donating substituents in substituted 2,5-diphenyl-1,3,4-oxadiazoles increase their efficiency as solutes in toluene scintillators.

The deviations for the halogenated compounds which gave values considerably below the correlation line (Fig. 3) might be due to significantly higher self-quenching for these compounds. It will be recalled that the comparison of maximum relative pulse height is meaningful only if fluor self-quenching was approximately the same for each fluor. A comparison of the slope of the lines of Figs. 1 and 2 with Fig. 3 shows that the pulse height varies much more with a change in the σ value of the solvent than with an equal change in the σ value of the fluor. The variation of the pulse height for the series of fluors shown in Fig. 3(a) and 3(b) can be attributed on the basis of Eq. (1) to changes in p_t, w_0, or q_f. Since the solvent composition is fixed it is reasonable to assume, on the basis of the previous discussion for solvents, that w_0 does not account for the variation in pulse height. From the data it is not possible to distinguish whether changes in q_f (particularly as reflected in p_i) or p_t are responsible for changes in the observed pulse height.

[5] F. N. Hayes, B. S. Roger, and P. C. Sanders, Nucleonics **13**, 46 (1955).
[6] F. N. Hayes, P. Ott, V. Kerr, and B. Rodger, Nucleonics **13**, 38 (1955).
[7] O. P. Shvaika and A. P. Grekov, optika i Spektroskopiya **7**, 483 (1959).

O_2 Vibration Relaxation in Oxygen-Argon Mixtures

MORTON CAMAC

Avco-Everett Research Laboratory, Everett, Massachusetts

(Received August 1, 1960)

This paper and the one following [M. Camac and A. Vaughan, J. Chem. Phys. **34**, 459 (1961)] discuss the use of a new experimental technique for the determination of O_2 vibration and dissociation rates. The concentration of O_2 in the ground vibrational state can be inferred from measurements of ultraviolet light transmission at 1470 A. O_2 has a strong continuous absorption band in this vacuum ultraviolet region. The vibrational relaxation rate of O_2 in shock-heated O_2-Ar mixtures was obtained from 1200°K to 7000°K. For Ar-O_2 collisions, the measured relaxation time τ_v can be fit by the Landau-Teller theory [L. Landau and E. Teller, Physik. Z. Sowjetunion **10**, 34 (1936)]

$$1/\tau_v = nC_1T^{1/6}[1-\exp(-2228T)]\exp(-(C/T)^{1/3}),$$

where n is the number of particles /cc and T is the temperature in °K. $C_1=1.2\times10^{-7}$ cc/particle-sec-(°K)$^{1/6}$ and $C=1.04\times10^7$ ($\pm30\%$)°K. The observed vibrational relaxation time for O_2-O_2 collisions is 5.0 ± 0.5 times faster than that for O_2-Ar collisions. The experimental results are compared to the theoretical predictions of Schwartz and Herzfeld [R. N. Schwartz, Z. I. Slawsky, and K. F. Herzfeld, J. Chem. Phys. **20**, 1591 (1952); R. N. Schwartz and K. F. Herzfeld, *ibid.* **22**, 767 (1954)]. At the lower temperatures, the O_2-O_2 rates given by Blackman [V. H. Blackman, J. Fluid Mech. **1**, 61 (1956)] have a different temperature dependence than the O_2-Ar rates obtained in this experiment.

I. INTRODUCTION

THE recent interest in the field of high-temperature gas dynamics and, in particular, the study of chemical kinetics of air and its constituents stems both from its importance in upper atmosphere phenomena and the aerodynamics of hypersonic flight, and from the academic interest in the reactions of these relatively simple molecules. The study of the reaction rates in gaseous collisions of diatomic molecules with simple particles permits a direct experimental and theoretical comparison. The theory of vibrational relaxation rates for diatomic molecules[1,2] has already advanced to the point where a direct comparison to experimental measurements can now be made.

In this past decade the application of the shock tube for the study of chemical reaction rates has grown very rapidly. It is an ideal experimental apparatus for studying very fast reaction kinetics at high temperatures, since it furnishes a well-understood method for heating gases to high temperatures very quickly to accurately known values of pressure and enthalpy. Several types of detection apparatus have been employed in conjunction with shock tubes in the quantitative investigation of oxygen reaction. Interferometric studies of the gas density have yielded information on the vibration[3] and dissociation[4,5] relaxation rates. Studies of emission from Schumann-Runge radiation[6–8] give information on the excitation of electronic states as well as other relaxation phenomena. Microwave absorption experiments[9] have determined the ionization rates in oxygen and oxygen-nitrogen mixtures.

The experiments described in this and the following[10] papers use an ultraviolet light absorption technique to determine the vibration and dissociation rates of O_2 in argon-oxygen mixtures.[11] Molecular oxygen strongly absorbs ultraviolet light radiation in a continuous broad wavelength band from about 1350 to 1650 A, while atomic oxygen and argon are transparent in this region. Data were obtained over the temperature range from 1200°K to over 8000°K.

It is instructive to compare this technique with the interferometric method for the study of oxygen relaxation rates. The ultraviolet light absorption method has two advantages. First, due to the strong ultraviolet light absorption, a 10-μ Hg change in the oxygen density can be observed. Thus, this system is about 100 times more sensitive to density changes than the interferometer. This permits measurements of reaction rates at correspondingly lower densities. Since the relaxation times vary inversely with density, operation at lower densities permit the extension of the rate measurements to higher temperatures. The second advantageous feature is that the absorption is sensitive only to molecular oxygen, even for dilutions to less than $\frac{1}{4}\%$ O_2 in argon. For such small percentages of O_2, the argon has essentially all the enthalpy and remains chemically inert. Thus, the chemical relaxation takes place at essentially constant temperature. This greatly simplifies the analysis of the data in the determination of relaxation rate constants.

A description of the experimental technique and the

[1] L. Landau and E. Teller, Physik. Z. Sowjetunion **10**, 34 (1936).
[2] R. N. Schwartz, Z. I. Slawsky, and K. F. Herzfeld, J. Chem. Phys. **20**, 1591 (1952); R. N. Schwartz and K. F. Herzfeld, *ibid.* **22**, 767 (1954).
[3] V. H. Blackman, J. Fluid Mech. **1**, 61 (1956).
[4] D. L. Matthews, Phys. Fluids **2**, 170 (1959).
[5] S. R. Byron, J. Chem. Phys. **30**, 1380 (1959).
[6] J. Keck, Avco-Everett Research Laboratory, Research Rept. 67, June, 1959.
[7] S. A. Losev, Doklady Akad. Nauk S.S.S.R. **120**, 1291 (1958).
[8] Cornell Aeronautical Laboratory, Inc., Rept. No. QM-997-A-1, September, 1957.
[9] S. C. Lin, Avco Research Laboratory, Research Report 33, June 1958; Proceedings of Plasma Sheath Symposium, Air Force Cambridge Research Center (1959).
[10] M. Camac and A. Vaughan, J. Chem. Phys. **34**, 459 (1961), following paper.
[11] M. Camac and C. C. Petty, Bull. Am. Phys. Soc. Ser. II, **3**, 286 (1958); IAS Preprint No. 802. M. Camac and A. Vaughan, Avco-Everett Research Laboratory, Research Rept. 84, December, 1959.

calibration of the apparatus is presented in the next section. Following this, the vibrational relaxation measurements are given. The results of this experiment are then compared with Blackman's data and with theory. Two items are noted in this comparison: (1) Landau-Teller's[1] prediction for the variation of the relaxation rate with temperature is confirmed in this experiment. Schwartz and Herzfeld's[2] calculation of the magnitude of the rates agree within a factor of 10. (2) The variation of the relaxation rate with temperature in O_2-Ar collisions as observed in this experiment differs from Blackman's[3] results for O_2–O_2 collisions at low temperatures.

II. EXPERIMENTAL TECHNIQUE AND APPARATUS

A. Ultraviolet Light Method

The ultraviolet light absorption method is similar to that of Davidson and his co-workers[12] who used visible light to measure iodine relaxation rates. The concentration of a specific chemical species is determined by its absorption of its characteristic radiation. Practically all molecules including the constituents of air absorb radiation in the far ultraviolet region.[13] The absorption coefficient of molecular oxygen at room temperature (that is, in the ground vibrational state) has been measured from 1000 A to 2500 A.[13] The Schumann-Runge system has a strong continuous absorption band from about 1350 to 1650 A (see Fig. 1). The two states associated with this transition are shown in a potential energy diagram in Fig. 2. Also shown are the low vibration levels for these two electronic states. The continuum absorption band occurs for a quantum with over 57 300 cm^{-1} wave number, i.e., shorter than 1750 A.

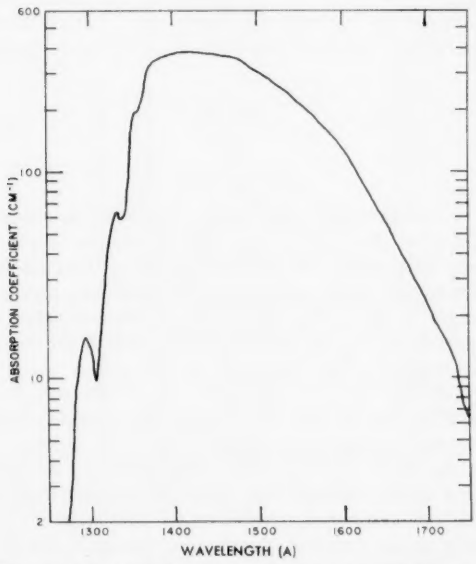

FIG. 1. The absorption coefficient per centimeter path of molecular oxygen at NTP as a function of wavelength, from footnote 13.

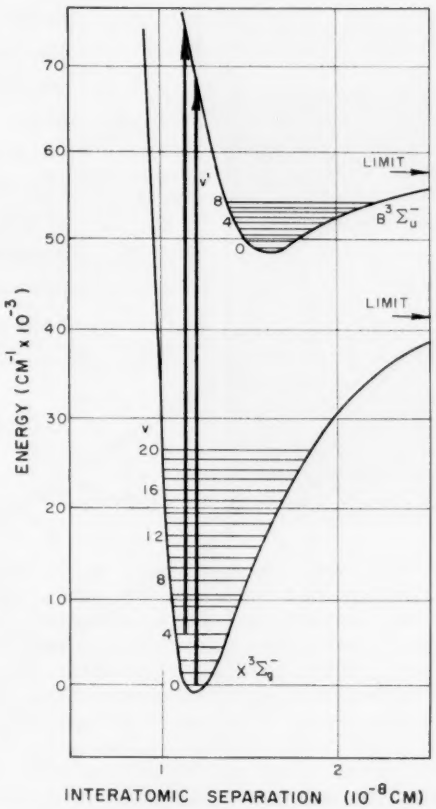

FIG. 2. The potential energy diagram for molecular oxygen showing the two electronic states which give rise to Schumann-Runge radiation. The energy in wave numbers is plotted as a function of interatomic separation in Angstroms. Also shown are the lower vibrational levels. Radiation at 1470 A corresponds to an energy change of 68 000 cm^{-1} as indicated by the arrows.

With the use of this potential energy diagram the absorption coefficient from the higher vibrational levels can be estimated.[14] A Morse potential is used to obtain the anharmonic wave functions for the vibration levels of the $X\,^3\Sigma_g^-$ ground electronic system. The wave functions for the continuum $B\,^3\Sigma_u^-$ state are approximated by δ functions at the potential energy line. Assuming the Franck-Condon principle for radiative transitions, the overlap integral of these two wave functions is directly proportional to the absorption coefficient. The amount of absorption from each state

[12] T. Carrington and N. Davidson, J. Phys. Chem. **57**, 418 (1953); D. Britton, N. Davidson, and Schott, Discussions Faraday Soc. **17**, 58 (1954).

[13] E. Watanabe, M. Zelikoff, and E. C. Y. Inn, Geophysical Research Papers, No. 21, AFCRC Tech. Rept. No. 53-23.

[14] G. Herzberg, *Spectra of Diatomic Molecules* (D. Van Nostrand Company, Inc., Princeton, New Jersey, 1950).

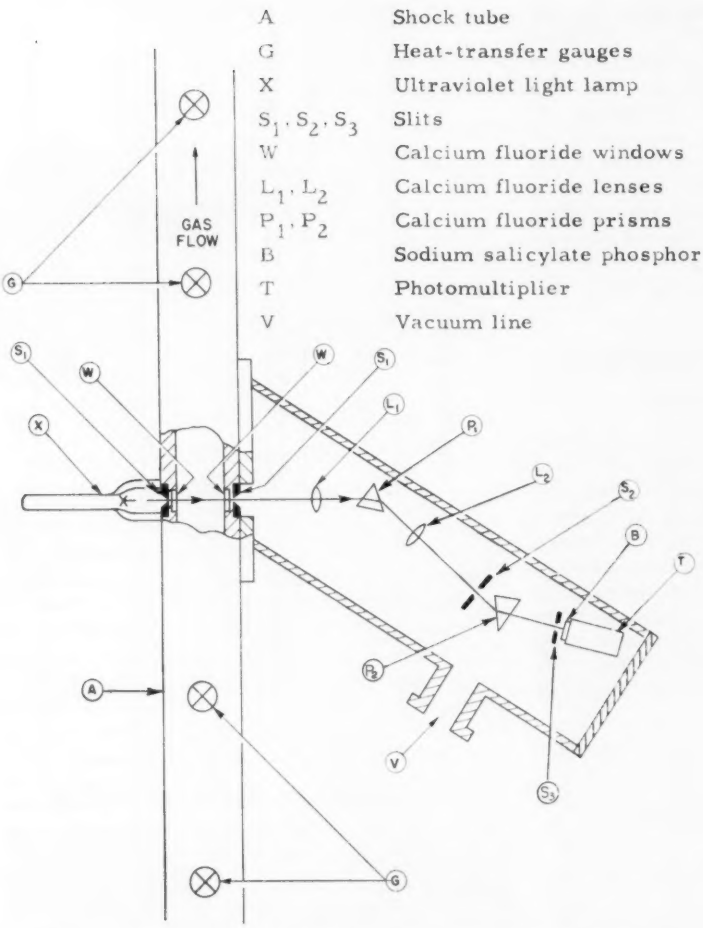

FIG. 3. The experimental arrangement for the ultraviolet light transmission experiment.

depends upon the wavelength of the radiation. Following this procedure, analysis[15,16] showed that the absorption from the first excited vibrational state is very small at about 1470 A. Thus, operation at this wavelength gives the most sensitive conditions for observing vibrational relaxation, since any depletion from the ground vibrational state into higher states will cause the largest change in the absorption coefficient. Thus, this experiment was performed using a 16-A wide band of radiation around 1470 A. The radiative molecular transition is illustrated in Fig. 2 by the vertical arrows for the ground and the fourth vibration level. It is also convenient to operate at this wavelength, since the experimental apparatus can be aligned and calibrated with the strong xenon resonance line at 1471 A.

As oxygen is heated to high temperatures the population in the rotational states changes by a large amount for each vibrational state. As will be seen later, it is important to know how the absorption coefficient of each vibrational state varies with the rotational population. The absorption coefficient should be practically independent of the rotational state. This can be qualitatively shown as follows: The selection rule for changes in molecular rotation in a photoabsorption process is $\Delta J=0, \pm 1$ where J is the rotational quantum number. The rotational energy peaks at $J=(T/1.40°\text{K})^{\frac{1}{2}}$ which corresponds to $J=85$ for $T=10\,000°\text{K}$. For $J=85$, the change in rotational energy in a photoabsorption process is 0.03 ev for $\Delta J=\pm 1$. The electronic and rotational energies simply add with only a small coupling term. Since the absorption of a 1470-A photon corresponds to an 8.5 ev change in the energy of the molecule, the 0.03 ev change in the potential energy diagram due to rotation is negligible. A corollary to the absorption coefficient being independent of the rotational distribution is that the absorption coefficient from each vibrational state is independent of the translational temperature of the gas. Experimental data in Sect. IIC show this temperature independence for the ground vibrational state.

[15] B. Kivel (private communication).
[16] H. DeWitt (private communication).

B. Experimental Arrangement

The apparatus for this experiment is shown schematically in Figs. 3 and 4. In Fig. 3, which gives details of the optical setup, the ultraviolet light source and monochromator detector system are shown affixed to opposite sides of the shock tube. The entire path from the light source to the detector, with the exception of the shock tube itself, was evacuated to a few microns pressure by a mechanical pump (indicated by V). An ultraviolet light beam from the lamp X traversed the 1.5-in. diameter shock tube A, parallel to the shock front, and was spectrally analyzed by the monochromator. The monochromator consisted of a collimating lens L_1 a camera lens, L_2, and two prisms, P_1 and P_2. The second prism was required to furnish further discrimination against stray visible light. The shock tube windows W and the monochromator optics were made of calcium fluoride. The ultraviolet detector consists of a thin layer of sodium salicylate phosphor, B (for conversion of the 1470-A radiation to visible light) deposited on the photomultiplier tube T, Dumont type 6291. This tube was situated within the vacuum housing of the monochromator. Slits S_1, 5 mm high and $\frac{1}{3}$ or 1 mm wide, were on either side of the shock tube. Slit S_2 was 1 mm wide passing a 16-A wide band. Slit S_3 (5 mm wide) discriminated against visible light.

Three kinds of ultraviolet light sources were employed in order to extend the operating range of the experiment: a xenon-filled microwave excited resonance lamp,[17] a hot cathode hydrogen discharge tube,[18] and a high-voltage Lyman discharge lamp. The xenon resonance lamp was made of Pyrex tubing with a calcium fluoride window cemented to one end and filled with pure xenon at about 10 mm Hg pressure. Activated uranium contained in a side tube acted as a getter for the removal of impurities[19] from the xenon discharge. The discharge was initiated by a Tesla coil and maintained by a Raytheon 2450-Mc 100-w "Microtherm" unit. A xenon resonance lamp gives line radiation at 1471 A. Since the intensity was rather low, this lamp was used only to align the monochromator. Slits S_2 and S_3 were adjusted to give the maximum ultraviolet reading when using the xenon 1471-A line radiation.

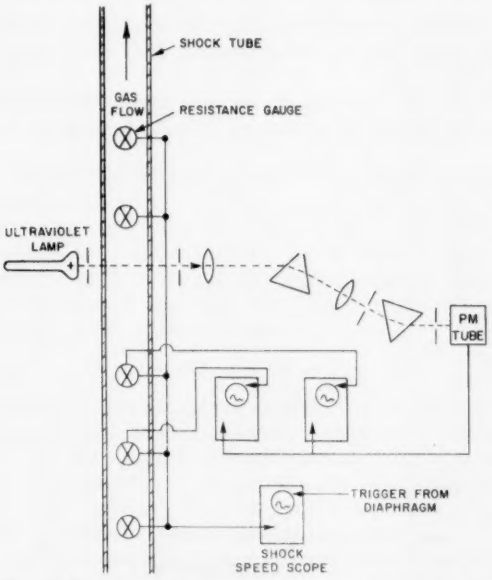

FIG. 4. The electrical circuitry for the ultraviolet light measurements.

FIG. 5. Oscillograms showing the ultraviolet light intensity as a function of time for the hydrogen (a) and Lyman (b) discharge lamp. The experimental measurements were made at the peak of the second cycle of the ringing Lyman lamp. The oscilloscope trace shows the end of the first cycle and the complete second cycle.

The hydrogen discharge tube had a 6-mm diam, 10-cm long Pyrex capillary containing flowing (tank) hydrogen gas at a pressure of 1 mm Hg. The lamp operated on a pulsed basis and was powered by a 250-μf 1000-v condenser. The best operation was obtained with a 200-amp initial tube current and a 2-msec decay time constant. The ultraviolet light output is shown in Fig. 5(a).

The Lyman lamp had a 6-mm diam, 10-cm long quartz capillary containing flowing (tank) helium at a pressure of 2 cm to 4 cm Hg. The lamp worked on a pulsed basis and was powered by a 100-μf 6000-v condensor. An inductance was used to lengthen the duration of the light pulse. The ultraviolet light output is shown in Fig. 5(b). The lamp was triggered so that the shock traversed the ultraviolet beam at the peak of the second cycle. The hydrogen and Lyman lamps were, respectively, 25 and 10 000 times more intense than the xenon lamp (for the 16-A band accepted). In order to keep the statistical "noise" fluctua-

[17] P. G. Wilkinson and Y. Tanaka, J. Opt. Soc. Am. **45**, 344 (1955).

[18] P. L. Hartman and J. R. Nelson, J. Opt. Soc. Am. **47**, 646 (1957).

[19] G. H. Dieke and H. M. Crosswhite, J. Opt. Soc. Am. **42**, 433 (1952).

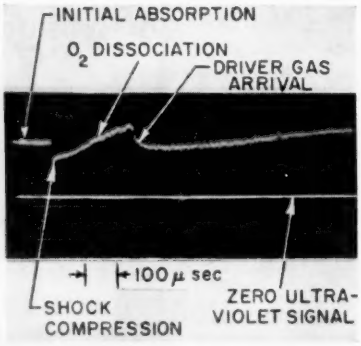

FIG. 6. Typical experimental oscillogram showing the variation of the ultraviolet light transmission with time.

tions relatively low when using the hydrogen lamp, the slits S_1 were 1 mm wide and the photomultiplier output has an integration time of about 1 μsec. Thus, the hydrogen lamp gave useful data from about 2 μsec after shock passage. The lamp output was essentially constant for all experimental test times (i.e., below 300 μsec). The Lyman lamp gave useful data down to 0.1 μsec after shock passage; $\frac{1}{3}$ mm wide slits S_1 were used, and the photomultiplier output had a 0.01-μsec rise time. This lamp was not usable for more than a 10-μsec period because of the short period of oscillation of the lamp.

Figure 6 shows a reproduction of an oscilloscope trace for a typical experiment, illustrating the manner in which the measurements were taken. The orientation of the trace is such that a downward deflection implies an increase in the concentration of oxygen molecules; i.e., a decrease in the vacuum ultraviolet transmission through the gas. The horizontal line at the bottom of the figure is a single oscilloscope sweep with the ultraviolet lamp turned off. This would correspond to an infinite O_2 concentration when the lamp is on. The data trace was triggered just prior to the arrival of the shock front at the test point. Before shock passage, the transmission was 73% due to the (room temperature) oxygen gas. The discontinuity in the trace corresponds to the time of arrival of the shock front and is due to the sudden increase in gas density. Following this discontinuity is a region in which the oxygen molecule concentration in the heated gas relaxes to its equilibrium value—the relaxation in this case being due to dissociation. For this run the gas had reached vibrational equilibrium during the time of transit of the shock wave across the slits. Toward the end of the trace there is an abrupt rise, indicating the arrival of the turbulent mixing region at the interface of the driver and the shocked gas. The noise shown in Fig. 6 is due to statistical counting fluctuations. The testing time for this experiment, i.e., the time between the arrival of the shock front and the arrival of the driver, is thus clearly shown in the data. Testing times when operating at an initial pressure of 1 mm Hg were above 50 μsec, while for a 2-cm Hg initial pressure over 200-μsec test time is observed. Boundary layer effects have been observed in these experiments.[10,11]

The shock wave speed was determined by six platinum strip heat transfer gauges G that lie flush with the wall of the shock tube. Each gauge consisted of a 1-×5-mm thin strip of platinum of about 5 ohms resistance, deposited on Pyrex, that carried a constant current of 0.2 amp. The sudden change in resistance of the platinum upon being heated by the shock-heated gas produced a change in voltage across the strip of about 10 mv. These signals were amplified and fed through a cathode follower and diode clamp. The signals from all the gates went to a single cable and were displayed on an oscilloscope with a single ratchet trace time-base. Time measurements of the position of the shock front were made to about $\frac{1}{3}$-μsec accuracy. The distance between gauges, ranging from 12.5 to 30 in., were measured to 0.01-in. accuracy. Thus, the shock velocity was determined with less than a 0.3% uncertainty.

Figure 4 shows a schematic diagram of the electronics used in this experiment. The oscilloscope for the shock-speed gauges is triggered by the bursting shock tube diaphragm. The two oscilloscopes for the ultraviolet light signal were triggered by signals from resistance gauges. Two scopes were used in order to obtain data with a low and fast sweeping time.

C. Calibration of the Apparatus

Several calibration steps are required for the evaluation of the data of this experiment. They are presented in this section.

First, the detection system must be sensitive only to the desired radiation around 1470 A. A graph of the

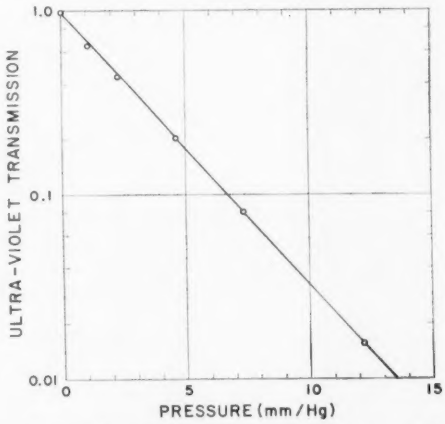

FIG. 7. Ultraviolet light transmission as a function of the gas pressure in the shock tube for a 21.5% O_2–78.5% Ar mixture at room temperature, 294°K. The straight line fit to the data point gives the room temperature absorption coefficient.

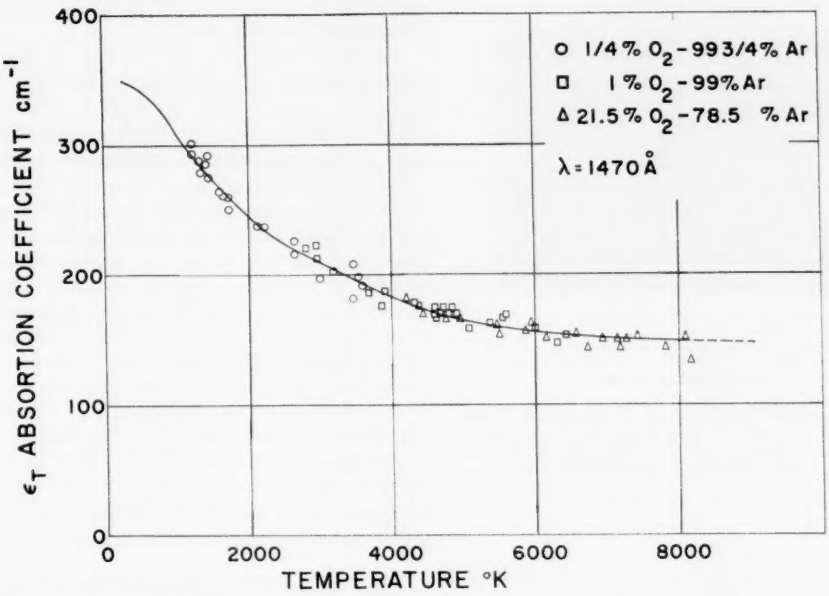

FIG. 8. The absorption coefficient ϵ_T of molecular oxygen per centimeter path at atmospheric density (2.69×10^{19} particles/cc, Loschmidt's number) plotted as a function of the gas temperature.

measured transmission of the light from the hydrogen discharge lamp as a function of the gas pressure in the shock tube is shown in Fig. 7. The exponential transmission is characteristic for a monochromatic light source, and the measured absorption coefficient agrees with that given by Watanabe, *et al.*[13] Less than 0.01% of the photomultiplier output was due to stray ultraviolet and visible light with the use of the double prism monochromator.

1. *Calibration for Dissociation Relaxation Data*

For the determination of the O_2 dissociation rates to be discussed in the following paper,[10] the transmitted ultraviolet light must be related to the concentration of O_2 in the shock tube. Let I be the intensity of the transmitted light; let I_0 be the transmission when there is a vacuum in the shock tube. These intensities are related by the exponential absorption law

$$I=I_0\exp(-\epsilon_T\rho d), \qquad (1)$$

where ϵ_T is the absorption coefficient of O_2 per centimeter of path at normal density (2.69×10^{19} particles/cc); ρ is the oxygen density per unit normal density; and d is the diameter of the shock tube (3.81 cm) that the light traversed. This relation is independent of the concentrations of atomic oxygen and argon.

The absorption coefficient ϵ_T is a function of temperature and experimentally determined values are given in Fig. 8 in a plot of ϵ_T versus T. The data points were obtained by measuring the gas transmission after the vibration relaxation was completed, but before an appreciable amount of dissociation. For example, in Fig. 6 this would correspond to the transmission just after shock passage. For the point at 294°K (room temperature), ϵ_T is determined from the data shown in Fig. 7.

The shock heated gas is elevated to high temperatures and many vibrational states become occupied. The absorption coefficient ϵ_T now has contributions

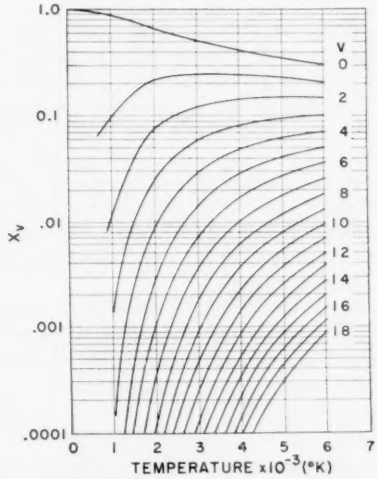

FIG. 9. The distribution of molecules in vibrational levels as a function of the gas temperature. X_v is the fraction of molecules in vibrational level, v.

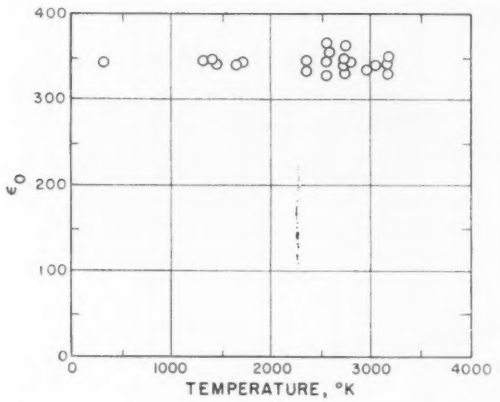

FIG. 10. The absorption coefficient for the ground vibrational state ϵ_0 is shown as a function of the gas temperature for 2.69×10^{19} particles/cc (Loschmidt's number). The point at 293° was obtained from Fig. 7. The other points are from shock tube runs.

from many states

$$\epsilon_T=\sum_{v=0}^{N}\epsilon_v X_v, \qquad (2)$$

where ϵ_v and X_v are the absorption coefficient and the fraction of oxygen molecules in the vth vibrational state. N is the total number of vibrational states. ϵ_T, given in Fig. 8, was determined when vibration, rotation, and translation were all in equilibrium at a temperature T. Figure 9 gives the equilibrium vibration values of X_v as a function of the temperature. At room temperature, $\epsilon_T=\epsilon_0$ (the absorption coefficient from the ground vibrational state), since $X_0=1$ and $X_{v>0}=0$.

2. *Calibration for Vibrational Relaxation Data*

A knowledge of the absorption coefficient during vibrational relaxation is required. The calibration for the vibrational relaxation analysis cannot be obtained directly but must be inferred from a combination of theory and experiment. For our analysis we have assumed that ϵ_T given by Fig. 8 and Eq. (2) is only a function of the vibrational temperature and *independent* of the translational temperature. This assumption is justified if both (1) a vibrational temperature exists, and (2) each ϵ_v in Eq. (2) is constant and independent of the temperature.

It has been shown[20] that a vibrational temperature T_v does exist during the relaxation time under the assumption of a parabolic potential. The X_v of Eq. (2) has a Boltzmann distribution of the form

$$X_v=[1-\exp(-h\nu/kT_v)]\exp(-vh\nu/kT_v), \qquad (3)$$

where ν is the vibrational frequency. For O_2, $(h\nu/k)=2228$°K. The distribution X_v in Fig. 9 can be used during the relaxation process with the abscissa having the vibrational temperature T_v.

The assumption that the ϵ_v in Eq. (2) are temperature independent is justified mainly from the theoretical discussion presented in Sect. II.A. This theoretical result is corroborated by measurements which show that ϵ_0 (the ground-state absorption coefficient) is constant with temperature. Values of ϵ_0 for rotational and translational equilibrium at elevated temperatures can be determined from measurements of the ultraviolet transmission before an appreciable amount of vibrational relaxation. Figure 10 shows experimental values of ϵ_0 up to 3000°K translational temperature. Note that ϵ_0 remains constant within a few percent of its room temperature value. This agreement with the theoretical predictions supports the assumption that each ϵ_v is temperature independent, and that ϵ_T of Fig. 8 is a function of only the vibrational temperature.

The absorption curve given in Fig. 8 has been analyzed in accordance with Eqs. (2) and (3), and the following results obtained: $\epsilon_1<0.1\epsilon_0$, $\epsilon_2+\epsilon_3\approx 0.8\epsilon_0$. The higher states contribute approximately $0.5\,\epsilon_0$.

III. VIBRATIONAL RELAXATION OF O_2 BY O_2 AND ARGON

A. Theory

In the analysis of vibrational relaxation it is generally accepted that the time sequence for the relaxation of the various modes behind strong shock fronts takes place in three distinct periods. First, within a few collisions the translational and rotational modes are equilibrated. Next, the vibrational mode adjusts, and finally, chemical relaxation brings the gas to complete thermodynamic equilibrium. It is shown in the following paper[10] that the vibration and dissociation rates become comparable at 8000°K and remain coupled above this temperature. In this paper only data below 7000°K are discussed and the analysis assumes that there is no O_2 dissociation during vibrational relaxation.

Theoretical investigations of the vibrational relaxation[1,2,20] assuming a simple harmonic oscillator system for the diatomic molecule have the following simple results. If initially the population of the vibrational levels follows a Boltzmann distribution, then a Boltzmann distribution X_v will persist through the entire relaxation process [see Eq. (3)]. Thus, a gas has a well-defined vibrational temperature T_v throughout the relaxation.

The energy in vibration E is given by

$$E=\frac{h\nu}{\exp(h\nu/kT_v)-1}, \qquad (4)$$

where $h\nu$ is the energy level spacing. The relaxation equation[1,2,20] has the simplest form when written in terms of the relaxation of the vibrational energy E

$$E-E_f=(E_i-E_f)\exp(-t/\tau)_v, \qquad (5)$$

[20] E. Montroll and K. Shuler, J. Chem. Phys. **26**, 454 (1957).

where E_i and E_f are the initial and final energies; t is the time; and τ_v is the vibrational relaxation time. The relaxation time is related to k_v, the number of vibrational transitions per second an O_2 molecule makes, by the formula

$$k_v = 1/\tau_v. \tag{6}$$

The number of transitions from the first to the ground vibrational states k_{10} is $k_{10} = k_v[1 - \exp(-h\nu/kT)]$. Introducing the quantity P_{10}, the probability per collision for de-excitation from the first to the ground state, then

$$\frac{1}{\tau_v[1 - \exp(-h\nu/kT)]} = k_{10} = ZP_{10}$$
$$= n(\pi r^2)(8kT/\mu\pi)^{\frac{1}{2}}P_{10}; \tag{7}$$

Z is the number of collisions an O_2 molecule makes per second; n the number of particles/cc; μ the reduced mass; and r the collision radius. Theoretical formulas for P_{10} have been proposed by Landau and Teller[1] having the temperature dependence

$$P_{10} = A_1 T^{-1/3} \exp -[(C/T)^{1/3}] \tag{8}$$

and by Schwartz and Herzfeld[2]

$$P_{10} = A_2 T^{-1/6} \exp(h\nu/2kT) \exp -[(C/T)^{1/3}], \tag{9}$$

where A_1, A_2, and C are constants which depend on the molecular constants. The explicit formula for C is[2]

$$C = [54\pi^4\mu(h\nu)^2/h^2k(\alpha^*)^2]; \tag{10}$$

$1/\alpha^*$ is the range of the exponential potential that was used to approximate the repulsive portion of the Lennard-Jones potential. Over the temperature range of this experiment, $\alpha^* \approx 17.5/r_0$, where r_0 is the intermolecular distance at which the Lennard-Jones potential has zero energy. From viscosity data, $r_0 = 3.433$ A for O_2-O_2 and 3.426 A for O_2-Ar, respectively, $\mu = 2.65 \times 10^{-23}$ g and 2.95×10^{-23} g for O_2–O_2 and O_2–Ar. Using these constants, C becomes

$$C = 8.4 \times 10^6 \text{ °K for } O_2\text{-}O_2 \text{ collisions}$$

and

$$C = 9.3 \times 10^6 \text{ °K for } O_2\text{-Ar collisions.} \tag{11}$$

Schwartz and Herzfeld[2] also present a table of P_{10} for several values of the temperature. These are also compared to our experimental values for P_{10} at the end of this section.

The temperature dependence of the relaxation time is obtained by combining Eqs. (7) and (8)[21]

$$\{n\tau_v[1 - \exp(-h\nu/kT)]\}^{-1} = C_1 T^{1/6} \exp -[(C/T)^{1/3}], \tag{12}$$

where $C_1 = r^2(8\pi k/\mu)^{\frac{1}{2}}A_1$. When combining Eqs. (7) and (9), the temperature-dependent factor before the exponential is $T^{1/3} \exp(+h\nu/2kT)$. The main dependence of the relaxation time with temperature is in the exponential factor $\exp -[(C/T)^{1/3}]$. This variation is observed in this experiment.

[21] Note that this formula differs from Eq. (31) of Blackman,[4] which is in error. The temperature-dependence factor $T^{1/6}$ is for constant density and not constant pressure as given by Blackman.

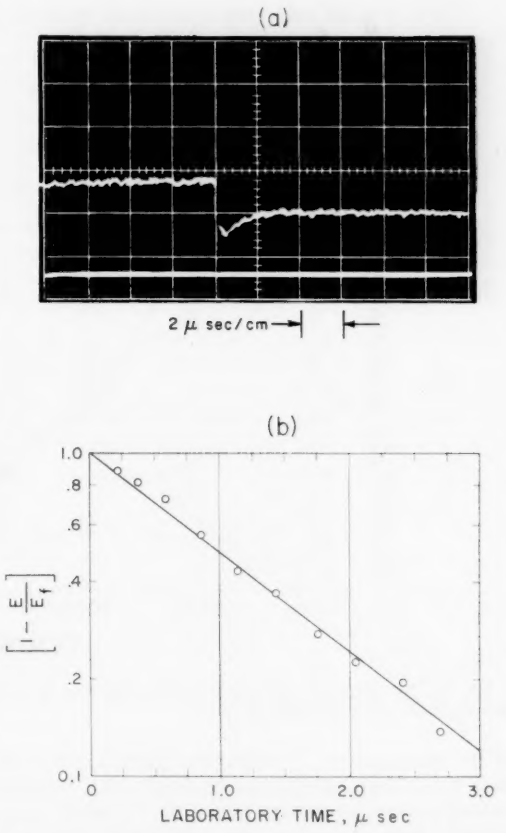

FIG. 11. Experimental data showing vibrational relaxation of oxygen in a 21.5% O_2–78.5% Ar mixture. Initial shock tube pressure was 0.93 mm Hg. The shock velocity was 2.51 mm/μsec corresponding to a temperature of 5180°K. Figure 11(a) shows the variation of the ultraviolet light transmission with time. The initial drop in transmission is due to the shock compression of the gas. The small increase in transmission is due mainly to the depopulation of the ground vibrational state during the relaxation. Figure 11(b) shows an analysis of the data where the $\log(1 - E/E_f)$ is plotted as a function of the laboratory time. E is the energy in vibration.

B. Experimental Method

The experimental measurements can be compared to the theory presented above. The data will be plotted according to Eq. (5), the simplest theoretical form for vibrational relaxation; that is, $\log(E_f - E)/(E_f - E_i)$ versus time. Since E_i is negligible in this experiment, this reduces to $\log(1 - E/E_f)$. The slope of the straight line fit to the data gives the vibrational relaxation time.

In each experimental run two quantities are measured: (1) the shock velocity along a 100-in. length

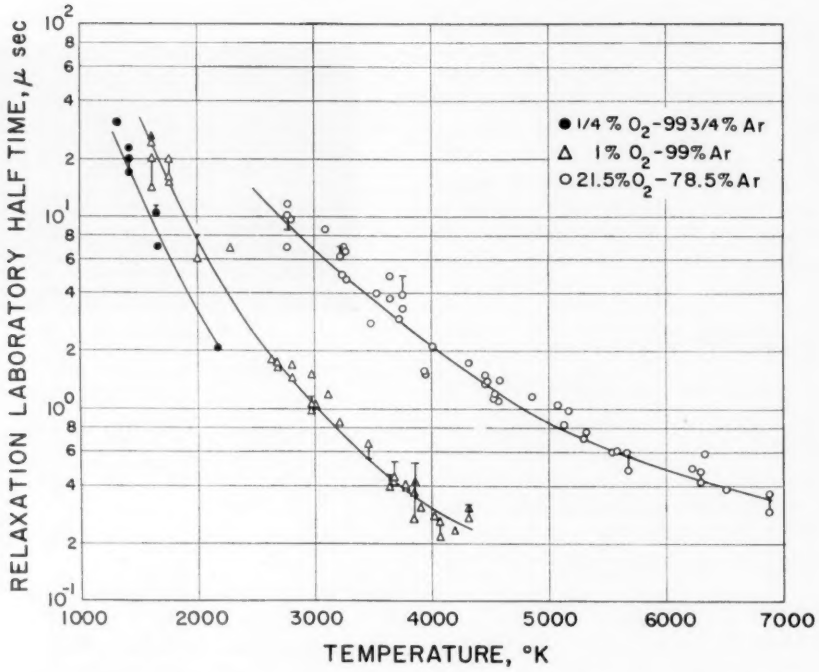

FIG. 12. The observed relaxation laboratory half-time in microseconds is plotted as a function of the gas temperature in degrees Kelvin for the vibration relaxation data.

of the tube, and (2) the ultraviolet light transmission with time. The temperature and density of the shock-heated gas can be computed from the measured shock velocity with the use of the conservation equations and the thermodynamic relations for O_2-Ar mixtures. The absorption coefficient of the gas ϵ_T can be determined from the ultraviolet light transmission data, ϵ_T is directly related to the vibrational energy E by Fig. 8 and Eq. (4), that is, the vibrational temperature, T_v, obtained from ϵ_T in Fig. 8, is converted into E by Eq. (4).

The details of the analysis sketched above are now presented. Starting with Eq. (1) the ultraviolet light transmission is

$$I = I_0 \exp(-\epsilon_T \rho d), \tag{13}$$

where ϵ_T is the absorption coefficient given in Fig. 8; ρ is the O_2 density normalized to atmospheric density; and d is the shock tube diameter 3.81 cm. The vacuum transmission I_0 is, in general, not observed, but can be related to the transmission I_1 of the initial unshocked gas

$$I_1 = I_0 \exp(-\epsilon_0 \rho_1 d), \tag{14}$$

where ρ_1 is the initial O_2 density and ϵ_0 is the absorption coefficient at room temperature. Eliminating I_0 in Eqs. (13) and (14), we obtain

$$\ln(I_1/I) = \epsilon_T \rho d - \epsilon_0 \rho_1 d. \tag{15}$$

The ratio I_1/I is obtained directly from the ultraviolet transmission oscillogram. For the vibrational relaxation analysis, (I_1/I) must be related to the quantity $(1-E/E_f)$,

$$1 - E/E_f = \exp(h\nu/kT_v) - \exp(h\nu/kT)/[\exp(h\nu/kT_v) - 1], \tag{16}$$

where T_v and T are the instantaneous vibrational and translational temperatures. These temperatures are determined from the conservation equations relating quantities across the shock front

$$\rho u = \rho_1 u_1, \tag{17}$$

$$\rho(RT + u^2) = \rho_1(RT_1 + u_1^2), \tag{18}$$

$$\{\tfrac{5}{2} + \phi + (\phi h\nu/kT_v)/[\exp(h\nu/kT_v) - 1]\} RT + \tfrac{1}{2}u^2 = [\tfrac{5}{2} + \phi] RT_1 + \tfrac{1}{2}u_1^2. \tag{19}$$

The unity subscript denotes the conditions ahead of the shock. In vibrational equilibrium, $T_v = T$; ϕ is the fraction of O_2 in the O_2-Ar mixture. Equations (16) and (19) are based on two simplifying assumptions: The vibration levels are calculated for a harmonic oscillator (parabolic) potential, and only the ground electronic state is populated. The additional error in the results due is these assumptions increases with

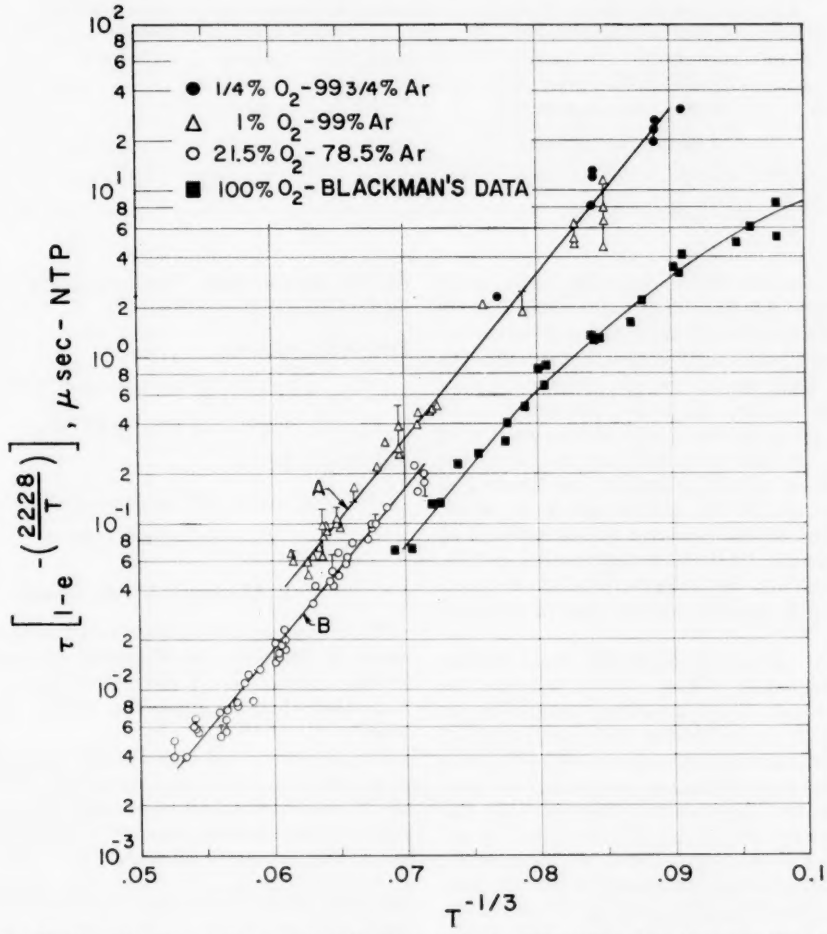

FIG. 13. The vibration relaxation results normalized to standard density, 2.69×10^{19} particles/cc, are plotted in the form $\log\tau[1-\exp(-2228°K/T)]$ vs $T^{-1/3}$. τ is the relaxation time in microseconds, and T is the temperature in degrees Kelvin.

temperature but would not introduce more than a 10% error in the relaxation rates at the highest temperatures (at 7000°K).

For each experimental run a calibration curve was plotted relating the ultraviolet data (I_1/I) to $(1-E/E_f)$. The numerical values of the initial gas conditions ρ_1, T_1, and ϕ, and the measured shock velocity u_1 were inserted in Eqs. (16)–(18) which were then solved for ρ and T as a function of T_v. These values for T and T_v were used with Eq. (16) to determine the variation of $(1-E/E_f)$ with T_v. Equation (15) for the ultraviolet transmission (I_1/I) was also made a function of T_v by noting that ρ and ϵ_T are functions of T_v. The calibration curve was obtained by cross plotting (I_1/I) and $(1-E/E_f)$ for the same value of T_v. With the use of this calibration curve, the experimental data were plotted to display the variation of $\log(1-E/E_f)$ with the laboratory time. The slope of the curve gives the vibrational relaxation time at the average translational temperature.

C. Measurements

O_2 vibrational relaxation measurements by means of the vacuum ultraviolet technique were made for three mixtures of oxygen with argon: $\frac{1}{4}\%$ O_2—$99\frac{3}{4}\%$ Ar; 1%O_2—99% Ar; and 21.5% O_2—78.5% Ar. The initial gas pressures for these mixtures were 8 cm, 2 cm, and 0.93 mm Hg, respectively, corresponding to an O_2 partial pressure of 0.2 mm Hg. The initial gas temperature was approximately 294°K. Thus, the gas transmission before shock passage was 0.73 for all runs. Measurements with pure oxygen have not been attempted, since the initial shock tube gas pressure would be too low for reliable shock tube operation. Preliminary measurements of N_2 vibrational relaxation

TABLE I. P_{10} vs temperature. P_{10}=fraction of collisions that de-excite the first vibrational level.

	T=1200°K	1800°K	2400°K	3000°K	4000°K	6000°K
O_2 in O_2 gas-theory[a]	5.2×10^{-5}	3.4×10^{-4}	2.2×10^{-3}	6.0×10^{-3}	...	...
O_2 in O_2 gas-exp	7.2×10^{-6}	5.4×10^{-5}	2.3×10^{-4}	7.2×10^{-4}	3.0×10^{-3}	1.7×10^{-2}
O_2 in Ar gas-exp	1.6×10^{-6}	1.2×10^{-5}	5.0×10^{-5}	1.6×10^{-4}	6.3×10^{-4}	3.5×10^{-3}

[a] See footnote 22.

in air have also been made[11] by observing the change in the gas density with time; the results show that O_2 is not more effective than N_2 in producing N_2 vibration.

For the low temperature runs (that is, the $\frac{1}{4}\%$ $O_2-99\frac{3}{4}\%$ Ar data) special care was taken to use pure gases. The gas mixture was passed through a liquid N_2 trap when filling the shock tube. A mass analysis of the gas used for these runs indicated less than 100 parts per million of all impurities combined. The partial pressure due to the residual gas in the shock tube at the time of shock passage was of the order of 0.2 μ Hg. Since the total gas pressure was 8 cm Hg, this corresponded to an impurity level of 25 ppm. Thus, the over-all impurity was between 25 ppm and 125 ppm.

Figure 11(a) shows an ultraviolet trace having vibrational relaxation. Figure 11(b) presents the analysis of this run. The slope of the straight-line fit to the data gives the relaxation time [see Eq. (5)]. Figure 12 shows the observed experimental relaxation data; the laboratory half-times are plotted as a function of the temperature. The relaxation time τ_v used in Eq. (5) is obtained by multiplying this half-time by $\rho^2/\phi\rho_1 \ln 2$, where ϕ is the fraction of O_2 in the mixture. This factor converts from laboratory to particle time and also normalizes to standard density.

Figure 13 shows a plot of the experimental relaxation data as well as Blackman's[3] results for pure O_2. $\text{Log}\tau_v[1-\exp(-2228°\text{K}/T)]$ is plotted versus $T^{-1/3}$ normalized to normal density ($n=2.69\times10^{19}$ particles/cc). Note that the experimental points lie along a straight line in agreement with the theory of Landau and Teller,[1] Eq. (12). The measured O_2 relaxation time τ for a muxture of O_2 and argon is related to the individual relaxation times τ_{O_2} and τ_{Ar} by the formula

$$1/\tau=\phi/\tau_{O_2}+(1-\phi)/\tau_{Ar}. \tag{20}$$

For $\phi=0.0025$ and 0.01, this equation reduces to $\tau=\tau_{Ar}$. However, for $\phi=0.215$, vibrational excitation by O_2-O_2 collisions are observed and a value for τ_{O_2} can be determined. It is observed that

$$\tau_{Ar}=(5.0\pm0.5)\tau_{O_2}, \tag{21}$$

that is, O_2 is five times more effective than argon in producing vibrational excitation. This ratio is also obtained by comparing our O_2-Ar data with Blackman's[3] pure O_2 results over the range of temperatures that the data overlaps. The data in Fig. 13 can be fit by the formula given in Eq. (12).

For O_2-Ar collisions

$$C_1=1.2\times10^{-7}\text{ cc/part-sec-(°K)}^{1/6}, \tag{22}$$

$$C=10.4(\pm30\%)\times10^6\text{ °K}. \tag{23}$$

For O_2-O_2 collisions

$$C_1=6.0\times10^{-7}\text{ cc/part-sec-(°K)}^{1/6} \tag{24}$$

$$C=10.4(\pm30\%)\times10^6\text{ °K}. \tag{25}$$

D. Comparison with Theory

These experimental results can be compared to the theory of Schwartz and Herzfeld.[2] Numerical values for their relation for C were presented in Eq. (11). Note that there is agreement within experimental error.

The theoretical and experimental values for P_{10} are compared in Table I. The theoretical values for P_{10} for O_2 relaxation in an O_2 gas were taken from the Schwartz and Herzfeld paper.[2,22] Experimental values for P_{10} were computed from Eq. (7)

$$P_{10}=(1/r^2)(\mu/8\pi kT)^{\frac{1}{2}}\{1/n\tau_v[1-\exp(-h\nu/kT)]\} \tag{26}$$

with $r=r_0=3.43$ A. Values for $\tau_v[1-\exp(-h\nu/kT)]$ were obtained from the curves designated by A and B in Fig. 13, with $n=2.69\times10^{19}$ part/cc. For O_2 collisions with Ar, curve A was used for temperatures up to 4000°K; curve B multiplied by 1.86 was used above 4000°K. For O_2 relaxation by O_2, curve B multiplied by 0.372 was used; below 2600°K curve B was extended parallel to curve A. These numerical factors were obtained by combining Eqs. (20) and (21). This table indicates a factor of 10 difference between theory and experiment over the entire range of temperatures.

E. Discussion

Schwartz and Herzfeld[2] used the parameters from Lennard-Jones potentials in their theoretical analysis. Since the Lennard-Jones parameters for argon and oxygen are very similar, the theory predicts essentially

[22] The theoretical values of P_{10} in Table I are four times larger than those presented in footnote 2 where a computational error was made. See paper of F. I. Tanczos, J. Chem. Phys. **25**, 439 (1956).

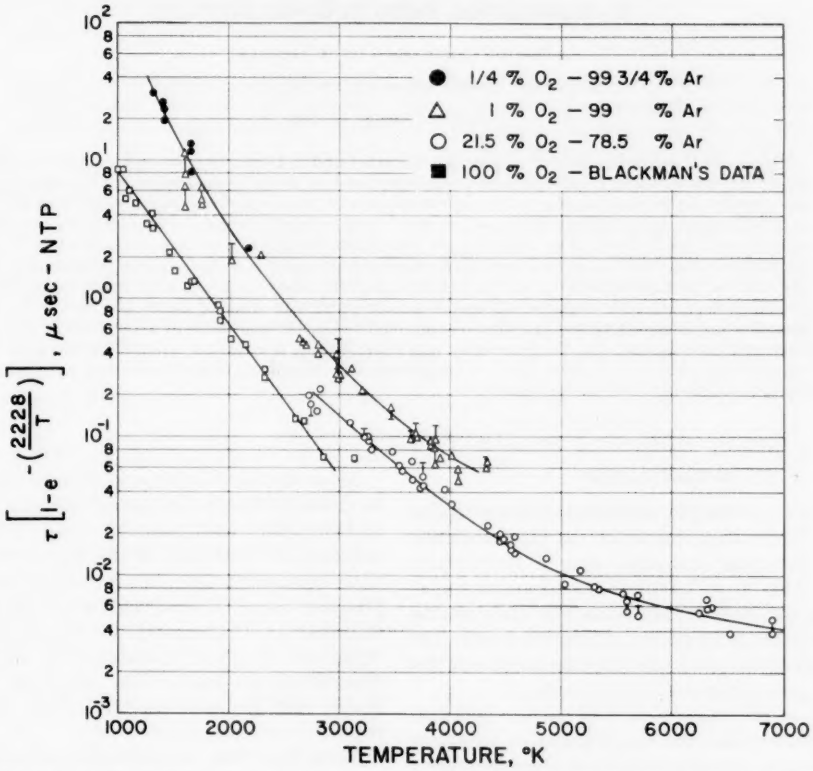

FIG. 14. The vibration relaxation results normalized to standard density are plotted in the form $\log\tau[1-\exp(-2228°K/T)]$ vs the temperature. τ is the relaxation time in microseconds and T is the temperature in degrees Kelvin.

the same value for P_{10} for O_2 collisions with oxygen and with argon. The factor of 4.75 difference in P_{10} may be due to a steeper slope to the repulsive core for the O_2-O_2 system or to the extra energy in rotation contributing to the O_2-O_2 rate.

It has been suggested by Widom[23] that a better line fit to the data is obtained by plotting $\log\tau_v$ at constant pressure as a function of temperature. Figure 14 shows a similar plot; obviously a straight line does not fit the results of this experiment. An extension of the straight line fit to Blackman's[3] data to high temperatures is inconsistent with our results above 3500°K.

Note that the data of Blackman[3] agree with the results of this experiment in the range where they overlap. However, at lower temperatures Blackman's data do not follow the same straight-line slope in the $T^{-1/3}$ plot as the O_2-Ar curve. This is an interesting difference and should be investigated further. For example, water vapor impurity could produce this change.[24] If these experimental results are correct, then O_2 vibrational relaxation in O_2-O_2 collisions does not follow the Landau-Teller theory[1] and resonance effects[2,22] become important.

[23] B. Widom, J. Chem. Phys. **27**, 940 (1957).

ACKNOWLEDGMENTS

Many people at this laboratory have contributed in obtaining the experimental data and in the data reduction. We especially want to thank Dr. C. C. Petty[11] (see footnote 11) for his participation in the early phases in this experiment. Dr. J. D. Teare[25] (private communication) supplied all the shock tube performance graphs which were required for data reduction.

[24] R. Taylor, Ph.D. thesis, California Institute of Technology, Pasadena, California.

[25] J. D. Teare (private communication); "Shock Wave calculations for High Temperature Gases," Proceedings of 2nd Shock Tube Symposium, sponsored by Air Force Special Weapons Center, Albuquerque, New Mexico, March 5–6, 1958.

O_2 Dissociation Rates in O_2-Ar Mixtures

MORTON CAMAC AND ARTHUR VAUGHAN*

Avco-Everett Research Laboratory, Everett, Massachusetts

(Received August 1, 1960)

Experimental measurements of the O_2 dissociation rate in shock-heated oxygen-argon mixtures were obtained with the ultraviolet light absorption technique described in the preceding article. The dissociation rate constant k_{Ar} for the reaction $O_2+Ar \rightarrow O+O+Ar$ can be fit over the temperature range from 3400°K to 7500°K by the theoretical formula $k_{Ar}=C(D/RT)^{n-1}\exp(-D/RT)$, where $C=6.0\times10^{21}\pm20\%$ cc/mole-sec and $n=1.5\pm0.2$. $D=5.116$ ev is the oxygen dissociation energy; R is the gas constant; and T is the temperature. This result is compared with the classical collision theory and the theories of Wigner and Keck. The rates for the dissociation of O_2 by O and O_2 were also determined; compared to the argon rate constant $k_O \approx 25k_{Ar}$, $k_{O_2} \lesssim 3k_{Ar}$. Our experimental results are compared with those of Byron and Matthews. The relaxation times for dissociation and vibration are observed to be comparable at about 8000°K. The experimental data indicate that the dissociation rate above 8000°K is at least a factor of two less than the expected rate when the vibration is not in equilibrium (the vibrational temperature being less than the translational temperature) during dissociation.

I. INTRODUCTION

THIS paper extends the ultraviolet light absorption method[1,2] to measurements of the O_2 dissociation rate in oxygen-argon mixtures over a temperature range from 3300°K to 7500°K. The concentration of molecular oxygen was determined as a function of time from a measurement of the uv absorption by O_2. The previous paper[1] presented a detailed description of the experimental technique used in this work.

The study of the reaction rates in gaseous collisions of diatomic molecules with simple particles should be amenable to a direct experimental and theoretical comparison. Several phenomenological theories of chemical relaxation rates of diatomic molecules have been proposed.[3–7] Footnote 4 gives an extensive bibliography. A correlation of these theories with experimental data is required for an evaluation of the important parameters underlying these theories. For example, a gross parameter of primary importance is the ratio of the cross section for dissociation to the kinetic cross section, usually referred to as the collision efficiency or steric factor. Also, a knowledge of the variation of the relaxation rates with temperature would furnish information on the contribution by the internal modes of motion to the dissociation process. These two items will be related to our experimental results on the dissociation of O_2 by argon.

More refined reaction rate theories discuss the rates of dissociation as a function of the state of vibrational[7] and electronic[4] excitation. The ideal experiment would measure the vibration of the population of some of these states with time; but this would be an ambitious program. Some information on this problem was obtained in this experiment by observing that there is significant coupling between the vibrational and dissociation processes. This occurs at temperatures above 8000°K where the relaxation rates for these reactions are comparable.

There have been several experimental investigations of O_2 chemical reactions at high temperatures. Interferometric studies on the gas density have yielded information on the O_2 dissociation[8,9] relaxation rates. Studies of emission from Schumann-Runge radiation[10–12] give information on the excitation of electronic states as well as other relaxation phenomena. Our results are in agreement with those of Byron where the data overlap. However, we have determined some of the relaxation rates to a greater precision and over a wider temperature range because of several advantages of the uv light method.[1]

II. THE DISSOCIATION OF O_2 BY ARGON

Theory

The dissociation of O_2 in a binary collision with another body M may be represented by the chemical equation

$$O_2+M \rightarrow O+O+M. \quad (1)$$

* Present address: University of Rochester, Rochester, New York.

[1] M. Camac, J. Chem. Phys. **34,** 447 (1961), preceding paper.

[2] M. Camac and C. C. Petty, Bull. Am. Phys. Soc. **3,** 286 (1958); IAS Preprint No. 802.

[3] E. D. Wigner, J. Chem. Phys. **5,** 720 (1937); **7,** 646 (1939).

[4] J. Keck, J. Chem. Phys. **29,** 410 (1958); Avco-Everett Research Laboratory, Research Report 66 (September, 1959).

[5] R. H. Fowler, *Statistical Mechanics* (The Macmillan Company, New York, 1936), 2nd ed., Chap. 18.

[6] R. H. Fowler and E. A. Guggenheim, *Statistical Thermodynamics* (Cambridge University Press, New York, 1939), Chap. 12.

[7] E. Bauer, Bull. Am. Phys. Soc. **5,** 228 (1960).

[8] S. R. Byron, J. Chem. Phys. **30,** 1380 (1959).

[9] D. L. Matthews, Phys. Fluids **2,** 170 (1959).

[10] J. Keck, Avco-Everett Research Laboratory, Research Report 67, June 1959.

[11] S. A. Losev, Doklady Akad. Nauk S.S.S.R. **120,** No. 6, 1291 (1958).

[12] Cornell Aeronautical Laboratory, Inc., Report No. QM-997-A-1 (September, 1957).

In oxygen-argon mixtures, collisions with O, O_2, and Ar will, in general, lead to the events represented by Eq. (1).

The kinetic equation for reactions of the above kind relates the rate of depletion of O_2 at constant temperature T and density ρ to the concentrations of the reacting species,

$$d[O_2]/dt\,|_{\rho,T} = -k_{Ar}[Ar][O_2] - k_{O_2}[O_2]^2 - k_O[O][O_2]. \quad (2)$$

Brackets denote the number density of the species indicated. The coefficients k_{Ar}, k_{O_2}, and k_O are the dissociation rate constants when the colliding bodies are Ar, O_2, and O, respectively.

For dilute concentrations of O_2, the second and third terms of Eq. (2) are negligibly small and the expression reduces to

$$d[O_2]/dt\,|_{\rho,T} = -k_{Ar}[Ar][O_2]. \quad (3)$$

Theories of dissociation and recombination of diatomic molecules in collision with other particles have been discussed by a number of authors.[3-7] Such a theory should use the atomic and molecular properties to predict the dissociation rate constant as a function of the temperature. The theories have used two general approaches: (a) the classical collision and statistical reaction rate, and (b) perturbation methods. The conclusions of the first group are within an order of magnitude of the reaction rates, while the second yields predictions that are many orders of magnitude smaller than the observed experimental values.

Classical Collision Theory[5,6]

The classical collision theory of the dissociation rate postulates that a molecule will dissociate during a collision if there is sufficient energy. The rate constant is obtained by calculating the number of collisions between dissociating molecules and other particles for which there is sufficient energy to cause dissociation. The result of this calculation gives the following relation for the number O_2 dissociations/cc/sec[6]

$$d[O_2]/dt = ZP\frac{(D/RT)^{t/2}}{(t/2)!}e^{-D/RT}; \quad (4)$$

Z = the number of collisions encountered by O_2 molecules/cc/sec; D = O_2 dissociation energy (5.116 ev); P, called the collision efficiency or steric factor, indicates the departure from the theory. The numerical value of t is determined by the number of degrees of freedom that supply energy to the dissociation process during a collision. Each rotational degree of freedom contributes unity to the value of t; each transverse translational degree of freedom also contributes unity; however, each vibrational degree of freedom contributes 2. The translational motion along the line of centers of the colliding bodies makes no contribution to t. Thus, for a collision of two particles involving q atoms

$$t \leq (3q-6+v), \quad (5)$$

where v is the number of vibrational degrees of freedom. The decrease by 6 arises from consideration of center-of-mass motion, motion along the line of centers, and conservation of angular momentum. The equal sign is used if all available energy consistent with conservation laws contribute to dissociation. Here t has a smaller value when some of the degrees of freedom do not transfer energy to the dissociation process. Equation (4) may be applied to the O_2—Ar system. For this case it has been postulated that the energy in vibration contributes but the transverse translation energy might not. Thus, there are two cases

$\frac{1}{2}t = 2$ for utilization of all energy consistent with conservation laws;
$\frac{1}{2}t = 1$ if energy in transverse translational degrees of freedom is not utilized. (6)

The number of collisions between O_2 and Ar, per cc per sec, is

$$Z = [O_2][Ar]\pi r^2(8kT/\pi\mu)^{\frac{1}{2}}, \quad (7)$$

where r = collision radius; μ = reduced mass of the O_2—Ar system. Equations (4) and (7) may be combined and compared with Eq. (3) giving the rate constant

$$k_{Ar} = r^2(8\pi kT/\mu)^{\frac{1}{2}}[P/(t/2)!](D/RT)^{t/2}e^{-D/RT}. \quad (8)$$

Since the choice of t and the collision radius are uncertain, we propose to use only the form of Eq. (8) to fit the experimental data. Equation (8) has the temperature dependence

$$k_{Ar} = C(D/RT)^{(n-\frac{1}{2})}e^{-D/RT}, \quad (9)$$

where C and n are constants to be determined by comparison with experiment.

Statistical Reaction Rate Theories

Of the various statistical reaction rate theories only those of Wigner[3] and Keck[4] are developed sufficiently to permit a detailed comparison with experimental data. They give rigorous numerical upper bounds to these rates without any unknown parameters. These theories are basically very similar and involve a phase space calculation of the molecular recombination rate. If the experimental rate lies close to their limit, then recombination occurs on almost every proper three-body collision. Wigner's upper bound for the recombination rate constant k_r for the reaction $O+O+Ar \rightarrow O_2+Ar$ is

$$k_r = 1.1\times10^{17}T^{-1}\ \text{cc}^2/\text{moles}^2\text{-sec}, \quad (10)$$

where T is the temperature in degrees Kelvin. As can be seen in Fig. 6, this bound is approximately 35 times higher than the observed rate constant.

Keck's upper bound for k_r is considerably smaller than Wigner's since he included the effect of the

rotational barrier which excluded many recombination paths considered by Wigner; he also considers recombination into stable excited electronic states of O_2. Keck separated the contribution to the rate constant k_r into two terms: (a) those recombination paths that use only the energy due to motion along the line of centers of the Ar-(2O) system; and (b) those that use only the transverse translational energy. The curve labeled "Keck A" (in Fig. 6) includes contributions from both these terms, while the curve "Keck B" has only the contributions from the translational energy along the line of centers. Note that both Keck's curves give upper bounds that are lower than Wigner's. In fact, the curve "Keck B" is only 3.5 times higher than the experimental data. Since the contribution from the transverse motion would be completely absent for a perfectly spherical molecule, this suggests that the "dumbbell" shape molecule assumed by Keck may be too asymmetrical. This is quite possible since specifications of the three-body interaction potential are one of the principal uncertainties in the theory. Another important effect which can lead to an overestimate of the rate in both the Wigner and Keck theories is the possibility that molecules may recombine and dissociate in the same collision.

Experimental Data

It is convenient to change the notation of Eq. (2). Let ϕ be the fraction of molecular oxygen in the initial mixture, and let N be the number of particles per cc before shock compression. The Ar, O_2, and O concentrations become

$$[\mathrm{Ar}]=(1-\phi)\Delta N$$
$$[\mathrm{O_2}]=(1-\alpha)\phi\Delta N$$
$$[\mathrm{O}]=2\alpha\phi\Delta N, \qquad (11)$$

where Δ is the density ratio across the shock, and α is the degree of dissociation of O_2. Equation (2) becomes

$$d\ln(1-\alpha)/dt_l = -N\Delta^2[(1-\phi)k_{\mathrm{Ar}}+(1-\alpha)\phi k_{\mathrm{O_2}}+2\alpha\phi k_{\mathrm{O}}], \qquad (12)$$

where the laboratory time, t_l, is used instead of the particle time t_p: t_l and t_p are related by the condition $t_p=\Delta t_l$. The reverse recombination reactions are not included and are never important, since the data were analyzed far from equilibrium conditions.

In this section the dissociation rate constant for argon k_{Ar} will be determined. Thus, only the data for the dilute O_2 mixtures are used; that is, for $\phi=0.0025$ and 0.01. The dissociation processes due to O_2 and O are negligible in first approximation and Eq. (12) reduces to

$$d\ln(1-\alpha)/dt_l=-\Delta^2 N k_{\mathrm{Ar}}. \qquad (13)$$

Moreover, the temperature and density ratio are essentially constant during the dissociation process for these dilute mixtures. Thus, Eq. (13) can be integrated

$$\ln(1-\alpha)=-(\Delta^2 N k_{\mathrm{Ar}})t_l=-t_l/\tau_d, \qquad (14)$$

where τ_d is the dissociation relaxation time. The experimental data will be analyzed with the use of Eq. (14).

For the analysis of the dissociation data we start with the transmission equation

$$I=I_0\exp[-\epsilon_T\Delta(1-\alpha)\rho_1 d], \qquad (15)$$

where I is the uv intensity transmitted through the gas and I_0 is the intensity with no gas absorption; α is the degree of dissociation of oxygen; ϵ_T is the absorption coefficient of O_2; Δ is the density ratio across the shock; ρ_1 is the initial O_2 density; and $d=3.81$ cm is the shock tube diameter. The absorption coefficient for O_2 has been determined experimentally over the temperature range from 293°K to 8000°K. The data are presented in footnote 1.

For given shock velocity and initial gas mixture the density and temperature in the shocked gas were calculated as functions of α assuming vibrational equilibrium.[13] The conservation equations relating quantities across the shock front are

$$\Delta u=u_1$$
$$\Delta u^2+(1+\alpha\phi)\Delta RT=u_1^2+RT_1$$
$$\{\tfrac{5}{2}+\phi+(\tfrac{3}{2}+D)\alpha\phi+(1-\alpha)\phi[(E_v+E_{el})/RT]\}RT+\tfrac{1}{2}u^2=(\tfrac{5}{2}+\phi)RT+\tfrac{1}{2}u_1^2.$$

The unity subscript denotes the conditions ahead of the shock; E_v and E_{el} are the energies in the vibrational and the electronic excitation of the bound states. All states were assumed to have equilibrium population at the translational temperature T. This simplified treatment neglected the depletion of the upper vibrational states and upper electronic states due to dissociation.

The results of such a calculation are shown in Figs. 1 and 2 for a 1% O_2 and 99% Ar mixture at an initial pressure of 2.0 cm Hg. Figure 1 shows the temperature of the gas and the density ratio across the shock as a function of the shock velocity for no dissociation and for full equilibrium. Because of the low percentages of O_2, both the density and the temperature remain relatively constant in the relaxation region, the temperature varying at most 190°K during dissociation. The ultraviolet transmission (I/I_0) is plotted as a function of shock velocity. in Fig. 2. Here I/I_0 was obtained from Eq. (15). The dashed line at 0.73 indicates the transmission of the initial unshocked gas. The lowest curve, marked $\alpha=0$, is the transmission assuming equilibrium

[13] J. D. Teare (private communication); "Shock wave calculations for high temperature gases," Proceedings of 2nd Shock Tube Symposium, sponsored by Air Force Special Weapons Center, Albuquerque, N. M., March 5–6, 1958.

vibration and electronic excitation but no dissociation. The top curve is for full chemical equilibrium. Note that for high shock velocities the final transmission approaches unity because the oxygen is essentially completely dissociated.

Figure 3 has two oscilloscope traces showing the ultraviolet light transmission versus time for a 1% O_2–99% Ar mixture. The shock velocities were 2.32 mm/μ sec and 2.61 mm/μ sec corresponding to equilibrium temperatures of 5045°K and 6320°K. Two traces were taken for each run. The lower traces was made by sweeping the oscilloscope with the light source off both before and after the run; thus, this trace would correspond to zero transmitted intensity with the lamp on. The upper trace was taken with the lamp on and initiated just prior to the passage of the shock front across the slits. The vertical deflection is proportional to the intensity of 1470 A ultraviolet light transmitted across the shock tube, an upward deflection corresponding to increased intensity. The variation of the intensity with time is explained as follows: The initial flat portion shows the transmission of the room temperature gas ahead of the shock front. At shock passage the transmission decreases because of the gas compression. For these runs the vibrational relaxation is not observed since equilibrium is reached during the shock wave transit time across the slits. The variation of transmission is due to O_2 dissociation. Note that for both runs shown chemical equilibrium is reached and the transmission becomes constant. The temperature was high enough so that in equilibrium the dissociation was essentially complete. Thus, the final flat portions of the upper traces represent the intensity which is observed with no absorption by the gas in the shock tube.

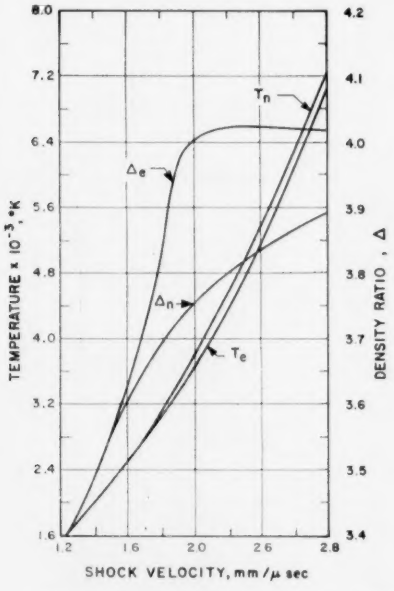

FIG. 1. Shock tube performance data for a 1% O_2-99% Ar mixture with the initial pressure at 2 cm Hg and temperature at 294°K. The gas temperature and density ratio across the shock are plotted as a function of the shock velocity in millimeters per microsecond. The curves designated by the subscript n show gas conditions with no O_2 dissociation. The subscript e are for full chemical equilibrium.

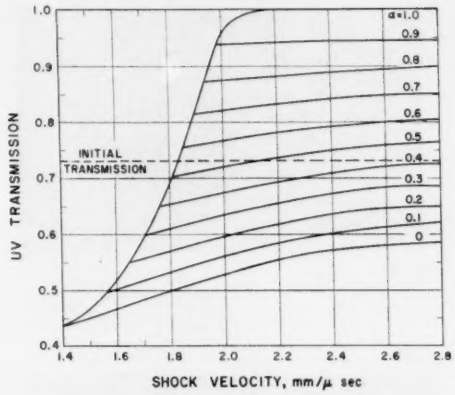

FIG. 2. Shock tube performance data for a 1% O_2-99% Ar mixture with the initial pressure at 2 cm Hg and initial temperature at 294°K. The ultraviolet light transmission is plotted as a function of the shock velocity in millimeters per microsecond. The curves are for values of α, the fraction of molecules dissociated. The dashed line indicates the transmission before shock passage.

These oscilloscope records are consequently self-calibrating. The ultraviolet transmission (I/I_0) at a time t is found by dividing the deflection measured from the base line at t by the deflection for complete dissociation. For the low shock velocity oscillograms where dissociation does not attain completion, the calibration was obtained from the transmission of the gas before the arrival of the shock. This initial transmission was checked repeatedly with high shock velocity runs where the gas became transparent.

With the use of the plot of ultraviolet transmission versus shock velocity (Fig. 2), the data of Fig. 3 can be converted to curves showing the O_2 dissociation with time. In Fig. 4, $\log(1-\alpha)$ is plotted as a function of t_l. These curves show a simple exponential behavior and the slope τ_d of the line drawn through the data is a direct measure of the relaxation rate. The dissociation rate constant k_{Ar} is calculated from the formula

$$k_{Ar} = (\Delta^2 N \tau_d)^{-1}, \tag{16}$$

which follows from Eq. (14).

In the analysis of the experimental data, Eq. (16) was used to calculate the dissociation rate constant. However, this is only an approximate formula since the effects of the dissociation by O_2 and O were neglected as well as the temperature drop (by as much as 190°K) due to the dissociation. These two effects give opposing corrections to Eq. (16) and essentially cancel. Equation

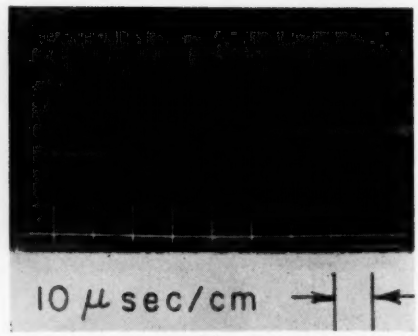

(a)

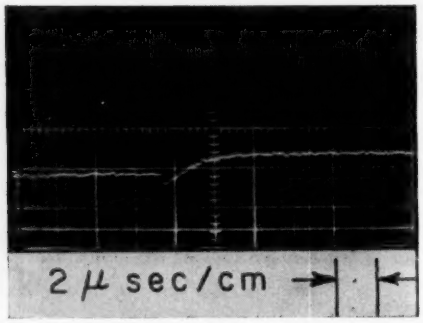

(b)

FIG. 3. Ultraviolet light oscillograms showing O_2 dissociation for the 1% O_2-99% Ar mixture at 2 cm Hg initial pressure. The shock velocities were 2.32 and 2.61 millimeters per microsecond for (a) and (b), respectively.

(16) gives accurate values for k_{Ar} when using the density ratio and the temperature for $\alpha=0$.

Results

The experimental determination of the dissociation rate k_{Ar} for the reaction $O_2+Ar\rightarrow 2O+Ar$ is shown in Fig. 5. These results include data from the $\frac{1}{4}$% and 1% O_2-Ar mixtures. Also shown are the experimental results of Byron.[8] The curve through the experimental data for k_{Ar} has the form suggested by the classical theory [see Eq. (9)]

$$k_{Ar}=C(D/RT)^{(n-\frac{1}{2})}e^{-D/RT}, \qquad (17)$$

where $C=6.0\times10^{13}$ ($\pm20\%$) cc/mole-sec, and $n=1.5\pm0.2$.

This value of n suggests that the classical collision theory use the exponent $(t/2)=1.5$. Comparing this value to predictions given in Eq. (6), we can conclude that almost all of the available energy consistent with conservation laws is used for dissociation. Note that $(t/2)$ should be less than 2 because the classical value for the energy in vibration is too large. For these experimental conditions $t/2$ should range from 1.7 to 1.8. The factor C can be separated into a collision term times a steric factor, P, as shown in Eq. (8). Using 2.06×10^{-8} cm (the radius of closest approach) for r, then $P=0.13$. For $r=3.43\times10^{-8}$ cm (the Lennard-Jones radius for zero potential), the P would be 0.05.

The recombination rate constant for the reaction $O+O+Ar\rightarrow O_2+Ar$ can be computed from the dissociation rate constant with the use of the equilibrium constant K: $k_r=k_d/K$. Figure 6 gives the recombination rate constant using the experimental dissociation rate and the equilibrium constant. Also shown are the theoretical curves of Wigner[2] and Keck[3] who give upper bounds for the recombination rate constant.

The upper limit proposed by Wigner is 35 times larger than the experimental data. Keck's proposed upper bounds to the recombination rate constant are 3.5 or 8 times larger assuming a spherical or dumbbell shape for the O_2 molecule. This is excellent agreement and substantiates the hypothesis that recombination occurs in almost every three-body collision. It should be noted that the same steric factor required for Keck's

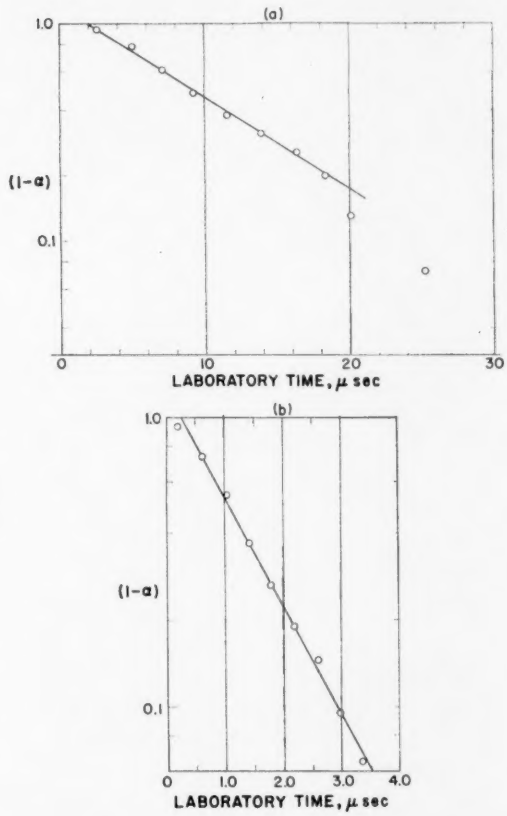

FIG. 4. Analysis of the data shown in Fig. 3. $\text{Log}(1-\alpha)$ is plotted as a function of the laboratory time. α is the degree of dissociation of O_2. The straight line fit to the data gives laboratory half-times of 7.3 μsec and 0.89 μsec for (a) and (b), respectively.

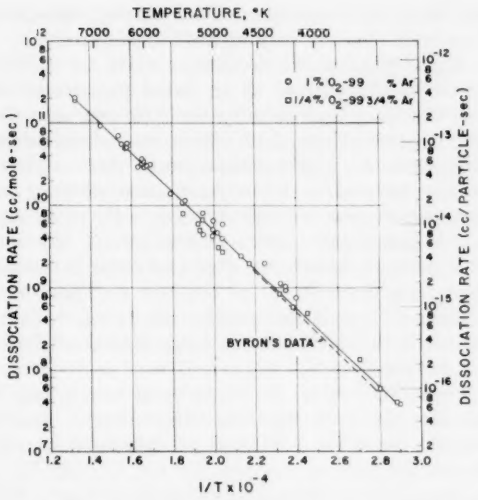
TEMPERATURE, °K
7000 6000 5000 4500 4000
o 1% O2-99 % Ar
□1/4% O2-99 3/4% Ar
BYRON'S DATA
DISSOCIATION RATE (cc/mole-sec)
DISSOCIATION RATE (cc/PARTICLE-sec)
1/T x 10^-4
1.2 1.4 1.6 1.8 2.0 2.2 2.4 2.6 2.8 3.0

FIG. 5. The dissociation rate constant for the reaction $O_2+Ar\rightarrow 2O+Ar$ is plotted as a function of $1/T$. The curve through the data has the form $k_{Ar}=6\times10^{13}(D/RT)e^{-D/RT}$ cc/mole-sec. Also shown is the data of Byron.[9]

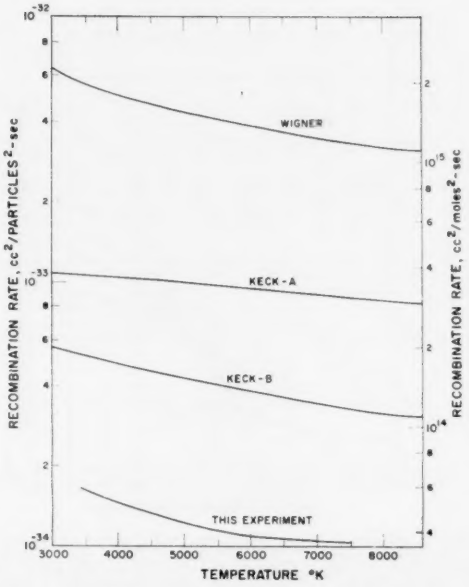

FIG. 6. The recombination rate for the reaction $O+O+Ar\rightarrow O_2+Ar$ is plotted as a function of temperature. The recombination rate is obtained from the dissociation rate measurements with the use of the equilibrium constant. Also shown are the theoretical curves of Wigner[3] and Keck.[4] The curve labeled "Keck A" [footnote 4, Fig. 9, curve $k^B(0)$] assumes that energy from all degrees contribute to the dissociation process. The curve "Keck B" [curve $k_P{}^B(0)$] assumes that the kinetic energy only along the line of centers of the 2O-Ar system contributes.

curve A is obtained with the classical dissociation collision theory.

III. THE DISSOCIATION OF O_2 BY O_2 AND O

This experiment also furnished some information on the dissociation rates of O_2 in collisions with O_2 and O. Data were obtained from runs using a 21.5% O_2–78.5% Ar mixture. A better determination of these rates could have been obtained by using pure oxygen; however, this was not possible with this experimental setup because of the large ultraviolet absorption coefficient. To have sufficient transmission the initial gas pressure must be less than 0.25 mm Hg which is too low for reliable operation of the 1.5 in. diameter shock tube.

The kinetic relation is given in Eq. (12). The rate constant k_{Ar} was fit by the formula given in Eq. (17). We shall assume similar temperature behaviors for k_O and k_{O_2}

$$k_O=C_1(D/RT)^{(n_1-\frac{1}{2})}e^{-D/RT} \tag{18}$$

$$k_{O_2}=C_2(D/RT)^{(n_2-\frac{1}{2})}e^{-D/RT}, \tag{19}$$

where C_1, n_1, C_2, and n_2 are unknown constants to be evaluated.

Substituting these formulas for k_{Ar}, k_O, and k_{O_2} into Eq. (12)

$$d\alpha/dl=\{(1-\alpha)\Delta^2N\phi C(D/RT)^{(n-\frac{1}{2})}e^{-D/RT}\}$$
$$\times\{[(\phi^{-1}-1)+(C_2/C)(D/RT)^{(n_2-n)}]$$
$$+\alpha[(2C_1/C)(D/RT)^{(n_1-n)}-(C/C)(D/RT)^{(n_2-n)}]\}. \tag{20}$$

Here Δ and T can also be expressed as a function of α,

$$\Delta=\Delta_0(1+a_1\alpha+a_2\alpha^2)$$
$$T=T_0-B\alpha; \tag{21}$$

Δ_0 and T_0 correspond to the no dissociation values (at $\alpha=0$); a_1 and a_2 are constants that depend on ϕ and the shock velocity; B depends only on ϕ. For $\phi=0.215$, $T=T_0-(4040°K)\alpha$.

Substituting Eq. (21) into Eq. (20) and integrating, we obtain the formula

$$\int_0^\alpha \frac{(1-B\alpha'/T_0)^{n-\frac{1}{2}}\exp[(D/RT)B\alpha'/(T_0-B\alpha')]}{\left(\frac{1}{\phi}-1+\frac{(1-\alpha')C_2}{C}\left[\frac{T_0-B\alpha'}{D/R}\right]^{n-n_2}+\frac{2\alpha'C_1}{C}\left[\frac{T_0-B\alpha'}{D/R}\right]^{n-n_1}\right)}\cdot\frac{d\alpha'}{(1-\alpha')(1+a_1\alpha'+a_2\alpha'^2)^2}=(\Delta_0{}^2N\phi k_{Ar}{}^0)l_L, \tag{22}$$

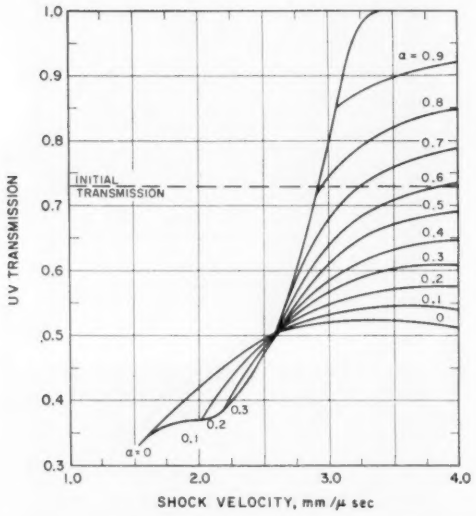

FIG. 7. Shock tube performance data for a 21.5% O_2-78.5% Ar mixture with the initial pressure at 0.93 mm Hg and initial temperature at 294°K. The ultraviolet light transmission is plotted as a function of the shock velocity. The curves are for values of α, the degree of O_2 dissociation. The dashed line indicates the transmission before shock passage.

where $k_{Ar}^0 = C(D/RT_0)^{(n-\frac{1}{2})}e^{-D/RT_0}$. The factors in parentheses on the right side are constant for each experimental run. The factors on the left side are functions of α only. The value of this integral was obtained numerically with an IBM 650 digital computer. The 21.5% O_2-78.5% Ar data were analyzed in two ways: by an integral method using Eq. (22), or by fitting calculated slopes to regions of data points. In the integral method an attempt was made to fit the entire experimental run starting from the time of shock passage.

Experimental Results

The transmission Eq. (15) is used in the analysis of the dissociation data. Figure 7 shows the variation of the ultraviolet transmission I/I_0 with shock velocity for several values of α. Note that while the 1% and $\frac{1}{4}$% O_2 transmission curves change uniformly with shock velocity, the 21.5% O_2 curves have large variations and even cross at the shock velocity of 2.6 mm/μsec. The crossover of the curves can be understood with the use of Eq. (15) where the product $\Delta(1-\alpha)$ appears; Δ increases with α, while $(1-\alpha)$ decreases. At 2.6 mm/μsec, the variation of Δ and $(1-\alpha)$ just compensate and I/I_0 remains constant. At lower shock velocities the variation in Δ is greater, and the transmission decreases. At higher shock velocities $(1-\alpha)$ decreases faster and the transmission increases. Because of this crossover, dissociation data cannot be obtained in the shock velocity range from 2.4 to 2.75 mm/μsec. Since the rates are too slow for shock velocities below 2.4 mm/μsec, dissociation data were obtained only above 2.75 mm/μsec.

Figure 8(a) shows dissociation data for a 21.5% O_2–78.5% Ar mixture at an initial pressure of 0.93 mm Hg. The shock velocity was 3.01 mm/μsec. Note that this run shows both vibration and dissociation relaxation. At higher temperatures this overlap is even greater and for shock velocities above 3.4 mm/μsec the analysis becomes difficult because the dissociation rate is comparable with the vibration rate. When the vibration and dissociation relaxation occur at the same time, then it is difficult to interpret the data. Thus, analysis of dissociation rates for the 21.5% O_2 data is limited to the shock velocity range from about 2.75 to 3.4 mm/μsec.

Figure 8(b) shows the variation of α with time for the data shown in Fig. 8(a). This curve is obtained with the use of Fig. 7. It is not possible to fit a straight line to the data as was done for the 1% and $\frac{1}{4}$% O_2 mixtures because of the large temperature (up to 4040° K) drop during the relaxation process. Also, O_2 and

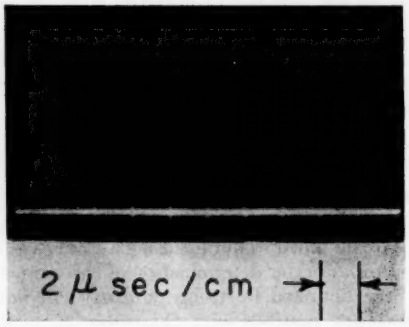

(a)

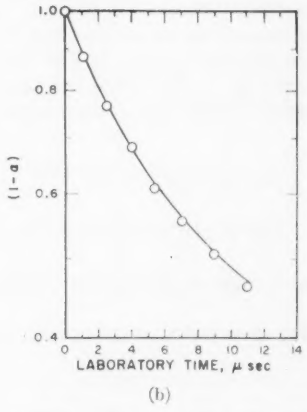

(b)

FIG. 8. Oscillogram showing the ultraviolet light transmission as a function of time for a 21.5% O_2-78.5% Ar mixture at initial pressure of 0.93 mm Hg. The shock velocity was 3.01 mm/μsec. The analysis of the data is shown in (b). The data points are from (a), while the curve is a theoretical fit.

O_2 participate in the O_2 dissociation process, and their contributions vary with α.

Equation (22) was used to make a theoretical fit to the data. Values for n_1, n_2, C_1, and C_2 were chosen to determine the best fit to the data. For all the runs analyzed, the data can be fit by neglecting the contribution of O_2–O_2 collisions to the dissociation. This puts an upper limit on the O_2 dissociation rate at about three times the argon rate in the temperature range from 6000°K to 7000°K. The value for k_O varies between 35 and 25 times k_{Ar} in the temperature range from 5000°K to 7500°K. For O_2–O collisions the best fit to the dissociation rate formula is $n_1=2.5$ and $C_1=1.8\times10^{14}$ cc/mole-sec. It is difficult to estimate the uncertainty in these results and it may be as much as 50%. Inserting these values for n_1 and C_1 into Eqs. (8) and (9), then the steric factor P becomes 0.8; other assumptions were a collision radius $r=2$ A, and $\mu=1.77\times10^{23}$ g.

The experimental dissociation rates of k_{O_2} and k_O are shown in Fig. 9. Also shown are the results of Byron[8] and Matthews,[9] their values for n were not determined experimentally but were based on uncertain theoretical arguments. The upper limit to our value for k_{O_2} is lower than expected by extrapolating Byron's or Matthews' data. This reduction may be due to a coupling of the vibration and dissociation processes at the higher temperatures which would tend to decrease the dissociation rates.

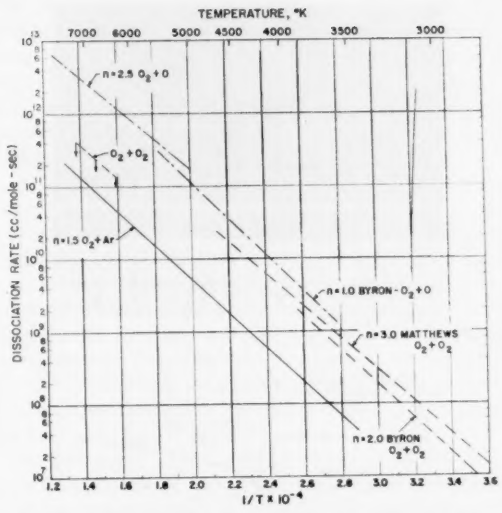

FIG. 9. The dissociation rate constant for O_2 collisions with Ar, O_2, and O are plotted as a function of $1/T$. Also shown are the data of Matthews[9] and Byron.[8] The curves have the temperature variation $k=C(D/RT)^{n-\frac{1}{2}}e^{-D/RT}$, where $D=5.116$ ev, the dissociation energy, and T is the temperature. Values of n are shown on the curves.

Coupling of Vibration and Dissociation at High Temperatures

In this section experimental data are presented which demonstrate that the dissociation rate depends upon the state of vibrational excitation. The effects of vibration-dissociation coupling have been discussed by Hammerling *et al.*[14] They assumed the following model: the dissociation of a diatomic molecule can occur from every vibrational level. The probability that dissociation occurs from any given level is assumed to be proportional to a Boltzmann factor corresponding to the binding energy of the level; thus, the rate of dissociation k is

$$k\propto\sum_{n=0}^{N}X_n\exp[-(D-E_n)/kT], \qquad (23)$$

where T is the translational temperature; N is the number of vibrational levels; $(D-E_n)$ is the energy difference between the nth vibrational level and the dissociation energy; and X_n is the relative population for the nth vibrational level. It can be shown that the dissociation rate is less than the equilibrium value when $T_v<T$.

Definite predictions of the changes in the dissociation rate can be made with Eq. (23). Consider the example of shock heating O_2 from room temperature to 10 000°K. Immediately after shock passage, the molecules remain predominantly in the ground vibrational state until thousands of collisions have occurred. During this time the dissociation rate is reduced by the factor

$$\{N[1-\exp(-h\nu/kT)]\}^{-1}$$
$$=\{40[1-\exp(-2228°/10\,000)]\}^{-1}=0.13, \qquad (24)$$

compared to the rate at vibrational equilibrium. If dissociation proceeds preferentially from the upper states (aside from the Boltzmann factor), then Eq. (23) must be modified and there would be an even larger reduction in the initial rate of dissociation.

Figure 10(a) shows an ultraviolet oscillogram obtained under conditions where the dissociation and vibrational rates are comparable. For this run P_1 was 0.93 mm Hg; the initial composition was 21.5% O_2–78.5% Ar. The shock velocity was 3.19 mm/μsec corresponding to about 8000°K translational temperature immediately following the shock with frozen vibration and dissociation. Figure 10(b) illustrates the coupling of dissociation and vibration. The dashed curves indicate how the data would appear if vibration and dissociation occurred separately. If there were no dissociation, then the data would follow the curve lebeled "vibration alone." This curve was determined by extrapolating the results of Fig. 13 in footnote 1. The curve labeled "dissociation alone" assumes vibration equilibrium and is based on an extrapolation of the data in Fig. 9. The experimental curve shows that

[14] P. Hammerling, J. D. Teare, and B. Kivel, Phys. Fluids **2**, 422 (1959).

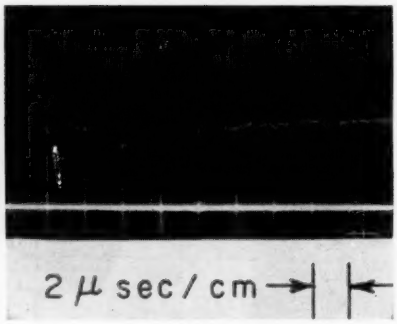

(a)

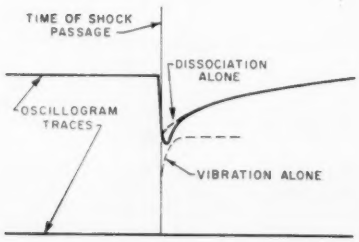

(b)

FIG. 10. Oscillogram showing the ultraviolet light transmission as a function of time for a 21.5% O_2-78.5% Ar mixture at initial pressure of 0.93 mm Hg. The shock velocity was 3.19 mm/μsec. Note that the vibration and dissociation rates indicated by dashed curves have comparable relaxation times at the shock front.

dissociation is in progress during the vibration relaxation.

It becomes difficult to analyze both the dissociation and vibration relaxation data under conditions where this coupling is important. The analysis of the vibration data requires a knowledge of the translational temperature and the gas density at all times. When dissociation proceeds during the vibration relaxation then the gas temperature changes and becomes uncertain. This sets an upper temperature of about 7500°K for which vibrational relaxation data can be obtained. Similarly, it is difficult to obtain dissociation data for temperatures above 8000°K because the absorption coefficient ϵ_T depends on the vibrational temperature T_v. Our analysis of the dissociation data assumed that the vibrational mode was always in equilibrium with translation. The I/I_0 calibration curves presented in Figs. 2 and 7 assume vibrational equilibrium.

Figure 11(a) illustrates the vibration-dissociation coupling at a higher shock velocity, 3.51 mm/μsec. The temperature was 9250°K for no dissociation. However, the gas temperature drops by 4040°K to 5210°K during the dissociation process. Above 8000°K, the data cannot be analyzed because of the vibration-dissociation overlap. When the gas temperature drops below 7500°K and the vibration relaxation rate becomes faster than the dissociation rate, then the analysis of the dissociation data can proceed in the usual way. We are thus able to measure the O_2 dissociation by O atoms below 7500°K by using the portion of the experimental data in this temperature range, even though the gas was initially shock heated to a much higher temperature. The analysis of the oscillogram is shown in Fig. 11(b). The rate constants presented in Fig. 9 were extrapolated to higher temperatures using the theoretical formula given in Eqs. (17), (18), and (19). Inserting these rates into the integral relation Eq. (22), the solid curve shown in Fig. 11(b) was obtained. The calculated curve is aligned with the experimental data below 7500°K. The extrapolation of the curve to $(1-\alpha)=1$ (no dissociation) is much steeper than the experimental data. The lack of agreement indicates that the observed rates are slower

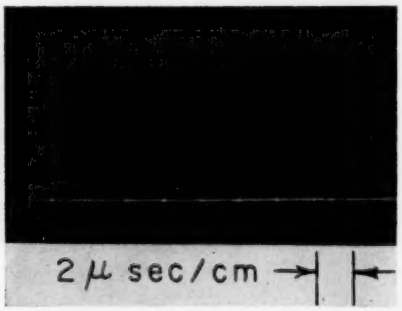

(a)

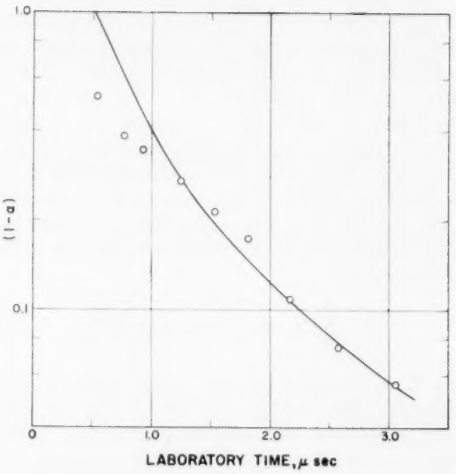

(b)

FIG. 11. (a) The oscillogram showing the ultraviolet light transmission as a function of time for a 21.5% O_2-78.5% Ar mixture at initial pressure of 0.93 mm Hg. The shock velocity was 3.51 mm/μsec corresponding to a temperature of 9250°K for no O_2 dissociation, i.e., $\alpha=0$. (b) Analysis of data showing $\log(1-\alpha)$ vs laboratory time. Note the computed curve goes to $\alpha=0$ at 0.5 μsec and not at the time of shock passage.

by more than a factor of 2. Thus, the dissociation process is slower when vibration has not reached equilibrium.

Quantitative data are difficult to obtain with the present experimental arrangement. The experimental rates are so fast that large errors arise due to the uncertainty in the position of the shock front, as well as in the curvature of the shock. To do a more precise experiment, a large diameter (greater than 6 in.) shock tube must be used which can operate at lower initial gas pressures. The experimental rates will be slower, thereby permitting a quantitative analysis.

IV. ACCURACY OF THE EXPERIMENT

This section considers the important factors that limit the accuracy of the experiment. The following items will be considered separately.

1. Accuracy of the shock velocity.
2. Statistical noise, electronic response, and slit width effects on ultraviolet transmission.
3. Shock wave velocity attenuation.
4. Boundary layer absorption of ultraviolet light.
5. The interaction of the boundary layer with the free stream conditions.
6. Contamination of the gas with nitrogen and other reacting species.

The over-all accuracy of the data is summarized at the end of this section.

1. The importance of an accurate knowledge of the shock velocity appears in the calculation of the recombination rate $k_r(=k_d/K)$, where K is the equilibrium constant and k_d is the dissociation rate. There is a T^{10} to T^{15} temperature variation in the equilibrium constant K. In addition the gas temperature varies quadratically with the shock velocity. Thus, any error in the shock velocity will result in a 20 to 30 times larger error in the recombination rate. In this experiment the shock velocity was measured at six stations. The separations between adjacent stations were from 10 to 30 in. and were measured to an accuracy of 0.01 in. The time of shock passage between stations was measured to an accuracy of 1/3 μsec. Thus, the error in determining the temperature from shock velocity measurements was approximately 0.6%.

2. The fluctuations in the ultraviolet oscilloscope traces are produced by statistical variations in the electron current from the photomultiplier cathode due to the low intensity of the ultraviolet lamp. The combination of noise fluctuations, the finite slit widths, and the electronic response produced an uncertainty in both the time of shock passage and also the ultraviolet light transmission just after shock passage. Estimation of the time of shock passage was based upon a judgment of the importance of these effects. The time of shock passage was mainly determined by calculating the shock transit time across the slit; one half of this transit time was added to the time that the oscillogram trace started to deviate from the initial absorption. For the 2 cm and 8 cm initial pressure runs, the observed shock front transit time was approximately equal to the ratio of the slit width to the shock velocity. For the runs at 0.93 mm initial pressure, the observed transit time was longer indicating a 1 mm curvature to the shock front.

3. The attenuation of the shock velocity affects the state of the gas behind the shock. This effect is discussed in detail elsewhere.[15] Both the temperature and density of the gas increase slowly. The density variation can be neglected but the temperature variation can be important because of the strong dependence of the equilibrium constant and the dissociation rate on the temperature. The effects of attenuation were applied to the 1% O_2–99% Ar mixture. There were significant corrections to the data after about 70 μsec from the time of shock passage.

4. The effect of the growth of the boundary layer can be observed in this experiment.[15] The free stream gas was shock heated to a very high temperature so that the dissociation was complete within a few microseconds. Thus, the free stream gas was completely transparent during most of the test time. When the initial gas pressure is 4 times greater than normal, the growth of the boundary layer is observed; there is absorption by the gas cooling and recombining in the boundary layer. Another source of boundary layer absorption is due to irregularities in the shock tube wall due to the insertion of windows. These irregularities produce additional absorption, but can be made smaller than the normal boundary layer effects. In the analysis of the data, this boundary layer absorption never required more than a 5% correction.

5. The absorption (discussed above) due to the boundary layer gas is relatively easy to correct.[15] However, the change in the free stream condition due to the boundary layer growth is more serious. The loss of gas on the shock tube walls produces a large negative displacement thickness and the free stream gas follows the flow pattern similar to a diverging channel. Since the flow is subsonic in shock coordinates, the gas temperature and density increase. The magnitude of the displacement thickness varies inversely as the Reynolds number based upon free stream conditions. Thus, this effect is largest for the low gas density runs. The growth of the boundary layer varies as the square root of the distance behind the shock; thus, these effects can be important very close to the shock front. Because of the uncertainty in calculating this effect, the analysis of the data was stopped where this effect was estimated to be important. It was important only for the 21.5% O_2–78.5% Ar data where the initial pressure was 0.93 mm. It should be noted that changes in the free stream temperature of the order of a few per cent produce very large changes in the reaction

[15] M. Camac and A. Vaughan, Avco-Everett Research Laboratory, Research Report 84 (December, 1959).

rates. Thus, for experiments such as this one where dissociation rates are measured, it is important to know the gas temperature very accurately.

6. The effects of having other molecular species in the O_2–Ar mixtures must be evaluated since both the gas absorption and the chemical rates can be affected. At 1470 A, N_2 is transparent but heated NO has an absorption coefficient of about 300/cm at NTP, about twice the absorption of heated O_2. Impurities such N_2 could effect the rates of chemical reaction because of the fast exchange reactions: $O+N_2 \rightleftarrows NO+N$ and $N+O_2 \rightleftarrows NO+O$. This permits another mechanism for the rapid dissociation of oxygen producing NO and O. Also, as oxygen dissociates and NO is produced through these exchange reactions, the absorption would not decrease as rapidly because of the increase of absorption due to the NO. It can be shown for the $\frac{1}{4}$% and 1% O_2 mixtures that these exchange reactions are not important. However, they can be serious for the 21.5% O_2 runs. The purity of the gas used for these runs was measured; the argon has less than 100 parts per million impurity and the oxygen had at most $\frac{1}{2}$% of N_2. This impurity was comparable to the residual gas pressure in the shock tube. The effects of these impurities on the dissociation rates are unimportant at high temperatures.

Summary of Corrections and Accuracy of Data

The major uncertainty in the evaluation of the experimental data is in the effects on the free stream due to shock velocity attenuation and the strong boundary layer interaction. This effect is strongest for the lowest initial gas density corresponding to the 21.5% O_2–78.5% Ar mixture. This can lead to uncertainties in the free stream temperature of several percent after 16-μsec test time.[15] Since the reaction rates have such a large temperature dependence this may lead to errors of 50% or more in the estimation of the dissociation rate constant.

The effect of boundary layer interaction is smaller for the 1% and $\frac{1}{4}$% O_2 mixtures and could be neglected for less than 70 microseconds laboratory time. For these mixtures, the major uncertainty is in the knowledge of the shock velocity and the statistical fluctuations of the ultraviolet oscilloscope trace. The uncertainty in the shock velocity was about $\frac{1}{3}$% which leads to an uncertainty in the rate constant by as much as 10%. The noise fluctuations in the ultraviolet trace lead to a larger uncertainty up to about 20% in the value of the degree of dissociation. The uncertainty in the time of shock passage gave up to a 10% error for the high temperature runs where the rates were very fast.

V. SUMMARY

This paper has presented experimental data from which the O_2 dissociation rates in O_2–Ar mixtures were determined. The dissociation rate constant k_{Ar} for the reaction $O_2+Ar \rightarrow O+O+Ar$ can be fit by the formula

$$k_{Ar}=6.0\times10^{13}(\pm20\%)\,(D/RT)^{1.0(\pm0.2)}e^{-D/RT}$$

cc/mole-sec

over the temperature range from 3300°K to 7500°K. $D=5.116$ ev is the dissociation energy of O_2. This dissociation rate was measured with sufficient precision to determine the temperature dependence aside from the Arrhenius factor. Using the classical collision theory, this dependence can be interpreted that all degrees of freedom aside from the limitations of conservation laws contribute energy to the dissociation process. The recombination rate for the reaction $O+O+Ar \rightarrow O_2+Ar$ can be inferred from the dissociation rate with the use of the equilibrium constant K where $k_r=k_d/K$. The recombination rate theory of Keck[4] predicts this recombination rate within a factor of 3.5 or 8 depending on the O_2 molecular model. It appears that the Keck theory, which predicts the recombination rate without any adjustable parameters, gives results sufficiently in agreement with experiment to establish the general validity of this approach. It also appears reasonable to hope that experiments on recombination and dissociation can provide the necessary clues for significant improvements in the theory, and that coupling of theory and experiment may eventually lead to information concerning three-body potentials.

The dissociation of O_2 by O_2 has been measured over a smaller temperature range from about 6000°K to 7000°K, while O_2 dissociation by O was observed from 5000°K to 7500°K. The dissociation rate constants compared to that of argon are

$$k_O \approx 25k_{Ar}, \qquad k_{O_2} \leq 3k_{Ar}.$$

The vibration and dissociation relaxation rates become comparable at about 8000°K temperature. Since the dissociation proceeds from many vibrational states, the dissociation rate should be less if the upper vibration levels have not reached equilibrium. The experimental data indicate that there is at least a factor of 2 decrease from the expected dissociation rate at high temperatures (above 8000°K) where vibration has not reached equilibrium. Only qualitative results could be obtained with our experimental apparatus. However, this ultraviolet method used with a larger diameter shock tube could give quantitative data on the vibration-dissociation coupling. In particular, it could ascertain whether dissociation proceeds predominantly from the upper or from the lower vibrational levels.

ACKNOWLEDGMENTS

We are indebted to Dr. J. D. Teare for supplying the extensive shock tube performance calculations which were required for data reduction, and to Dr. C. C. Petty who participated in the early stages of this work. We sincerely thank the many people who have contributed to the job of obtaining and reducing the experimental data.

Electron Spin Resonance Study of *p*-Phenylene-Diamine Positive Ion

M. T. MELCHIOR* AND A. H. MAKI

Mallinckrodt Laboratory, Harvard University, Cambridge, Massachusetts

(Received July 5, 1960)

The mono-positive radical ion of *p*-phenylene diamine has been prepared by controlled potential electrolysis and studied by electron spin resonance. This ion has been formed in acetonitrile solution with sodium perchlorate as supporting electrolyte and the controlled potential electrolysis has been carried out in the microwave cavity of the ESR spectrometer. The ion exhibits a complex hyperfine structure in dilute solution; the observed spectrum consists of about 75 hyperfine components. Isotropic hyperfine coupling constants have been assigned for the three types of interacting nuclei: the aromatic ring protons, amine protons, and the nitrogen nuclei. The large nitrogen hyperfine interaction observed is in marked contrast to Würster's Blue cation, for which this interaction is vanishingly small. ESR spectra of deuterated derivatives have been obtained and employed in making the assignment. The magnitude of the nitrogen hyperfine interaction relative to that of the amine protons is shown to be consistent with the mechanism of a π-σ electron exchange interaction on the nitrogen atom. Electrochemical generation allows the study of the relatively unstable ion-radical, whereas other methods of preparation have been less successful.

INTRODUCTION

THE early, very comprehensive work of Michaelis and co-workers on one-electron oxidation-reduction processes revealed many classes of organic compounds showing this behavior. Among the types of molecules studied were the *N*-methyl derivatives of *p*-phenylene diamine (PPD)[1]: $NH_2C_6H_4NH_2$

The product of a one-electron oxidation of these compounds is a positive radical ion, the stability of which was found to be greatly dependent on the *p*H of the solution, as well as on the nature of the *N* substituents. The *p*H dependence of the stability of the positive ion results from the complicating effects of various protonic equilibria which may exist in the system. Unsubstituted PPD forms a relatively unstable positive ion, while it is well known that the *N*,*N*,*N*′,*N*′-tetramethyl derivative forms a positive ion so stable it can be isolated as a perchlorate salt (Würster's Blue perchlorate). The other *N*-methyl derivatives show intermediate behavior.

The same one-electron oxidation behavior has been observed in aqueous solutions of unsubstituted PPD by polarographic oxidation at a rotating platinum electrode.[2] An inflection point attributable to a partial superposition of two single-electron electrode processes is observed in the current-potential curve. The separation of these electrode processes is strongly dependent on *p*H; and under the proper *p*H conditions the polarogram consists of two distinct oxidation waves, each attributable to a one-electron electrode process. The product of the first process is presumably the paramagnetic positive radical-ion.

Because of its exceptional stability, Wüster's Blue cation has been the subject of several investigations by electron spin resonance (ESR).[3–7] The best resolved spectrum has recently been obtained by Hausser[6] and exhibits isotropic hyperfine interactions with all magnetic nuclei in the molecule. Hyperfine coupling constants observed were 1.9 gauss for the aromatic ring protons, 6.8 gauss for the methyl protons, and 0.28 gauss for the N^{14} nuclei.

The mechanism of the isotropic hyperfine interaction with aromatic ring protons has been discussed at great length,[8–11] and it has been shown that a reasonable mechanism involves a $\pi-\sigma$ electronic exchange interaction at the contiguous carbon atom. The magnitude of the isotropic hyperfine coupling constant A_{H_i} has been represented in terms of ρ_{C_i}, the unpaired π-electron spin density at the contiguous carbon atom:

$$A_{H_i}=Q\rho_{C_i}, \tag{1}$$

where Q is an approximate constant. Estimates of the magnitude of Q have ranged from -22 to -30 gauss.

McLachlan[12] has carried out a valence bond calculation for the case of hyperfine coupling of methyl protons and has arrived at the same linear dependence of the hyperfine coupling constant on the unpaired π-electron spin density at the contiguous carbon atom. McLachlan has extended these results to an interpretation of the ESR spectra[4] of *N*-substituted PPD derivatives using simple molecular orbital (MO) theory, with reasonable success.

* National Institutes of Health Predoctoral Fellow.

[1] L. Michaelis, M. P. Schubert, and S. Granick, J. Am. Chem. Soc. **61**, 1981 (1939).

[2] R. E. Parker and R. N. Adams, Anal. Chem. **28**, 828 (1956).

[3] S. I. Weissman *et al.*, J. Chem. Phys. **21**, 2227 (1954).

[4] S. I. Weissman, J. Chem. Phys. **22**, 1135 (1954).

[5] K. H. Hausser, Archives des Sciences **12**, 195 (1959).

[6] K. H. Hausser (private communication).

[7] T. R. Tuttle, Jr., J. Chem. Phys. **30**, 331 (1959).

[8] B. Venkateraman and G. K. Fraenkel, J. Chem. Phys. **24**, 737 (1956).

[9] H. M. McConnell, J. Chem. Phys. **24**, 764 (1956).

[10] H. M. McConnell and D. B. Chestnut, J. Chem. Phys. **28**, 107 (1958).

[11] H. M. McConnell, J. Chem. Phys. **28**, 1188 (1958).

[12] A. D. McLachlan, Mol. Phys. **1**, 233 (1958).

In this paper the ESR spectrum of the positive ion of unsubstituted PPD is reported. This radical is prepared by controlled potential electrolytic generation[13] in acetonitrile at a polarizable platinum electrode contained within the ESR spectrometer. The resulting spectrum is completely interpreted with the aid of the ESR spectra of several deuterated derivatives. In marked contrast to the Würster's Blue ion, a rather large hyperfine interaction due to N^{14} is evident. The comparative ease of observing relatively unstable radicals by this electrolytic technique is also of interest.

EXPERIMENTAL METHOD

The electrolytic generation method for the ESR study of organic free radical-ions has been applied to the examination of nitroaromatic negative ions, and is reported elsewhere.[13] As applied here, the electrode process is an oxidation and occurs at a polarizable platinum electrode.

Because of the complicating effects of protonic equilibria in aqueous media, there is much to be gained by working with an aprotic solvent such as acetonitrile. The polarogram of PPD in acetonitrile consists of two separate, well-defined oxidation waves, each attributable to a single electron electrode process. The polarographic data indicated that the positive radical-ion of PPD could be prepared by a controlled potential electrolysis at the proper potential. Polarographic data was obtained at room temperature using a Sargent model XXI recording polarograph with appropriate span voltage and current sensitivity. Oxidation was carried out at a rotating platinum electrode with 0.1 *N* sodium perchlorate as supporting electrolyte. An aqueous saturated calomel reference cell (SCE) was used throughout.

The electrochemical cell used to carry out the controlled electrolysis was essentially the same as that previously described.[13] As designed for oxidative electrolysis, this cell contains a fire-polished platinum wire sealed into a 3-mm Pyrex capillary instead of the mercury pool previously employed. The electrode section was enclosed in a quartz jacket and centered in the microwave cavity of the ESR spectrometer, which was the same as previously described.[13]

Acetonitrile was purified by the method of Wawzonek and Runner.[14] Sodium perchlorate (Fischer, grade 2), used as supporting electrolyte, was obtained as the monohydrate. This was dried 24 hr at 120°C, recrystallized from absolute ethanol (Gold Seal), and again dried at 120°C for 24 hr. A blank polarogram using this electrolyte (0.1*N*) in acetonitrile showed no interfering oxidizable impurities.

P-phenylene diamine (Eastman, practical grade) was recrystallized three times from water. Because of the tendency toward air oxidation, it was necessary to expel oxygen by continuously passing prepurified nitrogen through the solution. The first recrystallization was accompanied by treatment with decolorizing carbon. The product of these recrystallizations was then sublimed under reduced pressure (1 mm) at 150°C. The result was a colorless nicely crystalline product.

First attempts at preparing *N,N,N',N'*-tetra*deutero*-PPD by a simple exchange technique revealed, with the help of infrared spectra, that the amine protons were extremely labile. Not only were the amine protons easily exchanged in neutral D_2O, but this position was so labile that the exchanged product underwent immediate back-exchange with the small amount of residual H_2O in the carefully dried acetonitrile, in which H_2O is an extremely weak proton donor. Considering that solutions used were about 2×10^{-3} *M* in deuterated product, the presence of even $10^{-2}\%$ H_2O in the solvent under conditions of fast proton-deuteron exchange is hardly negligible. In light of these facts, this product was obtained quite simply. The controlled potential electrolysis and ESR observation were made on a solution of PPD in a mixed solvent of 4% D_2O and 96% acetonitrile. The D_2O used was of 99.5% isotopic purity. This amount of D_2O was sufficient to provide essentially complete exchange of the amine protons with the excess of deuterons (greater than 100/1), but apparently was insufficient to appreciably affect the stability of the radical.

PPD-d^8 (per*deutero* PPD) was prepared by refluxing a solution of 300 mg of PPD in 30 ml of 1.0 *M* D_2SO_4 in D_2O under nitrogen for 10 days. The resulting solution was neutralized with carefully dried Na_2CO_3 and taken to dryness under reduced pressure. The free diamine was sublimed from the inorganic residue at 150°C and 1 mm pressure. To prevent back-exchange of the amine deuterons, the electrolysis and ESR observation of this compound was carried out in acetonitrile containing 4% D_2O.

The spectrum of 2,3,5,6-tetra*deutero*-PPD positive ion was obtained from a solution of per*deutero* PPD in 4% H_2O-96% acetonitrile. Because of the tendency toward air oxidation, thorough degassing of all solvents was necessary before addition of diamine samples. This initial degassing was followed by an extensive degassing of the solution in the electrochemical cell through a fine capillary extending just below the electrode region. A continuous stream of nitrogen flowed over the surface of the solution in the electrolysis cell during the electrolysis.

Nitrogen (Linde Prepurified) used for degassing was passed over hot copper gauze, through a drying column and through an acetonitrile presaturator.

RESULTS

The polarogram of a solution of 2.2 m*M* PPD in acetonitrile with 0.1 *M* sodium perchlorate as supporting electrolyte consists of two distinct oxidation

[13] D. H. Geske and A. H. Maki, J. Am. Chem. Soc. **82**, 2671 (1960).

[14] S. Wawzonek and M. E. Runner, J. Electrochem. Soc. **99**, 457 (1952).

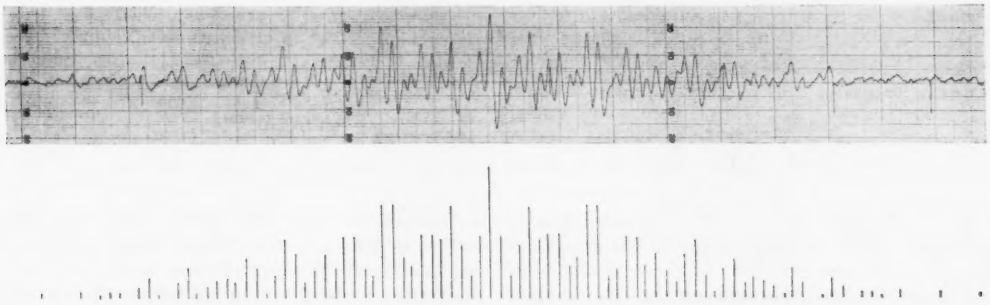

FIG. 1. Observed ESR spectrum of electrolytically generated *p*-phenylene diamine positive ion (above) and calculated spectrum (below).

waves. The first has a half-wave potential of 0.24 v vs SCE and a limiting current of 13.0 μa; the second has a half-wave potential of 0.85 v vs SCE and a limiting current of 10.7 μa. These limiting current values correspond to current constants of 5.91 and 4.86 μa liters millimoles^{-1}, respectively. Although the limiting current constant for a platinum electrode is not expressible in terms of measurable quantities, a given electrode can be calibrated using the limiting current constant obtained from a known reaction. The oxidation of iodide ion in acetonitrile is a known one-electron process. The limiting current constant for this process at the platinum electrode used was 4.81. It is apparent that the polarogram of PPD represents two distinct one-electron processes. On the basis of this evidence, it was postulated that the product of the first process is the desired radical-ion, $(NH_2C_6H_4NH_2)^+$. The clear definition and separation of the two oxidation waves indicated it would be possible to prepare this ion in the microwave cavity by controlled potential electrolysis. For this purpose a potential of 0.55 v vs SCE was chosen.

The ESR spectrum of a 1 m*M* solution of PPD electrolyzed at 0.55 v consists of about 75 hyperfine components. Some degree of power saturation was observed, and reduced microwave power levels were used for the best resolved spectra. A typical spectrum is shown in Fig. 1. The width (peak to peak) of the hyperfine components is slightly less than 0.2 gauss. The total width between centers of outermost observed lines is 41.70 gauss.

The ESR spectrum of the positive ion of *N*,*N*,*N*′,*N*′-tetra*deutero*-PPD is shown in Fig. 2. This spectrum consists of 35 nearly equally spaced hyperfine components. The total measured width is 35.4 gauss. The concentration was 2.96 m*M*. The apparent asymmetry in line intensities is believed to be due to second-order effects which alter slightly the positions of hyperfine components on the low- and high-field sides of the spectrum. This effect is most marked here since each line is a resultant of several very closely spaced hyperfine components.

The ESR spectrum of 2,3,5,6-tetra*deutero*-PPD positive ion is shown in Fig. 3. This spectrum consists of seven rather broad lines. Further splittings are observed under conditions of higher resolution, but the signal is very weak. This spectrum was obtained from a 10m*M* solution and observed with a rather large field modulation amplitude. The total width of the observed

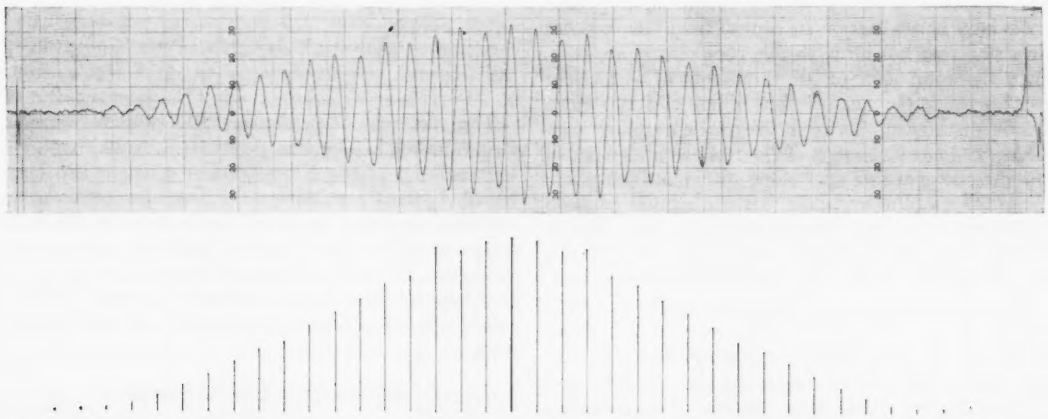

FIG. 2. Observed ESR spectrum of *N*,*N*,*N*′,*N*′-tetra-*deutero*-*p*-phenylene diamine positive ion (above) and calculated spectrum (below).

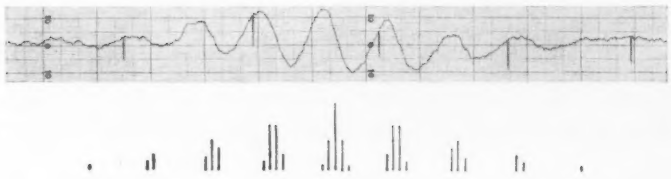

FIG. 3. Observed ESR spectrum of 2,3,5,6-tetra*deutero* *p*-phenylene diamine positive ion (above) and calculated spectrum (below).

pattern is 32.8 gauss. The separation between lines is about 6 gauss and the average line width about 2.5 gauss.

The totally deuterated compound was also studied and only the envelope of the total absorption was observed. The total width of this spectrum, corrected for the large modulation amplitude used, is 30.6 gauss.

DISCUSSION

Observation of an ESR spectrum from an electrolyzed solution of PPD confirms not only that the product of the first electrode process is a free radical, but also that the radical formed is relatively long-lived in the aprotic medium. Interpretation of the hyperfine structure confirms the hypothesis that the electrode process can be represented by the removal of one electron from the diamine molecule:

$$NH_2C_6H_4NH_2 \xrightarrow{-1e} [NH_2C_6H_4NH_2]^+.$$

In order to assign isotropic hyperfine coupling constants to fit the observed ESR spectrum of PPD positive ion, it was necessary to assume hyperfine interactions with all magnetic nuclei in the molecule. There are three sets of such nuclei: four amine protons, four aromatic ring protons, and two N^{14} nuclei. The total possible number of hyperfine components from three sets of equivalent nuclei, each with a total nuclear spin of 2, is 125. That fewer than this number of lines were observed indicates accidental coincidences in line positions, transitions too weak to be observed, or both. The predicted intensity of the outermost hyperfine line is only 1/108 that of the central line; thus it is not surprising that not all hyperfine components are seen. Since the total spin of all three sets of equivalent nuclei is the same, measurement of line positions alone cannot distinguish between the three coupling constants. The measurements of the relative intensities of hyperfine components does allow specific identification of the N^{14} coupling constant. To distinguish between the hyperfine coupling constants for the two types of protons, more information is needed, i.e., the effect of deuterium substitution in the ring and amine positions.

The parameters obtained from the spectrum of PPD positive ion are 5.29 gauss for N^{14} and 5.88, 2.13 gauss for the two proton coupling constants. These parameters were obtained by averaging the low-field and high-field values from four spectra. The spectrum predicted from this assignment is shown below the observed spectrum in Fig. 1. Lines predicted to fall in an interval less than 0.15 gauss have been combined in the predicted spectrum. The agreement is to within a few hundredths of a gauss for reasonably intense lines. Since the calculated spectra do not include the second-order effects, there is some slight deviation from the predicted spectrum at extreme fields.

To distinguish the two proton coupling constants, and to fully verify the above assignment, the ESR spectra of the positive ions of *N,N,N',N'*-tetra*deutero*-PPD; 2,3,5,6-tetra*deutero*-PPD; and per*deutero*-PPD were obtained. The isotropic hyperfine constant for a nucleus of magnetic moment μ_k and the nuclear spin I_k is given by

$$A_k = (8\pi/3)(\mu_k/I_k) \mid \phi_k(0) \mid^2, \qquad (2)$$

where $\mid \phi_k(0) \mid^2$ is the probability density of the unpaired electron spin at the kth type of nucleus. Assuming that the mechanism of hyperfine coupling is identical for H and D, i.e., that $\mid \phi_H(0) \mid^2$ and $\mid \phi_D(0) \mid^2$ are equal in a given position, Eq. (2) yields

$$A_D/A_H = (\mu_D I_H/\mu_H I_D) = 0.187. \qquad (3)$$

On using Eq. (3) and the observed hyperfine coupling constants for PPD positive ion, the hyperfine structure could be predicted for the deuterated species for the two possible assignments of proton coupling constants. The spectra predicted for the tetra-deuterated derivatives are shown below the corresponding observed spectra in Figs. 2 and 3. The spectra observed lead to the following unambiguous assignment for the PPD positive ion:

$$A_N = 5.29 \text{ gauss},$$

$$A_{H(\text{amine})} \equiv A_H = 5.88 \text{ gauss},$$

$$A_{H(\text{ring})} \equiv A_{H'} = 2.13 \text{ gauss}.$$

The spectrum of per*deutero*-PPD positive ion was also calculated. The line positions are not favorable for resolution of the N^{14} interaction alone as had been hoped. Under the existing conditions of resolution, the coupling constants predict a single flat absorption 30 gauss in width. The observed spectrum appeared as predicted. The width of this spectrum cannot be attributed to anything but an isotropic hyperfine interaction of the magnitude reported above for the nitrogen nucleus.

Proton Hyperfine Interaction

The application of Eq. (1) to this system has been examined. This equation has been applied with consider-

able success employing a value of -28 gauss for Q (aromatic protons).[12,15] In his work,[12] McLachlan has used a value of $Q=\pm 25$ gauss for an interpretation of the hyperfine interaction of amine protons and N-methyl protons in PPD positive ion derivatives. A simple MO calculation similar to that of McLachlan was carried out in connection with this work. A planar configuration was assumed with six carbon $2p$ and two nitrogen $2p$ atomic orbitals used as the basis for an LCAO variational calculation. All resonance integrals (β) were assumed equal and the nitrogen Coulomb integral, α_N, was treated as the only parameter of the calculation. On employing Eq. (1) with $Q=-28$ gauss and the observed value of $A_{H'}$ an "experimental" value of the unpaired π-electron density at the 2,3,5,6 positions was obtained. This value was $\rho_C=0.076$. The value of α_N was then adjusted to give this value of ρ_C; the value chosen in this way being $\alpha_N=\alpha_C+0.85\beta$, where α_C is the carbon Coulomb integral. Using this parameter, the unpaired π-electron spin density in the nitrogen $2p_z$ orbital was calculated to be $\alpha_N=0.236$. Employing this value and Eq. (1) with McLachlan's value of $Q=-25$ gauss for the amine protons results in a value of -5.9 gauss for A_H. Although this quantitative agreement with experiment cannot be taken too seriously, it is evidence that Eq. (1) can be applied to this type system and that simple MO theory gives a reasonable description of the ESR spectrum of the positive ion of PPD. Since this ion is analogous to an even alternant hydrocarbon radical-ion, it is expected that simple MO theory should give a reasonable description of the unpaired spin distribution.[15,16]

Hyperfine Interaction of the N^{14} Nucleus

The theory of the isotropic hyperfine coupling mechanism of the N^{14} nucleus has not previously been examined. The situation is more complex than that of the proton coupling mechanism due to the possibility of unpaired spin density in a π orbital on the nitrogen atom itself.

The condition for isotropic hyperfine coupling with the nitrogen nuclei requires [cf. Eq. (2)] a nonvanishing of $|\phi_N(0)|^2$, the unpaired electron spin density at the nitrogen nucleus. A nonvanishing value of $|\phi_N(0)|^2$ requires that there be unpaired electron spin density in an s-type orbital at the nitrogen nucleus. The explanation of the nonvanishing value of unpaired spin density at the nuclei of aromatic protons has been given in terms of a $\pi-\sigma$ electronic exchange interaction at the contiguous carbon atom.[9,10] In the case of the nitrogen interaction, there are two ways unpaired spin density can be transmitted into the σ system and thus into an orbital with nitrogen $2s$ character. The two possible mechanisms are: (i) a $\pi-\sigma$ electronic exchange interaction on the contiguous carbon atom, transmitting unpaired spin polarization into the C—N bond; and (ii) a $\pi-\sigma$ interaction on the nitrogen atom, transmitting unpaired spin polarization into all three nitrogen σ bonds.

It is interesting to try to compare the relative effectiveness of mechanisms (i) and (ii) in leading to the observed values of A_N and A_H. Since it seems reasonable to assume that hyperfine coupling with the amine protons proceeds through a $\pi-\sigma$ interaction on the nitrogen atom, as has been assumed above, it has been assumed that mechanism (ii) gives the main contribution of unpaired spin density at the nitrogen nucleus. Mechanism (i) is ignored for the time being. It is possible to calculate the ratio A_N/A_H without a detailed examination of the mechanism involved since, on the basis of this assumption, mechanism (ii) is responsible for both the nitrogen and amine proton hyperfine interactions. From Eq. (2)

$$A_N/A_H=(\mu_N/\mu_H)(I_H/I_N)\times\frac{|\phi_N(0)|^2}{|\phi_H(0)|^2}$$

$$=0.0723\times\frac{|\phi_N(0)|^2}{|\phi_H(0)|^2}. \quad (4)$$

It is assumed that the PPD positive ion is planar, so that the hybridization of the nitrogen atom is sp^2. The three hybrid σ orbitals are the appropriate orthogonal linear combinations of atomic orbitals $(2s)_N$, $(2p_x)_N$ and $(2p_y)_N$. It is further assumed that the N—H bond orbitals are nonpolar and of the form

$$\psi_\sigma=\frac{1}{(2)^{\frac{1}{2}}(1+\Delta)^{\frac{1}{2}}}\{(sp^2)_N+(1s)_H\}, \quad (5)$$

where Δ is the overlap integral.

Given a certain electron spin polarization, $\rho(\psi_\sigma)$, transmitted into the ψ_σ bond orbital, under the assumptions above, Eq. (4) becomes

$$A_N/A_H=-0.0723\times\frac{|2s_N(0)|^2}{|1s_H(0)|^2}, \quad (6)$$

where $2s_N(0)$ and $1s_H(0)$ are the values of the $2s$ wave function at the nitrogen nucleus and of the $1s$ wave function at the hydrogen nucleus, respectively. The negative sign arises since any electron spin polarized at the nitrogen nucleus will result in a polarization of opposite sign at the hydrogen nucleus. The value of $|2s_N(0)|^2$ can be estimated from the self-consistent field wave function[17] and $|1s_H(0)|^2$ can be estimated from the Schrödinger function $(\pi a_0^3)^{-1}$. The results are

$$|2s_N(0)|^2=33.4\times10^{24}\ \text{cm}^{-3},$$

$$|1s_H(0)|^2=2.15\times10^{24}\ \text{cm}^{-3}.$$

Then $A_N/A_H=-1.12$.

[15] G. K. Fraenkel and B. Segal, Ann. Rev. Phys. Chem. **10**, 435 (1959).

[16] H. M. McConnell and H. H. Dearman, J. Chem. Phys. **28**, 51 (1958).

[17] D. R. Hartree and N. Hartree, Proc. Roy. Soc. (London) **A193**, 299 (1948).

The absolute value of this ratio may be compared with the experimental ratio of 0.900. This encouraging result suggests that mechanism (ii) is mainly responsible for the nitrogen hyperfine interaction in the PPD positive ion. Mechanism (i) would be expected to contribute a spin polarization at the nitrogen nucleus opposite in sign to that contributed by mechanism (ii) and because it would not be expected to appreciably contribute to A_H, the main effect of the introduction of mechanism (i) would be the lowering of A_N/A_H. The vanishingly small value of A_N in Würster's Blue cation may be mainly due to the competing mechanisms (i) and (ii). In this case, the effect of mechanism (i) would be expected to be enhanced by the indirect transmission of spin polarization into the nitrogen sp^2 orbitals via the methyl groups as well as the adjacent ring carbon atom. This effect, along with any differences in electron distribution, may account for the surprising contrast between the ESR spectra of Würster's Blue and PPD positive ions. Explanation of the vanishingly small value of A_N in Würster's Blue cation on the basis of the N^{14} quadrupole moment[11] would seem to be disproved by the present work and the most recent result on Würster's Blue.[6]

Having made the assumption that the nitrogen hyperfine interaction in PPD positive ion is interpretable by means of a $\pi-\sigma$ exchange interaction on the nitrogen atom, it is possible to use an expression of the form of Eq. (1) for this interaction. A value of $Q_N=22.4$ gauss fits the experimental data when compared with the simple MO theory used. As suggested previously, however, the mechanism of nitrogen hyperfine interaction is probably too complex for such an expression.

To the extent that mechanism (ii) is mainly responsible for both the nitrogen and amine proton hyperfine interactions in PPD positive ion, it would seem that the ratio A_N/A_H should be nearly a constant for compounds related to PPD. Work to test this prediction is anticipated, including studies of related *p*-phenylene diamine derivatives.

ACKNOWLEDGMENTS

We gratefully acknowledge the support of this work by research grants from the National Institutes of Health and the National Science Foundation.

THE JOURNAL OF CHEMICAL PHYSICS VOLUME 34, NUMBER 2 FEBRUARY, 1961

Infrared Spectra of Alkyldiboranes. IV. 1,1-Dimethyl- and 1,1-Diethyldiboranes

WALTER J. LEHMANN,* CHARLES O. WILSON, JR.,† AND I. SHAPIRO*

Research Laboratory, Olin Mathieson Chemical Corporation, Pasadena, California

(Received July 21, 1960)

The infrared spectra of five isotopic variants of two 1,1-dialkyldiboranes, viz., $(CH_3)_2B_2{}^{10}H_4$, $(CH_3)_2B_2H_4$, $(CH_3)_2B_2D_4$, $(CD_3)_2B_2H_4$, and $(CD_3)_2B_2D_4$, and the corresponding diethyl compounds, are reported and frequency assignments are made. A method for purification of these compounds also is described. The intensity ratio of the 923 to 2096-cm^{-1} bands in $(CH_3)_2B_2H_4$ served as a simple preliminary criterion for the absence of other alkyldiboranes. The strong bridge-stretching frequencies of the 1,1-dialkyldiboranes at 1550 cm^{-1} are unique in being ca 50 cm^{-1} lower than corresponding B—H′ bands in other alkyldiboranes. Another B—H′ absorption, at 2100 cm^{-1}, is quite intense compared with other alkyldiboranes.

INTRODUCTION

PREVIOUS papers of this series [1–3] discussed compounds in which alkyl groups replaced not more than one of the two terminal hydrogens on each boron. In the 1,1-dialkyldiboranes (i.e., the *unsym*-dialkyldiboranes), both hydrogen atoms on one end of the molecule have been replaced, while the opposite end is unsubstituted and is like diborane. Thus the compounds in the present discussion have vibrational character intermediate between that of diborane and totally alkylated diborane (i.e., tetraalkyldiborane). It was especially interesting to note the effects that 1,1-*di*-substitution has on the vibrations of the unsubstituted part of the molecule and on the vibrations of the nearby bridge.

EXPERIMENTAL

The room-temperature reaction of diborane and trialkylborane in a 5:1 molar ratio resulted in a mixture of alkyldiboranes, of which 1,1-dialkyldiborane was the

* Present address: Chemistry Department, Hughes Tool Company—Aircraft Division, Culver City, California.

† Present address: National Engineering Science Company, Pasadena, California.

[1] W. J. Lehmann, C. O. Wilson, Jr., and I. Shapiro, J. Chem. Phys. **32**, 1088 (1960), first paper of this series.

[2] W. J. Lehmann, C. O. Wilson, Jr., and I. Shapiro, J. Chem. Phys. **32**, 1786 (1960), second paper of this series.

[3] W. J. Lehmann, C. O. Wilson, Jr., and I. Shapiro, J. Chem. Phys. **33**, 590 (1960), third paper of this series.

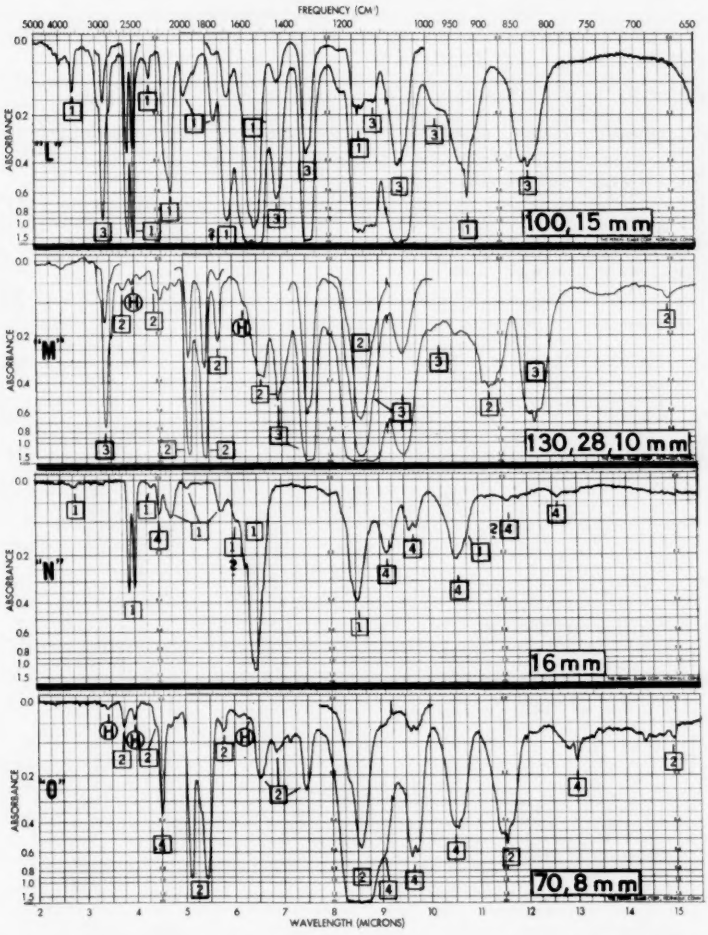

FIG. 1. Infrared spectra of 1,1-dimethyldiboranes; pressures reported for 5-cm cells.

"*L*"—$(CH_3)_2B_2H_4$	[1] —B_2H_4	(*H*) protium-impurity bands
"*M*"—$(CH_3)_2B_2D_4$	[2] —B_2D_4	
"*N*"—$(CD_3)_2B_2H_4$	[3] —CH_3	
"*O*"—$(CD_3)_2B_2D_4$	[4] —CD_3	

most abundant.[4] (Small quantities of 1,2-dialkyldiborane also were formed.) The dimethyldiboranes were removed from the mixture by distillation through a −115°C trap and condensation in a −120°C trap. The corresponding temperatures for the diethyldiboranes were −72° and −80°C.

Since it was difficult to separate the two kinds of dialkyldiboranes by fractional condensation, excess diborane was added to the mixture to convert the 1,2-dialkyldiborane to monoalkyldiborane according to the equation

$$(RBH_2)_2 + B_2H_6 \rightleftharpoons 2RB_2H_5.^5$$

This procedure was the reverse of the method used in the preparation of the 1,2-compounds.[3] Fractionation of the monoalkyldiboranes and the 1,1-dialkyldiboranes was then readily accomplished, the whole process being repeated until the mass spectrum as well as the infrared spectrum indicated sufficient purity. The vapor pressure of $(C_2H_5)_2B_2H_4$ was found to be 46.1 mm of Hg at 0°C, in agreement with a recently reported value.[6]

The 1,1-dialkyldiboranes were fairly stable with respect to *decomposition*, but a small amount of hydrogen was produced during several months of storage. Furthermore, the 1,1-compounds disproportionated much faster than the 1,2-compounds. Within a few

[4] H. I. Schlesinger and A. O. Walker, J. Am. Chem. Soc. **57,** 621 (1935).

[5] We use the form $(RBH_2)_2$ for the 1,2-dialkyldiboranes, to distinguish them from the 1,1-dialkyldiboranes, $R_2B_2H_4$.

[6] I. J. Solomon, M. J. Klein, and K. Hattori, J. Am. Chem. Soc. **80,** 4520 (1958).

TABLE I. Infrared bands of 1,1-dimethyldiboranes.

"K"	"L"		"M"		"N"		"O"		
$(CH_3)_2B_2{}^{10}H_4$	$(CH_3)_2B_2H_4$		$(CH_3)_2B_2D_4$		$(CD_3)_2B_2H_4$		$(CD_3)_2B_2D_4$		Assignment[b]
cm^{-1}	cm^{-1}	intensity[a]	cm^{-1}	intensity[a]	cm^{-1}	intensity[a]	cm^{-1}	intensity[a]	
4032	3984	(11)	~4000	(2)					
3636	3610	(25)			~3600	(19) b			$-B_2H_4$ (combination)
3040	3040	ssh	3049	sh					
2958	2958	(200)	2950	(120)			2940	(5)	CH_3 stretch. asym; protium imp. in "O"
2841	2841	ssh	2849	sh					CH_3 stretch. sym.
2732	~2740	sh							$-B_2H_4$ (combination)
			2681	(10)			2681	(17)	$-B_2D_4$ (combination) (partly imp. in "O")
2577	2571	(470)			2571	(440)			BH_2 stretch. asym
			2532	(8)			2525	(12)	B—H (single) stretch. (protium imp.)
2500	2494	(450)			2488	(410)			BH_2 stretch. sym
			2421	(6)					
2315	2304	(18)			2299	(19)			$-B_2H_4$ (combination)
			2262	(11*i*)			2273	sh	$-B_2D_4$ (combination
			2208	(14)	2212	(100)	2217	(100)	CD_3 stretch. asym
							2203	sh	
			2137	(11)	2141	sh	2132	(17)	CD_3 stretch. sym and $-B_2D_4$ (comb.)
2102	2096	(120)			2105	(110)			B—H′ sym in-phase
			2070	(9)			2070	(11)	$-B_2D_4$ (combination)
1992	1985	(28)			1975	(22) b			B—H′ sym out-of-phase
			1965	(200)			1953	(260)	BD_2 stretch. asym
1912	1905	sh	1887	wsh			1883	sh	part. $(MeBD_2)_2$ imp. in "M"
			1842	(230) *A*?			1842	(270)	BD_2 stretch. sym
1789	1764	(44)			1745–1725	(100) b			B—H′ asym out-of-phase
			1754	(34)			1733	(20)	$-B_2D_4$ (combination)
1712	1686	(190) *A*?			~1645	(125) sh	1718	sh	$-B_2H_4$ (combination)?
					1597	pip	1639	(10) b	
			1600	sh			1595	sh	B—H′ (single) asym (protium imp.)
1555	1546	(1500) *A*			1548	(1500)			B—H′ asym out-of-phase
			1530–1505	(55) b			1530	(60)	B—D′ sym in-phase
1437	1441	(130) *A*?	1443	(80)			1460	(37*i*)	CH_3 def. asym and B—D′ sym out-of-phase
							1400	(30*i*)	impurity
							1340	(73) *A*?	B—D′ asym out-of-phase?
1330	1326	(480)	1328	(440)					CH_3 def. sym
1319	1316	ssh	1321	sh					
					1253	(38)			
1212	1212	(26*i*)			1215	sh			
							1200	sh	prob. B_2D_6 imp.
					1186	sh			
~1167	1163	(260) *A*			1170	(490)			BH_2 def.
			1159	(~1400) *A*			1167	(1400)	B—D′ asym in-phase
~1157	1126	(210) *B*	~1125	sh	1093	(240)	1110	sh	BC_2 stretch. asym
~1080	~1064	(560)	1055	(200) *A*?					CH_3 rock.
	1053	pip							
					1042	(155)	1042	(180)	CD_3 def. asym
					1028		1031		
			992	sh					$(CH_3BD_2)_2$ imp.
980	976	(36) sh	975	wsh					CH_3 rock.
			946	(30)					impurity
					948	(260)	948	(125) *A*	CD_3 def. sym
931	923	(130) *C*			~925	sh			BH_2 wag. (out-of-plane)
									impurity
			899	pip			867	(155)	BD_2 def.
			~882	(65) *A*					

TABLE I.—*Continued*

"K"	"L"		"M"		"N"		"O"		
$(CH_3)_2B_2{}^{10}H_4$	$(CH_3)_2B_2H_4$		$(CH_3)_2B_2D_4$		$(CD_3)_2B_2H_4$		$(CD_3)_2B_2D_4$		Assignment[b]
cm^{-1}	cm^{-1}	intensity[a]	cm^{-1}	intensity[a]	cm^{-1}	intensity[a]	cm^{-1}	intensity[a]	
					864	w			CD_3 rock.?
							836	pip	impurity
							823	wb	
837	829	(85) *A*	821	(110) *A*	794	w	770	(43)	BC_2 stretch. sym
			730	wb					
							694	(28)	impurity
			669	(30) *C*			668	(26)	BD_2 wag. (out-of-plane)

[a] Approximate intensities expressed as absorbance $\times 10^5$ divided by cell length in cm and sample pressure in mm. Abbreviations: w—weak, s—strong, sh—shoulder b—broad, v—very; *i*—apparent intensity increased by overlap with other band(s); *A*, *B*, *C*—apparent band types.
[b] B—H′ and B—D′ refer to bridge stretchings.

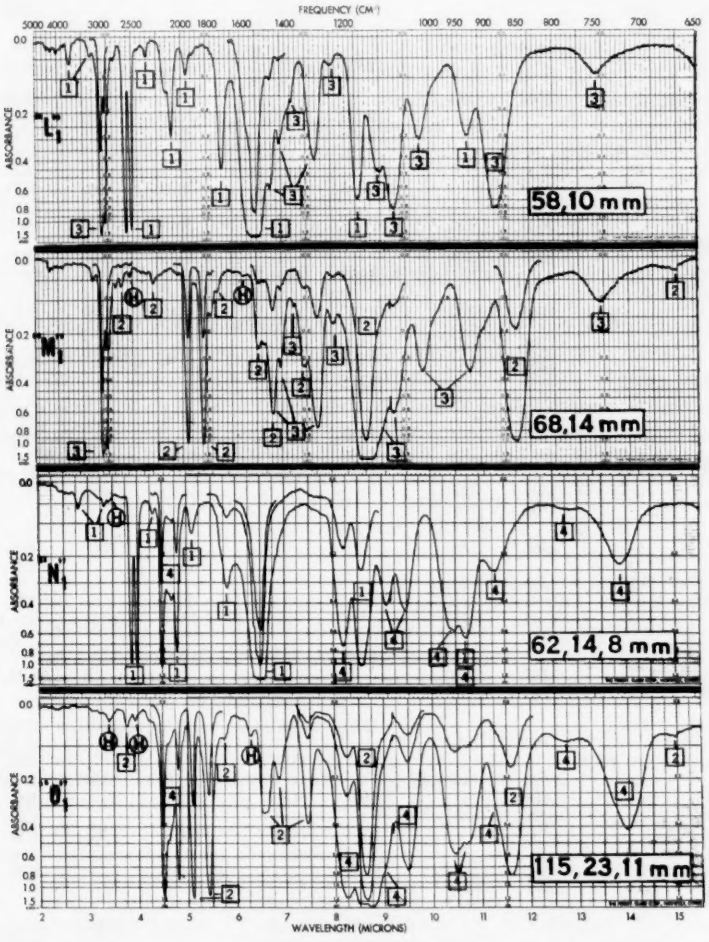

FIG. 2. Infrared spectra of 1,1-diethyldiboranes; pressures reported for 5-cm cells.
"L_1"—$(C_2H_5)_2B_2H_4$ [1] —B_2H_4 (*H*) protium-impurity bands
"M_1"—$(C_2H_5)_2B_2D_4$ [2] —B_2D_4
"N_1"—$(C_2D_5)_2B_2H_4$ [3] —C_2H_5
"O_1"—$(C_2D_5)_2B_2D_4$ [4] —C_2D_5

TABLE II. Infrared bands of 1,1-diethyldiboranes.

"K_1" $(C_2H_5)_2B_2{}^{10}H_4$	"L_1" $(C_2H_5)_2B_2H_4$		"M_1" $(C_2H_5)_2B_2D_4$		"N_1" $(C_2D_5)_2B_2H_4$		"O_1" $(C_2D_5)_2B_2D_4$		
cm^{-1}	cm^{-1}	intensity[a]	cm^{-1}	intensity[a]	cm^{-1}	intensity[a]	cm^{-1}	intensity[a]	Assignment[b]
3623	3623	(22)			3571	(20)			$-B_2H_4$ (combination)
3145	3145	(15)	3125	(15)	~3100	(12)			
~3030	~3030	wsh	3030	wsh	3012	(18)			$-B_2H_4$ (combination)
2958	2958	(700)	2958	(650)					CH_3 stretch. asym
2932	2932	ssh	2924	sh	2924	(14)	2924	(7)	CH_2 stretch. asym; protium imp. in "N_1" and "O_1"
2882	2882	(410)	2882	(370)					CH_3 stretch. sym.
2849	2841	sh	2841	sh					CH_2 stretch. sym.
2747	2747	(17)			~2740	wb			$-B_2H_4$ (combination)
			2732	(20)					
			2652	(19)			2646	(9)	$-B_2D_4$ (combination)
2591	2577	(600)			2577	(320)			BH_2 stretch. asym
			2532	(13)			2538	(7)	B—H (single) (protium imp.)
2512	2506	(540)			2506	(320)			BH_2 stretch. sym
2439	2427	bsh							
			~2350	wb			2353	(7)b	
2330	2315	(15)			2315	(25)			$-B_2H_4$ (combination)
			2262	(18)					$-B_2D_4$
					2222	(430)	2222	(350)	CD_2 stretch. asym
					2164	sh	2164	sh	CD_2 stretch. asym
2137	2128	(50)sh			2132	pip			
2086	2079	(100)			2083	(270)	2079	(150)	B—H′ sym in-phase; CD_3 and CD_2 stretch. sym
			2041	(12)			2041	wsh	$-B_2D_4$ (combination)
			1957	(300)			1953	(260)	BD_2 stretch. asym
1965	1957	(31)			1953	(40)			B—H′ sym out-of-phase
1923	1908	sh							
			1845	(300)			1842	(220)	BD_2 stretch. sym
			1795	(43*i*)					
			1754	(38*i*)			1739	(14)	$-B_2D_4$ (combination)
1733	1718	(160)			1715	(110)			B—H′ asym out-of-phase
			1605	w			1592	(13)	B—H′ (single) asym imp. (other $R_xB_2H_y$)
	1580	sh			1570	sh			
					1550	ssh	1550	sh	
1548	1543	(1700)			1538	(1500)			B—H′ asym in-phase
			1531	(74*i*)			1530–1510	(58)b	B—D′ sym in-phase
			1504	(70*i*)					
			1464	(180)			1456	(35*i*)	B—D′ sym out-of-phase
1475	1473	(210*i*)pip							CH_3 asym and CH_2 def.
1435	1433	(110*i*)pip	1435	(97)pip					
1385	1383	w pip	1381	w pip					CH_3 def. sym
			1342	(97*i*)			1344	(67)	B—D′ asym out-of-phase?
					~1300	bsh	1290	bsh	
1310	1302	(140)	1295	(220) *A*?					CH_2 wag. and/or twist.
1248	1245	(24)	1244	(50)					
					1220	(240)	1215	(230*i*)	CD_2 wag. and/or twist.
			1190	bsh					sl. B_2D_6 imp.
1172	1168	(240) *A*?			1167	(360)			BH_2 def.
			1152	(1400) *A*?			1159	(1450) *A*?	B—D′ asym in-phase
1136	1114	(165*i*) *B*?	~1110	sh	1101	(130)	1111	sh	BC_2 stretch. asym
1087	1078	(280) *A*?	1081	(180*i*)					CH_3 rock.
					1055	(145)	1055	(130)	CD_3 asym (and CD_2?) def.
1024	1019	(105)	1017	(100) *A*					CH_3 rock.
985	985	bsh	~985	bsh					
					955	(190*i*)	957	(100*i*)	CD_3 rock.
933	928	(100) *C*?			935	(210*i*)			BH_2 wag. (out-of-plane)
							937	(88*i*)	CD_3 rock.
896	881	(250)	927[c]	(100) *A*	883	(80*i*)	~887	vwsh?	C—C stretch. v. sl. $(EtBD_2)_2$ imp.
			905	w					
			852[d]	(270)			863	(140)	BD_2 def.

TABLE II.—*Continued*

"K_1"	"L_1"		"M_1"		"N_1"		"O_1"		
$(C_2H_5)_2B_2{}^{10}H_4$	$(C_2H_5)_2B_2H_4$		$(C_2H_5)_2B_2D_4$		$(C_2D_5)_2B_2H_4$		$(C_2D_5)_2B_2D_4$		
cm^{-1}	cm^{-1}	intensity[a]	cm^{-1}	intensity[a]	cm^{-1}	intensity[a]	cm^{-1}	intensity[a]	Assignment[b]
					780	wb	787	wb	CD_2 rock.?
751	745	(31)	744	(32)	721	(74)	715	(73)	BC_2 stretch. sym
			721	vwsh					v. sl. B_2D_6 imp.
			670	w			670	w	BD_2 wag. (out-of-plane)

[a] Approximate intensities expressed as absorbance×10^{3}divided by cell length in cm and sample pressure in mm. Abbreviations: w—weak, s—strong, sh—shoulder, b—broad, v—very; *i*—apparent intensity increased by overlap with other band(s); *A*, *B*, *C*—apparent band types.

[b] B—H′ and B—D′ refer to bridge stretchings.

[c] Probably shifted by Fermi resonance from approx 900 cm^{-1}.

[d] Probably shifted by Fermi resonance from approx 880 cm^{-1}.

hours, absorption peaks of diborane and trialkyldiborane were observed. Small amounts of other alkyldiboranes, which probably also were present, were obscured in the infrared spectra, but these compounds have been reported by others.[6]

The infrared spectra were recorded on a Perkin-Elmer model 21 spectrophotometer equipped with NaCl optics. The spectra of the four dimethyldiboranes containing isotopically normal boron are reproduced in Fig. 1, and the corresponding diethyldiborane spectra are shown in Fig. 2. The measured wave numbers, plus those of the B^{10}-enriched compounds, are listed in Tables I and II. Our spectrum of $(C_2H_5)_2B_2H_4$ is in good agreement with a previously published spectrum.[6] Intensities were obtained for each band by dividing the value of $\log_{10} I_0/I$ (i.e., the optical density, or absorbance) by the cell length in cm and by the pressure in mm of Hg, then multiplying by 10^5. Since no pressure measurement had been obtained for the $(CD_3)_2B_2H_4$ sample, we arbitrarily fixed the intensity of the strongest peak (1548 cm^{-1}) at 1500 units. (This value was arrived at through correlation with other spectra.)

Under our operating conditions, we found that a minimum intensity ratio of the sharp 923-cm^{-1} peak to the 2096-cm^{-1} absorption in $(CH_3)_2B_2H_4$ is a good preliminary criterion of purity, since all other isotopically normal methyldiboranes have medium-intensity absorption maxima near the former value, but none at the latter. In our reported spectrum this intensity ratio is 120/130, or 0.923. It should be kept in mind that this numerical factor is a function of instrumental parameters and operating conditions.

Continuing the scheme introduced in earlier papers of this series,[1–3] we will henceforth use the designations "*K*" through "*O*" for the 1,1-dimethyldiboranes, and "K_1" through "O_1" for the corresponding ethyl compounds (see headings of Tables I and II).

MOLECULAR SYMMETRY

Examination of molecular models and the consideration that ethane has the staggered form, indicate that the most probable configuration for 1,1-dimethyldiborane has two planes of symmetry (point group C_{2v})[7]—the plane of the BH_2 group and the plane of the BH_2B ring. Three of the vibrational species—A_1, B_1, and B_2—are Raman and infrared active, while the fourth—A_2—is only Raman active. This latter species includes BH_2 and BC_2 twisting, out-of-phase out-of-plane methyl rocking, and some internal methyl modes. If the molecule has a lesser symmetry (owing to partial rotation of the methyl groups), either C_s or C_1, then all vibrations are Raman and infrared active, but their infrared intensities would be very similar to those of the C_{2v} model.

On using the accepted dimensions of the diborane molecule[8] and reasonable values for the boron-methyl distance,[9] we calculated the principal moments of inertia for $(CH_3)_2B_2H_4$ to be 106, 115, and 218×10^{-40} g cm^2. 1,1-Dimethyldiborane thus is a slightly asymmetric top with the minor axis along the B—B bond (change of dipole moment along this axis produces *A*-type bands of species A_1), the intermediate axis perpendicular to the BH_2B ring (type *B* bands of species B_1), and the major axis perpendicular to the H_2BBC_2 plane (type *C* bands of species B_2).

The symmetry of 1,1-diethyldiborane is not established, and the band contours (Fig. 2) generally are not clearly defined.

ASSIGNMENTS

In accordance with the scheme introduced previously,[1] mostly through simple comparison of the spectra in Figs. 1 and 2, we can assign the observed bands to the molecular fragments $-B_2H_4$, $-B_2D_4$, $-CH_3$ or $-C_2H_5$, and $-CD_3$ or $-C_2D_5$ (labeled [1] to [4] in Figs. 1 and 2).

[7] G. Herzberg, *Infrared and Raman Spectra of Polyatomic Molecules* (D. Van Nostrand Company, Inc., Princeton, New Jersey, 1945).

[8] K. Hedberg and V. Schomaker, J. Am. Chem. Soc. **73,** 1482 (1951).

[9] H. A. Levy and L. O. Brockway, J. Am. Chem. Soc. **59,** 2085 (1937); see also S. H. Bauer and J. M. Hastings, J. Am. Chem. Soc. **64,** 2686 (1942).

Vibrations of the $-B_2H_4$ (and $-B_2D_4$) Fragments

The sharpness and clear separation of the two absorptions representing symmetric and asymmetric terminal stretchings—approx 2490 and 2570 cm^{-1} for B—H and approx 1845 and 1960 cm^{-1} for B—D—are characteristic of the 1,1-dialkyldiboranes. The presence of a doublet here is the most obvious indication that one is not dealing with 1,2-dialkyldi boranes.[10]

Another characteristic feature of the 1,1-dialkyldiboranes is the considerable intensity increase (as may be predicted from symmetry considerations) of the B—H′ (and B—D′) symmetric in-phase bridge stretching ("breathing") vibration at approx 2100 (and 1530) cm^{-1}.

The very strong (asymmetric, in-phase) bridge vibrations are found at approx 1550 and 1160 cm^{-1} for B—H′ and B—D′, respectively, somewhat lower than the values of approx 1600 and 1200 cm^{-1} for most other alkyldiboranes[1-3,11] and diboranes.[12]

The other two bridge stretchings are found at 1950–1990 (and 1440–1465) cm^{-1} for the B—H′ (and B—D′) symmetric out-of-phase vibration and at 1715–1790 (and approx 1340?) cm^{-1} for the B—H′ (and B—D′) asymmetric in-phase vibration. The former are slightly higher than in most of the alkyldiboranes, while the latter have somewhat enhanced intensities.

In monoalkyldiboranes, the BH_2 and BD_2 deformation vibrations were assigned to the 1140–1180 and 876–883 cm^{-1} regions, respectively, and in the present compounds very similar bands were observed. In most of the 1,1-dimethyldiboranes these bands have clearly visible *A*-type contours. The relatively low value in $(C_2H_5)_2B_2D_4$, 852 cm^{-1}, is probably due to resonance with 927 cm^{-1}; the nonperturbed frequencies are perhaps 880 and 900 cm^{-1}, respectively.

The BH_2 (out-of-plane) wagging motion is responsible for a prominent type *C* band at 923 cm^{-1} in $(CH_3)_2B_2H_4$, very similar in all respects to the 946-cm^{-1} band of $CH_3B_2H_5$. Just as in $CD_3B_2H_5$, the BH_2 absorption is masked in $(CD_3)_2B_2H_4$; it probably is responsible for the approx 923 cm^{-1} shoulder on the low-frequency side of the 950-cm^{-1} band. In the ethyl compounds, $(C_2H_5)_2B_2{}^{10}H_4$, $(C_2H_5)_2B_2H_4$, and $(C_2D_5)_2B_2H_4$, this band appears at 930 cm^{-1} and has lost its *C*-type contour. The BD_2 wagging vibration is assigned to the weak bands at approx 670 cm^{-1}, slightly lower than in the monoalkyl-diboranes (695 cm^{-1}).

In the spectra of the boron-deuterated compounds [$(CH_3)_2B_2D_4$, $(CD_3)_2B_2D_4$, $(C_2H_5)_2B_2D_4$, and $(C_2D_5)_2B_2D_4$], residual boron-protium content is responsible for B—H (single) stretching bands at approx 2530 cm^{-1}, which is approximately the average of the BH_2 asymmetric and symmetric frequencies. Likewise, we observe B—H′ (single) bands at 1600 cm^{-1}. The decrease of this value as compared to other alkyldiboranes is in harmony with a similar diminution of the B—H′ asymmetric in-phase frequency.

Relatively weak absorptions at approx 3600, 3030, 2740, and 2310 cm^{-1} represent combinations and/or overtones of $-B_2H_4$ vibrations, while bands at approx 2660, 2260, 2050, and 1740 cm^{-1} correspondingly represent $-B_2D_4$ (BH/BD frequency ratios of 1.34 ± 0.02). The fairly prominent bands at 1712 and 1886 cm^{-1} in $(CH_3)_2B_2{}^{10}H_4$ and $(CH_3)_2B_2H_4$ and probably the shoulder at approx 1645 cm^{-1} in $(CD_3)_2B_2H_4$ seem to be related to $-B_2H_4$, but they are absent in the corresponding ethyl compounds, and no parallel is found in the $-B_2D_4$ compounds (expected near 1250 cm^{-1}).

Vibrations of the Methyl Groups

The C—H (and C—D) asymmetric and symmetric stretching vibrations produce a peak and a shoulder at approx 2950 and 2840 (and at 2210 and 2140) cm^{-1}.

The CH_3 asymmetric deformation bands are located, as expected,[1,3,13] at about 1440 cm^{-1}, and the much stronger absorptions of the symmetric vibrations are found apparently as doublers at approx 1320 cm^{-1}. The corresponding CD_3 vibrations result, respectively, in doublets at approx 1035 cm^{-1} and what appear to be *A*-type bands at 948 cm^{-1}. In branched-chain hydrocarbons, i.e., when more than one methyl group is attached to the same carbon—an approx 16-cm^{-1} splitting of the CH_3 symmetric deformation band has been reported.[14]

The very strong group [3] bands at approx 1050 cm^{-1}, matching similar bands in other methyldiboranes,[3,11] are assigned to methyl rocking motions. All these bands have about the same B^{10}-isotope shifts (approx 15 cm^{-1}) as the CH_3 rocking mode at 970 cm^{-1} in trimethylborane.[13] In $(CH_3)_2B_2H_4$ and especially in $(CH_3)_2B_2D_4$ these bands appear to have *A*-type contours, which would classify them as belonging to in-plane (i.e., in the BC_2 plane), in-phase (species A_1) vibrations. In $B(CD_3)_3$ the corresponding CD_3 rocking modes are assigned[15] to 870 cm^{-1}, and to approx 850 cm^{-1} in[1] $CD_3B_2H_5$ and $CD_3B_2D_5$ (described as in-plane modes in these latter compounds). Thus we tentatively assign the weak 864 cm^{-1} band in $(CD_3)_2B_2H_4$ to CD_3 rocking. In $(CD_3)_2B_2D_4$ it probably is masked by the BD_2 deformation band at 867 cm^{-1}. Additional CH_3 rocking modes may be represented by the approx 975-cm^{-1} bands in $(CH_3)_2B_2H_4$ and $(CH_3)_2B_2D_4$.

There remain two series of methyl bands, in the 1100 and 800 cm^{-1} regions, which we assign to BC_2 asymmetric and symmetric stretching vibrations. In trimethylborane the asymmetric and symmetric BC_3

[10] I. Shapiro, C. O. Wilson, Jr., and W. J. Lehmann, J. Chem. Phys. **29,** 237 (1958).
[11] W. J. Lehmann, C. O. Wilson, Jr., and I. Shapiro, J. Chem. Phys. (to be published).
[12] W. J. Lehmann, J. F. Ditter, and I. Shapiro, J. Chem. Phys. **29,** 1248 (1958).
[13] W. J. Lehmann, C. O. Wilson, Jr., and I. Shapiro, J. Chem. Phys. **28,** 777 (1958).
[14] L. J. Bellamy, *The Infrared Spectra of Complex Molecules* (John Wiley & Sons, Inc., New York, 1958).
[15] W. J. Lehmann, C. O. Wilson, Jr., and I. Shapiro, J. Chem. Phys. **31,** 1071 (1959).

(*sic*!) vibrations are observed[13,15] at 1156 and 675 cm^{-1}, respectively. The former has a B^{10} shift of 29 cm^{-1} to 1185 cm^{-1}; the latter appears only in the Raman spectrum. This leaves no doubt about assignment of the type *B* band in $(CH_3)_2B_2H_4$ at 1126 cm^{-1} (isotope shift of 31 cm^{-1} to 1157 cm^{-1} in $(CH_3)_2B_2{}^{10}H_4$) to the BC_2 asymmetric stretching vibration. In $(CH_3)_2B_2D_4$ this absorption is almost completely masked by the very strong B—D′ vibration at 1159 cm^{-1}. In $(CD_3)_2B_2H_4$ and $(CD_3)_2B_2D_4$, it has shifted to 1093 and 1110 cm^{-1}, respectively. The BC_2 symmetric stretching frequencies in the series $(CH_3)_2B_2{}^{10}H_4$ to $(CD_3)_2B_2D_4$ decrease steadily from 837 to 770 cm^{-1}.

Vibrations of the Ethyl Groups

Again the C—H and C—D stretching bands are at the expected[2,3,15,16] values of 2840–2960 cm^{-1} and 2080–2220 cm^{-1} and show the expected splitting.

The asymmetric CH_3 and CH_2 deformations are found at 1475 and 1435 cm^{-1} (the former coincides in $(C_2H_5)_2B_2D_4$ with a B—D′ band), while the symmetric bands are mere pips at approx 1380 cm^{-1}. The CD_3 asymmetric and/or CD_2 deformations appear as fairly intense bands at 1055 cm^{-1} (CH/CD) frequency ratio of approx 1.38). In $(C_2D_5)_2B_2H_4$ and $(C_2D_5)_2B_2D_4$, as in previously analyzed ethyldiboranes[2,3] we are unable to arrive at an assignment for the CD_3 symmetric deformation motions. The bands at 955 cm^{-1} are eliminated from serious consideration by the high CH/CD frequency ratio of 1.45.

The prominent band at 1300 cm^{-1} (B^{10} shift of 8 cm^{-1}) and the weaker one at 1245 cm^{-1} represent wagging and twisting motions of the CH_2 group, as in other ethyldiboranes; and again the 1300-cm^{-1} band is considerably enhanced in the boron-deuterated compound. In triethylborane these bands are slightly higher, at 1325 (B^{10} shift of 8 cm^{-1}) and 1290 cm^{-1}. The corresponding CD_3 wagging and/or twisting frequency in $(C_2D_5)_2B_2H_4$ and $(C_2D_5)_2B_2D_4$ is at 1220 cm^{-1}, which compares with 1238 cm^{-1} in $B(C_2D_5)_3$, not observed in mono- and 1,2-diethyldiboranes.

The bands at approx 1080 (B^{10} shift of 9 cm^{-1}) and 1020 cm^{-1} (B^{10} shift of 5 cm^{-1}) are assigned to CH_3 rocking. Both these bands are observed in other ethyldiboranes, with generally increasing intensities (especially of the former) in more highly ethylated diboranes, and somewhat lower wave numbers (ca 1025–1060 and 980 cm^{-1}, respectively) in tri- and tetraethyldiboranes. In triethylborane CH_3 rocking has been assigned to 1022 cm^{-1} (B^{10} shift of 5 cm^{-1}) and approx 975 cm^{-1}, coupled with some C—C stretching. In $(C_2D_5)_2B_2H_4$ and $(C_2D_5)_2B_2D_4$ the CD_3 rocking bands appear at approx 955 and 935 cm^{-1}. The latter is superimposed on the BH_2 wagging band in $(C_2D_5)_2B_2H_4$. In $B(C_2D_5)_3$ the CD_3 wagging modes have been assigned to 945 and approx 900 cm^{-1}.

[16] W. J. Lehmann, C. O. Wilson, Jr., and I. Shapiro, J. Chem. Phys. **28**, 781 (1958).

The strong band in $(C_2H_5)_2B_2H_4$ at 881 cm^{-1} is probably a C—C stretching band partly coupled with other motions. It is slightly lower than in triethylborane and other ethyldiboranes (904–943 cm^{-1}). In $(C_2H_5)_2B_2D_4$, we assign the 927-cm^{-1} band to this vibration and ascribe its elevated value to resonance with the BD_2 deformation at 852 cm^{-1}, a markedly low value for the latter vibration. As mentioned previously, the unperturbed values of the two vibrations are located at about 900 and 880 cm^{-1}, respectively. In $(C_2D_5)_2B_2H_4$ the C—C band is at 883 cm^{-1}, and it probably appears as a shoulder at about 887 cm^{-1} in $(C_2D_5)_2B_2D_4$.

No bands are observed in the vicinity of 800 cm^{-1} that might be assigned to CH_2 rocking, but weak bands at approx 780 in $(C_2D_5)_2B_2H_4$ and $(C_2D_5)_2B_2D_4$ could be due to CD_2 rocking.

The two BC_2 stretching vibrations have not yet been assigned. The asymmetric oscillation is easily singled out at 1114 cm^{-1} in $(C_2H_5)_2B_2H_4$ by its large B^{10} shift of 22 cm^{-1}. In $(C_2D_5)_2B_2H_4$, it is found at 1101 cm^{-1}, but in $(C_2H_5)_2B_2D_4$ and $(C_2D_5)_2B_2D_4$ only weak shoulders at approx 1110 cm^{-1} are discernible. These frequencies closely match those in the triethylboranes and are slightly lower than those in the corresponding methyl compounds. The symmetric BC_2 frequency decreases from 751 cm^{-1} in $(C_2H_5)_2B_2{}^{15}H_4$ to 715 cm^{-1} in $(C_2D_5)_2B_2D_4$ and is about 10% lower than in the dimethyldiboranes. A similar frequency drop is observed in going from trimethyl- (675 cm^{-1}) to triethylborane (620 cm^{-1}).

CONCLUSION

Examination of the assignments listed in Tables I and II and comparison with those for other alkyldiboranes allow some generalizations regarding vibrations of the nonalkylated parts of the 1,1-dialkyldiborane molecules. The terminal B—H stretching frequencies are only slightly lowered (on the order of approx 10–20 cm^{-1}) by progressive alkylation of the *other* end of the molecule. The BH_2 deformation band remains characteristically at approx 1170 cm^{-1}. The infrared-active BH_2 (out-of-plane) wagging frequency in the 920–970 cm^{-1} region is diminished by approx 20 cm^{-1} for each methyl group substituted on the far end. These observations are corroborated by parallel trends in the BD frequencies. Similar generalizations can be made for the ethylenic CH_2 (and CD_2) vibrational modes in deuterated and alkylated ethylenes.[13,17–19]

The approx 50-cm^{-1} reduction in the strong bridge-stretching frequency and the intensification of B—H′ absorption at approx 2100 cm^{-1} have been mentioned previously.

[17] E. G. Hoffmann, Ann. Chem. Liebigs **618**, 276 (1958).

[18] N. Sheppard and D. M. Simpson, Quart. Revs. (London) **6**, 1 (1952).

[19] B. L. Crawford, Jr., J. E. Lancaster, and R. G. Inskeep, J. Chem. Phys. **21**, 678 (1953).

THE JOURNAL OF CHEMICAL PHYSICS VOLUME 34, NUMBER 2 FEBRUARY, 1961

Note on the Calculation of Saturation Effects in Magnetic Resonance

M. J. STEPHEN

Department of Chemistry, Columbia University, New York, New York

(Received March 7, 1960)

A simple method using diagrams is described for calculating saturation parameters in spin systems. Results are derived for the multiresonance case. The lattice is regarded as inducing transitions among the various spin levels and the transition probabilities are assumed known. The method is particularly useful in complicated spin systems as are found in organic free radicals. For a free radical in solution with one odd electron and N equivalent nuclei under conditions where the intramolecular electron nuclear dipole-dipole interaction and g factor anisotropy contribute to the relaxation, the dependence of the saturation parameters of the electron resonance spectrum on the nuclear quantum number m_J is given by an expression of the form $Am_J^2+Bm_J+C$. Such behavior has been found experimentally.

I. INTRODUCTION

THE purpose of this note is to describe a simple method for calculating saturation parameters in spin systems. Results are derived for the s-tuple resonance case at high temperatures, i.e., when s rf fields are applied to the spin system. The method is very convenient in complicated spin systems such as exist in organic free radicals. In many cases some relaxation probabilities are much more important than others and then an expansion of the saturation parameters in terms of the ratio of the small to the large relaxation probabilities is easily obtained. Measurement of these saturation parameters can be made and comparison with theory can lead to information about the important relaxation mechanisms.[1]

Lloyd and Pake[2] have suggested a method for calculating the saturation parameter in the presence of a single rf field but for large spin systems the calculation becomes prohibitively long. Bloch[3] has pointed out that at high temperatures the equations governing the population of the various spin levels are just Kirchoff's equations for an electric circuit. Thus an alternative method for obtaining saturation parameters is to set up the analogous electric network. In practice, however, this method is not very useful as the measurements on the network cannot be made with sufficient accuracy.

The method of calculation of saturation parameters developed here depends on certain mathematical results. These results are described in the following and illustrated by application to double resonance in a 4-level system and single resonance in parabenzosemiquinone which has recently been studied experimentally.[1] The proofs are relegated to the Appendix. An interesting result is obtained for a system of one odd electron interacting with N equivalent nuclei in a strong magnetic field. The dominant relaxation in such systems usually corresponds to electron spin flips but intramolecular dipole-dipole interaction may also contribute. Then the saturation parameter, to first order in the dipole interaction, for a transition $m_s=-\frac{1}{2}\rightarrow m_s=\frac{1}{2}$. $m_J\rightarrow m_J$ is of the form $\Omega_{m_J}=Am_J^2+Bm_J+C$. Where m_s and m_J are the electron spin and nuclear spin quantum numbers and A, B, and C are constants. Such a dependence on m_J has been found experimentally.[1]

II. THEORY

The basic assumption is that the spin level populations are governed by the familiar rate equations. These equations may be justified from the well-known Boltzmann equation for the density matrix if the off diagonal elements of the density matrix are neglected.[3,4] Thus if Q_j is the fractional population of level j and W_{jk}' is the probability of making a transition from j to k in unit time then the Q_j obey the set of equations,[2]

$$\dot{Q}_j=\sum_k{}'W_{kj}'Q_k-Q_j\sum_k{}'W_{jk} \tag{1}$$

W_{jk}' includes the transitions induced by any rf field and thus

$$W_{kj}'=W_{kj}+V_{kj}, \tag{2}$$

where W_{kj} is the lattice induced transition probability and V_{kj} is that induced by the rf field. In order for the spin system to attain a Boltzmann distribution in the absence of rf fields it is necessary to assume that

$$W_{kj}=W_{jk}\exp\{\beta\omega_{kj}\}, \tag{3}$$

where $\beta=\hbar/kT$, T is the lattice temperature and $\omega_{kj}=\omega_k-\omega_j$ is the frequency difference between the levels k and j. When temperature effects are neglected the lattice induced transition probabilities will be denoted by $\bar{W}_{kj}=\bar{W}_{jk}$. Owing to the essentially infinite temperature of the rf oscillator it is possible to neglect any spontaneous emission and so $V_{jk}=V_{kj}$.

In magnetic resonance in order to obtain the power absorbed we require the relative population of two

[1] J. W. H. Schreurs and G. K. Fraenkel (to be published).
[2] J. P. Lloyd and G. E. Pake, Phys. Rev. **94**, 579 (1954).
[3] F. Bloch, Phys. Rev. **102**, 104 (1956).
[4] A. G. Redfield, IBM J. Research and Development **1**, 19 (1957).

levels in the presence of the rf fields applied to the system. The saturation factor is defined in the usual way for the levels i and j by

$$Z_{ij}(V)=\frac{Q_i(V)-Q_j(V)}{Q_i(0)-Q_j(0)}, \tag{4}$$

where $Q(V)$ and $Q(0)$ are the relative populations in the presence and absence of rf fields V, respectively. In the limit of high temperature the dependence of Z_{ij} on the applied rf fields $V_{\alpha\beta}\cdots$ is given by (see Appendix)

$$Z_{ij}(V_{\alpha\beta}, V_{\gamma\delta}\cdots)=\frac{1+\sum_{\alpha\beta}V_{\alpha\beta}\chi_{\alpha\beta}{}^{(ij)}+\sum_{\alpha\beta<\gamma\delta}\sum V_{\alpha\beta}V_{\gamma\delta}\chi_{\alpha\beta,\gamma\delta}{}^{(ij)}+\cdots}{1+\sum_{\alpha\beta}V_{\alpha\beta}\Omega_{\alpha\beta}+\sum_{\alpha\beta<\gamma\delta}\sum V_{\alpha\beta}V_{\gamma\delta}\Omega_{\alpha\beta,\alpha\delta}+\cdots}. \tag{5}$$

The constants $\chi_{\alpha\beta}{}^{(ij)}$, $\Omega_{\alpha\beta}$, etc., are the saturation parameters of the spectrum and depend on the lattice induced transition probabilities $\bar{W}_{kj}$. The summations in (5) extend over all applied rf fields. It is shown in the Appendix that $\chi_{ij}{}^{(ij)}=0$; $\chi_{ij,\gamma\delta}{}^{(ij)}=0$, etc., so that V_{ij} does not appear in the numerator of (5) and thus the spectrum saturates. In the case of a single rf field applied to two levels (5) reduces to the well-known results

$$Z_{\alpha\beta}(V_{\alpha\beta})=1/(1+V_{\alpha\beta}\Omega_{\alpha\beta}) \tag{6}$$

$$Z_{ij}(V_{\alpha\beta})=(1+V_{\alpha\beta}X_{\alpha\beta}{}^{(ij)})/(1+V_{\alpha\beta}\Omega_{\alpha\beta}). \tag{7}$$

Equation (6) describes the ordinary saturation behavior of a pair of levels and (7) describes the change in the relative populations of levels ij when transitions are induced between the pair $\alpha\beta$, including the Overhauser effect.

The method of evaluation of the saturation parameters consists in noting that each of them may be represented by a sum of diagrams. We will call each energy level a vertex and represent each relaxation probability by a line on a diagram joining the appropriate two vertices. In the case of finite temperature the direction of the line must be specified. Thus W_{kj} is represented by a line from vertex k to vertex j. By each diagram is meant the product of all relaxation probabilities appearing in the diagram. A sum of diagrams is the sum of all such terms. For a system of n vertices the only diagrams we need consider are of the following type (see Appendix). (a) There are n vertices and $n-1$ lines in each diagram. (b) There is at least one line attached to each vertex. (c) There are no disconnected diagrams (i.e., in each diagram we can go from any vertex to any other via some path. (d) The diagrams have no closed sections (i.e. starting at any vertex there is no closed path bringing us back to that vertex.)

These rules can easily be interpreted physically. Disconnected diagrams are absent because we suppose that each level of the system can be reached by relaxation in some way. Diagrams with closed sections do not occur because in going round a closed section no energy would be lost or gained by the system and thus there would be no contribution to relaxation.

We now define the following sums of the foregoing type of diagrams (a bar over a quantity indicates that temperature effects are neglected and thus the directions of the lines in the diagrams are immaterial):

$\bar{N}$ = sum of all diagrams of the foregoing type

$\bar{N}(\alpha\beta)$ = sum of all diagrams of the foregoing type containing the line $\alpha-\beta$ with $\bar{W}_{\alpha\beta}=\bar{W}_{\beta\alpha}=1$

$\bar{N}(\alpha\beta,\gamma\delta)$ = sum of all diagrams of the foregoing type containing the lines $\alpha-\beta$ and $\gamma-\delta$ with $\bar{W}_{\alpha\beta}=\bar{W}_{\beta\alpha}=\bar{W}_{\gamma\delta}=\bar{W}_{\delta\gamma}=1$, etc.

Then

$$\Omega_{\alpha\beta}=\bar{N}(\alpha\beta)/\bar{N};\quad \Omega_{\alpha\beta,\gamma\delta}=\bar{N}(\alpha\beta,\gamma\delta)/\bar{N}, \text{ etc.} \tag{9}$$

In order to define the parameters $X_{\alpha\beta,\gamma\delta\ldots}{}^{(ij)}$ we need the following sums of diagrams:

$\bar{N}_{j,\alpha\beta,i}(\alpha\beta)$ = sum of all diagrams in $\bar{N}(\alpha\beta)$ in which the path $j\to i$ goes via $\alpha-\beta$ in that order.

$\bar{N}_{j,\alpha\beta,i}(\alpha\beta,\gamma\delta)$ = sum of all diagrams in $\bar{N}(\alpha\beta,\gamma\delta)$ in which the path $j\to i$ goes via $\alpha-\beta$ in that order and this path does not include $\gamma-\delta$.

$\bar{N}_{j,\alpha\beta,\gamma\delta,i}(\alpha\beta,\gamma\delta)$ = sum of all diagrams in $\bar{N}(\alpha\beta,\gamma\delta)$ in which the path $j\to i$ goes via $\alpha-\beta$ and $\gamma-\delta$ in that order, etc. (10)

For convenience we introduce the following summation convention:

$$\sum_{(rs)}\bar{N}_{j,rs,i}(\alpha\beta)=\bar{N}_{j,\alpha\beta,i}(\alpha\beta)+\bar{N}_{j,\beta\alpha,i}(\alpha\beta).$$

The summation indices can only take on the values of the pairs of indices occurring in the brackets. Thus in

$$\sum_{(rs)}\sum_{(tu)}\bar{N}_{j,rs,tu,i}(\alpha\beta,\gamma\delta)$$

we can have $rs=\alpha\beta$, $\beta\alpha$, $\gamma\delta$, $\delta\gamma$ with corresponding values for the pair tu leading to 8 terms in all.

Then

$$\chi_{\alpha\beta}{}^{(ij)}=\Omega_{\alpha\beta}+(1/\bar{N})\sum_{(rs)}\bar{N}_{j,rs,i}(\alpha\beta)\,(\omega_{sr}/\omega_{ji})$$

$$\chi_{\alpha\beta,\gamma\delta}{}^{(ij)}=\Omega_{\alpha\beta,\gamma\delta}+(1/\bar{N})\left[\sum_{(rs)}\bar{N}_{j,rs,i}(\alpha\beta,\gamma\delta)\,(\omega_{sr}/\omega_{ji})+\sum_{(rs)}\sum_{(tu)}\bar{N}_{j,rs,tu,i}(\alpha\beta,\gamma\delta)\left(\frac{\omega_{sr}+\omega_{ut}}{\omega_{ji}}\right)\right], \tag{11}$$

etc. Note that as $\bar{N}_{j,ji,i}(ij,\ \gamma\delta\cdots)=\bar{N}(ij)$ that

$$\chi_{ij}{}^{(ij)}=\chi_{ij,\gamma\delta}{}^{(ij)}\cdots=0.$$

Under certain conditions the expressions (11) can be simplified. Thus in an electron double resonance experiment we monitor the electron resonance while nuclear frequencies are applied to nuclear resonances, i.e., ij refer to the electron resonance and $\alpha\beta$, $\gamma\delta$, etc., refer to the nuclear resonance levels. It is permissible to neglect terms in $\omega_{\text{nuc}}/\omega_{\text{el}}$ and thus

$$\chi_{\alpha\beta}{}^{(ij)}=\Omega_{\alpha\beta};\quad \chi_{\alpha\beta,\gamma\delta}{}^{(ij)}=\Omega_{\alpha\beta,\gamma\delta},\ \text{etc.}\quad (\alpha\beta,\gamma\delta\neq ij). \tag{12}$$

In the other case where ω_{ij} refers to a nuclear frequency and $\omega_{\alpha\beta}$ to an electron frequency, the $\Omega_{\alpha\beta}$, $\Omega_{\alpha\beta,\gamma\delta}$ may be omitted in (11). This shows that the relative population of the levels ij is enhanced by a factor $\omega_{\text{el}}/\omega_{\text{nuc}}$ which is just the well-known Overhauser effect.

With the definitions (8) and (10) and Eqs. (9) and (11), the evaluation of any saturation parameter reduces to drawing and summing all the appropriate diagrams. For an n level system if all relaxation probabilities W_{kj} are nonzero, then the total number $\bar{N}$ of such diagrams is n^{n-2} which for large spin systems is very large. But in actual practice a number of relaxation probabilities are either forbidden or small and this number is greatly reduced. Also, if some relaxation probabilities are larger than others, then useful expansions can be obtained by first drawing the diagrams containing the largest number of large relaxations and so on. These rules will be illustrated in the following and their usefulness demonstrated on systems of practical interest.

III. EXAMPLES

As an illustration of some of the foregoing rules we consider a 4-level system and calculate the relative population of levels 1 and 2 when rf fields are applied to levels 12 and 23. From (5)

$$Z_{12}(V_{12},\ V_{23})=\frac{1+V_{23}\chi_{23}{}^{(12)}}{1+V_{12}\Omega_{12}+V_{23}\Omega_{23}+V_{12}V_{23}\Omega_{12,23}}. \tag{13}$$

The 16 possible diagrams and the terms they represent are given in Eq. (14).

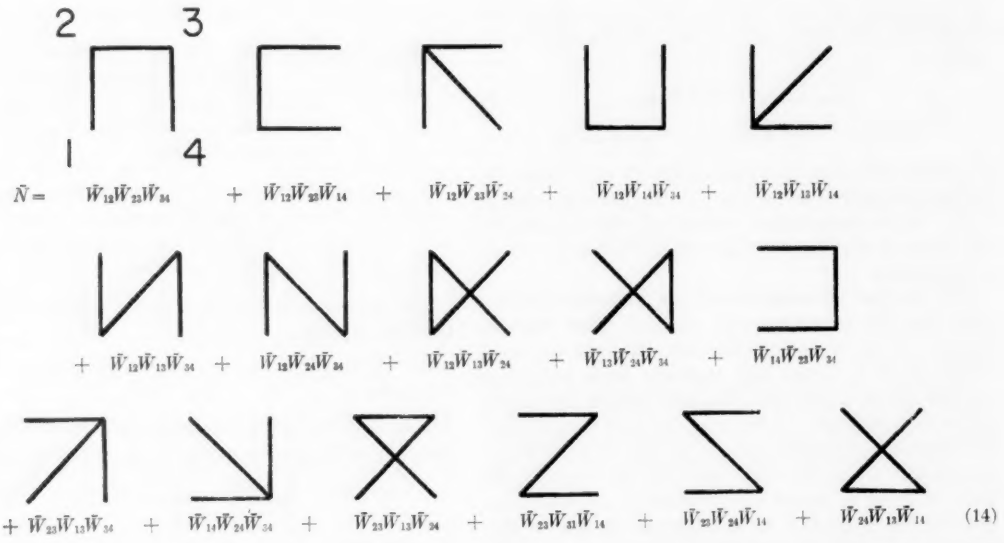

$$\bar{N}=\bar{W}_{12}\bar{W}_{23}\bar{W}_{34}+\bar{W}_{12}\bar{W}_{23}\bar{W}_{14}+\bar{W}_{12}\bar{W}_{23}\bar{W}_{24}+\bar{W}_{12}\bar{W}_{14}\bar{W}_{34}+\bar{W}_{12}\bar{W}_{13}\bar{W}_{14}$$
$$+\bar{W}_{12}\bar{W}_{13}\bar{W}_{34}+\bar{W}_{13}\bar{W}_{24}\bar{W}_{34}+\bar{W}_{12}\bar{W}_{13}\bar{W}_{24}+\bar{W}_{13}\bar{W}_{24}\bar{W}_{34}+\bar{W}_{14}\bar{W}_{23}\bar{W}_{34}$$
$$+\bar{W}_{23}\bar{W}_{13}\bar{W}_{34}+\bar{W}_{14}\bar{W}_{24}\bar{W}_{34}+\bar{W}_{23}\bar{W}_{13}\bar{W}_{24}+\bar{W}_{23}\bar{W}_{31}\bar{W}_{14}+\bar{W}_{23}\bar{W}_{24}\bar{W}_{14}+\bar{W}_{24}\bar{W}_{13}\bar{W}_{14} \tag{14}$$

For $\bar{N}(12)$ and $\bar{N}(23)$ we pick out all those diagrams containing the line 12 and 23 and put $\bar{W}_{12}=1$ and $\bar{W}_{23}=1$, respectively. Thus

$$\bar{N}(12)=\bar{W}_{23}\bar{W}_{34}+\bar{W}_{23}\bar{W}_{14}+\bar{W}_{23}\bar{W}_{24}+\bar{W}_{14}\bar{W}_{34}+\bar{W}_{13}\bar{W}_{14}$$
$$+\bar{W}_{13}\bar{W}_{34}+\bar{W}_{24}\bar{W}_{34}+\bar{W}_{13}\bar{W}_{24} \tag{15}$$

and $\bar{N}(23)$ is obtained by cyclic interchange of the subscripts. $\bar{N}(12,\ 23)$ is the sum of all diagrams containing both lines 1–2 and 2–3 with $\bar{W}_{12}=\bar{W}_{23}=1$. Thus

$$\bar{N}(12,\ 23)=\bar{W}_{34}+\bar{W}_{14}+\bar{W}_{24}. \tag{16}$$

In order to complete the calculation of $\chi_{23}{}^{(12)}$, we require $\bar{N}_{2,32,1}(23)$ and $\bar{N}_{2,23,1}(23)$. $\bar{N}_{2,32,1}(23)=0$ because it is impossible to draw such diagrams without repeating lines. $\bar{N}_{2,23,1}(23)$ is the sum of all diagrams in which the path 2→1 goes via vertex 3 with $\bar{W}_{23}=1$. Such diagrams in (14) are numbers 10, 11, 13, and 14.

Thus

$$\bar{N}_{2,23,1}(23)=\bar{W}_{14}\bar{W}_{34}+\bar{W}_{13}\bar{W}_{34}+\bar{W}_{13}\bar{W}_{24}+\bar{W}_{13}\bar{W}_{14}. \quad (17)$$

Thus from (9) and (11)

$$\Omega_{12}=\bar{N}(12)/\bar{N},$$

$$\Omega_{23}=\bar{N}(23)/\bar{N},$$

$$\Omega_{12,23}=\bar{N}(12,23)/\bar{N}$$

$$\chi_{23}^{(12)}=\Omega_{23}+(\bar{N}_{2,23,1}(23)/\bar{N})(\omega_{32}/\omega_{21}). \quad (18)$$

As an illustration of the usefulness of this diagram technique we will calculate the saturation parameters for the free radical para-benzo semiquinone. This radical contains one odd electron and four equivalent protons so that the electron resonance spectrum at high field consists of five lines and each transition may be denoted by the total nuclear quantum number m_J which takes on the values $-2, -1, 0, 1, 2$. The assumed relaxation pattern is shown in Fig. 1. The various relaxation mechanisms included have been discussed elsewhere.[5] Briefly M includes all mechanisms which relax the odd electron independently of the nuclei. The relaxation K and K_0 are due to electron nuclear dipole-dipole interaction and $K_0=K(1+\omega^2\tau_c^2)$, where ω is the electron resonance frequency and τ_c the rotational correlation time. The parameter L, which leads to an asymmetry in the saturation behavior of the spectrum, arises out of a cross term between the g factor anisotropy and the above dipole-dipole interaction. Recent measurements of the saturation parameters in this molecule indicate that $M \gg K$, L so in evaluating Ω we will only retain terms linear in K/M and L/M. We will consider in detail only the calculation of $\Omega_{12}=\bar{N}(12)/\bar{N}$ corresponding to the transition $m_J=-2$.

The largest terms in $\bar{N}$ will correspond to those diagrams containing the largest number of vertical relaxations, i.e., with the basic pattern of five vertical relaxations. To complete the diagram we must add one cross relaxation in each section which may be added in any way. A typical such diagram is shown in Fig. 2(a). Thus the contribution of these diagrams (4^4 in number) is

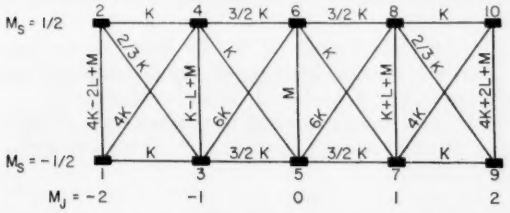

FIG. 1. Relaxation probabilities in para-benzo semiquinone. Energy levels, indicated by filled rectangles, are labeled by M_s, M_J.

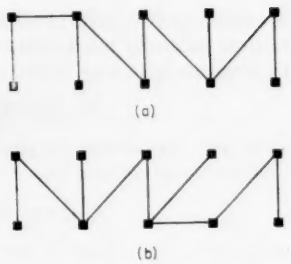

FIG. 2. (a) (b) Typical diagrams in the calculation of saturation effects on para-benzo semiquinone.

$$6M(M+4K-2L)(M+4K+2L)(4M+4K-4L)$$
$$\times(4M+4K+4L)(\tfrac{1}{6}\alpha^4)\simeq\tfrac{32}{3}M^5\alpha^4(1+10K/M), \quad (19)$$

where $\alpha=(6K_0+14K)$ and is the sum of the cross relaxations in the central two sections. $\alpha/3$ is the sum of the cross relaxations in the outer two sections. The next set of diagrams in $\bar{N}$ will come from those diagrams with the basic pattern where one vertical relaxation is missing. These diagrams are completed by adding five cross relaxations. A typical diagram is shown in Fig. 2(b). There are five such basic patterns as there are five vertical relaxations and each gives the same contribution to $\bar{N}$ of $\frac{128}{3}M^4\alpha^3\delta$, where

$$\delta=\tfrac{1}{4}(3K_0^2+14KK_0+8K^2).$$

To first order in K/M this is all that is required.

To calculate $\bar{N}(12)$ we must only consider diagrams containing the line 1–2. The most important of these will have the vertical relaxation pattern of five vertical relaxations as in Figure 1(a) but with $\bar{W}_{12}=1$. Thus the total contribution of this type is obtained from (19) by replacing the term $(M+4K-2L)$ by unity thus giving $\frac{32}{3}\alpha^4M^4[1+(6K/M)+(2L/M)]$. Next we sum all diagrams in which one solid vertical relaxation is missing as in Fig. 1(b) (except for the line 1–2 which must always be present). There are four such basic patterns and each contributes exactly as in $\bar{N}$, i.e., $\frac{128}{3}M^4\alpha^3\delta$. Thus it is found to first order in K/M and L/M that

$$\Omega_{12}=\bar{N}(12)/\bar{N}\simeq(1/M)[1-(1/M)(4K-2L+4\delta/\alpha)] \quad (20)$$

This result is easily generalized to the case of a molecule with N equivalent nuclei of spin $\frac{1}{2}$. On denoting the electron resonance transition by the nuclear quantum number m_J, we have to first order in K/M and L/M

$$\Omega_{m_J}=(1/D_{m_J}M)[1-(1/M)(Km_J^2-Lm_J+N\delta/\alpha)] \quad (21)$$

where D_{m_J} is the degeneracy of the level m_J. Complete expansions in powers of K/M and L/M for some simple spin systems are given in footnote 5. The dependence of

[5] M. J. Stephen and G. K. Fraenkel, J. Chem. Phys. **32**, 1435 (1960).

the saturation behavior of the electron resonance on the nuclear quantum number m_J shown in (21) is found experimentally in some cases.

IV. APPENDIX

We will here obtain the results described in Sec. II. Written in matrix form Eq. (1) is

$$\dot{Q}=-AQ, \tag{A.1}$$

where Q is the column vector of the Q_j and A is a matrix having elements

$$A_{jj}=\sum_k{}'W'_{jk}; \qquad A_{jk}=-W_{kj}'. \tag{A.2}$$

We will only be interested in the steady-state population of the levels so that we only need study the equation

$$AQ=0 \tag{A.3}$$

with normalization condition $\sum_i Q_i=1$. If n is the total number of energy levels in the system a convenient solution of (A.3) when the rank of A is $n-1$ is[5]

$$Q_i(V)=B_{ii}(V)/\sum_k B_{kk}(V), \tag{A.4}$$

where $B_{ii}(V)$ is the ith diagonal cofactor of the matrix A. $Q_i(V)$ is a function of any rf fields as is shown by including a V in brackets. When temperature effects are neglected, i.e., W_{kj} is replaced by $\bar{W}_{kj}$, then $B_{ii}(V)$ will be denoted by $\bar{B}_{ii}(V)$.

The method of evaluation of (A.4) depends on two simple theorems.

(i) Theorem 1. The expansion of $B_{ii}(V)$ contains only positive terms provided all the W_{kj}' are positive. This is a simple extension of a theorem proved by Ledermann.[6]

(ii) Theorem 2. Each term of $\bar{B}_{ii}(V)$ can be represented by a diagram of the type listed under (a)–(d) in Sec. II.

Proof

The order of the matrix A is n and so clearly each term of $\bar{B}_{ii}(V)$ is a product of $n-1$ relaxation probabilities and the corresponding diagram will thus contain $n-1$ lines. All diagonal cofactors of the matrix $\bar{A}$ are equal,[5] i.e.,

$$\bar{B}_{11}(V)=\bar{B}_{22}(V)\cdots=\bar{B}_{nn}(V). \tag{A.5}$$

Consider

$$\bar{B}_{11}(V)=\begin{vmatrix} \sum_{k=1}^{n}{}'\bar{W}_{2k}' & -\bar{W}_{32}'\cdots \\ \\ -\bar{W}_{23} & \sum_{k=1}^{n}{}'\bar{W}_{3k}'\cdots \\ \vdots & \end{vmatrix}. \tag{A.6}$$

Expansion on diagonal elements $\bar{W}_{j1}'$ shows that each term contains $\bar{W}_{j1}'$ and no term has $(\bar{W}_{j1}')^2$. This combined with (A.5) proves (a). Further, in constructing a term we must take an entry from each column of (A.6) and so each term must be of the form

$$\bar{W}_{2\beta}'\bar{W}_{3\gamma}'\cdots\bar{W}_{n\phi}' \tag{A.7}$$

and using (A.5) again shows that each term must also be of the form

$$\bar{W}_{1\alpha}'\bar{W}_{3\gamma}'\cdots\bar{W}_{n\phi}', \quad \text{etc.}, \tag{A.8}$$

and so each index $1\cdots n$ is represented in each term. This proves (b). We can use this result to prove (c). Suppose a term is written

$$\bar{W}_{2\alpha}'\bar{W}_{3\gamma}'\cdots\bar{W}_{n\phi}'. \tag{A.9}$$

We know each index must occur so let $\alpha=1$ and suppose index 1 does not occur again. Then index 2 must occur again in some other W because (A.9) can be written from (A.8) in the form

$$\bar{W}_{12}'\bar{W}_{2\beta}'\bar{W}_{4\delta}'\cdots\bar{W}_{n\phi}'.$$

This process may be continued and shows that starting at some vertex we can always find some path to any other vertex and (c) follows.

Type (d) is really a consequence of (a)–(c). Suppose a diagram has a closed section involving s vertices. This requires s lines and leaves $n-s$ vertices and $n-s-1$ lines. Each vertex must have at least one line leaving it and in order to obtain a connected diagram we must now join $n-s+1$ vertices with $n-s-1$ lines which is clearly impossible and (d) follows.

The proof is completed by showing that the number of terms in a determinant $\bar{B}_{ii}$ is equal to the number of the above diagrams. This is not difficult and it is found that the number of such diagrams (and terms in the determinant $\bar{B}_{ii}$) is n^{n-2} where n is the number of vertices, i.e., the order of matrix A.

The extension to finite temperature is easily made. In this case $W_{kj}\neq W_{jk}$ and the directions of the lines in the diagrams must be specified. By an examination similar to that made above the terms occurring in $\bar{B}_{ii}(V)$ we obtain the following additional rule for drawing the diagrams corresponding to any cofactor of $\bar{B}_{ii}(V)$

(e) In each diagram of $B_{ii}(V)$ there are no lines *leaving* vertex i, and there is only one line *leaving* every other vertex. This leads to a unique set of diagrams.

It is now straightforward to evaluate any cofactor occurring in (A.4) as a function of the rf fields acting on the system:

$$B_{ii}(V_{\alpha\beta}, V_{\gamma\delta})=N_i+\sum_{\alpha\beta}V_{\alpha\beta}N_i(\alpha\beta) +\sum_{\alpha\beta<\gamma\delta}\sum V_{\alpha\beta}V_{\gamma\delta}N_i(\alpha\beta,\gamma\delta)+\cdots, \tag{A.10}$$

where summations extend over all rf fields acting on the system. The N_i, etc., are defined in (8) except

[6] W. Ledermann, Proc. Cambridge Phil. Soc. **46**, 581 (1950).

that rule (e) is taken into account (finite temperature) and thus a subscript i is attached.

The saturation factor $Z_{ij}(V)$ defined in (4) is, in the limit of high temperature, using (A.4) and (A.5) given by

$$Z_{ij}(V)=\frac{1}{\bar{B}(V)}\left(\frac{B_{ii}(V)-B_{jj}(V)}{\beta\omega_{ji}}\right)_{\beta\to 0}. \qquad (A.11)$$

To evaluate $B_{ii}-B_{jj}$ we notice that there is a one-to-one correspondence between the diagrams of B_{ii} and B_{jj}, the only difference being in the direction of the lines. To convert a diagram of type i into a diagram of type j, according to (e), all we do is reverse all the lines along the path connecting j and i.

Then it is easy to see that

$$\begin{aligned}
N_j&=N_i\exp(\beta\omega_{ij})\\
N_{i,\alpha\beta,j}(\alpha\beta)&=N_{j,\beta\alpha,i}(\alpha\beta)\exp[\beta(\omega_{ij}+\omega_{\beta\alpha})]\\
N_{i,\alpha\beta,j}(\alpha\beta,\gamma\delta)&=N_{j,\beta\alpha,i}(\alpha\beta,\gamma\delta)\exp[\beta(\omega_{ij}+\omega_{\beta\alpha})]\\
N_{i,\alpha\beta,\gamma\delta,j}(\alpha\beta,\gamma\delta)&=N_{j,\delta\gamma,\beta\alpha,i}(\alpha\beta,\gamma\delta)\\
&\quad\times\exp[\beta(\omega_{ij}+\omega_{\beta\alpha}+\omega_{\delta\gamma})]. \qquad (A.12)
\end{aligned}$$

The $N_{i,\alpha\beta,j}(\alpha\beta)$ are defined in (10) except again the temperature is considered finite. So that by (e) $N_{i,\alpha\beta,j}(\alpha\beta)$ = sum of all diagrams in $N_j(\alpha\beta)$ in which the path $i\to j$ goes via $\alpha-\beta$ in that order, etc.

Thus using (A.12) we have to first order in β

$$\begin{aligned}
N_i-N_j&=\beta\bar{N}\omega_{ji}\\
N_i(\alpha\beta)-N_j(\alpha\beta)&=\beta[\bar{N}(\alpha\beta)\omega_{ji}+\sum_{(rs)}\bar{N}_{j,rs\,i,}(\alpha\beta)\omega_{sr}]\\
N_i(\alpha\beta,\gamma\delta)-N_j(\alpha\beta,\gamma\delta)&\\
=\beta[\bar{N}(\alpha\beta,\gamma\delta)\omega_{ji}&+\sum_{(rs)}\bar{N}_{j,rs,i}(\alpha\beta,\gamma\delta)\omega_{sr}\\
+\sum_{(rs)}\sum_{(tu)}&\bar{N}_{j,rs,tu,i}(\alpha\beta,\gamma\delta)(\omega_{sr}+\omega_{ut})]. \qquad (A.13)
\end{aligned}$$

Using these results in (A.11) leads to Eq. (5).

ACKNOWLEDGMENT

The author would like to thank Professor G. K. Fraenkel for much useful discussion.

THE JOURNAL OF CHEMICAL PHYSICS VOLUME 34, NUMBER 2 FEBRUARY, 1961

Mean Free Path and Ultrasonic Vibrational Relaxation in Liquids and Dense Gases

W. M. MADIGOSKY AND T. A. LITOVITZ*

U. S. Naval Ordnance Laboratory, White Oak, Silver Spring, Maryland

(Received July 11, 1960)

Measurements of ultrasonic absorption and velocity in CO_2 yielded values of the vibrational relaxation times over a range of densities from 400 to 610 amagats at 25°C and 50.2°C. On the basis that only binary collisions are important it is found that the Enskog theory for determining collision times in the dense fluid failed to account for the results. Application of the Eyring-Hirschfelder cell model of the liquid accounted well for the density dependence of the relaxation frequency but gave values of mean free path which were too large. It is proposed that for mean free path calculations a realistic cell model must not use fixed walls as the Eyring and Hirschfelder model does but rather moving walls. When this modification is included excellent agreement is obtained for both CO_2 and CS_2. It is further shown that attractive forces do not play the role in determining the collision efficiencies in a liquid or dense gas that they do in the dilute gas. After correcting for the reduced effect of attractive forces, it is found that the collision efficiencies for the dilute gas agree with values obtained for the liquid and dense gas.

I. INTRODUCTION

THE theory of vibrational relaxation in gases has been successfully developed by Schwartz and Herzfeld.[1] They assume that the transfer of energy between vibrational and translational degrees of freedom is due to binary collisions and derive an expression for the probability of energy transfer per collision (P^*). Litovitz[2] has suggested that this concept of binary collisions can account for the vibrational relaxation times in dense gases and liquids if proper attention is given to the finite size of the molecule. He assumed that the collision efficiency P^* is the same in the liquid as in the gas except for a factor which is related to the effect of attractive forces on P^*. In addition, he uses a cell model to calculate the mean free path in the liquid. Actually, if the binary collision assumption is

* Also of Physics Department, Catholic University of America, Washington, D. C.

[1] K. F. Herzfeld and T. A. Litovitz, *Absorption and Dispersion of Ultrasonic Waves* (Academic Press, Inc., New York, 1959).

[2] T. A. Litovitz, J. Acoust. Soc. Am. **26**, 469 (1956).

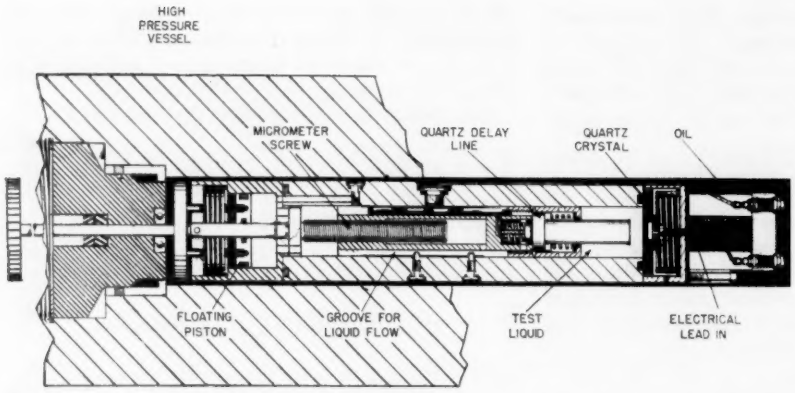

FIG. 1. High-pressure variable path acoustic system.

true, the ultrasonic data become an excellent means of measuring the mean free path of dense gases and liquids.

Bass and Lamb[3] offer data comparing relaxation times in the gas and liquid state which they suggest indicate limitations of the cell model. One of the disadvantages in this comparison of gas and liquid data is that in no case has the relaxation time been continuously measured from dilute gas densities up to very high gas or liquid densities. Henderson and Peselnick[4] and Henderson and Klose[5] made measurements in CO_2 over a large range of densities but did not reach a sufficiently high density region where the mean free path deviates significantly from the kinetic theory value.

In this investigation the relaxation time in CO_2 has been measured from a region which overlaps the data of Henderson and Klose up to higher densities where the mean free path is no longer calculable by simple kinetic theory. Our purpose is to investigate the limitations of the cell model theory for determining the mean free path using the measured vibrational relaxation time in dense gases and liquids.

II. APPARATUS

The sound absorption was measured at frequencies from 5 to 55 Mc by a pulse-echo technique similar to that employed by Litovitz *et al.*[6] The high pressure variable path acoustic system is shown in Fig. 1. It is similar to that used by Litovitz and Carnevale[7] with the exception that instead of a reflector a second quartz crystal and a fused quartz delay line has been added. Highly absorbing liquids may be more readily studied by the two-crystal method because it provides a "one-way" sound path. The quartz delay line provides a time delay in the echo pattern that separates the acoustic pulses from the direct electromagnetic feed-through of the transmitter pulse. The delay line is an optically polished fused quartz rod flat to one-fifth of a wavelength, parallel to within 20×10^{-6} in. and approximately 2 in. long and $\frac{1}{2}$ in. in diameter with a chrome-gold plated shoulder on one end. The delay line fits into a holder containing a spring, and the assembly is screwed onto the end of the moving piston. The transmitting crystal is bonded to the quartz delay line and is electrically connected to the transmitter by means of a spring mounted metallic button and a sliding electrical contact. The sound wave travels down the quartz delay line, through the liquid, and is detected by the large receiving crystal. Absorption measurements are made by varying the acoustic path length in the test liquid, accomplished by turning the micrometer screw, and comparing the height of the received echoes with the output of a standard pulsed signal generator.

The CO_2 was used as both the test liquid and pressure transmitting fluid. As obtained the gas was certified to contain less than 0.06 mg of water vapor per liter of CO_2. It was further dried at tank pressure by passing it through a tube filled with Drierite. The gas was then admitted into a HART (Rotterdam, Holland) gas compressor capable of producing pressures to 45 000 psi. The HART compressor uses two upright pressure chambers and a tube connected to the upper and extending inside the lower chamber. The upper chamber was filled with the test gas and the lower with mercury. Oil was pumped into the lower chamber, which in turn forced the mercury up the tube into the upper chamber, thereby compressing the CO_2 gas. The compressed gas was then admitted into the pressure vessel. The whole process was recycled until the desired pressure was reached. At no time was the gas under test in contact with the pumping oil. The pressure vessel was "flushed out" several times before final filling.

The gas pressure was measured with an oil-free, 0–20 000 psi, 16-in. Heise Bourdon tube gauge calibrated to within 15 psi. For pressures higher than

[3] R. Bass and J. Lamb, Proc. Roy. Soc. (London) **A247**, 168 (1958).
[4] M. C. Henderson and L. Peselnick, J. Acoust. Soc. Am. **29**, 1074 (1957).
[5] M. C. Henderson and T. Z. Klose, J. Acoust. Soc. Am. **31**, 29 (1958).
[6] T. A. Litovitz, T. Lyon, and L. Peselnick, J. Acoust. Soc. Am. **26**, 566 (1954).
[7] T. A. Litovitz and E. H. Carnevale, J. Acoust. Soc. Am. **26**, 816 (1955).

20 000 psi a 0–50 000 U. S. gauge was used. The temperature was controlled to 0.1°C by circulating water through a jacket surrounding the pressure vessel.

III. EXPERIMENTAL PROCEDURE AND RESULTS

When the absorption can be accounted for by a single thermal relaxation mechanism in addition to nonrelaxing mechanisms, it may be represented by the following expression

$$\alpha/f^2=\frac{v}{v_0^2}\frac{(\gamma-1)C'}{(C_p-C')f_0}\frac{1}{1+f^2/f_0^2}+B. \tag{1}$$

Here α is the absorption coefficient, f the frequency of the sound wave, f_0 the effective relaxation frequency which is obtained directly from the absorption measurements, v the velocity at any frequency f, v_0 the low-frequency velocity, γ the ratio of specific heats, C' the relaxing infrared specific heat, C_p the specific heat at constant pressure, and B any absorption that remains at infinite frequency including that due to shear viscosity. It was found that for CO_2 B may be neglected. Hence, Eq. (1) may be rewritten,

$$(f^2/\alpha)(v/v_0^2)=I+Sf^2, \tag{2}$$

where I and S are constants. When $(f^2/\alpha)(v/v_0^2)$ is plotted against f^2, the effective relaxation frequency f_0 is given by

$$f_0=(I/S)^{\frac{1}{2}}, \tag{3}$$

where I and S are the intercept and slope, respectively, of the best straight line.

The true relaxation frequency (the rate in which the system returns to equilibrium) is given by

$$f_r=[(C_p-C')/C_p]f_0. \tag{4}$$

The relaxing vibrational specific heat may be calculated from the slope and intercept by the equation

$$C'=C_p/[\pi(\gamma-1)(I/f_0)^{\frac{1}{2}}+1]. \tag{5}$$

Values of the specific heat at constant volume and pressure as a function of density and temperature were taken from Michels and De Groot.[8]

Figure 2 is a phase diagram of carbon dioxide.[9] The critical point occurs at 31°C and approximately 73 atm. The relaxation frequency has been measured as a function of density at one temperature above and one below the critical temperature. The data at 25°C were taken in the liquid region A to B shown in Fig. 2. The 50.2°C data were taken in the region marked CD, where one has a gas above the critical temperature but at densities comparable to those existing in the liquid state. The necessary density data were taken from Michels *et al.*[10,11]

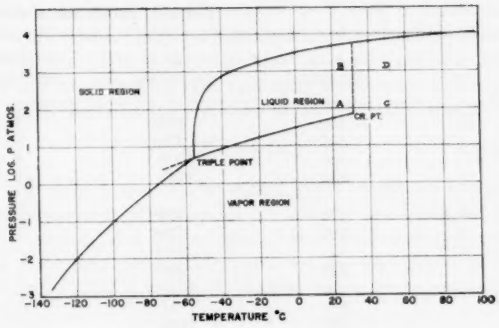

FIG. 2. Phase diagram of CO_2.

In order to apply Eq. (2) correctly one must also measure the velocity throughout the dispersion region. However, in using the present technique, it was found that the uncertainty in any particular velocity reading was comparable to the total dispersion. Hence the following procedure was used to correct for the dispersion. Initially, the effects of dispersion were neglected by assuming $v=v_0$ in Eq. (2) and thus a first approximation to the effective relaxation frequency (f_0') was achieved. This value was then used, together with a knowledge of the low-frequency velocity V_0 and the dispersion ratio V_∞/V_0,[12] to estimate the velocity at any given frequency from the relation

$$\frac{(f/f_0')^2}{1+(f/f_0')^2}=\frac{V^2-V_\infty^2}{V_\infty^2-V_0^2}\left(\frac{V_\infty}{V}\right)^2. \tag{5a}$$

Knowing the approximate frequency dependence of the velocity, one can now plot Eq. (2) taking the dispersion into account. The values of the intercept I and the effective relaxation frequency f_0 reported in Table I are the corrected values. The values of the low frequency velocity v_0 in the high density region were taken by the authors and those at lower densities were taken by Henderson *et al.*[13] Together, they constitute the only velocity data available in the high density region.

It should be noted that an error in the low-frequency velocity v_0 does not directly affect the corrected effective relaxation frequency since it appears in the same manner in both the intercept and slope of Eq. (3).

In column 6 of Table I the relaxing vibrational specific heat C' obtained at each density point is tabulated. The uncertainty in the value of C' is directly related to any uncertainty in the low-frequency velocity v_0. If one assumes that the vibrational specific heat is independent of density, then the average value of C'

[8] A. Michels and S. R. De Groot, Appl. Sci. Research **A1**, 94 (1948).

[9] E. L. Quinn and C. L. Jones, *Carbon Dioxide* (Reinhold Publishing Company, New York, 1936), p. 63.

[10] A. Michels and C. Michels, Proc. Roy. Soc. (London) **A153**, 201 (1936).

[11] A. Michels, C. Michels, and H. Wouters, Proc. Roy. Soc. (London) **A153**, 214 (1936).

[12] W. E. Farrel, M.A. thesis, Catholic University (1957).

[13] M. C. Henderson (private communication).

TABLE I. Tabulation of various relaxation parameters in CO_2.

T°C	ρ amagats	v_0 meters/sec	$I\times10^{-7}$ (mc²/neper)	f_0 (mc)	C'	f_r (mc)
25	460	595[a]	3.2	13.5	2.54	12.1
	540	900[a]	6.2	19.7	2.47	17.2
	580	1090	8.4	24.1	2.51	20.8
	610	1240	11.2	29.1	2.49	25.2
50.2	400	464[a]	2.6	13.4	2.46	12.1
	480	720[a]	4.5	19.1	2.42	16.7
	520	876[a]	6.4	22.5	2.25	19.5
	540	960	7.4	25.1	2.30	21.7
	576	1124	10.0	30.6	2.33	26.4
	580	1142	10.0	30.6	2.33	26.4
	588	1180	11.2	32.4	2.24	27.8

[a] Footnote 13.

at 50.2° is 2.33. This agrees well with the 2.35 result observed by Henderson[5] at the same temperature. Both values are slightly higher than the 2.21 predicted by Wooley.[14] The average value of C' at 25°C is 2.50, and the theoretical value given by Wooley is 1.97. It is not understood why the average value of C' is higher in the liquid at a lower temperature than in the dense gas at a higher temperature. This result may be due to experimental error, although the authors believe this is not the explanation.

IV. COMPARISON OF DATA TO GAS KINETIC THEORY PREDICTIONS

The time it takes the internal degrees of freedom (the vibrational mode in the case of CO_2) to return from an excited state to equilibrium with the external degrees of freedom is called the "relaxation time," τ. This thermal relaxation time in the case of binary collisions may be expressed by

$$\tau=1/\bar{N}P^*, \tag{6}$$

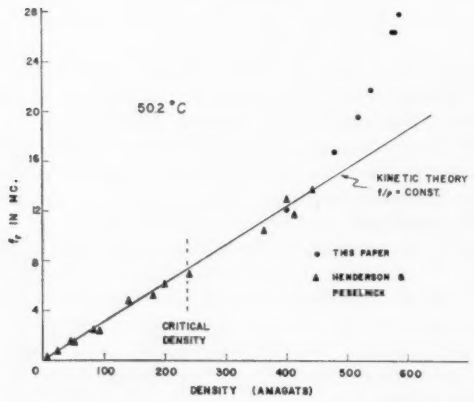

FIG. 3. Plot of the relaxation frequency vs amagat density for CO_2 at 50.2°C.

[14] H. W. Wooley, J. Research Natl. Bur. Standards **52**, 289 (1954).

where $\tau=1/(2\pi f_r)$, $\bar{N}$ is the number of collisions per second, and P^* the total probability that a collision is effective in producing a vibrational energy transfer to translational energy (or transition probability).

For the number of collisions per second we may use

$$\bar{N}=\bar{v}/L_f, \tag{7}$$

where L_f is the mean free path and $\bar{v}$ is the average velocity of the molecules.

When considering the gas kinetic theory we shall in all cases use the results of the Sutherland model which gives,

$$L_f=[\sqrt{2}\pi\sigma^2\rho(1+C/T)]^{-1} \tag{8}$$

and

$$\bar{v}=(8RT/\pi M)^{\frac{1}{2}}, \tag{9}$$

where σ is the hard-sphere molecular diameter, ρ the molecular density, and C is the Sutherland constant. If one assumes that the collision efficiency P^* is independent of density (this is reasonable since for low density it should only depend on the mechanics of the collision involved and not on surroundings), then by Eqs. (6)–(9) we see that gas kinetic theory predicts that

$$f_r/\rho=\text{constant}. \tag{10}$$

Henderson and Peselnick[4] have measured the relaxation frequency in gaseous CO_2 at 50.8°C up to 440 amagats, from which they conclude that f_r/ρ is constant at a value of 30.9 kc/a.u. over the entire range of densities. The amagat unit is defined as the ratio of the density to the density at standard conditions.

Figure 3 shows the relaxation frequencies of Table I at 50.2° plotted against the density expressed in amagats. At this temperature the CO_2 remains a gas over the entire density range covered. Included in the graph are the values reported by Henderson and Peselnick.[4] The critical density occurs at 237 a.u. The straight line is that of Henderson and Peselnick $f_r/\rho=30.9$ kc/a.u.

The data indicate that there is a large departure from the gas kinetic theory ($f_r/\rho=$ const) in the high-density region above 400 a.u. Furthermore, this departure is in the same direction and of the same general

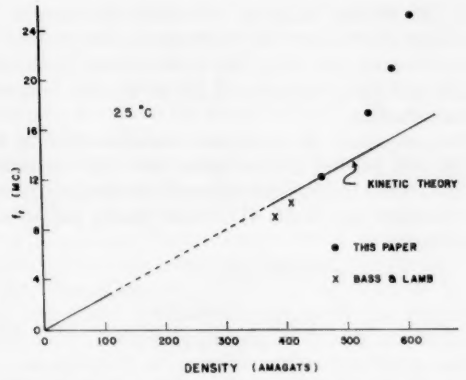

FIG. 4. Plot of the relaxation frequency vs amagat density for CO_2 at 25°C.

shape as that obtained by Litovitz, Carnevale and Kendall[15] for liquid CS_2. One also concludes that Henderson and Peselnick, limited to 10 000 psi by their pressure vessel, could not go to high enough densities to observe this deviation.

In Fig. 4 we see the same type of deviation from the gas kinetic theory in the liquid state. The discontinuity in the density that occurs when liquifying the gas is from 120–380 a.u. The straight line $f_r/\rho = 26.35$ kc/a.u. is the gas value reported by Shields[16] for CO_2 at 25°C.

V. EVALUATION OF COLLISION TIMES IN THE LIQUID AND DENSE GAS

If one assumes that only binary collisions and not the cooperative action of molecules are important, then Eq. (6) holds for the liquid and dense gas as well as for the normal gas state. It is in the evaluation of $\bar{N}$ for the liquid or dense gas that we encounter difficulty. Two possible approaches in evaluating $\bar{N}$ will be discussed. The first attempts to calculate the ratio of the collision frequency $\bar{N}$ in the gas and liquid states directly from P-V-T data using the Enskog theory. The latter approach proposes a modified cell model for the liquid state which allows a direct calculation of the mean free path.

(1) Use of Enskog Theory to Predict $\bar{N}$

Enskog has successfully used a semiempirical extension of his rigid-sphere theory to predict the viscosity of dense gases.[17] He assumes that a dense gas is made up of rigid spherical molecules of diameter σ and that only binary collisions take place. Because of these assumptions two effects become important when considering dense gases: (a) there is an instantaneous transport energy and momentum during a collision and (b) the frequency of collisions is increased because of the finite size of the molecules and decreased because of the shielding of one molecule by others. Enskog derives the following equation of state for rigid spheres

$$pv/RT = 1 + (b_0/v)\,Y, \tag{11}$$

where $b_0 = (\frac{2}{3})\pi n\sigma^3$ is the second virial coefficient and n is the number of molecules per mole, p the pressure, v the volume, and Y the ratio of the collision frequency in the dense gas to that given by gas kinetic theory, Eq. (8). The quantity Y is unity for a dilute gas and increases with increasing density. Enskog suggests that in the case of a real gas the pressure p in Eq. (11) be replaced by the "thermal pressure," $T(\partial p/\partial T)_v$. Hence the dimensionless quantity

$$y \equiv (b_0/v)Y = (v/RT)[T(\partial p/\partial T)_v] - 1 \tag{12}$$

may be evaluated from the experimental P-V-T data. This quantity is by definition related to f_a, the relaxation frequency for hard spheres in the dense gas by

$$y = (b_0/v)\,(\bar{N}_a/\bar{N}_b) = (b_0/v)\,(P_b^*/P_a^*)\,(f_a/f_b), \tag{13}$$

where the subscript a refers to the value in the dense gas and b to that given by gas kinetic theory, Eq. (8). Dividing both f_a and f_b by the molecular density and using the kinetic theory Eq. (10) ($f_b/\rho = K$) we find that

$$y = K^{-1}(b_0/v)\,(P_b^*/P_a^*)\,(f_a/\rho) = (\tfrac{2}{3})\pi K^{-1}\sigma^3(P_b^*/P_a^*)f_a, \tag{14}$$

where $b_0/(v\rho) = (\frac{2}{3})\pi\sigma^3$, σ is the molecular diameter and K is the constant in Eq. (10). If we assume that at high densities the ratio of the collision efficiencies is independent of pressure, then we may write

$$y = Cf_a, \tag{15}$$

where C is a constant.

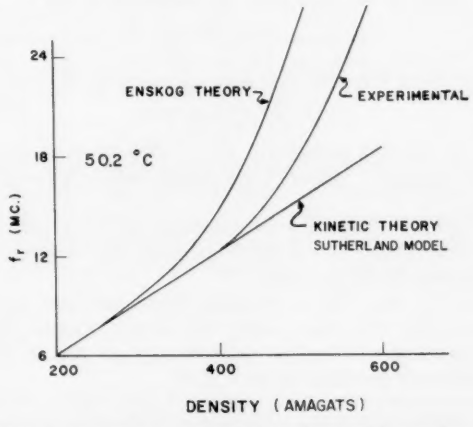

FIG. 5. Comparison of the Enskog theory with experimental results.

[15] T. A. Litovitz, E. H. Carnevale, and P. A. Kendall, J. Acoust. Soc. Am. **26**, 465 (1956).
[16] F. D. Shields, J. Acoust. Soc. Am. **29**, 450 (1956).
[17] J. O. Hirschfelder, C. F. Curtiss, and R. B. Bird, *Molecular Theory of Gases and Liquids* (John Wiley & Sons, Inc., New York, 1954).

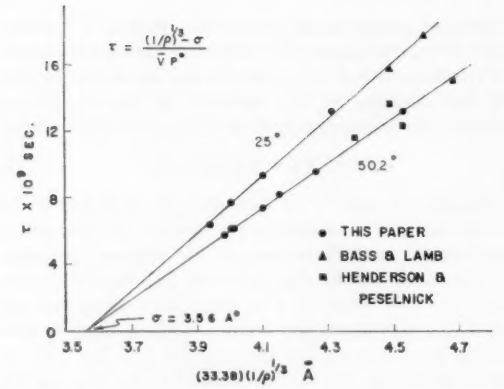

FIG. 6. Plot of relaxation time vs the mean distance between molecular centers in A for CO_2 at 25 and 50.2°C.

The procedure followed was to calculate y from the P-V-T data and then to adjust the constant, C, in Eq. (15) so that experiment and theory agree at some given density. The results of fitting the data and experiment at the critical density[18] are shown in Fig. 5. We see that values of f_a calculated using the Enskog theory are in poor agreement with the experimental values of the relaxation frequency at high densities.

(2) Use of Cell Model to Calculate L_f

A rigid-sphere model of the liquid state has been proposed by Eyring and Hirschfelder.[17] For short intervals of time the thermal motions of a molecule of diameter σ are assumed to be confined within a shell-like arrangement of nearest neighbors. Assuming that all molecules occupy the lattice points of a cubic cell the center molecule or "wanderer" is free to move a distance of $2(V/N)^{\frac{1}{3}}-2\sigma$, where V is the volume, N the number of molecules in that volume, σ the diameter of the rigid sphere molecule, and $(V/N)^{\frac{1}{3}}=(1/\rho)^{\frac{1}{3}}$ the mean distance between molecular centers. The mean free path for the fixed wall cell model is given by

$$L_f=2[(1/\rho)^{\frac{1}{3}}-\sigma]. \tag{16}$$

Combining Eq. (16) with Eqs. (6) and (7), we have

$$\tau=(2/\bar{v}P^*)[(1/\rho)^{\frac{1}{3}}-\sigma]. \tag{17}$$

If the collision probability P^* is independent of pressure, a plot of τ versus $(1/\rho)^{\frac{1}{3}}$ should result in a straight line.

Figure 6 shows the experimental data for carbon dioxide plotted in the above manner. Two important observations can be made.

1. The data fit the straight lines extremely well; hence, Eq. (17) does predict the correct pressure dependence in CO_2 for both high-density gas and in the liquid state just as it did for CS_2.[15]

2. The abscissa intercept is a direct measurement of the molecular diameter σ. Furthermore, since both lines have the same intercept, this value is identical for the liquid and highly compressed gas at the two temperatures measured.

Not only does the molecular diameter agree in the liquid and gas but it also agrees with that predicted by the kinetic theory hard-sphere Sutherland equation[19] for viscosity (see Table II). From kinetic theory one has that

$$\eta=0.499m\rho\bar{v}L_f$$
$$=0.499\frac{2(\pi mkT)^{\frac{1}{2}}}{\pi^2\sigma^2(1+C/T)}, \tag{18}$$

where η is the viscosity, m the mass per molecule, $\bar{v}$ the average velocity, and C Sutherland's constant. Both Sutherland's constant and the molecular diameter may be calculated by use of Eq. (18) and a knowledge of the viscosity at two different temperatures.

In Fig. 7 are plotted several curves of the mean free path L_f divided by the molecular diameter σ as a function of the amagat density. The upper is determined from the cell model [Eq. (16)], and the middle is

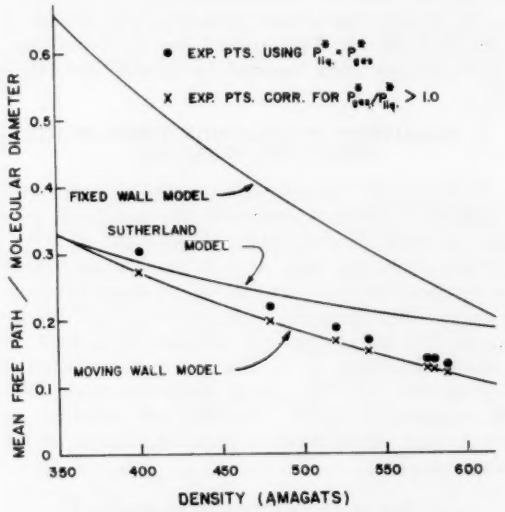

FIG. 7. Comparison of the mean free path divided by the molecular diameter as a function of density predicted by kinetic theory [Eq. (8)], fixed wall cell model [Eq. (16)], and modified cell model [Eq. (24)]. Included are experimental data assuming $P^*_{liq}=P^*_{gas}$ and the same data corrected for the fact that $P^*_{liq}\neq P^*_{gas}$.

[18] Enskog suggested that b_0 be evaluated by fitting the minimum in the curve of η/ρ, where η is the viscosity, as a function of y. This occurs at the critical density.

[19] Collision diameters obtained from the hard sphere cell model theory should not be directly compared with those listed by Hirschfelder, who used a function $\Omega^{(2,2)*}$ in place of $1+C/T$. This is because Hirschfelder's viscosity relation is not for hard spheres, but rather for a Lennard-Jones molecule that has a repulsive term varying with the intermolecular distance. To be consistent one must compare the effective hard sphere collision diameters obtained from the cell model theory with those obtained from the attracting hard sphere viscosity relation of Sutherland.

determined from gas kinetic theory (Sutherland model). The two sets of points are experimental values of L_f/σ obtained from acoustic data by (a) assuming $P^*_{\text{liq}} = P^*_{\text{gas}}$ and (b) correcting for the fact that attractive forces play no role in the liquid and thus $P^*_{\text{gas}}/P^*_{\text{liq}} > 1.0$. (See Sec. VI.)

One finds that even though the cell model predicts a density dependence in agreement with experimental values, the magnitude of $(L_f/\sigma)_{\text{cell}}$ is larger than $(L_f/\sigma)_{\text{acoustic data}}$. The Sutherland model though giving better agreement in magnitude does not give the proper density dependence of (L_f/σ). The fact that the fixed wall cell model predicts so accurately the pressure dependence of the relaxation time causes one to look for a modification of the cell model rather than propose an entirely new model.

(3) Modification of the Cell Model for Movable Walls

A description of the liquid state in terms of fixed wall cells is somewhat unrealistic. A better approximation would be that of a wandering molecule trapped in not fixed, but moving walls. Each nearest molecule that makes up the cubic cell is itself a "wanderer" which is in turn trapped within a moving wall cage made up of its nearest neighbors.

These ideas are clarified if one considers the one-dimensional array of molecules shown in Fig. 8. If we fix our attention on any one molecule, then the average length the molecule will travel before suffering a collision (the mean free path) is given by

$$L_f = \sum_{j=1}^{\infty} p_j l_j, \tag{19}$$

where l_j is the jth distance a particles moves and p_j is the probability that the given molecule will move the distance l_j. A few of the different possibilities are shown in Fig. 8.

If one assumes that the black molecule (n_0) moves to the right, two different situations may occur. If the nearest neighbor n_1 goes to the left, the black molecule will move a distance $l_1 = \delta/2$ before it suffers a collision and the probability of this occurring is $p_1 = \frac{1}{2}$. If n_1 goes to the right, there are two additional possibilities. With n_1 moving to the right, n_2 may move to the left. If this happens, the black molecule (n_0) will move a distance of $l_2 = \delta$ before it suffers a collision. The probability of this event taking place is $p_2 = \frac{1}{4}$. If, however, n_2 moves to the right, we must consider the motion of n_3. If n_3 moves to the left, $l_3 = (\frac{3}{2})\delta$ and $p_3 = \frac{1}{8}$; or to the right, $l_4 = 2\delta$ and $p_4 = \frac{1}{16}$. The same procedure is followed until all possibilities are taken into account. One soon sees that the distance l_j follows the relation

$$l_j = (j/2)\delta$$

and the probabilities p_j become

$$p_j = (\tfrac{1}{2})^j. \tag{20}$$

FIG. 8. First four possible motions of a linear array of free molecules. In each case the distance moved is given by l_j and the probability of moving that distance l_j is given by p_j.

Thus the mean free path is

$$L_f = \sum_{j=1}^{\infty} (\tfrac{1}{2})^j (j/2)\delta = (\delta/4) \sum_{j=1}^{\infty} j(\tfrac{1}{2})^{j-1}. \tag{21}$$

To evaluate the sum one uses the relation

$$\sum_{j=1}^{\infty} j x^{j-1} (d/dx) \sum_{j=1}^{\infty} x^j = (d/dx)\left(\sum_{j=0}^{\infty} x^j - 1\right)$$
$$= (d/dx)[(1-x)^{-1} - 1] = 1/(1-x)^2; \quad (x^2 < 1). \tag{22}$$

Letting $x = \frac{1}{2}$ one obtains

$$L_f = (\delta/4)[1/(1-\tfrac{1}{2})^2]$$

or

$$L_f = \delta.$$

If the first collision takes place at the value l_j, one would also like to know what is the probable value of the mean free path of the particle for the next collision. In order to calculate this one follows exactly the same procedure and finds, for example, that given $l_1 = \delta/2$,

$$(L_f \mid l_1 = \tfrac{1}{2}\delta) = \tfrac{1}{2}\cdot\tfrac{1}{2}\delta + [\tfrac{1}{2}\cdot\tfrac{1}{2}\cdot\delta + \tfrac{1}{2}\cdot\tfrac{1}{2}\cdot\tfrac{1}{2}(3\delta/2) + \cdots]$$

or in the limit

$$(L_f \mid l_1 = \delta/2) = \delta. \tag{23}$$

The same result is found for $l_1 = \delta, (\frac{3}{2})\delta, \cdots$. This says that the mean free path is the same after each successive collision (i.e., it has no memory of its past). Thus in all cases the mean free path is given by

$$L_f = \delta = (\bar{x} - \sigma),$$

where $\bar{x}$ is the average distance between molecular centers. This may be extended to a three-dimensional model by replacing $\bar{x}$ by $(V/N)^{\frac{1}{3}}$ the average distance between molecular centers in a cubic lattice. Hence the mean free path in three dimensions is given by

$$L_f = [(1/\rho)^{\frac{1}{3}} - \sigma]. \tag{24}$$

Thus

$$\tau = [(1/\rho)^{\frac{1}{3}} - \sigma]/\bar{v}P^*, \tag{25}$$

where $(1/\rho) = (V/N)$. Thus the moving wall model gives a value of L_f which is one-half the value obtained from the fixed wall cell model. It does, however,

TABLE II. Comparison of collision efficiencies of the liquid and dense gas with the dilute gas.

	T°C	$\sigma_{\text{cell model}}$ (A)	$\sigma_{\text{Sutherland}}$ (A)	P^*_{gas}	$(P^*_{\text{gas}}/P^*_{\text{liq}})_{\text{exp}}$	$1+(C/T)$	$\exp[\epsilon(KT)]$	$(P^*_{\text{liq}})_{\text{cal}}$	$(P^*_{\text{liq}})_{\text{exp}}$
CO_2	25	3.56±0.02	3.54[a]	1.75[b,c]	1.1	1.67	1.89	1.55[b]	1.54[b]
CO_2	50.2	3.56±0.02	3.54	2.08[d]	1.1	1.62	1.80	1.87	1.88
CS_2	25	4.32[e]	4.13[f]	10.9[g]	2.5	2.53	5.14	5.4	4.4[h]

[a] Calculated by Eq. (18) and viscosity data of footnote 17.
[b] All values should be multiplied by 10^{-6} sec^{-2}.
[c] Footnote 16.
[d] Footnote 4.
[e] Footnote 2.
[f] Calculated by Eq. (18) and viscosity data of *Handbook of Chemistry and Physics* (Chemical Rubber Publishing Company, Cleveland, Ohio, 1949), p. 1763.
[g] F. A. Angona, J. Acoust. Soc. Am. **25,** 1116 (1954).
[h] Application of the modified cell model using $\sigma=4.32$ (see footnote 2) to the liquid data of J. H. Andreae, E. L. Heasell, and J. Lamb, Proc. Phys. Soc. (London) **B69,** 625 (1956).

yield the same molecular diameter, σ, and pressure dependence of relaxation frequency as the fixed wall cell model discussed in Sec. V.

The lowest curve in Fig. 7 is that of L_f/σ, calculated from Eq. (24). The 10% agreement between Eq. (24) and the "circled" experimental points is satisfactory considering the assumption made ($P^*_{\text{gas}}=P^*_{\text{liq}}$) in calculating the experimental values of L_f/σ. Actually, it is shown in Sec. VI that P^*_{liq} should not be equal to P^*_{gas} because attractive forces have much less effect in the liquid than in the dilute gas. Taking the results of Sec. VI into consideration gives the excellent agreement shown by the "corrected" values of $(L_f/\sigma)_{\text{exp}}$.

One interesting result is that the Sutherland model mean free path is close to the cell model value over a surprisingly large range of moderate densities. For CO_2 these two theories predict values of L_f which agree within 5% over a range of densities from 150 to 350 amagats. This accounts for the results of Henderson and Peselnick[4] who found that the kinetic theory mean free path gave good results up to approximately twice the critical density. As one continues to go up in pressure, the gas kinetic theory value based on the Sutherland model is no longer appropriate and one must go over to the cell model theory. The cell model, of course, breaks down at low densities when a given molecule is no longer effectively trapped in a cage.

VI. COMPARISON OF TRANSITION PROBABILITIES IN THE LIQUID AND DENSE GAS VERSUS THE DILUTE GAS

The modified cell model correctly predicts the pressure dependence of the relaxation time and gives an acceptable value of the mean free path in the liquid. It also enables us to make a calculation of the transition probability in the liquid or dense gas. Using Eq. (25) the transition probability, P^*, may be calculated from the average velocity and the slope of the lines in Fig. 6. Values obtained in this manner are compared with the appropriate gas transition probabilities in Table II. The gas transition probabilities were calculated from ultrasonic data, the viscosity relation,

$$\eta=1.271 p t_c \tag{26}$$

and

$$P^*_{\text{gas}}=t_c/\tau, \tag{27}$$

where $t_c=1/\bar{N}$ is the time between collision, η the viscosity in poise and p the pressure in dynes per cm^2. A similar comparison is listed for CS_2. For CO_2 the transition probabilities P^*_{gas} and P^*_{liq} agree within 10%; however, in CS_2 the agreement is not good. In both CS_2 and CO_2 the transition probabilities P^*_{gas} are larger than P^*_{liq}.

Litovitz[2] has suggested that the attractive forces probably do not play a role in determining P^*_{liq}, and therefore this could account for the difference between P^*_{gas} and P^*_{liq}. Schwartz and Herzfeld[1] have calculated the following expression for P^* in the gas state,

$$P^*=(1.294)(r_c/r_0)^2\frac{1}{Z_0 Z_{\text{osc}} Z'_{\text{tr}}}\frac{\exp[\epsilon/(kT)]}{1+C/T} \tag{28}$$

with the abbreviations

$$Z_{\text{osc}}=\frac{M_B M_C(M_A+M_B+M_C)}{(M_B{}^2+M_C{}^2)M_A}(1/\pi^2)(\theta'/\theta)$$

and

$$Z'_{\text{tr}}=\pi^2(\theta/\theta')^2(3/2\pi)^{\frac{1}{2}}(T/\theta')^{1/6}\exp[\tfrac{3}{2}(\theta'/T)^{\frac{1}{3}}-(\theta/2T)],$$

where C is Sutherland's constant, r_c is the distance of closest approach, r_0 is the zero of the Lennard-Jones curve, ϵ is the depth of the Lennard-Jones potential well, $\theta=h\nu/k$, $\theta'=0.8153\,M\theta^2 l^2$, the M's are the molecular weights of the triatomic molecule, l is the characteristic length of the vibrator which is around 0.2 A, and Z_0 is a geometrical factor approximately equal to three. Further explanation may be found in the text of footnote 1.

If the thermal relaxation mechanism is the same in the liquid as in the gas, then Eq. (28) is applicable in the liquid state except that the factors $(1+C/T)^{-1}$

and $\exp[\epsilon/(KT)]$ are not needed. The Sutherland correction factor $(1+C/T)^{-1}$ accounts for the long-range attractive forces which cause collisions between slow moving molecules that otherwise would not have collided. The factor $\exp[\epsilon/(KT)]$ accounts for the increased effective collision velocity arising from the presence of attractive forces. These factors are not effective in the liquid state since molecules are too close for these attractive forces to play a role. Thus one should write,

$$P^*_{\text{liq}} = P^*_{\text{gas}} \frac{1+C/T}{\exp[\epsilon/(KT)]}, \tag{29}$$

where P^*_{liq} should be the same as the value of P^* for dense gas. If this assumption is correct, one can calculate the expected P^*_{liq} or $P^*_{\text{dense gas}}$ if the value of P^*_{gas} is known. The calculated liquid values are listed in Table II. Excellent agreement is found between $(P^*_{\text{liq}})_{\text{cal}}$ and $(P^*_{\text{liq}})_{\text{exp}}$ for both CO_2 and CS_2. The effect of the attractive forces in CO_2 is only 10% while in CS_2 it is over 100%. Application of this correction to the data for CO_2 resulted in the excellent agreement between experimental and modified cell model mean free paths shown in Fig. 7.

One can now attempt to understand the results of Bass and Lamb.[3] They have measured the relaxation times of several substances in the liquid state. Following Henderson they assumed that the relaxation frequency was still proportional to the density even up into the liquid state. This would mean that the product $(\rho\tau)_{\text{liq}}$ would be a constant. Using the data of other investigators in the gas state they calculated the ratio $(\rho\tau)_{\text{liq}}/(\rho\tau)_{\text{gas}}$. This was found to be consistently greater than 1.0 for the substances considered. When considering their calculations one should note that Bass and Lamb did not go to a region of sufficiently high density for the actual mean free path to deviate significantly from the kinetic theory value. This alone would limit their results to $(\rho\tau)_{\text{liq}} \simeq (\rho\tau)_{\text{gas}}$. However, at the densities they reached the molecules are nevertheless close enough so that the attractive forces no longer play an important role. Therefore, one can write, (since at these densities $\rho_{\text{liq}}/\rho_{\text{gas}} \cong L_{\text{gas}}/L_{\text{liq}}$)

$$(\rho\tau)_{\text{liq}}/(\rho\tau)_{\text{gas}} = (\rho_{\text{liq}} P^*_{\text{gas}}/\rho_{\text{gas}} P^*_{\text{liq}})(L_{\text{liq}}/L_{\text{gas}}) \cong P^*_{\text{gas}}/P^*_{\text{liq}}. \tag{30}$$

Thus in this region of densities the ratio of

$$(\rho\tau)_{\text{liq}}/(\rho\tau)_{\text{gas}}$$

is larger than 1.0 owing to the change in the role of attractive forces in going from gas to dense gas or liquid and not to a failure in the cell model theory.

A further interesting finding of Bass and Lamb is the indication that in SO_2 where one has two vibrational relaxation times present their respective ratios $(\tau_{\text{gas}}/\tau_{\text{liq}})$ are not the same. This conclusion is open to some question because of the difficulty in getting good values for both relaxation times in the gas phase. Recent measurements by Henderson[20] cast some doubt on the original gas data obtained by Lambert and Salter[21] and used by Bass and Lamp to make this comparison.

SUMMARY

Measurements of ultrasonic absorption and velocity in CO_2 were made over a density range from 400 to 610 amagats at 25°C and 50.2°C. Large departures from the gas kinetic theory assumption that $f_r/\rho =$ const were found in this density region. Use of the Enskog theory for calculating the collision times in the dense phase showed this theory to be inadequate to account for the data.

A modified version of the Eyring-Hirschfelder cell model was found to give an excellent fit to the data. This modification consists of allowing the walls to move back and forth rather than be fixed. Good agreement was found between the collision efficiencies of both CS_2 and CO_2 in the gas and liquid phase when the effect of attractive forces was taken into account.

[20] M. C. Henderson, International Congress on Acoustics Stuttgart (1959).

[21] J. D. Lambert and R. Salter, Proc. Roy. Soc. (London) **A243**, 78 (1957).

Energy Levels for Internal and Over-All Rotation of Two-Top Molecules. I. Microwave Spectrum of Dimethyl Silane*

LOUIS PIERCE

Department of Chemistry, University of Notre Dame, Notre Dame, Indiana

(Received August 15, 1960)

A method is given for analyzing barrier-dependent "tunnel effect" splittings in rotational spectra of molecules with two equivalent tops. The perturbation treatment is an extension of the "principal axis" method for single-top molecules, and is limited to torsional states in which the two principal torsional quantum numbers are identical. Tables of perturbation coefficients are given from which the effects of top-top coupling on the rotational spectrum may be calculated. The microwave spectra of six isotopic species of dimethyl silane have been investigated in the region 8 to 25 kMc. Changes in moments of inertia with isotopic substitution yield the following structural parameters:

SiC	1.867±0.002 A	CSiC	110°59′±10′
SiH	1.483±0.005 A	HSiH	107°50′±20′
CH	1.095±0.005 A	HCH	108°0′±20′,

$2\theta = 110°59' \pm 1°$,

where 2θ is the angle between the symmetry axes of the methyl groups. From splittings in the rotational spectrum the angle 2θ is found to be 110°50′±20′. Analysis of splittings for $(CH_3)_2SiH_2$, $(CH_3)_2SiD_2$, and $(CH_3)(CD_3)SiH_2$ indicates that coupling between tops is very small. Assuming *no* coupling, the barrier to internal rotation is 1647±3 cal/mole. From Stark effect measurements the dipole moment is found to be 0.75±0.01*D*.

THE results of a large number of microwave studies[1] of single-top asymmetric rotor molecules, such as acetaldehyde (CH_3CHO), have demonstrated that by far the most important mechanism for the production of barrier-dependent "tunnel effect" splittings in the rotational spectrum is that of coupling between angular momenta of internal and over-all rotation. A rather elegant and very practical method for the analysis of rotational spectra of single-top molecules has been developed by Wilson and his co-workers.[2] This method, sometimes referred to as the "principal axis" method, treats top-frame coupling by perturbation theory, and because the necessary perturbation sums have been extensively tabulated,[2b,3] it has the great advantage that much of the analysis of spectra can be carried out by using standard techniques and tables developed for rigid asymmetric rotor molecules.

The present work is the first of a series of papers which will deal with the problem of analyzing "tunnel-effect" splittings in the rotational spectra of two-top molecules such as dimethyl silane [$(CH_3)_2SiH_2$] and ethyl silane ($CH_3CH_2SiH_3$). These molecules have a unique feature not present in single-top molecules; the possibility of coupling between tops as well as between tops and frame. In our approach to the two-top problem, we try to make as much use as possible of the theory and tables[2b,3] developed for single-top molecules. This objective requires in the zeroth order that the tops be independent, so that our treatment is limited to cases where top-top coupling is relatively "weak."

In this paper consideration is limited to rotational spectra arising from torsional states (of molecules with equivalent tops) in which the two principal torsional quantum numbers are identical (vv states). The results given here will be in part applicable to, but not adequate for, torsional states in which the two principal torsional quantum numbers are different (vv' states). Work on the vv' problem is in progress and will be reported in IV of this series. Numbers II and III will deal with the analysis of rotational spectra of the two kinds of molecules with nonequivalent tops; (a) $(CH_3)(CD_3)$S-type molecules,[4] and (b) $CH_3CH_2SiH_3$-type molecules.[5] In so far as vv states of molecules with equivalent tops are concerned, Swalen and Costain have already shown that in the absence of top-top coupling, analysis of rotational spectra requires only single-top perturbation coefficients.[6] In this work the effects of top-top coupling in both the kinetic and

* This research was made possible by a grant from the National Science Foundation.

[1] For literature references and summaries of microwave barrier studies, see E. B. Wilson, Jr., Proc. Natl. Acad. Sci. U. S. **43**, 816 (1957), "The Problem of Barriers to Internal Rotation in Molecules," *Advances in Chemical Physics* (Interscience Publishers, Inc., New York, 1959), Vol. II; C. C. Lin and J. D. Swalen, Revs. Modern Phys. **31**, 841 (1959).

[2] (a) R. W. Kilb, C. C. Lin, and E. B. Wilson, Jr., J. Chem. Phys. **26**, 1695 (1957); (b) D. R. Herschbach, J. Chem. Phys. **31**, 91 (1959).

[3] (a). D. R. Herschbach, *Tables for the Internal Rotation Problem* (Department of Chemistry, Harvard University, Cambridge, Massachusetts, 1957); J. Chem. Phys. **27**, 975 (1957); (b) R. W. Kilb, *Tables of Degenerate Mathieu Functions* (Department of Chemistry, Harvard University, Cambridge, Massachusetts, 1956). Copies of these tables are available on request to Professor E. B. Wilson, Jr.

[4] M. Hayashi and L. Pierce, Symposium on Molecular Structure and Spectroscopy, Ohio State University (1960).

[5] D. H. Petersen and L. Pierce, Symposium on Molecular Structure and Spectroscopy, Ohio State University (1960).

[6] J. D. Swalen and C. C. Costain, J. Chem. Phys. **31**, 1562 (1959). See also P. Kasai and R. J. Myers, *ibid.* **30**, 1096 (1959).

potential energy are considered.[7] The effects of coupling in the kinetic energy are shown to be expressable in terms of products of tabulated[2b] single-top perturbation sums, and also quite often to be completely negligible. Perturbation sums from which the effects of coupling in the potential energy can be calculated have been evaluated. The theoretical results are applied to the analysis of the rotational spectrum of dimethyl silane.

I. THEORY

1. Notation

$g=x, y, z$ refers to principal axes of the entire molecule.

I_g = principal moments of inertia of the entire molecule.

I_α = moment of inertia of either internal top about its symmetry axis.

λ_{gk} = direction cosines between kth top and the principal axes.

$$r=1-\sum_g \lambda_{gk}^2 I_\alpha/I_g, \qquad (k=1 \text{ or } 2).$$

$$q=-\sum_g \lambda_{g1}\lambda_{g2} I_\alpha/I_g.$$

P_g = components of the total angular momentum along the principal axes.

p_k = total angular momentum of kth top along its symmetry axis.

$$\mathcal{P}_k=\sum_g P_g \lambda_{gk} I_\alpha/I_g.$$

v_k = principal torsional quantum number of the kth top.

σ_k = a symmetry index giving the periodicity of the torsional wave function for the kth top.

α_k = angle of internal rotation for kth top.

2. Model and Hamiltonian

The model adopted for molecules such as $(CH_3)_2SiH_2$ or $(CH_3)_2S$ consists of two equivalent rigid symmetric tops attached, with symmetry axes not coincident, to a rigid asymmetric framework. There are then, five degrees of freedom; three for over-all rotation and two for internal torsion or rotation. The kinetic energy[2b,8] for the model may be written as (see Notation above)

$$H_r+F[(p_1-\mathcal{P}_1)^2+(p_2-\mathcal{P}_2)^2]+F'[(p_1-\mathcal{P}_1)(p_2-\mathcal{P}_2)+(p_2-\mathcal{P}_2)(p_1-\mathcal{P}_1)], \quad (1)$$

where H_r is the rigid rotor Hamiltonian

$$H_r=aP_x^2+bP_x^2+cP_y^2, \qquad (I^r). \quad (2)$$

The quantities $p_1-\mathcal{P}_1$ and $p_2-\mathcal{P}_2$ represent, respectively, the angular momenta of tops 1 and 2 relative to the framework. F and F' are inverse reduced moments of inertia for internal rotation and are conveniently defined by the equation

$$F_\pm=F\pm F'=\hbar^2/2(r\pm q)I_\alpha. \quad (3)$$

The tops are assumed to have threefold symmetry so that the Fourier expansion of the potential energy gives

$$V(\alpha_1,\alpha_2)=V_0+\tfrac{1}{2}V_3(2-\cos 3\alpha_1-\cos 3\alpha_2)+V_3'\cos 3\alpha_1\cos 3\alpha_2+V_3''\sin 3\alpha_1\sin 3\alpha_2+\text{terms in } 3n\alpha_1,\ 3n\alpha_2; \qquad n=2,3,\cdots. \quad (4)$$

Implicit in the perturbation treatment described below are the assumptions that: (a) terms in $V(\alpha_1,\alpha_2)$ having higher than threefold symmetry in α_1 or α_2 are negligibly small,[9] (b) the barrier to internal rotation is relatively high so that top-frame coupling may be treated as a perturbation, (c) $V_3'\ll V_3^*$, $V_3''\ll V_3^*$ and, $F'\ll F$, where $V_3^*=V_3-2V_3'$, so that top-top coupling terms as well may be treated by perturbation theory. With these assumptions a very appropriate form for the Hamiltonian is

$$H=H_r+2F_+(p_+-\mathcal{P}_+)^2+2F_-(p_--\mathcal{P}_-)^2+\tfrac{1}{2}V_3^*(2-\cos 3\alpha_1-\cos 3\alpha_2)+V_3'(1-\cos 3\alpha_1)(1-\cos 3\alpha_2)+V_3''\sin 3\alpha_1\sin 3\alpha_2, \quad (5)$$

where

$$\mathcal{P}_\pm=\tfrac{1}{2}(\mathcal{P}_1\pm\mathcal{P}_2),$$

and

$$p_\pm=\tfrac{1}{2}(p_1\pm p_2).$$

Except for the occurrence of top-frame coupling terms $-4F_\pm p_\pm \mathcal{P}_\pm$ the Hamiltonian is separable into purely rotational and purely torsional parts. Thus in high barrier cases, it would be practical to treat these terms by perturbation theory. However, one of the principal objectives of this paper is to make fullest possible use of existing theoretical methods and tables[2b,3] for single-top molecules, and to do this it proves necessary to treat both top-top and top-frame coupling terms by perturbation theory. Consequently, we choose the zeroth-order Hamiltonian as

$$H^{(0)}=H_r+F(p_1^2+p_2^2)+\tfrac{1}{2}V_3^*(2-\cos 3\alpha_1-\cos 3\alpha_2), \quad (6a)$$

[7] In the perturbation treatment of footnote 6 (Swalen and Costain) a portion of the top-top kinetic energy coupling terms are retained and the rest disregarded. One of the results of the present investigation shows that in general, it will be a much better approximation (for vv states) to disregard *all* rather than just part of these coupling terms. See also, L. Pierce, J. Chem. Phys. **31**, 547 (1959).

[8] B. L. Crawford, J. Chem. Phys. **8**, 273 (1940).

[9] This assumption seems justifiable in view of the fact that for single-top molecules, spectra have thus far been satisfactorily interpreted by using only a V_3 term in the Fourier expansion of the potential energy. See for example, D. R. Herschbach and J. D. Swalen, J. Chem. Phys. **29**, 761 (1958).

TABLE I. Symmetry of the torsional basis functions.

	Function[a]		Species	
			+	−
$v=v'$:	$v0v0$		A_1A_1	
	$v0v1$, $v1v0$, $v0v-1$, $v-1v0$		EE	
	$v1v1$, $v-1v-1$		A_1E	
	$v1v-1$, $v-1v1$		EA_1	
$v\neq v'$:	$(1/\sqrt{2})(v0v'0\pm v'0v0)$		A_1A_1	A_2A_2
		or[b]	A_1A_2	A_2A_1
	$(1/\sqrt{2})(v1v'1\pm v'1v1)$ $(1/\sqrt{2})(v-1v'-1\pm v'-1v-1)$		A_1E	A_2E
	$(1/\sqrt{2})(v1v'-1\pm v'1v-1)$ $(1/\sqrt{2})(v-1v'1\pm v'-1v1)$		EA_1	EA_2
	$v1v'0$, $v'0v1$, $v-1v'0$, $v'0v-1$		EE	
	$v0v'1$, $v'1v0$, $v'-1v0$, $v0v'-1$		EE	

[a] $v\sigma_1v'\sigma_2=U_{v\sigma_1}(\alpha_1)U_{v'\sigma_2}(\alpha_2)$.

[b] The first alternative if v and v' have the same parity, the second alternative if v and v' have opposite parity.

and the perturbation Hamiltonian as

$$H^{(1)}=2F_+\mathcal{P}_+^2+2F_-\mathcal{P}_-^2-4F_+p_+\mathcal{P}_+-4F_-p_-\mathcal{P}_- +F'(p_1p_2+p_2p_1)+V_3'(1-\cos3\alpha_1) \times(1-\cos3\alpha_2)+V_3''\sin3\alpha_1\sin3\alpha_2. \quad (6b)$$

Each of the basis functions for the perturbation treatment then, consists of a rotational factor (asymmetric rotor functions) and a torsional factor for each of the tops (periodic Mathieu functions). In standard one-top notation the two torsional factors are

$$U_{v_1\sigma_1}(\alpha_1)U_{v_2\sigma_2}(\alpha_2),$$

where

$$U_{v\sigma}(\alpha)=\exp(i\sigma\alpha)\sum_k A_k^v\exp(3ik\alpha), \quad \sigma=0,\pm1, \quad (7)$$

and the A_k^v depend only on a reduced barrier parameter s, where

$$s=4V_3^*/9F.$$

3. Symmetry Considerations

The application of symmetry principles to rotation-internal rotation levels of two-top molecules has been discussed in detail by Myers and Wilson.[10] They have shown that for molecules such as $(CH_3)_2SiH_2$ or $(CH_3)_2S$, the group **I** of the Hamiltonian (5) is the direct product of two simple groups, i.e., $\mathbf{C}_{3v}\times\mathbf{C}_{3v}$. The reader is referred to their paper for derivation of the possible species for energy levels, their statistical weights, and selection rules. For our purposes, the only required elaboration of their work is the determination of the transformation properties of the zeroth-order torsional functions

$$U_{v\sigma_1}(\alpha_1)U_{v'\sigma_2}(\alpha_2); \qquad U_{v'\sigma_1}(\alpha_1)U_{v\sigma_2}(\alpha_2) \quad (8)$$

under the operations of the group **I**. For high barriers (high s) the zeroth-order torsional energy levels are ninefold degenerate when $v=v'$ and eighteen fold degenerate when $v\neq v'$. Using the following relations;

$$\begin{aligned} U_{v0}(-\alpha)&=(-1)^vU_{v0}(\alpha)\\ U_{v1}(-\alpha)&=U_{v-1}(\alpha)\\ U_{v0}(\alpha+2\pi n/3)&=U_{v0}(\alpha)\\ U_{v1}(\alpha+2\pi n/3)&=w^nU_{v1}(\alpha)\\ U_{v-1}(\alpha+2\pi n/3)&=w^{2n}U_{v-1}(\alpha), \end{aligned} \quad (9)$$

where $n=1$, 2 and $w=\exp(2\pi i/3)$, it can be shown that when (a) $v'=v$, the nine functions (8) contain the irreducible representations A_1A_1, A_1E, EA_1 and EE once each; (b) $v'\neq v$ and $vv'=ee$ or oo, the eighteen functions (8) contain the irreducible representations A_1A_1, A_2A_2, A_1E, EA_1, A_2E, EA_2 once each and EE twice; (c) $v'\neq v$ and $vv'=eo$ or oe, the eighteen functions (8) contain the irreducible representations A_1A_2, A_2A_1, A_1E, EA_1, A_2E, EA_2 once each and EE twice. The linear combinations of (8) which transform as irreducible representations of **I** are given in Table I.

It is important to note that while the top-frame coupling operators of $H^{(1)}$ belong to the totally symmetric species of **I**, their individual factors do not. Thus p_+ and $\mathcal{P}_+$ belong to the species A_1A_2, p_- and $\mathcal{P}_-$ belong to the species A_2A_1, while $p_\pm\mathcal{P}_\pm$ is in A_1A_1. The nonzero matrix elements of $p_\pm$ and $\mathcal{P}_\pm$ are given in Table II. Note that the dipole moment is of species A_1A_2 so that the p_+ connections of Table II are also the selection rules.

Finally we note that there is a class of molecules with two equivalent tops having less symmetry than $(CH_3)_2SiH_2$. Two examples are dimethyl amine and *cis* 2,3-epoxybutane. Sage[11] has shown that for such

TABLE II. Nonzero matrix elements of $p_\pm$ and $\mathcal{P}_\pm$.[a]

p_+ or $\mathcal{P}_+$	p_- or $\mathcal{P}_-$
$A_1A_1\leftrightarrow A_1A_2$	$A_1A_1\leftrightarrow A_2A_1$
$A_2A_2\leftrightarrow A_2A_1$	$A_2A_2\leftrightarrow A_1A_2$
p_+	p_-
$A_1E\leftrightarrow A_1E$	$A_1E\leftrightarrow A_2E$
$A_2E\leftrightarrow A_2E$	$EA_1\leftrightarrow EA_1$
$EA_1\leftrightarrow EA_2$	$EA_2\leftrightarrow EA_2$
$EE\leftrightarrow EE$	$EE\leftrightarrow EE$

[a] For $p_\pm$ the symmetry species refer to species of the zeroth-order torsional functions, while for $\mathcal{P}_\pm$ they refer to species of asymmetric rotor functions. Note that there are only four species of asymmetric rotor functions.

[10] R. J. Myers and E. B. Wilson, Jr., J. Chem. Phys. **33,** 186 (1960).

[11] M. Sage, thesis, Harvard University (1960).

molecules the group $\mathbf{I}'$ of the Hamiltonian (5) is also the direct product of two simple groups; in this case $\mathbf{C}_{3v}\times\mathbf{C}_3$. The effective rotational Hamiltonians given in the next section are equally applicable to $(CH_3)_2SiH_2$ or dimethyl amine type molecules. They are labeled, however, according to the symmetry of the torsional sublevels under $\mathbf{I}$. Their symmetry under $\mathbf{I}'$ is easily obtained if we note that the relation between the species of $\mathbf{C}_{3v}$ and its subgroup $\mathbf{C}_3$ is

$$A_1\rightarrow A,\quad A_2\rightarrow A,\quad E\rightarrow E_a+E_b.$$

4. Perturbation Treatment

The methods employed here for two-top molecules are a natural extension of the so-called principal axis method for single-top molecules. Therefore, we shall, before proceeding to the problem of two-tops, briefly review the perturbation treatment of top-frame coupling in single-top molecules. In the "semirigid" approximation the Hamiltonian is

$$H=H_r+F(p-\mathcal{P})^2+V(\alpha). \tag{10}$$

Treating the terms $-2Fp\mathcal{P}$, $F\mathcal{P}^2$, and the asymmetric part of H_r as perturbations, the Hamiltonian matrix is off-diagonal in the rotational (symmetric top) quantum number K and the principal torsional quantum number v. The boundary condition of invariance under $\alpha\rightarrow\alpha+2\pi$ requires that the zeroth-order torsional functions be periodic Mathieu functions, which for tops of threefold symmetry have the form (7) and are either of period $2\pi/3$ in α ($\sigma=0$, A species of C_3), or 2π in α ($\sigma=\pm1$, E species). For each value of v there are then two torsional sublevels, $vA(\sigma=0)$ and $vE(\sigma=\pm1)$, and physically, the separation of these levels may be regarded as a result of "tunneling" through the potential barrier.

Approximate v diagonalization of (10) is effected by applying successive Van Vleck transformations[12] to reduce the off-diagonal matrix elements of $-2Fp\mathcal{P}$ to an order high enough so that they may be neglected. If, in applying the Van Vleck transformations, the spacing of rotational levels is considered negligible compared to the spacing of torsional levels, then the Hamiltonian matrix approximately factors into smaller matrices $H_{v\sigma}$, one for each torsional state, where $H_{v\sigma}$ has the form[2b]

$$H_{v\sigma}=H_r+F\sum_n W_{v\sigma}^{(n)}\mathcal{P}^n. \tag{11}$$

Formally, the neglect of rotational energy differences allows $\mathcal{P}$ to be regarded as a parameter rather than as an operator for the purpose of approximate v diagonalization, so that the $W_{v\sigma}^{(n)}$ are simply the usual nth-order perturbation sums encountered in nondegenerate perturbation theory.[13] Herschbach[2b] has shown that, for sufficiently high s, the $W_{v\sigma}^{(n)}$ are simply proportional to the vA, vE torsional energy difference; thus making apparent the fact that "tunneling" affects rotational spectra indirectly via the top-frame coupling term.

The two-top problem differs from the one-top problem in two fundamental ways. First, regardless of whether coupling terms are included or not, there are four species of purely torsional functions for $v=v'$, and eight species for $v\neq v'$. Thus in general the rotational spectrum should consist of quartets for torsional states with $v=v'$ and octets for torsional states with $v\neq v'$, as opposed to doublets for any torsional state of a single-top molecule. Second, and more important, is the fact that with more than one top, terms are introduced into the Hamiltonian which have no analogs in the one-top Hamiltonian. Regarded as perturbations, these top-top coupling terms will affect "tunneling rates" and thus, through the top-frame coupling terms, will have an effect on the rotational spectrum.

The present perturbation treatment of two-top molecules will be restricted to finding effective rotational Hamiltonians for torsional states having $v=v'$. First let us assume that top-top coupling terms are negligible, i.e., set F', V_3', and V_3'' equal to zero. In this approximation $H^{(1)}$ reduces to $-4F(p_+\mathcal{P}_++p_-\mathcal{P}_-)+2F(\mathcal{P}_+^2+\mathcal{P}_-^2)$. Application of the Van Vleck transformation reduces matrix elements of $H^{(1)}$ which are off-diagonal in v to second order so that if rotational energy differences are neglected, the effective rotational Hamiltonian to second order has the form[14,15]

$$H_{vv}=H_r+F\sum_n[w_{vv}^{(+n)}\mathcal{P}_+^n+w_{vv}^{(-n)}\mathcal{P}_-^n],\quad n=0,1,2. \tag{12}$$

[12] E. C. Kemble, *Fundamental Principles of Quantum Mechanics* (McGraw-Hill Book Company, Inc., New York, 1937), p. 395.

[13] $W_{v\sigma}^{(2)}$ is not exactly a second-order perturbation coefficient. The term $F\mathcal{P}^2$ contributes only in the first order to $H_{v\sigma}$ and this contribution is lumped together with the second-order contribution of $-2Fp\mathcal{P}$ so that

$$W_v^{(2)}=4\Sigma\mid p_{vv'}\mid^2/(W_v^{(0)}-W_{v'}^{(0)})+1.$$

[14] For simplicity, one term, which ordinarily will be negligibly small for molecules that can be treated by the present theory, has been omitted from Eq. (12). This term has the form $Fw_{vv}^{(x2)}(\mathcal{P}_+\mathcal{P}_-+\mathcal{P}_-\mathcal{P}_+)$ where $w_{vv}^{(x2)}=W_{v1}^{(2)}-W_{v0}^{(2)}$ if $\Gamma_{vv}=EE$ and $w_{vv}^{(x2)}=0$ if $\Gamma_{vv}=A_1A_1$, A_1E_1 or EA_1. By suitably rotating the principal axes, this term can be absorbed into H_r. Usually this rotation will be negligibly small. For example, in the case of dimethyl silane, a rotation of considerably less than one minute of arc in the a–b plane is required to remove the $\mathcal{P}_+\mathcal{P}_-$ cross terms for the ground torsional state.

[15] In the absence of top-top coupling, the effective rotational Hamiltonian may be written in the alternative form

$$H_{vv}=H_r+F\Sigma_n[W_{v\sigma_1}^{(n)}\mathcal{P}_1^n+W_{v\sigma_2}^{(n)}\mathcal{P}_2^n],$$

where $\sigma_1\sigma_2$ is taken as 00, 10, 11, and 1−1 for $\Gamma_{vv}=A_1A_1$, EE, A_1E, and EA_1, respectively. This form of H_{vv} contains the term in $(\mathcal{P}_+\mathcal{P}_-+\mathcal{P}_-\mathcal{P}_+)$ which is omitted in Eq. (13) (see the preceding footnote), i.e., it is correct to the second order ($n=2$). In the third and higher orders it is only approximately correct because it neglects certain cross terms between $\mathcal{P}_1$ and $\mathcal{P}_2$. We have not investigated the perturbation coefficients for these cross terms.

TABLE III. Definition of the $w_{vv'}^{(\pm n)}$ in terms of the $W_{vv'}^{(n)}$.[a]

$\Gamma_{vv'}$	$w_{vv'}^{(1)}$	$w_{vv'}^{(-1)}$	$w_{vv'}^{(\pm 2)}$
A_1A_1	0	0	$2W_{v0}^{(2)}$
A_1E	$2W_{v1}^{(1)}$	0	$2W_{v1}^{(2)}$
EA_1	0	$2W_{v1}^{(1)}$	$2W_{v1}^{(2)}$
EE	$W_{v1}^{(1)}$	$W_{v1}^{(1)}$	$(W_{v0}^{(2)}+W_{v1}^{(2)})$

[a] The perturbation sums $W_{vv'}^{(n)}$ are defined and tabulated in footnotes 2b and 3a.

For every v there are four such Hamiltonians, H_{vv}; one for each of the torsional sublevels $vv(A_1A_1)$, $vv(EA_1)$, $vv(A_1E)$, and $vv(EE)$. In each case the $w_{vv}^{(\pm n)}$ are simple linear combinations of the $W_{vv'}^{(n)}$ defined and tabulated by Herschbach.[2b] The appropriate linear combinations are listed in Table III according to the symmetry of the torsional sublevels. While in general the rotational spectra will consist of quartets, it should be noted that the odd n terms will not contribute, except in the second or higher order in the H_r (asymmetric rotor) basis, to the rotational energy levels. Thus, if the matrix elements of the odd n terms in the H_r basis are small compared to the spacing of levels that they connect, the rotational spectrum will consist of symmetrical triplets.

If top-top interaction terms are included in $H^{(1)}$ the effective rotational Hamiltonian becomes

$$H_{vv}=H_r+F\sum_n[W_{vv}^{(+n)}\mathcal{P}_+^n+W_{vv}^{(-n)}\mathcal{P}_-^n], \quad n=0, 1, 2, \tag{13}$$

where the $W_{vv}^{(\pm n)}$ are comprised of the $w_{vv}^{(\pm n)}$ plus a power series in the parameters

$$x=F'/F=-q/r$$
$$y=V_3'/V_3^*$$
$$z=V_3''/V_3^*. \tag{14}$$

To the first order in x, y, and z we define the $W_{vv}^{(\pm n)}$ as

$$W_{vv}^{(\pm n)}=w_{vv}^{(\pm n)}+xX_{vv}^{(\pm n)}+yY_{vv}^{(\pm n)}+zZ_{vv}^{(\pm n)}. \tag{15}$$

The $X_{vv}^{(\pm n)}$ and $Y_{vv}^{(\pm n)}$ are defined in Tables IV and V. Here $Z_{vv}^{(\pm n)}$ can be shown to be identically zero for $n=0$, 1, 2. Thus it appears that the coupling term $V_3''\sin 3\alpha_1 \sin 3\alpha_2$ gives rise to no $\mathcal{P}_\pm^n$ dependence in the effective rotational Hamiltonian for torsional states with $v=v'$. (It is, however, a very important term for states with $v=v'\pm 1$.)

The $W_{vv}^{(\pm n)}$, unlike the $w_{vv}^{(\pm n)}$, cannot be regarded as simple nth-order perturbation coefficients. The $X_{vv}^{(\pm n)}$ and $Y_{vv}^{(\pm n)}$ are actually perturbation sums of the $(n+1)$st rather than nth order. In this regard the $X_{vv}^{(\pm n)}$ are somewhat special. Because top-frame coupling terms are multiplied by $F_\pm=F(1\pm x)$, a rather large $x\mathcal{P}_\pm^n$ dependence is obtained in the nth order. However, a portion of the $(n+1)$st order contributions arising from cross terms between $F'(p_1p_2+p_2p_1)$ and the top-frame coupling terms cancels this large $x\mathcal{P}_\pm^n$ dependence, so that the $X_{vv}^{(\pm n)}$ are composed of only $(n+1)$st-order perturbation sums. Fortunately, the $X_{vv}^{(\pm n)}$ are very easy to evaluate because they can be expressed as linear combinations of products of perturbation sums of lower order than the $(n+1)$st. They are, in fact, linear combinations of products of the $W_{vv'}^{(n)}$ which have been extensively tabulated by Herschbach.[2b] Inspection of Tables III and IV shows that the order of magnitude of the $X_{vv}^{(\pm n)}$ is $\sim[W_{vv}^{(2)}][w_{vv}^{(\pm n)}]$. Since $W_{vv}^{(2)}\ll 1$ for high s and low v, it is apparent that it will often be an excellent approximation to set $F'=0$ for $v=v'$ torsional states. However, for $v=v'\pm 1$ the terms in F' like those in V_3'' become very important.

Unfortunately, we have found no obvious way to simplify the $Y_{vv}^{(\pm n)}$. It is necessary to evaluate them directly from the matrix elements of p and p^2 tabulated by Herschbach[3a] and Kilb.[3b] The $Y_{vv}^{(\pm n)}$ are defined in Table V as functions of the expectation value of an operator $\Theta=(1-\cos 3\alpha)$ and the perturbation sums $\gamma_{vv}^{(n)}$, $\delta_{vv}^{(2)}$. The sums, $\gamma^{(1)}$, have been calculated for $v=0$ and 1 at 14 values of s, $16\leqq s\leqq 100$. The sums, $\gamma^{(2)}$, are much more difficult to evaluate and have thus far been calculated for $v=0$, and 1 at only four s values, $s=20$, 28, 40, and 60. For $s>20$ and $v=0$, or 1 the $\delta_{vv}^{(2)}$ are negligible. Calculation of γ's and δ's is still in progress and a complete report will be given in II of this series. Table VI lists empirical formulas from which the $Y_{vv}^{(\pm n)}$ may be calculated. These formulas reproduce the $Y_{vv}^{(\pm n)}$ thus far computed to about 2%.

TABLE IV. Definition of the $X_{vv'}^{(\pm n)}$ in terms of the $W_{vv'}^{(n)}$.[a]

$\Gamma_{vv'}$	$X_{vv'}^{(1)}$	$X_{vv'}^{(-1)}$	$X_{vv'}^{(\pm 2)}$
A_1A_1	0	0	$\pm 2[W_{v0}^{(2)}]^2$
A_1E	$2W_{v1}^{(2)}W_{v1}^{(1)}$	0	$\pm 2[W_{v1}^{(2)}]^2+3W_{v1}^{(1)}W_{v1}^{(3)}$ $\mp 2[W_{v1}^{(1)}]^2W_{v1}^{(d)}$
EA_1	0	$-2W_{v1}^{(2)}W_{v1}^{(1)}$	$\pm 2[W_{v1}^{(2)}]^2-3W_{v1}^{(1)}W_{v1}^{(3)}$ $\mp 2[W_{v1}^{(1)}]^2W_{v1}^{(d)}$
EE	$W_{v0}^{(2)}W_{v1}^{(1)}$	$-W_{v0}^{(2)}W_{v1}^{(1)}$	$\pm 2W_{v0}^{(2)}W_{v1}^{(2)}\mp[W_{v1}^{(1)}]^2W_{v0}^{(d)}$

[a] The perturbation sums $W_{vv'}^{(n)}$ are defined and tabulated in footnotes 2b and 3a.

TABLE V. Definition of $Y_{vv}^{(\pm n)}$.

Γ_{vv}	$Y_{vv}^{(1)}$ [apart from a factor of $-(9/2)s$]	$Y_{vv}^{(-1)}$ [apart from a factor of $-(9/2)s$]	$Y_{vv}^{(\pm 2)}$ [apart from a factor of $9s$]
A_1A_1	0	0	$2\langle\Theta\rangle_{v0}\gamma_{v0}^{(2)}$
A_1E	$2\langle\Theta\rangle_{v1}\gamma_{v1}^{(1)}$	0	$2[\langle\Theta\rangle_{v1}\gamma_{v1}^{(2)}\pm\delta_{v1}^{(2)}]$
EA_1	0	$2\langle\Theta\rangle_{v1}\gamma_{v1}^{(1)}$	$2[\langle\Theta\rangle_{v1}\gamma_{v1}^{(2)}\mp\delta_{v1}^{(2)}]$
EE	$\langle\Theta\rangle_{v0}\gamma_{v1}^{(1)}$	$\langle\Theta\rangle_{v0}\gamma_{v1}^{(1)}$	$\langle\Theta\rangle_{v0}\gamma_{v1}^{(2)}+\langle\Theta\rangle_{v1}\gamma_{v0}^{(2)}$

$$\langle\Theta\rangle_{vv'}=(v\sigma\mid\Theta\mid v\sigma)$$

$$\gamma_{vv'}^{(1)}=\left\{\sum_{v'}{}'\frac{p\Theta+\Theta p}{\Delta'}\right\}_{\sigma}$$

$$\gamma_{vv'}^{(2)}=\left\{\sum_{v',v''}{}'\frac{pp\Theta+p\Theta p+\Theta pp}{\Delta'\Delta''}-\langle\Theta\rangle_{v}\sum_{v'}{}'\frac{pp}{(\Delta')^2}-\langle p\rangle_{v}\sum_{v'}{}'\frac{p\Theta+\Theta p}{(\Delta')^2}\right\}_{\sigma}$$

$$\delta_{vv'}^{(2)}=\tfrac{1}{2}[\gamma_{vv'}^{(1)}]^2-\langle\Theta\rangle_{vv}\langle p\rangle_{vv}\sum_{v'}{}'\frac{p\Theta+\Theta p}{(\Delta')^2}$$

$$\Delta'=W_v^{(0)}-W_{v'}^{(0)}$$

$p\Theta=(v\mid p\mid v')(v'\mid\Theta\mid v)$, etc.

It is interesting to note that the $Y_{vv}^{(\pm 1)}$ contribution to $W_{vv}^{(\pm 1)}$ is percentagewise virtually identical to the $Y_{vv}^{(\pm 2)}$ contribution to the $W_{vv}^{(\pm 2)}$. Thus the problem of estimating V_3' for a two-top molecule is similar to the problem of estimating V_6 for a single-top molecule; in general, measurements for more than one torsional state are required. The $vv=11$ state of a $(CH_3)_2$-type isotopic species would, together with the $vv=00$ state, provide an excellent determination of V_3' as well as V_3. However, rotational transitions from the 11 state would, in general, be weak and difficult to assign. For $(CD_3)_2$-type molecules the study of the 11 state is more feasible, but it is likely that in molecules for which the present theory is applicable, no splittings would be observed for $vv=00$. The study of $vv'=01$ states is probably the best way to get at V_3'. However, the present treatment does not suffice to interpret rotational spectra arising from 01 states.

Unsymmetrical isotopic substitution can be used to get some information about V_3' without the necessity of studying excited torsional states. For the ground torsional state of a $(CH_3)_2$-molecule species the ratio of $Y_{00}^{(\pm n)}$ to $w_{00}^{(\pm n)}$ is roughly -1.7 to -1.8 in the range $30<s<100$, while for $(CH_3)(CD_3)$-type molecules the corresponding ratio (for the CH_3 group) is about -1.3. This difference is sufficient to obtain a crude estimate of V_3' from only ground-torsional-state rotational spectra.

II. MICROWAVE SPECTRUM OF DIMETHYL SILANE

1. Experimental

Samples of $(CH_3)_2SiH_2$ and $(CH_3)_2SiD_2$ were prepared by reducing $(CH_3)_2SiCl_2$ with $LiAlH_4$ and $LiAlD_4$ in ethyl ether at 0°C. $(CH_3)(CD_3)SiH_2$ was prepared by reacting CD_3MgI with CH_3SiH_2Cl in ethyl ether at 0°C. The CH_3SiH_2Cl was prepared in the manner described by Kilb and Pierce.[16]

Spectra were observed with a conventional Stark-modulated (100 kc) spectrometer employing phase-sensitive detection. Frequency measurements were made with a crystal-controlled microwave frequency standard which was monitored by the 10 Mc WWV signal. Weak absorptions due to $Si^{29,30}$ and C^{13} isotopic species were measured in natural abundance on a re-

TABLE VI. Formulas for $\langle\Theta\rangle_{v\sigma}\gamma_{v\sigma'}^{(n)}$.[a]
$B_n\langle\Theta\rangle_{v\sigma}\gamma_{v\sigma'}^{(n)}/W_{v\sigma'}^{(n)}=a+bs+c/s^b$

n	$v\sigma$	$v\sigma'$	a	b	c
1	00	01	−1.7613	−0.0013124	2.4382
1	01	01	−1.8003	−0.0010086	3.5604
1	10	11	−6.0296	0.0043701	48.7719
1	11	11	−5.6873	0.0019475	37.3250
2	00	00	−1.8744	−0.0000943	4.6211
2	01	01	−1.8510	−0.0005313	4.6724
2	10	10	−4.7380	−0.0077923	15.5627
2	11	11	−4.3747	−0.0114064	6.8513

$B_n\{\langle\Theta\rangle_{v\sigma}\gamma_{v\sigma'}^{(n)}+\langle\Theta\rangle_{v\sigma'}\gamma_{v\sigma}^{(n)}\}/(W_{v\sigma}^{(n)}+W_{v\sigma'}^{(n)})=a+bs+c/s^b$

n	$v\sigma$	$v\sigma'$	a	b	c
2	00	01	−1.9232	0.0004219	6.1163
2	10	11	−2.6808	−0.0285468	−34.4660

[a] For $n=1$, these formulas are accurate to 1% in the range $16\leq s\leq 100$. For $n=2$, the formulas are accurate to about 3% in the range $20\leq s\leq 60$.
[b] $s=4V_3^*/9F$. $B_1=-(9/2)s$, $B_2=9s$.

[16] R. W. Kilb and L. Pierce, J. Chem. Phys. **27**, 108 (1957).

cording potentiometer and may be uncertain by as much as ±0.20 Mc. Spectra of the enriched isotopic species were displayed and measured on an oscilloscope with an estimated uncertainty of less than 0.05 Mc. Special effort was made to get accurate splittings, and for the enriched isotopic species the splittings are estimated to be uncertain by less than 0.02 Mc. Several absorption frequencies for $(CH_3)_2SiH_2$ and $(CH_3)(CD_3)SiH_2$ were reported in a previous communication.[7] These frequencies have been remeasured and the new values given here are somewhat more accurate.

2. Spectra and Dipole Moment

Apart from the fact that each rotational transition is a triplet (except in the case of $(CH_3)(CD_3)SiH_2$), the ground-state rotational spectrum of dimethyl silane is typical of an asymmetric rotor with "*b*"-type transitions. Below $J=4$ the transitions were positively identified by their character Stark effects. Transition frequencies for $(CH_3)_2SiH_2$, $(CH_3)_2SiD_2$, and $(CH_3)(CD_3)SiH_2$ are listed in Table VII.

The *Q*-branch series for these species cannot be reproduced very accurately with the rigid rotor approximation. Deviations of measured frequencies from the rigid rotor values are as large as 5 Mc in the case of the $6_{06}\rightarrow 6_{15}$ transition. No centrifugal distortion corrections have been applied. For these three species rotational constants have been calculated from the $O_{00}\rightarrow 1_{11}$, $1_{01}\rightarrow 1_{10}$ and $2_{02}\rightarrow 2_{11}$ transition frequencies (a small correction for internal rotation was applied to these frequencies). Centrifugal distortion effects are small for these low J transitions and in the structure analysis used here these small effects largely tend to cancel.

TABLE VII. Ground-state rotational transitions (Mc).[a]

Transition	$(CH_3)_2SiH_2$[b]	$(CH_3)_2SiD_2$[b]	$(CH_3)(CD_3)SiH_2$[c]
$1_{01}\rightarrow 1_{10}$	11 857.06	8 993.41	10 397.79
	11 858.19	8 994.12	10 398.58
	11 859.33	8 994.82	
$2_{02}\quad 2_{11}$	12 978.49	10 112.93	11 309.18
	12 979.76	10 113.72	11 310.02
	12 981.03	10 114.53	
$3_{03}\quad 3_{12}$	14 792.71	11 958.60	12 776.79
	14 794.11	11 959.51	12 777.78
	14 795.50	11 960.42	
$4_{04}\quad 4_{13}$	17 441.16	14 695.69	14 909.62
	17 442.72	14 696.75	14 910.75
	17 444.27	14 697.84	
$5_{05}\quad 5_{14}$	21 068.32	18 462.82	17 823.41
	21 070.13	18 464.11	17 824.74
	21 071.97	18 465.35	
$6_{06}\quad 6_{15}$	25 771.55		21 604.75
	25 773.65		21 606.33
	25 775.75		
$0_{00}\quad 1_{11}$	21 649.82	18 438.12	19 082.67
	21 651.08	18 438.86	19 083.52
	21 652.35	18 439.63	
$2_{12}\quad 3_{03}$	22 403.80	24 013.39	19 664.24
	22 402.90	24 012.92	19 663.69
	22 402.03	24 012.43	

[a] Estimated uncertainty: ±0.05 Mc.
[b] The triplet components are listed in the order (A_1E+EA_1), EE, A_1A_1 (according to the symmetry of the torsional sublevel).
[c] The doublet components are listed in the order E, A (in single-top notation).

TABLE VIII. Ground-state transitions measured in natural abundance (Mc).[a]

Transition	$(CH_3)_2Si^{29}H_2$	$(CH_3)_2Si^{30}H_2$	$(C^{13}H_3)(CH_3)SiH_2$
$4_{04}\rightarrow 4_{13}$	17 394.96	17 353.41	17 180.01
	(17 396.51)[b]	17 354.68	17 181.68
	(17 398.06)[b]	17 356.26	17 183.30
$5_{05}\quad 5_{14}$	21 086.34	21 106.76	20 646.21
	21 088.16	21 108.42	20 647.95
	21 089.93	21 110.22	20 649.83
$6_{06}\quad 6_{15}$			24 142.60
			25 144.60
			(25 146.60)[b]
$0_{00}\quad 1_{11}$	21 489.88	21 337.99	21 379.40
	21 491.07	21 339.18	21 380.70
	21 492.33	21 340.20	21 382.00

[a] Estimated uncertainty: ±0.20 Mc.
[b] Obscured by a nearby strong absorption line. Frequency estimated from splitting for a barrier of 1660 cal/mole.

The measured spectra of $Si^{29,30}$ and C^{13} species are given in Table VIII. Since mostly high J transitions were measured for these species the rotational constants had to be calculated in a different manner. It was assumed that centrifugal distortion effects were for these species identical to those for the parent species, $(CH_3)_2SiH_2$. The transition frequencies thus empirically corrected were analyzed in the rigid rotor approximation. Rotational constants and moments of inertia are listed in Table IX.

The assignments of transitions to $Si^{29,30}$ and C^{13} species were not confirmed by temperature dependence studies. However, in the case of the Si^{29} and Si^{30} isotopic species each transition can be used to calculate the b coordinate of the silicon atom, and all lines are in excellent (±0.0010 A) agreement with each other on the value of b_{Si}. Furthermore, the observed change in $I_a+I_b-I_c$ (see Table IX) when Si^{29} or Si^{30} replaced Si^{28} is in the theoretically expected direction for an atom lying on or very near a principal axis.[17] In the case of the C^{13} species the assignment of Table I gives, when Kraitchman's equations are used, a b coordinate for the carbon atom which is in excellent agreement with the value obtained from the first moment equation (see Sec. II. 3). In all three cases comparison of the Stark effect and triplet spacing with that of the parent species clearly indicated that J values were correctly assigned.

The dipole moment of dimethyl silane was determined from Stark effect measurements on the $O_{00}\rightarrow 1_{11}$

[17] V. W. Laurie and D. R. Herschbach, Symposium on Molecular Structure and Spectroscopy, Ohio State University (1960).

TABLE IX. Rotational constants (Mc) and moments of inertia (amu A²).[a]

	a	b	c
$(CH_3)_2SiH_2$	16754.24	5945.44	4896.50
$(CH_3)_2Si^{29}H_2$	16606.85	5945.56	4883.83
$(CH_3)_2Si^{30}H_2$	16467.26	5945.50	4871.52
$(C^{13}H_3)(CH_3)SiH_2$	16605.08	5785.65	4775.22
$(CH_3)_2SiD_2$	13716.25	5749.07	4722.39
$(CH_3)(CD_3)SiH_2$	14740.79	5198.82	4342.47

	I_a	I_b	I_c	$I_a+I_b-I_c$
$(CH_3)_2SiH_2$	30.1733	85.0283	103.2433	11.9583
$(CH_3)_2Si^{29}H_2$	30.4411	85.0266	103.5111	11.9566
$(CH_3)_2Si^{30}H_2$	30.6992	85.0274	103.7727	11.9538
$(C^{13}H_3)(CH_3)SiH_2$	30.4444	87.3766	105.8654	11.9555
$(CH_3)_2SiD_2$	36.8563	87.9326	107.0498	17.3762
$(CH_3)(CD_3)SiH_2$	34.2947	97.2395	116.4155	15.1187

[a] Corrected for internal rotation effects. Conversion factor: 505 531 Mc amu A².

and $1_{10}\rightarrow 1_{01}$ transitions of the common isotopic species. The apparatus was calibrated with OCS. Using the dipole moment of OCS as determined by Marshall and Weber,[18] the dipole moment of dimethyl silane was calculated to be $0.75\pm0.01D$.

3. Structure of Dimethyl Silane

The preferred method of calculating structures from ground-state rotational parameters involves the use of changes in moments of inertia with isotopic substitution rather than moments of inertia as such.[19,20] The data obtained for dimethyl silane are more than sufficient to employ this technique. The coordinates [in the principal axis system of $(CH_3)_2SiH_2$ of the carbon and silicon atoms] were obtained from Kraitchman's equations.[21] In the case of the carbon atom, changes in the a and b moments of inertia were used, while for the silicon atom the change in the a moment was used.

The various alternative combinations of ΔI's give only slightly different values for the carbon and silicon coordinates simply because the change in $I_a+I_b-I_c$ is small for C^{13} or $Si^{29,30}$ substitution and because the carbon and silicon coordinates are large (>0.5 A).

TABLE X. Atom coordinates [$(CH_3)_2SiH_2$ principal axes]. (A)

	a	b	c
Si	0	0.5218	0
C	±1.5385	−0.5351	0
H(Si)	0	1.3954	±1.1983
$H_a(CH_3)$	±1.5711	−1.1785	±0.8857
$H_s(CH_3)$	±2.4400	0.0858	0

[18] S. A. Marshall and J. Weber, Phys. Rev. **105**, 1502 (1957).
[19] C. C. Costain, J. Chem. Phys. **29**, 864 (1958).
[20] L. Pierce, J. Mol. Spectroscopy **3**, 575 (1959).
[21] J. Kraitchman, Am. J. Phys. **21**, 17 (1953).

However, use of changes in a rather than c moments is preferable because of the fact that the former are more accurately determined.

Substitution of deuterium atoms for the silicon hydrogens produces a large change in $I_b+I_c-I_a$ (0.03 amu A). This change is much larger than the experimental uncertainties in the moments of inertia. Consequently, each of the coordinates adopted for these atoms is the average of coordinates calculated from two combinations of ΔI's.

In calculating the coordinates of the methyl hydrogen atoms, it was assumed that methyl groups were symmetric with symmetry axes coincident with the SiC bond axes. The CH distance and HCH angles were then varied to give the best possible (least-square) fit of differences in moments of inertia between $(CH_3)_2SiH_2$ and $(CH_3)(CD_3)SiH_2$. The fit obtained was excellent. Deviations were less than 0.01 amu A². Tilting the methyl group symmetry axes by as little as one degree resulted in a significantly poorer fit of the ΔI's.

TABLE XI. Structure of dimethyl silane.[a]

CSi	1.867±0.002 A	CSiC	110° 59′±10′
SiH	1.483±0.005 A	HSiH	107° 50′±20′
CH	1.095±0.005 A	HCH	108° 0′±20′

$2\theta^b = 110°\ 50'\pm 20'$

Structural checks [$(CH_3)_2SiH_2$]

	obs	calc
I_a (amu A²)	30.0941	30.1733
I_b	84.8421	85.0283
I_c	102.7705	103.2433

$\Sigma m_i b_i = 0.009$ amu A

[a] Conversion factor: 505 531 Mc amu A². Atomic masses taken from C. H. Townes and A. L. Schawlow, *Microwave Spectroscopy* (McGraw-Hill Book Company, Inc., New York, 1955).
[b] 2θ = angle between the symmetry axes of the two methyl groups.

Coordinates of atoms in the $(CH_3)_2SiH_2$ principal axis system are given in Table X, and bond distances and angles in Table XI.

4. Internal Rotation Analysis

The operators $\mathcal{P}_\pm$ in the case of $(CH_3)_2SiH_2$ and $(CH_3)_2SiD_2$ can be written

$$\mathcal{P}_+ = \beta P_x$$
$$\mathcal{P}_- = \alpha P_z, \tag{16}$$

where

$$\alpha = \lambda_{z1} I_a / I_z = -\lambda_{z2} I_a / I_z$$

and

$$\beta = \lambda_{x1} I_a / I_x = \lambda_{x2} I_a / I_x.$$

TABLE XII. Internal barrier calculations. Multiplet separation (Mc).[a]

Transition	$(CH_3)_2SiH_2$ obs	$(CH_3)_2SiH_2$ calc	$(CH_3)_2SiD_2$ obs	$(CH_3)_2SiD_2$ calc	$(CH_3)(CD_3)SiH_2$ obs	$(CH_3)(CD_3)SiH_2$ calc
$1_{01}\rightarrow 1_{10}$	1.14	1.15	0.71	0.72	0.79	0.77
$2_{02}\ 2_{11}$	1.27	1.27	0.80	0.80	0.84	0.86
$3_{03}\ 3_{12}$	1.40	1.40	0.91	0.91	0.99	0.98
$4_{04}\ 4_{13}$	1.56	1.58	1.08	1.07	1.13	1.12
$5_{05}\ 5_{14}$	1.83	1.81	1.27	1.27	1.33	1.33
$6_{06}\ 6_{15}$	2.10	2.11			1.58	1.58
$0_{00}\ 1_{11}$	1.27	1.27	0.76	0.78	0.84	0.85
$2_{12}\ 3_{03}$	0.89	0.88	0.48	0.47	0.55	0.54
V_3 (cal/mole)[b]	1649±3		1646±3		1647±3	
2θ[c]	110° 26′		111° 10′		110° 52′	
I_a (amu A^2)	3.1635		3.1635		3.1635 (CH_3) 6.3221 (CD_3)	
F (kMc)	174.95		172.25		173.01 (CH_3) 94.91 (CD_3)	
F' (kMc)	−11.18		−8.69		−10.59	
α	0.086113		0.070809		0.073085 (CH_3) 0.157128 (CD_3)	
β	0.021224		0.020334		0.019850 (CH_3) 0.034002 (CD_3)	
s	43.95		44.53		44.37 (CH_3) 80.89 (CD_3)	

[a] Estimated uncertainty: <0.02 Mc.
[b] Assuming $V_3'=0$.
[c] 2θ=angle between symmetry axes of the methyl groups.

Because of the smallness of α and β, for the transitions of Table VII, the separation of internal and over-all rotation need only be carried out to second order, i.e., in Eq. (13) only terms with $n\leqq 2$ need be retained.[14,15] For $J>3$, Eq. (13) may further be simplified by dropping the $n=1$ term, in which case the effective rotational Hamiltonian has the pseudo-rigid rotor form

$$H_{vv}\approx H_r+FW_{vv}^{(2)}[\beta^2P_x^2+\alpha^2P_z^2]. \qquad (17)$$

(The terms which make $W_{vv}^{(2)}\neq W_{vv}^{(-2)}$ are negligibly small for dimethyl silane.) For $J<3$, the rather small effect (0.06 Mc max) of the terms in αP_z may be exactly evaluated from equations given in references 2b or 16. In all cases the βP_x term is negligible.

The $X_{vv}^{(\pm n)}$ are for dimethyl silane completely negligible in comparison with the $w_{vv}^{(\pm n)}$. Assuming $V_3'=0$, the splittings are reproduced to within the small experimental uncertainty of ±0.02 Mc by taking $V_3=1649\pm 3$ cal/mole for $(CH_3)_2SiH_2$ and $V_3=1646\pm 3$ cal/mole for $(CH_3)_2SiD_2$. The uncertainty of ±3 cal/mole represents only the effect of errors in measurement of splittings. Uncertaintites in structural parameters, I_a in particular, could affect the value of V_3 by as much as 30 cal/mole.

In the case of $(CH_3)(CD_3)SiH_2$, if top-top coupling terms are ignored, the effective rotational Hamiltonian can be taken as the single-top Hamiltonian (11). This is so because tunnel effects due to the CD_3 group in the ground state are negligibly small. Analysis of the $(CH_3)(CD_3)SiH_2$ splittings yield a barrier $V_3=1647\pm 3$ cal/mole, which is in excellent agreement with the values obtained for $(CH_3)_2SiH_2$ and $(CH_3)_2SiD_2$. The calculations for all three species are summarized in Table XII.

It was pointed out in Section I.4 that there is a small but significant difference in the $V_{vv}^{(\pm n)}$ contribution to $W_{vv}^{(\pm n)}$ for $(CH_3)_2$- and $(CH_3)(CD_3)$-molecular species. This fact allows us to make a crude estimate of V_3' for dimethyl silane. For all three species the $W_{vv}^{(\pm n)}$ are believed to be experimentally determined with an accuracy of 1%. To within this accuracy the $W_{vv}^{(\pm n)}$ can be fitted by taking

$$V_3^*=1647\pm 3 \text{ cal/mole}$$

$$V_3'=0\pm 60 \text{ cal/mole}$$

$$V_3=1647\mp 120 \text{ cal/mole}.$$

Table XII lists a value of 2θ for each of the three isotopic species. In analyzing the splittings, two parameters were used; V_3 and the ratio α/β. The calculated splittings are quite sensitive to α/β and thus to the angle between the symmetry axes of the tops and the principal axes of the molecule. The three values of 2θ are in excellent agreement with each other and give an average 2θ of 110°50′±20′ which is also in good agreement with 2θ as determined from changes in moments of inertia. Thus apart from a small experimental error, the methyl group symmetry axes can be said to be coaxial with their SiC bond axes.

ACKNOWLEDGMENTS

The author is pleased to acknowledge the work of Dr. Michiro Hayashi on the two-top problem. Table VI of this paper is based entirely on Dr. Hayashi's calculations.

THE JOURNAL OF CHEMICAL PHYSICS VOLUME 34, NUMBER 2 FEBRUARY, 1961

Spin Density in Pyrene Negative Ion*

G. J. HOIJTINK

The Free University, Amsterdam, Netherlands

AND

J. TOWNSEND AND S. I. WEISSMAN

Washington University, St. Louis, Missouri

(Received July 7, 1960)

Improved resolution has permitted assignment of all proton hyperfine coupling constants in pyrene negative ion. The results are accounted for by a simple calculation of configurational interaction.

ALTHOUGH the correspondence between the spin distribution in uninegative anions of many even alternant hydrocarbons and the predictions of Hückel's molecular orbital theory is satisfactory,[1] a serious discrepancy exists for the ion of pyrene (Fig. 1).

In the Hückel approximation the singly occupied orbital is antisymmetric in the plane passing through positions 2, 12, 15, and 7 and a splitting into 25 lines by the protons at positions 3, 4, etc., is predicted. Earlier observations showed that the spectrum consisted of more than 25 lines[1] but because of imperfect resolution a complete analysis was not possible. Because of recent improvements in the experimental methods, we have been able to obtain well-resolved spectra exhibiting all 75 lines compatible with the symmetry of the molecule. The spectrum is well represented by coupling constants 4.75 and 2.08 oe for protons of types 1 and 4, respectively, and -1.09 oe for protons of type 2. The assignment of the large coupling constant to position 1 has been verified by isotopic substitution.[1] Assignment of a negative coupling constant to positions 2 and 7 is not required from the pattern of splitting but is consistent with the length of the spectrum (29.5 oe) and the calculations, to be outlined below. Several theoretical treatments[2–4] yield negative spin densities at positions in radicals at which the simple Hückel treatment predicts zero spin density. A simple calculation of configuration interaction predicts a spectrum in good agreement with our observations. The principal configuration of the ground state of a mononegative ion containing $2n$ carbon atoms is described by the antisymmetrized product

$$\psi_N = |\,\phi_1\bar{\phi}_1\cdots\phi_j\bar{\phi}_j\cdots\phi_{n+1}\,|\,,$$

in which each ϕ is the usual combination of atomic orbitals

$$\phi_j(v) = \sum_s C_{sj}\phi_s(v).$$

Molecular orbitals obeying the SCF conditions described by Lefebvre[5] yield a ψ_N which contains no singly excited configurations. However, doubly excited configurations

$$\psi_v = 6^{-\frac{1}{2}}\{2\,|\,\phi_j\bar{\phi}_{n+1}\phi_k\,|\,-\,|\,\phi_j\bar{\phi}_k\phi_{n+1}\,|\,+\,|\,\phi_k\bar{\phi}_j\phi_{n+1}\,|\,\}$$
$$\times j\leq n; \qquad k\geqslant n+2$$

interact with ψ_N. Inclusion of ψ_v leads to nonvanishing spin density ρ_t at those carbon atoms t where spin density vanishes when ψ_N alone is considered,

$$\rho_t = 2\sum_j\sum_k \frac{\langle j, n+1\,|\,k, n+1\rangle}{E_v - E_N} C_{tj}C_{tk}$$

$$\langle j, n+1\,|\,k, n+1\rangle$$
$$= \iint \phi_j(1)\phi_{n+1}(1)\,(l^2/r_{12})\phi_k(2)\phi_{n+1}(2)\,d\tau_1 d\tau_2.$$

Since SCF orbitals are not available we use Hückel orbitals. In order that ρ_t should not vanish, the matrix element and the coefficient $C_{tj}C_{tk}$ must not vanish. The two pairs of Huckel orbitals for pyrene[6] $j=7$, $k=13$ and $j=4$ $k=10$ contribute strongly to the spin densities at positions 2 and 7. We estimate[7,8]

$$\langle j, n+1\,|\,k, n+1\rangle = 0.246 \text{ ev}.$$

The energies of the excited configuration is approximated by the appropriate one-electron excitation energies $Ev - En = 5.6$ ev ($\beta = 2.5$ ev). These energies yield $\rho_2 = \rho_7 = -0.039$. If we take the constant of proportionality between ρ and the proton coupling constant to be 27 oe (the total splitting in naphthalene negative ion) we estimate the coupling constant at positions 7

* This work was supported by the U. S. Air Force through the Air Force Office of Scientific Research of the Air Research and Development Command and by an Equipment Loan Contract with ONR.

[1] E. de Boer and S. I. Weissman, J. Am. Chem. Soc. **80**, 4549 (1958); E. de Boer, J. Chem. Phys. **25**, 190 (1956); thesis, The Free University, Amsterdam, 1957.

[2] P. Brovetto and S. Ferroni, Nuovo cimento **5**, 142 (1957).

[3] R. Lefebvre, H. H. Dearman, and H. M. McConnell, J. Chem. Phys. **32**, 176 (1960), and related papers.

[4] G. J. Hoijtink, Mol. Phys. **1**, 157 (1958).

[5] R. Lefebvre, J. chim. phys. **54**, 168 (1957).

[6] R. Daudel and C. A. Coulson, *Dictionary of Molecular Constants* (Mathematical Institute, Oxford, 1955).

[7] R. Pariser and R. G. Parr, J. Chem. Phys. **21**, 466, 767 (1953).

[8] R. Pariser, J. Chem. Phys. **24**, 250 (1956).

FIG. 1. dX''/dH vs H for pyrene negative ion. The cation is potassium, the solvent THF, the temperature 190° K, the concentration between 10^{-5} and 10^{-4} M.

and 2 to be 1.05 oe. The value 1.09 yields good agreement with the observed spectrum.

The present consideration shows that even Lefebvre's SCF—MO's are not self-consistent so far as the electron spin is concerned. Such a self-consistency can be reached only when α and β spin electrons are described by different sets of MO's. For a more detailed discussion on this subject we may refer to a recent paper by McLachlan.[9]

[9] A. D. McLachlan, Mol. Phys. (to be published).

THE JOURNAL OF CHEMICAL PHYSICS VOLUME 34, NUMBER 2 FEBRUARY, 1961

Application of the Free-Electron Theory to Three-Dimensional Networks*

J. A. HOERNI†

Gates and Crellin Laboratories of Chemistry,‡ California Institute of Technology, Pasadena, California

(Received March 21, 1960)

The free-electron network theory is generalized to permit its application to covalent and metallic crystals. General expressions for the case where the various branches of the network have different lengths and potentials are derived. Delta function discontinuities of potential at the junctions of the branches are introduced to describe the effective field acting on valence electrons. The general equations can be applied to various special cases, such as the Kronig and Penney potential or the behavior of π electrons in planar organic molecules. The free-electron network theory is used to derive the energy band structure of diamond in the interpolation scheme proposed by Slater. Energy band features are in semiquantitative agreement with those obtained by other methods. Some discrepancies in the sequence of energy levels in different theories are pointed out. The discussion includes the possible application of the free-electron network theory to more complicated crystals.

I. INTRODUCTION

IN recent years the free-electron network theory (FE theory) has met with considerable success in dealing with conjugated systems of double bonds in planar organic molecules.[1] In this theory, it is assumed that the motion of the mobile π electrons is restricted to infinitely narrow channels (the branches of the network) joining the centers of bonded atoms, the effective potential being chosen conveniently as zero within the channels and infinitely high elsewhere. The solutions to the Schrödinger equation are one-dimensional waves propagating along the branches and the eigenvalues of the wavelength (or the energy) are determined from the boundary conditions for the various waves at the junction of several branches. The success of the FE theory has been attributed to the formal analogy between its equations and those of the LCAO MO theory.

The possibility of applying the FE theory to periodic structures has been suggested by Coulson.[2] From the particular case of π electrons in graphite, he shows that the FE and LCAO MO theories are here again in agreement, and he concludes that many features of the energy bands in crystals are to a large extent independent of the theoretical model chosen. No essentially new result, however, is brought out by the consideration of graphite, since, as in previous cases, the correspondence of FE wave functions with MO's formed from only $2p_z$

* This work was supported by the Office of Naval Research.

† Present address: Fairchild Semiconductor Corporation, Palo Alto, California.

‡ Contribution No. 2355.

[1] K. Ruedenberg and C. W. Scherr, J. Chem. Phys. **21**, 1565, 1582 (1953).

[2] C. A. Coulson, Proc. Phys. Soc. (London) **A67**, 608 (1954).

AO's is studied. In general, MO's in a crystal have to be expressed as the combination of several AO's of different types on each atom. Furthermore, the number of valence electrons occupying FE orbitals is often larger than one per atom, so that the use of orbitals of correspondingly higher energy is required. As will be shown for the case of diamond (where there are four valence electrons per atom, involving in the LCAO treatment the $2s$, $2p_x$, $2p_y$, and $2p_z$ AO's), these two factors bring out some features of the FE theory that were not apparent in previous applications.

II. GENERAL FORMULATION OF THE FREE-ELECTRON THEORY

Let us consider an arbitrary system of n atoms numbered in a suitable way. Let V_{pq} be the potential on the branch (pq), of length D_{pq}, between two atoms p and q, and x_{pq} be the branch coordinate, the point $x_{pq}=0$ coinciding with the midpoint of the branch and x_{pq} increasing toward atom q if $q>p$. Solutions of the one-dimensional Schrödinger equation along this branch are of the type

$$\phi_{pq}(x_{pq}) = A_{pq}\exp ik_{pq}x_{pq} + B_{pq}\exp(-ik_{pq}x_{pq}), \quad (1)$$

where k_{pq} is related to the energy E by

$$k_{pq}=[2m(E-V_{pq})]^{\frac{1}{2}}/\hbar. \quad (2)$$

The condition of continuity between the various branch functions ϕ_{pq}, ϕ_{pr}, $\cdots$ meeting at a junction p requires that they all take an equal value ϕ_p at this point. It will be convenient to express A_{pq} and B_{pq} in (1) in terms of the values ϕ_p and ϕ_q taken by ϕ_{pq} at the points $p[x=-\frac{1}{2}D_{pq}]$ and $q[x=\frac{1}{2}D_{pq}]$, namely,

$$A_{pq}=(2i)^{-1}\csc k_{pq}D_{pq}[\phi_q \exp i\tfrac{1}{2}k_{pq}D_{pq} - \phi_p \times \exp(-i\tfrac{1}{2}k_{pq}D_{pq})]$$

$$B_{pq}=(2i)^{-1}\csc k_{pq}D_{pq}[\phi_p \exp i\tfrac{1}{2}k_{pq}D_{pq} - \phi_q \times \exp(-i\tfrac{1}{2}k_{pq}D_{pq})]. \quad (3)$$

The first derivatives of the branch functions meeting at junction p also satisfy a boundary condition. If there is a delta function potential singularity $C_p\delta$ at the junction, the condition is

$$\sum_q \phi_{pq}' = C_p\phi_p. \quad (4)$$

In (4), the summation is taken over the atoms q joined by branches to atom p, and ϕ'_{pq} is the derivative (calculated at point p) taken in the direction pointing away from the junction. By differentiating (1), making the substitution (3), and applying Eq. (4), we obtain

$$(\sum_q k_{pq}\cot k_{pq}D_{pq} + C_p)\phi_p - \sum_q (k_{pq}\csc k_{pq}D_{pq})\phi_q = 0. \quad (5)$$

Equations (5) are the fundamental equations of our problem. They form a system of n homogeneous linear equations in the unknowns $\phi_1, \phi_2, \cdots, \phi_n$. Since the k_{pq} can be expressed in terms of the energy, Eq. (2), the condition that the determinant of the coefficients in (5) vanishes yields the energy eigenvalues E^i. For every E^i, Eqs. (5) can be solved for a set of values $\phi_1{}^i, \phi_2{}^i, \cdots \phi_n{}^i$ (on a relative scale), from which, after substitution in (3), the branch functions $\phi_{pq}{}^i$, Eq. (1), can be obtained. The normalization condition

$$\sum_{(pq)} \int |\phi_{pq}{}^i|^2 dx_{pq} = 1 \quad (6)$$

(where the summation is taken over all branches) fixes the as yet undetermined absolute scale for the $\phi_q{}^i$.

It will be seen from Eq. (2) that k_{pq} is imaginary for $E<V_{pq}$. In this case the trigonometric factors in Eq. (5) can be expressed in terms of hyperbolic factors, and the branch functions (1) in terms of exponential functions.

Let us now show that in a crystal the order of the system of equations (5) is equal to the number of atoms per unit cell. According to Bloch's theorem, the values ϕ_p and $\phi_{p'}$ taken by a solution on two equivalent atoms p and p' separated by a lattice translation $\mathbf{a}_l$, differ by a phase factor only:

$$\phi_{p'}=\phi_p \exp i\mathbf{K}\cdot\mathbf{a}_l. \quad (7)$$

For a crystal containing N unit cells, $\mathbf{K}$ takes N permissible values filling uniformly the first Brillouin zone. The energy bands are obtained from the relationship between the FE energy E and the practically continuous variable $\mathbf{K}$.

It results from (7) that whenever an atom p is bonded to an atom q' in a neighboring unit cell, the amplitude $\phi_{q'}$ in (5) is to be replaced by $\phi_q \exp i\mathbf{K}\cdot\boldsymbol{\varrho}$, where $-\boldsymbol{\varrho}$ is the translation bringing atom q' in coincidence with the corresponding atom q which lies in the same unit cell as atom p. The order n of the system (5) is therefore equal to the number of atoms per unit cell, the coefficients of every ϕ_q including possible contributions of several atoms q', q'', $\cdots$ bonded to atom p but located in other unit cells. Group theoretical methods can be used to factorize further the determinantal equation for the system (5) in case that the crystal has symmetry properties other than translational symmetry. The factorization depends on the value of $\mathbf{K}$ since it can be shown that the functions (1) form a basis for a representation of the group of the wave vector $\mathbf{K}$. (This group is defined as the subgroup formed by all symmetry operations that leave $\mathbf{K}$ invariant. For $\mathbf{K}=0$, it coincides with the crystal point group; for $\mathbf{K}$ parallel to a mirror plane, it reduces to C_{1h}, etc.) Since the solutions are normalized to unity over the entire crystal, Eq. (6), they are normalized to $1/N$ over one unit cell.

III. SOME APPLICATIONS

The determinantal equation for the system (5) is in general complicated. It becomes considerably simpler,

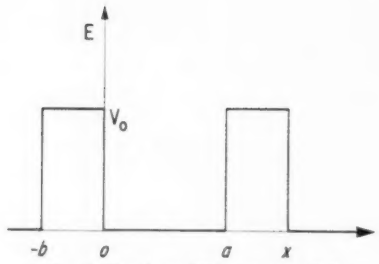

FIG. 1. Kronig and Penney potential.

however, in special cases which we shall briefly review here:

(a) In most previous applications of the FE theory, all the branches are supposed to have the same length and the potential is taken as constant over the whole network (except for delta function discontinuities at the junctions). Equation (5) reduce to

$$(\mathfrak{N}_p \cos kD + k^{-1}C_p \sin kD)\phi_p - \sum \phi_q = 0, \qquad (8)$$

where $\mathfrak{N}_p$ is the number of branches meeting at junction p. If there are no discontinuities, $C_p=0$, and Eqs. (8) are identical with the equations derived by Ruedenberg and Scherr.[1] The parameters C_p were first introduced in Eq. (4) by Kuhn[3] and correlated later with delta function discontinuities by Frost[4] and Coulson.[5]

(b) Let us consider the case of a monoatomic crystal where a given atom p is joined by branches of constant potential to equivalent atoms q', q'', $\cdots$ which can be reached by lattice translations $\pm\mathbf{a}_l$ $(l=1, 2, 3)$. Because of (7), the system (5) is of order unity and the determinantal equation reads

$$\sum_l \cot k|\mathbf{a}_l| + \tfrac{1}{2}k^{-1}C = \sum_l \csc k|\mathbf{a}_l| \cos \mathbf{K}\cdot\mathbf{a}_l, \qquad (9)$$

an expression quoted by Coulson[2] for the case $C=0$. Further specialization of (9) to cubic lattices with first neighbor interactions is immediate.

(c) The familiar Kronig and Penney potential[6] is related to the problem of a one-dimensional diatomic crystal, where the two interatomic distances a and b correspond to branch potentials 0 and V_0, respectively, and the C_p are zero (Fig. 1). For the energy range $E<V_0$, the solutions are of the exponential type over the interval $-b<x<0$. By applying (5) to the amplitudes ϕ_0 and ϕ_a for the atoms located at $x=0$ and a, we obtain

$$(k\cot ka+\gamma\coth\gamma b)\phi_0 - \{k\csc ka+\gamma\,\mathrm{csch}\gamma b \times \exp[-iK(a+b)]\}\phi_a = 0$$

$$-[k\csc ka+\gamma\,\mathrm{csch}\gamma b\exp iK(a+b)]\phi_0 + (k\cot ka+\gamma\coth\gamma b)\phi_a = 0,$$

where $k=(2mE)^{\frac{1}{2}}/\hbar$ and $\gamma=(2m)^{\frac{1}{2}}(V_0-E)^{\frac{1}{2}}/\hbar$. The determinantal equation reduces to

$$(\gamma^2-k^2)(2\gamma k)^{-1}\sin ka\sinh\gamma b + \cos ka\cosh\gamma b = \cos K(a+b). \qquad (10)$$

It should be noted that the present derivation of (10) is simpler than the original treatment in footnote reference 6, which entails the solution of a determinant of the fourth order.

(d) In the previous example, the limit $b\to 0$, $V_0\to\infty$ (their product remaining finite) corresponds to the case of a linear chain of equidistant similar atoms with delta function discontinuities on each atom. Since the crystal is monoatomic, (8) can be used and reduces here to

$$\cos ka + \tfrac{1}{2}Ca\,(\sin ka)/ka = \cos Ka. \qquad (11)$$

By comparing (11) with the limiting value of (10), it is found that $C=2mV_0b/\hbar^2$. Here again the present derivation of (11) bypasses the cumbersome determinantal expansion used in footnote reference 6.

IV. NODAL SOLUTIONS

Let us consider again the special case as discussed above where all branches have the same length D and potential $V_0=0$. For FE wave lengths equal to $2D$, $2D/2$, $2D/3$, $\cdots$, we may have solutions with nodes on each atom center of the system. These nodal solutions cannot be determined by means of Eqs. (8), since all the ϕ_q vanish, but they are obtained directly by substituting (1) in (4). In the case $\lambda=2D$, the nodal branch functions are

$$\phi_{pq}(x_{pq}) = A_{pq}\cos(\pi x_{pq}/D), \qquad (12)$$

and the substitution of (12) in (4) yields

$$\sum A_{pq}=0, \qquad (13)$$

where the summation is taken over all branches pq meeting at junction p. As before, the amplitude $A_{pq'}$ of a bond not located in the same unit cell as atom p is equal to the amplitude of the corresponding bond in the same unit cell as atom p, multiplied by a suitable translation factor $\exp i\mathbf{K}\cdot\boldsymbol{\varrho}$. Hence, Eqs. (13) form a system of n equations in m unknowns, n and m being the number of atoms and bonds, respectively, per unit cell. If Eqs. (13) are of rank, r, they posses $m-r$ independent solutions. In general, the rank of Eqs. (13) is equal to the number of equations (or atoms) n, so that we reach the important result: For a given $\mathbf{K}$ value, the number of degenerate nodal solutions with $kD=\pi$ is equal to the difference between the number of bonds and the number of atoms per unit cell. Therefore, the degeneracy of the nodal solutions in the Brillouin zone is equal to the same difference for the whole crystal. If two or more of Eqs. (13) are linearly dependent, r is smaller than n, and the number of nodal solutions in correspondingly larger. Solutions associated with

[3] H. Kuhn, J. Chem. Phys. **22,** 2098 (1954).
[4] A. A. Frost, J. Chem. Phys. **22,** 1613 (1954); **23,** 985 (1955); **25,** 1150 (1956).
[5] C. A. Coulson, Proc. Phys. Soc. (London) **A68,** 1129 (1955).
[6] R. de L. Kronig and W. G. Penney, Proc. Roy. Soc. (London) **A130,** 499 (1931).

different **K** values are automatically orthogonal. The solutions for a given **K** can be orthogonalized in an infinite number of ways. For special values of **K**, they can be sorted out according to the various irreducible representations of the group of the wave vector **K**. The set of solutions obtained in this way is not unique, however, if more than one solution belongs to a given symmetry type.

V. CASE OF DIAMOND

The diamond structure is formed of two interpenetrating face-centered cubic lattices. The smallest (rhombohedral) unit cell contains two atoms 1 and 2 of coordinates $(0, 0, 0)$ and $(\frac{1}{2}a, \frac{1}{2}a, \frac{1}{2}a)$, the edge of the cubic unit cell being $2a$. The three neighbors of atom 1, other than atom 2, are brought into coincidence with atom 2 by the translations $(0, a, a)$, $(a, 0, a)$ and $(a, a, 0)$, whereas the three neighbors of atom 2, other than atom 1, are brought into coincidence with atom 1 by the translations $(0, -a, -a)$, $(-a, 0, -a)$ and $(-a, -a, 0)$. Since we consider first order interactions (i.e., draw branches between nearest neighbors only), all branches have the same length and potential, and Eqs. (8) can be used. Due to the substitutions (7), these equations reduce to

$$(4\cot kD+k^{-1}C)\phi_1-(\csc kD)(1+e^{-i(\xi+\eta)}+e^{-i(\eta+\zeta)}+e^{-i(\zeta+\xi)})\phi_2=0$$

$$-(\csc kD)(1+e^{i(\xi+\eta)}+e^{i(\eta+\zeta)}+e^{i(\zeta+\xi)})\phi_1+(4\cot kD+k^{-1}C)\phi_2=0, \quad (14)$$

where $\xi=K_xa$, $\eta=K_ya$, and $\zeta=K_za$. The determinantal equation is

$$(\cos kD+\tfrac{1}{4}Ck^{-1}\sin kD)^2=\cos^2\tfrac{1}{2}\xi\cos^2\tfrac{1}{2}\eta\cos^2\tfrac{1}{2}\zeta+\sin^2\tfrac{1}{2}\xi\sin^2\tfrac{1}{2}\eta\sin^2\tfrac{1}{2}\zeta, \quad (15)$$

and yields the relation between $E(=\hbar^2k^2/2m)$ and **K**. In addition, we also have nodal solutions of energy $E=\hbar^2\pi^2/2mD^2$. Since there are two atoms and four bonds per unit cell, the degeneracy of these solutions for each **K** value is twofold.

In choosing a suitable value of C in (14), we have followed Slater's suggestion[7] that the parameters of an approximate theory can be estimated from more accurate calculations which are available for certain points of high symmetry in the Brillouin zone. For diamond, the most reliable energy values have been obtained by Herman[8] for the center of the Brillouin zone, using the orthogonalized plane waves method. We have chosen a value of C such that the relative separation of the three lowest energy levels is correctly reproduced in the FE theory. The resulting value, $C=1.77$ A^{-1}, can then be substituted in (15) to calculate the energy at various points in the Brillouin zone. Figure 2 shows the FE energy curves along axes [100] and [111]. For comparison the dashed curves show the values that Slater and Koster obtained by

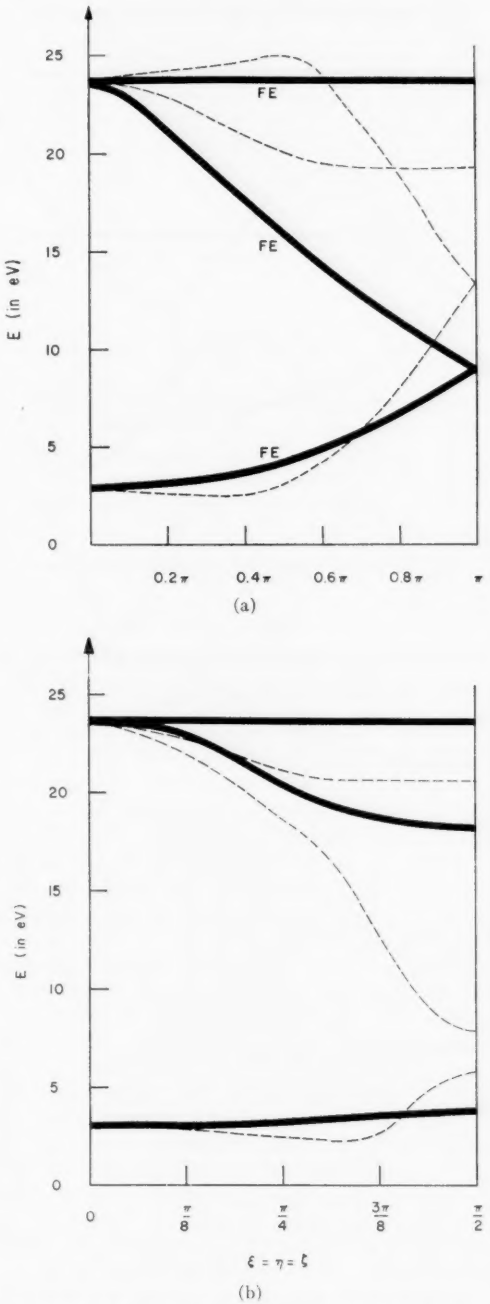

FIG. 2. Variation of energy with wave vector for the diamond valence band using the FE theory. Slater and Koster's results are shown by dashed lines: (a) 100 direction; (b) 111 direction.

[7] J. C. Slater and G. F. Koster, Phys. Rev. **94**, 1498 (1954).
[8] F. Herman, Phys. Rev. **88**, 1210 (1952).

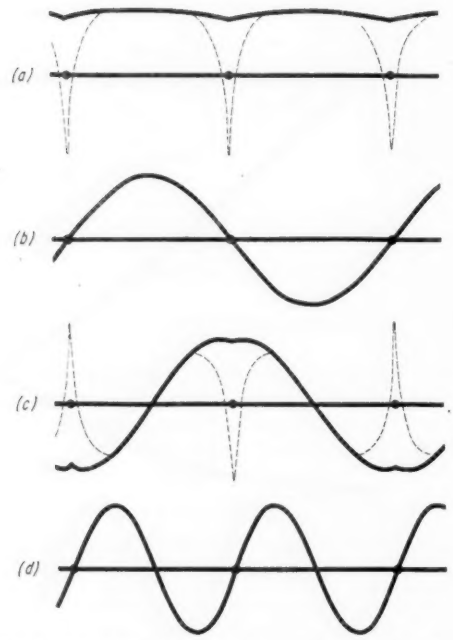

FIG. 3. Plot of FE orbitals for the center of the Brillouin zone in order of increasing energy. Orbitals are plotted along one of the staggered chains of atoms running in the ⟨110⟩ direction of the diamond lattice. Corresponding LCAO orbitals (formed by symmetric and antisymmetric combinations of $2s$ and $2p$ orbitals) are shown by dashed lines in the cases where they depart significantly from the FE orbitals.

using the LCAO method as an interpolation scheme.[7] Both theories predict that diamond should be an insulator and are in qualitative agreement in their description of the features of the valence band.[9] A notable exception relates to the existence of a doubly degenerate band of zero width in the FE treatment. A similar result was obtained by Kimball[10] by using the cellular method. This characteristic results from a common topological feature, namely, that the points at which Kimball matched his solutions on different atomic polyhedra are the same as the points of intersection of these polyhedra by the FE network.[11] For the conduction band both the FE and cellular methods predict that at the center of the Brillouin zone there is a nondegenerate level below a triply degenerate level (of same energy as another zero width band). This result does not agree with the sequence of levels deduced from the more accurate orthogonalized plane wave method, and will be discussed in the next section.

The value of the parameter C in (15) was chosen so as to reproduce the relative separation of the three lowest energy levels. In order to also reproduce their absolute separation, we can expand the energy scale by replacing the free electron mass m in (2) by an effective mass m^*. As would be expected from the usual behavior of valence electrons in solids, the resulting value $m^*/m=0.67$, is smaller than unity.

VI. DISCUSSION

It has been found above that the constant C is positive in the case of diamond. Therefore, the delta function discontinuities of potential at the atomic centers repel the electrons of the network, in apparent contradiction to the fact that atomic potentials are attractive. The explanation lies in our disregard of the inner electrons in filling the FE orbitals. The states of lowest energy are filled by valence electrons in the FE theory, whereas they are occupied by $1s$ electrons in the LCAO theory. In the latter case, the valence electrons do not approach the atomic centers because of the presence of nodes in the atomic $2s$ and $2p$ orbitals. An equivalent effect on FE orbitals without introduction of additional nodes is obtained by adding a repulsive potential term at the atomic centers.[12] This is shown on Fig. 3 where the four FE orbitals of lowest energy and the corresponding LCAO orbitals for the central point of the Brillouin zone have been plotted along one of the staggered chains of carbon atoms running in the ⟨110⟩ directions. In cases (a) and (c) the repulsive delta function potential clearly brings the FE orbitals into closer agreement with the LCAO orbitals. In cases (b) and (d), the repulsive potential does not affect the FE orbitals since these are zero at the atomic centers. The agreement with LCAO orbitals is then brought about by the same number of nodes in each orbital. If we assume that the number of nodes (including atomic nodes) is a measure of the energy of LCAO as well as FE orbitals, we can understand why the sequence of energies for the cases (c) and (d) is different in the FE and LCAO case. The number of nodes per bond in the FE case is one and two in cases (c) and (d) respectively, whereas in the LCAO case it is three and two. The opposite trend takes place because the FE theory reproduces the atomic nodes of the $2p$ orbitals but not those of the $2s$ orbitals. Clearly an exact node correspondence could be obtained by including inner electrons when filling the FE orbitals; however, the qualitative agreement between the energy behavior of the two theories would be lost. For instance, the LCAO bevels obtained by the symmetric and antisymmetric combinations of $1s$ orbitals have almost the same energy, whereas the corresponding FE energies would differ by the amount $h^2/8mD^2$.

An equivalent discussion of correspondence of wave functions has been given by Slater in the case of the $3s$

[9] Results in essential agreement with the LCAO treatment have been obtained by G. G. Hall [Phil. Mag. **43**, 338 (1952); **3**, 429 (1958)] using the method of equivalent orbitals.

[10] G. E. Kimball, J. Chem. Phys. **3**, 560 (1935).

[11] More recent work on the cellular method by V. Zehler [Ann. Physik **13**, 229 (1953)] has established that the zero-width band gets a finite width when more matching points on the polyhedra are used.

[12] The same procedure was used by H. Helmann [J. Chem. Phys. **3**, 61 (1935)] to obtain nodeless wave functions of valence electrons in light atoms.

orbital in metallic sodium.[13] This orbital can be closely approximated by a plane wave, which does not, however, have the same number of nodes as the corresponding LCAO orbital. The success of any approximate free-electron treatment is a measure of the more or less close resemblance of the electronic orbitals to a free wave (whether in the form of a three-dimensional plane wave in the case of sodium or of a one-dimensional network wave in the case of diamond). The network form of the wave will be more suited to open structures with strongly directed bonds whereas the three-dimensional form will apply to close packed structures with more uniform electronic density. The free-wave character is most pronounced when there is a large energy difference between the valence and the inner electrons, and will be expected to decrease in the case of the atoms of higher atomic number (for instance silicon and germanium).

Finally, we will mention two properties of the FE model that make its application to more complicated networks rather uncertain. First the occurrence of a widespread degeneracy associated with the nodal solutions in the case of a network of identical branches is an unattractive feature for the study of complicated structures. The resulting zero-width bands may be only partly occupied and no significant prediction about the metallic or insulating character of the crystal can be made. Since the nodal solutions vanish at atomic centers, they are insensitive to the introduction of delta function potential discontinuities at these points. The degeneracy might be removed in certain cases by taking into account possible variations in length and potential of the various branches of weak potential between an atom and its next nearest neighbors. This is not always possible, however, as can be seen simply in the diamond case. The branches joining second neighbor atoms form two interpenetrating networks, each of which is identical to that for a fcc lattice. The nodal solutions for these two networks, plus the original first neighbor (diamond) network, are finite on any one network and identically zero on the other two. It follows that the nodal solutions which are finite on the first neighbor network are identical to those obtained without consideration of second-neighbor interactions.

The second weakness of the FE theory is that a network made of infinitely narrow branches fails to account for the transverse properties of the wave functions of real bonds with finite width. In a linear chain of atoms, for example, the FE orbitals for $2p\pi$ bonds have an infinitely higher energy than the orbitals for all $ns\sigma$ and $np\sigma$ bonds. The correct energy sequence could only be obtained by using branches of finite width; this procedure would, however, complicate the matching of branches at an atom center. Since the distinction between σ and π bonds seems scarcely worth making in the simple FE theory, it will be expected that energy band features based on that distinction will not be reproduced correctly. Such is, for example, the case for the zero-width bands found in diamond. The corresponding LCAO treatment makes use of combinations of $2p\sigma$ and $2p\pi$ orbitals and leads indeed to finite band widths (Fig. 2). Even when only σ bonds are under consideration, the concept of infinitely narrow branches can lead to difficulties. Consider two possible orbitals for the cross-shaped potential well shown in Fig. 4. Although the p-type orbital on the left has a lower energy than the d-type orbital on the right, both go over to FE orbitals of same wavelength and energy for a vanishing width of the members of the cross. This lack of bond interactions in the FE theory could somehow be corrected by introducing second-neighbor interactions of the type described previously.

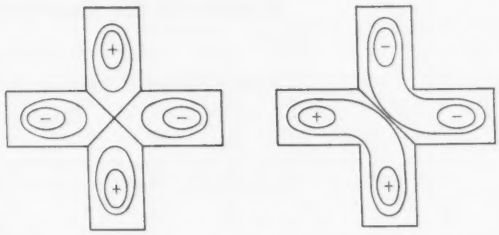

FIG. 4. Contour lines for p and d orbitals in a cross-shaped potential well.

It should be pointed out that each of the suggested refinements to the FE method introduces new parameters of sometimes doubtful physical significance, so that the simplicity and convenience of the original treatment are lost. Whereas the theory has met with considerable success in dealing with planar organic molecules, it is unlikely that it would as readily apply to the larger variety of orbitals met in three-dimensional structures, except in such simple cases as the diamond structure. Our results show that the FE theory can then be used as a rapid and simple tool in getting an estimate of energy bond features.

ACKNOWLEDGMENT

The author wishes to thank Professor Linus Pauling for suggesting this problem and for several helpful discussions.

[13] J. C. Slater, Revs. Modern Phys. **6**, 209 (1934).

Kinetics of the Reactions of Alkyl Iodides with HI*

SIDNEY W. BENSON AND EDWARD O'NEAL

Chemistry Department, University of Southern California, Los Angeles, California

(Received June 27, 1960)

A reexamination of Ogg's data on the kinetics of the reactions of RI+HI→RH+I_2 where R=CH_3, C_2H_5 or $n-C_3H_7$, shows that the mechanism is a simple I-atom catalyzed, radical reaction with the steps

$$I+RI \underset{2}{\overset{1}{\rightleftarrows}} R+I_2$$

$$R+HI \xrightarrow{3} RH+I.$$

The rate expression is

$$d(I_2)/dt = k_1k_3K^{\frac{1}{2}}(RI)(HI)/[k_2(I_2)+k_3(HI)],$$

where K is the equilibrium constant for dissociation of I_2. Values are obtained for k_1, and the inhibition ratio k_3/k_2 at one temperature and for k_1k_3/k_2 over a temperature range. Using some entropy estimates, values are deduced for A_1, A_2, A_3, and A_4 (reverse of step 3) all of which seem quite reasonable and self-consistent. The difference (E_3-E_2) appears to lie between 0 and 2 kcal/mole while E_1 is in excess of the estimated endothermicity of reaction (1) by not more than 1.5 kcal mole. There seems to be good agreement with independent data on the kinetics of pyrolysis of alkyl and aryl iodides which also turn out to be I-atom catalyzed, radical reactions.

I. INTRODUCTION

THE gas-phase reactions of both alkyl and aromatic iodides, RI with HI appear to go quantitatively to produce parent hydrocarbon plus iodine and in addition seem to be kinetically well-behaved. In view of this, it is surprising that so little attention has been devoted to their study. The only quantitative investigation has been reported by Ogg[1] who measured the rates for MeI, EtI, and *n*-PrI over the temperature range 250–320°C. and over a considerable range of compositions. He found that over the region of about 10 to 70% reaction the rate law could be fitted quite well to the equation,

$$d(I_2)/dt = k_0(RI)(HI). \qquad (1)$$

However, the apparent second-order rate constants k_0, obtained in this way decreased with increasing $(HI)_0$ the initial concentration of HI and Ogg made a further decomposition into the composite rate law

$$d(I_2)/dt = [K_1+K_2/(HI)_0](RI)(HI). \qquad (2)$$

This seemed to fit the data quite well over most of the composition range. However, the constants K_2 appeared to fall off with decreasing pressure and in addition the data during the first 10% of the reaction yielded slower rates. This latter was interpreted as an induction period despite the fact that there was no important effect of surface on the reaction, and that the mechanism proposed by Ogg did not allow for such an in-tion period.[2]

The first term on the rhs of Eq. (2) was interpreted by Ogg as a true, four-center, bimolecular reaction between RI and HI analogous to the classical four-center reaction of HI. The second term involving $(HI)_0$, the initial concentration of HI was attributed to a simultaneous free radical path with the suggested mechanism:

$$\begin{aligned}
&\text{initiation:} && RI \xrightarrow{k_i} R+I \\
&\text{propagation:} && R+HI \xrightarrow{k_3} RH+I \\
&\text{inhibition:} && R+I_2 \xrightarrow{k_2} RI+I \\
&\text{termination:} && 2I+M \xrightarrow{k_t} I_2+M. \qquad (3)
\end{aligned}$$

Applying the stationary state treatment to this mechanism, the rate of formation of I_2 is given by

$$d(I_2)/dt = k_ik_3(RI)(HI)/[k_3(HI)+k_2(I_2)]. \qquad (4)$$

To obtain the form of Eq. (2) Ogg then assumed that $k_2=k_3$. Since the stoichiometry of the over-all reaction requires that $(I_2)+(HI)=(HI)_0$, Eq. (4) then reduces to

$$d(I_2)/dt = k_i(RI)(HI)/(HI)_0, \qquad (5)$$

in agreement with Eq. (2). The apparent decrease with decreasing pressure of the value of the rate constant K_2 which is now equal to k_i was then attributed to that of a first-order rate constant in the region of pressure dependence.

There are many difficulties in the interpretation proposed by Ogg. In the first place, the Arrhenius A factors obtained for the bimolecular step corresponding to K_1 [Eq. (2)] are all of the order of 2×10^{11} l/mole/

* This work has been supported by grants from the U. S. Atomic Energy Commission and the Office of Ordnance Research, U. S. Army.

[1] R. A. Ogg, Jr., J. Am. Chem. Soc. **56**, 526 (1934).

[2] Ogg suggested that there was an anomalously slow mixing of reactants which could also account for such an effect.

TABLE I. Values of $f(x, K_{3.2})$ as a function of x and $K_{3.2}$ at $(I_2)_0=0$.[a]

$K_{3.2}$	0	0.05	0.10	0.20	0.30	0.40	0.50	0.60	0.70	0.80	1.00	f_{Av}[b]
0.25	0	0.78	0.97	1.12	1.15	1.15	1.13	1.11	1.08	1.05	1.00	1.10
0.20	0	0.93	1.13	1.24	1.25	1.22	1.18	1.14	1.10	1.06	1.00	1.19
0.15	0	1.15	1.34	1.40	1.35	1.29	1.23	1.17	1.12	1.08	1.00	1.30
0.10	0	1.54	1.66	1.60	1.48	1.37	1.28	1.21	1.15	1.09	1.00	1.47
0.05	0	2.27	2.18	1.87	1.64	1.47	1.35	1.25	1.17	1.10	1.00	...
0	0	4.48	3.16	2.24	1.83	1.58	1.42	1.29	1.20	1.12	1.00	...

[a] Values of $f(x, K_{3.2})$ for $(I_2)_0/(HI)_0=y\neq 0$ can be obtained from the above table by assuming that the run with added $(I_2)_0$ corresponds to a hypothetical run in which the initial (HI) is $(HI)_0'=(HI)_0+(I_2)_0=(HI)_0(y+1)$. The extent of reaction x is now equal to $(y+1)x-y$ where x' is the extent of reaction in the hypothetical reaction so that x has the initial value $y/(y+1)$. Fifty percent reaction ($x=0.50$) is then equivalent to $x=(y+0.5)/(y+1)$.

[b] f_{Av} is taken over the range 10% to 60% reaction.

$$f(x, K_{3.2})=x^{\frac{1}{2}}/[1-(1-K_{3.2})(1-x)] \text{ for } y=(I_2)_0/(HI)_0=0.$$

sec[3] which is implausibly high for a four-center reaction. The analogous HI reaction has A factors about ten fold less and for the more complex case of an alkyl iodide plus HI, transition state calculations, even with the loosest type of complex do not give A factors in excess of about 10^9 l/mole/sec. In addition the activation energies E_1 are in the range of 29 to 33 kcal/mole which are implausibly small for the type of four-center reaction involved[4] relative to that for 2 HI.

Far worse are the values obtained for k_i (i.e., K_1). The activation energies, E_i which must be minimum values for the C—I bond dissociation energies were 43 kcal, the same for all RI. Current thermodynamic data for alkyl iodides and alkyl radicals suggest that the relevant bond dissociation energies are about 55 kcal/mole for CH_3I and 54 kcal for EtI and PrI. In addition the assumption that $k_2=k_3$, is known to be in error both from subsequent work by Ogg[5] and from unpublished results in these laboratories on acetone photolysis in the presence of HI.[6]

Finally, the Arrhenius factors A_i were all about 10^{12} sec^{-1} which is implausibly low for a simple bond-breaking, unimolecular reaction.

All of these considerations lead us to seek a different interpretation for the reaction of alkyl iodides with HI.

II. FREE RADICAL MECHANISM

Using our present knowledge of the rate constants for elementary step reactions together with relevant bond dissociation energies, the following seems to be the most reasonable mechanism for the reaction of RI with HI:

$$\text{initiation:} \quad I_2+M \rightleftharpoons 2I+M \qquad (K)$$

$$\text{propagation:} \quad I+RI \underset{2}{\overset{1}{\rightleftharpoons}} R+I_2$$

$$R+HI \underset{4}{\overset{3}{\rightleftharpoons}} RH+I. \qquad (6)$$

Applying the stationary-state hypothesis to this system we find for the rate of production of I_2[neglecting Eq. (4)]

$$\frac{d(I_2)}{dt}=\frac{k_1k_3K^{\frac{1}{2}}(RI)(HI)(I_2)^{\frac{1}{2}}}{k_2(I_2)+k_3(HI)}, \qquad (7)$$

where K is the equilibrium constant for I atom production.

If we make use of the stoichiometry to eliminate $(I_2)=(I_2)_0+(HI)_0-(HI)$ where $(I_2)_0$ is the initial concentration of I_2 we can write

$$\frac{d(I_2)}{dt}=\frac{k_1k_3K^{\frac{1}{2}}(RI)(HI)}{k_2(HI)_0^{\frac{1}{2}}} \times\left\{\frac{\{1-[(HI)/(HI)_0]+[(I_2)_0/(HI)_0]\}^{\frac{1}{2}}}{1+[(I_2)_0/(HI)_0]+[(k_3/k_2)-1][(HI)/(HI)_0]}\right\} \qquad (8)$$

$$=\frac{k_1k_3K^{\frac{1}{2}}(RI)(HI)}{k_2(HI)_0^{\frac{1}{2}}}f(x, K_{3.2}). \qquad (9)$$

In Eq. (9) we have set $f(x, K_{3.2})$ equal to the expression in parenthesis in Eq. (8) with $x=1-(HI)/(HI)_0$ being the fraction of reaction and $K_{3.2}=k_3/k_2$. The function, $f(x, K_{3.2})$ can now be shown to be a very slowly varying function of x over most of the range of reaction so long as $(I_2)_0/(HI)_0$ is much less than unity. In Table I are tabulated values of $f(x, K_{3.2})$ as a function of x for different, probable values of $K_{3.2}$

[3] These were originally reported as tenfold higher due to an error in reduction of units. This was also true of k_0 which is corrected here.

[4] The complex involves a Walden inversion on the carbon atom by the H atom of the HI.

[5] R. R. Williams, Jr. and R. A. Ogg, J. Chem. Phys. **15**, 696 (1947).

[6] Over a broad range of temperatures k_2/k_3 is of the order of ten for all the alkyl radicals in good agreement with expectations from simple transition state models.

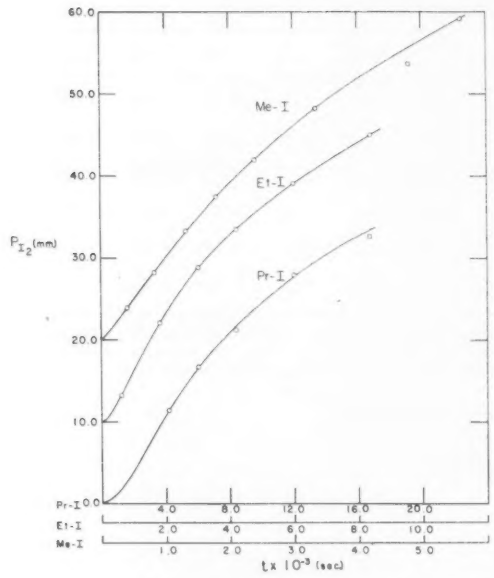

FIG. 1. Some typical pressure-time data for the reactions of HI with MeI (280°C), top curve, EtI (260°C) middle curve and *n*-PrI (290°C), bottom curve. Abscissa as time in ksec. Note different scales for each reaction. Ordinates P_{I_2} (mm Hg).

and zero initial I_2. The footnote indicates the way to calculate $f(x, K_{3.2})$ for added initial I_2.

It can be seen that for values of $K_{3.2}$ between 0.25 and 0.15, $f(x, K_{3.2})$ is reasonably constant between 10% and 70% reaction. For values of $K_{3.2}$ between 0.25 and 0.50 this would no longer be true nor would it be true for values of $K_{3.2}$ much less than 0.12. Ogg actually reported that his rate data during the first 10% of reaction fell below his second-order plots and this is precisely what is observed here for $f(x, K_{3.2})$ in this region. Because of this initial "slow" rate, Ogg calculated his second-order rate constants from data between 10% and about 60% reaction. In the last column of Table I we have calculated f_{av}, the average values of $f(x, K_{3.2})$ over the interval 10% to 60% reaction. In the range of $K_{3.2}$ between 0.25 and 0.10, the average deviation of $f(x, K_{3.2})$ from this mean value is about ±5% which is within the analytical precision of Ogg's data.[7] It thus appears that the apparent second-order rate law which Ogg observed arises from a neglect of the initial stages of the reaction, together with the fortuitous circumstance that the inhibition constant $K_{3.2}$ for the three systems studied is about 0.15 practically independent of temperature.

If the original data were available it would be possible to make a direct test of the rate law given by Eq. (7). Ogg reported such data only for three runs, one for each of the alkyl iodides. To use these data we have recast Eq. (7) into the following form,

$$Q = (\mathrm{RI})(\mathrm{I_2})^{\frac{1}{2}}/\mathrm{R_{I_2}} = (1/k_1K^{\frac{1}{2}}) + (1/k_1K^{\frac{1}{2}})(k_2/k_3)[(\mathrm{I_2})/(\mathrm{HI})], \quad (10)$$

where $\mathrm{R_{I_2}} = d(\mathrm{I_2})/dt$. On plotting the raw data in the form (I_2) against time, a smooth curve may be drawn through the experimental points. In the three runs mentioned such plots are shown in Fig. 1. The dotted lines indicate the extrapolation through the origin and show the initially slow rate. By drawing tangents to these smoothed curves it is possible to get R_{I_2} the instantaneous rate of formation of I_2. From the curves themselves and the over-all stoichiometry of the reaction it is then possible to compute the instantaneous values of (I_2), (RI), and (HI) as well. From all of these data the function Q may be calculated as well as the corresponding values of the ratio $(I_2)/(HI)$. If the proposed rate law is correct then Q should be a linear function of the ratio $(I_2)/(HI)$.

Plots of Eq. (10) for the three runs are shown in Fig. 2. It can be seen that the data do fall on straight lines with positive intercepts. From the values of the slopes we can obtain the quantities $k_2/k_3k_1K^{\frac{1}{2}}$ and from the intercepts of the values of $k_1K^{\frac{1}{2}}$. The ratio of these two quantities yields the values of the inhibition constant $k_3/k_2 = K_{3.2}$. It is 0.15 for both CH_3I and EtI and 0.11 for *n*-PrI at the temperatures given. It will be noted from Table I that these values of $K_{3.2}$ are just

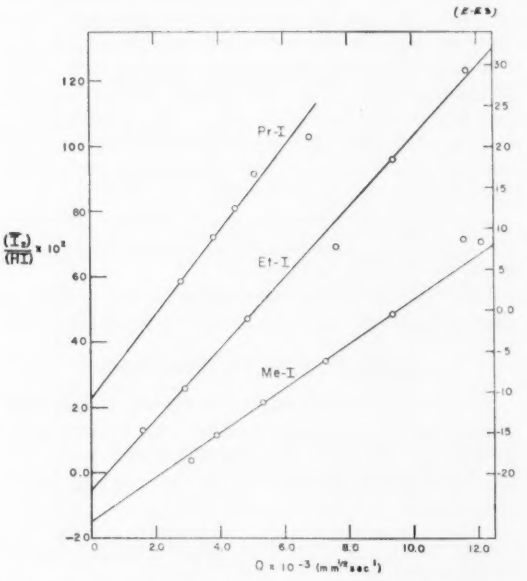

FIG. 2. Test of the rate expression [Eq. (10)] for the reactions of the alkyl iodides with HI. Data from Fig. 1. For MeI use left-hand ordinate and multiply abscissa by 10. For EtI subtract 10 from left-hand ordinate and multiply abscissa by 10. For *n*-PrI use right-hand ordinate and abscissa as shown. Ordinates: $(I_2)/(HI) \times 10^2$. Abscissa: $Q = (RI)(I_2)^{\frac{1}{2}}/R_{I_2}$ in units of $(mm\ Hg)^{\frac{1}{2}}$ sec $\times 10^{-3}$.

[7] This deviation is, however, systematic rather than random, so that Ogg's data will be biased by his range of observation and his weighting of points.

TABLE II. Kinetic data from pressure-time curves.

RI	T (°C)	$k_1\times10^{-3}$ [a]	$-\log K^{\frac{1}{2}}$ [b]	k_3/k_2
MeI	280	1.60	5.28	0.15
EtI	260	6.8	5.54	0.15
n-PrI	290	12.9	5.16	0.11

[a] Units for k_1 are liter/mole/sec.
[b] K is in units of moles/liter, calculated from thermodynamic data in the NBS circular No. 500.

TABLE III. Over-all rate constants for the reaction of CH_3I with HI.

T (°C)	Initial pressures (mm Hg) CH_3I	HI	$k_0\times10^{a}$	$k_0(HI)_0^{\frac{1}{2}}\times10^{2}$ [b]	
320.0	195.0	235.1	2.16	1.72	
	241.1	164.1	2.84	1.89	
	292.7	103.8	3.68	1.95	
	312.8	49.6	6.18	2.27[c]	
	66.1	109.3	3.28	1.78	
	85.2	47.0	5.20	1.86	
	15.2	30.8	8.05	2.32[c]	
	32.4	15.8	9.65	2.00	
	5.9	10.0	14.2	2.34[c]	
	10.4	5.9	16.1	2.03	Av=1.89
310.0	194.5	216.4	1.30	1.00	
	249.7	148.6	1.64	1.05	
	256.7	120.7	1.82	1.05	
	298.7	55.5	2.92	1.14	Av=1.06
300.0	300.0	265.0	0.718	0.618	
	202.4	219.4	0.790	0.619	
	302.9	72.4	1.41	0.634	
	363.7	54.1	1.75	0.682[c]	
	101.8	219.7	0.765	0.600	
	48.7	116.2	0.837	0.477[c]	
	52.6	62.6	1.02	0.426[c]	
	199.3	85.9	1.14	0.559	
	21.8	68.8	1.14	0.500[c]	
	124.0	51.0	1.20	0.452[c]	
	136.3	50.2	1.32	0.495[c]	
	11.1	41.4	1.49	0.509[c]	
	227.5	56.4	1.49	0.592	
	36.6	13.4	3.32	0.64[c]	
	3.0	5.1	5.4	0.63[c]	
	11.6	5.5	6.6	0.82[c]	
	4.6	2.4	7.2	0.594[c]	
	11.0	3.3	9.6	0.91[c]	Av=0.60
290.0	187.5	206.8	0.417	0.319	
	238.9	151.8	0.499	0.328	
	278.0	103.6	0.646	0.351	
	326.9	48.5	1.03	0.383[c]	Av=0.333
280.0	185.7	239.0	0.225	0.187	
	218.2	208.5	0.231	0.180	
	263.6	120.4	0.298	0.176	
	317.3	56.6	0.473	0.192	Av=0.182
270.0	167.3	254.9	0.108	0.092	
	143.0	202.8	0.119	0.092	
	261.1	111.9	0.159	0.091	
	311.7	57.5	0.244	0.101	Av=0.092

[a] Units of k_0 in liter/mole/sec.
[b] Units of $(HI)_0$ in moles/liter.
[c] Data not used in obtaining the average values listed for $k_0(HI)_0^{\frac{1}{2}}$.

TABLE IV. Over-all rate constants for the reaction of C_2H_5I with HI.

T (°C)	Initial pressures (mm Hg) C_2H_5I	HI	$k_0\times10^{a}$	$k_0(HI)_0^{\frac{1}{2}}\times10^{2}$ [b]	
300.0	53.1 (6.666×10^{-2})	158.2	4.60	3.06	
	43.6	151.5	4.78	3.10	
	33.8	127.6	5.38	3.22	
	89.4	92.9	6.58	3.35	
	102.7	59.3	7.77	3.06	
	82.8	52.3	9.26	3.54	
	101.5	31.9	11.96	3.57	
	15.9	38.0	11.24	3.67	Av=3.32
	36.7	16.2	19.7	4.20[c]	
	4.3	11.8	22.7	4.10[c]	
	4.0	9.0	26.9	4.26[c]	
	4.7	6.9	32.3	4.5[c]	
	7.7	5.3	33.5	4.07[c]	
	4.5	6.1	35.9	4.7[c]	
290.0	27.0	153.5	2.64	1.75	
	48.1	152.9	2.76	1.82	
	92.9	146.0	2.82	1.82	
	70.4	109.0	3.23	1.80	
	109.1	47.5	5.29	1.95	Av=1.83
	24.3	27.5	7.64	2.12[c]	
	41.3	19.9	10.0	2.37[c]	
	4.7	4.3	24.6	2.72[c]	
	6.8	4.1	25.2	2.72[c]	
280.0	78.9	177.7	1.50	1.07	
	48.7	148.5	1.56	1.01	
	76.6	68.3	2.19	0.95	
	79.5	46.9	2.83	1.04	
	115.1	41.1	3.12	1.07	
	14.1	38.9	3.12	1.04	
	21.8	27.6	3.92	1.11	
	31.9	19.0	4.85	1.14	
	3.7	5.3	7.5	0.92	
	4.8	3.7	9.8	1.01	Av=1.04±0.05
270.0	75.6	170.4	0.815	0.578	
	80.3	100.6	0.934	0.509	
	78.8	64.4	1.16	0.506	
	78.0	60.1	1.24	0.523	
	82.9	57.2	1.22	0.503	
	76.5	31.2	1.75	0.530	Av=0.525±0.019
260.0	35.9	166.3	0.429	0.306	
	45.9	118.7	0.500	0.298	
	90.5	87.8	0.529	0.272	
	84.6	57.2	0.632	0.262	
	84.2	48.1	0.695	0.264	Av=0.280±0.15
250.0	92.1	178.9	0.264	0.196	
	82.9	135.1	0.277	0.180	
	101.0	55.8	0.366	0.142[c]	Av=0.174

[a] Units of k_0 in liter/mole/sec.
[b] Units of $(HI)_0$ in moles/liter.
[c] Data not used in computing the averages listed for $k_0(HI)_0^{\frac{1}{2}}$.

in the range where $f(x, K_{3.2})$ will be nearly constant over the range of decomposition studied.[8] Table II

[8] The lower value for *n*-PrI makes the "constancy" of $f(x, K_{3.2})$ for this case a rather poor approximation and as we shall see later, the "corrected" rate constants of Ogg for *n*-PrI show a consistent trend with initial HI concentration.

TABLE V. Over-all rate constants for the reaction of n-C_3H_7 iodide with HI.

Initial pressure (mm Hg)					
T (°C)	n-C_3H_7I	HI	$k_0\times10^a$	$k_0(HI)_0^{\frac{1}{2}}\times10^{2\,b}$	
300.0	44.5	168.4	4.07	2.78	
	44.6	131.4	5.03	3.06	
	42.3	89.5	6.88	3.19[c]	
	42.0	66.0	8.38	3.47[c]	Av=2.92
290.0	42.2	172.6	2.21	1.55	
	44.4	110.8	3.17	1.78	
	43.5	77.7	4.05	1.90[c]	
	46.0	46.0	6.17	2.24[c]	Av=1.67
289.0	47.7	169.1	1.22	0.85	
	46.1	115.1	1.62	0.94	
	46.5	71.0	2.19	0.99[c]	
	43.4	31.3	4.39	1.32[c]	Av=0.89
270.0	50.6	181.7	0.623	0.46	
	43.9	127.6	0.765	0.47	
	49.3	73.6	1.09	0.51[c]	
	45.3	44.1	1.76	0.63[c]	Av=0.47
260.0	43.1	176.5	0.312	0.226	
	39.6	166.8	0.334	0.236	
	49.2	122.6	0.395	0.240	
	43.6	68.7	0.612	0.278[c]	
	46.1	42.6	0.835	0.299[c]	
	42.5	30.1	1.06	0.319[c]	Av=0.234

[a] Units of k_0 in liter/mole/sec.
[b] Units of $(HI)_0$ in moles/liter.
[c] Averages are obtained from runs in which $(HI)_0^{\frac{1}{2}}>100$ mm Hg. Marked data have been excluded from the reported averages.

summarizes the data obtained from these plots together with the values of k_1, obtained by using the known values of the equilibrium constant K for I_2 dissociation.

In the absence of other raw data, a more detailed test of the proposed mechanism is restricted to an analysis of values of the over-all, apparent, second-order rate constants k_0 reported by Ogg. A method for such testing is available from Eq. (9). If the function $f(x, K_{3.2})$ is insensitive to temperature in the range studied and nearly independent of x as seems indicated by Table I, then the constants k_0 given by Ogg should be inversely proportional to $(HI)_0^{\frac{1}{2}}$. In Tables III, IV, and V are listed Ogg's values of k_0 and the product $k_0(HI)_0^{\frac{1}{2}}$ for the different iodides.

For CH_3I and C_2H_5I (Tables III and IV) it can be seen that the product $k_0(HI)_0^{\frac{1}{2}}$ is reasonably constant over a rather remarkable range of compositions and initial pressures of reactants. The average precision of the rate constants at each temperature is about $\pm10\%$. This precision is a combination of the errors inherent in the photometric determination of I_2 vapor which is probably about $\pm5\%$, and the errors arising from the weighting used by Ogg in assigning values to k_0. Since his k_0 includes the function $f(x, K_{3.2})$ which is not truly constant but also varies by some $\pm10\%$ in the range of reaction covered (10–60%) this order of precision is all that can be expected.

There does seem to be a tendency at the higher temperatures towards systematically higher values of $k_0(HI)_0^{\frac{1}{2}}$ at lower total pressures which may reflect some heterogeneity in the reaction system or instrumental difficulties or possible complexities in the mechanism. These do not appear to be serious for CH_3I and C_2H_5I as we shall see when we consider the numerical values of the rate constants.

In the case of n-C_3H_7I (Table V) there is a real trend of the data towards higher rate constants with decreasing $(HI)_0$. The trend, at constant $(n\text{-}C_3H_7I)_0$, amounts to a 30% increase in apparent rate constant with a fourfold decrease in $(HI)_0$. Because of this large effect we have chosen in our subsequent analysis to use the data for $(HI)_0>100$ mm Hg,[9]. Effects like this for n-C_3H_7I are to be expected because of the low value of $K_{3.2}$ and the consequent real variation of $f(x, K_{3.2})$ for this case.[10] This does not however rule out the possibility of further complexities in the mechanism of the n-C_3H_7I reaction.

From Eq. (9) we see that the "constants" $k_0(HI)_0^{\frac{1}{2}}$ are equal to $k_1k_3K^{\frac{1}{2}}f(x, K_{3.2})/k_2$, so that if we divide the former by the average value of $f(x, K_{3.2})$ taken from Table I we will obtain $k_1k_3K^{\frac{1}{2}}/k_2$. Table VI summarizes

TABLE VI. Over-all averaged rate constants for the reaction RI+HI.[a,b]

Alkyl iodide	T (°C)	$k_0(HI)_0^{\frac{1}{2}}\times10^2$	$(k_1k_3K^{\frac{1}{2}}/k_2^{\frac{1}{2}})\times10^3$	$(k_1k_3/k_2)\times10^{-2}$
CH_3I	320.0	18.9	14.5	9.6
	310.0	10.6	8.1	6.9
	300.0	6.0	4.61	5.06
	290.0	3.33	2.56	3.70
	280.0	1.82	1.40 (1.26)[c]	2.67
	270.0	0.92	0.71	1.87
C_2H_5I	300.0	33.2	25.5	28.0
	290.0	18.3	14.1	20.4
	280.0	10.4	8.0	15.3
	270.0	5.25	4.04	10.6
	260.0	2.80	2.15 (1.97)[c]	7.8
	250.0	1.74	1.34	7.5
C_3H_7I	300.0	29.2	20.3	22.3
	290.0	16.7	11.6 (9.8)[c]	16.8
	280.0	8.9	6.2	11.8
	270.0	4.7	3.26	8.6
	260.0	2.34	1.62	5.9

[a] All rate constants and concentrations expressed in units of moles, liters and seconds.
[b] Here $f(x, K_{3.2})$ has been set equal to 1.30 for MeI and EtI and to 1.44 for n-PrI.
[c] These values are obtained from the intercepts of the pressure-time curves given in Figs. 1 and 2.

[9] This analysis is not affected if we use all the data, or alternatively only the lower $(HI)_0$ values. The activation energies remain unaffected. For consistency we have also in the cases of MeI and EtI, only used the higher pressure data in averaging.

[10] Note that for fixed $(n\text{-}C_3H_7I)_0$ and variable $(HI)_0$, at high values of $(HI)_0$ (see Table I), $f(x, K_{3.2})$ is weighted towards small values of x, while at low values of $(HI)_0$, it is systematically weighted towards larger values of x. Depending on where $f(x, K_{3.2})$ reaches its maximum, this could easily account for the trend observed.

TABLE VII. Over-all rate constants for the reaction of C_2H_5I+HI in the presence of added I_2 at 270°C.

Initial pressure (mm Hg)						
C_2H_5I	HI	I_2	$y=(I_2)_0/(HI)_0$	$k_0\times10$	$k_0\times(HI)_0^{\frac{1}{2}}\times10^3$	corrected[a] $k_0\times(HI)_0^{\frac{1}{2}}\times10^3$
81.1	46.0	16.0	0.348	1.25	4.54	5.15
80.8	43.2	16.1	0.376	1.30	4.68	5.20
74.9	29.8	10.5	0.368	1.53	5.96	5.00
80.4	28.0	12.9	0.461	1.59	6.22	5.25
88.1	18.9	14.1	0.746	1.81	8.35	5.25 Av=5.17

[a] These values have been obtained by multiplying the preceding column by the ratio $f(x, y, K_{3,2})/f(x, K_{3,2})$ where the numerator is obtained by the method described in the footnote to Table I using the appropriate value of y and the denominator $f(x, K_{3,2})=1.30$ for C_2H_5I.

these data for all runs. If in addition we further divide by the thermodynamically calculated values of $K^{\frac{1}{2}}$ for the dissociation of I_2, we will have the values of the ratio k_1k_3/k_2. These latter are given in the last column of Table VI.

A further check on the mechanism is now possible since the two independent methods of plotting the data should give the same values of the composite constant $(k_1k_3K^{\frac{1}{2}}/k_2)$. The values in parentheses, marked with a superscript b (Table VI, column 4) show the values of this constant at the indicated temperature, computed from the time-pressure data (Fig. 1, 2). The difference in the two different values varies from 10 to 15% which may be taken as excellent agreement.

A final check on the mechanism is available from a series of runs made by Ogg using C_2H_5I+HI in the presence of varying amounts of added I_2, all at 270°C.

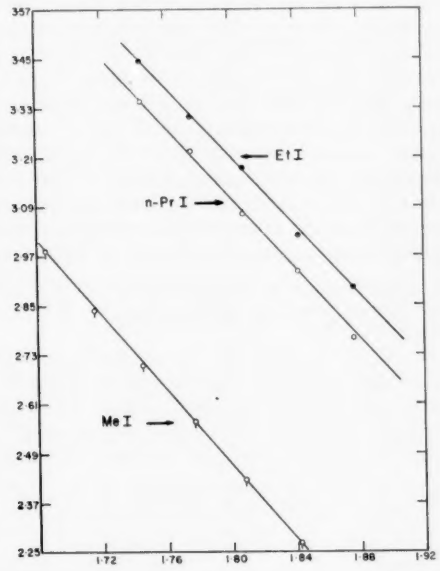

FIG. 3. Arrhenius plots of $\log(k_1k_3/k_2)$ vs $1/T$ for MeI (bottom curve), EtI (top) and *n*-PrI (middle curve) with HI. Abscissa: ^1T $(°K^{-1})\times10^3$. Ordinates: $\log(k_1k_3/k_2)$.

The presence of initially added I_2 can be treated according to Eq. (8) by using a modified value of $f(x, K_{3,2})$ which will now depend on the value of $y=(I_2)_0/(HI)_0$. The footnote in Table I describes the way in which this can be done. The data for the runs with added I_2 are listed in Table VII and it can be seen that the rate constants are quite constant and that in addition the average value calculated, of 5.17×10^{-3} from these constants for the "corrected" rate constant, agrees quite well with the value 5.25×10^{-3} for the "uninhibited" rate constant at 270°C for C_2H_5I (Table IV).

III. THE INDIVIDUAL RATE CONSTANTS AND ARRHENIUS PARAMETERS

The composite rate constants, listed in the last column of Table VI can be fitted to an Arrhenius equation by plotting the logarithms of these quantities against the reciprocal of the absolute temperature. Such plots are shown in Fig. 3 for the three different iodides and it can be seen that the data fit quite well to the Arrhenius equation. From the slopes and intercepts of this plot it is possible to get an activation energy E_0 and an Arrhenius A-factor, A_0. These over-all Arrhenius parameters are related to the Arrhenius parameters for the individual step reactions by the following relations,

$$E_0=E_1+E_3-E_2 \tag{11}$$

$$\log A_0=\log A_1+\log(A_3/A_2). \tag{12}$$

These data are listed in Table VIII.

From various estimates of the entropies of the relevant species it is possible to compute the entropy changes in steps 1 and 2 and also steps 3 and 4. These values are probably reliable to ±1.5 eu, the principal uncertainties arising from the entropies of the alkyl free radicals. From the estimated $\Delta S_{1,2}$ and the measured A_1A_3/A_2 it is possible to calculate A_3 with an uncertainty of a factor of two. Log A_3 is shown in Table VIII and the values seem both reasonable and self-consistent for this type of metathesis reaction.

From the over-all entropy change in the reaction

TABLE VIII. Summary of rate and thermodynamic data for the RI+HI reactions.[a]

RI	$k_1\times10^{-3}$ (calc)[b]	$k_1\times10^{-3}$[c]	k_3/k_2[c]	log (A_1A_3/A_2)	$E_1+E_3-E_2$ (kcal/mole)	$\Delta S_{1.2}$[d]	$\Delta S_{3.4}$[d]	log A_3	log A_4	E_1(max)[e] (kcal/mole)
CH_3I	1.80	1.60	0.15	10.65	20.8	5.3	−9.0	9.47	11.49	20.5 (19)
C_2H_5I	5.2	6.8	0.15	10.81	19.3	7.6	−10.3	9.11	11.41	18.2 (18)
n-C_3H_7I	11.1	12.9	0.11	10.84	19.6	9.0	−11.5	8.64	11.21	18.5 (18)

[a] A_1, k_1, k_3, A_4 in units of liter/mole/sec.
[b] Calculated from the values of k_3/k_2 above and the curves in Fig. 3.
[c] Calculated from the slopes and intercepts in Fig. 2 (time-pressure data). These are for the specific temperature 280°C (MeI), 260°C (EtI), and 290°C (n-PrI).
[d] Calculated from data and estimates compiled by S. W. Benson, *Foundations of Chemical Kinetics* (McGraw-Hill Book Company, Inc., New York, 1960) Appendix D. ΔS in units of cal/mole °K, at standard pressure of 1 atm.
[e] Calculated from k_1 (col. 3) and assumption that $A_1\leq2\times10^{11}$ l/mole/sec. The values in parentheses are minimum values of E_1 estimated from $\Delta H_{1.2}$.

$\Delta S_{1.2}+\Delta S_{3.4}$ and A_1A_3/A_2 it is possible to compute A_4 with an uncertainty which is less than $\pm30\%$.[11] Values of logA_4 are given in Table VIII and while they appear high by a factor of about 2[12] they seem self-consistent.

If it is assumed that the Arrhenius A factor for reaction 1 cannot exceed 2×10^{11}/mole sec, then from the values of k_1 in Table VIII it is possible to compute maximum values of E_1, the activation energy for this reaction. These are listed in Table VIII and it will be noted that they are from 0.3 to 1.1 kcal/mole less than the values of $E_0=E_1+(E_3-E_2)$. Since E_3-E_2 is expected to be zero or not more than 2 kcal, this agreement is excellent.[13]

The minimum value of E_1 will be given by $\Delta H_{1.2}$, the enthalpy change in reaction 1. It is unfortunately the case that there are very few reliable data available on ΔH_f^0 of alkyl iodides. For the alkyl radicals the uncertainties in ΔH_f^0 are about ±1 kcal. Using the data that are available one obtains the values given in the last column of Table VIII (in parentheses). It is remarkable, considering all of the uncertainties, that the values of E_1 (max) are so closely bracketed by E_0 and $\Delta H_{1.2}$. These minimum values of E_1 give corresponding minimum values for A_1 which are very close to 8×10^{10} liter/mole/sec, for all the alkyl iodides. These latter imply, as might be expected, that the ratio $A_3/A_2\leq0.7$.

The maximum and minimum values of E_1 bracket E_3-E_2 in the range from 0.3 to about 2 kcal in accordance with expectations for these types of reactions.

The maximum information which can be obtained from a quantitative study of the kinetics of the present type of system are values for k_1, k_3/k_2, and their respective Arrhenius parameters. In order to obtain bond energies it will be necessary to have an absolute measurement of either k_2 or k_3. However it is very likely that E_2 is not in excess of about 0.6 kcal, so that the kinetic information should be useful in fixing $\Delta H_{1.2}$ to within ±1 kcal.

Despite the necessary crudity of the present data, it appears that the activation energies are within the above limits of error and that the A factors are correct to within a factor of about three. These estimates gain support from an allied study of the pyrolysis of alkyl and aryl iodides which also turn out to be I_2 catalyzed, free radical reactions. We hope to be able to report on the latter in the near future.[14] In the meanwhile it would appear that kinetic studies of the iodide systems should be very fruitful and we have undertaken to repeat some of the present measurements as well as extending them to some other important iodides.

[11] The reason for the improvement is that for the over-all process the radical species disappear and the only uncertain values are the entropies of the alkyl iodides.
[12] The comparison here is with A factors for reactions involving atom attack on molecules leading to abstraction. These latter are mostly in the range of 10^{11} liter/mole/sec. See S. W. Benson, *Foundations of Chemical Kinetics* (McGraw-Hill Book Company, Inc., New York, 1960).
[13] The uncertainties in E_0 are about ±2 kcal, arising mainly from the method of employing Ogg's data.
[14] Preliminary results are within 1.5 kcal of the activation energies reported here for the same reactions and A factors are within a factor of three.

Reaction of Cyclopropane with Iodine and Some Observations on the Isomerization of Cyclopropane*

SIDNEY W. BENSON

Chemistry Department, University of Southern California, Los Angeles, California

(Received June 27, 1960)

The kinetic and thermodynamic data of Ogg and Priest on the system I_2+cyclopropane$\rightleftharpoons ICH_2CH_2CH_2I$ are reexamined. Using an entropy for $ICH_2CH_2CH_2I$, estimated from additivity rules of 93.0±1.5 eu, and the experimental value of K_{eq}, $\Delta H°$ is found to be −19.4±0.9 kcal. This gives $H_f°(ICH_2CH_2CH_2I) = 8.2$ kcal/mole and the use of group additivity rules allow the values of $\Delta H_f°$ for EtI and n-C_3H_7I to be fixed at −3.3±0.5 and −8.3±0.5 kcal/mole, respectively. For CH_3I, $\Delta H_f° = 1.6 \pm 1$ kcal/mole. The kinetic mechanism is also reexamined and from entropy and energy estimates for the free radical species, values of all of the rate constants are evaluated. These are in good agreement with values for similar reactions. It is proposed that the I_2-catalyzed isomerization of cyclopropane proceeds through the step $I + ICH_2CH_2CH_2I \rightarrow HI + ICH_2-CH=CH_2 + I$, followed by a rapid, atom-catalyzed reaction of allyl iodide with HI to give propylene. The rate constants for such a step are also in good agreement with those for similar reactions. Extension of the data to cyclopropane-propylene isomerization is made and it is shown that the most reasonable path involves the trimethylene radical as an intermediate. Its lifetime is, however, very short$\sim 10^{-11}$ sec. Slater's model for this reaction is shown to be implausible. These data indicate an activation energy for the cyclization of the trimethylene free radical of about 8 kcal. This is reasonable only if the end CH_2 groups in trimethylene are interacting via a "bent" bond. In such case the activation energy arises from the necessity for eclipsed configurations. A similar analysis is made for cyclobutane and the tetramethylene radical with compatible results. For cyclopropane the strain energy is 30 kcal and for cyclobutane 28 kcal.

INTRODUCTION

RECENT investigations in these laboratories of the reactions of simple hydrocarbon radicals with I_2 and HI have led to a reappraisal of the kinetics of the reactions of alkyl radicals with HI[1] and the pyrolysis of alkyl iodides.[2] The results of these studies lead to the conclusion that both sets of reactions can be analyzed in terms of simple free radical mechanisms catalyzed by I atoms made available by the rapid, reversible equilibrium $I_2 \rightleftharpoons 2I$. Ogg and Priest[3] have studied the equilibrium and kinetics in the system

$$\text{cyclopropane} + I_2 \rightleftharpoons \text{1,3-diiodopropane} \qquad (1)$$

and have shown that the mechanism is also one of simple I-atom catalysis. However, incorrect information concerning bond energies and mechanisms of related systems led them to draw erroneous conclusions from their results. It is the purpose of the present paper to reexamine their results in the light of the new, correct data now available and to consider some of the implications of these findings for the well-studied isomerization of cyclopropane to propylene.

EQUILIBRIUM CONSTANT

The equilibrium constant for reaction (1) can be estimated from known thermodynamic data for cyclopropane (Δ) and I_2, together with additivity rules for 1,3-diiodopropane (PI_2). These data are listed in Table I. From the values of K_{eq}, we calculate $\Delta H° = -15.0$ kcal/mole, $\Delta S° = -26.1$ eu (i.e., cal/mole-°K), and $\Delta C_p° = 2.6$ eu. At 265°C, which is the middle of the range measured by Ogg and Priest (OP), these become $\Delta H = -14.4$ kcal/mole, $\Delta S = -24.6$ eu. The experimental values reported by OP are $\Delta H = -18.5 \pm 4$ kcal/mole and $\Delta S = -26.2 \pm 7$ eu, in excellent agreement with the estimated values.

The large uncertainties in the values reported by OP arise from the fact that they could only measure the equilibrium over a 30°C range in temperature. Below 250°C equilibrium is too slowly attained while above 280°C the side reaction of I-atom catalyzed isomerization of cyclopropane to propylene is so fast that it interferes seriously with the attainment of equilibrium. This isomerization reaction is in fact a serious source of error in the absolute measurement of K_{eq} for reaction (1) at any temperature.

OP observed that the total pressure in the reaction system, starting with I_2+cyclopropane, reached a minimum value as PI_2 was formed and then slowly climbed back to the initial total pressure as cyclopropane was almost completely isomerized to propylene. For their measure of K_{eq}, they took a point very close to the minimum pressure value, estimated from the rate constants for the reaction. They also reported values of the total pressure and an analysis of the cyclopropane/propylene ratio measured much later. If we use these latter values to compute K_{eq} we obtain values much lower than those found near the pressure minimum. Both sets are reported in Table II.

It can be seen that there is a drift away from equilibrium as time elapses so that the "long-time" values are not necessarily the best values. It can also be seen that the drift is most rapid at the higher temperatures. The implication of this drift is that once we get close to

* This work has been supported by grants from the Atomic Energy Commission and the Office of Ordnance Research, U. S. Army.

[1] S. W. Benson and E. O'Neal, J. Chem. Phys. (to be published).

[2] S. W. Benson (to be published).

[3] R. A. Ogg, Jr., and W. J. Priest, J. Chem. Phys. **7**, 736 (1939).

TABLE I. Thermodynamic data of interest.[a]

Compound	ΔH_f° (kcal/mole)	S° (cal/mole °K)	C_p° (cal/mole °K)
I_2	14.9	62.3	8.8
HI	6.2	49.3	7.0
H	52.1	27.4	5.0
I	25.5	43.2	5.0
cyclopropane	12.7[b]	56.8[b]	13.3[c]
propylene	4.9	63.8	15.3
propane	−24.8	64.5	17.6
$\cdot CH_2—CH_2—CH_2\cdot$[e]	67.0	68	17.6
n-C_3H_7I[d]	−8.3	80.1	21.3
$ICH_2CH_2CH_2I$[d]	8.2 (12.6)	93.0	24.7
$ICH_2CH_2CH_2\cdot$[f]	37.6	81.5	22

[a] Unless otherwise noted, all values are from the NBS Circular No. 500 or the A.P.I. compilation. Standard states are ideal gases at 1 atm, 25°C.

[b] J. W. Linnett, J. Chem. Phys. **6**, 682 (1938). See also G. B. Kistiakowsky and W. W. Rice, *ibid.*, **8**, 610 (1940).

[c] J. W. Knowlton and F. D. Rossini, J. Research Natl. Bur. Standards **43**, 113 (1949). See also J. R. Lacher, A. Kianpour, and J. D. Park, J. Phys. Chem. **61**, 1124 (1957).

[d] Estimated from bond additivity rules (S° and C_p°). ΔH_f° estimated from ΔH° for reaction (1) and group additivity rules. (See footnote 5). The value in parenthesis for PI_2 is based on the older and less reliable data for C_2H_5I.

[e] ΔH_f° is estimated by assuming that the bond dissociation energies in C_3H_8 are the same as in C_2H_6. C_p° and S° are based on additivity rules.

[f] ΔH_f° is estimated by assuming that the H-bond dissociation energy in C_3H_7I is the same as in C_2H_6. C_p° and S° are based on additivity rules.

equilibrium, the rate at which PI_2 is removed by the side reaction is faster than the rate at which it reacts to produce cyclopropane+I_2. If the converse were true we would get a drift towards "high" values of K_{eq}. We shall discuss this in more detail.

There is a third method of obtaining ΔH, the enthalpy change in reaction (1), with better precision than either of the previous two methods. This is to use OP's values of K_{eq} at any fixed temperature, together with an estimated value for ΔS of reaction (1). It seems reasonable to suppose that the values of K_{eq} obtained by OP are not in error by more than ±30%. An error of 30% in K_{eq} at 263°C would produce an error of ±0.28 kcal/mole in ΔF. Now $\Delta H=\Delta F+T\Delta S$ and if we assume that the error in ΔS is not more than ±1.5 eu, this would produce an error in ΔH of ±0.8 kcal/mole. The net expected error in ΔH from both these sources is thus ±0.85 kcal. Using our own estimated value of $\Delta S(265°K)=-24.6$ eu, and OP's value of $K_{eq}(265°C)=740$ liters/mole$=16.7$ atm^{-1}, we find $\Delta H(265°C)=-18.8$ kcal/mole and $\Delta H°=-19.4$ kcal/mole±0.9 kcal/mole. Using this value, we reassign ΔH_f° (PI_2) = 8.2 kcal/mole.

In Table II are listed the values of K_{eq} at each temperature calculated from these values of ΔH and ΔS. It can be seen that these values are in excellent agreement with the experimental values reported by OP.

The value of S° used for PI_2 is estimated from additivity rules for bond entropies[4] which have a reliability for compounds such as PI_2 of about ±1.5 eu. However the estimated value for ΔH_f° (PI_2) is based on a very poor value for ΔH_f° (C_2H_5I) obtained from combustion data.[5] Using the present value of ΔH_f° (PI_2) = 8.2 kcal/mole, we can calculate a new value for additivity purposes for the group C—C(H)$_2$I of 6.8 kcal/mole and for bond additivity we assign the value of 13.1 kcal/mole to the C—I bond. These yield values of $\Delta H_f^\circ(C_2H_5I)=-3.3$ kcal/mole and $\Delta H_f^\circ(CH_3I)=1.6$ kcal/mole, respectively, which are in much better agreement with bond energy data than the values −0.3 kcal/mole (EtI) and 4.9 kcal/mole (MeI) listed by the NBS Circular No. 500.

KINETICS OF THE REACTION

The mechanism proposed by OP for the reaction of cyclopropane (Δ) with I_2 is

$$I_2 \underset{2}{\rightleftharpoons} 2I$$

$$I + \text{cyclo-}C_3H_6 \underset{4}{\overset{3}{\rightleftharpoons}} ICH_2CH_2CH_2\cdot$$

$$ICH_2CH_2CH_2\cdot + I_2 \underset{6}{\overset{5}{\rightleftharpoons}} I(CH_2)_3I + I. \qquad (2)$$

The stationary-state concentration of 3-I-propyl radical (IP·) is given by

$$(IP\cdot)=\{[k_3(\Delta)+k_6(PI_2)](I)/[k_4+k_5(I_2)]\}, \qquad (3)$$

which leads to the rate law

$$d(PI_2)/dt=\frac{k_3(\Delta)(I)}{1+k_4/k_5(I_2)}\{1-[(PI_2)/K_e(I_2)(\Delta)]\}, \qquad (4)$$

$$\xrightarrow[k_4\ll k_5(I_2)]{} K_e^{\frac{1}{2}}k_3(\Delta)(I_2)^{\frac{1}{2}}\{1-[(PI_2)/K_e(I_2)(\Delta)]\}, \qquad (5)$$

TABLE II. Equilibrium constants for reaction (1).

Run No.	Temp. °K	K_{eq}(liter/mole)×10^{-2} Reported by OP[a]	Calculated from[b] "long-time" composition	Calculated from "best" thermodynamic data
E 1	279.2	5.55	2.35	
E 2	279.2	5.50	2.27	5.2
E 10	270.2	6.06	3.39	
E 11	270.2	6.36	3.41	6.9
E 9	261.6	7.5	4.8	
E 12	261.6	8.9	5.7	9.0
E 14	253.1	12.2	7.4	
E 15	253.1	11.8	9.9	11.2

[a] Calculated from compositions estimated shortly after the pressure minima.
[b] Calculated from "final" compositions reported by OP.

[4] S. W. Benson and J. H. Buss, J. Chem. Phys. **29**, 546 (1958).

[5] D. Berthelot, Ann. chim. et phys. **21**, 296 (1900); Thomsen, *Thermochem. Untersuchungen* (Barth, Leipzig, 1883). There are astonishingly few data on the heats of formation of iodides in the literature.

where K_i is the equilibrium constant for the dissociation of I_2 and K_e is the equilibrium constant for the overall reaction (1). Since Eq. (5) is the form observed by OP for the experimental rate law, they assumed that $k_4 \ll k_5(I_2)$. We shall show that this is justifiable from independent considerations.

From the observed rates, the quantity $k_3K_i^{\frac{1}{2}}$ was found to be given by (units of liter$^{\frac{1}{2}}$ mole$^{\frac{1}{2}}$-sec)

$$\log k_3K_i^{\frac{1}{2}} = 11.57 - (35\ 200/4.575T). \quad (6)$$

Employing the value for K_i calculated from Table I[6] we obtain

$$\log k_3 = 9.62 - (17\ 500/4.575T). \quad (7)$$

Again, from Table I we find $\Delta H_{3.4}$ (265°K) $= +0.3$ kcal/mole and $\Delta S_{3.4}(265°K) = -16.3$ eu. This gives for k_4(units of sec^{-1})

$$\log k_4 = 11.52 - (16\ 100/4.575T). \quad (8)$$

For reactions 5 and 6 in Eq. (2) we can calculate from the data in Table I,

$$\Delta H_{5.6}(265°C) = 19.0 \text{ kcal/mole},$$

$$\Delta S_{5.6}(265°C) = -7.1 \text{ eu}.$$

From our work on the reactions of I atoms with alkyl iodides[1,2] we find that the Arrhenius A factors are all of the order of magnitude of 10^{11} liter/mole-sec with activation energies which appear to be equal to the endothermicity of the reaction. On the basis of these data, we will assign k_6 and k_5 as follows,

$$\log k_6 = 11.0 - (19\ 500/4.475T), \quad (9)$$

$$\log k_5 = 9.5 - (500/4.575T). \quad (10)$$

The assignment of 0.5 kcal/mole activation energy for the exothermic reaction 5 is based on the use of collision theory.

In terms of the above rate constants we can now examine the experimental finding that $k_4 \ll k_5(I_2)$. At 265°C, and an average (I_2) concentration of 0.1 atm, the ratio of rates of reaction 5 to 4 is about 50:1 so that the assigned rate constants are consistent with the experimental observation that reaction 4 is indeed negligible relative to 5. In fact, one would have to go to temperatures in excess of 350°C and I_2 concentrations of less than 10 mm Hg before the competition would be observable.[7]

I_2 CATALYZED ISOMERIZATION

There are two reasonable paths for the observed isomerization of cyclopropane to propylene which was observed in the studies of OP. Both of these proceed through the intermediate formation of allyl iodide with the formation of a small stationary concentration of HI. Once allyl iodide is formed in the system it may be expected to undergo very rapid I_2-catalyzed reaction with HI to form propylene.[8]

The first path is

$$\begin{aligned} &I\cdot CH_2\cdot CH_2{-}CH_2\cdot + I \xrightarrow{7} ICH_2CH{=}CH_2 + HI, \\ &I + ICH_2CH{=}CH_2 \underset{9}{\overset{8}{\rightleftharpoons}} I_2 + \cdot CH_2CHCH_2\cdot, \\ &\cdot CH_2CHCH_2\cdot + HI \xrightarrow{10} CH_3CH{=}CH_2 + I. \end{aligned} \quad (11)$$

If we assume, following Shaw's observations, that the conversion of allyl iodide to propylene will be rapid, then the rate of formation of propylene will be given by the rate of reaction 7 in Eq. (11). Adding reaction 7 to our previous scheme Eq. (2), we then find for the rate of isomerization,

$$\begin{aligned} d(C_3H_6)/dt &= k_7(IP\cdot)(I) \\ &= k_7K_iK_{6.5}(PI_2)\{1 + [k_3(\Delta)/k_6(PI_2)]\}. \end{aligned} \quad (12)$$

Using our data for K_i, $K_{6.5}$, k_6, and k_3, together with a value for k_7 (265°C) of about 2×10^{10} liters/mole-sec, we find that the half-life for conversion of PI_2 to $C_3H_6+I_2$ by this mechanism is about 500 hr. This value is about 50 times larger than the half-life observed by OP and we conclude that it is too slow.

The second path is that followed by the I_2-catalyzed pyrolysis of n-C_3H_7I,[2,9]

$$\begin{aligned} &I + CH_3CH_2CH_2I \xrightarrow{11} CH_3\dot{C}HCH_2I + HI, \\ &CH_3\dot{C}HCH_2I \xrightarrow{12} CH_3CH{=}CH_2 + I. \end{aligned} \quad (13)$$

Here reaction 12 in Eq. (13) is extremely rapid since the iodopropyl radical is unstable with respect to the decomposition by about 5 kcal/mole. In fact, it is likely that 12 may participate in lowering the activation energy for reaction 11 by about 4 kcal/mole. If we assume that PI_2 has the same rate law as that observed by Ogg and Jones for n-C_3H_7I, we find for the rate of production of allyl iodide,

$$-d(PI_2)/dt = k_0(PI_2)(I_2)^{\frac{1}{2}}, \quad (14)$$

with $k_0 = 10^{12.3}e^{-38\,000/RT}$ liter$^{\frac{1}{2}}$/mole$^{\frac{1}{2}}$-sec.[9] At 265°C with $I_2 \sim 0.1$ atm, this gives a half-life for PI_2 disappearance of about 7 hr, in excellent agreement with the observed rate of isomerization.

The stationary state concentration of HI can be shown to be very low[2] and it can also be shown that the rate of production of n-C_3H_7I via reaction 13 in

[6] This value for K_i is about sevenfold larger than that used by OP. Their value of K_i was estimated from the data of M. Bodenstein and H. Starck, Z. Elektrochem. **16**, 961 (1910) and is less reliable than the present statistically calculated value.

[7] The photochemical studies of OP are in agreement with these conclusions.

[8] A. Shaw, Master's thesis, University of Manchester, 1948, has observed that allyl iodide undergoes very rapid pyrolysis at temperatures as low as 150°C.

[9] J. L. Jones and R. A. Ogg, Jr., J. Am. Chem. Soc. **59**, 1931 (1937).

Eq. (15) is unimportant,

$$ICH_2CH_2CH_2\cdot + HI \xrightarrow{13} ICH_2CH_2CH_3 + I. \quad (15)$$

PYROLYSIS OF CYCLOPROPANE

The very elegant work of RSW[10] on the geometrical isomerization of *trans* cyclopropane-d_2 indicates that the rate of opening of the ring to form the trimethylene free radical is some 16 times faster than the rate of production of propylene when both reactions are in their high-pressure limits. It seems quite reasonable then to suppose that both reactions have a common mechanism,

$$\text{cyclopropane} \underset{b}{\overset{a}{\rightleftharpoons}} \cdot CH_2CH_2CH_2\cdot,$$

$$\cdot CH_2CH_2CH_2\cdot \xrightarrow{c} CH_3CH=CH_2, \quad (16)$$

where k_c is smaller than k_b. The rate of formation of propylene (P) is given, using a stationary-state treatment, by

$$d(P)/dt = k_c k_a(\Delta)/(k_b+k_c) = k_p(\Delta), \quad (17)$$

where $k_p = k_a(k_c/k_b)/(1+k_c/k_b)$. If we identify k_a with the rate of geometrical isomerization, then we can use the data of RSW to obtain the value of the ratio k_c/k_b(~444°C) as 0.057, or in Arrhenius form

$$\log(k_c/k_b) = -0.84 - (1300/4.575T). \quad (18)$$

Now RSW give k_a in Arrhenius form as (444°C): $\log k_a = 16.0 - 64\,200/4.575T$. But from the data in Table I $\Delta S°_{a.b} = 11.2$ eu, and $\Delta H°_{a.b} = 54.3$ kcal/mole. At 444°C, these are $\Delta S_{a.b} = 14.0$ eu, and $\Delta H°_{a.b} = 56.0$ kcal/mole. Combining these data we find for k_b (444°C): $\log k_b = 13.0 - 8200/4.575T$.

We observe that the frequency factor for the ring closure, reaction *b*, is 10^{13} sec^{-1}, a quite reasonable result for this unimolecular process. In addition there is an activation energy of 8.2 kcal/mole for the ring closure which we shall comment on later. Together with the relation in Eq. (18) for the ratio k_c/k_b, this yields for k_c(444°C),

$$\log k_c = 12.2 - 9500/4.575T.$$

The frequency factor of $10^{12.2}$ sec^{-1} for the isomerization of the trimethylene radical is again a quite reasonable number for this process which involves a bridged hydrogen migrating from the central C atom to one of the terminal C atoms. Correcting for the symmetry change of 8 from the radical to the bridged structure, the intrinsic frequency factor[11] becomes $10^{11.3}$ sec^{-1} which is just the order of magnitude that would be calculated from a simple transition-state model. The activation energy of 9.5 kcal/mole is of course considerably lower than would be expected for the isomerization of an alkyl radical but it must be recognized that the process is assisted by the concomitant double bond formation. The transition state is probably

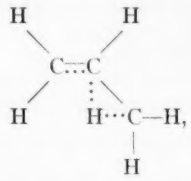

with an estimated entropy of about 6 to 8 eu, lower than that of propylene. The large decrease in entropy arises from the loss in free rotation of the two end methylene groups.

The large frequency factor of 10^{16} sec^{-1} for reaction *a*, the opening of the cyclopropane ring, implies that the transition state for this process[12] is very close in structure to the trimethylene radical, again a quite reasonable result.

Two objections have been raised to the above mechanism. Smith[13] has suggested that the *cis-trans* isomerization occurs via a twisting of the D and H atoms attached to one of the ring carbons without ring rupture. There are two difficulties with such a process. The first involves the energetics. Any reasonable frequency assignment for the CH_2 twist (900 to 1200 cm^{-1}) yields a value for the activation energy of about 100 to 150 kcal/mole which cannot be reconciled with any acceptable anharmonicities to the observed value of 64 kcal. An even more serious difficulty is that the frequency factor for such a process will never be in excess of 10^{15} sec^{-1} which is an order of magnitude too low.

The second objection comes from the work of Slater,[14] who has used his model for unimolecular reactions to show that the pressure dependence for a C—C bond split in cyclopropane will persist to much higher pressures than has been observed. The Slater theory, however, is based on the assumption that there is no energy transfer between "normal" coordinates and this is probably not correct for large molecules. In fact, the findings of RSW may be considered as an experimental refutation of this hypothesis. In addition, the frequency factor predicted by Slater is low by a factor of 3 even for his own model of isomerization.[15]

[10] B. S. Rabinovitch, E. W. Schlag, and K. B. Wiberg, J. Chem. Phys. **28**, 504 (1958).

[11] See S. W. Benson, J. Am. Chem. Soc. **80**, 5157 (1958).

[12] Part of this factor comes from the change in symmetry which contributes a factor of 12.

[13] F. T. Smith, J. Chem. Phys. **29**, 235 (1958).

[14] N. B. Slater, Proc. Roy. Soc. (London) **A218**, 224 (1953).

[15] The Slater model, based on "normal" coordinates, is always inadequate to explain the very large frequency factors which are observed for the decomposition of molecules such as N_2O_4, N_2O_5, C_2H_6, etc. See S. W. Benson, *Foundations of Chemical Kinetics* (McGraw-Hill Book Company, Inc., New York, 1960). In addition, the vibrational analysis of Slater is based in part on symmetry arguments deduced from the symmetry of the ground state, cyclopropane. The considerable distortion in going to his proposed transition state involves a change in symmetry of the molecule and the symmetry restrictions for the ground state structure no longer apply. In particular much of the degeneracy is removed.

An equally serious argument aginst the Slater model is based on energetic considerations. The only way in which the C—H bond in cyclopropane can be simultaneously stretched and deformed to permit transfer to an adjacent CH_2 group without drastic ring deformation would require energies in excess of 120 kcal. The low energy path for this process requires rupture of a C—C bond and considerable C=C, double bond formation. But this latter process is equivalent to the prior formation of the trimethylene free radical.

The free radical mechanism has some interesting implications for the trimethylene radical. The lifetime of this radical at 444°C, calculated from the fast, unimolecular step k_b is about $10^{-11.3}$ sec. This is at least 100 fold less than collision times at 1 atm. Thus, the trimethylene radical, once formed, will not have a chance to come into thermal equilibrium but will instead react adiabatically. Its energy content is fixed by the energized cyclopropane molecules which gave rise to it. Even the slower conversion to propylene (k_c) is essentially adiabatic. Its stationary concentration is also extremely low [$\sim\times 10^{-14}(\Delta)$], so low in fact that it would require 1 atm pressure of a radical scavenger which would react at every collision to compete with the isomerization reaction. This explains quite well the negative results which have attended the attempts to observe such competing steps.

ENERGETICS OF THE TRIMETHYLENE RADICAL. STRAIN ENERGIES IN SMALL RINGS

The $\Delta H_f°$ ($ICH_2CH_2CH_2\cdot$) given in Table I is based on the assumption that the C—H bond energy in the parent compound n-C_3H_7I is not affected by the I atom three carbon atoms away and is thus the same as that in C_3H_8 (or C_2H_6), namely 98 kcal. This assumption is in agreement with presently known bond energy data and seems quite reasonable on structural grounds.[4] If we now further assume that the C—I bond in the radical is the same as that in n-C_3H_7I we arrive at a value of 66 kcal for $\Delta H_f°(\cdot CH_2CH_2CH_2\cdot)$. An independent estimate can be obtained by applying these same assumptions to the end C—H bonds in C_3H_8 and these lead to the listed value of 67.0 kcal in good agreement.[16]

These values yield maximum estimates for the energy of cleaving cyclopropane to trimethylene free radical of 54 kcal/mole. They are maximum since the only effect of the $—CH_2\cdot$ radical end group on the terminal bond would be a weakening effect. If, for example, we estimate the interaction of the terminal methylene free radicals, treating them as two free radicals at a distance of 2.51 A which would be the distance in propane, we obtain a value of about 21 kcal. This is based on the use of a Morse function with $D=84$ kcal/mole and $a=1.95$ A^{-1}. A Lennard-Jones potential gives a value of about 8 kcal.

If the interaction of the two end radicals were this simple it would be impossible to account for an activation energy for the ring closure to cyclopropane of 8.2 kcal/mole since the bond energy-distance relation increases much more rapidly than does the C—C—C bond angle strain energy.[17] A reasonable alternative is to treat the interaction as occurring through a bent bond.[18] In such a case the interaction is about 3 kcal for a Lennard-Jones potential and about 10 kcal for a Morse Potential. In addition, at the "bent-bond" distances the bond energy grows less slowly than the C—C—C angle strain energy and a small activation energy appears reasonable.

An energetically equivalent point of view is to observe that the barrier to the rocking of groups in molecules can be looked upon as arising from the weakening of the bond holding the group to the molecule. This distortion energy estimated for the angle between the end $—CH_2\cdot$ groups in trimethylene is more than enough to compensate for the attractive interactions calculated above.

Another source of activation energy can be considered if one assumes that the methylene interaction is not significant until the eclipsed configuration is reached. Assuming that the energy to eclipse the two end methylene groups, relative to the central

group is about equal to the barrier in ethane or propane, namely $2\times 3=6$ kcal, this could account for the major fraction of the observed activation energy.

If we identify the difference in energies for a normal C—C bond ($\sim$82 kcal) and that in cyclopropane (54 kcal) as the strain energy in the small ring we obtain a value of 28 kcal. It is interesting to note that a simple calculation of the C—C—C angle strain energy based on a Hooke's law model using the force constant of 0.72×10^5 d/cm[19] yielded a value of 48 kcal for the angle strain in cyclopropane. This is undoubtedly an upper limit since it neglects any harmonicity in the bending.

The same type of argument may be applied to cyclobutane. For the tetramethylene free radical $\Delta H_f°=62$ kcal/mole while $\Delta H_f°$ (cyclobutane) $=6.3$ kcal/mole. The energy to open the ring is thus 56 kcal. The strain energy is then estimated as $82-56=26$ kcal, just 2 kcal/mole less than in cyclopropane. The kinetics of decomposition of cyclobutane has been found to be a first order reaction,[20] with an activation energy of 62.5

[16] F. H. Seubold, Jr., J. Chem. Phys. **21**, 1616 (1953); **22, 945 (1954)**, has obtained similar values by the same argument.

[17] This is in essential agreement with the findings of H. O. Pritchard and A. F. Trotman-Dickenson, Proc. Roy. Soc. (London) **A218**, 416 (1953).

[18] L. Pauling, *The Nature of the Chemical Bond* (Cornell University Press, Ithaca, New York, 1960), 3rd ed.

[19] This is calculated from the bending frequency of 400 cm^{-1} for the angle deformation and reduced to units of C–C distance.

[20] F. Kern and W. D. Walters, J. Am. Chem. Soc. **75**, 6196 (1953).

kcal and a frequency factor of $10^{15.6}$ sec^{-1}. If we assume that this reaction proceeds through the formation of an intermediate tetramethylene free radical then 62.5 kcal is an upper limit to the bond dissociation energy. At 450°C, this latter is estimated to be 58.5 kcal[21] so that the maximum value for the activation energy of splitting $(CH_2)_4$ into $2C_2H_4$ would be 4 kcal. This is reasonable in view of the exothermicity of the reaction (37 kcal).[22]

The data do not permit of an estimation of the activation energy for ring closure of the tetramethylene radical, but the data indicate that it cannot exceed 4 kcal.[23] The energy required to convert butane from the gauche to the totally eclipsed, planar configuration may be estimated at about 9 to 10 kcal. However the end C—C distance is only 2.57 A at this point, only 0.06 A longer than in trimethylene and the bent-bond distance corresponds to greater interaction than in the latter case so that 4 kcal is not an unreasonable figure.[24] Finally, the frequency factor of $10^{15.6}$ sec^{-1} would be quite reasonable in terms of the intermediate radical formation, although a loose complex of 2 quasi-ethylene species would also fit the data.

It is interesting to note that similar estimates of the strain energy in ethylene oxide yield the value of 29 kcal. Two independent values in good agreement are obtained starting with either C_2H_5OH or CH_3OCH_3. For the cyclic paraffins, the strain energies are C_5H_{10} (6.5 kcal); C_6H_{12} (0.6 kcal); C_7H_{14} (6.5 kcal); C_8H_{16} (10 kcal); C_9H_{18} (12 kcal).

[21] Based on $\Delta C_p^\circ \sim 6$ eu.

[22] The activation energies for less exothermic reactions, the addition of alkyl radicals to olefins are about 7 kcal.

[23] Experiments on the *cis-trans* isomerization of dideuterocyclobutane are obviously in order to resolve this.

[24] The estimated angle strain energy to deform $(CH_2)_4$ to cyclobutane, calculated as in the previous case is only 11 kcal so that once the planar configuration is established the bond energy increases more rapidly than the angle strain energy.

X-Ray Diffraction Study of Lead Sulfide-Arsenic Sulfide Glasses*

JOHN I. PETZ

Department of Physics, University of Arkansas, Fayetteville, Arkansas

R. F. KRUH

Department of Chemistry, University of Arkansas, Fayetteville, Arkansas

AND

G. C. AMSTUTZ

Department of Geology, University of Missouri School of Mines and Metallurgy, Rolla, Missouri

(Received June 29, 1960)

The structures of arsenic sulfide glass, two synthetic glasses, $PbS \cdot 5As_2S_3$ and $2PbS \cdot 5As_2S_3$, and a natural glass, $5PbS \cdot 3As_2S_3$, have been studied by x-ray diffraction. Arsenic is found to have three sulfur neighbors in the first three glasses, just as in crystalline arsenic sulfide. The natural glass and crystalline lead sulfide are similar in that lead is situated in octahedral holes among closely packed sulfurs. The increased ratio of sulfur to arsenic in the natural glass results in four sulfur neighbors for each arsenic. The lead-sulfur distance is about 3.1 A, and that for arsenic-sulfur is about 2.3 A.

TO our knowledge, there have been no previous reports of structure determinations of sulfide glasses, and their study is desirable so that existing theories of the glassy state[1,2] might be applied to other than familiar oxide systems. Moreover, the natural occurrence of glasses other than silicates is extremely rare, so that structural information for the natural glass, $5PbS \cdot 3As_2S_3$, revoredite, might help to understand why it is unusual and perhaps how it was formed.[3] And finally, the lead sulfide-arsenic sulfide glasses have interesting physical properties, such as transparency in the infrared[4,5] and semi- and photoconductivity,[6] understanding of which might be aided were structural data available.

In undertaking to provide the necessary structural

* This work was supported by the U. S. Atomic Energy Commission.

[1] W. H. Zachariasen, J. Am. Chem. Soc. **54**, 3841–51 (1932); B. E. Warren, J. Appl. Phys. **8**, 645–655 (1937), J. Am. Ceram. Soc. **24**, 256–261 (1941).

[2] Although presently applied only to silicates, the theory of L. W. Tilton, J. Research Natl. Bur. Standards **59**, 139–154 (1957), is noteworthy.

[3] G. C. Amstutz, P. Ramdohr, and F. de las Casas, Bol. Soc. Geol. Peru **32**, 25–33 (1957); G. C. Amstutz, Abstracts, Am. Crystallographic Assn. Meeting, Milwaukee (1958).

[4] R. Frerichs, J. Opt. Soc. Am. **43**, 1153–1157 (1953).

[5] F. W. Glaze, D. H. Blackburn, J. S. Osmalov, D. Hubbard, and M. H. Black, J. Research Natl. Bur. Standards **59**, 83–92 (1957).

[6] N. A. Goryunova and B. T. Kolomiets, Izvest. Akad. Nauk SSSR, Ser. Fiz. **20**, 1496–1500 (1956).

TABLE I. Modification function.

s	0	1	2	3	4	5	6	7	8	9	10	11	12
$M(s)$	1.000	1.056	1.221	1.476	1.766	2.026	2.219	2.353	2.446	2.503	2.525	2.497	2.414

information we examined a series of varying composition in the hope of lessening the uncertainty which often accompanies the interpretation of a single determination.

EXPERIMENTAL

Glasses of As_2S_3, $PbS \cdot 5As_2S_3$, and $2PbS \cdot 5As_2S_3$ were prepared by melting appropriate amounts of finely ground arsenic sulfide and lead sulfide in evacuated Pyrex tubes and quenching in a blast of compressed air. Heating for only 10–15 min gave samples from which no crystal diffraction could be detected.

The natural glass comes from the Cerro de Pasco Mine, Peru, and its density is 5.21 g cm^{-3}; densities for the prepared glasses are 3.20, 3.35, and 3.70 g cm^{-3}, respectively.

The diffraction of Mo $K\alpha$ x rays was measured with a diffractometer especially designed for the study of liquids.[7] Times required to obtain 3200 counts/min were recorded at equal angular intervals, with a background counting rate of about 4 counts/min.

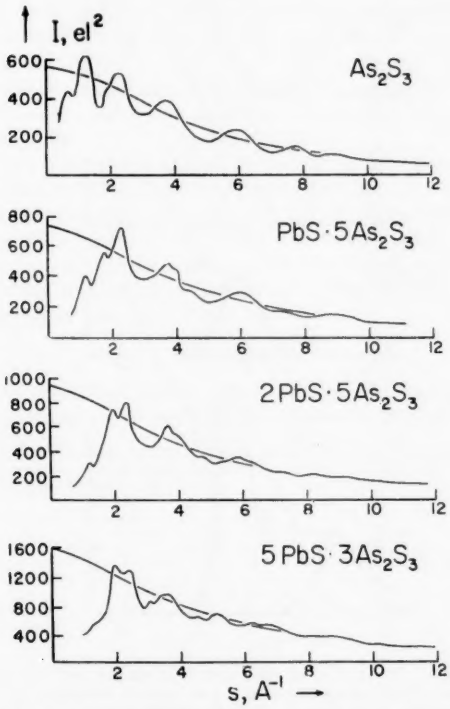

FIG. 1. Coherent intensities for the several glasses. The smooth curves are the calculated independent coherent scattering.

[7] P. C. Sharrah, J. I. Petz, and R. F. Kruh, J. Chem. Phys. **32**, 241–246 (1960).

TREATMENT OF DATA

Normalized intensities were obtained by correcting[8] the observed intesnities for background and polarization aed then scaling to the calculated scattering of independent atoms. Figure 1 shows plots of the observed coherent intensity I and the calculated independent coherent intensity Σf^2. Before evaluating the Fourier sine transform of the intensity function, $s(I-\Sigma f^2)$, the function was multiplied by a modification function, $M(s)$, given in Table I, which partially eliminates the effect of intra-atomic scattering and sharpens the resulting electron distribution function. The modification function was chosen arbitrarily and was the same for each set of data. Its application has been carefully developed by Waser and Schomaker,[9] who show how exactly to predict the effect of any such modification upon peak shapes in the distribution function. The formalism of Waser and Schomaker was used to calculate the expected peak shape, $T(r)$, for each kind of atom pair according to the formula

$$T(r) = \pi^{-1} \int f_i f_j M(s) \cos rs ds.$$

Integration to the maximum experimental value of s automatically includes the effect on peak shape of the high-angle limit.

Calculated peak areas are shown in Table II, and seem to be internally consistent. The electron density distribution functions were obtained at intervals of $\pi/30$ A in r by numerical evaluation of the Fourier sine transform with an increment of 0.05 A^{-1} in s. This

TABLE II. Pair contributions to electron distribution function (in el^2).

	Pb–Pb	As–As	S–S	Pb–As	Pb–S	As–S
I.	6640	1040	220	2650	1200	480
II.	6640	1040	220	2624	1214	480

I. Calculated according to formalism of Waser and Schomaker (footnote 9).
II. Product Z_iZ_j, assuming effective atomic number Z_i for Pb, As, and S to be the square roots of the first three numbers in I, namely 81.5, 32.2, and 14.9.

[8] For highly absorbing specimens the absorption correction is negligible for the Bragg-Brentano geometry used in this work.

[9] J. Waser and V. Schomaker, Revs. Modern Phys. **25**, 671–690 (1953).

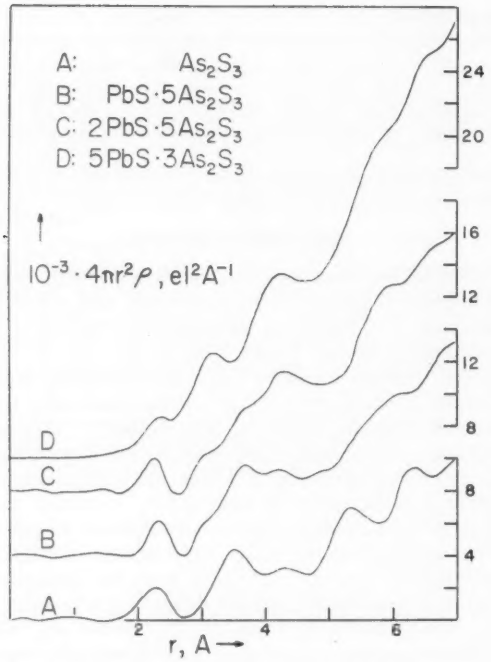

FIG. 2. Electron distributions for the several glasses.

calculation, as well as that of the peak shapes, was done by an IBM 650 computer.

RESULTS

The sharpened electron distribution functions are shown in Fig. 2, and the inner portions of these curves are reproduced on a larger scale in Fig. 3 to show the comparison with calculated peak shapes. The three prepared glasses exhibit discrete peaks (at about 2.3 A) each of which corresponds in area to three arsenic-sulfur pairs per arsenic, that is, to three sulfur neighbors for each arsenic. This is the same as found by Morimoto in crystalline arsenic sulfide[10] although in the molecules As_4S_4[11] and As_4S_6[11] and the ion AsS_3^{3+} [12] the arsenic-sulfur distance is shorter, namely, 2.23 A in the first, and 2.25 A in the last two.

For each of these three glasses the next prominent peak is at about 3.5 A, and it is due to arsenic-arsenic and sulfur-sulfur pairs. Assuming that glassy arsenic sulfide contains an arrangement of alternating arsenic and sulfur similar to that in the crystal and that 3.5 A is the mean distance between like atoms, one calculates a representative value of 99° for the As–S–As and S–As–S angles, which agrees with previous determinations [11,12] (e.g., 103°, 93°, 101°, 100°, 114°). If one further assumes that, just as in the crystal, each arsenic has three arsenic neighbors at distances near 3.5 A and then subtracts their contribution from the peak at 3.5 A, the remaining area corresponds to fourteen sulfur-sulfur pairs in this range. In Fig. 3 the solid curve lying beneath the second peak for arsenic sulfide is the sum of the peaks expected for three arsenic-arsenic pairs and fourteen sulfur-sulfur pairs. We find that four arsenic-arsenic pairs and eleven sulfur-sulfur pairs would fit equally well, but prefer to believe that the coordination in the glass is similar to the coordination found in the crystal, because the further maxima, as well as the previously cited features, are consistent with the arrangement of near neighbors in the crystal. The peak at 5.3 A, for example, is probably due to arsenic's next nearest sulfur neighbors.

The intercomparison of the several distribution functions shows the development, with increasing lead concentration, of important interactions at about 3.1 and 4.3 A. The former can be identified as a lead-sulfur contact distance, and in Fig. 3 the expected peak shapes for six sulfur neighbors per lead are superimposed on the curves for the binary glasses at about 3.1 A. Especially for $PbS·5As_2S_3$ and $2PbS·5As_2S_3$, the fact that

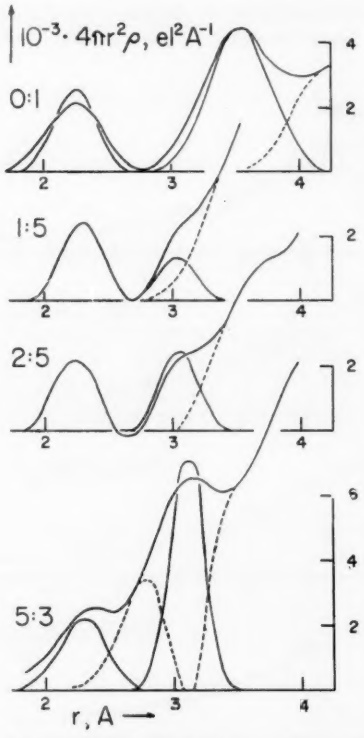

FIG. 3. Comparison of calculated peak shapes with observed electron distribution functions. Each curve is identified by the appropriate ratio of lead sulfide to arsenic sulfide. For the 1:5 and 2:5 glasses the calculated peak shape for three sulfur neighbors per arsenic has not been drawn in at 2.3 A since it coincides so closely with the function. The peak at 2.3 A for arsenic sulfide is also for three sulfur neighbors per arsenic, but that for the 5:3 glass is for four sulfurs per arsenic. The dotted lines show the difference between the function and the calculated peaks.

[10] N. Morimoto, X-sen Kondankai, Osaka University, Japan **5**, 115–118 (1949).
[11] C. Lu and J. Donohue, J. Am. Chem. Soc. **66**, 818–827 (1944).
[12] D. Harker, J. Chem. Phys. **4**, 381–390 (1936).

the calculated peaks account for the observed shoulders and that the difference curve (shown by dashed line) joins the function smoothly makes the assignment of six sulfur neighbors reasonable.

The first peak in the distribution function for the natural glass is more closely fitted by one calculated for four sulfur neighbors per arsenic, and the higher ratio of sulfur to arsenic either enables or induces arsenic to adopt tetrahedral coordination (see below). The difference curve for the natural glass shows a large peak at 2.8 A, one whose presence might not have been suggested had the trend in arsenic-sulfur and lead-sulfur interactions not been established in the other glasses. The area of this peak corresponds to 1.4 arsenic-lead pairs per lead atom, and we believe that this value is significantly close to the stoichiometric ratio of arsenic to lead in the mineral, namely, 1.2. The fact that 2.8 A falls so close to the expected separation ($3.1\times\frac{1}{2}\sqrt{3}=2.7$) of octahedral and tetrahedral holes in nearly close-packed sulfurs makes this assignment rather appealing.

The large peak at 4.3 A is at very nearly the proper distance ($\sqrt{2}\times 3.1=4.4$) for sulfur-sulfur and lead-lead pairs in such an arrangement. If we say that lead occupies octahedral holes at random, we would expect only $(5/14)\times 12$ lead-lead pairs per lead atom, and if we use this value together with 12 sulfur-sulfur pairs per sulfur atom to calculate the expected peak area at 4.3, the value of 7200 el^2 is obtained. Although the actual limits of this interaction cannot be assigned but arbitrarily, this value accounts substantially for the area under the curve in this region.

Even though the inequality of the arsenic-sulfur and arsenic-lead distances emphasizes the departure from the face-centered cubic array of sulfurs that occurs in crystalline lead sulfide we propose that the natural glass contains approximately close-packed sulfurs,[13] with the random occupation of octahedral holes by lead and tetrahedral holes by arsenic.

DISCUSSION

In crystalline arsenic sulfide, chains of alternating arsenic and sulfur are bridged by sulfur to form a two-dimensional net with each arsenic at the apex of a shallow triangular pyramid. Since the short-range order in the glass is evidently quite similar to that of the crystal, it is likely that the net's deformation to produce a glass is largely a matter of favorable entropy, rather than energy. The glass' easy formation is consistent with the notions of Zachariasen,[1] and the radius ratio, 0.36, is in the range which Goldschmidt[14] cited for glass-formers, 0.2–0.4.

The two prepared binary glasses are apparently quite similar to arsenic sulfide glass itself—even in the latter the sulfur to arsenic ratio is only 1.7:1, little more than in As_2S_3. In the natural glass, however, the ratio jumps to 2.33:1, and there is little resemblance of its distribution function to that of arsenic sulfide. Rather the proposed short-range structure has much in common with that of crystalline lead sulfide.

Indeed, its existence is not nearly so consistent with Zachariasen's criteria, and it is rather surprising that so much lead sulfide can be added to the arsenic sulfide without causing devitrification, considering the fact that the natural glass contains more lead sulfide than baumhauerite, $4PbS\cdot 3As_2S_3$, a well-known crystalline mineral.[15] According to Winter[16] one explanation for this is that the natural glass may have been formed by rapid cooling. The stalactitic growth pattern of this natural material does not confirm this suggestion, however, and annealing experiments[3] have not led to any detectible devitrification.

In conclusion, the probable similarity between glassy As_2O_3 and As_2S_3 should be pointed out. A more convincing report[17] on the oxide might have made for easier comparison with the sulfide (it is impossible to evaluate the coordination number from the distribution function since the ordinate scale is not given), but on the basis of a comparison of distances between atoms in the crystal and in the glass the threefold pyramidal coordination of arsenic has been proposed for the oxide glass as well.

[13] The reference to approximate close-packing is not to imply long-range ordering but is made in the sense due to Bernal, Proc. Roy. Inst. **37**, 355–393 (1959).

[14] V. M. Goldschmidt, Skrifter Norske Videnskaps-Akad. Oslo. I. Mat.-Natur. Kl. **1926**, 7–156 (1927).

[15] The mineral gratonite, $9PbS\cdot 2As_2S_3$, is also crystalline, and it, too, is found in Cerro de Pasco. C. Palache and D. J. Fisher, Am. Mineralogist **25**, 255–265 (1940).

[16] A. Winter, J. Am. Ceram. Soc. **40**, 54–58 (1957).

[17] H. Bötticher, K. Plieth, E. Reuber-Kürbs, and I. N. Stranski, Z. anorg. u. allgem. Chem. **266**, 302–312 (1951).

Infrared Spectrum of $Co(CO)_3NO$

ROBIN S. MCDOWELL, W. D. HORROCKS, JR., AND JOHN T. YATES

Spectroscopy Laboratory and Department of Chemistry, Massachusetts Institute of Technology, Cambridge, Massachusetts

(Received July 14, 1960)

The infrared spectra of $Co(CO)_3N^{14}O$ and $Co(CO)_3N^{15}O$ vapor are reported from 10 000 to 280 cm^{-1} and all fundamentals assigned. The two C–O stretches and the N–O stretch are at 2108, 2047, and 1822 cm^{-1}, respectively. Exchange with $C^{13}O$ indicates that a strong band at 2010 cm^{-1} is due to the C^{13}–O stretch of the isotopic species $Co(CO)_2(C^{13}O)NO$. A normal coordinate treatment has been carried out, and the force constants determined.

INTRODUCTION

SOME time ago Magee[1] investigated the infrared absorption spectrum of cobalt tricarbonyl nitrosyl and made a complete vibrational assignment by analogy with the assignment of frequencies in nickel carbonyl by Crawford and Cross.[2] Since that time the work of Jones[3,4] and Pistorius[5] has shown the Crawford and Cross assignments to be in error, and consequently the fundamentals of $Co(CO)_3NO$ assigned by Magee on that basis are incorrect. We thought it worthwhile to reinvestigate the vibrational spectrum of $Co(CO)_3NO$ and also to prepare and study the N^{15}-substituted compound, $Co(CO)_3N^{15}O$, in order to facilitate the assignment of the fundamentals. An exchange experiment with C^{13}-labeled CO was also performed to establish definitely the assignments in the C—O stretching region.

Recently Barraclough and Lewis[6] succeeded in synthesizing and recording the spectrum of $Mn(CO)(NO)_3$, the fourth member of the pseudo-nickel carbonyl series: $Ni(CO)_4$, $Co(CO)_3NO$, $Fe(CO)_2(NO)_2$, $Mn(CO)(NO)_3$. A complete understanding of the spectrum of the second member of this series is of interest. We have carried out a normal coordinate analysis and the approximate force constants of $Co(CO)_3NO$ have been calculated.

EXPERIMENTAL

Cobalt carbonyl nitrosyl was prepared according to the dithionate method of Bor and Mohai,[7] in which an ammoniacal solution of cobalt nitrate is treated with $Na_2S_2O_4$ and then with CO. On passing through NO, the gaseous product is carried off and collected in a dry ice-acetone trap.

The compound was also obtained directly from crystalline $Co_2(CO)_8$ which was prepared by reaction of a suspension of cobalt carbonate in petroleum ether with hydrogen and CO at high pressure. The procedure of Wender *et al.*[8] was followed, except that a lower loading pressure was used (2300 psi vs 3500 psi); this decreased the yield to 16%. The cystalline $Co_2(CO)_8$ obtained melted at 52.8–53.8°C. When this compound is brought into contact with gaseous NO and heated to 50°C, $Co(CO)_3NO$ is immediately formed.[9] After purification of the products obtained from each synthesis by pumping on the solid $Co(CO)_3NO$ at −20°C and by trap-to-trap distillation, the $Co(CO)_3NO$ obtained from the two methods of preparation gave identical spectra. The compound melted sharply between −0.9 and −0.4°C, in agreement with Mond and Wallis' value[9] (but not with that of Gilmont and Blanchard,[10] who report −11°C). The compound exhibits the ability to supercool at least 15 deg below its freezing point. Because $Co(CO)_3NO$ decomposes slowly in air,[1] the compound was handled in a vacuum system and stored under vacuum at 80°K.

When an excess of $Co_2(CO)_8$ is used in the second method of preparation, the reaction is quantitative and no NO can be detected in the spectrum of the unpurified product. Consequently $Co(CO)_3N^{15}O$ was prepared exclusively by this method, using 98.2% $N^{15}O$ obtained from Isomet Corporation, Palisades Park, New Jersey.

The substitution of $C^{13}O$ into $Co(CO)_3NO$ (partial pressure 10 mm) was carried out in the gas phase by exchange with $C^{13}O$ (53% C^{13}) at a partial pressure of 35 mm. The $C^{13}O$ was prepared from $C^{13}O_2$ (obtained from enriched barium carbonate, Isomet Corporation) according to the method of Bernstein and Taylor[11] by reduction over zinc dust at 425°C.

The spectrum of $Co(CO)_3NO$ vapor was obtained at various pressures up to 80 mm in 10-cm cells. A Beckman DK-2 spectrometer fitted with a wavelength marker and calibrated with water vapor was used in the near infrared (1–2.85μ). In the infrared proper, a Perkin-Elmer Model 112 with LiF (2.8–5.7μ), KBr (13.5–24μ), and CsBr (22–35μ) prisms and a Baird model AB-2 with NaCl prism (5–15μ) were used. The $C^{13}O$ substitution studies near 5μ were made on a

[1] C. B. Magee, Ph.D. thesis, Purdue University (1954); Dissertation Abstr. **15**, 991 (1955).
[2] B. L. Crawford and P. C. Cross, J. Chem. Phys. **6**, 525 (1938).
[3] L. H. Jones, J. Chem. Phys. **23**, 2448 (1955).
[4] L. H. Jones, J. Chem. Phys. **28**, 1215 (1958).
[5] C. W. F. T. Pistorius, Spectrochim. Acta **15**, 717 (1959).
[6] C. G. Barraclough and J. Lewis, J. Chem. Soc. (to be published).
[7] G. Bor and B. Mohai, Acta Chim. Acad. Sci. Hung. **8**, 355 (1956); from Chem. Abstr. **50**, 13643e (1956).
[8] I. Wender, H. W. Sternberg, S. Metlin, and M. Orchin, Inorg. Syntheses **5**, 190 (1957).
[9] R. L. Mond and A. E. Wallis, J. Chem. Soc. **121**, 32 (1922).
[10] P. Gilmont and A. A. Blanchard, Inorg. Syntheses **2**, 239 (1946).
[11] R. B. Bernstein and T. I. Taylor, Science **106**, 498 (1947).

Perkin-Elmer Model 12B with a CaF_2 prism and with a grating substituted for the Littrow mirror. These instruments were calibrated as described by Downie *et al.*[12] The region 58–115 cm^{-1} (89–172μ) was examined on the far-infrared instrument described by Lord and McCubbin,[13] using CsBr and KRS-5 reststrahlen filters.

The infrared spectrum of $Co(CO)_3N^{14}O$ is shown in Fig. 1, and the frequencies of both isotopic species are tabulated in Table I. The results of $C^{13}O$ substitution on the spectrum in the 5μ region are shown in Fig. 2.

DISCUSSION OF RESULTS

Electron-diffraction study[14] of $Co(CO)_3NO$ indicates that the C–O and N–O groups are arranged tetrahedrally about the Co atom; the point group is thus C_{3v}. Fourteen fundamental frequencies are expected, of which six will be A_1, one A_2, and seven E; all except the A_2 mode are infrared active. The numbering of the fundamentals and their approximate description is given in Table II, together with the frequency assignments as discussed below.

In the region 2200–1800 cm^{-1} there are four strong bands, of which three must be ν_1, ν_2, and ν_8. The bands at 2108 and 2047 cm^{-1} are assigned as ν_1 and ν_8 respectively by analogy with $Ni(CO)_4$, in which the

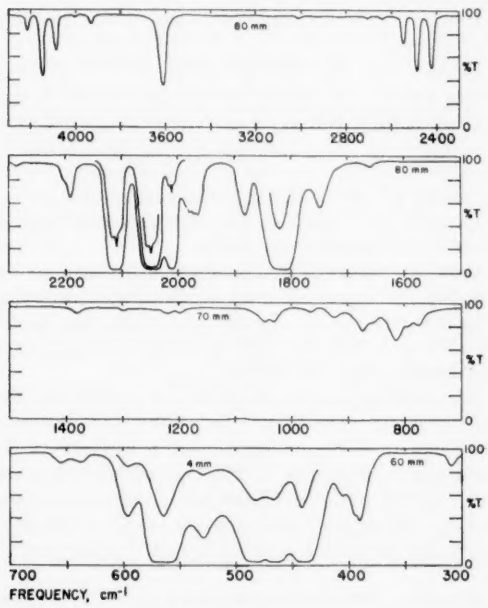

FIG. 1. Spectrum of $Co(CO)_3N^{14}O$ vapor, 4300–300 cm^{-1}. Path length 10 cm, pressures as shown.

[12] A. Downie, M. Magoon, L. Purcell, and B. L. Crawford, J. Opt. Soc. Am. **43**, 941 (1953).
[13] R. C. Lord and T. K. McCubbin, J. Opt. Soc. Am. **47**, 689 (1957).
[14] L. O. Brockway and J. S. Anderson, Trans. Faraday Soc. **33**, 1233 (1937).

TABLE I. Observed infrared bands of $Co(CO)_3NO$.

$\nu Co(CO)_3N^{14}O$	$k\times10^4$ [a]	Assignment	$\nu Co(CO)_3N^{15}O$
5385 cm^{-1}	0.1	$3\nu_2$	5287 cm^{-1}
4523	0.1	$2\nu_8+\nu_{12}$	4250
4211	0.6	$2\nu_1$	4209
4144	3.3	$\nu_1+\nu_8$	4142
4083	1.7	$2\nu_8$	4083
4003	0.1	$2\nu C^{13}—O$	4003
3931	0.4	$\nu_1+\nu_2$	3891
3615	4.3	$2\nu_2$	3542
3014	0.1	$\nu_8+2\nu_4$	...
2703	0.2	$\nu_1+\nu_3$	2697
2640	0.1	$\nu_8+\nu_3$	2636
2548	1.8	$\nu_1+\nu_{12}$	2547
2488	3.6	$\nu_8+\nu_{12}$	2488
2420, broad	3.2	$\nu_8+\nu_5$; $\nu_8+\nu_{12}-\nu_6$; $\nu_2+\nu_3$	2434; 2410; 2375
2285	0.3	$\nu_2+\nu_{11}$	...
2190	2.4	$\nu_1+\nu_{13}$	2189
2108	(s)	ν_1	2107
2047	(vs)	ν_8	2047
2010	(s)	$\nu C^{13}—O$	2010
1980	4.0	$\nu_8-\nu_{14}$	1980
1972	4.1	$\nu_8-\nu_6$	1973
1966	4.2	$\nu_8-\nu_{13}$	1967
1881	4.0	$\nu_2+\nu_{14}$	1844
1822	(vs)	ν_2	1786
1748	3.1	$\nu_2-\nu_6$	1709
1660	0.2	$\nu_8-\nu_5$	1654
1379	0.3	$3\nu_{11}$; $\nu_2-\nu_{12}$	...
1297	0.1	$3\nu_{12}$	...
1223	0.2	$\nu_2-\nu_3$	1190
1194	0.1	$2\nu_3$?	...
1048	0.6	$\nu_4+\nu_9$; $2\nu_{10}$	(1036 sh)
1030	0.6	$\nu_9+\nu_{11}$	1020
965	0.2	$2\nu_4$	...
924	0.3	$2\nu_{11}$; $\nu_4+\nu_{12}$	922
874	1.2	$2\nu_{12}$; $\nu_7+\nu_{11}$; $\nu_4+\nu_5$; ?	(875 sh); 864
814	1.4	$2\nu_7$	815
793	0.7	$2\nu_{12}-\nu_{13}$; $\nu_4+\nu_5-\nu_{13}$	790
773	0.8	$2\nu_5$	772
654	0.4	$\nu_3+\nu_{14}$	...
637	0.4	$\nu_9+\nu_6$	629
594	5.5	ν_3	591
565	73	ν_9	555
528	9.0	ν_{10}	526
483	36	ν_4	482
467	35	ν_{11}	467
442	51	ν_{12}	442
405	(w, sh)	$\nu_4-\nu_6$	405
393	(w, sh)	$\nu_{11}-\nu_6$	...
390	3.9	ν_5	390
309	0.8	$\nu_5-\nu_{13}$	308

[a] k = optical density$\times t^{-1}\times P^{-1}$; t = path length in cm; P = pressure in mm Hg; s = strong; vs = very strong; w = weak; sh = shoulder.

C—O stretches occur at 2128 and 2057 cm^{-1}.[4] The band at 1822 cm^{-1}, which shifts downward in the N^{15} compound, is the N–O stretch, ν_2. Jones[3] has suggested that a strong band at 2018 cm^{-1} in $Ni(CO)_4$ is not a fundamental as previously suggested,[2] but is the C^{13}–O stretching frequency of the isotopic species $Ni(C^{12}O)_3(C^{13}O)$. In $Co(CO)_3NO$ this band occurs at 2010 cm^{-1}. In order to check Jones' assignment, a study was made of the substitution of $C^{13}O$ for $C^{12}O$ in $Co(CO)_3NO$ by exchange, the results of which are shown in Fig. 2. The marked increase of intensity of the 2010 cm^{-1} band indicates that it is indeed due to the

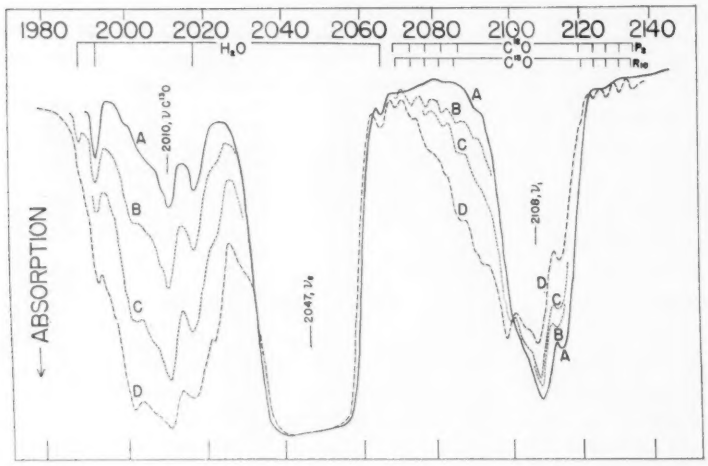

FIG. 2. Spectrum of $Co(CO)_3N^{14}O$ in the 2000 cm^{-1} region, showing the effect of isotopic substitution. Curve A: spectrum of $Co(CO)_3NO$ (10-mm, 18-cm path length). Curves B, C, D: spectra taken 3, 10, and 29 hours, respectively, after addition of 53% $C^{13}O$ at 35-mm pressure.

C^{13}–O stretching frequency of the species $Co(C^{12}O)_2(C^{13}O)NO$. Several other bands are observed to grow in order a period of time, the strongest of which is at 2090 cm^{-1}; these are probably due to species such as $Co(C^{12}O)(C^{13}O)_2NO$.[8]

Using the interatomic distances given by Brockway and Anderson,[14] the moments of inertia have been calculated, and $Co(CO)_3NO$ is found to be a quasi-spherical top. The rotational constants are $A=0.0349$ and $B=0.0354$ (0.0352 for $Co(CO)_3N^{15}O$). Thus no observable difference is expected between the contours of A_1 and E vibrations: these will both have the P—Q—R structure of spherical tops. This is observed. The P—R branch spacing of symmetric top molecules can be calculated as described by Gerhard and Dennison,[15] and is found in this case to be 10.7 cm^{-1}. The spacings observed for ν_1 and ν_8 are 10.7 and 10.8 cm^{-1}, respectively. In contrast the P—R spacing of the bond at 2010 cm^{-1}, which does not arise from a symmetric top molecule, is 12.1 cm^{-1}.

TABLE II. Fundamental frequencies of $Co(CO)_3NO$.

Symmetry	Assignment	Description	Frequency, cm^{-1} N^{14}	N^{15}
A_1	ν_1	sym. C—O stretch	2108	2107
	ν_2	N—O stretch	1822	1786
	ν_3	Co—N stretch	594	591
	ν_4	sym. C—O bend	483	482
	ν_5	sym. Co—C stretch	390	390
	ν_6	sym. C—Co—C deform.	(76)	(76)
A_2	ν_7	C—O twist	(410)	(410)
E	ν_8	degen. C—O stretch	2047	2047
	ν_9	N—O bend	565	555
	ν_{10}	degen. Co—C stretch	528	526
	ν_{11}	degen. C—O bend	467	467
	ν_{12}	degen. C—O bend	442	442
	ν_{13}	C—Co—N deformation	(81)	(81)
	ν_{14}	C—Co—C deformation	(67)	(67)

[15] S. L. Gerhard and D. M. Dennison, Phys. Rev. **43**, 197 (1932).

A normal coordinate treatment[5] indicates that the inactive F_1 frequency in $Ni(CO)_4$ should fall near 400 cm^{-1}; in $Co(CO)_3NO$ this frequency splits into an inactive A_2 vibration ν_7 and an E vibration. The first overtone of ν_7 will be infrared-active and a band of medium intensity appears at 814 cm^{-1}; this is the only band in this region which does not shift downward on N^{15}-substitution, as is expected for the A_2 vibration. Consequently 814 is assigned as $2\nu_7$, which places ν_7 near 410 cm^{-1}.

In the region 300–600 cm^{-1}, there are seven strong bands, which from their intensities must be the fundamentals ν_3 to ν_5 and ν_9 to ν_{12}. The peak at 390 cm^{-1} is assigned as the symmetric Co—C stretch, ν_5, by analogy with $Ni(CO)_4$, which has a symmetric Ni—C stretch at 381 cm^{-1}. Similarly the peak at 467 cm^{-1} is assigned as a CO bend ν_{11} the corresponding peak in $Ni(CO)_4$ occurring at 461 cm^{-1}.

From the observed isotope shifts, the peaks at 594 and 565 cm^{-1} are taken as fundamentals involving primarily motions of the nitrogen atom. We assign 594 as ν_3 and 565 as ν_9; this gives the best agreement with the product rule calculation.

The small separation of the bands at 467 and 483 cm^{-1} suggests that they must belong to different symmetry species; consequently 483 is assigned as the remaining A_1 frequency, ν_4. The peak at 442 is assigned as the second type E CO bend, ν_{12}; ν_{11} and ν_{12} are separated by only 25 cm^{-1} and probably are in Fermi resonance. The remaining peak at 528 cm^{-1} is assigned as ν_{10}.

A number of bands in the observed spectrum can best be explained as combinations of the above fundamentals with the C–Co–C and C–Co–N deformations, expected to lie below 100 cm^{-1}. The values 81, 76, and 67 cm^{-1} appear repeatedly in these combinations, and accordingly these frequencies are assigned as ν_{13}, ν_6, and ν_{14}, respectively. An attempt was made to observed these fundamentals directly, using 40 mm of $Co(CO)_3NO$

TABLE III. Symmetry force constants of $Co(CO)_3NO$.

$F_{11}=17.34$ md/A	$F_{88}=16.15$ md/A
$F_{22}=14.00$ md/A	$F_{99}=0.90$ md·A·rad^{-2}
$F_{33}=3.87$ md/A	$F_{10,10}=3.10$ md/A
$F_{44}=0.60$ md·A·rad^{-2}	$F_{11,11}=0.54$ md·A·rad^{-2}
$F_{55}=2.55$ md/A	$F_{12,12}=0.51$ md·A·rad^{-2}
$F_{66}=0.19$ md·A·rad^{-2}	$F_{13,13}=0.21$ md·A·rad^{-2}
$F_{77}=0.45$ md·A·rad^{-2}	$F_{14,14}=0.17$ md·A·rad^{-2}

in a 10-cm cell with polyethylene windows. In the region 58–115 cm^{-1} no definite absorption was observed, although there was the suggestion of a weak peak at 69 ± 1 cm^{-1}. These fundamentals are apparently of very low intensity.

This completes the assignment of the fundamentals. Most of the remaining observed bands are assigned straightforwardly as combinations and overtones; these assignments are given in Table I.

A check of the assignments can be made by use of the Teller-Redlich product rule.[16] The observed product ratios are 0.9728 for the A_1 species and 0.9786 for the E species, using the observed fundamentals; the calculated values are 0.9690 and 0.9752, respectively. Since a number of the fundamentals do not shift on N^{15} substitution, the product rule cannot provide a rigorous check of the assignments; the agreement between the calculated and observed values is good, however, suggesting that at least those bonds which show appreciable shifts are correctly assigned.

TABLE IV. Observed and calculated fundamental frequencies.

	$Co(CO)_3N^{14}O$		$Co(CO)_3N^{15}O$	
	Observed	Calculated	Observed	Calculated
ν_1	2124[a]	2123	2124[a]	2123
ν_2	1849[a]	1860	1816[a]	1822
ν_3	594	588	591	585
ν_4	483	477	482	476
ν_5	390	393	390	392
ν_6	(76)	75	(76)	75
ν_7	(410)	410	(410)	410
ν_8	2070[a]	2066	2070[a]	2066
ν_9	565	600	555	591
ν_{10}	528	528	526	523
ν_{11}	467	463	467	463
ν_{12}	442	444	442	444
ν_{13}	(81)	80	(81)	80
ν_{14}	(67)	67	(67)	67

[a] Estimated zero-point frequencies.

[16] G. Herzberg, *Infrared and Raman Spectra* (D. Van Nostrand Company, Inc., Princeton, New Jersey, 1945), pp. 231 ff.

CALCULATION OF FORCE CONSTANTS

A normal coordinate analysis was carried out using Wilson's[17] F and G matrix method and employing the symmetry coordinates and G-matrix elements of Magee.[1] The internal coordinates are as follows: r_1, r_2, r_3, the C–O distances; R_1, R_2, R_3, the Co–C distances; r', the N–O distance; R', the Co–N distance; β_1, β_2, β_3, the C—Co—N angles; α_{12}, α_{13}, α_{23}, the C—Co—C angles; γ_1, γ_3, γ_5, the Co—C—O angles in the σ_v plane; γ_2, γ_4, γ_6, the respective Co—C—O angles perpendicular to the σ_v plane; Δ_1 and Δ_2, the Co—N—O angles normal to one another. The values of the molecular parameters used in evaluating the G-matrix elements are those of Brockway and Anderson.[14] The symmetry coordinates in terms of the internal displacement coordinates are:

A_1: $S_1=3^{-\frac{1}{2}}(r_1+r_2+r_3)$

$S_2=r'$

$S_3=R'$

$S_4=3^{-\frac{1}{2}}(\gamma_1+\gamma_3+\gamma_5)$

$S_5=3^{-\frac{1}{2}}(R_1+R_2+R_3)$

$S_6=6^{-\frac{1}{2}}(\alpha_{12}+\alpha_{13}+\alpha_{23}-\beta_1-\beta_2-\beta_3)$

A_2: $S_7=3^{-\frac{1}{2}}(\gamma_2+\gamma_4+\gamma_6)$

E: $S_{8a}=6^{-\frac{1}{2}}(2r_1-r_2-r_3)$

$S_{8b}=2^{-\frac{1}{2}}(r_2-r_3)$

$S_{9a}=\Delta_1$

$S_{9b}=\Delta_2$

$S_{10a}=6^{-\frac{1}{2}}(2R_1-R_2-R_3)$

$S_{10b}=2^{-\frac{1}{2}}(R_2-R_3)$

$S_{11a}=6^{-\frac{1}{2}}(2\gamma_1-\gamma_3-\gamma_5)$

$S_{11b}=2^{-\frac{1}{2}}(\gamma_3-\gamma_5)$

$S_{12a}=6^{-\frac{1}{2}}(2\gamma_2-\gamma_4-\gamma_6)$

$S_{12b}=2^{-\frac{1}{2}}(\gamma_6-\gamma_4)$

$S_{13a}=6^{-\frac{1}{2}}(2\beta_1-\beta_2-\beta_3)$

$S_{13b}=2^{-\frac{1}{2}}(\beta_2-\beta_3)$

$S_{14a}=6^{-\frac{1}{2}}(2\alpha_{23}-\alpha_{12}-\alpha_{13})$

$S_{14b}=2^{-\frac{1}{2}}(\alpha_{13}-\alpha_{12})$.

The values of the symmetry valence force constants calculated using the above symmetry coordinates and

[17] E. B. Wilson, J. C. Decius, and P. C. Cross, *Molecular Vibrations* (McGraw-Hill Book Company, Inc., New York, 1955).

TABLE V. Distribution of potential energy among the symmetry coordinates.

	S_1	S_2	S_3	S_4	S_5	S_6
			A_1 Vibrations			
ν_1	0.950	0.000	0.000	0.000	0.050	0.000
ν_2	0.000	0.912	0.088	0.000	0.000	0.000
ν_3	0.006	0.063	0.639	0.183	0.079	0.030
ν_4	0.000	0.017	0.192	0.747	0.005	0.039
ν_5	0.045	0.007	0.078	0.005	0.865	0.000
ν_6	0.000	0.000	0.003	0.065	0.002	0.930

	S_8	S_9	S_{10}	S_{11}	S_{12}	S_{13}	S_{14}
				E Vibrations			
ν_8	0.932	0.000	0.068	0.000	0.000	0.000	0.000
ν_9	0.017	0.680	0.228	0.008	0.023	0.040	0.004
ν_{10}	0.042	0.282	0.586	0.003	0.074	0.002	0.011
ν_{11}	0.000	0.007	0.000	0.889	0.059	0.024	0.021
ν_{12}	0.008	0.000	0.113	0.061	0.773	0.002	0.043
ν_{13}	0.000	0.027	0.000	0.039	0.004	0.831	0.099
ν_{14}	0.000	0.004	0.004	0.000	0.068	0.101	0.823

neglecting all off-diagonal elements are given in Table III.

The frequencies calculated using the above set of symmetry force constants are given in Table IV, together with the observed fundamentals. The observed frequencies are those of Table II except for ν_1, ν_2, and ν_8; for these frequencies the combination bands $\nu_1+\nu_2$ and $\nu_1+\nu_8$ and the overtones enable us to estimate the anharmonic corrections and to assign the approximate zero-order frequencies[18] as $\omega_1=2124$, $\omega_8=2070$ cm^{-1}; $\omega_2=1849$ cm^{-1} for $Co(CO)_3N^{14}O$ and 1816 cm^{-1} for $Co(CO)_3N^{15}O$. The agreement between the observed and calculated frequencies is good except for ν_9, which is some 35 cm^{-1} off. The observed isotope shifts are reproduced very closely.

In terms of the valency force field similar to that used by Jones[4] for $Ni(CO)_4$, $F_{CO}=16.55$ md/A, and the interaction constant $F_{CO,CO}=0.40$ md/A. This is in reasonable agreement with Jones' values for $Ni(CO)_4$ of $F_{CO}=17.29$ md/A and $F_{CO,CO}=0.22$ md/A; the interaction constant is positive, as would be expected from a consideration of the resonance involved. $F_{NO}=14.00$ md/A and $F_{Co-N}=3.87$ md/A; this is higher than $F_{Co-C}=2.92$ md/A, as would be expected considering that the Co—N bond length is 4% shorter than the Co—C bond length. Stammreich *et al.*[19] found F_{Co-C} to be 3.55 md/A in $Co(CO)_4^-$. The interaction constant $F_{Co-C,Co-C'}=-0.18$ md/A while Jones obtained $F_{Ni-C,Ni-C'}=0.1$ md/A. The Co—C—O deformation force constants have not been solved for explicitly in terms of any assumed interaction constants, but F_{Co-C-O} falls in the range 0.45–0.54 md/A/rad^{-2}, while Jones obtained $F_{Ni-C-O}=0.4\pm1$ md/A/rad^{-2} for $Ni(CO)_4$. In terms of our units Stammreich obtained 0.97 md/A/rad^{-2} for F_{Co-C-O} in $Co(CO)_4^-$. We find $F_{Co-N-O}=0.90$ md/A/rad^{-2} and it is interesting that this is considerably higher than F_{Co-C-O}. Finally, we find that the skeletal deformation constant $F_{C-Co-N}=0.21$ md/A/rad^{-2} and F_{C-Co-C} falls in the range 0.17 to 0.19 md/A/rad^{-2} with interaction constants not considered.

The above force constants are probably not accurate to better than 5% and might be improved by including certain off-diagonal interaction constants. A least-squares improvement of the force constants using data from the N^{15}-substituted compound was contemplated, but the inavailability of computer time made this impractical. The present set of force constants, though approximate, is the best available.

Table V gives the distribution of potential energy among the normal coordinates as determined from the L-matrix elements, for $Co(CO)_3N^{14}O$. It will be seen that the C—O and N—O stretches and the deformations are relatively unmixed, while the Co—N and degenerate Co—C stretches and the N—O bend show a large amount of mixed character.

ACKNOWLEDGMENTS

This research was carried out in the Spectroscopy Laboratory at MIT and the authors thank Professor R. C. Lord for the use of these facilities. Thanks are also due Professor C. W. Garland and Professor F. A. Cotton for their encouragement, and the Chemistry Department of MIT, which provided financial support. The autoclave reaction for the preparation of $Co_2(CO)_8$ was carried out with the assistance of Zenon Jacura. Some of the calculations were done at the MIT Computation Center. One of us (W.D.H.) wishes to thank the Monsanto Chemical Company and the National Science Foundation for fellowship support.

[18] See pp. 210 ff. of work cited in footnote 16.

[19] H. Stammreich, K. Kawai, Y. Tavares, P. Krumholz, J. Behmoires, and S. Bril, J. Chem. Phys. **32**, 1482 (1960).

A Closed General Solution of the Probability Distribution Function for Three-Dimensional Random Walk Processes*

CHI-HUA HSIUNG, HSIEN-CHIH HSIUNG, AND ADON A. GORDUS

Department of Chemistry, The University of Michigan, Ann Arbor, Michigan

(Received June 27, 1960)

A closed general solution of the probability distribution function for three-dimensional random walk processes is derived. In addition: (1) For the particular case of equal-length displacements, the exact solution is compared with the Gaussian approximation for $n=3$, 5, and 10 steps. (2) The general solution is utilized in calculating the probability distribution of gamma-ray energies resulting in the Cl^{35} (n, γ) Cl^{36} process. (3) For five unequal steps of fractional length: 0.582, 0.135, 0.131, 0.092, and 0.060 (which is somewhat characteristic of the fractional energies of gamma rays resulting from neutron capture), the exact solution is compared with a Gaussian, a modified Gaussian, and a five equal-step approximation. (4) There are presented the specific solutions for all possible unequal-length random displacements involving $n=2$, 3, and 4 steps.

INTRODUCTION

WE have been interested in using the random walk model to evaluate the probability distribution of the recoil energy imparted to an atom in a molecule as a result of neutron-capture gamma-ray emission. Cobble and Boyd[1] have discussed this problem with regard to the $Br^{81}(n, \gamma)Br^{82}$ process. In the case of cascade gamma emission there exists (in many cases) a finite probability that the atom activated by neutron absorption receives a relatively small recoil energy and thus fails to dissociate from the parent molecule.[2] If neutron-capture gamma-ray data are available for the process of interest, and if the gamma-ray emission is spherically symmetrical, then the probability distribution of energies can be calculated in terms of the random walk model.

If the ith step is of length l_i and in a random direction in space, then, according to Rayleigh,[3,4] the probability distribution function will be

$$W_n(R) = (2\pi^2 R\prod_{i=1}^{n} l_i)^{-1}\int_0^{\infty} \{[\prod_{i=1}^{n} \sin(l_i\rho)]\sin(R\rho)/\rho^{n-1}\}d\rho, \quad (1)$$

where R is the vector sum of n random displacements l_i ($i=1$ to n), ρ is a dummy variable of spatial integration, and $W_n(R)$ is the probability distribution function specifying the total vector displacements resulting from the n random vector displacements l_i.

To our knowledge, analytical solutions of this integral have been derived for only a small number of special cases. Chandrasekhar[4] solved the integral for the case of an infinite number of equal-length random displacements. The integrals involving three, four, and six equal-length steps were solved by Rayleigh.[3,4] Campbell[5] presented solutions, based on work by O'Connor,[6] for the integrals involving two and three unequal-length, as well as five equal-length, random vector displacements.[7] Rayleigh[3] suggested a method for evaluating $W_n(R)$ which is workable in principle, yet in practice becomes so tedious that it might be considered impractical for n greater than about 4. The direct numerical integration of Eq. (1) was found to be too time-consuming even using an IBM-704 computer. In an attempt to simplify the calculations, we derived a closed general solution for $W_n(R)$.

CLOSED GENERAL SOLUTION

We examine the integral first where n is even, and then where n is an odd number.

Case I: n an Even Number

Through the use of simple trigonometric relationships, the numerator of the integrand of Eq. (1) can be expressed as a sum of sin terms,

$$[\prod_{i=1}^{n} \sin(l_i\rho)]\sin(R\rho) = (1/2^n)\sum_{j=1}^{2^{n-1}} [\sin(a_j\rho)-\sin(b_j\rho)], \quad (2)$$

* This work was supported in part by a grant from The University of Michigan, Memorial Phoenix Project, and by the U. S. Atomic Energy Commission, Division of Research.

[1] J. W. Cobble and G. E. Boyd, J. Am. Chem. Soc. **74**, 1282 (1952).

[2] A. A. Gordus and J. E. Willard, J. Am. Chem. Soc. **79**, 4609 (1957).

[3] Lord Rayleigh, Phil. Mag. **37**, 321 (1919) or *Scientific Papers of Lord Rayleigh* (Cambridge University Press, New York, 1920), VI, p. 604.

[4] S. Chandrasekhar, Revs. Modern Phys. **15**, 1 (1943).

[5] I. G. Campbell, Nucleonika **2**, 605 (1957); Chem. Abstr. **52**, 11600i (1958); U. S. Atomic Energy Comm. Nuclear Sci. Abstr. **12**, 6505 (1958).

[6] D. O'Connor, Rept. No. 12/I-B, Polish Acad. Sci., Inst. Nuclear Research, Warsaw; U. S. Atomic Energy Comm. Nuclear Sci. Abstr. **12**, 9942 (1958).

[7] The equation presented in the work cited in footnote 5 (apparently obtained from the work cited in footnote 6) for three unequal-vector lengths is incomplete. It is applicable only in the case of $(l_1+l_2)>l_3$. The solution of the integral for the case of $l_3>(l_1+l_2)$ is somewhat different. At the time of writing we had not received a copy of footnote 6.

where both a_j and b_j are algebraic sums consisting of $(n+1)$ terms of R, l_1, l_2, $\cdots$, l_n. The first quantity in each algebraic sum is always positive and the signs of subsequent l's are determined by the following rules:

1. The number of negative signs in each a_j term is even when $n/2$ is even and odd when $n/2$ is odd.
2. The number of negative signs in each b_j term is even when $n/2$ is odd and odd when $n/2$ is even.

Thus, from Eqs. (1) and (2),

$$W_n(R)=(2^{n+1}\pi^2R\prod_{i=1}^{n}l_i)^{-1}\sum_{j=1}^{2^{n-1}}\left[\int_0^\infty\frac{\sin(a_j\rho)}{\rho^{n-1}}d\rho-\int_0^\infty\frac{\sin(b_j\rho)}{\rho^{n-1}}d\rho\right]. \tag{3}$$

The general integration form of Eq. (3),

$$\int_0^\infty\frac{\sin(x\rho)}{\rho^{n-1}}d\rho,$$

can be evaluated by means of integration by parts and is divergent. Since $W_n(R)$ is convergent, it is anticipated that the divergency in the integral will disappear upon summing the a_j and b_j integrals,

$$\begin{aligned}\int_0^\infty\frac{\sin(x\rho)}{\rho^{n-1}}d\rho&=\lim_{y\to0,z\to\infty}\left[x^{n-2}\int_y^z\frac{\sin(x\rho)}{(x\rho)^{n-1}}xd\rho\right]\\
&=\lim_{y\to0,z\to\infty}x^{n-2}\left\{-\left[\frac{\sin(x\rho)}{(n-2)(x\rho)^{n-2}}+\frac{\cos(x\rho)}{(n-2)(n-3)(x\rho)^{n-3}}\right]\right.\\
&\qquad+\left[\frac{\sin(x\rho)}{(n-2)(n-3)(n-4)(x\rho)^{n-4}}+\frac{\cos(x\rho)}{(n-2)(n-3)(n-4)(n-5)(x\rho)^{n-5}}\right]\\
&\quad+\cdots+(-1)^k\left[\frac{\sin(x\rho)}{(n-2)(n-3)\cdots(n-2k)(x\rho)^{n-2k}}+\frac{\cos(x\rho)}{(n-2)(n-3)\cdots(n-2k-1)(x\rho)^{n-2k-1}}\right]+\cdots\\
&\qquad\left.+(-1)^{(n/2)-1}\left[\frac{\sin(x\rho)}{(n-2)(n-3)\cdots(2)(x\rho)^2}+\frac{\cos(x\rho)}{(n-2)(n-3)\cdots(2)(1)(x\rho)}\right]\right\}_{\rho=z}^{\rho=y}\\
&\qquad+\lim_{y\to0,z\to\infty}\frac{(-1)^{(n/2)-1}}{(n-2)!}\left[x^{n-2}\int_z^y\frac{\sin(x\rho)}{x\rho}xd\rho\right]\\
&=\lim_{y\to0,z\to\infty}x^{n-2}\sum_{k=1}^{(n/2)-1}(-1)^k\left[\frac{(n-2k-1)!\sin(x\rho)}{(n-2)!(x\rho)^{n-2k}}+\frac{(n-2k-2)!\cos(x\rho)}{(n-2)!(x\rho)^{n-2k-1}}\right]_{\rho=z}^{\rho=y}\\
&\qquad+\frac{(-1)^{(n/2)-1}}{(n-2)!}\left[\frac{x^{n-2}\mid x\mid}{x}\int_0^\infty\frac{\sin\rho}{\rho}d\rho\right].\end{aligned}$$

Therefore,

$$\int_0^\infty\frac{\sin(x\rho)}{\rho^{n-1}}d\rho=\lim_{y\to0,z\to\infty}x^{n-2}\sum_{k=1}^{(n/2)-1}(-1)^k\left[\frac{(n-2k-1)!\sin(x\rho)}{(n-2)!(x\rho)^{n-2k}}+\frac{(n-2k-2)!\cos(x\rho)}{(n-2)!(x\rho)^{n-2k-1}}\right]_{\rho=z}^{\rho=y}+\frac{(-1)^{(n/2)-1}\pi x^{n-3}\mid x\mid}{2(n-2)!}. \tag{4}$$

On substituting Eq. (4) into Eq. (3),

$$\begin{aligned}W_n(R)=(2^{n+1}\pi^2R\prod_{i=1}^{n}l_i)^{-1}\sum_{j=1}^{2^{n-1}}&\left\{a_j^{n-2}\lim_{y\to0,z\to\infty}\sum_{k=1}^{(n/2)-1}(-1)^k\left[\frac{(n-2k-1)!\sin(a_j\rho)}{(n-2)!(a_j\rho)^{n-2k}}+\frac{(n-2k-2)!\cos(a_j\rho)}{(n-2)!(a_j\rho)^{n-2k-1}}\right]\right.\\
&\left.-b_j^{n-2}\lim_{y\to0,z\to\infty}\sum_{k=1}^{(n/2)-1}(-1)^k\left[\frac{(n-2k-1)!\sin(b_j\rho)}{(n-2)!(b_j\rho)^{n-2k}}+\frac{(n-2k-2)!\cos(b_j\rho)}{(n-2)!(b_j\rho)^{n-2k-1}}\right]\right\}_{\rho=z}^{\rho=y}\\
&+[(-1)^{(n/2)-1}/2^{n+2}\pi R(n-2)!\prod_{i=1}^{n}l_i]\sum_{j=1}^{2^{n-1}}[a_j^{n-3}\mid a_j\mid-b_j^{n-3}\mid b_j\mid]. \qquad (5)\end{aligned}$$

We now proceed to evaluate the limits of the first two terms on the right-hand side of Eq. (5). These two terms vanish as ρ approaches infinity, thus leaving only the negative limit of these two terms as ρ approaches zero. On calling this limit S, we have

$$S=\sum_{j=1}^{2^{n-1}}\left\{-a_j^{n-2}\lim_{y\to 0}\sum_{k=1}^{(n/2)-1}(-1)^k\left[\frac{(n-2k-1)!\sin(a_j\rho)}{(n-2)!(a_j\rho)^{n-2k}}+\frac{(n-2k-2)!\cos(a_j\rho)}{(n-2)!(a_j\rho)^{n-2k-1}}\right]\right.$$
$$\left.+b_j^{n-2}\lim_{y\to 0}\sum_{k=1}^{(n/2)-1}(-1)^k\left[\frac{(n-2k-1)!\sin(b_j\rho)}{(n-2)!(b_j\rho)^{n-2k}}+\frac{(n-2k-2)!\cos(b_j\rho)}{(n-2)!(b_j\rho)^{n-2k-1}}\right]_{\rho=y}\right.\text{.}$$

Since the summations are over finite terms, the order of summation may be interchanged. Thus,

$$S=\lim_{y\to 0}\sum_{k=1}^{(n/2)-1}(-1)^{k+1}\frac{(n-2k-2)!}{(n-2)!}\left[(n-2k-1)\sum_{j=1}^{2^{n-1}}\left(a_j^{2k-2}\frac{\sin(a_j\rho)}{\rho^{n-2k}}-b_j^{2k-2}\frac{\sin(b_j\rho)}{\rho^{n-2k}}\right)\right.$$
$$\left.+\sum_{j=1}^{2^{n-1}}\left(a_j^{2k-1}\frac{\cos(a_j\rho)}{\rho^{n-2k-1}}-b_j^{2k-1}\frac{\cos(b_j\rho)}{\rho^{n-2k-1}}\right)\right]_{\rho=y}. \quad (6)$$

However, the terms of the form $[\sin(W_j\rho)/\rho^{n-2k}]_{\rho=0}$ are indeterminants. Evaluating them through the use of the l'Hôpital rule, we obtain

$$[\sin(W_j\rho)/\rho^{n-2k}]_{\rho=0}=[W_j/(n-2k)][\cos(W_j\rho)/\rho^{n-2k-1}]_{\rho=0}. \quad (7)$$

On substituting the form of Eq. (7) into (6), we find

$$S=\lim_{y\to 0}\sum_{k=1}^{(n/2)-1}\frac{(-1)^{k+1}(n-2k-2)!(2n-4k-1)}{(n-2)!(n-2k)(\rho^{n-2k-1})_{\rho=y}}\sum_{j=1}^{2^{n-1}}[a_j^{2k-1}\cos(a_j\rho)-b_j^{2k-1}\cos(b_j\rho)]_{\rho=y}.$$

Thus,

$$S=\sum_{k=1}^{(n/2)-1}\frac{(-1)^{k+1}(n-2k-2)!(2n-4k-1)}{(n-2)!(n-2k)(\rho^{n-2k-1})_{\rho=y}}\sum_{j=1}^{2^{n-1}}(a_j^{2k-1}-b_j^{2k-1}). \quad (8)$$

However, if one examines the a_j and b_j terms, one finds that

$$\sum_{j=1}^{2^{n-1}}(a_j-b_j)=0$$
$$\sum_{j=1}^{2^{n-1}}(a_j^3-b_j^3)=0$$
$$\cdots$$
$$\sum_{j=1}^{2^{n-1}}(a_j^{n-3}-b_j^{n-3})=0.$$

Therefore,

$$\sum_{j=1}^{2^{n-1}}(a_j^{2k-1}-b_j^{2k-1})=0 \quad \text{for} \quad k=1 \quad \text{to} \quad [(n/2)-1].$$

The successive use of l'Hôpital's rule permits evaluation of the indeterminant. Accordingly,

$$\lim_{\rho\to 0}\frac{1}{\rho^{n-2k-1}}\sum_{j=1}^{2^{n-1}}[a_j^{2k-1}\cos(a_j\rho)-b_j^{2k-1}\cos(b_j\rho)]=\lim_{\rho\to 0}\frac{-1}{(n-2k-1)\rho^{n-2k-2}}\sum_{j=1}^{2^{n-1}}[a_j^{2k}\sin(a_j\rho)-b_j^{2k}\sin(b_j\rho)]$$
$$=\lim_{\rho\to 0}\frac{-1}{(n-2k-1)(n-2k-2)\rho^{n-2k-3}}\sum_{j=1}^{2^{n-1}}[a_j^{2k+1}\cos(a_j\rho)-b_j^{2k+1}\cos(b_j\rho)]$$

$= \cdots$ etc. Consequently, for any specific value of k, the process is continued until the denominator becomes ρ times a constant. Under these conditions $\rho = \rho^{n-2k-2m+1}$ and the indeterminant becomes

$$\lim_{\rho\to 0} \frac{(-1)^m \sum_{j=1}^{2^{n-1}} [a_j^{2k+2m-1}\cos(a_j\rho) - b_j^{2k+2m-1}\cos(b_j\rho)]}{(n-2k-1)(n-2k-2)\cdots(n-2k-2m+2)\rho^{n-2k-2m+1}} = \frac{(-1)^m(n-2k-2m+1)!}{\rho(n-2k-1)!} \sum_{j=1}^{2^{n-1}} (a_j^{2k+2m-1} - b_j^{2k+2m-1}). \quad (9)$$

Since $\rho^{n-2k-2m+1} = \rho$, then

$$n-2k-2m+1 = 1 \quad \text{and} \quad m = \tfrac{1}{2}(n-2k),$$

when

$$k = 1, \qquad m = \tfrac{1}{2}(n-2) \quad \text{and} \quad 2k+2m-1 = n-1.$$

Thus,

$$\sum_{j=1}^{2^{n-1}} (a_j^{2k+2m-1} - b_j^{2k+2m-1}) = 0.$$

For any value of k,

$$2k+2m-1 = 2k+n-2k-1 = n-1.$$

Therefore, this summation is always equal to zero. Thus, Eq. (9) remains an indeterminant. However, further use of l'Hôpital's rule leads to

$$\lim_{\rho\to 0} \frac{1}{\rho^{n-2k-1}} \sum_{j=1}^{2^{n-1}} [a_j^{2k-1}\cos(a_j\rho) - b_j^{2k-1}\cos(b_j\rho)] = \left[\frac{(-1)^{[(n-2)/2]+1}}{(n-2k-1)!} \sum_{j=1}^{2^{n-1}} [a_j^n \sin(a_j\rho) + b_j^n \sin(b_j\rho)] \right]_{\rho=0} = 0.$$

Therefore, Eq. (8) yields

$$S = 0$$

or

$$W_n(R) = \frac{(-1)^{(n/2)-1}}{2^{n+2}\pi R(n-2)! \prod_{i=1}^{n} l_i} \sum_{j=1}^{2^{n-1}} (a_j^{n-3} \mid a_j \mid - b_j^{n-3} \mid b_j \mid). \quad (10)$$

When $n/2$ is even, $(-1)^{(n/2)-1} = -1$; when $n/2$ is odd, this term $= +1$.

However, according to the rules defining the a_j and b_j terms, it is found that a_j terms for $n/2$ equal to an even number are the same as b_j terms for $n/2$ equal to an odd number, and vice versa. Therefore, Eq. (10) may be stated in a general manner irrespective of the evenness or oddness of $n/2$.

Hence, the general solution for n equal to an even number is

$$W_n(R) = [2^{n+2}\pi R(n-2)! \prod_{i=1}^{n} l_i]^{-1} \sum_{j=1}^{2^{n-1}} (a_j^{n-3} \mid a_j \mid - b_j^{n-3} \mid b_j \mid), \quad (11)$$

where

1. both a_j and b_j are algebraic sums consisting of $(n+1)$ terms of $R, l_1, l_2, \cdots, l_n$;
2. there are a total of 2^{n-1} different a_j and 2^{n-1} different b_j terms;
3. the first quantity in each a_j or b_j term is always positive;
4. the total number of negative signs in each a_j term is an odd number, $[1, 3, 5, \cdots, (n-1)]$;
5. the total number of negative signs in each b_j term is an even number, $[0, 2, 4, \cdots, n]$.

Case II: n an Odd Number

The deriviation is similar to that of Case I. By using simple trigonometric relationships, the numerator of the integrand of Eq. (1) is expressed as a series of cosine terms,

$$[\prod_{i=1}^{n} \sin(l_i\rho)] \sin(R\rho) = (1/2^n) \sum_{j=1}^{2^{n-1}} [\cos(c_j\rho) - \cos(d_j\rho)], \quad (12)$$

where both c_j or d_j consist of $(n+1)$ terms of $R, l_1, l_2, \cdots, l_n$. The first quantity R in each term is always positive and the signs of subsequent l's are determined by the following rules:

(1) The number of negative signs in each c_j term is even when $(n-1)/2$ is even and odd when $(n-1)/2$ is odd.

(2) The number of negative signs in each d_j term is even when $(n-1)/2$ is odd and odd when $(n-1)/2$ is even. Thus, from Eqs. (1) and (12),

$$W_n(R) = (2^{n+1}\pi^2 R\prod_{i=1}^{n} l_i)^{-1} \sum_{j=1}^{2^{n-1}} \left(\int_0^\infty \frac{\cos(c_j\rho)}{\rho^{n-1}} d\rho - \int_0^\infty \frac{\cos(d_j\rho)}{\rho^{n-1}} d\rho \right). \tag{13}$$

The general integration form of Eq. (13) is

$$\int_0^\infty \frac{\cos(x\rho)}{\rho^{n-1}} d\rho,$$

which is divergent.

As in Case I, integration by parts results in

$$\int_0^\infty \frac{\cos(x\rho)}{\rho^{n-1}} d\rho = x^{n-2} \lim_{y\to 0, x\to\infty} \left\{ \sum_{k=1}^{(n-1)/2} \left[\frac{(-1)^k (n-2k)!\sin(x\rho)}{(n-2)!(x\rho)^{n-2k+1}} + \frac{(-1)^k (n-2k-1)!\cos(x\rho)}{(n-2)!(x\rho)^{n-2k}} \right] + \frac{\sin(x\rho)}{(x\rho)^{n-1}} \right\}$$
$$+ [(-1)^{(n-1)/2}\pi/2(n-2)!] x^{n-3} \mid x \mid. \tag{14}$$

This general solution (14) may be utilized in Eq. (13). The indeterminate expression which results is evaluated as in Case I, using the rule of l'Hôpital successively. The final result is, for $(n-1)/2$ equal to an even number,

$$W_n(R) = [2^{n+2}\pi R(n-2)!\prod_{i=1}^{n} l_i]^{-1} \sum_{j=1}^{2^{n-1}} (c_j{}^{n-3} \mid c_j \mid - d_j{}^{n-3} \mid d_j \mid). \tag{15}$$

For $(n-1)/2$ equal to an odd number, $W_n(R)$ is equal to the negative of Eq. (15). Reciprocity relationships again exist so that c_j's for $(n-1)/2$ equal to an even number are the same as d_j's for $(n-1)/2$ equal to an odd number. Thus, the over-all expression is identical for both $(n-1)/2$ even or odd, and for n equal to an odd number the solution is Eq. (15). The restrictions are:

1. both c_j and d_j are algebraic sums consisting of $(n+1)$ terms of $R, l_1, l_2, \cdots, l_n$;
2. there are a total of 2^{n-1} different c_j and 2^{n-1} different d_j terms;
3. the first quantity in each c_j or d_j term is always positive;
4. the total number of negative signs in each c_j term is an odd number, $[1, 3, 5, \cdots, n]$;
5. the total number of negative signs in each d_j term is an even number, $[0, 2, 4, \cdots, (n-1)]$.

General Solution

On comparing Eqs. (11) and (15) and their respective conditions, it is seen that the solution is of the same general form, with conditions 4 and 5 differing only slightly. It is therefore possible to combine these two cases in the form of one general equation valid for any finite value of $n \geq 2$. Thus,

$$W_n(R) = [2^{n+2}\pi R(n-2)!\prod_{i=1}^{n} l_i]^{-1} \sum_{j=1}^{2^{n-1}} (M_j{}^{n-3} \mid M_j \mid - N_j{}^{n-3} \mid N_j \mid), \tag{16}$$

where

1. both M_j and N_j are algebraic sums consisting of $(n+1)$ terms of $R, l_1, l_2, \cdots, l_n$;
2. ther are a total of 2^{n-1} different M_j and 2^{n-1} different N_j terms;
3. the first quantity in each M_j or N_j term is always positive;
4. the total number of negative signs in each M_j term is an odd number, $[1, 3, 5, \cdots, (n-1)_e$ or $(n)_o]$;
5. the total number of negative signs in each N_j term is an even number, $[0, 2, 4, \cdots, (n)_e$ or $(n-1)_o]$, where e and o represent n equal to an even or odd number, respectively.

Given in the Appendix are the complete solutions for $n=2$, 3, and 4 unequal-length random vector displacements.

Equal-Length Displacements

A case of particular interest occurs when all displacements are of equal length. The probability distribution function, Eq. (1), is therefore

$$W_n(R) = (2\pi^2 Rl^n)^{-1} \int_0^\infty \{[\sin^n(\rho l)] \sin(R\rho)/\rho^{n-1}\} d\rho. \tag{17}$$

We examine the general solution, Eq. (16). If we choose R as the first quantity in the M_j and N_j terms, the remaining quantities are all l's. According to the condition for M_j, the number of negative l's is odd, $[1, 3, 5, \cdots, (2s-1), \cdots, (n-1)_e$ or $(n)_0]$. Therefore,

the number of positive l's in any M_j term is $n-(2s-1)$, where

$$s=1, 2, 3, \cdots, (n/2)_e \quad \text{or} \quad [(n+1)/2]_o.$$

As a result, the net number of l's is

$$n-(2s-1)-(2s-1)=n+2-4s,$$

and $M_s=R+(n+2-4s)l$.

The number of possible combinations of positive l's and negative l's that will result in M_s [i.e., n total l's, of which $(2s-1)$ are negative] is the binomial coefficient

$$\binom{n}{2s-1}.$$

Therefore,

$$\sum_{j=1}^{2^{n-1}} M_j^{n-3} \mid M_j \mid = \sum_{s=1}^{(n/2)_e \text{ or } [(n+1)/2]_o} \binom{n}{2s-1} M_s^{n-3} \mid M_s \mid. \tag{18}$$

Regarding the N_j terms, the number of negative l's is even, $[0, 2, 4, \cdots, (2s-2), \cdots, (n)_e \text{ or } (n-1)_o]$ where $s=1, 2, 3, \cdots, [(n/2)+1]_e$ or $[(n+1)/2]_o$. Therefore, in a manner similar to that above, the net number of l's in any N_s term is: $n-(2s-2)-(2s-2)=n+4-4s$ and $N_s=R+(n+4-4s)l$. The number of possible combinations of positive l's and negative l's that will result in N_s is

$$\binom{n}{2s-2}.$$

Therefore,

$$\sum_{j=1}^{2^{n-1}} N_j^{n-3} \mid N_j \mid = \sum_{s=1}^{[(n/2)+1]_e \text{ or } [(n+1)/2]_o} \binom{n}{2s-2} N_s^{n-3} \mid N_s \mid. \tag{19}$$

The probability distribution function is

$$W_n(R)=[2^{n+2}\pi(n-2)!Rl^n]^{-1}\left\{\sum_{s=1}^{(n/2)_e \text{ or } [(n+1)/2]_o}\binom{n}{2s-1}[R+(n+2-4s)l]^{n-3} \mid R+(n+2-4s)l \mid \right.$$
$$\left. -\sum_{s=1}^{[(n/2)+1]_e \text{ or } [(n+1)/2]_o}\binom{n}{2s-2}[R+(n+4-4s)l]^{n-3} \mid R+(n+4-4s)l \mid \right\}. \tag{20}$$

Equations (16) and (20), when reduced to special cases, result in expressions identical to those stated in the literature.[4,5]

Evaluation of Probability

The probability that the total displacement is between 0 and R as a result of n random vector displacements is,

$$P_n(R)=\int_0^R 4\pi R^2 W_n(R)\,dR. \tag{21}$$

The probability distribution is,

$$dP_n(R)/dR=4\pi R^2 W_n(R). \tag{22}$$

COMPARISON WITH APPROXIMATIONS

Equal Random Steps

A Gaussian distribution is perhaps the most commonly utilized approximation of the probability distribution (PD), Eq. (22). In this case,[4]

$$W_n(R)=[1/(2\pi n\langle l^2\rangle_{Av}/3)^{\frac{3}{2}}]\exp[-3R^2/2n\langle l^2\rangle_{Av}]. \tag{23}$$

Figure 1 is the percent error in the Gaussian approximation of the probability distribution for $n=3$, 5, and 10 equal-length random vector displacements. For this plot: percent error $=100[(PD)_{ex}-(PD)_g]/(PD)_{ex}$, where $(PD)_{ex}$ is the exact and $(PD)_g$ the Gaussian calculated value.

Similarly, Fig. 2 is the percent error in the Gaussian approximation of the probability for $n=3$, 5, and 10 equal-length random vector displacements. Here: percent error $=100[P_{ex}-P_g]/P_{ex}$, where the subscripts have the same meaning as above.

Five Unequal Steps

To illustrate the error in various approximations of an unequal-step random walk we have chosen five steps of fractional lengths: 0.582, 0.135, 0.131, 0.092, and 0.060. These five steps are characteristic of the relative magnitudes of the gamma rays emitted following neutron capture. Specifically, these steps correspond to the 5.01, 1.16, 1.13, 0.79, and 0.51 Mev gamma-ray cascade in the $Cl^{35}(n,\gamma)Cl^{36}$ process discussed below.

Figure 3 illustrates the probability distribution calculated via (a) the exact expression, Eqs. (16) and (22); (b) Eq. (20), assuming each of the five steps to be of equal length, 0.2 R_{max}; (c) the Gaussian distribution for $\langle l_i^2\rangle_{Av}=0.0771$; and (d) a modified Gaussian dis-

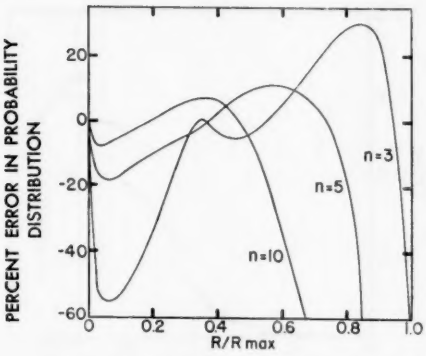

FIG. 1. Percent error in probability distribution for a Gaussian distribution vs the fraction of the maximum possible resultant vector length for three, five, and 10 equal-length random vectors.

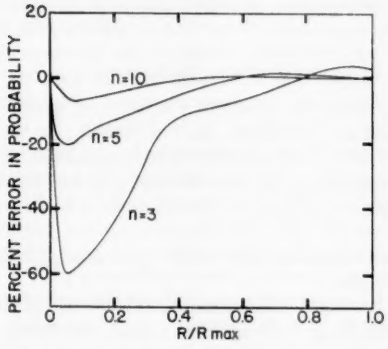

FIG. 2. Percent error in probability for a Gaussian distribution vs the fraction of the maximum possible resultant vector length for three, five, and 10 equal-length random vectors.

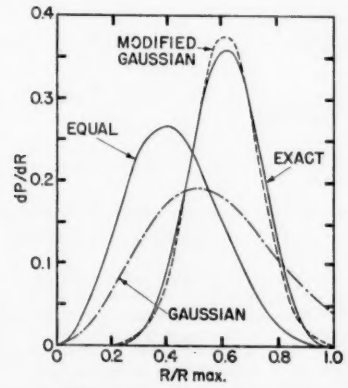

FIG. 3. Probability distribution of gamma-ray energy (in units of Mev^{-1}) calculated according to different methods vs the fraction of the maximum possible resultant gamma-ray energy for five random gamma rays. Refer to text for individual gamma-ray energies.

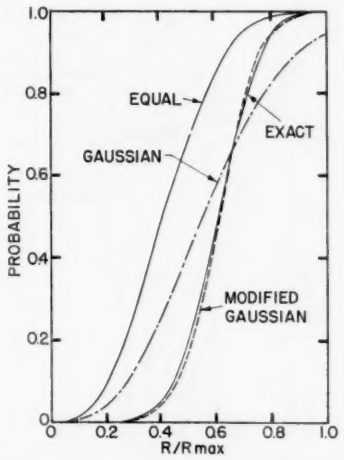

FIG. 4. Probability of gamma-ray energy calculated according to different methods vs the fraction of the maximum possible resultant gamma-ray energy for five random gamma rays. Refer to text for individual gamma-ray energies.

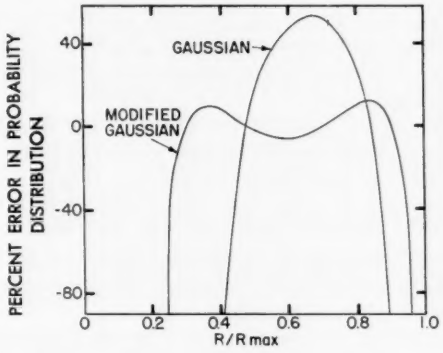

FIG. 5. Percent error in probability distribution in terms of the exact calculation vs the fraction of the maximum possible resultant gamma-ray energy for the approximate solutions given in Fig. 3.

TABLE I. Gamma-ray cascades[a] from $Cl^{35}(n, \gamma)Cl^{36}$

Energies (Mev)	% Occurrence[b]
8.55	3.71
7.78, 0.79	10.33
7.40, 1.16	18.54
6.96, 1.60	2.52
6.64, 1.95	15.23
5.72, 2.87	3.84
5.28, 3.34	17.10
6.64, 1.16, 0.79	11.26
6.15, 0.51, 1.95	7.42
5.01, 1.65, 1.95	2.12
6.15, 0.51, 1.16, 0.79	2.38
5.01, 1.13, 0.51, 1.95	1.59
5.01, 1.65, 1.16, 0.79	3.18
5.01, 1.13, 0.51, 1.16, 0.79	0.79

[a] See footnote 12.

[b] Based on Table I of work cited in footnote 12 (b).

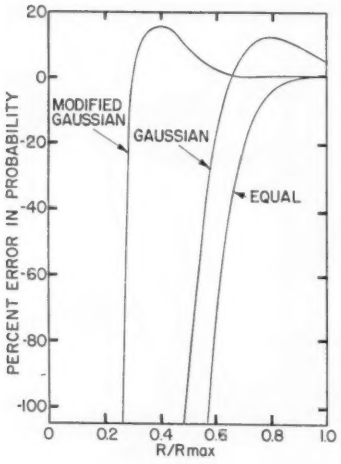

FIG. 6. Percent error in probability in terms of the exact calculation vs the fraction of the maximum possible resultant gamma-ray energy for approximate solutions given in Fig. 4.

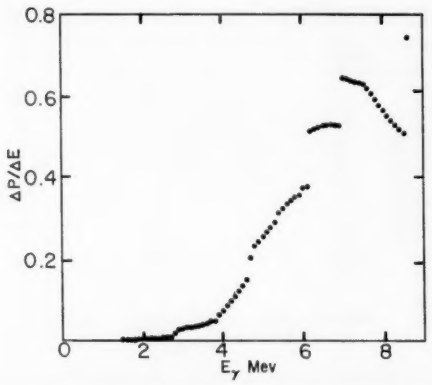

FIG. 7. Summed probability distribution of gamma-ray energies (in units of Mev^{-1}) vs the net gamma-ray energy for the 14 gamma cascades of the $Cl^{35}(n,\gamma)Cl^{36}$ process as given in Table I.

tribution in which the four small steps are approximated by a Gaussian distribution with $\langle l_i^2\rangle_{Av}=0.0119$ and the large step, $l_1=0.582$, is combined with the Gaussian function.[8] Figure 4 is the probability for these same four calculations.

The percent errors in the Gaussian and modified Gaussian approximations relative to the exact calculation for the probability distribution (Fig. 3) are depicted in Fig. 5. Similarly, the percent errors in the Gaussian, modified Gaussian, and five equal-step approximations relative to the exact calculation for the probability (Fig. 4) are depicted in Fig. 6.

It is occasionally necessary to utilize the distribution function in various theoretical investigations. For example, we anticipate a need for the gamma-ray recoil energy distribution in evaluating the high energy kinetics of chemical reactions activated by nuclear transformations.[2] Therefore, it is desirable to determine whether any of the mathematically simplified random-walk approximations are sufficiently in agreement with the exact calculation to permit their use. As noted in Figs. 5 and 6, for this five-step gamma cascade, the modified Gaussian distribution serves as the best approximation.

The modified Gaussian is calculated as follows: The large step is designated l_1 and, according to the original form of the Markoff process,[4]

$$W_n(R)=(8\pi^3)^{-1}\int_{-\infty}^{+\infty}\exp(i\boldsymbol{\rho}\cdot\mathbf{R})\,A_n(\rho)\,d\boldsymbol{\rho}, \tag{24}$$

where, for the remaining $(n-1)$ steps,

$$A_{n-1}(\rho)=\prod_{j=2}^{n}\int_{-\infty}^{+\infty}\tau_j(r_j)\,\exp(i\boldsymbol{\rho}\cdot\mathbf{r}_j)\,d\mathbf{r}_j. \tag{25}$$

For a Gaussian distribution,

$$\tau_j(r_j)=[1/(2\pi l_j^2/3)^{\frac{3}{2}}]\exp(-3\,|\,r_j\,|^2/2l_j^2). \tag{26}$$

Thus,

$$A_{n-1}(\rho)=\exp[-(\rho^2\sum_{j=2}^{n}l_j^2)/6] \tag{27}$$

and

$$A_1=\sin(\rho l_1)/\rho l_1. \tag{28}$$

Therefore,

$$A_n=A_1\cdot A_{n-1} \tag{29}$$

and

$$W_n(R)=(8\pi^2R)^{-1}\int_{-\infty}^{+\infty}\frac{\sin(\rho R)\,\sin(\rho l_1)}{\rho l_1}\exp[-\rho^2(n-1)\,\langle l^2\rangle_{Av}/6]\rho d\rho.$$

$$W_n(R)=\frac{1}{8\pi^{\frac{1}{2}}Rl_1[(n-1)\,\langle l^2\rangle_{Av}/6]^{\frac{1}{2}}}\left\{\exp\left[\frac{-3(R-l_1)^2}{2(n-1)\,\langle l^2\rangle_{Av}}\right]-\exp\left[\frac{-3(R+l_1)^2}{2(n-1)\,\langle l^2\rangle_{Av}}\right]\right\}. \tag{30}$$

[8] The authors are indebted to Professor G. E. Uhlenbeck for suggesting this approximation.

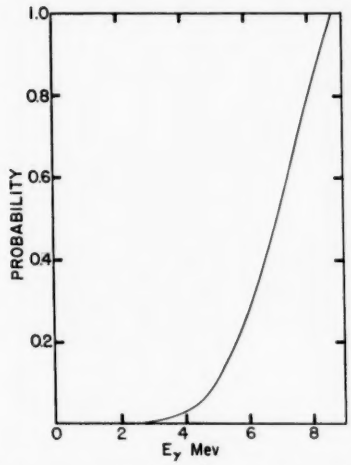

FIG. 8. Summed probability of gamma-ray energies vs the net gamma-ray energy for the 14 gamma cascades of the $Cl^{35}(n,\gamma)Cl^{36}$ process as given in Table I.

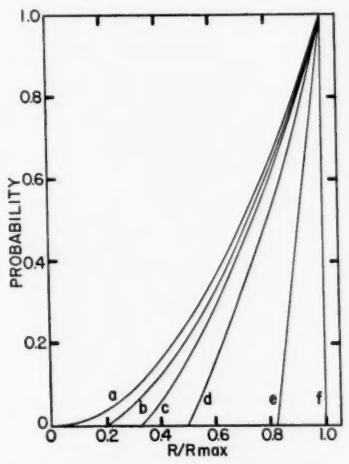

FIG. 9. Probability vs the fraction of the maximum possible resultant vector length for various random walks involving the two steps: A and B, (a) $A=B$, (b) $A=\frac{3}{4}B$, (c) $A=2B$, (d) $A=3B$, (e) $A=10B$, (f) $B=0$.

Cl^{36} GAMMA RECOIL

Our original purpose in evaluating the random-walk expression was to obtain data regarding the distribution of recoil energy imparted to an atom as a result of cascade-gamma emission in (n,γ) activation processes.[9,10] Such information is needed in order to evaluate more quantitatively hot-atom reaction mechanisms.[11] In addition, this information is of importance in investigations of the failure to bond rupture following neutron activation,[2] where the fraction of (n,γ) activated atoms which fail to dissociate from their parent compound should be related to the fraction of the atoms which receive a gamma-recoil energy less than some threshold energy.

Unfortunately, to date very little neutron-capture

TABLE II. Probability distribution function for three unequal-length random steps.

R-range	Applicability[a]	$W_3(R)$
$0\rightarrow(A-B-C)$	1	0
$0\rightarrow(-A+B+C)$	2	$\dfrac{1}{8\pi ABC}$
$(A-B-C)\rightarrow(A-B+C)$	1	$\dfrac{R-A+B+C}{16\pi RABC}$
$(-A+B+C)\rightarrow(A-B+C)$	2	
$(A-B+C)\rightarrow(A+B-C)$	1 or 2	$\dfrac{1}{8\pi RAB}$
$(A+B-C)\rightarrow(A+B+C)$	1 or 2	$\dfrac{-R+A+B+C}{16\pi RABC}$

[a] 1 is where $A>(B+C)$; 2 is where $A<(B+C)$.

TABLE III. Various cases for four unequal-length steps.

Case	Conditions[a]
1	$A>(B+C+D)$ and $B>(C+D)$
2	$A>(B+C+D)$ and $(C+D)>B$
3	$(A+D)>(B+C)$, $(B+D)>A$, and $B>(C+D)$
4	$(A+D)>(B+C)$, $(B+C)>A$, $A>(B+D)$, and $B>(C+D)$
5	$(B+C+D)>A$, $A>(B+C)$, and $B>(C+D)$
6	$(A+D)>(B+C)$ and $(C+D)>A$
7	$(A+D)>(B+C)$ and $(B+D)>A>(C+D)>B$
8	$(A+D)>(B+C)>A>(B+D)$ and $(C+D)>B$
9	$(B+C+D)>A>(B+C)$ and $(C+D)>B$
10	$(B+C)>(A+D)$, $(B+D)>A$, and $B>(C+D)$
11	$(B+C)>(A+D)$, $A>(B+D)$, and $B>(C+D)$
12	$(B+C)>(A+D)$ and $(C+D)>A$
13	$(B+C)>(A+D)$ and $(B+D)>A>(C+D)>B$
14	$(B+C)>(A+D)$, $A>(B+D)$, and $(C+D)>B$

[a] Where $A>B>C>D$.

[9] This type of calculation recently has been considered by Zvara (footnote 10) for the $Cl^{35}(n,\gamma)Cl^{36}$ process. Zvara, however, limits the calculations to cascades involving only two and three gamma rays. He approximates a cascade of four gamma rays by a three-step calculation. Zvara performed the calculations in terms of the recoil energy of the activated atom. Therefore, his equations can be transformed into the form given in this paper by an appropriate change in the variable.

[10] I. Zvara, Vestnik Moskov. Univ., Ser. Mat., Mekhan., Astron., Fiz. i Khim. **13**, No. 6, 127 (1958); Chem. Abstr. **53**, 15083f (1959); U. S. Atomic Energy Comm. Nuclear Sci. Abstr. **14**, 3046 (1960).

[11] J. E. Willard, Ann. Rev. Phys. Chem. **6**, 141 (1955).

TABLE IV. Probability distribution function for four unequal-length random steps.

R-Range	Applicability—Case:[a] 1	2	3	4	5	6	7	8	9	10	11	12	13	14	$W_4(R)$
$0\rightarrow(A-B-C-D)$	×	×													0
$0\rightarrow(-A+B+C-D)$										×	×	×	×	×	$\frac{1}{8\pi ABC}$
$0\rightarrow(-A+B+C+D)$					×				×						$\frac{-A+B+C+D}{16\pi ABCD}$
$0\rightarrow(A-B-C+D)$			×	×		×	×	×							
$(A-B-C-D)\rightarrow(A-B-C+D)$	×	×													$\frac{(R-A+B+C+D)^2}{64\pi RABCD}$
$(-A+B+C+D)\rightarrow(A-B-C+D)$					×				×						
$(A-B-C+D)\rightarrow(-A+B+C+D)$				×				×							$\frac{8DR-(R+A-B-C+D)^2}{64\pi RABCD}$
$(-A+B+C-D)\rightarrow(A-B+C-D)$										×		×	×		
$(-A+B+C-D)\rightarrow(-A+B+C+D)$											×			×	
$(A-B-C+D)\rightarrow(A-B+C-D)$			×			×	×								$\frac{R-A+B+C}{16\pi RABC}$
$(-A+B+C+D)\rightarrow(A-B+C-D)$	×	×			×				×						
				×				×			×			×	
$(A-B+C-D)\rightarrow(-A+B+C+D)$			×			×			×			×			$\frac{4CD-(A-B)^2-(R-C-D)^2}{32\pi RABCD}$
$(A-B+C-D)\rightarrow(A+B-C-D)$					×						×				
$(A+B-C-D)\rightarrow(-A+B+C+D)$					×						×				$\frac{-[(R-A-B-C-D)(3R+A+B+C+D)+4(A^2+B^2+C^2+D^2)]}{64\pi RABCD}$

$(A-B+C-D)\rightarrow(A+B-C-D)$	× × × ×	$\dfrac{8CD-(R-A+B-C-D)^2}{64\pi RABCD}$
$(A-B+C-D)\rightarrow(A-B+C+D)$	× × × ×	
$(-A+B+C+D)\rightarrow(A+B-C-D)$	× × × ×	
$(-A+B+C+D)\rightarrow(A-B+C+D)$	× × × ×	
$(A+B-C-D)\rightarrow(A-B+C+D)$	× × × × × ×	$\dfrac{4CD-(R-A)^2-(B-C-D)^2}{32\pi RABCD}$
$(A-B+C+D)\rightarrow(A+B-C-D)$	× × × × × ×	$\dfrac{1}{8\pi RAB}$
$(A+B-C-D)\rightarrow(A+B-C+D)$	× × × × × ×	$\dfrac{8CD-(R-A-B+C+D)^2}{64\pi RABCD}$
$(A-B+C+D)\rightarrow(A+B-C+D)$	× × × × × × × ×	
$(A+B-C+D)\rightarrow(A+B+C-D)$	× × × × × × × × × × × × × ×	$\dfrac{A+B+C-R}{16\pi RABC}$
$(A+B+C-D)\rightarrow(A+B+C+D)$	× × × × × × × × × × × × × ×	$\dfrac{(R-A-B-C-D)^2}{64\pi RABCD}$

[a] Refer to Table III for conditions governing each case.

gamma-ray data are available and most of what has appeared in the literature is incomplete. One process, which has been studied in great detail, however, is the $Cl^{35}(n,\gamma)Cl^{36}$ reaction. The neutron-capture gamma-ray emission is spherically symmetrical and the gamma-ray scheme is fairly complex. We have chosen this activation process to illustrate a particular use of the previously derived random-walk (or to be more precise for this application: random flight) equation.

The random-walk equation requires the use of momentum vectors. However, in the particular case of gamma-ray emission the energy of a gamma ray differs from the momentum by only a multiplicative constant (the velocity of light). Therefore, the gamma-ray energies were used in the calculation.

We utilized the data of Groshev *et al.*[12], arbitrarily limiting the possible gamma cascades to the 14 listed in Table I. For convenience and accuracy, the 14 gamma-ray energy probability distributions and probabilities were calculated separately with the aid of an IBM-704 computer and then added according to the abundances given in Table I. It should be emphasized, however, that these calculations could have been performed with little effort using a desk calculator. The summed probability distribution of gamma-ray energies is depicted in Fig. 7, the summed probability in Fig. 8.

It is of interest to note the "step function" nature of the results of Fig. 7. For example, the jump at 6.24 Mev is a result of the initial contribution from the 7.40+1.16 Mev gamma cascade. The jump at 6.99 Mev results from the 7.78+0.79 Mev cascade.

APPENDIX

Presented below are the complete solutions of $W_n(R)$ for $n=2$, 3, and 4 random-length vectors calculated via Eq. (16). It should be noted that the signs and magnitudes of the M_j and the N_j terms vary as a result of variations in R and as a result of these variations, $W_n(R)$ is a piecewise continuous curve with respect to R. Consequently $W_n(R)$, and thus $dP_n(R)/dR$ and $P_n(R)$, must be evaluated in segments.

Two Random Steps

For two random-length vectors, $l_1=A$ and $l_2=B$ where $A>B$, the solutions are trivial. There are $2^{2-1}=2M_j$ and $2N_j$ terms. They are $M_1=R-A+B$, $M_2=R+A-B$, $N_1=R+A+B$, $N_2=R-A-B$. $W_2(R)=0$ in the range $0<R<(A-B)$, and $=1/(8\pi RAB)$ in the range $(A-B)<R<(A+B)$.

Depicted in Fig. 9 are the probabilities for various two-step processes.

Three Random Steps

For the process involving three random steps there exist two possible cases. Assuming $(l_1=A)>(l_2=B)>(l_3=C)$, then these two cases are: 1. Where $A>(B+C$; or), 2. Where $A<(B+C)$.

The four M_j and four N_j terms are:

M_j	N_j
$M_1=R+A+B-C$	$N_1=R+A+B+C$
$M_2=R+A-B+C$	$N_2=R+A-B-C$
$M_3=R-A+B+C$	$N_3=R-A+B-C$
$M_4=R-A-B-C$	$N_4=R-A-B+C.$

As an illustration, let us consider the calculation of $W_3(R)$ in the range $(A+B-C)\rightarrow(A+B+C)$, the solution being valid for both cases (1) and (2).

$$W_3(R)=(32\pi RABC)^{-1}\sum_{j=1}^{j=4}(\,|\,M_j\,|\,-\,|\,N_j\,|\,)$$

$$=\frac{M_1+M_2+M_3-M_4-N_1-N_2-N_3-N_4}{32\pi RABC}$$

$$=(-R+A+B+C)/16\pi RABC.$$

The calculated values of $W_3(R)$ for all four ranges for each case are given in Table II.

Four Random Steps

For the process involving four random steps there exist eight M_j and eight N_j terms. Calling $l_1=A$, $l_2=B$, $l_3=C$, and $l_4=D$, and assigning $A>B>C>D$, there exist 14 different complete solutions depending on the particular numerical values for A, B, C, and D. These 14 cases are listed in Table III.

For each of these cases the range of $W_4(R)$ is divided into eight segments. In many instances, certain solutions of $W_4(R)$ are common to more than one of the above cases. The complete solutions of $W_4(R)$ for all 14 possible cases are given in Table IV.

[12] (a) L. V. Groshev, B. P. Adyasevich, and A. M. Demidov, Proc. Intern. Conf. Peaceful Uses Atomic Energy, Geneva, 1955 (United Nations, New York, 1956); (b) R. E. Segel, Phys. Rev. **113**, 844 (1959).

THE JOURNAL OF CHEMICAL PHYSICS VOLUME 34, NUMBER 2 FEBRUARY, 1961

Electronic Structures and Spectra of Some Nitrogen-Oxygen Compounds*

K. LENORE MCEWEN†

Department of Chemistry, University of Montreal, Montreal, Canada, and

Department of Chemistry, University of Saskatchewan, Saskatoon, Canada

(Received May 3, 1960)

The electronic structures and spectra of nitrite ion, nitrosomethane, nitrosamine, and nitrate ion have been calculated by a semiempirical method, which includes both the π-electron system and, in a more limited manner, the σ-electron system. The calculated transition energies and intensities for the first three compounds above agree fairly satisfactorily with experiment. For nitrate ion, however, it seems possible that the lowest observed transition may be a very low energy $n\rightarrow\sigma^*$ transition, σ^* being an antibonding σ orbital, rather than one of the $n\rightarrow\pi^*$ transitions considered in the present work.

INTRODUCTION

THE group of molecules and ions whose electronic structures and spectra are to be examined theoretically in the present work have three types of valence electrons: π electrons, and bonding and nonbonding σ electrons. The π-electron system is of course separated by symmetry from the σ-electron system. The two subdivisions of the σ-electron system, on the other hand, are usually not separated by symmetry; they are, however, separated to some extent because of energy considerations.

A method has been evolved over the past few years for predicting the electronic transition energies of compounds containing π electrons.[1,2] This method involves the calculation of suitable molecular orbitals for the π system of a molecule, then the combination of these into many-electron determinantal wave functions, and finally the calculation of those linear combinations of many-electron configurations which are approximations to the stationary states of the molecule. In order that some account may be taken of the effect on the π electrons of the σ-electron arrangement, it is assumed that the various atoms are in appropriate valence states and the various interaction terms of the Hamiltonian are then, where possible, estimated from empirical data.[1,3]

Turning to the σ-electron system, the method of choosing empirically the various one-center terms of the Hamiltonian can readily be adapted here; it is more difficult, however, to find unambiguous ways of testing approximations for the two-center terms. Nonbonding electrons within the σ system have been brought into the theory in the case of carbonyl compounds[4] where interactions with the σ-bonding electrons could reasonably be ignored, and in the case of nitrogen heterocycles,[5] nitromethane, and nitrogen dioxide[6] where they could not. In the last mentioned paper it appeared that although the nonbonding σ orbitals are allowed by symmetry to mix with the σ-bonding orbitals, they in fact remain fairly well separated. One important consequence of this result is that our ability to calculate σ-nonbonding orbitals and their energies may be relatively unimpaired by the present difficulty in determining the most suitable interaction terms between σ-bonding atomic orbitals.

THEORY

π and σ Molecular Orbitals

The molecular orbitals ψ_i for a molecule with a closed shell ground configuration may be obtained, in the LCAO approximation, from equations of the form[7]

$$\sum_\nu F_{\mu\nu}c_{i\nu}=E_i\sum_\nu c_{i\nu}S_{\mu\nu}, \tag{1}$$

where the μ, ν, etc., are atomic orbitals. The ψ_i are required to be orthonormal, and we will in the present work be interested only in real ψ_i. The molecular orbital energies E_i are solutions of the secular determinant

$$|F_{\mu\nu}-ES_{\mu\nu}|=0, \tag{2}$$

the $S_{\mu\nu}$ being overlap integrals, and the $F_{\mu\nu}$ being given by

$$F_{\mu\nu}=H_{\mu\nu}^{\text{core}}+\sum_{\eta\delta}P_{\eta\delta}\{(\mu\nu\,|\,\eta\delta)-\tfrac{1}{2}(\mu\delta\,|\,\eta\nu)\}. \tag{3}$$

In this expression $H_{\mu\nu}^{\text{core}}$ is the interaction between an electron with distribution $[\mu(1)\nu(1)]$ and the molecular core; the two-electron integrals are defined by

$$(\mu\nu\,|\,\eta\delta)=\iint\mu(1)\eta(2)\,(e^2/r_{12})\nu(1)\delta(2)d\tau_1d\tau_2,$$

* Presented in part at the Conference on Molecular Quantum Mechanics, Boulder, Colorado, June, 1959.

† National Research Council Post Doctorate Fellow (1957–1959). Present address: Department of Chemistry, University of Saskatchewan, Saskatoon, Canada.

[1] R. Pariser and R. G. Parr, J. Chem. Phys. **21**, 466, 767 (1953); **23**, 711 (1955).

[2] J. A. Pople, Trans. Faraday Soc. **49**, 1375 (1953); Proc. Phys. Soc. (London) **A68**, 81 (1955).

[3] W. Moffitt, Proc. Roy. Soc. (London) **A210**, 245 (1951).

[4] J. W. Sidman, J. Chem. Phys. **27**, 429 (1957).

[5] T. Anno, J. Chem. Phys. **29**, 1161 (1958); T. Anno and A. Sadô, *ibid.* **29**, 1170 (1958).

[6] K. L. McEwen, J. Chem. Phys. **32**, 1801 (1960).

[7] G. G. Hall, Proc. Roy. Soc. (London) **A205**, 541 (1951); C. C. J. Roothaan, Revs. Modern Phys. **23**, 61 (1951).

and the $P_{\eta\delta}$ are expressions for the electron distribution of the molecule, i.e.,

$$P_{\eta\delta}=2\sum_i c_{i\eta}c_{i\delta},$$

where the $c_{i\eta}$ are the LCAO coefficients of the orbital ψ_i.

The π-electron system of a molecule can often be treated fairly satisfactorily by ignoring differential overlap [1,2]; in this work we will ignore differential overlap for both the π- and σ-electron systems. Since our interest is in those molecular orbitals which involve predominantly π-type interactions, this sweeping neglect of overlap does not involve much more than the usual neglect of π-electron overlap.

In the approximation of zero differential overlap the $F_{\mu\mu}$ and $F_{\mu\nu}$ are given by

$$F_{\mu\mu}=\alpha_\mu+\tfrac{1}{2}P_{\mu\mu}(\mu\mu\,|\,\mu\mu)+\sum_{\mu'\neq\mu}P_{\mu'\mu'}\{(\mu\mu\,|\,\mu'\mu')-\tfrac{1}{2}(\mu\mu'\,|\,\mu\mu')\}+\sum_{\nu\nu'}\{P_{\nu\nu}(\mu\mu\,|\,\nu\nu)+P_{\nu\nu'}(\mu\mu\,|\,\nu\nu')\} \quad (4)$$

and

$$F_{\mu\nu}=\beta_{\mu\nu}-\tfrac{1}{2}P_{\mu\nu}(\mu\mu\,|\,\nu\nu). \quad (5)$$

If only one atomic orbital per atom is involved then Eq. (4) becomes the same as that obtained by Pople.[2] The α_μ and $\beta_{\mu\nu}$ in the preceding expressions represent the interaction of an electron on one and two centers, respectively, with the core potential H^{core}. Here $\beta_{\mu\nu}$ is taken as zero unless μ and ν are on adjacent centers. The one-center integral α_μ is given by the expression

$$\alpha_\mu=-I_\mu-\sum_{\nu\neq\mu}(n_\nu:\mu\mu)-Z_{\mu'\neq\mu}\{(\mu\mu\,|\,\mu'\mu')-\tfrac{1}{2}(\mu\mu'\,|\,\mu\mu')\}-\sum_{\nu\neq\mu}Z_\nu(\mu\mu\,|\,\nu\nu), \quad (6)$$

where I_μ is the appropriate valence state ionization potential, Z_ν is the number of electrons denoted by ν to the system under consideration, and $(n_\nu:\mu\mu)$ is the penetration integral between an electron in μ and the atom with orbital ν.

On using Eqs. (4), (5), and (6), one could find for the π system, solutions for Eq. (1) which are self-consistent in the π approximation; this is normally done assuming a nonpolar σ-bond structure. One might then adopt the cyclic method suggested by Parr and Lykos[8,9] for obtaining mutually self-consistent π- and σ-electron distributions. This procedure seems premature for the present problem, in view of our lack of knowledge of which σ-electron integrals are suitable; if, however, the first set of self-consistent π orbitals are used in calculating the σ-electron Hamiltonian, still assuming a nonpolar σ-bond structure and ideal valence states, then a first approximation to the nonbonding σ orbitals may be obtained. The main reason for calculating self-consistent π orbitals, rather than using Hückel orbitals in conjunction with this Hückel-type approximation for the σ system, is that the π-electron distributions calculated using such self-consistent orbitals often reproduce the main features of the electron distribution of the molecule; for example, they often yield a realistic though rough approximation to the dipole moment.[4,6]

In contrast then, with our treatment of the π system, where the various $P_{\eta\delta}$ in Eqs. (4) and (5) represent the self-consistent π distribution, Eq. (1) is solved for the nonbonding σ orbitals using a much cruder method of estimating those $P_{\eta\delta}$ which represent the σ-electron distribution. Initial molecular orbitals are assumed which will combine to give nonpolar localized σ-bonding orbitals of the type $1/\sqrt{2}(N_{sp^2}+O_r)$, and nonbonding orbitals which are either pure O_t, O_s, or N_{sp^2}, where O_r and O_t are oxygen $2p$ orbitals and O_s is an oxygen $2s$ orbital. The nitrogen and oxygen $2p$ orbitals are indicated in Fig. 1. When the approximation is extended to include a methyl or an amino group at X (in the diagram), then the artificial molecular orbitals assumed are those which combine to give nonpolar localized orbitals of the form $(1/\sqrt{2})(C_{sp^3}+N_{sp^2})$ or $(1/2)(N'_{sp^2}+N_{sp^2})$. The above conditions will not uniquely specify the various σ-molecular orbitals; they will, however, be sufficient to specify the various $P_{\eta\delta}$. This approximate initial σ-electron distribution may well be too rough to allow one to calculate realistic σ-bonding orbitals, it seems likely, however, that the σ-nonbonding orbitals will be affected less than the σ-bonding orbitals by the initially assumed electron distribution in the σ bonds.

We will now consider briefly certain types of interactions which will arise in the present work, which would not occur in an exclusively π-electron treatment. The nonpolar σ-electron distribution enters the π-electron calculation only through certain terms in the expression for $F_{\mu\mu}$, namely, those quantities in Eq. (4) represented by $P_{\nu\nu'}(\mu\mu\,|\,\nu\nu')$. Because of the simple σ-electron distribution we have chosen, terms involving $P_{\nu\nu'}$ arise only when there is a doubly occupied nitrogen sp^2 nonbonding orbital, so that $(\nu\nu')$ represents $(NsNy)$; the resulting two-center quantities may conveniently

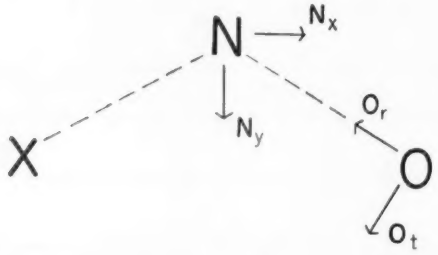

FIG. 1. The $2p$ orbitals of nitrogen and oxygen in the compound XNO, where X is oxygen, methyl, or amino. The direction of the arrow indicates the positive direction of the orbital.

[8] R. G. Parr and P. G. Lykos, J. Chem. Phys. **24**, 1166 (1956).
[9] Recently Parks and Parr have applied this method to the formaldehyde molecule. [J. Chem. Phys. **32**, 1657 (1960).]

be included in the penetration integrals. Similarly two-center quantities involving $P_{N_sN_y}$ which arise in the various $F_{\mu\mu}$ of the σ system, may also be included in the penetration integrals.

Finally, in the σ-electron calculation there arise interaction terms of the type $F_{\mu\mu'}$; it has been pointed out previously,[6] however, that these quantities, when nonzero, are rather small due to cancellation among contributing interactions. For this reason the terms $F_{\mu\mu'}$ will be ignored in the present work.

CONFIGURATION INTERACTION

Having obtained a set of molecular orbitals in the manner described one can form the many-electron configurations which interact to give approximations to the various stationary states of the molecule. Since the σ orbitals are not self-consistent, there will be interactions which arise because of the difference between the calculated σ-electron distribution and the true distribution. We have already decided that the present calculation cannot be expected to predict reliably the electron distribution of the σ-bonding system, and so it will be consistent to ignore the matrix elements which correct for changes in the σ-bonding electron distribution. It is expected that the perturbation energies arising from such interactions would be small, both because the σ-electron polarity is expected to be small, and also because it happens that all the excited σ-electron configurations with the correct symmetry needed to interact with the ground configuration, are of very high energy.

Our configuration interaction calculation is then reduced to only those interactions arising between configurations in which electrons are excited from π orbitals and nonbonding σ orbitals into the antibonding π^* orbital.

INTEGRALS OVER ATOMIC ORBITALS

Empirically determined values are used for all the required valence-state ionization potentials and one-center coulomb repulsion integrals. The latter quantities are estimated using Pariser's approximation[10]

$$(\mu\mu \mid \mu\mu) = I_\mu - A_\mu, \tag{7}$$

where A_μ is the appropriate valence-state electron affinity. Integrals of the type $(\mu\mu \mid \bar{\mu}\bar{\mu})$ and $(\mu\bar{\mu} \mid \mu\bar{\mu})$, where $\bar{\mu}$ is a $2p$ orbital on atom n_μ at right angles to μ, are readily estimated using valence-state ionization potentials, together with the identity

$$(\mu\mu \mid \mu\mu) - (\mu\mu \mid \bar{\mu}\bar{\mu}) = 2(\mu\bar{\mu} \mid \mu\bar{\mu}).[11] \tag{8}$$

The various specific valence-state ionization potentials used will be mentioned in the section dealing with the calculations.

[10] R. Pariser, J. Chem. Phys. **21**, 568 (1953).
[11] R. G. Parr and F. G. Fumi, J. Chem. Phys. **21**, 1265 (1953).

Turning to the two-center integrals, π-orbital coulomb repulsion integrals $(\mu\mu \mid \nu\nu)$ are estimated by the method of Pariser and Parr,[1] at large distances theoretically calculated values are used, while at shorter distances the values are adjusted downward so that at $r_{\mu\nu}=0$ the magnitude of $(\mu\mu \mid \nu\nu)$ approaches $\frac{1}{2}\{(\mu\mu \mid \mu\mu)+(\nu\nu \mid \nu\nu)\}$. The integrals $(\mu\mu \mid \bar{\nu}\bar{\nu})$, where μ is a π orbital and $\bar{\nu}$ a $2p$ orbital perpendicular to μ and $r_{\mu\nu}$, are obtained using an identity similar to that in Eq. (8), together with the calculated value of $(\mu\bar{\mu} \mid \nu\bar{\nu})$ as taken from the tables of Roothaan.[12] Two-center coulomb repulsion integrals not involving π electrons are also taken from the tables of Roothaan, as are penetration integrals.

The resonance integrals $\beta_{NO}(\pi)$ are chosen semi-empirically so as to correspond to values which have proved suitable in π-electron calculations for C=O and C=C bonds. It has been found that the approximate value for β of -2.9 to -3 ev, gives good results for the electronic spectra of ethylene[1] and formaldehyde,[4] both of which contain pure double bonds. The value $\beta=-3$ ev, is adopted for a pure N—O double bond, of length approximately 1.18 to 1.20 A.[13] Other N—O resonance integrals are then assigned values based on the assumption that for a given pair of atoms $\beta_{NO}\alpha S_{NO}$, the overlap integrals being obtained from the tables of Mulliken *et al.*[14]

CALCULATIONS AND RESULTS

Nitrite Ion

The electronic structure of the nitrite ion has been calculated using the experimentally determined bond lengths and angles, $r_{NO}=1.23$ A and $\measuredangle_{ONO}=116°$.[15]

The magnitudes of the nitrogen one-center quantities required for the π-electron calculation depend on whether the nitrogen valence state is $N(s^2xyzV_3)$ or $N(sxy^2zV_3)$. Since we are assuming the nitrogen to be sp^2 hybridized, the value used here for a quantity $\mathcal{E}$ (either an ionization potential or a coulomb repulsion integral) is the linear combination $\mathcal{E}=\frac{1}{3}\mathcal{E}(s^2p^3)+\frac{2}{3}\mathcal{E}(sp^4)$. The two quantities I_N and $(NN \mid NN)$ for the π-electron calculations are obtained from the energies of the following two pairs of processes:

$$N(s^2xyzV_3) \rightarrow N^+(s^2xyV_2);$$
$$N^-(s^2xyz^2V_2) \rightarrow N(s^2xyzV_3); \tag{9}$$

and

$$N(sxy^2zV_3) \rightarrow N^+(sxy^2V_2);$$
$$N^-(sxy^2z^2V_2) \rightarrow N(sxy^2zV_3); \tag{10}$$

[12] C. C. J. Roothaan, *Two-Center Coulomb Integrals* (Special Technical Report of the Laboratory of Molecular Structure and Spectra, University of Chicago, Chicago, Illinois, 1955); *ibid.*, J. Chem. Phys. **19**, 1445 (1951).
[13] G. W. Wheland, *Resonance in Organic Chemistry* (John Wiley & Sons, Inc., New York, 1955).
[14] R. S. Mulliken, C. A. Reike, D. Orloff, and H. Orloff, J. Chem. Phys. **17**, 1248 (1949).
[15] M. R. Truter, Acta Cryst. **5**, 132 (1952).

TABLE I. Integrals over atomic orbitals for NO_2^-.

$I_N(\pi)$	14.16 ev	$(N_\pi N_\pi \mid O_\pi O_\pi)$	8.88 ev	$(O':O_sO_s)$	0.04 ev
$I_N(x, y)$	14.49	$(O_\pi O_\pi \mid O_\pi' O_\pi')$	6.58	$(N:O_tO_t)$	1.45
$I_N(s)$	27.5	$(N_\pi N_\pi \mid O_tO_t)$	8.68	$(N:O_rO_r)$	5.09
$I_O(\pi)$	17.21	$(O_\pi O_\pi \mid O_t'O_t')$	6.58	$(N:O_sO_s)$	2.70
$I_O(t)$	14.21	$(O:N_\pi N_\pi)$	0.91	$(O_rO_r \mid N_yN_y)$	12.54
$I_O(s)$	32.3	$(N:O_\pi O_\pi)$	1.57	$(O_rO_r \mid N_xN_x)$	13.22
$(N_\pi N_\pi \mid N_\pi N_\pi)$	12.81	$(O':O_sO_\pi)$	0.05	$(O_rO_r \mid N_sN_s)$	12.30
$(N_sN_s \mid N_sN_s)$	13.6	$(O:N_xN_x)$	3.94	$\beta(O_\pi N_\pi)$	−2.9
$(N_\pi N_\pi \mid N_\sigma N_\sigma)$	11.31 (est.)	$(O:N_yN_y)$	1.97	$\beta(_\pi N_\sigma)$	−4.56
$(N_\pi N_\pi \mid N_sN_s)$	12.81	$(O:N_sN_s)$	2.27	$\beta(O_rN_s)$	−4.82
$(O_\pi O_\pi \mid O_\pi O_\pi)$	14.52	$(O':O_rO_r)$	0.05	$\beta(O_sN_\sigma)$	−5.82
$(O_\pi O_\pi \mid O_tO_t)$	12.76	$(O':O_tO_t)$	0.06	$\beta(O_sN_s)$	−5.05

the energies of these processes are taken from the tables of Skinner and Pritchard,[16] as are the required quantities for the oxygen valence state $O(s^2x^2yzV_2)$. For the various σ-electron atomic ionization potentials it is convenient to begin with the nitrogen valence state $N(sp^4)$ and then to correct the various nitrogen diagonal matrix elements for changes in electron interaction which arise when sp^2 hybridization is introduced. All of the valence state energies will of course be rather approximate when applied to the nitrite ion, since the various atoms have some excess charge.

The N—O bond length of 1.23 A is slightly longer than the value assumed for a normal N—O double bond (i.e., 1.18 A to 1.20 A), and we therefore will use the value $\beta=-2.9$ ev, for the π-electron resonance integral, instead of $\beta=-3.0$ ev, which we have chosen for a normal double bond. The various quantities required in the calculation are presented in Table I. It is convenient to list resonance integrals involving N_π and N_σ (the latter being parallel to the N—O bond) instead of quantities involving N_x and N_y.

TABLE II. Molecular orbitals for nitrite ion.

Symmetry	Wave function	Energy (ev)
	π orbitals	
B_1	$b_1=0.629\,N_\pi+(0.778/\sqrt{2})\,(O_\pi+O_\pi')$	−10.56
	$b_1^*=0.778\,N_\pi-(0.629/\sqrt{2})\,(O_\pi+O_\pi')$	6.70
A_2	$a_2=(1/\sqrt{2})\,(O_\pi-O_\pi')$	−6.31
	Nonbonding σ orbitals	
A_1	$a_1=0.540\,O_t^+ +0.244\,O_r^+ -(0.790/\sqrt{3})\,(N_s-\sqrt{2}N_y)$ $+(0.157/\sqrt{3})\,(\sqrt{2}N_s+N_y)$	−11.08
	$a_1^*=0.825\,O_t^+ -0.337\,O_r^+ +0.007\,O_s^+$ $+(0.454/\sqrt{3})\,(N_s-\sqrt{2}N_y)-(0.011/\sqrt{3})\,(\sqrt{2}N_s+N_y)$	−4.75
B_2	$b_2=0.989\,O_t^- -0.146\,O_r^- +0.006\,O_s^- -0.014N_x$	−6.31

The molecular orbitals and their energies for the nitrite ion are presented in Table II. The symmetry orbitals involving O_t, O_r, and O_s are expressed in abbreviated form, for example $O_t^\pm=\sqrt{\frac{1}{2}}(O_t\pm O_t')$. The nitrogen orbitals are presented in the orthogonal linear combinations $\sqrt{\frac{1}{3}}(N_s-\sqrt{2}N_y)$ and $\sqrt{\frac{1}{3}}(\sqrt{2}N_s+N_y)$. An asterisk, for example in a_1^*, denotes antibonding character.

The molecular orbitals and energies in Table II have been used to calculate the various low energy states of the molecule, and these are presented in Table III, together with the calculated oscillator strengths for transitions from the ground state, as well as observed transition energies and oscillator strengths. The $\pi\rightarrow\pi^*$ transition oscillator strengths were calculated assuming zero overlap, with the formula developed by Mulliken.[17] The $n\rightarrow\pi^*$ oscillator strengths were calculated employing values for the transition dipoles $\langle N_s \mid r \mid N_\pi\rangle$ and $\langle O_s \mid r \mid O_\pi\rangle$ which are derived using Slater orbitals for N_s, N_π, O_s, O_π. The experimental oscillator strengths quoted have been estimated from the experimental intensity data.

The notation χ_0 is adopted for the first approximation to the ground state, where

$$\chi_0=\mid a_1\bar{a}_1a_1^*\bar{a}_1^*b_2\bar{b}_2a_2\bar{a}_2b_1\bar{b}_1\mid,$$

the normalizing coefficient and the σ-bonding orbitals being omitted for the sake of brevity. A singlet configuration in which an a_2 electron has been excited is represented as follows,

$$(a_2^{-1}b_1^*)=(1/\sqrt{2})\{\mid a_1\bar{a}_1a_1^*\bar{a}_1^*b_2\bar{b}_2b_1\bar{b}_1a_2\bar{b}_1^*\mid + \mid a_1\bar{a}_1a_1^*\bar{a}_1^*b_2\bar{b}_2b_1\bar{b}_1b_1^*\bar{a}_2\mid\},$$

while a singlet configuration involving a two-electron

[16] H. A. Skinner and H. O. Pritchard, Trans. Faraday Soc. **49**, 1254 (1953); Chem. Revs. **55**, 745 (1955).

[17] R. S. Mulliken and C. A. Reike, Repts. Progr. Phys. **8**, 231 (1941).

TABLE III. Electronic transitions of the nitrite ion.

Symmetry	State wave function	Calculated transition energy	f.	Observed[a] transition energy	f.
$^1A_1$	$0.990\,\chi_0+0.037(b_1^{-1}b_1^*)-0.135(a_2^{-2}b_1^{*2})-0.078(b_1^{-2}b_1^{*2})$	0	...	...	...
	$0.846(b_1^{-1}b_1^*)-0.102\,\chi_0-0.523(a_2^{-2}b_1^{*2})$	8.31 ev	0.09	...	...
$^1B_2$	$0.981(a_2^{-1}b_1^*)+0.195(b_1^{-1}a_2^{-1}b_1^{*2})$	5.75	0.39	5.95 ev	0.20
$^1B_1$	$(a_1^{*-1}b_1^*)+0.06(a_1^{*-1}b_1^{-1}b_1^{*2})$	2.93	0.003	3.50	0.0005[b]
	$(a_1^{-1}b_1^*)+0.05(a_1^{-1}b_1^{-1}b_1^{*2})$	8.46	0.04	...	...
$^1A_2$	$0.986(b_2^{-1}b_1^*)+0.168(b_2^{-1}b_1^{-1}b_1^{*2})$	4.40	0	4.20	0.0004
$^3A_1$	$^3(b_1^{-1}b_1^*)$	7.33	0	...	...
$^3B_2$	$^3(a_2^{-1}b_1^*)$	3.78	0	...	...
$^3B_1$	$^3(a_1^{*-1}b_1^*)$	2.36	0	...	...
	$^3(a_1^{-1}b_1^*)$	7.92	0	...	...
$^3A_2$	$^3(b_2^{-1}b_1^*)$	4.26	0	...	...

[a] H. L. Friedman, J. Chem. Phys. **21**, 319 (1953).
[b] This transition has been shown to have a transition dipole of B_1 symmetry [see J. W. Sidman, J. Am. Chem. Soc. **79**, 2669, 2674 (1957)].

TABLE IV. Atomic orbital integrals for CH_2NO and NH_2NO.

$I_{N^{+}(\pi)}$	24.38 ev	$(N_xN_x \mid O_\tau O_\tau)$	13.48 ev	$(C{:}N_\pi N_\pi)$	0.52 ev
$I_{(Cy)}$	11.26	$(N_yN_y \mid O_\tau O_\tau)$	12.57	$(C{:}N_xN_x)$	1.95
$I_{(C\sigma)}$	21.34	$(N_\sigma N_\sigma \mid O_\tau O_\tau)$	12.57	$(C{:}N_yN_y)$	1.00
$(N_\pi N_\pi' \mid N_\pi N_\pi')$	12.74	$(N_xN_x \mid C_\tau C_\tau)$	11.27	$(C{:}N_\sigma N_\sigma)$	1.11
$(C_\pi C_\pi \mid N_\pi N_\pi)$	8.33	$(N_yN_y \mid C_\tau C_\tau)$	10.45	$(N{:}C_\tau C_\tau)$	3.27
$(O_\pi O_\pi \mid C_\pi C_\pi)$	5.95	$(N_\sigma N_\sigma \mid C_\tau C_\tau)$	10.45	$(N{:}C_\sigma C_\sigma)$	1.45
$(N_\pi N_\pi \mid O_\pi O_\pi)$	9.06	$(N_xN_x \mid C_\sigma C_\sigma)$	10.14	$(N'{:}N_\pi N_\pi)$	0.52
$(N_\pi N_\pi \mid N_\pi N_\pi')$	7.85	$(N_yN_y \mid C_\sigma C_\sigma)$	9.50	$(N'{:}N_xN_x)$	1.93
$(O_\pi O_\pi \mid N_\pi N'_\pi)$	6.02	$(N_\sigma N_\sigma \mid C_\sigma C_\sigma)$	9.50	$(N'{:}N_yN_y)$	1.07
$(N{:}O_\pi O_\pi)$	1.70	$(N_xN_x \mid N_\tau N_\tau')$	10.96	$(N'{:}N_\sigma N_\sigma)$	1.17
$(N{:}O_t O_t)$	1.58	$(N_yN_y \mid N_\tau N_\tau')$	10.25	$(N{:}N_\pi N_\pi')$	0.85
$(N{:}O_\tau O_\tau)$	5.60	$(N_\sigma N_\sigma \mid N_\tau N_\tau')$	10.37	$(N{:}N_\tau N_\tau')$	2.61
$(N{:}O_\sigma O_\sigma)$	2.97	$(N_xN_x \mid N_\sigma N_\sigma')$	10.09	$(N{:}N_\sigma N_\sigma')$	1.41
$(O{:}N_\pi N_\pi)$	1.00	$(N_yN_y \mid N_\sigma N_\sigma')$	9.52	$(N'{:}O_\pi O_\pi)$; $(C{:}O_\pi O_\pi)$	0.03
$(O{:}N_xN_x)$	4.52	$(N_\sigma N_\sigma \mid N_\sigma N_\sigma')$	9.62	$(N'{:}O_t O_t)$; $(C{:}O_t O_t)$	0.05
$(O{:}N_yN_y)$	2.03	$\beta(N_\pi N_\pi'), \beta(N_\pi C_\pi)$	−1.60	$(N'{:}O_\tau O_\tau)$; $(C{:}O_\tau O_\tau)$	0.04
$(O{:}N_\sigma N_\sigma)$	2.52	$\beta(N_\pi N_\tau'), \beta(N_\sigma C_\tau)$	−2.85	$(N'{:}O_\sigma O_\sigma)$; $(C{:}O_\sigma O_\sigma)$	0.05
$\beta(N_\pi O_\pi)$	−3.0	$\beta(N_\pi N_\sigma'), \beta(N_\sigma C_\sigma)$	−3.15	$(H{:}C_\tau C_\tau)$	0.81
$\beta(N_\sigma O_\tau)$	−4.72	$\beta(N_\sigma N_\tau'), \beta(N_\sigma C_\tau)$	−3.15	$(H{:}C_\sigma C_\sigma)$	1.29
$\beta(N_\sigma O_\sigma)$	−6.03	$\beta(N_\sigma N_\sigma'), \beta(N_\sigma C_\sigma)$	−2.93	$(H{:}N_\pi N_\pi')$	0.83
$\beta(N_\sigma O_\tau)$	−4.99	$(O{:}N_\pi N_\pi')$	0.03	$(H{:}N_\tau N_\tau')$	1.38
$\beta(N_\sigma O_\sigma)$	−5.24	$(O{:}C_\tau C_\tau)$; $(O{:}N_\tau N_\tau')$	0.05	$(H{:}N_\sigma N_\sigma')$	1.58
		$(O{:}C_\sigma C_\sigma)$; $(O{:}N_\sigma N_\sigma')$	0.05		

TABLE V. Molecular orbitals for CH_3NO and NH_2NO.

Symmetry	Wave function	Energy
	Nitrosomethane	
A'	$n=0.617\ O_t+0.220\ O_\tau+0.141\ C_I-0.015\ N_s$	
	$-(0.729/\sqrt{3})(N_s-\sqrt{2}N_y)+(0.139/\sqrt{3})(\sqrt{2}N_s+N_y)$	-18.24 ev
	$n^*=0.755\ O_t-0.131\ O_\tau+0.006\ O_s-0.328\ C_I+0.006\ N_s$	
	$+(0.552/\sqrt{3})(N_s-\sqrt{2}N_y)-(0.025/\sqrt{3})(\sqrt{2}N_s+N_y)$	-14.03
A''	$\pi=0.628\ N_\tau+0.779\ O_\tau$	-18.06
	$\pi^*=0.779\ N_\tau-0.628\ O_\tau$	-2.86
	Nitrosamine	
A'	$n=0.469\ O_t+0.246\ O_\tau+0.164\ N_I'+0.044\ N_s$	
	$-(0.825/\sqrt{3})(N_s-\sqrt{2}N_y)+(0.119/\sqrt{3})(\sqrt{2}N_s+N_y)$	-18.41
	$n^*=0.837\ O_t-0.123\ O_\tau+0.005\ O_s-0.354\ N'_I$	
	$-0.107\ N_s+(0.378/\sqrt{3})(N_s-\sqrt{2}N_y)$	
	$-(0.062/\sqrt{3})(\sqrt{2}N_s+N_y)$	-13.91
A''	$\pi_1=0.416\ N_\tau'+0.641\ N_\tau+0.645\ O_\tau$	-18.06
	$\pi_2=0.886\ N_\tau'-0.127\ N_\tau-0.446\ O_\tau$	-14.91
	$\pi^*=0.204\ N_\tau'-0.757\ N_\tau+0.621\ O_\tau$	-2.15

excitation is represented by, for example

$$(a_1^{*-1}a_2^{-1}b_1^{*2})=(1/\sqrt{2})\{\,|\,a_1\bar{a}_1b_2\bar{b}_2b_1\bar{b}_1b_1^*\bar{b}_1^*a_1^*\bar{a}_2\,| + |\,a_1\bar{a}_1b_2\bar{b}_2b_1\bar{b}_1b_1^*\bar{b}_1^*a_2\bar{a}_1^*\,|\,\}.$$

In these configurations a_1, $\bar{a}_1$, etc. are used to differentiate between α and β spin.

Nitrosomethane and Nitrosamine

There is no experimental information available concerning the bond lengths and bond angles of nitrosomethane and nitrosamine, and it has therefore been necessary to assume structures for each molecule. The molecular dimensions assumed are

CH_3NO: $r_{NO}=1.18$ A; $\measuredangle ONC=120°$; $r_{CN}=1.47$ A

$N'H_2NO$: $r_{NO}=1.18$ A; $\measuredangle ONN'=120°$; $r_{N'N}=1.47$ A.

The one-center interaction integrals employed for the N—O group are the same here as for the nitrite ion, since the valence states are taken to be the same. The two-center integrals are different because of the shorter internuclear distance. The resonance integrals $\beta_{CN}^{(\pi)}$ and $\beta_{N'N}^{(\pi)}$ are estimated by the formula suggested by Pariser and Parr[1] for carbon-carbon bonds. The interaction integrals which differ from those used in the NO_2^- calculation are presented in Table IV.

In choosing a value for $I_{N'+}$, the second ionization potential of the amino nitrogen, and for $(N_\tau'N_\tau'\,|\,N_\tau'N_\tau')$, it seems advisable to retain the uncharged character of the atom. The experimentally determined second ionization potential, 28.86 ev,[18] for the process

$$N^+(sxyz)\rightarrow N^{++}(sxy),$$

refers of course to the nitrogen positive ion, as does the value of 16.77 ev estimated for the integral $(N_\tau'N_\tau'\,|\,N_\tau'N_\tau')$ using Eq. (8). Rather than these quantities, it seems preferable to use for

$$(N_\tau'N_\tau'\,|\,N_\tau'N_\tau')$$

the value 12.74 ev, which is obtained by Eq. (7), using the ionization potential and electron affinity of $N(sp^4V_3)$ [see Eq. (10)], and which is therefore suitable for the uncharged atom. The second ionization potential may similarly be estimated for an uncharged nitrogen atom by the following equation, using the value 12.74 ev for $(N_\tau'N_\tau'\,|\,N_\tau'N_\tau')$,

$$I_{N'+}=E\{N(sxyz^2)\rightarrow N^+(sxyz)\}+(N_\tau'N_\tau'\,|\,N_\tau'N_\tau')=24.83\text{ ev},$$

where E is the energy of the process indicated in brackets. The other nitrogen ionization potentials which we require are listed in Table I.

The notation C_τ and N_τ' in Table IV refers to that carbon or amino nitrogen $2p$ orbital directed toward the central nitrogen atom. It has been found that if a detailed calculation is done, including the symmetry orbital $H=\sqrt{\frac{1}{3}}(H_{1s}+H_{1s}'+H_{1s}'')$ or $H=\sqrt{\frac{1}{2}}(H_{1s}+H_{1s}')$ in the case of nitrosomethane and nitrosamine, respectively, and if the contributions from C_s and C_τ (or N_s' and N_τ') are expressed instead in terms of $C_I=\frac{1}{2}(C_s+\sqrt{3}C_\tau)$ and $C_{II}=\frac{1}{2}(\sqrt{3}C_s-C_\tau)$ [or $N_I'=\sqrt{\frac{1}{3}}(N_s'+\sqrt{2}N_\tau')$ and $N_{II}'=\sqrt{\frac{1}{3}}(\sqrt{2}N_s'-N_\tau')$] then nonbonding σ orbitals are obtained which have fairly large contributions from C_I (or N_I'), fairly small contributions from H, and negligible contributions from C_{II} (or N_{II}'). If the calculation is repeated ignoring C_{II} (or N_{II}') and H, then, except for some loss of detail at the methyl (or amino) end of the molecule, the resulting nonbonding molecular orbital wave functions are substantially unchanged, as are the orbital energies. For this limited purpose of obtaining nonbonding orbitals, then, the orbitals C_{II} (or N_{II}') and H have not been included, and the substituent contribution to the wave function is expressed in terms of C_I (or N_I').

The molecular orbitals obtained for nitrosomethane and nitrosamine are given with their energies in Table V; and the various state wave functions with energies under 8 ev are given in Table VI, together with their transition energies from the ground state, and the related oscillator strengths. Also presented in Table VI are the available experimental data for $N(CH_3)_2NO$ and CF_3NO.

The notation n, n^* for the nonbonding σ orbitals, and π, π^* for the π orbitals is adopted here because it is

[18] C. E. Moore, Natl. Bur. Standards (U. S.) Circ. 467 (1949).

TABLE VI. States of CH_3NO and NH_2NO.

Symmetry	State wave function	Calc transition energy	Calc f.	Obs transition energy	Obs f.
	Nitrosomethane				
$^1A'$	$0.985\,\chi_0+0.021(\pi^{-1}\pi^*)-0.171(\pi^{-2}\pi^{*2})$	0	...	...	...
	$(n^{*-2}\pi^{*2})+0.03(\pi^{-1}\pi^*)$	4.98 ev	0.0002	4.0[a] ev	0.00005
$^1A''$	$(n^{-1}\pi^*)$	6.32	0.01	...	...
	$(n^{*-1}\pi^*)$	2.08	0.002	1.71[a]	0.0004
$^3A'$	$^3(\pi^{-1}\pi^*)$	4.26	0	...	.
$^3A''$	$^3(n^{*-1}\pi^*)$	1.36	0	...	. .
	$^3(n^{-1}\pi^*)$	5.60	0	...	...
	Nitrosamine				
$^1A'$	$0.990\,\chi_0-0.049(\pi_2^{-2}\pi^{*2})-0.120(\pi_1^{-2}\pi^{*2})-0.072(\pi_1^{-1}\pi_2^{-1}\pi^{*2})$	0	...	...	...
	$0.931(\pi_2^{-1}\pi^*)+0.158(\pi_1^{-1}\pi^*)+0.275(\pi_2^{-2}\pi^{*2})-0.181(\pi_1^{-2}\pi^{*2})$	5.65	.18	5.34[b]	0.10
	$(n^{*-2}\pi^{*2})$	7.12	~0	...	...
$^1A''$	$(n^{-1}\pi^*)$	7.11	0.02	...	...
	$(n^{*-1}\pi^*)$	2.97	0.002	3.46[b]	0.002
$^3A'$	$^3(\pi_2^{-1}\pi^*)$	4.93	0	...	...
	$^3(\pi_1^{-1}\pi^*)$	5.74	0	...	...
$^3A''$	$^3(n^{*-1}\pi^*)$	2.23	0	...	...
	$^3(n^{-1}\pi^*)$	6.23	0	...	...

[a] J. Mason, J. Chem. Soc. **1957,** 3904. These data are for CF_3NO.
[b] R. N. Haszeldine and J. Jander, J. Chem. Soc. **1954,** 691. These data are for $(CH_3)_2N{\cdot}NO$.

TABLE VII. Integrals over atomic orbitals for nitrate ion (see Fig. 2).

I_{N^+}	28.86 ev	$(N_yN_y \mid O_rO_r)$	13.65 ev	$(O':O_sO_s)$	0.05 ev
$(N_\pi N_\pi \mid N_\pi N_\pi)$	16.77	$(N_xN_x \mid O_rO_r)$	12.11	$(O':N_xN_x)$	4.31
$(O_\pi O_\pi \mid N_\pi N_\pi)$	9.66	$(N_sN_s \mid O_rO_r)$	12.30	$(O':N_yN_y)$	1.60
$(O_\pi O_\pi \mid O_\pi'O_\pi')$	6.54	$(N:O_tO_t)$	1.34	$(O':N_sN_s)$	2.27
$(O:N_\pi N_\pi)$	0.91	$(N:O_rO_r)$	4.81	$\beta(O_rN_y)$	−5.34
$(N:O_\pi O_\pi)$	1.14	$(N:O_sO_s)$	2.43	$\beta(O_rN_s)$	−5.16
$(O':O_\pi O_\pi)$	0.05	$(O':O_tO_t)$	0.04	$\beta(O_sN_y)$	−6.67
$\beta(O_\pi N_\pi)$	−3.0	$(O':O_rO_r)$	0.06	$\beta(O_sN_s)$	−5.50

simpler than the purely symmetry designation. The orbitals n^*, π^* have antibonding character. The first approximation to the ground state for nitrosomethane is of course,

$$\chi_0 = |\cdots\pi\bar{\pi}n\bar{n}n^*\bar{n}^*|.$$

Nitrate Ion

The nitrate ion has been shown to have a symmetrical planar structure, with N—O bond lengths of 1.21 A.[19]

A preliminary π-electron calculation indicates that, provided one may to a rough approximation ignore σ-electron polarization, the nitrogen atom in this ion is in the form N^+. In this situation we should consider modifying the various atomic orbital interaction integrals so that they may be appropriate to the atoms as they exist in the ion. We have seen in the calculation for nitrosamine that the values for I_{N^+} and $(NN \mid NN)$ can be chosen so as to be suitable for either a charged or an uncharged nitrogen atom. A similar procedure could be followed to modify I_O and $(OO \mid OO)$ to suit a case where the oxygen has a negative charge; it has been pointed out previously,[6] however, that the corrections to the one-center integrals may be expected to be less important for a negatively charged atom than for a positively charged one, and for this reason only the nitrogen one-center integrals will be modified.

[19] N. Elliott, J. Am. Chem. Soc. **59,** 1380 (1937).

TABLE VIII. Molecular orbitals and energies for nitrate ion.

Symmetry	Orbital	Energy
A_2''	$\pi_1=0.679\ N_\pi+(0.734/\sqrt{3})(O_\pi+O_\pi'+O_\pi'')$	−14.76 ev
	$\pi^*=0.734\ N_\pi-(0.679/\sqrt{3})(O_\pi+O_\pi'+O_\pi'')$	5.33
E''	$\pi_2=\sqrt{\frac{1}{2}}(O_\pi'-O_\pi'')$	−8.52
	$\pi_{-2}=\sqrt{1/6}(2O_\pi-O_\pi'-O_\pi'')$	
A_2'	$n_1=\sqrt{(\frac{1}{3})}(O_t+O_t'+O_t'')$	−8.44
E'	$\left\{\begin{matrix}n_2=0.023\ N_y-0.004\ O_s'^+ +0.282\ O_r'^+ -0.959\ O_t'^+ \\ n_{-2}=0.023\ N_x-\dots\end{matrix}\right\}$	−8.35

Table VII gives the values of the atomic orbital interaction integrals used for NO_3^-. For the σ-electron system the positive charge on the nitrogen was ignored in evaluating the integrals, and the one-center quantities are found in Tables I and IV. The π-electron polarity was of course included in calculating the σ-system matrix elements through the final two summations in Eq. (4).

By using the parameters in Table VII, the molecular orbitals for NO_3^- were calculated, and are presented in Table VIII. Of the degenerate pair of E' wave functions n_2 and n_{-2}, only n_2 is shown in detail in Table VIII, and the following notation is adopted for one set of E' symmetry orbitals,

$$O_t'^+=\sqrt{\tfrac{1}{2}}(O_t'-O_t''); \qquad O_r'^+=\sqrt{\tfrac{1}{6}}(2O_r-O_r'-O_r'');$$
$$O_s'^+=\sqrt{\tfrac{1}{6}}(2O_s-O_s'-O_s'').$$

The orbitals O_t, O_t', and O_t'' are directed as indicated in Fig. 2.

The first approximation to the ground state is taken to be

$$\chi_0=|\cdots\pi_1\bar{\pi}_1\pi_2\bar{\pi}_2\pi_{-2}\bar{\pi}_{-2}n_1\bar{n}_1n_2\bar{n}_2n_{-2}\bar{n}_{-2}|.$$

In Table IX are found the various states of the nitrate ion, together with predicted transition energies and oscillator strengths. Also in Table IX are found the observed transitions and their intensities.

DISCUSSION

Nitrite Ion

It would be of interest to obtain an estimate of the importance of a resonance integral between the two oxygen O_t orbitals in the nitrite ion, an effect which has been ignored in the present calculation. Possibly the discrepancy between the predicted splitting of the states $^1B_1$(2.93 ev) and $^1A_2$(4.40 ev) of 1.47 ev, and the observed splitting of 0.70 ev, (see Table III) is due partly to the neglect of this resonance integral. A resonance integral $\beta(O_tO_t')\simeq-0.3$ ev would improve the agreement between the calculated and observed energies for the two lowest observed nitrite ion transitions.

Nitrosomethane

The identification of the observed low energy nitrosomethane band with the singlet→singlet $n^*\rightarrow\pi^*$ transition is made mainly because of intensity considerations, since the results of the energy calculation indicate that both the triplet and the singlet ($n^*\rightarrow\pi^*$) configuration are in the correct energy range for this transition. The present assignment of this lowest observed transition is the same as that suggested by Orgel.[20]

Turning to the very weak band at higher energy; this could arise from the singlet→triplet $\pi\rightarrow\pi^*$ transition predicted in this general energy region, or it could perhaps be due to the singlet doubly excited state which has some ($\pi^{-1}\pi^*$) character. The fact that the calculated energy of this state (Table VI) is somewhat high may be due to the unsuitability of the various parameters which have been used for accurate calculation of doubly excited state energies.

It is unfortunate that there is no spectral data for nitrosomethane in the region 2000 to 1800 A, since it would be of interest to check the energy of the transition $n\rightarrow\pi^*$, predicted in Table VI at 6.32 ev. Nitrosomethane is the only one of the compounds studied here for which both the $n^*\rightarrow\pi^*$ and the $n\rightarrow\pi^*$ transitions might be expected to be clearly observable, since in the other compounds there would probably be a strong $\pi\rightarrow\pi^*$ transition in the same region as the $n\rightarrow\pi^*$ transition.

Nitrate Ion

In attempting to identify the low-energy band which has been observed for nitrate ion, there are three types of data to consider: the energy, λ_{max} at 4.1 ev.,

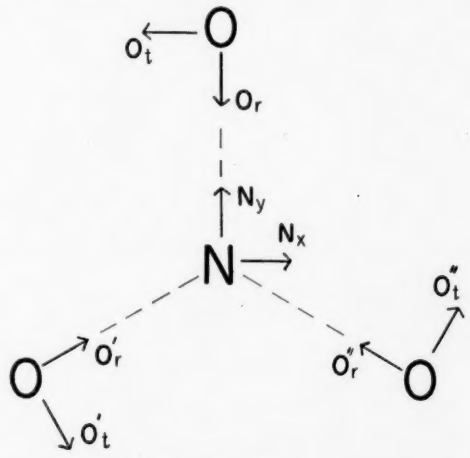

FIG. 2. The $2p$ orbitals of nitrogen and oxygen for nitrate ion. The direction of the arrow indicates the positive direction of the orbital.

[20] L. E. Orgel, J. Chem. Soc. **1953**, 1276.

TABLE IX. Transition energies for nitrate ion.

Symmetry	State wave function	Calc transition energies (ev)	Calc f.	Obs[a] transition energies (ev)	Obs[a] f.
A_1'	$0.993\,\chi_0+0.026(\pi_1^{-1}\pi^*)+0.116(\pi_2^{-2}\pi^{*2})$	0	...	...	...
E'	$0.965(\pi_2^{-1}\pi^*)+0.263(\pi_1^{-1}\pi_2^{-1}\pi^{*2})$	6.22	0.34	6.26	0.15
A_1''	$(n_1^{-1}\pi^*)-0.151(n_1^{-1}\pi_1^{-1}\pi^{*2})$	4.95	0	...	...
E''	$(n_2^{-1}\pi^*)-0.151(n_2^{-1}\pi_1^{-1}\pi^{*2})$	4.86	0	...	...
		...	...	4.10	0.0001
$^3A_1''$	$^3(n_1^{-1}\pi^*)$	4.95	0	...	...
$^3E''$	$^3(n_2^{-1}\pi^*)$	4.85	0	...	...
$^3E'$	$^3(\pi_2^{-1}\pi^*)$	4.40	0	...	...

[a] R. P. Buck, S. Singhadeja, and L. B. Rogers, Anal. Chem. **26**, 1240 (1954).

the intensity, $\log\epsilon_{max}=0.9$, and the observed polarization of the transition, E'.[21] Possible upper states for the transition include the $n\rightarrow\pi^*$ states and the triplet $^3(\pi^{-1}\pi^*)$ state in Table IX.

There is some reason to feel that the calculated $n\rightarrow\pi^*$ transition energies should be more reliable in the case of nitrate ion than for the other compounds studied in the present work. This is because in nitrate ion the lower orbital involved is in each case practically completely nonbonding, so that the importance of any errors in our choice of σ-electron parameters should be at a minimum. It seems likely that the $n\rightarrow\pi^*$ transitions predicted at 4.9 ev, (Table IX) would be masked by the tail of the allowed $\pi\rightarrow\pi^*$ transition.

On turning to the intensity and polarization data, both of the $n\rightarrow\pi^*$ transitions are symmetry forbidden; one of them, however, the $A_1'\rightarrow E''$ transition, could possibly receive some $A_1'\rightarrow E'$ character by vibrational perturbation. We should then not rule out the possibility that the observed transition is $A_1'\rightarrow E''$.

There is however, an additional possibility that we should consider, for the lower energy nitrate band. This is a weakly allowed $n\rightarrow\sigma^*$ transition, from an E' orbital shown in Table VIII to an A_1' σ-antibonding orbital. This latter orbital would be an antibonding combination of Ns, O_r and O_s atomic orbitals, and it should be of very low energy because of the low energy of all the component diagonal matrix elements. A rough calculation indicates that this $n\rightarrow\sigma^*$ transition in NO_3^- may be one or two electron volts lower than the corresponding $n\rightarrow\sigma^*$ transition in a less symmetrical compound; so that in nitromethane, for example, this weak transition may perhaps be covered up by the strongly allowed $\pi\rightarrow\pi^*$ band. If this suggestion is correct, then the lowest energy transition of NO_3^- would be symmetry allowed, although with a very small transition moment, of symmetry E'.

[21] J. A. Friend and L. E. Lyons, J. Chem. Soc. **1959**, 1572.

Infrared Spectrum and Thermodynamic Properties of Ruthenium Tetroxide

M. H. ORTNER

Vitro Laboratories, Division of Vitro Corporation of America, West Orange, New Jersey

(Received August 15, 1960)

The infrared spectrum of liquid ruthenium tetroxide was determined over the range 300 to 5000 cm^{-1}. Fundamental bands were observed at 330 and 913 cm^{-1}, and were assigned to the infrared active $\nu_3(F_2)$ and $\nu_4(F_2)$ vibrations. A combination band $[\nu_3+\nu_1](F_2)$ at 1792 cm^{-1} permitted an assignment of the Raman-active $\nu_1(A_1)$ frequency in agreement with earlier work. The final $\nu_2(E)$ Raman-active fundamental was calculated by the OVFF method, and the set of observed and calculated frequencies were utilized to calculate thermodynamic functions for the ideal gas from 298.16°K to 1000°K.

INTRODUCTION

RUTHENIUM-tetroxide and osmium tetroxide are the only known neutral molecules of the type MO_4, although anions of the same general formula are common. Several investigations of the infrared[1,2] and Raman[1,3] spectrum of OsO_4 have been reported, and the vibrational assignments $\nu_1(A_1)=965$ cm^{-1}, $\nu_2(E)=335$ cm^{-1}, $\nu_3(F_2)=954$ cm^{-1}, $\nu_4(F_2)=335$ cm^{-1} have been made. The occurrence of two of the vibrational fundamentals of OsO_4 in the ir and two in the Raman, supports the x-ray diffraction[4] and electron diffraction[5] evidence of a tetrahedral structure. By analogy with OsO_4, RuO_4 should also have tetrahedral symmetry and show a simple ir absorption pattern. Dodd,[2] recently reported a study of the ir spectrum of RuO_4 in the gas phase and in solution in the range 5–15 μ. The bands observed in solution at 914, 1794, and 1831 cm^{-1} were assigned to the modes $\nu_3(F_2)$, $2\nu_3(A_1+E+F_2)$, and $\nu_3+\nu_1(F_2)$, respectively. The assignment of the combination band yields the value $1794-914=800$ cm^{-1} for the totally symmetric, Raman-active $\nu_1(A_1)$ vibration. Due to the color and photochemical instability of RuO_4 it is unlikely that a direct determination of the remaining Raman-active $\nu_2(E)$ mode can be made. For this reason, in the present study, the ir spectrum of RuO_4 was redetermined over the range 300–5000 cm^{-1} to identify the frequency of the remaining $\nu_4(F_2)$ infrared fundamental. The experimental values for $\nu_3(F_2)$ and $\nu_4(F_2)$ were then utilized in an orbital valency force field calculation of the Raman-active fundamentals, thus confirming Dodd's assignment for $\nu_1(A_1)$; thermodynamic functions for RuO_4 were calculated from the spectroscopic data.

TABLE I. Infrared spectrum of RuO_4 [frequency (cm^{-1})].

Assignment	This study	Dodd
ν_4 (F_2)	330	...
ν_3 (F_2)	913	914 (sol'n.), 960 (vapor)
$\nu_3+\nu_1$ (F_2)	1792	1794 (sol'n.)
$2\nu_3$	1820	1831 (sol'n.)

EXPERIMENTAL

The RuO_4 was prepared by a method similar to those reported by Shechter[6] and Marshall.[7] Ruthenium metal or RuO_2 (supplied by A. D. Mackay) was roasted in air at 700°C to drive off any volatiles. The sample was transferred to a nickel crucible and slurried in molten KOH. Potassium nitrate was added slowly and the mixture heated to red heat. The melt was then cooled, dissolved in water, and acidified with H_2SO_4. The ruthenate solution was filtered, added to a distilling flask, and oxidized to the volatile octavalent state using $K_2S_2O_8$ and a silver catalyst. The pot temperature was held at 70°–80°C and a steam of dry N_2 or O_2 was used to carry the RuO_4 vapors from the still. The vapors were condensed in a tube immersed in a dry ice-acetone bath. The crude condensate which contained some water was treated several times with concentrated H_2SO_4 and the H_2SO_4 decanted after cooling to 10°C. The partially dried RuO_4 was finally redistilled with the vapors passing through a drying tube before freezing.

The spectrum from 650–5000 cm^{-1} was determined in a Beckman Model IR-4 spectrophotometer. The sample was prepared by spreading a film of liquid RuO_4 between two KBr plates. (Attempts to press solid KBr-RuO_4 pellets and to prepare a Nujol mull led to rapid decomposition.) In the region 300–500 cm^{-1}, the spectrum was obtained in a Perkin-Elmer Model 112G spectrometer equipped with a CsBr fore prism and a 750 cm^{-1} grating, in zero order, in the double pass monochromator. The instrument was flushed with nitrogen to reduce the water vapor background, and the sample was contained between two CsBr plates separated by a 1-mm AgCl spacer. The

[1] L. A. Woodward and H. C. Roberts, Trans. Faraday Soc. **52**, 615 (1956).
[2] R. E. Dodd, Trans. Faraday Soc. **55**, 1480 (1959).
A. Langseth and B. Qviller, Z. physik. Chem. (Leipzig) **27**, 90 (1934).
[4] A. Zalkin and D. H. Templeton, Acta. Cryst. **6**, 106 (1953).
[5] R. Glauber and V. Schomaker, Nature **170**, 290 (1952).
[6] H. Schechter, J. Chem. Soc. (London) **74**, 3055 (1952).
[7] E. D. Marshall and R. R. Rickard, Anal. Chem. **22**, 795 (1950).

TABLE II. Thermodynamic properties of RuO_4.

	298.16°K	400°K	500°K	600°K	700°K	800°K	900°K	1000°K
				Heat capacity (cal/g mol°K)				
Translation	4.97	4.97	4.97	4.97	4.97	4.97	4.97	4.97
Rotation	2.98	2.98	2.98	2.98	2.98	2.98	2.98	2.98
Vibration	10.19	12.45	13.92	14.92	15.60	16.08	16.42	16.69
Total	18.14	20.40	21.87	22.87	23.55	24.03	24.37	24.64
				-Free energy function (cal/g mol°K)				
Translation	36.25	37.71	38.82	39.72	40.49	41.15	41.74	42.26
Rotation	17.46	18.34	19.01	19.55	20.01	20.41	20.76	21.07
Vibration	3.21	4.18	5.75	7.27	8.73	10.08	11.29	12.61
Total	56.92	60.23	63.58	66.54	69.23	71.64	73.79	75.94
				Enthalpy (cal/g mol)				
Translation	1 481	1 987	2 483	2 980	3 476	3 973	4 470	4 966
Rotation	889	1 192	1 490	1 788	2 086	2 384	2 682	2 980
Vibration	1 395	2 553	3 873	5 323	6 859	8 441	10 052	11 734
Total	3 765	5 732	7 846	10 091	12 421	14 798	17 204	19 680
				Entropy (cal/g mol°K)				
Translation	41.23	42.69	43.80	44.70	45.47	46.13	46.72	47.24
Rotation	20.48	21.36	22.03	22.57	23.03	23.43	23.78	24.09
Vibration	7.89	10.56	13.49	16.15	18.53	20.63	22.46	24.34
Total	69.60	74.61	79.32	83.42	87.03	90.19	92.96	95.67

instrument was calibrated following the values given by Downie and Crawford[8] for water vapor bands.

RESULTS AND DISCUSSION

The bands observed in the present study are compared with Dodd's[2] values in Table I.

The agreement between the two sets of values is quite good, and the position of ν_4 is about where it is expected by analogy with Woodward's determination $\nu_4(F_2)=335$ cm^{-1} for OsO_4.

Dodd's assignment $\nu_1(A_1)=880$ cm^{-1} and the frequency of the remaining $\nu_2(E)$ Raman-active vibrations were then determined by carrying out an orbital valency force field calculation, utilizing the F_2 vibrational equations given by Heath and Linnett,[9] and the experimentally determined $\nu_4(F_2)=330$ cm^{-1} and $\nu_3(F_2)=913$ cm^{-1} frequencies.[10] This calculation results in the values $\nu_1(A_1)=890$ cm^{-1} and $\nu_2(E)=293$ cm^{-1}, thus confirming Dodd's assignment for $\nu_1(A_1)$.

[8] A. R. Downie, M. C. Magoon, T. Purcell, and B. Crawford, Jr., J. Opt. Soc. Am. **43**, 941 (1953).

[9] D. F. Heath and J. W. Lincett, Trans. Faraday Soc. **44**, 561, 878 (1948).

[10] In terms of Heath and Lincett's[9] nomenclature we have used the values $B/R=2A/13$ and $k^{81}=3$ A.

Thermodynamic Properties of RuO_4(g)

With the exception of fragmentary data for the solid,[11] no thermodynamic data for RuO_4 are available in the literature. For this reason, the spectroscopic and structural data available for the molecule were utilized to calculate the heat capacity, enthalpy, entropy, and free energy function of the ideal gas over the range 298.16°K–1000°K by the standards methods of statistical thermodynamics.[12] The frequencies used to calculate the vibrational partition function were $\nu_1(A_1)=880$ cm^{-1}, $\nu_2(E)=293$ cm^{-1}, $\nu_3(F_2)=913$ cm^{-1}, $\nu_4(F_2)=330$ cm^{-1}.

Calculation of the rotational partition function requires a value for the moment of inertia which, in turn, depends upon the Ru—O bond distance and the geometry of the molecule. Infrared studies leave little doubt that RuO_4 is tetrahedral; however, the length of the Ru—O band has been the subject of some dispute.

Silverman and Levy[13] studied the related molecule $KRuO_4$ by x-ray diffraction and found the bond dis-

[11] L. Brewer, Chem. Revs. **52**, 1 (1953).

[12] I. Mayer and M. Mayer, *Statistical Mechanics* (John Wiley & Sons, Inc., New York, 1940).

[13] M. D. Silverman and H. A. Levy, J. Am. Chem. Soc. **76**, 3318 (1954).

tance to be 1.79 A. Braune and Stute[14] obtained a value of 1.66 A by electron diffraction; however, this measurement is uncertain. Brockway[15] found the four bonds of OsO_4 to be equal to 1.66±0.05 A, while a rough calculation[2] based on the rotational contour of the ν_3 band of RuO_4 lead to a bond length of 1.85 A. In the absence of better data, we have used the value 1.66 A for the Ru—O bond distance, which leads to the value 54.28×10^{-115} g^3cm^6 for the product of the principal moments of inertia.

The thermodynamic functions calculated from these data are summarized in Table II. Contributions due to nuclear spin and isotope mixing were neglected. The value of the standard entropy at 298.16°K is close to that expected, based upon the value 65.65 eu for OsO_4 reported by Anderson and Yost.[16]

ACKNOWLEDGMENTS

This work was supported by a subcontract from Phillips Petroleum Company, prime contractor to the U. S. Atomic Energy Commission. We acknowledge with thanks the assistance provided by R. Bauman of the Polytechnic Institute of Brooklyn in running the spectrum of RuO_4 in the cesium bromide region.

[14] H. Braune and A. Stute, Angew. Chem. **51**, 528 (1938).
[15] L. O. Brockway, Revs. Modern Phys. **8**, 260 (1936).
[16] L. H. Anderson and D. M. Yost, J. Am. Chem. Soc. **60**, 1822 (1938).

THE JOURNAL OF CHEMICAL PHYSICS VOLUME 34, NUMBER 2 FEBRUARY, 1961

Molecular Association in Alkali Halide Vapors

SHELDON DATZ,* WILLIAM T. SMITH, JR., AND ELLISON H. TAYLOR

Chemistry Division, Oak Ridge National Laboratory,† Oak Ridge, Tennessee, and

Department of Chemistry, University of Tennessee, Knoxville

(Received July 5, 1960)

Molecular association equilibria in alkali halide vapors were studied by measuring the temperature dependence of the molecular weights of gaseous NaCl, NaBr, NaI, KCl, KI, RbCl, and CsCl. The molecular weights were determined by measurement of the absolute pressure exerted by a known weight of completely vaporized salt contained in an isothermal fused silica bulb of known volume. The pressure sensing element was a fused silica manometer containing molten gold. The apparatus was used in the temperature range of 1175° to 1430°K and pressures of from 10 to 40 mm were measured with a precision of ±0.05 mm. The temperature dependence of the equilibrium constants for the reaction $(MX)_2 \rightleftharpoons 2MX$ yielded dissociation energies (evaluated at 1300°K) ranging from 48.0 kcal $mole^{-1}$ for NaCl to 34.7 for CsCl. The entropies of dissociation were found to fall within a small range, varying from 28.3 eu for NaCl to 25.0 for KI, and a statistical calculation of the entropy changes based on an ionic model was found to agree well with the experimental values. It is shown that these systems may be adequately described with an electrostatic model, although closer attention should be paid to the nature of polarization interactions.

INTRODUCTION

ALTHOUGH the presence of polymeric species in alkali halide vapors has been well established by many recent investigations, several discrepancies still exist between the different thermodynamic values reported for the molecular association equilibria. The values obtained by Miller and Kusch[1] (hereinafter referred to as MK) from analyses of the velocity distributions in alkali halide molecular beams were found to be inconsistent with the trends in dissociation energies calculated by Milne and Cubicciotti[2] (MC) and with the trends in the dissociation entropies calculated by Bauer, Diner, and Porter[3] (BDP) and by others.[2,4] Much valuable information has been obtained from mass spectrometric investigations[5–9] of the composition of the vapor in equilibrium with the solid, but uncertainties in ionization cross sections and mode of dissociation upon electron impact prevent quantitative evaluation of the degree of association.

The present work was undertaken with the object of measuring the characteristics of the equilibria by a

* This paper is based on a thesis presented to the University of Tennessee, Knoxville, Tennessee, by S. Datz in partial fulfillment of the requirements for the Ph.D. degree.

† Operated for the U. S. Atomic Energy Commission by the Union Carbide Corporation.

[1] R. C. Miller and P. Kusch, J. Chem. Phys. **25**, 860 (1956); **27**, 981 (1957).
[2] T. A. Milne and D. Cubicciotti, J. Chem. Phys. **29**, 846 (1958).
[3] S. H. Bauer, R. M. Diner, and R. F. Porter, J. Chem. Phys. **29**, 991 (1958).
[4] S. A. Rice and W. Klemperer, J. Chem. Phys. **27**, 643 (1957).
[5] J. Berkowitz and W. A. Chupka, J. Chem. Phys. **29**, 653 (1958).
[6] L. Friedman, J. Chem. Phys. **23**, 477 (1955).
[7] T. A. Milne, H. M. Klein, and D. Cubicciotti, J. Chem. Phys. **28**, 718 (1958).
[8] R. F. Porter and R. C. Schoonmaker, J. Chem. Phys. **29**, 1070 (1958); **30**, 283 (1959).
[9] W. A. Chupka, J. Chem. Phys. **30**, 458 (1959).

more simple and direct method for a sufficient number of salts to reveal any systematic trends. Aside from the intrinsic value of the results themselves, they can also be used to assess the applicability of the various theoretical models that have been proposed to explain the behavior of these vapors. In this work, the vapor-phase association equilibria of seven alkali halides were studied by the measurement of average molecular weights as a function of temperature and pressure. The molecular weights were determined by measurement of the absolute pressure exerted by a known weight of completely vaporized salt contained in an isothermal silica bulb of known volume.

The salts studied were NaCl, NaBr, NaI, KCl, KI, RbCl, and CsCl. These were chosen to enable correlation of changes in thermodynamic functions with changes in cation and anion. The measurement of a complete range of cation and anion variation was prevented by the reactivity of the lithium halides and the alkali fluorides with the silica container. The results for NaI and a general description of the apparatus have been previously published.[10]

APPARATUS

Fused silica was used for the bulb because of its high-temperature dimensional stability, its nonreactivity with halide vapors, and its ability to be degassed and sealed off at high temperatures.

The requirement on the pressure sensing device of operating with an accuracy of ± 0.1 mm above the condensation temperature of the vapor in the bulb was met by a molten gold manometer, observed through a window in the furnace and balanced by argon pressure which could be measured by an external mercury manometer. The choice of molten gold was made on the basis of its melting point, its lack of chemical reactivity, and its low vapor pressure over the required temperature range.

The silica apparatus, the gold manometer, and the furnace arrangement are shown in Fig. 1. The principal difference between this apparatus and that described previously[10] is the inclusion of an evacuated outer bulb surrounding the bulb which contained the salt vapor. This jacket reduced the area through which ambient gas could diffuse into the measuring volume, so that the corrections due to leakup during an experiment were much reduced and in most cases were not measurable.

SAMPLE PURITY

Those halides which were available in the form of pure single crystals from the Harshaw Company were used without further purification. In these cases, a large single crystal was cleaved and a single piece of the crystal, removed from the center, constituted a sample. Single crystals of pure NaI, RbCl, and CsCl were not readily available and were prepared by heating the reagent grade salt under vacuum to 500°C and then melting it in an argon atmosphere. Optically clear crystals were selected and a single piece cleaved from the center of a crystal constituted a sample. Spectroscopic analyses indicated that all of the halides examined, with the exception of RbCl, contained less than 0.1% of impurities. The RbCl, prior to purification, contained 0.6% Cs and 0.4% K, but the purified sample was too small to allow satisfactory analysis.

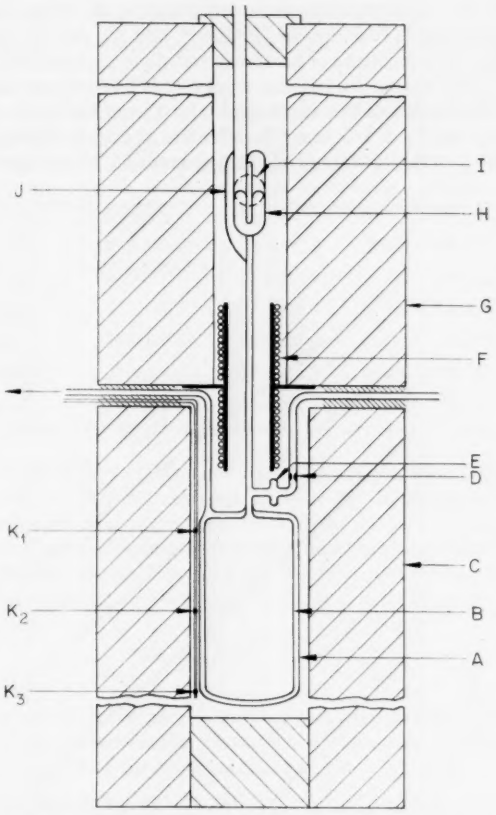

FIG. 1. Bulb and gold manometer apparatus. A, Evacuated buffer bulb; B, measuring bulb; C, bulb furnace; D, seal-off; E, sample loading tube; F, intermediate furnace; G, manometer furnace; H, gold manometer; I, viewing port; J, silica support rod; K_1, K_2, K_3, thermocouples.

RESULTS

If it is assumed that the gases under study consisted of only monomeric and dimeric alkali halide molecules and were sufficiently dilute to be treated as ideal gas mixtures, then the equilibrium constant for the reaction

$$(MX)_2 \rightleftharpoons 2MX$$

is $K_d=(P/R'T)(N_m^2/N_d)$, where K_d is the equilibrium constant expressing concentrations in moles liter^{-1}, P

[10] S. Datz and W. T. Smith, J. Phys. Chem. **63**, 938 (1959).

is the experimentally observed pressure, R' is the gas constant in liter atm mole^{-1} deg^{-1}, and N_m and N_d are the mole fractions of monomer and dimer, respectively.

The change in internal energy ($\Delta E°$) accompanying dissociation of the dimer is obtained from the slope of the log K_d vs $1/T$ line. The standard change in entropy for a standard state of one atmosphere ($\Delta S°$) is obtained

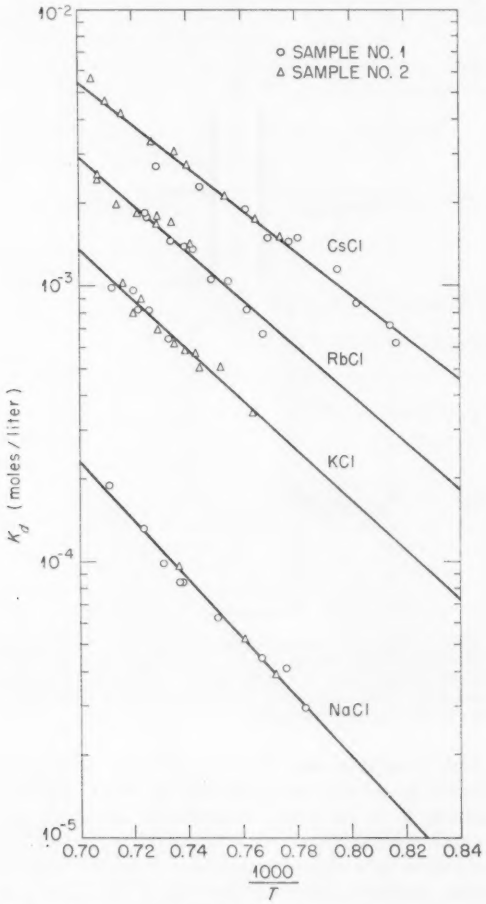

FIG. 2. Dimer dissociation equilibrium constant vs reciprocal temperature for sodium-, potassium-, rubidium-, and cesium chlorides.

from the zero intercept of this line (α) from

$$\Delta S° = \alpha + R(1 + \ln R'T),$$

where R is in cal mole^{-1} deg^{-1}.

In Table I, the sample weights and volumes and the ranges of experimental temperature, pressure and mole fraction of dimer are listed for each of the seven alkali halides studied. The equilibrium constants obtained are plotted vs reciprocal temperature in Figs. 2–4.

The values of the equilibrium constants at 1300°K and a summary of the standard energy and entropy

TABLE I. Range of measurements.

No.	Sample	Wt (mg)	Vol. (cc)	Press. (mm)	Temp. (°K)	Mole fract. N_d
NaCl	1	8.24	795	8.80–11.75	1277–1406	0.60–0.32
	2	6.74	795	7.65–8.75	1296–1357	0.53–0.40
NaBr	1	40.3	685	26.00–33.20	1293–1421	0.36–0.17
	2	60.2	685	34.40–43.75	1317–1434	0.37–0.18
NaI	1	42.0	796	17.60–24.05	1212–1353	0.49–0.21
	2	20.0	836	8.25–11.35	1179–1337	0.41–0.16
KCl	1	29.0	685	36.75–39.60	1364–1404	0.32–0.26
	2	15.8	685	19.20–22.90	1310–1397	0.32–0.18
KI	1	37.8	675	20.85–27.05	1226–1385	0.24–0.08
	2	61.45	675	35.90–43.50	1292–1408	0.23–0.10
RbCl	1	21.2	675	17.50–20.25	1302–1380	0.21–0.10
	2	32.0	675	28.30–31.10	1350–1415	0.17–0.11
CsCl	1	40.5	760	19.50–24.85	1224–1371	0.24–0.09
	2	67.2	760	35.50–43.25	1291–1418	0.19–0.08

changes for dissociation, together with the standard errors in these quantities obtained from a least-squares treatment, are presented in Table II. A statistical treatment of the data showed no significant differences between the points obtained from the two different samples of the halides used. An additional column lists the standard error of fit σ_f. Considering the limited range of the measurements in the log K_d vs $1/T$ coordinate system, the value of σ_f may be interpreted as approximating the average deviation in logK_d.

DISCUSSION

Equation of State

Under the conditions of pressure and temperature used in this work, deviations from ideality of the gases

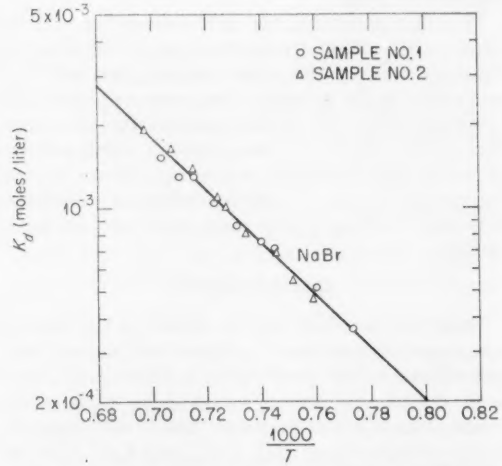

FIG. 3. Dimer dissociation equilibrium constant vs reciprocal temperature for sodium bromide.

studied were assumed to be due solely to chemical reaction. The validity of this assumption may be assessed by considering those conditions under which the greatest deviations from ideal gas behavior might be expected, namely the highest pressure (40 mm), the lowest temperature (1200°K), the highest polarizability ($\alpha = 10\times10^{-24}$ cc), and the highest permanent dipole moment ($\mu = 10\times10^{-18}$ esu cm). If the behavior of the monomer gas is represented by the Van der Waals equation of state, it is clear that corrections due to intrinsic molecular volume and London dispersion forces[11] are negligible.

The large permanent dipole moment would be expected to make the most significant contribution to deviation from ideality. To determine the magnitude of this correction, it is assumed that the total interaction may be estimated by summing the contributions of strong and weak interactions. The weak interaction is defined as that for which the potential energy ϵ can be represented by[12]

$$\epsilon = -\tfrac{2}{3}(\mu^4/r^6kT),$$

where r is the intermolecular distance and k is Boltzmann's constant. This relation will be valid in the region where $\mu^2/r^3 < kT$, and, for the purposes of this calculation, it will be assumed to hold for intermolecular separations greater than 10 A, since at this distance the interaction energy is already less than one-half the thermal energy. The Van der Waals a can be obtained by summing all the interactions for a mole of gas

$$a = 2\pi N_0^2 \int_{\delta}^{\infty} -\epsilon r^2 dr,$$

where N_0 is Avogadro's number and δ is the lower limit of the intermolecular distance for which the equation is valid. For the weak interaction, the solution is

$$a = (4\pi/9)(N_0^2/kT)(\mu^4/3)$$
$$= 3.62\times10^9 D^4/T\delta^3 \text{ atm cc}^2 \text{ mole}^{-2},$$

where D is the dipole moment in debyes and δ is in angstrom units. Upon inserting the parameters presently under consideration, the value of a/V^2 is found to be 8×10^{-6} atm, which amounts to the negligible correction of 0.02%.

In order to evaluate the contribution of forces experienced at internuclear distances of less than 10 A (strong interactions), it is necessary to calculate the probability of finding two molecules within this distance of each other in the gas under consideration. If a random spatial distribution is assumed, the average number of molecules to be found within a sphere of radius $\bar{r}$ is given by

$$P(\bar{r}) = 3\pi N_0 \bar{r}^3/\bar{V}.$$

When $\bar{r}$ is 10 A, $P(\bar{r})$ will be 3×10^{-3}. Since $P(\bar{r})$ is small compared to unity, its magnitude may be taken as the probability of two dipoles being within 10 A of each other at any time. Hence, if the distribution were truly random, the departure from ideality due to the strong interaction is negligible. However, when two dipoles are sufficiently close to interact strongly, the randomness of the distribution is destroyed, but this is

TABLE II. Summary of experimentally derived thermodynamic functions for dimer dissociation.

MX	Evaluated at 1300°K ΔE° (kcal mole^{-1})	ΔS° (cal mole^{-1} deg^{-1})	$-\log K_d$	Standard error of fit σ_f
NaCl	48.0±1.7	28.3±1.3	4.378	0.029
NaBr	42.9±1.3	28.8±0.9	3.410	0.025
NaI	40.2±1.2	27.1±1.0	3.312	0.033
KCl	41.2±2.3	27.1±1.7	3.500	0.027
KI	34.7±0.9	25.0±0.7	2.846	0.025
RbCl	39.4±2.0	27.3±1.5	3.130	0.031
CsCl	34.7±1.0	25.3±2.8	2.791	0.037

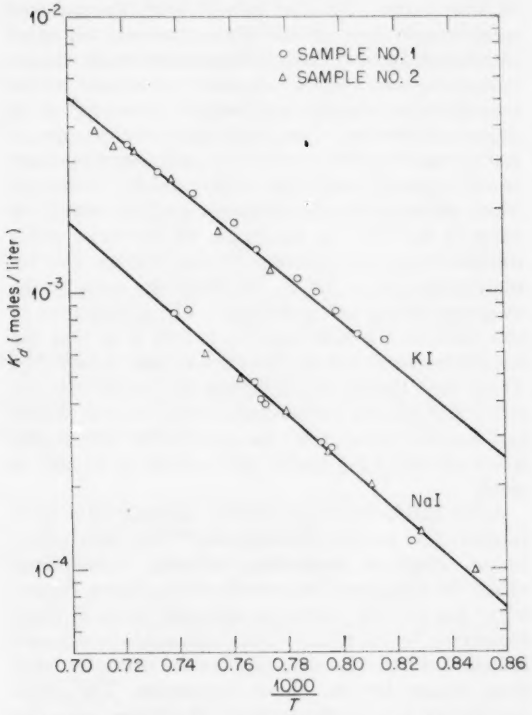

FIG. 4. Dimer dissociation equilibrium constant vs reciprocal temperature for sodium- and potassium iodides.

[11] J. C. Slater and J. G. Kirkwood, Phys. Rev. **40**, 387 (1932).
[12] H. Margenau, Revs. Modern Phys. **11**, 1 (1939).

tantamount to molecular association. Therefore, the only force which is sufficiently large to cause deviation from ideality is that which causes chemical reaction. Under these circumstances, the alkali halide gas may be considered "species-perfect," i.e., a reacting mixture in which each component behaves as an ideal gas.[13]

Trimer Formation

It has been assumed that the only molecular species present in any appreciable concentrations are those of monomer and dimer. If trimer molecules were also present, the derived quantities would, of course, be considerably less significant. However, two arguments can be presented which indicate that trimer molecules are not present in appreciable concentrations under the conditions of this experiment.

First, since the equilibrium concentration of trimer should be dependent on the total pressure, it would be expected that the equilibrium constant, calculated on the assumption that only monomer and dimer were present, would vary with pressure in the presence of large amounts of trimer. The equilibrium constants so calculated from the measurements do not appear to be sensitive to total pressure which was varied by a factor of two by varying the sample size at constant temperature.

A second and better argument can be adduced from extrapolated values of trimer concentrations measured at lower temperatures and pressures by Berkowitz and Chupka.[5] In their work, a mass spectrographic analysis of the alkali halide vapor composition was made by electron bombardment of a molecular beam emanating from an effusion cell which was maintained at a temperature corresponding to an equilibrium vapor pressure of 10^{-2} mm. If it is assumed that the ionization cross section for the three species is the same, an equilibrium constant for the reaction,

$$(MX)_3 \rightleftharpoons 3MX, \tag{1}$$

can be calculated, at the given temperature. At the higher temperatures encountered in this work, the equilibrium constant can be calculated if ΔE_t°, the change in internal energy for this reaction, is known. An estimate of this quantity may be obtained from the work of Milne and Cubicciotti[14] who, on the basis of a simple electrostatic model, calculated the expected energy changes for the reactions

$$(MX)_2 \rightleftharpoons 2MX \tag{2}$$

and

$$(MX)_3 \rightleftharpoons (MX)_2 + MX. \tag{3}$$

These values were calculated for the alkali chlorides, and the energy change for reaction (3) was found to be 3 to 4 kcal mole^{-1} less than that for corresponding reaction (2). Since reaction (1) is simply the sum of reactions (2) and (3), it was assumed for the purposes of the extrapolation that

$$\Delta E_t^\circ = 2\Delta E^\circ - 4 \text{ kcal mole}^{-1},$$

where ΔE° is the dimer association energy found in the present work. Of all the experimental conditions encountered in this work, the case of sodium bromide at a temperature of 1315°K and a pressure of 35 mm would be expected to yield the maximum value of the mole fraction of trimer. Even in this case, the mole fraction of trimer should be only 3×10^{-3}.

Comparison with Previous Investigations

Since 1300°K is within the temperature range of measurement for all of the salts investigated in the present work, it was chosen as the reference temperature, and, to facilitate comparison of the results with the previously published work, all the reported results were adjusted to their corresponding values at this temperature. The adjustment of the other values to this temperature requires a knowledge of the heat capacities of the reactants and products as a function of temperature, but the lack of both thermal and spectroscopic data on the dimer prevents an exact calculation. However, in this temperature range, change in heat capacity may be adequately computed by the assumption of classical equipartition of energy in all degrees of freedom. The justification of this approximation can be demonstrated by estimating the maximum expected departure from classical behavior, which will occur in the vibrational mode for which the value of $hc\omega/kT$ is a maximum. Of the cases under consideration, this criterion is most closely met by sodium chloride at 920°K, for which the value of the monomer frequency[15] is 366 cm^{-1}. The contribution of this mode to the heat capacity is 0.98 R so that the error introduced even in this extreme case is only 2%. Thus, even though the difference in temperature between the present measurements and those of Miller and Kusch is about 450°, the error in the corrections, which are about 1.8 kcal to ΔE° and 0.8 eu to ΔS°, is small.

Alkali halide dimer dissociation entropies have been computed by previous investigators[2–4] but these calculations employed somewhat arbitrary assumptions about the vibrational frequencies of the dimer. Berkowitz[16] has recently arrived at different values of these frequencies by calculations from a plausible model, and it seemed worthwhile to recalculate the entropies using these values for the dimer frequencies. The other parameters used in the entropy calculations were the monomer vibrational frequencies obtained by Rice and

[13] G. Scatchard, *Equilibrium in Solutions* (Massachusetts Institute of Technology, Cambridge, Massachusetts, 1940).

[14] T. A. Milne and D. Cubicciotti, J. Chem. Phys. **30**, 1625 (1959).

[15] S. A. Rice and W. Klemperer, J. Chem. Phys. **27**, 573 (1957).

[16] J. Berkowitz, J. Chem. Phys. **32**, 1519 (1960).

Klemperer,[15] the monomer internuclear distances determined by Honig *et al.*,[17] and the dimer configurations previously computed by Berkowitz.[18] The experimental and calculated values of the dimer dissociation entropies obtained in this investigation are given in Table III together with those obtained by other investigators.

The agreement between the experimental and calculated values obtained in this investigation is quite good, the calculated values lying within the experimental standard error in all cases except KI and CsCl. The calculations of BDP and MC are consistently higher, the difference ranging from 2.1 to 3.2 eu for the former and 2.8 to 3.9 eu for the latter. The differences between these calculations and those calculated herein are due almost entirely to the differences in the vibrational entropy contributions. The large internal discrepancies found in the entropies determined by MK were attributed by BDP to probable errors in the determination of the dimer dissociation energies. The values obtained by Barton and Bloom,[19] while not in gross disagreement with other determinations, cannot be weighted as heavily due to the paucity of data reported.

The dimer dissociation energies determined in this investigation and those of other workers are listed in Table IV. Since the stability of the dimer is due primarily to electrostatic forces, it would be expected that the dissociation energy should be approximately proportional to the reciprocal of the anion-cation internuclear distance, and a plot of these two variables is shown in Fig. 5. The values obtained in the present work display the expected monotonic increase with decreasing interionic separation. The lack of systematic variation in the results of MK had been noted previously by BDP, who recalculated the dissociation energies, using their calculated entropy values and assuming that the equilibrium constants measured by MK were correct. The recalculated energies show good agreement with the present values for KCl, KI, RbCl, but the values for NaI, and NaCl remain significantly lower. In the case of NaCl, the discrepancy has been partially mitigated by the higher value found experimentally by Eisenstadt, Rao, and Rothberg,[20] using the technique and apparatus developed by MK.

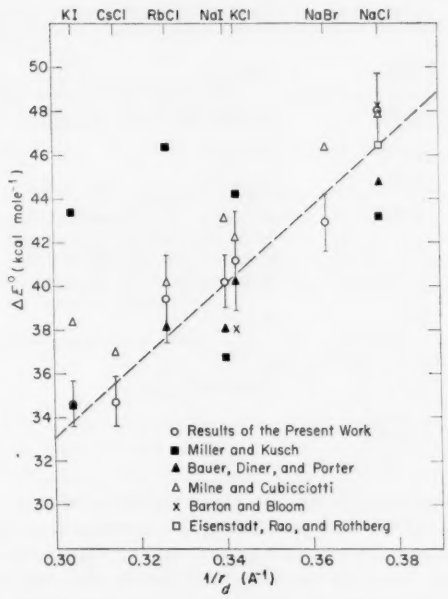

FIG. 5. Dimer dissociation energy vs the reciprocal of the anion-cation separation in the dimer.

TABLE III. Comparison of dimer dissociation entropies at 1300°K (in cal mole^{-1} deg^{-1})

	This work		MK[b]	BDP[c]	MC[d]	Barton[e]
MX	(exptl)[a]	(calc)[a]	(exptl)	(calc)	(calc)	(exptl)
NaCl	28.3±1.3	28.02	28.8±1.0	30.45	31.1	30.0±0.7
NaBr	28.8±1.0	28.01			31.8	
NaI	27.1±1.0	28.04	27.6±4.2	29.21	30.8	
KCl	27.1±1.7	27.29	34.1±0.8	29.62	30.8	25.5±1.0
KI	25.0±0.7	27.20	39.2±1.1	28.25		
RbCl	27.3±1.5	26.81	38.9±0.6	29.45	30.3	
CsCl	25.3±1.0	26.45			29.2	

[a] Values obtained in this work.
[b] See footnote 1.
[c] See footnote 3.
[d] See footnote 2.
[e] See footnote 19.

The dimer dissociation energies calculated by MC agree especially well with the present results for NaCl, KCl, and RbCl, but are higher by about 2 kcal mole^{-1} for CsCl and about 3 kcal mole^{-1} for NaBr, NaI, and KI. A possible cause for this discrepancy may be found by considering the assumptions used in the calculation. The theory used by MC was identical to the one which had been used by Pauling[21] in his treatment of gaseous alkali halide monomers. Pauling found that the binding energies in the monomers were calculable from a relatively simple formula which contained just the coulombic attractive energy and a repulsive term. The repulsive term contained the quantity

$$n = n_+ + n_-,$$

where n_+ and n_- are constants characteristic of the cation and anion, respectively, and independent of the particular combination of the two. These constants were empirically evaluated and a self-consistent set of

[17] A. Honig, M. Mandel, M. L. Stitch, and C. H. Townes, Phys. Rev. **96,** 629 (1954).
[18] J. Berkowitz, J. Chem. Phys. **29,** 1386 (1958).
[19] J. L. Barton and H. Bloom, J. Phys. Chem. **63,** 1785 (1959).
[20] M. Eisenstadt, V. S. Rao, and G. M. Rothberg, J. Chem. Phys. **30,** 604 (1959).
[21] L. Pauling, Proc. Natl. Acad. Sci. India **25,** Sec. A, Pt. I, 1 (1956).

TABLE IV. Comparison of dimer dissociation energies at 1300°K (in kcal mole^{-1}).

MX	(Exptl)[a]	MK[b] (Exptl)	Eisenstadt[c] (Exptl)	BDP[d] (Calc)	MC[e] (Calc)	Barton[f] (Exptl)
NaCl	48.0±1.7	43.1±0.9	46.4±0.6	44.7	47.9	48.3±0.8
NaBr	42.9±1.3				46.3	
NaI	40.2±1.2	36.7±3.4		38.0	43.1	
KCl	41.2±2.3	44.2±0.7		40.2	42.2	38.0±0.6
KI	34.7±0.9	43.4±0.9		34.5	38.3	
RbCl	39.4±2.0	46.3±0.5		38.1	40.1	
CsCl	34.7±1.1				36.9	

[a] Values obtained in this work.
[b] See footnote 1.
[c] See footnote 20.
[d] See footnote 3.
[e] See footnote 2.
[f] See footnote 19.

binding energies for the alkali halide monomers was obtained. In their calculation, MC assumed that these values could be applied equally well in the calculation of the bond strengths in the dimers. Although the contribution of polarization to the total energy is not explicitly mentioned in the Pauling formulation, it is implicitly included in the values of n_+ and n_-. Thus, the assumption made by MC is equivalent to the supposition that the polarization energy per bond is the same in monomer and dimer. However, in the dimer the nature of the polarization interaction is considerably more complex, since each ion is interacting with three other ions and the magnitude of the polarizability for each interaction is reduced by the presence of the other interactions. The fact that the calculated energies are too high indicates that the contribution of the polarization energy per bond is less in the dimer than in the monomer and, as would be expected, the discrepancies are larger for molecules containing ions with higher polarizabilities. However, considering the simplicity of the model the agreement is remarkably good.

CONCLUSIONS

The relatively small range in the values of the dimer dissociation entropies for the series of alkali halides investigated is in accord with the predictions of previous theoretical calculations. The absolute values of the experimentally determined entropy changes are in agreement with calculations based on dimer vibrational frequencies predicted by Berkowitz, but are significantly lower than those calculated heretofore.

The trend observed in the dissociation energies is consistent with an electrostatic model for the dimer, exhibiting a monotonic increase with decreasing anion-cation internuclear distance. A comparison of the total Coulombic energy of the dimer (calculated from the sum of the four anion-cation attractive energies minus the anion-anion and cation-cation repulsive terms) exhibits a similar trend. The results also indicate that a complete theoretical treatment of the dimer dissociation energies must take into account the detailed nature of the polarization interactions in the dimer.

The diminution of the dimer energy with internuclear distance is reflected in the reduction of the bond restoring force constants and is therefore accompanied by a reduction in the vibrational contribution to the dissociation entropy. This effect is partially compensated by the increase in the translational and rotational entropy contributions due to the larger masses of the ions. However, the net effect is a decrease in the entropy so that there is a relatively small change in the equilibrium constants throughout the series of alkali halides studied.

ACKNOWLEDGMENT

It is a pleasure to thank Dr. R. E. Minturn for his aid during the early part of this work and for his abiding interest since.

Temperature Dependence of the Proton Spin-Lattice Relaxation Time in Liquid Butyl Alcohols*

ROBERT A. BERNHEIM,† H. S. GUTOWSKY, AND IAN J. LAWRENSON

Noyes Chemical Laboratory, University of Illinois, Urbana, Illinois

(Received August 12, 1960)

The proton T_1 has been measured by rf pulse methods at 20 Mc for *n*-butyl, *iso*-butyl, *sec*-butyl, and *tert*-butyl alcohol over their liquid range. The observed temperature dependences of T_1 correspond to activation energies of 3.9, 4.8, 5.2, and 7.3 kcal/mole, respectively, for the *n*, *iso*, *sec*, and *tert* alcohols. The T_1 results and a comparison of them with known dielectric dispersion data indicate that the spin-lattice relaxation is produced by molecular motions which are restricted by hydrogen bonding and steric effects to reorientations mainly about the C−O and C−C bonds of the heavy atom skeleton.

I. INTRODUCTION

IN early nuclear magnetic resonance studies, it was pointed out[1] that the correlation time τ_c for nuclear spin relaxation is related to the dielectric relaxation time τ_D. Therefore, in principle, studies of the nuclear spin relaxation and of dielectric relaxation in the same system are complementary. The present work was started with this in mind. The systems chosen were *n*-butyl, *iso*-butyl, *sec*-butyl, and *tert*-butyl alcohols. This choice was made because (a) dielectric relaxation times had been measured for the first three alcohols of this series over a wide temperature range,[2] and (b) the compounds are isomers with considerably different molecular shapes, so that something might be learned about the importance of steric effects upon the molecular motions in the associated liquids.

The activation energy for the relaxation process is found to be different for each alcohol, and the differences are interpreted as resulting from steric influences upon the molecular motions and hydrogen bonding in the liquids. Steric effects were also found in the dielectric relaxation time studies.[2] However, the proton T_1 depends upon the motions of all the protons in the molecule, and thus reflects the dynamic structure of the whole heavy atom molecular skeleton, while the dielectric relaxation depends mainly upon the C-O-H motions which are influenced to a greater extent by the hydrogen bonding. Therefore, it is not surprising that the activation energies governing T_1 are smaller than those for the dielectric relaxation, and that the T_1 results supplement the information obtained from the dielectric study.

II. EXPERIMENTAL

The samples of the butyl alcohols used were all reagent grade. Before use, they were dried over calcium hydride and redistilled. The constant boiling fractions were collected, thoroughly degassed by freezing in liquid nitrogen under vacuum, and sealed in 9-mm Pyrex tubes. In the experiments, the temperature of the samples was controlled by means of a gasflow cryostat,[3] and was within ±0.5°C for each T_1 measurement. The temperature was measured by a copper-constantan thermocouple embedded in a small well in the side of the sample tube.

The proton spin-lattice relaxation times were measured at a proton resonance frequency of 20 Mc, using spin-echo apparatus described elsewhere.[4] At high temperatures, where T_1 is of the order of seconds, the method of two 90° pulses was used,[5] while at lower temperatures, where T_1 is short, it was more convenient to use the "null" method of a 180° pulse followed by a 90° pulse.[6] Although the two methods give values of T_1 which may differ in magnitude by as much as 10%, the variation of T_1 with temperature is the same for each method.

Different apparent values of T_1 are found in the two methods because the sample does not see a completely homogeneous radio-frequency field H_1. In the null method, any inhomogeneities in H_1 make it difficult to determine the "null point," because of the resultant small tail following the 90° pulse at what would otherwise be the true null. However, if the null point is defined in a consistent manner, the variation of T_1 between compounds, or with temperature in the same compound, will be the same as for the 90°–90° method, although the numerical values obtained by the two methods will differ by a constant factor near unity. This factor may be determined experimentally by

* Acknowledgment is made to the donors of the Petroleum Research Fund, administered by the American Chemical Society, for partial support of this research. This work was also supported in part by the Office of Naval Research and by the National Science Foundation.

† DuPont Teaching Fellow in Chemistry. Present address: Department of Chemistry, Columbia University, New York.

[1] N. Bloembergen, E. M. Purcell, and R. V. Pound ,Phys. Rev. **73**, 679 (1948).

[2] W. Dannhauser and R. H. Cole, J. Chem. Phys. **23**, 1762 (1955).

[3] E. R. Andrew and R. G. Eades, Proc. Roy. Soc. (London) **A216**, 398 (1953).

[4] J. Buchta, H. S. Gutowsky, and D. E. Woessner, Rev. Sci. Instr. **29**, 55 (1958).

[5] E. L. Hahn, Phys. Today **6**, No. 11, 4 (1953).

[6] H. Y. Carr and E. M. Purcell, Phys. Rev. **94**, 630 (1954).

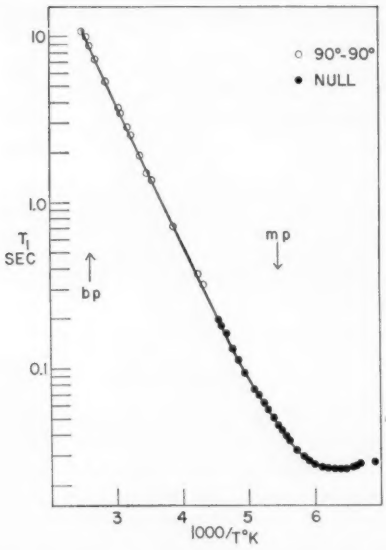

FIG. 1. Temperature dependence of the proton T_1 observed in *n*-butyl alcohol, at a resonance frequency of 20 Mc. The methods used to measure T_1 are indicated in the figure.

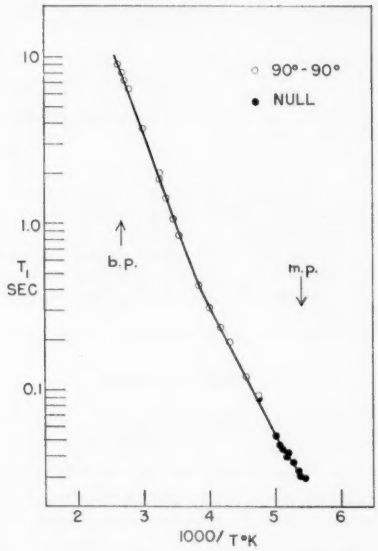

FIG. 3. Temperature dependence of the proton T_1 observed in *sec*-butyl alcohol, at a resonance frequency of 20 Mc. The methods used to measure T_1 are indicated in the figure.

measurements by both methods at one temperature. Subsequent measurements by the null method can then be multiplied by this factor to make the two sets of values agree. This has been done for the experimental points shown in Figs. 1 to 4.

Measurements of T_1 were made over the entire liquid range for each of the four butyl alcohols. The samples were also super-heated and super-cooled to extend this range. At low temperatures, measurements were made as the temperature decreased, until the resonance line broadened suddenly, indicating the transition to a solid or glass phase, at a temperature about 10° below the freezing point. At high temperatures, measurements were made on samples superheated to about 15° above the boiling point.

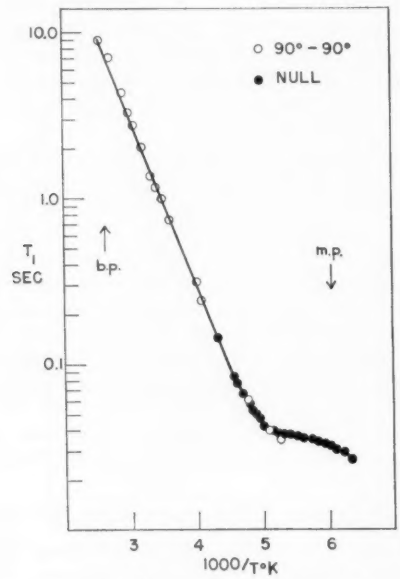

FIG. 2. Temperature dependence of the proton T_1 observed in *iso*-butyl alcohol, at a resonance frequency of 20 Mc. The methods used to measure T_1 are indicated in the figure.

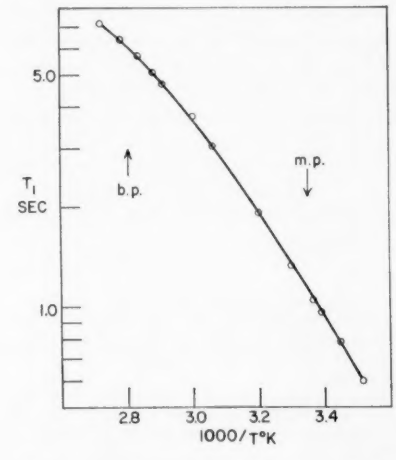

FIG. 4. Temperature dependence of the proton T_1 observed in *tert*-butyl alcohol, at a resonance frequency of 20 Mc. The method of two 90° pulses was used to measure T_1.

Each of the isomers contains at least two sets of structurally different protons, which in principle should have different T_1's.[1,7] However, no evidence was found for the existence of more than one T_1 in any of the samples. The height of the induction decay following the second 90° pulse in each case obeyed the simple formula $A_2 \propto -\exp(-t/T_1)$, within experimental error, over a range of time t of about $3T_1$. This agrees with the work of Powles and Cutler,[8] who measured T_1, T_2, and the diffusion coefficient for a series of primary alcohols, including *n*-butyl, at room temperature. Only in the case of methyl alcohol did they observe two T_1's of 2.5 and 8.5 sec, corresponding to the relaxation of the methyl and hydroxyl protons, respectively.

The effects of self-diffusion in the alcohols[8] are sufficiently pronounced in comparison to the relatively long T_2's that we were discouraged from attempting to measure the latter with our present apparatus. There is no reason to believe that T_2 does not equal T_1, but it would be of some interest to check on this point. There is the possibility that the molecular association and the dynamic equilibrium involving it could give $T_2<T_1$ because of a spread in the proton chemical shifts. The *t*-butyl alcohol would probably be the best candidate for this because of its having only one intramolecular chemical shift.

Some of our early experiments using the method of two 90° pulses on samples at high temperatures did give results consistent with two T_1's. However, the results were not very reproducible, and the effect was traced to the condensation of vapor at the top of the long sample tubes used at first. This cooler liquid ran back into the sample volume within the rf coil and gave a shorter T_1 than the rest of the liquid there. Except for this instrumental effect, no multiple T_1's were found either while obtaining the results reported or in several special searches. However, our experience with the "spurious" double T_1 suggests that the apparatus and methods used would not resolve multiple T_1's unless their ratio was greater than about 1.5 and their relative amplitudes differed by no more than a factor of about 5. Therefore, the "single" T_1's reported are most likely an average for all of the protons in the molecule, except possibly the tertiary and hydroxyl protons. The latter would be expected to have considerably longer T_1's than the protons in the CH_3 and CH_2 groups, but their contribution to the signal amplitude is relatively small to affect the apparent T_1 or to be resolved.

III. RESULTS AND DISCUSSION

Proton Spin-Lattice Relaxation

The values of $\log T_1$ observed for the protons in the butyl alcohols are plotted in Figs. 1–4 as a function of the reciprocal temperature.[9] The normal melting and boiling points are indicated by the arrows in the figures. The curves for all four compounds have linear portions corresponding to an exponential temperature dependence of T_1, particularly for the *n*-butyl and *iso*-butyl alcohols at high temperatures. Also, the curves for these two compounds exhibit a T_1 minimum. That for *n*-butyl alcohol falls at 158.5°K; it is well defined and has a width slightly greater than that predicted on the basis of a single correlation time.[1] On the other hand, that for *iso*-butyl alcohol is a relative minimum only, the T_1 decreasing further at lower temperatures.

TABLE I. Activation energies in kcal/mole obtained from the temperature dependence of the proton T_1 and from dielectric relaxation time studies[a] for the butyl alcohols.

	n	*iso*	*sec*	*tert*
E_a (T_1)	3.85	4.75	5.20	7.25
Temp.[b]	210–400	240–390	280–380	284–320
E_a (τ_{D1})	6.29	6.72	8.26	...
Temp.	200–270	220–270	220–270	...
E_a (τ_{D2})	11.4	13.	...	...
Temp.	136–163	134–155	...	...

[a] The dielectric constant results are taken from the work cited in footnote 2.
[b] The temperatures given are the range in °K of the linear portion of the curve from which E_a was calculated.

The spin-lattice relaxation time is given by an expression of the form[1,9]

$$1/T_1 = A[\tau_c/(1+\omega_o^2\tau_c^2) + 4\tau_c/(1+4\omega_o^2\tau_c^2)], \qquad (1)$$

where A is a constant involving the interproton separations, τ_c is the correlation time for the relaxation process, and ω_o is the resonant angular frequency. From Eq. (1), it follows[10,11] that the straight-line portions of the $\log T_1$ vs $1/T$ curves correspond to Arrhenius plots of rate constants. Assuming only one significant thermally activated relaxation process, the activation energy of the process is obtained from the linear slope. The resultant value of E_a is given in Table I for each of the four butyl alcohols, along with the temperature range for which E_a is applicable. The values increase from 3.85 to 7.25 kcal/mole in the sequence *n*-butyl<*iso*-butyl<*sec*-butyl<*tert*-butyl, demonstrating that the shape of the molecule does exert a major effect upon the motions governing the spin-lattice relaxation.

An important consideration in the interpretation of these results is the nature of the molecular motions responsible for the observed T_1 values. Appreciable insight into this question may be gained by considering

[7] P. S. Hubbard, Phys. Rev. **109**, 1153 (1958), and prior work cited therein.
[8] J. G. Powles and D. Cutler, Arch. sci. (Geneva) **12**, 135 (1959).
[9] E. O. Stejskal and H. S. Gutowsky, J. Chem. Phys. **28**, 388 (1958).
[10] H. S. Gutowsky and G. E. Pake, J. Chem. Phys. **18**, 162 (1950).
[11] E. O. Stejskal, D. E. Woessner, T. C. Farrar, and H. S. Gutowsky, J. Chem. Phys. **31**, 55 (1959).

the minimum values of T_1. Equation (1) predicts a minimum value for T_1 when $\omega_0\tau_c=0.6158$. Moreover, the constant A can be evaluated from the relevant internuclear distances and the correlation function describing the dynamic process to which the relaxation is attributed.[1] In this manner, one predicts,[9] for a resonance frequency of 20 Mc, a value of about 10 msec for a T_1 minimum produced by random tumbling of CH_3 groups, and 20 msec for CH_2 groups. If one assumes that the T_1 observed for *n*-butyl alcohol is an average of that for three protons in a methyl group and six protons in three CH_2 groups, random molecular tumbling would give a T_1 minimum of 17 msec. This predicted value is significantly less than the observed minimum of 26 msec. However, restriction of the motions to random reorientations about axes perpendicular to the interproton vectors increases the predicted T_1 by a factor[9] of $\frac{4}{3}$, giving a value of 23 msec, which is in satisfactory agreement with experiment.

This type of restricted rotation model can be extended successfully to the results for *iso*-butyl alcohol. In this case, two relaxation processes are operative, one producing the minimum T_1 of 38 msec observed at about 180°K, and the other causing the further decrease to 28 msec at 158°K, the lowest temperature at which T_1 was measured in the liquid. These results can be explained in a manner very similar to those found for solid *t*-butyl chloride.[11] The "high temperature" minimum of 38 msec is much too large for random molecular tumbling, but is reasonable for restricted reorientations of the heavy atom skeleton about the C—O and C_2C—C bonds. The further decrease in T_1 at lower temperatures is assigned to reorientations of the methyl groups about their threefold axes.

The T_1's observed for the four alcohols are almost all on the high-temperature, high-frequency side of the minimum. That is, τ_c is generally too short to produce the optimum relaxation. Therefore, it is of interest that the *sec*- and *tert*-butyl alcohols, which have considerably larger activation energies than the *n*- and *iso*-butyl alcohols, do not exhibit T_1 minima, while the latter do. This means that the frequency factor in the Arrhenius equation describing the motions for the *sec*- and *tert*-butyl alcohols must be larger than the factor for the *n*- and *iso*-butyl alcohols, in order to compensate for the differences in E_a which would otherwise increase τ_c enough to give T_1 minima for the *sec*- and *tert*-butyl alcohols. In fact, a careful intercomparison of the T_1 curves in Figs. 1–4 indicates that the frequency factors for the relaxation process increase in the sequence *n*-butyl<*iso*-butyl<*sec*-butyl<*tert*-butyl, which is the same order as was found for the activation energies.

The frequency factors provide an indirect confirmation of the restricted reorientation model proposed to explain the T_1 minima observed. In order to see this, let us compare the *n*- and *tert*-butyl alcohols. The cross-sectional area of the *tert*-butyl group is two or three times as large as that of an extended, "straight" *n*-butyl chain. Therefore, one would expect a larger E_a for rotation of the *tert*-butyl group about the C—O bond than for the *n*-butyl group, as observed. However, the *n*-butyl group is relatively flexible and will not rotate easily unless it is extended rather than bent or coiled. Therefore, there will be a large entropy of activation and a low apparent frequency factor for the *n*-butyl group reorientation, but not for the rigid and highly symmetrical C_3C framework of the *tert*-butyl group. This too agrees with experiment.

Mention was made earlier of the T_1 measurements by Powles and Cutler[8] on a series of primary alcohols at room temperature. Their T_1 value for *n*-butyl alcohol agrees closely with the value reported here. They also measured the diffusion coefficient for the alcohols with results which led them to suggest that motions of the links of the carbon chain determined the spin relaxation and the diffusion. However, more recent measurements on three primary alcohols,[12] including *n*-butyl, indicate that the earlier diffusion coefficient measurements are in error, reopening the question of any relation between diffusion and spin relaxation. Our results suggest that any such relation is a relatively indirect one.

Comparison of Spin-Lattice and Dielectric Relaxation

It is of interest to compare the results in the preceding section with the dielectric relaxation time studies of Dannhauser and Cole.[2] They found that two dielectric dispersions could be resolved for the *n*-butyl and *iso*-butyl alcohols. The primary dispersion occurs at the lower frequency, and is Debye-like in character, indicating that it is the result of a single process or motion. The second dispersion occurs at higher frequencies and was observable only at low temperatures, just below the melting point in the supercooled liquid. When the high-frequency dispersion is plotted after the manner of Cole and Cole,[13] the complex dielectric constant loci show a depression angle of about 20°, indicating that there is a distribution of motions responsible for the dielectric relaxation.

The principal, low-frequency dispersion must be due to motion of the hydroxyl group, for that is where the electric moment of the molecule is situated. Dannhauser and Cole proposed that the process involves reorientation of the hydroxyl moments by rupture of the intermolecular hydrogen bonds and subsequent formation of a new bond with the oxygen of another molecule. The temperature dependence of the low frequency relaxation time τ_{D_1} does not follow a simple rate process at temperatures near the melting point, indicating the onset of local structure in the liquid, which ultimately develops into the glassy state. At high temperatures,

[12] D. W. McCall and D. C. Douglass, J. Chem. Phys. **32**, 1876 (1960).

[13] K. S. Cole and R. H. Cole, J. Chem. Phys. **9**, 341 (1941)

the process is simple and activation energies can be evaluated. The results,[2] included in Table I, lie in the range 6 to 8 kcal/mole, and are comparable with hydrogen bond energies. The values are larger than those obtained from the spin-lattice relaxation, but they show the same trend, namely *n*-butyl<*iso*-butyl<*sec*-butyl<*tert*-butyl. Therefore, it appears that the molecular configuration has a similar effect upon the dielectric and spin-lattice relaxation, E_a being larger for the less eccentric groups.

Unfortunately, all of the available measurements of the high-frequency relaxation time τ_{D_2} lie in the temperature range where there are major departures from simple rate processes. Dannhauser and Cole[2] suggested that discussion of these be postponed until data at higher frequencies and temperatures were available. However, similar results for ethyl and iso-propyl alcohol have been ascribed[14] to reorientation of the oxygen-alkyl group moment during the shift of the hydrogen bond from the electron orbital of the bridged oxygen atom to the other orbital not used by either the alkyl group or the proton of the alcohol molecule.

A detailed comparison of the correlation times is possible for *n*-butyl alcohol. One can evaluate τ_c, for the spin-lattice relaxation, as a function of temperature by using the relation that at the T_1 minimum $\omega_0\tau_c=0.6158$ and assuming that $\tau_c=\tau_0\exp(E_a/RT)$. Also, it is known that if one mechanism is responsible for both the spin-lattice and dielectric relaxation the correlation times are related, namely $3\tau_c=\tau_D$. In this manner, values of τ_D were calculated for *n*-butyl alcohol from the T_1 values. These values are given in Fig. 5, as a function of reciprocal temperature, from 158.5°K to 250°K. Also given in the figure are values of τ_{D_1} and τ_{D_2} obtained in the dielectric relaxation studies.[2]

It is seen that the curve for τ_D is quite distinct from the curves for both τ_{D_1} and τ_{D_2}, indicating that different molecular motions are involved in the three relaxation processes. Moreover, the apparent frequency factor for the spin-lattice relaxation is somewhat smaller than that for the primary dielectric dispersion. This is what one would expect, because the entropy of activation for rotation of the butyl chain about the C—C and C—O bonds should be greater than that for the breaking and making of the hydrogen bonds.

General Comments

The restricted rotational motions proposed to account for the spin-lattice relaxation are compatible with the dielectric relaxation studies and with what is known about the molecular association of the alcohols by the hydrogen bonding. It is significant that larger values of E_a are found from the dielectric relaxation than from the spin-lattice relaxation. Therefore, it is reasonable to postulate that the hydrogen bonding is strong enough to "tie down" the hydroxyl end of the molecules and limit the motions of the alkyl groups primarily to the less hindered reorientations about the C—O and C—C bonds.

This introduces an important point not previously commented upon. The association equilibrium, $nA \leftrightarrows A_n$, where A represents the monomeric alcohol molecule, is itself temperature-dependent. Therefore, it is probable that the apparent activation energies include a temperature-dependent term. For relatively short temperature intervals such a term can be absorbed in the apparent activation energy, E_a, which is the linear slope calculated from the $\log T_1$ or $\log\tau_D$ versus $1/T$ curves. Over larger temperature intervals, the temperature dependence of the activation energy becomes readily discernible, as in Figs. 3 and 4, for the *sec*- and *tert*-butyl alcohols. While this interpretation of the curvature is probably qualitatively correct, more detailed studies are required to answer such quantitative questions as why the curve for *sec*-butyl alcohol is concave upwards while that for *tert*-butyl alcohol is concave downwards.

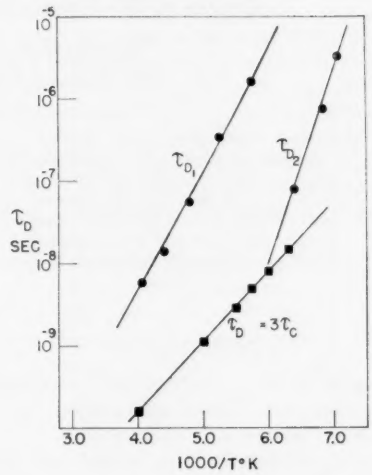

FIG. 5. Temperature dependence of the dielectric relaxation times τ_{D_1} and τ_{D_2} for *n*-butyl alcohol (Dannhausser and Cole, footnote 2) compared with τ_D calculated from the observed proton spin-lattice relaxation time.

[14] F. X. Hassion and R. H. Cole, J. Chem. Phys. **23**, 1756 (1955).

Origin of the Green Bands in the Boron-Oxygen System*

W. E. KASKAN, J. D. MACKENZIE, AND R. C. MILLIKAN

General Electric Research Laboratory, Schenectady, New York

(Received July 28, 1960)

A study has been made of the effect of oxygen on the intensity of absorption in the green or "*fluctuation*" bands by the gas phase in equilibrium with $B_2O_3(l)$. The reaction which forms the substance responsible for the bands from $B_2O_3(l)$ in the presence of oxygen was found to be 70 kcal/mole endothermic, in the range 1660–1950°K, in agreement with other work. At constant temperature the absorptivity was found to depend on the $\frac{1}{4}$ power of the oxygen pressure. This is interpreted as evidence that the absorbing species is BO_2. The oscillator strength of the transition is estimated as 0.003.

I. INTRODUCTION

THE green bands or "fluctuation" bands, from systems containing boron and oxygen have been known for a long time. They have been observed in flames, arcs, discharges, and afterglows.[1] Recently Margrave and co-workers have studied these bands in both emission and absorption in the gas at equilibrium with liquid B_2O_3 at high temperatures.[1–3] From measurements on a tube open to the atmosphere, they determined that the heat of formation of the source of these bands with respect to liquid boric oxide is in the range from 60–90 kcal/mole.[1,3] Furthermore, Soulen has stated that the bands appear even when no oxygen is present.[1] From these data it was concluded that the bands are due to $B_2O_3(g)$ since the heat of vaporization of B_2O_3 in this temperature range (1500 to 2000°K) is known to be about 85 kcal/mole.

On the other hand, Kaskan and Millikan[4] have made observations on the green bands in trimethyl borate-air flames and have concluded that they cannot be due to $B_2O_3(g)$. This conclusion was based in part on the fact that the bands were much weaker in rich flames than in lean, and in part on the fact that the molecule responsible for the bands behaved like a free radical. They concluded that the simplest possibility was the triatomic molecule BO_2.

The disagreement between these two sets of observations might be the result of the weak dependence of the formation of BO_2 from liquid B_2O_3 on the oxygen concentration. The reaction would be

$$\tfrac{1}{2}B_2O_3(l)+\tfrac{1}{4}O_2\rightarrow BO_2, \qquad (1)$$

for which ΔH would be about 65 kcal/mole if the heat of formation of BO_2 were taken as -85 kcal/mole,[4] as previously suggested. It was with this point in mind that the present experiments were undertaken and the principal purpose of this work was to investigate the effect of O_2 on the intensity of the green bands over liquid B_2O_3.

II. EXPERIMENTAL

A. Preparation of the Sample

Mallinckrodt A.R.-grade H_3BO_3 was first dehydrated by the gradual heating of the charge in a platinum crucible to about 1000°C until a bubble-free melt was obtained. Dry N_2 (~2 ppm H_2O) was then allowed to bubble through the melt via a $\frac{1}{8}$-in. i.d. platinum tubing for 4 hr at 1300°C. At this stage of the dehydration treatment, the water content was estimated to be less than 0.1% by infrared analysis.[5] Spectrographic analysis indicated that the upper limits for Li, Na, Ca, Pt, Pb, Sn, and Fe were 0.001% for K, Rb, Sr, and Ba, 0.01%, and for Cs 0.1%. A final vacuum dehydration treatment was made by heating the liquid B_2O_3 for 8 hr at 900–1000°C and at a pressure of about 10^{-6} mm.

The dehydrated B_2O_3 was then transferred to a semicylindrical platinum boat ($2\frac{1}{2}$ in. long, $\frac{5}{8}$ in. wide and $\frac{1}{4}$ in. deep giving an exposed area of 10 cm^2) in a dry box and stored in dry N_2 before use.

In the present experiments, the boat was placed in the center of a Morganite "Impervious Mullite" tube of length 22 in. and i.d. $\frac{3}{4}$ in. The latter was in turn placed inside a horizontal Pt-40% Rh resistance furnace of length 12 in. and i.d. $1\frac{1}{4}$ in. Temperature was controlled by a Variac transformer and measured by a Pt-10% Rh thermocouple placed in between the Mullite and the furnace tubes. The two ends of the Mullite tube were sealed onto glass tubings of similar diameter which were in turn connected to adaptors having side arms for gas flow and flat end windows via standard ground-glass joints.

Most of the observations were made with atmos-

* This research was partially supported by the U. S. Air Force, Aeronautical Research Laboratory, Wright Air Development Center.

[1] For a recent review, as well as for other matters pertinent to the present investigation, see J. R. Soulen, Ph.D. thesis, University of Wisconsin, 1955. (University of Michigan Microfile Publication No. 16 212, University of Michigan, Ann Arbor, Michigan.)

[2] J. R. Soulen, P. Sthapitanonda, and J. L. Margrave, J. Phys. Chem. **59**, 132 (1955).

[3] J. R. Soulen and J. L. Margrave, J. Am. Chem. Soc. **78**, 2911 (1956).

[4] W. E. Kaskan and R. C. Millikan, J. Chem. Phys. **32**, 1273 (1960); Eighth Combustion (International) Symposium (to be published).

[5] J. D. Mackenzie, J. Phys. Chem. **63**, 1875 (1959).

pheres of oxygen, argon, or mixtures of the two. Oxygen (99.2%) and argon (99.99%) were taken directly from cylinders, metered with critical flow orifices, combined, and passed through a dry-ice trap before reaching the furnace. A bypass was provided so that the flow rate through the furnace could be varied, and the effluent gas from the furnace was bubbled through an oil trap in order to monitor the flow. Whenever a change in atmosphere was made, the new gas was flushed through the furnace for several minutes, at a rate sufficient to displace all of the gas in the furnace in 10–20 sec, until a steady state was reached, as indicated by constancy of the absorption. Then the flow rate was cut to about one bubble/sec and the observation was only made when the (new) steady state was reached.

B. Optical Arrangement

Light from a tungsten strip filament lamp was collimated by a lens and passed down the axis of the tube, after which it was gathered by another lens and focussed on the slit of a Jarrell-Ash 0.5-m Ebert grating monochromator. The lamp was operated at a brightness temperature of 2600°K in order to ensure that the bands were always reversed. Diaphragms were placed at both ends of the furnace to limit the beam of light to the center of the tube and to minimize light from the furnace walls at the slit. Slits of 10-A bandpass were used with the monochromator in order to smear the absorption in a band to a single peak. For convenience, all measurements were made with the strong 5470 A band, since all of the bands appear to behave similarly.[1,2,4]

Since the band contains many strong lines which stand out above the average absorption, the use of the wide slits should cause deviations from Beer's law at high absorption. In spite of this, the wide slits were used because of the increased reproducibility they afforded. Most of the measurements involved less than about 30% absorption, so that this error should not be too serious.

In the initial arrangement, a monitor beam was provided which passed from the lamp to the monochromator without going through the furnace. This proved to be useless because of the slow deposition of a whitish deposit on the windows. In order to obtain the absorption, it was necessary to adopt a procedure whereby the intensity which would have been transmitted without absorption (but with scattering) could be determined. This was done in the following way. First the spectrum was scanned from 5300 to 5700 A for each measurement. These two wavelengths are about halfway between the peak of the observed band and those of the other strong bands lying on either side of 5470 A, and should be only weakly absorbed, if at all. The absorption at 5700 A was measured in a case corresponding to very strong absorption at 5470 A (~50%) by observing the change in transmission when the gas above the $B_2O_3(l)$ was changed from pure argon to pure oxygen, and found to be about 8%. In reducing the data, it was assumed that there was always an absorption at 5700 A in proportion to that observed at 5470, and the unabsorbed, i.e., incident minus scattered, intensity at 5700 A was corrected accordingly. Thus, the incident intensity at 5470 A was calculated from the corrected I_{5700} and that spectral distribution for the lamp which had been observed before the windows became clouded.

Even after this had been done there remained one source of error in that the ratio of intensities, I_{5700}/I_{5470}, without any absorption, had increased by 6% in the period during which the experiments were performed. This is presumably due to stronger scattering at the lower wavelengths by the window deposit. No correction for this effect was made, since the rate of clouding of the windows was unknown. In both runs however, the low absorption experiments, in which knowledge of the unabsorbed intensity is critical, were done first while the windows were still fairly clear so that it is felt that this source of error was not serious.

III. RESULTS

Two runs were made, each with a different B_2O_3 sample in a different tube. In the first run the furnace was heated with a flow of dry argon through it, up to a temperature of 1660°K. At this point a very small absorption was observed at 5470 A, amounting to perhaps 1 or 2%. Then the gas through the furnace was changed to pure oxygen while the monochromator was set on the peak of the 5470 band. Within a few seconds of the time that oxygen entered the furnace, there was an abrupt increase in absorption to about 10%. The absorption continued to increase slowly for several minutes after this before reaching a steady state. This behavior was generally observed whenever the oxygen content of the purging gas was increased. The effect was found to be reversible, but with the difference that when switching from a gas of high to one of a lower oxygen content, the time to reach a steady state was much longer, amounting to in some cases as much as 15 min. This qualitative experiment proves that O_2 has an effect on the intensity of absorption without showing precisely what the effect is. The recordings obtained are illustrated in Fig. 1.

The absorption in the 5470 band was measured as a function of the partial pressure of oxygen in oxygen-argon mixtures, the total pressure always being 1 atm. The data are shown in Fig. 2 where the logarithm of the absorptivity is plotted against the logarithm of the partial pressure of oxygen. The absorptivity is defined as $\ln I_0/I$, where I_0 and I are the incident and transmitted intensities. The length of the data points show the uncertainty in absorptivity which is to be expected from the uncertainty in the intensity measurements alone. In no case did the absorption amount to more than 30% so that Beer's law should be approximately

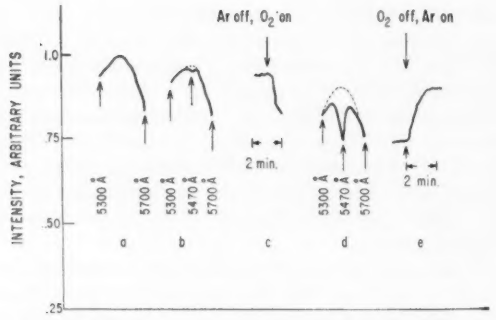

FIG. 1. Sample recordings, traced from the original. Photocell noise of about 2% of signal not reproduced. (a), (b), and (d) are scans from 5300 to 5700 A, and (c) and (e) are recordings of the transmitted intensity at the band peak, 5470 A, with time increasing left to right. Here (a) shows the spectral distribution of the lamp through the furnace with the sample in argon below 1500°K; (b) shows the small peak observed with the sample in argon at 1750°K; (c) shows the abrupt decrease in transmission at 5470 A when the argon was replaced with oxygen; (d) is the scan of the spectrum when the steady state was reached after (c) (the dotted line is the reconstruction of the no-absorption distribution); (e) shows the increase in transmission at 5470 A observed after (d) when the oxygen was replaced with argon. The general decrease of transmission with time is due to the fogging of the windows.

obeyed. It can be seen that although there is considerable scatter, the data fit the form required by reaction (1).

The temperature dependence of the absorption in the presence of pure oxygen was then investigated. Observations were made first at the lower temperatures and the furnace was flushed with pure argon while being adjusted to the next temperature. It was observed that the residual absorption peak, which remained even after flushing for some time with argon, increased with increasing temperature, until at 1950°K it amounted to about 10%. It was not clear whether this was really characteristic of an oxygen-free system, because at the high temperature the falling off of the absorption upon the removal of oxygen in the gas stream was quite slow, so that a steady state in argon

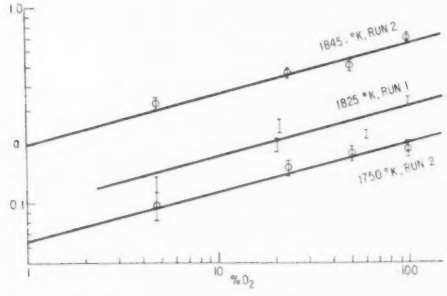

FIG. 2. Log-log plot of the absorptivity α ($=\ln I_0/I$) of the 5470 band against percent O_2 in O_2–A mixtures at 1 atm. Uncircled points are run 1 and circled points run 2. Height of data points indicates uncertainty due to photocell noise alone.

may not have been reached. In each case, however, the increase in absorption was quite abrupt when switching from argon to oxygen.

The temperature dependence is shown in Fig. 3. The errors in absorptivity are indicated as in Fig. 2, and the temperatures are those measured at the center of the furnace. Since the absorptivity is a measure of density, it has been multiplied by $T/1665$ to convert it to a quantity proportional to pressure. It is seen that the data conform to a straight line whose slope corresponds to a heat of reaction of 70 kcal/mole. This is consistent with the findings of Soulen and Margrave,[3] which were apparently obtained with a furnace open to the atmosphere.[1]

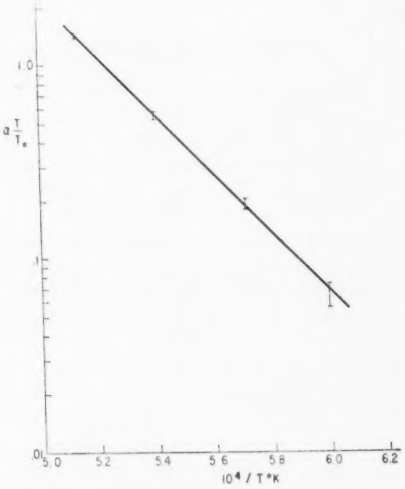

FIG. 3. Semilog plot of the function $\alpha T/T_0$ against $10^4/T$, where α is the absorptivity ($\ln I_0/I$) of the 5470 band in the presence of pure oxygen, T is the temperature measured in the center of the furnace, and T_0 is 1665°K. Height of the data points is the uncertainty due to photocell noise alone.

After these experiments had been completed, observations were made with dry air, moist argon, and moist oxygen. The dry air point (21% O_2) is shown in Fig. 2. Moisture was added by bubbling the feed gas through water at 24°C. Before the addition of water was made, the furnace was flushed for some time with dry argon. At a temperature of 1850°K a residual absorption of about 5% remained under these conditions. When the feed gas was switched to moist argon, this absorption nearly disappeared. After this the furnace was purged with moist O_2 and the absorption appeared strongly. A measurement of this absorption showed it to be within experimental error the same as dry oxygen alone, so that it is not shown.

When the tube and sample of run 1 were examined after the experiment, it was found that the B_2O_3 had either spilled or evaporated to such an extent that the platinum boat was glued to the furnace, and the furnace

walls in the vicinity of the boat appeared to be coated with B_2O_3. Thus, the exposed area of liquid B_2O_3 was probably considerably more than that estimated previously.

On reducing the data for run 1, it was felt that the time to reach a steady state on changing feed gas composition had been underestimated, particularly in the oxygen-dependence part of the run. For this reason a second run was made using a new sample in a second tube. The procedure was similar to that in the first run, with measurements being made at the lower temperature first, starting with the lower oxygen concentrations. Several times, however, the purge gas was changed to pure argon to check the reversibility of the oxygen effect, with the same result as previously. In run 2, however, it was observed that at 1850°K, when the oxygen content was increased at the higher concentrations, the absorption would overshoot, and then slowly decrease to a steady value. In the worst case about 15 min were required to reach the steady state. There was no noticeable temperature change associated with the overshoot.

The data for run 2 are also shown in Fig. 2. These points represent the steady state which was eventually reached. It can be seen that there is less scatter than for run 1, and that the data at both temperatures conform well to a line with a slope of $\frac{1}{4}$, as would be required if BO_2 was the absorber.

IV. DISCUSSION

In interpreting the results, the assumption is made that the system was at chemical equilibrium at the time the measurements were made. That this is probably not entirely justified is indicated by the overshoot observed in the absorption when the oxygen content of the purging gas was suddenly increased. The appearance of the tubes after the experiments indicates some transfer of B_2O_3 from the boat to other parts of the tube. It is conceivable that some B_2O_3 diffused upstream and deposited on the walls of the tube during a low oxygen measurement, and then was rapidly removed as the oxygen concentration was increased, giving rise to an increased optical depth of the absorber. On the other hand, it is conceivable that a cloud of particles may have condensed and scattered light from the beam. Such clouds have been observed in a system similar to the present one.[6] The presence of such a cloud would not have affected the results, since the spectrum was scanned in each case and the measured absorption shown to be due to the 5470 A band, and not to scattering. In any case, the data presented have been obtained in a consistent manner so it is felt that they can be interpreted by assuming that equilibrium was reached.

These experiments clearly show the effect of oxygen on the formation of the substance which is responsible for the green bands. They further show that the concentration of this substance depends on the $\frac{1}{4}$ power of the O_2 pressure. This is exactly what one should expect with the green bands arising from BO_2. One can only speculate that this behavior has not been previously observed because: (a) The bands are not strongly dependent on the O_2 pressure and (b) oxygen apparently is removed only with difficulty once it has been admitted into the furnace. The effect of water vapor on the intensity of the bands shows that the substance responsible for them does not contain hydrogen, which of course was expected. The decrease in intensity of absorption when water vapor was added is probably to be ascribed to the reaction

$$H_2O+BO_2 \rightarrow HBO_2+OH. \qquad (2)$$

Finally, the heat of formation of BO_2 which can be deduced from the heat of reaction (1) as obtained from Fig. 3 is -74 kcal/mole in satisfactory agreement with the value of about -85 which would have been predicted from the measurements made in flames.

It is of interest to estimate both the amount of BO_2 present and the oscillator strength of the green bands. The thermal functions of BO_2 have been computed[7] by assuming, by analogy with the known structure of the isoelectronic molecule[8,9] CO_2^+ that: BO_2 is linear; its vibrational frequencies are 1400, 1100, and 600 cm^{-1} for the unsymmetric stretch, symmetric stretch, and bending vibrations, respectively; the ground state is $^2\Pi$ and the spin splitting is 100 cm^{-1}. From these functions and those for $B_2O_3(l)$ and O_2, the heat of formation of BO_2 as measured here, the equilibrium constant for reaction (1) was computed as a function of temperature.

TABLE I. Temperature and partial pressure of BO_2 as a function of distance from the center of the tube in the presence of pure oxygen. P_{BO_2} computed as described in text.

Distance from center, cm	T°K	P_{BO_2} (atm)
0	1845	4.0×10^{-3}
1.2	1835	3.7
2.5	1825	3.2
3.8	1804	2.6
5.1	1778	1.9
6.3	1754	1.5
7.6	1715	0.9
8.9	1660	0.45
10.1	1550	0.1

[6] D. White, D. E. Mann, P. N. Walsh, and A. Sommer, J. Chem. Phys. **32**, 481 (1960).

[7] These computations were carried out on an IBM 704 computer at the General Electric Company Flight Propulsion Division in Cincinnati, Ohio, and were supplied to us by W. G. Browne.

[8] S. Mrozowski, Phys. Rev. **60**, 730 (1941); **62**, 270 (1942); **72**, 682, 691 (1947).

[9] F. Bueso-Sanllehi, Phys. Rev. **60**, 556 (1941).

For the case $P_{O_2}=1$ atm, these are numerically equal to the BO_2 pressure in atmospheres. In Table I is shown a temperature distribution along one half the furnace for a center temperature of 1845°K (the distribution was symmetrical about the center), and the corresponding equilibrium BO_2 pressures in the presence of 1 atm of O_2. By integration, it was determined that the amount of BO_2 present in the experiment was equivalent to a 1-cm path through 7.3×10^{-3} atm of BO_2 at 300°K. This value, when combined with the peak absorption of 60%, the approximation of the band as a triangle with a base of 500 cm^{-1} wide, and the assumption that the 5470 band represents 25% of the strength of the transition, leads to an oscillator strength (or "f" number) of 0.003.

In summary, it is felt that fairly conclusive evidence has been obtained to show that the green bands are due to BO_2.

ACKNOWLEDGMENTS

The authors wish to express their gratitude to W. I. Foss and W. K. Murphy for assistance with the experimental work, and to W. G. Browne for his cooperation in computing the thermal functions.

THE JOURNAL OF CHEMICAL PHYSICS VOLUME 34, NUMBER 2 FEBRUARY, 1961

Transferability of Urey-Bradley Force Constants. VI. The Silyl Halides

JOHN OVEREND* AND JAMES R. SCHERER

Chemical Physics Research Laboratory,† The Dow Chemical Company, Midland, Michigan

(Received August 12, 1960)

Urey-Bradley force constants have been fitted, by least squares, to the observed vibrational frequencies of SiH_3F, SiH_3Cl, SiH_3Br, SiH_3I and their fully deuterated analogs. The force constants have been correlated with other molecular parameters and, in the case of the nonbonded hydrogen-halogen repulsions, have been discussed in terms of an inverse-power potential function.

INTRODUCTION

In a previous paper,[1] in which we reported Urey-Bradley force constants for the methyl halides, we remarked on the values of the carbon-hydrogen stretching force constants. These increase regularly through the series from fluoride to iodide, but the value of K_{CH} for CH_3F is quite a bit lower than is suggested by a correlation of K_{CH} vs the degree of hybridization of the carbon atom, the latter determined from the experimental values of the interbond angles. However, the fact that the carbon-hydrogen stretching force constant is strongly correlated with the hydrogen-halogen nonbonded interaction made us wonder whether this trend in K_{CH} was real or whether it arose through forcing a fit to the *UBFF*. In an attempt to shed further light on this problem we have calculated force constants for the silyl halides where one might expect the greater separation of the hydrogen and halogen atoms to result in a considerably lower nonbonded interaction constant.

We used a least-squares procedure described previously[2,3] to fit the UBFC's to the observed vibrational frequencies. Data for SiH_3F, SiH_3Cl, and SiH_3Br were taken from Newman, O'Loane, Polo, and Wilson,[4] and those for the deuterated species SiD_3F and SiD_3Cl were taken from Newman, Polo, and Wilson.[5] Linton and Nixon[6] have studied the infrared spectra of SiH_3I and SiD_3I, and we have taken the vibrational frequencies of these molecules from their assignment.

The bond lengths for the fluoride, chloride, and bromide were taken from the work cited in footnote 4, and for the iodide we used Dixon and Sheppard's[7] values. In no case does the observed geometry differ much from the tetrahedral configuration and accordingly all angles were assumed to be tetrahedral.

The potential energy was expressed in the Urey-Bradley form as

$$2V=\sum_i[2K_i'r_i\Delta r_i+K_i(\Delta r_i)^2]+\sum_{i<j}[2H_{ij}'\Delta\alpha_{ij}+H_i(\Delta\alpha_{ij})^2]+\sum_{i<j}[2F_{ij}'q_{ij}\Delta q_{ij}+F_{ij}(\Delta q_{ij})^2], \quad (1)$$

* Present address: Department of Chemistry, University of Minnesota, Minneapolis 14, Minnesota.

† Formerly Spectroscopy Laboratory.

[1] J. Overend and J. R. Scherer, J. Chem. Phys. **33,** 446 (1960).

[2] J. Overend and J. R. Scherer, J. Chem. Phys. **32,** 1289 (1960).

[3] J. R. Scherer and J. Overend, J. Chem. Phys. **32,** 1720 (1960).

[4] C. Newman, J. K. O'Loane, S. R. Polo, and M. K. Wilson, J. Chem. Phys. **25,** 855 (1956).

[5] C. Newman, S. R. Polo, and M. K. Wilson, Spectrochim. Acta **15,** 793 (1959).

[6] H. R. Linton and E. R. Nixon, Spectrochim. Acta **12,** 41 (1958).

[7] R. N. Dixon and N. Sheppard, J. Chem. Phys. **23,** 215 (1955).

TABLE I. Urey-Bradley force constants; K and F in units of md/A, H and κ in 10^{-11} ergs/(radian)^2.

	SiH_3F		SiH_3Cl		SiH_3Br		SiH_3I	
	$\bar{\phi}_i$	$\sigma\{\bar{\phi}_i\}$	$\bar{\phi}_i$	$\sigma\{\bar{\phi}_i\}$	$\bar{\phi}_i$	$\sigma\{\bar{\phi}_i\}$	$\bar{\phi}_i$	$\sigma\{\bar{\phi}_i\}$
K_{SiH}	2.580	0.085	2.640	0.074	2.692	0.047	2.702	0.037
K_{SiX}	4.752	0.249	2.492	0.321	2.020	0.292	1.618	0.204
H_{HX}	0.353	0.130	0.311	0.172	0.360	0.045	0.275	0.123
H_{HH}	0.385	0.032	0.395	0.024	0.429	0.028	(0.400)	...
F_{HX}	0.288	0.123	0.213	0.132	(0.190)	...	0.137	0.085
F_{HH}	0.040	0.029	0.042	0.022	(0)	...	0.027	0.005
κ[a]	0.114	0.072	0.048	0.039	(0)	...	0.052	0.020

[a] The values of κ have been scaled by a factor of $81/32\sqrt{2}$ as described in footnote 1, and consequently are not directly comparable with those given in footnote 8.

TABLE II. SiH_3F and SiD_3F. Observed frequencies, best estimates, dispersions, and errors in cm^{-1}.

Mode		ν_{obs}	$\bar{\nu}_i$	$\sigma\{\bar{\nu}_i\}$	e_i	ν_{obs}	$\bar{\nu}_i$	$\sigma\{\bar{\nu}_i\}$	e_i
A_1	ν_1	2206	2209	16	−3	1577	1572	11	5
	ν_2	990	992	18	−2	888	889	18	−1
	ν_3	872	871	18	1	704	704	16	0
E	ν_4	2196	2210	16	−14	1615	1596	12	19
	ν_5	943.4	953	19	−9.6	(764)[a]	680	12	84
	ν_6	728.1	722	15	6.1	549	554	13	−5

[a] This frequency is an erroneous estimate; see text.

TABLE III. SiH_3Cl and SiD_3Cl. Observed frequencies, best estimates, dispersions, and errors in cm^{-1}.

Mode		ν_{obs}	$\bar{\nu}_i$	$\sigma\{\bar{\nu}_i\}$	e_i	ν_{obs}	$\bar{\nu}_i$	$\sigma\{\bar{\nu}_i\}$	e_i
A_1	ν_1	2201	2208	13	−7	1581	1571	9	10
	ν_2	949	949	15	0	702	703	14	−1
	ν_3	551	552	13	−1	538	537	13	1
E	ν_4	2195	2209	13	−14	1616	1596	9	20
	ν_5	954.4	960	15	−5.6	(734)[a]	686	11	48
	ν_6	664	659	12	5	488	492	10	−4

[a] This frequency is an erroneous estimate; see text.

and again we assumed $F' = -0.1F$. After removing the dependent variables Δq_{ij} and introducing the minimum condition, the potential energy is left as a function of seven parameters, viz., two stretching force constants K_{SiH} and K_{SiX}, two bending force constants H_{HX} and H_{HH}, two nonbonded interactions F_{HX} and F_{HH} and the intramolecular tension[8] κ.

The absence of frequency data for SiD_3Br necessitates that values be supplied for some of the force constants of SiH_3Br. We first set H_{HH} and κ equal to zero, but these constraints were insufficient to admit a stable solution and our final set of force constants shown in Table I were obtained with the additional constraint that $F_{HBr} = 0.190$ md/A; this value was determined from a correlation of F_{HX} vs the Pauling electronegativity of the halogen atom. See Fig. 1. We also found that it was necessary to supply a value of one force constant in order to achieve a stable solution for SiH_3I, and we chose to constrain H_{HH} at a value of 0.400×10^{-11} erg/(radian)^2. In Tables II–V we show, for each molecule, the observed frequencies $(\nu_i)_{obs}$, the best estimates of the frequencies $\bar{\nu}_i$, the dispersions $\sigma\{\bar{\nu}_i\}$, and the errors $e_i = [(\nu_i)_{obs} - \bar{\nu}_i]$.

UBCF for the bromine derivatives of silane have been obtained previously by Murata and Kawai[9] in a treatment in which they freely transferred values from SiH_4 and $SiBr_4$. For comparison with the present results, the values they find are $K_{SiH} = 2.65$, $K_{SiBr} = 2.02$, $F_{HH} = 0.049$, $F_{HBr} = 0.140$ md/A, and $H_{HH} = 0.392$, $H_{HBr} = 0.285 \times 10^{-11}$ erg/(radian)^2.

DISCUSSION

Before discussing the values of the force constants obtained in this study, we shall pause to review the

[8] T. Shimanouchi, J. Chem. Phys. **17**, 245 (1949).

[9] H. Murata and K. Kawai, J. Chem. Phys. **23**, 2451 (1955).

TABLE IV. SiH_3Br. Observed frequencies, best estimates, dispersions, and errors in cm^{-1}.

Mode		ν_{obs}	$\bar{\nu}_i$	$\sigma\{\bar{\nu}_i\}$	e_i
A_1	ν_1	2200	2179	18	21
	ν_2	930	913	18	17
	ν_3	430	430	26	0
E	ν_4	2196	2216	19	−20
	ν_5	950.4	957	25	−7
	ν_6	632.6	647	20	−14

vibrational assignments of SiH_3F and SiH_3Cl. Newman, Polo, and Wilson,[5] rejecting the previous assignments of Andersen and Bak,[10] proposed new assignments which are consistent with the infrared spectra. We believe their assignments to be in the main part correct but in both SiD_3F and SiD_3Cl, the "best estimate" we calculate for ν_5 is quite a bit lower than their suggested value which was adjusted to fit the Teller-Redlich product rule; see Tables II and III. In both molecules we gave this frequency a low weight $(0.2/\lambda_5)$ in the least-squares refinement, and the derived force constants are not significantly affected by this disparity. In their published spectrum of SiD_3F, Newman *et al.* show a typical perpendicular-band structure at about 675 cm^{-1} as a shoulder on a stronger parallel band, and it seems reasonable to assign this to ν_5.[11] Unfortunately, it is not possible to fix this frequency with any degree of certainty wthout a rotational assignment. There is no evidence of a corresponding band in their published spectrum of SiD_3Cl although it could possibly be obscured by an impurity band at about 660 cm^{-1}.

The silicon-hydrogen stretching force constants, K_{SiH}, shown in Table I, increase slightly from fluoride to iodide, but the total range of this variation is only 0.12 md/A, which is not much greater than the dispersion and certainly much less than the 0.48 md/A range in the methyl halides. The presently accepted values of the interbond angles[4,7] are all close to 108°40′, which suggests that, if the bonding orbitals of the silicon atom are hybrids of $3s$ and $3p$ atomic orbitals, the degree of hybridization is similar for all molecules and very close to sp^3. Thus we cannot usefully display the K_{SiH} force constants in a plot against the degree of hybridization in the same way as the K_{CH} ones.

However, although the values of F_{HX} again show a regular correlation with the electronegativity of the halogen atom (cf. Fig. 1), as we expected, the silyl-halide values are much lower than the methyl-halide ones. Thus it is not inconsistent to suppose that the variations in K_{CH} and K_{SiH} are spurious, deriving entirely from variations in the force constant F_{HX} through correlations which show up in the statistical analysis. But it does seem significant that the former variations in the methyl halides should parallel the variation in the HCX bond angle, and that in the silyl halides, where there are no significant differences between the HSiX angles, the variation in K_{SiH} should scarcely exceed the dispersion.

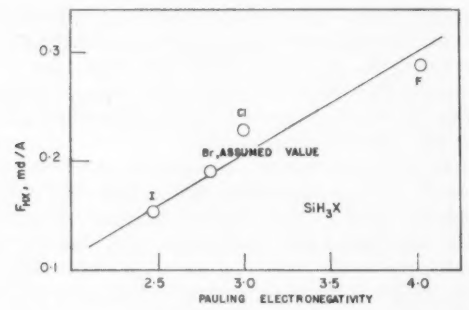

FIG. 1. Correlation of hydrogen-halogen repulsive force constant with Pauling electronegativity of halogen.

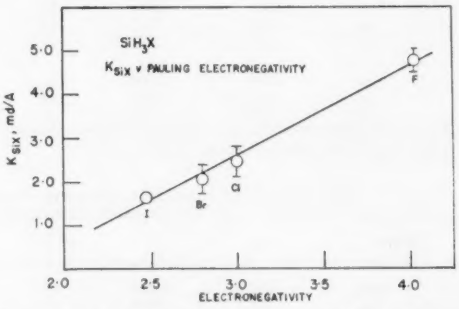

FIG. 2. Correlation of silicon-halogen stretching force constant with Pauling elecrronegativity of halogen.

We have correlated the silicon-halogen stretching force constant with the Pauling electronegativity of the halogen atom, see Fig. 2 and, as with the methyl halides, we find that the relationship is pleasingly linear.

At present, considerable interest centers on the form of the nonbonded Urey-Bradley potential. The simplifying assumption is that $F'=0.1F$ derives from a postulated potential of the form

$$V(r_{ij}) = k[r_0/r_{ij}]^9, \qquad (2)$$

but recent evidence indicates that in certain cases the exponent should be considerably lower. For example, Hisatsune[12] has found in several nitrogen oxides that F' is more negative than $-0.1F$. Such results suggest that the exponent in Eq. (2) is less than the assumed value of 9. The present force constants, taken in conjunction with those of the methyl halides, shed some further light on this problem.

[10] F. A. Andersen and B. Bak, Acta. Chem. Scand. **8**, 738 (1954).

[11] In fact, the values they took for $\Pi(\nu/\nu^1)$ in the E class vibrations of silyl fluoride and chloride, see footnote 5, Table II, are in error and should be 2.531 and 2.598, respectively (M. K. Wilson, private communication).

[12] I. C. Hisatsune (private communication).

TABLE V. SiH_3I and SiD_3I. Observed frequencies, best estimates, dispersions, and errors in cm^{-1}.

Mode		ν_{obs}	$\bar{\nu}_i$	$\sigma\{\bar{\nu}_i\}$	e_i	ν_{obs}	$\bar{\nu}_i$	$\sigma\{\bar{\nu}_i\}$	e_i
A_1	ν_1	2191.8	2197	5	−5	1575	1563	3	12
	ν_2	903	903	6	0	664	665	6	−1
	ν_3	362	363	5	−1	351.5	350	5	2
E	ν_4	2205	2213	5	8	1607	1600	3	7
	ν_5	941	942	5	−1	675	675	4	0
	ν_6	592	592	5	0	435	435	4	0

If we assume that the nonbonded repulsive potential has the general form

$$V(r_{ij}) = k[r_0/r_{ij}]^x \tag{3}$$

we find that

$$F_{ij} = [\partial^2 V/\partial(r_{ij})^2] = kx(x+1)r_0{}^x r_{ij}{}^{-(x+2)}, \tag{4}$$

and if we further assume that for any particular halogen atom, the parameters k and r_0 in Eq. (4) are the same in both the methyl halides and the silyl halides,[13] we obtain the relationship

$$(x+2) = \frac{\log[F_{ij}{}^1/F_{ij}{}^2]}{\log[r_{ij}{}^2/r_{ij}{}^1]}, \tag{5}$$

where the superscipts 1 and 2 refer, respectively, to the methyl and silyl compounds. Substituting values of F_{ij} and r_{ij} in Eq. (5) we can evaluate x for each halogen; the results are summarized in Table VI. The dispersions of the F_{ij} have been propagated through Eq. (5) to yield an estimate of the dispersion of the exponent, $\sigma\{x\}$. Unfortunately, these are so high that little significance can be attached to the results although they do suggest, like Hisatsune's results, that F' should be taken at about $-0.2F$ rather than $-0.1F$. The values of F_{ij} obtained in this analysis are predicted on the latter assumption, but in our experience, the value of F_{ij} is not particularly sensitive to F_{ij}'.

TABLE VI. The exponent of r_{ij} in the hydrogen-halogen repulsive potential; Eq. (3).

	F_{ij}		r_{ij}			
X	CH_3X	SiH_3X	CH_3X	SiH_3X	x	$\sigma\{x\}$
F	1.118	0.288	2.047	2.506	4.7	5.3
Cl	0.567	0.213	2.353	2.897	2.7	7.5
Br	0.483	0.190	2.485	3.043	2.6	...
I	0.393	0.137	2.666	3.257	3.3	8.2

[13] It is with some trepidation that we make this assumption; clearly the values of the force constants indicate that the SiH bonds are much weaker than the CH bonds, and chemical evidence shows that the silyl hydrogen is more acidic than the methyl one. However, one might argue that these phenomena are manifestations of the lower electron density about the silicon atom, and that the electron clouds of the hydrogen and halogen atoms are similar in the two molecules.

At this stage the experimental data do not warrant a more extended analysis of the repulsive potential but further studies are presently in progress, which we hope will lead to detailed information on the form of the repulsive potential.

ACKNOWLEDGMENTS

We should like to thank Dr. J. C. Evans and Dr. L. K. Frevel for helpful discussions, and Dr. N. Wright and Dr. W. J. Potts for their continued encouragement in this work.

Determination of Relative Electronic Transition Probabilities by Impact Methods

F. H. DORMAN AND J. D. MORRISON

Division of Chemical Physics, C.S.I.R.O. Chemical Research Laboratories, Melbourne, Australia

(Received July 20, 1960)

The possibility of obtaining relative electronic transition probabilities from ionization efficiency data is discussed. It is claimed that measurements of relative maximum ionization cross section lack much theoretical significance. It is shown that the factors determining the detailed form of the ionization efficiency curves need to be considered, and that when this is done it should be possible to calculate relative transition probabilities from the experimental data. An illustration is given of such a calculation for several states of excited and ionized krypton and xenon.

INTRODUCTION

WHEN the molecules of a gas undergo collisions with photons or electrons, energy may be absorbed in transitions to excited or ionized states. The primary data most easily obtained from impact studies are the ionization efficiency curves. These curves relate the amount of ionization produced per incident particle to the energy of the particles. By means of a mass spectrometer, the curve of total ionization for a given molecule may be resolved into separate curves for parent, and for fragment ions, for different degrees of charge, and sometimes for different amounts of kinetic energy possessed by dissociating fragment ions. Up to the present time, no very serious consideration has been given to the possibility that any quantitative estimate could be made, for a given molecule, of the relative probabilities of the various possible transition reactions leading to ionization. Such estimates, if they could be made, could clearly be of some theoretical interest. Except for a few measurements of relative maximum ionization efficiencies, the most recent by Fox,[1] it has been customary to use ionization efficiency curves to measure only threshold energies.

Recent developments have led to a much better understanding of ionization phenomena. The shape of the ionization probability for a single process has been determined.[2] The various excited states of a given ionic species are indistinguishable in so far as the mass spectrometer is concerned, but it has proved possible to detect their presence from the occurrence of changes in the amount of ionization, and even to resolve vibrational levels within these states.[3] Quite detailed interpretations of the efficiency curves for the single ionization of simple molecules have been made in terms of the upper-state potential energy curves. More recently, it has been shown that the shapes of ionization probability curves depend on the class of process giving rise to the ionization, and that any particular process may thereby be identified.[4] The fact that all ionization probability curves do not have the same shape reduces the significance of any comparison of maximum ionization efficiencies. The additional knowledge now available makes it reasonable nevertheless to hope that it may be possible to obtain, from impact data, some comparison of relative transition probabilities.

To do this, one must first establish that where several ionization processes can occur simultaneously, their probabilities are additive. Obviously, if competition between processes could occur, the ionization efficiency curve would not give a true picture of the relative probabilities for any reactions above the least energetic. Fortunately, if such competition did occur, it should be evident from the shape of the ionization efficiency curves, and in only two cases does there seem to be the slightest indication of it.[5] Where all the processes compared are of the same kind, the problem is then the trivial one of measuring the relative heights of a series of steps, or a set of gradients, etc. The comparison of processes of different kinds, with differing forms of the ionization probability curve, is not so obvious. A precisely similar problem is encountered in spectroscopy, in comparing the probabilities for bound-bound and bound-free transitions. It will be shown that the latter may be divided into different classes by a simple criterion, which follows naturally from the collision mechanism.

Any attempt to determine relative electronic transition probabilities from ionization efficiency curves requires that the experimental conditions of their measurement be considered carefully. Mass spectrometers are notoriously subject to discriminatory effects of various kinds, and these effects are far more serious when the over-all shape of the ionization efficiency is being examined, than when only the thresholds are of interest.

DEVELOPMENT OF METHOD

The ionization efficiency is defined, for a given ionic species, as the number of ions produced per ionizing

[1] R. E. Fox, *Advances in Mass Spectrometry*, edited by J. D. Waldron (Pergamon Press, London, 1959), p. 397 ff.; R. E. Fox, J. Chem. Phys. **33**, 200 (1960).

[2] W. M. Hickam, R. E. Fox, and T. Kjeldaas Jr., Phys. Rev. **96**, 63 (1954); K. Watanabe, *ibid.* **22**, 1504 (1954); J. D. Morrison, J. Appl. Phys. **28**, 1409 (1957).

[3] J. D. Morrison, Revs. Pure and Appl. Chem. (Australia) **5**, 22 (1955); H. Hurzeler, M. G. Inghram, and J. D. Morrison, J. Chem. Phys. **28**, 76 (1958).

[4] H. Hurzeler, M. G. Inghram, J. D. Morrison, and H. Stanton, J. Chem. Phys. **33**, 821 (1960); F. H. Dorman, J. D. Morrison, and A. J. C. Nicholson, *ibid.* **32**, 378 (1960).

[5] P. T. Smith, Phys. Rev. **36**, 1293 (1930); J. D. Morrison, J. Chem. Phys. **19**, 1305 (1951).

particle, per unit path length, per unit gas pressure. In a given apparatus, the geometry of the source is fixed, and the gas pressure is maintained constant, but neither the effective path length nor the pressure is known with any accuracy. Accordingly, all the ionization efficiencies obtainable are on a relative scale. An observed ionization efficiency curve is assumed to be made up by the sum of a number of probability curves for single processes of ionization and/or excitation, all of which lead to the same indistinguishable ionic species. Fairly satisfactory experimental grounds exist for believing that this is so, and that all processes of the same class have the same shape of ionization probability curve, at least to a first approximation.

It is possible to distinguish three separate factors which determine the form of the ionization probability curve for a given single process. The first of these, to be termed here the freedom factor, has been studied in some detail.[4,6] It is determined solely by the number of electrons liberated in the primary reaction involving transfer of energy and is related to the number of degrees of freedom available for the removal of excess energy from the collision complex. It appears to be almost, if not entirely, independent of the structure of the atom or molecule concerned, of whether the reaction was induced by photon or electron impact, or of any interaction between the separating electrons. The second factor, which will be termed the structural factor, does seem to be dependent in a not yet clearly defined way, on various molecular properties. Some of these are the mass and size of the atom or molecule being ionized, whether angular momentum has to be transferred during the collision, and the lifetime of the collision complex, while there are possibly others which have not yet been identified. The freedom factor and the structural factor are intrinsic to the process of energy transfer. The third factor is experimental, and is associated with the fact that the beam of exciting or ionizing particles is not perfectly monoenergetic, but possesses an effective energy spread.

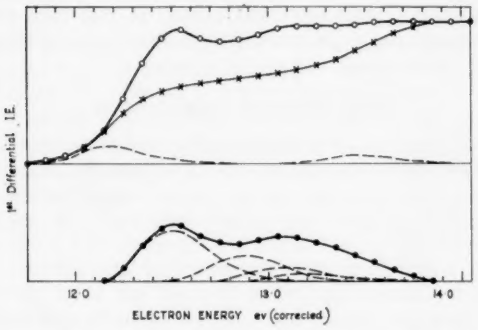

FIG. 1. Curve ○,○,○: Experimental 1st differential I.E. curve for Xe^+. Curve ×,×,×: 1st differential I.E. curve for Xe^+ assuming only two ionization processes (to give $^2P_{\frac{1}{2}}$ and $^2P_{\frac{3}{2}}$ ions). This is produced by summing two 1st differential I.E. curves for He^+ placed at the correct energies and adjusted to coincide with the Xe^+ curve at the beginning and end of the experimental curve. Curve – – –: Differential of curve ×,×,× (i.e., 2nd differential curve). The areas under the two peaks are proportional to the probabilities of the ionization processes. Curve ●,●,●: Residual curve obtained by subtracting curve ×,×,× from curve ○,○,○. Curve – – –: A series of 2nd differentials of the He^+ curve placed at the energies corresponding to the spectroscopic levels which autoionize, and adjusted so that their sum corresponds to curve ●,●,●. The areas under these peaks are proportional to the probabilities of the autoionization processes. For clarity only four curves are shown.

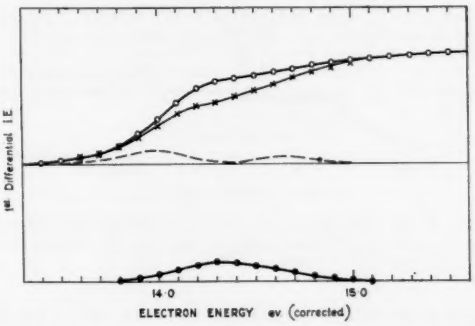

FIG. 2. Curve ○,○,○: Experimental 1st differential I.E. for Kr^+. Curve ×,×,×: 1st differential I.E. curve for Kr^+ assuming only two ionization processes, to give $^2P_{\frac{1}{2}}$ and $^2P_{\frac{3}{2}}$ ions. This is produced by summing two 1st differential I.E. curves for He^+ placed at the correct energies, and adjusted to coincide with the Kr^+ curve at the beginning and end of the experimental curve. Curve – – –: Differential of curve ×,×,× (i.e., 2nd differential curve). The areas under the two peaks are proportional to the probabilities of the ionization processes. Curve ●,●,●: Residual curve obtained by subtracting curve ×,×,× from curve ○,○,○. It is not possible to separate the contribution from the individual processes of autoionization.

For a transition to a discrete upper state with well-defined energy, it is convenient to regard the ionization probability as the integral of three functions of the ionizing energy, each dependent on only one of the three factors cited. The first of these functions, relating the probability of energy transfer to the freedom factor, is believed to be given by the nth integral[7]

$$P(E) \propto \int \cdots \int_0^E \delta(E-E_c) \cdot dE^n.$$

For $n>1$ this equals $(E-E_c)^{n-1}/(n-1)!$ when $E>E_c$, where E_c is the threshold energy for the process, $\delta(E-E_c)$ is a delta function centered on E_c, and n the freedom factor, is the number of electrons leaving the collision complex. For example, for a process of direct single ionization by electron impact $A+e \rightarrow A^+ + 2e$, $n=2$. The second function appears to be of the general form $\exp-[(E-E_c)/E_c]S$, where S, the structural factor, seems to be proportional to the total number of electrons in the molecule being ionized. The

[6] J. D. Morrison and A. J. C. Nicholson, J. Chem. Phys. **31**, 1320 (1959); F. H. Dorman, J. D. Morrison, and A. J. C. Nicholson, *ibid.* **31**, 1335 (1959).

[7] cf. S. Geltman, Phys. Rev. **102**, 171 (1956); G. H. Wannier, *ibid.* **100**, 1180 (1956).

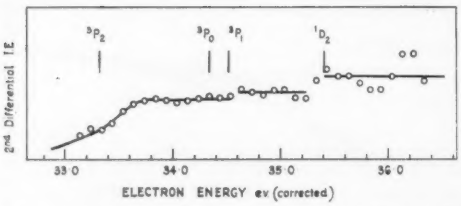

FIG. 3. 2nd differential I.E. curve for Xe^{2+} showing increases due to presence of excited states of the ion. The known states are superposed in the figure.

third is the energy distribution function $m(U)$ for the particles in the ionizing beam, and this can be determined experimentally with some measure of accuracy. One can write therefore for the ionization probability as a function of the observed energy V

$$p(V)$$

$$=\int P(E)\cdot\{\exp-[(E-E_c)/E_c]S\}\cdot m(E-V)\cdot dE.$$

Of the three functions on the rhs, the second is in all cases a comparatively slowly varying function of the energy, so that when small scale details are being considered, as for example in the immediate neighbourhood of the threshold, the first and third are by far the more important.

The ionization efficiency for a given ionic species can then be written as

$$i(V)=K_1p_1(V)+K_2p_2(V)+K_3p_3(V)+\cdots.$$

Where all the possible processes have the same freedom factor, the coefficients K_s will give a set of measures of the relative probabilities for transitions from the ground state of the neutral molecule to the various levels of that particular ion, which are closely related to the oscillator strengths as defined by spectroscopists.[8]

Where transitions with differing freedom factors are compared, it is necessary to take into account the form of the various $P(E)$. For a single transition with freedom factor zero,

$$K=\int i(V)dV$$

by definition of a δ-function and the requirement that

$$\int m(U)dU=1.$$

For the general case of a transition with freedom factor n

$$K\doteq\int_{E_c-\Delta U/2}^{E_c+\Delta U/2}\frac{d^n\{i(V)\}}{dV^n}\cdot dV.$$

The energy distribution function $m(U)$ has appreciable value only over a limited energy range ΔU, and it is therefore necessary to carry out this integration only over this energy range. The expression is an approximation because of the structural factor but the smaller S, the better this approximation. It emerges therefore that the units in which K is measured depend on the freedom factor n for the process, being relative transition probability per unit energy to the nth power. This is closely analogous to the calculation of oscillator strengths for bound-free transitions in spectroscopy, although in the latter case only processes of freedom factor unity have been treated.

It may be pointed out here that the continuum observed spectroscopically for ionization will have this usual form only for bound-free transitions with freedom-factor unity. For other bound-free transitions where the freedom factor exceeds one, as for example, double, triple ionization by photon impact, the intensity of continuous absorption above the ionization limit will be governed by precisely the same considerations which determine the threshold law for ionization.

The case of transitions to upper states which are continuous, as for example to a molecular state above its dissociation limit, may be dealt with by a slight extension of the treatment above. In this case the electronic transition probability is obtained as a function of the energy.

EXPERIMENTAL APPLICATION

The conclusions of the preceding section can now be used in the interpretation of some experimental results. Curves measured by photon impact would be more satisfactory, since the energy spread can be much

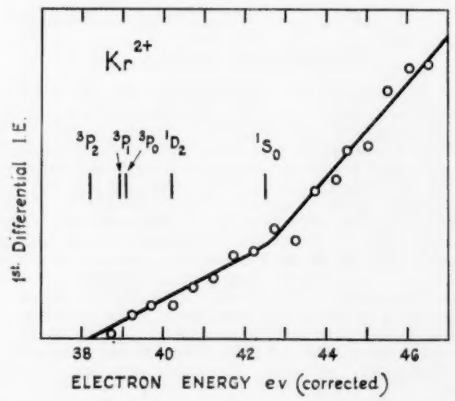

FIG. 4. 1st differential I.E. curve for Kr^{2+} showing change in gradient at an excited state of the ion. The known states are superposed in the figure.

[8] E. U. Condon and G. H. Shortley, *The Theory of Atomic Spectra* (Cambridge University Press, New York, 1953), Chap. IV; A. C. G. Mitchell and M. W. Zemansky, *Resonance Radiation and Excited Atoms* (Cambridge University Press, New York, 1934), Chap. III ff.

smaller, and since the freedom factors are all one less than for electron impact. However, no atoms have been studied in adequate detail, because of the difficulties of obtaining photons of energies greater than 11 ev. At present, most of the data recorded using electron impact involves an energy spread of 0.3 ev half-width. It will be shown that in a favorable case, a surprisingly large amount of information can nevertheless be obtained from such data.

The ionization efficiency curves for Kr^+ and Xe^+ are interesting, in that it is plain that two different kinds of processes, with differing freedom factors, are occurring simultaneously, namely, direct single ionization and autoionization. All the levels present in the neighborhood of the ionization threshold are known from spectroscopic data. They consist of the $^2P_{\frac{1}{2}}$ and $^2P_{\frac{3}{2}}$ states of the ion, and members of two series of excited states of the neutral atom lying between these.[9] The effective electron energy spread, and its effect on a process of freedom factor 2, can be obtained from the ionization efficiency curve for the reaction $He+e\rightarrow He^+ + 2e$. The attempt can then be made to approximate the observed ionization efficiency curve for Xe^+ by the curve

$$i(V)=F(E-v)=K_1 p(E-E_{c_1})+K_2 p(E-E_{c_2}) +K_3(\Delta/\Delta E)\cdot\{p(E-E_{c_3})\}+\cdots.$$

The shape of $p(E-E_c)$ is given by the curve for He^+, E_{c_1} and E_{c_2} are the ionization potentials of the $^2P_{\frac{1}{2}}$ and $^2P_{\frac{3}{2}}$ states of the Xe^+ ion, and E_{c_3}, E_{c_4}, etc., are the energies of the autoionizing states. The quantity v is included to take into account the experimental uncertainties in the absolute values of the energy scale. If a unique solution can be obtained, the coefficients K_1, K_2, etc., will give the relative transition probabilities desired.

It is more convenient experimentally and the problem is simplified if one attempts to synthesize the first differential ionization efficiency for Xe^+ by a sum made up of the first and second differentials of the ionization efficiency for He^+. The solution may proceed in either of two ways. In the first, the absolute energy scale may be fixed by the known difference between the spectroscopic ionization potentials of Xe^+ and He^+, then by a process of trial and error the values of the K's which give the best fit to the curve for Xe^+ may be calculated. The sum K_1+K_2 is fixed, and so is the upper limit to K_1. It is not necessary to use the absolute energy scale, and in the second by making use only of the known spacings of the Xe levels, the best values of the K's and the constant v can be determined. The consistency of the results found by both methods is excellent. Experimental errors set the limit to the precision with which the K's may be determined. The breakdown of the curve is shown in Fig. 1. The case of Kr^+ is much less satisfactory, because of the very close spacing of the levels. It is not possible to resolve the separate contributions due to the autoionization, and the uncertainty in the values of K_1 and K_2 is much greater. The curve is shown in Fig. 2. It is very clear that when better energy resolution can be obtained, these uncertainties will be largely removed, and it will be unnecessary to know the position of the levels beforehand.

For the case of the process $Xe+e\rightarrow Xe^{2+}+3e$, the second differential ionization efficiency consists of a series of steps, each of which can be related to a transition to a known energy state of the doubly charged ion. These is no sign of any processes with freedom factor different from 3. This curve is shown in Fig. 3. The desired transition probabilities are given by the heights of these steps. For doubly charged krypton, the scatter in the experimental points is too great to permit a satisfactory second differential to be obtained. Two straight lines can be drawn through the points for the first differential, and the intercepts of these can be related to two of the known states of the ion. The contributions of the first four levels can not be separated. The relative transition probabilities are measured by the increases in gradient at the energy states. This curve is shown in Fig. 4.

For triply and higher charged krypton and xenon, there has been no attempt to detect higher states above the lowest. The ionization efficiency curves have been fitted with curves of the form $i(V)=K(V-E_c)^k/k!$, where k is the appropriate degree of ionization ($k=$

TABLE I. Relative electronic transition probabilities as defined in text calculated from experimental data for various states of Kr and Xe. The value for the $^2P_{\frac{1}{2}}$ state of the singly charged ion is arbitrarily made to be unity for both atoms.

Charge on ion	State	Relative electronic transition probability (K) Kr	Xe	Unit
0	$6d^1(\frac{3}{2})$	4×10^{-1}	6×10^{-1}	$(ev)^{-1}$
	$7d^1(\frac{3}{2})$		3×10^{-1}	
	$8d^1(\frac{3}{2})$		1.5×10^{-1}	
	$9d^1(\frac{3}{2})$		9×10^{-2}	
	$10d^1(\frac{3}{2})$		6×10^{-2}	
	$11d^1(\frac{3}{2})$		4×10^{-2}	
1	$^2P_{\frac{1}{2}}$	2	2	$(ev)^{-2}$
	$^2P_{\frac{3}{2}}$	1	1	
2	$^3P_2$	3×10^{-2}	9×10^{-2}	$(ev)^{-3}$
	$^3P_1, ^3P_0$		1.5×10^{-2}	
	$^1D_2$		3×10^{-2}	
	$^1S_0$	2×10^{-2}	...	
3		5×10^{-6}	2×10^{-4}	$(ev)^{-4}$
4		1×10^{-10}	3×10^{-8}	$(ev)^{-5}$
5		2×10^{-13}	2×10^{-11}	$(ev)^{-6}$
6		6×10^{-16}	1×10^{-13}	$(ev)^{-7}$

[9] C. E. Moore, Natl. Bur. Standards (U. S.), Circ. 467 (1958).

$n-1$), the K's then giving the transition probabilities. The curves for $k$fold ionization must in addition be normalized by dividing each by k, to take into account the fact that multiply-charged ions require more than one electron for neutralization when they arrive at the collector of the mass spectrometer. All of the values determined have been summarized in Table I.

It is interesting to compare these results with the few data already available. Kr^+ and Xe^+ have been studied by Fox, Hickam, and Kjeldaas,[10] and Kr^+ by Frost and McDowell,[11] both using the retarding-potential-difference method. The ratio of the probabilities for transitions to the $^2P_{\frac{3}{2}}$ and $^2P_{\frac{1}{2}}$ states are listed by the former as 0.8/1.0 for Kr^+ and 2.8/1.0 for Xe^+. The curves shown by the latter seem to indicate a ratio for Kr^+ of 0.3/1.0. Fox *et al.* make the observation that autoionization is significant in Kr^+ but not in Xe^+. The rather interesting finding is made in the present work, that of the two series of excited states in Xe which might undergo autoionization, probably only one does so. This seems to be supported by a recent spectroscopic study.[12]

EXPERIMENTAL TECHNIQUE

Mass spectrometers are well known to be subject to a number of discriminatory effects, which make the accurate measurement of even relative ionization efficiencies at best a hazardous procedure. Voltage discrimination effects in the mass analyzer may be serious. They are usually minimized by using a constant value of ion-accelerating voltage, and by studying ions with differing m/e by varying the magnetic field. The methods employed to keep low the spread in energies of the ionizing electron beam may also have discriminatory effects. In this work, oxide cathodes consisting of BaO–SrO on a nickel base were used, giving trap currents never in excess of 5 μA. The electron beam and the ion repellers were pulsed at 150 kc in order to achieve relatively field-free conditions in the ionization source. This technique certainly discriminates against certain fragment ions formed with initial kinetic energy, and it is just possible that it might also affect some ions arising by autoionization mechanisms. Tests made at other values of ion-repeller pulse voltage, and at different frequencies, indicated that this was not so for the rare gas ions.

Surface conditions in the ionization source were found to be a most important factor in determining the shape of ionization efficiency curves at energies well above threshold. The procedure finally adopted was to use the ionization efficiency for Xe^+ as a test curve, this being run alternately with the other ions studied. The shape of this curve was found to deteriorate slightly even after only four or five hours of running, whereupon the source was disassembled and cleaned with abrasives. The instrument used, and the other techniques employed were the same as those described in earlier papers.[6] By using these methods, consistent results were obtained.

It is believed that if only parent ions are studied, reasonably reliable values can be obtained for the relative transition probabilities for a given ionic species. Relating the probabilities for transitions to states of the singly charged ion, to those of states of the multiply charged ion may be expected to involve a slightly greater error. The results quoted in this paper are not intended to be taken as final values, but merely as an illustration that with improved energy resolution, such measurements should become readily possible.

[10] R. E. Fox, W. M. Hickam, and T. Kjeldaas, Jr., Phys. Rev. **89**, 555 (1953).
[11] D. C. Frost and C. A. McDowell, Proc. Roy. Soc. (London) **A232**, 227 (1955).
[12] M. Ogawa (personal communication).

Stabilities of Gaseous Molecules in the Pb-Se and Pb-Te Systems*

RICHARD F. PORTER†

Department of Chemistry, Cornell University, Ithaca, New York

(Received August 8, 1960)

Mass spectrometric analyses of the vaporization products of phases near compositions PbSe and PbTe indicate that these substances vaporize primarily as molecular PbSe(g) and PbTe(g), respectively. Ion fragmentation processes originating from electron bombardment of vapors effusing from a conventional Knudsen cell interfere with quantitative determination of thermochemical dissociation energies of PbSe(g) and PbTe(g). The use of double oven-type Knudsen cells provided a means for the study of the dissociation of PbSe(g) and PbTe(g) into the gaseous elements. Dissociation energies of PbSe(g) and PbTe(g) were found to be 61.5±2.5 and 51.4±2.0 kcal/mole, respectively. The dissociation energy of $Te_2(g)$ was found to lie close to the published spectroscopic value.

RECENTLY some attention has been focused on the high temperature thermodynamic properties of metallic compounds of selenium and tellurium. Information related to one aspect, the vaporization behavior, is quite limited. The available data indicate that stoichiometry of vaporization may vary considerably from one metallic compound to another. Compounds of ZnSe, CdSe, and HgSe,[1,2] for example, vaporize by complete decomposition to gaseous elements while Bi_2Te_3 and Bi_2Se_3[3] vaporize in a complex manner with the formation of gaseous BiTe and BiSe, respectively. Inghram and Drowart[2] have reviewed the mass spectrometric work on vaporization and have suggested that the selenides and tellurides are analogous to the corresponding oxides with the expectation that the gaseous diatomic metal selenide or telluride would be less stable than the oxide.

Vapor pressure data for PbSe[4] and PbTe[5] have recently been reported. Bond energies from spectroscopic data[6,7] indicate that PbSe(g) and PbTe(g) are of sufficient stability to become important vaporization products. These energies, however, are obtained from long extrapolations of vibrational levels and are thus subject to considerable uncertainty. The present work was undertaken to provide information on the identification and stability of the vaporization products from PbSe and PbTe. In these studies, the mass spectrometric-Knudsen effusion technique was employed.

EXPERIMENTAL

For these experiments, graphite effusion cells were found to be quite satisfactory containers for PbTe and PbSe. Samples of the solid compounds were prepared by heating approximately equal molar mixtures of the components in graphite containers *in vacuo* prior to mass spectrometric observations. The mass spectrometer used for vapor analyses is a 60°, 12-inch direction focusing instrument with an electron bombardment-type ion source. Descriptions of the experimental procedure have been given previously.[8] Background ion currents, due to ionization of residual gases in the instrument, are distinguished from ions formed from the sample vapor, which occur at the same mass positions, with a movable shutter located between the effusion cell and the ion source.

Two types of effusion cells were used. For preliminary experiments, a single graphite oven of the conventional design was employed. Subsequent observations suggested the need for a double oven-type cell. Milne[9] has discussed the use of double oven cells in mass spectrometric work. The design of this cell is indicated in Fig. 1. For these latter experiments, the upper chamber of the cell was heated directly by radiation and electron bombardment from tungsten filaments. The temperature of the cooler lower portion of the cell was determined primarily by thermal conduction from the upper region. Temperatures were measured with a thermocouple fastened to a tantalum ring at the base of the upper chamber. A graphite cup with several exit holes for vapor was placed over the entrance channel to the upper oven. The purpose of this cup was to deflect vapor molecules flowing into the upper chamber and thus insure that they would undergo a number of wall collisions prior to effusion from the orifice.

* This research was supported by the United States Air Force through the Air Force Office of Scientific Research of the Air Research and Development Command under contract.

† Alfred P. Sloan Research Fellow.

[1] P. Goldfinger, M. Ackerman, and M. Jeunehomme, University of Brussels, Tech. Rept. AFf61(052)-19 (January, 1959).

[2] M. G. Inghram and J. Drowart, *Proceedings of an International Symposium on High Temperature Technology* (McGraw-Hill Book Company, Inc., New York, 1959), p. 219.

[3] R. F. Porter and C. W. Spencer, J. Chem. Phys. **32**, 943 (1960).

[4] V. P. Zlomanov, B. A. Popovkin, and A. N. Novoselova, Zhur. Neor. Khim. (English translation, The Chemical Society, London) 1231 (1959).

[5] A. S. Dashinkin and A. V. Novoselova, Zhur. Neor. Khim. (English translation, The Chemical Society, London) 1229 1959).

[6] A. G. Gaydon, *Dissociation Energies and Spectra of Diatomic Molecules* (Chapman and Hall, Ltd., London, 1953), 2nd ed.

[7] G. Herzberg, *Spectra of Diatomic Molecules* (D. Van Nostrand Company, Inc., Princeton, New Jersey, 1950), 2nd ed.

[8] R. F. Porter and R. C. Schoonmaker, J. Phys. Chem. **62**, 234 (1958).

[9] T. Milne, J. Chem. Phys. **28**, 717 (1959).

TABLE I. Ion current data for PbTe system.

Type cell	Condensed phase composition	Temp °K	$PbTe^+/Pb^+$ [a]	$PbTe^+/Te^+$ [a]	Pressure calibration (atm)	Apparent K (diss.)	Apparent ΔE_0^0 (diss.) kcal/mole
Single oven	Pb≈Te	1000	11.0	40.0	$PbTe=2.1\times10^{-4}$ [b]	9.6×10^{-7}	47.7
Single oven	Pb>Te	963	4.7	35.2	$Pb=6.3\times10^{-6}$ [c]	3.6×10^{-7}	47.9
Double oven	Pb≈Te	1129	1.9	2.3	PbTe [d]	2.0×10^{-6}	52.1
Double oven	Pb≈Te	923	17.0	14.7	$PbTe=2.1\times10^{-5}$ [b]	1.7×10^{-7}	47.2

[a] Ionizing electron energy=100 volts.
[b] Vapor pressure data from reference 5.
[c] Vapor pressure data from reference 10.
[d] Calibrated at $T=935$°K using vapor pressure data of reference 5.

With the double oven technique, it is possible to obtain a condition in which the vapor is heated to a high temperature but is at a pressure well below that corresponding to solid-vapor equilibrium.

RESULTS (PbTe)

Single Ovens

The major ion observed on electron impact of vapors from a conventional effusion cell containing PbTe was $PbTe^+$. Linear extrapolation of appearance potential curves indicates a threshold at 8.2±0.5 volts which is interpreted as an ionization potential for PbTe(g). Ions of Pb^+ and Te^+ were also observed but were always lower in ion intensity than $PbTe^+$ as indicated in Table I. A serious problem that is encountered in these experiments with single ovens is the unknown extent of ion fragmentation to form the minor ion species, Pb^+ and Te^+. Evidence that fragmentation is important is suggested by the data in Table I which show that the observed $PbTe^+/Te^+$ ratio is relatively insensitive to the presence of excess Pb in the system. Since appearance potentials for Pb^+ and Te^+ from fragmentation of PbTe(g) are expected to be close to the ionization potentials of the elements, the range of electron energy is limited for study of the atomic ionization processes. This problem of ion fragmentation was minimized by further experimentation with double ovens.

Double Ovens

Three experimental procedures were employed with double ovens. These were as follows:

(1) PbTe in upper oven and tellurium in lower oven;
(2) PbTe in upper and lower oven;
(3) PbTe and tellurium in lower oven; tellurium in upper oven.

In the first series of experiments, $Te_2(g)$ leaked into the heated upper chamber containing PbTe(s) and thus the vapor phase from PbTe was enriched with $Te_2(g)$. The effect on the $PbTe/Pb^+$ and $PbTe^+/Te^+$ ratios is shown in Table I. As indicated, the $PbTe^+/Pb^+$ ratio is increased over that found in the single oven experiments. This should be a consequence of a shift in the vapor equilibrium toward lower Pb(g) pressures. These data indicate, therefore, that a small amount of Pb(g) was present in the vapor phase in experiments with single ovens. The $PbTe^+/Pb^+$ ratio observed under conditions with excess Te_2 should set the maximum limit on the contribution of ion fragmentation to Pb^+ from PbTe(g).

In the second series of experiments, a small sample of PbTe was evaporated from the upper chamber to obtain a sensitivity calibration of the mass spectrometer. The temperature of the cell was then raised until $PbTe^+$ was again observable from vapors originating in the lower chamber. A typical mass spectrum of vapor effusing from the upper chamber under these conditions is indicated in Table I. The ratios $PbTe^+/Pb^+$ and

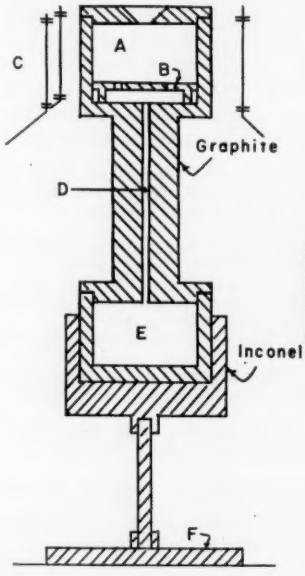

FIG. 1. Double oven assembly. A, upper chamber; B, deflection cup; C, tungsten filaments; D, gas channel; E, lower chamber; and F, base plate insulated to support high voltage.

$PbTe^+/Te^+$ were found to be decreased considerably from those observed in single oven experiments. This effect is attributed to an increase in the degree of dissociation of PbTe(g). Ion currents of Pb^+ and Te^+ are now assumed to be proportional to the partial pressures of Pb(g) and Te(g). The near equality of Pb^+ and Te^+ indicates that Pb and Te are in nearly equal concentration as is to be expected by the dissociation mechanism.

In the final series of experiments, tellurium vapor from the upper chamber was used for a sensitivity calibration with Te_2^+. The cell was then heated to a higher temperature until Te_2^+ and Te^+ reappeared. At still higher temperatures, Pb^+ and $PbTe^+$ appeared. Typical ion current data for Te_2^+/Te^+ ratios are given in Table II and subsequent data including Pb^+ and $PbTe^+$ are given in Table III. The increase in Te_2^+/Te^+ as a function of cell temperature clearly shows that $Te_2(g)$ is dissociating in the upper chamber (the Te_2^+/Te^+ ratio observed for pure tellurium in single ovens was about 20 for 100-volt ionizing electrons).

TABLE II. Thermochemical data for $Te_2(g)=2\,Te(g)$ from double oven experiments.

Temp. °K	Te_2^+/Te^+	$P_{Te_2(g)}$ (atm)	K_{diss}	ΔS_T° entropy units	ΔE_0° kcal/mole Te_2
1019	6.2	2.5×10^{-6}	1.3×10^{-6}	24.5	51.2
1097	1.3	7.1×10^{-6}	8.6×10^{-6}	24.6	51.0
1151	0.65	5.3×10^{-6}	1.4×10^{-5}	24.6	52.4
1171	0.87	3.6×10^{-6}	1.7×10^{-5}	24.7	53.0

HEATS OF DISSOCIATION OF $Te_2(g)$ AND PbTe(g)

The heat of dissociation of PbTe(g) was evaluated by third-law procedures involving the thermodynamic cycle:

$$Te_2(g)=2Te(g), \qquad \Delta H_1 \qquad (1)$$

$$Pb(g)+Te_2(g)=PbTe(g)+Te(g). \qquad \Delta H_2 \quad (2)$$

The heat of dissociation of PbTe(g) is $\Delta H_1-\Delta H_2$. For reaction (1) we may express

$$K_{eq}=P_{Te}^2/P_{Te_2}.$$

From the relationship of ion current to pressure, we have

$$P_{Te(g)}=c(P_{Te_2(g)})(I_{Te^+}/I_{Te_2^+}),$$

where c is a constant incorporating relative ionization cross sections of Te and Te_2, and ion detection efficiencies of Te^+ and Te_2^+. For calculations involving dimer-monomer relationships, this constant is assumed to be approximately 1.4.[10] For reaction (1), values of ΔS_T° were taken from the tabulations of Stull and Sinke.[11] These values, combined with $\Delta F^\circ=-RT\ln K_{eq}$ and heat capacity data,[11] give ΔE_0° values listed in Table II. From these data, the value of ΔE_0° recommended is 52.0±2.0 kcal/mole Te_2. For reaction (2), we have

$$K_{eq}=(P_{Te})(P_{PbTe})/(P_{Pb})(P_{Te_2})$$
$$\approx(I_{Te^+})(I_{PbTe^+})/(I_{Pb^+})(I_{Te_2^+}).$$

This relationship is assumed to hold since geometrical and ion sensitivity terms cancel uniquely and ionization cross section and ion detection efficiency terms cancel to a good level of approximation. Values of ΔS_T° for reaction (2) were obtained from tabulated entropies[11] for Pb, Te, and Te_2 and a calculated entropy for PbTe. This latter quantity was calculated with a vibration frequency, $\omega=212$ cm^{-1},[7] and an estimated Pb—Te bond distance of 2.9 A. For reaction (2), we find $\Delta S^\circ_{1000-1200}=+3.0\pm0.5$ entropy units. Experimental values of K_{eq} for reaction (2) were found to be temperature insensitive and ranged between 2.4 and 4.5 in the temperature range studied. Combining free energy and entropy increments gives, for reaction (2), $\Delta H_T^\circ=+0.6\pm1.0$ kcal/mole. The dissociation energy of PbTe is then calculated to be $\Delta E_0^\circ=51.4\pm2.0$ kcal/mole.

TABLE III. Typical ion current data observed from double oven experiments (sample of PbTe+Te in lower chamber).

Temp. °K	I_{Te^+}	I_{Pb^+}	$I_{Te_2^+}$	I_{PbTe^+}
1171	100	23	87	47
1151	100	22	65	63

An alternative method for evaluation of the dissociation energy of PbTe was to compute directly K_{eq} for the reaction $PbTe(g)=Pb(g)+Te(g)$ from the partial pressures of PbTe, Pb, and Te calculated from ion currents of $PbTe^+$, Pb^+, and Te^+, respectively, and a sensitivity calibration with $PbTe^+$. These calculations are given in Table I. As expected, ion current data from single experiments lead to lower values for ΔE_0° than do data from double oven experiments unless a contribution to ion fragmentation effects is included. The value of ΔE_0^0 in Table I from double oven experiments, however, is in good agreement with that obtained by the previously outlined procedure.

TABLE IV. Comparison of ion current ratios for PbSe system from single and double oven experiments.

Type cell	Temp. °K	$PbSe^+/Pb^+$	$PbSe^+/Se^+$
Single oven	895	8.8	82.5
Double oven	1353	3.1	13.0

[10] See, for example, R. C. Schoonmaker, A. H. Friedman, and R. F. Porter, J. Chem. Phys. **31**, 1586 (1959).

[11] D. R. Stull and G. C. Sinke, Advances in Chem. Ser. No. 18, (1956).

TABLE V. Computations of ΔE_0° for PbSe=Pb+Se from double oven data.

Temp °K	$PbSe^+/Pb^+$	$PbSe^+/Se^+$	$PbSe^+/Se_2^+$	P_{PbSe}[a] (atm)	K (diss.)	ΔS_T° (entropy unit)	ΔE_0° kcal/mole
1177	2.8	10.5	8.1	3.0×10^{-6}	2.1×10^{-7}	22.7	60.6
1243	4.3	21.2	10.3	7.7×10^{-6}	1.7×10^{-7}	22.7	64.5
1228	3.8	21.2	15.5	7.7×10^{-6}	1.9×10^{-7}	22.7	63.5

[a] Pressure calibrations obtained with sample in upper oven at temperatures between 900°K and 950°K. Vapor pressure data of footnote 4 were used.

PbSe

Experimental techniques for study of PbSe were similar to those employed for PbTe. The $PbSe^+$ ion was the major species produced by electron impact of vapors from single ovens. Ion currents of Pb^+, Se_2^+, and Se^+ were also observed, but were in lower abundance than $PbSe^+$. Data were obtained from double oven experiments using PbSe in the upper chamber for calibration purposes. After obtaining a sensitivity calibration, the temperature of the cell was raised to the range 1180°K to 1450°K for observations of vapors originating from a PbSe sample in the lower chamber. A comparison of ion current ratios obtained from single and double ovens is shown in Table IV. As indicated, the ratios $PbSe^+/Pb^+$ and $PbSe^+/Se^+$ are lower in double oven experiments. Ion fragmentation to form Pb^+ or Se^+ under double oven conditions is thus assumed to be of minor importance for evaluation of thermodynamic data. The data were used to calculate ΔH_T° for the reaction

$$Pb(g)+Se_2(g)=PbSe(g)+Se(g). \qquad (3)$$

For this reaction, we have

$$K_{eq}=(P_{PbSe})(P_{Se})/(P_{Pb})(P_{Se_2})$$
$$=(I_{PbSe^+})(I_{Se^+})/(I_{Pb^+})(I_{Se_2^+}).$$

In the temperature range 1200°K to 1450°K, experimental values of K_{eq} were found to be quite insensitive to temperature. From ten series of ion current measurements, we find $K_{eq}=2.0\pm0.7$. For reaction (3), the standard entropy change, using $\omega=278$ cm^{-1} [7] and an estimated Pb—Se bond length of 2.6 A for PbSe(g), is found to be $+3.7\pm0.5$ entropy units. Combining free energy and entropy increments gives for reaction (3), $\Delta H^\circ_{1200-1450°K}=+3.1\pm1.0$ kcal/mole. Gaydon[6] gives a dissociation energy for Se_2 of 2.8 ± 0.1 ev or 64.6 kcal/mole. This value, combined with ΔH for reaction (3), gives, for the dissociation energy of PbSe(g), 61.5 ± 2.5 kcal/mole. Values of the dissociation energies of PbSe(g), determined from sensitivity calibrations with $PbSe^+$, are given in Table V. At the highest temperature, dissociation energies obtained by the latter procedure tended toward higher values. A decrease in the sensitivity of the mass spectrometer and/or change in geometrical arrangement of the furnace, is probably responsible for this trend. These effects, however, are not reflected in K_{eq} values for reaction (3), since they tend to cancel. Results of the calculations in Table V are confirmatory and support the spectroscopic $D_0(Se_2)$ used in conjunction with reaction (3), although they do not permit us to set better limits of precision than that quoted by Gaydon. Attempts to determine $D_0(Se_2)$, by the procedure used for Te_2 was abandoned because of the high volatility of $Se_2(g)$ and the low degree of dissociation obtainable.

DISCUSSION

It is interesting to compare the bonding in the gaseous diatomic selenides and tellurides of lead with those of bismuth. In Table VI we compare, for the diatomic molecules, their experimental dissociation energies and energies of formation from the gaseous diatomic elements. It is evident, from the latter quantities, that, for the Pb molecules, there are stabilization factors which are not as pronounced in the Bi molecules. On the basis of Pauling's[12] electronegativity scale and the assignment of an electronegativity of 2.4 for Se, we calculate, from the data for the selenides, electronegativities of 1.5 and 2.1 for Pb and Bi, respectively. These values are also obtained from the telluride data if a value of 2.3 is assigned to Te. Although these values are qualitatively consistent with periodic trends,[13] they indicate a larger difference for Pb and Bi than previously reported. This may simply reflect departures from single bond character in these molecules. A better comparison of Pb and Bi would perhaps

TABLE VI. Comparisons of thermodynamic data for diatomic Pb and Bi selenides and tellurides.

Molecule	ΔE_0° (dissociation) kcal/mole	$\Delta E_0^\circ(\frac{1}{2}M_2+\frac{1}{2}Y_2=MY)$ kcal/mole MY	Ref.
PbSe	61.5 ± 2.5	-17.7[a]	This work
BiSe	53.8 ± 2.0	-1.8	3
PbTe	51.4 ± 2.0	-14.0[a]	This work
BiTe	47.5 ± 2.0	-0.9	3
TeSe	57.9 ± 2.0	$+0.4$	3

[a] $D_0(Pb_2)=1.0$ ev taken from footnote 14.

[12] L. Pauling, *The Nature of the Chemical Bond* (Cornell University Press, Ithaca, New York, 1945), 2nd ed.
[13] L. Brewer, Chem. Revs. **52**, 47 (1953).

be obtained from an investigation of the reaction $Pb(g)+Bi_2(g)=PbBi(g)+Bi(g)$ since the presnet data suggest that PbBi(g) is a fairly stable molecule.

Using published data for PbO[14] and PbS,[6] we have, for PbO, PbS, PbSe, and PbTe, dissociation energies of approximately 4.3, 3.3, 2.7, and 2.2 ev, respectively. The trend toward lower bond strengths from oxide to telluride is thus apparent. A similar trend is found for diatomic molecules of bismuth with group VI elements.

Gaydon[6] has suggested a dissociation energy of 2.3± 0.2 ev for $Te_2(g)$. A thermochemical value for the dissociation energy obtained in the present work is in close agreement with the spectroscopic value although the thermochemical data set somewhat narrower limits of uncertainty. These results for $Te_2(g)$ also agree within experimental error with the value of 49±2 kcal/mole obtained by Goldfinger and co-workers[1] from studies of CdTe vapors.

[14] J. Drowart and R. E. Honig, J. Phys. Chem. **61**, 980 (1957).

ACKNOWLEDGMENT

Helpful discussions with Professor Paul Goldfinger and Dr. F. E. Stafford are gratefully acknowledged.

THE JOURNAL OF CHEMICAL PHYSICS VOLUME 34, NUMBER 2 FEBRUARY, 1961

Infrared Spectrum of Lithium Fluoride Monomer by Matrix Isolation*

MILTON J. LINEVSKY

Space Sciences Laboratory, General Electric Company, Philadelphia, Pennsylvania

(Received August 11, 1960)

A method has been developed which can be used to observe the infrared spectrum of high temperature vapors. It combines the techniques of matrix isolation with that of Knudsen effusion. The infrared spectrum of matrix isolated lithium fluoride has been observed in argon, krypton, xenon, and nitrogen matrices. The observed frequencies in the various matrix materials are shifted approximately 7% to 14% from the measured gas fundamental at 900 cm^{-1}. These shifts can be explained by the interactions of the trapped molecule with its surrounding neighbors, based on a model which estimates the change in magnitude of the electrostatic, inductive, and dispersive interactions during the course of a molecular vibration. These effects are particularly large in lithium fluoride due to its sizable dipole moment.

I. INTRODUCTION

CONVENTIONAL techniques for observing the infrared spectrum of vapor species in equilibrium with materials at high temperatures are usually difficult. They consist mainly of heating the substance in a furnace until the vapor pressure of the desired molecular species is sufficiently high to give an observable spectrum. The chief disadvantages of these methods are reaction with the furnace walls, complexity of the spectrum due to hot bands, highly excited rotational-vibrational interactions, and achieving a sufficiently high concentration of species so that a spectrum can be observed.

The technique of Knudsen effusion offers a convenient method for producing vapor species from high-temperature materials, and also mitigates several of the difficulties of the furnace method. Reaction with the container can be more easily controlled since a variety of different container materials and liners can be used. Since the Knudsen cell is small, it can be easily heated by induction or electron bombardment, and can be conveniently mounted within a vacuum system. Once a molecular beam of vapor species is produced by this method, its infrared spectrum can be observed using the techniques of matrix isolation as described by Becker and Pimentel.[1] The beam is condensed simultaneously with a stream of matrix gas on a window cooled to liquid helium temperatures. The ratio of matrix gas to effusion species is maintained sufficiently large so that effective isolation of the effusing molecules is obtained. When a sufficiently dense deposit is formed, the infrared spectrum of the condensed film is observed.

Lithium fluoride was chosen as the initial material to be examined by this technique.

II. EXPERIMENTAL

Apparatus

A schematic drawing of the apparatus appears in Fig. 1. It consists essentially of a double Dewar, a cold finger on which the matrix and molecular beam are condensed, and a Knudsen cell which generates the molecular beam. The Dewar is made of Pyrex and is silvered down to the silver chloride window ports.

* This work was performed under a contract with the U. S. Air Force Ballistic Missile Division.

[1] E. D. Becker and G. C. Pimentel, J. Chem. Phys. **25**, 224 (1956).

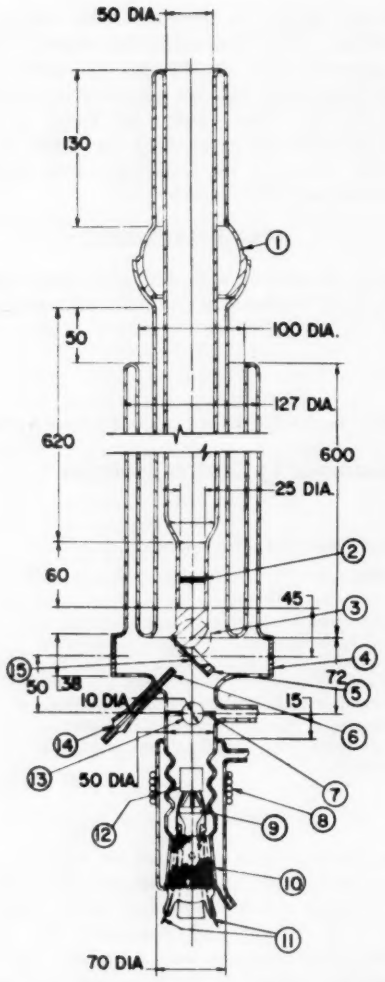

FIG. 1. Cross section of experimental apparatus: 1, 102/75 ball and socket joint; 2, kovar to glass seal; 3, pumping line; 4, AgCl window; 5, doughnut; 6, matrix jet; 7, nickel disk; 8, induction coil; 9, quartz stage; 10, 45/50 tapered joint; 11, thermocouple leads; 12, Knudsen cell; 13, shutter; 14, 14/35 tapered joint; 15, silver chloride cold window (all dimensions in millimeters).

The Knudsen cell, $\frac{3}{4}$ in. in diam and $\frac{3}{4}$ in. in height, is made of platinum-10% rhodium and is supported on a quartz stage. The Knudsen cell assembly can be removed from the Dewar by loosening the 45/50 tapered joint. This tapered joint is fitted with a rubber O ring which provides the vacuum seal. A nickel disc having a 1-cm diam hole serves as a collimator for the beam issuing from the Knudsen cell. The beam can be turned on and off by means of an externally controlled shutter activated by a solenoid.

The Knudsen cell is inductively heated by means of a 15-kw Lepel induction heater operating at a frequency of 300 kc. The Pyrex container surrounding the cell is water-jacketed in order to prevent excessive heating in this area.

The output of the platinum-platinum 10% rhodium thermocouple is continuously recorded and monitored. The couple is welded directly to the base of the Knudsen cell and the temperature can be maintained to any present value.

The matrix gas, which enters the Dewar in the form of a small jet, and the beam from the cell, are condensed simultaneously on the silver chloride window. A constant flow of matrix gas is maintained by allowing the gas to flow through a small fixed leak from a large reservoir before entering the Dewar. The evacuation of the Dewar is provided by a three-stage oil diffusion pump and mechanical pump.

In order to facilitate cooling, the "doughnut" is hollow and liquid helium is allowed to fill it. There is a hole through the center of the "doughnut" so that light from the source can strike the cool window and pass through the condensed film. The "doughnut" is attached to the cold finger and can be properly positioned (in relation to the effusing beam and the light entering the window ports) by rotating the cold finger.

A copper-constantan thermocouple is soldered to the bottom of the "doughnut" which allows temperature measurements above 20°K. This has been found useful in observing the effect of warmup on the spectrum. No attempt was made to measure the temperature of the matrix directly.

Liquid helium is siphoned through a cap into the cold finger in a conventional manner using a vacuum-jacketed transfer tube. The evaporation losses are approximately 25 cc/min when the outer Dewar is filled with liquid nitrogen.

The infrared spectrometers used were Models 12 and 12G (grating) Perkin-Elmer Spectrometers, using slightly modified optics with an intermediate focus so that the source to entrance slit distance could be increased to 1 m.

Lithium Fluoride Isolation

Approximately 2.5 g of lithium fluoride, obtained from spectroscopic-grade windows manufactured by the Frank Cook Company, were loaded into the Knudsen cell. The lid of the cell was welded directly to the body of the cell after filling with LiF. The orifice diameter was approximately 0.075 cm.

The melting point of LiF provided a convenient calibration for the Pt-Pt 10% Rh thermocouple. The melting point was taken as 848±1°C, as reported by Douglas and Deever.[2] Isolation of LiF was accomplished by using argon, krypton, xenon, and nitrogen matrices; in all cases the ratio of matrix to lithium fluoride was maintained greater than 300:1. This ratio

[2] T. B. Douglas and J. L. Deever, J. Am. Chem. Soc. **76**, 4826 (1954).

was estimated by using the Knudsen effusion relationship and a calibration of the flow through the fixed leak in the matrix gas line. The matrix gases were all Matheson research-grade materials and were used without further purification.

The Knudsen cell containing the LiF was degassed in place, at a temperature at least 100°C above which depositions were carried out. The pressure in the Dewar was always less than 10^{-5} mm during isolation. Spectra of the isolated lithium fluoride were observed with both spectrometers in the region of 2μ to 15μ.

III. RESULTS AND DISCUSSION

Typical spectra, in various matrices, are shown in Fig. 2. Table I gives the conditions under which the spectra were obtained and the resulting observed frequencies. In all cases the absorption bands disappeared when the cold finger was warmed up to approximately 40°K, and did not reappear upon recooling to liquid helium temperatures. It is felt that diffusion in the solid, even at these temperatures, is sufficient to destroy the effects of matrix isolation. No spectrum was observed in the pure LiF condensate (matrix excluded). The spectrum of the pure condensed matrices was checked yielding negative results. An extremely weak band at 767 cm^{-1} was observed in the rare gas matrices after long periods of deposition (>1 hr). This band has only been observed with the grating instrument and its validity remains somewhat questionable.

The band observed in argon at 840 cm^{-1} may be due to LiF which may possibly occupy two slightly different sites in the matrix, or it could conceivably be due to resolution of rotational structure.

The fundamental frequency for LiF monomer in the gas phase has been reported by Vidale[3] to be about 900 cm^{-1}. When this is compared to the frequencies given in Table I, it is apparent that sizeable shifts in the fundamental frequency are produced by the various matrices.

The magnitude of these shifts can be explained

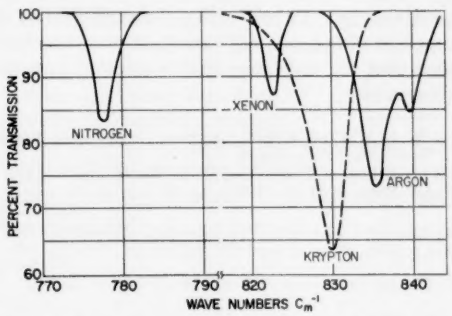

FIG. 2. Infrared spectrum of lithium fluoride in various matrices.

[3] G. Vidale, J. Phys. Chem. **64**, 314 (1960).

TABLE I. Observed infrared bands for LiF in various matrices.

Matrix gas	Knudsen cell temperature °K	LiF deposited[a] grams	Frequency[b] cm^{-1}
Argon	1150±5	6×10^{-5}	835 840 (767-very weak)
Krypton	1183±5	8×10^{-5}	830 (767-very weak)
Xenon	1190±5	3×10^{-5}	823
Nitrogen	1190±5	3×10^{-5}	778

[a] Values estimated from Knudsen effusion equations and LiF vapor pressure data.
[b] All bands are of approximately the same intensity when normalized to equivalent amounts of deposited lithium fluoride.

qualitatively based on the following approach. When a molecule is trapped in a matrix, there is an interaction energy between the trapped molecule and the molecules or atoms of the matrix. Semiclassically, this interaction energy can be attributed to a dispersion effect, an electrostatic effect, and an induction effect, depending upon the polar nature and the polarizability of the interacting species. The magnitude of the interaction energy of the trapped molecule with the sourrounding matrix will, in general, be different for different vibrational levels and when the molecule undergoes a vibrational transition, this difference in interaction energy must be added to the energy of transition. Therefore, the frequency of transition will be shifted by an amount equal to the difference in interaction energy between the two states.

In the inert matrices (A, Kr, Xe), the interaction energy between LiF and the inert atoms will consist primarily of a dispersion term and an induction term, the latter being made up essentially of a dipole-induced dipole contribution. The potential energy associated with this interaction is given by[4]

$$\Phi_{\text{ind}}=-[\alpha\mu^2(3\cos^2\theta+1)/2r^6], \tag{1}$$

where α is the polarizability of the matrix atom, μ is the dipole moment of LiF, r is the LiF-matrix nearest-neighbor distance, and θ is the polar angle of dipole. Therefore

$$\Delta\nu_{\text{ind}}=(\Delta\Phi_{\text{ind}}/hc)=-[\alpha(\mu_1^2-\mu_0^2)(3\cos^2\theta+1)]/2r^6hc. \tag{2}$$

Braunstein and Trischka[5] give for Li^7F^{19} values of $(\mu^2I)_{v=0}=837.1\times10^{-76}$ and $(\mu^2I)_{v=1}=872.3\times10^{-76}$ where I is the moment of inertia of Li^7F^{19} in a given vibrational state. The latter can be calculated from the spectroscopic parameters given by Vidale[3]; this leads

[4] J. O. Hirschfelder, C. F. Curtiss and R. B. Bird, *Molecular Theory of Gases and Liquids* (John Wiley & Sons, Inc., New York, 1954).
[5] R. Braunstein and J. W. Trischka, Phys. Rev. **98**, 1092 (1955).

to a value for $\mu_1^2-\mu_0^2$ of approximately 1.1×10^{-36}. In order to evaluate Eq. (2), several assumptions must be made as to the nature of the LiF-matrix condensate. First, it is assumed that the LiF occupies a substitutional site in the rare gas lattice, and second, that the distance between LiF and the matrix neighbor is the same as the nearest-neighbor distance in the matrix lattice. Strictly speaking, these assumptions are not necessarily valid; however, for the purpose of estimating this interaction energy their inclusion seems justifiable. Since $kT\ll\Phi_{\text{ind}}$ the induced dipoles can be considered to be perfectly aligned so as to maximize the interaction energy. The rare gases crystallize in a face-centered cubic configuration and consequently, the angular dependent term $(3\cos^2\theta+1)$ can be evaluated based on this structure. This leads to an angular dependent factor of 2 per nearest-neighbor regardless of the LiF orientation. This is not surprising since the fcc configuration is almost spherically symmetric. Since the energy varies as $1/r$,[6] the effective number of nearest neighbors for a fcc structure is 14.45 (see footnote 4). The expression for $\Delta\nu_{\text{ind}}$ now becomes

$$\Delta\nu_{\text{ind}}=-\frac{14.45\times1.1\times10^{-36}\times5.034\times10^{15}\alpha}{d_0^6}, \qquad (3)$$

where d_0 is the nearest-neighbor distance in a pure matrix lattice. Using the values of the polarizabilities[6] of argon, krypton, xenon (1.63×10^{-24}, 2.36×10^{-24}, 4.01×10^{-24}) and values of d_0 of A, Kr and Xe (3.83 A, 3.95 A, 4.34 A)[4] respectively, Eq. (3) leads to a frequency shift of the order of -45 cm^{-1} in each of the three rare gas matrices. It is to be observed that the shifts do not change appreciably going from one rare gas to another since α/r^6 remains almost constant. The observed shifts in argon, krypton, and xenon are -65 cm^{-1}, -70 cm^{-1}, and -77 cm^{-1}; therefore, this would indicate that the dispersion part of the shift would amount to -20 cm^{-1} to -30 cm^{-1} in the respective matrices.

In the case of the nitrogen matrix the observed shift amounts to -122 cm^{-1} The interaction energy of LiF in nitrogen contains both the inductive and dispersion terms as discussed above and, in addition, should contain an electrostatic term due to the dipole-quadrapole interactions. The magnitude of the frequency shift due to the dipole-quadrapole interaction can be estimated in the following manner. The potential energy associated with a dipole-quadrapole interaction is given by[4]

$$\Phi_{\text{elec}}=(3\mu_a Q_b/4d_0^4)[\cos\theta_a(3\cos^2\theta_b-1)-2\sin\theta_a\sin\theta_b\cos\theta_b\cos(\phi_a-\phi_b)], \qquad (4)$$

where Q_b is the quadrapole moment of N_2, and θ_a, θ_b, ϕ_a, ϕ_b are the polar angles associated with the dipole (LiF) and quadrapole (N_2) and d_0 is the nearest neighbor distance in N_2 lattice. Nitrogen below 35°K crystallizes in a face-centered cubic structure[7] and since kT is again much less than Φ_{elec} (allowing maximum interaction), the angular dependent term of the potential can be evaluated for any LiF orientation. This leads to a value of approximately -1 per nitrogen molecule for this angular contribution, regardless of the LiF position. For a $1/r^4$ potential, the effective number of nearest neighbors (see footnote 4) is 25.34. The frequency shift due to this interaction potential is therefore

$$\Delta\nu_{\text{elec}}=(\Delta\Phi_{\text{elec}}/hc)=-\frac{95.67\times10^{15}Q_{N_2}\Delta\mu_{0\text{-}1}}{d_0^4}. \qquad (5)$$

The value of $\Delta\mu$ is approximately 0.1×10^{-18} as obtained from the data of Braunstein and Trischka.[5] Using the values[4] of $Q_{N_2}=1.49\times10^{-26}$, and $d_{N_2}=4$ A, Eq. (5) leads to a frequency shift of approximately -55 cm^{-1}.

The dipole-induced dipole contribution can be evaluated in a manner similar to that of the rare gases and leads to a shift of approximately -40 cm^{-1}. By difference, the shift due to the dispersion forces amounts to approximately -30 cm^{-1}.

It is interesting to note that the relatively large shifts in the vibrational fundamental of LiF are primarily a result of the rather large changes in μ and μ^2 for this molecule Pimentel[1] has measured shifts of the order of 1% in hydrogen halides, and since the dipole moments of these materials are much smaller than those of LiF, the shifts are reduced. For example in HCl, using the dipole moment functions of Benedict, Herman, Moore, and Silverman,[8] the dipole-induced dipole and quadrapole-dipole effects lead to a shift of approximately -13 cm^{-1}. The observed shift of HBr[1] trapped in nitrogen is -14 cm^{-1}. It may also be concluded that the dispersion effects are also correspondingly reduced.

[6] *Landolt-Bornstein, Zahlenmerte und Functionen*, edited by E. Schmidt, (Springer-Verlag, Berlin, Germany, 1951).

[7] G. W. G. Wyckoff, *Crystal Structures* (Interscience Publishers, Inc., New York, 1951), Vol. 1.

[8] W. S. Benedict, R. Herman, G. E. Moore, and S. Silverman, J. Chem. Phys. **26**, 1671 (1957).

Electron Spin Resonance of Some Vanadyl Porphyrins*

E. M. ROBERTS AND W. S. KOSKI

The Johns Hopkins University, Baltimore, Maryland

AND

W. S. CAUGHEY

Department of Physiological Chemistry, The Johns Hopkins School of Medicine, Baltimore, Maryland

(Received July 25, 1960)

The electron spin resonance spectra of the vanadyl complexes of etioporphyrin II, vanadyl mesoporphyrin IX dimethyl ester, and deuteroporphyrin IX dimethyl ester have been studied and found to be identical to within experimental error. Unlike the corresponding copper complexes, the vanadyl complexes give no observable nitrogen hyperfine effects. An explanation is proposed for the lack of this hyperfine structure, and an approximate method is suggested for evaluating the bonding parameters.

INTRODUCTION

RECENTLY the electron-spin resonance spectrum of copper etioporphyrin II (Cu Etio II) was analyzed for the spin Hamiltonian parameters.[1] A notable feature of that spectrum is the nitrogen hyperfine structure. From the spacings of the nitrogen hyperfine structure, it was found that the coefficient, α, of the $3d_{x^2-y^2}$ atomic orbital in the ground-state molecular orbital is 0.86.

O'Reilly has determined the spin Hamiltonian parameters for vanadyl etioporphyrin I (VO Etio I).[2] This compound shows no nitrogen hyperfine structure. Thus the amount of directly available information concerning the metal-nitrogen bonds in the vanadyl porphyrin is correspondingly less than in the copper porphyrin.

In this paper a corresponding study has been made of vanadyl etioporphyrin II (VO Etio II) vanadyl mesoporphyrin IX dimethyl ester, and vanadyl deuteroporphyrin IX dimethyl ester. An explanation for the lack of nitrogen hyperfine effects is proposed and an approximate method is suggested for obtaining α.

EXPERIMENTAL

A Varian Model V 4500 EPR spectrometer utilizing 100-kc modulation was used for all measurements reported here. The magnetic field was monitored with a Harvey-Wells Electronic Inc. model G-501 proton resonance gaussmeter. Each spectrum was preceded by a spectrum of a benzene solution of DPPH for which the g_0 value is accurately known.

The preparation of the vanadyl porphyrins will be described in detail elsewhere.[3] However, since the state of purity is critically important here, it should be mentioned that in each case the vanadyl complexes were prepared from the respective metal-free porphyrins of a high state of purity. The resulting vanadyl complexes were purified by chromatography on calcium carbonate columns and recrystallization several times from chloroform-methanol to give products whose carbon, hydrogen, and nitrogen analyses are in excellent agreement with calculated values. The deuteroporphyrin IX dimethyl ester and mesoporphyrin IX dimethyl ester complexes melted at 250° and 248–249°, respectively.

All of the electron spin resonance measurements were made on benzene and castor oil solutions ranging in concentration from 10^{-3} to 10^{-2} M.

DISCUSSION AND RESULTS

Benzene solutions of the vanadyl complexes of etioporphyrin II, mesoporphyrin IX dimethyl ester, and deuteroporphyrin IX dimethyl ester yield electron spin resonance spectra which are described by the spin Hamiltonian

$$\mathcal{H}_s = g_0 \beta H S_z + a\mathbf{S}\cdot\mathbf{I},$$

where

$$a = \tfrac{1}{3}(A+2B)$$

and

$$g_0 = \tfrac{1}{3}(g_{\parallel}+2g_{\perp}).$$

Here, A and B are the usual hyperfine coupling constants of the central metal nucleus. The eight hyperfine components are given by

$$H(m) = H_0 - am - a^2/2H_0(63/4 - m^2)$$

for each molecule; here m is the z component of the nuclear spin. The above three compounds have identical spectra. For these compounds $g_0 = 1.975_5$ and $|a| = 0.0089$ cm^{-1}. From a castor oil solution of each molecule, we obtain $g_{\parallel} = 1.947_4$, $g_{\perp} = 1.988_5$, $|A| = 1.58 \times 10^{-2}$ cm^{-1}, and $|B| = 0.54 \times 10^{-2}$ cm^{-1}. These values are in agreement with those obtained for VO Etio I.[2]

* This investigation was supported in part by a research grant from the Division of General Medical Sciences, Public Health Service.

[1] E. M. Roberts and W. S. Koski, J. Am. Chem. Soc. **82**, 3006 (1960).

[2] D. E. O'Reilly, J. Chem. Phys. **29**, 1188 (1958); **30**, 591 (1959).

[3] W. S. Caughey (to be published).

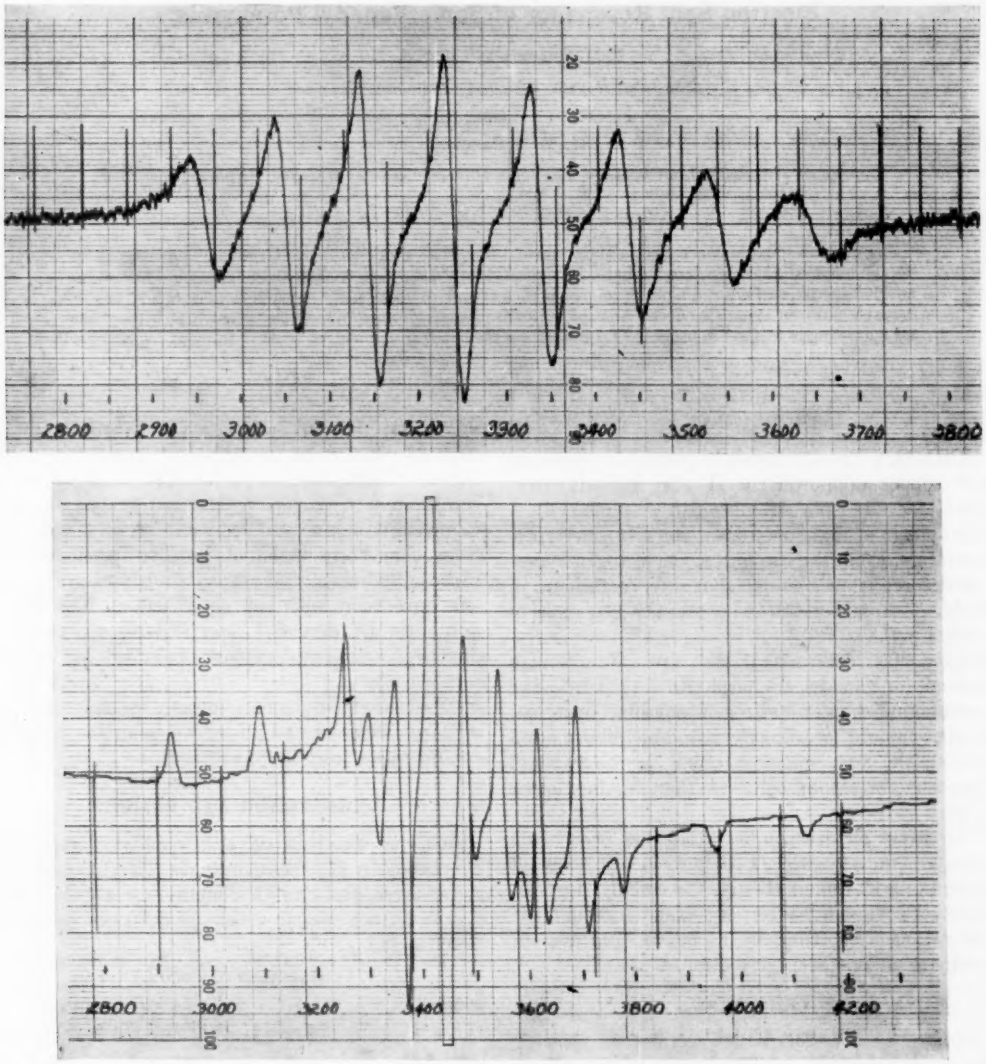

FIG. 1. Electron spin resonance spectra of vanadyl etioporphyrin II in benzene solution (upper curve) and in castor oil solution (lower curve) at 20°C. The horizontal ordinate gives the value of the field in gauss.

The spectra for the compounds reported on here, have the same appearance as those for VO Etio I. Typical spectra obtained for these compounds are given in Fig. 1.

The symmetry group of VO Etio II is C_{2v}. The assumption that the symmetry of the electric field in the vicinity of the metal atom is C_{4v}, leads to two principal values of the g tensor. Since neither the presence of the ester groups nor replacing the alkyl substituents in the 2 and 4 positions with hydrogens affects the electron-spin resonance data, the assumption of C_{4v} symmetry is valid in the cases studied. It seems possible, however, that electron-attracting or electron-donating groups attached directly to the ring might well affect the spectrum.

Under the assumption of C_{4v} symmetry the ground state of the unpaired electron is given by a bonding molecular orbital containing the $3d_{xy}$ atomic orbital and the nitrogen $2p_x$ and $2p_y$ atomic orbital. This molecular orbital forms the basis for the B_2 representation and has nodes at the vanadium and nitrogen nuclei. Thus it is not surprising that the solution spectra shows no nitrogen hyperfine structure. In the case of Cu Etio II, the ground-state molecular orbital does not have nodes at the nitrogen nuclei; hence, a nitrogen hyperfine structure would be expected. The hyperfine

components due to the vanadium nuclei may be explained by promoting an electron from the bonding A_1 molecular orbital to the antibonding A_1 orbital.[1]

The bonding B_2 orbital state will be taken to be

$$|B_2\rangle=\beta|d_{xy}\rangle+(1-\beta^2)^{\frac{1}{2}}/2[|\tau_1\rangle+|\omega_2\rangle-|\tau_3\rangle-|\omega_4\rangle], \quad (1)$$

where the τ's and ω's are nitrogen $2p_x$ and $2p_y$ atomic orbitals, respectively. Atoms 1 and 2 are on the $+y$ and $+x$ axes, respectively. Atoms 3 and 4 are on the $-x$ and $-y$ axes, respectively.

In relating the g values to the bonding parameters, various energy level differences of the crystal field appear. No detailed knowledge of the latter energy differences is available for the paramagnetic porphyrins. In order to avoid this difficulty, we define an average excitation energy ΔE such that

$$(\Delta E)^{-1}\langle 0|L_j^2|0\rangle=\sum_{n\neq 0}|\langle 0|L_j|n\rangle|^2/E_n-E_0 \times(j=x,z). \quad (2)$$

From the general formula for g_{jj},[4] we obtain with $|0\rangle=|B_2\rangle$

$$g_{\parallel}=2.0023\{1-\lambda/\Delta E_\sigma(3\beta^2+1)\} \quad (3a)$$

$$g_{\perp}=2.0023\{1-\lambda/2\Delta E_\pi(\beta^2+1)\}, \quad (3b)$$

where $\Delta E_\sigma(\Delta E_\pi)$ is the average excitation energy to states whose wave functions have maxima in (out of) the plane of the four nitrogens. If bonding is neglected by placing $\beta=1$, these equations become identical to equations deduced from an ionic model if ΔE_σ and ΔE_π are replaced by the proper energy differences.[5]

The spin-orbit coupling constant, λ, has been determined not to be less than $+200$ cm^{-1}.[5] We accept this value for lack of a better one. A method is now needed to approximate ΔE_σ or ΔE_π. Calculation of these quantities from first principles does not seem feasible. Any approximation to their values, however, should be dependent on the given molecule. The following empirical method is suggested. Define a quantity

$$\langle\Delta E\rangle_{Av}=\sum_i^i P_i\Delta E_i/\sum_i^i P_i, \quad (4)$$

where P_i and ΔE_i are the transition probability and energy of the ith absorption peak in the visible and ultraviolet spectrum of the particular molecule. The association $\langle\Delta E\rangle_{Av}\leftrightarrow\Delta E_\pi$ is proposed as an approximation.

In order to test the above association we have calculated the bonding parameter α for copper etioporphyrin II and copper phthalocyanine, using the following equation for $g_\perp$ which is the analogue of Eq. (3b)

$$g_\perp=2.0023\{1-\lambda/\Delta E_\pi[0.667\alpha^2+0.033\alpha+0.333]\}, \quad (5)$$

where it has been assumed that the overlap between the ligand hybrid orbitals and the copper $d_{x^2-y^2}$ orbital is the same for both the porphyrin and the phthalocyanine. Calculations using hydrogenlike orbitals show an overlap value of 0.1.[1] From the absorption spectra we obtain $\langle\Delta E\rangle_{Av}$ values of 24 560 cm^{-1} and 33 300 cm^{-1} for copper etioporphyrin II and copper phthalocyanine,[6] respectively. Here, λ is -828 cm^{-1}. Using $g_\perp=2.061_6$ we get $\alpha=0.88$ for the copper porphyrin. Using $g_\perp=2.045$ we get $\alpha=0.87$ for the phthalocyanine. Experimentally we can obtain α from the nitrogen hyperfine spectra. For copper etioporphyrin II we have found $\alpha_{exp}=0.86$.[1] For copper phthalocyanine we have found $\alpha_{exp}=0.89$.[6] Thus the association of ΔE_π with $\langle\Delta E\rangle_{Av}$ is in good agreement with experiment.

From the data on the vanadyl porphyrins,[7] we obtain $\langle\Delta E\rangle_{Av}=27\,000$ cm$^{-1}\leftrightarrow\Delta E_\pi$ which with $g_\perp=1.988_6$ and $\lambda=200$ cm^{-1} gives $\beta=0.94$. If the A_1 orbitals were appreciably covalent, a small amount of nitrogen hyperfine structure would be expected due to configuration interaction. However, since none can be observed, the A_1 orbital may be considered to consist only of the vanadium $3d_{z^2}$ and $4S$ orbitals and oxygen $2p_z$ and $2S$ orbitals.

If VO Etio I is in the presence of pyridine, a weak complex is formed and a new transition appears in the optical spectrum.[6] Similar solvent effects have been noted for other metalloporphyrins.[8] It is expected that ΔE_π will be affected by the complexed pyridine but that ΔE_σ will remain almost the same. If further it is assumed that β remains unchanged, we may predict g_0 for the presence of pyridine. The new $\langle\Delta E\rangle_{Av}$ is 26 500 cm^{-1} which leads to $g_0=1.974$ for VO Etio II in the presence of pyridine. The agreement of the latter result with experiment may be fortuitous since the copper porphyrins show no solvent effect in the electronic spectrum.

The calculations made above are consistent with experiment but data on more compounds are needed to make an accurate estimation of the validity of these calculations.

[4] A. Abragam and M. H. L. Pryce, Proc. Roy. Soc. (London) **A205**, 135 (1951).

[5] M. B. Palma-Vittorelli, M. U. Palma, and D. Palumbo, Nuovo cimento **3**, 718 (1956).

[6] P. E. Fielding and F. Gutman, J. Chem. Phys. **26**, 411 (1957).

[7] J. G. Erdman and A. H. Corwin, J. Am. Chem. Soc. **68**, 1885 (1946).

[8] W. S. Caughey and R. M. Deal (unpublished).

[9] E. M. Roberts and W. S. Koski (to be published).

NMR Spectra of 1,1,4,4-Tetramethylcyclohexyl-*cis* and *trans*-2,6-diacetate

J. I. MUSHER

Lyman Laboratory, Harvard University, Cambridge, Massachusetts

(Received March 14, 1960)

The high resolution NMR spectra of 1,1,4,4-tetramethylcyclohexyl-*cis* and *trans*-2,6-diacetate have been studied and provide a series of coupling constants which are then compared with values predicted by theory. Relative chemical shifts of equatorial and axial protons are also given.

I. INTRODUCTION

KARPLUS and Anderson[1] and Karplus[2] have calculated on the basis of valence-bond theory values for the NMR coupling constants between protons bonded to a single carbon atom as a function of H—C—H angle and between protons on successive carbon atoms as a function of the dihedral angle between the two C—C—H planes. The existing experimental evidence is somewhat in accord with their results, with particularly good agreement for the methane coupling constant where $J_{\text{exptl}}=12.4\pm0.6$ cps[3] and $J_{\text{theor}}=12.5$ cps. The only other value in the literature for this tetrahedral H—C—H angle is 12.0 cps.[4] The H—C—C—H proton-proton couplings for dihedral angles $\phi=60°$ and $\phi=180°$ corresponding to $J_{ea}=J_{ee}$ and J_{aa}, respectively, in cyclohexane derivatives[5] are 1.7 cps and 9.2 cps from the theory; Karplus refers to experimental values based on first order calculations of J_{ea} and $J_{ee}=2$–4 cps and $J_{aa}=5$–8 cps from the acetylated sugars of Lemieux *et al.*[6] Other similar values have also been obtained by Cohen *et al.*[7] based on the assumption that $J_{ea}=J_{ee}$, and in footnote 4 there is a $J_{aa}=9.2$ cps which is identical with that predicted theoretically. The coupling constants from a series of substituted ethanes[8] are in the range 6.0–7.4 cps, while the Karplus values predict 4.2 cps.

In order to provide experimental values of these coupling constants based on an explicit spectral analysis considering all the interacting spins as a single system, a pair of substituted cyclohexanes has been studied. The *cis*- and *trans*-isomers of 1,1,4,4-tetramethylcyclohexyl-2,6-diacetate are (in the time average for the *trans*-isomer) symmetrical along the plane through the axial bonds on the 1 and 4 carbons, and the system of six ring protons can therefore be reduced to two identical (again in the time average for the *trans*-isomer) closed 3-spin systems. There is of course, negligible coupling expected between the protons separated by four bonds across this plane of symmetry. The analysis is facilitated by the fact that protons on the same carbon with an acetoxy group appear considerably to low field from the position of methylene protons. Thus the 2 and 6 protons are well separated from the pairs of 3 and 5 protons and the 3-spin systems are reduced to the form of ABX in the nomenclature of Pople *et al.*[9] The spectrum from the *cis*-isomer has been analyzed explicitly, providing coupling constants and chemical shifts; the former can be compared with the theoretical estimates of Karplus. The spectrum from the *trans*-isomer can only be analyzed if the coupling constants and chemical shifts for half of the molecule are assumed to be identical with those for the *cis*-isomer.

II. EXPERIMENTAL DETAILS

The high-resolution NMR spectra of 1,1,4,4-tetramethylcyclohexyl-*cis*- and *trans*-2,6-diacetate in degassed CCl_4 solution were taken at 60 Mc. A spectrum of each isomer is shown in Fig. 1 and peak positions are indicated relative to internal hexamethyldisiloxane. The peak separations were calibrated by the use of audio sidebands from a variable frequency oscillator whose frequency was monitored with a cycle counter. The field was swept upfield and downfield on alternate calibrations to eliminate the effect of drift. Eight calibrations were made for each spectrum and the standard deviations of the multiplet separations were reduced to less than 0.1 cps for the *cis*-isomer. The standard deviations for the multiplet separations and for the peak positions relative to the standard are indicated in parentheses in the figure. The four lines

[1] M. Karplus and D. H. Anderson, J. Chem. Phys. **30**, 6 (1959).
[2] M. Karplus, J. Chem. Phys. **30**, 11 (1959).
[3] M. Karplus, D. H. Anderson, T. C. Farrar, and H. S. Gutowsky, J. Chem. Phys. **27**, 597 (1957).
[4] R. U. Lemieux, R. K. Kullnig, H. J. Bernstein, and W. G. Schneider, J. Am. Chem. Soc. **80**, 6098 (1958).
[5] Cyclohexane rings, or oxygen containing saturated rings, possess two distinct types of substituents (or protons): those perpendicular to the pseudoplane of the chair (the usual ring structure, appearing as a zigzag or chair from end on) called axial (a), and those skew to the ring, called equatorial (e). When the ring inverts by a simultaneous rotation about all the C−C bonds the axial substituents become equatorial and the equatorial substituents become axial. The system is generally in the conformation of lowest energy when it has the greatest number of substituents equatorial.
[6] R. U. Lemieux, R. K. Kullnig, H. J. Bernstein, and W. G. Schneider, J. Am. Chem. Soc. **80**, 2237 (1958).
[7] A. D. Cohen, N. Sheppard, and J. J. Turner, Proc. Chem. Soc. **1958**, 118.
[8] R. E. Glick and A. A. Bothner-By, J. Chem. Phys. **25**, 362 (1956).
[9] J. A. Pople, W. G. Schneider, and H. J. Bernstein, *High-resolution Nuclear Magnetic Resonance* (McGraw-Hill Book Company, Inc., New York, 1959).

of very low intensity in the *cis*-isomer appear in only four of the spectra and their separations from the adjacent peaks show standard deviations of less than 0.3 cps. Attempts to find these lines of low intensity for the *trans*-isomer were not successful.

III. RESULTS AND DISCUSSION

A cyclohexane ring containing an equatorially oriented substituent is usually of lower energy than the same ring containing the substituent axially oriented, with the energy difference between the two forms (called conformers) depending upon the bulk of the substituent. Since the ring is able to invert from one conformer to the other with all equatorial bonds becoming axial and vice versa, an equilibrium will exist between the two conformers. Although a given molecule with one conformation energetically favorable (1–2 kcal/mole is a representative energy difference between conformers for a single substituent) may invert rapidly, it will still spend the greater portion of the time (by the Boltzmann factor) in the energetically favorable conformer. The 1,1,4,4-tetramethylcyclohexyl-*cis*-2,6-diacetate has conformers with both acetoxy groups either equatorial or axial and because of the considerably higher energy of the diaxial conformer, this molecule can be considered rigid (in the time average sense) in the conformer with both acetoxy groups equatorial. This rigid molecule is symmetrical about the axial plane through the 1,4 carbons and since these carbons have no protons directly bonded to them there will be negligible coupling across the plane of symmetry. Thus the 6-spin system can be reduced to a 3-spin system of double intensity which is of the form ABX, where X denotes the 2 proton, A the axial 3 proton, and B the equatorial 3 proton as indicated in Fig. 1.

There are 14 possible resonances of nonzero intensity in such a case, 12 of which are present in our spectrum. The assignment of peaks is straightforward following p. 134 of Pople *et al.*[9] and their numbers in reverse order for the different transitions are indicated in the figure. Peaks number 3 and 5 overlap, peak number 8 lies under one of the methyl peaks and peak number 7 is too weak to observe. Performing the calculations for the coupling constants based on the experimental values of $2\,|\,D_+-D_-\,|$, $2(D_++D_-)$, $|\,J_{AX}+J_{BX}\,|$ and the separations between peaks 4 and 6, and for the chemical shifts based on peaks 10 (or 11) and 6 (or 4), the following values are obtained:

$$J_{AB}=12.36\pm0.2 \text{ cps}$$

$$J_{AX}=12.35\pm0.1 \text{ cps}$$

$$J_{BX}=4.25\pm0.1 \text{ cps}$$

$$\nu_A=-76.12\pm0.2 \text{ cps}=-1.269\pm0.003 \text{ ppm}$$

$$\nu_B=-84.00\pm0.2 \text{ cps}=-1.400\pm0.003 \text{ ppm}$$

$$\nu_X=-280.83\pm0.2 \text{ cps}=-4.681\pm0.003 \text{ ppm}.$$

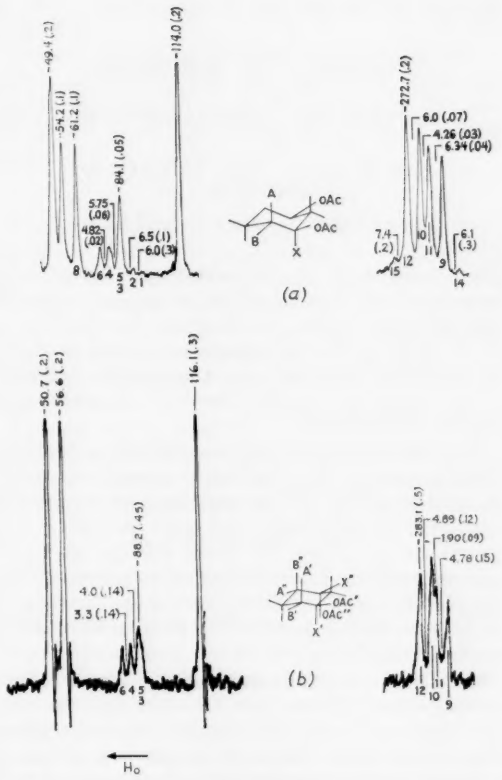

FIG. 1. The 60 Mc/sec NMR spectra of (a) 1,1,4,4-tetramethylcyclohexyl *cis*-2,6-diacetate and (b) 1,1,4,4-tetramethylcyclohexyl *trans*-2,6-diacetate. The peak positions are indicated in cps relative to internal hexamethyldisiloxane. The numbers in parentheses are the standard deviations for the experimental values presented, and the numbers under the peaks correspond to the transitions for an ABX system as noted in text.

The standard deviation for the value of $2(D_++D_-)$ is 0.3 cps; however this has only a small effect on J_{AB} and an almost neglibigle effect on the other coupling constants. A change in the value of $2(D_++D_-)$ by 1.0 cps changes J_{AB} by $\sim$0.5 cps and changes J_{AX} and J_{BX} by only $\sim$0.05 cps. There is negligible error introduced by the use of an ABX analysis rather than an ABC analysis as machine calculations have indicated. The unusual effect of unequal splittings (considerably greater than the standard deviations) in the X spectrum cannot be explained by any means presently available. In practice only the averages of these splittings enter into the calculations and thus this phenomenon is neglected here. On the basis of this discussion the expected error in the coupling constants is most probably within ±0.1 cps for J_{AX} and J_{BX} and ±0.2 cps for J_{AB}. The chemical shifts should also be valid to ±0.2 cps with ν_A–ν_B valid to ±0.1 cps.

These coupling constants compare with the theoretical values using the usual cyclohexane angles, as

follows:

Theoretical	Experimental
$J_{AB}=12.5$ cps	$J_{AB}=12.36\pm0.2$ cps
$J_{AX}=9.2$ cps	$J_{AX}=12.35\pm0.1$ cps
$J_{BX}=1.7$ cps	$J_{BX}=4.25\pm0.1$ cps.

The agreement for J_{AB} is good despite (or probably because of) the neglect of the noncontact terms as pointed out by Karplus and Anderson. For the H—C—C—H couplings the agreement is not very good and this cannot be compensated for by possible distortion of the cyclohexane ring structure due to the presence of the other substituents.

These experimental values can be used to predict a coupling constant for substituted ethanes representing the average of the coupling constant over the internal rotation of the CH_3 group. The result obtained is 6.98 cps which lies within the range 6.0–7.4 cps found experimentally for substituted ethanes, and within the very narrow range of 6.93–7.00±0.10 cps for most of the experimental $J_{CH_3-CH_2}$'s. The Karplus calculations predict 4.2 cps.

We turn now to the spectrum of 1,1,4,4-tetramethylcyclohexyl-*trans*-2,6-diacetate. The two conformers of this isomer are energetically identical (one is the mirror image of the other) and each has one acetoxy group equatorial and one axial. Since the resonances of protons adjacent to axial acetoxy groups usually appear 0.4–0.7 ppm to low field from those of protons adjacent to equatorial acetoxy groups,[4,10] the presence of a single multiplet for the 2 and 6 protons signifies that the ring is rapidly inverting between its two conformers and that the spectrum observed is that of the time-average molecule. Were the molecule rigid, that is, inverting slower than ~16 cps, which would imply a barrier to inversion of >~16 kcal/mole, two sets of low field multiplets would be present. Since it is only the time-average molecule that affects the spectrum, this isomer, too, can be considered as a 3-spin ABX system of double intensity because of time-average symmetry along the 1,4 axial plane.

Because of the absence of peaks 14 and 15 an explicit analysis of the spectrum is not possible. It is necessary to provide $J_{AB}{}^{av}$ in order to determine the remaining time-average parameters $J_{AX}{}^{av}$, $J_{BX}{}^{av}$, $\nu_A{}^{av}$, and $\nu_B{}^{av}$ while $\nu_X{}^{av}$ is determined directly from the spectrum. Setting $J_{AB}{}^{av}=J_{AB}$ from the *cis*-isomer=12.36 cps and using the experimental values of $2|D_+-D_-|$, $|J_{AX}+J_{BX}|$, the separations between peaks 4 and 6 and the chemical shifts of peaks 10 (or 11) and 6 (or 4), we obtain the following time-average values:

$$J_{AX}{}^{av}=7.57 \text{ cps}$$
$$J_{BX}{}^{av}=4.01 \text{ cps}$$
$$\nu_A{}^{av}=-81.13 \text{ cps}=-1.352 \text{ ppm}$$
$$\nu_B{}^{av}=-88.95 \text{ cps}=-1.482 \text{ ppm}$$
$$\nu_X{}^{av}=-288.94 \text{ cps}=-4.816 \text{ ppm}.$$

If the assumption that $J_{AB}{}^{av}=J_{AB}$ from the *cis*-isomer is valid, these coupling constants should be accurate to ±0.2 cps and the chemical shifts to ±0.4 cps.

What is really of interest, however, is not the time-average couplings and chemical shifts, but those for the rigid molecule, i.e., the molecule fixed in either (mirror image) single conformer. We have already denoted by a J the coupling constants from the *cis*-isomer and by a J^{av} the coupling constants from the time-average *trans*-isomer. Let us now denote by a J' the coupling constants on the side of the molecule with the acetoxy group equatorial and by a J'' the coupling constants on the side of the molecule with the acetoxy group axial; the same notation shall hold for chemical shifts ν. Since ring inversion can be considered as reflection in the 1,4 axial plane, ring inversion just requires all primed couplings and shifts to go into double primed ones and vice versa. We shall now assume that the primed parameters take the same values as the parameters calculated for the *cis*-isomer. This is only so if the two halves of the ring can be considered independently and hence the primed half of the *trans*-isomer is identical to half of the *cis*-isomer, which is probably quite valid for the coupling constants, but is apt to be a few cps in error for the chemical shifts. Thus $J'_{AB}\equiv J_{AB}$ and by the assumption above $\equiv J_{AB}{}^{av}=J''_{AB}$, $J'_{AX}\equiv J_{AX}$, $J'_{BX}\equiv J_{BX}$, $\nu'_A\equiv\nu_A$, $\nu'_B\equiv\nu_B$ and $\nu'_X\equiv\nu_X$. Since there are equal populations at all times in both the primed and double primed systems $J^{av}=(J'+J'')/2$. If all coupling constants are assumed positive we obtain:

$$J''_{AX}=2.8 \text{ cps}$$
$$J''_{BX}=3.8 \text{ cps}$$
$$\nu''_A=-86.2 \text{ cps}=-1.436 \text{ ppm}$$
$$\nu''_B=-93.9 \text{ cps}=-1.565 \text{ ppm}$$
$$\nu''_X=-297.1 \text{ cps}=-4.951 \text{ ppm}.$$

Because of the nature of the assumptions involved, no estimate of the error can be given.

It should be noted that the coupling constants for the same dihedral angles between the C—C—H planes are not identical if the usual tetrahedral angles are not greatly distorted, since $J(\phi=60°)=4.25$, 3.8, and 2.8 cps for $J_{BX}\equiv J'_{BX}$, J''_{BX}, and J''_{AX} respectively. It is also interesting to note that $\nu''_A>\nu''_B$ even though

[10] J. I. Musher, J. Am. Chem. Soc. (to be published).

A″ is equatorial and B″ is axial. This is contrary to the general expectation for greater shielding for axial protons than for equatorial protons which is the case for the *cis*-isomer: $\nu_A > \nu_B$, where here A is axial and B is equatorial. This shows that it is not generally correct that an axial proton is differently shielded than an equatorial proton. For this reason a ring molecule cannot be assumed to be rapidly inverting merely on the basis of a sharp line resonance for a system containing both axial and equatorial protons.[11–13] Instead, low-temperature measurements[14] are necessary to verify that these protons are differently shielded and that the sharp spectrum observed does signify ring inversion.

The chemical shifts for the rigid *trans*-isomer of the acetoxy and X protons using the above rough approximations are as follows:

$$\nu''_X(\text{equat}) = -297.1 \text{ cps} = -4.952 \text{ ppm};$$

$$\nu'_X(\text{axial}) = -280.8 \text{ cps} = -4.680 \text{ ppm};$$

$$\nu''_{\text{acetoxy}}(\text{axial}) = -118.2 \text{ cps} = -1.970 \text{ ppm};$$

$$\nu'_{\text{acetoxy}}(\text{equat}) = -114.0 \text{ cps} = -1.900 \text{ ppm}.$$

This agrees with the observation of Lemieux *et al.*[4] that axial acetoxy groups show resonances at lower fields than do equatorial acetoxy groups and is also in accord with the observations that an equatorial proton on the same carbon as an (axial) acetoxy group has its resonance at lower field than that of an axial proton on the same carbon as an (equatorial) acetoxy group.[4,10,15]

There is no unambiguous assignment possible for the methyl peaks; however, by comparison with the methylcyclohexanols[10] it is expected that the low field peaks belong to the protons on the 1-methyl groups.

IV. CONCLUSIONS

Three proton-proton coupling constants have been found, one of which, $J(\phi_{H-C-H} = 109°28') = 12.36 \pm 0.2$ cps, compares favorably with the theoretical value and two of which, $J_{aa} = J(\phi_{H-C-C-H} = 180°) = 12.35 \pm 0.1$ cps and $J_{ea} = J(\phi_{H-C-C-H} = 60°) = 4.25 \pm 0.1$ cps, do not. The chemical shift between axial and equatorial protons is 0.131 ± 0.002 ppm with the axial proton at higher field.

Another set of coupling constants is determined approximately and also differs from those predicted by the theory. An axial proton is found to occur at lower field than an equatorial proton, contrary to expectation.

V. ACKNOWLEDGMENTS

We should like to thank Dr. R. P. A. Sneeden, who very kindly provided the 1,1,4,4-tetramethylcyclohexyl-2,6-diols[16] from which the acetates were made by standard procedures. We are also grateful to Dr. A. A. Bothner-By of the Mellon Institute, on whose equipment the spectrum of the *cis*-isomer was made. This investigation was supported in part by a fellowship from the National Cancer Institute, Public Health Service, and by the joint program of the Office of Naval Research and the U.S. Atomic Energy Commission.

[11] J. I. Musher and R. E. Richards, Proc. Chem. Soc. **1958**, 230.
[12] J. I. Musher, Spectrochim. Acta **16**, 835 (1960).
[13] S. Brownstein and R. Miller, J. Org. Chem. **24**, 1886 (1959).
[14] F. R. Jensen, D. S. Noyce, C. S. Sederholm, and A. J. Berlin, J. Am. Chem. Soc. **82**, 1256 (1960).
[15] J. N. Shoolery and M. T. Rogers, J. Am. Chem. Soc. **80**, 5121 (1958).
[16] A. W. Allan, R. P. A. Sneeden, and J. Colvin, J. Chem. Soc. **1959**, 2186.

Luminescence in a Scintillation Solution Excited by α and β Particles and Related Studies in Quenching*

ISADORE B. BERLMAN

Radiological Physics Division, Argonne National Laboratory, Argonne, Illinois

(Received August 15, 1960)

The relative intensity of the light pulses produced by α and β particles in a scintillating solution of 2,5-diphenyloxazole (PPO) in xylene has been investigated as a function of the concentration of the solute. The α/β ratio is substantially smaller than that found in organic plastic scintillators. From the data the dynamic quenching parameter has been calculated. Several independent experiments, i.e., measurements pertaining to mean lifetime of fluorescence, uv excitation, and pulse heights, were undertaken to study the mechanisms of quenching by oxygen in a scintillating solution. The best interpretation of the oxygen effect is consistent with the existence of dynamic quenching of the solvent and of the solute.

INTRODUCTION

AN interesting and challenging aspect of the scintillation process in organic solutions is the fact that the ratio of the luminescence yield per unit energy loss for α and β particles, namely the α/β ratio, is less than unity and varies with the solute concentration.[1-3] Although no definitive theory has as yet been presented which completely explains this anomaly, several explanations have been proposed. Galanin and Chizhikova[2] have demonstrated that the small light yield under α-particle excitation for a solution of terphenyl in xylene can be explained by two quenching processes occurring in time intervals which are short and long by comparison to the time of energy transfer; these are called static and dynamic quenching, respectively. Galanin[4] postulates that the short-term quenching component is the result of a "thermal spike." Kallman and Brucker[5] in explaining the low fluorescent yield on excitation by α particles had also assumed the existence of a static quenching component. Birks[6] has extended these concepts to specify that the short-term process affects principally the short-lived second- and third-excited electronic levels of the solvent without affecting noticeably the longer-lived first-excited level from which energy-transfer takes place.[7]

In an earlier publication[8] it was concluded that the efficiency of energy transfer in a solution of PPO and xylene is a linear function of the solute concentration and is independent of whether primary excitation is provided by ultraviolet or electron excitation. In this article, the experimental values of the energy transfer taking place in the above solution when excited by α particles are tabulated as a function of the solute concentration, as are the α/β ratios.

Several independent experimental techniques have been marshalled to investigate the mechanism of oxygen quenching in an aerated scintillating solution.

THEORY

The luminescent yield, L, of a scintillating solution excited by β particles is given by

$$L=L_\beta[p_t/(p_e+p_q+p_t)]\cdot[P_e/(P_e+P_i+P_q)], \quad (1)$$

where p_t, p_e, and p_q are the probabilities/sec, respectively, for energy transfer from the solvent to the solute, for solvent emission of the excitation energy, and for both inter- and intramolecular quenching of the solvent, and P_e, P_i, and P_q are the analogous probabilities, respectively, for emission from the solute, for internal quenching of the solute, and for self-quenching of the solute. P_q is concentration dependent and L_β is a factor proportional to the number of first excited electronic states and to the light collection efficiency of the apparatus. The first set of brackets in Eq. (1) is the expression for the efficiency of energy transfer from xylene to PPO, whereas the last bracketed term expresses the quantum yield of the solute.

The luminescent yield on α-particle excitation can be expressed in a form analogous to Eq. (1), i.e.,

$$L=L_\alpha[p_t/(p_e+p_q+p_t+p_{q_\alpha})]\cdot[P_e/(P_e+P_i+P_q)], \quad (2)$$

in which p_{q_α} is the probability/sec for dynamic quenching of the solvent when the solution is excited by α particles, and L_α is a factor wholly analogous to L_β and the remaining p's and P's have the same meaning as in Eq. (1). It should be noted that the energy-transfer efficiency at a specific solute concentration is smaller when the solution is excited by α particles than when excited by β particles because of the added term, p_{q_α}. Furthermore, it is assumed that (within the accuracy of this experiment), there is no measurable long-term quenching of the solute resulting from α-particle excitation.

* Work performed under the auspices of the U. S. Atomic Energy Commission.

[1] C. T. Reynolds, Nucleonics **10**, 46 (1952).
[2] M. D. Galanin and Z. A. Chizhikova, Optics and Spectroscopy **4**, 196 (1958).
[3] I. M. Rozman and S. F. Kilin, Uspekhi Fiz. Nauk **69**, 459 (1959).
[4] M. D. Galanin, Optics and Spectroscopy **4**, 758 (1958).
[5] H. Kallmann and G. J. Brucker, Phys. Rev. **108**, 1122 (1957).
[6] J. B. Birks (private communication).
[7] S. G. Cohen and A. Weinreb, Proc. Phys. Soc. (London) **B69**, 593 (1956).
[8] I. B. Berlman, J. Chem. Phys. **33**, 1124 (1960).

On adding a quenching substance such as oxygen to the scintillating solution and on exciting the solution with β particles, Eq. (1) become

$$L=L_\beta'[p_t/(p_e+p_q+p_t+p_q')]\cdot[P_e/(P_e+P_i+P_q+P_q')], \quad (3)$$

where p_q' is the probability/sec for solvent quenching, and P_q' is the probability/sec for solute quenching. If static quenching takes place, $L_{\beta'}<L_\beta$. On testing a similar solution with α particles Eq. (2) becomes

$$L=L_\alpha'[p_t/(p_e+p_q+p_t+p_{q_\alpha}+p_q')]\cdot[P_e/(P_e+P_i+P_q+P_q')], \quad (4)$$

where p_{q_α} is assumed to have the same value as in a nitrogenated solution. If static quenching is operative then $L_\alpha'<L_\alpha$.

EXPERIMENTAL PROCEDURE

The scintillating solution under investigation was a solution 2,5-diphenyloxazole (PPO) in paraxylene. The solvent, *p*-xylene, was purified with two distillations in each of which the first and last 20% of the distillate were discarded. After the second distillation, prepurified nitrogen was passed through a cold trap and bubbled through the xylene. Oxygen-free conditions were maintained by storing and handling the solutions in a nitrogen-filled glove box. The solute PPO was used without further purification.

A highly reflecting and easily demountable cell, shown in Fig. 1, was used in making the measurements. The right-cylindrical cup, (internal height of 1.15 in. and internal diameter 1.13 in.) was made from Teflon, a type of material which is inert to the standard organic scintillating solvents and is one of the best diffuse reflectors available.[9] The cell was sealed with a quartz window placed on the shoulder of the cup and held in position by a fluorothene retaining ring which compressed the Teflon against the outer rim of the quartz disk.

Cm^{244} was used as the α-particle source because it is less of a health hazard than Po^{210} and is easily deposited on stainless steel. Cm^{244} in an acetone solution was sputtered[10] on the flat end of a partially threaded stainless steel rod, and then flamed. By rotating the rod in the cell it was possible to position accurately the source close to the window (approximately 0.008 in.) and, therefore, to investigate very thin sample solutions. The β source was a Cs^{137} source deposited on a similar rod positioned approximately $\frac{1}{8}$ in. from the window to accomodate the relatively large range of the internal-conversion β particles. The energy of the α particle was measured to be 5.80±0.05 Mev in a Frisch grid chamber; the β-particle energy was taken to be 624 kev.

[9] W. R. Anderson and I. B. Berlman, J. Opt. Soc. (to be published).

[10] D. J. Carswell and J. Milsted, J. Nuclear Energy **4**, 51 (1957).

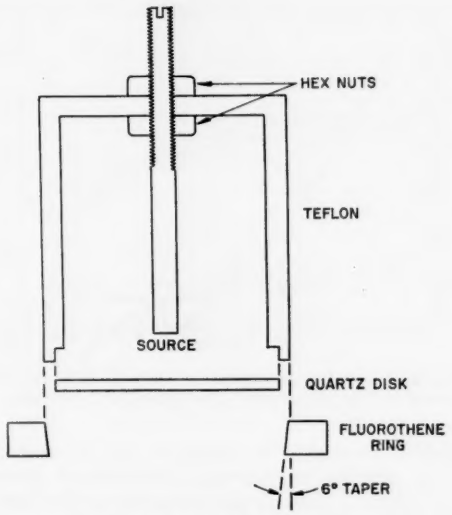

FIG. 1. Teflon cell with source holder.

A 6292 photomultiplier tube and associated electronic apparatus in conjunction with a 20-channel pulse-height analyzer was used to record the α and β light-pulse spectra produced in the cell. See Fig. 2.

The apparatus used in the fluorescence lifetime and uv measurements are described in the work cited in footnote 8.

RESULTS

A. Nitrogenated Solutions

1. Excitation with β Particles

A meaningful comparison between Eq. (1) and the experimental data requires independent evaluation of the parameters involved. In this experiment this has been done for the self-quenching parameter, $P_q/(P_e+P_i)$, and the efficiency for energy transfer parameter, ϵ: The remaining parametric expression, $L_\beta P_e/(P_e+P_i)$, was determined by normalizing the equation at one of the experimental values.

The self-quenching parameter was obtained from the emission intensity excited by 3130-A radiation in solutions containing progressively larger concentrations of PPO. Since the PPO is directly excited by the incident radiation a decrease in the quantum yield with an increase in the solute concentration is to be attributed to self-quenching. A value of $P_q/(P_e+P_i)=0.006C$, where C is the concentration of the solute in g/liter, was obtained.

Experimental values of the efficiency of energy transfer, defined as $\epsilon=p_t/(p_e+p_q+p_t)$, are given in the work cited in footnote 8. These values correspond approximately to $p_t/(p_e+p_q)=7.0C$, where C is the concentration of the solute, and are independent of the mode of excitation, uv or pulsed electrons.

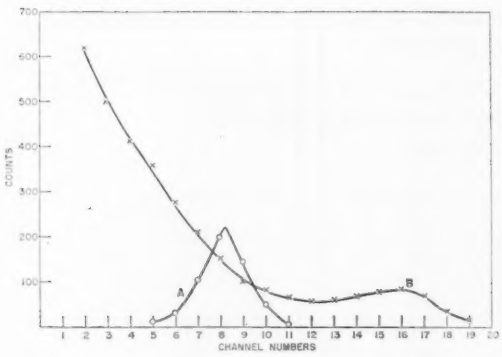

FIG. 2. Curve A is an example of the pulse-height spectrum produced by Cm^{244} α particles; curve B by Cs^{137} β particles.

Substitution of these values in Eq. (1) and comparison with the experimentally determined values of β-ray produced pulse heights vs concentration leads to curve B (Fig. 3) which is a plot of

$$L=217[7.0C/(1+7.0C)]\cdot(1+0.006C)^{-1}, \quad (5)$$

where $L_\beta P_e/(P_e+P_i)=217$ is the result of normalizing Eq. (1) at the experimental value of 1 g/liter.

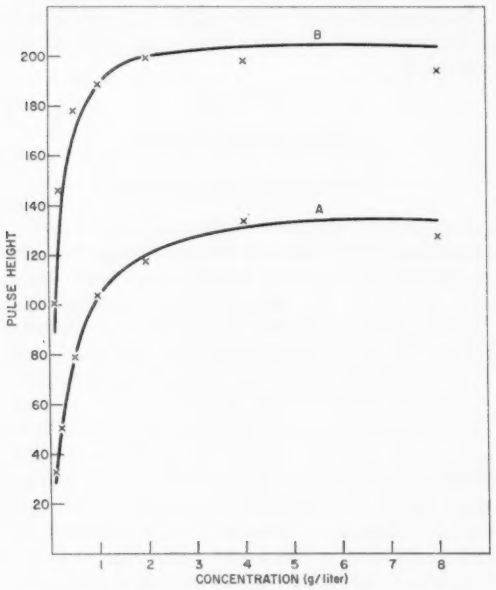

FIG. 3. Luminescent yield from nitrogenated solution versus PPO concentration when excited by α particles, curve A, and β particles, curve B. Curve A is a plot of

$$L=148\left(\frac{2.33C}{1+2.33C}\right)\cdot\left(\frac{1}{1+0.006C}\right).$$

Curve B is a plot of

$$L=217\left(\frac{7.0C}{1+7.0C}\right)\cdot\left(\frac{1}{1+0.006C}\right).$$

The deviations between the theoretical curve and the experimental points is to be ascribed to the necessity of using a sample thickness of $\frac{1}{8}$ in. to stop the 624 kev electrons; within this distance, as shown in a separate experiment performed with uv excitation, radiation transfer as well as absorption and re-emission take place at low and high solute concentrations, respectively. This fact was further confirmed experimentally by repeating the measurements of pulse heights vs solute concentration with a sample 0.008 in. thick. The results, based on a determination of the maximum pulse height in the pulse height spectrum, although not as precise as the method used for the thicker samples, indicated a better fit between the experimental points and the calculated curve.

2. *Excitation with α Particles*

In this case, after retaining the values of $p_t/(p_e+p_q)$ and $P_q/(P_e+P_i)$, the following equation was found to describe adequately the experimentally determined pulse heights as a function of the solute concentration,

$$L=148[7.0C/(1+7.0C+2.0)]\cdot(1+0.006C)^{-1}$$
$$=148[2.33C/(1+2.33C)]\cdot(1+0.006C)^{-1}, \quad (6)$$

in which $p_{q_\alpha}/(p_e+p_q)=2.0$ and $L_\alpha P_e/(P_e+P_i)=148$ are the result of normalizing the light-output curve at the concentration of 1 g/liter and of tailoring the theoretical curve for the best fit with the experimental points. Since thin sample are used and two parameters are required for the normalization, the fit between the mathematical curve and the data is much better than in the case of excitation by β particles, as shown by curve A in Fig. 3.

TABLE I. Calculated efficiencies of energy transfer and the α/β ratios as a function of the solute concentration.

Concentration of PPO (g/liter)	$\epsilon(\beta)$	$\epsilon(\alpha)$	α/β ratio
0.1	0.41	0.19	0.035
0.2	0.58	0.32	0.038
0.5	0.78	0.54	0.048
1.0	0.88	0.70	0.059
2.0	0.93	0.82	0.064
4.0	0.97	0.90	0.072
8.0	0.98	0.95	0.071

In columns 2 and 3 of Table I are tabulated the efficiencies of energy transfer, namely $\epsilon=7.0C/(1+7.0C)$ and $\epsilon=2.33C/(1+2.33C)$, as a function of the solute concentration under: (1) excitation by β particles and (2) excitation by α particles, respectively. The α/β ratios shown in column 4 of Table I are computed from the experimentally determined pulse heights and have an uncertainty of approximately 5%.

To obtain the α/β ratio in a plastic scintillator of thicknesses similar to those used for solutions, two disks, 0.125 in. and 0.005 in. in thickness were freshly machined from a sample of Pilot B plastic scintillator[11] and excited, respectively, by β and α particles. Each plastic sample was positioned between the source and the quartz window of the teflon cell; mineral oil being used to provide optical coupling between the sample and the window. The experimentally determined value value of the α/β ratio is 0.095 ± 0.004.

B. Aerated Solutions

1. Experiments Involving uv and Lifetime Measurements

Oxygen, a molecule known to quench the excitation energy of a scintillation solution,[12] was introduced by bubbling air through the solution. To differentiate the quenching component affecting the solute from that affecting the solvent, independent experiments were performed using uv excitation and lifetime measurements as in the work cited in footnote 8.

To determine the magnitude of oxygen quenching of PPO, solutions of PPO in nitrogenated and aerated xylene were irradiation with 3130-A radiation to excite the solute directly and the resultant intensities of the emission spectra were compared; from the decrease of the emission intensity the oxygen quenching parameter was found to be $P_q'/(P_e+P_i)=0.12\pm0.01$. The type of quenching may be described primarily as dynamic quenching, since the measured mean lifetime of PPO is decreased by oxygen.

As an aid in interpreting what mechanisms are operative when excitation is produced by ionizing radiation the following experiment was performed with uv radiation to determine the magnitude of the oxygen quenching on the first excited state of the solvent molecule. A solution sample, 0.05 mm in thickness, was excited with 2650-A radiation and the resultant radiation spectrum was recorded under aerated and nitrogenated conditions. The intensity of the emission spectrum from the aerated sample slowly increased with time until an equilibrium condition was obtained, i.e., $p_q'/(p_e+p_q)$ decreased from a value of 2.8 to 0.9 in approximately 10 min. At no time did the magnitude of the spectrum from an aerated sample approach that from the nitrogenated sample. On shutting off, by use of a shutter, the incident radiation for a few minutes and then continuing the excitation, the magnitude of the emission spectrum returned again to a low value. When a thicker sample of xylene, 1 mm, was illuminated under similar circumstances the intensity of the emission spectrum did not increase with time. An explanation compatible with these observations will be given in the section entitled Discussion.

Lifetime measurements of nitrogenated and aerated xylene samples were made by means of pulsed electron techniques[8] in an attempt to determine directly the magnitude of the dynamic quenching parameter. Normally, in performing this experiment with nitrogenated solutions the sample is covered with a double thickness of 0.0025-in. aluminum foil. The pulsed-electron beam passes through the two layers of foil. In measuring the mean lifetime of aerated solutions the experiment was performed with and without the aluminum foil covering the solution, and lifetimes of 8.2 and 6.3 nanosec, respectively, were obtained. From these values and the value of the lifetime of nitrogenated xylene, 20.2 nanosec, the value of the quenching parameter $p_q'/(p_e+p_q)$, was obtained; namely, 1.5 and 2.2, respectively.

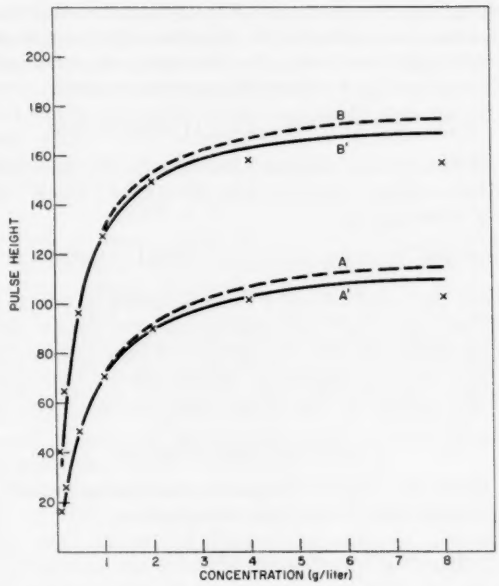

FIG. 4. Luminescent yield from an aerated solution versus PPO concentration when excited by α particles and β particles. Curve A is a plot of

$$L=148\left(\frac{7.0C}{1+7.0C+2.0+2.8}\right)\cdot\left(\frac{1}{1+0.12+0.006C}\right).$$

Curve A′ is a plot of

$$L=140\left(\frac{7.0C}{1+7.0C+2.0+2.3}\right)\cdot\left(\frac{1}{1+0.12+0.006C}\right).$$

Curve B is a plot of

$$L=217\left(\frac{1}{1+7.0C+2.5}\right)\cdot\left(\frac{2}{1+0.12+0.006C}\right).$$

Curve B′ is a plot of

$$L=208\left(\frac{7.0C}{1+7.0C+2.1}\right)\cdot\left(\frac{1}{1+0.12+0.006C}\right).$$

2. Experiment with β Particles

The equations $p_q'/(p_e+p_q)=2.5$ and $P_q'/(P_e+P_i)=0.12$, which are obtained from independent measure-

[11] Pilot Chemical Company, Waltam 54, Massachusetts.

[12] R. W. Pringle, L. D. Black, B. L. Funt, and S. Sobering, Phys. Rev. **92**, 1582 (1953).

ments, are incorporated in Eq. (3) and the resultant equation is compared to the experimentally determined pulse heights as a function of the solute concentration. Curve B of Fig. 4 depicts this equation, namely,

$$L=217[7.0C/(1+7.0C+2.5)]\cdot(1+0.12+0.006C)^{-1}.$$

If the excited xylene molecules are statically quenched by the oxygen molecules then $L_\beta'<L_\beta$. Curve B' in Fig. 4 is a plot of

$$L=208[7.0C/(1+7.0C+2.1)]\cdot(1+0.12+0.006C)^{-1},$$

where the values 208 and 2.1 were obtained by tailoring the calculated curve to fit the experimental value to the same degree that Eq. (5) agrees with its experimental values. It is noted that as L_β' is made smaller, the value of the ratio $p_q'/(p_e+p_q)$ is also made smaller.

3. *Experiment with α Particles*

Curve A in Fig. 4 depicts the relationship between the experimental points and the equation

$$L=148[7.0C/(1+7.0C+2.0+2.8)]\cdot(1+0.12+0.006C)^{-1},$$

where the following equalities have been used: $p_{q_\alpha}/(p_e+p_q)=2.0$ and $p_q'/(p_e+p_q)=2.8$.

Assuming that the excited xylene molecules are statically quenched by the oxygen molecules then $L_\alpha'<L_\alpha$. Curve A' is a plot of

$$L=140[7.0C/(1+7.0C+2.0+2.3)]\cdot(1+0.12+0.006C)^{-1}.$$

It is noted also that in this case as L_α' is made smaller so is the value of $p_q'/(p_e+p_q)$.

DISCUSSIONS

In the literature, the α/β ratios have usually been obtained with a Po^{210} α particles and Cs^{137} β particles. Although the α particles from our Cm^{244} source have a slightly larger energy than the particles from Po^{210}, the α/β ratio should not be noticeably different since the numerator and the denominator each have dimensions of energy^{-1}.

The α/β ratios reported here were determined under optimum experimental conditions involving the use of a highly purified solvent in thin nitrogenated samples wherein the ratios, in contrast to experiments reported heretofore, are 20 to 30% lower than those published for organic crystals and plastic scintillators, and vary rather sharply with solute concentration (cf. Galanin and Chizhikova's[2] contention that the α/β ratios in fluorescent solutions and the fluorescent plastics are essentially equal). The present procedure leaves little doubt as to experimental mistakes since it was checked in two ways: (1) the α-particle energy available to the solution was accurately calibrated and (2) the α/β ratio of a Pilot B plastic scintillator was measured and found to be in the range normally given, i.e., 0.10 ± 0.01.

A possible objection to the procedure in measuring the α/β ratio of the fluorescent plastic is the use of a very thin sample in conjunction with the α source. Since the Pilot B plastic scintillator contains a wavelength shifter, the fluorescence spectrum emerging from a thin sample might be expected to differ from that from a thicker sample: namely, the spectrum would not be completely shifted to the longer wavelengths. It was found, however, that the use of a $\frac{1}{8}$-in. sample did not increase the pulse height.

The variation in the value of the α/β ratio with the solute concentration, as shown in column 4 of Table I, is the result of the dynamic quenching parameter, p_{q_α}, affecting in greater measure the efficiency of energy transfer at the lower solute concentrations as shown in column 3. At values of the solute concentration greater than 4 g/liter, p_{q_α} becomes ineffective and the limiting value of the α/β ratio is determined by the static quenching, i.e., by L_α/L_β, each referred to unit energy.

The ratio $p_{q_\alpha}/(p_e+p_q)=2.0$ was experimentally determined under oxygen-free conditions. By assuming, with some trepidation, that p_{q_α} has the same value in an aerated solution as in a nitrogenated solution and correcting for the dynamic quenching of oxygen the following value is obtained, $p_{q_\alpha}/(p_e+p_k)=0.57$, where p_k includes the added dynamic quenching of oxygen. The value of this ratio is slightly less than the value, 0.85, obtained by Galanin and Chizhikova[2] for aerated solutions of terphenyl in xylene.

If p_{q_α} is the result of a thermal effect then it is logical to assume that the value of p_{q_α} is the same in aerated as in nitrogenated solution. However, if p_{q_α} is the result of radicals and radiation products then it may have a slightly different value in the two cases. Our assumption has been that it has the same value in both cases. The magnitude of p_{q_α} is somewhat dependent on the value specified for $p_t/(p_e+p_q)$.

In the experiments in which thin aerated xylene samples were illuminated with 2650-A radiation the magnitude of the quenching parameter $p_q'/(p_e+p_q)$ was not constant, but decreased with time. If one assumes that dynamic quenching is the principal process acting to reduce the emission, then this quenching parameter equals 2.8, although after a few minutes it decreases to a value of 0.9. An explanation compatible with these observations is that a photochemical reaction takes place between an excited xylene molecule and an oxygen molecule which results in partially or totally *inactivating* the oxygen molecule as a quenching agent. This phenomenon is not observed when a large volume of liquid is exposed to the incident radiation because of the larger reservoir of oxygen; moreover, in the case of thin cells when the short wavelength excitation is temporarily removed by means of a shutter,

more oxygen diffuses into the illuminated area and the emission is again reduced. It has come to the author's attention that a similar effect has been reported by G. M. Almy, H. O. Fuller, and G. D. Kinzer [J. Chem. Phys. **8**, 37 (1940)].

The same interpretation is applicable to the results obtained in the measurements of the mean lifetime of aerated xylene. When the thin sample is uncovered, the oxygen in the solvent (depleted by the repeated bursts of electrons) is replaced by fresh oxygen which can diffuse into the solution through the surface of the liquid; whereas the oxygen in the solution covered with the aluminum foil is progressively depleted during the finite time that is required to complete the measurement. Hence, since there is also the possibility of quenching by gaseous radiation products such as ozone or by radiation products involving oxygen in the solution, in the former case and the possibility of oxygen depletion in the latter, the values of $p_q'/(p_e+p_q)$ obtained by this method are open to objection.

When excitation is produced in an aerated solution by α and β particles the value of the dynamic quenching parameter of oxygen, 2.6 ± 0.2, as obtained from an experiment using uv excitation, may be used to adequately explain the results. It is entirely possible that a small percent ($\leq 5\%$) of excited xylene molecules may be statically quenched by the oxygen molecules. Concomitant with this assumption it must be assumed that the dynamic quenching parameter is slightly less than the value of 2.6 ± 0.2, as shown in Eqs. (7) and (8). An explanation consistent with this reduction in the dynamic quenching parameter is that certain short-lived processes, acting immediately after the passage of the α or β particles, *inactivate* some of the oxygen in the vicinity of the α and β tracks so that the energy-transfer process takes place in an environment partially depleted of oxygen, much the same as with massive uv radiation. Although it is known that radiation products readily combine with oxygen (as reported by Gordon *et al.*[13]) it is impossible at this time to specify whether or not the reaction time would be much shorter than the energy-transfer time, or whether the noted effect is the result of other processes such as subexcitation electrons.

A simple calculation of the number of oxygen molecules which would be removed by an α-induced reaction of the type $H+O_2$ with a G value of 2 in a cylindrical volume with a radius of five molecules and a height equal to the length of the α-particle track shows that most of the oxygen would be removed. In the case of a β-particle track the relatively large length of the track militates against inactivating an appreciable amount of the oxygen if one assumes that energy is lost continuously along the track. However, since a large fraction of the energy of the electron is lost in clusters and spurs, such as delta rays, it is possible that a small fraction of the oxygen in their vicinity is also inactivated. In any event more detailed work is contemplated to define more clearly the process involved.

In conclusion, the necessity of including P_q' in Eqs. (7) and (8), in conjunction with the observation that the mean lifetime of PPO is decreased by oxygen, implies that the solute is dynamically quenched by oxygen molecules. Thus, the total effect of oxygen can be interpreted to be principally dynamic quenching of the excited solvent and solute molecules: Static quenching of the solvent, if present, is small and of the order of $\leq 5\%$.

ACKNOWLEDGMENTS

The author wishes to thank L. D. Marinelli for his advice and encouragement. Grateful acknowledgement is made to R. F. Barnes for preparing the sources, W. L. Buck for the use of the lifetime measuring apparatus, to Dr. A. Weinreb and Dr. L. M. Dorfman for stimulating discussions, and to H. F. Lucas, Jr., for measuring the energy of the α particles.

[13] S. Gordon, A. R. Van Dyken, and T. F. Doumani, J. Phys. Chem. **62**, 20 (1958).

THE JOURNAL OF CHEMICAL PHYSICS VOLUME 34, NUMBER 2 FEBRUARY, 1961

Pauling's Model and the Thermodynamic Properties of Water

HENRY S. FRANK AND ARVIN S. QUIST*

Department of Chemistry, University of Pittsburgh, Pittsburgh, Pennsylvania

(Received June 28, 1960)

A statistical-thermodynamic treatment is given of the model for liquid water recently proposed by Pauling, in terms of a variable distribution of water molecules between the two states—framework water and interstitial water—for which this model provides. This treatment shows that, with simple assumptions, the model can give a satisfactory representation of the *P-V-T* properties of water over limited ranges of temperature and pressure. The properties (enthalpies and entropies) which are derived for framework and interstitial water, respectively, also seem physically reasonable. The simple model is less successful in representing the heat capacity of water and the partial molal properties of nonpolar solutes. The fact that water is a liquid, however, requires that some molecules be in a "third state," and it is suggested that if this third state is taken into consideration the shortcomings of the simple model can be remedied. Adoption of the Pauling model would seem to have as a corollary the likelihood that the structural "transition," purportedly found in liquid water just above 30°C, may be real.

1. INTRODUCTION

THE existence of a structured, or ice-like, component in liquid water has long[1] been postulated to account for the phenomenon of maximum density and related effects. This fundamental notion has been employed in a variety of forms,[2] all more or less, but none completely, successful in meeting the twin requirements of physical acceptability and ability to explain in detail the things that water actually does. Pauling has recently[3] put forward a new modification of it, suggesting that liquid water has a stucture, or range of structures, similar to those of the so-called gas hydrates,[4] which consist of a framework of ordered water, so made up as to contain voids in which nonhydrophilic molecules—Kr, Cl_2, C_2H_5Cl, among many others—are trapped, so to speak, in a clathrate structure. These have been called krypton hydrate, chlorine hydrate, etc. In this sense, according to Pauling's suggestion, liquid water can be regarded as a "water hydrate," consisting of some such framework as is found in the clathrate crystals, with the enclosed sites occupied by unbonded water molecules.

The frameworks in question may be thought of as based upon a pentagonal dodecahedron of 20 water molecules, each participating in 3 hydrogen bonds, one such bond lying in each of the 30 edges of the solid figure. The inside of such a dodecahedron contains a void of about 5 A in unobstructed diameter. Dodecahedra may form additional hydrogen bonds with each other, or by fusing together (sharing pentagonal faces), and may also be joined through bridge waters hydrogen-bonded to them. Such linkage, fusion and bridging give rise to fully bonded structures containing other types of voids, one of which, for example, may be described as the inside of a tetrakaidecahedron, which has 12 pentagonal and 2 hexagonal faces. These are "large" voids (6 A or more of free diameter), as contrasted with the "small" ones in the dodecahedra. Structures of this general class have also been found by Jeffrey and his co-workers[5] to characterize the high hydrates of such salts as tetra isoamyl ammonium fluoride (38 H_2O), and tri-*n*-butyl sulfonium fluoride (20 H_2O), and the suggestion that liquid water contains them is an attractive one.

Pauling[3] has stated that certain properties of water—density, and dispersion of dielectric constant—can be accounted for by his model, but there has as yet been no attempt, so far as we are aware, to see whether, or how, it can provide for the density maximum or for the "structural compressibility,"[6] which are among the most characteristic features which water displays. It is the purpose of this essay to show how, with certain reasonable interpretations, the model can be made to satisfy such requirements.

2. STATISTICAL AND THERMODYNAMIC TREATMENT

We follow Frank and Wen[7] in postulating that the formation of bonded structure in liquid water is a cooperative process in which "flickering clusters" of

* Present address: Department of Chemistry, University of Nebraska, Lincoln, Nebraska.

[1] For a review of the theories of water structure up to 1927 see H. M. Chadwell, Chem. Revs. **4**, 375 (1927).

[2] See, for example, the outline given by F. S. Feates and D. J. G. Ives, J. Chem. Soc. **1956**, 2798.

[3] (a) *Hydrogen Bonding*, edited by D. Hadzi (Pergamon Press, London, 1959), p. 1; (b) L. Pauling, *The Nature of the Chemical Bond* (Cornell University Press, Ithaca, New York, 1960), 3rd Ed., p. 472.

[4] (a) L. Pauling and R. E. Marsh, Proc. Natl. Acad. Sci. U. S. **38**, 112 (1952); (b) W. S. Claussen, J. Chem. Phys. **19**, 259, 662, 1425 (1951); (c) M. von Stackelberg and H. R. Müller, *ibid.* **19**, 1319 (1951); (d) Z. Elektrochem. **88**, 25 (1954).

[5] "Polyhedral clathrate 'ice' structures in some high hydrates" by G. A. Jeffrey, D. Feil, and R. K. McMullan, at the International Union of Crystallography, Cambridge Meeting, August 14–24, 1960. See *Acta Crystallographica* for abstract.

[6] (a) L. Hall, Phys. Rev. **73**, 775 (1948); (b) T. A. Litovitz and E. H. Carnevale, J. Appl. Phys. **26**, 816 (1955); (c) A. H. Smith and A. W. Lawson, J. Chem. Phys. **22**, 351 (1954).

[7] (a) H. S. Frank and W. Y. Wen, Discussions Faraday Soc. **24**, 133 (1957); (b) H. S. Frank, Proc. Roy. Soc. (London) **A247**, 481 (1958).

varying extent form, relax, and reform in a temporal sequence, and a spatial pattern, determined by the energy fluctuations which are constantly taking place. In these terms, Pauling's model may be regarded as specifying a particular class to which such flickering clusters may be imagined to belong. For our present purpose the only necessary feature of this class is that in it some fraction of the water is in the form of unbonded (monomeric) molecules which are interior to a bonded framework and may be described as occupying interstitial sites in it. We shall therefore use the term "Pauling model" to refer to any assumed structure in which this is true. Since it is this feature of the clusters which is under study we make the further simplifying assumption that a snapshot would find the water sample made up entirely of such clusters—we shall treat a quasi-solid model, and ignore the possible presence of any molecules which are not either framework water or interstitial water in the sense just described. The phenomena in which we are interested, however, require the existence of an equilibrium which can be shifted by changes in temperature and pressure, and there must therefore be some feature of the model which is describable in terms of a variable parameter. This need is met by assuming that the quasi-crystal is imperfect in the sense that some of the interstitial sites are left vacant. Such a possibility is suggested by the experimental observation[8] that an acetone hydrate can apparently lose variable amounts of acetone without impairment of the water framework. The following discussion is therefore of an imperfect quasi-crystal of the Pauling class, with a variable degree of occupancy of interstitial sites.

Let the sample consist of N molecules, of which the fraction f composes the framework, and the fraction $(1-f)$ the monomeric, or nonframework, portion. If V_{fr} is the volume (per mole of H_2O) of the framework, then, on this representation, the molal volume of the liquid (around 18 cc) is $V_l=fV_{fr}$. The framework is assumed to provide a definite number of interstitial sites, this being specified in terms of a parameter ν, the number of framework waters per site, making the number of sites present in a water sample of N molecules equal to Nf/ν. Among these sites are distributed $N(1-f)$ monomeric molecules. Making the simplest assumptions, namely, that all sites are occupied with equal probability and that the probability that a given site will be occupied is the same whether or not any other site is occupied, the number of ways in which the monomers can be distributed among the sites is

$$(Nf/\nu)!/[N(1-f)]![Nf/\nu-N(1-f)]!,$$

k times the logarithm of this number will be, in this model, the counterpart of the entropy of mixing of a binary liquid mixture. Employing the customary approximations, it is, per mole of water,

$$S^M=R\left[f/\nu\ \ln\frac{f/\nu}{f/\nu-(1-f)}-(1-f)\ \ln\frac{(1-f)}{f/\nu-(1-f)}\right]. \tag{1}$$

This has the required properties of going to zero as $f\rightarrow 1$, and as $(1-f)\rightarrow f/\nu$, i.e., as $f\rightarrow[\nu/(\nu+1)]$. The lower limit to f corresponds to the formal physical property of the model that it must break down if more of the framework "melts" than corresponds to filling all of the sites in what remains.

Still keeping to the simplest assumptions, one may use Eq. (1) to write, for the molal Gibbs free energy of the liquid,

$$F=f\{F_{fr}^\circ+\alpha[(1-f)/f]\}+(1-f)F_m^\circ$$
$$-RT\left[f/\nu\ \ln\frac{f/\nu}{f/\nu-(1-f)}-(1-f)\ \ln\frac{(1-f)}{f/\nu-(1-f)}\right]. \tag{2}$$

Here F_{fr}° and F_m° are hypothetical standard molal free energies of (empty) framework and pure "standard" monomer, respectively. If the framework is not empty its molal free energy will be altered in proportion as sites have been filled, and the term $\alpha[(1-f)/f]$ in the first bracket is designed to account for this. Equation (2) rearranges to

$$F=F_m^\circ+\alpha+f(\Delta F^\circ-\alpha)$$
$$-RT\left[f/\nu\ \ln\frac{f/\nu}{f/\nu-(1-f)}-(1-f)\ \ln\frac{(1-f)}{f/\nu-(1-f)}\right], \tag{3}$$

where $\Delta F^\circ=F_{fr}^\circ-F_m^\circ$, the standard free energy change, per mole of H_2O, for the transformation of monomeric water into empty framework. It is related to f by an equilibrium constant expression, which can be obtained by minimizing F with respect to f, i.e., setting $(\partial F/\partial f)_{P,T}=0$.[9]

Carrying out this operation leads to

$$(\Delta F^\circ-\alpha)/RT=\nu^{-1}\ln\frac{f/\nu}{f/\nu-(1-f)}+\ln\frac{(1-f)}{f/\nu-(1-f)}. \tag{4}$$

This also has required formal properties, namely, that $\Delta F^\circ\rightarrow-\infty$ as $f\rightarrow 1$, and $\Delta F^\circ\rightarrow+\infty$ as $f\rightarrow[\nu/(\nu+1)]$; the framework must be infinitely stable (energetically) with respect to the monomer to prevent any of the latter from forming, and the monomer must be infinitely stable with respect to the framework if the last interstitial site is to be filled. [In practice, of course, if the monomer

[8] Unpublished work in this laboratory.

[9] This method of proceeding from an assumed entropy of mixing to an equilibrium constant can be employed in analyzing other models for liquid water. Such an analysis shows that the equilibrium constant employed by Hall,[6a] Litovitz and Carnevale,[6b] and Smith and Lawson,[6c] namely,

$$[f/(1-f)]=\exp(-\Delta F^\circ/RT)$$

corresponds to simple mole-fraction entropy of mixing of icelike and unicelike components, and no heat of mixing, and therefore suffers from whatever defects these assumptions contain.

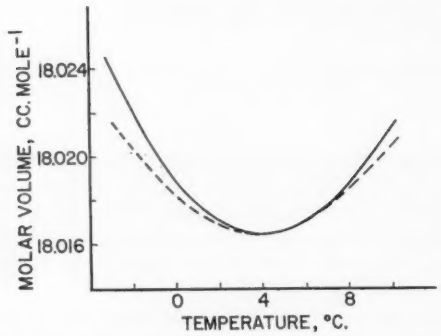

FIG. 1. Change of volume of water with temperature. —— experimental; ------ calculated, as described in text.

were so overwhelmingly "preferred," the framework would break down. This is an eventuality which Eq. (4) can not take account of, since it lies outside the model discussion of which the equation is a part.]

Of special interest is the question how, on this model, f will be influenced by changes in such intensive parameters as temperature and pressure. Letting ξ be such a parameter, and differentiating both sides of Eq. (4) with respect to it (ν being kept constant), leads to

$$\partial f/\partial\xi = -\nu f(1-f)[f/\nu-(1-f)] \times(\partial/\partial\xi)[(\Delta F^\circ-\alpha)/RT]. \quad (5)$$

It is instructive to compare this expression with the corresponding one found for the "simple" model referred to in footnote 9. There the equilibrium constant $[f/(1-f)] = \exp(-\Delta F^\circ/RT)$ leads to

$$\partial f/\partial\xi = -f(1-f)(\partial/\partial\xi)(\Delta F^\circ/RT). \quad (5a)$$

The extra factor $[f-\nu(1-f)]$ in (5) causes the latter to make f respond much more slowly to changes in ξ than it does in (5a), and will, in fact, bring f to a dead stop at $f=[\nu/(\nu+1)]$. This relative insensitivity of f to external changes is characteristic of the Pauling model.

Proceeding, Eq. (5) can be particularized to

$$(\partial f/\partial T)_P = f(1-f)[f-\nu(1-f)][(\Delta H^\circ-\alpha)/RT^2] \quad (6)$$

and

$$(\partial f/\partial P)_T = f(1-f)[f-\nu(1-f)](-V_{fr}/RT). \quad (7)$$

In (6) ΔH° is $H_{fr}^\circ - H_m^\circ$, and α has been treated as independent of temperature. It will be negative, as will ΔH°, and the latter ought to be somewhat the larger in absolute magnitude, so that $(\partial f/\partial T)_P$ will be negative, in agreement with expectation.

In (7) ΔV° has been set equal to V_{fr}, for on this model the interstitial water has the interesting formal property of occupying no volume. This property is employed again in obtaining expressions for the structural expansibility, α^{st}, and the structural compressibility, β^{st}, i.e. the contributions to these quantities which arise from the shifting of the structural equilibrium. They are easily evaluated as

$$\alpha^{st} = (1/V)(\partial V/\partial T)_P{}^{st} = (1/V)\times V_{fr}(\partial f/\partial T)_P = (\partial \ln f/\partial T)_P = (1-f)[f-\nu(1-f)][(\Delta H^\circ-\alpha)/RT^2] \quad (8)$$

and

$$\beta^{st} = -(1/V)(\partial V/\partial P)_T{}^{st} = (-1/V)\times V_{fr}(\partial f/\partial P)_T = -(\partial \ln f/\partial P)_T = (1-f)[f-\nu(1-f)](V_{fr}/RT). \quad (9)$$

A corresponding expression for the "structural" part of the heat capacity is

$$C_P{}^{st} = (\Delta H^\circ-\alpha)(\partial f/\partial T)_P = f(1-f)[f-\nu(1-f)]R[(\Delta H^\circ-\alpha)/RT]^2. \quad (10)$$

3. NUMERICAL APPLICATION

The fact that equations like (8)–(10) can be written shows that, in principle, the provision of a variable degree of occupancy of interstitial sites enables a Pauling model to display some of the special qualitative features of liquid water. To go beyond this it is necessary to make more specific assumptions, and, as an illustration of what kind of results can be obtained, we have chosen, for a framework, that described by Pauling and Marsh[4a] for chlorine hydrate. This has a unit cell of 11.88 A (at 4°C), containing 46 water molecules. It affords 6 "spheroidal" cavities, each of which is able to contain a Cl_2 molecule, and 2 smaller cavities interior to dodecahedra. We allow 2 interstitial waters to enter each of the larger cavities, but leave the smaller ones unoccupied. This assumption makes $\nu = (46/12) = 3.83$, and $V_{fr} = (11.88)^3\times10^{-24}\times 6.02\times10^{23}\div 46 = 22.0$ cc/mole at 4°C. With this choice, f will always be near 18.0 cc/22.0 cc = 0.818. This contrasts with $f\approx0.25$, which Litovitz and Carnevale[6b] find necessary on the simple mixture model in order to explain their inferred values of β^{st}. Our values of f and ν make $\Delta F^\circ-\alpha$, according to Eq. (4), equal to +1180 cal/mole at 0°C.

4. EXPANSIBILITY

Equation (8) shows that the structural expansibility will be negative in the expected case where $(\Delta H^\circ-\alpha) < 0$. The density maximum of water will therefore occur if, or when, this negative structural expansibility just balances the positive expansibility of the framework. To make a numerical check it is thus necessary to make an assumption regarding the latter. We have chosen to write $V_{fr} = 22.0[1+33\times10^{-5}(t-4)+33\times10^{-7}(t-4)^2]$ cc/mole, where t is the centigrade temperature. In Eq. (6), also, we have taken $\Delta H^\circ-\alpha$ as −2210 cal/

mole, independent of temperature. With these assumptions, starting from the volume of a mole of water at any temperature, the volume at any other temperature may be computed as $V(t)=f(t)\times V_{\text{fr}}(t)$. The result obtained with the constants quoted is shown in Fig. 1, where equality between V_{calc} and V_{exp} was forced at 4°C. The fit could be improved by further juggling of constants, or by making ΔH° temperature-dependent, but there would be no point in this as the agreement is already better than the model itself (see below).

5. DERIVED PROPERTIES OF FRAMEWORK AND MONOMER

Our assumptions, and the requirements of fitting the volume-temperature curve of water, lead to $\Delta F^\circ-\alpha=+1180$ cal/mole and $\Delta H^\circ-\alpha=-2210$ cal/mole for removing an interstitial water and incorporating it into the framework, at 0°C. ΔS° for this process is therefore $(-2210-1180)/273=-12.43$ eu. But S_l, the molal entropy of the liquid, is $fS_{\text{fr}}+(1-f)S_m^\circ+\Delta S^M=S_m^\circ+f\Delta S^\circ+\Delta S^M$. The last term can be evaluated from Eq. (1), and comes out equal to 0.18 eu, S_l is therefore equal to $S_m^\circ-0.818\times12.43+0.18=S_m^\circ-10.1$ eu, but S_l is equal to $S_{\text{ice}}+527$ eu and $S_{\text{ice}}=S^\circ(g)-34.6$ eu, so that $S_m^\circ=S^\circ(g)-19.2$ eu. Here $S^\circ(g)$ is the standard entropy of water vapor at 0°C and a hypothetical pressure of 1 atm, i.e., a hypothetical volume $V/N-(22\,400)/6.02\times10^{23}=3.72\times10^{-20}$ cm^3 $=3.72\times10^4$ A^3 per molecule. If the interstitial molecules in this model are taken as being in a physical state corresponding to that of a perfect gas except that each is confined in a "harmonic-oscillator free-volume box" of volume v, then,[10] remembering that occupancy of interstitial sites is not "communal," whereas the occupancy of V/N is, and that the effective box size varies with temperature, $S^\circ(g)-S_m^\circ=19.2$ eu $=4.575\log\{(3.72\times10^4)/[v\times(2.718)^4]\}$. This makes $v=1.425$ A^3, or (1.13 A).[3] This is clearly of the right order of magnitude. One thing that this means is that no appreciable restriction of rotation can be ascribed to the interstitial molecules without either making considerable and implausible changes in our constants or, alternatively, ascribing unreasonably large dimensions to the cavities. The idea that interstitial molecules should be able to rotate freely is not, however, unreasonable since (a) they should be in rather symmetrical fields, and (b) the dipole moment of the molecule tends to be "averaged out" in most of the rorational states,[11] and it is of considerable interest that evidence which seems to require the existence of freely rotating molecules has been found experimentally by Hughes, Palevsky, *et al.*[12] in their study of the scattering of cold neutrons by liquid water.

Another entropy comparison can be made. From the numbers given above, $S_{\text{fr}}-S_m^\circ=-12.43$ eu, and $S_{\text{ice}}-S_m^\circ=-15.37$ eu. This gives $S_{\text{fr}}-S_{\text{ice}}=2.94$ eu. Some such difference is to be expected. Hibben[13] gives the "hindered translation" frequencies observed in Raman spectra of ice and water, respectively, as 205 cm^{-1} and 144 cm^{-1}. On our model, the latter frequency would have to be ascribed to the framework. This change in frequency for a mole of monochromatic oscillators at 0°C corresponds to an increase in entropy of 0.68 eu. The approximate agreement between our 2.94 eu and what would arise from this softening of vibrations in three directions is amusing, but the complexity of the low-frequency Raman spectra of ice, as analyzed by Ockman,[14] and of water as revealed by neutron scattering,[12] makes it impossible to say more than that the framework might well have the entropy which this model, and this assignment of parameters, gives to it.

The same kind of arithmetic can be done with heats, taking note of the fact that H_m° and α never occur separately. This corresponds to the property of the model which permits monomers to exist only when occupying interstitial sites, and causes $(H_m^\circ+\alpha)$ to be, in effect, a single quantity—a sort of partial molal enthalpy of the monomer-in-its-site. Using $\Delta H^\circ-\alpha=-2210$ cal/mole and $f=0.82$, we get $H_l=H_m^\circ+\alpha+f(\Delta H^\circ-\alpha)=H_m^\circ+\alpha-1810$ cal/mole. Since, at 0°C, $H(g)-H_l=10\,800$ cal/mole, this means that $H(g)-(H_m^\circ+\alpha)=9$ kcal/mole, approximately. The inference from entropies, that the monomers are freely rotating, means that this binding must arise from van der Waals-type forces. Such forces, in ice, with 4 nearest neighbors, are commonly thought to account for some 3 kcal/mole of binding energy. Here, with many more neighbors, a stronger binding is to be expected, though, in view of the looseness of fit of monomers in sites, it is difficult to say how close to 9 kcal/mole a predicted value will be.

The other number of interest, $H_{\text{fr}}^\circ-H_{\text{ice}}$, comes out approximately 1 kcal/mole. This is an essentially reasonable quantity, though in this case the computation from Hibben's frequency shift falls far short of accounting for it.

6. ISOTHERMAL COMPRESSIBILITY

A treatment parallel to that in Sec. 4 uses the relation $(\partial\ln V/\partial P)_T=(\partial\ln f/\partial P)_T+(\partial\ln V_{\text{fr}}/\partial P)_T$, along with

[10] H. S. Frank, J. Chem. Phys. **13**, 478 (1945).

[11] Cf. J. H. Van Vleck, "Electric and Magnetic Susceptibilities" (Oxford University Press, New York, 1932), p. 184. This suggests the interesting idea that these interstitial water molecules are in rotational states that make them "nonhydrophilic," a notion which would accord with v. Stackelberg's thesis (footnote reference 4d) that only nonhydrophilic substances form clathrate hydrates.

[12] D. J. Hughes, H. Palevsky, W. Kley, and E. Tunkelo, Phys. Rev. **119**, 872 (1960). This evidence consists of the observation of a group of scattered neutrons which have gained a sharply-defined, but very small, amount of energy from the water sample. The amount of energy in question, $(0.5\pm0.15)\times10^{-3}$ ev or 4.0 ± 1.2 cm^{-1}, is so small that it is difficult to imagine any other process that a rotational transition with which it might be associated. Borst [L. B. Borst, Phys. Rev. Letters **4**, 131 (1960)] has suggested a particular mechanism by which such a transition might be induced.

[13] J. H. Hibben, J. Chem. Phys. **5**, 166 (1937).

[14] N. Ockman, Advances in Phys. **7**, 199 (1958).

TABLE I.[a]

t °C	P kg/cm²	V_{calc} cm³/mole	V_{obs} cm³/mole	β_{calc} cm²/kg $\times 10^6$	β_{obs} cm²/kg $\times 10^6$	β^{st}_{calc}	$\beta^{st}_{L \text{ and } C}$
0	1	18.019	18.019	53.0	53.0	22.4	35.8
0	1000	17.255	17.252	39.7	38.8	12.0	27.7
0	2000	16.737	16.685	31.0	31.2	6.2	21.5
30	1	18.095	18.095	47.0	47.0	16.1	29.5
30	1000	17.399	17.400	36.9	35.8	8.9	23.4
30	2000	16.905	16.859	29.9	29.2	4.8	18.2

At 1 atm $V_{fr}=V_{fr4^\circ C}[1+33\times10^{-5}(t-4)+33\times10^{-7}(t-4)^2]$

At0°C $V_{fr}=V_{fr\ P=1}[1-30.6\times10^{-6}P+3.0\times10^{-9}P^2]$

At 30°C $V_{fr}=V_{fr\ P=1}[1-30.9\times10^{-6}P+3.0\times10^{-9}P^2]$

[a] Data are from N. E. Dorsey, *Properties of Ordinary Water Substance* (Reinhold Publishing Corporation, New York, 1940), pp. 198, 254.

the experimental value of the compressibility at 1 atmosphere, and a numerical value of $(\partial \ln f/\partial P)_T$ obtained from Eq. (7), to get a value for $(\partial \ln V_{fr}/\partial P)_T$ at atmospheric pressure. Making an assumption about its pressure-dependence $\{V_{fr}=V_{fr}^\circ[1-30.6\times10^{-6}\ P+3\times10^{-9}P^2]\}$ enables Eq. (7) to be integrated and f also obtained as a function of P. This leads to computed values for $V(P)=f(P)\times V_{fr}(P)$ which are shown in Table I, where they are compared with experimental results. In column 7 are computed values of β^{st}, obtained by inserting appropriate numbers for f and V_{fr} into Eq. (9). Litovitz and Carnevale[6b] have estimated values of β^{st} from their treatment of sound absorption data, and these are also shown. They are uniformly larger than our computed values, a fact which may be related to the somewhat problematical estimates of relaxation times which enter into the sound-absorption calculations.

7. HEAT CAPACITY

The first real disagreement between the numbers the model can give and an observed property of water is found in the heat capacity. From the identity $(\partial/\partial T)(F/T)=-H/T^2$, and Eq. (3), it follows, remembering that we have taken α independent of T, that

$$H=H_m^\circ+\alpha+f(\Delta H^\circ-\alpha). \tag{11}$$

Another differentiation, and use of Eq. (10), gives

$$C_P=C_{Pm}^\circ+f\Delta C_P^\circ+C_P^{st}, \tag{12}$$

which might have been inferred by inspection. Now C_{Pm}° can be estimated on the basis of the physical description inferred above for the monomeric water, and can hardly exceed $\frac{9}{2}R-\frac{3}{2}R$ from three fully excited degrees of rotational freedom and $3R$ corresponding to elastic binding to the equilibrium position in a site. The latter treats each molecule as a three-dimensional harmonic oscillator. Departures from this description should be in the direction of a stronger-than-quadratic potential energy law (containment in a box) rather than toward dissociative anharmonicity, and should therefore decrease C_{Pm}°, so that the value estimated for this quantity should be an upper limit [since the monomer "occupies no volume" in this model there will be no (C_P-C_V) contribution], $C_{P_{fr}}^\circ$ can also be estimated after a fashion from a sort of analogy to the values obtained above for the entropy and enthalpy of the framework as compared with those of ice. It would seem that such a guess must make $C_{P_{fr}}^\circ=12.0$ cal/deg mole at the largest, and this would make $\Delta C_P^\circ\approx+3.0$ units. Insertion of values of f and $(\Delta H^\circ-\alpha)$ into Eq. (10) gives a value for C_P^{st} of about 0.55 cal/deg mole All told, then, C_P for liquid water comes out to $9+0.82\times3+0.55=12$ cal/deg mole at the highest, in gross disagreement with the true value of about 18 units. The relationship between this discrepancy and the shortcomings of the model will be touched on below.

8. REACTION TO NONPOLAR SOLUTES

Another characteristic property of water is that nonpolar gases dissolved in it have unusually low partial molal entropies, a phenomenon which has been ascribed[15] to a shifting of the water-structure equilibrium in the direction of greater "ice-like-ness." Since methane shows a pronounced effect of this kind,[15b] and since its molecule should be small enough to fit into one of the interstitial sites which the Pauling model provides for monomeric water, a straightforward test of the model for such an entropy effect is possible. This begins, as before, by writing an expression for a number of configurations. Let N_2 be the number of solute molecules dissolved in a sample consisting of N_1 water molecules, of which a fraction f are in the framework, and $1-f$ are monomers. Then, permitting either a solute molecule or a water monomer to occupy an interstitial site, and assuming equal probabilities of occupancy, the number of ways the solute and mono-

[15] (a) H. S. Frank and M. W. Evans, J. Chem. Phys. **13**, 507 (1945); (b) W. F. Claussen and M. F. Polglase, J. Am. Chem. Soc. **74**, 4817 (1952).

mer molecules can occupy the $N_1 f/\nu$ sites is

$$(N_1 f/\nu)!/[N_1(1-f)]!N_2![N_1 f/\nu - N_1(1-f) - N_2]!$$

This leads to an entropy of mixing equal to

$$S^M = R\left[n_1 f/\nu \ln\frac{f/\nu}{f/\nu-(1-f)-y} - n_1(1-f)\ln\frac{1-f}{f/\nu-(1-f)-y} - n_2\ln\frac{y}{f/\nu-(1-f)-y}\right], \quad (13)$$

where n_1 and n_2 are the numbers of moles, respectively, of water and solute, and y is the mole ratio n_2/n_1. The total entropy of the solution is then (keeping to simple assumptions as before)

$$S = n_1 f S_{fr}^\circ + n_1(1-f)S_m^\circ + n_2 S_2^\circ + S^M, \quad (14)$$

where S_2° is an appropriate standard molal entropy of the pure solute. This leads to an equilibrium condition for f identical with Eq. (4) except that the denominator in the logarithm becomes $[f/\nu-(1-f)-y]$. Using this, the result of differentiating Eq. (14) with respect to n_2 is

$$\bar{S}_2 = S_2^\circ - R\ln y + n_1(\partial f/\partial n_2)[(\Delta H_1^\circ - \alpha_1)/T] + R\ln[f/\nu-(1-f)-y]. \quad (15)$$

Again, $(\partial f/\partial n_2) = (1/n_1)(\partial f/\partial y)$, and $\partial f/\partial y$ is obtained from the analog of Eq. (4) as

$$\frac{f(1-f)(\nu+1)}{1-y[\nu f-(1-f)]}.$$

The "excess" partial molal entropy is therefore

$$\bar{S}_2^E = \bar{S}_2 - S_2^\circ + R\ln y = \frac{f(1-f)(\nu+1)}{1-y[\nu f-(1-f)]}\frac{\Delta H_1^\circ-\alpha_1}{T} + R\ln[f/\nu-(1-f)-y], \quad (16)$$

which, at infinite dilution, becomes

$$\bar{S}_2^{E\circ} = f(1-f)(\nu+1)\frac{\Delta H_1^\circ-\alpha_1}{T} + R\ln[f/\nu-(1-f)]. \quad (17)$$

Substituting the numerical values used previously, this gives $\bar{S}_2^{E\circ} = -4.4-5.3 = -10.7$ eu. This is clearly of the right order of magnitude for methane,[15a] and is the effect we were looking for. It has the interesting property, however, that only about half of the lowering comes from causing monomeric water to form a new framework, while the other half comes from the barring out of some of the water from its "solvent function." This is reasonable in this case, but the treatment falls down in other ways. It is unable to explain the fact that experimental values of $\bar{S}_2^{E\circ}$ become progressively more negative as the solute molecule becomes bigger. Neither can it deal with the way in which this trend continues far beyond solute sizes which can be accommodated in frameworks so far described. Moreover, (16) gives the wrong dependence of $\bar{S}_2^E$ on concentration, and differentiation with temperature does not lead to a $C_{P_2}^E$ which has the properties of the experimentally observed[7] heat capacities. The last-mentioned fact is perhaps not surprising in view of the failure of the model to give good results for C_P of pure water.

9. DISCUSSION

It is clear from the foregoing that a simple Pauling model can be formulated in a way which enables a reasonably satisfactory account to be given of many of the thermodynamic properties of water from 0°C to, say, 30°C. There is no reason, of course, to suppose that the particular framework chosen for numerical testing is the "right" one, and a different choice would have given different values of ν and of V_{fr}, which would have led to different values for $\Delta F^\circ-\alpha$, $\Delta H^\circ-\alpha$, etc., but might well have given equally good numerical results for expansibility and compressibility. Indeed, in view of the variety of the solid frameworks which have already been identified, it seems likely that a more realistic application of the model would take into account the coexistence of a variety of frameworks in the liquid, and that the effective values of ν and of V_{fr} should be averages, possibly temperature-dependent in their weighting.

The "flickering" character of any framework structure, which is required by the fact that the water under discussion is a liquid, and is supported by theoretical considerations,[7] is another feature which the present treatment has left out of account. To include it would require consideration of a third "state" or group of states, made up of water molecules which have just melted from a Pauling cluster and have not yet been incorporated into a new one. This "State III" is itself presumably complex, and characterized by an average molal enthalpy and molal entropy intermediate between the values characteristic of framework and of monomers. The proportions in which its representatives are present must be determined by another equilibrium constant, or set of constants, and must be both temperature- and pressure-dependent. It seems possible to suppose that not much of "State III" is present at 0°C, and that the success of the tests reported above arises in part from this circumstance. As temperature rises, however, the restriction imposed by the Pauling model, namely, the lower limit on f, accompanied by the very slow rate of decrease of f with increase in temperature, must become more and more difficult to maintain, and this must tend to force more and more of the water into the "State III" form. Such a process would furnish a natural explanation for the finding of Sec. 7, that water has a higher heat capacity than the simple model can account for, since "State III" might well have a high-intrinsic heat capacity, and since there would be at least one additional structural shift which

would absorb heat. Correspondingly, the ascribing of appropriate properties to "State III" could furnish a sort of escape hatch for evading the limitations of the simple treatment in accounting for the partial molal properties of nonpolar solutes.

The "strait jacket" feature of the simple model $\{f \gtrless [\nu/(\nu+1)]\}$, and the need, with rising temperature, for water to be able to escape from it, suggests another interesting possibility. This is that there may actually be a qualitative change, over a short temperature interval, in the "significant structures"[16] of which water is principally composed, leading to some sort of pseudo-transition. Arguments for such "transitions" in liquid water have been reported from time to time,[17] and in every case one of them has seemed to appear just above 30°C. In no individual case, however, has the evidence seemed conclusive, and the idea of such transitions has not received general acceptance, in part, presumably, because no very plausible theoretical picture could be advanced which would call for, or explain, such a phenomenon. Adoption of the Pauling model as essentially correct at low temperatures might well, however, imply the existence of just such a transition, for when, with the gradual accumulation of "State III," the framework fraction f fell below a certain critical value (lower, of course, than $\nu/(\nu+1)$, since, at this stage, not all of the water would be subject to the restriction) the (cooperative) stability of the Pauling frameworks ought to fall off rather rapidly, leaving the various structures we have lumped together as "State III" as the only material present. This might, in turn, give rise to the anomalies in expansibility and in thermal behavior at which the experimental results have hinted, and the temperature range just above 30°C seems intuitively to be about where this might plausibly be imagined to take place.

10. CONCLUDING REMARKS

As compared with other water models which have been proposed, this one seems to have definite merits:

1. As pointed out by Pauling, it is attractive from the structural standpoint, being consistent with observed x-ray results, and representing most of the water molecules as doing something that water molecules are known to do.

2. It provides naturally for a single cooperative relaxation process, the forming and dissolution of clusters, and this, as has been shown,[7b] opens the way to a unified discussion of dielectric, viscosity, and diffusion properties.

3. It is the only model we know of which provides, without forcing, a straightforward explanation of all of the neutron-scattering results of Hughes, Palevsky, *et al.*[12] These indicate (a) the existence of a framework capable of supporting solidlike normal modes of vibration, (b) the probable existence of some freely rotating molecules,[18] and (c) the absence of any component (which the neutron can see) which is undergoing diffusional motion. The last finding corresponds exactly to the properties of both framework and interstitial water, but does not rule out "State III," since a diffusional effect involving up to, say, 10% of the molecules in cold water (and 25% at 45°C) cannot be excluded on the basis of the measured curves.

4. While it cannot compete with Eucken's[19] elaborate matching of P-V-T data, it is able, with relatively few assumptions (and these very limited in their degree of

[16] H. Eyring, T. Ree, and N. Hirai, Proc. Natl. Acad. Sci. U. S. **44**, 683 (1958).

[17] See e.g., (a) M. Lavergne and W. Drost-Hansen, Naturwissenschaften **43**, 511 (1956); (b) Footnote 2; (c) S. R. Gupta, G. J. Hills, and D. J. G. Ives, Discussions Faraday Soc. **24**, 147 (1957); (d) F. Franks and D. J. G. Ives, J. Chem. Soc. **1960**, 741.

[18] This probability has been challenged on the grounds that such freely rotating monomers should produce observable gaslike infrared absorption and Raman scattering effects which are not, in fact, observed. (a) So far as concerns the infrared data, the IR-active gas-phase frequencies are 3756 cm^{-1} (2.66 μ) and 1595 cm^{-1} (6.27 μ), and correspond to the liquid absorption bands found, for example, by Fox and Martin [J. J. Fox and A. E. Martin, Proc. Roy. Soc. (London) **A174**, 234 (1940)], extending, respectively, from 2.7 μ to 3.4 μ, and from 5.2 μ to 6.4 μ approximately, the latter with a marked shoulder which is still falling very slowly at 7.2 μ (this shoulder is even more pronounced in ice). These liquid bands should of course be dominated by the absorption of hydrogen-bonded framework, and the question is therefore why the "gaslike" absorption of 15–20% of monomers does not appear as separate bands or as distinguishable structure in the observed bands. What is actually to be expected, however, will depend on what is assumed (or can be known) about shifts in frequency [cf. E. Greiner, W. Lüttke, and R. Mecke, Z. Elektrochem. **59**, 23 (1955)] and changes in intensity [cf. W. B. Person, J. Chem. Phys. **28**, 319 (1958)] in going into the particular kind of "condensed" state here in question. For example, application to the 3756 cm^{-1} frequency of the "normal" dielectric constant correction of Greiner *et al.* (even for a high-frequency value of D) would bring it near 2.8 μ, into the rising limb of the high-frequency band of Fox and Martin. It therefore seems too soon to give categorical answers to the questions raised by infrared spectra. (b) The low-frequency Raman studies of Stoicheff [unpublished work; cf. footnote 23 of footnote reference 12] show a maximum scattering intensity near 5 cm^{-1}, corroborating the neutron-scattering results, but a much feebler scattering at the higher frequencies where the maximum should lie if it corresponded to the population of rotational states which an equilibrium thermal distribution would give. This raises questions of interpretation. It should be kept in mind, however, that the distribution over rotational states of the monomers postulated in this paper should differ from the normal distribution, characteristic of a gas at the temperature of the sample, for two reasons: (1) the formation of the clusters which are imagined to contain these interstitial monomers always corresponds to a local energy density which is slightly lower than the average, since it is such local fluctuations which call the clusters into existence, and (2) the "disproportionation" into framework and monomers must exercise some sorting influence, preferentially incorporating into the framework molecules in states which have large Stark effects and are therefore strongly subject to electrostatic influences, and leaving behind as monomers molecules which are in the "nonhydrophilic" states referred to in footnote reference 11. Our inference of a large rotational entropy for the monomers implies, of course, that such sorting is not too drastic so far as numbers are concerned, but says nothing about excitation functions for Raman scattering.

It is clear that questions regarding the existence and properties of freely rotating molecules in liquid water are far from being closed. It also seems that the ultimate usefulness of the Pauling model may well depend on the way in which such questions are finally resolved.

[19] A. Eucken, Nachr. Ges. Wiss. Göttingen **1946**, p. 38.

arbitrariness) to give a better-than-qualitative result in this respect.

From the standpoint of model-construction, on the other hand, the need to include "State III" is a blemish. This is particularly true in view of the way the specific nature of "State III" (which must be partly structured, but is otherwise unspecified) had to be appealed to *ad hoc* to escape from the heat capacity and nonpolar-solute difficulties. It is necessary to remember, however, that water is extremely versatile in what it can do, and that it is known to do different things in different temperature ranges (cf. the crossing of the vapor-pressure curves of H_2O and D_2O at 220°C).[20] From this standpoint, the danger of oversimplification is one which the model maker must be on guard against, and the appearance of "State III" may be accepted, if not welcomed, as evidence that that danger has been avoided.

Note added in proof. Since the foregoing was written the work of van der Waals and Platteeuw has come to our attention [*Advances in Chemical Physics*, edited by I. Prigogine, (Interscience Publishers, New York, 1959) Vol. 2 Chap. 1, and other references there cited], in which they treat the clathrates as solutions (of variable composition) of enclosed component in framework. Our statistical treatment is essentially equivalent to theirs, and the value of $F^\circ_{fr} - F_{ice}$ derived from our figures, about 200 cal/mole, is very similar to the corresponding $\Delta\mu$ values they quote, of 0.167 and 0.19 kcal/mole for the 12 A and 17 A frameworks respectively. The degree of occupancy of sites in our model is also great enough, according to their criterion, to make the clathrate framework stable with respect to ice at 0°C.

[20] I. Kirschenbaum, *Physical Properties and Analysis of Heavy Water* (McGraw-Hill Book Company, Inc., New York, 1951), p. 25.

ACKNOWLEDGMENTS

We are grateful to the National Science Foundation for a grant under which the work of one of us (ASQ) was supported, and to Dr. Boris Stoicheff for informing us, in advance of publication, of the results of his Raman-effect measurements. Discussions with him, with Dr. Harry Palevsky, and with Professor George C. Pimentel are also gratefully acknowledged.

THE JOURNAL OF CHEMICAL PHYSICS VOLUME 34, NUMBER 2 FEBRUARY, 1961

Crystal Spectra of Metal Coordination Compounds. III. Nickel Complexes with Salicylaldehyde and Its Imines

J. FERGUSON

Division of Chemical Physics, C.S.I.R.O. Chemical Research Laboratories, Melbourne, Australia

(Received August 12, 1960)

Polarized single crystal absorption spectra are reported for three nickel complexes: *bis*-N-methylsalicylaldiminato-nickel (II), *bis*-salicylaldiminato-nickel (II), and diaquo-*bis*-salicylaldehydato-nickel (II). The analysis of the bands of an orthorhombic form of *bis*-N-methyl-salicylaldiminato-nickel (II) (described for the first time) results in the assignment of the two visible absorption bands to $^1A_g \rightarrow {}^1B_{1g}$ and $^1A_g \rightarrow {}^1B_{3g}$, respectively. This assignment is discussed in relation to the simple crystal field model and a possible refinement of the model has been suggested. The analysis of the band observed with *bis*-salicylaldiminato-nickel (II) is consistent with the assignment of those in *bis*-N-methylsalicylaldiminato-nickel (II). The analysis of the visible absorption band of diaquo-*bis*-salicylaldehydato-nickel (II) shows that the theoretical assignment is incorrect although an unambiguous assignment cannot be made from the crystal spectrum.

INTRODUCTION

THREE quantities are needed to characterize an excited electronic state of an ion in the field of its ligands: the energy above the ground state, the magnitude of the transition moment, and its direction. So far, the validity of crystal field theory has been tested mainly by comparing the first two quantities with experiment. A much more severe test of the theory is to compare the theoretical and observed directions of the transition moment which can only be done with single crystals of known structure. The aim of the present communication is to report measurements of the crystal absorption spectra of three nickel complex compounds for which an extensive theoretical treatment is available.[1-3] These measurements were designed to test the theoretical assignments on the grounds of symmetry and are particularly powerful providing the correct assumption is made about the mechanism of the transition. This will be the accepted one[4] which invokes *u*

[1] G. Maki, J. Chem. Phys. **28**, 651 (1958).
[2] G. Maki, J. Chem. Phys. **29**, 162 (1958).
[3] G. Maki, J. Chem. Phys. **29**, 1129 (1958).
[4] J. H. Van Vleck, J. Phys. Chem. **41**, 67 (1937); A. D. Liehr and C. J. Ballhausen, Phys. Rev. **106**, 1161 (1957).

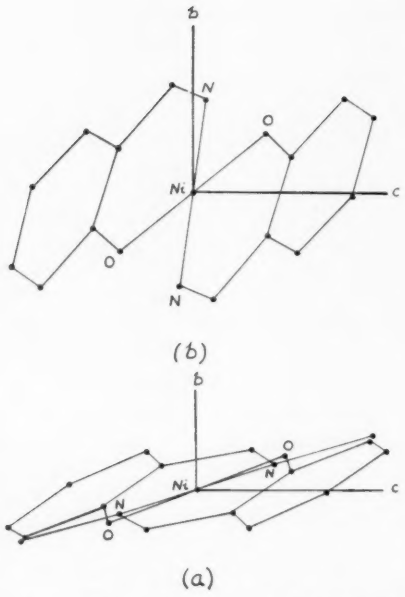

FIG. 1(a). Projection of the molecule of *bis*-N-methyl-salicylaldiminato-nickel (II) on the well-developed (100) face; (b) projection of the molecule of *bis*-salicylaldiminato-nickel (II) on the well-developed (100) face.

vibrations, i.e., those which are antisymmetric with respect to inversion through the center of symmetry.

EXPERIMENTAL

The complexes were prepared by standard methods.[5,6] The orthorhombic form of *bis*-N-methylsalicylaldiminato-nickel (II), which has not been described in the literature, was obtained by crystallization from hot concentrated ethanol solution.

The crystal spectra were measured with a Beck reflecting microscope and a Hilger constant deviation spectrometer fitted with a 1-P22 photomultiplier. The power supply and ac amplifier have been described recently.[7] A piece of polaroid was used as analyser. The experimental method has been outlined previously.[8]

CRYSTAL STRUCTURES

The crystal structure of the monoclinic form of *bis*-N-methylsalicylaldiminato-nickel (II), hereafter called I, has recently been reported.[9] The well-developed face is (100) and Fig. 1(a) shows the projection of the molecule on this face.

The orthorhombic form of I has the cell dimensions, $a=24.46$, $b=9.25$, and $c=6.60$ A with four molecules per unit cell.[10] The calculated density is 1.45 and that observed 1.44. The crystal is isomorphous with the corresponding copper complex described by Stackelberg[11] and more recently by Lingafelter.[12] The molecular planes lie exactly in the (001) crystal plane with the long axis of the molecule making a small angle with the *a* axis. The nickel ions are 3.30 A apart along the *c* axis. The crystal is diamagnetic.[13]

The crystal structure of *bis*-salicylaldiminato-nickel (II), hereafter called II, has been determined by Stewart and Lingafelter.[14] The crystal is monoclinic with the (100) face well-developed. Figure 1(b) shows the projection of the molecule on this face.

The structure of diaquo-*bis*-salicylaldehydato-nickel (II), hereafter called III, has been determined by J. M. Stewart, E. C. Lingafelter, and J. D. Breaze-

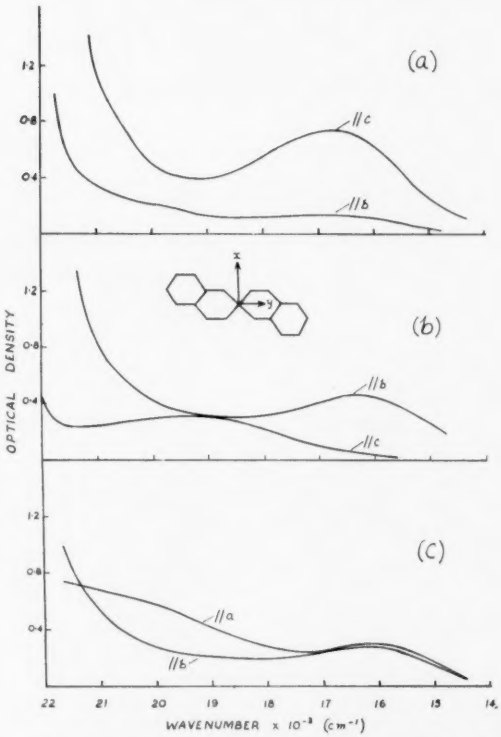

FIG. 2. Spectra of crystals of *bis*-N-methyl-salicylaldiminato-nickel (II). (a) Monoclinic form, light incident on the (100) face; (b) orthorhombic form, light incident on the (100) face; and (c) orthorhombic form, light incident on the (001) face.

[5] G. N. Tyson and S. C. Adams, J. Am. Chem. Soc. **62**, 1228 (1940).
[6] W. Klemm and R. R. Radatz, Z. anorg. u. allgem. Chem. **250**, 121 (1942).
[7] G. F. Box and A. Walsh, Spectrochim. Acta **16**, 255 (1960).
[8] J. Ferguson, J. Chem. Phys. **32**, 528 (1960).
[9] E. Frasson, C. Panattoni, and L. Sacconi, J. Phys. Chem. **63**, 1908 (1959).

[10] The author is most grateful to his colleague, Dr. A. McL. Mathieson, for making the x-ray examination of the crystals.
[11] M. v. Stackelberg, Z. anorg. u. allgem. Chem. **253**, 136 (1947).
[12] Professor E. C. Lingafelter (personal communication).
[13] The magnetic measurements were kindly done by R. C. Croft of the Mineral Chemistry Division.
[14] J. M. Stewart and E. C. Lingafelter, Acta Cryst. **12**, 842 (1959).

dale.[15] The well-developed (100) face of the crystal has the shape of a square with the crystal axes along the diagonals. The salicylaldehyde molecules and the nickel ion lie exactly in the (010) plane and the nickel-water bonds lie exactly along the b axis.

CRYSTAL SPECTRUM OF *BIS*-N-METHYL-SALICYLALDEHYDATO-NICKEL (II)

Monoclinic Form

The crystals are dichroic and appear green with the electric vector parallel to the b axis and yellow with it perpendicular to this axis. The spectrum is shown in Fig. 2(a).

Maki[3] has assigned the transition at 16 800 cm^{-1} to $^1A_g \rightarrow {}^1B_{3g}$ and the shoulder at about 20 500 cm^{-1} to $^1A_g \rightarrow {}^1B_{1g}$, while Ballhausen and Liehr[16] have used strong field formalism to assign the bands to $^1A_g \rightarrow {}^1B_{1g}$ and $^1A_g \rightarrow {}^1A_g$, respectively. Before discussing these assignments, it is necessary to consider the crystal spectrum of the orthorhombic form.

Orthorhombic Form

The crystals are strongly dichroic and appear red with the electric vector parallel to the needle axis c and green with it perpendicular to this axis (parallel to the b axis). The spectrum of the crystal is shown in Fig. 2(b) for light incident on the (100) face.

In order to make an unambiguous assignment of the two absorption bands, thin sections were cut, with a microtome, perpendicular to the needle axis, i.e., parallel to the (001) plane. Figure 2(c) shows the absorption spectrum for light incident on this face.

It is apparent from Figs. 2(b, c) that the band at 16 500 cm^{-1} is polarized parallel to the a and b crystal axes and not along the c axis, while the band at 19 600 cm^{-1} is polarized parallel to the a and c crystal axes and not along the b axis.

TABLE I. Vibronic representations in D_{2h} (product of ground electronic state, excited electronic state and perturbing vibration).

Symmetry representation of perturbing vibration	Symmetry representation of the product of ground and excited electronic wave functions			
	A_g	B_{1g}	B_{2g}	B_{3g}
$b_{1u}(z)$	B_{1u}	A_u	B_{3u}	B_{2u}
$b_{2u}(y)$	B_{2u}	B_{3u}	A_u	B_{1u}
$b_{3u}(x)$	B_{3u}	B_{2u}	B_{1u}	A_u

[15] The author wishes to thank Professor E. C. Lingafelter for communicating details of the structure in advance of publication.

[16] C. J. Ballhausen and A. D. Liehr, J. Am. Chem. Soc. **81**, 538 (1959).

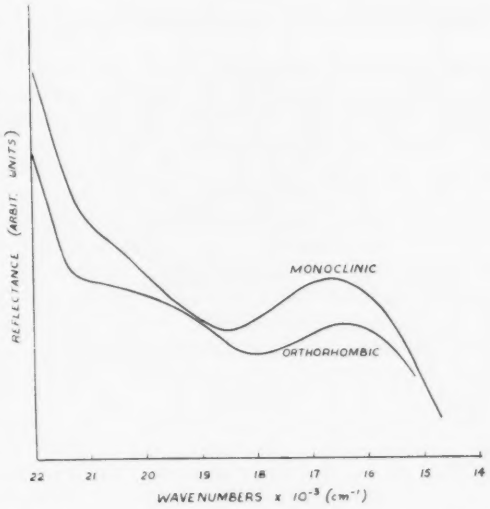

FIG. 3. Diffuse reflectance spectra of the monoclinic and orthorhombic forms of *bis*-N-methyl-salicylaldiminato-nickel (II).

Assignment of the Bands

The orthorhombic form is more important for an assignment of the bands because of the very fortunate orientation of the molecules in the crystal. The molecular plane lies exactly parallel to the (001) plane so that the c axis is normal to the molecular plane. The structure analysis of the isomorphous copper compound[10] shows that the line bisecting the internal N-Cu-O angle makes an angle of about 10° with the a axis while the line bisecting the external N-Cu-O angle makes the same angle with the b axis. In the monoclinic form, the plane of the molecule is not perpendicular to the well-developed face and the molecule makes a small projection on the b axis. However, the relative projections of the molecule on the well-developed face of each of the crystals are similar.

It is evident from Fig. 2(b, c) that for the higher energy band, at 19 600 cm^{-1}, the in-plane absorption is anisotropic and it is polarized in a direction close to the line bisecting the internal N-Ni-O angle. The *vibronic* symmetry is then best described under the point group D_{2h}, with axes in the plane chosen as shown in Fig. 2(b). The analysis of the bands will now be made with the assumption that both the electronic and vibrational force fields are also described by the same symmetry operations. Other possibilities will be considered later.

The mechanism of the transition is assumed to be that of perturbation of the g electronic levels by u vibrations which belong to the representations b_{1u}, b_{2u}, or b_{3u}. The ground electronic state of the molecule is diamagnetic and belongs to the representation A_g while the possible excited states belong to the four g representations. Table I gives the vibronic symmetry for the combination of one quantum of a u vibration and the

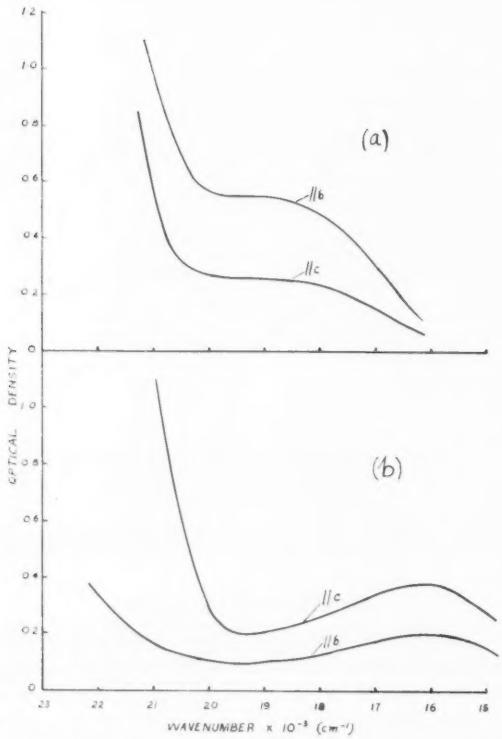

FIG. 4(a). Crystal spectrum of *bis*-salicylaldiminato-nickel (II); (b) crystal spectrum of diaquo-*bis*-salicylaldehydato-nickel (II).

direct product of the ground and excited electronic representations.

The absorption band at 16 500 cm^{-1} is polarized in the molecular plane, i.e., vibronic species B_{2u} and B_{3u}. Table I shows that this is expected for an electronic combination of species B_{1g}, so the electronic transition is assigned to $^1A_g \rightarrow {}^1B_{1g}$. The higher energy band at 19 600 cm^{-1} is observed with the electric vector parallel to the a and c axes and not along the b axis, i.e., along the molecular y and z axes (species B_{2u} and B_{1u}), and the electronic transition is therefore assigned to $^1A_g \rightarrow {}^1B_{3g}$.

It is, of course, possible that the symmetries of the vibrational and electronic force fields are not the same. In this event, the vibronic symmetry will be determined by the operations which are common to both groups. One possibility is that the electronic field is D_{4h} and the vibrational field D_{2h}, but this seems unlikely for the following reason. The band at 19 600 cm^{-1} with upper state B_{3g} in D_{2h} symmetry can only come from a degenerate E_g level in D_{4h} symmetry. There is no sign in the spectrum of the B_{2g} component nearby so that the splitting of the degenerate level is greater than a few thousand cm^{-1} and it is very unlikely that such a large splitting can be induced by a vibrational distortion. Another possibility, in which the electronic field is D_{2h} but with axes along metal-ligand bonds, is eliminated because the vibronic symmetry in common with the vibrational field D_{2h} [axes chosen as in Fig. 2(b)] would be C_{2h}. Similarly, the case of vibrational field D_{4h} and electronic field D_{2h} with axes along metal-ligand bonds would give a resultant vibronic symmetry of D_{2h}, but with axes along bonds.

The spectrum of the monoclinic form of the complex can be interpreted in the same way, but as the bands are at slightly higher energy the analysis is not clear. The low energy band is not completely polarized perpendicular to the b axis as there is weak absorption parallel to this axis. Reference to Fig. 1 shows that the latter absorption must arise from the small projection that the molecular y axis makes on the b axis, while the former arises from the active molecular x component. The polarization of the band is then that expected for the transition $^1A_g \rightarrow {}^1B_{1g}$. The higher energy band appears to be polarized parallel and perpendicular to the b axis and this would be true for either of the assignments $^1A_g \rightarrow {}^1B_{3g}$ and $^1A_g \rightarrow {}^1A_g$.

The difference between the energies of the bands of the two crystal forms is more clearly shown by the diffuse reflectance spectra in Fig. 3. The bands of the orthorhombic form lie at lower energy than the monoclinic form and the shift is greater for the higher energy transition. This difference in energy must be related to nickel-nickel interaction, since the x-ray data show a nickel-nickel distance of 3.30 A along the c axis in the orthorhombic form. In a sense, each molecule is solvated by molecules above and below the molecular plane, but this axial perturbation is insufficient to force the cross-over to a triplet ground state.

CRYSTAL SPECTRUM OF *BIS*-SALICYLALDIMINATO-NICKEL (II)

The molecule does not have the favorable projection on the well-developed face as does I. In addition, the bands are at higher energy than those of I so that only one band is observed and the other must lie under the stronger ligand absorption. If this transition is assigned to $^1A_g \rightarrow {}^1B_{1g}$, the same as for I, then the band should be nearly twice as intense parallel to the b axis as perpendicular to it. Figure 4(a) shows the spectrum of the crystal and confirms this prediction.

CRYSTAL SPECTRUM OF DIAQUO-*BIS*-SALICYLALDEHYDATO-NICKEL (II)

The orientation of the molecules in the crystal is favorable for an assignment on grounds of symmetry because the salicylaldehyde molecules lie exactly in the (010) plane and the two water molecules lie exactly along the b crystal axis. Figure 4(b) shows the spectrum parallel and perpendicular to this axis.

Maki[2] has reported the spectrum of the powder and assigned the absorption band at 16 100 cm^{-1} to the transition $^3B_{3g} \rightarrow {}^3B_{2g}$ in D_{2h} symmetry. If this is correct,

then the allowed vibronic states belong to the representations B_{2u} and B_{3u} and the transition should be polarized in the molecular (xy) plane.[2] The absorption band should therefore be strongly polarized parallel to the c axis, but Fig. 4(b) shows that the transition also appears for light polarized perpendicular to the c axis with the polarization ratio c/b about 2. The only possible assignment within D_{2h} is ${}^3B_{3g}\rightarrow{}^3B_{1g}$.

DISCUSSION

The polarization of the crystal absorption bands of I and their analysis suggests that the electronic field has D_{2h} symmetry, with the in-plane symmetry axes bisecting ligand-metal-ligand bond angles. This choice is difficult to reconcile with the simple crystal field model which considers the ligands as point dipoles. However, if account is taken of the likely spatial orientation of all the ligand orbitals, then a field consistent with the observed symmetry is obtained. Each ligand is assumed to have three in-plane orbitals, approximately sp^2 hybrid orbitals, and one out-of-plane p_π orbital. With the further assumption that the fields of the nitrogen and oxygen orbitals are approximately the same, then the orientation of the ligand orbitals is such that the symmetry of the resultant field is D_{2h} in the observed sense (one nonbonding orbital directed towards the metal with angles of about 120° between it and the other in-plane orbitals).

Unfortunately, the model used by Maki[3] is not supported by the analysis of the crystal spectrum. Another attempt including one other ligand orbital (the other nonbonding oxygen orbital and its equivalent nitrogen bonding orbital) would be useful, but probably too lengthy. On the other hand, a molecular orbital approach is probably more easily managed and the effect of additional ligand orbitals amounts to the inclusion of in-plane π-bonding. It should be noted that there is evidence for the latter from an analysis of the paramagnetic resonance absorption of *bis*-salicylaldiminatocopper (II).[17]

A comparison can be made between the use of weak and strong field methods. Ballhausen and Liehr[16] have used the latter to predict two excited singlet states, ${}^1B_{1g}$ and ${}^1A_g$. The method fails to account for the observed ${}^1B_{3g}$ state and no ${}^1A_g$ state has been found. It seems clear, therefore, that a weak field formulation of the problem is required because of its inclusion of excited state configurations of the nickel ion.

The analysis of the crystal absorption spectrum of III also shows disagreement with the theoretical assignment. However, Maki[2] has calculated a ${}^3B_{1g}$ state to lie at slightly lower energy than the ${}^3B_{2g}$ state, and there is the possibility that the observed band in the crystal represents this transition. It would be polarized along the molecular x and y axes, i.e., parallel to the c and b crystal axes, respectively. Maki achieved the best energy fit by considering the molecule to have D_{2h} symmetry, but with a marked difference in the effect of the two oxygen atoms in each salicylaldehyde molecule ion. An attempt to fit the spectrum along the lines suggested for I would be worthwhile. It should be noted that the band can also be assigned to ${}^3A_{2g}\rightarrow{}^3T_{1g}$ in O_h symmetry[2] or ${}^3B_{2g}\rightarrow{}^3E_g$ in D_{4h}; the results do not give an unambiguous indication of the vibronic symmetry.

ACKNOWLEDGMENTS

The author wishes to thank Dr. E. G. McRae for a critical reading of the manuscript and helpful comments. He has also benefited from discussions with Dr. N. S. Ham, Dr. R. L. Martin, and Dr. A. L. G. Rees. It is a pleasure to thank Dr. A. M. Mathieson for his help in the problems associated with x-ray structure determinations.

[17] A. H. Maki and B. R. McGarvey, J. Chem. Phys. **29**, 35 (1958).

THE JOURNAL OF CHEMICAL PHYSICS VOLUME 34, NUMBER 2 FEBRUARY, 1961

Step Formation during the Growth of $BaTiO_3$ Crystals

R. C. DeVries and G. W. Sears

General Electric Research Laboratory, Schenectady, New York

(Received April 29, 1960)

The growth behavior of barium titanate crystals from molten potassium fluoride at 1000°C may be described in some detail by the Frank growth mechanism. In particular the role of reentrant twin angles as growth step sources was examined. A finite supersaturation is required for the operation of this source and the event must occur by an easier nucleation process than homogeneous two-dimensional nucleation.

THE screw dislocation theory of crystal growth was originally developed by F. C. Frank[1] to account for growth of a crystal from its own vapor. The theory recognized that growth can only occur by the spreading of partially completed surface layers.[2] The empirical fact that growth does occur at low supersaturations[3] could only be accounted for by a mechanism that produced new growth steps at low supersaturations, since steps are destroyed when they grow to the periphery of a crystal plane. Frank commented that real crystals should contain screw dislocations and that a step must proceed from the point of emergence of a screw dislocation either to the edge of a crystal or to a screw of opposite hand. Thus the growth of crystals at low supersaturations was controlled by their line imperfections. Frank[4] also recognized that the reentrant angle formed at an emergent twin boundary might also furnish a source of steps at low supersaturations.

The range of validity of Frank's[1] mechanism has been extended to much more general crystal growth processes than growth from the vapor. In the present paper it is demonstrated that the growth of $BaTiO_3$ crystals from a 0.1 mole fraction solution of $BaTiO_3$ in molten KF solution at 1000°C occurs by the layer spreading mechanisms. Different sources of growth steps are described. In particular the effectiveness of reentrant angles at twin boundaries is qualitatively established.

EXPERIMENTAL

The morphology of the $BaTiO_3$ twin crystals grown by the Remeika[5] technique from a 0.1 mole fraction solution of $BaTiO_3$ in KF has been described by Curien and LeCorre[6] and by White.[7] Crystallographically, twinning on {111} type planes is combined with a {100} habit (Fig. 1).

The topology of the crystal surfaces on opposite sides of the thin plate-like wings of the twinned crystal is noticeably different. On the reentrant angle side (side *A* in Figs. 1 and 2) growth layers spread upward along the wings from the reentrant angle. A heavily stepped surface results. The reentrant angle serves as a source from which growth layers originate and spread over the crystal surface.

In contrast the outer surfaces of the butterfly wings are remarkably smooth and no stepped structure corresponding to partially completed layers is normally visible at 500× magnification. The difference between the two surfaces is illustrated by the schematic cross section of a wing in Fig. 2(b). In this view it is seen that the crystal wing is wedge shaped with one flat surface and one stepped surface. It is clear that the step generation processes are very different on opposite sides of the thin plate-like crystal.

The growth behavior on the two faces of a butterfly wing can be modified by allowing small equant crystals of $BaTiO_3$ to impinge upon the growing faces. This experiment was carried out in the following way. Butterfly twin crystals were grown by slow cooling[8] (~30°/hr) of a 0.1 mole fraction solution of $BaTiO_3$ in molten potassium fluoride in the temperature range of 1000–1100°C. The twinned crystals grew rapidly at quite constant thickness of 100μ or less until they reached a lateral dimension of about 1 cm. At this stage thickening began to occur on the inside surfaces at the reentrant twin boundary and the lateral growth rate slowed down by several orders of magnitude.

The cooling rate was then sharply increased to ~100°/hr in the temperature range of 1000°C to 950°C so that new crystals nucleated and grew in the solution over the butterfly twins. The new crystals were generally equant and untwinned.[8] The previous cooling rate of ~30°/hr was then resumed.

After the temperature had reached about 900°C the crucible was quickly removed from the furnace, the excess molten potassium fluoride solution was decanted from the assemblage of $BaTiO_3$ crystals in the bottom of the crucible, and the crucible was replaced in the furnace. The furnace power was turned off, and the crucible and furnace were allowed to cool to near room temperature. The remaining potassium fluoride was

[1] F. C. Frank, Discussions Faraday Soc. **5**, 48 (1949).
[2] J. W. Gibbs, *Collected Works* (Longmans Green and Company, London, 1928), p. 325.
[3] M. Volmer and W. Schultze, Z. Physik. Chem. (Leipzig) **156A**, 1 (1931).
[4] F. C. Frank, Discussions Faraday Soc. **5**, 186 (1949).
[5] J. P. Remeika, J. Am. Chem. Soc. **76**, 940 (1954).
[6] H. Curien and Y. LeCorre, Bull. soc. franc. mineral et crist. **78**, 604 (1955).
[7] E. A. D. White, Acta Cryst. **8**, 845 (1955).
[8] R. C. DeVries, J. Am. Ceram. Soc. **42**, 547 (1959).

dissolved in water, and the $BaTiO_3$ crystals were examined microscopically.

It was found that some of the equant crystals formed during the 100°/hr cooling had impinged upon the surfaces of the butterfly twin wings. At each impingement site it was seen that growth layers and their associated growth steps had been formed and had spread outward over the surrounding surface. This behavior is shown in Fig. 3 at 600×. The local thickening rate had markedly increased. No centers of thickening were observed where a second crystal had not impinged upon a wing surface. If equant $BaTiO_3$ crystals were never nucleated and grown, local growth centers were never observed on the outer surfaces of butterfly wings. The occurrence of growth centers was also observed at impingement sites of equant crystals on the reentrant surfaces of butterfly wings.

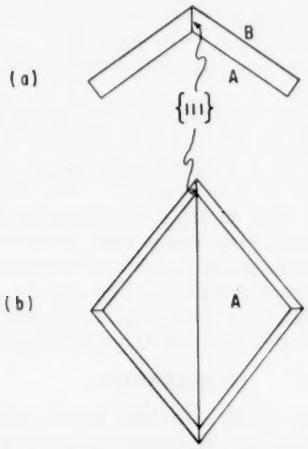

FIG. 1. (a) Cross section of a singly twinned crystal of $BaTiO_3$; (b) is a perspective view of the twinned crystal as seen looking into the reentrant angle formed by the adjacent "wings". The crystal faces are all {100} type. The twin plane is {111}. Side *A* is reentrant face and side *B* is the external angle face.

DISCUSSION

The possibility that reentrant angles associated with emergent twin boundaries might serve as a source of growth steps at low supersaturations was recognized by Frank.[4] DeVries[8] has observed that reentrant twin boundaries do in fact serve as a source of growth steps for barium titanate crystals. He also found that those combinations of twin plane and adjacent faces not forming reentrant angles do not act as a source of growth steps. The region of supersaturation necessary for the action of a reentrant as a step source was not considered. More recently it has been demonstrated[9-11] that twin boundaries are also a source of growth steps

[9] A. I. Bennett and R. L. Longini, Phys. Rev. **116,** 53 (1959).
[10] R. S. Wagner, Acta Met. **8,** 57 (1960).
[11] D. R. Hamilton and R. G. Seidenstricker, J. Appl. Phys. **31,** 1165 (1960).

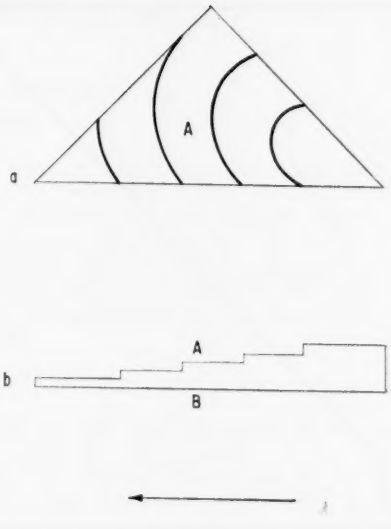

FIG. 2. Plan (a) and cross section (b) of a wing of a twinned crystal of $BaTiO_3$. The curved lines on the *A* surface as shown in (a) are the growth layers forming the steps in (b). *A* and *B* have the same significance as in Fig. 1. The arrow indicates the direction of growth of the crystal.

in the production of long laths of germanium from a slightly supercooled melt.

Consider the growth history of a butterfly twin. The macroscopic butterfly twin grows from a parent crystallite that contains a twin boundary. It is not known whether the original nucleus was twinned or whether twinning occurred during the initial growth of the nucleus by a faulted two-dimensional nucleation.[12] The plate-like wings probably grow by the action of a

FIG. 3. Growth layers on the outer surfaces (*B* of Fig. 1) of a twinned crystal. The layers are associated with a randomly oriented smaller crystal which impinged and stuck to the twinned crystal. The smaller crystal was actually removed during handling so that the black area is a hole in the surface of the larger crystal. (600×)

[12] G. W. Sears, J. Chem. Phys. **31,** 157 (1959).

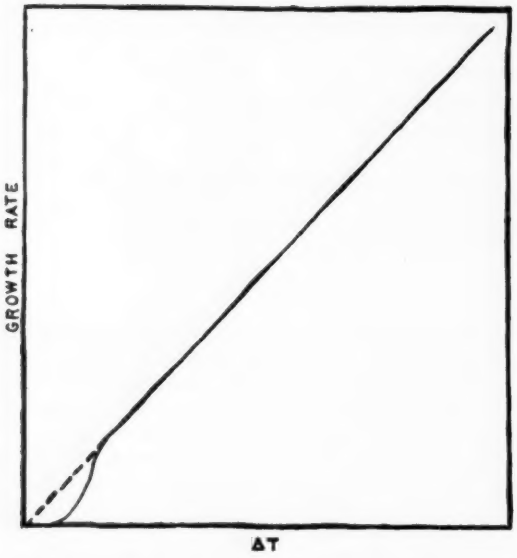

FIG. 4. Growth rate by screw dislocation mechanism as a function of supercooling.

planar set of screw dislocations.[13] However, it is certain that the lateral extension of the butterfly wings occurs at supersaturations that are insufficient to cause steps to originate from the reentrant angle associated with the twin boundary. If both growth sites were operative at the supersaturation existent in the potassium fluoride solution, the final morphology would have been approximately equant.

Emergent screw dislocations offer the easiest possible growth mechanism, i.e., the step generation mechanism that will operate at the lowest supersaturation. Burton, Cabrera, and Frank[14] have theoretically calculated the growth rate by the screw dislocation mechanism as a function of supersaturation as shown in Fig. 4. Since dislocations offer the easiest mechanism by which lateral wing growth can occur, and the reentrant twin is only operative after the wings have developed, it is certain that a finite supersaturation is required for the action of a reentrant as a source of growth steps. On the other hand the reentrant serves as a source of steps at supersaturations which are quite insufficient to cause an appreciable rate of two dimensional nucleation.

It is observed that growth steps are very rapidly generated on the external faces of butterfly wings after secondary crystals have impinged upon these surfaces. This fact demonstrates that two dimensional nucleation was not occurring at an appreciable rate prior to the impingement event. Not only were the steps not observed, but thickening occurred at a very slow rate if at all.

When impingement occurred on the inside faces of the butterfly wings, the same rapid step generation and thickening was observed. Since the step generation associated with crystal impingement is caused by those screw dislocations defining the interface between the two crystals.[15,16] It is corroborated that a screw dislocation serves as an easier step source than a reentrant twin boundary.

This same growth behavior is operative in growth of germanium laths.[9,11] It was observed by Bennett and Longini that in a slightly supercooled melt (~8°C) lath extension by the action of a twin boundary occurred much more rapidly than thickening by a two dimensional nucleation mechanism. It was noted that opposite ends of a twinned parent lath were not equivalent in their growth behavior. This may be correlated with the presence or absence of a reentrant angle at the emergent twin boundary at opposite ends of a lath.

CONCLUSIONS

It has been shown that the growth behavior of $BaTiO_3$ crystals from their supersaturated solution in molten potassium fluoride at approximately 1000°C may be described in some detail by the Frank crystal growth mechanism. Similarly the growth of germanium crystals from a slightly supercooled melt also can be described by the Frank mechanism.

[13] J. B. Newkirk and G. W. Sears, Acta Met. **3,** 110 (1955).
[14] W. K. Burton, N. Cabrera, and F. C. Frank, Phil. Trans. Roy. Soc. (London) **243,** 299 (1951).
[15] J. B. Newkirk, Acta Met. **3,** 121 (1955).
[16] G. W. Sears and R. V. Coleman, J. Chem. Phys. **25,** 635 (1956).

THE JOURNAL OF CHEMICAL PHYSICS VOLUME 34, NUMBER 2 FEBRUARY, 1961

Nuclear Quadrupole Coupling in the NH_3 Molecule*

YOSHIFUMI KATO

Osaka Municipal Technical Research Institute, Osaka, Japan

(Received April 4, 1960)

The electric field gradient q at the position of the nitrogen nucleus in the NH_3 molecule is evaluated by using four representative molecular orbitals expressed as linear combinations of atomic orbitals. The integrals over atomic orbitals are carried out by the method of Barnett and Coulson. When the electric quadrupole moment $Q(N^{14})$ of the nitrogen nucleus is determined from the experimental nuclear quadrupole coupling constant eQq, all $Q(N^{14})$ values obtained by us fall into the range of values already found by several authors. The most reliable computed value of $Q(N^{14})$ may be 0.94×10^{-26} cm², which can be obtained from the wave function including configuration interaction given by Kaplan. The polarization effect of the inner shell pointed out by Sternheimer is also evaluated by the use of Slater atomic orbitals. There is some discussion about the bond equivalent orbitals of NH_3.

I. INTRODUCTION

As the quadrupole coupling constant of the nitrogen atom by means of atomic beam techniques has not yet been measured, we can evaluate the electric quadrupole moment of the nitrogen nucleus $Q(N^{14})$ by calculating the electric field gradient at the position of the nitrogen nucleus in a molecular environment. The values of the nuclear quadrupole moment of N^{14} obtained by other authors are given in Table I. Townes

TABLE I. Values of the electric quadrupole moment of N^{14}.

Molecule	$(eQq/h)_{N^{14}}$	Quadrupole moment $Q(N^{14})$ (in 10^{-26} cm²)	Reference
Cyanides		2	a
NF_3	−7.07 Mc	1	b
HCN	−4.58 Mc	0.71	c

[a] C. H. Townes, A. N. Holden, and F. R. Merritt, Phys. Rev. **74,** 1113 (1948).
[b] J. Sheridan and W. Gordy, Phys. Rev. **79,** 513 (1950).
[c] A. Bassompierre, J. chim. phys. **51,** 614 (1954); Compt. rend. **239,** 1298 (1955); *ibid.* **240,** 285 (1955); Discussions Faraday Soc. **19,** 260 (1955).

et al.[1] and Sheridan *et al.*[2] have determined the $Q(N^{14})$ value from Townes and Dailey's theory[3] for calculating the field gradient at a nucleus, which is based on the assumptions of an appropriate coupling energy per unbalanced p electron and s-p hybridization with a reasonable electronic structure. On the other hand, Bassompierre[4] has calculated the electric field gradient in the HCN molecule by using the molecular orbitals (MO) consisting of linear combinations of atomic orbitals (LCAO) which have been set up by the self-consistent field (SCF) method.[5]

As seen in Table I, these estimates have not given a quantitatively consistent result. In the field gradient calculation in molecules, it is necessary to get the detailed behavior of the electric charge distribution near the nucleus. Especially in the LCAO MO scheme, the contributions of the p electrons to each MO should be given precisely because of the larger dependence of the field gradient on those electrons. In Bassompierre's HCN molecule calculation, the nitrogen and carbon 1s orbitals were considered as inner shells and not used in constructing the MO's.

The NH_3 molecule is used in the present calculation of the electric field gradient since there exist fairly good wave functions[6–9] and a reasonably accurate experimental value of eQq.

II. EVALUATION OF THE q VALUE

In the ground state the NH_3 molecule has threefold symmetry around the principal axis of symmetry. The NH bond distance (R) and the angle of H—N—H (α) at the equilibrium position are 1.916 A and 106°47′, respectively.[10] We have only to calculate the mean value of $\partial^2V/\partial z^2(=q)$, where z is taken along the principal axis of symmetry including the nitrogen nucleus as the origin, and V is the electrostatic potential in the molecule. The electric field gradient q can be divided into two parts,

$$q=q_n+q_e, \tag{1}$$

where q_n and q_e, respectively, represent the electric field gradients of the protons and all the electrons in the molecule. One can express q_n simply by the following

* Part of the results are reported by Y. Kato and O. Nakahara, J. Phys. Soc. Japan **14,** 690 (1959).
[1] C. H. Townes, A. N. Holden, and F. R. Merritt, Phys. Rev. **74,** 1113 (1948).
[2] J. Sheridan and W. Gordy, Phys. Rev. **79,** 513 (1950).
[3] C. H. Townes and B. P. Dailey, J. Chem. Phys. **17,** 782 (1949).
[4] A. Bassompierre, J. chim. phys. **51,** 614 (1954); Compt. rend. **239,** 1298 (1955); **240,** 285 (1955); Discussions Faraday Soc. **19,** 260 (1955).
[5] C. C. J. Roothaan, Revs. Modern Phys. **23,** 69 (1951).
[6] A. B. F. Duncan, J. Chem. Phys. **27,** 423 (1957).
[7] H. Kaplan, J. Chem. Phys. **26,** 1704 (1957).
[8] J. Higuchi, J. Chem. Phys. **24,** 535 (1956).
[9] A. B. F. Duncan and J. A. Pople, Trans. Faraday Soc. **49,** 217 (1953).
[10] G. Herzberg, *Infrared and Raman Spectra of Polyatomic Molecules* (D. Van Nostrand Company, Inc., New York, 1945), p. 439.

TABLE II. Calculated values of the nuclear part q_n of the electric field gradient.

	Static nuclei	Vibrating nuclei (I)[a]	(II)[b]
q_n (in a.u.)	$-0.24688e$	$-0.22412e$	$-0.23133e$

[a] The value averaged about simple harmonic oscillation.
[b] The value averaged about the inversion doubling.

formula in the case of static nuclei,

$$q_n = 3e(3\cos^2\beta - 1)R^{-3}. \tag{2}$$

Here e is the proton charge and β the angle between the z axis and an NH bond. However, it is also possible to take into account the effect of the nuclear vibration in the molecule. This can be done approximately by averaging over the symmetric bending vibration corresponding to $\nu_2(a_1) = 950$ cm^{-1}, since this vibrational mode is predominant at ordinary temperatures. Here q_n has been averaged over the lowest vibrational state in the following two ways: one is the average about the simple harmonic oscillation using the normal coordinates obtained by McKean and Schatz,[11] and the other is the average about the inversion doubling using the results of Manning.[12] In the latter, the vibration ν_2 is assumed to be expressed as a one-dimensional oscillator moving in a potential field with double minima. The vibrational wave function used is as follows,

$$\psi_v = (1-x)^{\tau/2-\lambda}F(x), \tag{3a}$$

$$F(x) = \sum_n a_n x^n, \qquad x \equiv \tanh^2(p/2\rho), \tag{3b}$$

where p is the distance from the nitrogen nucleus to the plane of the protons, and τ and ρ are the constants obtained by Manning. Here λ is assumed to be -0.40 for the symmetric lowest vibrational state $v = O_s$. The values of q_n obtained are given in Table II.

One can write q_e in the LCAO MO scheme as follows,

$$q_e = -2e\sum_{i,p,q} \alpha_{ip}\alpha_{iq}\int \chi_p^*(3\cos^2\theta_z - 1)r_N^{-3}\chi_q d\tau \tag{4a}$$

$$= -2e\sum_i q_{\phi_i}', \tag{4b}$$

where i stands for the suffix of the occupied MO: $\phi_i = \sum_p \alpha_{ip}\chi_p$. Here χ's represent AO's and r_N is the length of a radius vector drawn from the nitrogen nucleus to the electron which is inclined at an angle θ_z from the z axis. In order to take the effect of the nuclear vibrations on q_e into account, we should know the adiabatic dependence of q_e on the normal coordinates of vibration. However this evaluation may be very difficult and we have therefore assumed q_e to be independent of the nuclear vibrations. This approximation is permissible since the electron distribution which gives a large effect on the electric field gradient is in the vicinity of the nucleus, and it would be scarcely perturbed by small vibrations of the protons.

Various electronic wave functions of NH_3 used in the calculation of q_e are shown in Table III, together with some molecular quantities obtained. The MO's are set up from the Slater or Hartree-Fock (H–F) AO's of the nitrogen atom and the 1s function of the free hydrogen atom. For practical computation, the H–F AO may be approximated reasonably well by a finite series of the Slater type AO's with a different exponent factor in each term, as Slater[13] has shown. Accordingly the following radial wave functions can be assumed as the H–F AO's of the nitrogen atom obtained by Hartree and Hartree,[14]

$$R_{1s} = 6.2940\exp(-22.0r) + 31.134\exp(-6.31r),$$

$$R_{2s} = 6.8841\exp(-6.82r) - r[8.9336\exp(-2.03r) - 5.8769\exp(-2.95r)],$$

$$R_{2p} = r[1.80911\exp(-1.387r) + 6.62040\exp(-2.950r)]. \tag{5}$$

According to this approximation, it can be found that for example, the value of the overlap integral between R_{1s} and R_{2s} becomes -0.00208. This result, however, does not give the validity of this approximation. The method of Barnett and Coulson[15] has been used for the evaluation of the field gradient integrals. All the 1s orbitals centered on the protons are expanded in terms of r_N, θ_z, and φ about the nitrogen nucleus. After the integrals have been reduced by considering orthogonality relations between the angular factors, the radial part is expressed by a few terms of the following form:

$$Z_{m,n,1+\frac{1}{2}}(\kappa,\alpha) = \int_0^\infty \exp(-\kappa t)\zeta_{m,n}(1, t{:}\alpha)t^{1+\frac{1}{2}}dt, \tag{6}$$

where $\zeta_{m,n}(1, t{:}\alpha)$ is a function composed of the standard Bessel functions of purely imaginary argument: $I_{n+\frac{1}{2}}$ and $K_{n+\frac{1}{2}}$. Use of this device makes possible the numerical integration of the radial part. One three-center integral $q_{h_i h_j}$ can also be expanded in the same manner and its radial part can be reduced to a doubly infinite series,

$$\sum_{n,n'=0}^{\infty}\int \zeta_{1,n}(1, r_N{:}R)\zeta_{1,n'}(1, r_N{:}R)r_N^{-2}dr_N, \tag{7}$$

[11] D. C. McKean and P. N. Schatz, J. Chem. Phys. **24**, 316 (1956).
[12] M. F. Manning, J. Chem. Phys. **3**, 136 (1935). The calculation of the behavior of symmetric double minimum problems has been carried out by several authors. The one by Manning has assumed the most reasonable potential and there is no approximation in the method used. Therefore we have adopted the results obtained by Manning. However, there are a few trivial mistakes in Eqs. (6) and (8) in his original paper.
[13] J. C. Slater, Phys. Rev. **42**, 33 (1932).
[14] D. R. Hartree and W. Hartree, Proc. Roy. Soc. (London) **A193**, 299 (1948).
[15] M. P. Barnett and C. A. Coulson, Trans. Roy. Soc. (London) **A243**, 221 (1951).

TABLE III. MO's of the NH_3 molecule and the molecular quantities.

Author	Duncan	Kaplan (I)	Kaplan (II)	Higuchi	Duncan and Pople
Method:	LCAO SCF	LCAO SCF	CI	LCAO SCF	Parameter
Basic AO	Slater	H-F	H-F		Slater
E_T[a]	99.2%	99.42%	99.44%		
D_e[b]	72.1%	79.3%	82.4%	68%	
μ[c]	1.486 D		1.82 D	1.97 D	1.461 D
ϵ_1[d]	9.94 ev		14.0 ev	13.1 ev	
ϵ_2[d]	16.2 ev		19.3 ev	18.2 ev	

[a] E_T is the calculated percentage of the total experimental energy.
[b] D_e is the calculated percentage of the experimental dissociation energy.
[c] μ represents the dipole moment. The experimental value=1.468 D.
[d] ϵ_1 and ϵ_2 represent the first and second ionization potentials, respectively. The experimental values: $\epsilon_1=10.25\sim11.0$ ev, $\epsilon_2=15\sim17$ ev.

TABLE IV. Numerical values of the field gradient integrals: $q_{ab}'\equiv(a\mid b)=\int\chi_a(3\cos^2\theta-1)r^{-3}\chi_b d\tau$ (in a.u.). The following abbreviated notations for AO's are adopted: $h_i=(H_i\colon 1s)$, $k=(N\colon 1s)$, $s=(N\colon 2s)$, $x=(N\colon 2px)$, $y=(N\colon 2py)$ and $z=(N\colon 2pz)$.

Author:	Duncan	Kaplan	Higuchi[a]	Duncan-Pople[b]
$(z\mid z)$	1.977300	2.366350	2.366350	1.741429
$(x\mid x)=(y\mid y)$	−0.988650	−1.183175	−1.183175	−0.870715
$(k\mid h_i)$	−0.013159	−0.013517	−0.012145	
$(s\mid h_i)$	−0.019449	0.016614	0.014929	−0.017595
$(z\mid h_i)$	0.061965	0.063806	0.068536	0.056694
$(x\mid h_1)$	0	−0.094011	0	0
$(x\mid h_2)$	−0.079637	0.047005	0.079604	−0.072687
$(x\mid h_3)$	0.079637	0.047005	−0.079604	0.072687
$(y\mid h_1)$	−0.091957	0	−0.091918	−0.083932
$(y\mid h_2)$	0.045978	−0.081416	0.045978	0.041966
$(y\mid h_3)$	0.045978	0.081416	0.045959	0.041966
$(h_i\mid h_i)$	−0.043780	−0.043780	−0.039339	−0.039533
$(h_i\mid h_j)$	-0.0161_1	-0.0161_1	-0.0157_8	

[a] The value at the angle $\alpha=105^\circ$.
[b] The value is q_{ab}'. The values without Sternheimer's correction are the same as those obtained by Duncan's orbitals.

the convergence is rather slow. However, we think it is sufficient to truncate the series after several terms because of the small contribution from this integral to q_e. The values of the field gradient integrals are tabulated in Table IV.

III. STERNHEIMER EFFECT IN NH_3

Duncan-Pople's MO's are based upon equivalent orbitals (EO).[16] The 1s orbital of the nitrogen atom is treated as an inner shell. The coefficients of AO's are determined under the condition of ortho-normalizing the orbitals and fitting the experimental value of the dipole moment. We have to take into account the shielding effect due to the quadrupole moment induced in the inner shell, in evaluating the field gradient q_e for Duncan-Pople's MO. This effect has been treated by Sternheimer.[17] According to the results of Sternheimer and Foley[18] for the Li_2 molecule, the correction to the field gradient can be calculated as the interaction of the quadrupole moment induced in the inner shell with the electric charge outside it. Then the field gradient is modified as follows:

$$q_n^s=3e[1-\gamma(R)](3\cos^2\beta-1)R^{-3}, \tag{8}$$

$$q_n^s=-2e\sum_{i,p,q}\alpha_{ip}\alpha_{iq}\chi_p^*[1-\gamma(r)](3\cos^2\theta_z-1)r_N^{-3}\chi_q d\tau, \tag{9a}$$

$$=-2e\sum_i q_{\phi_i}{}'_s, \tag{9b}$$

[16] J. E. Lennard-Jones, Proc. Roy. Soc. (London) **A198,** 1 (1949); **A198,** 14 (1949); **A202,** 155 (1950); **A202,** 166 (1950).

[17] R. M. Sternheimer, Phys. Rev. **80,** 102 (1950); **84,** 244 (1950); **95,** 736 (1954).

[18] R. M. Sternheimer and H. M. Foley, Phys. Rev. **92,** 1460 (1953).

TABLE V. Calculated values of the electronic part q_e (in a.u.) of the electric field gradient and the nuclear quadrupole moment $Q(N^{14})$ (in 10^{-26} cm^2).

MO	Duncan	(I) Single conf.	Kaplan (II) CI	Higuchi	Duncan-Pople Without St. correction	Duncan-Pople With St. correction
q_{ϕ_1}' [a]	0.03164	0.05705		0.05325		
q_{ϕ_2}'	1.65282	1.86075		1.66497	1.20830[c]	1.06463[c]
q_{ϕ_3}'	0.00002	0.00007		0		
$q_{\phi_5}'=q_{\phi_7}'$	−0.49357	−0.54882		−0.54519	−0.22137[d]	−0.19670[d]
q_e	−1.39467e	−1.61045e	−1.60973e	−1.25567e	−1.08839e	−0.94909e
q[b]	−1.62600e	−1.84178e	−1.84106e	−1.48700e	−1.31972e	−1.15536e
$Q(N^{14})$	1.07	0.94	0.94	1.17	1.32	1.50

[a] The subscript of q' is described for convenience. ϕ_1, ϕ_2, and ϕ_3 are the MO's of A_1 type, and ϕ_5 and ϕ_7 the MO's of E type.
[b] For q_n, the value averaged on the inversion doubling is used.
[c] The value $q'(1)$ by lone pair orbital.
[d] The value $q'(b_i)$ by a bonding EO. Therefore $q_e=-2e[q'(1)+3q'(b_i)]$.

where

$$\gamma(r)=1/Q\left[\int_0^r Q_i dr'+r^5\int_r^\infty Q_i r'^{-5}dr'\right]. \qquad (10)$$

Here $\gamma(r)$ is Sternheimer's correction factor; $Q_i(r')dr'$ means the induced quadrupole moment due to the $1s$ electrons between r' and $r'+dr'$. Adopting Slater AO's for the nitrogen atom, Q_i can be given as follows:

$$Q_i(r')=(16/15)Q\exp(-2t')t'^3(1+t'/3), \qquad t'\equiv\delta_1 r', \qquad (11)$$

where $\delta_1(=6.7)$ is the orbital exponent of the nitrogen $1s$ orbital. Then $\gamma(r)$ can be easily integrated using Eq. (11),

$$\gamma(r)=(2/3\delta_1)[1-(e^{-2t}/3)(4t^4+4t^3+6t^2+6t+3)] -(16/9\delta_1)t^5\{-E_1(-2t)\}, \qquad t\equiv\delta_1 r, \qquad (12)$$

where $\{-E_i(x)\}$ is a logarithmic integral. The $\gamma(r)$ function is smoothly varying up to a finite value $\gamma(\infty)=8/15\delta_1$ as shown in Fig. 1, together with Q_i. We can therefore carry out the integrals in Eq. (9a) by numerical integration. The value of the $q_{ab}'^s$ elements are also tabulated in Table IV.

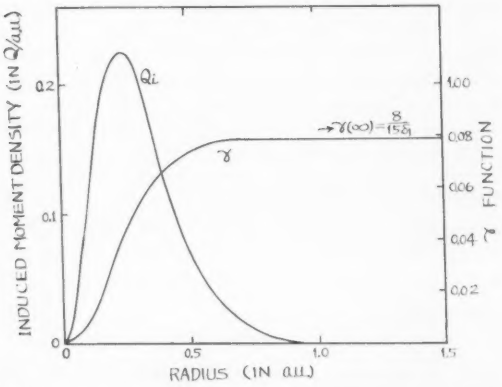

FIG. 1. Induced quadrupole moment density Q_i and $\gamma(r)$ function.

IV. RESULTS AND DISCUSSION

Table V shows the contributions of the occupied MO's to q_e, together with the value of $Q(N^{14})$. The value of $Q(N^{14})$ can be determined by using the experimental value[19] (4.0842 Mc/sec) of the nuclear quadrupole coupling constant eQq in NH_3. As shown in Table V, the major part of the total field gradient q is due to the electrons, and the contributions of the protons to q are small. Furthermore the effect of the vibrational average on q_n is not too large, as seen in Table II. We are not always able to compare the accuracy of the two cases of the vibrational average. The average about the inversion doubling may be more accurate in regard to the vibrational wave function used than is the average using the harmonic oscillation, but the former has used an approximation concerning the displacement of the nuclei. Here we have estimated the value of q by taking an average about the inversion doubling. This gives rise to a variation of less than 1% in the value of $Q(N^{14})$, as compared with the other contributions to q_n.

The value of q_e from Duncan's MO is slightly different from that obtained by Kaplan's MO (I) as shown in Table V. These MO's differ from each other in regard to the basic AO's. Accuracy of the calculated q_e value will depend on the molecular wave function used. The better the wave function, the more accurate one would expect the values of the molecular quantities to be. Kaplan's MO's give better values in the total

[19] G. R. Gunther-Mohr, R. L. White, A. L. Schawlow, W. E. Good, and D. K. Coles, Phys. Rev. **94**, 1184 (1954).

energy and binding energy than Duncan's MO's but the other molecular quantities are not always better as seen in Table III. However, in a molecule containing an atom with p electrons, such as the nitrogen atom, their contributions to each MO are predominant for the estimation of q_e. The Slater function would not be as good as the H-F function in the vicinity of a nucleus. The behaviors of these radial functions times r are shown in Fig. 2. There is an appreciable difference between the $2p$ functions in spite of there being almost no distinct difference between the $1s$ and $2s$ functions. This fact will cause the difference between the values of q_e from Duncan's and Kaplan's MO's. The value of q_e from Kaplan's wave function (II) including configuration interaction (CI) among 13 states is nearly equal to that from his single configuration. This will not be surprising since the best one determinant wave function gives the major part of the configuration mixing, and the rest of the state functions give almost no contribution.[20] The circumstances are the same as the small energy change resulting from the inclusion of CI.[21] The value of q_e by Higuchi's MO is calculated for $\alpha=105°$, namely, $\beta=66°24'$. In his work, many integrals are calculated approximately and the $1s$ orbital of nitrogen is separated as an inner shell in the energy calculation. Now, by using the results of the MO calculation by Higuchi, the dependence of the field gradient on the angle β is shown in Fig. 3. As seen in Fig. 3, q is intensely dependent upon the angle β. The value of q at the equilibrium angle ($\beta_e=67°58'$) becomes $-1.65e$ a.u. in Fig. 3. This gives 1.05×10^{-26} cm^2 as the value of $Q(N^{14})$ and approaches the values of the above MO's. In this respect, it seems to be meaningless to take into consideration the Sternheimer effect for q_e by Higuchi's MO.

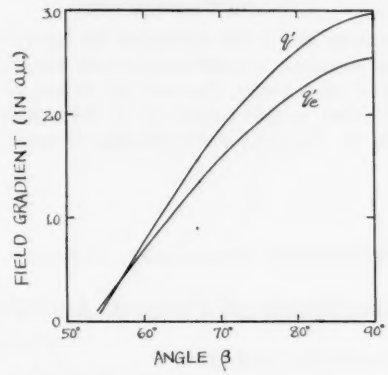

FIG. 3. Dependence of the electric field gradients q' and q_e' upon the angle β between the z axis and an NH bond.

In view of the above consideration, the best value of q_e is presumably that from Kaplan's wave function (II) including CI. This yields 0.94×10^{-26} cm^2 as the most reliable value of the electric quadrupole moment of N^{14}.

The value of q_e by Duncan-Pople's MO is smaller apart from the sign value, than the others. This MO is set up to agree with the value of the experimental dipole moment. The value of a molecular dipole moment would be rather more dependent on the distribution of the whole charge than on the local behavior near the nucleus in the molecule. This could result in a worse estimate of q_e. The Sternheimer effect makes the value of q_e still smaller. This correction induces a change of about 12% in the total field gradient. Then there has been an attempt to improve the results in the following way. The dipole moment does not vary much in the neighborhood of the equilibrium angle β_e as shown by Higuchi.[8] In general, there is no need for the direction of the bonding orbitals to coincide with the direction of the NH bond. If the bonding EO's are assumed to be bent only a small amount towards the direction of increasing angle β, the value of the field gradient will be improved surprisingly as shown in Fig. 3. This depends not so much upon the variation in the direction of the EO's as upon the increase of the p character in the lone pair orbital. In view of this fact, it would be rather desirable for MO's obtained by the EO method to be described as somewhat bent outwards.

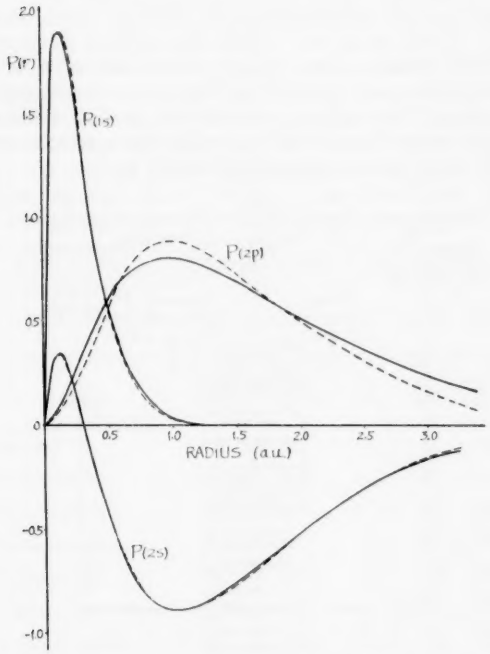

FIG. 2. Comparison of normalized Slater type functions $P(1s)$, $P(2s)$ and $P(2p)$ of nitrogen (in broken line) with the corresponding Hartree-Fock functions (in full line). All $P(r)$ functions express r times the radial functions. The Slater $2s$ function is that orthogonalized to the $1s$ function.

[20] H. Kaplan (private communication).
[21] F. O. Ellison and H. Shull, J. Chem. Phys. **23**, 2348 (1955), see work cited in footnote 7.

V. ACKNOWLEDGMENTS

The author would like to express his hearty thanks to Dr. O. Nakahara with whom the work was originally begun and who kindly checked the values of many integrals used in this paper. He is very grateful to Professor H. Narumi for his valuable discussions and his continual guidance, and to Professors H. Takeyama and H. Murata for their helpful discussions and continual encouragement throughout this work. He also wishes to thank Professor H. Kaplan for valuable information from his unpublished data and for his continual interest.

THE JOURNAL OF CHEMICAL PHYSICS VOLUME 34, NUMBER 2 FEBRUARY, 1961

Time Spectra of Positrons Annihilating in Organic Liquids Containing Halogens*

J. H. ORMROD† AND B. G. HOGG

Allen Physics Laboratories, University of Manitoba, Canada

(Received July 21, 1960)

Measurements have been made of the mean life τ_2, and the percent I_2, of positrons forming triplet positronium in propyl halides and in benzene-carbon tetrachloride solutions. The experimental variations of I_2 in the propyl halides can be predicted assuming a semiempirical equation of the form $100-4/3I_2=AN_1+2.4N_2$, where A is the *annihilation factor* of the parent molecule and N_1 and N_2 are the percent volumes of the parent and halide, respectively. A equal to 0.36 is needed for the propyl parent. This equation also predicts correctly the experimental values for the benzyl halides if A equal to 0.53 is used as the benzyl *annihilation* factor. The quenching of I_2 in the benzene-carbon tetrachloride solutions is much greater than that computed by the equation and the variation in quenching closely resembles that obtained in aqueous nitrate-ion solutions.

INTRODUCTION

LET us consider a positron which has been emitted from a Na^{22} nucleus and which is incident on the liquid under study. This positron will lose energy mainly by inelastic collisions and eventually it will be in an energy region where both direct annihilation and positronium formation cross sections are important and possibly competing factors. At still lower energies only direct annihilation may occur.[1] If positronium is formed as the positron loses energy, then statistically it is three times more likely to be triplet than singlet positronium. Positronium in the triplet state annihilates with a mean life of $\sim 10^{-7}$ sec[2] while singlet positronium will decay with a mean life of $\sim 10^{-10}$ sec.[3]

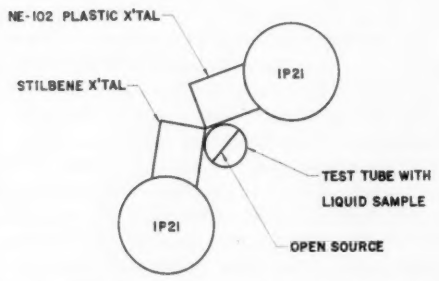

FIG. 1. Geometry of detectors and source, showing location of open Na^{22} source.

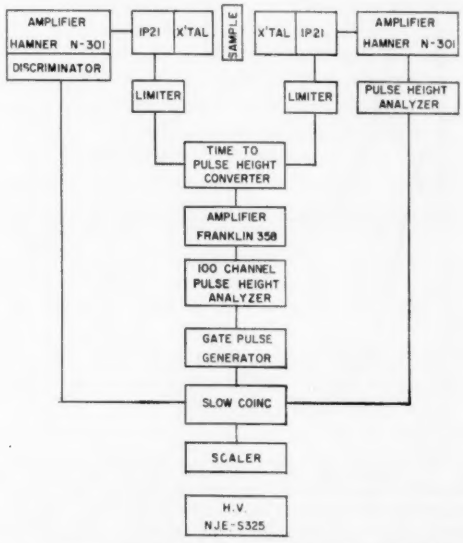

FIG. 2. Block diagram of delayed coincidence circuit.

* This work was supported by the Defense Research Board of Canada.

† Holder of a Northern Electric Fellowship, 1959–60. Now at McMaster University, Hamilton, Canada.

[1] R. A. Ferrell, Revs. Modern Phys. **28**, 308 (1956).

[2] A. Ore and J. L. Powell, Phys. Rev. **75**, 1696 (1949).

[3] J. A. Wheeler, Ann. N. Y. Acad. Sci. **48**, 219 (1946).

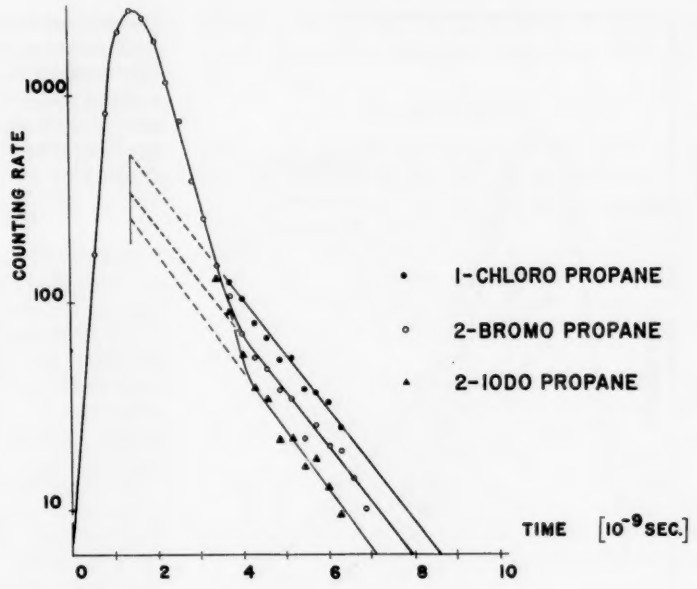

FIG. 3. Decay of positrons in propyl halides.

Delayed coincidence experiments by Bell and Graham[4] indicated that in most liquids a measurable time delay occurred for approximately 30% of the positrons entering the sample. The mean lifetime recorded for the long lived component was several millimicroseconds in each case. The measurement of the mean life of the long component (τ_2) gives the mean life associated with the conversion (thought to be mainly by collision and pickoff[4]) of the triplet state to the fast decaying single state. The percentage of positrons (I_2) forming positronium can be obtained from analysis of the delayed coincidence curve.

Subsequent experiments[5,6] have shown that there can be wide variations in I_2 for liquids. Experiments by Millett and co-workers[7] have indicated a systematic variation in I_2 in the benzyl halides.

TABLE I. Experimental and calculated values of $(100-4/3I_2)$ for benzyl[7] and propyl halides.

Sample	Parent, % vol	Halide, % vol	I_2 obs	$100-4/3I_2$ exp	$100-4/3I_2$ calc
Benzene	100	0	35±2	53	53
Fluoro-benzene	93.3	6.7	24±2	68	66
Chloro-benzene	85	15	14±2	81	82
Bromo-benzene	82	18	6±2	92	88
Iodo-benzene	77	23	4±2	95	97
Dichloro-benzene	75.6	24.4	0	100	100
1 propyl chloride	83	17	23±2	69	71
2 propyl bromide	80	20	16±2	79	77
2 propyl iodide	75	25	12±2	84	87

[4] R. E. Bell and R. L. Graham, Phys. Rev. **90**, 644 (1953).
[5] H. S. Landes, S. Berko and A. J. Zuchelli, Phys. Rev. **103**, 828 (1956).
[6] R. E. Green and R. E. Bell, Can. J. Phys. **35**, 398 (1957).

EXPERIMENTAL

The positron source used in this experiment was 3μ-C of Na^{22}. Mica sandwich sources of 2–3 mg/cm^2 thickness were found unsuitable since the adhesives used to close the source eventually succumbed to the attack of the liquids under study. It was found that open sources could be used satisfactorily. The $Na^{22}Cl$ in aqueous solution was deposited on a piece of mica 3 mg/cm^2 and evaporated to dryness. For the liquids tested the activity remained with the mica. The source was inserted in a test tube containing the sample and mounted with respect to the detectors as indicated in Fig. 1.

The time delays were measured with a fast-slow coincidence circuit. A block diagram of the circuit appears in Fig. 2. The 1.28-Mev nuclear γ ray from Ne^{22} occurs simultaneously (as far as our circuit resolution is concerned) with the emission of the positron. This radia-

TABLE II. Benzene-carbon tetrachloride solutions.

CCl_4, % vol	$\tau_2(10^{-10}$ sec±.2)	I_2(%±3)
0	23.0	36
0.50	17.7	29
0.77	17.5	26
1.06	16.5	24
2.50	17.7	16
4.45	17.9	11
6.50	18.0	8
100	...	0

[7] C. R. Hatcher, W. E. Millet and L. Brown, Phys. Rev. **111**, 12 (1958).

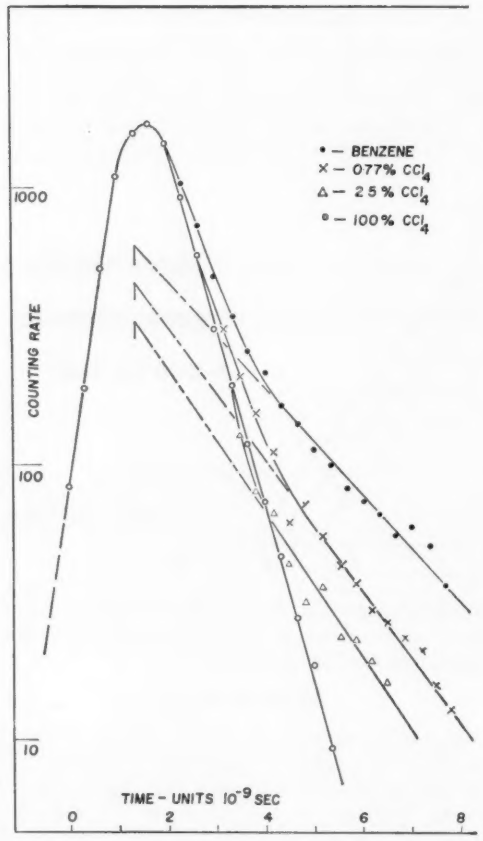

FIG. 4. Decay of positrons in benzene-carbon tetrachloride solutions.

tion was detected in the right hand (1.28-Mev channel) detector which consisted of NE 102 plastic. The pulse from the anode of the 1P21 was limited and sent on to the time to pulse height converter.[5] A pulse was also taken from the last dynode of the 1P21 and its energy analyzed to pass down the 1.28-Mev channel provided its energy was 0.52 Mev or higher.

With the annihilation of the positron one of the 0.511-Mev γ rays may reach the stilbene crystal on the left hand channel (0.511-Mev channel). A limited pulse from this channel was also fed to the pulse height converter. If the pulses from the 0.511- and 1.28-Mev detectors overlapped, a pulse would be passed on to the integrator. The size of the pulse from the integrating circuit is a measure of the time delay.

The 0.511-Mev side channel received a pulse from the last dynode of its 1P21 and if the pulse lay between 0.2 and 0.5 Mev it was amplified and sent on to the slow coincidence circuit. The 100 channel kicksorter recorded an event if it received a triggering pulse from the gate pulse generator within 10^{-6} sec of receiving a pulse from the amplifier in the fast coincidence circuit. The instrument proved to be linear over a range of 5 mμsec and gave τ_2 and I_2 values for water and benzene in good agreement with previous workers.[6,7] The resolving time of the apparatus, the full width at half-height for a Co^{60} curve, was $2\tau_0=1.2\times10^{-9}$ sec.

RESULTS AND DISCUSSION

The propyl halide curves are shown in Fig. 3. The τ_2's were obtained from a least-squares fit of the tails and the I_2's were obtained by projecting the tails back to zero time and computing the ratio of the area under the tail to the total area under the whole curve.[6] Zero time was taken from curves obtained for positron annihilations in copper. It is clear from Fig. 3 that a similar variation of I_2 observed in the benzyl halides exists for the propyl halides.

These results may be interpreted as follows. The fate of a positron passing through a halogenated compound could be described by attributing an *annihilation factor*, A to the parent (benzyl, propyl group etc) and a constant annihilation factor, B to the halide. Then the number of positrons annihilating can be written as

$$100-4/3I_2=AN_1+BN_2. \qquad (1)$$

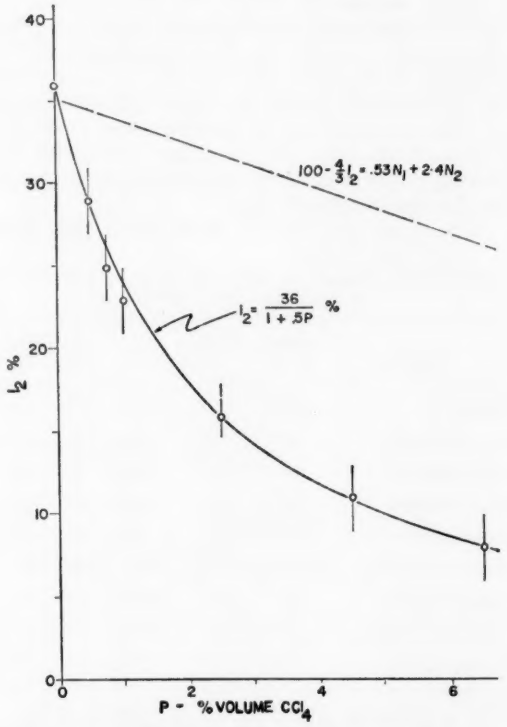

FIG. 5. Comparison of results of positron decays in benzene-carbon tetrachloride with Eq. (1) and Eq. (2).

[5] G. Jones, Ph.D. thesis, University of British Columbia, 1960.

N_1 and N_2 are the percent volume[9] of parent and halide, respectively, and N_1+N_2 must equal 100%. I_2 is the percent of the positrons forming triplet positronium and $4/3I_2$ is the percent of entering positrons that form both singlet and triplet positronium. The equation simply states that the number of positrons annihilating directly depends on the environment in which the positron finds itself and the time spent in that environment.

In Table I a comparison is made between the experimental values for $100-4/3I_2$ and those calculated from Eq. (1). In applying the equation $A=0.53$ for the benzyl parent, $A=0.36$ for the propyl parent and $B=2.4$ for the halides. There is good agreement between the experimental and calculated values in all cases.

A further test of Eq. (1) was then undertaken by studying a number of benzene-carbon tetrachloride solutions. Delayed coincidence curves for some concentrations of these solutions are shown in Fig. 4 and the results for all concentrations tested are in Table II.

An examination of Table II and the graphical representation of this table in Fig. 5 reveals that a much larger quenching of the τ_2 component occurs for a given concentration of carbon tetrachloride than is predicted by Eq. (1). An excellent fit of the experimental data can be obtained however from the following equation:

$$I_2=36/1+0.5P\%, \tag{2}$$

where P is the percent volume of the carbon tetrachloride. The form of Eq. (2) is identical with that obtained by Green and Bell[6] for different concentrations of nitrate ions in aqueous solution. They proposed a mechanism whereby removal of positrons by chemical combination of positrons with nitrate ions occurred. We have been dealing with organic liquids and it seems unlikely that such an ionic reaction can occur appreciably here.

It may be that some form of chemical association can occur to provide the positron a means of fast annihilation. Another plausible mechanism would be to assume that the halide inhibits positronium formation by allowing the positron to pass through the energy band where the formation of positronium is possible. This inhibition would be larger for the heavier halides since percentagewise more of the liquid would be dominated by the halide.

In conclusion we may say that for the liquid organic halogen compounds studied it is possible to correctly predict the percentage of promptly annihilating positrons by Eq. (1). When dilution experiments with benzene-carbon tetrachloride solutions are performed more positrons annihilate directly than was predicted by the equation.

[9] The volume of the halide was calculated using the appropriate ionic radius, see L. Pauling, *Nature of the Chemical Bond* (Cornell University Press, Ithaca, New York, 1948), 2nd ed., p. 346. The ionic radius is approximately equal to the sum of the covalent radius plus the radius of a positronium atom.

Intensities of Infrared Bands of Some I_2-Alkylbenzene Charge-Transfer Complexes

E. E. FERGUSON

Department of Physics, University of Texas, Austin, Texas

AND

IKE Y. CHANG

Department of Chemistry, University of Texas, Austin, Texas

(Received August 22, 1960)

The intensities of the infrared bands corresponding to symmetric ring breathing and symmetric methyl stretching modes have been measured for charge-transfer complexes of iodine in benzene, toluene, the xylenes, mesitylene and 1,2,4 trimethylbenzene, durene, penta-, and hexamethylbenzene. The ring breathing mode intensity is found to decrease and the methyl stretching mode intensity to increase with methyl substitution. These results are interpreted in terms of a previously proposed "electron vibration" infrared absorption mechanism [E. E. Ferguson and F. A. Matsen, J. Chem. Phys. **29,** 105 (1958); J. Am. Chem. Soc. **82,** 3268 (1960)] extended to include π-electron interaction with methyl group electrons.

INTRODUCTION

THE effect of dissolved I_2 and Br_2 on the infrared spectrum of benzene[1] and I_2 on C_6D_6[2] has been found to be principally the enhancement of two inactive vibrations $\nu_1(a_{1g})$ and $\nu_{10}(e_{1g})$, which occur weakly in the pure liquid aromatic as a consequence of breakdown of selection rules in the liquid phase. These enhanced bands are attributed to the approximately 3% concentration of binary complex in solution and not to other halogen solvent perturbation effects for the following reasons: (1) The effect of varying the concentration of a wide variety of solvents on the inactive fundamentals of benzene has been found to be a nearly uniform change in intensity of all the observed inactive fundamentals, rather than specific enhancement of certain vibrations as occurs in the case of halogenbenzene solutions.[3,4] In particular, the inactive ν_{10} and $\nu_9(e_{2g})$ of roughly the same intensity in pure liquid benzene were influenced approximately in the same manner in all the noncomplexing solvents studied. (2) The enhanced intensities are too large to be attributed to a solvent effect when one considers that the solubility of I_2 in benzene is less than 5 mol percent. (3) Recent measurements[5] on ν_1 and ν_{10} in solid benzene-iodine complex yield intensities comparable to those for the liquid.

Since the iodine-enhanced vibrations in benzene (ν_1 and ν_{10}) are precisely those which would become active in going from D_{6h} to C_{6v} symmetry, this observation has been used as an argument for the C_{6v} "axial" geometry.[1,2] The argument for axial symmetry has recently been criticized by Morcillo and Gallego[6] on the grounds that three vibrations of benzene should become active under the symmetry reduction $D_{6h} \rightarrow C_{6v}$, the third being a C–H stretching frequency. This is true; however, a weak C–H band (as an enhanced band of complex in only 3% solution would be) would not be expected to be detectable since benzene has an active C–H stretching mode $\nu_{20}(e_{1u})$ at 3080 cm^{-1} along with many e_{1u} combination bands which can be in Fermi resonance with ν_{20} so that there is a region of strong absorption from about 3000–3100 cm^{-1}. This is clearly shown in the spectrum of Morcillo and Gallego, for example. The formal lowering of symmetry from $D_{6g} \rightarrow C_{6v}$ by I_2 attachment to the π-electron system of benzene is expected to be less significant for a C–H stretching vibration than for ring deformation modes, so that enhancement of ν_2 might not be observable even without the interference. According to the electron vibration model[7,8] donor infrared band intensities of charge-transfer complexes are interpreted in terms of variation of vertical ionization potential during vibration. Clearly, a hydrogen stretching is second order with respect to a carbon-carbon stretching as far as effect on π-electron energy is concerned. In any case, the failure to observe ν_2 is not significant with respect to symmetry, as it would be active for models of all proposed symmetries of benzene-halogen complexes. One of the authors (E.E.F.) previously searched for this band without success using a quartz prism with good resolution. Recently, Ellis[5] failed to observe any significant enhancement in the infrared spectrum of the solid in this region.

The C_{6v} symmetry has been objected to on theoretical grounds by Mulliken.[9] Aono,[10] however, has recently made energy calculations which support the C_{6v} geom-

[1] E. E. Ferguson, J. Chem. Phys. **25,** 577 (1956).
[2] E. E. Ferguson, J. Chem. Phys. **26,** 1357 (1957).
[3] E. E. Ferguson, J. Chem. Phys. **26,** 1265 (1957).
[4] J. K. Thompson and A. D. E. Pullin, J. Chem. Soc. **314,** 1658 (1957).
[5] G. E. Ellis, M.A. thesis, University of Texas, Austin, Texas, (1960).
[6] J. Morcillo and E. Gallego, Anales real soc. españ. fís. y quím. (Madrid) **55, B645** (1959).
[7] E. E. Ferguson and F. A. Matsen, J. Chem. Phys. **29,** 105 (1958).
[8] E. E. Ferguson and F. A. Matsen, J. Am. Chem. Soc. **82,** 3268 (1960).
[9] R. S. Mulliken, J. Am. Chem. Soc. **74,** 811 (1952).
[10] S. Aono, Progr. Theoret. Phys. (Kyoto) **22,** 313 (1959).

etry. In addition, Hassel[11] found by means of x-ray diffraction that the near Br atom in a solid $Bz \cdot Br_2$ complex lies on the sixfold axis. The I_2 is only loosely bound to the benzene and the C_{6v} symmetry probably only means that the near I atom lies on the axis with the far atom behaving essentially as a free rotator.

Qualitative observations on I_2·alkylbenzene spectra have been reported earlier.[12,13] Since there now exists a satisfactory theoretical model for infrared intensities,[7,8] these data are of increased interest and have been remeasured quantitatively and extended.

EXPERIMENTAL

All aromatic compounds except benzene were Eastman Kodak reagent grade and were used without purification. The benzene and CS_2 were redistilled. The iodine was resublimed reagent grade.

All spectra were obtained on a Perkin-Elmer model 112 single-beam double-pass spectrometer with NaCl prism. The 4, 5, and 6 methylbenzenes, being solids, were studied in CS_2 solution. Spectral slit widths ranged from 3 to 7 cm^{-1}. Since this is comparable to the half-widths of the bands measured, an error is introduced into the measured intensities. However, integrated intensities corrected for this slit-width error using the corrections given by Ramsay[14] for Lorentz band shapes agree within experimental error with the results obtained. A very large uncertainty has been assigned to all of the measurements because of the inherent difficulty in measuring very weak infrared bands. This difficulty is aggravated here because one is measuring band "enhancements," i.e., changes in weak band intensities due to the addition of I_2. Therefore, the uncertainties in measurement vary considerably (with respect to percentage) from band to band, depending principally on this ratio of enhanced intensity to the intensity of the band in the absence of iodine.

Finally, there remains the problem of determining the concentrations of complex. Table I shows the equilibrium constants used and their sources. In view of the previously mentioned measuring difficulties, it does not appear likely that the concentration determinations contribute a significant factor to the uncertainty of the results. A measurement of the relatively strong 1300 cm^{-1} mesitylene-iodine band intensity in pure liquid and various volume fractions of CS_2 showed an appreciable solvent effect on the apparent equilibrium constant, the CS_2 apparently competing for the I_2 and hence decreasing the amount of complex formed. The solvent effect was assumed to be the same for the 4, 5, and 6 methylbenzenes as for mesitylene and the equilibrium constants accordingly

TABLE I. Equilibrium constant.[a]

	Benzene	Toluene	Ethylbenzene	*o*-Xylene	*p*-Xylene	*m*-Xylene	Mesitylene	1,2,4-Trimethylbenzene	Durene	Pentamethylbenzene	Hexamethylbenzene
Andrews and Keefer[b]	0.15	0.16	...	0.27	0.31	0.31	0.82	...	0.63	0.88	1.35
Tamres, Virzi, and Searles[c]	0.15	...	...	...	...	...	0.58	...	...	0.94	1.47
Benesi and Hildebrand[d]	0.168	...	...	...	...	...	0.70	...	...	...	...
Value used in this work	0.15	0.16	0.16[e]	0.27	0.31	0.31	0.70±0.12	0.47[f]	0.63	0.91±0.03	1.41±0.06

[a] Defined as $[Ar \cdot I_2]/[Ar] \cdot [I_2]$ and is in units of reciprocal moles per liter where $[Ar \cdot I_2]$, $[Ar]$, and $[I_2]$ are molar concentrations of complex, aromatic compound, and iodine, respectively. The dimensionless equilibrium constant originally given by Tamres and Hildebrand is defined as $[Ar \cdot I_2]/N[I_2]$ where N is mole fraction of aromatic compound.
[b] J. Am. Chem. Soc. **74**, 4502 (1952).
[c] J. Am. Chem. Soc. **75**, 4358 (1953).
[d] J. Am. Chem. Soc. **71**, 2703 (1949).
[e] Assumed same as that of toluene.
[f] Taken as average of *p*-xylene and durene.

[11] O. Hassel, J. Mol. Phys. **1**, 241 (1958).
[12] W. Haller, G. Jura, and G. C. Pimentel, J. Chem. Phys. **22**, 220 (1954).
[13] E. E. Ferguson, Spectrochim. Acta **10**, 123 (1957).
[14] D. A. Ramsay, J. Am. Chem. Soc. **74**, 72 (1952).

TABLE II. Summary of integrated band intensities for I_2 charge-transfer complexes.

Donor	Symmetric ring breathing vibration ν (cm^{-1})	Symmetric ring breathing vibration A (darks)[a]	Symmetric C—CH_3 stretching vibration ν (cm^{-1})	Symmetric C—CH_3 stretching vibration A (darks)
Benzene	992	190±20		
Toluene	1002	130±20	1210	95±20
p-Xylene	836	120±70	1204	250±40
m-Xylene	1000	100±20	1250	190±60
o-Xylene	733	masked	1223	230±80
Mesitylene	998	80±50	1300	350±30
1,2,4-Trimethylbenzene	746	30±20	1250	320±50
Durene	738	70±40	1266	520±100
Pentamethylbenzene	580	50±40	1292	630±100
Hexamethylbenzene	560	50±40	1296	730±100
Ethylbenzene	1005	70±30		
Other measured intensities				
p-Xylene	943	90±20	Not assigned as fundamental by Pitzer and Scott	
Mesitylene	880	700±200	Not assigned as fundamental by Pitzer and Scott	
m-Xylene	1265	60±20	Possibly Fermi resonance combination with 1250	
1,2,4-Trimethylbenzene	942	90±30	Possibly the symmetric ring breathing mode	
Benzene	850	640±200	$\nu_{10}(e_{1g})$ not previously reported	

[a] Dark = cm^{-1}/millimole/cm^2.

were corrected for this effect. The Van Laar-Hildebrand-Scatchard equation[15] was used to evaluate the ratio of activity coefficient of complex to that of aromatic compound and iodine, and thus the equilibrium constant in terms of activities could be estimated for the given volume fraction of CS_2. Since only semiquantitative results are reported for these latter compounds, this procedure will not be elaborated. The final data are reported in Table II.

ASSIGNMENT OF FREQUENCIES

The frequency assignments of the totally symmetric ring breathing and methyl carbon-ring carbon stretching vibrations for benzene, toluene, the xylenes, and mesitylene were taken from Pitzer and Scott.[16] The hexamethylbenzene assignments are from Kohlrausch.[17] For 1,2,4-, 1,2,4,5-, and pentamethylbenzene vibrational assignments have not been made. The symmetric methyl stretching modes in Table II are in very little doubt because of the relative constancy of this frequency and the fact that the vibration yields a characteristically strong Raman band in each case.[18] The ring breathing modes are also probably correct as they correspond in each case to the strongest Raman band in the spectrum,[18] which is characteristic. There is some question in the case of 1,2,4-trimethylbenzene where a strong Raman band at 942 cm^{-1} corresponds to an enhanced infrared band in the complex and may, in fact, be the symmetric ring breathing mode. The intensity of this alternate choice is in somewhat better agreement with the intensity trends observed in the iodine-complex spectra.

RESULTS AND CONCLUSIONS

The most interesting correlation of the data (Table II) is the fairly consistent decrease in intensity of the symmetric ring breathing mode with increasing methyl substitution. This, at first sight, is a surprising result since the complex strength is well known to increase with methyl substitution. The molar polarizations, and hence, dipole moments of iodine complexes, are known to increase in the order: benzene, *p*-xylene, and mesitylene,[19] for example. Hence, one would normally expect the change of dipole moment during molecular vibration to also increase in that order. Suppose, e.g., that the near iodine atom was attached preferentially

[15] See, for example, J. H. Hildebrand and R. L. Scott, *Solubility of Nonelectrolytes* (Reinhold Publishing Corporation, New York, 1950), 3rd ed., p. 450.

[16] K. S. Pitzer and D. W. Scott, J. Am. Chem. Soc. **65**, 803 (1943).

[17] K. W. F. Kohlrausch, *Ramanspektren* (Becker and Erler, Leipzig, 1943).

[18] K. W. F. Kohlrausch and A. Pongratz, Monatsch. Chem. **65**, 6 (1934).

[19] G. W. Nederbragt and J. Pelle, J. Mol. Phys. **1**, 97 (1958).

to one carbon atom (or carbon-carbon bond) such that the complex symmetry was lower than C_{6v}, as in Mulliken's[9] oblique model "O." Then the carbon ring would have a dipole moment in its plane which would change during ring breathing vibration and absorb infrared radiation in the usual manner. One should expect such "localization" to be stronger, the stronger the complex, and hence the ring breathing mode absorption intensity to increase. This effect very likely would be aided in those cases where charge asymmetry of the ring is caused by addition of alkyl groups.

This observed effect may be accounted for by an extension of the electron vibration model[7,8] which has been found to be in semiquantitative agreement with the symmetric ring breathing mode intensity in Bz-I_2 complex,[7] and for the I_2, Br_2, Cl_2 stretching mode intensities in these halogen-benzene complexes.[8] This model does not require axial symmetry, in fact, does not have anything to say about symmetry, but is consistent with a C_{6v} model. In brief, the mechanism is as follows: A variation in molecular geometry (a vibration) leads to a variation in vertical ionization potential of the aromatic donor. It follows that the electron charge transfer from donor to acceptor will vary, and consequently infrared absorption will occur due to what might be called an "electron vibration" mechanism. The frequency, of course, is the molecular vibration frequency, but the direction of dipole moment change does not have to be parallel to nuclear displacement, and in fact may be nearly perpendicular. In a discussion of acceptor infrared bands, vertical electron affinity replaces vertical ionization potential in the above discussion.

According to this model, when the carbon ring "breathes" the vertical ionization potential decreases (sign is irrelevant, i.e., increase in I.P. would give same result). Hence, the ring donor has a greater tendency to transfer π-electron charge to the halogen acceptor and the dipole moment increases, the periodic repetition giving rise to the infrared activity.

When methyl groups are added to the benzene ring they normally are sources of electrons as is evidenced by the decrease in ionization energy with methyl substitution. However, the methyl groups, being more polarizable than hydrogen atoms, can also probably act as sinks. Such a combined source-sink role for methyl groups would have the effect of reducing, with methyl substitution, the change in vertical ionization energy with vibrational displacement. Here one might consider such π-electron-methyl group interactions as hyperconjugation or induction. It is probably safer in this case to avoid the possibly controversial concepts and simply say that there must be interaction to some extent between the methyl and carbon π-electrons, which qualitatively is all that is necessary. It follows that an increase in the number of methyl groups will decrease the breathing mode intensity, as is in fact observed.

The π-electron-methyl electron coupling can also be invoked to account for the other outstanding feature of the data, the strong iodine enhancement of the symmetric ring carbon-methyl carbon stretching vibrations. Here the coupling is invoked in an inverse fashion, namely, as the carbon-carbon single-bond length changes, the π-electron charge density in the ring will be changed due to the interaction between π and methyl electrons. Hence, the donor-acceptor charge transfer will vary and infrared absorption will result. In this case, the trend for intensities to increase with number of methyl groups is predicted, in agreement with observation. Within the accuracy of the measurements, the intensities are, in fact, a linear function of the number of methyl groups. A value of about 100 darks per methyl group fits all of the nine observed symmetric methyl stretching intensities.

It will be noted in Table II that there are a few other vibrations enhanced, in addition to the ring breathing and symmetric methyl stretching modes. Other modes should interact with (or perturb) the π system and hence this might be expected. In view of the uncertainty of the assignments of many of these fundamentals, the large uncertainty in the intensity measurements, and the qualitative nature of the model proposed, it does not appear feasible to attempt a detailed explanation of the results.

The only one of these which is disturbing is the quite strong mesitylene band at 880 cm^{-1}. This band is atypical in its appearance in the complex spectra, being extremely broad. The band was not assigned as a fundamental by Pitzer and Scott and we have no explanation of its peculiar behavior. It does seem very likely that the fundamental assignments are in error and that, in fact, the band is an inactive fundamental of mesitylene.

The symmetric ring mode of ethylbenzene complex with I_2 was also measured and is included in Table II. This intensity seems too low to be consistent with the herein proposed mechanism since one might expect the π-electron interaction to be less with an ethyl than with a methyl group. Certainly this would be so if one thinks in terms of a hyperconjugative interaction mechanism in which case the intensity in ethylbenzene should have returned to essentially the benzene value. We have assumed the equilibrium constant to be the same as for toluene and perhaps this assumption is not valid. On the whole, however, it is felt that the proposed model explains sufficient data to be given serious consideration.

The 850 cm^{-1} band intensity of benzene-iodine complex, not previously reported, is included in Table II.

ACKNOWLEDGMENTS

The authors wish to express their appreciation to Professors R. S. Mulliken, M. J. S. Dewar, and F. A. Matsen for very helpful discussions.

Evaluation of Electrostatic Energy Levels of f^6

JOHN B. GRUBER AND JOHN G. CONWAY

Lawrence Radiation Laboratory and Department of Chemistry, University of California, Berkeley, California

(Received August 19, 1960)

The 119 electrostatic energy levels for an nf^6 configuration have been calculated for three different sets of Slater F_k ratios: $4f^6$ hydrogenic $-F_4/F_2=0.1381$, $F_6/F_2=0.01511$; $5f^6$ hydrogenic $-F_4/F_2=0.1422$, $F_6/F_2=0.0161$; and $5f^6$ based on a Hartree-Fock calculation for the normal uranium atom $-F_4/F_2=0.159$, and $F_6/F_2=0.0204$. A tentative theoretical analysis of the absorption spectra of Eu IV can be made by using $\zeta=1360$ cm^{-1} and $F_2=370$ cm^{-1}. The results of our work show clearly that the intermediate field matrices are essential to a quantitative analysis of the Eu IV and Am IV spectra, and that Zeeman studies are needed to identify certain levels.

INTRODUCTION

THE absorption and fluorescence spectra of Eu IV and Am IV have been reported in a number of papers.[1–5] However, a theoretical analysis of the absorption-spectra data (arising from $4f\rightarrow 4f$ transitions) has not been attempted, and only a complete analysis of the ^7F ground term and ^5D term by B. R. Judd[6] has been made from the fluorescence data of

TABLE I. Pure electrostatic energy levels for the $4f^6$ configuration. Assumption: $4f$ hydrogenic radial distribution function. Energy levels in terms of F_2.

Term	Energy	Term	Energy	Term	Energy	Term	Energy	Term	Energy
^7F	0	^1I	114.5	^3H	148.3	^3H	181.7	^3H	250.4
^5D	51.70	^3D	114.6	^5F	148.6	^1L	183.6	^1G	251.4
^5L	57.64	^1N	117.5	^1M	148.7	^1H	185.0	^3G	253.6
^5G	60.69	^3H	118.2	^3D	151.3	^3M	186.7	^1I	257.7
^5H	68.93	^3G	118.9	^1I	151.6	^3L	194.3	^3G	268.3
^5I	78.03	^3M	121.7	^1F	153.4	^3I	198.8	^3P	269.1
^5F	78.89	^3K	121.8	^1G	154.5	^3K	199.3	^1S	269.7
^5K	88.05	^1L	122.6	^1K	155.8	^3P	200.0	^1D	277.2
^3P	88.57	^3I	126.7	^3I	157.6	^1G	202.6	^1L	277.6
^3O	95.37	^1G	126.8	^3K	162.3	^1L	203.4	^1G	277.7
^5G	96.52	^3L	128.2	^3F	163.6	^3G	204.0	^3D	278.7
^3M	97.67	^3H	130.1	^1F	164.5	^1N	208.2	^1F	279.4
^3K	99.56	^1M	130.8	^3H	167.1	^3F	213.4	^3F	300.4
^3D	99.73	^3F	131.2	^1S	168.4	^1F	221.7	^1D	304.4
^3F	101.2	^5S	132.2	^1G	170.1	^1P	222.5	^1G	322.8
^3H	101.4	^3P	132.7	^3P	170.6	^3H	222.8	^1H	325.5
^3I	101.5	^1H	133.2	^1D	171.4	^3D	228.3	^3F	334.3
^5P	104.5	^3I	135.6	^3D	174.9	^1H	233.9	^3P	337.2
^3N	106.7	^3L	136.1	^3G	175.0	^1D	236.4	^1I	337.4
^3G	107.5	^1D	136.7	^5G	177.3	^3I	237.5	^3H	337.9
^5H	110.1	^3F	137.7	^3F	178.6	^3F	241.1	^1G	372.3
^3K	112.6	^1I	142.1	^5D	180.7	^1I	241.3	^1D	395.3
^1S	113.9	^5I	144.4	^1K	180.9	^3K	242.6	^1S	462.2
^1Q	114.1	^3G	145.7	^1I	181.4	^1K	246.5		

[1] H. Gobrecht, Ann. Physik **28**, 673 (1937).
[2] O. Deutschbein, Ann. Physik **36**, 183 (1939).
[3] E. V. Sayre and S. Freed, J. Chem. Phys. **24**, 1211 (1956).
[4] D. M. Gruen, J. G. Conway, R. D. McLaughlin, and B. B. Cunningham, J. Chem. Phys. **24**, 1115 (1956).
[5] B. Stover and J. G. Conway, J. Chem. Phys. **20**, 1490 (1952).
[6] B. R. Judd, Mol. Phys. **2**, 407 (1959).

TABLE II. Pure electrostatic energy levels for the $5f^6$ configuration. Assumption: $5f$ hydrogenic radial distribution function. Energy levels in terms of F_2.

Term	Energy	Term	Energy	Term	Energy	Term	Energy	Term	Energy
^7F	0	^1S	120.2	^5F	150.8	^1L	188.1	^1G	255.1
^5D	54.76	^1I	120.5	^3H	151.7	^1H	189.3	^3G	255.7
^5L	60.04	^3H	122.6	^1M	152.9	^3M	190.4	^1I	261.8
^5G	63.56	^3G	122.9	^3D	154.7	^3L	197.7	^3G	270.9
^5H	71.03	^1N	123.2	^1I	156.4	^3I	202.0	^3P	272.6
^5I	80.21	^3K	125.6	^1F	158.4	^3P	203.8	^1S	273.8
^5F	81.29	^3M	125.7	^1G	159.2	^3K	204.4	^1D	280.7
^5K	90.06	^1L	127.9	^1K	160.7	^1G	206.5	^3D	280.7
^3P	94.53	^3I	130.5	^3I	161.0	^3G	207.6	^1L	281.0
				^3K	166.5				
^5G	98.73	^1G	131.9	^3F	167.3	^1L	207.7	^1G	282.0
^3O	99.50	^3L	132.0	^1F	168.5	^1N	212.4	^1F	282.1
^5D	101.8	^3H	133.8	^3H	170.7	^3F	216.6	^3F	303.8
^3M	102.0	^3F	134.7	^1S	172.6	^1F	225.2	^1D	307.5
^3K	104.0	^5S	135.0	^3P	173.9	^1P	225.6	^1G	326.4
^3I	105.7	^1M	135.3	^1G	174.4	^3H	226.0	^1H	328.3
^3F	105.8	^3P	136.6	^1D	175.4	^3D	231.3	^3F	336.3
^5P	106.1	^1H	137.6	^3G	178.1	^1H	238.1	^3P	338.8
^3H	106.2	^3I	139.6	^3D	178.3	^3I	240.0	^1I	341.2
^3N	110.6	^3L	140.1	^5G	178.7	^1D	240.7	^3H	341.4
^5H	111.8	^3F	141.6	^5D	181.7	^3K	243.5	^1G	374.6
^3G	112.0	^1D	142.4	^3F	181.8	^3F	244.1	^1D	399.1
^3K	115∫8	^1I	147.0	^1K	184.5	^1I	244.8	^1S	467.7
^3D	118.5	^5I	147.0	^3H	185.4	^1K	250.0		
^1Q	119.0	^3G	148.9	^1I	185.4	^3H	253.4		

Sayre and Freed.[3] As a start in analyzing the absorption spectra, we have evaluated the 119 pure electrostatic energy levels for an nf^6 configuration. Tentative theoretical assignments can then be made for Eu IV and Am IV based on several assumptions.

When the calculation of pure electrostatic energy levels for configurations with more than two f electrons is carried out following the methods outlined by Condon and Shortley, we find the work exceedingly tedious and laborious.[7] However, the necessary theory to handle such a problem is available in the papers of Racah who has shown how states of f^n may be classified by group-theoretical methods.[8] Several papers are now available which describe how Racah's theory can be used.[9]

Elliott, Judd, and Runciman have re-evaluated all the pure electrostatic energy levels from f^2 to f^4 and the two lowest multiplicities of the f^5 and f^6 configurations.[9] Also, B. G. Wybourne has calculated the doublet electrostatic energy matrices for f^5 and triplet and singlet matrices for f^6.[10] In this paper, a complete evaluation of the f^6 configuration energy matrices has been made independently by the authors, and actual energy levels in terms of F_2, the Slater radial integral, are presented on the assumption of various Slater F_k ratios.

ELECTROSTATIC ENERGY LEVELS

Three different Slater F_k ratios were used in our calculations. For $4f^6$, the $4f$ hydrogenic radial distribution function yields, $F_4/F_2=0.1381$ and $F_6/F_2=0.01511$; for $5f^6$ the $5f$ hydrogenic radial distribution function yields $F_4/F_2=0.1422$, and $F_6/F_2=0.01610$; and from Cohen's relativistic Hartree-Fock calcula-

[7] E. U. Condon and G. H. Shortley, *The Theory of Atomic Spectra* (Cambridge University Press, Cambridge, England, 1953).

[8] G. Racah, Phys. Rev. **76**, 1352 (1949).

[9] J. P. Elliott, B. R. Judd, and W. A. Runciman, Proc. Roy. Soc. (London) **A240**, 509 (1957).

[10] B. G. Wybourne, Johns Hopkins University, Baltimore, Maryland (private communication, 1960) (to be published).

TABLE III. Pure electrostatic energy levels for the $5f^6$ configuration. Assumption: Slater ratios from Hartree-Fock calculation for the normal uranium atom. Energy levels in terms of F_2.

Term	Energy	Term	Energy	Term	Energy	Term	Energy	Term	Energy
^7F	0	^3H	140.4	^3H	166.3	^1I	205.9	^1K	266.5
^5D	67.21	^3G	140.6	^1I	168.0	^3M	206.9	^3H	266.9
^5L	70.14	^3K	141.2	^3D	169.6	^1L	207.6	^1G	272.6
^5G	72.24	^3M	142.8	^1M	171.4	^1H	208.0	^1I	280.0
^5H	80.01	^1I	144.8	^3I	176.0	^3L	213.1	^3G	283.6
^5I	89.52	^1S	145.5	^1I	176.7	^3I	216.7	^3P	288.5
^5F	91.36	^3I	146.2	^1F	179.0	^3K	217.5	^3D	291.3
^5K	98.83	^1N	147.2	^1G	179.6	^3P	220.5	^1S	292.7
^5G	108.4	^5S	147.6	^3K	180.2	^3G	223.5	^1F	295.1
^5D	111.2	^3L	147.9	^1K	181.9	^1G	223.9	^1D	296.7
^5P	113.4	^3F	149.8	^3F	183.1	^1L	226.7	^1L	296.8
^3O	116.8	^3H	149.9	^5G	185.3	^3F	231.0	^1G	301.3
^3P	118.5	^1L	149.9	^3H	185.7	^1N	231.5	^3F	319.6
^5H	119.4	^3P	152.5	^1F	186.2	^1P	239.8	^1D	322.6
^3M	119.9	^1G	153.1	^5D	187.7	^3H	240.6	^1H	342.0
^3I	123.5	^1M	154.2	^3P	188.2	^1F	240.6	^1G	343.6
^3K	123.5	^1H	156.2	^1S	191.1	^3D	244.7	^3F	347.3
^3F	124.5	^3I	157.3	^3G	192.1	^3I	252.2	^3P	348.5
^3H	125.5	^3L	157.5	^1D	192.6	^1H	256.8	^3H	357.8
^3N	127.0	^3F	158.5	^3D	193.0	^3F	257.7	^1I	359.7
^3G	130.4	^5I	158.7	^1G	193.3	^3I	259.4	^1G	387.6
^3K	131.6	^5F	160.7	^3F	195.8	^1D	259.8	^1D	418.2
^3D	134.6	^3G	162.8	^1K	201.3	^1I	260.6	^1S	494.6
^1Q	139.9	^1D	166.3	^3H	202.0	^3G	266.0		

tion for the normal uranium atom, Marrus *et al.* obtained from an IBM-704 program, $F_4/F_2=0.159$ and $F_6/F_2=0.0204$.[11] The additional assumption is made that the F_k ratios obtained from the Hartree-Fock calculation will not change appreciably in going from the uranium atom with three f electrons to the Am IV, $5f^6$, for example. However, one should expect the probability-density-distribution function to become sharper in going from an atom to the ion, which has only a partly filled f shell of electrons, but the question of whether the F_k ratios will become larger or smaller cannot be answered simply. A Hartree-Fock calculation for a *trans*-uranium ion is sorely needed. Thus, the use of these uranium-atom ratios may be open to error, but at least it will give us some indication of the shift of the pure electrostatic energy-level spectrum as we go from the $4f^6$ to the $5f^6$ configuration.

[11] Richard Marrus, William A. Nierenberg, and Joseph Winocur, "Hyperfine structure of americium-241," UCRL-9207 (May 1960).

The energy matrices are in terms of the parameters E^0, E^1, E^2, and E^3, which Racah has defined as:

$$E^0=F_0-10F_2-33F_4-286F_6 \quad (1)$$

$$E^1=\tfrac{1}{9}[70F_2+231F_4+2002F_6] \quad (2)$$

$$E^2=\tfrac{1}{9}[F_2-3F_4+7F_6] \quad (3)$$

$$E^3=\tfrac{1}{3}[5F_2+6F_4-91F_6]. \quad (4)$$

We can divide Eqs. (1) through (4) by F_2, substitute the proper set of F_k ratios, and obtain numerical secular equations which can be solved by an IBM-650 program.

The theoretical results are given in Tables I, II, and III. Each table gives the configuration considered and the assumption made for that calculation. It should be noted that several numerical errors were found under the f^6 column in Table III of Elliott *et al.*

These errors have been corrected and all other energy levels for nf^6 rechecked.

From Figs. 1–6, which show the electrostatic energy-level spectra, we note the marked change in position of terms as we go from a $4f^6$ configuration to a $5f^6$ configuration. The spectrum on the right is that of a $5f^6$ configuration, based on the uranium atom Hartree-Fock, (H–F), F_k ratios. All spectra are normalized to the ground term, $^7F=0$. In general, as we go from $4f^6$ to $5f^6$, the energy spectrum moves in the direction of greater F_2. In many cases, quintets, triplets, and singlets appear in different order from the ground term.

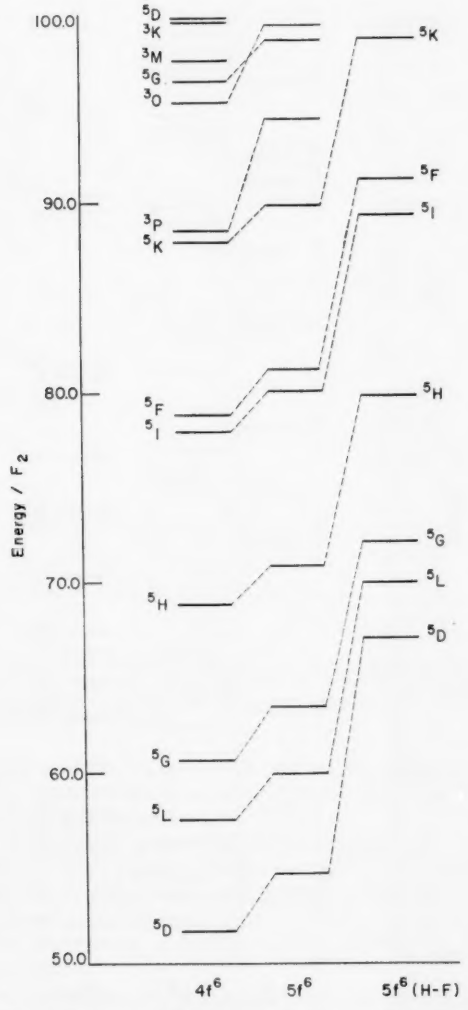

FIG. 1. Pure electrostatic energy level spectra based on the $4f$ and $5f$ hydrogenic F_k ratios, and the $5f$ F_k ratios obtained from a Hartree-Fock calculation for the normal uranium atom. Energy levels are in terms of F_2.

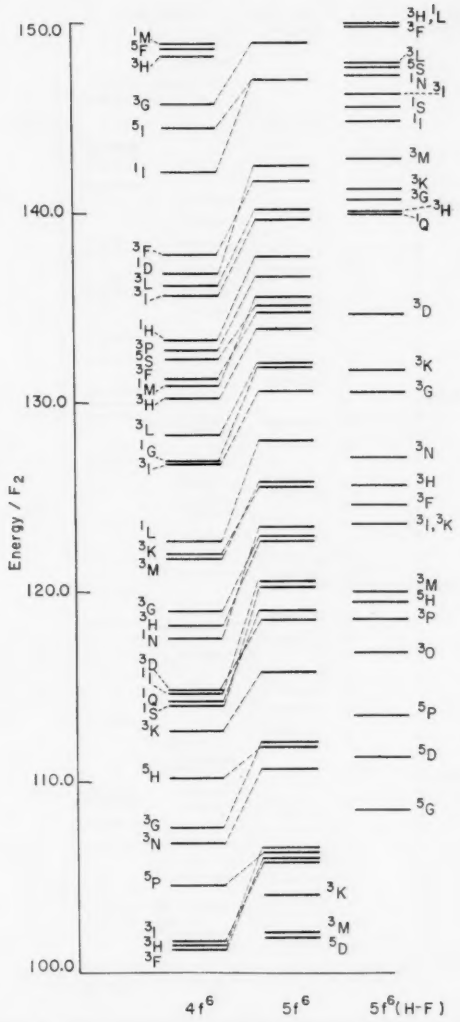

FIG. 2. Pure electrostatic energy level spectra based on the $4f$ and $5f$ hydrogenic F_k ratios, and the $5f$ F_k ratios obtained from a Hartree-Fock calculation for the normal uranium atom. Energy levels are in terms of F_2.

TERM ANALYSIS

There is no question that an intermediate-field calculation of the 301 J levels for f^6 is necessary in order to completely interpret the absorption spectra of Eu IV and Am IV. However, until the intermediate-field matrices are completed, we can use some pieces of experimental and theoretical information now at our disposal to give us at least a tentative term assignment for some of the J levels of Eu IV.

The Sayre and Freed J-level assignments for Eu IV are based on the polarized and axial absorption spectra

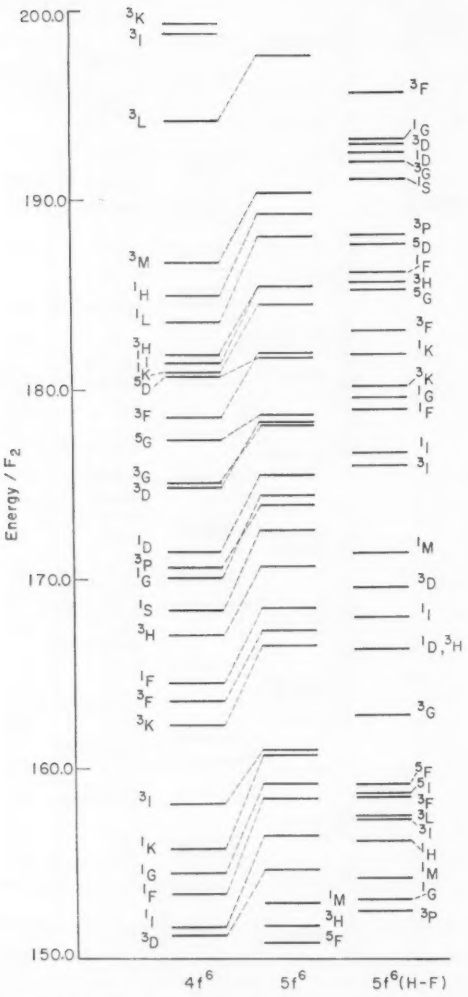

FIG. 3. Pure electrostatic energy level spectra based on the $4f$ and $5f$ hydrogenic F_k ratios, and the $5f$ F_k ratios obtained from a Hartree-Fock calculation for the normal uranium atom. Energy levels are in terms of F_2.

of $Eu(C_2H_5SO_4)_3 \cdot 9H_2O$[9]. Such polarized data, consistent with a given point symmetry, identifies J levels 1, 2, and 3 uniquely and larger J values only indicatively.

We have found the $5f$ hydrogenic ratios to give the best values to the electrostatic energy levels for Eu IV. From a least-squares fit, Wybourne in his analysis of Nd IV, $4f^3$ also obtained Slater ratios close to the $5f$ hydrogenic ratios.[12] If the reasonable values of $\zeta = 1360$ cm^{-1} [13] and $F_2 = 370$ cm^{-1} are used for Eu IV, we obtain an L–S plot of energy levels in units of F_2 which appears in Fig. 7.

It should be pointed out that a term assignment in intermediate field is based on that L–S level which provides the largest eigenvector contribution to a given J level. In Fig. 7, however, for Eu IV we have made the assignments in terms of the parent L–S level since the exact eigenvectors are not known. The goodness of fit in some cases would indicate that the L–S level will probably also be the intermediate level. Several of the theoretical levels have been evaluated according to first-order perturbation theory. Judd has calculated the de-

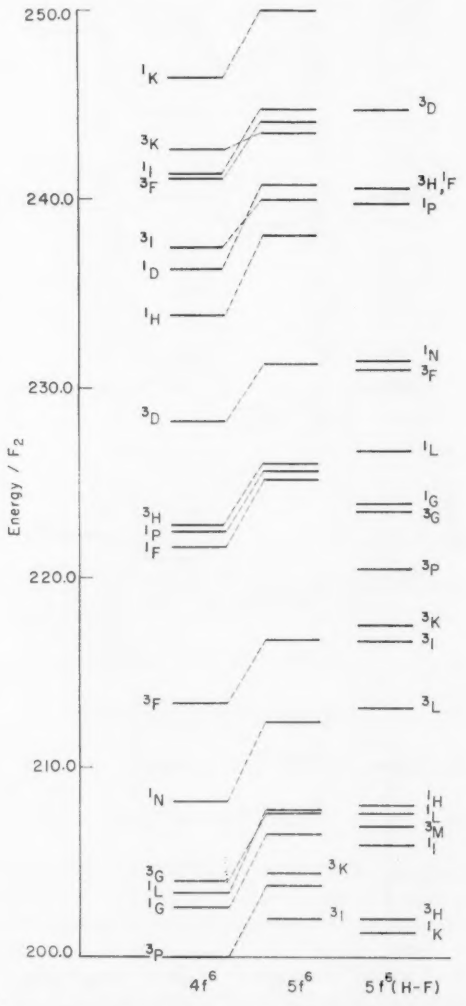

FIG. 4. Pure electrostatic energy level spectra based on the $4f$ and $5f$ hydrogenic F_k ratios, and the $5f$ F_k ratios obtained from a Hartree-Fock calculation for the normal uranium atom. Energy levels are in terms of F_2.

[12] B. G. Wybourne, J. Chem. Phys. **32**, 639 (1960).
[13] B. R. Judd, Proc. Phys. Soc. (London) **A69**, 157 (1956).

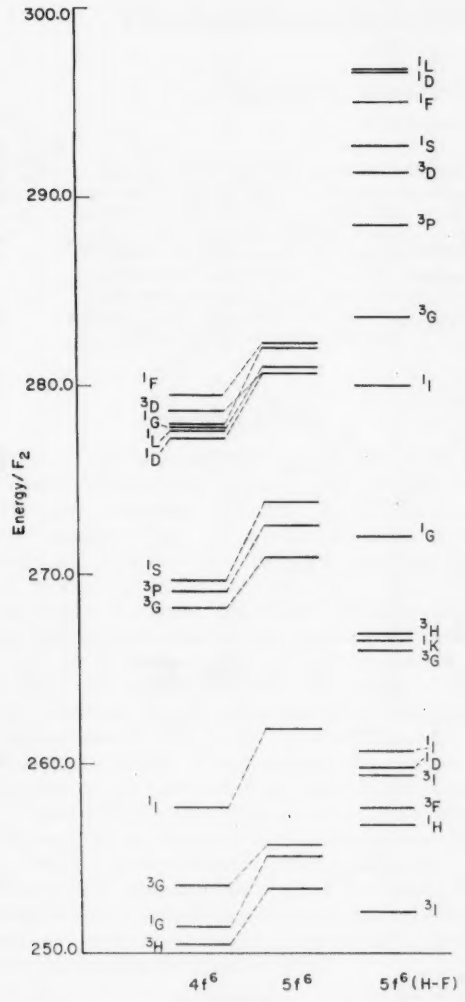

FIG. 5. Pure electrostatic energy level spectra based on the $4f$ and $5f$ hydrogenic F_k ratios, and the $5f$ F_k ratios obtained from a Hartree-Fock calculation for the normal uranium atom. Energy levels are in terms of F_2.

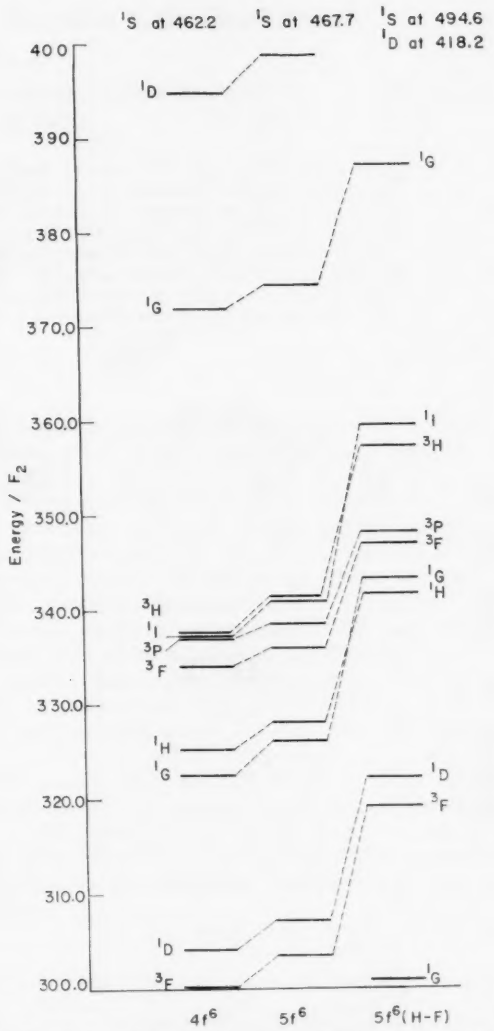

FIG. 6. Pure electrostatic energy level spectra based on the $4f$ and $5f$ hydrogenic F_k ratios, and the $5f$ F_k ratios obtained from a Hartree-Fock calculation for the normal uranium atom. Energy levels are in terms of F_2.

pression of the $^7F_0$ by the $^5D_0$ and obtains 1324 cm^{-1}.[14] This correction has been made to the experimental data of Sayre and Freed.

On the basis of the data and assumptions just considered, we can make a limited number of assignments. The $^5D_{0,1,2}$ which have been studied and identified by various workers agrees fairly well with our plot.[15,16] Also we presume to identify the $^5G_2$, $^5G_3$, $^5F_2$, $^3P_2$, and possibly the $^5H_3$ from the Sayre and Freed data. However, it is impossible to unequivocally identify such levels as the $^5I_{4,5,6,7}$, $^5L_{6,7}$, and $^5H_{4,5,6,7}$ because of the complex absorption spectra pattern. Zeeman experiments must be done on such levels if further analysis is to be made. Complications in the analysis of Eu IV data result from the intermixing of crystal quantum sublevels of different nearby J levels. Also F_k ratios should be determined from the experimental data.

The right-hand side of Fig. 7 represents Am IV energy levels using values of 2600 cm^{-1} for ζ_{nf} and 225 cm^{-1} for F_2. The experimental infrared energy levels

[14] B. R. Judd, Lawrence Radiation Laboratory, Berkeley (private communication, 1960).
[15] K. H. Hellwege, U. Johnsen, H. G. Kahle, and G. Schaack, Z. Physik **148**, 112 (1957).
[16] H. G. Kahle, Z. Physik **155**, 145 (1959).

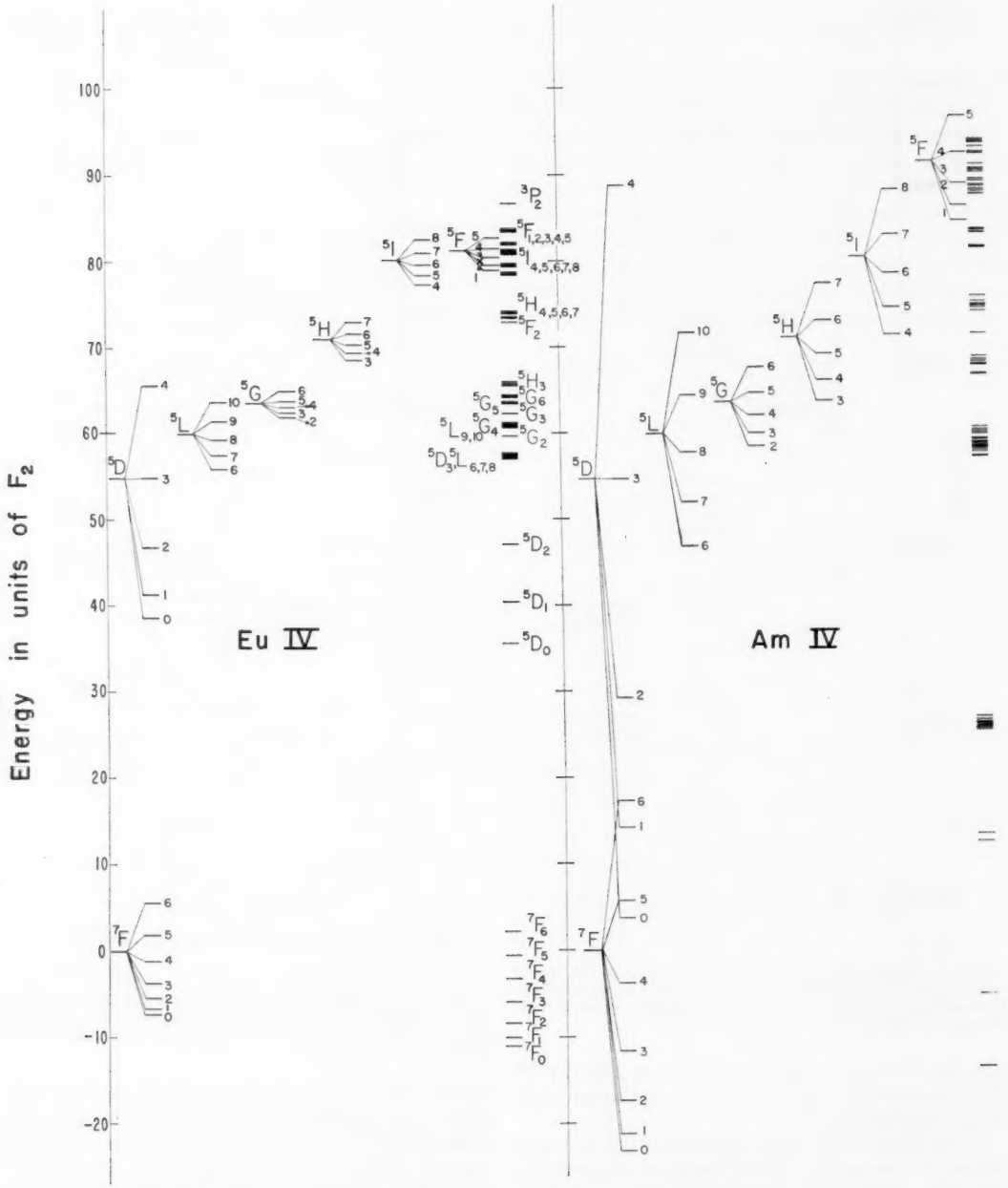

FIG. 7. Comparison of the *L–S* Landé energy levels with experimental levels for Eu IV and Am IV.

are unpublished work of the authors; other levels shown are from Stover and Conway.[5] It is apparent that nothing can be derived from the L–S model even in the ground state of Am IV. However, the polarized absorption spectra of Am IV in $LaCl_3$, which allow experimental identification of the ^7F levels, will be made available shortly for an intermediate field calculation of Am IV energy levels.

Vibrational Relaxation of Carbon Monoxide in the Shock Tube*

D. L. MATTHEWS†

Palmer Physical Laboratory, Princeton University, Princeton, New Jersey

(Received July 20, 1960)

The rate of approach to vibrational equilibrium of suddenly heated CO has been studied using a shock tube and interferometer in the temperature range 2200–4900° K. Care was taken to ensure purity of the gas, so that the effect of impurities could be considered negligible. The measured relaxation times, which ranged nearly exponentially from 50 μsec at 2200° to 2 μsec at 4900°, agree fairly well with the results of Windsor *et al.*, who covered the range 1400°–3000° using a somewhat different method. Both sets of measurements show satisfactory agreement with Landau-Teller theory as refined by Herzfeld *et al.* Separate experiments were performed with CO to which was added about one percent of H_2, N_2, O_2, CO_2, and H_2O, one at a time. CO_2 produced a slight reduction and H_2O a very marked reduction in the relaxation time; the others produced no observable effect.

I. INTRODUCTION

THE use of the shock tube and interferometer to observe microsecond relaxation processes in gases is, by now, a standard technique. As a shock wave passes through a gas, the transitional modes reach equilibrium in two or three collisions, while the rotational modes take about ten times longer. The vibrational modes, however, take about 10^3 times longer again than the rotational, so that rotation and translation are effectively in equilibrium at every moment of the vibrational relaxation process. As energy is taken up by vibration, the gas cools, and the accompanying density increase is observed by the interferometer.

The first reliable measurements on vibrational relaxation in CO were made by Windsor, Davidson, and Taylor (WDT),[1] who recognized the marked effect of H_2O and CO_2 as impurities in reducing the relaxation time. WDT observed infrared emission from the first overtone of the vibration behind a reflected shock. The present study observed density behind an incident shock and worked at higher temperatures, though partly overlapping the range of WDT.

II. THEORY

The theory divides itself into two parts: (A) obtaining a relaxation time from the experimental data, and (B) calculating the relaxation time by considering molecular collisions.

(A) The derivation which follows is not new,[2] but it is given here to show what approximations are involved. The basic rate equation governing relaxation in an internal mode is

$$dE'/dt = -[\tau(T)]^{-1}[E' - E'(T)], \qquad (1)$$

where E' is the energy actually present in the internal mode, $E'(T)$ is the energy which would be in the internal mode if there were thermodynamic equilibrium at the temperature T, and $\tau(T)$ is the relaxation time at translational temperature T. Just behind a shock wave passing through a pure gas, E' (in vibration) is small and subsequently increases at the expense of energy in the remaining "external" modes (translation plus rotation, which are in equilibrium with each other at each point of the relaxation). Let the specific heat at constant pressure (the pressure changes 5% or less in the relaxation zone) be $C = C' + \bar{C}$, where C' is the internal heat capacity and $\bar{C}$ the external. In the present case $\bar{C} = 3.5R$ and is independent of temperature. Then, $dE' = C'dT' = -\bar{C}dT$, where T' is the internal temperature, $\leq T$, associated with E', and the second equality states that the increase in internal energy is supplied entirely from the external modes. Integrating from T to the equilibrium temperature, T_b, one obtains

$$E_b' - E' = -\bar{C}(T_b - T). \qquad (2)$$

On the other hand, $dE'(T) = C'dT$, and

$$E_b' - E'(T) = \bar{C}'(T_b - T), \qquad (3)$$

since $E_b' = E_b'(T)$. Here $\bar{C}'$ is the average value of C' between T and T_b; an arithmetic average suffices because C' does not change rapidly with T. Subtracting Eq. (2) from (3) one obtains $E' - E'(T) = \bar{C}(T_b - T)$, where $\bar{C}$ is the average value of C between T and T_b. Substituting this and $dE' = \bar{C}dT$ in Eq. (1), one obtains the final result

$$d[\ln(T - T_b)]/dt = -\bar{C}/(\bar{C}\tau), \qquad (4)$$

where τ is the relaxation time at temperature T.

(B) The theory of vibrational relaxation to be used here is due to Schwartz and Herzfeld[3] who elaborated

* Most of this work was supported by the Office of Naval Research. It was completed at Carleton University, Ottawa, Canada.

† Now at Radio Physics Laboratory, Defence Research Telecommunications Establishment, Shirley Bay, Ottawa, Canada.

[1] M. W. Windsor, N. Davidson, and R. L. Taylor, Seventh Symposium (International) on Combustion (Butterworths Scientific Publications, Ltd., London, 1959), p. 80.

[2] K. F. Herzfeld and T. A. Litovitz, *Absorption and Dispersion of Ultrasonic Waves* (Academic Press, Inc., New York, 1959).

[3] R. N. Schwartz and K. F. Herzfeld, J. Chem. Phys. **22**, 767 (1954).

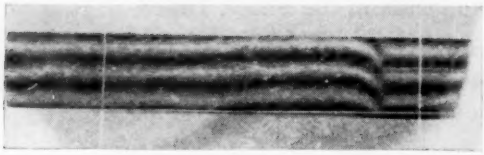

FIG. 1. Vibrational relaxation behind a shock in CO moving to the right. Upward fringe shift means increasing density. Approximate mean temperature and pressure in the relaxation zone: 3200°K and 2 atm. Approximately twice actual size (channel height $\frac{1}{4}$ in.). The horizontal boundaries to the fringes are the top and bottom of the channel.

on a method originated by Landau and Teller.[4] This theory is presented in complete detail, with certain modifications and corrections from the original paper, in the book by Herzfeld and Litovitz,[2] together with a comparison with experimental data and a complete discussion of the assumptions and limitations. The formula for the relaxation time (Herzfeld and Litovitz,[2] p. 299) is

$$\tau = Z\tau_c = 2.0\times10^{-15}(r_0/r_c)^2 T^{2/3}[1-\exp(-\theta/T)]^{-1} \times \exp[\tfrac{3}{2}(\theta'/T)^{\frac{1}{3}} - (\tfrac{1}{2}\theta+\epsilon/k)\,T^{-1}],$$

in which all temperature-independent quantities have been included in the initial constant. The quantities r_0 and ϵ are the parameters in the Lennard-Jones intermolecular potential $4\epsilon[(r_0/r)^{12}-(r_0/r)^6]$, while r_c, which depends on the Kelvin temperature T, is the intermolecular distance at the turning point in a collision. In this calculation $r_0=3.590$ A, $\epsilon/k=110$°K.[5] These are the values usually employed; the use of other pairs of Lennard-Jones parameters only changes the resulting τ by 20 or 30%. The characteristic vibrational temperature $h\nu/k$, 3080°K for CO, is represented by θ, while $\theta'=0.815M\theta^2l^2$. Here M is the reduced molecular weight, 14 for CO, and l represents the effective range of the repulsive intermolecular force. This range is weakly dependent on the temperature and the particular intermolecular potential. Using method B of Herzfeld and Litovitz,[6] which they prefer as yielding slightly better over-all agreement with experiment, l is found to be 0.192–0.194 A over the whole range 1500–5000°K. The time between collisions for a single particle τ_c is given by $7.76\times10^{-7}\eta$, where η is the viscosity; thus one can calculate Z, the number of collisions per particle per vibrational transition. The initial numerical factor in the expression for τ includes a steric factor 5.9 as calculated by the method of the work cited in footnote 2, Sect. 64, in which rotational transitions during the collision are taken into account. The $T^{2/3}$ term includes the usual $T^{\frac{1}{2}}$ dependence of the collision frequency.

The theory involves several approximations, especially in the assumption that the collision partner is an atom rather than a molecule. Also, the relaxation time obtained is extremely sensitive to the form of the intermolecular potential. In view of all this, the agreement of the theory, which contains no adjustable parameters, with experiment has been remarkable,[7] especially at higher temperatures where it is within a factor of 4 for O_2, N_2, CO_2, N_2O, COS, CS_2, and (as will be seen) CO, and within a factor of 12 for Cl_2. There is a definite need for more accurate calculations. There are other theoretical approaches,[8,9] but they have so far been applied only to homonuclear molecules.

If one assumes a harmonic oscillator, the transition probability for deactivation from the first excited state to the ground state is given by

$$(k_{10})^{-1}=\tau[1-\exp(-\theta/T)];$$

the factor in brackets is about 0.5 at 4500° and 0.9 at 1500°.

III. EXPERIMENTAL TECHNIQUE

The shock tube and interferometer used in this study have been described previously.[10] They have been improved by reducing the leak rate to less than 10μ per hour and by making the density measurements more accurate. The latter was accomplished by using a Baird-Atomic interference filter of about 50-A bandwidth centered at 3742 A. At this wavelength the refractive index, by interpolation in Koch's[11] data, is 1.0003483 at 0°C and 760 mm. The geometrical path length in the gas was 1.372 in. The combined inaccuracies in these data do not exceed two parts in 10^3, or about five times better than the accuracy of reading the fringe position (about 1/30 fringe in a shift of four fringes).

The driver gas for the shock was helium or a mixture of half helium and half hydrogen by volume at pressures of a few thousand cm Hg; the CO was initially at a pressure of one or two cm Hg. Shock Mach numbers of 5.5 to 9.5 were used. The shock tube converged from a vertical dimension of 3.2 in. to $\frac{1}{4}$ in. about 2 ft before the windows (rather than $\frac{3}{4}$ in. as in the work cited in footnote 10).

As the shock wave passed the windows, a spark of about 0.1-μsec duration was fired, producing an interferometric "snapshot" as shown in Fig. 1. A picture was also taken of the fringes before arrival of the shock. Thin-film resistance thermometers separated by a known distance were used in conjunction with a suitable chronograph to measure the velocity of the shock

[4] L. Landau and E. Teller, Physik. Z. Sowjetunion **11**, 18 (1936).

[5] J. O. Hirschfelder, C. F. Curtiss, and R. B. Bird, *Molecular Theory of Gases and Liquids* (John Wiley & Sons, Inc., New York, 1954), p. 1111.

[6] See work cited in footnote 2, p. 281.

[7] See work cited in footnote 2, pp. 325–328.

[8] Morris Salkoff and Ernest Bauer, J. Chem. Phys. **30**, 1614 (1959).

[9] J. G. Parker, Phys. Fluids **2**, 449 (1959).

[10] D. L. Matthews, Phys. Fluids **2**, 170 (1959); Ph.D. thesis, Princeton University, Princeton, New Jersey, 1958.

[11] John Koch, Arkiv Mat. Astron. Fysik **10**, No. 1 (1914).

to better than 1%. The initial pressure and temperature of the CO were measured to about 0.5% in p_1 and 0.1% in T. The important question of purity is discussed in Sect. V.

IV. INTERPRETATION OF DATA

If the temperature were constant or the relaxation rate independent of temperature, the approach of T to equilibrium would be strictly exponential, according to Eq. (4). Actually, neither of these conditions holds, so that plotting $\ln(T-T_b)$ against distance behind the shock (distance being proportional to time) is not expected to produce a straight line. The graph is very nearly linear, however, at the lower temperatures, where the temperature change in the relaxation zone is small, and even at the highest temperatures the slope does not change by more than a factor of two in the relaxation zone. Figure 2 shows a typical situation. The density is computed from the observed fringe shift; $1/\rho$ is proportional to T within the pressure change during relaxation, which does not exceed 5%, so that the ordinate is effectively $\ln(T-T_b)$, as in Eq. (4). The curvature is seen to be in the right direction. By taking the slope of this curve at, say, its midpoint, the relaxation time is calculated from the formula

$$\tau = t(\bar{C}/\bar{C})(\rho/\rho_1)(p/p_1)p_1/(760d \times \text{slope}).$$

Here, t is the time required for the shock to travel the measured distance d, and ρ/ρ_1 and p/p_1 are the density and pressure ratios, across the shock, associated with the point in the relaxation for which the slope (in cm) was taken. The pressure before the arrival of the shock

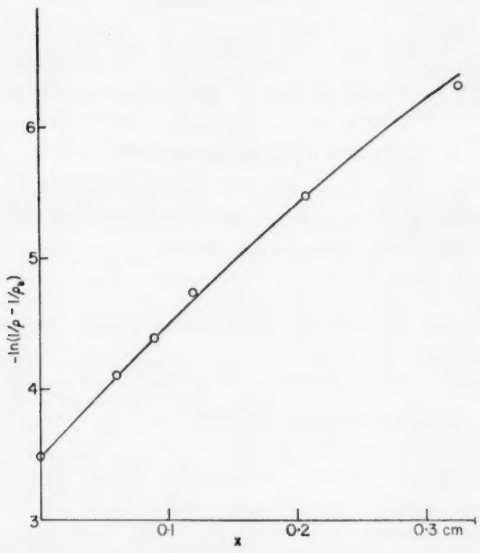

FIG. 2. A typical relaxation process: effectively ln (actual translational temperature minus equilibrium temperature) is plotted as a function of distance behind the shock. $\tau = 6.4$ μsec.

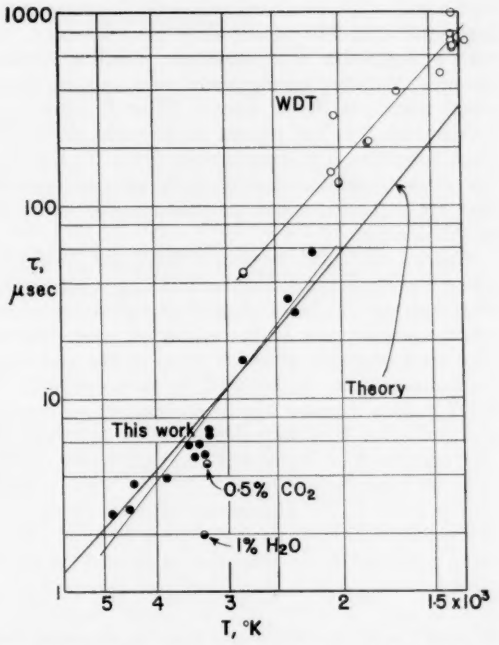

FIG. 3. Vibrational relaxation time at atmospheric pressure as a function of T (horizontal scale $\propto T^{-\frac{1}{3}}$), experimental and theoretical. Least-squares straight lines have been fitted to the two sets of experimental data.

is p_1 mm Hg. One writes p in the form $(p/p_1)p_1$ because p_1 and p/p_1 rather than p itself are known.[12] The factor $\bar{C}/\bar{C}$ has already been explained; the factor ρ/ρ_1 converts shock speed to particle speed (by mass conservation); and $p/760$ converts the observed relaxation time to that at one atmosphere pressure. The relaxation time obtained from this expression is associated with the (translational) temperature at the point in the relaxation process where the slope was measured.

The equilibrium state of shock-excited CO has been calculated by Griffith and Kenny[12] as a function of Mach number. Since the Mach number and the density ratio were measured independently in these experiments, these calculations provide a valuable check of experimental consistency in those photographs in which the whole relaxation zone is visible. In spite of a slight falloff in density after the relaxation zone, such as appears in Fig. 1, the directly observed maximum density ratio always agrees to better than 2% with that calculated. Where the relaxation evidently continues beyond the boundary of the picture, the graph as in Fig. 2 is observed to be quite straight as expected, which indicates that any disturbances are relatively unimportant.

According to the theory, it can be seen that a plot of $\log\tau$ against $T^{-\frac{1}{3}}$ should be nearly linear. Figure 3 is

[12] Wayland C. Griffith and Anne Kenny, Tech. Rept. II-23, Department of Physics, Princeton University, Princeton, New Jersey, 1957.

such a plot with the actual values of T shown on the horizontal axis. The results show good linearity, but with a suggestion of a curvature which is concave upwards. Widom[13] has suggested that data on vibrational relaxation should have a $T^{\frac{1}{3}}$ or T dependence rather than $T^{-\frac{1}{3}}$. The present data would show even more curvature if plotted against $T^{\frac{1}{3}}$ or T, but it is the author's opinion that no data are yet available that are accurate enough to give a useful indication on this question.

Figure 3 also shows the data of WDT and the theory. The relaxation times quoted by WDT have been multiplied here by $\tilde{C}/\bar{C}$ and plotted as a function of the average temperature in the relaxation zone, whereas they were originally given in terms of the unrelaxed temperature. The factor $\tilde{C}/\bar{C}$ is necessary even in WDT's data because the concentration of excited particles which they measured increases with time not only because of excitation but also because the density increases, making the excitation rate appear faster than it really is. The discrepancy between the two sets of points is probably little greater than the experimental error. Considering the differences in method the agreement is satisfactory. It should be noted that each set of data is most accurate towards lower temperatures, because τ is there much longer than the resolving time of the apparatus; also, because in the author's data there is none of the curvature of Fig. 2 at the lowest temperatures, so there is no question as to what the slope is. There is no curvature because there is not enough temperature change in the relaxation zone to cause much change in τ.

V. PURITY

Matheson assayed reagent-grade CO was used, stated to contain 0.05 mole % H_2, 0.26M CO_2, and $<0.002\%$ N_2. The CO was admitted to the shock tube through several feet of copper refrigeration tubing immersed in liquid nitrogen, which arrangement presumably removed the CO_2 impurity. The shock tube was usually fired about 5 min after filling, by which time it would have leaked about 1μ. The leak rate of the shock tube was much the same over periods of minutes or days, so that the leak was mostly real rather than virtual. Since the usual pressure of CO was 10 to 20 mm before arrival of the shock, the total impurity level can have been only 0.01% higher than that of the original (CO_2 free) gas, and it is most unlikely that even this 1 part in 10 000 consisted entirely of H_2O, the only impurity known to have a very large effect. The effect of 0.5% of added CO_2 and of roughly 1% of H_2O are shown in Fig. 3 as well. As one would expect, these effects at 3300° are considerably less than found by WDT at 1400°. It is questionable whether the CO_2 had any effect at all at 3300°. The effect of H_2O is thought to be due to near-resonant transfer of vibrational energy between CO and H_2O molecules, and a calculation on this hypothesis[14] agrees with the observations to half an order of magnitude, or within the experimental and theoretical uncertainties. More experiments are needed on this type of impurity effect. The addition of $\frac{1}{2}$ to 1% of O_2, H_2, and N_2 at about 3300° produced no noticeable effect, nor did allowing the shock tube to leak for one hour before firing, or omitting the liquid nitrogen trap for the CO, or using C.P. rather than reagent-grade CO. The points with these various impurities or possible impurities are not distinguished in the figure from those using the purest gas (except, of course, the two with added CO_2 and H_2O). The H_2O impurity due to leaks, already discussed, could hardly have exceeded 1 part in 20 000, and its effect is considered negligible. The effect of CO_2 may also be neglected since the omission of the cold trap had no effect, and the addition of CO_2 little or none.

VI. CONCLUSION

This study and that of WDT provide values of the vibrational relaxation time in CO in the range 1400–4900°K, considered reliable within a factor of 2. Any error remaining is unlikely to be due to impurity.

VII. ACKNOWLEDGMENT

R. L. Taylor has given the author valuable help in clarifying the foregoing discussion of the work of WDT.

[13] B. Widom, J. Chem. Phys. **27**, 940 (1957).

[14] R. L. Taylor (private communication).

THE JOURNAL OF CHEMICAL PHYSICS VOLUME 34, NUMBER 2 FEBRUARY, 1961

On the Nature of the Crystal Field Approximation*

C. M. HERZFELD AND H. GOLDBERG† ‡

U. S. National Bureau of Standards and Physics Department, University of Maryland, College Park, Maryland

(Received August 12, 1960)

A new method is developed for the treatment of molecular interactions, and is applied to a system consisting of a hydrogen atom in a $2p$ state and a hydrogen molecule in the ground state. The interaction of these two species is calculated using ordinary crystal field theory and also the new method. A comparison of the results shows some of the shortcomings of the conventional crystal field theory, and provides corrections to it. The new method consists of (1) expanding all electron terms of the total Hamiltonian for the system which involve interactions between the atom and the molecule, thus transforming the interaction Hamiltonian into sums of products of one-electron operators, and (2) of using properly antisymmetrized wave functions made up of products of atom and molecule eigenfunctions. The calculations show the effect of the neglect of overlap and exchange in ordinary crystal field theory.

1. INTRODUCTION

CRYSTAL field theory and its extension ligand field theory, have been extraordinarily useful tools in the analysis of the magnetic and optical properties of solids.[1] Only in recent years, however, have its foundations been examined critically. The theory has several obvious shortcomings: It is a blend of classical electrostatic theory of solids and quantum mechanics. The perturbation on the reference ion ("Auf-Ion", in Bethe[2]) is calculated classically, and its effect on the reference ion is calculated quantum mechanically. Therefore the theory neglects the overlap of electron charge distributions, and it neglects the Pauli exclusion principle by ignoring the exchange of the electrons of the reference ion with the electrons of the neighbors of the reference ion. Furthermore, in the usual calculation of the parameters of the theory from an electrostatic model, the potential is expanded in a Taylor's series in a nonrigorous manner, because the expansion is limited to the region where the electrons of the reference ion are interior to the charge distribution formed by the neighbors of the reference ion.

In recent years these questions of the foundations of crystal field theory have received considerable attention. Kleiner[3] has made a careful calculation of a crystal field parameter, using the conventional theory and good ion wave functions. His results were disappointing. Later Tanabe and Sugano[4] obtained more satisfactory results in a calculation of a crystal field parameter, based on molecular orbitals for the complex consisting of the reference ion and its nearest neighbors. Phillips[5] has pointed out that the point charge model of ordinary crystal field theory gives in fact a good estimate of the crystal field parameters. Quite recently, Jarrett[6] has shown how to include exchange in crystal field theory. Finally, Koster[7] has explained that crystal field theory is "nothing but" an application of a generalization of the Wigner-Eckart theorem.

The present paper represents an effort to show explicitly the effect of some of the approximations used in crystal field theory. This is done by treating a simple system explicitly, using a modified molecular orbital technique. The system treated here consists of a hydrogen atom in the $2p$ state and a hydrogen molecule in its ground state. We thus deal with a three-electron problem. The interaction of these two species is treated in two ways: First, with an extension of ordinary crystal field theory which has proved useful in the study of the spectra of trapped atoms,[8] then with our modified MO technique. The two results are compared.

The modified MO technique used by us appears to be new in some respects and may be generally useful for the study of atomic and molecular interactions. Much of the present paper is devoted to describing it. The basic idea of the method is this. The total Hamiltonian for the 3 electrons and 3 nuclei of the system is written down. Then the two-electron terms in the Hamiltonian which describe the interactions between electrons from the atom and electrons from the molecule, and the one-electron terms describing interactions of the electrons of one species with the nuclei of the others species, are expanded in a Taylor's series, assuming that the charge distributions of atom and molecule do not overlap. This exhibits the two-electron operators as sums of products of one-electron operators and simplifies the one-electron operators mentioned. A wave function which is a product of an eigenfunction

* This research was supported by the Free Radical Research Program at the National Bureau of Standards, under contract with the Department of the Army.

† Based in part on a thesis submitted to the University of Maryland in partial fulfillment of the requirements for the degree of Doctor of Philosophy in Physics.

‡ Present address: Department of Physics, University of Buffalo, Buffalo, New York

[1] W. Low, *Paramagnetic Resonance in Solids* (Academic Press, Inc., New York, 1960); W. Moffitt and C. J. Ballhausen, Ann. Rev. Phys. Chem. **7**, 107 (1956).

[2] H. A. Bethe, Ann. Physik **3**, 133 (1929).

[3] W. H. Kleiner, J. Chem. Phys. **20**, 1784 (1952).

[4] Y. Tanabe and S. Sugano, J. Phys. Soc. Japan **11**, 864 (1956).

[5] J. C. Phillips, J. Phys. Chem. Solids **11**, 226 (1959).

[6] H. S. Jarrett, J. Chem. Phys. **31**, 1579 (1959).

[7] G. F. Koster, Phys. Rev. **109**, 227 (1958).

[8] C. M. Herzfeld, Phys. Rev. **107**, 1239 (1957); H. Goldberg and C. M. Herzfeld, Bull. Am. Phys. Soc. II, **3**, 180 (1958).

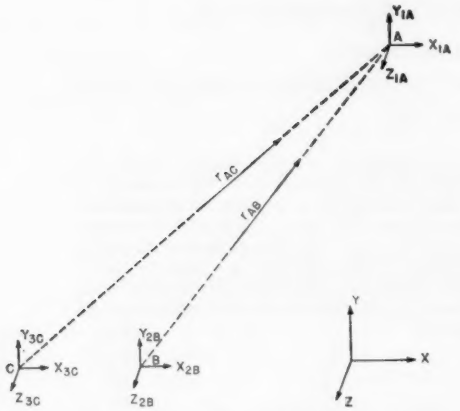

FIG. 1. The system $H-H_2$. The nucleus of the hydrogen atom is located at A.

for the free atom and a molecular orbital wave function for the free molecule, and which is properly antisymmetric under the exchange of any pair of electrons, is used to calculate the matrix elements of the expanded Hamiltonian. We suggest the obvious designation EH–SA–MO (Expanded Hamiltonian-Separated Atom-Molecular Orbital) method. The fundamental result is the following: The eigenvalues of the expanded Hamiltonian contain three types of terms. First, the eigenvalues of the free atom and molecule. Second, terms which are analogous to those obtained in conventional crystal field theory. Third, terms which involve the overlap and exchange, and which are, therefore, correction terms to the crystal field result. In this paper we concentrate on the formal results alone, because of the considerable complexities of the formal calculation. We will leave a discussion of numerical results for a later publication. Also, because of the complexities of the formal calculation, we present here only the chief results. Details of certain calculations, as well as certain special results are published elsewhere.[9]

2. THE HAMILTONIAN

The total Hamiltonian of the system consisting of a hydrogen atom and a hydrogen molecule at rest can be written as follows,

$$\mathbf{H}=\mathbf{H}_A+\mathbf{H}_M+\mathbf{H}_I, \tag{2.1}$$

where

$$\mathbf{H}_A=-(\hbar^2/2m)\nabla_1^2-e^2/r_{1A}$$

$$\mathbf{H}_M=-(\hbar^2/2m)(\nabla_2^2+\nabla_3^2)-e^2/r_{2B}-e^2/r_{2C}-e^2/r_{3B}-e^2/r_{3C}+e^2/r_{BC}+e^2/r_{23}$$

$$\mathbf{H}_I=-e^2/r_{2A}-e^2/r_{3A}-e^2/r_{1B}-e^2/r_{1C}+e^2/r_{12}+e^2/r_{13}+e^2/r_{AB}+e^2/r_{AC}. \tag{2.2}$$

[9] H. Goldberg and C. M. Herzfeld, NBS Technical Note 67, October 1960.

Here we label the nucleus of the atom with A and the nuclei of the molecule with B and C. The coordinates are defined in Fig. 1. For the present treatment we assume that all nuclear coordinates remain fixed, hence all terms which depend only on these are parameters of the problem.

It is convenient for our treatment to transform all electron coordinates in the following manner: The coordinates of electron 1 are referred to nucleus A, those of electron 2 to nucleus B, and those of electron 3 to nucleus C. These transformations are formally quite trivial. A typical example is

$$x_{1B}=x_{AB}+x_{1A}$$

$$y_{1B}=y_{AB}+y_{1A}$$

$$z_{1B}=z_{1A}. \tag{2.3}$$

For the other relations used, see Sec. II.3 of the work cited in footnote 9.

$\mathbf{H}_I$ is now expanded in a Taylor's series about nucleus A. This expansion is the most crucial part of the present analysis. We carry out the expansion by assuming that the charge distributions of the atom and the molecule do not overlap. This assumption is also used in ordinary crystal field theory. It is convenient and gives a simple result. The assumption is, of course, not realistic, and furthermore, it is inconsistent with the wave functions we use, which do overlap. This inconsistency also exists in ordinary crystal field theory. It can, of course, be removed by a proper treatment of the various regions of convergence, but the ensuing complications of a rigorous treatment are not worthwhile at present. At any rate, this feature of our method of analysis is *no worse* than conventional crystal field theory. The expansion of $\mathbf{H}_I$ is carried out in standard manner.[10] The basic assumption of nonoverlap of charge distributions limits the expansion to the regions, where

$$r_{1A}<r_{AB}-r_{2B}$$

$$r_{1A}<r_{AC}-r_{3C}. \tag{2.4}$$

Consider now r_{1B}^{-1}, for example. It can be written, using the transformations of Eq. (2.3), as

$$r_{1B}^{-1}=r_{AB}^{-1}[1+r_{1A}^2r_{AB}^{-2}+2(x_{1A}x_{AB}+y_{1A}y_{AB})r_{AB}^{-2}]^{-\frac{1}{2}}.$$

We invoke the conditions of Eq. (2.4), and expand the term in parentheses in a power series in

$$[r_{1A}^2+2(x_{1A}x_{AB}+y_{1A}y_{AB})]r_{AB}^{-2}.$$

Similarly, we expand r_{1C}^{-1}, r_{2A}^{-1}, r_{3A}^{-1}, r_{12}^{-1}, and r_{13}^{-1} of Eq. 2.2. The results are displayed in Table I. For the sake of clarity we will group terms in $\mathbf{H}_I$ by their order in this expansion, and collect, within each order the terms in a given degree in the electron coordinates r_{1A} measured from A. The terms of zero and first order in

[10] J. O. Hirschfelder, C. F. Curtiss, and R. B. Bird, *Molecular Theory of Gases and Liquids* (John Wiley & Sons, Inc., New York, 1954), Chap. 12.

the expansion vanish identically. The second-order terms contain the $\mathbf{r}_{1A}$ only in first degree. Hence they contribute in crystal field theory only via configuration interaction.[8] The contribution of higher order terms will be discussed in detail in Sec. 3.

It is an important result that all terms in the expanded form of $\mathbf{H}_I$ are one-electron operators, except the purely nuclear terms, which are parameters depending on the geometry only. This result seems to have general usefulness for the discussion of certain problems, because it eliminates from the start the necessity to consider complicated integrals over the coordinates of several electrons. The general expanded form of $\mathbf{H}_I$ is the following,

$$\mathbf{H}_I=\sum_{k,l,m} H_A{}^{kl}(H_B{}^{ml}+H_C{}^{ml}), \qquad (2.5)$$

where $H_A{}^{kl}$ is the lth term of a homogeneous polynomial of kth degree in $\mathbf{r}_{1A}$, $H_B{}^{ml}$ and $H_C{}^{ml}$ are the lth terms of homogeneous polynomials of mth degree in $\mathbf{r}_{2B}$ and $\mathbf{r}_{3C}$, respectively. Clearly, $k+m$ is the order of the lth term in the expansion of $\mathbf{H}_I$.

The details of the terms in Eq. (2.5) depend entirely on the nuclear configuration. In the present paper, and in reference 9, we treat two special configurations in detail. These configurations are (1) the T model, where the atom nucleus lies on the perpendicular bisectrix of the molecule axis, and (2) the linear model, where all three nuclei lie on a line. All detailed comparisons between the EH–SA–MO treatment and the crystal field treatment are limited to these two special cases. The explicit form of the expanded $\mathbf{H}_I$ for these two models is quite complicated. It is displayed in full in Appendix B of the work cited in footnote 9.

The interaction Hamiltonian can be written explicitly for the two special configurations which we treat.

The Hamiltonian for the T model can be written as follows,

$$\mathbf{H}_I=\sum_{k,r}\alpha_k{}^r P_k{}^{\pm}\mathbf{r}_A+\sum_{k,l,r,s}(\alpha_{kl}{}^{rs}Q_{kl}{}^{\pm}\mathbf{r}_A+\alpha_k{}^{rs}P_k{}^{\pm}\mathbf{r}_A s_A)$$
$$+\sum_{k,l,m,r,s,t}(\alpha_k{}^{rst}P_k{}^{\pm}\mathbf{r}_A s_A l_A+\alpha_{kl}{}^{rs}Q_{kl}{}^{\pm}\mathbf{r}_A s_A+\alpha_{klm}{}^{r}T_{klm}\mathbf{r}_A)$$
$$+\cdots. \qquad (2.6)$$

In this equation the symbols $\mathbf{r}_A$, s_A, and l_A stand for coordinates measured from atom A. Each can take on independently the values x_A, y_A, and z_A. The symbols P_k, Q_{kl}, and T_{klm} stand for the following functions of coordinates measured from the molecule nuclei,

$$P_k{}^{\pm}=k_B\pm k_C, \qquad Q_{kl}{}^{\pm}=k_B l_B\pm k_C l_C,$$

and

$$T_{klm}{}^{\pm}=k_B l_B m_B\pm k_C l_C m_C,$$

where k, l, and m can take on independently the values x, y, and z. When no sign is written as superscript, the $+$ sign will be understood to be present. The symbols α are constant parameters which depend only on the nuclear coordinates. Their explicit form must be obtained from Appendix B of the work cited in footnote 9. A factor of e^2, common to all terms on the right side, has been omitted from Eq. (2.6).

TABLE I. Expansion of $H_I(1, 2, 3)$.

Second-Order terms:

$$(\mathbf{r}_{1A}\cdot\mathbf{r}_{2B})r_{AB}{}^{-3}+(\mathbf{r}_{1A}\cdot\mathbf{r}_{3C})r_{AC}{}^{-3}-3V_{1A}V_{2B}r_{AB}{}^{-1}-3U_{1A}U_{3C}r_{AC}{}^{-1}$$

Third-Order terms:

$$3/2\left\{\begin{matrix} r_{AB}{}^{-3}[V_{1A}r_{2B}{}^2-V_{2B}r_{1A}{}^2-2(V_{1A}-V_{2B})\mathbf{r}_{1A}\cdot\mathbf{r}_{2B}] \\ +r_{AC}{}^{-3}[U_{1A}r_{3C}{}^2-U_{3C}r_{1A}{}^2-2(U_{1A}-U_{3C})\mathbf{r}_{1A}\cdot\mathbf{r}_{3C}]\end{matrix}\right\}$$
$$+15/2[r_{AB}{}^{-1}V_{1A}V_{2B}(V_{1A}-V_{2B})+r_{AC}{}^{-1}U_{1A}U_{3C}(U_{1A}-U_{3C})].$$

Fourth-order terms:

$$-3/4\left\{\begin{matrix} r_{AB}{}^{-5}[2\mathbf{r}_{1A}\cdot\mathbf{r}_{2B}(r_{1A}{}^2+r_{2B}{}^2-\mathbf{r}_{1A}\cdot\mathbf{r}_{2B})-r_{1A}{}^2r_{2B}{}^2] \\ r_{AC}{}^{-5}[2\mathbf{r}_{1A}\cdot\mathbf{r}_{3C}(r_{1A}{}^2+r_{3C}{}^2-\mathbf{r}_{1A}\cdot\mathbf{r}_{3C})-r_{1A}{}^2r_{3C}{}^2]\end{matrix}\right\}$$

$$+15/4\left\{\begin{matrix} r_{AB}{}^{-3}[2\mathbf{r}_{1A}\cdot\mathbf{r}_{2B}(V_{1A}-V_{2B})^2 \\ \quad +r_{1A}{}^2V_{2B}(2V_{1A}-V_{2B})+r_{2B}{}^2V_{1A}(2V_{2B}-V_{1A})] \\ +r_{AC}{}^{-3}[2\mathbf{r}_{1A}\cdot\mathbf{r}_{3C}(U_{1A}-U_{3C})^2 \\ \quad +r_{1A}{}^2U_{3C}(2U_{1A}-U_{3C})+r_{3C}{}^2U_{1A}(2U_{3C}-U_{1A})]\end{matrix}\right\}$$

$$-35/4\left\{\begin{matrix} r_{AB}{}^{-1}V_{1A}V_{2B}(2V_{1A}{}^2-3V_{1A}V_{2B}+2V_{2B}{}^2) \\ +r_{AC}{}^{-1}U_{1A}U_{3C}(2U_{1A}{}^2-3U_{1A}U_{3C}+2U_{3C}{}^2)\end{matrix}\right\}.$$

$\alpha=x_{AB}r_{AB}{}^{-2}$	$V_{1A}=\alpha x_{1A}+\beta y_{1A}$
$\beta=y_{AB}r_{AB}{}^{-2}$	$V_{2B}=\alpha x_{2B}+\beta y_{2B}$
$\gamma=x_{AC}r_{AC}{}^{-2}$	$U_{3C}=\gamma x_{3C}+\delta y_{3C}$
$\delta=y_{AC}r_{AC}{}^{-2}$	$U_{1A}=\gamma x_{1A}+\delta y_{1A}$
$u=x_{1A}r_{1A}{}^{-2}$	$W_{AB}=x_{AB}u+y_{AC}v$
$v=y_{1A}r_{1A}{}^{-2}$	$W_{AC}=x_{AC}u+y_{AC}v$
	$W_{2B}=x_{2B}u+y_{2B}v$
	$W_{3C}=x_{3C}u+y_{3C}v$

The linear model Hamiltonian can be written

$$\mathbf{H}_I=\sum_{P,k,r}(\alpha_{Pk}{}^r k_P\mathbf{r}_A)+\sum_{P,k,l,r,s}(\alpha_{Pkl}{}^r k_P l_P\mathbf{r}_A+\alpha_{Pk}{}^{rs}k_P\mathbf{r}_A s_A)$$
$$+\sum_{P,k,l,m,r,s,t}(\alpha_{Pklm}{}^r k_P l_P m_P\mathbf{r}_A+\alpha_{Pkl}{}^{rs}k_P l_P\mathbf{r}_A s_A$$
$$+\alpha_{Pk}{}^{rst}k_P\mathbf{r}_A s_A l_A)+\cdots. \qquad (2.7)$$

Here k, l, and m can range independently over x, y, and z. P can stand for nucleus B or C. Again a factor of e^2 has been omitted. The difference between Eq. (2.6) and (2.7) arises, of course, from the lack of equivalence of nuclei B and C in the linear model. In Eqs. (2.6) and (2.7) the electron labels have been omitted. They are given by the convention discussed before Eq. (2.3).

3. THE MATRIX ELEMENTS

The choice of wave function is obviously of great importance in the calculation of the matrix element.

We choose a set of functions which must satisfy the following requirements: (1) The wave functions for the whole system must satisfy the Pauli exclusion principle. (2) They must go over into eigenfunctions of $\mathbf{H}_A$ and $\mathbf{H}_M$, as the separation of the two species becomes large. (3) They must be fairly simple. The compromise we choose is a properly antisymmetrized product of atom and molecule functions. A typical member of the set is

$$|x,1,2,3\rangle=3^{-\frac{1}{2}}N_x\{|2p_x,1,+\rangle|M,2,3\rangle$$
$$+|2p_x,2,+\rangle|M,3,1\rangle+|2p_x,3,+\rangle|M,1,2\rangle\}. \quad (3.1)$$

Here $|2p_x,i,+\rangle$ is an atomic hydrogen $2p_x$ function, centered on nucleus A of the atom, of electron i, with $m_s=+\frac{1}{2}$; $|M,2,3\rangle$ is a molecular wave function discussed below, N_x is a normalization constant,

$$N_x=\{1-\langle 2p_x|BC\rangle^2\}^{-\frac{1}{2}}. \quad (3.2)$$

The set $|j,1,2,3\rangle$, with $j=1,2,3$ standing for x,y,z, respectively, form the complete set of functions used, except for the spin degeneracy of the atom. All results of this paper are independent of the value of m_s of the hydrogen atom. Hence we will generally ignore this quantum number in the discussions to follow, except where otherwise stated.

The molecular wave function $|M,2,3\rangle$ deserves special consideration. It has been useful to specialize this function slightly more by assuming for it the following form

$$|M,2,3\rangle=2^{-\frac{1}{2}}N_M|BC,2\rangle|BC,3\rangle$$
$$\times[\alpha(2)\beta(3)-\beta(2)\alpha(3)]. \quad (3.3)$$

Here N_M is a normalization constant, $|BC,i\rangle$ is a molecular orbital for electron i, $\alpha(i)$ and $\beta(i)$ are spin functions for electron i with $m_s=+\frac{1}{2}$ and $-\frac{1}{2}$, respectively. We assume, therefore, explicitly that the molecular orbitals for the two electrons of the molecule are identical. This form of the molecular wave function makes it possible to utilize fully the fact that the expanded Hamiltonian contains only one-electron terms. The molecular orbital $|BC\rangle$ can be specialized further, if desirable, by assuming that

$$|BC\rangle\approx\{|1s,B\rangle+|1s,C\rangle\},$$

where $|1s,B\rangle$ is a hydrogen atom $1s$ function centered on nucleus B, etc. This assumption is not needed for the general results presented here.

In general the set of three functions of Eq. (3.1) does not form an orthogonal set, but such a set is easily constructed from them. But for the two special geometrical configurations under examination, these three functions do form an orthonormal set.

The general result obtained by our analysis is the following. When the matrix elements of the Hamiltonian of Eq. (2.1), with $\mathbf{H}_I$ expanded as discussed in Sec. 2, are formed using the wave functions of Eqs. (3.1), and (3.3) the following is obtained,

$$\langle i|\mathbf{H}|j\rangle=N_iN_j\{(E_A+E_M)(\delta_{ij}-a_{ij})$$
$$+\sum_{k,l,m}\langle 2p_i|H_A{}^{kl}|2p_j\rangle\langle BC|H_B{}^{ml}+H_C{}^{ml}|BC\rangle$$
$$-\tfrac{1}{2}\langle 2p_i|H_B{}^{ml}+H_C{}^{ml}|BC\rangle\langle BC|H_A{}^{kl}|2p_j\rangle$$
$$-\tfrac{1}{2}\langle 2p_i|BC\rangle\langle BC|H_B{}^{ml}+H_C{}^{ml}|BC\rangle\langle BC|H_A{}^{kl}|2p_j\rangle\}. \quad (3.4)$$

In this equation E_A and E_M are the eigenvalues of $\mathbf{H}_A$ and $\mathbf{H}_M$, respectively, the Kronecker symbol δ_{ij} has its usual meaning, and $a_{ij}=\langle 2p_i|BC\rangle\langle BC|2p_j\rangle$. All electron labels have been dropped, because each term in Eq. (3.4) is a one-electron term. The derivation of Eq. (3.4) is quite elementary and straightforward and is given in Appendix F of the work cited in footnote 9. The result is correct through the fourth order in the expansion of $\mathbf{H}_I$.

When the functions $|j,1,2,3\rangle$ do not form an orthogonal set, the matrix elements given above must be combined in a straightforward manner to obtain the correct matrix elements of $\mathbf{H}$. For the two special nuclear configurations under study here, the functions do form an orthogonal set, and Eq. (3.4) gives the correct matrix elements directly. For these two configurations a direct check also shows that $\langle i|\mathbf{H}|j\rangle=\langle i|\mathbf{H}|i\rangle\delta_{ij}$. In these cases it is possible to rewrite Eq. (3.4) in the following way,

$$\langle i|\mathbf{H}|i\rangle=\langle i|H^0|i\rangle+N_i{}^2\langle i|\mathbf{H}^c|i\rangle$$
$$-\tfrac{1}{2}N_i{}^2\langle i|\mathbf{H}'|i\rangle. \quad (3.5)$$

Here

$$\langle i|\mathbf{H}^0|i\rangle=E_A+E_M$$
$$\langle i|\mathbf{H}^c|i\rangle=\sum_{k,l,m}\langle 2p_i|H_A{}^{kl}|2p_i\rangle$$
$$\times\langle BC|H_B{}^{ml}+H_C{}^{ml}|BC\rangle$$
$$\langle i|\mathbf{H}'|i\rangle=\sum_{k,l,m}\langle 2p_i|H_A{}^{kl}|BC\rangle$$
$$\times\langle BC|H_B{}^{ml}+H_C{}^{ml}|2p_i\rangle$$
$$+\langle 2p_i|BC\rangle\langle BC|H_B{}^{ml}+H_C{}^{ml}|BC\rangle\langle BC|H_A{}^{kl}|2p_i\rangle; \quad (3.6)$$

$\langle i|\mathbf{H}^0|i\rangle$ is the Hamiltonian when the two species are far apart, $\langle i|\mathbf{H}^c|i\rangle$ is the close analog of the crystal field Hamiltonian, and $\langle i|\mathbf{H}'|i\rangle$ is a correction which involves three-center integrals and overlap between atom and molecule functions which arises from the antisymmetric wave function. The exact form of the terms H_A, H_B, and H_C can be obtained from Eqs. (2.6) and (2.7) for the two models under consideration. The evaluation of the integrals which arise can be simplified considerably by first deriving a set of selection rules appropriate for the two models. These selection rules are obtained by considering the parities of

TABLE II. Selection rules for matrix elements.

1. T model. Nonvanishing elements.

$\langle BC \mid P_x^- \mid BC\rangle \neq 0 \qquad \langle BC \mid Q_{kk} \mid BC\rangle \neq 0$

$\langle BC \mid T_{xkk}^- \mid BC\rangle \neq 0 \qquad \langle 2p_y \mid BC\rangle \neq 0$

$\langle 2p_i \mid P_k \mid BC\rangle = \delta_{ik}\langle 2p_i \mid P_k \mid BC\rangle$

$\langle 2p_i \mid Q_{kl} \mid BC\rangle = [\delta_{i1}\delta_{k1}\delta_{l2}+\delta_{i2}\delta_{k1}+\delta_{i3}\delta_{k3}\delta_{l2}]\langle 2p_i \mid Q_{kl} \mid BC\rangle$

$\langle 2p_i \mid T_{klm} \mid BC\rangle = \delta_{i2}\delta_{lm}\langle 2p_i \mid T_{klm} \mid BC\rangle$

$\langle 2p_i \mid r_A \mid BC\rangle = \delta_{ir}\langle 2p_i \mid r_A \mid BC\rangle$

$\langle 2p_i \mid r_A s_A \mid BC\rangle = [\delta_{i1}\delta_{r1}\delta_{s2}+\delta_{i2}\delta_{rs}+\delta_{i3}\delta_{r2}\delta_{s2}]\langle 2p_i \mid r_A s_A \mid BC\rangle$

2. The linear model. Nonvanishing elements.

$\langle BC \mid x_P \mid BC\rangle \neq 0 \qquad (= \tfrac{1}{2}x_{BC} \text{ if } P=B, = -\tfrac{1}{2}x_{BC} \text{ if } P=C)$

$\langle BC \mid r_P^2 \mid BC\rangle \neq 0 \qquad \langle BC \mid x_P y_P^2 \mid BC\rangle \neq 0$

$\langle BC \mid x_P^3 \mid BC\rangle \neq 0 \qquad \langle BC \mid x_P z_P^2 \mid BC\rangle \neq 0$

$\langle 2p_z \mid BC\rangle \neq 0$

$\langle 2p_i \mid k_P \mid BC\rangle = \delta_{ik}\langle 2p_i \mid k_P \mid BC\rangle$

$\langle 2p_i \mid k_P l_P \mid BC\rangle = [\delta_{i1}\delta_{k1}+\delta_{i2}\delta_{k2}\delta_{l1}+\delta_{i3}\delta_{k3}\delta_{l1}]\langle 2p_i \mid k_P l_P \mid BC\rangle$

$\langle 2p_i \mid k_P l_P m_P \mid BC\rangle = \delta_{ik}\delta_{lm}\langle 2p_i \mid k_P l_P m_P \mid BC\rangle$

$\langle 2p_i \mid r_A \mid BC\rangle = \delta_{ir}\langle 2p_i \mid r_A \mid BC\rangle$

$\langle 2p_i \mid r_A s_A \mid BC\rangle = [\delta_{i1}\delta_{rs}+\delta_{i2}\delta_{r2}\delta_{s1}+\delta_{i3}\delta_{r3}\delta_{s1}]\langle 2p_i \mid r_A s_A \mid BC\rangle$

$\langle 2p_i \mid r_A s_A t_A \mid BC\rangle = \delta_{is}\delta_{st}\langle 2p_i \mid r_A s_A t_A \mid BC\rangle$

the integrands in the matrix elements with respect to reflections in three mutually perpendicular planes which intersect in the center of the molecule. The selection rules are listed in Table II. The usual selection rules for $\langle 2p_i \mid r_A^n \mid 2p_j\rangle$ also hold.

When the selection rules of Table II are used to evaluate the matrix elements of Eqs. (3.6) the following results are obtained. For the T model,

$$\langle i \mid \mathbf{H}^e \mid i\rangle = e^2\sum_{r,k}\langle 2p_i \mid r_A^2 \mid 2p_i\rangle \times\{\alpha_1^{rr}\langle BC \mid P_x^- \mid BC\rangle+\alpha_{kk}^{rr}\langle BC \mid Q_{kk} \mid BC\rangle\}. \quad (3.7)$$

The expressions for $\langle i \mid \mathbf{H}' \mid i\rangle$ are quite complicated. A typical element, $\langle y \mid \mathbf{H}' \mid y\rangle$, is displayed in Appendix 1. For the rest, see Tables III.2 and III.5 of footnote 9. For the linear model,

$$\langle i \mid \mathbf{H}^e \mid i\rangle = e^2\sum_{P,r,k}\langle 2p_i \mid r_A^2 \mid 2p_i\rangle \times\{\alpha_{P1}^{rr}\langle BC \mid x_P \mid BC\rangle+\alpha_{Pkk}^{rr}\langle BC \mid k_P^2 \mid BC\rangle\}. \quad (3.8)$$

Again, the expressions for $\langle i \mid \mathbf{H}' \mid i\rangle$ are quite complicated, and can be found in Table III.6 of footnote 9. They have the same general form as the typical element $\langle y \mid \mathbf{H}' \mid y\rangle$ of the T model displayed in Appendix 1.

4. COMPARISON WITH THE CRYSTAL FIELD APPROXIMATION

It is instructive to compare, for the two special geometries, the results of the crystal field approximation and of the present approximation. This comparison shows in explicit detail some of the features which are left out in the usual crystal field calculation.

The crystal field Hamiltonian appropriate for the two special models considered here has the following form,

$$\mathbf{H} = eC+\sum_k e\alpha_k k_A+\sum_{r,s} eA_{rs}r_A s_A. \quad (4.1)$$

As before, k_A, r_A, and s_A are electron coordinates measured from nucleus A. The values of the constants C, α_k, and A_{rs} depend on the detailed geometry. They can be derived in the usual way, and are listed in Appendix 2. Their calculation is discussed in general, and given in considerable detail by Goldberg and Herzfeld.[11]

The matrix elements of the crystal field are calculated in the usual manner, using the functions $\mid 2p_x, +\rangle \mid 2p_y, +\rangle, \mid 2p_z, +\rangle$ as a basis. If we denote the integral $\langle 2p_s \mid r_A^2 \mid 2p_s\rangle$ by I_{rs}, and use elementary relations between the integrals of this type, we can readily derive the following results. The nonvanishing matrix elements for the T model, and hence the eigenvalues of Eq. (4.1) are

$$H_{11} = eI_{xy}(3A_{11}+A_{22}+A_{33}) = 2eI_{xy}A_{11},$$
$$H_{22} = eI_{xy}(A_{11}+3A_{22}+A_{33}) = 2eI_{xy}A_{22},$$
$$H_{33} = eI_{xy}(A_{11}+A_{22}+3A_{33}) = -2eI_{xy}(A_{11}+A_{22}), \quad (4.2)$$

where the second equality holds because the electrostatic potential satisfies Laplace's equation. We disregard here the effect of the constant, and of the linear terms in Eq. (4.1) which contribute only in a higher order of approximation. Two crystal field splitting parameters are obtained,

$$H_{11}-H_{22} = 2eI_{xy}(A_{11}-A_{22})$$
$$H_{22}-H_{33} = 2eI_{xy}(A_{22}-A_{33}) = 2eI_{xy}(A_{11}+2A_{22}). \quad (4.3)$$

The corresponding results for the linear model are

$$H_{11} = 2eI_{xy}A_{11}$$
$$H_{22} = H_{33} = -eI_{xy}A_{11}. \quad (4.4)$$

Only one splitting parameter is obtained, since one state retains a twofold orbital degeneracy in this case,

$$H_{11}-H_{22} = 3eI_{xy}A_{11}. \quad (4.5)$$

The eigenvalues and splittings obtained from the expanded Hamiltonian-separated atom method are a good deal more complicated. First we present the results for the T model. Define as follows,

$$A_{rr}' = e\sum_k\{\alpha_{kk}^{rr}\langle BC \mid Q_{kk} \mid BC\rangle+\alpha_1^{rr}\langle BC \mid P_x^- \mid BC\rangle\}. \quad (4.6)$$

Then the expression for $\langle i \mid \mathbf{H}^e \mid i\rangle$ [Eq. (3.7)] can be

[11] H. Goldberg and C. M. Herzfeld, NBS Technical Note in preparation.

written as

$$\langle i \mid \mathbf{H}^e \mid i \rangle = \sum_r eI_{ir}A_{rr}'. \tag{4.7}$$

The diagonal matrix elements, and therefore, eigenvalues of the Hamiltonian for the complete system (Eq. 2.1, with $\mathbf{H}_I$ in expanded form) are

$$\begin{aligned}
H_{11} &= E_A + E_M + N_x^2 eI_{xy}[3A_{11}' + A_{22}' + A_{33}'] - \tfrac{1}{2}N_x^2 H_{11}', \\
H_{22} &= E_A + E_M + N_y^2 eI_{xy}[A_{11}' + 3A_{22}' + A_{33}'] - \tfrac{1}{2}N_y^2 H_{22}', \\
H_{33} &= E_A + E_M + N_z^2 eI_{xy}[A_{11}' + A_{22}' + 3A_{33}'] - \tfrac{1}{2}N_z^2 H_{33}'.
\end{aligned} \tag{4.8}$$

This result is to be compared with Eqs. (4.2). First of all, Eq. (4.8) contains the eigenvalues E_A and E_M. This difference is a trivial consequence of the differences in the Hamiltonians (2.1) and (4.1). Next, both sets of equations contain terms in I_{xy}. These depend on the crystal field parameters A_{rr} and their molecular orbital analogs A_{rr}' in the same way. These terms in Eq. (4.8) also depend on overlap through the normalization constants. The A_{rr}' may not satisfy Laplace's equation (at least it is not obvious whether they do or not), hence the simplification of Eqs. (4.2) cannot be carried out here. Finally, Eqs. (4.8) contain the correction terms H_{rr}', which have no analog in crystal field theory.

The splittings can be readily calculated, and using Eq. (3.2), are

$$\begin{aligned}
H_{11} - H_{22} &= 2eI_{xy}(A_{11}' - A_{22}') \\
&\quad - \frac{\langle 2p_y \mid BC\rangle^2}{1 - \langle 2p_y \mid BC\rangle^2}(eI_{xy})[A_{11}' + 3A_{22}' + A_{33}'] \\
&\quad - \tfrac{1}{2}(H_{11}' - H_{22}'N_y^2), \\
H_{22} - H_{33} &= 2eI_{xy}(A_{22}' - A_{33}') \\
&\quad + \frac{\langle 2p_y \mid BC\rangle^2}{1 - \langle 2p_y \mid BC\rangle^2}(eI_{xy})[A_{11}' + 3A_{22}' + A_{33}'] \\
&\quad - \tfrac{1}{2}(H_{22}'N_y^2 - H_{33}').
\end{aligned} \tag{4.9}$$

This result is to be compared with Eq. (4.3). Again the first terms in (4.9) are exact analogs of Eq. (4.3). Then, Eqs. (4.9) contain terms in the parameters A_{rr}' which depend on the overlap $\langle 2p_y \mid BC\rangle$. Finally, Eqs. (4.9) contain the "correction" terms in H_{rr}', which depend both on overlap and on the three-center integrals introduced by the antisymmetric wave functions.

The results for the linear model are quite similar in general form to those for the T model. Now define

$$A_{rr}' = e\sum_{P,k}\{\alpha_{P1}{}^{rr}\langle BC \mid x_P \mid BC\rangle + \alpha_{Pkk}{}^{rr}\langle BC \mid k_P{}^2 \mid BC\rangle\}. \tag{4.10}$$

Then eigenvalues of the complete Hamiltonian [Eq. (2.1), with $\mathbf{H}_I$ is expanded form] are of exactly the same form as Eqs. (4.8) for the T model. In the linear model we must obtain one singly and one doubly degenerate level. This is a result of symmetry considerations alone, and depends in no way on the method used to calculate the splittings. In analogy with the crystal field result we assume that the levels H_{22} and H_{33} are degenerate, though this is not obvious. By considering the behavior of our solution as the separation of the species increases it seems very likely that this is the correct assignment. These conclusions will be tested in later work. The splitting calculated on this basis is

$$\begin{aligned}
H_{11} - H_{22} &= 2eI_{xy}(A_{11}' - A_{22}') \\
&\quad + \frac{\langle 2p_x \mid BC\rangle^2}{1 - \langle 2p_x \mid BC\rangle^2}(eI_{xy})(3A_{11}' + 2A_{22}') \\
&\quad - \tfrac{1}{2}N_x^2(H_{11}' - H_{22}').
\end{aligned} \tag{4.11}$$

This result again contains a term analogous to the crystal field result, Eq. (4.5), an additional term which depends on overlap and the correction terms H_{rr}' which depend on overlap and arise from exchange.

5. DISCUSSION

The comparison of the crystal field calculations with the EH–SA–MO calculations of Sec. 4 shows that the chief difference between the two is the complete neglect of wave function overlap and electron exchange between species in the crystal field calculation. This result is not surprising, but it is instructive to see explicitly the effects of this neglect, and to see explicitly the corrections necessary to take these two effects into account.

The method we have used makes contact with several other theories which arise in different contexts. The expanded Hamiltonian method is quite generally used in the discussion of properties of gases,[10] though there usually without consideration of the effect of exchange. Recently, however, several attempts have been made to treat the quantum mechanical many-electron problem in ways similar to this, particularly by Pluvinage,[12] and by Walsh and Borowitz.[13] The separated atom wavefunctions for our system are close analogs of the functions first used by Moffitt.[14]

It is clear that this work must be extended in several directions. First of all, the results of this paper depend to a considerable extent on the details of the system studied, and have, therefore, the status of a particular example, rather than that of a general theory. Various generalizations are, therefore, required. For example, the case where the reference ion has many electrons must be treated. Second, all results obtained so far have been formal. These formal results are instructive, and certainly shed light on the nature of the crystal field approximation, but they must be subjected to numerical treatment. Finally, the EH–SA–MO method should be applied to certain other interaction problems of special interest. Such results will be reported later.

---

[12] P. Pluvinage, Ann. Phys. **12**, 145 (1950).
[13] P. Walsh and S. Borowitz, Phys. Rev. **115**, 1206 (1959).
[14] W. Moffitt, Proc. Roy. Soc. (London) **A210**, 245 (1951).

The results obtained in this paper are applicable to one type of case of a reference ion having many electons. This is the strong field case of crystal field theory, where the Coulomb repulsion between the electrons of the reference ion which are in an unfilled shell are weaker than the perturbations of these electrons by the neighboring species. In this case the electrons of the reference ion are effectively decoupled, and their interaction with the surroundings will be given in a qualitative way by our results.

In summary, it appears that the expanded-Hamiltonian separated-atom molecular orbital method of this paper explains some of the shortcomings of the conventional crystal field theory, and provides explicit expressions for some necessary corrections in the special cases considered.

APPENDIX 1

Matrix Element H_{22}'

T Model (*in this Appendix* $\psi_{BC} = |BC\rangle$)

$$
\begin{aligned}
H_{22}' = e^2\{ & (2p_y \mid \alpha_2^2 P_y \mid \psi_{BC})(\psi_{BC} \mid y_A \mid 2p_y) \\
& + (2p_y \mid \psi_{BC})(\psi_{BC} \mid \alpha_{11}^2 Q_{xx} + \alpha_{22}^2 Q_{yy} + \alpha_{33}^2 Q_{zz} \mid \psi_{BC})(\psi_{BC} \mid y_A \mid 2p_y) \\
& + (2p_y \mid \alpha_2^{11} P_y \mid \psi_{BC})(\psi_{BC} \mid x_A^2 \mid 2p_y) + (2p_y \mid \alpha_2^{22} P_y \mid \psi_{BC})(\psi_{BC} \mid y_A^2 \mid 2p_y) \\
& + (2p_y \mid \alpha_2^{33} P_y \mid \psi_{BC})(\psi_{BC} \mid z_A^2 \mid 2p_y) \\
& + (2p_y \mid \psi_{BC})(\psi_{BC} \mid \alpha_{11}^{11} Q_{xx} + \alpha_{22}^{11} Q_{yy} + \alpha_{33}^{11} Q_{zz} \mid \psi_{BC})(\psi_{BC} \mid x_A^2 \mid 2p_y) \\
& + (2p_y \mid \psi_{BC})(\psi_{BC} \mid \alpha_{11}^{22} Q_{xx} + \alpha_{22}^{22} Q_{yy} + \alpha_{33}^{22} Q_{zz} \mid \psi_{BC})(\psi_{BC} \mid y_A^2 \mid 2p_y) \\
& + (2p_y \mid \psi_{BC})(\psi_{BC} \mid \alpha_{11}^{33} Q_{xx} + \alpha_{22}^{33} Q_{yy} + \alpha_{33}^{33} Q_{zz} \mid \psi_{BC})(\psi_{BC} \mid z_A^2 \mid 2p_y) \\
& + (2p_y \mid \alpha_{112}^2 T_{xxy} + \alpha_{222}^2 T_{yyy} + \alpha_{332}^2 T_{yzz} \mid \psi_{BC})(\psi_{BC} \mid y_A \mid 2p_y) \\
& + (2p_y \mid \alpha_{11}^{11} Q_{xx} + \alpha_{22}^{11} Q_{yy} + \alpha_{33}^{11} Q_{zz} \mid \psi_{BC})(\psi_{BC} \mid x_A^2 \mid 2p_y) \\
& + (2p_y \mid \alpha_{11}^{22} Q_{xx} + \alpha_{22}^{22} Q_{yy} + \alpha_{33}^{22} Q_{zz} \mid \psi_{BC})(\psi_{BC} \mid y_A^2 \mid 2p_y) \\
& + (2p_y \mid \alpha_{11}^{33} Q_{xx} + \alpha_{22}^{33} Q_{yy} + \alpha_{33}^{33} Q_{zz} \mid \psi_{BC})(\psi_{BC} \mid z_A^2 \mid 2p_y) \\
& + (2p_y \mid \alpha_2^{112} P_y \mid \psi_{BC})(\psi_{BC} \mid y_A x_A^2 \mid 2p_y) + (2p_y \mid \alpha_2^{222} P_y \mid \psi_{BC})(\psi_{BC} \mid y_A^3 \mid 2p_y) \\
& + (2p_y \mid \alpha_2^{233} P_y \mid \psi_{BC})(\psi_{BC} \mid y_A z_A^2 \mid 2p_y) \\
& + (2p_y \mid \alpha_{11}^2 Q_{xx} + \alpha_{22}^2 Q_{yy} + \alpha_{33}^2 Q_{zz} \mid \psi_{BC})(\psi_{BC} \mid y_A \mid 2p_y) \\
& + (2p_y \mid \psi_{BC})(\psi_{BC} \mid \alpha_1^{222} P_x^- \mid \psi_{BC})(\psi_{BC} \mid y_A^3 \mid 2p_y) \\
& + (2p_y \mid \psi_{BC})(\psi_{BC} \mid \alpha_1^{112} P_x^- \mid \psi_{BC})(\psi_{BC} \mid y_A x_A^2 \mid 2p_y) \\
& + (2p_y \mid \psi_{BC})(\psi_{BC} \mid \alpha_1^2 P_x^- \mid \psi_{BC})(\psi_{BC} \mid y_A \mid 2p_y) \\
& + (2p_y \mid \psi_{BC})(\psi_{BC} \mid \alpha_1^{11} P_x^- \mid \psi_{BC})(\psi_{BC} \mid x_A^2 \mid 2p_y) \\
& + (2p_y \mid \psi_{BC})(\psi_{BC} \mid \alpha_1^{22} P_x^- \mid \psi_{BC})(\psi_{BC} \mid y_A^2 \mid 2p_y) \\
& + (2p_y \mid \psi_{BC})(\psi_{BC} \mid \alpha_1^{33} P_x^- \mid \psi_{BC})(\psi_{BC} \mid z_A^2 \mid 2p_y) \\
& + (2p_y \mid \psi_{BC})(\psi_{BC} \mid \alpha_1^{233} P_x^- \mid \psi_{BC})(\psi_{BC} \mid y_A z_A^2 \mid 2p_y)\}.
\end{aligned}
$$

$$
\begin{aligned}
\alpha_2^2 &= r_{AB}^{-5}(x_{AB}^2 - 2y_{AB}^2) \\
\alpha_{11}^2 &= (3/2) r_{AB}^{-5} y_{AB} - (15/2) r_{AB}^{-7} y_{AB} x_{AB}^2 \\
\alpha_{22}^2 &= (9/2) r_{AB}^{-5} y_{AB} - (15/2) r_{AB}^{-7} y_{AB}^3 \\
\alpha_{33}^2 &= (3/2) r_{AB}^{-5} y_{AB} \\
\alpha_2^{11} &= -(3/2) r_{AB}^{-5} y_{AB} + (15/2) r_{AB}^{-7} x_{AB}^2 y_{AB} \\
\alpha_2^{22} &= -(9/2) r_{AB}^{-5} y_{AB} + (15/2) r_{AB}^{-7} y_{AB}^3 \\
\alpha_2^{33} &= -(3/2) r_{AB}^{-5} y_{AB} \\
\alpha_{11}^{11} &= (9/4) r_{AB}^{-5} - (45/2) r_{AB}^{-7} x_{AB}^2 + (105/4) r_{AB}^{-9} x_{AB}^4 \\
\alpha_{22}^{11} &= -3 r_{AB}^{-5} + (105/4) r_{AB}^{-9} x_{AB}^2 y_{AB}^2
\end{aligned}
$$

$$\alpha_{33}^{11}=(3/4)r_{AB}^{-5}-(15/4)x_{AB}^{2}r_{AB}^{-7}$$

$$\alpha_{11}^{22}=-3r_{AB}^{-5}+(105/4)r_{AB}^{-9}y_{AB}^{2}x_{AB}^{2}$$

$$\alpha_{22}^{22}=(9/4)r_{AB}^{-5}-(45/2)r_{AB}^{-7}y_{AB}^{2}+(105/4)r_{AB}^{-9}y_{AB}^{4}$$

$$\alpha_{33}^{22}=(3/4)r_{AB}^{-5}-(15/4)r_{AB}^{-7}y_{AB}^{2}$$

$$\alpha_{11}^{33}=(3/4)r_{AB}^{-5}-(15/4)r_{AB}^{-7}x_{AB}^{2}$$

$$\alpha_{22}^{33}=(3/4)r_{AB}^{-5}-(15/4)r_{AB}^{-7}y_{AB}^{2}$$

$$\alpha_{33}^{33}=(9/4)r_{AB}^{-5}$$

$$\alpha_{112}^{2}=6r_{AB}^{-5}-(105/2)r_{AB}^{-9}x_{AB}^{2}y_{AB}^{2}$$

$$\alpha_{222}^{2}=-(3/2)r_{AB}^{-5}+15r_{AB}^{-7}y_{AB}^{2}-(35/2)r_{AB}^{-9}y_{AB}^{4}$$

$$\alpha_{233}^{2}=-(3/2)r_{AB}^{-5}+(15/2)r_{AB}^{-7}y_{AB}^{2}$$

$$\alpha_{2}^{112}=6r_{AB}^{-5}-(105/2)r_{AB}^{-9}x_{AB}^{2}y_{AB}^{2}$$

$$\alpha_{2}^{222}=-(3/2)r_{AB}^{-5}+15r_{AB}^{-7}y_{AB}^{2}-(35/2)r_{AB}^{-9}y_{AB}^{4}$$

$$\alpha_{2}^{233}=(3/2)r_{AB}^{-5}+(15/2)r_{AB}^{-7}y_{AB}^{2}$$

$$\alpha_{1}^{222}=(15/2)r_{AB}^{-7}x_{AB}y_{AB}-(35/2)r_{AB}^{-9}x_{AB}y_{AB}^{3}$$

$$\alpha_{1}^{112}=(15/2)r_{AB}^{-7}3x_{AB}y_{AB}-(35/2)3r_{AB}^{-9}x_{AB}^{3}y_{AB}$$

$$\alpha_{1}^{2}=-3r_{AB}^{-5}x_{AB}y_{AB}$$

$$\alpha_{1}^{11}=-(3/2)r_{AB}^{-5}3x_{AB}+(15/2)r_{AB}^{-7}x_{AB}^{3}$$

$$\alpha_{1}^{22}=(15/2)r_{AB}^{-7}y_{AB}^{2}x_{AB}$$

$$\alpha_{1}^{33}=-(3/2)r_{AB}^{-5}x_{AB}$$

$$\alpha_{1}^{223}=(15/2)r_{AB}^{-7}x_{AB}y_{AB}.$$

APPENDIX 2

The Crystal Field Constants

The constants are derived on the basis of the following model. The molecular charge distribution is described by a positive charge ϵ on each nucleus B and C, whose coordinates in the center of molecule system are $x_B=a$, $x_c=-a$, and a negative charge -2ϵ at the origin. The magnitude of ϵ is such that the quadrupole moment of the point charge distribution has the same magnitude as that of the molecule. The nucleus A of the atom is located at x_0, y_0, $z_0(=0)$, in the center of molecule system.

1. The T Model

$$C=\sum_i \epsilon_i/d_i \qquad \alpha_1=\alpha_3=0$$

$$\alpha_2=2y_0\epsilon\left[\frac{1}{(a^2+y_0^2)^{\frac{3}{2}}}-\frac{1}{y_0^3}\right]$$

$$A_{11}=\epsilon\left\{\frac{3a^2}{(a^2+y_0^2)^{5/2}}-\left[\frac{1}{(a^2+y_0^2)^{3/2}}-\frac{1}{y_0^3}\right]\right\}$$

$$A_{22}=\epsilon\left\{3y_0^2\left[\frac{1}{(a^2+y_0^2)^{5/2}}-\frac{1}{y_0^5}\right]-\left[\frac{1}{(a^2+y_0^2)^{3/2}}-\frac{1}{y_0^3}\right]\right\}$$

$$A_{33}=-\epsilon\left\{\frac{1}{(a^2+y_0^2)^{3/2}}-\frac{1}{y_0^3}\right\}$$

$$A_{12}=A_{23}=A_{13}=0.$$

2. The linear Model

$$C=\sum_i \epsilon_i/d_i \qquad \alpha_2=\alpha_3=0$$

$$\alpha_1=-\epsilon\left[\frac{1}{(x_0+a)^2}-\frac{2}{x_0^2}+\frac{1}{(x_0-a)^2}\right]$$

$$A_{11}=\epsilon\left[\frac{1}{(x_0+a)^3}-\frac{2}{x_0^3}+\frac{1}{(x_0-a)^3}\right]$$

$$A_{22}=A_{33}=-(\tfrac{1}{2})\epsilon\left[\frac{1}{(x_0+a)^3}-\frac{2}{x_0^3}+\frac{1}{(x_0-a)^3}\right]$$

$$A_{12}=A_{23}=A_{13}=0.$$

THE JOURNAL OF CHEMICAL PHYSICS VOLUME 34, NUMBER 2 FEBRUARY, 1961

Concentration Dependence of NMR Spin-Lattice Relaxation Times in Solutions*

R. W. MITCHELL AND M. EISNER

Agricultural and Mechanical College of Texas, College Station, Texas

(Received August 8, 1960)

Spin-lattice relaxation times for protons in benzene, cyclohexane, chlorobenzene, bromobenzene, and *o*-dichlorobenzene in solution with carbon tetrachloride and carbon disulfide are empirically fitted to theoretical curves based on the Hill and molecular sphere models of molecular motion. The results indicate that the Hill model properly accounts for the variation of both the rotational and translational relaxation times with concentration of solute.

INTRODUCTION

THE Hill model[1,2] for molecular motion in liquids gives results that agree closely with experimentally determined values for the viscosities and diffusion coefficient of solutions and for the dielectric correlation times of polar molecules in nonpolar solvents. In a previous investigation, we have shown that this model gives reasonable values for the rotational correlation times obtained from NMR relaxation time measurements of molecules in dilute solutions.[3] As a more severe test of this model, we have investigated the concentration dependence of T_1 which involves the variation with concentration of both the rotational and translational correlation times.

According to the Hill model, the nuclear rotational correlation time of a solute molecule B in solution with a solvent A should be

$$\tau_r=(f_A K_{AB}{}^2\eta_{AB}\sigma_{AB}+f_B K_{BB}{}^2\eta_B\sigma_B)/kT, \qquad (1)$$

where

$$K_{AB}{}^2=I_{AB}I_B/(I_{AB}+I_B, \quad K_{BB}{}^2=I_{BB}I_B/(I_{BB}+I_B),$$

f_A and f_B are the mole fractions of solvent and solute, respectively, I_{AB} is the moment of inertia of an A and B molecule during collision (figured about the center of mass of B), I_{BB} is the moment of inertia of two B molecules during collision, η_B is the viscosity of the pure solvent, σ_B is the cube root of the volume per molecule for the pure solvent, and the quantity $\eta_{AB}\sigma_{AB}$ is defined by

$$\eta_m\sigma_m=f_A{}^2\eta_A\sigma_A+f_B{}^2\eta_B\sigma_B+2f_Af_B\eta_{AB}\sigma_{AB}, \qquad (2)$$

where η_m, η_A, and η_B are the viscosities of the mixture, solvent, and solute, respectively, σ_m is the average distance between molecules in the mixture, and σ_A and σ_B are the respective distances between molecules of the pure solvent and pure solute.

The dependence of the translational correlation time on the physical properties of the solution are contained in the diffusion constant D which is given by the Hill theory to be

$$D=kT/6(\eta_{AB}\sigma_{AB}f_A+\eta_B\sigma_Bf_B). \qquad (3)$$

* This research was supported by the U. S. Air Force through the Air Office of Scientific Research of the Air Research and Development Command under a contract. It is taken from a dissertation submitted by R. W. Mitchell to A. and M. College of Texas in partial fulfillment of the Ph.D.degree.

[1] N. E. Hill, Proc. Phys. Soc. (London) **67B**, 149 (1954).
[2] N. E. Hill, Proc. Phys. Soc. (London) **28B**, 207 (1955).
[3] R. W. Mitchell and M. Eisner, J. Chem. Phys. **33**, 86 (1960).

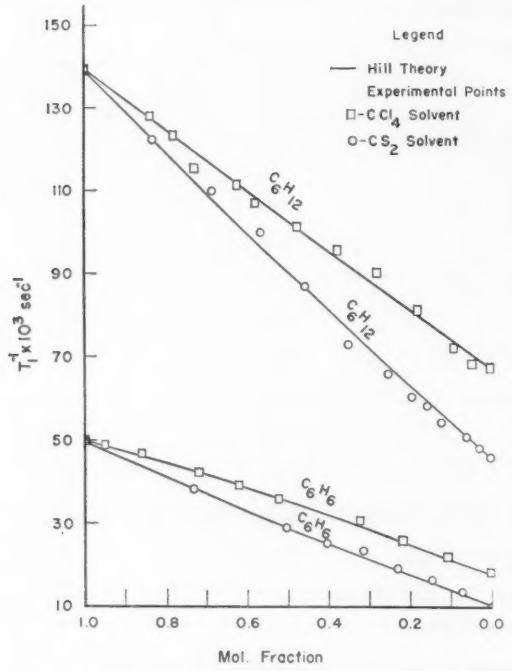

FIG. 1. Comparison of the Hill theory with experimental values of T_1^{-1} at 30°C for protons in C_6H_6 and C_6H_{12} as a function of concentration. The theoretical curves were fitted to the experimental value for T_1^{-1} at $f=1$ and at $f=0$.

RELATIONS OF T_1 TO PHYSICAL PROPERTIES OF SOLUTIONS

From the dependence of the rotational and translational relaxation times on their respective correlation times, one can write for the spin-lattice relaxation time T_1, of a solute molecule in a solution of nonmagnetic solvent nuclei,

$$1/T_1 = A\tau_r + BV/D, \qquad (4)$$

where V is the volume fraction of solute and A and B are constants. The formulas of Gutowsky and Woessner[4] can be employed to calculate A and B; however, because of the uncertainties in the molecular parameters, we shall select these constants to fit the experimental data for T_1. Equation (4), in conjunction with Eqs. (1) and (3), gives the theoretical dependence of T_1 on the physical properties of the solution. The theoretical curves for the solutions employed in this investigation are presented in Figs. 1 through 4. The points which are shown in these figures represent the experimentally determined values of T_1. The values of A and B, in Eq. (4), were selected so that the theoretical curves would pass through the experimental points at $V=1$ and at $V=0$. While the volume fraction of solute is the natural choice for the independent variable, the mole fraction of solute was used here because the curves turned out to be almost linear with this choice of variable.

The theoretical values for A and B in Eq. (4) are independent of the solvent for a given solute molecule, so the values obtained by fitting this equation to the experimental points for the CS_2 and CCl_4 solutions will provide a test of the reliability of the Hill theory. However, since the values of A and B are not as significant as the values of $T_1^{-1}{}_{\text{rot}}$ and $T_1^{-1}{}_{\text{trans}}$ which can be calculated from A and B, the latter quantities have been presented in Table I. The values obtained for $T_1^{-1}{}_{\text{rot}}$ and $T_1^{-1}{}_{\text{trans}}$ from the data on the CS_2 solutions agree with the corresponding ones obtained from the data on the CCl_4 solutions within the limits of uncertainty; thus, A and B are independent of the solvent for each of the solute molecules as predicted.

The relative values of $T_1^{-1}{}_{\text{rot}}$ and $T_1^{-1}{}_{\text{trans}}$ in Table I demonstrate the importance of the translational mechanism for relaxation for the solutions investigated. With the exception of C_6H_{12}, the translational contribution to the relaxation is larger than the rotational contribution. It is significant that the Hill theory curves in Figs. 1 to 4 fit the experimental data for C_6H_{12}, for which the rotational relaxation is dominant, equally as

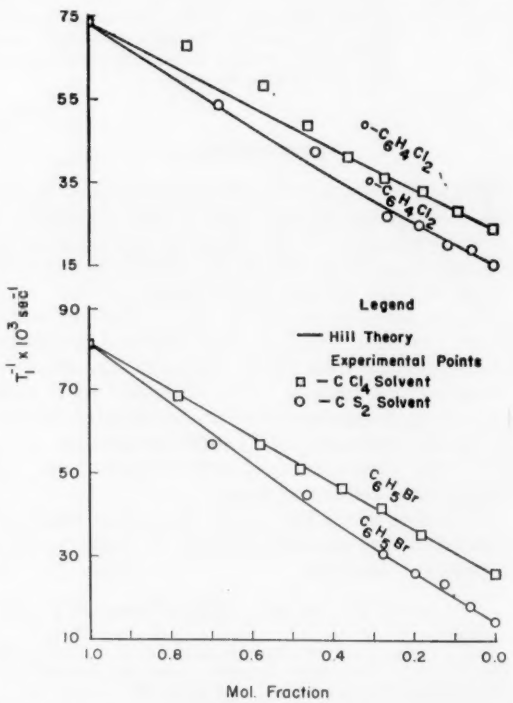

FIG. 2. Comparison of the Hill theory with experimental values of T_1^{-1} at 30°C for protons in o-$C_6H_4Cl_2$ and C_6H_5Br as a function of concentration. The theoretical curves were fitted to the experimental values of T_1^{-1} at $f=1$ and $f=0$.

[4] H. S. Gutowsky and D. E. Woessner, Phys. Rev. **104**, 843 (1956).

well as for the other molecules, for which the translational relaxation is dominant. It follows that the Hill theory predicts the proper dependence of both $T_{1\,\mathrm{rot}}$ and $T_{1\,\mathrm{trans}}$ on the physical properties of the solutions over the whole range of concentrations.

DEPENDENCE OF T_1 ON SOLUTION VISCOSITY

The usual expression used by NMR workers to estimate the rotational correlation time is the Debye time, and the Stokes-Einstein relation is commonly used for the diffusion constant. Both of these results are obtained by treating the molecule as a sphere imbedded

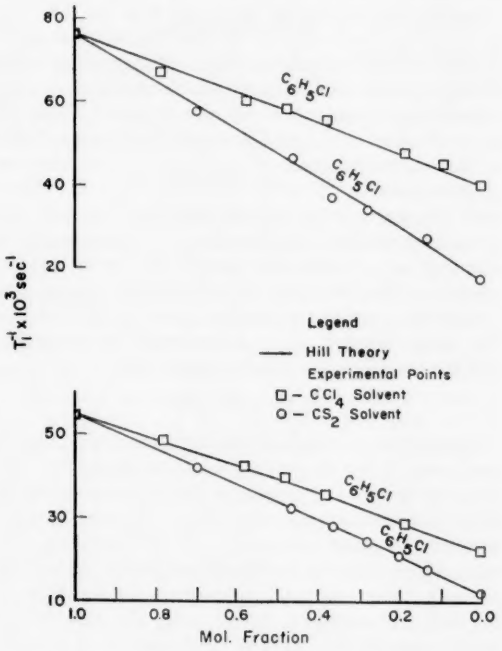

FIG. 3. Comparison of the Hill theory with experimental values of T_1^{-1} at 30°C (upper graphs) and 10°C (lower graphs) for protons in C_6H_5Cl as a function of concentration. The theoretical curves were fitted to the experimental values of T_1^{-1} at $f=1$ and $f=0$.

in a viscous medium. We shall refer to these results as the "molecular sphere model." According to this model, τ_r is directly proportional to the solution viscosity η while D is inversely proportional to η. Making use of these relations, Eq. (4) can be written as

$$1/T_1 = A'\eta + B'\eta V$$

or (5)

$$1/\eta T_1 = A' + B'V.$$

Hence, this model predicts $(\eta T_1)^{-1}$ to be a linear function of the volume fraction of solute.

From the experimental points presented in Fig. 5, it is clear that $(\eta T_1)^{-1}$ is not a linear function of the volume fraction of solute for the $C_6H_{12}-CS_2$ and

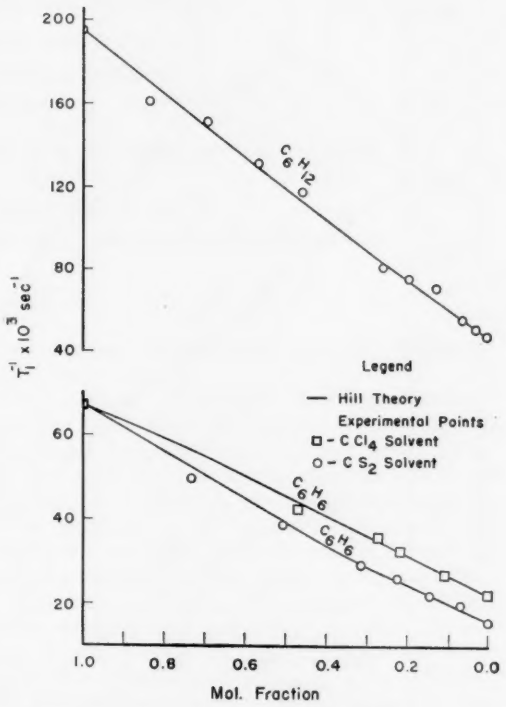

FIG. 4. Comparison of the Hill theory with experimental values of T_1^{-1} at 10°C for protons in C_6H_{12} as a function of concentration. The theoretical curves were fitted to the experimental values at $f=1$ and $f=0$.

$C_6H_6-CS_2$ solutions. On the other hand, the data for $C_6H_{12}-CCl_4$ and $C_6H_6-CCl_4$ fit Eq. (5) reasonably well. It should be noted that the viscosity variation is rather small for the CCl_4 solutions compared with that of the CS_2 solutions. Only the curves for the C_6H_6 and

TABLE I. Translational and rotational relaxation times at $V=1$ obtained from fitting T_1 data to the Hill theory.

Molecule	Solvent	$T_1^{-1}{}_{\mathrm{trans}} \times 10^3$ (sec^{-1})	$T_1^{-1}{}_{\mathrm{rot}} \times 10^3$ (sec^{-1})	Averages $T_1^{-1}{}_{\mathrm{trans}}$	Averages $T_1^{-1}{}_{\mathrm{rot}}$
C_6H_{12}	CS_2(30°C)	26	113	37	102
	CCl_4(30°C)	48	91		
C_6H_6	CS_2(30°C)	29	20	30	19
	CCl_4(30°C)	31	18		
	CS_2(10°C)	34	34	39	29
	CCl_4(10°C)	45	23		
C_6H_5Cl	CS_2(30°C)	36	19	32	23
	CCl_4(30°C)	28	27		
	CS_2(10°C)	49	27	39	37
	CCl_4(10°C)	29	47		
C_6H_5Br	CS_2(30°C)	52	29	53	28
	CCl_4(30°C)	54	27		
o–$C_6H_4Cl_2$	CS_2(30°C)	43	30	44	29
	CCl_4(30°C)	45	29		

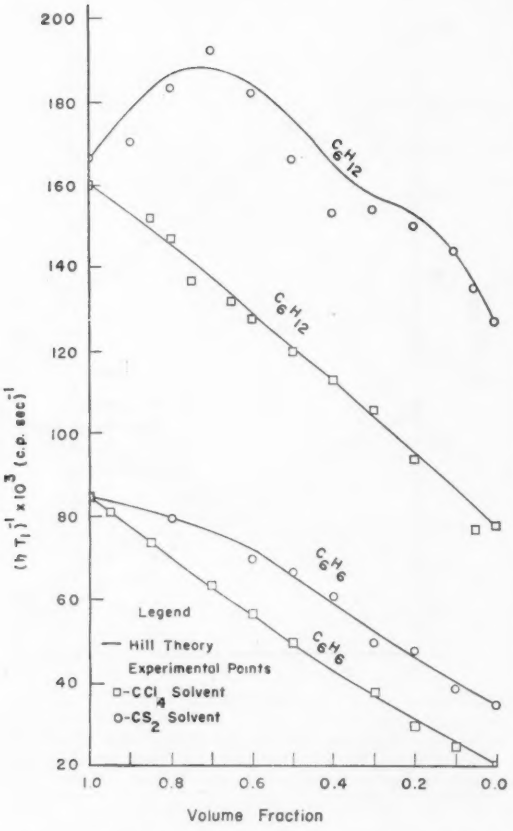

FIG. 5. Comparison of the Hill theory with experimental values of $(\eta T_1)^{-1}$ at 30°C for protons in C_6H_6 and C_6H_{12} as a function of concentration. The theoretical curves were fitted to the experimental values of $(\eta T_1)^{-1}$ at $V=1$ and $V=0$.

C_6H_{12} solutions were presented in Fig. 5, since the behavior of $(\eta T_1)^{-1}$ for these curves was typical of all of the solutions. Namely, for those solutions having a wide viscosity variation $(\eta T_1)^{-1}$ was nonlinear, while for those solutions exhibiting little viscosity variation, the data for $(\eta T_1)^{-1}$ were represented reasonably well by Eq. (5). The solutions used by Anderson and Arnold[5] (H_2O-D_2O) and by Giulotti, Lanzi, and Tosca[6] ($C_6H_5Cl-CCl_4$) fell into the latter class and supported the conclusion that the molecular sphere model accurately predicted the variation of T_1 with concentration.

It is interesting to observe the variation of $(\eta T_1)^{-1}$ with volume fraction predicted by the Hill theory. These curves, which are presented in Fig. 5, do not agree with the experimental results as well as those of Figs. 1 through 4; in fact, the curve for $C_6H_{12}-CS_2$ does not agree with the data within the experimental uncertainty. These results can be understood when one considers that the values of A and B in Eq. (4) were selected here to fit $(\eta T_1)^{-1}$ to the experimental points at $V=1$ and $V=0$, while, for the corresponding curves of Figs. 1 to 4, A and B were selected to fit T_1^{-1} to the experimental points at $V=1$ and at $V=0$. These different choices of A and B amount to different choices of the relative amounts of rotational and translational contributions to the total relaxation time T_1. Therefore, the introduction of the solution viscosity as a parameter for these solutions causes a distortion in the shape of the experimental curves and in the relative weights of the Hill theory rotational and translational contributions to the relaxation time. It is clear that the usual choice of ηT_1 as a parameter for presenting NMR relaxation time data is a poor one.

CONCLUSIONS

The success of the Hill model in predicting the dependence of the nuclear spin-lattice relaxation time upon the physical properties of the solutions employed in this investigation provides a basis for using T_1 measurements to study anomalous solution behavior. One point which deserves further investigation is the temperature dependence of T_1. Although the variation of T_1 with concentration agrees with the Hill theory equally well at 10°C and 30°C, the values of $T_{1\text{rot}}$ do not appear to have the same temperature dependence as the inner viscosity.

[5] W. A. Anderson and J. T. Arnold, Phys. Rev. **101**, 511 (1956).
[6] L. Giulotti, G. Lanzi, and L. Tosca, J. Chem. Phys. **24**, 632 (1956).

Diffusion of Hydrogen through Palladium

R. C. HURLBERT AND J. O. KONECNY

Shell Development Company, Emeryville, California

(Received July 27, 1960)

Diffusion rates F (cm³ STP/cm² min) of hydrogen from the upstream pressure P (atm) into vacuum through a palladium sheet of thickness L (microns) are represented by

$$\log F = 3.70 + 0.68 \log P - 623/T - \log L,$$

except for very thin membranes. Explanations are suggested for the wide discordance of earlier results in the study of the diffusion of hydrogen through palladium.

INTRODUCTION

THE diffusion of hydrogen through palladium membranes has been investigated by numerous authors with quite divergent results. Observations have generally been expressed in the form

$$F = k_n(P_u^n - P_d^n)/f(L), \qquad (1)$$

where F is the flow rate per unit surface area, k_n the diffusion constant, $f(L)$ a function f of the membrane thickness L, P_u and P_d the pressures of hydrogen on the upstream and downstream side of the membrane, and n a constant. There is, however, a lack of agreement concerning the function $f(L)$, and the values reported for n vary considerably. According to Silberg and Bachman[1] and also Holt *et al.*[2] the rates are essentially independent of the membrane thickness, while according to Lombard and Eichner[3] and Winkelman[4] they are inversely proportional to it. The values reported[5] for n range from 0.5 to 1. The value of 0.5 may be taken to imply that the transport of hydrogen through the bulk of the metal is rate determining and that equilibrium is established at the surface—an equilibrium between hydrogen gas and an ideal solution of hydrogen atoms (or protons) in the metal. A value of 1, on the other hand, implies a slow, rate determining surface reaction of hydrogen with palladium. Such conflicting conclusions about $f(L)$ and n are not surprising because the diffusion rates reported by different authors sometimes differ by orders of magnitude. For example, the rates reported for a 50-μ membrane at 300°C by Jost and Widman,[6] Silberg and Bachman,[1] Barrer[7] and ourselves are in the ratio of 0.005:0.01:0.3:1.

Our values are seen to be higher than those of other authors. The exceptionally high diffusion rates through specially prepared membranes, reported by de Rosset,[8] could not be confirmed.

Our experience indicates that these large discrepancies arise mainly from two sources of error, namely, poisoning of the palladium surface and the accumulation of nondiffusing gases on the upstream side of the membrane. Volatile metals, like zinc are severe poisons for the diffusion, so that the use of silver solder for brazing the membrane, as in the work of Silberg and Bachman,[1] may profoundly reduce the rates and lead to spurious results. Apart from poisoning by volatile metals, diffusion rates generally decline with diffusion time, not infrequently to a small fraction of the initial value. This effect is apparently due to the accumulation of nondiffusing gases upstream because it disappears when a bleed of more than 10% is taken from the main stream of hydrogen at a point close to the upstream surface. With this precaution, diffusion rates are reproducible within 10% or better. A similar bleed has been used before by Lombard and Eichner.[9] However, some of the connections in the heated zone of their apparatus were brazed, so that poisoning of the palladium membrane may have occurred. Their values for the rates of diffusion are, indeed, somewhat low.

The present work describes the effect of upstream pressures from 1 to 7 atm and of membrane thickness from 10 to 150 μ on diffusion rates into vacuum at 350°C. The effect of temperature on diffusion rates through membranes of different thickness has also been determined. The results show that the surface reaction is not rate limiting for membranes thicker than 20 μ.

DESCRIPTION OF THE APPARATUS

The apparatus consisted essentially of three parts: The palladium disk holder, a purification train for hydrogen, and suitable pressure equipment with flow reading and controlling devices. The disk holder, shown in Fig. 1, was a flange made of stainless steel, bolted together. The palladium membrane, about 4

[1] P. A. Silberg and C. H. Bachman, J. Chem. Phys. **29,** 777 (1958).
[2] A. Holt, E. C. Edgar, and J. B. Firth, Z. physik. Chem. **82,** 534 (1913).
[3] V. Lombard and C. Eichner, Bull. soc. chim. France [4] **53,** 1194 (1933).
[4] A. Winkelman, Ann. Physik **6,** 115 (1901).
[5] V. Lombard and C. Eichner, Compt. rend. **196,** 1998 (1933).
[6] W. Jost and A. Widman, Z. physik. Chem. (Leipzig) **B45,** 285 (1940).
[7] R. M. Barrer, Trans. Faraday Soc. **36,** 1235 (1940).
[8] A. J. de Rosset, U. S. 2,824,620 (1958).
[9] V. Lombard and C. Eichner, Bull. soc. chim. France [4], 51, 1462 (1932); [4], 55, 945 (1934); [5], 2, 1555 (1935); [5] 3, 2203 (1936); [5], 4, 1276 (1937).

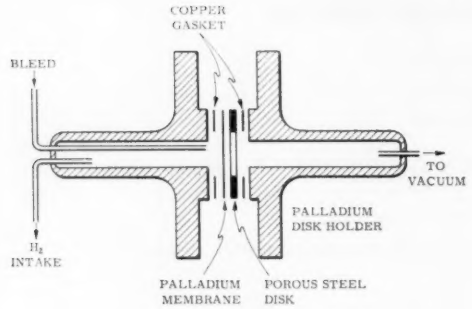

FIG. 1. Palladium disk holder.

cm² in area, was backed with a disk of porous stainless steel, welded into a solid steel ring. Copper gaskets were used for a hermetic seal.

Hydrogen was purified by passage over fine, hot copper and then through a liquid nitrogen trap. Subsequent investigation showed that the purification was actually unnecessary. Experiments described in Table I were carried out with commercial hydrogen.

In the earlier phase of this work, completed in 1954, diffusion rates were determined by the direct measurement of hydrogen flow from a pressure of 810 mm Hg upstream into vacuum downstream. Automatic control devices were used to maintain constant pressure over the required extended periods of time. The investigation was resumed in 1959 with a simplified apparatus. Hydrogen, maintained at constant pressure upstream, was allowed to flow into a 3-liter, initially evacuated receiver downstream. The rates of diffusion into vacuum were determined graphically from suitable plots of downstream pressure against time. The values reported here are generally averages of several experiments made with at least two membranes of the same thickness.

Agreement between the two methods was satisfactory. In both cases the results were reproducible within 10% or better.

Palladium sheets sometimes displayed low permeability when first used owing, probably, to impurities on the surface. However, constant reproducible rates were obtained by exposing all membranes to air at 300°C for a few minutes before the admission of hydrogen.

TABLE I. Diffusion rates as a function of pressure.[a]

P_u atm	F cm³ STP/cm² min	$F/P_u^{0.5}$	$F/P_u^{0.68}$
1.54	27.0	21.8	20.0
2.68	38.1	23.2	19.4
4.38	56.1	26.8	20.6
5.89	66.5	27.4	20.1
7.18	68.3	25.3	17.8

[a] Membrane thickness 24 μ, temperature 350°C.

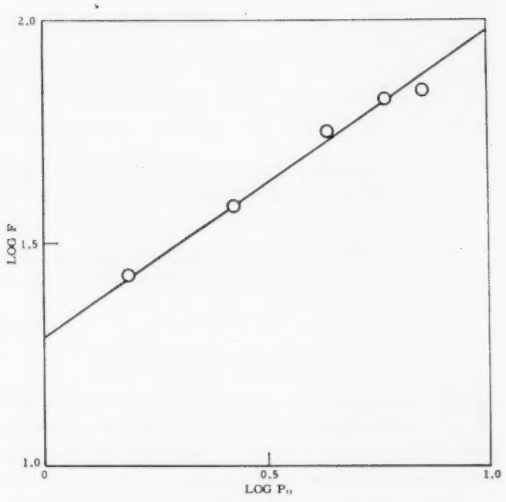

FIG. 2. Diffusion rate (cm³ STP/cm² min) vs upstream pressure (atm).

RESULTS

The effect of upstream pressure P_u on diffusion rates F into vacuum through a 24-μ membrane and at 350°C is shown in Table I. Although the ratio $F/P_u^{0.5}$ changes only to a small extent with P_u, a definite trend in its values is discernible. The plot of log$F$ against logP_u, shown in Fig. 2, is satisfactorily linear and has a slope of 0.68. The relation between diffusion rates and pressure in the given experimental range may therefore be expressed by the equation

$$F = kP_u^{0.68}. \tag{2}$$

The value of the diffusion constant k depends on the thickness of the membrane and the temperature.

With the exception of the thinnest membrane, the values of kL, shown in Table II, are practically constant and the data can be fitted with the equation

$$k = 480/L. \tag{3}$$

However, the plot of k against $1/L$, shown in Fig. 3, indicates that k begins to approach a limiting value

TABLE II. Diffusion constants as a function of thickness.[a]

L microns	k cm³ STP/cm² min atm$^{0.68}$	$10^{-2}\,kL$
11.4	28.9[b]	3.3
24	19.6[b]	4.7
27	17.5[c]	4.7
50	8.9[c]	4.5
79	5.3[b]	4.2
106	4.6[c]	4.9
127	4.1[b]	5.2
154	3.8[c]	5.9

[a] Temperature 350°C, P_u 1.1 to 1.7 atm.
[b] Measured by the second method.
[c] Measured by the first method.

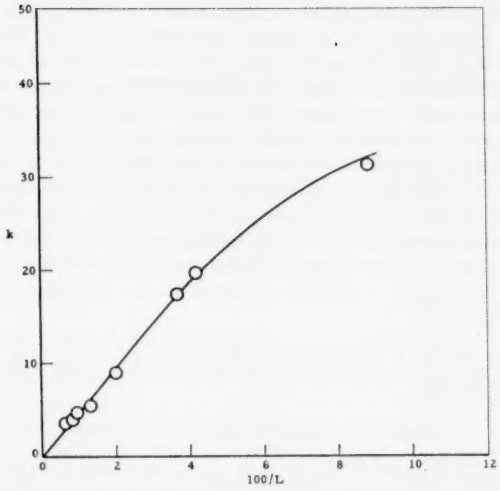

FIG. 3. Diffusion constant (cm^3 STP/cm^2 min $atm^{0.68}$) vs the reciprocal of the membrane thickness (microns).

when L is reduced below 20 μ. The value of kL for the 11.4-μ membrane, confirmed by repeated measurements, is markedly smaller than the value predicted by Eq. (3).

The effect of temperature on k at different values of membrane thickness is summarized in Table III and shown in Fig. 4 in the form of the conventional Arrhenius plots. The activation energy, calculated from these graphs, is 2850 cal.

Contamination of the upstream side of the diffusion cell with silver solder reduces hydrogen flow to a small fraction of the normal value. Hydrogen sulfide is an extremely effective poison, even at concentrations as low as 5×10^{-5} mole % in hydrogen. The effect of such a trace amount on the flow rate of hydrogen through a 24-μ membrane at 350°C and at 1.7-atm hydrogen upstream is shown in Fig. 5. The poisoning is associated with the formation of a grey surface film on the membrane and is practically irreversible.

DISCUSSION

The following discussion will be restricted to a fairly simple model, sufficient to represent the available data. More elaborate models have been developed by Wang[10] and recently by Ash and Barrer.[11] Much more extensive and accurate information will be required for an adequate discussion of these models.

TABLE III. Diffusion rates as a function of temperature.[a]

t °C	k, cm^3 STP/cm^2 min $atm^{0.68}$			
	$d=27$	$d=50$	$d=106$	$d=154$
225	9.8	4.8	2.6	1.9
300	14.1	7.5	3.9	2.6
350	17.5	8.9	4.6	3.8
425	22.0	11.4	6.4	4.8
500	26.5	13.8	7.9	6.5

[a] Measured by the first method; $P_u=1.07$ atm.

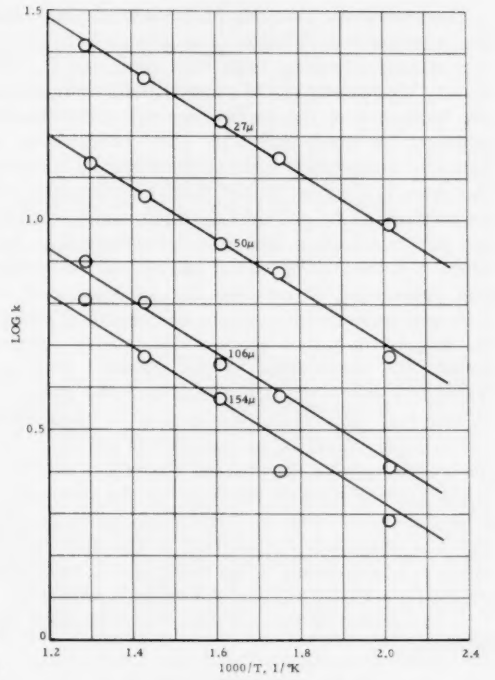

FIG. 4. Arrhenius plot of the diffusion constants (cm^3 STP/cm^2 min $atm^{0.68}$) for membranes of different thickness.

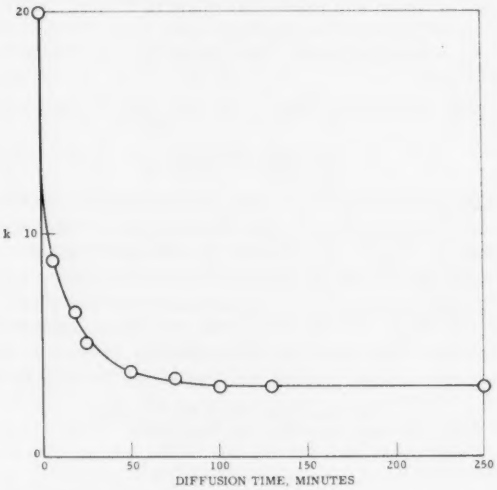

FIG. 5. The poisoning of the permeability by hydrogen sulfide. Diffusion constant (cm^3 STP/cm^2 min $atm^{0.68}$) vs diffusion time.

[10] T. Wang, Proc. Cambridge Phil. Soc. **32**, 657 (1936).
[11] R. Ash and R. M. Barrer, Phil. Mag. [8], **4**, 1197 (1959).

The basis of our first simplification is the observation that experimental diffusion rates give no indication of approaching a limiting value with increasing P_u, even at very high pressures.[12] We may therefore assume that the fraction θ of the surface covered with adsorbed hydrogen is small and that the concentration of hydrogen immediately beneath the surface is far below the saturation value. Under these circumstances θ is proportional to P_u, and the rate of adsorption of hydrogen per unit surface area may be expressed as $k_f P_u$ where k_f is the specific rate of adsorption. The adsorption presumably[13,14] involves the dissociation of the hydrogen molecule into protons and electrons, perhaps by way of hydrogen atoms. The reverse reaction, namely the evaporation of the adsorbed hydrogen, therefore, involves the recombination of two atoms and its rate may plausibly be assumed to be proportional to θ^2. It may, therefore, be expressed as $k_r\theta^2$ where k_r is the specific rate for the process. The rate of migration of the protons through the metal to the downstream surface is proportional to their concentration gradient and may therefore be expressed in the form $k_t(\theta/L)$ where k_t is a constant. (The value of θ at the downstream surface is zero at zero downstream pressure.)

In the course of the diffusion θ is stationary and therefore

$$d\theta/dt = k_f P_u - k_r\theta^2 - k_t(\theta/L) = 0. \quad (4)$$

Solving for θ/L we obtain

$$F = k_t(\theta/L) = -(k_t^2/2k_rL^2) + k_t[(k_fP_u/k_rL^2) + (k_t/2k_rL^2)^2]^{\frac{1}{2}}. \quad (5)$$

This equation assumes a very simple form for sufficiently small and sufficiently large L. With decreasing L it approaches the limiting value k_fP_u. This means that F is determined by the rate of the surface reaction alone.

For sufficiently large L the flow rate F approaches the value

$$F = k_t(k_f/k_r)^{\frac{1}{2}}(P_u^{\frac{1}{2}}/L). \quad (6)$$

Equation (6) can be derived more simply by dropping the term $k_t(\theta/L)$ in Eq. (4). Physically this approximation for large L implies that the diffusion through the solid is rate determining and that equilibrium between hydrogen gas and dissolved hydrogen is maintained at the surface. The change of the rate with pressure is therefore determined by the solubility isotherm. The square root law applies only to an ideal solution of protons in palladium. Actually, the value of $F/P_u^{\frac{1}{2}}$ increases slowly with pressure, as shown in Table I. This result is in agreement with Moon's analysis[15] of the solubility data reported by Gillespie[16,17] and Sieverts[18] and their co-workers. His analysis shows that the activity coefficient of the hydrogen in palladium, regarded as protons or atoms, is less than unity at all but very high temperatures or very low hydrogen pressures. The deviations of the solubility from the square root law at 350°C, extrapolated from Moon's equation, have the same direction and order of magnitude as the deviations observed in the diffusion experiments.

In the range $1 \leqslant P_u \leqslant 7$ atm and for $L \geqslant 20$ μ and $T \geqslant 623$°K a combination of all the results leads to the expression

$$\log F = 3.70 + 0.68 \log P_u - 623/T - \log L \quad (7)$$

for F (in cm³ STP/cm² min; P_u in atm and L in microns). The factor 0.68 in the pressure term applies strictly only at 350°C and in the experimental pressure range, and probably decreases to the limiting value of $\frac{1}{2}$ with increasing temperature. However, Eq. (17) is expected to reproduce the rates quite well also at somewhat higher temperatures.

At the time of this writing, de Rosset[12] published a paper on the diffusion of hydrogen through a 20-μ membrane at pressures ranging from 1 to 21 atm downstream and from 1 to 46 atm upstream. The rates reported for low pressures are about one half of the rates determined in this work although a bleed was used also in his experiments. Except for this deviation factor, most of de Rosset's results can be well represented by Eq. (1) with n equal to 0.68, though de Rosset expresses his results in a more complicated manner.

After a large number of discordant results on the diffusion of hydrogen through palladium have been reported in the past, the main features appear to be experimentally and theoretically well established. The detailed description still remains a problem for the future.

ACKNOWLEDGMENTS

The authors gratefully acknowledge the advice of Dr. Otto Redlich and the assistance of K. D. Vickery and A. J. Pane in making the measurements.

[12] A. J. de Rosset, Ind. Eng. Chem. **52,** 525 (1960).
[13] R. E. Norberg, Phys. Rev. **86,** 745 (1952).
[14] I. Isenberg, Phys. Rev. **79,** 736 (1950).
[15] K. A. Moon, J. Phys. Chem. **60,** 502 (1956).
[16] L. T. Gillespie and F. P. Hall, J. Am. Chem. Soc. **48,** 1207 (1926).
[17] L. T. Gillespie and L. S. Galstaun, J. Am. Chem. Soc. **58,** 2565 (1936).
[18] A. Sieverts and G. Zapf, Z. physik. chem. (Leipzig) **A174,** 359 (1935).

Vapor Pressure of Silicon and the Dissociation Pressure of Silicon Carbide*

STANLEY G. DAVIS,† DONALD F. ANTHROP,‡ AND ALAN W. SEARCY

Department of Mineral Technology and Radiation Laboratory, University of California, Berkeley, California

(Received June 13, 1960)

The vapor pressure of silicon and the dissociation pressure of silicon carbide have been obtained from total weight loss experiments with Knudsen effusion cells. Combination of the measured data with known entropies yields at 298°K for the heat of sublimation of silicon to silicon atoms 108.4±3 kcal and for the heat of the reaction $SiC_{(s)}=Si_{(g)}+C_{(s)}$ 126.0±3 kcal. From the pressure studies and from phase equilibria for the condensed phase silicon-carbon system, the heats of formation for both the cubic and hexagonal modifications of silicon carbide are concluded to be −15.0±2 kcal.

ELUCIDATION of the vaporization equilibria for silicon and the silicon-carbon phase system is of exceptional interest. Direct determinations of the vapor pressure of silicon have yielded values for the heat of sublimation at 298°K that range from 90[1] to 105±12[2] kcal. A mass spectrometer investigation demonstrated that silicon atoms are the principal vapor species at temperatures below 2000°K, although several molecular species were observed.[2]

Until recent years no gaseous carbide molecules other than hydrocarbons and carbides of elements more electronegative than carbon had been identified in high-temperature vapors. But experiments by Ruff[3] indicated that carbon is present in silicon carbide vapor at concentrations higher than can be explained as due to elemental carbon molecules and atoms. More recently, Kleman[4] tentatively identified some of the spectroscopic bands obtained by heating silicon in a graphite furnace as bands of SiC_2 molecules. Such gaseous silicon carbide molecules are of especial interest because of their probable role in production of pure silicon carbide crystals by vapor transport mechanisms.[5]

This paper reports results of Knudsen effusion investigations both of the vapor pressure of silicon in a silicon carbide-coated graphite Knudsen effusion cell and of silicon carbide-graphite mixtures in a graphite cell. The silicon carbide-graphite mixtures provide silicon carbide dissociation pressure data from which the heat of dissociation of silicon carbide can be calculated. Combination of this heat with the heat of formation of silicon carbide yields an indirectly determined value for the heat of sublimation of silicon and thus provides a test of the consistency of the data.

While this work was in progress detailed information about silicon carbide evaporation became available as a result of a mass spectrometric investigation by Drowart, De Maria, and Inghram.[6] Those investigators have measured ion intensities for Si^+, SiC^+, SiC_2^+, Si_2^+, Si_2C^+, $Si_2C_2^+$, Si_3^+, $Si_2C_3^+$, and Si_3C^+ produced by heating silicon carbide in graphite at 2100–2300°K and have calculated, among other things, dissociation energies for the gaseous molecules and the heat of sublimation of silicon to silicon atoms. This heat of sublimation yields calculated silicon vapor pressures that are about a factor of 10 lower than pressures calculated from the direct mass spectrometer determinations made by Honig,[2] and are about a factor of 100 lower than found in earlier measurements.[7,8] Although these results agree to within the wide uncertainty limits placed by Honig on his data, better agreement would certainly be expected.

The relative concentrations of gas species in a complex vapor mixture cannot be evaluated from Knudsen effusion experiments in which only the total weight loss is measured as a function of time. But total weight loss experiments, when the relative concentrations of vapor species are known, can give more precise measurements of the absolute pressure of the principal vapor species, in this system silicon atoms, than can a mass spectrometer. Absolute pressure measurements with mass spectrometers are usually estimated to be correct to within a factor of two; however, in a recent investigation, the usual method for calculation of absolute pressures from ion intensities was shown to yield pressures that differed by as much as a factor of four from pressures calculated by an independent method.[9] Determinations of sample weight changes in total weight loss experiments should be correct to within 20%. Accordingly, total weight loss experiments complement the mass spectrometric experiments The total weight loss measurements can be corrected for

* Support for this research was provided by the U. S. Atomic Energy Commission.

† Department of Chemistry, Rutgers University, Camden, New Jersey.

‡ General Electric Fellow.

[1] L. Brewer, Paper No. 3 in *Chemistry and Metallurgy of Miscellaneous Materials: Thermodynamics*, edited by L. L. Quill (McGraw-Hill Book Company, Inc., New York, 1950).

[2] R. E. Honig, J. Chem. Phys. **22**, 1610 (1954).

[3] O. Ruff, Trans. Electrochem. Soc. **68**, 87 (1935).

[4] B. Kleman, Astrophys. J. **123**, 162 (1956).

[5] J. A. Lely, Ber. deut. keram. Ges. **32**, 229 (1955).

[6] J. Drowart, G. de Maria, and M. G. Inghram, J. Chem. Phys. **29**, 1015 (1958).

[7] O. Ruff and M. Konschak, Z. Electrochem. **32**, 515 (1926).

[8] E. Bauer and R. Brunner, Helv. Chim. Acta **17**, 958 (1934).

[9] W. A. Chupka, J. Berkowitz, and C. F. Giese, J. Chem. Phys. **30**, 827 (1959).

the contributions of minor species, as revealed by the mass spectrometer, to yield silicon atom pressures that should be more reliable than can be obtained by either weight loss or mass spectrometer measurements alone.

EXPERIMENTAL

All samples of silicon carbide were prepared by direct synthesis from the elements in degassed graphite effusion cells. Spectroscopic analyses of the silicon showed 0.02% boron, 0.01% calcium, 0.01% aluminum, and lesser amounts of other metals to be present. The graphite used in the runs tabulated was National Carbon Company spectroscopic grade powder that had been heated at 2150°C for about 80 min before being mixed with silicon.

The mixtures were held at 1400°C for ½ hr and then held for 1 hr at 1900°C to complete silicon carbide formation. Samples used for silicon carbide dissociation studies showed strong diffraction patterns of cubic silicon carbide and faint or weak patterns of graphite.

When silicon was melted alone in graphite crucibles the crucibles cracked. But silicon mixed with silicon carbide could be heated successfully in crucibles that had already been used for silicon carbide dissociation studies. For this reason, silicon vapor pressures were measured by use of a mixture of silicon carbide and silicon in a graphite effusion cell. The solubility of carbon in liquid silicon is reported to be less than 0.1 atomic percent in the temperature range of our experiments.[10] This concentration of carbon will not significantly reduce the vapor pressure of silicon.

The effusion cell was a cup-shaped crucible, ¾ in. i.d. and 11/16 in. deep. The cell lid was drilled with a cylindrical effusion channel. Three graphite pieces surrounded the crucible and lid to reduce evaporation and oxidation by residual gases. Five-mil tantalum sheet served as radiation shields.

The inner cell and lid were weighed with a reproducibility of 0.01 to 0.02 mg. Blank runs showed crucibles remained at constant weight to within 0.05 mg/hr. An open, loaded crucible gained weight upon exposure to moist air. Accordingly, to minimize adsorption of moisture, the assembly was allowed to cool for 2 hr or more under high vacuum before the diffusion pump was cooled. Dried air was then admitted to the vacuum line, and the unit to be weighed was stored over Indicating Drierite. The weight change during storage was no greater in several days than the reproducibility of weighing.

For the silicon carbide and some silicon experiments the air was dried by Indicating Drierite, and the unit weighed was sample plus crucible plus lid plus a brass orifice-cover. This unit gained usually less than 0.02 mg in 6 min of standing in the balance case. In the last seven of the silicon runs the air was dried by $CaCl_2$, $Mg(ClO_4)_2$, P_2O_5, and liquid N_2, in series, and the unit weighed was sample plus crucible plus lid, all inside a tared weighing bottle to prevent exchange of air. When this procedure was used, weight changes during handling were not measurable.

The silicon carbide samples became stratified during effusion runs, and accordingly these sample mixtures were stirred between runs in order to reduce impedance to vaporization (see Discussion section).

The silicon vapor pressure experiments were made in cells that contained from 0.22 to 0.45 mole of silicon per each mole of silicon carbide present. These samples were usually stirred between runs. Seven of the silicon vapor pressure measurements were conducted with short degassing runs after mixing of the samples; no systematic difference is apparent between the vapor pressures thus measured and vapor pressures measured without this operation. The remainder of the procedure followed in each study was similar to that described in a previous publication.[11]

EXPERIMENTAL RESULTS

In Table I are summarized the data and calculations for those measurements of the dissociation pressure of silicon carbide which were considered most reliable. Six early measurements are not included because weight changes of the lid were comparable in magnitude to the weight losses of the cells. For six of the tabulated runs the weight of the lid remained constant to within ±0.06 mg. In one run the lid gained 0.61 mg and in another the lid gained 0.95 mg. Fourteen more runs are not included because those runs were made with samples that had not been recently stirred, and experience demonstrated that the rates of weight losses from such runs decrease with time. The results of these 14 untabulated dissociation pressure measurements are consistent with the data reported in Table I, with the reservation that the apparent pressures do decrease as a function of time when the heating periods are long.

The pressures recorded in Table I are silicon partial pressures calculated from the observed weight losses corrected for the concentrations of molecules found by Drowart *et al.* Because reliable entropy data are available for the reaction, the heat of reaction can be calculated most precisely by use of each dissociation pressure measurement with the known entropy of reaction, and no special advantage would accrue from accumulation of measurements for an extended temperature range.[12] In calculation of ΔH_{298} the thermodynamic functions of the report of Humphrey and co-workers[13] for silicon carbide in the cubic modification were used. Data for solid carbon and gaseous silicon were taken from the tabulations of Stull and Sinke.[14]

[10] R. L. Scace and G. A. Slack, J. Chem. Phys. **30,** 1551 (1959).

[11] A. W. Searcy and R. A. McNees, Jr., J. Am. Chem. Soc. **75,** 1578 (1953).

[12] L. Brewer and A. W. Searcy, J. Chem. Ed. **26,** 548 (1959).

[13] G. L. Humphrey, S. S. Todd, J. P. Coughlin, and E. G. King, Bureau of Mines Report of Investigations 4888 (1952).

[14] D. R. Stull and G. C. Sinke, *Thermodynamic Properties of the Elements* (American Chemical Society, Washington, D. C., 1956).

TABLE I. Calculation of the heat of the reaction $SiC_{(s)}=Si_{(g)}+C_{(s)}$ at 298°K.

Temp. (°K)	Time (sec×10⁻³)	Weight loss (g×10³)	P_{Si} (atm×10⁶)	$-\Delta[(F-H_{298})/T]$	ΔH_{298} (kcal)
2117[a]	2.82	1.89	7.09	36.68	127.5
2118[a]	3.87	3.18	9.98	36.68	126.2
2122[b]	5.70	4.48	9.17	36.67	126.7
2124[c]	11.03	3.25	11.6	36.67	125.9
2124[c]	11.52	3.45	12.3	36.67	125.6
2166[b]	1.99	4.26	28.3	36.64	124.4
2170[b]	3.45	5.52	18.2	36.64	126.6
2171[c]	6.00	3.62	24.1	36.64	125.4

[a] Orifice area 0.0317 cm², Clausing factor 0.391.
[b] Orifice area 0.0314 cm², Clausing factor 0.390.
[c] Orifice area 0.00935 cm², Clausing factor 0.410.

TABLE II. Calculation of the heat of sublimation of silicon at 298°K.

Temp. (°K)	Time (sec×10⁻³)	Weight loss (g×10³)	P_{Si} (atm×10⁶)	$-\Delta[(F-H_{298})/T]$	ΔH_{298} (kcal)
1848[a]	10.98	3.12	3.91	34.316	109.2
1855[a]	10.09	4.21	5.75	34.289	108.1
1858[a]	10.74	3.73	4.79	34.277	108.9
1861[b]	11.58	5.74	7.04	34.265	107.7
1877[b]	7.50	4.26	8.09	34.205	107.9
1881[a]	6.78	2.69	5.48	34.189	109.6
1884[b]	6.90	4.47	9.23	34.178	107.8
1932[b]	5.52	5.69	14.8	33.993	108.4
1934[b]	5.40	8.48	22.5	33.985	106.9
1956[b]	10.20	9.37	13.2	33.903	110.0
2003[b]	3.66	10.70	41.9	33.732	107.7

[a] Orifice area 0.0317 cm², Clausing factor 0.385.
[b] Orifice area 0.0310 cm², Clausing factor 0.382.

Table II contains a summary of the calculations of the heat of sublimation of silicon obtained from the evaporation of liquid silicon in a carbon crucible that was internally coated with silicon carbide. The high-temperature heat capacity data of Olette[15] for solid and liquid silicon were used in calculation of ΔH_{298}. The silicon pressures of the table were corrected for the concentration of molecules that should be present in the vapor.[6] The corrections amount to approximately 5%. The observed pressures are reduced by an additional 6% to correct for the weight loss observed when silicon was heated in a crucible that had no effusion orifice. This weight loss apparently resulted primarily from escape of silicon through the crack between the lid and the effusion cell proper since a concentric graphite crucible inside which the closed cell was placed showed negligible weight changes during the heating cycles.

When the average heat of formation for silicon carbide recommended by Humphrey[13] is used with the silicon carbide dissociation pressures, the heat of sublimation of silicon at 298°K is calculated to be 112.6± 0.9 kcal compared to 108.4±0.8 kcal calculated from the direct determinations. The uncertainties listed are average deviations, not expected limits of error. The vapor pressures of silicon calculated from both our direct and indirect determinations are plotted in Fig. 1 with the calculated pressures of Honig and Drowart.

DISCUSSION

The absolute uncertainties in these heat values that result from errors in the pressure measurements alone are estimated to be ±3 kcal, but the relative errors should be smaller. Common systematic errors, such as

[15] M. Olette, Compt. rend. **244**, 1033 (1957).

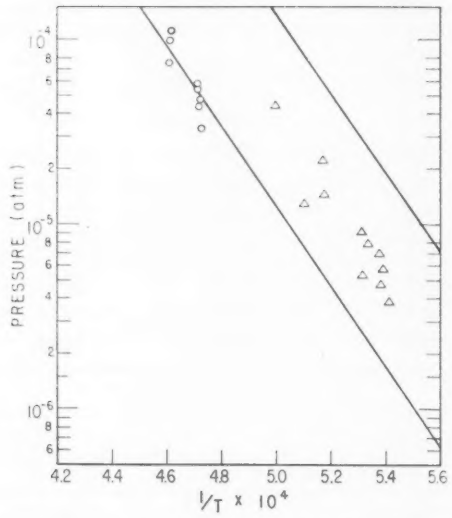

FIG. 1. Partial pressure of Si atoms over silicon. Pressures calculated from direct determinations of the research are designated by Δ. Pressures of Si calculated from SiC dissociation studies of this research and the heat of formation of SiC are designated by ○. The upper curve is that calculated by Honig; the lower curve is that calculated by Drowart.

errors in observed temperatures, should introduce in our directly and indirectly determined heats errors that are in the same direction and of nearly the same magnitude. To rationalize the markedly different values, errors peculiar to the different materials studied must be sought. Furthermore, the direction of these errors must be such as to give rise either to spuriously high weight losses in the liquid silicon evaporation experiments or to spuriously low weight losses in the silicon carbide dissociation experiments.

The most probable source of error unique to the silicon evaporation experiments would be reaction of silicon vapor with the carbon of the crucible during the effusion experiments with a resultant decrease, rather than increase, in weight loss of the cell. Conceivably, however, if the rate of diffusion of silicon through silicon carbide and graphite is high, a quantity of silicon comparable with the quantity of silicon lost through the effusion hole could diffuse through the crucible walls. Our demonstration that only 6% as much material escaped from a closed crucible as from an open crucible proves that such diffusion was not a serious source of error.

A low evaporation coefficient for silicon from a silicon carbide surface could give rise to a low apparent dissociation pressure. However, according to the results of Drowart and co-workers, silicon is the main species that evaporates from silicon carbide, and a low evaporation coefficient for this main vapor species should cause a lower apparent pressure for those runs made with the cell of larger hole area. But our experiments with cells in which different hole areas were used indicate no systematic change in the apparent pressure as a function of hole area. Apparently, the evaporation coefficient of silicon on silicon carbide is sufficiently close to unity to allow us to obtain essentially the equilibrium evaporation rates in our cells. (No data obtained by us or by Drowart *et al.* eliminate the possibility of low evaporation coefficients for the minor molecular species.)

An impedance to the escape of silicon vapor through a carbon layer could also reduce the rate of escape of silicon from silicon carbide. Carbon layers could form either on each individual crystallite of silicon carbide or in a separate (macroscopic) zone in the hottest portion of the sample. A macroscopic layer of carbon was observed to grow on the upper surface of the sample as a result of heating. This upper surface was slightly hotter than the lower portion of the sample because the heating coil was offset slightly to keep the lid at the sample surface temperature.

Immediately after the sample was remixed, when no macroscopic layer of carbon was yet interposed between the silicon carbide grains and the effusion hole, the impedance to evaporation of silicon must have been provided by the effusion chamber, by the Knudsen orifice, and by the microlayers of carbon on each silicon carbide crystal at the sample surface. A microlayer of high impedance would have an experimental effect like that of a low evaporation coefficient, except that the impedance of the microlayer should increase with time. Since yellow silicon carbide could be observed as a separate layer after effusion runs, microlayering was presumably unimportant relative to the macrolayering effect.

The macrolayer impedance should be negligible immediately after sample mixing and should have increased as the layer increased in thickness. Experiments on the rate of loss of silicon from silicon carbide

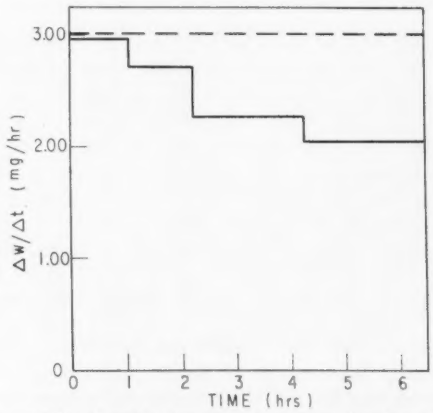

FIG. 2. Plot of weight loss per unit time vs time from SiC at 2118°K. The dotted line is the weight loss calculated for holes of this area from the effusion studies used in calculation of the heat of dissociation of silicon carbide. (Area = 0.0317 cm².)

as a function of time demonstrate that within the normal time of our evaporation experiments this impedance effect was indeed small. Figure 2 shows a plot of $\Delta W/\Delta t$ vs time, from a hole of area 0.0317 cm^2 and Clausing correction 0.391, where ΔW is the weight evaporated in a time period Δt at constant temperature. The value of dW/dt at time$=0$, rather than $\Delta W/\Delta t$, is the quantity that is required for equilibrium measurements. But the closer the approach to zero time, the more completely the effusion hole should govern the rate of weight loss.[16] The slope of dW/dt must approach zero near $t=0$. Examination of Fig. 2 demonstrates that during the first two hours after our sample had been stirred, the average rate of weight loss from a crucible with this hole area was probably at least 80% of the equilibrium value. The longest run used with this approximate hole area lasted less than two hours. The impedance effect of macroscopic layering should be less noticeable in the crucibles that had smaller holes. Longer runs with 0.00935 cm^2 area holes yielded calculated heats that revealed no dependence on time of the runs.

The discrepancy between the direct and indirect determinations of the heat of sublimation of silicon cannot be brought into agreement by the assumption that the contribution of silicon carbide molecules to evaporation from the silicon plus silicon carbide mixture is higher than has been calculated. At constant temperature, the ratio of the pressure of Si_2C to the pressure of silicon atoms is essentially independent of the increase in silicon partial pressure that results from introducing liquid silicon into the system. The introduction of liquid silicon must decrease the ratios of the pressures of SiC, Si_2C_2, Sl_2C_3, and SiC_2 to the pressure of silicon atoms. In principle, if the partial pressure of Si_2, Si_3, or Si_3C were assumed to be higher than found by Drowart *et al.*, our silicon atom partial pressures above silicon as calculated from the silicon carbide dissociation studies and as calculated from direct silicon evaporation would be brought into better agreement because the ratio of the pressures of these molecules to the pressure of silicon atoms is greater at increased silicon atom pressures. We should then make a proportionately larger correction for molecules in the vapor above the silicon plus silicon carbide mixture. But Honig has found the Si_2 and Si_3 molecule concentrations to be low compared to the silicon atom concentration in silicon vapor,[2] and the partial pressure of Si_3C reported by Drowart *et al.* would have to be increased by more than an order of magnitude to affect significantly the silicon atom pressures calculated from the total weight losses. The established reliability of mass spectrometer measurements makes an error of a factor of 10 appear very improbable.

[16] D. J. Meschi and A. W. Searcy, High Temperature Symposium, 135th Annual Meeting, American Chemical Society, Boston (April, 1959).

An attempt to determine the carbon concentration in the vapor by collection and chemical analysis was unsuccessful. Six samples collected on the glass tube wall above our cells showed carbon contents varying from 5 to 30 wt%, although the collections were made under apparently identical conditions. A vapor that consisted entirely of Si_2C would not contain more than 18% carbon. The excessive carbon deposit may have been the product of gas transport of carbon from the outer graphite crucible, which was exposed to the furnace residual atmosphere.

No explanation has been found for the discrepancy in the heats of sublimation for silicon calculated from the direct vapor pressure measurements and from the dissociation pressure measurements. The excellent agreement of the dissociation pressure data with data of Drowart *et al.* encourages adoption of the conclusion that the pressure measurements are substantially correct and that the heat of disproportionation of silicon carbide to solid carbon and atomic silicon gas is 126.0±3 kcal per mole. Furthermore, an unpublished mass spectrometer investigation of silicon evaporation that has been reported since the completion of our investigations leads to a heat of sublimation for silicon of 107±3 kcal,[17] in excellent agreement with our directly determined value of 108.4±3. The best interpretation of data at present appears to be to presume that both sets of measurements are substantially correct and that the discrepancy between heats of sublimation of silicon calculated from the direct and indirect determination is to be sought, at least in part, in thermal data exterior to the present investigation.

HEAT OF FORMATION OF SILICON CARBIDE

The discordant values for the heat of sublimation of silicon can be reconciled by the hypothesis that the heat of formation of silicon carbide at 298°K is more negative than -13 ± 1 kcal, the reported value.[13] Independent evidence for belief that the heat of formation may be more negative than -13 can be adduced.

The temperature of dissociation[10,18] of hexagonal silicon carbide to graphite and a liquid solution of about 20 at. % carbon in silicon can be used with heat capacity and entropy data to obtain a lower limit to the heat evolved in formation of silicon carbide from silicon and carbon. Because decomposition is to graphite and a silicon-rich solution, the free energy of the reaction $Si_{(l)}+C_{(s)}=SiC_{(s)}$ must be negative at the decomposition temperature. Unfortunately, the recent investigations yield discordant decomposition temperatures, 3100°K[10] and 2810°K.[18] A lower limit to the stability of silicon carbide can be calculated from each of these decomposition temperatures.

[17] J. Drowart and G. De Maria, quoted by M. G. Inghram in Advance Papers of An International Symposium on High Temperature Technology, Asilomar, California (October, 1959).

[18] C. E. Lowell of National Carbon Research Laboratory as quoted by E. L. Piper in Prog. Rept. No. 2.

Kelley[19] has calculated, from the heat capacity measurements of Olette,[15] that $S_{2000}-S_{298.15}$ for liquid silicon is 18.49. From the tables of Stull and Sinke and of Humphrey *et al.* ΔS for the reaction at 2000°K is found to be -8.79 cal deg^{-1}, and ΔC_p, if Olette's value for C_p of liquid silicon is employed, is $+0.9$ cal deg^{-1}. The entropy of formation of silicon carbide is then calculated to be 8.5 cal deg^{-1} at 2810°K and 8.4 at 3100°K. From the lower decomposition temperature the heat of the reaction $Si_{(s)}+C_{(s)}=SiC_{(s)}$ is calculated to be ≤ -12.7 at 298°K; and from the higher temperature, ≤ -15.5 kcal.

The cubic and hexagonal modifications of silicon carbide are almost equally stable toward decompositions.[10] Since the two modifications have nearly identical entropies and heat capacities, the heats of formation at 298°K must differ by at most a few hundred calories. The vapor pressure and condensed phase data are consistent with a standard heat of formation of -15 ± 2 kcal at 298°K for both modifications.

If the heat of formation of silicon carbide is -15 and the heat of sublimation of silicon is 108.4 kcal, the heat of dissociation of silicon carbide to silicon vapor and carbon solid at 298°K is calculated to be 123.4 instead of 126.0 kcal. The most probable source of this remaining discrepancy lies in the dissociation pressure measurements, but the discrepancy is now within our expected uncertainties and its source, or sources, can only be a subject of speculation until more information becomes available.

[19] K. K. Kelley (private communication).

ACKNOWLEDGMENT

Dr. Donald Menzer of the National Carbon Research Laboratory in Parma, Ohio, kindly supplied us with carbon analyses of sublimates.

THE JOURNAL OF CHEMICAL PHYSICS VOLUME 34, NUMBER 2 FEBRUARY, 1961

Thermodynamics of the Vaporization of Cr_2O_3: Dissociation Energies of CrO, CrO_2, and CrO_3*

R. T. GRIMLEY, R. P. BURNS, AND MARK G. INGHRAM

Department of Physics, University of Chicago, Chicago, Illinois

(Received August 12, 1960)

The vaporization of Cr_2O_3 under neutral and oxidizing conditions has been studied using mass spectrometric methods. The vaporization proceeds with the formation of Cr, CrO, CrO_2, O, and O_2 as the principal gaseous species. Under oxidizing conditions CrO_3 was also observed. Dissociation energies of the gaseous molecules are $D_0^0(CrO)=101.1\pm7$ kcal/mole, $D_0^0(CrO_2)=227.1\pm15$ kcal/mole, and $D_0^0(CrO_3)=341\pm20$ kcal/mole.

INTRODUCTION

THE vaporization properties of Cr_2O_3 have not previously been reported. Brewer[1] has suggested that, under neutral or oxidizing conditions, the dissociative vaporization of $Cr_2O_3(s)$ to CrO(g), Cr(g), and O_2 is likely with species such as $Cr_xO_2(g)$ and $Cr_xO_3(g)$ also possible. In addition, recent studies of Margrave[2] have indicated that Cr_2O_3 vaporizes congruently.

Spectroscopic evidence suggesting the existence of CrO in the gaseous state was first presented by Eder and Valenta.[3] Somewhat later, Ghosh,[4] using a linear Birge-Sponer extrapolation, determined the dissociation energy of CrO to be 87.2 kcal/mole (3.78 ev). More recently, Huldt and Lagerqvist,[5] using a spectroscopic flame technique, have reported a value of 101.5 ± 11 kcal/mole (4.4 ± 0.5 ev) for $D_0^0(CrO)$. Based on additional information, Brewer[6] re-evaluated the data of Huldt and Lagerqvist and arrived at a higher value of $D_0^0(CrO)=122\pm9$ kcal/mole (5.3 ev). In a later publication, Lagerqvist and Huldt[7] obtained the higher value of 122 kcal/mole. Texts frequently used as reference sources for dissociation energies list the following values as most probable: Gaydon,[8] 97 kcal (4.2 ± 0.5 ev); Cottrell,[9] 97 kcal, and Herzberg,[10] 87 kcal (3.78 ev). In the present investigation the equilibrium partial pressures of the gaseous species

* Supported in part by the Office of Ordnance Research, U. S. Army, and in part by the National Science Foundation.

[1] L. Brewer, Chem. Revs. **52**, 1 (1953).

[2] J. L. Margrave (private communication).

[3] J. M. Eder and E. Valenta, *Atlas typischer Spektra* (Wien, 1911).

[4] C. Ghosh, Z. Physik **78**, 521 (1932).

[5] L. Huldt and A. Lagerqvist, Arkiv Fysik **3**, 525 (1951).

[6] L. Brewer, UCRL-8356 (1957).

[7] A. Lagerqvist and L. Huldt, Z. Naturforsch. **8a**, 493 (1953).

[8] A. G. Gaydon, *Dissociation Energies and Spectra of Diatomic Molecules* (Chapman and Hall, Ltd., London, 1953).

[9] T. L. Cottrell, *The Strength of Chemical Bonds* (Butterworths Scientific Publications, London, 1958).

[10] G. Herzberg, *Spectra of Diatomic Molecules* (D. Van Nostrand Company, Inc., Princeton, New Jersey, 1950).

formed in the vaporization of $Cr_2O_3(s)$ have been measured under neutral and oxidizing conditions, and the dissociation energies of the gaseous molecules have been determined.

EXPERIMENTAL TECHNIQUE

Details of the mass spectrometric technique have been described in a previous publication.[11] In the present experiments, molybdenum Knudsen cells were used for both the neutral vaporizations and those carried out under oxidizing conditions. In order to minimize reaction of the molybdenum with the vapor species, an internal Knudsen cell of Morganite recrystallized alumina was used. The effusion hole in the alumina lid was 1 mm in diameter. Since the interior of the cell was completely covered with Cr_2O_3 shortly after operating temperatures were attained, the ratio of the effusion orifice to the evaporating surface area was approximately 1×10^{-3}. Temperatures were measured by sighting on blackbody holes in the crucible with a Leeds and Northrup optical pyrometer which was previously calibrated against a National Bureau of Standards calibrated lamp. Samples of both Baker's Analyzed and Fisher Certified Reagent-Grade Cr_2O_3 were used during the course of the experiments.

EXPERIMENTAL RESULTS

The investigation was carried out as two distinct series of measurements: (1) vaporization of $Cr_2O_3(s)$ under neutral conditions; and (2) vaporization of $Cr_2O_3(s)$ in the presence of an independently variable oxygen partial pressure. The atomic and molecular ions produced by electron bombardment of the species effusing from the Knudsen cell under neutral conditions were Cr^+, CrO^+, CrO_2^+, O^+, and O_2^+. The identity of the species was confirmed by mass measurement and isotope abundance determinations. Under oxidizing conditions CrO_3^+ was also detected. In order to distinguish between ions resulting from simple ionization and those produced by dissociative ionization, ionization efficiency curves were ascertained under neutral and oxidizing conditions and at different temperatures. Appearance potentials determined by the linear extrapolation procedure, using the spectroscopic ionization potentials of chromium[12] (6.7 ev) and mercury (10.4 ev) as references, are as follows: CrO^+, 8.4 ± 0.5 ev; CrO_2^+, 10.3 ± 0.5 ev; CrO_3^+, 11.6 ± 0.5 ev; and O^+, 13.7 ± 0.5 ev. The appearance potential of O^+ corresponds, within 0.1 ev, to the spectroscopic ionization potential of the oxygen atom.[13] Examination of the ionization efficiency curve for O^+ gave no evidence to indicate the formation of O^+ by any process other than simple ionization of atomic oxygen. Since the CrO_2^+ ion was the oxide species of highest mass observed under neutral conditions, and since the ionization potential does not indicate fragmentation, we attribute the observed peak to simple ionization of the $CrO_2(g)$ molecule. The ionization curves for Cr^+ and CrO^+ measured under neutral conditions show no evidence of fragmentation. However, with the addition of oxygen the ensuing equilibrium shift results in a large increase in the CrO_2 partial pressure, whereas the partial pressure of Cr is strongly suppressed. Under such conditions the dissociative ionization of CrO_2 can be detected. Thus, two processes are responsible for the formation of CrO^+: 1, simple ionization of CrO which occurs at 8.4 ev; and 2, dissociative ionization of CrO_2 which occurs at 13.5 ev. In the case of Cr^+, a possibility exists that three processes account for its formation: (1) simple ionization of Cr which occurs at 6.7 ev; (2) dissociative ionization of CrO_2; and (3) dissociative ionization of CrO. The intensities of the parent Cr^+ and CrO^+ peaks are obtained by linear extrapolation of measurements made before the onset of fragmentation. For purposes of calculation, the fragment contribution to the Cr^+ peak was assumed to arise completely from CrO_2. It should be noted, however, that under neutral conditions where the CrO_2 molecule is much less important than under oxidizing conditions, fragmentation corrections have only a slight effect on the absolute values of the dissociation energies (<1 kcal). The appearance potential of CrO_3^+ is in the range commonly observed for MO_3^+ type ions which are formed by simple ionization of the corresponding neutral molecule. In addition, since no higher oxide species were observed which might produce CrO_3^+ by dissociative ionization, the ion is attributed to simple ionization of the CrO_3 molecule.

In the course of the initial heating of the samples, a change in the relative intensities of the gaseous species was noted. A careful check of the system revealed peaks that were attributed to SO, SO_2, and SO_3. These were formed as a result of the decomposition of a small quantity of sulfate salts in the samples. A pre-bake out as well as a vacuum bake out in the mass spectrometer were found adequate to remove the impurity. Intensity measurements and ratios were then closely reproducible over long periods of time. Partial pressures were calculated from the corrected ion intensities by use of the relation

$$\frac{P_1}{P_2}=\frac{I_1^+T_1\sigma_2S_2(E_2-A_2)}{I_2^+T_2\sigma_1S_1(E_1-A_1)},$$

where P = partial pressure in atm, I^+ = corrected ion intensity, σ = relative cross section, S = multiplier efficiency corrected for molecular effects where necessary, A = appearance potential in ev, and E = energy of the ionizing electrons in ev. Relative ionization cross sec-

[11] Mark G. Inghram and Jean Drowart, "*Mass Spectroscopy Applied to High Temperature Chemistry*," appearing in *International Symposium on High Temperature Chemistry at Asilomar, California* (McGraw-Hill Book Company, Inc., New York, 1960).

[12] C. E. Moore, Natl. Bur. Standards (U. S.), Circ. No. 467, **I** (1949).

[13] C. E. Moore, Natl. Bur. Standards (U. S.), Circ. No. 467, **II** (1952).

TABLE I. Partial pressures of species in equilibrium with Cr_2O_3(s): Dissociation energies of CrO and CrO_2.

T°K	P_{Cr} (atm)	P_{CrO} (atm)	P_{CrO_2} (atm)	P_{O_2} (atm)	P_O (atm)	$D_0°(CrO)$ kcal/mole	$D_0°(CrO_2)$ kcal/mole
1839	4.30×10^{-7}	8.24×10^{-8}	9.08×10^{-8}	2.24×10^{-8}	5.25×10^{-8}	100.1	226.2
1862	7.08×10^{-7}	1.63×10^{-7}	1.77×10^{-7}	3.18×10^{-8}	8.12×10^{-8}	100.7	226.9
1883	1.08×10^{-6}	2.51×10^{-7}	1.82×10^{-7}	2.25×10^{-8}	1.37×10^{-7}	101.3	227.9
1887	1.08×10^{-6}	2.44×10^{-7}	2.80×10^{-7}	5.06×10^{-8}	1.57×10^{-7}	100.3	226.7
1917	1.88×10^{-6}	4.44×10^{-7}	3.19×10^{-7}	4.79×10^{-8}	2.05×10^{-7}	101.3	227.0
1925	2.20×10^{-6}	5.53×10^{-7}	5.79×10^{-7}	6.57×10^{-8}	2.65×10^{-7}	101.1	227.9
1936	2.90×10^{-6}	7.42×10^{-7}	5.32×10^{-7}	6.92×10^{-8}	3.22×10^{-7}	101.3	226.9
1939	2.93×10^{-6}	7.69×10^{-7}	5.33×10^{-7}	7.04×10^{-8}	3.19×10^{-7}	101.4	227.0
1959	3.98×10^{-6}	1.08×10^{-6}	1.10×10^{-6}	8.58×10^{-8}	4.30×10^{-7}	101.6	228.9
1963	4.60×10^{-6}	1.24×10^{-6}	8.20×10^{-7}	1.00×10^{-7}	5.00×10^{-7}	101.5	226.9
1998	7.75×10^{-6}	2.03×10^{-6}	1.33×10^{-6}	1.64×10^{-7}	8.40×10^{-7}	101.1	226.6
2029	1.19×10^{-5}	3.44×10^{-6}	2.09×10^{-6}	2.43×10^{-7}	1.34×10^{-6}	101.3	226.8
2059	1.83×10^{-5}	5.58×10^{-6}	3.51×10^{-6}	4.10×10^{-7}	2.10×10^{-6}	101.1	226.6

TABLE II. Dissociation energies of CrO, CrO_2, and CrO_3 determined under oxidizing conditions.

T°K	P_{Cr} (atm)	P_{CrO} (atm)	P_{CrO_2} (atm)	P_{CrO_3} (atm)	P_{O_2} (atm)	P_O (atm)	$D_0°(CrO)$ kcal/mole	$D_0°(CrO_2)$ kcal/mole	$D_0°(CrO_3)$ kcal/mole
1890	3.24×10^{-8}	4.20×10^{-8}	6.39×10^{-7}	1.18×10^{-8}	2.57×10^{-6}	1.36×10^{-6}	99.6	228.4	340.6
1911	5.91×10^{-8}	7.85×10^{-8}	8.38×10^{-7}	1.24×10^{-8}	2.28×10^{-6}	1.53×10^{-6}	100.4	228.8	341.1
1942	1.11×10^{-7}	1.44×10^{-7}	1.28×10^{-6}	1.51×10^{-8}	3.68×10^{-6}	1.92×10^{-6}	101.0	227.9	342.5

tions[14] used in the calculations were: Cr=28.1; O=3.29; O_2=6.58; CrO=31.4; CrO_2=34.7; CrO_3=38.0; and Ag=34.8. The quantitative vaporization of a known amount of silver was used to determine the sensitivity of the mass spectrometer.

Pressure data for the neutral Cr_2O_3 system are presented in Table I and Fig. 1. Table I presents only those partial pressures of Cr, CrO, CrO_2, and O measured simultaneously at the same temperatures, while Fig. 1 presents all the data taken in several experiments. The data taken under oxidizing conditions are presented in Table II.

DISCUSSION

The present work is in substantial agreement with the prediction of Brewer[1] with regard to the vapor species observed over Cr_2O_3(s). The reproducibility and constancy of ion intensities over long periods of time indicate an invariant system.

Dissociation energies for CrO and CrO_2 which were obtained from the neutral vaporization studies are listed in Table I. The free energy functions used in these calculations were taken from Stull and Sinke[15] in the case of Cr(g) and O(g). For CrO(g) and CrO_2(g), the free energy functions of Brewer and Chandrasekharaiah[16,17] were employed. These were determined by use of the vibrational frequency of ω=895.5 cm^{-1}, and an interatomic distance of r_e=1.627 A.[18] For the calculation of the CrO_2 free energy functions, a linear model was assumed with fundamental frequencies of ω_1=785 cm^{-1}, ω_2=259 cm^{-1}, and ω_3=996 cm^{-1} which were obtained using a valence force method. The value of the interatomic Cr–O distance was assumed to be the same in CrO_2 as for CrO. Similarly, free energy functions for CrO_3 were estimated from a planar symmetric model with a Cr–O distance of 1.627 A and vibrational frequencies of ω_1=875 cm^{-1}, ω_2=500 cm^{-1}, ω_3=920 cm^{-1}, and ω_4=425 cm^{-1}. As a verification of the dissociation energies obtained under neutral conditions, dissociation energies for CrO, CrO_2, and CrO_3 were determined under oxidizing conditions and these values are summarized in Table II. A slight, but unexplained, temperature trend is noted in these data. With the exception of CrO_3 which can be measured only under oxidiz-

[14] J. W. Otvos and D. P. Stevenson, J. Am. Chem. Soc. **78**, 546 (1956).
[15] D. R. Stull and G. C. Sinke, Advances in Chem. Ser. No. 18 78, 144 (1956).
[16] L. Brewer and M. S. Chandrasekharaiah, UCRL-8713 (Rev.) 1960.
[17] M. S. Chandrasekharaiah and L. Brewer, UCRL-8736 (1959).
[18] M. Ninomiya, J. Phys. Soc. Japan **10**, 829 (1955).

ing conditions, the dissociation energies obtained under neutral conditions are considered the most reliable since fragmentation corrections are small under these conditions.

The average third-law dissociation energy, $D_0°(CrO)$, which is calculated from the ΔH_0^b for the reaction $CrO(g) \rightarrow Cr(g) + \frac{1}{2}O_2(g)$ and the dissociation energy of O_2[15], is 101.1 ± 7 kcal/mole, whereas the second-law least-squares value is 97.2 kcal/mole. Using the reaction $CrO(g) \rightarrow Cr(g) + O(g)$, one calculates the third law $D_0°(CrO)$ to be 97.4 kcal/mole, while the second-law least-squares value is 101 kcal/mole. The $D_0°(CrO) = 101.1 \pm 7$ kcal/mole is considered to be the most reliable value. The linear Birge-Sponer extrapolation method used by Ghosh[4] to obtain a value of $D_0° = 87.2$ kcal/mole is acknowledged to be of limited value in many cases. As was noted earlier, Huldt *et al.* first reported a $D_0°(CrO)$ of 101 kcal/mole. But, on re-examination and in consideration of the transition probabilities measured by Estabrook,[19] these workers revised their value to 122 kcal/mole. The redetermined value brings Huldt *et al.* into agreement with the somewhat earlier calculation of Brewer.[6] A prime assumption in the determination of dissociation energies by the flame technique used by Huldt *et al.* is that the only gas phase species containing chromium are Cr and CrO. At the oxygen partial pressures mentioned by Huldt *et al.*, the partial pressure of $CrO_2(g)$ certainly cannot be neglected. Thus, in this particular case, a basic assumption of the calculation is shown to be incorrect. Therefore, it is not surprising that Huldt *et al.* are in disagreement with the presently determined value of 101.1 kcal/mole.

No values for the dissociation energies of CrO_2 and CrO_3 have been reported in the literature. If the $\Delta H_0°$ for the reaction $CrO_2(g) \rightarrow Cr(g) + O_2(g)$ is used in conjunction with $D_0°$ for O_2, the third-law value of the atomization energy of CrO_2 is 227.1 ± 15 kcal/mole. Similarly, for the atomization reaction $CrO_2(g) \rightarrow Cr(g) + 2O(g)$ the third-law value is 220.7 kcal/mole, whereas the second-law value is 231.8 kcal/mole. It is to be noted that the $D_0°(CrO_2)$ calculated from a thermodynamic cycle which uses the reaction $\frac{1}{2}Cr_2O_3(s) + \frac{1}{4}O_2(g) \rightarrow CrO_2(g)$ is 236 kcal/mole. The most plausible explanation of this result appears to be either reduced Cr_2O_3 activity or a nonstoichiometric solid phase. Earlier the heat of vaporization of chromium was considered suspect, but a subsequent measurement of the $\Delta H_0°_{vap}$ by the mass spectrometer yielded a value of 94.2 kcal/mole which shows excellent agreement with the most recent determinations of Gulbransen and Andrew[20] and of Speiser, Johnston, and Blackburn.[21] Because of the reproducibility of the results obtained by gas phase equilibria in both the neutral and oxidizing system, and because the results are independent of the composition of the condensed phase, the gas phase results are considered the most accurate. As in the case of the CrO calculations, the energies calculated by use of the measured O_2 pressures are deemed more reliable than those determined by use of the measured O pressures. Thus the value of $D_0°(CrO_2) = 227.1 \pm 15$ kcal/mole is recommended.

Using the $\Delta H_0°$ for the gas phase reaction $CrO_3(g) \rightarrow Cr(g) + \frac{3}{2}O_2(g)$ and the $D_0°$ for O_2, we obtain 341 ± 20 kcal/mole for $D_0°$ of $CrO_3(g)$.

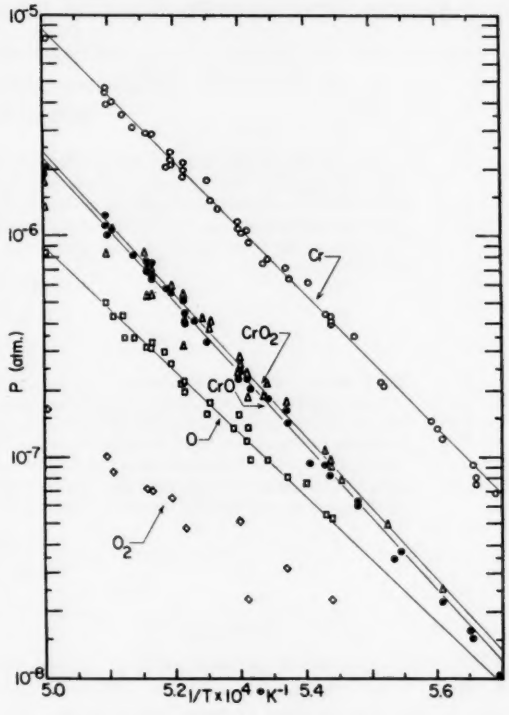

FIG. 1. Partial pressures (atm) of the vapor species over $Cr_2O_3(s)$ under neutral conditions as a function of $1/T \times 10^4$ deg K^{-1}.

[19] F. B. Estabrook, Astrophys. J. **115,** 571 (1952).

[20] E. A. Gulbransen and K. F. Andrew, J. Electrochem. Soc. **99,** 402 (1952).

[21] R. Speiser, H. L. Johnston, and P. Blackburn, J. Am. Chem. Soc. **72,** 4142 (1950).

Vacuum Ultraviolet Photolysis of Ethane: Molecular Detachment of Hydrogen

H. OKABE AND J. R. MCNESBY

National Bureau of Standards, Washington, D. C.

(Received August 16, 1960)

The primary process of direct ethane photolysis by Xe radiation (1470 A and 1295 A) was studied at room temperature. The hydrogen and methane isotopic compositions from a mixture of C_2H_6–C_2D_6 and from CH_3CD_3 were measured mass-spectrometrically. The results show that, contrary to the previously proposed mechanism, almost all (>95%) of the hydrogen is formed intramolecularly, and preferentially from the same carbon atom. Methane is also formed by a molecular process. Then the primary processes may be written as

$$C_2H_6 \rightarrow CH_3CH + H_2 \quad (1)$$

$$C_2H_6 \rightarrow C_2H_4 + H_2 \quad (2)$$

$$C_2H_6 \rightarrow CH_4 + CH_2. \quad (3)$$

The absence of C_2D_6 in the products of the photolysis of CH_3CD_3 places an upper limit on $\varphi_{CD_4}/\varphi_{CD_3H+CH_2D}$ of about unity assuming all methyl radicals form ethane by recombination. The effect of the product ethylene on the composition of hydrogen isotopes from C_2H_6–C_2D_6 mixtures was examined, since any atomic hydrogen produced may be reacting rapidly with ethylene. The sample was purified and very low conversion (0.01%) was made. The result shows almost no change in the composition of the hydrogen isotopes in the products, indicating that the hydrogen forming step is largely molecular. It is suggested that higher hydrocarbons may be produced by the following reactions

$$CH_2 + C_2H_6 \rightarrow C_3H_8 \quad (4)$$

$$CH_3CH + C_2H_6 \rightarrow C_4H_{10}. \quad (5)$$

THE primary process in direct ethane photolysis using xenon resonance readiation (1470 A and 1295 A) has been studied at room temperature. The isotopic compositions of the hydrogen and methane (present to the extent of 3% of the hydrogen) products were measured in photolysis of C_2H–C_2D mixtures and in CH_3CD_3.

Current views on the primary process in ethane photolysis are due to Faltings[1]

$$C_2H_6 \xrightarrow{h\nu} 2CH_3 \quad (1)$$

and to Wijnen[2]

$$C_2H_6 \xrightarrow{h\nu} C_2H_5 + H. \quad (2)$$

Such primary processes seemed necessary to explain the appearance of the major products, hydrogen, methane, ethylene, propane, and butane.

EXPERIMENTAL

A water-cooled xenon resonance lamp with nickel electrodes containing 20μ of Xe and 1 mm of Ne was used as the radiation source. The pressure of ethane was measured with an Alphatron gauge. A filter cell situated between the lamp and reaction vessel was either evacuated or filled with methane to remove the 1295-A resonance line. Lithium fluoride windows were used to isolate the lamp, filter cell, and reaction vessel. The latter was about 4 cm in diameter and 15 cm in length and was connected to a Toepler pumping system by means of a brass bellows valve. Both the reaction vessel and the lamp were prevented from becoming contaminated with mercury vapor by means of an oil diffusion pump. A vacuum ultraviolet monochromator was employed to demonstrate the absence of the 1849-A line of mercury. Only the fraction of products volatile at 77°K was pumped into the sample flask for mass spectrometer analysis. Phillips research-grade ethane and Merck C_2D_6 and CH_3CD_3 were used in this work. Specifications on the deuterated materials were 99% D/(D+H).

RESULTS AND DISCUSSION

The experiments we wish to report are summarized in Table I and provide evidence for an entirely different mechanism of ethane photolysis.

Hydrogen Analysis

It is apparent that H_2 and D_2 are the major hydrogen species formed in photolysis of C_2H_6—C_2D_6 mixtures. The presence of only minor amounts of HD indicates that hydrogen is mainly formed intramolecularly. This conclusion, of course, requires the assumption that the primary processes are the same for both C_2H_6 and C_2D_6 photolysis. The C_2D_6 contained 6.5% C_2D_5H, a sufficiently large impurity to account for much of the HD, on the basis of an entirely intramolecular mechanism. An additional observation of interest is the isotope effect amounting to a factor of two in favor of H_2.

The question of the detailed way in which H_2 and D_2 are formed was investigated by means of the photol-

[1] K. Faltings, Ber. deut. Chem. ges. **72B**, 1207 (1939).
[2] M. H. J. Wijnen, J. Chem. Phys. **24**, 851 (1956).

TABLE I. Photolysis of ethane with Xe resonance radiation at room temperature.

(A) C_2H_6—C_2D_6 mixture

	Ethane press. (mm Hg)		Exposure time	Decomposition[d]	Isotopic analysis (percent) Hydrogen			Methane[e]			
Expt.	C_2H_6	C_2D_6	(min)	%	H_2	HD	D_2	CH_4	CH_3D	CD_3H	CD_4
1	18.7	15.4	200	1.0	69.6	1.9	28.5	65	5	7	23
2[a]	19.7	17.7	120	0.8	66.9	1.7	31.3	71	9	3	17
3[b]	19.2	13.0	90	0.4	73.7	1.6	24.6	68	12	Trace	20
4	15.1	20.2	60	0.3	58.1	3.3	38.5	58	4	8	30
5[c]	16.8	11.0	1	0.05	82.0	2.5	15.5	...	...	...	...
6[c]	27.8	47.0	0.5	0.01	56.3	3.7	40.0	...	...	...	...

(B) CH_3CD_3

Expt.	Ethane press. (mm Hg)	Exposure time (min)	Decomposition (%)	Isotopic analysis of hydrogen (%) H_2	HD	D_2
7	7.5	60	2.0	58.6	16.4	25.0
8	40.8	170	0.3	58.5	16.9	24.6

[a] Methane filter was used to isolate radiation at 1470-A wavelength.

[b] The sample was preirradiated for 2 hr and the noncondensable products at −195°C were pumped off.

[c] The sample was purified. Traces of ethylene were removed by means of gas chromatography.

[d] Percent decomposition is not strictly related to exposure time since the lamp intensity was not constant from experiment to experiment. The values are based upon ϕ hydrogen = 1.

[e] Since the amount of methane produced is small (~3% of hydrogen) the analysis is less accurate than that of hydrogen. Light intensity at the front window of reaction vessels ~10^{14} quanta sec^{-1} cm^{-2}.

ysis of CH_3CD_3. If the mechanism is

$$CH_3CD_3 \xrightarrow{h\nu} CH_2\overset{H\cdots D}{\cdots}CD_2 \rightarrow HD + CH_2CD_2, \qquad (3)$$

only HD should be observed. However if both hydrogen atoms come from the same carbon atom the reactions are

$$CH_3CD_3 \xrightarrow{h\nu} H_2 + CHCD_3 \qquad (4)$$

$$CH_3CD_3 \xrightarrow{h\nu} D_2 + CH_3CD. \qquad (5)$$

Experiments (7) and (8), in which H_2 and D_2 are seen to be the predominant species, show that reactions (4) and (5) are responsible for the production of most of the intramolecularly formed hydrogen with (3) playing a minor role. The source of ethylene would then be isomerization of ethylidene.

Methane Analysis

In the C_2H_6—C_2D_6 experiments, it is evident that CH_4 and CD_4 are the predominant methanes. The absence of C_2D_6 in the products of the photolysis of CH_3CD_3 places an upper limit on $\phi_{CD_4}/\phi_{CD_3H+CH_3D}$ of about unity assuming all methyl radicals form ethane by recombination.

Back[3,4] has called attention to the possibility that any H atoms produced might be scavenged by small ethylene impurities or by ethylene produced in the reaction. He concludes that H atoms will not be scavenged effectively if the reactants are pure and if the extent of reaction is less than 0.05%. Experiments (5) and (6) were carried out on ethylene free mixtures of C_2H_6 and C_2D_6 at very low conversions and it is found that the percentage of HD is not greatly increased, although the question is somewhat obscured by the rise in the percentage of H_2. The proportion of H_2 fluctuates in these two experiments probably because of the varying amounts of H_2 impurity in the samples.

The isotopic methanes produced imply they are formed by reactions like (6)

$$CH_3CH_3 \rightarrow CH_4 + CH_2. \qquad (6)$$

It is of interest to speculate on the mechanism of formation of propane and butane, since evidence for methyl and ethyl radicals is negative. The mechanism proposed is

$$CH_2 + C_2H_6 \rightarrow CH_3CH_2CH_3 \qquad (7)$$

$$CH_3CH + C_2H_6 \rightarrow CH_3CH_2CH_2CH_3. \qquad (8)$$

It is therefore suggested that the chemistry subsequent to the primary process is controlled largely by methylene and ethylidene insertion reactions.[5]

[3] R. A. Back, Can. J. Chem. **37**, 1834 (1959).

[4] R. A. Back, J. Phys. Chem. **64**, 124 (1960).

[5] For a summary, see A. F. Trotman-Dickenson, *Free Radicals* (Methuen and Co., Ltd., London, 1959), p. 125.

Pressure Induced Color Centers in CaF_2 and BaF_2†

S. MINOMURA AND H. G. DRICKAMER

Department of Chemistry and Chemical Engineering, University of Illinois, Urbana, Illinois

(Received July 29, 1960)

The effect of pressure to 52 800 atm has been studied on x-irradiated CaF_2 and BaF.. The three bands discovered by Smakula are little affected by pressure or bleaching. There are two new bands induced by pressure, which are greatly enhanced by any change in pressure. These bands show a marked blue shift with increasing pressure. Each can be bleached by light of its own frequency, and restored by reapplication of pressure. It is suggested that the pressure-induced bands are due to electrons associated with pressure-induced lattice defects, while the bands discovered by Smakula are associated with colloidal deposits or impurities.

INTRODUCTION

SMAKULA[1] has studied three absorption bands of the color centers produced in CaF_2 and BaF_2 crystals by x-ray irradiation in the region from 220 mμ to 1000 mμ (580 mμ, 400 mμ, and 335 mμ in CaF_2; 670 mμ, 480 mμ, and 380 mμ in BaF_2). On the other hand, Mollwo[2] has found two absorption bands in natural CaF_2 crystals by additive coloring (525 mμ and 370 mμ). According to Smakula, as compared with alkali halides, the absorption spectra of colored CaF_2 and BaF_2 show some similar and some different properties and the nature of the color centers may be generally the same as in alkali halides with electrons trapped in lattice defects.

The authors have measured the effect of pressure on the absorption bands of the color centers produced in CaF_2 and BaF_2 crystals by x-ray irradiation up to 52 800 atm and found two pressure-induced absorption bands in each crystal. The frequency shift, the intensity change with pressure, and the light bleaching for the new absorption bands are discussed.

EXPERIMENTAL PROCEDURE

Harshaw synthetic CaF_2 and BaF_2 crystals and natural CaF_2 crystals were used in this experiment. The crystals were cleaved to the thickness of about 0.5 mm and irradiated by x rays (50 kv, 35 ma) for a time ranging from 60 to 243 hr at a distance of about 25 mm.

The high pressure optical techniques have been discussed previously.[3] The following photomultipliers and

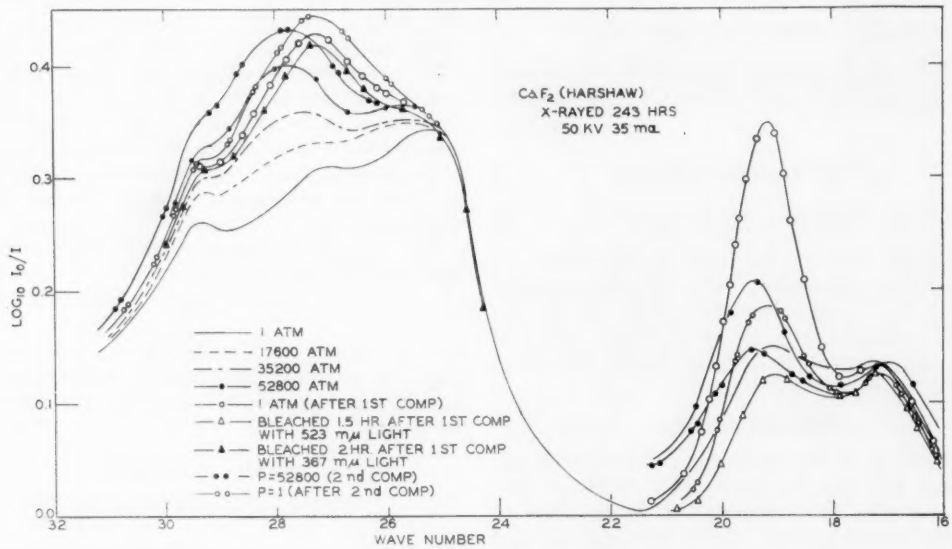

FIG. 1. Spectra of CaF_2.

† This work was supported in part by the U. S. Atomic Energy Commission.

[1] A. Smakula, Phys. Rev. **77**, 408 (1950).

[2] E. Mollwo, Gottingen Nachrichten **1**, 79 (1934).

[3] R. A. Fitch, T. E. Slykhouse, and H. G. Drickamer, J. Opt. Soc. Am. **47**, 1015 (1957).

TABLE I. The absorption peaks of the color centers in CaF_2 and BaF_2 crystals at 1 atm.

CaF_2	mμ	580	523[a]	400	367[a]	340
	cm^{-1}	17241	19125	25000	27250	29411
BaF_2	mμ	660	559[a]	470	420[a]	380
	cm^{-1}	15151	17880	21276	23820	26315

[a] Pressure-induced bands.

light sources were used in three regions of wavelength: RCA7102 and W lamp (1000–600 mμ); RCA1P28 and W lamp (660–400 mμ); and RCA1P28 and H_2 lamp (410–300 mμ).

RESULTS

The peaks of the absorption spectra at one atmosphere of the color centers in CaF_2 and BaF_2 crystals in the region from 1000 mμ to 300 mμ, are given in Table I.

In addition to the three bands found by Smakula there are two pressure-induced bands. Figure 1 shows typical results for CaF_2. The bands in BaF_2 are similar but are shifted to lower energy and have greater overlap. The bands described by Smakula show very little shift and only a small change in intensity with pressure. They are also not very susceptible to bleaching. In contrast to this, the pressure-induced bands grow steadily in intensity with increasing pressure. This growth is accompanied by a shift to higher energy (see Fig. 2). Upon releasing pressure the (pressure-induced) bands return to their original energy, but with a marked further increase of intensity.

The pressure-induced bands can be bleached by light of their own wavelength, but the band at 367 mμ is not bleached by 523 mμ light, and vice versa. There is little bleaching of the Smakula bands. A second compression of the crystal after bleaching restores the bands.

In Fig. 3 are plotted $\ln\nu/\nu_0$ vs $\ln\rho/\rho_0$ for the pressure-induced bands. Bridgman's compressibility data for

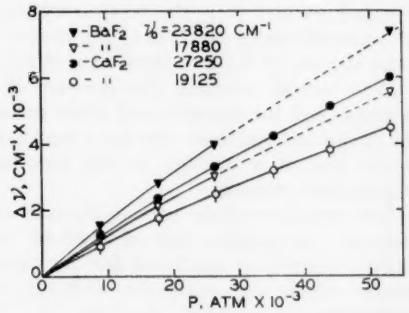

FIG. 2. $\Delta\nu$ vs pressure. Pressure-induced bands in CaF_2 and BaF_2.

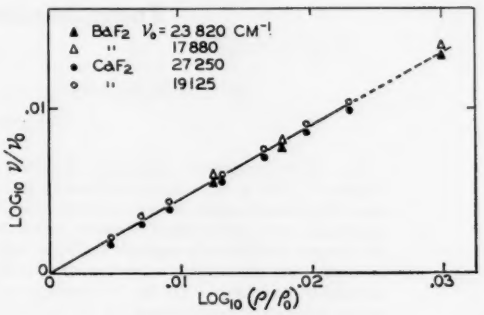

FIG. 3. $\text{Log}_{10}(\nu/\nu_0)$ vs $\log_{10}(\rho/\rho_0)$. Pressure-induced bands in CaF_2 and BaF.

CaF_2[4] to 30 000 kg/cm² and for BaF_2[5] to 12 000 kg/cm² were extrapolated to 52 800 atmospheres.

Within the accuracy of the extrapolation one obtains a straight line of slope 0.444. This slope is somewhat smaller than that obtained for the F or M center in alkali chlorides or bromides[6,7] but the fluorides may well behave differently.

It should be noted that there is apparently a phase transition in BaF_2 near 30 800 atm, as the light cuts off at that point and is restored at 35 200 atm. There seemed to be no discontinuity in the shifts at these pressures.

DISCUSSION

The properties of the pressure-induced bands (the shift to higher frequency with increasing pressure, the growth with pressure change, and the bleaching) all indicate that these centers are associated with electrons trapped at lattice defects. From the bleaching characteristics there is no connection between the high and low energy centers such as that between the F and M centers in alkali halides.

The bands consistent with Smakula's observations seem to be associated with colloidal metal deposits or impurity ions in the lattice.

The pressure-induced color centers are probably formed by dispersion of electrons from colloidal metal to pressure-induced lattice defects by processes such as the following

$$\text{Ca}+2V^-\rightarrow\text{Ca}^{++}+2(V^-+e),$$

where V^- is a negative ion vacancy, e is an electron, and (V^-+e) is a color center. The process is not reversible with pressure at room temperature, but the electrons are released from the color centers by light of the appropriate energy.

[4] P. W. Bridgman, Proc. Am. Acad. Arts Sci. **77**, 187 (1949).
[5] P. W. Bridgman, *The Physics of High Pressure* (G. Bell and Sons, Ltd., London, 1949), p. 163.
[6] R. A. Eppler and H. G. Drickamer, J. Chem. Phys. **33**, 1734 (1960).
[7] S. Minomura and H. G. Drickamer, J. Chem. Phys. **33**, 290 (1960).

Thermoluminescence in Dolomite

W. L. MEDLIN

Socony Mobil Oil Company, Inc., Field Research Laboratory, Dallas, Texas

(Received August 8, 1960)

The thermoluminescent properties of dolomite have been investigated by coprecipitating impurities which are likely to serve as activators with an otherwise pure sample. Only impurities which are likely to occur in natural samples were considered. The effects of cation and anion vacancies were also investigated and found to be unimportant. Divalent manganese was found to be the only activator of importance and its presence satisfactorily explains the important features of glow curves for natural samples. The results of luminescent efficiency as a function of activator concentration were determined. It was found that concentration quenching of the Mn^{++} luminescence is characteristic of an isolated activator site. Quenching of the manganese luminescence by Fe^{++}, Co^{++}, and Ni^{++} was also observed and quantitative results were compiled. All impurity ion concentrations were determined by colorimetric procedures. The presence of Co^{++} or Ni^{++} with Mn^{++} produces high-temperature glow peaks which roughly coincide with similar peaks observed in natural samples. However, it appears more likely that the peaks in natural samples are due to lattice defects resulting from deformation pressures. Isothermal decay curves were measured for all of the glow peaks due to Mn^{++} and found to have the form predicted for a second-order decay process. However, the behavior of one of the decay parameters as a function of activation time is different from the predicted behavior. The trap depth energies and frequency factors associated with most of the glow peaks due to Mn^{++} have also been determined.

I. INTRODUCTION

THIS work is a continuation of studies of the thermoluminescent properties of common rock minerals. Previous articles describing the properties of calcite[1] and anhydrite[2] have established the importance of a few impurity ions in accounting for most of the thermoluminescent characteristics in these crystals. It has also been shown that some nonimpurity defects such as vacancies, etc., are of importance.

In order to determine which of the impurities commonly found in natural samples can influence the thermoluminescent properties, it is necessary to develop a means of adding each impurity to an otherwise pure synthetic sample. In dolomite, as in calcite, the methods for doing this are practically limited to coprecipitation techniques since decomposition of the mineral at temperatures as low as 450°C prevents the use of diffusion methods. Until recently a means of precipitating dolomite from solution was not available. However, a recently published paper[3] describes a method which has proved to be satisfactory for this purpose.

The thermoluminescent characteristics of the dolomite samples were studied by means of glow curves and isothermal decay measurements.[4] The activation source was an Mo x-ray tube operated at 35 kv and 20 ma. All of the samples were activated for 5 min for the glow curve measurements which were made at a heating rate of 0.5 deg/sec. X-ray powder patterns were obtained for all of the synthetic samples in order to eliminate samples where the crystallinity was poor or where there was any trace of other minerals such as calcite or magnesite.

[1] W. L. Medlin, J. Chem. Phys. **30**, 451 (1959).
[2] W. L. Medlin, Phys. and Chem. Solids (to be published).
[3] W. L. Medlin, Am. Mineral **44**, 979 (1959).
[4] W. L. Medlin, J. Chem. Phys. (to be published).

II. EXPERIMENTAL PROCEDURE AND RESULTS

Dolomite samples containing no more than 20 ppm of any undesired impurity were prepared by slowly raising the *p*H of a calcium chloride-magnesium chloride solution at an elevated temperature and CO_2 pressure. The magnesium chloride solution was prepared from high-purity magnesium rods and the calcium chloride solution was prepared from high-purity $CaCO_3$ reagent.[5]

The dolomite precipitations were carried out in a 1-liter autoclave and required 12 hr for completion at 220°C and 60 atm CO_2 pressure. The sample solutions contained 0.04 g/ml urea, 0.1 g/ml NaCl, 0.5 g/ml calcium, and 0.18 g/ml magnesium as chlorides The presence of the urea which controls the *p*H of the solution at elevated temperatures, results in corrosion of the stainless steel walls of the autoclave chamber. To prevent contamination by these corrosion products the sample solutions were placed in Pyrex test tubes with glass covers. The water level in the autoclave chamber (for thermal contact with the walls) was kept low enough to remain below the tops of the sample tubes. Dolomite samples of 0.5 g or more were obtained by using 25-ml sample solutions. The presence of NaCl which suppressed the formation of other carbonates such as calcite and magnesite was not a source of contamination since it is available in very pure form in the reagent-grade material.

The concentrations of the various impurity ions in the dolomite precipitates were determined by the colorimetric procedures developed for the calcite investigation[1] which were applicable with only a few minor changes.

[5] Both the magnesium rods and the $CaCO_3$ reagent were supplied by Johnson Mathey Company, London.

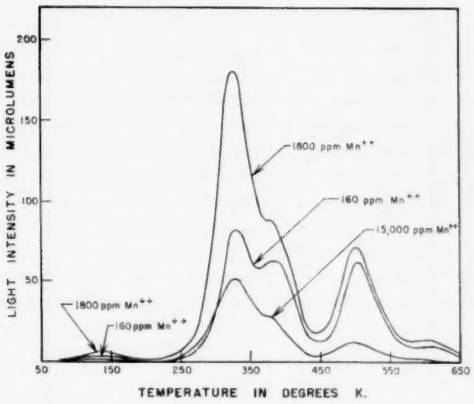

FIG. 1. Glow curves for synthetic dolomite samples containing various concentrations of Mn^{++}.

Of the impurities which normally occur in natural dolomite samples, Mn^{++} was the only ion which produced thermoluminescence. Other ions which were investigated were Pb^{++}, Zn^{++}, Cd^{++}, Sb^{+++}, Co^{++}, Ni^{++}, Fe^{++}, Fe^{+++}, Bi^{+++}, Cu^{++}, Li^{+}, Al^{+++}, Ag^{+}, and Sn^{++}. All of these impurities were added as chlorides except for Ag^{+} and Pb^{++} whose chlorides are insoluble. These ions were added as nitrates to $CaNO_3$ and $MgNO_3$ solutions and $NaNO_3$ was substituted for NaCl without any adverse effects.[5]

Since it is well known that the presence of divalent ions in the monovalent lattices of the alkali halides provides cation and anion vacancies, it is reasonable to assume that omission defects will be introduced in dolomite by the inclusion of quadrivalent ions. The addition of Sn^{4+} ions to produce cation vacancies and $P_2O_7^{4-}$ ions to provide anion vacancies had no effect on the glow curve. Therefore it is doubtful that vacancy defects account for any of the glow peaks observed in natural samples.

The presence of Mn^{++} in the dolomite lattice results in four distinct glow peaks at 330°K, 380°K, 500°K, and 600°K and one very broad, low-temperature peak

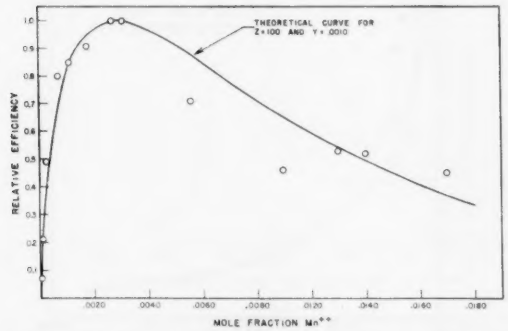

FIG. 2. Efficiency of thermoluminescence as a function of activator concentration for the 330°K glow peak due to Mn^{++}.

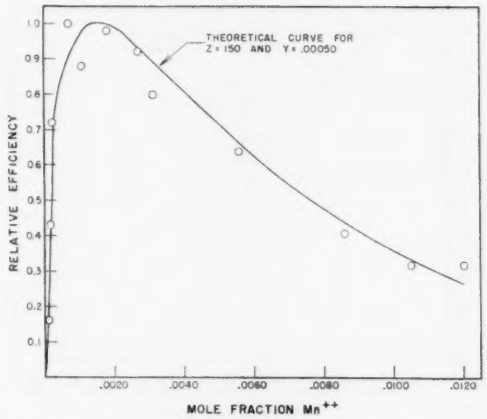

FIG. 3. Efficiency of thermoluminescence as a function of activator concentration for the 380°K glow peak due to Mn^{++}.

at about 140°K. These are illustrated in Fig. 1 for three different Mn^{++} concentrations. The broad peak which appears at 140°K for low concentrations is replaced by an almost continuous level of emission from 77°K to 250°K as the Mn^{++} concentration is increased. The glow peaks at 330°K, 380°K, and 500°K are of roughly equal intensity at low Mn^{++} concentrations but at higher concentrations the 330°K peak becomes more prominent and obscures the 380°K peak to some extent.

The results of annealing the dolomite samples at temperatures near the decomposition range had no effect on the glow curves. The samples were heated for two hours at temperatures up to 450°C.

Plots of relative intensity of emission vs Mn^{++} concentration are shown in Figs. 2–5 for the 330°K, 380°K, 500°K, and 600°K glow peaks, respectively. The theoretical curves shown here are based on the relation for concentration quenching derived by Johnson and Williams,[6]

$$\eta = \{c(1-c)^z/[c+\gamma(1-c)]\},$$

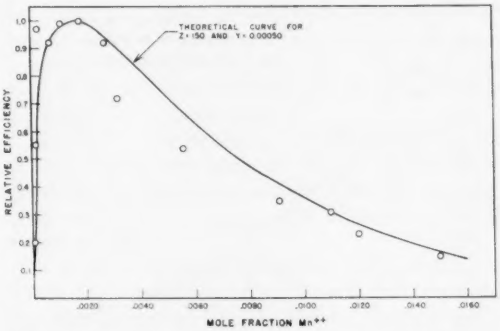

FIG. 4. Efficiency of thermoluminescence as a function of activator concentration for the 500°K glow peak due to Mn^{++}.

[6] P. D. Johnson and F. E. Williams, J. Chem. Phys. **18**, 1477 (1950).

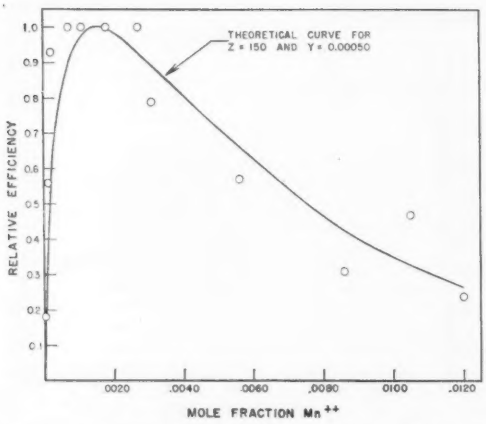

FIG. 5. Efficiency of thermoluminescence as a function of activator concentration for the 600°K glow peak due to Mn^{++}.

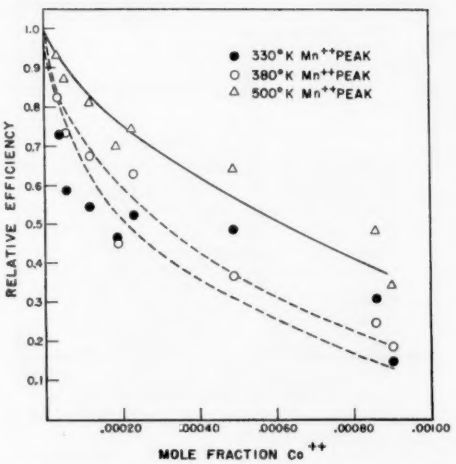

FIG. 7. Quenching effect due to Co^{++} in the presence of Mn^{++}.

where η is the efficiency of luminescence and c is the activator concentration. The best fit to the experimental points was obtained by varying the parameters z and γ. The value assigned to z represents the number of nearest neighbor cation sites surrounding a Mn^{++} impurity site which cannot be occupied by another Mn^{++} ion without quenching the luminescence. The values obtained for the Mn^{++} peaks in dolomite are of the same order as those determined for Mn^{++} in calcite.[1]

The results for the 380°K peak were obtained by initially warming the samples at the normal rate (0.5 deg/sec) to 360°K and then cooling rapidly to 300°K. This procedure empties nearly all of the traps corresponding to the 330°K glow peak and thus removes this source of interference.

The quenching effects of Fe^{++}, Fe^{+++}, Co^{++}, and Ni^{++} were investigated by coprecipitating various concentrations of each of these impurities with constant amounts of Mn^{++}. The Mn^{++} concentration was maintained within suitable limits of 0.003 mole percent which corresponds approximately to the optimum concentration for all of the Mn^{++} glow peaks (cf. Figs. 2–5).

It was found that Fe^{++}, Co^{++}, and Ni^{++} are all effective in suppressing the Mn^{++} luminescence but Fe^{+++} has no effect. The relative effects of Fe^{++}, Co^{++}, and Ni^{++} are illustrated in Figs. 6, 7, and 8, respectively for the 330°K, 350°K, and 500°K glow peaks due to Mn^{++}.

The presence of appreciable quantities of FeO and Fe_2O_3 resulted in some absorption of the Mn^{++} luminescence in samples containing Fe^{++} or Fe^{+++}. To account for this a thermoluminescent internal standard was mixed with these samples to provide a suitable normalization factor. The standard used for

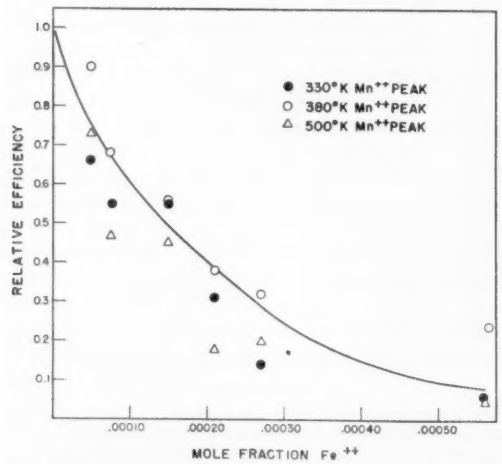

FIG. 6. Quenching effect due to Fe^{++} in the presence of Mn^{++}.

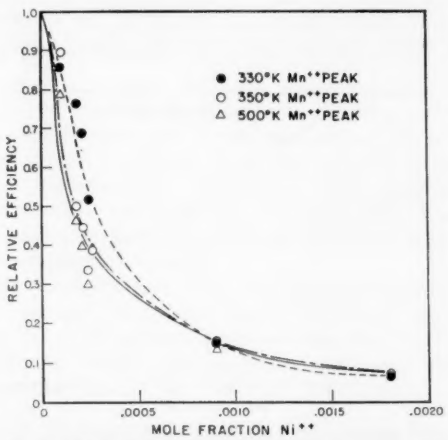

FIG. 8. Quenching effect due to Ni^{++} in the presence of Mn^{++}.

this purpose was $CaSO_4$ containing approximately 100 ppm Sb^{+++}. The glow curve for this material has been thoroughly investigated and consists of two glow peaks at 200°K and 350°K.[2] The latter peak is the most prominent and was used for the normalization corrections. This method is subject to errors as large as 20% and therefore is useful in correcting for only rather large discrepancies. The errors in this case include those which are inherent in repeating glow peak intensities (5–10%) as well as errors in adding the proper amount of internal standard to the samples. Since thermoluminescence is primarily a volume effect, it is not completely correct to add the standard on a weight basis (the procedure used here) since the sample density varies with average crystal size. The corrections for the data of Fig. 6 amounted to factors as large as 2.5 for the largest Fe^{++} concentrations.

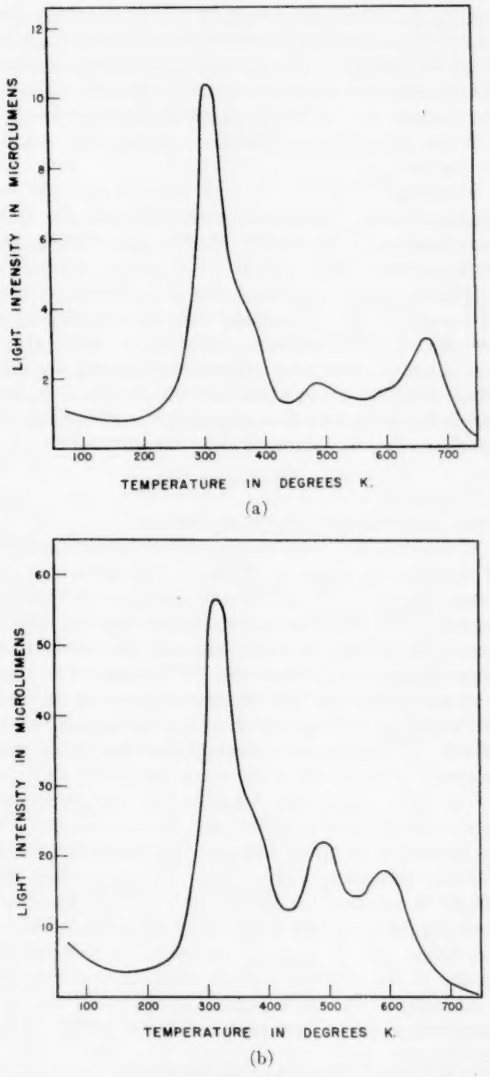

FIG. 9. (a) Glow curves for synthetic dolomite sample containing Co^{++} in the presence of Mn^{++}. (b) Glow curve for synthetic dolomite sample containing Ni^{++} in the presence of Mn^{++}.

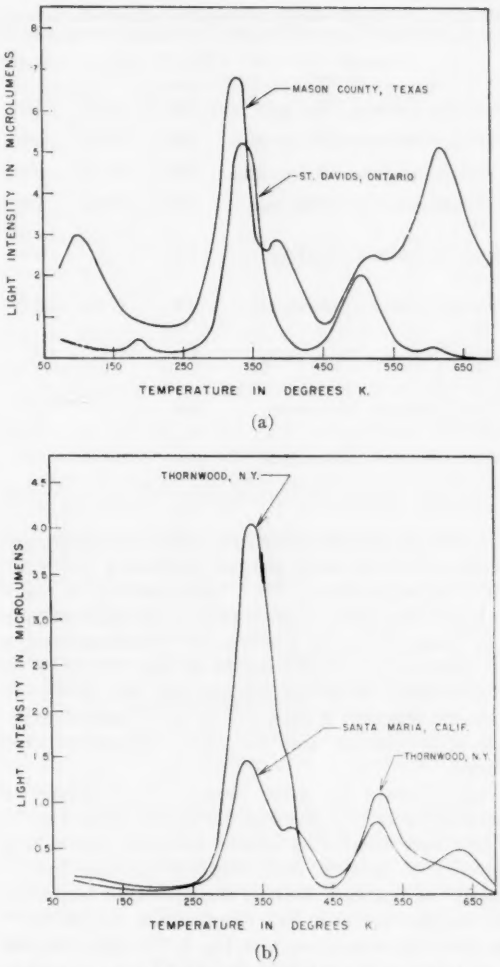

FIG. 10. (a) and (b) Glow curves for some natural dolomite samples.

The Mn^{++} concentration was determined for each of the samples containing Fe, Co, or Ni and it was found that the variations involved (300–500 ppm) were small enough to be neglected in accordance with the results of Figs. 2–5.

In addition to suppressing the 330°K, 380°K, and 500°K Mn^{++} glow peaks, Co^{++} and Ni^{++} introduce new high-temperature peaks in the presence of Mn^{++}. For Co^{++} the result appears as an enhancement of the 600°K glow peak due to Mn^{++} whereas Ni^{++} introduces a new peak at 660°K. In both cases the original Mn^{++} peak at 600°K is masked to such an extent that

TABLE I. Trap depth energy and frequency factor measurements.

Sample	T_g in °K	$\mathcal{E}$ in ev	ν in sec^{-1}
Synthetic dolomite (1100 ppm Mn)	330	0.55	10^7
Synthetic dolomite (1100 ppm Mn)	500	1.3	10^{11}
Synthetic dolomite (1100 ppm Mn)	600	1.7	10^{12}
Synthetic dolomite (11 000 ppm Mn)	330	0.50	10^7
Synthetic dolomite (11 000 ppm Mn)	500	1.2	10^{10}
Synthetic dolomite (11 000 ppm Mn)	600	1.5	10^{10}
Natural dolomite (Thornwood, N. Y.)	330	0.54	10^7
Natural dolomite (Thornwood, N. Y.)	500	1.4	10^{12}
Natural dolomite (Thornwood, N. Y.)	600	1.7	10^{12}

it cannot be determined whether it has been suppressed. Glow curves for some samples containing Co^{++} and Ci^{++} in the presence of Mn^{++} are illustrated in Fig. 9.

For a fixed Mn^{++} concentration the high-temperature peaks vary with Co^{++} or Ni^{++} concentration in the same manner as the curves of Figs. 2–5 which are characteristic of an isolated activator ion. Similar results are observed if the Co^{++} or Ni^{++} concentrations are held constant and the Mn^{++} concentration is varied.

Glow curves for some representative samples of naturally occurring dolomite are illustrated in Fig. 10. These were selected as typical examples from a large number of outcrop and well-core samples from a variety of locations. Most of the significant features of all the glow curves in Fig. 10 are clearly due to Mn^{++} as shown by comparison with Fig. 1. The high-temperature peaks between 600°K and 650°K are exceptions. They could be explained by the presence of Co^{++} or Ni^{++} (cf. Fig. 9) but spectrographic analysis has shown that none of the natural samples contained sufficient quantities of these impurities to account for the observed intensities. It seems more likely that the peaks are due to lattice defects produced by deformation strains of the type described by Handin *et al.*[7] for calcite. In support of this it was observed that these peaks generally occurred in well-core specimens where such deformations are prevalent and were not usually found in outcrop samples.

The minor peak at 180°K in the glow curve of the St. Davids, Ontario, sample in Fig. 10 was also observed in occasional synthetic samples. However, its appearance could not be correlated with the presence of any particular impurity and it is probably associated with some type of nonimpurity defect. Another point of interest is the suppressed intensity of the 380°K peak in the St. Davids, Ontario, sample. It may be significant that this particular sample was much better crystallized than any of the others.

In general, the intensity of thermoluminescence in natural samples is lower by one or two orders of magnitude than the levels observed for synthetic samples containing the optimum amount of manganese. Spectrographic analyses have shown that this is the result of the relatively low Mn^{++} concentrations (10–100 ppm) as well as the presence of iron in most of the samples.

The results obtained here are of interest in interpreting the correlations reported by Lewis[8] for the glow peaks in natural samples of calcite-dolomite mixtures. From the results of the present study and the previous investigation of calcite[1] it is clear that the observed correlations are due solely to mineralogical differences and are not related to differences in impurity content in the two minerals.

Empirical values of the trap depth $\mathcal{E}$ and the frequency factor ν have been determined for the traps associated with the 330°K, 500°K, and 600°K glow peaks due to Mn^{++}. Values for $\mathcal{E}$ were determined graphically from the initial rise in intensity for each of the glow peaks. Assuming that the trapping levels are discrete, the emission intensity at temperatures well below the glow peak is proportional to $\exp(-\mathcal{E}/kT)$ where k is Boltzmann's constant and T is the temperature.[9] Assuming that there is negligible retrapping, the value of ν can be computed from the relation[10]

$$\nu = (\mathcal{E}/kT_g)\exp(\mathcal{E}/kT_g),$$

where T_g is the glow peak temperature.

The results for some synthetic and natural samples of dolomite are given in Table I. The agreement between the synthetic and natural samples is within the limits of experimental error. Values for the 380°K Mn^{++} peak were not obtainable by this method because of interference from the 330°K peak.

It can be observed that the low-temperature emission (77°K–250°K) due to Mn^{++} cannot be completely removed by heating to temperatures less than that required to empty all of the traps associated with the 330°K Mn^{++} peak. For example, in a sample heated at the normal rate to 300°K and then cooled to 77°K by immersion in liquid nitrogen, the low-temperature emission reappears with reduced intensity when the sample is reheated. A similar phenomenon has been observed for traps due to Zn^{++} in anhydrite.[2] Since a correlation can be observed between the reduced intensity of the low-temperature emission and the loss in intensity of the 330°K peak, it appears that thermal transitions occur at temperatures below 330°K which

[7] J. Handin, D. V. Higgins, D. R. Lewis, and P. K. Weyl, Bull. Geol. Soc. Am. **66**, 1571 (1955).

[8] D. R. Lewis, J. Phys. Chem. **60**, 698 (1956).

[9] J. T. Randall and M. H. F. Wilkins, Proc. Roy. Soc. (London) **184A**, 390 (1945).

[10] E. I. Adirovitch, J. phys. radium **17**, 705 (1956).

transfer electrons from the deeper to the shallower traps. It would be expected, on the basis of this explanation, that the traps corresponding to the 330°K peak could be emptied at an appreciable rate at temperatures well below the glow peak. This has been confirmed by annealing activated samples at temperatures as low as 200°K where it is observed that the rate of emptying the traps for the 330°K peak is much faster than predicted for the measured value of δ (cf. Table I). Incidentally, the same phenomenon occurs in the calcite-Mn^{++} system where a low-temperature emission (77°K–230°K) is reproduced under the conditions described above provided the traps associated with a peak at 340°K are not all emptied.

The decay of luminescence as a function of time at constant temperature has been investigated for all of the glow peaks in dolomite and has the form predicted for a second-order decay process,[10]

$$I = I_0[b/(b+t)]^n,$$

where b and n are constants for a given temperature and activation time. It is of interest to investigate the dependence of b and n on temperature and degree of trap filling (i.e., activation time). The close spacing of all of the dolomite glow peaks makes it difficult to investigate the effects of temperature variation over very large ranges because of interference between neighboring peaks. Results for the 330°K and 500°K glow peaks are given in Table II for two activation times and two temperatures near the glow peaks. The observed increase in b with activation time contradicts the behavior expected for a second-order decay process which predicts a decrease in b for an increase in the number of initially filled traps.

TABLE II. Decay parameter measurements.

Impurity	T_g in °K	Activation temp. in °K	Activation time in min	b in sec	n
1100 ppm Mn^{++}	330	270	0.75	40	0.91
1100 ppm Mn^{++}	330	270	5.0	70	0.71
1100 ppm Mn^{++}	330	300	0.75	70	1.3
1100 ppm Mn^{++}	330	300	5.0	110	1.1
1100 ppm Mn^{++}	500	480	0.75	50	0.94
1100 ppm Mn^{++}	500	480	5.0	110	0.99
1100 ppm Mn^{++}	500	530	0.75	10	1.1
1100 ppm Mn^{++}	500	530	5.0	40	1.1

III. CONCLUSIONS

The thermoluminescent properties of dolomite are very similar to those of calcite. Nearly all of the important features of the glow curves in natural samples are due to the presence of Mn and Fe. Manganese which is found in trace amounts in nearly all natural samples accounts for glow peaks at 330°K, 380°K, 500°K, and 600°K as well as a more or less constant level of emission below 300°K. Fe^{++}, Co^{++}, and Ni^{++} suppress the manganese luminescence (Fe^{+++} has no effect) and Co^{++} and Ni^{++} in the presence of Mn^{++} account for new high temperature glow peaks. But the results for Co^{++} and Ni^{++} are of little interest in interpreting the glow curves of natural samples because they are rarely present in large enough concentrations.

In the appropriate temperature range, thermal transitions occur between the traps associated with the 330°K glow peak and the traps corresponding to the emission below 300°K. These transitions make it possible to empty the traps corresponding to the 330°K peak at appreciable rates at temperatures as low as 200°K.

Isothermal decay curves for the emission due to all of the prominent glow peaks for Mn^{++} have the form predicted for a second-order process. However, the behavior of one of the decay parameters as a function of activation time is different from the predicted behavior.

IV. ACKNOWLEDGMENTS

The author wishes to thank I. M. Gurney, W. R. Hornbuckle, and J. J. McAlpin for their assistance and Socony Mobil Oil Company, Inc., for permission to publish this paper.

Cation-Electron Interaction in Metal-Ammonia Solutions

J. JORTNER

Department of Physical Chemistry, Hebrew University, Jerusalem, Israel

(Received August 10, 1960)

The problem of electron binding in the field of a cation in metal solutions is treated on the basis of an interstitial ion model. The energy levels and charge distribution of the unpaired electron are computed by a self-consistent field treatment for electron binding in a continuous dielectric medium employing one parameter wave function. Comparison with experimental results and with theoretical treatment based on a molecular model is presented. The adequacy of the continuous model is discussed.

INTRODUCTION

IT is fairly well established that in dilute metal-ammonia solutions the ionization of the alkali metal to solvated cations and electrons bound to the solvent is practically complete in the concentration region below $10^{-3}M$[1,2]. The concentration dependence of the paramagnetic susceptibility[3,4] and the electrical conductivity[5–7] was recently interpreted[8,9] by assuming that at higher concentration cation-electron interaction occurs. This "ion-pair" is involved in the mechanism of spin pairing, which occurs either by F_2 center[9] or by dimer formation.[8] The NMR experiments of McConnel and Holm[10] definitely indicate the existence of charge distribution of the unpaired electron on the alkali cation. Quantum mechanical calculations led to the values of -0.28 ev,[8] -0.10 ev,[11] and -0.61 ev[11] for the binding energy of the electron in the ground state of the monomer.

The purpose of this note is to present a treatment of the energy levels and charge distribution of an electron trapped in the field of a cation in solution. The present approach is based on a self-consistent field treatment for electron binding in the field of a positive point charge in a continuous dielectric medium. This formulation of the problem is equivalent to the computation of the energy levels of an electron bound in the field of an interstitial ion in a crystal[12–14]. The present approach involves the application of the static method.[15,16] The dynamic interactions between the electron and the nuclear motion of the solvent molecules are not taken into account. The present treatment is based on the assumption that the form of the potential well is solely determined by long-range interactions. Spherical symmetry of the potential is assumed, and one parameter wave functions are employed.

GROUND STATE

In the ground state of the system the potential $V(r)$ is determined by the charge Ze of the cation and the wave function of the electron chosen as

$$\psi_0(r) = (\mu^3/\pi)^{\frac{1}{2}} e^{-\mu r}. \tag{1}$$

The potential is then obtained from the total field acting on the electron,

$$-\text{grad}V(r) = (Ze/D_{0p}r^2) - \{[Z-q(r)]\beta e/r^2\}, \tag{2}$$

where

$$\beta = (1/D_{0p}) - (1/D_s) \tag{3}$$

$$q(r) = \int_0^r |\psi_0(r)|^2 4\pi r^2 dr; \tag{4}$$

D_s and D_{0p} are the static and optical dielectric constants of the medium.

Using Hartree's atomic units the following expression is obtained,

$$V(\mu, r) = -(D_{0p}r)^{-1} + \frac{\beta(1+\mu r)e^{-2\mu r}}{r}. \tag{5}$$

The total energy of the bound electron is computed from the variation integral

$$W_{1s}(\lambda, \mu) = \int \psi_1[-\tfrac{1}{2}\Delta + V(\mu, r)]\psi_1 4\pi r^2 dr, \tag{6}$$

where

$$\psi_1(r) = (\lambda^3/\pi)^{\frac{1}{2}} e^{-\lambda r}. \tag{7}$$

The reference state is that of a free electron placed at infinity from the cation, while the dielectric medium

[1] M. C. R. Symons, Quart. Revs. (London) **13**, 99 (1959).
[2] J. Jortner, J. Chem. Phys. **30**, 839 (1959).
[3] S. Freed and N. Sugarman, J. Chem. Phys. **11**, 354 (1943).
[4] C. A. Hutchison and R. C. Pastor, J. Chem. Phys. **21**, 1959 (1953).
[5] C. A. Kraus, J. Am. Chem. Soc. **43**, 749 (1921).
[6] C. A. Kraus, J. Chem. Ed. **30**, 83 (1953).
[7] E. C. Evers and P. W. Frank, J. Chem. Phys. **30**, 61 (1959).
[8] E. Becker, R. A. Lindquist, and B. J. Alder, J. Chem. Phys. **25**, 971 (1956).
[9] M. F. Deigen and Y. A. Tsvirko, Ukrain Fiz. Zhur. **1**, 245 (1956).
[10] H. M. McConnel and C. A. Holm, J. Chem. Phys. **26**, 1517 (1957).
[11] W. E. Blumberg and T. P. Das, J. Chem. Phys. **30**, 251 (1959).
[12] N. F. Mott and R. W. Gurney, *Electronic Processes in Ionic Crystals* (Oxford University Press, New York, 1948), p. 85.
[13] R. Kubo, J. Phys. Soc. Japan **3**, 254 (1948).
[14] J. H. Simpson, Proc. Roy. Soc. (London) **A197**, 269 (1949).
[15] H. Frohlich, Phil. Mag. Suppl. **3**, 325 (1954).
[16] J. H. Simpson, Proc. Roy. Soc. (London) **231**, 308 (1955).

has attained the nuclear configuration forming the potential well presented by Eq. (5).

The best wave function of this form is obtained by solving for λ the equation

$$[\delta W(\lambda, \mu)/\delta\lambda]_\mu = 0, \tag{8}$$

and for self-consistency of the field then setting $\lambda = \mu$. Hence

$$\lambda = \tfrac{1}{16}[(5/D_{0p}) + (11/D_s)] \tag{9}$$

$$W_{1s} = -\tfrac{1}{512}[(5/D_{0p}) + (11/D_s)][(15/D_{0p}) + (1/D_s)]. \tag{10}$$

The Bohr radius of the bound electron is $r_B = 1/\lambda$.

In order to check the validity of the variational treatment, the calculation was repeated using the wave function

$$\psi_0 = (\mu^3/7\pi)^{\frac{1}{2}}(1+\mu r)e^{-\mu r}. \tag{11}$$

By applying Eqs. (2) and (6),

$$V(\mu, r) = -(D_{0p}r)^{-1} + \beta(r^{-1} + \tfrac{19}{14}\mu + \tfrac{5}{7}\mu^2 r + \tfrac{1}{7}\mu^3 r^2)e^{-2\mu r}. \tag{12}$$

And by the solution of the variational integral (8) with $\psi_1(\lambda)$ of the form (11) we readily obtain

$$\lambda = \tfrac{7}{8}[(0.2170/D_{0p}) + (0.4259/D_s)] \tag{13}$$

$$W_{1s} = (3\lambda^2/14) - (9\lambda/14D_{0p}) + 0.2145\beta\lambda. \tag{14}$$

The Bohr radius of the bound electron presented by a wave function (11) is given by $r_B = [(5)^{\frac{1}{2}}+1]/2\lambda$.

For liquid ammonia at -33°C we set

$$D_s = 22 \quad D_{0p} = n^2 = 1.76 \quad \text{and} \quad \beta = 0.523.$$

The results of the calculations using the wave function of the type (1) and (11) are presented in Table I. No significant lowering of the energy is observed by applying the wave function (11). This result indicates the adequacy of the variational treatment using the potential function defined by Eq. (2).

It is interesting to consider the period of the bound electron in the ground state which can be approximately presented by

$$\tau = 512\pi\hbar^3/[(5/D_{0p}) + (11/D_s)]^2 \tag{15}$$

for liquid ammonia at -33°C $\tau \sim 3.10^{-13}$ sec. The comparison of this value with the relaxation time of liquid ammonia 1, 3.10^{-12} sec at -40°C,[17] yields a justification for the static approximation employed in the present treatment.

OPTICAL EXCITATION ENERGY

The energy of the first excited state ($2p$ state in our approximation) was calculated by using the wave functions

$$\psi_{2p} = (\alpha^5/\pi)^{\frac{1}{2}} r e^{-\alpha r} Y_{2m}(\theta\phi). \tag{16}$$

The vertical electronic transition is subjected to the restrictions of the Franck-Condon principle. Thus we have computed the energy of the excited state in the nuclear configuration of the ground state. In this approximation Eqs. (2) and (4) remain unchanged; the potential corresponds to the ground state, while the charge distribution is given by Eq. (16).

As the energy of the excited state is not very susceptible to the behavior of the potential function at small distances, the calculation was carried out by using only the potential $V(\mu, r)$ presented by Eq. (5). The energy of the excited state W_{2p} is given by

$$W_{2p} = \tfrac{1}{2}\alpha^2 - (\alpha/2D_{0p}) + \tfrac{1}{2}\beta\alpha(1+X)^{-4} + \beta\mu(1+X)^{-5}, \tag{17}$$

where $X = \mu/\alpha$; X was then obtained from

$$\delta W/\delta\alpha = \alpha - (2D_{0p})^{-1} + \tfrac{1}{2}\beta(15X^2+6X+1)(1+X)^{-6} = 0. \tag{18}$$

Thus we calculate for the excited state

$$\alpha = 0.200 \text{ a.u.} \qquad r_B = 5.24 \text{ A} \qquad W_{2p} = -0.51 \text{ ev.}$$

The first electronic transition in the monomer is expected to occur at

$$h\nu = W_{2p} - W_{1s}, \tag{19}$$

thus the calculated value for $h\nu$ is about 1.1 ev.

THERMAL AND OPTICAL DISSOCIATION ENERGIES

The binding energy $-W_{1s}$ of the electron in the ground state represents the optical dissociation energy corresponding to a vertical ionization process. The thermal dissociation energy of the monomer involves the formation of an unbound electron and a normally solvated cation. The thermal and optical dissociation energies are related by

$$-H = W_{1s} + \chi, \tag{20}$$

where χ is the electrostatic energy required to transform the configuration of the dielectric medium which is in equilibrium with the alkali cation to the configuration which forms the potential well $V(\mu, r)$. For the calculation of χ we applied the theory of Marcus[18] for the electrostatic free energy of nonequilibrium states. This

TABLE I. Calculations for the electron binding in the ground state.

Wave function	λ a.u.	W_{1s} ev	r_B a.u.
(1)	0.209	−1.52	4.79
(11)	0.334	−1.65	4.85

[17] K. Fish, C. Miller, and C. P. Smyth, J. Chem. Phys. **29**, 745 (1958).

[18] R. A. Marcus, J. Chem. Phys. **24**, 979 (1956).

TABLE II. Density of unpaired electron spin on Na^+ nucleus.[a]

Wave function	$\lvert\psi_{1s}\rvert^2$	$\langle 1s \mid \psi_{1s}\rangle$	$\langle 2s \mid \psi_{1s}\rangle$	$\lvert\psi_{1s}\rvert^2$
(1)	0.00202	0.0212	0.160	0.107
(11)	0.00170	0.0161	0.137	0.096

[a] Charge density expressed in a.u. units (Bohr radius)$^{-3}$.

theory leads to the general result[19] for the work required to transform a system which is in equilibrium in respect of a charge distribution ρ^0 to a nonequilibrium state where the permanent orientation polarization[1] is in equilibrium with the charge distribution ρ,

$$\chi=\frac{\beta}{8\pi}\int(E_c-E_c^0)^2dv, \tag{21}$$

where

$$\operatorname{div}E_c=4\pi\rho$$
$$\operatorname{div}E_c^0=4\pi\rho^0. \tag{22}$$

For the present case

$$E_c^0=e/r^2. \tag{23}$$
$$E_c=e[1-q(r)]/r^2.$$

Hence

$$\chi=\frac{\beta e^2}{2}\int_{R_0}^{\infty}\frac{|\,q(r)\,|^2}{r^2}dr. \tag{24}$$

Assuming that the configuration of the primary solvation layer of the cation M^+ is not affected by the introduction of the electron we set $R_0=r_{M^+}+2r_{NH_3}$. Hence R_0 and thus χ will be slightly dependent on the nature of the cation. For Na^+ ion $R_0=3.80$ A. Using the wave function (1) we obtained $\chi=0.72$ ev and $H=0.80$ ev.

It is interesting to compare this result with the value of the thermal dissociation energy of the bound electron in infinitely dilute metal ammonia solutions. A self-consistent field treatment using one parameter wave function of the form (1) yielded the result of 0.845 ev for the thermal dissociation energy of the electron bound to the polarized dielectric medium. Thus the calculated energy change accompanying the thermal process

$$\text{Na am}\rightarrow\text{Na}^+\text{ am}+E\text{ am} \tag{25}$$

is 0.045 ev.

HYPERFINE INTERACTIONS WITH THE Na NUCLEI

It is interesting to compare the charge distribution predicted on the basis of the simple variational wave functions (1) and (11) with the experimental results obtained from NMR Knight shifts in this system.[10] The calculation method is based on the general treatment of Gourary and Andrian.[20,11] The wave function ψ_{1s} of the unpaired electron is orthogonalized with respect to all the other electrons ψ_i of the system using Schmidt's orthogonalization process. Neglecting overlap between adjacent molecules and the ion the orthogonalized wave function ϕ_{1s} of the unpaired electron is presented by

$$\phi_{1s}=\frac{\psi_{1s}-\langle\psi_{1s}\mid\psi_i\rangle\psi_i}{(1-\sum_i\langle\psi_{1s}\mid\psi_i\rangle^2)^{\frac{1}{2}}}, \tag{26}$$

ϕ_{1s} admixes into its components the orbital wave functions of all the electrons of the system with the same spin.

The Na^+ atomic orbitals were represented by Tubis' wave functions[21]

$$(1s)=19.95e^{-10.66r}$$
$$(2s)=6.52e^{-3.36r}-4.31e^{-9.64r}. \tag{27}$$

For NH_3 molecule central field wave functions were employed.[22] However their effect on the unpaired electron density on the sodium ion nucleus is negligible. The results of these calculations employing for ψ_{1s} the wave function (1) and (11) used for energy calculations are summarized in Table II.

DISCUSSION

The direct comparison of the results obtained on the basis of the interstitial ion model with experimental data is rather difficult because of the relative low concentration of this species. The application of the equilibrium constants[8] derived from conductivity and magnetic data indicates that the concentration of the monomer unit does not exceed 10% of the total metal concentration.[23]

The comparison of our results with previous treatment[11] based on a molecular model indicates that the present approach yields higher values for the binding energy of the electron in the ground state. The optical dissociation energy is comparable with the energy corresponding to the photoelectric threshold which is about 1.5 ev.[24] However this comparison should be accepted with reservation as the inner potential of liquid ammonia is unknown, and the role of other species e.g., e centers and dimers in this process has to be considered. For the energy change accompanying the thermal process[21] inspection of the equilibrium constants[8] for K solutions yields $\Delta H=0$, $\Delta G=-0.09$ ev. The agreement with the theoretical value 0.045 ev is fair.

The present treatment indicates that the absorption band of the system, arising from a $1s\rightarrow 2p$ transition,

[19] J. Jortner (unpublished).

[20] B. S. Gourary and F. J. Andrian, Phys. Rev. **105**, 1180 (1957).

[21] A. Tubis, Phys. Rev. **102**, 1049 (1956).

[22] K. S. Pitzer, J. Chem. Phys. **29**, 453 (1958).

[23] H. C. Clark, A. Horsfield, and M. C. R. Symons, J. Chem. Soc. **1959**, 2478.

[24] G. K. Teal, Phys. Rev. **71**, 138 (1947).

should lie at 1.1 ev. Thus this band should be placed at higher energy than that corresponding to the first transition of the bound electron in infinitely dilute solution ($h\nu = 0.8$ ev).[1,2]

Recently Clark, Horsfield and Symons[23] have demonstrated that addition of 0.1M sodium iodide to sodium ammonia solutions results in the formation of a new absorption band at 1.55 ev. This band was tentatively ascribed to the monomer unit. The results of the theoretical calculation support this assignment. However it should be pointed out that in liquid ammonia solutions ion-pair formation is rather extensive. The dissociation constants of some alkali halides in liquid NH_3 are of the order of 10^{-3}.[25] Thus under the experimental conditions of Symons *et al.* the role of the centers involving Na^+I^- ion pairs has to be considered. Electron binding in the field of a Na^+I^- ion pair may be analogous to that of a D center[26] (an F center whose nearest-neighbor cation is missing). The absorption band recorded in NaI solution[23] shows a fine structure and one of these bands may be due to electron binding in the field of an ion pair. More experimental work is needed to establish this point.

The charge distribution obtained on the basis of the present treatment indicates that the maximum probability for the location of the bound electron is in the region of 2.5 A. This result is similar to that obtained by Blumberg and Das[11] on the basis of a molecular model. The result obtained for the electron spin density on the Na^+ nucleus is of the same order of magnitude as the values of 0.014 and 0.066 a.u. obtained by application of the molecular model in agreement with experimental data.[11] Direct comparison is still impossible as the equilibrium constants for Na ammonia solutions at room temperature are unknown. However it appears that the present treatment overestimates the charge distribution on the Na nucleus.

We wish to compare the charge distribution of the unpaired electron in the interstitial ion with the 3s sodium atom orbital. This alkali atom wave function is an example of spatially diffuse charge distribution. Within the ionic radius of Na^+ ion (1.85 a.u.) there is included only 4.3% of the total charge.[27] For the wave functions employed in our treatment 5% of the total electronic charge is included within the ionic radius of the sodium ion. This comparison yields a certain justification for the employment of a point charge model for the alkali cation. In the present treatment the basic difficulty rises because of the application of the static and optical dielectric constants inside the sodium ion core. The closed electronic shells of the cation will tend to repel the unpaired electron from the origin of the binding center. The application of high-dielectric constant in the potential function in that region is qualitatively similar to the effect of interelectronic repulsion.

All the previous models employed for the study of metal solutions were static. Experimental data indicate the existence of a rapid exchange between solvent molecules in the vicinity of the binding center of the electron (the e centers or the monomer) and the solvent molecules in the bulk. These include the absence of NMR lines at unshifted position[10] and the extreme narrowness of the ESR band.[28] The present static model is however suitable for the calculation of the optical absorption spectrum and of the mean charge distribution of the center.

ACKNOWLEDGMENT

I am greatly indebted to Professor H. C. Longuett-Higgins for his interest in this work and for valuable discussions on the nature of metal ammonia solutions.

[25] V. F. Hindza and C. A. Kraus, J. Am. Chem. Soc. **71**, 1565 (1949).
[26] L. Pincherle, Proc. Roy. Soc. (London) **A64**, 648 (1951).
[27] L. Dexter, Phys. Rev. **108**, 707 (1957).
[28] J. Kaplan and C. Kittel, J. Chem. Phys. **21**, 1429 (1953).

Bonding in Cubic Complexes*

JOSEPH H. MACEK AND GEORGE H. DUFFEY

Physics Department, South Dakota State College, Brookings, South Dakota

(Received June 29, 1960)

Symmetry arguments yield the general *spdf* σ bond orbitals for A in cubic AB_8. The valence orbitals needed include $1s$, $3np$, $3d$, and $(4-3n)f$. The greatest strength, 3.934, is found when n is 27/55. Incomplete hybridization, splitting of valence levels of A, and π bonding in a cubic field are also discussed.

SEVERAL structures for AB_8 complexes have been discussed.[1-7] More symmetric than these is the cubic arrangement, which we shall consider here. We shall suppose that s, p, d, and f valence orbitals of central atom A are available and that either covalent or ionic bonding occurs.

The cubic structure is oriented, as in Fig. 1, so it is symmetrically placed with respect to the rectangular coordinate axes. The B groups are numbered as shown. The bond between A and the ith B is called bond i. In covalent bonding, the bond orbital labeled ψ_i is used for this bond.

The s, p, d, and f orbitals of A are labeled as in Eisenstein's paper,[8] so that the homogeneous-polynomial subscripts describe their nonradial variations. Such variations determine whether and how much an atomic orbital can contribute to forming a bond orbital.

Since by symmetry the eight σ cubic-bond orbitals are equivalent, each contains the same amount of s. And since our structure is symmetrically placed with respect to nodal planes $x=0$, $y=0$, and $z=0$, d_{zz}, d_{yz}, d_{xy}, and f_{xyz} contribute equally to each bond orbital. Likewise, p_z plus $f_{z(5z^2-3r^2)}$, p_x plus $f_{x(5x^2-3r^2)}$, and p_y plus $f_{y(5y^2-3r^2)}$ contribute equally. Following convention,[8] we represent these f orbitals as $f_{\delta 1}$, $f_{\delta 2}$, and $f_{\delta 3}$, respectively.

These simple considerations are upheld by the group theoretical treatment,[8-10] according to which the s orbital spans the A_{1g} representation, the f_{xyz} orbital the A_{2u} one, the d_{zz}, d_{yz}, d_{xy} orbitals the F_{2g} one, and p_z, p_x, p_y or $f_{\delta 1}$, $f_{\delta 2}$, $f_{\delta 3}$ the F_{1u} one. These representations make up the σ reducible representation.

Choosing signs properly, we thus obtain the normalized, orthogonal bond orbitals

$$\psi_1=[1/(8)^{\frac{1}{2}}][s+(\cos\alpha)(+p_z+p_x+p_y)+d_{zz}+d_{yz}+d_{xy}+f_{xyz}+(\sin\alpha)(-f_{\delta 1}-f_{\delta 2}-f_{\delta 3})], \quad (1)$$

$$\psi_2=[1/(8)^{\frac{1}{2}}][s+(\cos\alpha)(+p_z-p_x+p_y)-d_{zz}+d_{yz}-d_{xy}-f_{xyz}+(\sin\alpha)(-f_{\delta 1}+f_{\delta 2}-f_{\delta 3})], \quad (2)$$

$$\psi_3=[1/(8)^{\frac{1}{2}}][s+(\cos\alpha)(+p_z-p_x-p_y)-d_{zz}-d_{yz}+d_{xy}+f_{xyz}+(\sin\alpha)(-f_{\delta 1}+f_{\delta 2}+f_{\delta 3})], \quad (3)$$

$$\psi_4=[1/(8)^{\frac{1}{2}}][s+(\cos\alpha)(+p_z+p_x-p_y)+d_{zz}-d_{yz}-d_{xy}-f_{xyz}+(\sin\alpha)(-f_{\delta 1}-f_{\delta 2}+f_{\delta 3})], \quad (4)$$

$$\psi_5=[1/(8)^{\frac{1}{2}}][s+(\cos\alpha)(-p_z+p_x+p_y)-d_{zz}-d_{yz}+d_{xy}-f_{xyz}+(\sin\alpha)(+f_{\delta 1}-f_{\delta 2}-f_{\delta 3})], \quad (5)$$

$$\psi_6=[1/(8)^{\frac{1}{2}}][s+(\cos\alpha)(-p_z-p_x+p_y)+d_{zz}-d_{yz}-d_{xy}+f_{xyz}+(\sin\alpha)(+f_{\delta 1}+f_{\delta 2}-f_{\delta 3})], \quad (6)$$

$$\psi_7=[1/(8)^{\frac{1}{2}}][s+(\cos\alpha)(-p_z-p_x-p_y)+d_{zz}+d_{yz}+d_{xy}-f_{xyz}+(\sin\alpha)(+f_{\delta 1}+f_{\delta 2}+f_{\delta 3})], \quad (7)$$

$$\psi_8=[1/(8)^{\frac{1}{2}}][s+(\cos\alpha)(-p_z+p_x-p_y)-d_{zz}+d_{yz}-d_{xy}+f_{xyz}+(\sin\alpha)(+f_{\delta 1}-f_{\delta 2}+f_{\delta 3})], \quad (8)$$

which apply if the hybridization of s, p, d, and f valence orbitals of A occurs. The over-all composition is $sp^{3n}d^{3}f^{4-3n}$ where the relationship between n and parameter α is

$$n=\cos^2\alpha. \quad (9)$$

According to Pauling and his adherents,[11-12] the energy of a covalent bond between atoms A and B is roughly a linear function of strength S, which is the value of the angular part of the bond orbital of A along the straight line between centers of A and B. Each cubic orbital from Eqs. (1)-(8), when its angular part is normalized to 4π, yields the results listed in Table I.

* Supported in part by the National Science Foundation.

[1] Reference 5b (J. L. Hoard) of L. E. Marchi, W. C. Fernelius, and J. P. McReynolds, J. Am. Chem. Soc. **65**, 329 (1943).

[2] G. H. Duffey, J. Chem. Phys. **18**, 746 (1950).

[3] J. L. Hoard and H. H. Nordsieck, J. Am. Chem. Soc. **61**, 2853 (1939).

[4] G. H. Duffey, J. Chem. Phys. **18**, 1444 (1950).

[5] G. H. Duffey, J. Chem. Phys. **19**, 963 (1951).

[6] G. H. Duffey, J. Chem. Phys. **19**, 553 (1951).

[7] L. E. Marchi, W. C. Fernelius, and J. P. McReynolds, J. Am. Chem. Soc. **65**, 329 (1943).

[8] J. C. Eisenstein, J. Chem. Phys. **25**, 142 (1956).

[9] J. H. Van Vleck, J. Chem. Phys. **3**, 803 (1935).

[10] M. G. Shirmazan and M. E. Dyatkina, J. Phys. Chem. (U.S.S.R.) **27**, 491 (1953). This paper was translated by M. Kasha, Department of Chemistry, Florida State University, Tallahassee, Florida.

[11] S. Glasstone, *Theoretical Chemistry* (D. Van Nostrand Company, Inc., Princeton, New Jersey, 1944).

[12] G. H. Duffey, J. Chem. Phys. **18**, 510 (1950).

The maximum strength, which is 3.934, occurs when n is 27/55.

Steric repulsion is greater in the cubic structure than in tetragonal antiprism,[2,5] or dodecahedral[4] structures, because the shortest distance between ligands is less (the arrangement in space is less efficient). Also, one can show that strength S, and hence the overlap of these orbitals with ligand orbitals, can be increased on going to such alternate structures. Nevertheless, a complex may be forced to assume a cubic structure by connections between the attached atoms.

The cubic structure is also favored if only the s and p valence orbitals mix, so that sp^3 bond orbitals result; for, such orbitals may form two tetrahedral structures—(a) one holding B atoms 1, 3, 6, 8 to A, and (b) the other holding B atoms 2, 4, 5, 7—which resonate with each other. A like resonance is exhibited by electron-deficient substances.[13] But, sp^3 hybrid orbitals cannot be distorted[14] to fit four of the dodecahedral bond positions. Indeed, if in the orbitals of Duffey,[4] one sets

$$\cos\alpha = \cos\beta = \cos\gamma = 1 \qquad (10)$$

to eliminate the contribution from d orbitals, tetrahedral orbitals are obtained undistorted. Likewise, the four sp^3 hybrids cannot be distorted to fit four of the tetragonal antiprism positions.

Let us now consider energy of the valence orbitals from the standpoint of crystal field-splitting theory.[15] In general, each orbital of a given symmetry species is shifted together because an electron in each interacts in like manner with the electron clouds of the ligands. Furthermore, the effect is large when the orbital is great in the direction of a ligand because the average electrostatic repulsion is then large. The p_x, p_z, and p_y orbitals of A are oriented equivalently with respect to the B's; therefore, the p level is not split. Since d_{xz}, d_{yz}, and d_{xy} are oriented equivalently, they are shifted

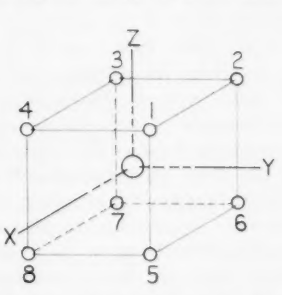

FIG. 1. Orientation chosen for cubic structure.

TABLE I. Properties of cubic bond orbitals.[a]

n	$\cos\alpha$	S
0.0000	0.0000	3.500
0.2000	0.4472	3.860
0.4000	0.6325	3.927
0.4909	0.7006	3.934
0.6000	0.7746	3.890
0.8000	0.8944	3.852
1.0000	1.0000	3.481

[a] The orbitals are of type $sp^{3n}d^{5}f^{1-3n}$.

together. Because of the large repulsion between electron clouds on the B's and these d electron clouds, the shift is upward—opposite to that observed in an octahedral field. Likewise, f_{xyz} is displaced upward. Since $f_{\delta 1}$, $f_{\delta 2}$, and $f_{\delta 3}$ belong to a different symmetry species, they are displaced upward a different amount. Because the remaining three f orbitals—$f_{z(x^2-y^2)}$, $f_{x(y^2-z^2)}$, and $f_{y(z^2-x^2)}$, which we label $f_{\epsilon 1}$, $f_{\epsilon 2}$, and $f_{\epsilon 3}$—have their nodal surfaces equivalently placed with respect to the B's, they are shifted together in bringing up the attached atoms. Since they are not used in σ-bond orbital formation, they do not interact as much with the electron clouds on the B's and so are more stable than the other f valence orbitals. The d orbitals $d_{3z^2-r^2}$ and $d_{x^2-y^2}$ have different nodal surfaces. However, the former is the linear combination of $d_{x^2-z^2}$ and $d_{y^2-z^2}$ that is orthogonal to $d_{x^2-y^2}$; and $d_{z^2-x^2}$, $d_{y^2-z^2}$ are obtainable from $d_{x^2-y^2}$ by covering operations of the group. Therefore, $d_{3z^2-r^2}$ and $d_{x^2-y^2}$ form the basis for the same irreducible representation.[8] Hence, they are shifted together—generally downwards because they are not used for σ bonds.

The π reducible representation breaks down into[8]

$$E_g + E_u + F_{1g} + F_{1u} + F_{2g} + F_{2u}. \qquad (11)$$

No basis functions for E_u and F_{1g} are found among the s, p, d, and f orbitals; only if higher orbitals are available can these species of π bonds be formed. Since d_{xz}, d_{yz}, and d_{xy} span the F_{2g} representation and these are already used for σ bonding, this kind of π bonds is not to be expected. But the F_{1u} representation is spanned by either p_x, p_z, p_y or $f_{\delta 1}$, $f_{\delta 2}$, $f_{\delta 3}$; so what is not used in σ bonding is available for π bonding. By Kimball's criterion,[16] the resulting π bonds are weak. In the strong class are the π bonds constructed from $d_{3z^2-r^2}$, $d_{x^2-y^2}$, which span E_g, and those from $f_{\epsilon 1}$, $f_{\epsilon 2}$, $f_{\epsilon 3}$, which span F_{2u}.

[13] L. Pauling, *The Nature of the Chemical Bond* (Cornell University Press, Ithaca, New York, 1960), 3rd ed.

[14] See J. W. Linnett and P. J. Wheatley, Trans. Faraday Soc. **45**, 33 (1949).

[15] For an introduction see F. Basolo and R. G. Pearson, *Mechanisms of Inorganic Reactions* (John Wiley & Sons, Inc., New York, 1958); R. G. Pearson, Chem. Eng. News **37**, No. 26, 72 (1959).

[16] H. Eyring, J. Walter, and G. E. Kimball, *Quantum Chemistry* (John Wiley & Sons, Inc., New York, 1944).

Letters to the Editor

THE Letters to the Editor section is subdivided into three parts entitled Communications, Comments and Errata, and Notes. These three sections are all subject to the same limitations on length. The textual material of each Letter is limited to a number of words equal to 950 minus the following: (a) 200 words for each average-sized figure; (b) 50 words for each displayed equation; (c) 7 words for each line of table including headings and horizontal rulings. No proof will be sent to the authors of "Communications" and "Comments and Errata." Proof will be sent to the authors of "Notes." The publication charge for Letters is $30 per page, with a minimum of $30 per Letter. If honored, the Institution will be entitled to 100 reprints without covers. See issues of May–September, 1957, for descriptions of categories.

Communications

EPR Studies of Spin Correlation in Some Ion Radical Salts

D. B. CHESNUT, H. FOSTER, AND W. D. PHILLIPS

E. I. duPont de Nemours and Company, Wilmington, Delaware

(Received November 22, 1960)

RECENTLY a new class of organic salts based on the strong π-electron acceptor tetracyanoquinodimethan (TCNQ)

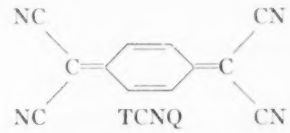

has been prepared[1] whose members are paramagnetic and exhibit high electrical conductivities.[2] Examples of these ion radical salts are $HN(C_2H_5)_3^+(TCNQ)_2^-$, $(\varphi_3PCH_3)^+(TCNQ)_2^-$, $(\varphi_3AsCH_3)^+(TCNQ)_2^-$, and (morpholinium)$^+$(TCNQ)$^-$. The EPR characteristics of these solid salts are attributable to the presence of entities residing in triplet rather than doublet electronic states.

The cations of these salts are diamagnetic, while the $(TCNQ)^-$ or $(TCNQ)_2^-$ anion is paramagnetic. However, the temperature dependence of the integrated EPR signal intensity I for the $HN(C_2H_5)_3^+(TCNQ)_2^-$ salt (Fig. 1) can be fitted to the expression

$$I \propto 1/T(e^{J/kT}+3), \tag{1}$$

with a value of $J=0.034$ ev[3] rather than to a $1/T$ temperature dependence expected for a doublet state. Equation (1) is characteristic of a coupled electron pair having a ground singlet state and a thermally accessible triplet state separated by the energy J.

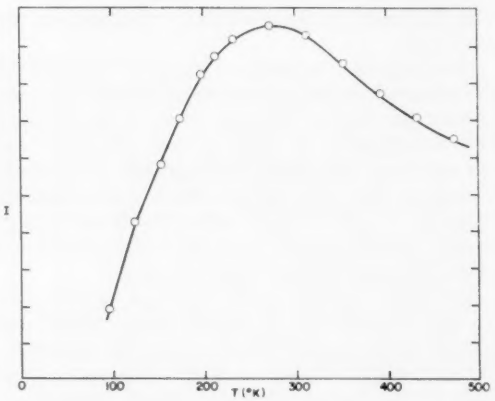

FIG. 1. Temperature dependence of the integrated EPR absorption intensity of the $HN(C_2H_5)^+(TCNQ)_2^-$ salt.

Below -150°C single crystals of the $\varphi_3PCH_3^+(TCNQ)_2^-$ and $\varphi AsCH_3^+(TCNQ)_2^-$ salts exhibit a doublet resonance spectrum[4] the spacing of which is dependent on the crystal orientation relative to the external field. If it is assumed that the doublet resonance arises from a zero field splitting in a triplet state, the angular dependence of the doublet spacing is described by the spin Hamiltonian

$$\mathcal{H}=\beta(g_xH_xS_x+g_yH_yS_y+g_zH_zS_z)+DS_z^2+E(S_x^2-S_y^2), \tag{2}$$

with $g_x=2.004_0$, $g_y=2.003_1$, $g_z=2.002_7$, $|D/hc|=0.0062$ cm^{-1} and $|E/hc|=0.00098$ cm^{-1} for the phosphonium salt. Within experimental error, identical values were observed for the parameters of the spin Hamiltonian of the arsonium salt. These values of $|D/hc|$ and $|E/hc|$ are to be compared with those observed for the phosphorescent state of naphthalene of, respectively, 0.1006 cm^{-1} and 0.0138 cm^{-1}.[5] Further confirmation of the triplet-state origin of the paramagnetism of these salts is provided by the observation of the $\Delta m=\pm 2$ transition. This resonance occurs at half the magnetic field required to observe the normal $\Delta m=\pm 1$ transitions (at constant frequency) and is weakly allowed due to the dipolar perturbation in the triplet state. A similar resonance also was observed for the phosphorescent state of naphthalene.[6]

As the temperature is raised above -150°C, the two peaks of the $\varphi_3PCH_3^+(TCNQ)_2^-$ and $\varphi_3AsCH_3^+(TCNQ)_2^-$ salts broaden, coalesce, and finally narrow at room temperature to a single, sharp resonance. The singlet-triplet separations for these molecules are identical and equal to 0.062 ev. This value of J yields a triplet state population of 4% at the temperature of

coalescence (about -100°C), a concentration sufficient to ascribe the temperature effect on the widths and spacing of the doublet resonances to exchange interactions between triplet entities in the solid. On the other hand, the (morpholinium)$^+$ (TCNQ)$^-$ salt yields a dipolar splitting[4] attributable to a thermally accessible triplet state with $J=0.40$ ev, that is observable without broadening or coalescence to 125°C. At 125°C, the paramagnetism of the morpholinium salt undergoes an irreversible change due presumably to chemical decomposition. A value of J of 0.40 ev would yield a 4% concentration of triplet states at about 800°C. Consistent with the above idea of concentration-dependent exchange interactions being responsible for the temperature dependences of the spectral characteristics of the phosphonium and arsonium salts, the $HN(C_2H_5)_3^+(TCNQ)_2^-$ salt with $J=0.034$ ev yields a single line with no evidence for dipolar splitting down to -180°C.

Details of the above and other solid state and solution EPR studies of TCNQ and its salts will be published shortly.

[1] D. S. Acker, R. J. Harder, W. R. Hertler, W. Mahler, L. R. Melby, R. E. Benson, and W. E. Mochel (to be published).

[2] R. G, Kepler, P. E. Bierstedt, and R. E. Merrifield (to be published).

[3] A value of $J=0.041$ ev is obtained for the

$$HN(C_2H_5)_3^+(TCNQ)_2^-$$

salt from direct susceptibility measurements.[2] The discrepancy is considered to be within the combined limits of accuracy of the two methods of measurement.

[4] Other, weaker lines are present in the spectrum that are attributed to the presence of paramagnetic organic impurities and, perhaps, crystal imperfections.

[5] C. A. Hutchison, Jr., and B. W. Mangum, J. Chem. Phys. **29**, 952 (1958).

[6] J. H. van der Waals and M. S. de Groot, Mol. Phys. **2**, 333 (1959).

Lithium Kinetic Isotope Effect in the Reaction of Ethyllithium with Benzyl Chloride*

ROBERT WEST AND WILLIAM GLAZE

Department of Chemistry, University of Wisconsin, Madison, Wisconsin

(Received November 21, 1960)

WE wish to report the first observation of a kinetic isotope effect in a reaction of an organolithium compound. The reaction studied was the coupling of ethyllithium and benzyl chloride to give *n*-propylbenzene and lithium chloride, in benzene as solvent[1]

$$C_2H_5Li+ClCH_2C_6H_5\rightarrow n\text{-}C_3H_7C_6H_5+Li^+Cl^-.$$

The reaction follows second-order kinetics (first order in each reactant) with $k=2.01\pm0.04\times10^{-4}$ mole^{-1} sec^{-1} at 25°C and $\Delta H_{act}=17.8$ kcal/mole. The reaction was allowed to proceed to half completion using ethyllithium containing approximately equal amounts of Li^6 and Li^7. The isotope ratio in the precipitated lithium chloride, and in the ethyllithium before and after reaction was determined mass spectrometrically using the electron-impact method after conversion of the lithium to lithium iodide.[2] Enrichment of Li^6 in the lithium chloride and Li^7 in the unreacted ethyllithium takes place. (Exchange of lithium isotopes was independently shown not to take place between lithium chloride and ethyllithium in benzene.) The observed kinetic isotope effect k_6/k_7 was 1.029 ± 0.008.

According to the statistical theory of kinetic isotope effects, the isotope effect for various models of a reaction can be calculated from a knowledge of the vibrational frequencies of the reacting species and the postulated transition states with and without isotopic substitution.[3] Bigeleisen has previously estimated a maximum isotope effect for reactions of organolithium compounds of 1.1, assuming complete bond breaking going from the ground to the transition state.[3] A better estimate of the maximum lithium isotope effect for organolithium compounds is made possible by our recent observation of the infrared spectra of organolithium compounds of lithium-6 and lithium-7. Previous workers have assigned bands at 880 cm^{-1} [4] and 1060 cm^{-1} [5] to the C-Li fundamental stretching bands. These assignments must be incorrect since the bands in question do not shift upon substitution of lithium-6 for lithium-7. However, ethyllithium-7 has complex absorption bands centering at 380 cm^{-1} and 540 cm^{-1} which do shift by about 20 cm^{-1} to higher frequency upon lithium-6 substitution, and so must represent vibrational modes involving lithium. Assuming that the 540 cm^{-1} band is the C–Li stretching mode and making the usual approximation that the temperature-independent term $\nu_6^{\ddagger}/\nu_7^{\ddagger}$ is equal to the square root of the inverse ratio of the reduced masses of the C–Li^6 and C–Li^7 bonds,[3] a maximum isotope effect of 1.07 can be calculated.

The observed isotope effect of 1.029 indicates considerable weakening of the carbon-lithium bond upon going to the transition state and implies probable participation of lithium in the rate-determining step, perhaps in removing a chloride ion from the benzyl chloride. Our observations are consistent either with a concerted bimolecular displacement mechanism, or with a rate-determining bimolecular step leading to formation of benzyl carbonium ion (the S_N1 and S_N2 mechanisms proposed by Cristol, Ragsdale, and Meek[6] for similar coupling reactions in ether). Mechanistic implications will be discussed more fully in a later publication.

* This research was supported by a grant from the Atomic Energy Commission.

[1] The authors are indebted to Professor Henry Gilman for suggesting the study of this particular reaction.

[2] These determinations were carried out at the Oak Ridge National Laboratory by arrangement with the Atomic Energy Commission. See A. E. Cameron, Rev. Sci. Instr. **25,** 1154 (1954) J. Am. Chem. Soc. **77,** 2731 (1955).

[3] J. Bigeleisen and M. Wolfsberg, Advances in Chem. Phys. **1,** 15 (1958).

[4] T. L. Brown and M. T. Rogers, J. Am. Chem. Soc. **79,** 1859 (1951).

[5] D. N. Shigorin, Spectrochim. Acta **14,** 198 (1959); D. N. Shigorin, T. V. Talalaeva, K. A. Kocheshkov, and A. N. Rodionov, Izvest. Akad. Nauk. S.S.S.R. Ser. Fiz. **22,** 1110 (1958).

[6] S. J. Cristol, J. W. Ragsdale, and J. S. Meek, J. Am. Chem. Soc. **73,** 810 (1951).

Comments and Errata

Photodecomposition of Biacetyl Vapor

JULIAN HEICKLEN

Department of Chemistry, University of California, Berkeley, California

AND

GERALD B. PORTER

Department of Chemistry, University of British Columbia, Vancouver, Canada

(Received September 19, 1960)

RECENTLY a paper has appeared[1] which reinterprets the data of Sheats and Noyes[2] on the photodecomposition of biacetyl vapor. The reinterpretation contends that the data can be explained by a wavelength and temperature-dependent decomposition of the initially formed excited state (I^1A_u) molecule instead of requiring two distinct decompositions, one wavelength dependent but essentially temperature independent and the other temperature dependent with only secondary dependence on wavelength.[3]

We disagree with Dubois' conclusions for the following reasons:

(1) At 3650 and 4358 A the fluorescence quantum yield is independent of temperature,[4] but photodissociation increases with increasing temperature. These two processes cannot originate from molecules in the same state. Phosphorescence does decrease as photodissociation increases. Since these two processes compete kinetically they must represent reactions of the same species, which would be molecules in the I^3B_u state. The situation is entirely different in the case of β-naphthylamine for which the fluorescence quantum yield does vary with temperature.[5]

(2) The reinterpretation[1] of the data at 3650 A is dependent on the quantitative use of extrapolated primary quantum yields at zero pressure at various temperatures. We feel this to be an unwarranted extension of the validity of the data. The primary quantum yield itself is calculated on the basis of a relatively complex mechanism which requires the estimation of rate constant ratios. The primary quantum yields at 26° have in fact been recalculated with the result that the intercept of a plot of the reciprocal of the primary quantum yield vs pressure is decreased from 15 to about 3,[3] but the corrected value was not used in the reinterpretation. This corrected value is certainly superior as it gives rise to a plot which is in excellent agreement with the emission data.

(3) The photo-oxidation of biacetyl[6] indicates that the intercept of reciprocal quantum yield-pressure plots at 3650 A should be very near to unity. For this reason, the experimental intercept values different from one are probably without significance.

(4) Recent data[7] confirm beyond question that the photodecomposition at 28° is a totally different kind of process in the main from the process at higher temperatures. Any calculation of an activation energy based on the assumption that they are the same is incorrect.

(5) The statement "...when a molecule contains little or no excess (over thermal) vibrational energy in its excited state, as is achieved by exciting near the O–O transition, the pressure effect on the primary quantum yield ϕ is negligible..."[1] is contrary to fact. In the first place the quantum yield of decomposition of molecules in the I^1A_u state is without doubt zero or very near to zero under these conditions. In this sense the statement is true since it would be zero under any conditions of pressure, as is shown by the absence of a pressure effect on the fluorescence at 4358 A at any temperature.[4] Experimentally, it is known that the pressure effect on the primary quantum yield in this type of molecule becomes greater, the longer the wavelength.[8]

(6) The concept of a vibrational temperature cannot be applied strictly to a photoexcited molecule, particularly at low pressures.[8] Although there may be intramolecular relaxation of vibrational energy among the various vibrational modes, the fact remains that, in the absence of perturbing collisions, all of the photoexcited molecules have the same total vibrational energy (with monochromatic radiation). This does not correspond to an equilibrium distribution at any temperature.

The authors are indebted to Professor W. A. Noyes, Jr., for valuable discussions.

[1] J. T. Dubois, J. Chem. Phys. **33,** 229 (1960).

[2] G. F. Sheats and W. A. Noyes, Jr., J. Am. Chem. Soc. **77,** 1421, 4532 (1955).

[3] J. Heicklen, J. Am. Chem. Soc. **81,** 3863 (1959).

[4] N. A. Coward and W. A. Noyes, Jr., J. Chem. Phys. **22,** 1207 (1954) and H. Okabe and W. A. Noyes, Jr., J. Am. Chem. Soc. **79,** 801 (1957).

[5] M. Boudart and J. T. Dubois, J. Chem. Phys. **23,** 223 (1955).

[6] G. B. Porter, J. Chem. Phys. **32,** 1587 (1960).

[7] Work performed at the Argonne National Laboratory and presented by M. S. Matheson, W. E. Mulac, and W. A. Noyes, Jr., before the Chemical Institute of Canada, Ottawa, Ontario, June, 1960.

[8] G. B. Porter and B. T. Connelly, J. Chem. Phys. **33,** 81 (1960).

Dichroism of 603 cm^{-1} Band of Polyvinyl Chloride

TAKEHIKO SHIMANOUCHI AND MITSUO TASUMI

Department of Chemistry, Faculty of Science, Tokyo University, Hongo, Tokyo, Japan

(Received October 25, 1960)

CRYSTALLINE syndiotactic polyvinyl chloride has two C—Cl stretching absorption bands at 638 and 603 cm^{-1}.[1-3] The latter band showed parallel dichromism for a film which was made of polyvinyl chloride polymerized at low temperature and was stretched about four times.[1]

However, Krimm observed perpendicular dichroism for this band[4] and Asahina and Enomoto[5] observed that the dichromism of this band tends to change with the degree of stretching. Therefore, we have repeated the measurement and found that for the highly syndiotactic polyvinyl chloride the dichroism of this band is reversed in the course of stretching the film.

The measurement was made by using a Perkin-Elmer 112G grating spectrometer equipped with a KBr foreprism; AgCl polarizer was used. The sample was prepared by S. Orihashi and the weakness of the 690 cm^{-1} band shows the high syndiotacticity. The results are shown in Figs. 1 and 2. The three C—Cl stretching vibration bands at 690, 638, and 615 cm^{-1} always have perpendicular dichroism. However, the 603 cm^{-1} band shows parallel dichroism when the film is stretched twice, and perpendicular dichroism when stretched five to seven times.

A similar inversion of dichroism has been found for the 963 and 1255 cm^{-1} bands.[5,6] The recent normal coordinate treatment[7] for the extended zigzag chain of

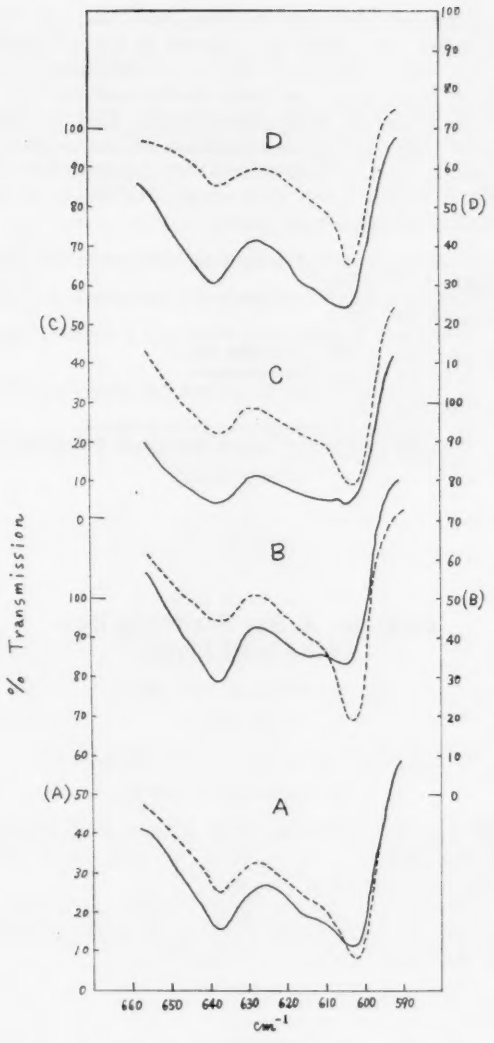

FIG. 1. Infrared spectra of stretched polyvinyl chloride films. (——) Absorption with electric vector perpendicular to stretching direction; (– – –) absorption with electric vector parallel to stretching direction. Stretching is twice at *A*, two and a half times at *B*, five times at *C* and seven times at *D*.

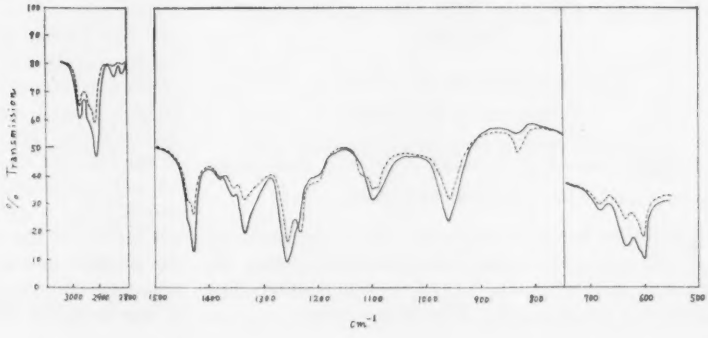

FIG. 2. Infrared spectrum of polyvinyl chloride film stretched seven times, 1500 to 500 cm^{-1} region was recorded with a Perkin-Elmer Model 21 double-beam spectrometer equipped with NaCl and CsBr optics.

syndiotactic polyvinyl chloride shows that the 638 and 603 cm^{-1} bands are assigned to the symmetric (A_1) and antisymmetric (B_1) C—Cl stretching vibrations, respectively, and both the 963 and 1255 cm^{-1} bands belong to the B_1-type vibration. This fact suggests that the initial orientation of the polyvinyl chloride chain is different from that obtained when the film is stretched to a great extent. The details of the results will be published later.

[1] T. Shimanouchi, S. Tsuchiya, and S. Mizushima, Kobunshi Kagaku **8**, 202 (1959).
[2] T. Shimanouchi, S. Tsuchiya, and S. Mizushima, J. Chem. Phys. **30**, 1365 (1959).
[3] S. Krimm, A. R. Berens, V. L. Folt, and J. J. Shipman, Chem. & Ind. (London) **1958**, 1512; **1959**, 433.
[4] S. Krimm (private communication).
[5] M. Asahina and S. Enomoto, J. Chem. Soc. Japan, Pure Chem. Sect. **81**, 1370 (1960).
[6] M. Tasumi and T. Shimanouchi (to be published).
[7] T. Shimanouchi and M. Tasumi, Bull. Chem. Soc. Japan (to be published).

Erratum: X-Ray Scattering by a Cell-Model Liquid

[J. Chem. Phys. **33**, 1086 (1960)]

L. H. Lund

Missouri School of Mines and Metallurgy, Rolla, Missouri

(Received November 18, 1960)

In Figs. 2–5, the values of "a" in the legends in each case should be the value of "a" indicated in the right top corner of each figure.

The expression for $p(r)$ preceding Eq. (8) is Gaussian in r. In the paper the r^2 appears to be an exponent for the square bracket in the exponential.

Erratum: Oxygen Diffusion in Periclase Crystals

[J. Chem. Phys. **33**, 905–6 (1960)]

Y. Oishi and W. D. Kingery

Ceramics Division, Department of Metallurgy, Massachusetts Institute of Technology, Cambridge, Massachusetts

(Received December 7, 1960)

On p. 906 incorrect numerical values are given by the activation entropy and activation energy for diffusion. Following Eq. (3), the correct values are $\Delta S^* = -21$ cal/deg and $\Delta H^* = 58$ kcal/mole.

Notes

Mass Spectrometric Test for an Intermediate in a Photochemical Reaction Involving Chlorine

Gus A. Ropp, C. E. Melton, and P. S. Rudolph

Chemistry Division, Oak Ridge National Laboratory, Oak Ridge, Tennessee*

(Received October 27, 1960)

During the course of studies aimed at developing techniques of direct application of a research mass spectrometer to problems in chemistry and radiation chemistry, a brief investigation was made of the photochemical reaction[1,2] of formic acid with chlorine,

$$\mathrm{HCOOH\ (monomer\ or\ dimer)} + \mathrm{Cl_2} \xrightarrow[\text{light}]{\text{visible}} 2\mathrm{HCl} + \mathrm{CO_2}.$$

The technique used was similar to that employed by Zemeny and Burton[3] and in some respects like the technique used by Kistiakowsky and Kydd.[4] The earlier investigators[1] had reported evidence for the presence of measurable quantities of a reaction intermediate which, they suggested, was probably chloroformic acid (ClCOOH). However, chloroformic acid is unstable, presumably because its structure includes a chlorine atom and a hydroxyl group attached to the same carbon atom. For this reason it seemed improbable to the present investigators that chloroformic acid could have been present as an intermediate in sufficient concentration to explain the experimental data of West and Rollefson.[1]

The reaction was therefore carried out in a 25-ml reaction chamber just before the gold foil leak leading into the ionization chamber of a research mass spectrometer.[5] The expansion bulb and the exit tube leading to the reaction chamber were always kept dark. With the light on, the progress of the reaction was readily followed by the changes in the mass spectrometric peaks corresponding to reactants and products.[6] Mass spectrometric peaks corresponding to chloroformic acid might have been expected if that compound had been formed during the reaction. Although chloroformic acid has not been isolated, a structurally similar chlorine compound, phosgene, yields the positive ion $[COCl_2]^+$ upon electron bombardment in the mass spectrometer.[7] However, no measurable concentration of the ions $[(Cl^{35}COOH)^+$ and $(Cl^{37}COOH)^+$, masses 80 and 82; $(Cl^{35}COO)^-$ and $(Cl^{37}COO)^-$, masses 79 and 81] that would be expected, on the basis of previous studies of the positive spectrum of phosgene[7] and the positive and negative spectra of formic acid,[8] to arise from chloroformic acid was found. Instead a series of ions including $(Cl^{35}HCOOH)^-$ and $(Cl^{37}HCOOH)^-$,

masses 81 and 83, $(Cl^{35}Cl^{35}HCOOH)^-$ and $(Cl^{35}Cl^{37}HCOOH)^-$, masses 116 and 118, and $[Cl^{35}Cl^{35}(HCOOH)_2]^-$ and $[Cl^{35}Cl^{37}(HCOOH)_2]^-$, masses 162 and 164, were observed with the light either on or off. These ions were very probably produced by negative ion-molecule reactions[9] between ionized chlorine and monomeric and dimeric formic acid molecules.

The extreme sensitivity of the research mass spectrometer and its adaptability for studying both positive and negative ions make it highly unlikely that an intermediate present in sufficient concentration to be detected by the methods employed by West and Rollefson would be overlooked in the study described here.

The presently described technique could be useful in examining other photochemical reactions for intermediates. The only proviso is that the intermediate sought for be capable of passing through the gold foil leak and yielding, under electron bombardment, representative positive or negative ions stable enough to reach the collector. Any species detected *only with the light on* could reasonably be attributed to some molecule or radical resulting from a photochemical process. Since natural chlorine contains 75% chlorine-35 and 25% chlorine-37, an ion containing one atom of chlorine can be identified readily because it gives rise to twin peaks, two mass units apart, with heights in 3:1 ratio. A similar characteristic pattern is observed if the ion contains two or more chlorine atoms or if it contains one or more bromine atoms.[5] Ions containing hydrogen can often be identified with the help of deuterium labeling.

The present method can also be applied in tests for intermediates in other types of reactions than those induced by visible light. The source of visible light can, for example, be replaced by a source of ultraviolet light, by a source of ionizing radiation, by a hot filament or by a catalytic surface in the reaction chamber, etc., with minor alterations of the apparatus. Recent work with a modified ion source has demonstrated that *the research mass spectrometer can be operated with the pressure as high as 1 mm inside the ionization chamber.*[10] With such a modified ion source, it should be possible to carry out a photochemically-induced reaction *inside the ionization chamber* by using a light pipe. With this arrangement it should be possible to detect intermediates such as free radicals that might be too unstable to pass through the gold foil leak of an ordinary mass spectrometer.

The authors acknowledge helpful discussions with Milton Burton, P. H. Emmett, and Russell Baldock.

* Operated by the Union Carbide Corporation for the U. S. Atomic Energy Commission.

[1] H. L. West and G. K. Rollefson, J. Am. Chem. Soc. **58**, 2140 (1936).
[2] Gus A. Ropp, C. J. Danby, and D. A. Dominey, J. Am. Chem. Soc. **79**, 4944 (1957).
[3] P. D. Zemeny and M. Burton, J. Phys. & Colloid. Chem. **55**, 949 (1951).
[4] G. B. Kistiakowsky and P. H. Kydd, J. Am. Chem. Soc. **79**, 4825 (1957).
[5] C. E. Melton, Gus A. Ropp, and P. S. Rudolph, J. Chem. Phys. **29**, 968 (1958).
[6] Under controlled conditions, relative reactions rates have been estimated by this method with sufficient precision to permit calculation of deuterium isotope effect ratios, k_H/k_D, when samples of formic acid and formic-*d* acid were used alternately. Details will be presented in a later communication.
[7] J. D. Morrison and A. J. C. Nicholson, J. Chem. Phys. **20**, 1021 (1952).
[8] Gus A. Ropp and C. E. Melton, J. Am. Chem. Soc. **80**, 3509 (1958).
[9] C. E. Melton and Gus A. Ropp, J. Am. Chem. Soc. **80**, 5573 (1958).
[10] C. E. Melton and P. S. Rudolph, J. Chem. Phys. **30**, 848 (1959).

Infrared Spectrum of Crystalline Boron Trichloride*

DAVID A. DOWS AND G. BOTTGER†

Department of Chemistry, University of Southern California Los Angeles, California

(Received August 31, 1960)

NOT long ago one of us concluded,[1] from a study of the infrared spectrum, that the crystal structure of BF_3 was not the same as that of the other boron trihalides, and that there existed strong interactions between adjacent molecules in the crystal. We have now made a study of the spectrum of BCl_3(s) which is of interest in connection with the previous work.

Samples of normal BCl_3 were purified by vacuum distillation. Enriched (90–95% boron-10) samples were prepared by conversion of the enriched BF_3 used previously by heating with $AlCl_3$ at 110°C for 20 hours. Spectra were obtained of the fundamental vibrational transitions above 400 wave numbers; the solid films were at about 84°K.

The spectra obtained showed for each of ν_2 and ν_3 a doublet due to the two boron isotopes; they were quite similar to the analogous spectra for BF_3 except that no shoulders appeared on the components of the doublets.

TABLE I. Observed frequencies in the infrared spectrum of crystalline BCl_3.

80% B^{11}	5–10% B^{11}	Gas[a]	Assignment
447.1	445.0	460	$\nu_2(B^{11})$
466.0	469.0	480	$\nu_2(B^{10})$
926	936	956	$\nu_3(B^{11})$
980	962	995	$\nu_3(B^{10})$

[a] See footnote 2.

No evidence was found for the appearance of the totally symmetric frequency ν_1, which is almost coincident with ν_2.[2] The other fundamental ν_4 lies below

the range of our observations.[2] In the BCl_3 crystal[3] the selection rules[1] are the same as those of the free molecule, and no reduction of degeneracy or splitting of bands (other than due to isotope effects) is predicted. The spectra are in full agreement with these predictions. Table I presents the observed frequencies and includes the gas phase fundamental frequencies.[2] All solid frequencies are believed accurate to one wave number, and differences to somewhat less.

There is clear evidence for intermolecular interaction in ν_2 and ν_3, and intermolecular force constants analogous to those of Table II in footnote 1 are easily obtained by the same method. They are, for ν_2 and ν_3, respectively (0.0072 ± 0.002) and (-0.066 ± 0.006), both in units of 10^{28} erg/g cm^2. These may be compared with the analogous values for BF_3, -0.034 and -0.14. By similar arguments to those used before, the ν_3 coupling constant is most likely due to dipole interactions, the band being quite intense. The ν_2 constant is much smaller *and of the opposite sign in* BCl_3. The latter point can be interpreted as further evidence for a unique BF_3 interaction. The positive sign of the constant in BCl_3 (as evidenced by the *direction* of the B^{10} or B^{11} frequency shift on changing isotopic composition) is consistent with a repulsive B···Cl interaction between molecules, but not with dipole interaction.

Further evidence of the qualitative difference between BF_3 and BCl_3 lies in the gas-solid frequency shifts of ν_2; the shift being relatively small (2%) in the latter, but large (8%) in the former compound. The BCl_3 entropy of vaporization is also normal (20 eu).

The results of this study support the conclusions reached before concerning the BF_3 crystal structure, and make even more interesting the possibilities of that structural problem.

* This work was supported by the Office of Ordnance Research, U. S. Army.

† Present address: Department of Chemistry, University of Washington, Seattle, Washington.

[1] D. A. Dows, J. Chem. Phys. **31**, 1637 (1959).
[2] R. E. Scruby, J. R. Lacher, and J. C. Park, J. Chem. Phys. **19**, 386 (1951).
[3] M. A. Rollier and A. Riva, Gazz. chim. ital. **77**, 361 (1947); M. Atoji, P. J. Wheatley, and W. N. Lipscomb, J. Chem. Phys. **27**, 195 (1957); C. Spencer and W. N. Lipscomb, *ibid.* **28**, 355 (1958).

The Torsional Oscillation Frequency of H_2O_2

DAVID CHIN AND PAUL A. GIGUÈRE

Department of Chemistry, Laval University, Québec, Canada

(Received September 16, 1960)

A FEW years ago the infrared spectrum of hydrogen peroxide vapor was measured from 2 to 23μ in this Laboratory.[1] Toward the long wavelengths a system of two bands was observed, one extending from 16μ with a well-resolved rotational structure, the other beginning around 20μ, of which only the nearest 5 or 6 peaks could be detected. On the basis of these incomplete data the bands were assigned to the torsional mode ν_4 of the H_2O_2 molecule, the doublet arising presumably from the double minimum in the curve of potential energy hindering free internal rotation. We have now carried these measurements out to 33μ by means of cesium bromide optics. The experimental arrangement was the same except that the salt windows of the absorption cell were covered with a thin film of polythene to protect them from attack by the peroxide vapor.

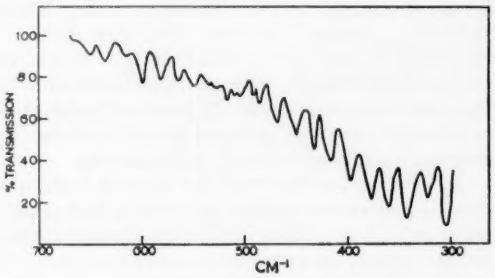

FIG. 1. The far-infrared spectrum of hydrogen peroxide vapor.

The new results (Fig. 1) confirm the previous ones as far as the first band is concerned, but for the lower frequency band the picture has changed entirely. Instead of what appeared as a weak satellite, we now find a strong, separate band with the expected spacing (18 cm^{-1}) of the rotational structure. As far as may be ascertained from the incomplete tracing its center lies at 314 cm^{-1}. Now, this band can only belong to the torsional oscillation, and the much weaker one at about 575 cm^{-1} is the first overtone. The anharmonicity seems a little low, 53 cm^{-1} compared to 87 cm^{-1} in N_2H_4 [2]; however, there is some uncertainty as to the center of the overtone band because of overlapping. Also it is somewhat surprising that the present value for ν_4 of H_2O_2 is well below the torsional frequency of N_2H_4, 376.7 cm^{-1}.

A significant feature of the two H_2O_2 bands is the absence of any measurable doubling as exists in the overtones of the OH stretching modes.[3,4] The explanation offered previously for this phenomenon, namely the double minimum in the potential curve, must be revised since it predicts a large doublet splitting for ν_4 and $2\nu_4$. Coupling between the modes involved and the torsional mode in the excited state would be an alternative explanation. That the actual splitting is smaller than the limit of resolution in the present work (0.7 cm^{-1}) agrees with previous conclusions[1,5,6] about

a fairly high *trans* barrier for H_2O_2. According to the perturbed-harmonic-oscillator approximation[7] the frequency 314 cm^{-1} for ν_4 leads to a barrier height of some 2.5 kcal, to be compared with the value 3.5 kcal derived from the calorimetric entropy.[8] Barrier heights of only a few hundred calories have been calculated from the microwave spectrum[9–11] although a reinterpretation of the data[12] has shown them to be equally compatible with a barrier of 2.8 kcal.

In condensed phases the torsional frequency of H_2O_2 will naturally be much higher than for the free molecule because of strong hydrogen bonds. It is, in fact, more than doubled: 635 cm^{-1} in the liquid[13] and 695 cm^{-1} in the crystal.[14] On the other hand, a very weak and diffuse band has been observed near 395 cm^{-1} for H_2O_2 trapped in an inert matrix[15] (conc. 1/60 in solid nitrogen at 20°K). The shift seems reasonable considering the type of forces involved.

We are grateful to the National Research Council of Canada for a generous grant.

[1] O. Bain and P. A. Giguère, Can. J. Chem. **33,** 527 (1955).
[2] A. Yamaguchi, I. Ichishima, T. Shimanouchi, and S. Mizushima, J. Chem. Phys. **31,** 843 (1959).
[3] L. R. Zumwalt and P. A. Giguère, J. Chem. Phys. **9,** 458 (1941).
[4] P. A. Giguère, J. Chem. Phys. **18,** 88 (1950).
[5] W. G. Penney and G. B. B. M. Sutherland, J. Chem. Phys. **2,** 492 (1934).
[6] E. N. Lassettre and L. B. Dean, J. Chem. Phys. **17,** 317 (1949).
[7] L. Pauling and E. B. Wilson, *Introduction to Quantum Chemistry* (McGraw-Hill Book Company, Inc., New York, 1935).
[8] P. A. Giguère, I. D. Liu, J. S. Dugdale, and J. A. Morrison, Can. J. Chem. **32,** 117 (1954).
[9] J. T. Massey and D. R. Bianco, J. Chem. Phys. **23,** 442 (1954).
[10] J. T. Massey and R. W. Hart, J. Chem. Phys. **23,** 942 (1955).
[11] E. Hirota, J. Chem. Phys. **28,** 839 (1958).
[12] G. E. Blomgren, Ph.D. thesis, University of Washington, 1956.
[13] R. C. Taylor, J. Chem. Phys. **18,** 898 (1950).
[14] P. A. Giguère and K. B. Harvey, J. Mol. Spectroscopy **3,** 36 (1959).
[15] T. Miyazawa (private communication).

Infrared Absorption of Nitrate Ions Dissolved in Solid Alkali Halides

A. Strasheim and K. Buijs

Chemical Physics Group of the National Chemical and Physical Research Laboratories, Pretoria, South Africa

(Received October 10, 1960)

FREQUENCY shifts in the infrared spectra of complex ions in solid solutions have recently been described by Ketelaar and van der Elsken[1] as being due mainly to the polarization of the matrix, i.e., long range forces. Maki and Decius[2] calculated the shifts for ν_3 of NCO^- due to interaction between dipole and induced dipole and found such small shifts that they had to conclude that, although the induction energy exerted a definitely measurable influence on the frequencies, the repulsive (short range) interactions were the more important. In addition to this evidence and to the temperature influence[2,3] upon the frequency, the following findings also seem to support the importance of short range forces.

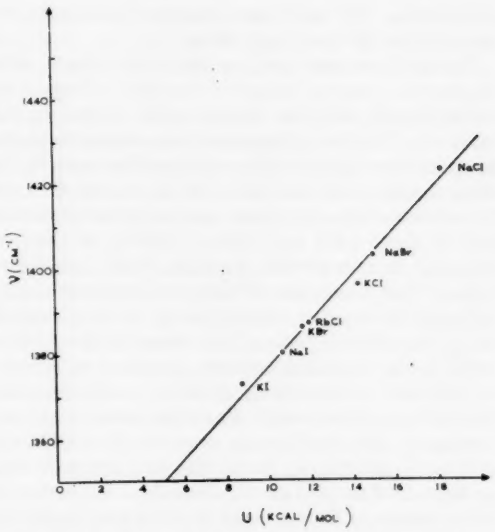

FIG. 1. ν_3 of the NO_3^- ion plotted against the combined contribution of repulsive, dipole-dipole, and dipole-quadrupole interaction energies to the lattice energy of the alkali halides.

During a study of the behavior of the asymmetrical stretching vibration (ν_3) of NO_3^- for nitrate ions dissolved in various alkali halides, it was found that a graph of the frequency versus the combined contribution of repulsive, dipole-dipole, and dipole-quadrupole interaction energies (given by the Born-Mayer equation) to the lattice energies,[4] yields a straight line [Fig. (1)].

Apart from the nitrate ion, this has also been found true for all the vibrations of NCO^-, NO_2^-, BH_4^-, and HF_2^- studied. Extrapolating we find a frequency of about 1325 cm^{-1} for ν_3 of a "free" NO_3^- ion. This value rises by about 2 cm^{-1}, if the correction derived by Maki and Decius[2] is applied for the polarization of the surrounding lattice by the changing dipole of the nitrate ion. The slope of the straight line is different for different vibrations and has as yet not been correlated with any parameter. From the observed correlation between the part of the lattice energy due to short range forces and the frequencies of complex ions in alkali halides, it can be concluded that these short range forces to which repulsive forces make the main

contribution, are, for the major part if not totally, responsible for the frequency shifts.

The solid solutions used for this type of study were prepared by pressing pellets of the nitrate form of an anion-changer with the desired alkali halide in the usual way. The ion exchange reaction during the pressing process results in a solid solution of the anion in the alkali halide. Amberlite IRA 400 in its nitrate form gives an excellent absorption band of dissolved nitrate ions at about 1400 cm^{-1} (ν_3), if 0.06% of the ion-exchanger is mixed with the alkali halide (thickness 1 mm). The absorption of this small amount of ion-exchanger is very low and can easily be compensated for by the chloride form of the ion-exchanger with a double beam spectrophotometer. Attached to Amberlite IRA 400, the nitrate ion shows a broad absorption band at about 1360 cm^{-1}. From the ratio of the intensities of this band due to attached nitrate (about 1360 cm^{-1}) and the one due to dissolved nitrate (varying from 1373 to 1423 cm^{-1}), the rate of ion-exchange can be estimated. It was found that this ratio decreased in the following order: NaCl, NaBr, KCl, RbCl, KBr, KI, the exchange for the last three being more or less complete. The lattice energies of the alkali halides decrease in the same order. If, however, the distance between the center of an oxygen atom and the surface of the nearest spherical cation is calculated for an undistorted nitrate-ion (with N–O distance of 1.218 A[5]) in an undistorted alkali halide lattice (the three-fold axis of the ion coinciding with that of the crystal), an increase in the following order is found: RbCl, KCl, NaCl, RbBr, KBr, NaBr, RbI, KI, NaI. From this it can be concluded that the activation energy of the ion exchange reaction depends on the lattice energy of the alkali halide and that spatial effects are only of second order.

[1] J. A. A. Ketelaar and J. van der Elsken, J. Chem. Phys. **30**, 336 (1959).
[2] A. Maki and J. C. Decius, J. Chem. Phys. **31**, 772 (1959).
[3] W. C. Price, W. F. Sherman, and G. R. Wilkinson, Spectrochim. Acta **16**, 663 (1960).
[4] F. Seitz, *The Modern Theory of Solids* (McGraw-Hill Book Company, Inc., New York, 1940), p. 88.
[5] R. L. Sass, R. Vidale, and J. Donohue, Acta Cryst. **10**, 567 (1957).

Use of Gaussian Orbitals for Atoms-in-Molecule Calculations

M. KRAUSS

National Bureau of Standards, Division of Chemistry, Washington, D. C.

(Received August 2, 1960

RELATIVELY simple applications of the "atoms-in-molecule" concept can yield accurate results for the total energy of diatomic molecules.[1] However, it has been shown that this is the result of the approximate cancellation of the differences between the results of the molecular and atomic calculations, using the same basis set, and the Hartree-Fock value.[2] If we do not extend the basis, or otherwise improve the basis atomic functions, the calculations must be calibrated for those molecules for which little or no experimental evidence exists. Since the Gaussian orbitals proposed by Boys[3] yield reasonable overlap densities in the bonding or interatomic region and are easily handled for polyatomic cases,[4] they should be suitable for this type of calculation. Before proceeding to a large computational program these procedures were tested on the H_2 molecule and the results are reported here.

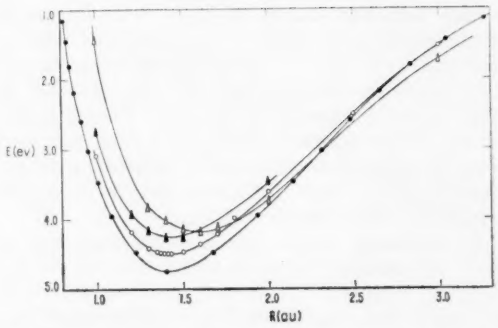

FIG. 1. Binding energy in ICC approximation. Experimental, ●; case I, △; case II, ▲; and case III, ○.

The calculations parallel those reported by Hurley[5] for Slater functions. Three calculations are reported. All are based on the wave functions

$$\Psi=\Psi_O+\alpha\Psi_S+\beta\Psi_C+\gamma\Psi_I, \tag{1}$$

which are defined by Hurley.[5] The atomic orbitals were chosen as follows:

$$a(\delta)=(2\delta/\pi)^{3/4}\exp(-\delta r_A^2),$$

$$a_x(\epsilon)=(2^{7/4}/\pi^{3/4})\cdot\epsilon^{5/4}\cdot x\cdot\exp(-\epsilon r_A^2), \text{ etc.} \tag{2}$$

For two of the cases the 1s functions were chosen as a linear combination of two 1s functions

$$a=N\{a(\zeta)+k\cdot a(\zeta\cdot\delta)\}. \tag{3}$$

In case I a one-Gaussian 1s function was used for Ψ_O and Ψ_I and in case II a two-Gaussian 1s function was used in Ψ_O and Ψ_I. For case III the two-Gaussian 1s function was used with all four of the Ψ's. In case III all nonlinear parameters were not completely minimized at all distances but only small improvements are expected if this is done. The results are compared with the experimental curve in Fig. 1. In Table I the Gaussian results are compared with those reported by Hurley for equilibrium separation.

The results are poorer than Hurley's, but considering the relative ease of the calculations, they show some promise. This is supported by the improvement in the energy from case II to case III which is of the same order as that found with Slater functions. It must also be noted that the internuclear separation and the shape in the neighborhood of the minimum is computed reasonably accurately in cases II and III. We are encouraged that calculations on more complicated systems can be properly calibrated to yield comparably accurate results.

TABLE I. Equilibrium constants for H_2.

	Binding energy (ev)	Nuclear separation (a.u.)
Weinbaum[a]	4.03	1.42
Hirschfelder-Linnett[b]	4.26	1.42
W-ICC[c]	4.42	1.41
HL-ICC[c]	4.72	1.40
I	−0.07	1.6
II	3.19	1.4
III	3.41	1.43
I-ICC	4.19	1.6
II-ICC	4.26	1.4
III-ICC	4.50	1.41
Experimental[d]	4.74	1.40

[a] S. Weinbaum, J. Chem. Phys. **1,** 593 (1933).
[b] J. O. Hirschfelder and J. W. Linnett, J. Chem. Phys. **18,** 130 (1950).
[c] See footnote 5. ICC-Intra-Atomic Correlation Correction.
[d] R. Rydberg, Z. Phys. **73,** 376 (1931).

[1] A. C. Hurley, Proc. Roy. Soc. (London) **A249,** 402 (1959); Revs. Modern Phys. **32,** 400 (1960).
[2] B. J. Ransil and M. Krauss, J. Chem. Phys. (to be published).
[3] S. F. Boys, Proc. Roy. Soc. (London) **A200,** 542 (1950).
[4] L. C. Allen, J. Chem. Phys. **31,** 736 (1959).
[5] A. C. Hurley, Proc. Phys. Soc. (London) **A69,** 49 (1956).

Comment on the Difference between the Bond Orders Calculated by SCF MO and Simple MO Method

MILAN RANDIĆ

Institute "Rudjer Bošković", Zagreb, Yugoslavia

(Received June 3, 1960)

PRITCHARD and Sumner[1] have calculated bond lengths in a number of aromatic hydrocarbons using a self-consistent field MO approximation (as developed by Pople[2]). With some disappointment it was noticed that on the average, calculated bond lengths are in no better agreement with experimental values than the bond lengths obtained applying simple MO (Hückel approximation).

However, at the time, no comparison between the two approximate methods was made. This is of interest since such comparison will give some information of redistribution of electrons after MO→SCF MO refinements.

Bond orders, as defined by Coulson[3] give, to some extent, a measure of electron distribution over a molecule, and refinements to wave functions will somehow reflect themselves in bond orders. It therefore seems worthwhile to investigate such changes regardless of the correlations with experimental quantities.

From SCF MO and simple MO we see that although there is no great difference between mean bond lengths calculated in the two approximations, there are considerable differences in the lengths of individual bonds.

For example, the results for naphthalene are given in Table I. Since in SCF calculations there is some electron repulsion included, a change from simple MO's to SCF MO's is related to partial inclusion of electron correlation (interaction) and this results in a change of bond lengths. Shorter bond lengths will have some additional double bond character, so to speak, while longer ones will have more single bond character. If we write down a valence structure for the molecule, writing single and double bonds according to an increase or a decrease in bond lengths, i.e., according to whether a bond has more single or more double bond character, on going from a MO to a SCF MO calculation we obtain the valence structures shown in Fig. 1.

In the cases of naphthalene, biphenylene, phenanthrene, chrysene, and coronene, we have as a result one of the conventional valence-bond structures for those molecules. In all these cases the refinement MO→SCF MO is equivalent to giving more weight to one of the

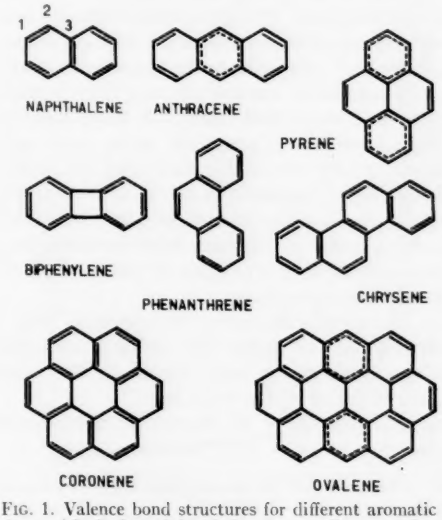

FIG. 1. Valence bond structures for different aromatic hydrocarbons with single and double bonds according to an increase or a decrease in bond lengths after an improvement from Hückel approximation to SCF MO is made.

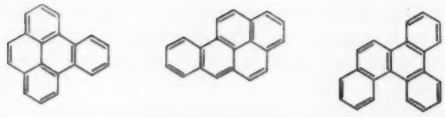

FIG. 2. Valence bond structures for some less common hydrocarbons with single and double bonds according to an increase or a decrease in bond lengths after an improvement from Hückel approximation to SCF MO is made.

stable Kekulé-type structures and it is very interesting that these structures are the ones with the maximum number of benzenoid rings. (The most stable structures as given by the Fries rule).

For anthracene, pyrene, and ovalene, the structures obtained are again in accordance with the Fries rule.

TABLE I. Bond lengths of naphthalene calculated by simple MO and SCF MO method.

Bond	MO	SCF	Difference
2–3	1.410	1.424	+0.014
1–1′	1.400	1.418	+0.018
1–2	1.377	1.364	−0.013
3–3′	1.417	1.396	−0.021

However, in these cases there are two or more equivalent valence bond structures and the resulting structure is a linear combination of these.

Hall[4] has calculated bond orders of some less common hydrocarbons using slightly different approximations. Again, when an SCF MO and simple MO bond length are compared, the same regularities are noted: Favored valence structures obtained after the improvement MO→SCF MO indicate the importance of structures with maximum number of rings fully benzenoid (Fig. 2). Hall states that from SCF bond orders one sees, with some exceptions, that larger bond orders are increased and the smaller decreased. In fact this rule has too many exceptions and is only partly true that larger bond orders indeed increase, but smaller ones either increase or decrease. As we have shown the change is related to the position of the bond in fully benzenoid valence structures.

From the correlation noted we conclude that the improvement on the simple MO method corresponds in VB theory to giving more weight to the valence structures favoured by the Fries rule.

I wish to thank Dr. J. N. Murrell for discussing the problem.

[1] H. O. Pritchard and F. H. Sumner, Proc. Roy. Soc. (London) **A226,** 128 (1954).
[2] J. A. Pople, Trans. Faraday Soc. **49,** 1375 (1953).
[3] C. A. Coulson, Proc. Roy. Soc. (London) **A169,** 413 (1939).
[4] G. G. Hall, Trans. Faraday Soc. **53,** 573 (1957).

Infrared Spectrum of Stannane

LEOPOLD MAY

Department of Chemistry, The Catholic University of America, Washington, D. C.

AND

CLYDE R. DILLARD*

Department of Chemistry, Brooklyn College, Brooklyn, New York

(Received October 20, 1960)

DURING the investigation of the infrared spectra of alkyltin hydrides, the problem of assigning the correct frequencies for the Sn—H stretching modes arose. The infrared spectrum of stannane (SnH_4) was examined to assist in this assignment.

Stannane was prepared by the reaction of lithium aluminum hydride with anhydrous stannic chloride following the procedure of Finholt *et al.*[1] The spectrum was measured with stannane at a pressure of 20 mm Hg in a potassium bromide cell. Spectra were obtained with a Perkin-Elmer infrared spectrophotometer, model 13, using sodium chloride and cesium bromide optics. Air was the blank in all runs.

The spectrum of stannane revealed two areas of major absorption. Each had three peaks which are characteristic of *P*, *Q*, and *R* branches found with similar molecules such as SiH_4.[2] The observed absorption maxima for ν_3 are 1813, 1860, and 1910 cm^{-1} and for ν_4, they are 677, 703, and 760 cm^{-1}. These bands are not sufficiently resolved to permit the direct calculation of *B*. Assuming valence forces,[3] ν_1 is calculated to be 1910 cm^{-1} and ν_2 is 829 cm^{-1}. The symmetrical Sn–H stretching frequency is 1910 cm^{-1} (calculated) and the degenerate mode is 1860 cm^{-1}.

From these same calculations, the force constants are $k=2.17\times10^5$ and $k_\delta/l^2=0.136\times10^5$ d/cm. Using Gordy's rule,[4]

$$k=1.67N(\chi_{Sn}\chi_H/d^2)^{3/4}+0.30,$$

where N is the bond order of 1.00, and the electronegativities χ are given by Gordy[4] (for tin, 1.7, and for hydrogen, 2.13), the internuclear distance d is 1.76 A. This compares favorably with the value of 1.700 A

TABLE I. Thermodynamic properties of SnH_4.

t °C	$-(F°-E_0°)/T$ cal $mole^{-1}$ deg^{-1}	$S°$ cal $mole^{-1}$ deg^{-1}	$Cp°$ cal $mole^{-1}$ deg^{-1}	$(H°-E_0°)/T$ cal $mole^{-1}$ deg^{-1}
−52	116.07	124.41	9.82	8.33
0	117.87	126.61	11.11	8.74
25	119.95	127.61	11.73	8.96
100	120.79	130.59	13.60	9.79
150	121.99	132.19	14.44	10.20
500	127.26	139.84	18.44	12.58
1000	136.54	153.13	22.87	16.59

which was reported by Lide[5] from the microwave studies of CH_3SnH_3 and the values of 1.70 and 1.694 A calculated from normal valence radii and calculated bond energies.[6]

Using the calculated value for the internuclear distance (1.76 A), the moment of inertia, I_0, is 13.91×10^{-40} g cm^2 and B is 2.01 cm^{-1}. The bond dissociation energy is 73.7 kcal/mole using the potential energy function of Lippincott and Schroeder.[7,8] This value compares favorably with the value of 71 kcal/mole given by Huggins.[6] Using the available data, the thermodynamic functions given in Table I are calculated assuming an ideal gas, rigid rotator, and harmonic oscillator.

* This research was supported in part by a grant from the Petroleum Research Fund administered by the American Chemical Society. Grateful acknowledgment is hereby made to the donors of said fund.

[1] A. E. Finholt, A. C. Bond, Jr., K. E. Wilzbach, and H. I. Schlesinger, J. Am. Chem. Soc. **69**, 2692 (1947).
[2] W. B. Steward and H. H. Nielsen, Phys. Rev. **47**, 828 (1935).
[3] G. Herzberg, *Infrared and Raman Spectra of Polyatomic Molecules* (D. Van Nostrand Company, Inc., Princeton, New Jersey, 1947), p. 182.
[4] W. Gordy, J. Chem. Phys. **14**, 305 (1946).
[5] D. R. Lide, Jr., J. Chem. Phys. **19**, 1605 (1951).
[6] M. L. Huggins, J. Am. Chem. Soc. **75**, 4123 (1953).
[7] E. R. Lippincott and R. Schroeder, J. Chem. Phys. **23**, 1131 (1955).
[8] E. R. Lippincott and R. Schroeder, J. Am. Chem. Soc. **78**, 5171 (1956).

Ferroelectricity in Mixed Bismuth Oxides with Layer-Type Structure

E. C. SUBBARAO

Westinghouse Research Laboratories, Pittsburgh, Pennsylvania

(Received September 26, 1960)

MATTHIAS[1] and Smolenskii and Kozhevnikova[2] have pointed out that the occurrence of ferroelectricity in oxides is favored when the crystal structure contains small, highly polarizable ions surrounded by oxygen octahedra, which are linked through corners. Perovskite, pyrochlore, and tungsten-bronze type structures, in which a number of oxide ferroelectrics were found, fit this description.

Aurivillius[3] found that perovskite-type structure units of the form $(Me_{x-1}R_xO_{3x+1})^{2-}$ and $(Bi_2O_2)^{2+}$ layers are stacked along the pseudotetragonal c axis in the crystal structure of some mixed bismuth oxides. The formula comprises $(Bi_2O_2)^{2+}(Me_{x-1}R_xO_{3x+1})^{2-}$, in which Me can be mono-, di-, or tri-valent ions, or a mixture thereof, and R represents Ti^{4+}, Nb^{5+}, Ta^{5+}, etc. The values of x can be 2, 3, 4 etc.

Several new compounds of this structure-type were synthesized by solid state reaction of the constituent oxides or carbonates between 1050° and 1175°C. X-ray diffraction powder patterns, obtained with Cu $K\alpha$ radiation, were indexed up to $2\theta=60°$, using pseudotetragonal cell parameters given in Table I. The value of $a\simeq 3.9$ A in all cases, whereas that of c depends upon the number of perovskite-type layers in the unit cell. The true symmetry of most of these compounds is probably orthorhombic. However, only the powder pattern of $PbBi_4Ti_4O_{15}$ shows an orthorhombic distortion with $b/a\simeq 1.005$.

Smolenskii *et al.*[4] recently reported ferroelectric behavior in $PbBi_2Nb_2O_9$ of this structure-type,[3] with a Curie temperature of 526°C. In the present work, the Curie point was placed at 550°C. The temperature dependence of dielectric constant of several compounds, measured on ceramic disks, has a behavior typical of ferroelectrics (Fig. 1). Dielectric constant maxima are observed at the (Curie) temperatures given in Table I. The polar axis is probably in the plane perpendicular to the c axis. At 250°C with an applied field of 30 kv/cm, reasonably saturated (D–E) hysteresis loops were observed only with $PbBi_2Ta_2O_9$ ceramics. The coercive field is perhaps large for other compounds, as for $PbTiO_3$. Ceramic disks, "poled" at 200°C under a dc field of 20 to 50 kv/cm, exhibit a weak but definite

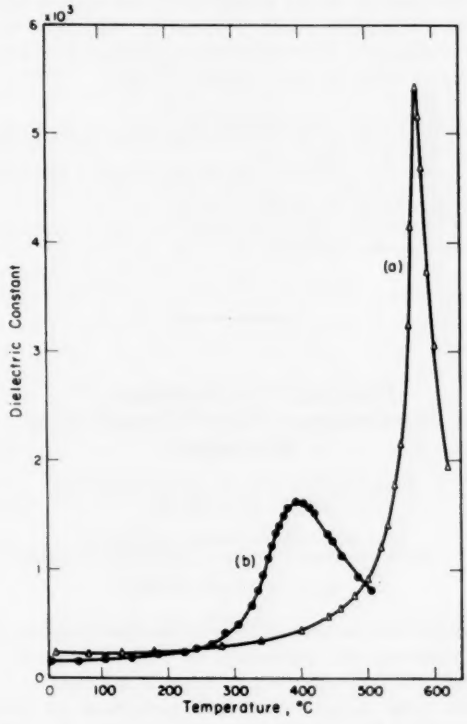

FIG. 1. Temperature dependence of dielectric constant of (a) $PbBi_4Ti_4O_{15}$ and (b) $BaBi_4Ti_4O_{15}$ ceramics.

piezoelectric response (d_{33} of the order of 10^{-11} coul/N).

$PbDy_2Nb_2O_9$, $La_4Ti_3O_{12}$,[5] and $PbBi_4Zr_4O_{15}$ could not be obtained with layer-type structure. The smaller Cd^{2+} (0.97 A) ions could not be substituted for Pb^{2+} (1.20 A) ions in $PbBi_2Ti_2NbO_{12}$. These data indicate the importance of Bi^{3+} ions for the formation of the

TABLE I. Properties of mixed bismuth oxides $(Bi_2O_2)^{2+}$ $(Me_{x-1}R_xO_{3x+1})^{2-}$.

x	Compound	Pseudotetragonal parameters, A		Curie temp, °C
		a	c	
2	$PbBi_2Nb_2O_9$	3.88_2	25.5_0	550
2	$PbBi_2Ta_2O_9$	3.88_2	25.3_0	430
3	$BaBi_3Ti_2NbO_{12}$	3.87_4	33.7_0	~270
3	$PbBi_3Ti_2NbO_{12}$	3.86_7	33.5_5	290
4	$BaBi_4Ti_4O_{15}$	3.84_9	41.6_5	395
4	$PbBi_4Ti_4O_{15}$	3.84_5	41.3_5	570

$(Me_2'O_2)^{2+}$ layers and the normal geometrical considerations for the stability of the perovskite-type units $(Me_{x-1}R_xO_{3x+1})^{2-}$.

A more detailed account of the layer type compounds and their solid solutions will be published later.

The author wishes to thank G. Shirane for many helpful discussions and J. Hrizo for assistance with measurements. This work was supported in part by contract with the Army Ordnance Corps.

[1] B. T. Matthias, Science **113**, 591 (1951).
[2] G. A. Smolenskii and N. V. Kozhevnikova, Doklady Akad. Nauk S.S.S.R. **76**, 519 (1951).
[3] B. Aurivillius, Arkiv Kemi **1**, 463, 499 (1949); **2**, 519 (1950).
[4] G. A. Smolenskii, V. A. Isupov, and A. I. Agranovskaya, Fiz. Tverdogo Tela **1**, 169 (1959).
[5] P. Popper, S. N. Ruddlesden, and T. A. Ingles, Trans. Brit. Ceram. Soc. **56**, 356 (1957).

Paramagnetic Resonance of Bis-Cyclopentadienyl Vanadium in Ferrocene*

H. H. DEARMAN,† W. W. PORTERFIELD,‡ AND H. M. MCCONNELL§

Gates and Crellin Laboratories of Chemistry,|| California Institute of Technology, Pasadena, California

(Received October 14, 1960)

IN this note we extend the previous observation of the paramagnetic resonance of bis-cyclopentadienyl vanadium (vanadocene) in benzene solution[1] to the solid state. Experiments were performed on single crystals of bis-cyclopentadienyl iron (ferrocene) that contained a small percentage of vanadocene.

Vanadocene was prepared by the method of Wilkinson *et al.*[2] The material was purified by repeated sublimations and subsequently handled either in evacuated containers or in an oxygen-free dry box. Crystals were grown by cosublimation of vanadocene and ferrocene in ampules partially immersed in a constant temperature bath maintained at 37°C. The spectra were obtained at room temperature with a spectrometer of conventional design which operated at 22.5 kMc, and the magnetic field modulation frequency was 400 cps. A cylindrical cavity operating on the TE_{011} mode was constructed so that it could be detached and the crystals mounted with the entire assembly in the dry box. Crystal alignment was carried out visually using the crystallographic information of Pfab and Fischer.[3]

There are two nonequivalent molecules per unit cell of ferrocene, and the fivefold molecular axes lie approximately on the b–c diagonals of the monoclinic cell. Figure 1 shows the magnetic field at which a resonance line occurs as a function of the angle made by the field direction and a vector in the (100) plane, when that plane is parallel to the plane of rotation of H_0. We note the absence of lines occurring at high magnetic fields (effective g factor <2.00). A similar behavior has been reported for the isoelectronic system Cr^{3+} in emerald,[4] where the splitting of the ground electronic quartet in zero applied magnetic field was much larger than the

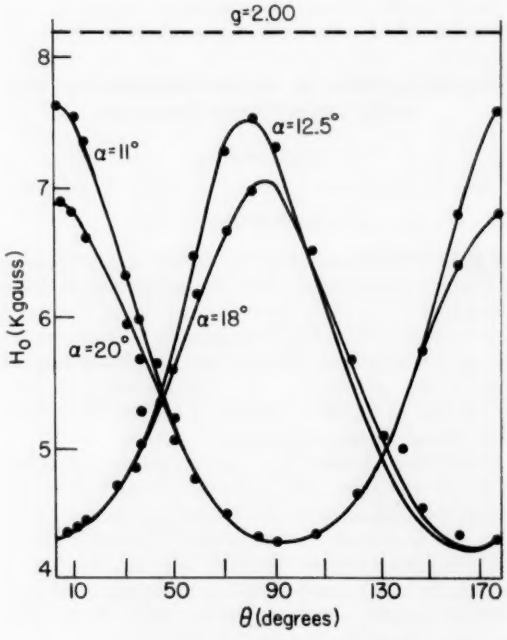

FIG. 1. Angular dependence of EPR spectra of $V(C_5H_5)_2$ in $Fe(C_5H_5)_2$ crystal; ● experimental, —— calculated.

energy of the incident radiation. The continuous curves in Fig. 1 were calculated using the formula of Geusic *et al.* which relates the effective g factor of the $-\frac{1}{2}\rightarrow\frac{1}{2}$ transition to the angle made by the magnetic field direction and the axis of the ligand field

$$g^{\text{eff}}=[g_{||}^2+(4g_{\perp}^2-g_{||}^2)\sin^2\theta]^{\frac{1}{2}} \times[1-\tfrac{1}{2}(g_{\perp}\beta H/2D)^2F(\theta)], \quad (1)$$

where

$$F(\theta)=\{[3\sin^2\theta(\sin^2\theta-\tfrac{1}{3})]/(\sin^2\theta+\tfrac{1}{3})\}.$$

Owing to errors in crystal alignment, the configuration in which the magnetic field was parallel to the fivefold axis was never achieved. If (100) makes the angle α with the rotation plane of H_0, the real angle θ between H_0 and the molecular axis is given in terms of the angle θ' read from the vernier by $\cos\theta=\cos\theta'\cos\alpha$. The fit of the angular dependence data to Eq. (1) allows the determination of the zero field splitting parameter, $|2D|=50\pm3$ kMc. Here we have made the assumption that the g factor is approximately isotropic and has the value 2.00 as determined in benzene solution[1] and as predicted by previous theoretical studies.[5]

The occurrence of a maximum of four lines instead of two (one from each molecule in the unit cell) is probably to be explained by crystal twinning. Another set of experiments in which the (100) plane was oriented approximately perpendicular to the plane of rotation of H_0 showed the following features: (1) the maxima in the angular dependence diagram appear at much lower magnetic fields; (2) the distance between maxima in angular units decreases markedly; (3) the minimum magnetic field at which a line is observed does not change from that shown in Fig. 1. These features suggest that the crystal studied was twinned such that the (100) plane of one member makes an angle of 30° (or 10°) with the (100) plane of the other.

Because the zero field splitting parameter depends only on the effective g factor evaluated at $\theta=90°$, its value is unaffected by the occurrence of the additional lines. Also any 180° rotation of H_0 makes certain attainment of the configuration in which the magnetic field is perpendicular to the axis of the ligand field.

* Supported by the National Science Foundation, the Office of Ordnance Research, U. S. Army, and the U. S. Public Health Service.

† Present address: Enrico Fermi Institute for Nuclear Studies, University of Chicago, Chicago 37, Illinois.

‡ Present address: Department of Chemistry, University of North Carolina, Chapel Hill, North Carolina.

§ Alfred P. Sloan Fellow.

|| Contribution No. 2636.

[1] H. M. McConnell, W. W. Porterfield, and R. E. Robertson, J. Chem. Phys. **30**, 442 (1959).

[2] G. Wilkinson, F. A. Cotton, and J. M. Birmingham, J. Inorg. & Nuclear Chem. **2**, 95 (1956).

[3] W. Pfab and E. O. Fischer, Z. anorg. Chem. **274**, 316 (1953).

[4] J. E. Geusic, M. Peter, and E. O. Schulz-DuBois, Bell System Tech. J. **38**, 291 (1959).

[5] R. E. Robertson and H. M. McConnell, J. Phys. Chem. **64**, 70 (1960).

Some Calculations for a One-Dimensional Salt Mixture

MILTON BLANDER

*Reactor Chemistry Division, Oak Ridge National Laboratory, Oak Ridge, Tennessee**

(Received August 22, 1960)

EXPERIMENTAL thermodynamic studies of binary mixtures of monovalent molten salts with a common anion, have indicated that the negative deviations from ideal solution behavior observed in phase diagrams of some alkali halides,[1] and negative heats of mixing[2] observed with molten nitrates, can be related to differences in the ionic sizes of the cations. A simple calculation was made by Förland[3] ascribing nonideality to the change of coulombic repulsive energy of next-nearest neighbor cations. Because of the long-range nature of coulombic interactions, it is necessary to extend Förland's calculations to an infinite array in order to assess the effect of interactions of longer range than next-nearest neighbors.

In this note are presented calculations of the coulombic energy of mixing of one molecule of a hypothetical salt BC, the salt consisting of an infinite linear array of hard charged spheres of interionic distance $r(1+\Delta)$, with a solvent AC, consisting of an infinite linear array of hard charged spheres with an interionic distance r. This model is clearly an unrealistic one for a real three-dimensional salt. However, certain results of the calculation based on the one-dimensional model have features in common with measurements on real molten salt mixtures,[2] and it is felt that this may not be fortuitous. The calculations, qualitatively, give an intuitive insight into one possible cause (i.e., coulombic interactions) for the deviations from ideality and it is hoped that these naive calculations may serve to provoke a more sophisticated approach.

The inset of Fig. 1 gives a picture of a portion of the infinitely dilute solution of one molecule of BC in the solvent AC. If ΔE is the coulombic energy of the solution minus the energy of the pure solvent and minus the average energy of one molecule of the pure solute, then ΔE may be calculated from the coulombic energies of the solution, solvent, and solute. After combining terms and simplifying the double summations involved, Eq. (1) was obtained for ΔE,

$$\Delta E=-e^2/r\left[2\sum_1^{\infty}\frac{1}{n+\Delta}(-1)^n - (1+2\Delta)\sum_1^{\infty}\frac{1}{n+2\Delta}(-1)^n - \left(\frac{1-\Delta}{1+\Delta}\right)\sum_1^{\infty}\frac{1}{n}(-1)^n\right]. \quad (1)$$

Figure 1 is a plot of values of $-\Delta Er/e^2$ as a function

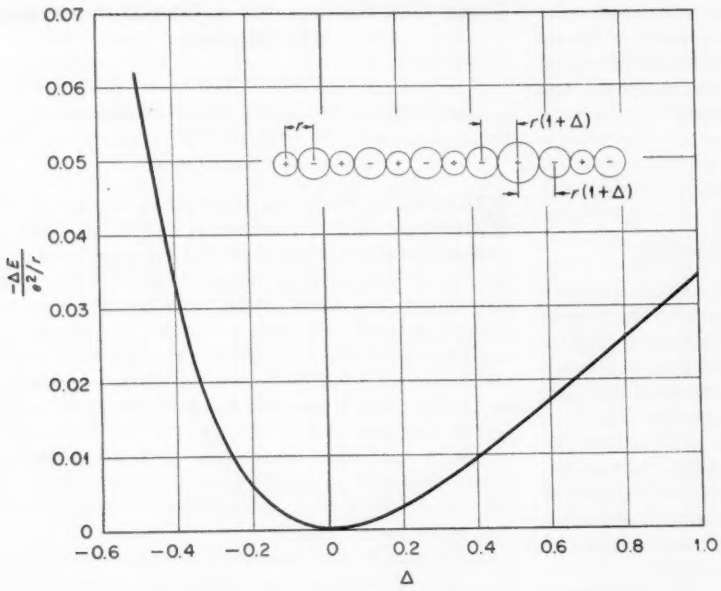

FIG. 1. The energy of solution as a function of Δ. (Inset is a section of the one-dimensional solution model.)

of Δ. ΔE is always negative, but is less negative than the calculated values of Förland, being approximately 0.4 times the magnitude. Thus, the interactions of longer range than the next-nearest neighbor repulsions, have a considerable effect on the total energy of mixing and need to be taken into account in any realistic theory.

In considering the mutual dissolution of two specific salts AC and BC, Eq. (1) leads to a somewhat more negative value of ΔE for the case when the solute is the salt with the larger cation, than when it is the salt with the smaller cation. For example, $-\Delta E/e^2$ when Δ is 0.25 and 0.50, is $0.00452/r_A$ and $0.0137/r_A$, respectively. The interchange of solute and solvent for these two cases leads to values of $-\Delta E/e^2$ of $0.00438/r_A$ and $0.0129/r_A$ (r_A is the interionic distance of the salt with the smaller cation). This asymmetry is in the same direction as the experimental measurements of the heat of solution.[2] Since the calculations of Förland, which take only next-nearest neighbor cation interactions into account, are symmetric, the asymmetry is caused by the interactions of longer range than next-nearest neighbors.

Polarization effects will contribute to the energy of solution. For example, the field intensity on all ions in the pure solute and solvent is zero but is not zero on the two anions adjacent to the solute cations in the mixture. For two given salts, the field intensity on the two anions adjacent to the solute cation, as calculated from the one-dimensional model, is greater when the solute has a larger cation than the solvent, than for the case when the solute cation is smaller than that of the solvent. This difference or asymmetry is due to the ions further away than next-nearest neighbors. If the anions are polarizable, it leads to an asymmetry in the energy of solution, due to polarization of electrons of the anions, or to the preferential residence of anions in lower energy minima (if thermal motions are taken into account).

It is hoped that these calculations will make clear the importance of long-range interactions in ionic mixtures and will lead to an intuitive insight into the physical basis for the observed negative deviations from ideality.

I would like to acknowledge many enlightening discussions with Dr. R. F. Newton, of the Oak Ridge National Laboratory.

* Operated for the United States Atomic Energy Commission by Union Carbide Corporation.

[1] See for example, A. G. Bergman and E. P. Dergunov, Compt. rend. acad. sci. U.R.S.S. **31**, 753 (1941).

[2] O. J. Kleppa and L. S. Hersh, J. Chem. Phys. (to be published).

[3] T. Förland, *On the Properties of Some Mixtures of Fused Salts* (N. T. H. Trykk, Trondheim, Norway, 1958), see work cited in footnote 2.

Near-Ultraviolet Solution Spectra of Pyridazine

ROBERT H. LINNELL

Department of Chemistry, University of Vermont, Burlington, Vermont

(Received August 31, 1960)

THE near-ultraviolet solution spectra of the diazines by Halverson and Hirt[1] indicate that the band

near 3330 A is due to a nonbonding electron transition and the band near 2500 A to a pi-electron transition. The solvent shift of the long-wavelength band on changing from hydrocarbon to water is striking in the case of pyridazine, with $\lambda_{max}=3400$ A (hexane) and 2990 A (H_2O). Significantly, the short-wavelength pi-electron band does not shift appreciably on changing from hydrocarbon to water solvent. This note is to suggest a particular kind of H bonding as the reason for the large solvent shift of the ultraviolet band due to transitions of nonbonding electrons ($n-\pi^*$ transition).

Considering pyridazine to have benzene bond angles with all C—C bonds 1.40 A, C—N bonds 1.36 A,[2] then the N—N bond is 1.46 A. This seems a little long compared to N—N of 1.48 A and 1.34 A for N=N[2] but the C-ring structure would be expected to stretch the N—N somewhat. For H_2O with an H—O—H angle of 105° and O—H of 0.96 A, the H—H distance is 1.52 A.[2] It should therefore be possible for one molecule of H_2O to form two H bonds with pyridazine with an N—H—O bond angle of 126° assuming an N—H length of 1.9 A. This calculated bond angle is not very sensitive to either the N—N or N—H length so it gives us a good order of magnitude at worst. This calculated bond angle should be favorable for H bonding. By comparison, the N—H—O=C angle is 122° in amido and imido compounds.[3] The proposed H-bond would be expected to involve only the nonbonding electrons as the spectral data indicate. Finally, we calculate the spectral shift involves about 10 kcal, which would therefore be 5 kcal per H-bond on this model, a reasonable value for such a bond.

A stable complex with a somewhat analogous structure is known, namely, the monohydrate of 1,10-phenanthroline. The dissociation pressure of this hydrate has been measured at several temperatures,[4] yielding $\Delta H=14.5$ kcal, or 7.25 kcal for each N—H bond, assuming each water to be bonded by two N. The near-ultraviolet absorption of 1,10-phenanthroline has a long-wavelength band, $\lambda_{max}=2650$ A and short-wavelength band, $\lambda_{max}=2280$ A (both in H_2O, *p*H 14). One might be tempted to propose that one (or both) of the observed near-ultraviolet absorption bands is a nonbonding electron transition. This can not be the case, however, since in cyclohexane, $\lambda_{max}=2640$ A and 2320 A[5] and in concentrated H_2SO_4 we find λ_{max} 2780 and 2240 A, so that we cannot attribute either band to an $n-\pi^*$ transition (see footnote 1 for discussion).

[1] Frederick Halverson and Robert C. Hirt, J. Chem. Phys. **19**, 711 (1951); **17**, 1165 (1949).

[2] Y. K. Syrkin and M. E. Dyatkina, *Structure of Molecules and the Chemical Bond* (Interscience Publishers, Inc., New York, 1950); Linus Pauling, *The Nature of the Chemical Bond* (Cornell University Press, Ithaca, New York, 1960), 3rd ed.

[3] George C. Pimentel and Aubrey L. McClellan, *The Hydrogen Bond* (W. H. Freeman & Company, San Francisco, California, 1960).

[4] J. S. Fritz, F. William Cagle, and C. F. Smith, J. Am. Chem. Soc. **71**, 2480 (1949).

[5] R. H. Linnell, R. B. Martin, and A. Kaczmarczyk (unpublished).

Effect of Magnetic Nonequivalence in A_2B_2 NMR Spectra*

DAVID M. GRANT

Department of Chemistry, University of Utah, Salt Lake City, Utah

AND

H. S. GUTOWSKY

Noyes Chemical Laboratory, University of Illinois, Urbana, Illinois

(Received October 26, 1960)

THE proton magnetic resonance spectra of β-propiolactone,[1] ethylene monothiocarbonate,[2] *trans*-dibromocyclopropane[3] and 2,3-dihydrofuran[3] have been interpreted by several workers on the basis of equal

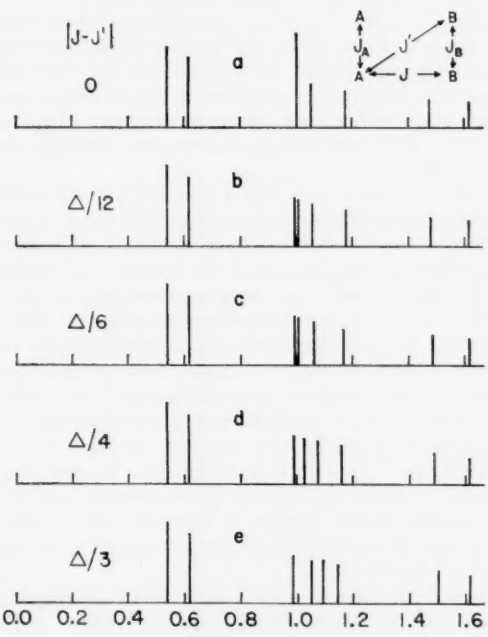

FIG. 1. Calculated high resolution NMR spectra for the A_2B_2 system, exhibiting the effects of magnetic nonequivalence $J \neq J'$. Only half of the spectrum is plotted; the other half is obtained by reflection at the left. The chemical shift between the A_2 and B_2 multiplets is defined as 2Δ cps, and the abscissa is given in units of Δ. In each of the calculated spectra it is assumed that

$$|J+J'|=|J_A+J_B|=|J_A-J_B|=\Delta.$$

cis and *trans* spin-spin coupling between the A and B nuclei in the A_2B_2 groups. These molecules have cyclic structures such that internal motional averaging about the carbon-carbon bonds is not possible, and, therefore, the *cis* coupling J is not necessarily the same as the *trans* J'. The proposed equality of the coupling constants ($J=J'$) has been explained in each case as accidental. However, the calculations summarized in Fig. 1 demonstrate that such a spectral assignment is not unique and that the magnetically equivalent A_2B_2 spectrum [Fig. 1(a)] can be duplicated with a magnetically nonequivalent assignment, $|J-J'|\neq 0$ [Fig. 1(b)–1(e)] provided that $|J_A+J_B|\gtrsim 5|J-J'|$ and $|J_A-J_B|\gtrsim 5|J-J'|$. The calculations in the figure assume that $J_B=0$; however, the results are similar for $J_B\neq 0$, if the conditions cited at the end of the previous sentence are met.

Comparison of the calculated spectra in Fig. 1(a)–1(e) reveals that the main effect of increasing $|J-J'|$ from zero is an initially very slow increase in the splitting of the pair of lines centered at $\nu=\Delta$, where 2Δ is the chemical shift in cps between the A_2 and B_2 sets. For $|J-J'|\lesssim\Delta/5$, this splitting is only about $(1/10)|J-J'|$. Thus, the question of magnetic equivalence is one of degree and experimental resolution. For example, if $|J+J'|=\Delta=10$ cps, and the resolution were 0.2 cps, $|J-J'|$ could be as large as 2 cps and the nonequivalence would not be apparent in the observed spectrum. In general, if this central pair of lines is not resolved, an upper limit can be placed upon $|J-J'|$, provided that approximate values are available for J_A, J_B and Δ.

Such arguments show that it is unlikely for each pair of AB coupling constants to be identical in all of the compounds mentioned, but there is evidence that they are about equal in some cases. For instance, one would expect the *cis* and *trans* coupling constants to have similar values in β-propiolactone because the corresponding constants have been found experimentally to be 4.9 and 5.9 cps in a substituted form of the compound, β-(p-nitrophenyl)-β-propiolactone.[4] In order for there to be a similar unobserved difference in β-propiolactone itself, it is necessary to have $|J_A-J_B|\gtrsim 5$ cps. The latter is reasonable, because the geminal coupling J_A between the α protons in β-(p-nitrophenyl)-β-propiolactone is 16.6 cps,[4] and a value of 11 cps or less for the β *geminal* coupling, J_B, is certainly feasible.

On the other hand, $|J-J'|$ might be of considerable magnitude in *trans*-dibromopropane because both $|J_A+J_B|$ and $|J_A-J_B|$ could be quite large. By designating the CH_2 group as A_2, we define J_A as the *geminal* coupling and J_B as the *trans*. Both of these can be sizeable, yet differ a good bit in magnitude. Of course, a reliable estimate of $|J-J'|$ in this compound would require at least approximate values for J_A and J_B in other substituted cyclopropanes.

The spectra presented here were computed on the Datatron 205 (University of Utah) and Illiac (University of Illinois) high-speed digital computers, using programs based upon an exact solution of the 4-spin system. A more detailed study of the NMR spectra of magnetically nonequivalent A_2B_2 groups is in progress and the results will be presented shortly.

*This work was supported in part by the Office of Naval Research and by the National Science Foundation. Also, acknowledgment is made to the donors of The Petroleum Research Fund, administered by The American Chemical Society, for partial support of this research.

[1] W. A. Anderson, Phys. Rev. **102**, 151 (1956). This case has been cited many, many times as one exhibiting accidentally degenerate coupling constants.

[2] P. L. Corio, Chem. Rev. **60**, 396 (1960).

[3] L. M. Jackman, *Applications of Nuclear Magnetic Resonance Spectroscopy in Organic Chemistry* (Pergamon Press, New York, 1959), p. 84.

[4] H. S. Gutowsky, M. Karplus, and D. M. Grant, J. Chem. Phys. **31**, 1278 (1959).

Correlation of Proton Magnetic Resonance Shifts with Group Dipole Moments in Substituted Ethylenes*

G. S. Reddy, C. E. Boozer, and J. H. Goldstein

Department of Chemistry, Emory University, Atlanta, Georgia

(Received October 20, 1960)

EMPIRICAL correlations of proton chemical shifts with various measures of electron withdrawing power of substituents such as electronegativity and dipole moments have been reported by a number of investigators.[1,2] Such correlations are of considerable theoretical interest as well as practical importance in the utilization of nuclear magnetic resonance data. We have been able to establish a linear relationship between the chemical shifts of the β protons in a series of substituted ethylenes, $H_2C{=}CHX$, and the group dipole moments of the substitutent X, where X=H, CH_3, Cl, OCH_3, CN, and C_6H_5. The shifts for vinyl chloride, vinyl cyanide, and methyl vinyl ether were obtained from analyses of their spectra using TMS as solvent and internal reference. The others were obtained from published data and converted to the same reference, using the value of +211.5 cps for the shift of TMS relative to water as the external reference.[3] The dipole moments used are those listed by Smyth.[4]

As shown in Fig. 1, the experimental *cis* and *trans* proton shifts each fall on a straight line when plotted against the dipole moments, except in the case of vinyl cyanide and styrene (solid circles and squares). However, when corrections for diamagnetic anisotropy of

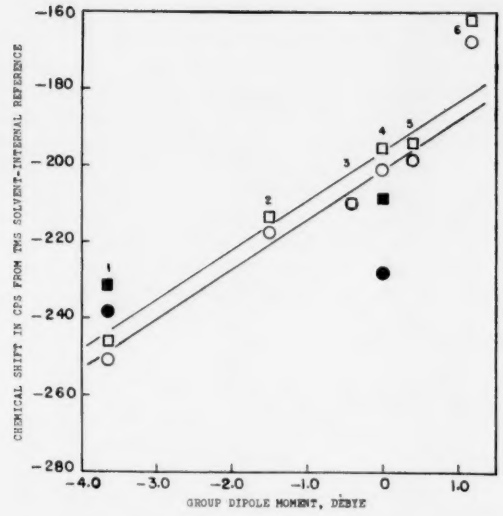

FIG. 1. Plot of group dipole moments vs resonance frequencies of the β protons in the series $H_2C{=}CHX$. The substituents and their group dipole moments are: (1) $C{\equiv}N = -3.6$, (2) $Cl = -1.5$, (3) $H = -0.4$, (4) $C_6H_5 = 0.0$, (5) $CH_3 = +0.4$, (6) $OCH_3 = +1.16$. These were calculated from values listed by C. P. Smyth, *Dielectric Behavior and Structure* (McGraw-Hill Book Company, Inc., New York, 1955). The circles and squares represent *cis* and *trans* proton shifts, respectively. The solid circles and squares in the case of vinyl cyanide and styrene are the chemical shifts before the corrections due to the anisotropy of the corresponding group were applied and the open circles are the shifts after the corrections were applied.

$C{\equiv}N$ and C_6H_5 are applied in the last two molecules, the resultant shifts (open circles and squares) also lie on the appropriate straight lines. The *cis* and *trans* plots are almost parallel, with the former lying towards the lower field.

In making the corrections for acrylonitrile we assumed as the value of the diamagnetic anisotropy factor $\Delta\chi$ for the nitrile group, the experimentally determined result for the acetylenic bond in methyl acetylene.[3] In the case of styrene, the anisotropy corrections were made on the basis of Ito's[5] estimation of the deshielding effect of the phenyl group on the ring protons assuming the plane of the benzene ring to be in the plane of the rest of the molecule.

In order for methylvinyl ether to fit even reasonably well with the series studied, it is necessary to make the CH_3O group, as a whole, positive with respect to ethylene. A similar situation occurs in *p*-chloroanisole, where the Cl and CH_3O group moments appear to augment, rather than cancel each other. It is evident that a very marked increase in shielding takes place at the β position in this molecule, the shift for these protons being about 100 cps higher than for, say, the vinyl halides.

* This work was supported by a Public Health Service Grant.

[1] L. H. Meyer and H. S. Gutowsky, J. Phys. Chem. **57**, 481 (1953).
[2] A. A. Bothner-by and C. Naar-Colin, J. Am. Chem. Soc. **80**, 1728 (1958).
[3] E. Whipple, Ph.D. dissertation, Emory University, 1959.
[4] C. P. Smyth, *Dielectric Behavior and Structure* (McGraw-Hill Book Company, Inc., New York, 1955).
[5] Kazuo Ito, J. Am. Chem. Soc. **80**, 3502 (1958).

Proton Hyperfine Splittings and Spin Densities of Pentaphenylcyclopentadienyl*

D. C. REITZ†

School of Chemistry, University of Minnesota, Minneapolis, Minnesota

(Received October 17, 1960)

A DILUTE liquid solution of the radical pentaphenylcyclopentadienyl(I) exhibits a symmetrical hyperfine spectrum of at least 33 lines separated by approximately 0.3 oe. The intensity of each line decreases as its distance from the center of the spectrum decreases. This is just the pattern one would expect if the ratios of the spin densities at the *o*, *m*, and *p* positions were similar to the same ratios in the odd-alternant radical triphenylmethyl.[1–5] If the proton splittings a_i of I have the approximate ratios $a_o = a_p = -2a_m$, then a spectrum of 41 lines decreasing in intensity from the center line would result. The intensity of the 3 or 4 lines on each end of the spectrum would be less than one-thousandth that of the central line, and would therefore be difficult to detect.

Table I lists the theoretical π-spin densities ρ_i at the various positions of I calculated from both simple Hückel MO theory[6] and Pauling-Wheland valence bond theory. The values listed in columns 1 and 3 result from all resonance integrals between adjacent orbitals being considered equal (all integrals between nonadjacent orbitals are neglected), and in columns 2 and 4 resonance integrals between orbitals on the 5 and 6 membered rings were reduced by one-half. This last approximation takes into account the nonplanarity

TABLE I. Theoretical and experimental spin densities of I.

Spin density	MO (1) planar	MO (2) twisted	VB (3) planar	VB (4) twisted	Obs (5)
ρ_1	0.033	0.018	0.114	0.030	0.030
ρ_2	0.001	0.001	−0.045	−0.016	0.015
ρ_3	0.029	0.014	0.071	0.027	0.030
ρ_4	0.008	0.008	0.004	−0.032	...
ρ_5	0.098	0.145	0.030	0.178	...

of the phenyl and cyclopentadienyl rings.[2] The only types of bond structures included in the valence bond calculations were

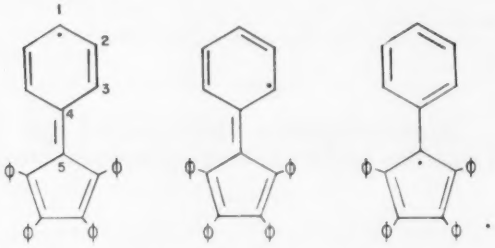

Column 5 lists the absolute values of the ρ_i calculated from the observed a_i by the relationship $a_i = Q\rho_i$. The observed values (assuming our analysis of the spectrum is correct) are $|a_o| = |a_p| = 0.72$ oe, $|a_m| = 0.36$ oe, and $|Q| = 24$ oe.

The pattern of spin-densities resulting from these calculations are close to what one obtains for odd-alternant systems[7]; the most conspicuous difference being the positive sign of ρ_4 in column 3. The twisted valence bond results (column 4) are in good agreement with experiment.

These results do not exclude the possibility that the molecule does not have D_{5h} symmetry. Liehr[8] and Snyder[9] have calculated the effects of Jahn-Teller distortions on the energy and spin densities of cyclopentadienyl (II). Their results indicate that the activation energy of a configurational conversion of II is only a few calories, however; the addition of 5 phenyl groups could result in a large enough activation energy for the molecule to be held in a deformed configuration.[10] If all the phenyl rings of I are not equivalent, there are several possible ratios of proton splittings which yield at least the 33 lines which may be observed.

The author wishes to thank Fricis Dravnieks for technical assistance, Professor John E. Wertz who made available the funds and equipment to support this work, and Professor Maurice Kreevoy for making the MO energies available and for several helpful conversations.

* This work was supported in part by a grant from the Air Force Office of Scientific Research.

† Present address: Radiation Physics Laboratory, Experimental Station, E. I. du Pont de Nemours & Company, Wilmington, Delaware.

[1] P. Brovetto and S. Ferroni, Nuovo cimento **5,** 142 (1957).
[2] F. C. Adam and S. I. Weissman, J. Am. Chem. Soc. **80,** 2057 (1958).
[3] D. C. Reitz, J. Chem. Phys. **30,** 1364 (1959).
[4] D. B. Chesnut and G. J. Sloan, J. Chem. Phys. **33,** 637 (1960).
[5] A. D. McLachlan, Mol. Phys. **3,** 233 (1960).
[6] M. Kreevoy, Tetrahedron **2,** 354 (1957).
[7] R. Lefebvre, H. Dearman, and H. McConnell, J. Chem. Phys. **32,** 176 (1960).
[8] A. D. Liehr, Z. physik Chem. (Frankfort) **9,** 338 (1956).
[9] L. C. Snyder, J. Chem. Phys. **33,** 619 (1960).
[10] Calculations by W. D. Hobey and A. D. McLachlan [J. Chem. Phys. **33,** 1694 (1960)] suggest that the addition of five phenyl groups to I will be much more likely to reduce the activation energy for interconversion than to increase it.

THE JOURNAL OF CHEMICAL PHYSICS

Heats of Mixing in Liquid Alkali Nitrate Systems
Solution at High Density to the Born-Green Equation
Quantum Calculations of the Velocity Dependence of the Scattering of Molecular Beams
Calculation of the Diamagnetic Susceptibility of H_2
Vibrational Relaxation in Liquids
Nuclear Magnetic Resonance Study of the Proton Transfer
Choice of Parameters for the Hückel a-Electron Method. Thiophene
Interpretation of Viscosity Data for Concentrated Polymer
Zero-Field Splitting of Molecular Zeeman Levels
Valence Bond Treatment on the B State of the Hydrogen Molecule
Theory of Light Scattering by Thin Rotating Macromolecules
Approximate Theory of Transport in Simple Dense Fluids
Spectroscopy of Fluorine Flames. I. Hydrogen-Fluorine Flame of HF
D. E. Mann, B. A.
Quasi-Lattice Model of Reciprocal Salt Systems. A
Effect of Solvent and Solute Structure on Scintillator
Substituted Styrene Plastic Scintillators with
Effect of Solvent and Solute Structure on Scintillation
Aromatic Liquid Organic Scintillators with
O_2 Vibration Relaxation in Oxygen-Argon Mixtures
O_2 Dissociation Rates in O_2-Ar Mixtures
Electron Spin Resonance Study of p-Benzoquinone-Diquinoyl
Infrared Spectra of Alkyldiboranes. IV. 1,1-Dimethyl- and
J. Walter J.
Note on the Calculation of Saturation Effects in
Mean Free Path and Ultrasonic Vibrational Relaxation
Energy Levels for Internal and Over-All Rotation in Silane
Spin Density in Pyrene Negative Ion
Application of the Free-Electron Theory to
Kinetics of the Reactions of Alkyl Iodides with HI
Reaction of Cyclopropane with Iodine and Some Observations on
X-Ray Diffraction Study of Lead Sulfide-Arsenic Sulfide
Infrared Spectrum of $Co(CO)_3NO$ Robin S. M
Closed General Solution of the Probability Distribution
Processes Calhoun
Electronic Structures and Spectra of Some Nitrogen-
Infrared Spectrum and Thermodynamic Properties of
Molecular Association in Alkali Halide Vapors
Temperature Dependence of the Proton Spin-Lattice
Robert A. Bern
Origin of the Green Bands in the Boron-Oxygen System
Transferability of Urey-Bradley Force Constants. VI. The
Determination of Relative Electronic Transition Probabilities
Stabilities of Gaseous Molecules in the Pb-Se and
Infrared Spectrum of Lithium Fluoride
Electron Spin Resonance of Some Vanadyl Porphyrins
NMR Spectra of 1,1,4,4-Tetramethylcyclohexyl-*cis* and